ISSN 0370—8691

NATIONAL ACADEMY OF SCIENCES OF THE REPUBLIC OF ARMENIA

Communications of the Byurakan Astrophysical Observatory

2

Erevan 2021

Communications of BAO, Vol. 68, Issue 2, 2021, pp. 139-142

Editorial

ComBAO board *

NAS RA V. Ambartsumian Byurakan Astrophysical Observatory (BAO)

Modern astronomy in Armenia began exactly 75 years ago, in 1946, when the Byurakan Astrophysical Observatory (BAO) was founded. The founder of the observatory was Viktor Ambartsumian (1908-1996), who at that time was already a world-renowned scientist and the author of many very famous works devoted to the study of various problems of astrophysics, theoretical physics, nuclear physics, mathematics. He became the first director of the observatory, and, naturally, his scientific experience and physical intuition played the main role in predetermining the directions for further scientific research of the new research center. In 1946, the design of the observatory complex began, and then construction. Famous architect Samvel Safaryan was the chief architect of the first stage of the observatory complex. In fact, he designed all the first buildings and telescope towers.

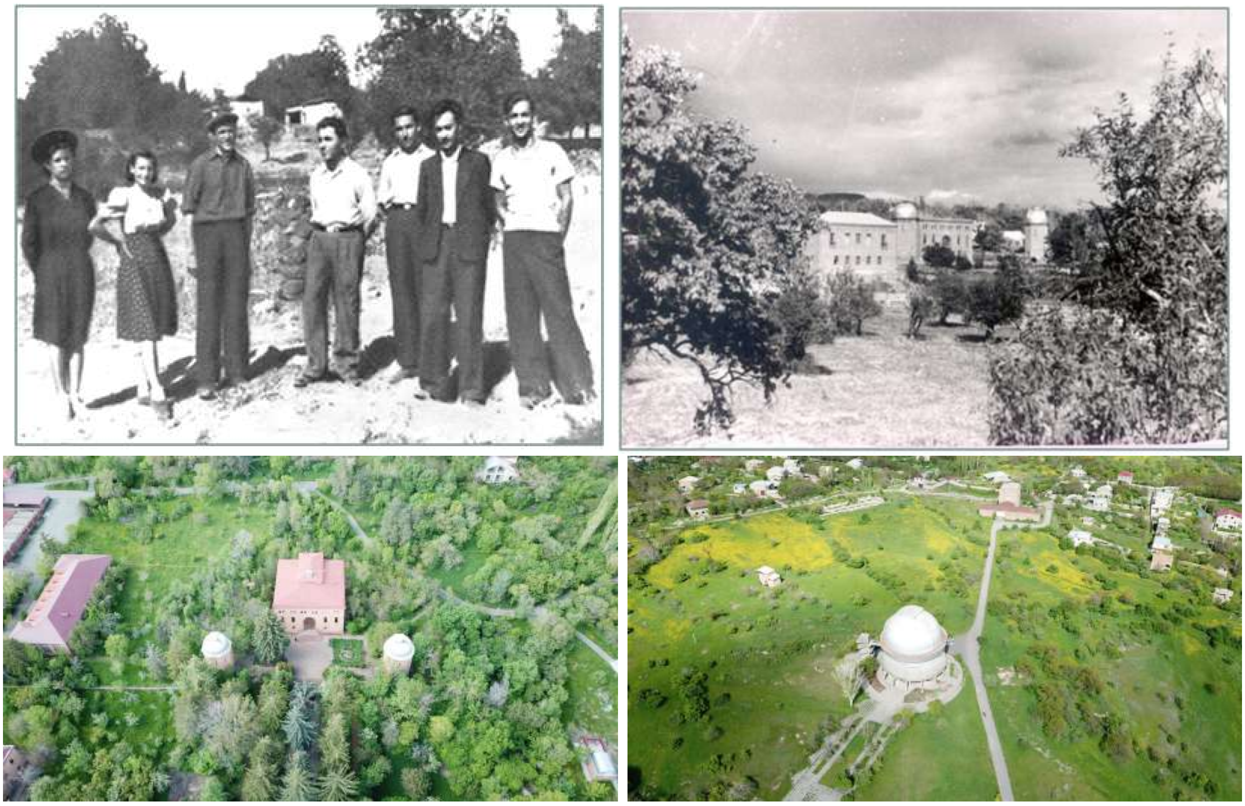

Figure 1. *Up left panel*: The Byurakan observatory here will be, 1946; *up right panel*: view of observatory in 1950s; *down panels*: view of observatory at present.

.

From the very beginning of the observatory's activities, the main target of astrophysical research has become non-stationary phenomena in cosmic objects and their systems. This was due to the fact that only non-stationary phenomena could prompt the correct path of evolution of cosmic structures in short-period observations. Completely new scientific results came immediately after the founding of the Byurakan Observatory. In 1947, Ambartsumian drew attention to some groupings of hot stars, the probability of accidental merging of which is practically zero. He called these new type systems stellar associations. The analysis of the dynamics of these systems showed that both the associations themselves and the stars

*combao@bao.am

included in these systems should be much younger than our Galaxy. Thus, it was shown for the first time that star formation processes are currently taking place in the Universe. The second important conclusion was that the formation of stars is not an individual process but it takes place in groups from much denser, so called, super-dense matter. Moreover, another essential conclusion made on the base of that research was one asserting that existing gas and dust are results of the same cosmogonic process.

Figure 2. Byurakan in winter.

The approach to problems of a cosmogonic nature, which was tested for the study of stellar associations, became the basis of the methodology for further research in Byurakan. The main thing in this methodology was the unbiased application of the entire arsenal of modern science for the analysis of observational data.It is this approach, using the methods of statistical mechanics, the dynamic features of the structures under consideration, that provided fairly reliable interpretations and predictions in the evolutionary chain. This applies to objects of all hierarchical levels of the Universe, from atomic nuclei and elementary particles to galaxies and galaxy clusters. All these structures show some physical properties that should become cornerstone if the main determinants of their evolutionary paths are considered. Thanks to the selected scientific topics, the methodology for conducting scientific research and the effective use of in fact not very large telescopes, the Byurakan observatory very quickly became widely known throughout the world.

The study of the dynamic properties of stellar associations and unexpected conclusions for the scientific community about the process of star formation had far-reaching consequences both for this area of scientific research and for the worldwide presentation of the Byurakan Observatory. Therefore, it is not surprising that many researchers began to visit the BAO, and in November 1951, the first international conference was held here. The conference was devoted to the stellar associations recently discovered in Byurakan and the spatial distribution of hot giants that make up the population of OB associations. Since then, about 90 symposia and conferences have been held in Byurakan, including symposia of the International Astronomical Union, as well as the congress of the European Astronomical Society.

The next area of research, begun at the BAO in the tradition of studying stellar associations, was a radical revision of the cosmogonic significance of galactic nuclei.This work began in the mid-1950s with determination of the relative number of multiple galaxies in clusters, which turned out to be excessively large compared to the estimate made for the equilibrium distribution. A detailed analysis based on the laws of physics, statistics and observational data again led to the conclusion that in many cases we are witnessing the decay of galactic nuclei, the ejection of huge masses from nuclei, etc. In other words, at the hierarchical level of galaxies, as in the case of young stars, the formation of galaxies occurs due to the decay of the denser matter of the core. This is how the term Active Galactic Nucleus (AGN) came into use for the first time. The results of the studies of this period were presented at the symposium of the International Astronomical Union IAU 29 "Non-stable phenomena in galaxies", which was organized in 1966 in Byurakan. All the most famous scientists working in this field attended this symposium.

Figure 3. IAU 29, 1966, Byurakan observatory.

At about the same time, on the initiative of Viktor Ambartsumian in Byurakan, Beniamin Markarian began a large observational project with the 1 m Schmidt telescope - a spectral sky survey, in order to search for galaxies with an ultraviolet excess in the spectrum. This project turned out to be one of the most successful observational campaigns, the result of which was the discovery of about 1500 galaxies, which today are known as the Markarian galaxies and are still being intensively studied all over the world. Today this survey (First Byurakan Survey, FBS) is included in the UNESCO documentary heritage "Memory of the World" and is one of the few scientific achievements included in the UNESCO heritage list.In addition to photographic plates, this survey is already available in digital form, carried out in international cooperation.

Both the discovery of newborn stars and the reassessment of the significance of galactic nuclei and the introduction of the concept of "Active galactic nuclei" undoubtedly made the Byurakan observatory famous. However, these are not the only innovations introduced into science by the Byurakan Observatory. A similar megaproject turned out to be the study of flare stars and the ultimate determination of the flare activity role in the evolutionary chain of non-stationary stars. The international observational campaign organized by the BAO made possible to prove that the flare activity of stars is a regular stage in the life of young stars. In the BAO and other observatories, many hundreds of flare stars have been revealed in star clusters and in the vicinity of the Sun during 70s and 80s. Unlike the 60s and 70s at present, there is no any doubt that this phenomenon is extremely common in the various types of stars.

In parallel with the major observational projects, from the very beginning, many works on theoretical astrophysics, as well as on the interpretation of observational data, were carried out at the BAO. Especially many articles have been published on the theory of radiation transfer. Many results have been obtained in the field of solving problems in the theory of radiation transfer under general laws of energy redistribution. Nonlinear problems, problems of non-stationary scattering, etc. are also considered. Moreover, unlike other scientific schools, in the BAO these problems were considered and are considered not by the method of the classical transfer equation, but using the Ambartsumian Invariance Principle, which turned out to be a rather powerfull tool for solving problems in this area. In 1981. in Byurakan an international symposium "The principle of invariance and its applications" was organized by J.-C. Pecker.

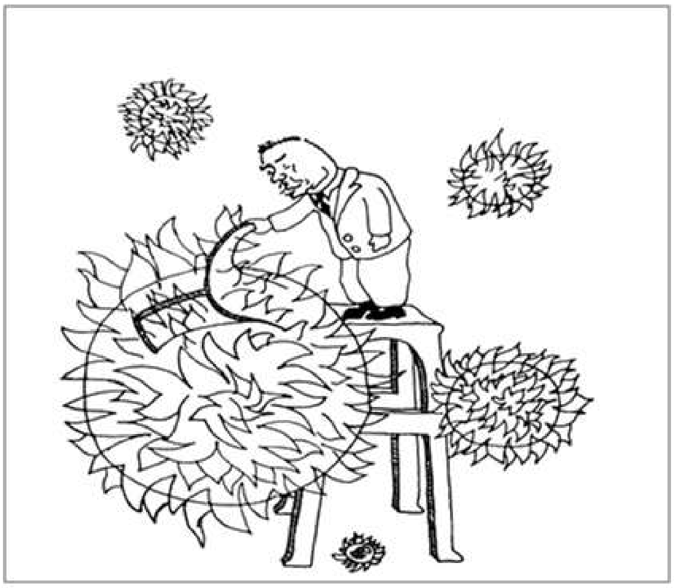

Figure 4. "The principle of invariance". Interpretation of by J.-C. Pecker.

Despite the fact that the Byurakan Observatory was created as a center for astrophysical research, very important conferences and symposia were held here that had no direct relation to astrophysics, like the research areas listed above. Such ones were the conferences, for example, devoted to the problems of communication with extraterrestrial civilizations. The first such conference was organized back in 1964. The second one had a completely different status. It was a first-class Soviet-American symposium attended by representatives of many branches of science. It was organized in 1971, and for the first time the topic studied was called "Communication with Extraterrestrial Intelligence" (CETI).

There is another interesting fact. Armenian astronomers at the Byurakan Observatory discovered many new cosmic objects, which are still being studied by many researchers around the world. We have already mentioned Markarian galaxies. There are also the Arakelian galaxies, the Ghazarian galaxies, the Parsamian cometary nebulae, the Gyulbudagian & Maghakian nebulae, the Shahbazian compact groups of compact galaxies, and others.

Communications of BAO, Vol. 68, Issue 2, 2018, pp. 143-149

Discovery and studies of stellar associations. The Key to Understanding Star Evolution

A.A. Akopian *

Byurakan Astrophysical Observatory, Armenia

Abstract

The review presents works carried out in BAO in the period 1947-70. It tells about the history and significance of one of the greatest discoveries of the twentieth century - stellar associations. Among the fundamental works of Ambartsumian and BAO studies of stellar associations occupy a special place. Their discovery radically changed the existing theories of star formation and evolution and "revived" the slowly dying (as previously assumed) Universe. The discovery of stellar associations proved that star formation occurs in our era. Ambartsumian's ideas clarified the existing and somewhat confusing theory of stellar evolution and gradually became one of the generally accepted directions of the theory of stellar evolution. For more than 75 years, scientists from the BAO and many observatories around the world have been studying stellar associations, but surprises and discoveries are not exhausted. Metaphorically, one can say that for a long time astronomers will follow the path illuminated by stellar associations.

Keywords: *stellar association, evolution*

1. Introduction

Over the 75-year history of the Byurakan Astrophysical Observatory (BAO), various scientific studies in the field of astrophysics have been carried out, many of which have gained great recognition in the former Soviet Union and the world. The first cycle of works - the discovery and study of stellar associations - stands apart among them. It was these works that brought the BAO world fame, and the director of the observatory, Victor Ambartsumian, rightfully took an honourable place among the greatest scientists of the 20th century. According to many scientists and experts in science, it is these works are the most significant contribution of Ambartsumian and BAO to world science.

On October 27, 1947, at the General Meeting of the Academy of Sciences of the USSR, Ambartsumian presented a report "Modern astrophysics and cosmogony", a revised version of which was published by the publishing house of the Academy of Sciences of Armenia under the title "Evolution of stars and astrophysics". In this work, Ambartsumian established and substantiated the existence of a new type of stellar system - stellar associations. In the subsequent works of Ambartsumian (1949-1959), the main ideas of this work were developed and presented to a wider circle of scientists.

The author of this review was faced with the difficulty task of presenting the achievements of the BAO in this area since they were repeatedly presented in the books and excellent articles of Ambartsumian, Mirzoyan and other famous scientists. The author was always interested in the question of why for the first article, among all possible attractive titles, Ambartsumian chose exactly this ("Evolution of stars and astrophysics"), changing the title of the report? The key change was the introduction of the phrase "evolution of stars". Maybe it meant that the main results of this work will impact the theory of evolution of stars and Ambartsumian wanted to emphasize it? Therefore, it was decided to present these achievements in light of the development of the ideas of the theory of stellar evolution.

The review presents the works carried out in BAO in the period 1947-70, which are of a more general and fundamental nature. The articles after 1970 are mainly devoted to individual associations or young non-stable stars and stellar systems that are part of associations. There are many high-quality works among them, which deserve separate consideration.

*aakopian57@gmail.com

doi: doi.org/10.52526/25792776-2021.68.2-143

2. Some historical remarks on the stellar evolution theory

In all areas of science (social, biology, etc.), evolutionary problems are the most attractive. Naturally, astronomy is no exception. The evolution of stars became the subject of fundamental research after the appearance of the H-R diagram. In 1911, Danish astronomer Hertzsprung published a diagram of the absolute luminosity of stars in the Pleiades and Hyades star clusters, versus their spectral type or effective temperature. In 1914 American astronomer Russell published a similar diagram for feld stars, and such plots are now known as Hertzsprung-Russell (H-R) diagrams. The H-R diagram, together with the theory of radiative equilibrium in stars (Schwarzschild K., Eddington), has become an important tool for understanding and interpreting stellar evolution.

The somewhat bizarre view of the diagram (Jeans used the geographic names of the world map to describe the diagram) shows the existence of clearly separated groups of stars with possible connections between them. It became obvious that any theory of evolution must be self-consistent with the H-R diagram.

Sometimes a joint analysis of the accumulated data and H-R diagram led to interesting results, such as Russell's brilliant hypothesis about the jump-like changes of stars in the process of evolution. According to Russell (1914) "...It is conceivable that at some particular epoch in a star's history there might be so rapid an evolution of energy - for example, of a radioactive nature - that it temporarily surpassed the loss by radiation and led to an expansion against gravity; but this would be, at most, a passing stage in its career, and it would still be true in the long run that the order of increasing density is the order of advancing evolution."

It must be admitted that at the beginning of the 20th century, there were no prerequisites for the development of the theory of evolution due to the lack of high-quality observational data on the distances, masses, luminosity, temperature, etc. of stars. But the main problems were associated with the lack of exact estimates of the age of stars/star systems and ignorance of the source of radiation energy of stars.

In the scheme of Russell (1914), evolution proceeds in the direction of "red giants - blue giants - red dwarfs". This scheme was consistent with Lockyer (1899, 1902) idea that stars reach their maximum luminosity by the middle of their life, as well as the generally accepted idea that a star contracts as a result of evolution ("... of all the propositions, more or less debatable, which may be made regarding stellar evolution, there is probably none that would command more general acceptance than this—that as a star grows older it contracts." - Russell (1914)). It follows from this scheme that the observed differences between the stars are because they are at different stages (different ages) of their development.

On the contrary, in the Jeans evolution scheme, it was suggested that the overwhelming majority of stars have almost the same age. According to Jeans (1929) "... There is rather distinct evidence of a special birth of stars at about the time when our Sun was born, and this leads naturally to the conjecture that the galactic system was born out of a spiral nebula whose main activity in producing stars centred around that epoch". Consequently, the observed differences between stars are associated with different initial conditions for star formation.

In both schemes, there are very vague ideas about the absolute age of stars and the rate of evolution, as well as a clearly predictable and sad future, described by Jeans in a "theatrical" (literally and figuratively) manner - "... perhaps the main drama of the Universe is over, and our fate is simply watch the unwanted ends of the lighted candles go out on an empty stage".

An important step in understanding the evolution of stars was revelation of Bethe (1939) that thermonuclear reactions, particularly the combustion of hydrogen, are the source of stellar energy. It seemed that this discovery could also solve the basic problems of stellar evolution. According to Gamow (1939) "... we can say that, due to the application of our present knowledge of nuclear physics, the problem of stellar energy sources and the main features of stellar evolution can be considered at present as practically solved".

Gamow developed his theory of evolution reasonably criticized by Lyttleton & Hoyle (1940). According to them "... **It has been customary during recent years for investigators on stellar evolution to devote attention to internal constitution with little or no regard for the dynamical features.** It appears that Prof. Gamow has followed essentially in this tradition and therefore confined his article to the modifications effected by the introduction of modern nuclear theory".

The importance of considering the dynamical characteristics of stars in the problems of evolution was accurately emphasized by Russell 20 years earlier. According to Russell (1919) studies of Galactic systems "... lead up to a single ultimate problem, which may be defined as the representation of the present positions and motions of the stars as a stage in the history of a dynamical system (whether in a steady state or not) and the deduction of the presumable history of the system in the past and the future. Among the subsidiary

doi: doi.org/10.52526/25792776-2021.68.2-143

problems connected with this are (a) the existence, character, distribution and gravitational influence of possible dark or absorbing matter in space; **(b) the relation between the age or evolutionary stage of a star and its position and motion within the galactic systems. The latter connects the problems of stellar and galactic evolution in such a way that any notable advance in the solution of one is likely to be of aid in that of the other, while an unfounded assumption regarding either will probably confuse the discussion of both.”**

Hoyle and Lyttleton also rightly criticized Gamow’s views about the ages of stars and star formation in our era. In turn, Gamow (1940) suggested that the mechanism of accretion of interstellar matter onto stars proposed by Hoyle and Lyttleton could not contribute significantly to the luminosity of the giant stars[1] Ironically, these prominent scientists, as it turned out, were closer to the truth in their critics of each other than in their works on this topic. In particular, according to Hoyle’s theory of accretion, the formation whole of stars in the Galaxy took place in the distant past, and all hot giants are also old stars.

Thus, Hoyle and his co-authors tried to solve one of two main problems associated with hot giant stars - the determination of the source of his high luminosity over a long time scale. Another problem was the existence of groups of O stars (or helium stars, as they were then called), investigated by Kapteyn (1914, 1918a,b,c). Given the rareness of such stars, it is unlikely that such groups could have formed accidentally.

Both problems found a brilliant solution in the works of Ambartsumian on stellar associations. Using his original approach (which he called ”observational”) to solving scientific problems, he considered these problems in conjunction with other characteristics of stars and their systems, in particular, with dynamical and kinematical ones. This led him to the discovery of stellar associations as a new type of star cluster, in which star formation processes are going at the present epoch. Ambartsumian approach to the problems of evolution was in complete harmony with Russell approach cited above. This approach sets them apart from other great astronomers of the time. Ambartsumian’s ideas clarified the existing and somewhat confusing theory of stellar evolution and gradually became one of the generally accepted mainstreams of the theory of stellar evolution.

3. Discovery of associations, their main characteristics

A stellar association is a spatial group of stars belonging to a certain physical type (relatively rare). The partial density of such stars (concentration per unit area of the celestial sphere) in the association is high, but it is less than the average density of whole of stars in a given region of the celestial sphere. As a result, the stars - members of the association are practically not connected with each other by the force of gravity, but experience the gravitational influence of other stars in this region, as a result of which the association disintegrates. Its constituent stars are scattered among the field stars. The calculation of the association disintegration time led to the conclusion that it does not exceed several million years.

Ambartsumian established the existence of associations of two types - O and T, the main stellar population of which consists of objects located at diametrically opposite ends of the H-R diagram - OB giant and T Tau type (red dwarf) stars, respectively. Ambartsumian was the first to establish that class O giants are born in groups - apparently, together with stars of lesser luminosity. The latter circumstance is confirmed by the fact that some of the O-associations contain many T Tau stars. Ambartsumian also noted the connection of T-associations with diffuse gaseous nebulae. This observational fact subsequently played a significant role in the development of theoretical concepts of stellar formations.

Analysis of relatively scarce data has led him to the conclusion that ”... stellar associations (and some clusters) are young systems of stars that somehow formed in our Galaxy, but did not form by combining previously independent stars. Consequently, stars belonging to associations and clusters did not exist before the appearance of the corresponding associations and clusters. On the other hand, these systems themselves are, by definition, composed of stars. We come to the inevitable conclusion that stars in open clusters (associations) are formed during the formation of this cluster (associations)”. From this, Ambartsumian made two conclusions, which are very important not only for astrophysics but also for the whole of natural science:

(i) Star formation in the Galaxy continues even now, in our epoch.

[1] Later Ambartsumian (1954c, after the discovery of stellar associations) criticized Hoyle’s theory of accretion for the same reason and noted that the very existence of stellar associations and their expansion refutes the theory of accretion (Ambartsumian, 1954b).

doi: doi.org/10.52526/25792776-2021.68.2-143

(ii) Stars are born in groups.

This was a refutation of the concept of the simultaneous origin of stars in the Galaxy. This work became a basis for astronomical studies of the evolution of stars and stellar systems by observing their development. This unorthodox view found support from various sides, including studies of the source of stellar (nuclear) energy and the study of the relative motions of the stars in the associations:

1) Based on the dynamic characteristics of associations, Ambartsumian pointed out that many associations cannot be bound by their own gravity and, therefore, must be in a state of expansion. He estimated their ages to be of the order of 10^7 years. For the O and B stars, ages of the same order had previously been estimated based on the luminosity and the energy sources, for instance, by Unsöld (1948). It is important to note that the "age" of a star, determined in this way, is actually an estimate of the duration of the evolutionary stage at which the star is at a given moment. Such estimates do not take into account the relation between the age / evolutionary stage of a star and its position and motion in galactic systems (see Russell's note above). Ignoring this circumstance sometimes can lead to erroneous conclusions, as in Gamow's theory of red giants.

2) Dynamical studies, such as those of Bok (1934) and Mineur (1939), have shown that clusters in the vicinity of the Sun with densities below about $0.1 M_{\odot}/pc^3$ are unstable. For densities an order of magnitude lower, their movements are governed by the gravitational field of the Galaxy, and not by the gravity of the members of the group themselves. It is important to note here that the disintegration of clusters because of the tidal effect (discussed these articles) leads to a change in the primary, presumably spherical shape of the cluster. Due to differential rotation, the clusters elongates and loses their spherical shape, which is not observed in the case of O-associations. It was this fact that allowed Ambartsumian to suggest that, in addition to the tidal mechanism, there is an internal mechanism of radially symmetric expansion of the association, which dominates over the tidal one and allows the association to retain a spherical shape. For such domination, the expansion rate must be of the order of $5 \div 10$ km/s.

3) The theoretical prediction (in 1947-49) of Ambartsumian about the dynamic instability of stellar associations and their expansion was confirmed as a result of an analysis of the motions (both tangential and radial) of stars carried out in Leiden (Blaauw, 1952, 1964, 1978) and Byurakan (Mirzoyan, 1966, Mirzoyan & Mnatsakanyan, 1970) observatories. Modern astrometric studies with the space observatories *HIPPARCOS* and *GAIA* have confirmed the results obtained on the dynamic instability of associations.

The study of associations and the analysis of observational facts (huge positive energy of associations and their expansion, the initially small volume of the region of formation, etc.) led Ambartsumian to an unconventional point of view on the origin and decay of stellar associations. He suggested that stars were formed from superdense bodies - a hitherto unknown state of matter, which contradicted the generally accepted view that star formation occurs due to the gradual compression of an interstellar gas cloud.

Ambartsumian views stimulated his opponents to develop their theories of the origin of associations and their expansion. Oort (1952, 1954), Opik (1953), and Zwicky (1953) suggested their own mechanisms of formation and expansion of stellar associations, based on the traditional view. In the modern theory of the formation of associations and their following expansion, some elements of all these mechanisms are included, but the basic idea is more close to Zwicky view.

4. Some important results of the early stage studies (1947-70)

The study of associations in the BAO can be conditionally divided into two stages: before 1970 and after it. Until 1970, articles were devoted to the fundamental problems of a) the formation and decay/expansion of associations, b) star formation in associations, c) the place and role of associations in the theory of evolution, etc. These works were carried out by a surprisingly small number of astronomers - the first disciples of Ambartsumian, who later became internationally recognized scientists. Among them were future academicians Markarian, Mirzoyan and Gurzadian.

The discovery of associations and group nature of star formation made it possible to directly study the nature and cosmogonic role of double and multiple stars, stellar chains, Trapezium-type systems, star

doi: doi.org/10.52526/25792776-2021.68.2-143

clusters, gaseous and cometary nebulae, non-stable stars, are stars, emission stars, globules, FUors and EXors, YSO etc. After 1970, the overwhelming majority of articles are devoted to these objects - members of associations. Drastically has increased the number of astronomers involved in these works, as well as published articles. The beginning of these works was laid in the works of Ambartsumian, in particular, in the work "Multiple systems of Trapezium type", which is an impeccable example of solving statistical problems. This article does not review these works. They deserve separate consideration.

Therefore, some important works of the first period are presented here to get a complete picture of the research of this period (1947-70).

In the 50s, Markarian, together with Ambartsumian, actively participated in the study of associations. It is worth noting his work on identifying associations between groups of OB (Markarian, 1951-52) stars and creating the first catalogue of OB stars. The first lists of O - associations were published by Markarian (1951), Morgan et al. (1953), and Code & Houck (1958). Because the nomenclatures used in these lists were differed each from other, Commission 37 (Star Clusters and Associations) of the International Astronomical Union, at the 1961 Berkeley Meetings, recommended the use of the Markarian nomenclature.

Another cycle of his works (1950-59) is devoted to the study of open stellar O-clusters in O-associations, in particular, their dynamic state and possible paths of evolution. The possible genetic relationships of associations and clusters were also considered.

In the sixties, Mirzoyan, another famous Armenian astrophysicist, actively joined the research of the associations. An interesting method for estimation of development rates of OB stars in stellar associations was proposed by him Mirzoyan (1961, 1964, 1965). Since the number of OB stars in individual associations is small, to increase the statistical reliability, he built one "synthetic association" from known associations and introduced the concept of the ageing function, which is actually the law of the change in the stream of stars with increasing distance from the nucleus of the "synthetic association" as a result ageing and rate gradient. Thus, thanks to this function, it is possible to estimate the rate of ageing of stars in associations.

Later, the velocity distribution of O-B stars in a "synthetic association" has been investigated by Mirzoyan & Mnatsakanyan (1970). They presented a method for the determination of the mean velocity of stars in spherically symmetric systems at different distances from the centre, using their residual radial velocities and the distribution projected on the celestial sphere and applied this method to the synthetic association. It was shown that the dependence of the mean space velocity of the stars on the distance from the centre of the system is a linearly increasing function. This can be regarded as another important evidence for the expansion of associations and their dynamical instability.

5. A brief chronology of the results of early studies of stellar associations

1) 1947-1949 Discovering of stellar associations - Ambartsumian

2) 1949-1950 Early studies of stellar association and connected stellar clusters and star groups - Ambartsumian, Markarian

3) 1950 - Ambartsumian and Markarian for the "... for the discovery and study of a new type of stellar systems (stellar associations), presented in a series of articles published in the journals: "Communication of the Byurakan Observatory", "Reports of the Academy of Sciences of the Armenian SSR", and "Soviet Astronomical Journal" (e.g. Ambartsumian, 1949, 1950, Ambartsumian & Markarian, 1949)" were awarded by the Soviet State prize[2].

4) 1951-52 - The first lists of O - associations were published by Markarian.

5) 1954 - Statistical study of multiple systems of Trapezium type - Ambartsumian.

6) 1950-54 - Studies of O type open clusters, their evolution and relation to host O association - Markarian.

7) 1961-1970 - Continuous formation and rates of development of stars in stellar associations: synthetic association, ageing function. Confirmation of expansion by analysis of radial motion - Mirzoyan; Mirzoyan and Mnatsakanian.

[2] https://ru.wikipedia.org/wiki/

doi: doi.org/10.52526/25792776-2021.68.2-143

6. Conclusion

The review presents works carried out in BAO in the period 1947-70. It tells about the history and significance of one of the greatest discoveries of the twentieth century - stellar associations. Among the fundamental works of Ambartsumian and BAO studies of stellar associations occupy a special place. Their discovery radically changed the existing theories of star formation and evolution and "revived" the slowly dying (as previously assumed) Universe. The discovery of stellar associations proved that star formation occurs in our era. Ambartsumian's ideas clarified the existing and somewhat confusing theory of stellar evolution and gradually became one of the generally accepted directions of the theory of stellar evolution. For more than 75 years, scientists from the BAO and many observatories around the world have been studying stellar associations, but surprises and discoveries are not exhausted. Metaphorically, one can say that for a long time astronomers will follow the path illuminated by stellar associations.

References

Ambartsumian V. A., 1947, The evolution of stars and astrophysics. Acad. Sci. ArmSSR, Yerevan

Ambartsumian V. A., 1949, Astronomicheskii Zhurnal, 26, 3

Ambartsumian V. A., 1950, Izv. Akad.Nauk USSR, Phys. Ser., 14, 15

Ambartsumian V. A., 1954a, in Liege International Astrophysical Colloquia. p. 293

Ambartsumian V. A., 1954b, Communications of the Byurakan Astrophysical Observatory, 13, 3

Ambartsumian V. A., 1954c, Communications of the Byurakan Astrophysical Observatory, 15, 3

Ambartsumian V. A., Markarian B. E., 1949, Communications of the Byurakan Astrophysical Observatory, 2, 3

Bethe H. A., 1939, Physical Review, 55, 434

Blaauw A., 1952, Bull. Astron. Inst. Neth. , 11, 405

Blaauw A., 1964, Annual Review of Astronomy and Astrophysics, 2, 213

Blaauw A., 1978, Internal Motions and Age of the Sub-Association Upper Scorpio. Problems of Physics and Evolution of the Universe., Edited by L.V. Mirzoyan, Yerevan, Publishing House of the Armenian Academy of Sciences, p. 101

Bok B. J., 1934, Harvard College Observatory Circular, 384, 1

Code A. D., Houck T. E., 1958, Publ. Astron. Soc. Pac. , 70, 261

Gamow G., 1939, Nature. , 144, 620

Gamow G., 1940, Nature. , 146, 97

Jeans J. H., 1929, The universe around us. Astronomy and Cosmogony, 428

Kapteyn J. C., 1914, Astrophys. J. , 40, 43

Kapteyn J. C., 1918a, Astrophys. J. , 47, 104

Kapteyn J. C., 1918b, Astrophys. J. , 47, 146

Kapteyn J. C., 1918c, Astrophys. J. , 47, 255

Lockyer N., 1899, Proceedings of the Royal Society of London Series I, 65, 186

Lockyer N., 1902, Philosophical Transactions of the Royal Society of London Series A, 198, 375

Lyttleton R. A., Hoyle F., 1940, Nature. , 146, 97

Markarian B. E., 1951, Communications of the Byurakan Astrophysical Observatory, 9, 3

Mineur H., 1939, Annales d'Astrophysique, 2, 1

Mirzoyan L. V., 1961, Communications of the Byurakan Astrophysical Observatory, 29, 81

Mirzoyan L. V., 1964, Communications of the Byurakan Astrophysical Observatory, 35, 75

Mirzoyan L. V., 1965, Astrophysics, 1, 70

Mirzoyan L. V., 1966, Transactions of the International Astronomical Union, Series B, 12B, 419

Mirzoyan L. V., Mnatsakanyan M. A., 1970, Astrophysics, 6, 221

Morgan W. W., Whitford A. E., Code A. D., 1953, Astrophys. J. , 118, 318

Oort J. H., 1952, Astrophys. J. , 116, 233

Oort J. H., 1954, Bull. Astron. Inst. Neth. , 12, 177

Opik E. J., 1953, Irish Astronomical Journal, 2, 219

Russell H. N., 1914, Nature. , 93, 281

Russell H. N., 1919, Proceedings of the National Academy of Science, 5, 391

Unsöld A., 1948, Zeitschrift für Astrophysik, 24, 278

Zwicky F., 1953, Publ. Astron. Soc. Pac. , 65, 205

Communications of BAO, Vol. 68, Issue 2, 2021, pp. 150-162

Statistical studies of flare stars and other flashing objects carried out at the Byurakan Observatory

A.A. Akopian *

Byurakan Astrophysical Observatory, Armenia

Abstract

The review briefly presents the statistical studies of flare stars and related objects carried out at the Byurakan Astrophysical Observatory, in particular: i) determination of the evolutionary status of flare stars, ii) an explanation of the observed difference between flare stars of the galactic field (type UV Cet) and flare stars of systems (open clusters, associations), iii) the connection between flare stars and T Tauri stars, iv) short-term and long-term (evolutionary) variability of flare activity, v) original statistical methods developed for the study of flare stars and their systems, vi) recent advances in research on flashing objects. This review does not present such important areas of research on flare stars as the determination of physical parameters, photometry and colorimetry of stars and their flares, detailed studies of individual stars, theoretical works on possible mechanisms of flares. These areas were well presented in many books and reviews by Ambartsumian and Mirzoyan.

1. Introduction

In the first years after the founding of the BAO, Ambartsumian's main research was related to the origin and development of celestial bodies. Analysis of the accumulated observational data allowed him in 1947 to discover in the Galaxy new type stellar systems, which he called "stellar associations". He established the existence of two types of associations - OB and T and predicted that they are dynamically unstable systems and have a relatively recent origin. The prediction by Ambartsumian (1947, 1949) about the dynamic instability of stellar associations and their expansion was confirmed as a result of the analysis of proper motions of associations stars, carried out in Leiden observatory by Blaauw and coworkers.

This led to the inevitable and fundamental conclusion about the continuous process of star formation at the present stage of the development of the Galaxy. This was a refutation of the concept of the simultaneous origin of stars in the Galaxy. This work indicated the fundamental possibility of observing and studying the development of stars and opened the door for astronomical studies of the evolution of stars and stellar systems, which seemed almost impossible within the framework of the old ideas about the origin of stars.

Ambartsumian drew attention to unusual continuous radiation - another feature of the physical nature of members of stellar associations, observed, in particular, in stars of the T Tauri and UV Ceti type/flare stars, as well as in cometary nebulae, and to the nonthermal origin of this continuous emission. The flare activity of UV Ceti type/flare stars is one of the most characteristic features of the red dwarf stars at the early stages of evolution. The radiation emitted from a UV Ceti type/flare star during the flare, which occurs between the long periods of the quiescent state of the star, shows physical similarity with the radiation of T Tauri type stars. But even during the quiescent state, the radiation spectrum displays some signs of chromospheric activity.

The physical similarity between the radiation of flare stars and rapid variations of the brightness of the T Tauri type stars (Ambartsumian, 1954), testifies the fact that in both cases similar processes of radiation take place, different from blackbody thermal radiation, at least during the flares. It is in itself an indication of the close genetic relationship between these two classes of stars. This conclusion has been confirmed by the investigations of Haro and coworkers (Haro, 1957, 1964). This aroused great interest in the origin of this entirely new phenomenon. Up to now, extensive studies of these objects are underway both at the Byurakan Observatory and the other observatories. Observations and statistical studies of flare stars strongly were stimulated when it had been shown by Ambartsumian (Ambartsumian, 1969, Ambartsumyan et al., 1970) that in a relatively young stellar aggregate of Pleiades ($\approx 5{\cdot}10^7$ years) almost all the red dwarf stars, fainter than a certain absolute magnitude, must be flare stars.

*aakopian57@gmail.com

doi: doi.org/10.52526/25792776-2021.68.2-150

Comparing the estimated number of flare stars with the available estimates of the total number of stars in the Pleiades led to the conclusion that the flare star stage (the stage of flare activity) is regular in the evolution of red dwarf stars, through which all of these stars pass. These results were so important for the evolution of red dwarfs that they initiated wide-field photographic observations at the observatories of Asiago (Italy), Byurakan (USSR, Armenia), and Tonantzintla (Mexico) to seek out and study flare stars in the regions of different ages stellar clusters and associations, and these studies were later undertaken at Abastumani (USSR, Georgia), Konkoly (Hungary), and Rozhen (Bulgaria). Besides the Pleiades system, other systems of flare stars, especially the systems of Orion, Praesepe, Hyades, etc., were studied in the international program. These observations led to the discovery of a large number of new flare stars and showed that they were unusually abundant in these systems. The regular observations of flare stars systems stopped in the early 80^{th} of the 20^{th} century because of cardinal changes of types of astrophysical detectors. These efforts ultimately yielded results that were important for understanding the development and evolution of red dwarf stars.

This review briefly presents the statistical studies of flare stars and related objects carried out at the Byurakan Observatory, in particular: a) determination of the evolutionary status of flare stars, b) an explanation of the observed difference between flare stars of the galactic field (type UV Cet) and flare stars of systems (open clusters, associations), c) the connection between flare stars and T Tauri stars, d) short-term and long-term (evolutionary) variability of flare activity, e) original statistical methods developed for the study of flare stars and their systems, f) recent advances in research on flashing objects. The basis for these studies was the data set of observations of flare stars obtained as a result of the collaboration of the Byurakan Observatory with other observatories.

This review does not present such important areas of research on flare stars as the determination of physical parameters, photometry and colorimetry of stars and their flares, detailed studies of individual stars, theoretical works on possible mechanisms of flares. These areas were well presented in many books and reviews by Ambartsumian and Mirzoyan.

2. Observations and observers/researchers

Observations of flare stars carried out in the Byurakan observatory can be combined into three groups: photographic, photoelectric and spectral.

2.1. Photographic observation

1) Main task - detection of the possible large, statistically significant number of flare stars and their flares in different systems of flare stars, simultaneous photometric observations of flare stars, their statistical, photometric and colorimetric studies.
2) Main targets - flare stars of star clusters and associations – the Pleiades, Orion association, NGC 7000 (Cygnus), Praesepe, Hyades, Taurus Dark Clouds
3) The telescopes used - 1 m Schmidt telescope (field of view is $4.1\,^\circ \times 4.1^\circ$) and 53 cm Schmidt telescope (field of view is $5^\circ \times 5^\circ$) with the Kodak plates 16 cm × 16 cm as detectors.
4) The method of detecting flare stars was a "chain" method, when several images of a star are obtained on a plate, each with an exposure of up to 10 minutes. Its alternative was the "tracks" method proposed by Chavushian, which is more informative but it was possible to apply only to a small sample of bright flare stars. The "track" method was rarely used.
5) Photometric bands - the majority of observation have been carried out in Johnson's photometric bands, mainly in the B band, allow to detect more flare stars and flare than in U and V bands.
6) The main observation period was the 70th of the last century. A significant part of the Byurakan observatory staff, headed by Ambartsumian and Mirzoyan, head of the Department of Physics of Stars and Nebulae, were involved in the observations. A group of astronomers of the Department of Physics of Stars and Nebulae (headed by Parsamian E.S.) actively collaborated with Mexican astronomers to study Orion flare stars and related objects. Here are the observers/researchers who participated in the studies: Chavushian, Erastova, Kazarian, Gasparian, Garibjanian, Hambarian, Melikian, Ohanian. Foreign astronomers also were involved in these observations and studies.

2.2. Phototelectric observation

1) Main task and targets - observation of UV Ceti, BY Dra type flare stars of solar vicinity with high photometric accuracy.
2) The telescopes used - 50 cm and 40 cm Cassegrain telescopes, 2.6 m telescope
3) Photometric bands - the majority of observation have been carried out in Johnson's photometric bands UVB.

doi: doi.org/10.52526/25792776-2021.68.2-150

4) The main observation period was the 70th and early 80th of the last century. Group members - Oskanian V.S.(head of group), Melkonian A.S., Oskanian A.A. Jr.

5) Important results - The expressing the sequence of flares of individual stars via Poisson law by Oskanyan & Terebizh (1971), based on the study of the longtime series of photoelectric observations of some flare stars in the vicinity of the Sun.

2.3. Spectral observation

Spectral observations began on the 80th of the 20th century. In contrary to photographic and photoelectric observations, spectral observations of flare stars are continued up to now.

1) Main task and targets - spectral observation of UV Ceti type flare stars of solar vicinity and their flares, discovering new flare stars in star-forming regions, detailed study of the physical characteristic of flare stars and their flares

2) The telescope used - 2.6m telescope

3) The members of the Department of Physics of Stars and Nebulae were involved in the spectral observations (Mirzoyan, Parsamian, Garibjanian, Melikian, Hambaryan, Ohanian). After the structural reformation of the observatory, the spectral observations continued by Melikian and his coworker A. Karapetian. Foreign astronomers also were involved.

3. Statistical studies of flare stars and related objects. Methods, applications and obtained results

In this section statistical methods developed at the Byurakan Observatory by Ambartsumian and followers for the study of flare stars and related objects are presented, in particular for the:

1) estimation of the unknown number of flaring objects,
2) determination the distribution function of the frequency of the flares,
3) study of the short- and long-time (evolutionary) variability of flare activity,
4) determining the spatial distribution of flare stars in the parent systems.

The basic assumption used in a) - c) is the Poissonian character of the flares sequence, both as with constant and variable parameter (intensity) of the Poissonian process.

3.1. Estimators of the unknown number of flare objects

Flare stars in stellar systems. Ambartsumian estimator Estimation of the total number of flare stars in the Pleiades has been obtained (Ambartsumian, 1969) under two following assumptions:

1) The sequence of flares at each flare star represents a random Poissonian process.
2) All flare stars of the given system have the same mean frequency of flares.

Ambartsumian estimator allows to estimate the number n_0 of flare stars flares of which have not been registered yet, via the known numbers n_1 and n_2 of stars which already showed, accordingly, one and two flares, as follows:

$$n_0 = \frac{{n_1}^2}{2n_2} \tag{1}$$

It should be noted that the first assumption is quite well-founded (Oskanyan & Terebizh, 1971). As to second assumption , one can give it up. Chavushian (1979) confirmed the heterogeneity of Pleiades cluster flare stars flares frequency. In this case, the number of stars in the system for which k flares each is observed over time t is equal to

$$n_k = N \int \varphi(\nu) \frac{(\nu t)^k e^{-\nu t}}{k!} d\nu \tag{2}$$

Ambartsumyan et al. (1970) using by Cauchy-Schwarz inequality have shown that when second assumption is incorrect, one can derive only the lower bound of the number of flare stars[1]. The upper

[1] Now Ambartsumian's estimator widely used in various branches of statistics, medical and social sciences, biology and ecology, linguistics, criminology, epidemiology, cryptography, etc. In these branches, this method, or closely related methods, are named in different ways: capture-recapture, mark-recapture, capture-mark-recapture, mark-recapture, sight-resight, mark-release-recapture etc.

doi: doi.org/10.52526/25792776-2021.68.2-150

bound of the flare stars number has been estimated in the assumption that the density of distribution of frequencies of flares is too slowly decaying exponential. Ultimately, the following inequality holds:

$$\frac{n_1^2}{n_2} > n_0 > \frac{n_1^2}{2n_2} \tag{3}$$

The application of this estimator to the Pleiades, based on observations by Ambartsumian & Mirzoyan (1971), Ambartsumyan (1970), Ambartsumyan et al. (1972, 1973), led, in particular, to the following conclusions Ambartsumian & Mirzoian (1975), Ambartsumyan et al. (1971):

1) The number of flare stars showed flares with a photographic amplitude of more than $0^m.6$ are observed, is about a thousand.
2) The mean flare rates for different flare stars in the Pleiades differ, but most of them experience, on average, one photographic flare every 3600 hours.
3) At a lower luminosity in the normal state outside the flares (at the minimum brightness), the average frequency of the observed flares is higher.

Comparing the estimated number of flare stars with the available estimates of the total number of stars in the Pleiades led to the above-mentioned conclusion that the flare star stage (the stage of flare activity) is regular in the evolution of red dwarf stars, through which all of these stars pass.

Table 1 gives the summary data for the two most studied systems, where T is the effective time of photographic observations, n - the number of discovered flare stars n'- number of registered flares, n_1- the number of flare stars for which one flare was recorded, n_2- the number of flare stars for which two flares were recorded, N - the estimate of the total number of flare stars, t- the mean discovery time of a new flare star, and r - the distance of the system (which were adopted in early studies).

Besides the estimation of flare stars number, also the relative number of T Tauri stars with flaring activity in the Orion association and other systems (e.g Ambartsumyan, 1970)(were estimated. It was shown that about 1/4 of Tauri stars in this system can produce "photographic" flares. This led, along with the arguments given by Haro (1957, 1964), to the conclusion that the flare star stage begins shortly before the end of the T Tauri stage and for a short time the star shows flare activity along with the T Tauri type activity. Now the genetic and evolutionary connections between T Tau and UV Cet stars appear to be more complex, but there is no doubt about their close relationship.

The Ambartsumian estimator can be used in the studies of other randomly flashing objects. As an example, in a statistical study of a sample of 1547 superflares of 270 solar-type stars found during an analysis of data on more than 80000 stars of the solar-type (obtained by the Kepler orbital observatory during the first 500 days of observations), the total number of stars capable of superflares and the superflare distribution frequency function were determined (Akopian, 2017). One may conclude that the number of stars capable of superflares is roughly 0.5% of the total number of all the solar-type stars that were studied. This most likely indicates that solar-type stars with superflares either have some rarely encountered feature(s) or are in a short-duration phase of their evolution. Unavoidable observational errors, incorrect classification of the stars, etc., can hardly affect the main conclusion that the overwhelming majority of solar-type stars cannot produce superflares over a time comparable to the lifetime of these stars.

Table 1. Results of photographic observations of flare stars

System	T (hrs)	n	n'	n_1	n_2	N	t (hrs)	r (pc)
Pleiades	3200	546	1495	287	92	995	5.9	125
Orion	1600	491	654	380	76	1441	3.3	500

Important mathematical and statistical properties of Ambartsumian estimator

Methods for the statistics of flare stars developed mainly at the Byurakan Observatory and originate in papers by Ambartsumian (1969), Ambartsumyan (1978). In terms of their scientific value and novelty, the mathematical methods developed by Ambartsumian for solving specific astrophysical problems in the statistics of flare stars are just as significant as the astrophysical results obtained using these methods. At a conference in honour of his sixtieth birthday in 1968, Ambartsumian (1969) gave a talk in which he proposed a clever and unexpectedly simple means of estimating the number of flare stars in stellar systems (Eq 1.) The most important mathematical and statistical properties of Ambartsumian estimator are:

1) Ambartsumian estimator gives the lower bound of the number n_0
2) Ambartsumian estimator is robust one. This important result was obtained by who has shown, that among possible estimators of type

$$n_0(t) = \frac{n_k(t) \cdot n_l(t)}{n_m(t)} \cdot c_{k,l,m}(t) \tag{4}$$

where the factor $c_{k,l,m}(t)$ generally depends on the kind of density of distribution of mean frequency of flares, robust estimators are those for which equality $k + l = m$ takes place; i.e. the estimator (**??**) is robust. According to (Ambartsumian, 1998) another robust estimator is

$$n_0(t) = \frac{n_1(t) \cdot n_2(t)}{n_3(t)} \tag{5}$$

1) Variation of n_0 has the following form (Bohning, 2010):

$$\sigma^2_{n_0} = \frac{n_1^3}{n_2^2}\left[1 + \frac{1}{4}\frac{n_1}{n_2}\left(1 - \frac{n_2}{N_{obs}}\right)\right] \tag{6}$$

where N_{obs}- a number already discovered flare stars.

1) The mean flare frequency can be determined from the expression $\langle \nu t \rangle = 2n_2/n_1$ (Ambartsumian, 1969) is a maximum likelihood estimate for the doubly truncated Poisson distribution in which no events with $k = 0$ and $k \geq 3$ are observed (Akopian, 1998).

Alternative estimators Ambartsumian's results stimulated works in this area. Several new estimators of the number of flare stars were published. The following estimator was obtained by Mirzoyan et al. (1977):

$$\begin{array}{c} N = \frac{\sum_{k=1} n_k}{1-e^{-\langle \nu t \rangle}}, \\ \frac{\langle \nu t \rangle}{1-e^{-\langle \nu t \rangle}} = \frac{n}{N_1} \end{array} \tag{7}$$

where $\langle \nu t \rangle$ is the solution of the second, transcendental equation of the equation system Eq(7), N−the total number of flare stars, n-total number of flares.

The estimate (7) was derived later in Akopian (1998), where other estimators based on a Poisson distribution also were suggested. The well-known estimators of the parameter νt truncated at the point $k = 0$ of the Poisson distribution were used. Estimators of the number of flare stars were obtained by assuming that these estimators are equal to the estimates for the non truncated Poisson distribution. Of the proposed estimates, the following estimator merits attention:

$$n_0 = n_1 \frac{\sum_{k=1} n_k}{\sum_{k=2} k n_k} = n_1 \frac{N_{obs}}{\sum_{k=2} k n_k}, \quad N = \frac{\sum_{k=1} n_k \sum_{k=1} k n_k}{\sum_{k=2} k n_k} = \frac{n N_{obs}}{\sum_{k=2} k n_k} \tag{8}$$

This estimate also gives a lower limit on the number of unknown flare stars (Akopian, 1998).

The problem of predicting the number $n_r(t)$ of flare stars, based on the data known for the observation time T, was solved by Mnatsakanyan (1986) and Mnatsakanyan & Mirzoyan (1988). According to the latter,

$$n_r(t) = \sum_{k=r}^{\infty} n_k(T) \cdot C_k^r \left(\frac{t}{T}\right)^r \left(1 - \frac{t}{T}\right)^{k-r}, \quad r = 0, 1... \tag{9}$$

$$N_{obs}(t) = \sum_{k=1}^{\infty} n_k(T) \cdot \left[1 - \left(1 - \frac{t}{T}\right)^k\right] \tag{10}$$

The detailed history of the Ambartsumian estimator and its analogues was given in Akopian (2018).

3.2. Determining the distribution function of the frequency of flares

Ambartsumian method. If each flare star is characterized by a mean frequency ν , then a cluster as a whole will be described by a distribution of the mean frequencies over the set of flare stars contained in it. Let us denote the normalized density of this distribution by $\varphi(\nu)$. Up to now, it has been essentially impossible to determine $\varphi(\nu)$by direct calculation because of the small number of detected flares for individual stars. In Ambartsumyan (1978) proposed a statistical method for determining $\varphi(\nu)$ based on solving the inverse problem which avoided this difficulty. To do this he used a function $m_i(t)$that gives the number of stars for which the $i-$th flares were observed during the interval from t to $t + 1$. The probability of this event is equal to the product of the probability that exactly (i - 1) flares have occurred up to the moment t by the probability that a flare will be detected in the interval from t to $t + 1$. Hence, for a Poisson process, the function $m_i(t)$ is given by

$$m_i(t) = N \int \nu \frac{(\nu t)^{i-1}}{(i-1)!} e^{-\nu t} \varphi(\nu) d\nu \tag{11}$$

In particular

$$m_1(t) = N \int \nu e^{-\nu t} \varphi(\nu) d\nu \tag{12}$$

doi: doi.org/10.52526/25792776-2021.68.2-150

will be the number of new flare stars of the given aggregate which are discovered per unit time, for only when a flare is observed can a star be included among the flare stars. Note that the number $m_1(0)$ (more precisely its mathematical expectation) is also equal to the mean number of all flares in the aggregate per unit time:

$$m_1(0) = N\nu_m = N \cdot \frac{n(t)}{t} \tag{13}$$

where ν_m is the mean of the mean frequencies of the flares in the set of stars and $n(t)$ is the total number of flares detected up to the time t.

Since evolutionary effects appear only after hundreds of thousands or millions of years, the physical state of the entire sample of flare stars can be considered practically unchanged throughout all our observations. Thus, $m_1(0)$ will characterize the density of flares in time, both at $t = 0$ and throughout the entire observation period. The mathematical expectation of $m_1(t)$ should fall off monotonically, for flares of already discovered stars are not counted in the calculation, since $m_1(0)$ denotes the number of flares per unit time of stars that have not been discovered up to time t, the number of which will fall off with increasing t. It follows directly from Eqs. (12) and (13) that the mathematical expectation of $m_1(t)$ is fully determined by the distribution $\varphi(\nu)$ of the frequencies and the following simple relationship exists between them:

$$\frac{m_1(t)}{m_1(0)} = \frac{\int \nu e^{-\nu t}\varphi(\nu)d\nu}{\int \nu\varphi(\nu)d\nu} = \frac{\int \nu e^{-\nu t}\varphi(\nu)d\nu}{\nu_m} \tag{14}$$

so the question of determining $\varphi(\nu)$ reduces to taking the inverse Laplace transform of the observed function $m_1(t)/m_1(0)$:

$$\varphi\left(\nu\right) = \frac{\nu_m}{\nu} L^{-1}\left[\frac{m_1(t)}{m_1(0)}\right] \tag{15}$$

where L^{-1} - is the inverse Laplace transform operator. Since the observation of the first flare of a star is the discovery of a new flare star, it follows that the chronology of the discoveries is the input data for determining the distribution of the flare frequency.

The function $m_1(t)/m_1(0)$ is subject to strong fluctuations, which are inevitable in a once-observed realization of this function so that preliminary smoothing is necessary when searching for a solution. Eq. (11) implies that the mathematical expectation of the numbers $m_i(t)$ and $m_{i+1}(t)$ for the same stars are related as follows:

$$\frac{dm_i(t)}{dt} = \frac{(i-1)m_i(t)}{t} - \frac{i \cdot m_{i+1}(t)}{t}, \tag{16}$$

In particular, for *i=1* :

$$\frac{dm_1(t)}{dt} = -\frac{m_2(t)}{t}, \quad m_1\left(t\right) = m_1(0) - \int_0^t \frac{m_2(t')}{t'}dt' \tag{17}$$

In this case, because the observed function is under the integral sign, the resulting $m_2(t)$ are much less susceptible to fluctuations than are those directly determined "by counting detections" in a single realization. Eq. (17) makes it possible to obtain a more reliable "detection" curve based on the chronology of second flares than that obtained from the chronology of detections. Let to note yet another, very simple to apply, but rarely used method for smoothing the function $m_1(t)$. It is easy to see that Eqs. (2), (12), and (13) imply that

$$\frac{m_1(t)}{m_1(0)} = \frac{n_1(t)}{n(t)} \tag{18}$$

where $n\left(t\right)$ is the total number of flares detected up to t and $n_1\left(t\right)$ is the number of singly flaring stars. For the Pleiades cluster, where about 500 flare stars are currently known, calculations have shown that the values $m_1(t)$given by Eq. (17) yield a smooth curve that is closely coincident with the smoothed curve of $m_1(t)$, determined by direct calculation. Both results are in satisfactory agreement with the assumption that $m_1(t)$ has the form

$$\frac{m(t)}{m(0)} = \frac{1}{\left(1+at\right)^b} \tag{19}$$

where $a = 0.0026$ and $b = 2/3$.

Ambartsumian proposed the following algorithm for determining the probability density of the mean flare frequencies $\varphi(\nu)$:

1) The function $m_1(t)/m_1(0)$ is computed by direct calculation,
2) The function $m_2(t)$is calculated and Eq. (17) is used to smooth the function $m_1(t)/m_1(0)$.
3) The inverse Laplace transform based on Eqs. (14) (15) is used to determine $\varphi(\nu)$.

doi: doi.org/10.52526/25792776-2021.68.2-150

The correctness of the resulting solution $\varphi(\nu)$ was verified using other observational data obtained independently of $m_1(t)$ and $m_2(t)$. In particular, knowing $\varphi(\nu)$, the ratios $n_k/n_1 = \int \varphi(\nu)\frac{(\nu t)^k e^{-\nu t}}{k!}d\nu \Big/ \int \varphi(\nu)\nu t e^{-\nu t}d\nu$ were determined and then compared with the observations.

The solution of Eq. (15) with an analytic form of the left side of Eq. (19) is given by

$$\varphi(\nu) = Ce^{-\nu s}\nu^{-4/3} \tag{20}$$

where the parameter s, which has the dimensions of time, turns out to be equal to s = 385 h for the Pleiades cluster. Eq.(20) implies that some part of the flare stars has mean frequencies of less than 0.001 h^{-1}.

This density function $\varphi(\nu)$ is singular at the point $\nu = 0$ so that the integral over the entire range of frequencies diverges. This meant that it was impossible to determine the value of C by normalization. Of course, for small νup, the real function should behave differently. T hours of observation cannot provide us with any significant information about the flare statistics of stars for which the mean interval between flares exceeds T. Thus, Ambartsumian suggested that the true function should have the form $\varphi(\nu) = Ce^{-\nu s}\nu^{-4/3}g(\nu)$ where $g(\nu)$ can be taken equal to unity for large ν and goes rapidly to zero as $\nu \to 0$. This made it possible, using normalization, to determine the product NC and to estimate the total number of flare stars in the Pleiades cluster with a flare frequency greater than a certain ν_0.

This method was later applied by Parsamyan (1980) to flare stars in the Orion association. As in the case of the Pleiades, the data are well fit by Eq.(19) with the constants $a = 0.00072$ and $b = 2/3$. Thus, a solution is obtained in the form of Eq. (20) with $s = 1389\ h$. Parsamian also determined the distribution function of the flare frequency of faint stars in the Pleiades cluster (Parsamian, 2002, Parsamyan, 1980). Here the chronology of the "first flares" was smoothed using the chronology of "third flares":

$$m_1(t) = m_1(0) + t\frac{dm_1(0)}{dt} + 2t\int_0^t \frac{m_3(t')}{t'^2}dt' - 2\int_0^t \frac{m_3(t')}{t'}dt' \tag{21}$$

This expression can be obtained from Eq. (16) through several transformations.

The probability of using chronologies of higher-order flares has been discussed by Arutyunyan (1984), with appropriate expressions given and numerical simulations carried out to establish the efficiency of the method.

Other methods of determination of distribution function of the frequency of flares.

1) It has been proposed by Mnatsakanyan & Mirzoyan (1988) rather than determine the distribution function, to solve the problem of predicting the number $n_k(t)$ (see Eq. (8)) of flare stars with time. This statement of the problem is based, in particular, on the fact that predicting the numbers $n_k(t)$ in the infinite future is equivalent to finding the function $\varphi(\nu)$:

$$n_k(T) \underset{T\to\infty}{\to} \frac{1}{T}\varphi\left(\frac{k}{T}\right) \tag{22}$$

According to the authors, their solution is practically unuseful for times exceeding $2T$. Moreover, due to the unavoidable fluctuations of observational data, such predictions limited by smaller time. This method was examined also by Mirzoyan & Hambarian (1995). It is shown that the chronology of flare star discoveries in the Pleiades cluster and the Orion association can be described satisfactorily by various distribution functions (gamma, binomial, decreasing exponential, and delta) for the mean frequencies of stellar flares. However, it has been found that this is due to the uncertainty in the observationally derived distribution function for the mean frequency of stellar flares. The most likely function is that derived by Ambartsumian, which has a physical basis.

2) Another method has been proposed in Akopian (2003) for determining the distribution function of the flare frequency of randomly flashing objects (flare stars, supernovae). This method essentially involves determining the unknown function through the statistical moments of the distribution. The distribution of the number of observed flares of flare stars, rather than the distribution of the corresponding frequencies, serves as an initial empirical distribution in the problem of determining the flare frequency distribution function. However, the moments of the flare frequency distribution function can be expressed in terms of the corresponding moments of the number of flares. For a sample of flaring objects with a frequency density distribution $\varphi(\nu)$, the moments of the distribution of the number of flares are, respectively, given by

$$\mu k_1 = \int \sum_{k=0}^{\infty} kp_k\varphi(\nu)d\nu,\ \ \mu k_j = \int \sum_{k=0}^{\infty}(k-\mu k_1)^j p_k\varphi(\nu)d\nu,\ j = 2,3,4 \tag{23}$$

where, in particular, μk_1 is the mean number of flares and μk_2 is the variation of in the number of flares.

doi: doi.org/10.52526/25792776-2021.68.2-150

Equations (1) and (23) yield some equations relating the moments of the flaring frequency to the moments of the flare number distribution function:

$$\begin{aligned}&\mu\nu_1 = \tfrac{\mu k_1}{t}, \quad \mu\nu_2 = \tfrac{(\mu k_2 - \mu k_1)}{t^2}, \quad \mu\nu_3 = \tfrac{(\mu k_3 - 3\mu k_2 + 2\mu k_1)}{t^3},\\ &\mu\nu_4 = \tfrac{(\mu k_4 - 6\mu k_3 - 6\mu k_2 \cdot \mu k_1 + 11\mu k_2 - 6\mu k_1 + 3\mu k_1^2)}{t^4},\end{aligned} \tag{24}$$

where $\mu\nu_1 = \int \nu\varphi(\nu)d\nu$, $\mu\nu_j = \int(\nu - \mu\nu_1)^j \varphi(\nu)d\nu$, $\quad$ j = 2, 3, 4

Substituting the empirical moments of the distribution of the number of flares into Eq. (24), one can obtain the corresponding empirical moments of the distribution function of the frequency of flares. Thus, the problem is reduced to determining the distribution functions using known distribution moments. This was done using the technique of curve fitting in the Pearson family of distributions by the method of moments. Numerical modelling has shown that the method is quite effective for determining the distribution function of the flare frequency. This method has been applied to the flare stars the Orion association and the Pleiades cluster, solar-type superflare stars.

3) In his first paper on the statistics of flare stars, Ambartsumian (1969) already pointed out the analogy between the statistics of flare stars and the statistics of supernovae (SNe). Here, according to Ambartsumian (1969), it is necessary to treat galaxies as “flaring objects” and replace the term “flare star” with “galaxy” and the concept of “stellar flare” with the concept of “supernova explosion in a galaxy” in the preceding discussions. In this way, a possible derivation by the analogy of the frequency distribution for different sets of galaxies could be examined.

However, despite this similarity, certain differences that owned to the specific features of the observational data, prevent using of the Ambartsumian method in its original form. First, as opposed to the total number of flare stars, the overall number of galaxies in a sample is known in most cases since a sample is constructed by the observer, under the problem that has been set. Second, the duration of the observation time for individual galaxies in the sample is different: in the case of flare stars, it is usually the same (there can be some important exceptions, as in the case of X-ray flare stars). Of course, the data can be cut off to a minimum common observation time, but this leads to a significant reduction of already scant data.

These differences have naturally revealed in the solution of the problem. In this case, we are in need to use censored data and methods for processing such data. In this task, a censored observation is one of a galaxy/star in which not a single SN explosions/ flare observed during the entire observation period. The unknown density distribution of the mean frequency (rate) $\varphi(\nu)$ is equal to the inverse Laplace transform of the survival function (Akopian, 1996):

$$\varphi(\nu) = L^{-1}\left[F_1(T)\right] \tag{25}$$

where $F_1(T) = 1 - M_1(T)$ is the survival or reliability function, and $M_1(T)$ is the distribution function of the times of first explosions /flares:

$$M_1(t) = \int_0^t \frac{m_1(t')}{N} dt' \tag{26}$$

Let us denote the nominal times at which SNe explosions/ flares are detected by t. Let T' be the time of the first SN explosion/ flare in a given galaxy/star if it has taken place, whereas if no explosion/ flare has not taken place then T' is the overall time of the observations of this galaxy/star, and let n be the number of galaxies/stars for which $T' > t$ while k is the number of galaxies/stars for which the first SN explosion/flare have been observed at the nominal time t. In this case, the estimate of the maximum reasonable survival function $F_1(T)$ is the Kaplan-Meier estimator:

$$F_1(T) = \prod^{T} \left(1 - \frac{k_i}{n_i}\right) \tag{27}$$

with the variation

$$var\left[F_1(T)\right] = \left[F_1(T)\right]^2 \sum^{T} \frac{k_i}{n_i(n_i - k_i)} \tag{28}$$

where $\sum$ denotes the sum over all i such that $t < T$. As yet, however, there are insufficient data for the use of these statistical methods, since supernova flares have only been observed in a small number of galaxies so far.

In the practical solution of inverse problems, it is useful to know preliminary information about the nature of the original function. The function $F_1(T)$ largely satisfies this condition: it, by definition, is a monotonically decreasing function of T and varies strictly within the range from 1 to 0. The possibility of estimating the uncertainty (28) of the determination $F_1(T)$ is also very important.

This method was used to determine X-ray flares frequency distribution of low-mass young stellar objects of Orion nebula and cloud L1688, which is a part of the complex of dark clouds ρ Oph (Akopian, 2012a,b).

doi: doi.org/10.52526/25792776-2021.68.2-150

3.3. Long- and short-term change in flare activity

Long-term change in flare activity due to stellar evolution The presence of systems of different ages makes it possible to trace the evolution of stars, in particular, how the flare activity of stars changes with time? The dependence of the luminosity of the brightest flare star on the age of the system containing these stars was pointed out by Haro (1964): there is a relation between the earliest spectral class of flare stars and the age of the system. Subsequently, Kunkel (1975) and Parsamyan (1976) confirmed the existence of the dependence of the luminosity of the system brightest flare star from the system age.

Later the dependence of the mean luminosity of flare stars of a given system on its age was established by Mirzoyan & Brutyan (1980) and then confirmed by Mirzoyan & Brutyan (1980) based on observational data of the nearest systems. It was shown that the observed luminosity function of flare stars is shifted toward lower luminosities as the system ages. Two best-studied subsystems of flare stars of various ages in Orion and Pleiades are compared. It is shown that the observed differences between them are in agreement with the evolutionary status of flare stars, presenting a stage in the evolution of red dwarf stars. It is detected that the mean frequency of flares increases towards low luminosity stars. For the same luminosity stars, the flare activity is lower in older stars. Based on these dependencies, Akopian (1999) has been proposed the method for determining the parameters of the initial luminosity function of flare stars.

The dependence of the maximum possible flare amplitude on luminosity was used by Parsamyan (1976, 1995) to determine the age of a stellar system from observations of the flare stars in it. The essence of this method is as follows: on a "flare amplitude-stellar magnitude" (Δm, m) diagram for all the flares of flare stars in a given system the upper envelope of the observed flare amplitudes can be fitted by the straight line:

$$\Delta m \ = \ \kappa m + \ \Delta m_0, \tag{29}$$

whose intersection point with the axis m determines the luminosity of the brightest flare star in the given system. Since the spectral class/luminosity of the brightest flare star in the system depends on the age T of the system, this implies that the slope κ of this line also depends on the age of the system. The available data yielded:

$$\kappa = 1.31 - 0.06 \lg T \tag{30}$$

This is giving a unique opportunity to find stellar system age if there are flare in the system. The method was adapted to determine the age of single flare stars not included in any system.

Ambartsumian (1969) postulated that during the evolution, the frequency of flares of a star undergoes secular (long-term) changes, the nature of which can be determined by comparing the frequencies of flares in populations of stars of different ages. Knowledge of the corresponding distribution functions allows, in principle, to implement this idea. An attempt of this kind was made in Akopian (2008), where the difference in the obtained functions for Orion and Pleiades flare stars was interpreted as a consequence of evolution.

Short-term change in flare activity due to stellar activity and stellar rotations - both axial and orbital. At the foundation of all the methods lies the detection of a departure of observational data from a theoretical Poisson distribution. At present, there are no reasons to reject the hypothesis that the distribution of flares has a random character.

To detect possible cyclicity in the flare activity of flare stars in the Pleiades, Mirzoyan & Oganyan (1977) divided the entire observational period into two approximately equal parts and calculated the theoretical ratios of the number of flare stars that each exhibit k flares in each interval ($n_{k,k}$) to the flare stars number that each exhibit $2k$ flares over the entire period (n_{2k}):

$$\frac{n_{k,k}}{n_{2k}} = \frac{(2k)!}{2k^{2k}k!k!} \tag{31}$$

A comparison of theoretical and observed ratios showed that the theoretically expected values are significantly larger than the corresponding observed ones for all values$k$. According to Mirzoyan & Oganyan (1977) this is consistent with the hypothesis of cyclicity of the flare activity of stars in the Pleiades.

A different approach was used by Parsamian & Andrews (1996). Flare stars of the Orion association that exhibiting five or more flares were chosen for further study. They divided the entire observational period into two parts and from the observed flare frequency in the first interval, they calculated the theoretically expected number of flares in the second interval and its dispersion. If the theoretically expected number of flares in the second interval differed significantly from the corresponding observed number, the given star was suspected of variable flare activity.

In both methods, the authors were not aimed to define the change point time of flaring activity. Such an attempt was made by in Akopian (1999, 2001), Akopian & Sargsyan (2002), where a piecewise-stationary Poisson process was involved to describe flare time-sequence of the flare stars of Orion Association and

Pleiades cluster. Consequently, the following question has been considered: is a sequence of flares a stationary or a piecewise-stationary Poisson process, in which a parameter of the Poisson distribution (the flare frequency) has different values in each time intervals of observations? This approach allows, in principle, to determine the probable change point of the flare activity and to estimate the significance level of the detected changes.

Methods of detecting probable cycles in the flaring activity of flare stars and determining the cycle durations are examined by Akopian (2010). A new method of detecting a cycle of flaring activity was proposed assuming periodic flaring activity (flare frequency) in the form $\nu(t) = v_0(1 + a\sin\omega t), \quad a > 1$. This method was applied to two flare stars of the Pleiades cluster, Ton 91 and Ton 377 (possible member of Hyades) based on data obtained during a long monitoring campaign of the Pleiades region performed in 60-80th of the last century.

In these works, the task was set to detect changes in the flare activity of stars, regardless of the mechanism of change. It was believed that, in the likeness of the Sun, stars should have their cycles of activity.

An analysis of the relationship between flare activity and the linear distance of the components of the flare star UV Ceti was carried out by Melikian et al. (2011). It was shown that the flare activity of a star depends on the distance between the components, a higher level of activity corresponds to a smaller distance between the components. This is a manifestation of the periodic variability of the flare frequency due to orbital rotation.

Since the flare frequency can be modulated by a periodic process (axial/orbital rotation of the star), the representation of the flare frequency as a periodic function of time seems to be more reasonable and the flare activity can be considered as a Poisson process with a periodic parameter.

It was recommended Akopian (2015) to use the following function as a periodic function of the flare frequency (parameter) of the Poisson distribution:

$$\nu\left(t\right) = \frac{\nu_0 exp\left[ksin\left(\omega_0 t + \vartheta\right)\right]}{I_0\left(k\right)} \qquad \left(k \geq 0,\ \omega_0 \geq 0,\ 0 \leq \vartheta \leq 2\pi,\ \nu_0 > 0\ \right) \tag{32}$$

where $k,\ \omega_0,\ \vartheta,\ \nu_0$ are constants, $I_0\left(k\right) = \int\limits_0^{2\pi} exp\left[ksin\left(u\right)\right]du$ - is the modified Bessel function of zeroth order of the first kind.

This function was chosen because it gives different forms of the periodic function depending on the value of k, from sinusoid to Dirac comb (Shah) function, which is undoubtedly the advantage of this function. Using this approach, Akopian (2015) suspected the existence of a possible periodicity of the frequency with a period equal to the period of the star's orbital or axial rotation for a few solar-type stars with superflares.

Data from the Kepler orbiting observatory are used in a statistical study of the periodic/cyclical variability of the flare frequency of 76 flare stars Akopian (2019). The corresponding periodic functions of the flare frequency are obtained and the possible periodicity of the flare frequency with a period equal to the rotation period of the star is verified. The periodicities of the flare frequency function turned out to be close to the periods of the axial rotation of the stars. For all stars without exception, the periodicity of the flare frequency has been confirmed. These results show that (a) the flare frequency is modulated by the axial rotation of the stars and (b) structural and physical changes in the active regions of these stars are relatively slow.

3.4. The spatial distribution of flare stars

The spatial distribution of stars in young stellar associations and clusters, where dynamical relaxation didn't occur yet, contains valuable information on the physical condition (both of stars and whole system) at their birth-time and subsequent evolution. From this point of view, the study of the spatial distribution of flare stars is of some interest.

Spatial distribution of UV Ceti - type flare stars in the solar vicinity and their origin. In the view of the formation of flare stars in stellar clusters and associations, the existence of UV Ceti-type stars in the vicinity of the Sun can have two possible explanations. According to the first hypothesis (Ambartsumian, 1957), these stars were formed in a system that still exists. In other words, UV Ceti-type stars in the vicinity of the Sun constitute a physical system at present. The second explanation (Herbig, 1962, Oskanyan, 1964), assumes that UV Ceti type stars were formed in systems now decayed and appeared in the vicinity of the Sun accidentally, as a result of the "parent" systems decay.

The solution to the problem can be obtained by determining the spatial distribution of stars. If it is uniform, then the second hypothesis is most likely true. If the spatial density of stars abruptly drops off at some distance (the edge of the stars cluster), then the first hypothesis is true. The first considerations Arakelian (1970), Garibdzhanian (1976) of the problem by BAO astronomers, led to a conclusion in favour

doi: doi.org/10.52526/25792776-2021.68.2-150

of the first explanation. The further study of the problem Mirzoyan et al. (1988) did not confirm the existence of a system of UV Ceti-type stars around the Sun. As became clear, that conclusion had been obtained as a result of an overestimate of the expected flare numbers produced by UV Ceti type stars in the galactic star field during photographic observations of various regions of the sky.

This result can be regarded as important evidence in favour of the hypothesis that UV Ceti type stars in the vicinity of the Sun, and in general, all flare stars of the galactic field, are formed in stellar clusters and associations. Consequently, there is the common origin of the flare stars in clusters/ associations and the UV Ceti type flare stars in the vicinity of the Sun. This allows supposing that they constitute a single class of stars having the common property of flare activity Mirzoyan (1981). Many parameters of flare stars of these two varieties differ very little, while the important differences between them can be successfully explained by differences in age, e.g. mean luminosity of flare stars of a system.

Spatial distribution of the Pleiades flare stars. The study of the distribution of flare stars in parent systems is of great importance for the problem of stellar evolution. Such a study carried out by Mirzoyan & Mnatsakanian (1971) for the Pleiades showed that flare stars are almost completely absent in the central part of the system. The radius of this cavity is 1.4 pc. The partial density of flare stars reaches a maximum at a distance of 1.5 pc from the centre of the system; then it decreases faster than $\sim r^{-2}$. The solution of the Abel equation was obtained by a method developed by Mnatsakanyan (1969), based on the well-known Plummer's method. The method gives a solution, which is a kind of average of all solutions that can be obtained using Plummer's method.

It has been supposed that the distribution of the flare stars in the system is a spheric-symmetrical one, the centre of the system being the geometrical centre of the known flare stars. It is almost coinciding with Alcyone. However, later studies of the problem didn't Mirzoyan (1981) confirm the results of the first work. The cavity disappeared when the number of discovered flare stars increased.

A study of the surface density of flare stars in the Pleiades by Chavushian et al. (1999a, 2004) led to the discovery of a density deficit at a distance of 3.2 pc from the centre of the cluster. The same feature was revealed in the spatial distribution of these stars. For the construction of flare stars spatial distribution, the one-dimensional distribution was constructed from observed surface distribution. It was shown that it is necessary for reliable construction of the one-dimensional distribution to solve Abel's equation. On its basis, the dependence of real space density distribution of flare stars on the distance from the cluster's centre is determined. As a result, 0.5 pc ($2.8\ pc \leq R \leq 3.5\ pc$) wide spherical layer with the deficit of flare stars was revealed. Preliminary consideration of the problem with new astrometric data from Gaia does not in contradiction with the obtained result.

3.5. Recent developments and possible applications of methods

Over the last decade, interest in flare stars and related objects has been renewed and increased sharply. Cosmic telescope research, modern observations on ground-based telescopes have shown that flare stars are also characterized by other manifestations of activity. X-ray and ultraviolet radiation were detected, indicating the presence of powerful corona and chromospheres in these stars. Flares have been directly recorded in a wide range of wavelengths - from hard X-rays and far-ultraviolet radiation to microwave radio emission. Cold spots have been found that manifest themselves in slow variations in the star's brightness with small amplitudes, and long-term cycles of activity have been discovered, similar to the 11-year solar cycle. This is mainly because of observations with the Kepler space telescope intended to search for exoplanets. Because of its unique characteristics, observations by the Kepler telescope simultaneously provide valuable and uniform data on variable stars and variable phenomena of almost all kinds, including flare stars and flare phenomena. A comparatively long series of almost continuous and uniform observations with high sensitivity, a large field, and a huge number of simultaneously observed objects facilitate comprehensive (both statistical and physical) studies of flare stars and flare phenomena. The complexity of these observations shows up not only and not so much in the number of characteristics of the data, as in the fact that data on very important physical parameters closely related to the variability of stars are obtained simultaneously. In the case of flare stars, these data can be used for the following:

– to obtain a light curve over a fairly long time, which in principle makes it possible to study the variation of flare activity during the stellar activity cycle (analogous to the solar activity cycle),

– estimate the rotation period and spottedness of stars, and, accordingly, the sizes and energy characteristics of active regions, and

– detect differential rotation and the migration of active regions, and study their relationship to flare activity.

This makes it possible to carry out more complete physical and statistical studies of the periodic/cyclical variability of the observed frequency of flares of flare stars, as well as to detect flares and flare objects of new types, in particular, solar-type stars with superflares.

In this process, the methods and approaches developed at the BAO for the study of flare stars will certainly be very useful.

doi: doi.org/10.52526/25792776-2021.68.2-150

References

Akopian A. A., 1996, Astrophysics, 39, 331

Akopian A. A., 1998, Astrophysics, 41, 47

Akopian A. A., 1999, Astrophysics, 42, 419

Akopian A. A., 2001, Astrophysics, 44, 106

Akopian A. A., 2003, Astrophysics, 46, 58

Akopian A. A., 2008, Astrophysics, 51, 48

Akopian A. A., 2010, Astrophysics, 53, 544

Akopian A. A., 2012a, Astrophysics, 55, 81

Akopian A. A., 2012b, Astrophysics, 55, 505

Akopian A. A., 2013, Astrophysics, 56, 488

Akopian A. A., 2015, Astrophysics, 58, 62

Akopian A. A., 2017, Astrophysics, 60, 118

Akopian A. A., 2018, Communications of the Byurakan Astrophysical Observatory, 65, 65

Akopian A. A., 2019, Astrophysics, 62, 518

Akopian A. A., Sargsyan L. A., 2002, Astrophysics, 45, 20

Akopyan A. A., 1995, Astrophysics, 38, 157

Ambartsumian V. A., 1947, The evolution of stars and astrophysics. Akad Nauk Arm SSR, Erevan

Ambartsumian V. A., 1949, Astronomicheskii Zhurnal, 26, 3

Ambartsumian V. A., 1954, Communications of the Byurakan Astrophysical Observatory, 13, 3

Ambartsumian V. A., 1957, in "Non-stable stars", ed. Herbig, G.H.. p. 177

Ambartsumian V. A., 1969, Stars, Nebulae, and Galaxies, Izd-vo. Akad Nauk Arm. SSR,, p. 283

Ambartsumian R. V., 1998, Editors addendum in "A life in astrophysics : selected papers of Viktor A. Ambartsumian", Publisher: New York, NY: Allerton Press,,

Ambartsumian V. A., Mirzoian L. V., 1975, in Proc. IAU Symp. 67 "Variable Stars and Stellar Evolution" ed. Sherwood, V. E. and Plaut, L., pp 3–14

Ambartsumian V. A., Mirzoyan L. V., 1971, in IAU Colloq. 15: New Directions and New Frontiers in Variable Star Research. p. 98

Ambartsumjan V. A., 1988, Scientific Works. Vol.3. Publisher, Address

Ambartsumyan V. A., 1970, Astrophysics, 6, 11

Ambartsumyan V. A., 1978, Astrophysics, 14, 209

Ambartsumyan V. A., Mirzoyan L. V., Parsamyan E. S., Chavushyan O. S., Erastova L. K., 1970, Astrophysics, 6, 1

Ambartsumyan V. A., Mirzoyan A. V., Parsamyan É. S., Chavushyan O. S., Erastova L. K., 1971, Astrophysics, 7, 189

Ambartsumyan V. A., Mirzoyan L. V., Parsamyan É. S., Chavushyan O. S., Erastova L. K., Kazaryan É. S., Oganyan G. B., 1972, Astrophysics, 8, 287

Ambartsumyan V. A., Mirzoyan L. V., Parsamyan É. S., Chavushyan O. S., Erastova L. K., Kazaryan É. S., Oganyan G. B., Yankovich I. I., 1973, Astrophysics, 9, 267

Arakelian M. A., 1970, Communications of the Byurakan Astrophysical Observatory, 41, 56

Arutyunyan G. A., 1984, Astrophysics, 21, 450

Bohning D., 2010, Scandinavian Journal of Statistics, 37, 221

Chavushian H. S., 1979, PhD thesis, Byurakan Astrophysical Observatory, Armenia.

Chavushian H. S., Broutian G. H., Oskanian A. V., 1999a, Astrophysics, 42, 264

Chavushian H. S., Oskanian A. V., Broutian G. H., 1999b, Astrophysics, 42, 404

Chavushian H. S., Pikichian H. V., Oskanian A. V., Broutian G. H., 2004, Astrophysics, 47, 313

doi: doi.org/10.52526/25792776-2021.68.2-150

Garibdzhanian A. T., 1976, Communications of the Byurakan Astrophysical Observatory, 49, 63

Haro G., 1957, "Non-stable stars", proceedings from IAU Symposium N. 3, ed. Herbig, G. H., p. 26

Haro G., 1964, "The Galaxy and the Magellanic Clouds", Proceedings of the IAU Symposium N. 20, ed.Frank, J. K., p. 26

Herbig G. H., 1962, Proceedings of a Symposium on Stellar Evolution, held in La Plata, ed. Sahade, J., p. 23

Kunkel W. E., 1975, "Variable Stars and Stellar Evolution"; Proceedings of the Symposium, Moscow, ed. Sherwood, V. E. and Plaut, L., p. 67

Melikian N. D., Tamazian V. S., Samsonyan A. L., 2011, Astrophysics, 54, 469

Mirzoyan L. V., 1981, Izvestiya Akademiya Nauk Armyanskoi, 16, 126

Mirzoyan A. V., 1993, Astrophysics, 36, 170

Mirzoyan L. V., Ambaryan V. V., 1988, Astrophysics, 28, 220

Mirzoyan L. V., Brutyan G. A., 1980, Astrophysics, 16, 67

Mirzoyan A. L., Hambarian V. V., 1995, Astrophysics, 38, 11

Mirzoyan L. V., Mnatsakanian M. A., 1971, Information Bulletin on Variable Stars, 604, 1

Mirzoyan A. L., Mnatsakanian M. A., 1990, "Flare Stars in Star Clusters, Associations, and the Solar Vicinity". Proceedings of the 137th. Symposium of the IAU, Armenia, ed. Mirzoian, L. V. and Pettersen, B. R. and Tsvetkov, M. K., p. 77

Mirzoyan L. V., Oganyan G. B., 1977, Astrophysics, 13, 333

Mirzoyan L. V., Chavushyan O. S., Erastova L. K., Oganyan G. B., Melikyan N. D., Natsvlishvili R. S., Tsvetkov M. K., 1977, Astrophysics, 13, 105

Mirzoyan L. V., Ambaryan V. V., Garibdzhanyan A. T., Mirzoyan A. L., 1988, Astrophysics, 29, 430

Mnatsakanyan M. A., 1969, Doklady Akademiia Nauk ArmSSR, 49, 33

Mnatsakanyan M. A., 1986, Astrofizika, 24, 621

Mnatsakanyan M. A., Mirzoyan A. L., 1988, Astrophysics, 29, 423

Oskanyan V. S., 1964, Publ. Astron. Observ. Beograd, 10

Oskanyan V. S., Terebizh V. Y., 1971, Astrophysics, 7, 48

Parsamian E. S., 2002, Astrophysics, 45, 15

Parsamian E. S., Andrews A. D., 1996, Irish Astronomical Journal, 23, 183

Parsamyan É. S., 1976, Astrophysics, 12, 145

Parsamyan É. S., 1980, Astrophysics, 16, 391

Parsamyan E. S., 1995, Astrophysics, 38, 206

doi: doi.org/10.52526/25792776-2021.68.2-150

Communications of BAO, Vol. 68, Issue 2, 2021, pp. 163-173

Search and Studies of the First Byurakan Survey Blue Stellar Objects

A. M. Mickaelian [*], G. A. Mikayelyan, H. V. Abrahamyan, and G. M. Paronyan

NAS RA V. Ambartsumian Byurakan Astrophysical Observatory (BAO), Byurakan 0213, Aragatzotn province, Armenia

Abstract

The First Byurakan Survey (FBS) 2^{nd} Part was devoted to search and studies of Blue Stellar Objects (BSOs) and Late-type Stars. Eleven lists of 1103 BSOs were published in Astrophysics in 1990-1996, found in FBS low-dispersion spectroscopic plates. The selection was carried out in the region with $+33° > \delta > +45°$ and $\delta >+61°$ with a surface of $\sim$4000 deg^2. As a result, the catalogue of the FBS BSOs was compiled. Its preliminary version has been available at CDS since 1999. We revised and updated the FBS BSOs catalogue with the new data from recently published optical and multiwavelength catalogues to give access to all available data and make further comparative studies of the properties of these objects possible. We made cross-correlations of the FBS BSOs catalogue with the MAPS, USNO-B1.0, SDSS, and 2MASS, as well as ROSAT, IRAS, NVSS, and FIRST catalogs, added updated SIMBAD and NED data for the objects, and provided accurate DSS1 and DSS2 positions and revised photometry. We also checked the objects for proper motion and variability. A refined classification for the low-dispersion spectra in the Digitized First Byurakan Survey (DFBS) was carried out. The revised and updated catalogue of FBS blue stellar objects contains 1101 objects. The FBS blue stellar objects catalogue can be used to study a complete sample of white dwarfs, hot subdwarfs, HBB stars, cataclysmic variables, bright AGN, and to investigate individual interesting objects.

Keywords: *Astronomical Data Bases: catalogs, Astronomical Data Bases: surveys, stars: subdwarfs, stars: white dwarfs, stars: cataclysmic variables, galaxies: quasars: general, galaxies: Seyfert*

Introduction: First Byurakan Survey (FBS)

The First Byurakan Survey (FBS), also known as Markarian survey, was the first systematic objective prism survey of the extragalactic sky. It was conducted by B. E. Markarian, V. A. Lipovetski and J. A. Stepanian in 1965-1980 at the Byurakan Astrophysical Observatory with the 1m (40") Schmidt telescope and 1.5° prism (Markarian, 1967, Markarian et al., 1989). At present, the FBS is the largest area spectral survey, covering 17,000 deg^2 of all the northern sky and part of the southern sky at high galactic latitudes, defined by δ > -15° and —b—> 15°. The limiting magnitude is 17.5^m–18^m, and the dispersion is 1800 Å/mm near Hγ. There are $\sim$40,000,000 spectra in all FBS plates corresponding to $\sim$20,000,000 objects; thus, each object has in average two spectra (Markarian et al., 1989). The FBS was conducted originally to search for galaxies with UV-excess (UVX). 1515 UVX galaxies have been discovered (Markarian et al., 1989, 1997, Mazzarella & Balzano, 1986). Studies of the Markarian galaxies early in the survey led to the spectral classification of Seyfert Galaxies (Weedman & Khachikyan, 1968), and to the first definition of starburst galaxies (Weedman, 1977).

The huge amount of spectral information contained in the plates allowed the development of several other projects based on the FBS, the most important being the discovery and investigation of blue stellar objects (Abrahamian & Mickaelian, 1996, Mickaelian, 2000). The FBS led to discovery of various important objects, like Markarian galaxies, FBS blue stellar objects (BSOs), late-type stars, identification of IRAS sources.

The nature of many FBS BSOs is still not clear. Moreover, the lists were published in Astrofizika and were not available for many years electronically. In 1999, the FBS catalog appeared in Vizier (Abrahamian et al., 1999), however with a number of uncertainties and with the old data given in the published papers only. Later in 2004, the accurate positions were measured for all FBS BSOs from two different epochs, DSS1

[*]aregmick@yahoo.com

doi: doi.org/10.52526/25792776-2021.68.2-163

and DSS2 images (Mickaelian, 2004). This revealed a number of proper motion objects, as well as variables and extended objects were revealed. After all these studies, a complete up-to-date catalog of the FBS BSOs was published in 2008 (Mickaelian, 2008), which combined the accurate positions, a reliable photometry, multiwavelength (X-ray, IR, and radio) data, and spectroscopic identifications.

At present the FBS plates have been digitized and the Digitized First Byurakan Survey (DFBS) has been created (Mickaelian et al., 2007). Its images and spectra are available on the DFBS web portal at Astronomical Observatory of Trieste at http://www.ia2-byurakan.oats.inaf.it/ and were used for the present study as well.

The FBS blue stellar objects

The second part of the FBS was devoted to the discovery and study of blue (UVX) stellar objects (Abrahamian & Mickaelian 1996 and references therein). It was carried out in 278 fields, in a 4009 deg^2 FBS area defined by $+33° < \delta < +45°$ and $\delta > +61°$). The discovery of new bright QSOs, Seyferts, planetary nebula nuclei (PNN), cataclysmic variables (CV), white dwarfs (WD), subdwarfs (sd), HBB (Horizontal Branch B) stars, and other interesting objects was the main purpose of this work. It was similar to the Palomar-Green (PG) survey (Green et al. 1986) but used a spectroscopic method of selection (which is more efficient), had a deeper magnitude limit, and larger area (though the Second part did not yet cover the whole FBS area so far). 1103 blue stellar objects (BSOs) have been selected, including 716 new ones. They have been published in 11 lists (Abrahamian & Mickaelian, 1993a,b, 1994a,b,c, 1995, 1996, Abrahamian et al., 1990a,b,c, 1991). The preliminary catalog of the FBS BSOs is available at the CDS (Abrahamian et al., 1999). And the revised and updated catalogue was published in 2008 (Mickaelian, 2008).

Spectroscopic observations proved the Second part of the FBS to be a rich source of QSOs, Seyferts, WDs, CVs, etc. (Mickaelian et al., 1999, 2001, 2002a, Sinamyan & Mickaelian, 2006, 2008a,b, 2009). Altogether, spectroscopic observations have been carried out for 406 FBS objects. Based on new spectroscopic observations, the local density of the bright QSOs and the completeness of the Bright Quasar Survey (BQS) (Schmidt & Green, 1983) have been re-estimated. We now have obtained a surface density of QSOs brighter than B=16.16 (completeness limit of the BQS) in a subarea of the FBS covering ∼2,250 deg^2, equal to 0.012 deg^{-2}, implying a completeness of 53±10% (Mickaelian et al., 1999, 2001).

Using the FBS low-dispersion spectra, a rare bright (V∼12.6) SW Sex subtype nova-like CV was discovered with a spectroscopic period within the period "gap" for such objects (Mickaelian et al., 2002b).

For a review of the FBS blue stellar objects see Mickaelian (2000) and an analysis of the samples of WDs and CVs see Mickaelian (2005). A full analysis of the FBS sample was given in Sinamyan & Mickaelian (2011).

The positions for FBS blue stellar objects (BSOs) published in the original papers were rather poor. This made finding the necessary objects very difficult. Later, accurate positions were measured and published for all 1101 FBS BSOs with an accuracy of 1" and better (Mickaelian, 2004). Moreover, both DSS1 and DSS2 (red and blue) positions were measured and the DSS1 and DSS2 positional accuracy was estimated in this paper.

However, the optical magnitudes for the FBS BSOs until recently were rather inaccurate, as well as the multiwavelength data were absent. The Sloan Digital Sky Survey (SDSS, http://www.sdss.org) now gives new photometric and redshift data for many FBS BSOs, which is also very useful for their further studies.

New data for the FBS objects

Accurate optical positions of the FBS BSOs made possible correct cross-correlation of the sample with all available modern catalogs and databases, like MAPS (Cabanela et al., 2003) and USNO-B1.0 (Monet et al., 2003), SDSS DR6 (Ahumada et al. 2020, online available at http://www.sdss.org/) and 2MASS (Cutri et al. 2003), ROSAT BSC (Voges et al., 1999) and FSC (Voges et al., 2000), IRAS PSC (IRAS, 1988) and FSC (Moshir & et al., 1990), NVSS (Condon et al., 1998) and FIRST (Becker et al., 2003) radio catalogs. We have also checked our objects in the catalogs of AGN (Véron-Cetty & Véron, 2006), WDs (McCook & Sion, 2006), CVs (Ritter & Kolb, 2003), and the catalogs of SDSS spectroscopically confirmed white dwarfs (Eisenstein et al., 2006), SDSS spectroscopically selected close binary systems (Silvestri et al., 2006), and the lists of SDSS cataclysmic variables (Szkody et al. 2007 and references therein). All these cross-correlations were necessary as not all data are in SIMBAD and NED, as found from other catalogs.

doi: doi.org/10.52526/25792776-2021.68.2-163

The identifications from various catalogs (QSO, WD, sd, CV, PN) also allowed to clarify the nature of many FBS objects. In addition, a number of FBS objects (mostly candidate QSOs) have been observed in SDSS and the spectra are available, however not all are classified. We have carried out the classification of these spectra and included the corresponding types in the FBS catalog too. We have also checked the objects for proper motions (PM) and variability, refined the classification using the Digitized First Byurakan Survey (DFBS, Mickaelian et al. 2007) spectra, updated the available data from SIMBAD and NED, and finally prepared a new catalogue of FBS blue stellar objects.

We have also corrected the names for three objects erroneously given in the previous version: FBS 0133+436 instead of FBS 0133+446, FBS 0223+365 instead of FBS 0223+355, and FBS 1600+382 instead of FBS 1609+382.

Accurate optical positions

For the new version of the catalogue, we give the accurate DSS1 (McGlynn & Scollick, 1994) and DSS2 (Lasker et al., 1996) red optical positions using our measurements (Mickaelian, 2004). Both measuremnets were needed to find the proper motions for many objects by comparison of positions from two epochs separated by about 40 years. These accurate positions, as already said and later shown, provided the possibility of correctly finding the corresponding associations in other known catalogues.

Proper motions

Proper motions (PM) are given in USNO-B1.0, calculated by measurements between POSS I and POSS II observations. However, based on our previous work (Mickaelian, 2004, Mickaelian & Gigoyan, 2006), when a number of PM from the USNO were not confirmed, we decided to cross-check them independently with our measurements from DSS1 and DSS2. We took the result as a real PM, if both data given in the USNO (in RA and DEC) matched. According to the USNO catalogue, 89 objects in our list have PM>60 mas/yr, including 52 with PM>100 mas/yr. However, by checking the DSS images, 21 objects were rejected. On the other hand, according to our measurements, more 11 objects have large PM not given in USNO catalogue. For objects having PM both by our measurements and USNO data, the agreement is within 30% (rms is 47 mas/yr and the systematic shift is only 7 mas/yr), which is rather reliable. This means that the USNO PM errors come from incorrect automatic identification of the object in plates of the two epochs, which happens especailly for large PM stars.

To increase the accuracy of the PM given in the catalogue, we have averaged the USNO and our measurements when available.

MAPS/USNO-B1.0 photometry

To have the best available photometric data for all our objects, we cross-correlated the FBS BSOs list with the Minnesota Automated Plate Scanner (MAPS) catalogue (Cabanela et al., 2003), and the USNO-B1.0 (Monet et al., 2003). MAPS is based on measurements from the POSS1, while USNO-B1.0 gives data from both POSS1 and POSS2. We carried out a statistical analysis of the photometric data provided by these two catalogues. When comparing their data from the POSS1 O (B) and E (R) images, we found a systematic shift. For the analysis, we used all FBS objects having USNO-B1.0 B1/B2/R1/R2 data and objects having MAPS (O and E) data.

First, we calculated the systematic shift between the MAPS (O and E) and USNO-B1.0 (B1 and R1) magnitudes. It is 0.01 and -0.05, respectively, which is negligible. So, we could trust these magnitudes and calculate the more accurate averages both for O (B) and E (R). Then we calculated the systematic shift between USNO B1 and B2, and between R1 and R2. It is 0.17 and 0.14, respectively, which we used for correction of the B2 and R2 magnitudes (as it was rather unlikely that B1 and R1 could have a systematic shift exactly similar to MAPS O and E). The corrected B2 and R2 were used together with MAPS O and E and USNO B1 and R1 to calculate the average B and R magnitudes, which we believe are the best ones available. Though both MAPS and USNO catalogs give 0.2 as their photometric errors, we find that the rms is about 0.48 for B magnitudes and 0.34 for R magnitudes, respectively.

doi: doi.org/10.52526/25792776-2021.68.2-163

Note that for all measurements we had eliminated possible variables or accidental large errors. Our conclusion is that R magnitudes are more accurate and that one should be careful with B magnitudes, and anyway a correction for the systematic shift is needed to calibrate them.

The rms between MAPS O and USNO B1 is 0.43, between MAPS E and USNO R1 0.50, which is very close to our estimates made for the BIS (Byurakan-IRAS Stars) catalog objects (Mickaelian & Gigoyan, 2006).

To reach the maximum possible photometric accuracy, we use the average between the MAPS O and USNO B1 as a B magnitude, and when MAPS is absent (for some low galactic latitude fields), we use the average between USNO B1 and corrected B2. The same was done for the red magnitudes. For an R magnitude, we take the average between MAPS E and USNO R1/R2, and when MAPS is absent, we use the corrected average USNO R1/R2. The values given in the catalogue are those calculated with the abovementioned principles.

Variability

The improvement of the USNO B2 and R2 magnitudes allowed us to investigate the sample for variability. We used the average MAPS O/E and USNO B1/R1 measurements for the POSS I observations, and corrected USNO B2/R2 measurements for the POSS II. Some accidental; errors were still present, which we found due to a study of the DSS1/DSS2 fields for possible defects. The variability flags given in the catalogue are based on these data. We did not use SDSS photometry, as the transformation of magnitudes into different bands caused additional errors.

To make a conclusion about the variability, we needed both USNO B and R differences between the two epochs (POSS1 and POSS2) to be large enough and to have nearly the same value (to exclude accidental errors). We took the 3-sigma limit (our measured rms both for B and R) for a confident variability (given as "var"), and 2-sigma limit for probable variability (var:).

Seventy objects matched these criteria; 21 are listed as genuine variables (var) and 49 as probable ones (var:). Of course, there still may be other variables that were not revealed by our approach (which showed approximately the same brightness during both observations). As it is well known, variable objects expected among the FBS BSOs are CVs and some white dwarfs (ZZ Cet stars), as well as a few possible blazars.

SDSS and 2MASS data

SDSS and 2MASS give accurate astrometric and photometric data for hundreds of million objects, thus being at present the largest and most useful catalogues. We have cross-correlated our sample with accurate positions with 5" search radius with SDSS DR16 and with 2MASS. Though the accuracy of these catalogs is higher, we left the radius larger to avoid accidental errors and losing any association, as a few objects among the FBS BSOs are still expected with larger than 3σ errors. In addition, there is a number of extended objects, as well as stars showing proper motion among the FBS BSOs resulting in worse accuracy.

We have found 510 SDSS objects as associations to the FBS BSOs and 970 2MASS objects. The first primary object in SDSS was taken. In addition, 120 SDSS objects have been observed spectroscopically and we were able to classify more FBS objects with unknown nature. SDSS five model magnitudes (*ugriz*) and 2MASS three NIR magnitudes (JHK) are now available.

SIMBAD and NED associations

A search for all FBS objects was made in SIMBAD and NED with a 60" search radius around their positions. In SIMBAD, we found 491 objects excluding FBS ones (the FBS objects are also included in SIMBAD and the data given are coming from our previous papers), including 62 extragalactic objects, 4 PN, 414 stars (158 WD, 110 sd, 39 CV, 24 main sequence stars, 83 of unknown type), 7 X-ray sources, and 4 radio sources.

In NED, we have found 196 objects, including 178 optical objects, 10 X-ray, and 8 radio sources. Optical objects include 88 extragalactic ones (including 65 having redshifts), 3 PN, 70 stars, and 17 unknown.

From both SIMBAD and NED objects, some were rejected due to incorrect associations (a neighboring object was taken, which was found from the DSS images), as well as ray and radio sources were combined with associations from non-optical catalogues. The combined SIMBAD/NED results give 522 objects (as

doi: doi.org/10.52526/25792776-2021.68.2-163

many objects were the same), including 509 optical ones: 68 extragalactic, 4 PN, 172 WD, 113 sd, 38 CV, 4 NHB (Normal or Horizontal Branch B stars), 18 other stars, and others are unknown BSOs. Thus, the nature of 414 FBS BSOs is known from other sources and later we have added data from our observations (see subsection "Classification of objects").

Classification of objects and sample content

All data described in the previous subsections were used to finally classify FBS BSOs, namely data from SIMBAD and NED databases, SDSS DR6, catalogs of AGN, PN, CV, WD (last online updates from Vizier), SDSS white dwarf and CV lists, etc. In addition, individual cross-correlations and DSS image check was carried out for Palomar-Green (PG, Green et al. 1986) objects, which have relatively inaccurate positions and were missed in our previous works. According to the new data, now we have 277 associations in PG, including 20 with very large PG positional errors. 24 more associations are found in Hamburg Quasar Survey (HQS, Hagen et al. 1995).

A spectroscopic study of the FBS BSOs was conducted in 1987-2000 with the Byurakan Astrophysical Observatory 2.6m telescope (BAO-2.6, UAGS and ByuFOSC spectrographs) and Observatoire de Haute-Provence 1.93m telescope (OHP-1.93, CARELEC spectrograph). Altogether, 485 slit spectra for 406 objects were obtained, both with photographic (in 1987-1991) and digital (in 1997-2000) receivers. The spectral coverage was 3300–6010Å(BAO-2.6 and UAGS), 4250–6950Å(BAO-2.6 and ByuFOSC), 4260–7910Å(OHP1.93 and CARELEC), and the spectral resolution was 6–7Åfor all spectra. Most of the observations were carried out in 1987-1991, however, to have better data, the photographic spectra were digitized and reduced in MIDAS as CCD ones (1850 pixels length). The details are given in Mickaelian et al. (1999, 2001), and Sinamyan & Mickaelian (2006, 2008a,b). In Table 1 we give the statistics of spectroscopic observations of the FBS BSOs.

Table 1. Statistics of all spectroscopic observations of FBS blue stellar objects.

FBS zones	**BAO-2.6 1987-1991**		**OHP-1.93 1997-1999**		**BAO-2.6 1998-2000**		**Total***	
	Objects	Spectra	Objects	Spectra	Objects	Spectra	Objects	Spectra
+35°	126	139	6	7	0	0	127	146
+39°	130	151	3	3	1	2	131	156
+43°	134	158	11	11	2	2	136	171
+63°÷+86°	-	-	9	9	3	3	12	12
Total	390	448	29	30	6	7	406	485

**Some objects have been observed using both photographic and digital methods, so the total is different from the sum of the numbers in the individual columns.*

As mentioned, altogether 509 objects were known, and 244 more (the new ones only) have been classified from our observations, bringing the total number to 753 (many objects with relatively low-quality spectra have been also re-classified and/or the classification was refined). The classification for WDs and subdwarfs is given as in Green et al. (1986) and McCook & Sion (2006).

Given that the SDSS spectra have $\sim$ 1Åresolution, for a final classification we have used these spectra when available, and then the other spectra in a decreasing order of resolution.

Thus, at present the physical types of more than 2/3 of our sample are known. These objects are: 217 WDs (DO, DOB, DBA, DAB, DA, DAZ, DZ, and DC subtypes), 371 subdwarfs (sdOA, SDOB, sdOC, sdOD, sdB-O, sdB, sdA, and unknown sd), 26 HBB, 6 NHB, 15 other stars (4 B-A and 11 F-G types, which were probably erroneously included in the sample), 38 CV, 5 PNN, 54 AGN (though including 3 HII; all with redshifts), and 14 Galaxies (given as "Gal", 7 with redshifts). According to their spectra, 6 objects are given as "cont" or "cont/Em" (possible AGN or CV), and one object is given as "nonstellar" (possible AGN). Table 2 gives the distribution of FBS BSOs by spectral types.

doi: doi.org/10.52526/25792776-2021.68.2-163

Table 2. Distribution of FBS BSO by spectral types.

Spectral Type	Zone $\delta = +35°$	Zone $\delta = +39°$	Zone $\delta = +43°$	Zone $\delta = +63° \div +86°$	Total	%
Star*		3	7	5	**15**	2.0
HBB / NHB	9	9	12	2	**32**	4.2
Sd	77	115	119	60	**371**	49.3
WD	40	41	41	95	**217**	28.8
CV	8	3	8	19	**38**	5.0
PNN		2	1	2	**5**	0.7
AGN**	11	10	14	19	**54**	7.2
Gal	2	5	2	5	**14**	1.9
cont / nonstellar	2	3	1	1	**7**	0.9
Total known	**149**	**191**	**205**	**208**	**753**	**100.0**
Unknown	61	20	28	241	350	
Total	**210**	**211**	**233**	**449**	**1103**	

* *contains the main sequence AFG stars.*
** *contains QSO, Sy and HII.*

The catalogue of the FBS BSOs

The revised and updated catalogue of the FBS blue stellar objects is given in Mickaelian (2008). The table is available in electronic form at the CDS. The catalogue consists of 1103 objects (the catalog in fact contains 1101 objects, as 2 pairs of objects turned to be identical however we have kept all objects in the list to allow users enter and find objects by all already accepted FBS names). The contents of the FBS catalogue are as follows:

1) First Byurakan Survey (FBS) blue stellar object (BSO) name.
2) FBS BSOs object name (hhmm+ddm).
3) The original paper number (1–11), where the object was published (see references for FBS lists).
4) FBS zone, where the object was found. Given by the central declination.
5) Comments on object names, including the two pairs of identical objects and alternative FBS names (erroneously used in previous publications).
6) DSS1 J2000 RA (hh:mm:ss.ss), accurate to 1" rms.
7) DSS1 J2000 DEC (dd:mm:ss.s), accurate to 1" rms.
8) DSS2 red J2000 RA (hh:mm:ss.ss), accurate to 1" rms.
9) DSS2 red J2000 DEC (dd:mm:ss.s), accurate to 1" rms.
10) Proper motion (PM) in RA, DEC, total yearly PM, and the position angle of the motion.
11) Galactic coordinates (l and b) (degrees).
12) Object classification into "stars" ("s") and "galaxies" ("g"). This is similar to MAPS classification, which gives an understanding of extension. This is important for magnitude measurements and may lead to large errors in case of misclassification (up to 3-4 magnitudes). Our type is a revised MAPS type based on careful study of the DSS1/DSS2 images.
13) FBS low-dispersion spectral (LDS) type, as explained e.g. in Mickaelian (2000).
14) Comments from inspection of DSS1/DSS2 images (binaries, nearby objects, possible variables, etc.).

doi: doi.org/10.52526/25792776-2021.68.2-163

15) Published FBS magnitude (corresponds to B).

16) MAPS O and E magnitudes based on our extension classification (i.e. taken from diameter or integral measurements).

17) USNO-B1.0 B1, R1 (POSS1 epoch), and B2, R2, and I (POSS2 epoch) magnitudes.

18) Summarizing B and R magnitudes derived from MAPS and USNO-B1.0 data.

19) Summarizing B-R color derived from MAPS and USNO-B1.0 data.

20) Variability flags ("var" or "var:").

21) SDSS ugriz model magnitudes from DR6.

22) 2MASS JHK photometry.

23) Other names and optical associations taken from SIMBAD, NED, etc.

24) Final spectroscopic classification based on known data from SIMBAD, NED, etc. and our observations: general type and subtype.

25) Redshifts of the FBS BSOs (extragalactic objects).

26) Associations with X-ray sources.

27) ROSAT X-ray count rate (photons per second).

28) Associations with IR sources (other than 2MASS).

29) IRAS (FSC when available) fluxes at 12, 25, 60, and 100 μm (Jansky).

30) Associations with radio sources.

31) Integral 21 cm flux from NVSS or FIRST (millijansky).

Study of the FBS BSOs sample

Fig. 1 presents the distribution of the FBS BSOs on the MAPS/USNO-B1.0 O/O-E color-magnitude diagram. Extragalactic objects (AGN and Gal, PNN, CVs, WDs, sd, HBB/NHB, and main sequence stars are marked differently. Objects of each group are in their typical location, however some of the CVs clearly move on the diagram due to their variability hence they may be located anywhere.

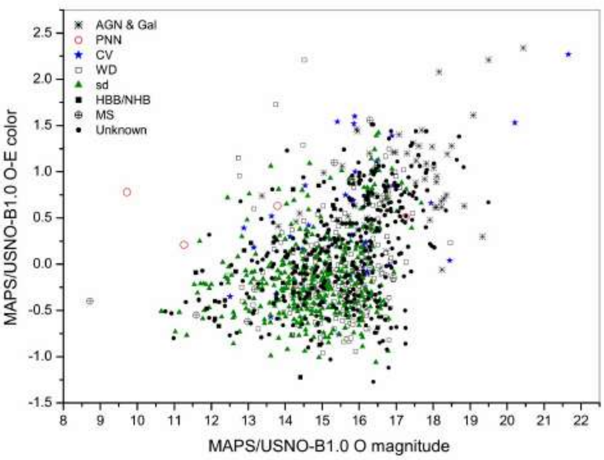

Figure 1. Combined MAPS/USNO-B1.0 *O-E* vs. *O* color-magnitude diagram for the FBS blue stellar objects. Asterisks: AGN and Gal; red open circles: PNN; blue stars: CVs; open squares: WDs; green triangles: subdwarfs; filled squares: HBB/NHB; open circles with crosses: main sequence (MS) stars; and filled circles: unclassified objects.

doi: doi.org/10.52526/25792776-2021.68.2-163

Fig. 1 shows some biases of the eye selection. Though most of objects show small color indices (O - E < 1.0), however, some selected objects have larger O-E. These are QSOs (selected by their peculiar SEDs), some WDs (selected by their broad absorption lines even without UV excess), and a few other objects.

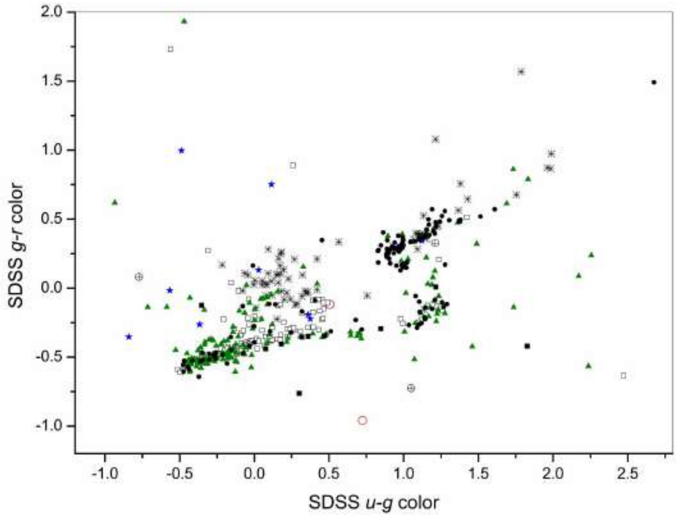

Figure 2. The SDSS u - g vs. g - r color-color diagram for 507 FBS blue stellar objects. The symbols are the same as on Fig. 1

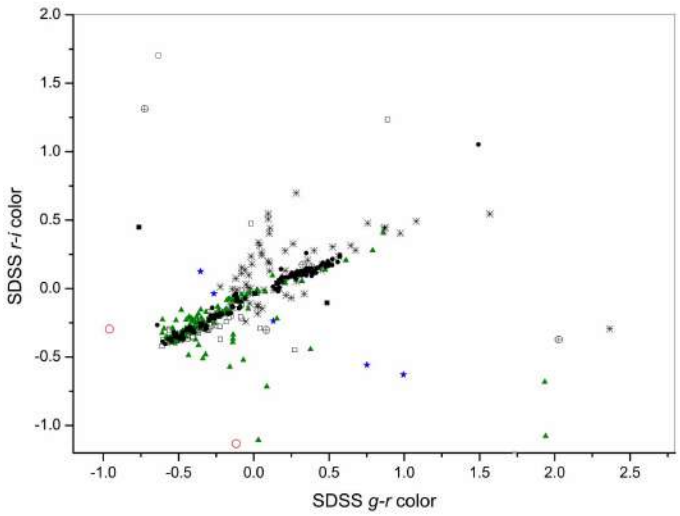

Figure 3. The SDSS g - r vs. r - i color-color diagram for 507 FBS blue stellar objects. The symbols are the same as on Fig. 1

Objects with unknown nature are marked by the filled circles. Their distribution indicates that still many new AGN, CVs, and WD are present in the FBS sample, as well as a few objects with extremely blue colors. Particularly, the faintest objects among the BSOs are either QSOs or CVs at their fainter brightness phase.

There is also a tendency showing that the fainter objects have redder colors. However, this can be also explained by the presence of extragalactic objects in the sample (which are fainter); as QSOs have small U - B color indices but relatively larger B - V ones (which is close to O - E used here). 139 objects (18.5%) out of 753 classified ones have O - E > 0.50, which may be considered as relatively non-blue ones. 48 are either extragalactic (AGN and Gal) or show peculiar SEDs (classified as cont or cont/Em:). Three others are PNN, 15 are CVs, 63 are WD/sd/HBBs (including several DZ dwarfs), and 10 are wrongly selected FG stars. If taken objects with O - E > 1.00, then only 55 objects are left, and 24 are extragalactic ones. Given that the rms accuracy of our derived MAPS/USNO-B1.0 photometric data is 0.4^m-0.5^m, we can conclude that the color criterion that corresponds to the selection of FBS BSOs was O - E < 0.50 and objects having larger color indices should not appear in the catalog and have been selected erroneously.

However, as the FBS BSOs are in fact UVX objects and not necessarily blue ones, we have plotted in

doi: doi.org/10.52526/25792776-2021.68.2-163

Fig. 2 and 3 the SDSS (model) u - g/g - r and g - r/r - i color-color diagrams for the 507 FBS objects measured in the SDSS (we have excluded 3 objects with obviously wrong data), including 387 classified and 120 unknown ones. As in Fig. 1, here too different types of objects are marked differently (by the same symbols). The extragalactic objects are much better separated (though some contamination by WDs and subdwarfs is present), which means that one can select new candidate AGN from the unknown FBS objects.

In fact, we do not use the SDSS data as main photometric ones, as it is not for all FBS objects and in addition the photometric accuracy rapidly decreases to the brighter magnitudes, where SDSS objects are saturated.

Fig. 4 gives the 2MASS J - H/H - K diagram for 970 FBS BSOs detected in 2MASS. It seems, 2MASS colors are the best separator for extragalactic objects among the blue stellar ones.

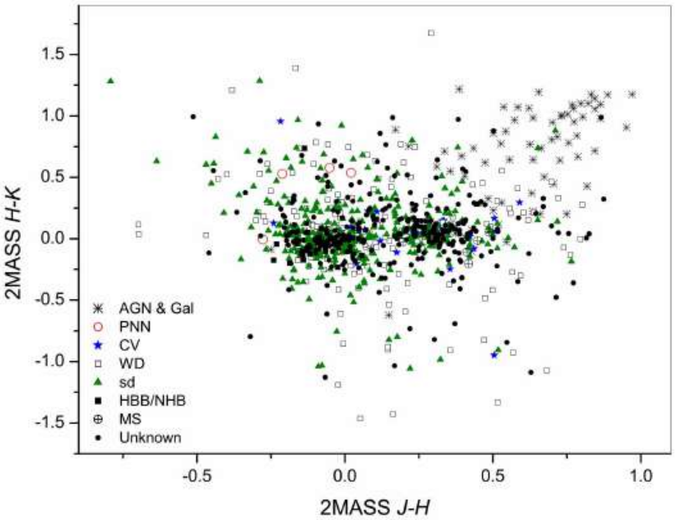

Figure 4. The 2MASS J - H vs. H - K color-color diagram for 970 FBS blue stellar objects. The symbols are the same as on Fig. 1

Based on the analysis of properties of the spectroscopically classified FBS objects and all available data from the multiwavelength catalogs, we have grouped the unknown FBS objects into subsamples of probable AGN (25 new objects are still expected), CVs (20 objects), WDs (101), subdwarfs (173), HBBs (15), and very few other objects.

Summary

Using newly obtained data on the FBS blue stellar objects, we have revised and updated the FBS sample giving the DSS1/DSS2 (accurate positions and proper motions), MAPS (optical photometry), USNO-B1.0 (optical photometry and proper motions), SDSS (ugriz magnitudes) and 2MASS (JHK photometry) catalogues, by re-classifying the objects by means of the slit spectra, and by updating other available data from SIMBAD, NED, X-ray, IR, and radio catalogues. An analysis of the MAPS and USNO-B1.0 photometric data led to a significant improvement of optical magnitudes, which may be used for other studies as well. The available photometric data for FBS BSOs allow us to follow their multiwavelength SEDs and to understand their nature, as not all objects have been observed spectroscopically.

The FBS catalogue contains the main available data for 1101 objects and will be useful as for study of its content so as for studies of individual objects, including AGN, CVs, WDs, etc.

Considering the spectroscopically known objects, our sample contains 7.2% AGN, 1.9% other galaxies, 5.0% CVs, and 28.8% WDs, slightly more than PG sample (6.8%, 1.9%, 3.7%, and 27.0%, respectively). However, this is the reason of more systematic works aimed at discovery of such interesting objects among the BSOs rather than hot subdwarfs, which are mostly the bye-products. Particularly our spectroscopic observations were aimed at discovery of new bright AGN (by pre-selection of candidates from X-ray and radio associations) as well as high proper motion objects (probable WDs), so that most of these objects have probably been already discovered. Hence, the PG and FBS samples are more or less similar by their content.

Most important changes and new details on the FBS BSOs will appear when applying Gaia data;

doi: doi.org/10.52526/25792776-2021.68.2-163

proper motions, parallaxes and distances, photometry and variability, and some physical characteristics are expected.

Acknowledgements

The authors acknowledge support from ANSEF grant in 2021-2022 (PS-astroex-2512) *"Discovery and study of new white dwarfs using Gaia accurate astrometry"*. The Digitized First Byurakan Survey (DFBS) is the digitized version of the Markarian survey (First Byurakan Survey, FBS) plates and is available online at http://www.ia2-byurakan.oats.inaf.it/.

References

Abrahamian H. V., Mickaelian A. M., 1991, Astrofizika, 35, 197

Abrahamian H. V., Mickaelian A. M., 1993a, Astrofizika, 36, 109

Abrahamian H. V., Mickaelian A. M., 1993b, Astrophysics, 36, 306

Abrahamian H. V., Mickaelian A. M., 1994a, Astrophysics, 37, 27

Abrahamian H. V., Mickaelian A. M., 1994b, Astrophysics, 37, 117

Abrahamian H. V., Mickaelian A. M., 1994c, Astrofizika, 37, 411

Abrahamian H. V., Mickaelian A. M., 1995, Astrofizika, 38, 201

Abrahamian H. V., Mickaelian A. M., 1996, Astrophysics, 39, 315

Abrahamian H. V., Lipovetskyi V. A., Stepanian J. A., 1990a, Astrofizika, 32, 29

Abrahamian H. V., Lipovetski V. A., Mickaelian A. M., Stepanian J. A., 1990b, Astrofizika, 33, 345

Abrahamian H. V., Lipovetski V. A., Mickaelian A. M., Stepanian J. A., 1990c, Astrofizika, 33, 213

Abrahamian H. V., Lipovetski V. A., Mickaelian A. M., Stepanian J. A., 1991, Astrofizika, 34, 13

Abrahamian H. V., Lipovetski V. A., Mickaelian A. M., Stepanian J. A., 1999, VizieR Online Data Catalog, p. II/223

Ahumada R., et al., 2020, Astrophys. J. Suppl. Ser. , 249, 3

Becker R. H., Helfand D. J., White R. L., Gregg M. D., Laurent-Muehleisen S. A., 2003, VizieR Online Data Catalog, p. VIII/71

Cabanela J. E., Humphreys R. M., Aldering G., Larsen J. A., Odewahn S. C., Thurmes P. M., Cornuelle C. S., 2003, Publ. Astron. Soc. Pac. , 115, 837

Condon J. J., Cotton W. D., Greisen E. W., Yin Q. F., Perley R. A., Taylor G. B., Broderick J. J., 1998, Astron. J. , 115, 1693

Cutri R. M., et al., 2003, VizieR Online Data Catalog, p. II/246

Eisenstein D. J., et al., 2006, Astrophys. J. Suppl. Ser. , 167, 40

Eritsyan M. A., Mickaelian A. M., 1993, Astrophysics, 36, 126

Green R. F., Schmidt M., Liebert J., 1986, Astrophys. J. Suppl. Ser. , 61, 305

Hagen H. J., Groote D., Engels D., Reimers D., 1995, Astron. and Astrophys. Suppl. Ser. , 111, 195

IRAS 1988, Joint IRAS Science Working Group. Infrared Astronomical Satellite Catalogs, The Point Source Catalog, Version 2.0, NASA RP-1190

Lasker B. M., Doggett J., McLean B., Sturch C., Djorgovski S., de Carvalho R. R., Reid I. N., 1996, in Jacoby G. H., Barnes J., eds, Astronomical Society of the Pacific Conference Series Vol. 101, Astronomical Data Analysis Software and Systems V. p. 88

Markarian B. E., 1967, Astrofizika, 3, 24

Markarian B. E., Lipovetsky V. A., Stepanian J. A., Erastova L. K., Shapovalova A. I., 1989, Soobshcheniya Spetsial'noj Astrofizicheskoj Observatorii, 62, 5

Markarian B. E., Lipovetsky V. A., Stepanian J. A., Erastova L. K., Shapovalova A. I., 1997, VizieR Online Data Catalog, p. VII/172

Mazzarella J. M., Balzano V. A., 1986, Astrophys. J. Suppl. Ser. , 62, 751

McCook G. P., Sion E. M., 2006, VizieR Online Data Catalog, p. III/235B

McGlynn T., Scollick K., 1994, in Crabtree D. R., Hanisch R. J., Barnes J., eds, Astronomical Society of the Pacific Conference Series Vol. 61, Astronomical Data Analysis Software and Systems III. p. 34

Mickaelian A., 1994, PhD thesis, Byurakan Astrophysical Observatory (BAO)

Mickaelian A. M., 2000, Astronomical and Astrophysical Transactions, 18, 557

doi: doi.org/10.52526/25792776-2021.68.2-163

Mickaelian A. M., 2004, Astron. Astrophys. , 426, 367

Mickaelian A. M., 2005, in Sion E. M., Vennes S., Shipman H. L., eds, Astrophysics and Space Science Library Vol. 332, White dwarfs: cosmological and galactic probes. pp 61–72, doi:10.1007/1-4020-3725-2_7

Mickaelian A. M., 2008, Astron. J. , 136, 946

Mickaelian A. M., Gigoyan K. S., 2006, Astron. Astrophys. , 455, 765

Mickaelian A. M., Sinamyan P. K., 2010, Mon. Not. R. Astron. Soc. , 407, 681

Mickaelian A. M., Eritsyan M. A., Abramyan G. V., 1991, Astrophysics, 34, 186

Mickaelian A. M., Gonçales A. C., Véron-Cetty M. P., Véron P., 1999, Astrophysics, 42, 1

Mickaelian A. M., Gonçalves A. C., Véron-Cetty M. P., Véron P., 2001, Astrophysics, 44, 14

Mickaelian A. M., Abrahamian H. V., Guibert J., Chesnel R., 2002a, Astrophysics, 45, 73

Mickaelian A. M., Balayan S. K., Ilovaisky S. A., Chevalier C., Véron-Cetty M. P., Véron P., 2002b, Astron. Astrophys. , 381, 894

Mickaelian A. M., et al., 2007, Astron. Astrophys. , 464, 1177

Mickaelian A. M., Mikayelyan G. A., Sinamyan P. K., 2011, Mon. Not. R. Astron. Soc. , 415, 1061

Monet D. G., et al., 2003, Astron. J. , 125, 984

Moshir M., et al. 1990, IRAS Faint Source Catalogue, p. 0

Nesci R., Mickaelian A., Rossi C., 2009, The Astronomer's Telegram, 2338, 1

Ritter H., Kolb U., 2003, Astron. Astrophys. , 404, 301

Schmidt M., Green R. F., 1983, Astrophys. J. , 269, 352

Silvestri N. M., et al., 2006, Astron. J. , 131, 1674

Sinamyan P. K., Mickaelian A. M., 2006, Astrophysics, 49, 333

Sinamyan P. K., Mickaelian A. M., 2008a, Astrophysics, 51, 37

Sinamyan P. K., Mickaelian A. M., 2008b, Astrophysics, 51, 226

Sinamyan P. K., Mickaelian A. M., 2009, Astrophysics, 52, 76

Sinamyan P. K., Mickaelian A. M., 2011, Astrophysics, 54, 403

Szkody P., et al., 2007, Astron. J. , 134, 185

Véron-Cetty M. P., Véron P., 2006, Astron. Astrophys. , 455, 773

Voges W., et al., 1999, Astron. Astrophys. , 349, 389

Voges W., et al., 2000, MPE, Garching, 7432, 3

Weedman D. W., 1977, Vistas in Astronomy, 21, 55

Weedman D. W., Khachikyan E. E., 1968, Astrophysics, 4, 243

doi: doi.org/10.52526/25792776-2021.68.2-163

Markarian survey and Markarian galaxies

A. M. Mickaelian *

NAS RA V. Ambartsumian Byurakan Astrophysical Observatory (BAO), Byurakan 0213, Aragatzotn province, Armenia

Abstract

Markarian survey (or the First Byurakan Survey, FBS) was the first systematic survey for active galaxies and was a new method for search for such objects. Until now, it is the largest objective prism survey of the sky (17,000 deg^2). It was carried out in 1965-1980 by B. E. Markarian and his colleagues and resulted in discovery of 1517 UV-excess (Markarian) galaxies. They contain many active galaxies, as well as powerful gamma-, X-ray, IR and radio sources (Mrk 180, 231, 421, 501, etc.), BCDGs (Mrk 116) and interacting/merging systems (Mrk 266, 273, etc.). They led to the classification of Seyfert galaxies into Sy1 and Sy2 and the definition of Starbursts (SB). Several catalogs of Markarian galaxies have been published (Bicay et al., 1995, Markarian et al., 1989, Mazzarella & Balzano, 1986, Petrosian et al., 2007) and they are accessible in all corresponding databases. Markarian survey also served as a basis for search for UVX stellar objects (including QSOs and Seyferts), late-type stars and optical identification of IR sources. At present the survey is digitized and DFBS database is available. We review the main characteristics of the Markarian survey, its comparison with other similar surveys and the importance of Markarian galaxies in modern astrophysics.

Keywords: *surveys – catalogues – techniques: spectroscopic – galaxies: active – galaxies: Seyfert – galaxies: Starburst – Virtual Observatory tools*

Introduction: Active Galaxies, AGN and their surveys

The history of active galaxies goes back to 1943, when Carl Seyfert published a list of 8 galaxies with broad emission lines (Seyfert, 1943). Later on, radio galaxies were discovered (Bolton et al., 1949). In 1956 Guillermo Haro published a list of blue galaxies (Haro, 1956). Viktor Ambartsumian (1958) paid attention to some active processes and observing data connected with the central regions of some galaxies: blue/UV colors, emission lines, radio emission, outflows, etc. He predicted that more such objects should exist and new forms of activity may be found; this idea was in fact the very beginning of the unified scheme suggested much later by Antonucci & Miller (1985). Similar discussions and direct indication on massive nuclei were given by Woltjer (1959). Predicted by Ambartsumian new types of active galaxies were the quasi-stellar objects (QSOs) discovered in 1963 (Schmidt, 1963) and the list of galaxies with anomalous colors (Markarian, 1963). To discover new such objects, find out what was their fraction and provide some statistics for further studies, Markarian conducted in 1965 a survey for UV-excess (UVX) galaxies. Some more types of active galactic nuclei (AGN) and other active galaxies were found in further works, such as BL Lac objects (Schmitt, 1968), Starburst (SB) galaxies (Weedman, 1977), LINERs (Heckman, 1980), etc.

The big variety of AGN types allows speaking about “AGN zoo”, as all these types have certain peculiarities and need a reliable classification. First attempts to classify Seyferts were done in mid-1960s, when differences between NGC 4151 and NGC 1068 were noticed (prototypes of Sy1 and Sy2). Later on Weedman & Khachikyan (1968) obtained the first spectra of Markarian galaxies and classified Seyferts into Sy 1/2 classes. Osterbrock (1981) introduced subclasses of Seyferts: 1.0, 1.2, 1.5, 1.8, 1.9 and 2.0. Later on Osterbrock & Pogge (1985) found galaxies with Sy 1 features having narrow Balmer and other permitted lines, Narrow-Line Seyfert 1 (NLS1) galaxies; these objects also show strong FeII and soft X-ray. We use NLS also for other subtypes of Sy1 (NLS1.2, NLS1.5, etc.), as well as NLQSOs have been observed. For narrow line AGN (Sy2, LINER and SB), the classification is given by so called diagnostic or BPT (Baldwin, Phillips, Terlevich) diagrams (Baldwin et al., 1981, Veilleux & Osterbrock, 1987). Anyway, due to the variety of their types and forms of activity, there is no final classification; very often classes refer to various properties, such as the morphology, optical spectrum, colour and/or spectral energy distribution (SED), radio loudness, polarization, etc.

*aregmick@yahoo.com

doi: doi.org/10.52526/25792776-2021.68.2-174

Markarian survey (First Byurakan Survey, FBS)

In 1965, Markarian started the first observations of the First Byurakan Survey (FBS), which was aimed at covering the northern extragalactic sky by objective prism plates to search for UVX galaxies. The first list was published in 1967 (Markarian, 1967) and altogether 15 lists of 1500 galaxies were published by Markarian, Lipovetski and Stepanian. The selection of the low dispersion (1800Å/mm at Hγ) provided a chance to follow SED and notice some broad (both emission and absorption) lines on one hand, and avoid overlaps on the other hand. Low-dispersion spectra cover the range 3400–6900 ÅÅ, and there is a sensitivity gap near 5300Å, dividing the spectra into red and blue parts. It is possible to compare these parts, easily distinguishing red and blue objects.

2050 Kodak IIAF, IIaF, IIF, and 103aF photographic plates in 1133 fields (4°×4° each, the size being 16cm × 16cm) have been taken. FBS covers 17,000 deg^2 of all the Northern Sky and part of the Southern Sky at high galactic latitudes (b>15°). The limiting magnitude on different plates changes in the range of 16.5^m–19.5^m in V, however for the majority it is 17.5^m–18^m. Each FBS plate contains low-dispersion spectra of some 15,000–20,000 objects, and there are some 20,000,000 objects in the whole survey.

We give in Table 1 the main observing and resulting characteristics of the FBS – Markarian survey. Though FBS spectra seem to be very similar, a thorough eye inspection with the help of 7$^\times$ lens provided opportunity to select peculiar spectra. To explain how difficult was the selection of peculiar spectra in the FBS, we give in Fig. 1 a standard FBS field and a collection of spectra of relatively rare interesting types of objects. Such spectra altogether are less than 5% among all in the FBS fields.

Table 1. Main observing and resulting characteristics of the FBS – Markarian survey.

Items	**Description**
Authors	B.E. Markarian, V.A. Lipovetskiy, J.A. Stepanian
Years	1965-1980
Telescope	BAO 102/132/213cm (40"/52"/84") Schmidt
Equipment	1.5° objective prism
Emulsions	Eastman Kodak IIAF, IIaF, IIF, 103aF
Plate size	4.1°×4.1°, 16cm × 16cm
Spectral range	3400-6900 ÅÅ with a sensitivity gap at 5300Å
Dispersion	1800 Å/mm at H$_\gamma$, 2500 Å/mm near H$_\beta$
Scale	96.8"/mm
Spatial resolution	2.4"
Limiting magnitude	17.5^m-18.0^m in V
Sky area	$\delta > -15°$, all RA except the Milky Way ($\lvert b\rvert > 15°$)
Total coverage	17,056 deg^2
Number of fields	1139 (each 16 deg^2), distributed by 28 declination zones
Number of plates	1874 (at least one plate with m=17 in each field)

Markarian survey was an outstanding study for all extragalactic (as well as galactic) astronomy; its main features may be given as:

- Markarian survey is the first systematic objective-prism survey,
- It is the largest objective-prism survey of the Northern sky (17,000 deg^2),
- It introduced a new method of search for active galaxies,
- Revelation of 1517 UVX galaxies: some 300 AGN and some 1000 HII galaxies,

doi: doi.org/10.52526/25792776-2021.68.2-174

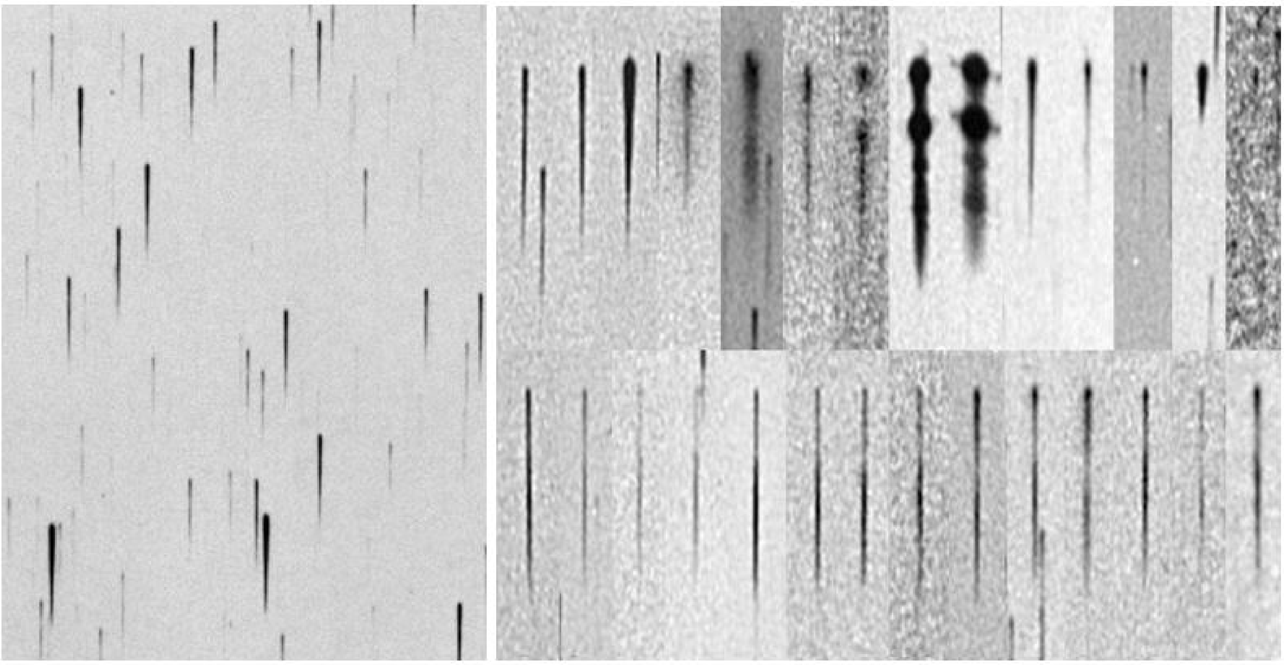

Figure 1. A standard FBS field showing similarity of most of the low-dispersion spectra and a collection of spectra of relatively rare interesting types of objects: Markarian galaxies, planetary nebulae, late-type stars (M and C), QSOs, CVs, white dwarfs and subdwarfs.

- Classification of Seyferts into Sy1 and Sy2 types (Weedman & Khachikyan, 1968),
- Definition of Starburst (SB) galaxies (Weedman, 1977),
- Discovery of many new Blue Compact Dwarf Galaxies (BCDG),
- Revelation of 1103 FBS Blue Stellar Objects (BSOs; Mickaelian 2008) and 1471 Late-type Stars (Gigoyan et al., 2019),
- Optical identification of 1577 IRAS sources (samples of Byurakan-IRAS Galaxies (BIG; Mickaelian & Sargsyan 2004) and Byurakan-IRAS Stars (BIS; Mickaelian & Gigoyan 2006)); discovery of many new AGN and ULIRGs.
- Markarian survey led to many other objective prism surveys with better spectral resolution and deeper limiting magnitudes, including the Second Byurakan Survey (SBS, Markarian et al. 1983, Stepanian 2005).

Markarian galaxies

Markarian galaxies have nuclei with excessive amounts of ultraviolet emission compared with other galaxies (so-called UV-excess). So far, 1517 Markarian galaxies are known, as well as many more similar UVX galaxies exist. Markarian galaxies have been published in a series of 15 papers in Astrophysics (Astrofizika) and then listed in several catalogs. We give in Table 2 all major lists and catalogs of Markarian galaxies providing accurate positional, morphological, photometric, multiwavelength data and images.

Fig. 2 shows the distribution of Markarian galaxies on the celestial sphere by equatorial coordinates RA and DEC and Fig. 3 shows the distribution of various types of Markarian galaxies by Galactic coordinates *lII* and *bII*.

Markarian galaxies have been studied by various observational methods, such as morphologically (e.g. Korovyakovskii et al. 1981), spectroscopically (Arakelyan et al. 1973, Markarian et al. 1988, Weedman & Khachikyan 1968 and references therein), as well as in different wavelength ranges (see below). Petrosian et al. (1989) have studied double and multiple structure of some Markarian galaxies. Carone et al. (1996) received spectra for the Sy1 galaxy Mrk 509 and studied its optical continuum and emission-line variability. Petrosian & Turatto (1986) investigated the relation of Markarian galaxies with Zwicky clusters. Santos-Lleó

doi: doi.org/10.52526/25792776-2021.68.2-174

Table 2. Lists and catalogs of Markarian galaxies.

Authors	**Years**	**Description**	**Number of objs.**
Markarian et al.	1967–1981	15 original lists of galaxies with UV-excess	1500
Kojoian et al.	1978–1984	Accurate optical positions	1500
Mazzarella & Balzano	1986	The first catalog of Markarian galaxies	1500
Markarian et al.	1989	The First Byurakan Survey. A catalogue of galaxies with UV-continuum	1517
Bicay et al.	1995	A multifrequency radio continuum and IRAS faint source survey of Mrk galaxies	899
Markarian et al.	1997	The FBS Catalogue of Markarian galaxies	1517
Petrosian et al.	2007	Markarian Galaxies. I. The Optical Database and Atlas	1544

Table 3. Most important Markarian galaxies for various matters of extragalactic astronomy.

Mrk galaxies	**Description**
Mrk 231	the closest ULIRG, BAL QSO and most luminous IR galaxy in the Local Universe
Mrk 421, 501	are among the highest known energy sources
Mrk 116 (=IZw18)	the most metal-deficient (BCDG) (Mrk and SBS)
Mrk 938	the first dynamic merger discovered observationally
Mrk 110	intermediate between NLS1 and BLS1 (FWHM=4900 km/s); understanding BLS1s and NLS1s differences
Mrk 6	shows variations of spectral lines typical of different types of objects (Sy2 & Sy1); very high H column density in X-rays
Mrk 926	one of the rare Sy1 galaxies having LINER properties
Mrk 766	one of the most important NLS1 galaxies
Mrk 273	a wonderful double-double nuclei galaxy
Mrk 266	has a multiple structure nuclear region
Mrk 231, 507	super strongest FeII emitters (FeII $\lambda4570$ / $H_\alpha > 2$)
Mrk 530, 993, 1018	change their spectra from Sy1.9 to Sy1.0

et al. (2001) have carried out a monitoring of the optical and NIR spectrum and MIR imaging of the Sy 1 galaxy Mrk 279. Some Markarian galaxies have also been reported to have jets.

Markarian galaxies are rather important for various extragalactic studies, such as: Mrk 231 is the most luminous infrared galaxy (ULIRG) in the Local Universe, Mrk 116 is the most metal-deficient blue compact dwarf galaxy (BCDG) (most of the BCDGs are Mrk and SBS galaxies), Mrk 421 and 501 are among the most powerful sources, etc. We give in Table 3 some selected Markarian galaxies that are most important for various matters of extragalactic astronomy. Detailed studies of these and similar objects are given in other papers of this symposium.

Altogether 292 Markarian galaxies are present in the Catalog of QSOs and AGN (Véron-Cetty & Véron, 2010) having activity types BLL, HPQ, QSO, Sy 1.0–1.2–1.5–1.8–1.9–2.0, NLS1, LINER, and HII. However, Markarian galaxies contain many more active ones, as not all have been classified for activity types.

doi: doi.org/10.52526/25792776-2021.68.2-174

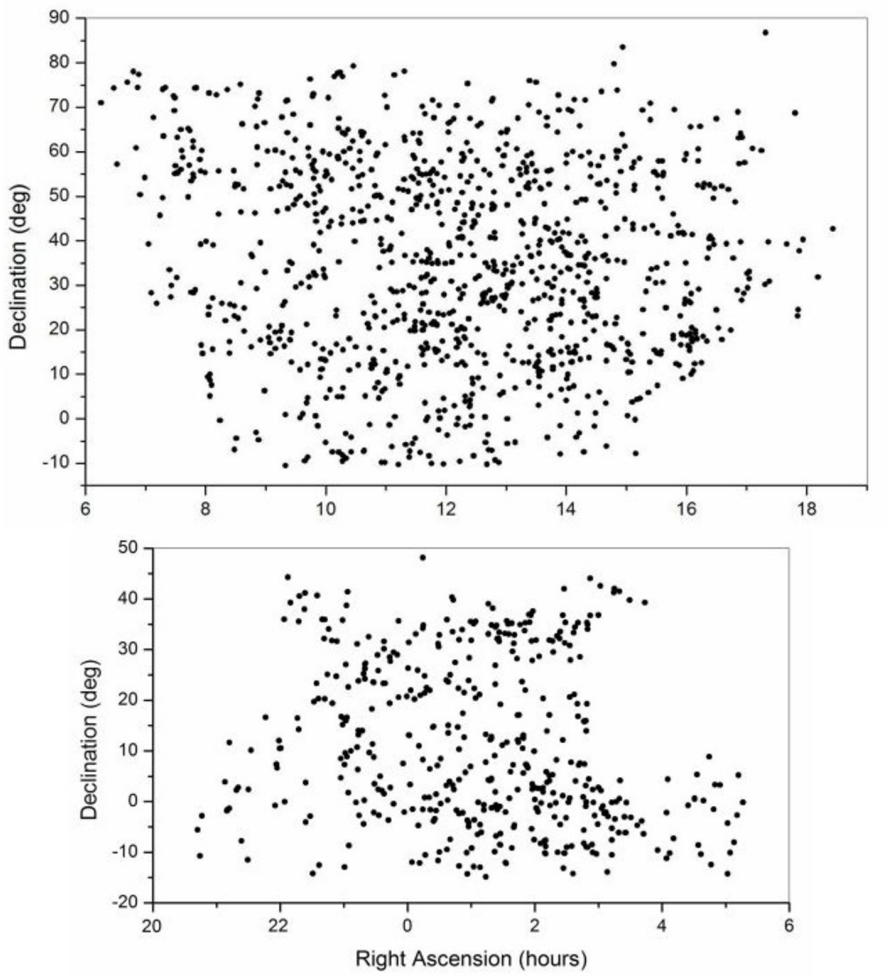

Figure 2. Distribution of Markarian galaxies on the celestial sphere by equatorial coordinates.

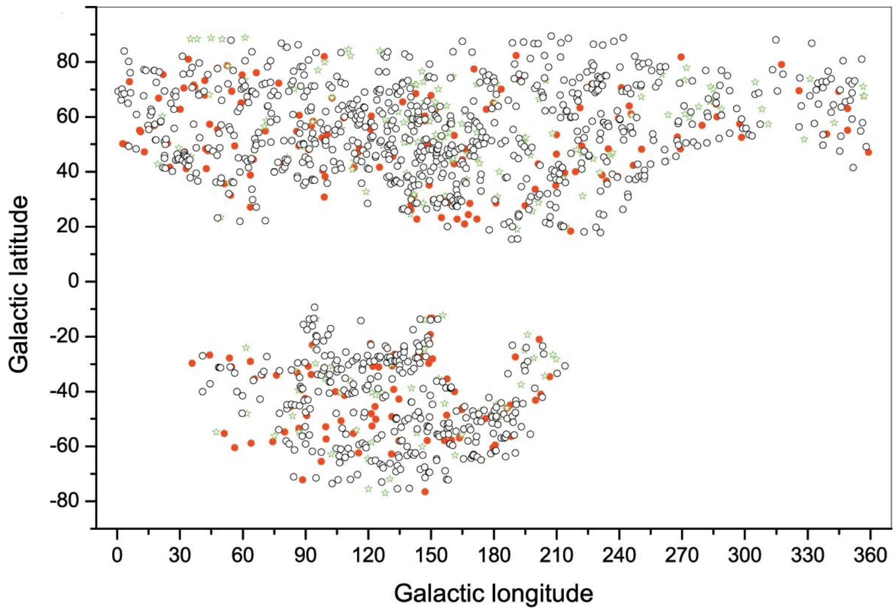

Figure 3. Distribution of Markarian galaxies on the celestial sphere by Galactic coordinates. Filled circles are AGN, stars are Starburst and HII galaxies, and open circles are galaxies without a sign of activity.

Studies of Markarian galaxies

Markarian galaxies have been observed in all wavelength ranges, from γ-ray to radio. E. g., they have been observed with the Arecibo radio telescope and for about 20% of them weak radio emission was detected (Tovmassian & Terzian, 1974). Kojoian et al. (1976) have studied the radio spectra of Markarian galaxies.

doi: doi.org/10.52526/25792776-2021.68.2-174

Kandalyan & Petrosyan (1989) have studied Markarian galaxies as FIR sources. They are targets for all modern ground-based and space telescopes as well. E. g. the blazars Markarian 421 and 501 have been detected in all high- and very high energy surveys, such as ROSAT (Voges et al., 1999, 2000), ASCA (Ueda et al., 2005), BeppoSAX (Ciliegi et al., 2003), Chandra (Evans et al., 2010), XMM (2010), INTEGRAL (Bird et al., 2010), Fermi (Nolan et al., 2012), as well as observations by systems as the High-Energy Stereoscopic System (H.E.S.S.; Aharonian et al. 2005), MAGIC, the Very Energetic Radiation Imaging Telescope Array System (VERITAS; Arlen et al. 2013), Nuclear Spectroscopic Telescope Array (NuSTAR; Harrison et al. 2013), etc.

We have carried out studies of Markarian galaxies (Mickaelian et al., 2013), including their revised spectral classification based on the SDSS spectra (Ahumada et al., 2020), studies of their multiwavelength (MW) properties, etc. Examples of MW SEDs for three famous Markarian galaxies (Mrk 180, Mrk 231 and Mrk 421) are given in Fig. 4. These SEDs have been built and taken from the Italian Space Agency (ASI) Data Science Center (ASDC, http://tools.asdc.asi.it/SED/) using the ASDC SED builder tool.

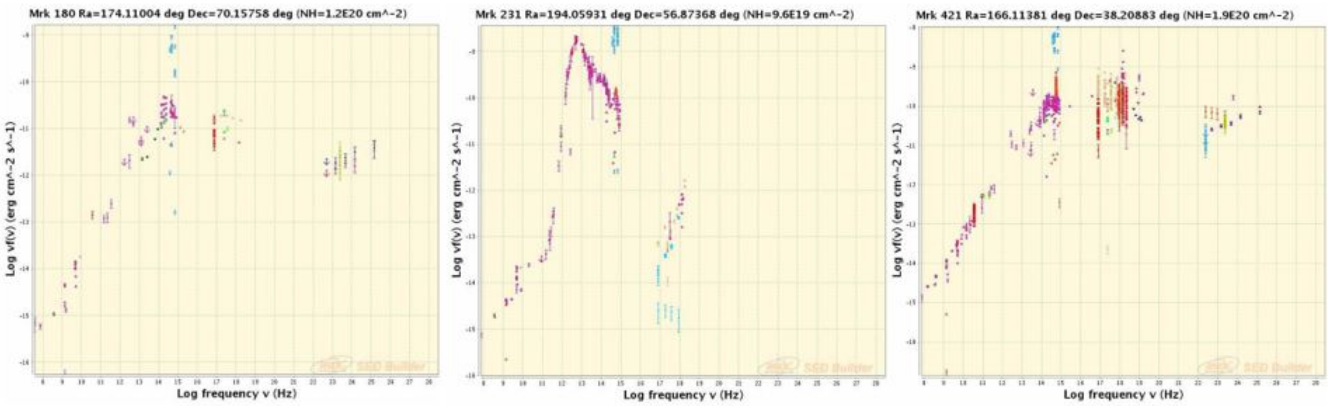

Figure 4. Spectral Energy Distribution (SED) of three famous Markarian galaxies: (from left to right) Mrk 180, Mrk 231 and Mrk 421.

Many more UVX and emission-line galaxies have been discovered in similar to Markarian surveys or by other studies. These are Arakelian galaxies having high surface bright- ness (Arakelian, 1975), Kazarian UVX galaxies (Kazarian et al., 2010), the University of Michigan emission-line galaxies (UM; MacAlpine & Feldman 1982), Case Low-Dispersion Northern Sky Survey galaxies (CG; Pesch et al. 1991), the Montreal blue galaxies (Coziol et al., 1994), SBS UVX and emission-line galaxies (Stepanian, 2005), Kiso UV galaxies (KUG; Miyauchi-Isobe et al. 2010), Hamburg/SAO emission-line galaxies (Pustilnik et al., 2005), GALEX UV-luminous galaxies (Hoopes et al., 2007), etc.

Digitized First Byurakan Survey – DFBS

The Digitized First Byurakan Survey (DFBS; Massaro et al. 2008, Mickaelian et al. 2007) is the digitized version of the Markarian survey (or FBS). It is a collaborative effort of the Byurakan Astrophysical Observatory, Universita di Roma "La Sapienza" and MIGG s.r.l. (Italy), Cornell University (USA), and Hamburger Sternwarte (Germany). It included scanning of the plates, high accuracy (1" rms) astrometric solution, extraction software for images and spectra, photometric and wavelength calibration of the spectra, classification, creation of DFBS catalog and database, construction of user interface and webpage. Later on, the Armenian Institute of Informatics and Automation Problems (IIAP) also joined the project to reproduce the DFBS database in Armenia in frame of the Armenian VO project. 1874 FBS plates have been scanned. We give in Table 4 the main scanning and resulting characteristics of the DFBS.

Fig. 5 shows a fragment of "bSpec" – DFBS spectra extraction and analysis dedicated software written by Giuseppe Cirimele.

For the classification, templates for main types of objects discovered from FBS have been used; UVX galaxies, QSOs, white dwarfs, subdwarfs, cataclysmic variables, car- bon stars, as well as stars of all spectral types (from O to M). The DFBS database is presently stored on a dedicated PC at Astronomical Observatory of Trieste (Italy) and can be accessed through web interface (http://www.ia2-byurakan.oats.inaf.it/).

doi: doi.org/10.52526/25792776-2021.68.2-174

Table 4. Main scanning and resulting characteristics of the DFBS.

Items	**Description**
Teams	Byurakan Astrophys. Obs., Univ. Roma "La Sapienza", Cornell Univ.
Years	2002-2007
Instrument	Epson Expression 1680 Pro scanner
Scanning options	1600 dpi (15.875μ pix size), 16 bit, transparency mode, "scanfits"
Plate size	9601×9601 pix, 176 MB file
Spectra	107×5 pix (1700μm in length)
Dispersion	33 Å/pix average (22-60 Å/pix), 28.5 at Hγ
Spectral resolution	50Å(average)
Astrometric solution	1" rms accuracy
Scale	1.542 "/pix
Photometry	0.3^m accuracy
Data volume	1874 plates, $\sim$ 400 GB
Number of objects	$\sim$ 20,000,000 ($\sim$ 40,000,000 spectra)

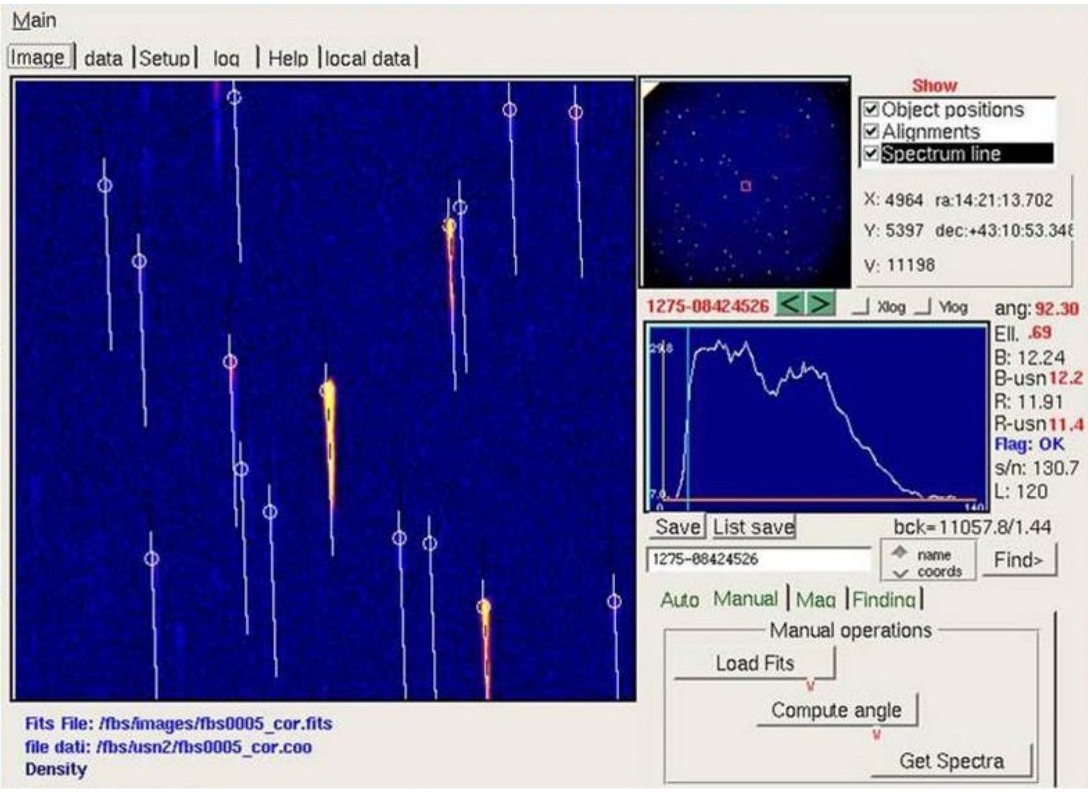

Figure 5. bSpec – DFBS spectra extraction and analysis software.

The user interface (the DFBS web portal) provides access to general information on the FBS and DFBS. It presently allows the following operations:

1) *DFBS sky coverage*,

2) *Plate list*,

3) *Explore*, allowing the display of a portion of plate around a given central RA, DEC position, interactive

doi: doi.org/10.52526/25792776-2021.68.2-174

selection of one or more spectra, their collection and downloading,

4) *Get Image*, allowing users to select a portion of a plate in FITS format and all the spectra of this portion present in the database for downloading, as well as downloading of the whole selected field,

5) *Get Spectra*, allowing downloading all the spectra in the database within a given distance from a selected central position (cone search). Fig. 6 shows two webshots from the DFBS web interface: modes "Explore" and "Get Spectra".

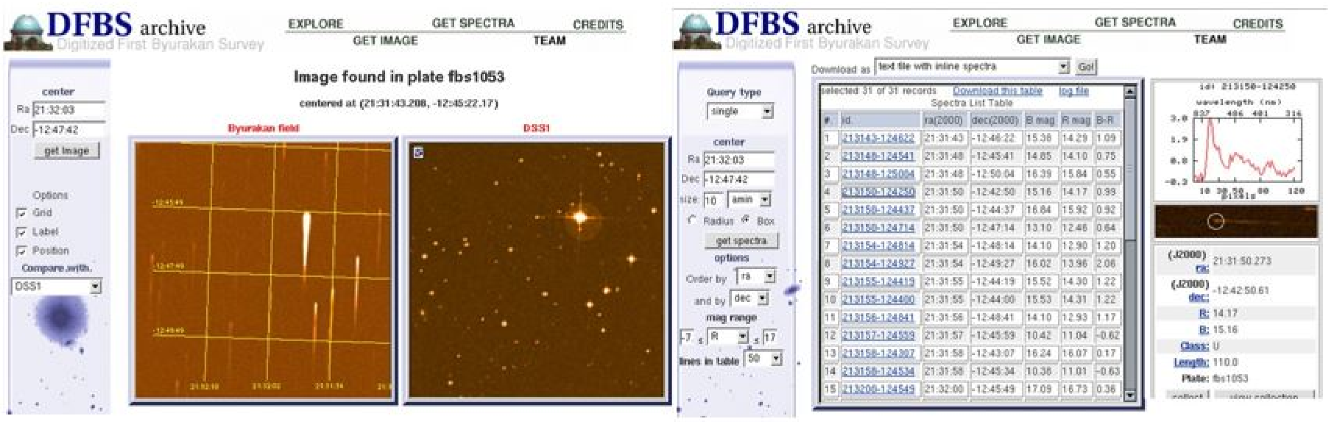

Figure 6. DFBS web interface: "Explore" and "Get Spectra" modes.

Summary and Conclusions

Markarian survey was the first systematic search for active galaxies, and Markarian galaxies led to discovery of many new AGN, spectral classification of Seyfert galaxies and definition of a new class of active galaxies, Starburst ones. Until now, Markarian survey is the largest area spectroscopic survey and the DFBS contains the largest number of spectra (some 20,000,000 objects).

We give in Table 5 a comparison of the main characteristics of large spectroscopic surveys. The first five surveys are objective prism ones and have been done using Kodak emulsions and only SDSS has been done with CCD using *u, g, r, i,* and *z* filters. In all cases, the most important goals were to discover active galaxies, as well as SDSS also has carried out the largest ever galaxy redshift survey (4.5 million objects). Such surveys are also an ideal tool for optical identifications of X-ray, IR, and radio sources; such projects have been carried out using FBS (Mickaelian, 1995) and HQS (Mickaelian et al., 2006, Zickgraf et al., 2003).

Markarian survey led to the discovery of 1517 UVX galaxies, including some 300 AGN and some 1000 HII galaxies. Classification of Markarian galaxies provided Sy1 and Sy2 types and the definition of Starburst galaxies. Many new BCDG were discovered as well. The continuation of the FBS for stellar objects revealed FBS Blue Stellar Objects and FBS Late-type Stars, as well as optical identifications of IRAS sources have been carried out resulted in discovery of new ULIRGs and AGN. Markarian survey also led to many other objective prism surveys.

Markarian galaxies are reliable objects for MW studies of active galaxies, as they are bright enough and have been detected in all ranges of electromagnetic radiation; from γ-ray to radio. In one of the recent works, we have collected all available MW data from all-sky or large-area catalogs and have built MW SEDs for Markarian galaxies using 38 photometric points (Fermi, INTEGRAL, ROSAT, GALEX FUV/NUV, UBV, POSS I/II OjEN, SDSS ugriz, 2MASS JHK, WISE w1/w2/w3/w4, Spitzer IRAC/MIPS, AKARI 9/18/65/90/140/160 μm, IRAS 12/25/60/100 μm, radio 4.85 and 1.4 GHz, 843, 612, 326, 152 and 38 MHz). These SEDs provide a possibility to group objects by their shapes and compare to existing physical properties to find various relations and refine the AGN classifications.

Other projects based on FBS observing material

As mentioned, as number of other projects were based on Markarian Survey:

doi: doi.org/10.52526/25792776-2021.68.2-174

Table 5. Comparison of the main characteristics of large area spectroscopic surveys.

Survey	**Years**	**Telescope** **Equipment**	**Sky area** **Surface** (deg^2)	**Disp. Hγ** Å/mm	**Sp. range** Å	**V$_{lim}$**
FBS	1965-1980	BAO 1m Schmidt 1.5 prism	$\delta > -15, \lvert b \rvert > 15$ 17,056	1800	3400-6900	17.5
SBS	1978-1991	BAO 1m Schmidt 1.5, 3, 4 prisms	$49 < \delta < 61, \lvert b \rvert > 30$ 965	1800/900/280	3400-6950	19.0
Case	1983-1995	KPNO 91cm 1.8 prism	$\delta > 30, \lvert b \rvert > 30$	1350	3400-5300	18.0
HQS	1985-1997	CAHA 81cm 1.7 prism	$\delta > 0, \lvert b \rvert > 20$ 14,000	1390	3400-5300	19.0
HES	1990-1996	ESO 1m Schmidt 4 prism	$\delta < 2.5, \lvert b \rvert > 30$ 9,000	280	3400-5300	18.0
SDSS	2000-2021	Apache Point 2.5m Double MOS	$\delta > 0, \lvert b \rvert > 30$ 14,555	res. 2.5Å	3000-10800	22.0

1) Second Byurakan Survey (SBS),

2) Second Part of the FBS: a) Search and studies for Blue Stellar Objects (BSO) and b) Search and studies for Late-Type Stars,

3) Optical Identifications of IRAS point sources (BIS and BIG objects, Byurakan-IR Stars and Byurakan-IR Galaxies, respectively),

4) Search for asteroids on the DFBS.

Many papers have been produced based on these studies and a number of catalogues have been published in peer-reviewed journals and VizieR.

Acknowledgements

The work was supported by the Science Committee of RA, in the frames of the research project No. 21AG-1C053 *"Revelation of the early stages of galaxy evolution by means of multiwavelength study of active galaxies"*.

References

Aharonian F., et al., 2005, Astron. Astrophys. , 437, 95

Ahumada R., et al., 2020, Astrophys. J. Suppl. Ser. , 249, 3

Ambartsumian V. A., 1958, in La structure et l'évolution de l'universe. pp 241–249

Antonucci R. R. J., Miller J. S., 1985, Astrophys. J. , 297, 621

Arakelian M. A., 1975, Communications of the Byurakan Astrophysical Observatory, 47, 3

Arakelyan M. A., Dibai É. A., Esipov V. F., 1973, Astrophysics, 9, 183

Arlen T., et al., 2013, Astrophys. J. , 762, 92

Baldwin J. A., Phillips M. M., Terlevich R., 1981, Publ. Astron. Soc. Pac. , 93, 5

Bicay M. D., Kojoian G., Seal J., Dickinson D. F., Malkan M. A., 1995, Astrophys. J. Suppl. Ser. , 98, 369

Bird A. J., et al., 2010, Astrophys. J. Suppl. Ser. , 186, 1

Bolton J. G., Stanley G. J., Slee O. B., 1949, Nature. , 164, 101

doi: doi.org/10.52526/25792776-2021.68.2-174

Carone T. E., et al., 1996, Astrophys. J. , 471, 737

Ciliegi P., Vignali C., Comastri A., Fiore F., La Franca F., Perola G. C., 2003, Mon. Not. R. Astron. Soc. , 342, 575

Condon J. J., Cotton W. D., Greisen E. W., Yin Q. F., Perley R. A., Taylor G. B., Broderick J. J., 1998, Astron. J. , 115, 1693

Coziol R., Demers S., Pena M., Barneoud R., 1994, Astron. J. , 108, 405

Cutri R. M., et al. 2012, VizieR Online Data Catalog, p. II/311

Evans I. N., et al., 2010, Astrophys. J. Suppl. Ser. , 189, 37

Gigoyan K. S., Mickaelian A. M., Kostandyan G. R., 2019, Mon. Not. R. Astron. Soc. , 489, 2030

Gyulzadyan M. V., Mickaelian A. M., Abrahamyan H. V., Mikayelyan G. A., Paronyan G. M., 2018, Communications of the Byurakan Astrophysical Observatory, 65, 392

Haro G., 1956, Astron. J. , 61, 178

Harrison F. A., et al., 2013, Astrophys. J. , 770, 103

Heckman T. M., 1980, Astron. Astrophys. , 500, 187

Hoopes C. G., et al., 2007, Astrophys. J. Suppl. Ser. , 173, 441

Kandalyan R. A., Petrosyan A. R., 1989, Astrophysics, 30, 196

Kazarian M. A., Adibekyan V. Z., McLean B., Allen R. J., Petrosian A. R., 2010, Astrophysics, 53, 57

Kojoian G., Sramek R. A., Dickinson D. F., Tovmassian H., Purton C. R., 1976, Astrophys. J. , 203, 323

Kojoian G., Chute P. A., Aumann C. E., 1984, Astron. J. , 89, 332

Korovyakovskii Y. P., Petrosyan A. R., Saakyan K. A., Khachikyan É. E., 1981, Astrophysics, 17, 121

MacAlpine G. M., Feldman F. R., 1982, Astrophys. J. , 261, 412

Markarian B. E., 1963, Communications of the Byurakan Astrophysical Observatory, 34, 3

Markarian B. E., 1967, Astrofizika, 3, 24

Markarian B. E., Lipovetskii V. A., Stepanian D. A., 1983, Astrofizika, 19, 29

Markarian B. E., Erastova L. K., Lipovetsky V. A., Stepanian J. A., Shapovalova A. I., 1988, Astrofizika, 28, 27

Markarian B. E., Lipovetsky V. A., Stepanian J. A., Erastova L. K., Shapovalova A. I., 1989, Soobshcheniya Spetsial'noj Astrofizicheskoj Observatorii, 62, 5

Markarian B. E., Lipovetsky V. A., Stepanian J. A., Erastova L. K., Shapovalova A. I., 1997, VizieR Online Data Catalog, p. VII/172

Massaro E., Mickaelian A. M., Nesci R., Weedman D., 2008, The Digitized First Byurakan Survey. ARACNE Editrice, Rome, 78 p.

Massaro E., Giommi P., Leto C., Marchegiani P., Maselli A., Perri M., Piranomonte S., Sclavi S., 2009, Astron. Astrophys. , 495, 691

Mazzarella J. M., Balzano V. A., 1986, Astrophys. J. Suppl. Ser. , 62, 751

McMahon R. G., Irwin M. J., Maddox S. J., 2000, VizieR Online Data Catalog, p. I/267

Mickaelian A. M., 1995, Astrophysics, 38, 349

Mickaelian A. M., 2000, Astronomical and Astrophysical Transactions, 18, 557

Mickaelian A. M., 2008, Astron. J. , 136, 946

Mickaelian A. M., Gigoyan K. S., 2006, Astron. Astrophys. , 455, 765

Mickaelian A. M., Sargsyan L. A., 2004, Astrophysics, 47, 213

Mickaelian A. M., Sargsyan L. A., 2010, Astrophysics, 53, 483

Mickaelian A. M., Gonçalves A. C., Véron-Cetty M. P., Véron P., 2001, Astrophysics, 44, 14

Mickaelian A. M., Hovhannisyan L. R., Engels D., Hagen H. J., Voges W., 2006, Astron. Astrophys. , 449, 425

Mickaelian A. M., et al., 2007, Astron. Astrophys. , 464, 1177

Mickaelian A. M., Abrahamyan H. V., Paronyan G. M., Harutyunyan G. S., 2013, Astronomische Nachrichten, 334, 887

Mickaelian A. M., Abrahamyan H. V., Gyulzadyan M. V., Paronyan G. M., Mikayelyan G. A., 2018, Astrophys. Space. Sci. , 363, 237

Miyauchi-Isobe N., Maehara H., Nakajima K., 2010, Publications of the National Astronomical Observatory of Japan, 13, 9

Nolan P. L., et al., 2012, Astrophys. J. Suppl. Ser. , 199, 31

doi: doi.org/10.52526/25792776-2021.68.2-174

Osterbrock D. E., 1981, Astrophys. J. , 249, 462

Osterbrock D. E., Pogge R. W., 1985, Astrophys. J. , 297, 166

Pesch P., Sanduleak N., Stephenson C. B., 1991, Astrophys. J. Suppl. Ser. , 76, 1043

Petrosian A. R., Turatto M., 1986, Astron. and Astrophys. Suppl. Ser. , 65, 349

Petrosian A. R., Sahakian K. A., Khachikian E. Y., 1989, in Osterbrock D. E., Miller J. S., eds, Vol. 134, Active Galactic Nuclei. p. 445

Petrosian A., McLean B., Allen R. J., MacKenty J. W., 2007, Astrophys. J. Suppl. Ser. , 170, 33

Pustilnik S. A., et al., 2005, Astron. Astrophys. , 442, 109

Santos-Lleó M., et al., 2001, Astron. Astrophys. , 369, 57

Schmidt M., 1963, Nature. , 197, 1040

Schmitt J. L., 1968, Nature. , 218, 663

Seyfert C. K., 1943, Astrophys. J. , 97, 28

Stepanian J. A., 2005, Rev. Mex. Astron. Astrofis. , 41, 155

Tovmassian H. M., Terzian Y., 1974, Publ. Astron. Soc. Pac. , 86, 649

Ueda Y., Ishisaki Y., Takahashi T., Makishima K., Ohashi T., 2005, Astrophys. J. Suppl. Ser. , 161, 185

Veilleux S., Osterbrock D. E., 1987, Astrophys. J. Suppl. Ser. , 63, 295

Véron-Cetty M. P., Véron P., 2010, Astron. Astrophys. , 518, A10

Voges W., et al., 1999, Astron. Astrophys. , 349, 389

Voges W., et al., 2000, IAU Circ., 7432, 3

Weedman D. W., 1977, Vistas in Astronomy, 21, 55

Weedman D. W., Khachikyan E. E., 1968, Astrophysics, 4, 243

Woltjer L., 1959, Astrophys. J. , 130, 38

XMM 2010, XMM-Newton Serendipitous Source Catalogue: 2XMMi–DR3 XMM-Newton Survey Science Centre Consortium, XMM-SSC, Leicester, UK

Zickgraf F. J., Engels D., Hagen H. J., Reimers D., Voges W., 2003, Astron. Astrophys. , 406, 535

Important papers on Markarian galaxies:

FBS lists (15)

Markarian B.E. – Galaxies with an Ultraviolet Continuum // Ap, 3, 24-38, 1967
Markarian B.E. – Galaxies with Ultraviolet Continuum. II // Ap, 5, 206-225, 1969
Markarian B.E. – Galaxies with ultraviolet continuum. III // Ap, 5, 286-301, 1969
Markarian, B. E.; Lipovetskii, V. A. –Galaxies with ultraviolet continuum. IV // Ap, 7, 299-310, 1971
Markarian, B. E.; Lipovetskii, V. A. – Galaxies with ultraviolet continuum. V // Ap, 8, 89-99, 1972
Markarian, B. E.; Lipovetskii, V. A. – Galaxies with ultraviolet continuum. VI // Ap, 9, 283-295, 1973
Markarian, B. E.; Lipovetskii, V. A. – Galaxies with ultraviolet continuum. VII // Ap, 10, 185-194, 1974
Markarian, B. E.; Lipovetskii, V. A. – Galaxies with ultraviolet continuum. VIII // Ap, 12, 241-254, 1976
Markarian, B. E.; Lipovetskii, V. A. – Galaxies with ultraviolet continuum. IX // Ap, 12, 429-442, 1976
Markarian, B. E.; Lipovetskii, V. A.; Stepanian, J. A. – Galaxies with ultraviolet continuum. X // Ap, 13, 116-125, 1977
Markarian, B. E.; Lipovetskii, V. A.; Stepanian, J. A. – Galaxies with ultraviolet continuum. XI // Ap, 13, 215-228, 1977
Markarian, B. E.; Lipovetskii, V. A.; Stepanian, J. A. – Galaxies with ultraviolet continuum. XII // Ap, 15, 130-141, 1979
Markarian, B. E.; Lipovetskii, V. A.; Stepanian, J. A. – Galaxies with ultraviolet continuum. XIII // Ap, 15, 235-250, 1980
Markarian, B. E.; Lipovetskii, V. A.; Stepanian, J. A. – Galaxies with ultraviolet continuum. XIV // Ap, 15, 363-376, 1980
Markarian, B. E.; Lipovetskii, V. A.; Stepanian, J. A. – Galaxies with ultraviolet continuum. XV // Ap, 17, 321-332, 1982

FBS catalogs (5)

Balzano & Mazzarella 1986

Markarian, B. E.; Lipovetsky, V. A.; Stepanian, J. A.; Erastova, L. K.; Shapovalova, A. I. – The First Byurakan Survey – a Catalogue of Galaxies with Ultraviolet Continuum // Com. SAO, 62, 5-121, 1989 (in Russian)

Markarian B.E. – Catalogue of Markarian Galaxies // VizieR On-line Data Catalog, VII/61A, 1994

Markarian, B. E.; Lipovetsky, V. A.; Stepanian, J. A.; Erastova, L. K.; Shapovalova, A. I. – First Byurakan Survey (FBS) // VizieR On-line Data Catalog, VII/172, 1997

Petrosian, A., McLean, B., Allen, R. J., MacKenty, J. W., ApJS 170, 33, 2007

doi: doi.org/10.52526/25792776-2021.68.2-174

Spectra of Markarian galaxies (9+)

Arakelian, M. A.; Dibay, Eh. A.; Esipov, V. F.; Markarian, B. E. – Spectra of Markarian galaxies. II // Ap, 6, 189-194, 1970

Arakelian, M. A.; Dibay, Eh. A.; Esipov, V. F.; Markarian, B. E. – Spectra of Markarian galaxies. III // Ap, 7, 102-108, 1971

Markarian, B. E.; Lipovetskii, V. A.; Stepanian, J. A. – Spectra of galaxies with ultraviolet continuum. I // Ap, 16, 1-7, 1980

Markarian, B. E.; Lipovetskii, V. A.; Stepanian, J. A. – Spectra of galaxies with ultraviolet continuum. II // Ap, 16, 353-359, 1981

Markarian, B. E.; Lipovetskii, V. A.; Stepanian, J. A. – Spectra of galaxies with ultraviolet continuum. III // Ap, 19, 129-133, 1983

Markarian, B. E.; Lipovetskii, V. A.; Stepanian, J. A. – Spectra of galaxies with ultraviolet continuum. IV // Ap, 21, 581-587, 1985

Markarian, B. E.; Erastova, L. K.; Lipovetskii, V. A.; Stepanian, J. A.; Shapovalova, A. I. – Spectra of galaxies with ultraviolet continuum. V // Ap, 22, 127-135, 1985

Markarian, B. E.; Erastova, L. K.; Lipovetskii, V. A.; Stepanian, J. A.; Shapovalova, A. I. – Spectra of galaxies with Ultraviolet Continuum. VI // Ap, 28, 14-21, 1988

Markarian, B. E.; Erastova, L. K.; Lipovetskii, V. A.; Stepanian, J. A.; Shapovalova, A. I. – Spectra of galaxies with Ultraviolet Continuum. VII // Ap, 28, 283-288, 1988

Khachikian/Weedman papers

FBS Seyferts (12)

Arakelian, M. A.; Dibay, Eh. A.; Esipov, V. F.; Markarian, B. E. – New Seyfert-type objects in the second Markarian's list // Astron. Circular, 568, 1-2, 1970 (in Russian)

Arakelian, M. A.; Dibay, Eh. A.; Esipov, V. F.; Markarian, B. E. – New Seyfert-type objects in the second and third Markarian's lists // Astron. Circular, 586, 1-3, 1970 (in Russian)

Arakelian, M. A.; Dibay, Eh. A.; Esipov, V. F.; Markarian, B. E. – New Seyfert-type objects in the third Markarian's list // Astron. Circular, 568, 2-4, 1970 (in Russian)

Markarian, B. E.; Lipovetskii, V. A.; Stepanian, J. A. – New Seyfert-type objects in list XII of galaxies with ultraviolet continuum // Astron. Letters, 5, 269-271, 1979

Markarian, B. E.; Lipovetskii, V. A.; Stepanian, J. A. – Seyfert-Type Objects from the 13th and 14th Lists of Galaxies with UV-Continuum // Astron. Circular, 1134, 6-8, 1980 (in Russian)

Afanasiev, V. L.; Lipovetskii, V. A.; Markarian, B. E.; Stepanian, J. A. – New Seyfert-Type Objects from Observations on BTA // Astron. Circular, 1039, 1-2, 1979 (in Russian)

Afanasiev, V. L.; Lipovetskii, V. A.; Markarian, B. E.; Stepanian, J. A. – Observations with the 6-m telescope of galaxies with ultraviolet continuum of Seyfert type // Ap, 16, 119-127, 1980

Markarian, B. E.; Stepanian, J. A.; Lipovetskii, V. A. – New Seyfert-Type Objects from the Last Lists of Galaxies with UV-Continuum // Astron. Circular, 1125, 4-6, 1980 (in Russian)

Markarian, B. E.; Stepanian, J. A.; Lipovetskii, V. A. – Faint Seyfert I Type Galaxies // Astron. Circular, 1168, 2-5, 1981 (in Russian)

Markarian, B. E.; Stepanian, J. A.; Lipovetskii, V. A. – Two New Remarkable Seyfert-Type Galaxies // Astron. Circular, 1233, 1-2, 1982 (in Russian)

Markarian, B. E.; Stepanian, J. A.; Lipovetskii, V. A. – Two New Remarkable Seyfert-Type Galaxies // Astron. Circular, 1237, 1, 1982 (in Russian)

Markarian, B. E.; Stepanian, J.; Lipovetski, V. I.; Shapovalova, A. I. – New Seyfert Galaxies from the First Byurakan Sky Survey // Astron. Circular, 1428, 7-8, 1986 (in Russian)

Markarian galaxies nature (4)

Markarian B.E. – On the nature of galaxies with ultraviolet continuum. I. Principal spectral and colour characteristics // Ap, 8, 100-105, 1972

Markarian B.E. – On the nature of galaxies with ultraviolet continuum: II. Objects with broad emission lines // Ap, 9, 1-8, 1973

Markarian, B. E.; Stepanian, J. A. – On the nature of galaxies with ultraviolet continuum. III. Surface brightness, morphology, and activity // Ap, 13, 372-379, 1977

Markarian B.E. – On the nature of galaxies with UV continuum having broad emission lines // A&A, 58, 139-143, 1977

FBS bright QSOs (2)

Markarian, B. E.; Stepanian, J. A.; Lipovetskii, V. A. – Bright Quasar Search and the FBS Continuation // Com. SAO, 61, 88-91, 1988 (in Russian)

Markarian, B. E.; Stepanian, J. A.; Lipovetskii, V. A. – Bright Quasar Search and the FBS Continuation // Proc. Conf.: QSO Physical Properties and Spectra, held at Special Astrophys. Obs., Moscow, 8-11 Sep 1987, Moscow, p. 88, 1989 (in Russian)

FBS general (3)

Markarian B.E. – Galaxies with the ultraviolet continuum // Proc. IAU S29: Non-stable Phenomena in Galaxies, Byurakan, May 4-12, 1966. Publ. House Acad. Sci. Arm. SSR Yerevan, p. 99-103, 1968 (in Russian)

Markarian, B. E.; Lipovetskii, V. A.; Stepanian, J. A. – Galaxies with UV-Continuum from Observations on BTA // Proc. Borjomi Meeting, 1981 (in Russian)

Lipovetsky, V. A.; Markarian, B. E.; Stepanian, J. A. – The First Byurakan Survey (FBS) and Search Problems for AGN // Proc. IAU S121: Observational Evidence of Activity in Galaxies, held in Byurakan, Armenia, USSR, 3-7 June 1986. Eds. E.Ye. Khachikian, K.J. Fricke & J. Melnick. Kluwer Academic Publishers, Dordrecht, p. 17, 1987

Markarian webpage created by A. M. Mickaelian and G. A. Mikayelyan in 2013: http://markarian.aras.am/

doi: doi.org/10.52526/25792776-2021.68.2-174

Communications of BAO, Vol. 68, Issue 2, 2021, pp. 186-235

Theoretical Astrophysics in the Byurakan Observatory (1946 - 2021)

A.G. Nikoghossian*

NAS RA V. Ambartsumian Byurakan Astrophysical Observatory (BAO), Byurakan 0213, Aragatzotn Province, Armenia

Abstract

The purpose of this review is to give a general idea of the results on theoretical astrophysics investigations carried out at the Byurakan Observatory during the period of its existence. A special place in the review is given to the research work in the Department of ”Theoretical Astrophysics”, founded in 1965. The review consists of two parts. The first part is mainly devoted to works on the theory of radiation transfer somehow related to Ambartsumian's ideas developed in his fundamental studies of the 40-50s of the last century. The second part presents, on the one hand, the results which are of importance for theoretical physics in general and, on the other hand, gives their application to the interpretation of observational data of various cosmic objects. In order to get an idea of the importance of each result, the background and prerequisites of the research are given, indicating its significance from the point of view of astrophysics. Naturally, the most important results are presented in more detail. At the same time, the review in one way or another includes almost all of the most important results obtained by various members of the department at different times. It should be noted that works on some other areas of theoretical astrophysics are not included in the review, since they are presented in other reviews of this series.

I. THEORY OF RADIATIVE TRANSFER

1. INTRODUCTION. PREREQUISITES.

The middle of the last century was marked by the rapid development of radiation transfer theory, which was increasingly being used in a wide variety of astrophysical research fields. Along with classical theory, which dates back to the works of its founders Schuster, Milne, Eddington in connection with modeling the stellar atmospheres, new more advanced and flexible methods, better adapted to numerical calculations, appeared. Around these years, when the Byurakan observatory was founded, Ambartsumian's fundamental works appeared (Ambartsumian, 1941; 1942a,b; 1943a,b; 1944a,b,c; 1947; see also his Scientific Papers, 1960), which developed new ideas and approaches to solving various, in particular, classical problems of the radiative transfer. Since then, the mentioned theory with variety of its applications have always been one of the main directions of theoretical studies in the observatory. The following is a comprehensive description of the observatory's achievements in this and adjacent areas.

The study of the equation of radiation transfer and its solutions in various forms occupied important place in the first works aimed at interpreting the stellar spectra. Of course, there were investigated first of all simplest and therefore the rough models, in which the medium assumed to be plane-parallel, stationary, homogeneous and purely absorbing. The last assumption substantially simplifies the problem of finding the field of radiation in the atmosphere, since in this case the state of the radiating gas obeys the equilibrium laws of Saha and Boltzmann with the local values of temperature and density. In this approximation, referred to as the approximation of LTE (local thermodynamic equilibrium), the source function, appeared in the transfer equation, is given by the Kirchhoff-Planck law. The situation changes drastically, when one takes into account the scattering of radiation which is of particular importance in the problem of the spectral line formation. Now the state of the radiating gas depends not only on the local values of thermodynamic parameters, but also on the field of radiation at the particular point, which establishes coupling between different volumes inside the atmosphere. The equation of radiation transfer in this case is integral-differential and its solution, in general, encounters great difficulties.

In spite of the rough assumptions, the first works in this direction in many respects contributed to the physical understanding of the studied processes and stimulated the development of theory. The approach, which was developed in them and became classical, consisted in finding the source function as a function of the depth in the atmosphere, which, in its turn, made it possible to determine the field of radiation in it. In the simplest cases of isotropic and monochromatic scattering the problem mathematically is reduced to the solution of an integral equation of Fredholm's

*nikoghoss@bao.sci.am

doi: doi.org/10.52526/25792776-2021.68.2-186

type with the kernel, which is the exponential integral depended on the modulus of a difference of the arguments. For instance, in the simplest case of isotropic scattering the problem of finding the radiation field in a semi-infinite atmosphere illuminated by a beam of parallel rays at angle of arccos ς is reduced, as it is known well, to the solution of the following integral equation

$$S(\tau,\varsigma) = \frac{\lambda}{2}\int_0^\infty \mathrm{Ei}\left(\left|\tau-\tau'\right|\right) S(\tau',\varsigma)\, d\tau' + \frac{\lambda}{4}e^{-\frac{\tau}{\varsigma}} \quad (1)$$

where λ is the single-scattering albedo (or the probability of the photon re-radiation during elementary act of scattering) and S is the source function. Its solution allows, in particular, determining the intensity of the radiation emerging from the atmosphere, i.e., the quantity, directly measured during the observations.

2. THE PRINCIPLE OF INVARIANCE

In contrast to conventional approach described above, Ambartsumian proposed the new method, named by him 'the principle of invariance', which allowed to find the outgoing intensity without the preliminary determination of the light regime at all depths in the atmosphere. By principle of invariance, he implies such transformation of the initial atmosphere, which does not influence the global optical characteristics of a medium (Ambartsumian, 1942a,b; 1943a,b, 1980). The application of principle significantly facilitates the solution of the problems of radiation transfer, revealing from the very beginning the structure of the desired solutions what, in its turn, is a great help in determining the field of radiation inside the atmosphere. As it was shown subsequently (see below, Sect. 5, and also (Nikoghossian, 1999), the principle of invariance is, in fact, a special case of the more general variational principle, connected with the translational transformation of optical depth.

The invariance principle was formulated for the first time by Ambartsumian (1943a) in treating the problem of diffuse reflection of light from a semi-infinite homogeneous atmosphere. Considerations underwent the principle based on the apparent fact that the addition to this medium a layer of infinitesimal optical thickness $\Delta\tau$, possessing the same properties as the original one, must not change its reflectivity. This thesis was referred by the author to as the principle of invariance. This implies that the total contribution of processes relevant to the added layer will be equal to zero.

The reflectance of a medium is characterized by the reflection function $\rho(\eta,\varsigma)$, where ς and η are respectively the cosines of the angles of incidence and reflection. Contribution of the all other possible processes is of the higher order of smallness with respect to $\Delta\tau$ and may be ignored. Then in the simplest case of isotropic scattering the condition of invariance of the reflection function for the semi-infinite atmosphere can be written in the form

$$(\eta+\xi)\,\rho(\eta,\xi) = \frac{\lambda}{2}\varphi(\eta)\,\varphi(\xi)\,, \quad (2)$$

where the function

$$\varphi(\eta) = 1 + \eta\int_0^1 \rho(\eta,\eta')\, d\eta' \quad (3)$$

is referred to as the Ambartsumian φ - function. The last two equations imply that the function φ satisfies the following functional equation

$$\varphi(\eta) = 1 + \frac{\lambda}{2}\eta\int_0^1 \frac{\varphi(\eta)\,\varphi(\eta')}{\eta+\eta'}d\eta', \quad (4)$$

usually called the Ambartsumian equation. Eq. (2) shows that the reflectance $\rho(\eta,\varsigma)$ is expressed through a function of one variable and is a symmetrical function of its arguments. The quantity $\eta\rho(\eta,\varsigma)\,d\eta$ possesses a probabilistic meaning, namely, it gives the probability that the quantum incident on the medium in the direction ς, will be reflected by it in the directional interval $(\eta,\eta+d\eta)$. In the same paper the principle of invariance was applied for solving the problem of the diffuse reflection and transmission for the medium of finite optical thickness. In this case the layer of infinitesimal optical thickness $\Delta\tau$ is added to one of boundaries while such layer is subtracted from the opposite side. For the reflectance $\rho(\eta,\varsigma)$ and diffuse part of transmittance $\sigma(\eta,\varsigma)$ this results (for convenience of the further discussion, we adopt here somewhat different notations)

$$\rho(\eta,\varsigma) = \frac{\lambda}{2}\frac{\varphi(\eta)\,\varphi(\varsigma)-\psi(\eta)\,\psi(\varsigma)}{\eta+\varsigma}, \qquad \sigma(\eta,\varsigma) = \frac{\lambda}{2}\frac{\psi(\eta)\,\varphi(\varsigma)-\varphi(\eta)\,\psi(\varsigma)}{\eta-\varsigma}. \quad (5)$$

The auxiliary functions $\varphi(\eta)$ and $\psi(\eta)$ are determined from the following system of functional equations

doi: doi.org/10.52526/25792776-2021.68.2-186

$$\varphi(\eta) = 1 + \frac{\lambda}{2}\eta \int_0^1 \frac{\varphi(\eta)\varphi(\eta') - \psi(\eta)\psi(\eta')}{\eta + \eta'} d\eta', \tag{6}$$

$$\psi(\eta) = \mathrm{e}^{-\frac{\tau_0}{\eta}} + \frac{\lambda}{2}\eta \int_0^1 \frac{\psi(\eta)\varphi(\eta') - \varphi(\eta)\psi(\eta')}{\eta - \eta'} d\eta', \tag{7}$$

where τ_0 is the optical thickness of the medium. These functions also are called the Ambartsumian functions. It is clear that the reflectance and transmittance, as well as the functions $\varphi(\eta)$ and $\psi(\eta)$, depend also on optical thickness of the medium, nevertheless, for brevity, τ_0 is not indicated explicitly among arguments. As has already been indicated, the starting point for the determination of the intensity of radiation outgoing from the medium is here not the equation of transfer, which allows finding the required quantity only after the regime of radiation is found for all depths in the atmosphere. It is obvious that, in view of the linearity of problem, knowledge of the functions of reflection and transmission makes it possible to determine the intensity of the outgoing radiation for any flux falling on the medium. On the other hand, formulas (2) and (5) give solution not only of one particular problem of diffuse reflection (for the semi-infinite medium) or the problem of diffuse reflection and transmission (for the finite medium). In fact, they make it possible to reveal the structure of the global optical characteristics of medium, as such, expressing in this case the unknown quantities through the functions of one variable. Approach itself in many respects contributed to the presence of a number of important relations connecting with each other different characteristics of the radiation field, in the problems of the radiative transfer theory most frequently encountered in the astrophysical applications. Some of them follow directly from invariance property. Such relationships were obtained in the different time by a number of the authors both abroad (Sobolev, 1963; Chandrasekhar, 1960; Preisedorfer, 1976; Rybicky, 1977; Ivanov, 1978) and in Byurakan observatory (Yengibarian & Mnatsakanian, 1974; Nikoghossian, 1995, 1997, 1999; Krikorian & Nikoghossian, 1996).

It should be noted that the relations (2), (4) were obtained by Ambartsumian earlier by another way in considering the scattering of light by the atmospheres of planets (Ambartsumian, 1942b). The way chosen in the mentioned work consists in the formal differentiation of the initial integral equation for the source function over the optical depth. From a purely mathematical point of view the way proposed is of large importance, since it shows, how the solution of the integral equation of the Fredholm-type with the difference kernel can be reduced to the solution of functional equation.

The idea on the invariant property of the global optical characteristics of the scattering and absorbing atmosphere with respect to the layer addition was employed in the problem of the radiation diffusion through the optically thick medium (Ambartsumian, 1941; 1944a). This research implies that the function $\varphi(\eta)$ admits a physical interpretation which concerns the angular distribution of the intensity of radiation transmitted through the optically thick atmosphere in the absence of true absorption. Various meanings can be ascribed to this function, of which the limb-darkening law for the Sun is one of astrophysical examples.

In various astrophysical problems one encounters, as it is known, the necessity to find the radiation field within the medium. An important advantage of the invariance principle is that knowledge of the intensities of radiation outgoing from a medium facilitates the solution of this problem essentially (see, e.g., Sobolev, 1959). For instance, being applied to Eq. (1), the invariance principle makes it possible to reduce the solution of this Fredholm-type integral equation to the solution of following Volterra-type equation for an auxiliary function $\Phi(\tau)$ related with the resolvent function of Eq.(1) (see, e.g., Sobolev, 1957)

$$\Phi(\tau) = L(\tau) + \int_0^\tau L(\tau - \tau')\Phi(\tau') d\tau', \tag{8}$$

where the kernel-function

$$L(\tau) = \frac{\lambda}{2}\int_0^1 \varphi(\varsigma) e^{-\frac{\tau}{\varsigma}} \frac{d\varsigma}{\varsigma} \tag{9}$$

is known well in the radiative transfer theory (Ivanov, 1969; Case & Zweifel, 1967). An explicit expression for the function $\Phi(\tau)$ was obtained in (Minin, 1958). For illustration, we limited our consideration by the simplest case of monochromatic scattering, though the described picture and conclusions remain valid for the much more general statement of the transfer problem. From the pure mathematical point of view, principle of invariance may be considered as a way reducing the boundary-value problem usually formulated for the source function to the solution of the initial-value or Cauchy problem.

The invariance principle has played an important role in the theory of radiative transfer. It has been especially effective as applied to relatively complicated problems in radiative transfer theory. According to the idea suggested in

doi: doi.org/10.52526/25792776-2021.68.2-186

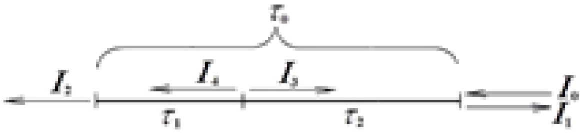

Figure 1: Schematic picture of the radiation transfer in two added layers

(Preisendorfer, 1976), this theory can be constructed so that it is based on the invariance principle, while the radiative transfer equation and the invariance relationships follow directly from it. Subsequently, as the theory developed, the feasibility of this approach became obvious and the direct use of this approach seemed preferable in some cases. The advantage of the approach lies in the profound intuitive content of the invariance principle and the existence of a close connection with the characteristic features of the physical problem under consideration, the symmetry property, and the boundary and initial conditions. In addition, as it is well known from physics, there is the relationship between invariance properties and conservation laws. In view of the importance of all these questions, they are examined them in more detail in Sect. 5 using radiative transfer in a plane-parallel atmosphere as an example.

3. THE LAYERS ADDING METHOD

As a result of Ambartsumian's studies in 1941-1948 on the theory of radiative transfer also another rather effective method, named by him the method of addition of layers, was proposed (Ambartsumian, 1944b). It gives response to the question, how the global optical characteristics of the absorbing and scattering media (coefficients of reflection and transmission) during their joining are added. It is obvious that this sufficiently general posing of the question appears naturally, if we abandon the requirement that the optical properties of a medium would remain unchanged during the addition to it of additional layer.

Because of importance of Ambartsumian's arguments in deriving the laws of addition of global optical characteristics for the further discussion, we present together with an explanatory figure the starting auxiliary equations written for the 1D homogeneous media. Fig.1 shows a medium of optical thickness τ_0 divided into two parts with thicknesses τ_1 and τ_2. Each of the media is characterized by reflection r and transmission q coefficients. The medium is illuminated externally and is supposed to be free of internal sources of energy. Based on some simple physical and probability arguments, one can write

$$I_1 = r(\tau_2) I_0 + q(\tau_2) I_3, \tag{10}$$

$$I_2 = q(\tau_1) I_4, \tag{11}$$

$$I_3 = r(\tau_1) I_4, \tag{12}$$

$$I_4 = q(\tau_2) I_0 + r(\tau_2) I_3. \tag{13}$$

In view of the fact that $I_1 = r(\tau_1 + \tau_2) I_0$, and $I_2 = q(\tau_1 + \tau_2) I_0$, it is easy to obtain the requisite addition laws for the reflection and transmission coefficients of scattering and absorbing media

$$q(\tau_1 + \tau_2) = \frac{q(\tau_1) q(\tau_2)}{1 - r(\tau_1) r(\tau_2)}, \tag{14}$$

$$r(\tau_1 + \tau_2) = r(\tau_2) + \frac{r(\tau_1) q^2(\tau_2)}{1 - r(\tau_1) r(\tau_2)}. \tag{15}$$

The quantities q, r have a probabilistic meaning and may be correspondingly interpreted as the probabilities of the transmission and reflection of a photon incident on the medium.

Replacing τ_2 by the infinitesimal Δ and passing to the limit when $\Delta \to 0$, one finds

$$\frac{\mathrm{d}q}{\mathrm{d}\tau_0} = -\left(1 - \frac{\lambda}{2}\right) q(\tau_0) + \frac{\lambda}{2} q(\tau_0) r(\tau_0), \tag{16}$$

$$\frac{\mathrm{d}r}{\mathrm{d}\tau_0} = \frac{\lambda}{2} - (2 - \lambda) r(\tau_0) + \frac{\lambda}{2} r^2(\tau_0). \tag{17}$$

doi: doi.org/10.52526/25792776-2021.68.2-186

The obtained system of non-linear differential equations satisfies the initial conditions $q(0) = 1, r(0) = 0$. Its solution is:

$$r(\tau_0) = r_0 \frac{1 - e^{-2k\tau_0}}{1 - r_0^2 e^{-2k\tau_0}}, \qquad q(\tau_0) = \left(1 - r_0^2\right) \frac{e^{-k\tau_0}}{1 - r_0^2 e^{-2k\tau_0}}, \tag{18}$$

where $k = (\lambda/4)\left(1 - r_0^2\right)/r_0$, and r_0 is the coefficient of reflection from a 1D semi-infinite atmosphere.

Thanks to their generality, these relations became a base for various modifications and stimulated the development of new methods in the radiative transfer theory. Some results obtained in the field are, in essence, nothing but elaboration of some special cases of the law of the layers addition. For instance, taking as one of the layers semi-infinite atmosphere and for another a layer of infinitesimal optical thickness, we are led to the problem considered in previous section, for which the invariance principle was formulated. When the infinitesimal layer is added to a finite layer, the requisite optical characteristics are found as the functions of optical thickness. Thus, the problem becomes 'imbedded' in a family of similar problems differing by the value of optical thickness. The generalization of this approach to the three-dimensional case was given by Chandrasekhar (1960). It underlies the method of *invariant imbedding* developed by Bellman and his co-authors (1960, 1963).

Finally, the method of addition of layers plays an important role in numerical solving the problems of radiation transfer in inhomogeneous atmospheres (see Sect.5.xvi). In this case the medium is divided into a number of layers in such a way as each of them can be regarded as homogeneous and the addition formulas (14), (15) are repeatedly applied (see, e.g., Bellman, Kalaba & Wing, 1960; Bellman; Kalaba & Prestrud, 1963; Van de Hulst, 1980; Nikoghossian, 2004). It is noteworthy that in the course of derivation of requisite optical parameters the fluxes appearing at the interfaces between adjacent layers are eliminated. Accordingly, in each application of the addition formulas one deals only with the intensities at the boundaries of the composite atmosphere. This is pointed out in some papers (Redheffer, 1962; Grant & Hrant, 1968; Peraiah, 1999) in which the addition formulas are treated in the case when the component layers are allowed to be inhomogeneous. In the last two works the law of addition of layers is called "the star product".

4. OTHER DIRECTIONS

i. Statistical description of the radiation diffusion. In astrophysical problems, it is often necessary to estimate various statistical averages which describe the diffusion of radiation in an atmosphere. It is especially important to get some idea of the average number of scattering events underwent by a photon as a result of multiple scattering. In one of his early papers, Ambartsumian (1948) derived for this value the formula

$$N = \lambda \frac{\partial \ln I}{\partial \lambda}, \tag{19}$$

where I is the intensity of radiation. This formula served as a starting point for the study of statistical mean values describing the process of the radiation diffusion in the scattering and absorbing medium. It has been shown in a series of papers that the invariance principle offers an effective method for determining the mean number of scattering events, as well as the average time, for a photon travel in a medium. In particular, it was found that Eq. (19) is only valid for estimating the average number of scattering events for "moving" photons, i.e., those which have not been thermalized in the medium (see below Sect. 5.iv).

ii. Anisotropic scattering. The first works on the principle of invariance concern the monochromatic and isotropic scattering. It was apparent, however, that the principle may also be applied under much more general assumptions on the elementary act of scattering. That is why as early as in the paper Ambartsumian (1943b) handles the problem of diffuse reflection of light from a semi-infinite plane-parallel atmosphere for anisotropic scattering with arbitrary phase function. It is noteworthy that here he employs the expansion of the phase function $x(\gamma)$ (γ is the angle of scattering) in a series of Legendre polynomials which was suggested earlier by him (Ambatsumian, 1941, 1942a)

$$x(\gamma) = \sum_{i=0}^{\infty} x_i P_i(\cos\gamma). \tag{20}$$

or with use of the summation theorem for spherical functions

$$x(\eta, \eta', \varphi - \varphi') = \sum_{m=0}^{\infty} \cos m(\varphi - \varphi') \sum_{i=m}^{\infty} c_{im} P_i^m(\eta) P_i^m(\eta'), \tag{21}$$

where the constants c_{im} are expressed through the coefficients x_i, and $P_i^m(\eta)$ are the associated Legendre polynomials.

doi: doi.org/10.52526/25792776-2021.68.2-186

Then an expansion similar to (21) holds for the reflection function

$$\rho\left(\eta,\eta',\varphi-\varphi'\right)=\sum_{m=0}^{\infty}\rho_m\left(\eta,\eta'\right)\cos m\left(\varphi-\varphi'\right). \tag{22}$$

Now the solution of the problem is written by means of the functions $\varphi_i^m(\eta)$

$$\rho_m\left(\eta,\eta'\right)=\frac{\lambda}{4}\sum_{i=m}^{\infty}(-1)^{i+m}c_{im}\frac{\varphi_i^m(\eta)\,\varphi_i^m(\eta')}{\eta+\eta'}, \tag{23}$$

which are determined from the following set of functional equations

$$\varphi_i^m(\eta)=P_i^m(\eta)+2\frac{(-1)^{i+m}}{2-\delta_{0m}}\int_0^1\rho_m\left(\eta,\eta'\right)P_i^m\left(\eta'\right)d\eta', \tag{24}$$

where δ_{km} is the Kronecker symbol.

In the same paper these results were illustrated in treating two special cases: the scattering with two-term and the Rayleigh phase functions, which are of astrophysical importance.

iii. **Non-LTE atmospheres**. Since the mid-60s, the principle of invariance began to be applied to solve various problems of radiation transport of interest to astrophysics. One of directions was non-linear problems relating with the transfer in the Non-LTE atmospheres, in which the effect of the radiation field in the medium on the local optical properties of the medium is taken into account. These problems are extremely complicated but also important from an astrophysical standpoint. The nonlinear effect shows up even in the case of a single spectral line (Ambartsumian, 1964a,b,c, 1966, 1988, 1998). In these papers Ambartsumian studies the possibility of generalizing the layers adding method to non-linear problems. It was shown, in particular, that finding the intensity of radiation emerging from a finite medium reduces to solving a quasilinear partial differential equation that includes both the derivative with respect to the limiting optical thickness and the derivative with respect to the intensity of the flux incident on the medium.

A special place in the non-linear theory of radiative transfer is occupied by so-called multilevel problems, in which radiation is redistributed over different lines as it diffuses in a medium. One of the simplest problems this type was examined by Ambartsumian (1964a). It was assumed that the medium consists of three-level atoms, with transitions between the two lowest levels being neglected. It was found that depending on the magnitude of the fluxes incident on the medium, it can become transparent in one of the lines. The approach employed for this problem involved first finding the radiation field and, therefore, the degree of excitation in the medium in terms of the ordinary linear theory for an arbitrary value of the actual optical thickness and then finding the latter as a function of limiting optical thickness and of the incident radiation flux. Ambartsumian called this approach *the method of self-consistent optical depths*.

5. DEPARTMENT OF THEORETICAL ASTROPHYSICS

The department of theoretical astrophysics in the Byurakan observatory was established in 1965 to further develop the theory of radiation transfer and its applications in interpreting the spectra of various space objects.

i. **Nonlinear problems**. The first works in the department studied the possibility of generalizing the method of addition of layers and invariance principle to nonlinear problems in which the effect of the radiation field in the medium on optical properties of the medium becomes essential. The problems are highly important from an astrophysical standpoint since the effect shows up even in the case of a single spectral line, when the density of the radiation is relatively high and induced emission processes begin to play an important role (Ambartsumian, 1964a,b, 1966). In this relatively simple situation the problem mathematically becomes linear by proper replacement of variables. In the simplest case of pure scattering in homogeneous atmospheres, the usual expression $q = 1/\left[1+(\tau/2)\right]$ for the transmission coefficient is replaced by

$$q=\frac{1+\alpha F}{1+\frac{\tau}{2}+\alpha F}, \tag{25}$$

where F is the intensity of the flux incident on the medium, $\alpha=(1/a)\left(1+g_2/g_1\right)$, g_1 and g_2 are the statistical weights of the upper and lower layers, respectively, and $a = 8\pi h\nu^3/c^2$ is the Planck factor, τ represents the limiting value of the optical thickness of the medium corresponding to the case when all the atoms lie in the lower state. The latter is introduced in nonlinear problems because the actual optical thicknesses depend on the radiation fluxes incident on the medium and are found after solving the problem. The method of self-consistent optical depths was used by Terebizh (1967) to solve two linearized transfer problems. An important result obtained in the area is that finding

doi: doi.org/10.52526/25792776-2021.68.2-186

the intensity of the radiation emerging from a finite medium now reduces to solving a quasilinear partial differential equation that includes both the derivative with respect to the limiting optical thickness and the derivative with respect to the intensity of the flux incident on the medium. The further progress in the theory is connected with relatively recently published works by Pikichyan (2010, 2016a,b,c, 2019).in which an alternative way of linearization of the problems was proposed and some inverse problems were treated.

The so-called multilevel problems, in which radiation is redistributed over different lines as it diffuses in a medium, occupy an important place in the nonlinear theory of radiative transfer. As it was above said, the simplest problems of this type was examined by Ambartsumian (1964b, 1996), and also (1988, 1998). It was found that, depending on the magnitudes of the fluxes incident on the medium with three-level atoms, the medium can become transparent in one of the lines.

The three-level problem of diffuse reflection from a semi-infinite atmosphere under more general assumptions particularly when all the transitions between energy levels are permitted has been examined using the invariance principle by Nikoghossian (1964, 1965). The problems were reduced to the solution of a partial quasilinear differential equations, the first integrals of which were found analytically. Later, the same problems, however, with use of the method of addition of layers were considered by Gros & Magnan (1981) and Magnan (1993) who developed a convenient numerical procedure for the solution. The three-level problem in the Schwarzschild-Shuster approximation for pure scattering was considered by Terebizh (1969).

ii. Homogeneous atmosphere. An important place in investigations of the department occupied an analytical work aimed at developing new schemes for the solution of classical problems of radiation transfer, facilitating the obtaining of the required solutions numerically. With limited computing capacity in the early years of the department, such work became particularly important. At the initial stage, relatively simple problems concerning mainly isotropic scattering of radiation in a *homogeneous* atmosphere were considered.

For instance, Danieian (1976) showed that the internal field of radiation in the finite medium illuminated by the parallel beam of rays can be found without integration over the optical depth. Approximate analytic solutions were derived by Mnatsakanian (1975, 1976) for determining the internal field of radiation in the medium of finite optical thickness under assumption that scattering is monochromatic and isotropic. Although these solutions are essentially asymptotic, in terms of the optical thickness of the medium, they are accurate within a few percent for the media of any thickness.

Due to the effectiveness of Ambartsumian's methods in the mentioned classes of problems, numerical algorithms for calculating fundamental φ - function for semi-infinite media, as well as φ - and ψ- functions for atmospheres of finite optical thickness, were developed (Danielian & Pikichyan, 1977; Andreasian & Danielian, 1978, 1983). Thus, for example, in the last of these works, a new scheme of numerical calculation of the φ- function was proposed, which has a relatively high convergence rate. A special place in the research was occupied by issues related to the study of properties and the definition of ways to facilitate the determination of Green's function (Pikichyan, 1978a, 1980). The Green function approach in the non-coherent transfer problems was considered in (Pikichyan, 1978b). The specific properties of homogeneous atmospheres were used by Pikichyan (1982a,b; 1983, 1984) to treat media of arbitrary geometrically and physical characteristics. The explicit expression for the resolvent function for the problem of radiation transfer in an atmosphere with horizontally homogeneities was obtained by Danielian (1989).

The structure of the functions characterizing the non-stationary field of radiation has been studied by Terebizh (1968). It was shown that the similarity principle allows to reduce the solutions of the vast class of problems to the solution for a special case for only one value of the scattering albedo.

iii. Anisotropic scattering. Following Ambartsumian's approach to the problems of anisotropic scattering in its general formulation was treated by Nikoghossian & Harutyunian (1978). The asymptotic behavior of Ambartsumian functions $\varphi_i^m(\eta)$ for large values of indices is employed in elaborating a simplified method of solving the problem of diffuse reflection of radiation from a semi-infinite atmosphere. The method was exemplified on the Henyey-Greenstein phase function

$$x(\gamma) = \frac{1-g^2}{(1+g^2-2g\cos\gamma)^{3/2}}, \tag{26}$$

where g is a parameter that determines the lengthening of the phase function. There was estimated the rate at which the functions $\varphi_i^m(\eta)$ approach to spherical functions $P_i^m(\eta)$ for large values of n, as well as, the dependence of the rate of convergence to true values of the reflection function on the degree of the phase functions elongation.

iv. Partial redistribution over frequencies and directions. It is well known that the multiple scattering of the line radiation in various astrophysical media undergoes redistribution over frequencies and directions. The transfer problem arisen in the general case of partial redistribution is similar in many respects to that for anisotropic scattering. This analogy is especially distinct when one uses the bilinear expansions of the redistribution functions. Thus, for

doi: doi.org/10.52526/25792776-2021.68.2-186

example, in the simplest case of a pure Doppler redistribution r_1 in Hummer's numeration (Hummer, 1962; Mihalas, 1970) it has been shown by Nikoghossian (1977) that the expansion

$$r_{\mathrm{I}}\left(x', x, \gamma\right) = \frac{1}{\sqrt{\pi} \sin \gamma} \exp\left\{\frac{x^2 + x'^2 - 2xx' \cos\gamma}{\sin^2\gamma}\right\} = \sum_{k=0}^{\infty} \cos^k \gamma \alpha_k(x) \alpha_k(x') \tag{27}$$

holds, where x and x' are the so-called dimensionless frequencies of the incident and scattered photons measured from the center of the spectral line in units of the Doppler width and

$$\alpha_k(x) = \left(2^k \sqrt{\pi} k!\right)^{-1/2} \exp\left(-x^2\right) H_k(x) \tag{28}$$

is an orthonormal system of functions with weight $\exp\left(x^2\right)$ expressed in terms of Hermite polynomials, $H_k(x)$. Analogous bilinear expansion was obtained in the same paper also for the case of the combined Doppler and damping effects ($r_{\mathrm{III}}(x, x, \gamma)$), the latter being due to radiation and collision.

$$r_{\mathrm{III}}\left(x', x, \gamma\right) = \frac{\sigma \csc\gamma}{\pi^{3/2} U(0, \sigma)} \int_{-\infty}^{\infty} \mathrm{e}^{-u^2} \frac{U\left(x \csc\gamma - u\mathrm{ctg}\gamma, \sigma \csc\gamma\right)}{\left(x' - u\right)^2 + \sigma^2} \mathrm{d}u, \tag{29}$$

where $U(x, \sigma)$ is the Voigt function with the parameter σ, Note that when $\sigma \rightarrow 0$, $r_{\mathrm{III}} \rightarrow r_{\mathrm{I}}$. The proper bilinear expansion has a form

$$r_{\mathrm{III}}(x', x, \gamma) = \frac{1}{U(0, \sigma)} \sum_{k=0}^{\infty} \cos^k \gamma \alpha_k\left(x', \sigma\right) \alpha_k(x, \sigma), \tag{30}$$

where

$$\alpha_k(x, \sigma) = \frac{\sigma}{\pi} \int_{-\infty}^{\infty} \frac{\alpha_k(u) \, \mathrm{d}u}{(x - u)^2 + \sigma^2} = (-1)^k \left(2^{k/2} \pi^{1/4} \sqrt{k!}\right)^{-1} \frac{\mathrm{d}^k U(x, \sigma)}{\mathrm{d}x^k}. \tag{31}$$

It is easy to see that the case $\gamma = 0$ corresponds to coherent scattering, while $\gamma = \pi/2$ - to the scattering with complete redistribution.

For directionally averaged redistribution laws, there was obtained

$$r_{\mathrm{I}}\left(x', x\right) = \int_{\max(|x|, |x'|)}^{\infty} \exp\left(-u^2\right) du = \sum_{k=0}^{\infty} A_k \alpha_{2k}\left(x'\right) \alpha_{2k}(x), \tag{32}$$

where $A_k = 1/(2k + 1)$. Analogously,

$$r_{\mathrm{III}}\left(x', x\right) = \frac{1}{\pi^2 U(0, x)} \int_0^{\infty} \exp\left(-u^2\right) f\left(x', u\right) f(x, u) \, du =$$

$$\frac{1}{U(0, x)} \sum_{k=0}^{\infty} A_k \alpha_{2k}\left(x', \sigma\right) \alpha_{2k}(x, \sigma), \tag{33}$$

where

$$f(x, u) = \mathrm{tg}^{-1} \frac{x + u}{\sigma} - \mathrm{tg}^{-1} \frac{x - u}{\sigma}. \tag{34}$$

In these non-coherent cases the one-dimensional problem of the spectral line formation in a semi-infinite atmosphere the analog of Ambartsumian equation (2) has a form

$$\frac{2}{\lambda}\left[\alpha(x) + \alpha\left(x'\right)\right] \rho\left(x', x\right) = r\left(x', x\right) + \int_{-\infty}^{\infty} \rho\left(x, x''\right) r\left(x'', x'\right) \mathrm{d}x' +$$

$$\int_{-\infty}^{\infty} r\left(x, x''\right) \rho\left(x'', x'\right) \mathrm{d}x'' + \int_{-\infty}^{\infty} \rho\left(x, x''\right) \mathrm{d}x'' \int_{-\infty}^{\infty} r\left(x'', x'''\right) \rho\left(x''', x'\right) \mathrm{d}x''', \tag{35}$$

where $r\left(x', x\right)$ is either of redistribution functions. Bilinear expansions of $r\left(x', x\right)$ reduce the problem to solving the infinite set of functional equations for the functions $\varphi_k(x)$

$$\varphi_k(x) = \alpha_{2k}(x) + \frac{\lambda}{2} \sum_{m=0}^{\infty} A_m \int_{-\infty}^{\infty} \frac{\varphi_m(x) \varphi_m\left(x'\right)}{\alpha(x) + \alpha\left(x'\right)} \alpha_{2k}\left(x'\right) dx', \tag{36}$$

where $\alpha(x)$ is the profile of the absorption coefficient. This is the natural generalization of equation (4) to the case of partial redistribution over frequencies. Using expansions of types (27) and (30) makes it much easier to solve the

doi: doi.org/10.52526/25792776-2021.68.2-186

corresponding transfer problems for the line-radiation (Yengibarian & Nikoghossian, 1972a,b,c; 1973a,b; Yengibarian, Nikoghossian & Gevorkian, 1975). Quasi-analytic and numerical methods have been developed for solving these problems (Nikoghossian & Harutyunian 1976, 1978, 1979; Harutyunian & Nikoghossian, 1978a,b; Nikoghossian, 1979, 1986a; Harutyunian, 1980a,b, 1985, 1991a,b; 1993, 1996). It was shown that the accuracy in solving the truncated set of equations (36) can be highly increased in view of the fact that to any fixed value of x there corresponds the number n beginning of which the functions $\varphi_k(x)$ may be replaced by the known functions $\alpha_{2k}(x)$. Physically this reflects the fact that the formation of the far wings of the spectral line is due to the single scattering. Mathematically, this follows from the asymptotic behavior of functions $\alpha_n(x)$ in Eq.(28)

$$\alpha_n(x) \approx 2^{(n+1)/2} n^{n/2} \exp\left[\left(x^2 - n\right)/2\right] \cos\left(\sqrt{2n+1}x - \frac{n\pi}{2}\right), \tag{37}$$

This allows reducing the solution of the infinite set of functional equations (36) to the set of equations of the form

$$\varphi_k^*(x) = \alpha_{2k}(x) + \frac{\lambda}{2}\sum_{m=0}^{N-1} A_m \int_{-\infty}^{\infty} \frac{\varphi_m^*(x)\varphi_m^*(x')}{\alpha(x)+\alpha(x')}\alpha_{2k}(x')\,dx' + \frac{\lambda}{2}\int_{-\infty}^{\infty} \frac{r(x',x)\alpha_{2k}(x')}{\alpha(x)+\alpha(x')}dx', \tag{38}$$

and makes it possible to construct solutions of various problems of line-radiation transfer in the general case of frequency redistribution..

The works carried out in the 60s in this direction in the Byurakan observatory allowed not only to develop effective mathematical methods for solving problems of spectral line formation for partial redistribution of radiation in frequencies and directions, but also to compare the obtained numerical results with the data in the commonly used assumption of completely incoherent scattering. For instance, Harutynian & Poghosyan (2018) numerically realized the algorithm for solving Ambattsumian's functional equations obtained for finite medium. Calculations were carried out for the particular case of the complete frequency redistribution. To this end, the authors elaborated the software package for calculating the nodes and corresponding weights of Hermite polynomials with high number of significant digits. The influence of the number of the used quadrature nodes, as well as the effect of the values of slab's thickness and the photon survival probability on the solution of problem were studied in details.

v. Statistical description of the radiation diffusion in an absorbing and scattering atmosphere. Ambartsumian's result Eq.(19) for determining the mean number of scattering events (MNSE) photons undergo during their diffusion in an absorbing and scattering atmosphere was treated and developed in a series of papers (Nikoghossian, 1984a,b, 1986b; Harutyunian & Nikoghossian, 1983, 1987). A new approach was elaborated to determining any statistical average characterizing a diffusion process in an atmosphere. It is based on invariance principle and extensive use of generating functions. It was shown that the method is applicable to determining the statistical averages of continuously distributed random variables as well, though it is then necessary to use appropriate characteristic functions. As an illustration, the problem of the average time of a photon travel (ATT) in an atmosphere under assumption that it spends time only in travelling between scatterings was treated by Nikoghossian (1986b). In the general case, when the photons are thermalizing not only in scatterings but also in flight, this average makes it possible to gauge the relative importance of energy dissipation in the medium and of energy flow through a boundary. Another important application of this average is associated with the problems, frequently encountered in astrophysical applications, of the radiation of an atmosphere subject to non-stationary energy sources. In these problems, knowledge of the ATT makes it possible to ascertain whether radiative equilibrium in the medium is established.

Under general assumptions concerning the elementary scattering event, equations were obtained in Nikoghossian's papers for determining the MNSE and ATT in a plain-parallel semi-infinite atmosphere. It was shown that, for moving photons (i.e. not for those being trapped in the course of multiple scattering) the problem simplifies and is reduced to differentiation of the reflectance correspondingly over the parameter λ for the MNSE and β – for ATT. Here we limit ourselves by presenting few results obtained on the base of invariance principle.

It has been shown that the formula Eq. (19) is valid only for 'moving' photons, i.e. those that have not been truly absorbed in the atmosphere and thermalized. The required values of MNSE and ATT for the photons reflected from a semi-infinite atmosphere satisfy integral-differential equations easily obtained by the mentioned formal differentiation of the proper equation for the reflectance ρ. A separate approach has been developed to account for the number of scatterings of thermalized photons, which, in turn, makes it possible to find the desired average characteristics for all photons, regardless of their further 'fate'. For instance, the requisite values of MNSE, $\langle N(\tau,x,\eta)\rangle$ and ATT $\langle\Omega(\tau,x,\eta)\rangle$ the photons with frequency-directional characteristics (x,η)moving at optical depth τ undergo and spent during their traveling in the semi-infinite atmosphere, are found from equations

$$\eta\frac{\partial\langle N(\tau,x,\eta)\rangle}{\partial\tau} = -v(x)\langle N(\tau,x,\eta)\rangle + \frac{\lambda}{2}\int_{-1}^{+1} d\eta' \int_{-\infty}^{\infty} r(x,\eta;x',\eta')\langle N(\tau,x,\eta')\rangle\,dx' + v(x), \tag{39}$$

doi: doi.org/10.52526/25792776-2021.68.2-186

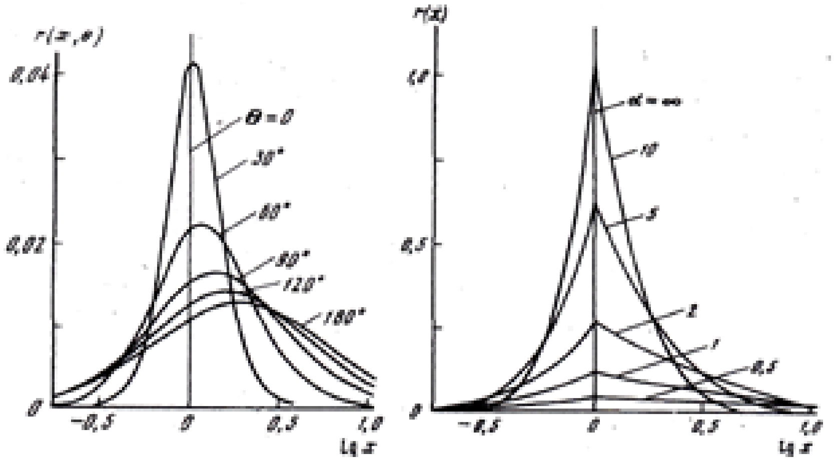

Figure 2: Frequency redistribution functions $r(x,\theta)$ and $r(x)$ for Compton scattering.

$$\eta \frac{\partial \langle \Omega(\tau,x,\eta)\rangle}{\partial \tau} = -v(x)\langle \Omega(\tau,x,\eta)\rangle + \frac{\lambda}{2}\int_{-1}^{+1} d\eta' \int_{-\infty}^{\infty} r(x,\eta;x',\eta')\langle \Omega(\tau,x,\eta')\rangle dx' + 1, \tag{40}$$

with the conditions $\langle N(0,x,\eta)\rangle = 0$, $\langle \Omega(0,x,\eta)\rangle = 0$ for $\eta > 0$. Note that the time intervals represent the mean time taken in free path between two successive scattering events for a photon in the line center. The obtained equations differ from the transfer equations only by free terms, so that many of methods of solution for the latter cover these equations as well. It was proved that there is a rather general relation connecting considered average statistical values

$$(1-\lambda)\langle N(\tau,x,\eta)\rangle + \lambda\beta\langle \Omega(\tau,x,\eta)\rangle = R_0(\tau,x,\eta), \tag{41}$$

where $R_0(\tau,x,\eta)$ yields the probability the photon at optical depth τ with characteristics (x,η) will be destroyed somewhere in the medium during its diffusion. Some of the presented results were generalized by Nikoghossian (2004b) to the case of inhomogeneous atmospheres.

vi. Compton scattering on free electrons. It is known that when interpreting the data obtained from observations of some astrophysical phenomena are widely used the mechanism of Compton scattering on electrons. In particular, this mechanism can be adopted to explain the sources of short X-ray bursts, X-ray radiation of quasars and nuclei of active galaxies (Zel'dovich & Syunyaev, 1970; Illarionov & Syunyaev, 1972; Basko, 1978). Before, the softening of the radiation in the course of multiple Compton scattering in the non-relativistic approximation was treated by Terebizh (1970).

It is of interest detection of the radiation spectra distortion caused by radiation scattering on free electrons and often referred to as "comptonization" of radiation. Especially .important in this case is the case of scattering on relativistic electrons, where the electrons transmit, in an average, some of the kinetic energy to the scattering photon. This phenomenon is commonly referred to as inverse Compton-effect.

To solve the problems of radiation transfer undergoing multiple Compton scattering, it is necessary to describe the elementary act of scattering, i.e., to know the law of the radiation redistribution on energy and directions. Under some simplifying assumptions the normalized redistribution function $r(x,\theta)$ analytically was derived by Harutyunian & Nikoghossian (1980)

$$r(x,\theta) = \frac{x}{2K_2(\alpha)\sqrt{1+x^2-2x\cos\theta}} \exp\left\{-\alpha\sqrt{\frac{1+x^2-2x\cos\theta}{2x(1-\cos\theta)}}\right\}, \tag{42}$$

where $\alpha = m_e c^2/kT_e$, $K_2(\alpha)$ is the cylindrical function of an imaginary argument of the second order, and x is the ratio of frequency of the scattered photon to that of the incident photon. Hence the redistribution law averaged over all direction is of the form

$$r(x) = \frac{|1-x|}{4K_2(\alpha)}\int_{x_0}^{\infty} e^{-\alpha t}\left(t^2-1\right)^{-3/2} dt,$$

where $x_0 = (1+x)/2\sqrt{x}$.

As it follows from Eq. (42), there is a drift in the frequency of the scattered photon towards high energy, the greater the scattering angle. These displacements are increasing also with decreasing α. It is also seen that when scattered

doi: doi.org/10.52526/25792776-2021.68.2-186

in the direction of motion of the original photon the energy of the latter does not change. The scattering indicatrix is lengthened in the opposite direction, the degree of which depends on the energy of electrons, Thus one can say that the most part of photons are scattered in the opposite direction with mostly increased energy. It is important to note that the redistribution function for the Compton scattering in this case depends only on the ratio of the scattered and incident photons energies. This implies that the global optical properties of the medium for this mechanism of scattering are also the functions of the mentioned ratio.

The problem of diffuse reflection from a semi-infinite medium with Compton scattering on free electrons was considered by Harutyunian & Nikoghossian (1981). The rigorous statement of the problem in terms of the invariance procedure was given.

The elementary events of photon scattering by a chaotically moving monoenergetic electron gas has been examined by Harutyunian (2006) to obtain the angle-averaged redistribution function. Expressions were obtained for the averaged redistribution function and its asymptotes which describe the redistribution function for low frequency radiation. The question of determining the frequency-dependent absorption coefficient was discussed, as well.

vii. Intensity fluctuations. Dynamically active media. The need to create a theory of radiative transfer in media with a complicated fine structure subject to random variations has long been felt. Already in the 1970's (Cram, 1972) it was shown that the observed profiles of chromospheric lines of ionized calcium cannot be explained in terms of the theory developed for homogeneous stationary media. It is quite evident that a satisfactory interpretation of other nonstationary phenomena in the solar atmosphere, such as chromospheric spicules, coronal streams, and polar plums would require a new theory. Problems involving the propagation of radiation in randomly inhomogeneous media also appear in other branches of astrophysics. Examples include the scattering of light on molecular clouds in the interstellar medium and the stochastic attenuation of galactic radiation as it travels over cosmologic distances.

The first papers in the area appeared in the frameworks of scientific collaboration between Meudon Observatory in France and Byurakan Observatory examined the line formation problems in multicomponent *static* media, i.e. the possible motions of structural elements were ignored (Nikoghossian, Pojoga & Mouradian, 1997, 1998a,b; Nikoghossian & Mouradian, 2000; Nikoghossian, 2002; Nikoghossian, Aboudarham & Mouradian, 2005). The direct implication of this research was interpretation of the EUV spectra of solar quiescent prominences (see below, Sect. 7, (**i**)).

An analytical procedure explored by Nikoghossian (2002) aimed at constructing the profiles of the spectral lines formed in a stochastic multicomponent atmosphere. A model one-dimensional problem was solved for the atmospheres in both local thermodynamic equilibrium (LTE) and non-LTE. The results previously obtained for the LTE atmosphere were generalized to include, in particular, correlations of the random variations in the physical properties of the structural elements. The line profiles formed in LTE stochastic atmosphere may have rather complicated shapes and, in general, differ significantly from those specific to the averaged homogeneous atmosphere. Particularly, it was shown that the stochastic multicomponent atmosphere may produce a kind of double-peaked profile, which is usually associated with the multiple scattering effects. The influence of the Markovian correlations between structural elements on the line profile was revealed.

The problem of the line formation in a stochastic non-LTE atmosphere was considered under assumption of the complete redistribution over frequencies with allowance for the absorption in continuum. For the line profile, a closed-form analytical expression was derived. The computed profiles were compared with those for a homogeneous deterministic atmosphere with preliminarily averaged physical properties. This allows one to conclude that the discrepancy between the line profiles relevant to these two cases may become significant, whereas the normalized profiles are fairly close to each other. The evident advantage of the model problem discussed in the cited papers is that it provides an important insight into specificity of the line radiation in an inhomogeneous atmosphere with randomly varied properties and it allows for various generalizations.

The theory was developed in (Nikoghossian, 2002, 2005) to determine the mean intensity and the relative mean square deviation (RelMSD) for the line radiation emerging from an one-dimensional atmosphere with randomly distributed inhomogeneities. Both the local thermodynamic equilibrium (LTE) and Non-LTE cases were considered. The results previously obtained for the LTE atmosphere were extended to encompass the more realistic situation when the random parameters describing the physical properties of structural elements may take an arbitrary number of possible values. The profiles of spectral lines constructed by solving the stochastic problem of radiative transfer in the LTE atmosphere allow one to check the accuracy of the commonly used approximations.

The LTE problem treating the number N of structural elements each of which is described by the optical thickness τ, and the power of the energy release, B (the value of B is assumed to be constant within each individual element) was presented by (Nikoghossian, Pojoga & Mouradian, 1999). The paper considers the simplest situation, when the pair of quantities (B,τ) takes randomly only two possible sets of values with some probabilities p_1 and p_2. For the averaged characteristics of the emerging radiation such as the mean intensity $\langle I_N \rangle$ and the RelMSD δ_N were found

doi: doi.org/10.52526/25792776-2021.68.2-186

$$\langle I_N \rangle = L_N \langle I_1 \rangle, \qquad \delta_N = \frac{M_N}{L_N^2}(1+\delta_1) + 2\frac{KA_N}{\langle I_1 \rangle L_N^2} - 1, \tag{43}$$

where the following notations are used

$$L_N = \left(1-\alpha^N\right)/(1-\alpha), \qquad M_N = \left(1-\beta^N\right)/(1-\beta), \qquad A_N = (L_N - M_N)/(\alpha-\beta), \tag{44}$$

and $\alpha = \langle \exp(-\tau) \rangle$, $\beta = \langle \exp(-2\tau) \rangle$, $K = \langle J \exp(-\tau) \rangle$, $J = \langle B(1-\exp(-\tau)) \rangle$.

An important salient trait inherent in Eqs. (43) is that the values of the mean intensity and the RelMSD for the multicomponent atmosphere with an *arbitrary* number of elements are determined by only a few parameters. These parameters for the general case of n realizations of (B,τ) are α, β, $\langle I_1 \rangle = \sum_{i=1}^n p_i J_i K = \sum_{i=1}^n p_i J_i (1-\exp(-\tau_i))$, and

$$\delta_1 = \frac{1}{2\langle I_1 \rangle^2} \sum_{i=1}^n p_i \sum_{k=1}^n p_k (J_i - J_k)^2. \tag{45}$$

All these five parameters are the average characteristics of a single structural element so that, in general, there must exist a great number of configurations, having a fixed number of components, that are characterized by the same values of the mean intensity and the RelMSD and, moreover, by the same behavior with varying N. The problem of determining the statistical characteristics of the line radiation formed in a multicomponent Non-LTE atmosphere was first treated for the case of conservative scattering. It was derived a closed-form analytical expression for the RelMSD of the outgoing intensity for an arbitrarily large number of structural elements in the medium.

The theoretical results were employed for interpreting some of the features specific to the spatial brightness fluctuations of prominences in extreme ultraviolet (EUV) lines (see Sect. 7.i). The estimates obtained for the mean value of the line-of-sight number of threads are in agreement with those inferred by the other authors. Some important conclusions on the multithread structure of prominences were drawn.

The theory was generalized afterwards to cover the frequency-dependent problem in (Nikoghossian, 2002; Nikoghossian, Aboudarham, Mouradian, 2007). It was particularly concluded that *when the intensity fluctuations of radiation escaping from a multicomponent atmosphere are due to random variations in the distribution of internal energy sources, the RelMSD of the measured intensity decreases monotonically from the center of the line to its wings, while if these fluctuations are resulted mostly from the difference in opacities of structural elements the run is opposite: the RelMSD grows towards wings.*

Further generalization of the theory concerns the dynamically active stochastic and multicomponent atmospheres (Nikoghossian, 2007a). Two types of problem for the LTE lines were discussed. In the first it was assumed that the realization of one or another type of non-thermal motion depends on the type of structural element and in the other this type of dependence is absent, i.e., it was supposed that the assumed random values of the velocity are distributed according to a law that is common to all the components.

The general effect of large-scale motions on spectral line profiles and on the scale of their spatial (or temporal) fluctuations was considered for spectral lines in LTE, which can be regarded, with a high probability, as valid for most of the non-hydrogen lines in the EUV spectrum of quiescent prominences. The theoretical results were compared with observational data obtained with the SUMER spectrometer in the SOHO space mission (Fig.3). The distinctive feature of the RelMSD of the radiation in a line formed in a dynamically active stochastic atmosphere is local "spikes" (maxima) in the wings of the line. The theoretical results obtained were compared with spectral observations of quiescent solar prominences obtained in framework of the SOHO space mission.

The "spikes" (local maxima) in the wings of the lines predicted by the above theory for non-thermal (hydrodynamic) motions can be seen distinctly. It can also be seen that for lines with a high effective formation temperature (i.e., the lines formed primarily in the surrounding corona), such as OVI λλ1032 Å, λλ1037 Å, and NV λλ1242 Å, the magnitude of these spikes appears to be smaller than for the lines formed entirely within the prominence. The appearance of isolated single spikes is an indication that the velocities of the non-thermal motions are only slightly greater than the thermal speed, if they exceed it at all.

viii. **Turbulent atmospheres**. The formation of spectral lines in a turbulent atmosphere with a spatially correlated velocity field were examined in a series of papers Nikoghossian (2007b,c, 2017). A new approach for solving this problem proposed in the first of these papers does not base on the Fokker-Planck formalism commonly used in the literature. The invariant imbedding method makes it possible to reduce the problem of finding the mean radiant intensity observed in a line to solving a system of differential equations. This possibility is based on determining the mean intensity of the radiation emerging from the medium for a fixed value of the turbulent velocity at its boundary (Yengibarian & Nikoghossian, 1969). A separate integral equation is derived for this quantity. The dependence of the line profile, integrated intensity, and width on the mean correlation length and the average value of the hydrodynamic velocity was studied. It was shown that the transition from a micro-turbulent regime to a macro-turbulent regime occurs within a comparatively narrow range of variation in the correlation length. Fig.4 demonstrates the dependence

doi: doi.org/10.52526/25792776-2021.68.2-186

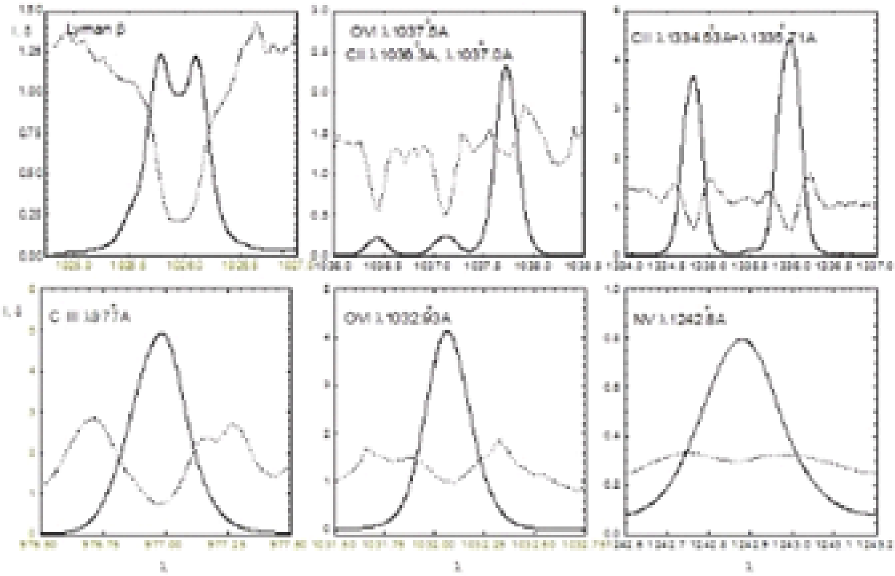

Figure 3: Statistical mean profiles (smooth curves) and the corresponding relative mean square deviations (dotted curves) for a series of relatively strong EUV lines of a solar prominence observed on August 10, 1999, as part of the SOHO space mission.

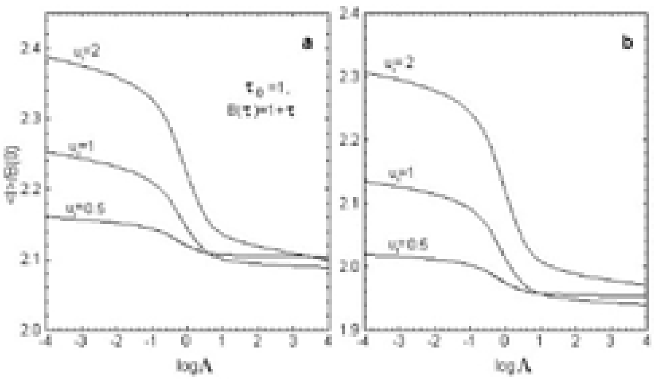

Figure 4: Integrated intensities of spectral lines observed at the boundaries $\tau = \tau_0$ (a), and $\tau = 0$ (b) of a turbulent atmosphere of optical thickness $\tau_0 = 1$, with the energy sources $B(\tau)$ that vary linearly with depth.

of intensities emergent from an atmosphere of optical thickness $\tau_0 = 1$ on the correlation length Λ. The sources of energy in the medium are assumed to be linearly varying with optical depth.

The proposed method yields a solution to the problem for a family of inhomogeneous atmospheres with different optical thicknesses, which makes it easy to determine the radiation field inside the turbulent medium. This approach can be generalized in various ways, in particular, it can be applied without significant changes to the case, where the correlation length depends on the position within the atmosphere.

The diffuse reflection of line radiation from a one dimensional semi-infinite turbulent atmosphere was examined in (Nikoghossian, 2007c) in two limiting regimes of micro- and macro-turbulence assuming that turbulence developed in the atmosphere is homogeneous. This means that the hydrodynamic velocity vector **v** is a random function that depends on depth, while the average characteristics of the velocity field are independent of depth in the atmosphere (Batchelor, 1970). Because of the homogeneity of the process, the correlation coefficient $l = |\tau - \tau'|$ (τ, τ' - optical depths) depends only on the distance ρ between two points. It was also assumed that the probability law according to which the hydrodynamic velocity u, measured in units of the mean thermal speed, takes one or another value is also independent of depth. In addition, it was supposed that the variations in the velocity inside the medium are correlated with one another. It was found the mean intensity of the radiation emerging from the boundary of the medium. The effect of the radiation on the velocity field was neglected. Formulated in this way, the problem models the case, often realized in astrophysics, where the optical depth of a radiating medium is large in the absence of turbulence.

doi: doi.org/10.52526/25792776-2021.68.2-186

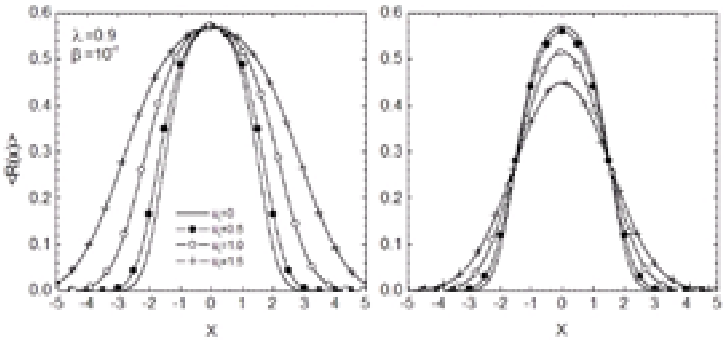

Figure 5: Profiles of lines formed during reflection from a semi-infinite micro-turbulent (left) and macro-turbulent (right) atmospheres. The central intensity of a line formed by reflection from a micro-turbulent atmosphere essentially remains unchanged as the average non-thermal velocity increases. In the macro-turbulent regime, the equivalent width of the line does not change.

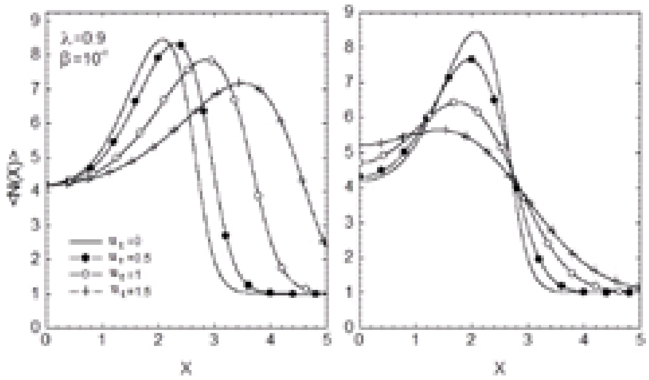

Figure 6: Mean number of scattering events experienced by a photon during diffusion in an atmosphere with micro- (left) and macro-turbulence (right). True absorption in the continuum is also treated as scattering.

The problem was solved by applying invariance principle. In addition to the observed spectral line profile, statistical averages describing the diffusion process in the atmosphere (mean number of scattering events, average time spent by a photon in the medium) were determined. The dependence of these quantities on the average hydrodynamic velocity and scattering coefficient was shown in Figs.4-7. It was shown that in the micro-turbulent regime the intensity at the line center depends only slightly on the mean non-thermal velocity. In both regimes, photons in the far wings undergo scattering more frequently than in a static atmosphere, although they spend, on average, less time in it.

The method of invariant imbedding used in the above-mentioned papers enables solution of the problem under rather general assumptions about the character of the turbulence, as well as about elementary scattering events and the distribution of energy sources in the medium. It was concluded that in the case of micro-turbulence, the reflectivity of the medium and its opacity are low over the entire frequency range. It was also found that the dependence of the observed characteristics on the correlation length is stronger when the medium is thicker and the average velocity of the turbulent motions is higher.

ix. Non-linear relations of the radiative transfer theory. As early as in 1977 Rybicky derived quadratic integrals of the transfer equation, however, some important points risen there remained unanswered for a long time. He studied the problems, for which the transfer equation admits integrals that involve quadratic moments of the radiation field. When the boundary conditions (or other constraints) are required to be met, the integrals convert into nonlinear relations of specific form for quantities characterizing the radiation field in the atmosphere. The so-called Q - and R- integrals involve as a particular case a certain class of 'surface' results, some of which were known well in the transfer theory.

Further generalization of Rybicki's results for monochromatic, isotropic scattering in the plane-parallel medium was given in (Ivanov, 1978). The so-called 'two-point' relations have been found that couple the intensities of equally directed radiation at two different depths in the atmosphere. The more general concept of 'bilinear integrals' (or relations) was introduced in (Nikoghossian, 1997) for quadratic integrals that connect the radiation fields of two separate transfer problems but referred to the same optical depth. Following the given terminology, it was reasonable to introduce also the concept of 'two-point bilinear integrals' for those coupling with each other the radiation fields

doi: doi.org/10.52526/25792776-2021.68.2-186

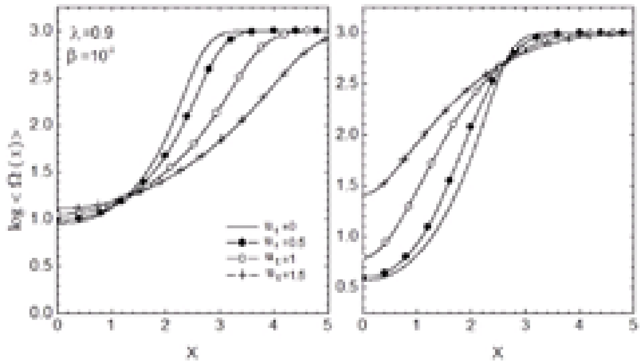

Figure 7: Average photon residence time in semi-infinite micro- (left) and macro-turbulent (right) atmospheres.

referred to both different transfer problems and diverse optical depths. Evidently this latter type of relations comprises all other types as the specific cases. Regardless of the new results, the main question on the physical nature of existence of quadratic and bilinear relations remained abstruse for a long time until appearing the mentioned Nikoghossian's paper. The idea that there must exist some relationship to the invariance principle suggested itself and is justified if for no other reason than that the majority of nonlinear equations in the transfer theory are associated in some or other way with the invariance technique. Most commonly these equations admit a plain physical interpretation and can be established by means of a direct use of the mathematical model of the physical process. Having this in mind, one may naturally be tempted to derive the requisite bilinear relations by the similar manner, thus making clear the physical significance of these relations. This kind of attempt has been made by Hubeny (1987a,b), who provided some intuitive insight into physical nature of quadratic results of the transfer theory.

The more general and mathematically rigorous derivation of quadratic and bilinear relations was given in (Krikorian & Nikoghossian, 1996, Nikoghossian, 1999) on the base of the principle of invariance. The authors elucidated the profound connection between invariance principle, quadratic relations and conservation laws resulting from general variational principle.

Due to the importance of the results obtained, it is expedient to reproduce here some of them for the simplest case of monochromatic, isotropic scattering in a semi-infinite, plane-parallel atmosphere. Suppose also that the atmosphere is homogeneous and does not contain energy sources. Turning to Eqs. (2), (3) and making use the expression for the zero-moment α_0 of $\varphi(\eta)$

$$\alpha_0 = \int_0^1 \varphi(\eta)\, d\eta = 2\left(1 - \sqrt{1-\lambda}\right)/\lambda, \tag{46}$$

one can derive

$$(1-\lambda)(\eta+\xi)\rho(\eta,\xi) = \frac{\lambda}{2}\left(1 - \int_0^1 \rho(\eta,\eta')\,\eta' d\eta'\right)\left(1 - \int_0^1 \rho(\xi,\eta')\,\eta' d\eta'\right). \tag{47}$$

Alongside with the reflection coefficient, it is of importance the function $Y(\tau,\eta,\mu)$ that characterizes the probability of the photon exit from atmosphere in the direction μ, if originally it was moving at depth τ with the directional cosine η. The symmetry property of the Y - function follows from the reciprocity principle and can be represented in the form:

$$|\eta|\, Y(\tau,\eta,\mu) = |\mu|\, Y(\tau,-\mu,-\eta) = |\mu|\, \tilde{Y}(\tau,\mu,\eta), \tag{48}$$

where for convenience it was introduced the function $\tilde{Y}$ with angular arguments referenced from inner normal direction. This function also admits a probabilistic interpretation, namely, $\tilde{Y}(\tau,\eta,\mu)\, d\eta$ is the probability that a photon incident on the atmosphere with the directional cosine μ will move (in general, as a result of multiple scattering) at depth τ within the directional interval $(\eta, \eta + d\eta)$. It is clear that $\tilde{Y}(0,\mu,\eta) = \eta\rho(\eta,\mu)$. In fact, $\tilde{Y}(\tau,\mu,\eta)\,/\,|\eta|$ is none other than the Green function for the source-free problem called also the surface Green function (Case & Zweifel, 1967). This quantity completely determines the radiation field throughout the semi-infinite atmosphere that is illuminated by the external mono-directional source of unit intensity. Taking into account that

$$Y(\tau,-\eta,\mu) = \int_0^1 Y(\tau,\eta',\mu)\,\rho(\eta',\eta)\,\eta' d\eta', \qquad \tilde{Y}(\tau,\mu,-\eta) = \eta \int_0^1 \tilde{Y}(\tau,\mu,\eta')\,\rho(\eta,\eta')\, d\eta'. \tag{49}$$

and using Eq. (47), it is easy to obtain

$$\int_{-1}^1 Y(\tau,\xi,\mu)\, Y(\tau',-\xi,\mu')\, d\xi = \frac{\lambda}{2}\left(\int_{-1}^1 Y(\tau,\xi,\mu)\, d\xi\right)\left(\int_{-1}^1 Y(\tau',\xi,\mu')\, d\xi\right). \tag{50}$$

doi: doi.org/10.52526/25792776-2021.68.2-186

We shall see below that the described procedure admits a simple physical interpretation which makes it possible to obtain the same result directly by means of some modification of invariance idea. The probabilistic meaning assigned to the function Y sets one thinking that some statistical explanation may be suggested for equation (50) as well. Indeed, this equation implies that $\lambda/2$ can be regarded as the correlation coefficient of two random events so that this result can be stated in the probabilistic language as follows.

Two random events of two photons exit from a semi-infinite atmosphere in certain fixed (diverse, in general) directions, if they were originally moving in opposite directions at some different optical depths, are correlated with the correlation coefficient equaled to $\lambda/2$.

The second fundamental result generating quadratic and bilinear R-relations, can be found by a similar manner from Eq. (47). Multiplication of this equation by $\tilde{Y}(\tau,\mu,\eta)\tilde{Y}(\tau',\mu',\xi)$, and integration over η and ξ in the range (0,1), in light of the second of Eqs. (49), yields

$$(1-\lambda)\int_{-1}^{+1}\tilde{Y}(\tau,\mu,\xi)\,\tilde{Y}(\tau',\mu',-\xi)\,d\xi = \frac{\lambda}{2}\left(\int_{-1}^{+1}\tilde{Y}(\tau,\mu,\xi)\,\xi\frac{d\xi}{|\xi|}\right)\left(\int_{-1}^{+1}\tilde{Y}(\tau',\mu',\xi)\,\xi\frac{d\xi}{|\xi|}\right). \tag{51}$$

With use of the reversibility property Eq. (48) in Eq. (51), one can obtain

$$(1-\lambda)\int_{-1}^{+1}Y(\tau,\xi,\mu)\,Y(\tau',-\xi,\mu',)\,\xi^2 d\xi = \frac{\lambda}{2}\left(\int_{-1}^{1}Y(\tau,\xi,\mu)\,\xi d\xi\right)\left(\int_{-1}^{1}Y(\tau',\xi,\mu')\,\xi d\xi\right). \tag{52}$$

Relations (51), (52) constitute a wealth of information about radiation fields in the source-free media. Some of their versatile consequences will be examined below. Here merely the special results following from these relations, when $\tau=\tau'$ and $\mu=\mu'$ are presented

$$\int_0^1 Y(\tau,\xi,\mu)\,Y(\tau,-\xi,\mu)\,d\xi = \frac{\lambda}{4}\left(\int_{-1}^{+1}Y(\tau,\xi,\mu)\,d\xi\right)^2, \tag{53}$$

$$(1-\lambda)\int_0^{+1}Y(\tau,\xi,\mu)\,Y(\tau,-\xi,\mu,)\,\xi^2 d\xi = \frac{\lambda}{4}\left(\int_{-1}^{+1}Y(\tau,\xi,\mu)\,\xi d\xi\right)^2. \tag{54}$$

Thus, we arrived at quadratic Q - and R - relations representing the prototypes of those obtained in (Rybicky, 1977). The derived bilinear and quadratic relations may be applied to different transfer problems of astrophysical interest to give a number of new results.

Let us start, for instance, with the problem of diffuse reflection from a semi-infinite atmosphere, which is illuminated from outside by parallel beam of radiation of unit intensity with directional cosine μ. Using superscripts '+' and '-' to denote the intensities with angular arguments $+\eta$ and $-\eta$, respectively, by virtue of the probabilistic meaning of function Y given above, one may write

$$I^+(\tau,\eta,\mu) = \tilde{Y}(\tau,\mu,-\eta)/\eta, \qquad I^-(\tau,\eta,\mu) = \tilde{Y}(\tau,\mu,\eta)/\eta \tag{55}$$

Now equations Eqs. (50) and (51) correspondingly yield

$$Q(\tau,\mu;\tau'\mu') = \lambda J(\tau,\mu)\,J(\tau',\mu'),$$

$$(1-\lambda)\,R(\tau,\mu;\tau'\mu') = \lambda H(\tau,\mu)\,H(\tau',\mu'), \tag{56}$$

where

$$J(\tau,\mu) = \frac{1}{2}\int_{-1}^{+1}\left[I^+(\tau,\eta,\mu)+I^-(\tau,\eta,\mu)\right]d\eta,$$

$$H(\tau,\mu) = \frac{1}{2}\int_{-1}^{+1}\left[I^+(\tau,\eta,\mu)-I^-(\tau,\eta,\mu)\right]\eta d\eta \tag{57}$$

are the mean intensity and flux, respectively; we introduced also two quadratic moments of the radiation field given by

$$Q(\tau,\mu;\tau'\mu') = \frac{1}{2}\int_{-1}^{+1}\left[I^+(\tau,\eta,\mu)\,I^-(\tau',\eta,\mu')+I^+(\tau',\eta,\mu')\,I^-(\tau,\eta,\mu)\right]d\eta, \tag{58}$$

$$R(\tau,\mu;\tau'\mu') = \frac{1}{2}\int_{-1}^{+1}\left[I^+(\tau,\eta,\mu)\,I^-(\tau',\eta,\mu')+I^+(\tau',\eta,\mu')\,I^-(\tau,\eta,\mu)\right]\eta^2 d\eta. \tag{59}$$

doi: doi.org/10.52526/25792776-2021.68.2-186

The angular arguments μ and μ', which specify the directions of incidence, enter into Eqs.(**??**) as a parameter so that the relations of this type can be written for arbitrary angular distribution of illuminating radiation. Moreover, they enable one to establish the relationship between radiation fields of two diverse problems with different angular distribution for incident radiation.

An important insight into the source-free problem and the group of related problems can be given upon the simple and physically intelligible formula, second of Eq. (49) which was employed in deriving Eqs.(**??**). By virtue of formulas Eq. (55) it can be rewritten as

$$I^{+}(\tau,\eta,\mu)=\eta\int_0^1 \rho(\eta,\varsigma)\, I^{-}(\tau,\varsigma,\mu)\, d\varsigma, \tag{60}$$

which states the obvious fact that, in the absence of internal sources, the upward radiation (and ultimately the radiation field at any optical depth τ is completely determined by the intensity of inward radiation. Indeed, taking account of that

$$I^{-}(\tau,\eta,\mu)=\lambda\int_0^{\tau} J(\tau,\mu)\, e^{-\frac{\varsigma-t}{\eta}}\frac{dt}{\eta}+\frac{1}{2}\delta(\eta-\mu)\, e^{-\frac{\tau}{\mu}} \tag{61}$$

and the source function $S(\tau,\mu)=\lambda J(\tau,\mu)$. The formula (61) being inserted into Eq. (60) yields

$$S(\tau,\mu)=\int_0^{\tau} L(\tau-t)\, S(t,\mu)\, dt+\frac{\lambda}{2}\varphi(\mu)\, e^{-\frac{\tau}{\mu}}. \tag{62}$$

Thus, knowledge of the reflectance of the atmosphere makes it possible to reduce the classical boundary-value problem of determining the internal field of radiation to the Volterra-type associated with an initial value problem. This result is not unexpected, however, and is important in the sense that similar equations may be written (see below) for some special internal-source problems as well while formula (60) is no more valid.

It has been shown that discussion similar to that given above be carried out for some other classic problems of the theory of radiative transfer. For instance, consider the atmosphere with the uniformly distributed internal sources of energy so that

$$S(\tau)=\lambda J(\tau)+(1-\lambda)\, B, \tag{63}$$

where $B=$ const is related to the Planck function. Two-point quadratic relations now have a form

$$Q(\tau,B;\tau',B')=\lambda S(\tau,B)\, S(\tau',B')-(1-\lambda)\, BB', \tag{64}$$

$$(1-\lambda)\, R(\tau,B;\tau',B')=\lambda H(\tau,B)\, H(\tau',B')+$$

$$(1-\lambda)\left[BK(\tau',B')+B'K(\tau,B)\right]-(1-\lambda)\, BB'/3, \tag{65}$$

where

$$K(\tau,B)=\frac{1}{2}\int_0^1\left[I^{+}(\tau,\eta,B)+I^{-}(\tau,\eta,B)\right]\eta^2 d\eta \tag{66}$$

is the K-*moment* and, for clarity, we marked B explicitly as an argument identifying the problem under consideration. It was shown that here again the source satisfies Volterra-type integral equation analogous to that of Eq. (62)

$$S(\tau,B)=\int_0^{\tau} L(\tau-t)\, S(t,B)\, dt+B\sqrt{1-\lambda}. \tag{67}$$

Using the same approach, two-point quadratic relations were derived also for the Milne problem and for the radiation transfer problem concerning the atmosphere with the exponential distribution of internal energy sources of the form $b(\tau,m)=(1-\lambda)\, Be^{-m\tau}$ with constant B and m. Sending the reader after Q - and R – non-linear relations to [17], we limit ourselves by presenting here the equations, counterparts of Eqs. (62), (67) for corresponding source functions

$$S(\tau,F)=\int_0^{\tau} L(\tau-t)\, S(t,F)\, dt+\left(\sqrt{3}/4\right)F, \tag{68}$$

where F is the constant factor in the Milne problem known as astrophysical flux, and

$$S(\tau,m)=\int_0^{\tau} L(\tau-t)\, S(t,m)\, dt+(1-\lambda)\, B\varphi\left(m^{-1}\right)e^{-m\tau}. \tag{69}$$

It must be emphasized that all the presented relations are valid if only $\lambda = const$, more generally, they are true wherever the local optical characteristics of the atmosphere do not change.

doi: doi.org/10.52526/25792776-2021.68.2-186

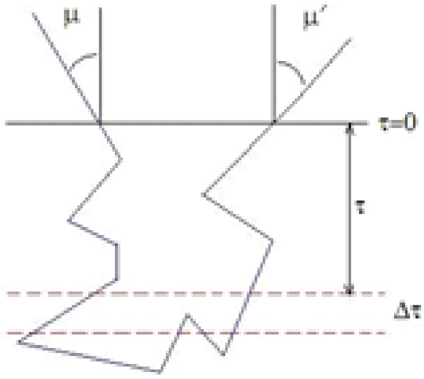

Figure 8: Derivation of the two-point bilinear Q relation.

x. The modified principle of invariance. The preceding results suggest an idea on that there must exist a close inter-connection between bilinear relations and the invariance principle. For this reason, let us return to the original formulation of the invariance principle given in the outset of the review. Consider a semi-infinite, plane-parallel and source-free homogeneous atmosphere. For simplicity of exposition, the probabilistic approach to the problem will be adopted.

Let a photon is incident upon the boundary plane $\tau = 0$ of the atmosphere at an angle $\cos^{-1}\mu$ (Fig.8) to the inner normal, and we are interested in the probability of the photon exit at some angle $\cos^{-1}\mu\prime$ to the upper normal direction. The classical formulation of the invariance principle assumes the addition (or removal) of a thin layer to (from) the surface of the atmosphere, presuming the optical properties of the layer and atmosphere to be the same. It is completely clear, however, that physically there is no difference whether we add (or remove) the layer to (from) the top of the atmosphere or do it somewhere within it with some selected layer $(\tau, \tau + \Delta)$. In the latter case we are interested in the probability of reflection subject to condition that the level τ intersected. Recalling the probabilistic meaning of functions Y and $\tilde{Y}$ introduced in the outset of this subsection, it is readily seen that the probability of the mentioned event is

$$d\mu \int_0^1 Y(\tau, -\varsigma, \mu') \, \tilde{Y}(\tau, \mu, \varsigma) \, d\varsigma. \tag{70}$$

Further, we must determine the same probability accounting of the elementary processes of interaction with the selected layer $(\tau, \tau + \Delta)$ and equate to that of the formula Eq. (70) in accordance with what have been said. One may distinguish three types of processes of the first order of $\Delta\tau$ associated with the layer.

a.The scattering photon passes the selected layer with no interaction.

b.The photon enters the selected layer by crossing the plane τ and is scattered in the layer in some direction specified by η.

c.The photon enters the selected layer from below, i.e. by crossing the plane $(\tau + \Delta\tau)$ and is scattered in the layer. The proper probabilities for these three events are derived in (Nikoghossian, 1997). By adding up the obtained values, after some simple transformation we arrive at the specific version of the bilinear Q – relation (50) written for $\tau = \tau'$.

$$\int_{-1}^1 Y(\tau, \xi, \mu) \, Y(\tau, -\xi, \mu') \, d\xi = \frac{\lambda}{2} \left(\int_{-1}^1 Y(\tau, \xi, \mu) \, d\xi \right) \left(\int_{-1}^1 Y(\tau, \xi, \mu') \, d\xi \right). \tag{71}$$

Finally, on setting $\tau = 0$ in and taking account of the boundary condition $Y(0, \zeta, \mu) = \delta(\zeta - \mu)$ we are led to invariance equation (2) for the reflection coefficient. We see that equation (71) is more informative (as compared to Eq. (**??**) and can be regarded as the extension of Ambartsumian's equation to all depths in the atmosphere.

xi. The variational formalism. As was above said, the theory of radiative transfer can be made to rest on the principles of invariance. It was shown that the invariance equation, being combined with some simple physical reasoning, makes it possible to derive the more informative quadratic and bilinear relations, for which the former equation is a special (surface) result. It turned out that the resulting Q - relations may be envisioned as a manifestation of a somewhat generalized version of the classical principle of invariance and can be obtained immediately. These facts indicate the fundamental nature of the invariance property of transfer problems and set one thinking that there must exists some general formulation of problems that implies both the equation of transfer and the principles of invariance as a kind of laws.

As it was shown by Nikoghossian (1999), the problems of transfer of radiation in the plane-parallel homogeneous atmosphere admit a variational formulation, the equation of transfer then being the Euler - Lagrange equation and the

doi: doi.org/10.52526/25792776-2021.68.2-186

bilinear Q - relation being the conservation law due to form-invariance of the suitable Lagrangian. In fact, a single functional comprises all the information on features of the problem and allows a systematic connection between symmetries and conservation laws. Being the first integrals of the Euler - Lagrange equation, the conservation laws may facilitate the solution of the problem under consideration and assist in its interpretation. Two salient problems, encountered in having recourse to the variational principle, are the existence of the principle for a given problem and the derivation of appropriate conservation laws. The former of these problems for systems of partial differential equations was solved by Vainberg (1964), who showed that this problem is equivalent to determining whether an operator is potential or not. The derivation of the conservation laws is based on Noether's theorem (see, Gelfand & Fomin, 1965), which suggests a systematic procedure for establishing these laws from a direct study of the variational integral. An important generalization of the Noether's theorem to encompass the integral-differential equations was given by Tavel (1971).

While the variational approach is widely used in various branches of theoretical physics, it was not the case in the field of the radiative transfer theory, with the only exception being the paper of Anderson (1973) who employs Tavel's results to establish the conservation law suitable for the case of non-isotropic scattering. The results of the rigorous mathematical theory in applying the Lagrangian formalism is used in (Krikorian & Nikoghossian, 1996) to the one-dimensional transfer problem. Due to the importance of the issue, let us consider it in more detail.

Let us start with the angle-dependent transfer equations for the function Y

$$\pm\eta\frac{dY(\tau,\pm\eta,\mu)}{d\tau} = -Y(\tau,\pm\eta,\mu) + \frac{\lambda}{2}\int_{-1}^{1} Y(\tau,\eta',\mu)\,\mathrm{d}\eta'. \tag{72}$$

From these equations one can easily obtain

$$\eta^2\frac{\mathrm{d}^2\Phi}{\mathrm{d}\tau^2} = -\Phi(\tau,\eta,\mu) - \lambda\int_0^1 \Phi(\tau,\eta',\mu)\,\mathrm{d}\eta', \tag{73}$$

where $\Phi(\tau,\eta,\mu) = Y(\tau,+\eta,\mu) + Y(\tau,-\eta,\mu)$.

One may readily check the self-adjointness of this equation so that the variational formulation is admitted. The Lagrangian density L corresponding to Eq. (73) was obtained in (Anderson, 1973)

$$L(\Phi,\Phi',\tau,\eta,\mu) = \Phi^2 + (\eta\Phi')^2 - 2\Phi U, \tag{74}$$

where

$$U(\tau,\mu) = \frac{\lambda}{2}\int_0^1 \Phi(\tau,\eta',\mu)\,\mathrm{d}\eta'. \tag{75}$$

In accordance with this result, the Euler-Lagrange equation has a form

$$\frac{\partial L}{\partial\Phi} - \frac{\mathrm{d}}{\mathrm{d}\tau}\frac{\partial L}{\partial\Phi'} + \lambda\int_0^1 \frac{\partial L}{\partial U}\mathrm{d}\eta' = 0. \tag{76}$$

One will make sure that insertion of the Lagrangian (74) into (76) yields the transfer equation (73). It is important that both the transfer equation (73) and the Lagrangian density (74) do not depend explicitly on τ, or stated differently, they are form-invariant under infinitesimal transformation

$$\tau \to \tau' = \tau + \delta\tau, \qquad \eta = \eta', \qquad \mu = \mu', \tag{77}$$

where the quantity $\delta\tau$ is allowed to be an arbitrary infinitesimal function of τ. This implies that the transformation Eq. (77), i.e. translation of the optical depth, is the symmetry transformation for Eq. (72) and suggests a certain conservation law as follows

$$\int_0^1 \left[L - \frac{\partial L}{\partial\Phi}\Phi'\right]\mathrm{d}\eta = \mathrm{const}, \tag{78}$$

which, in view of (74), takes a form

$$\int_0^1 \left[\Phi^2(\tau,\eta,\mu) - \eta^2\Phi'^2(\tau,\eta,\mu) - 2U(\tau,\mu)\Phi(\tau,\eta,\mu)\right]\mathrm{d}\eta = \mathrm{const}, \tag{79}$$

or

$$\int_0^1 Y(\tau,\varsigma,\mu)\,Y(\tau,-\varsigma,\mu)\,\mathrm{d}\varsigma = \frac{\lambda}{4}\left(\int_{-1}^{+1} Y(\tau,\varsigma,\mu)\,\mathrm{d}\varsigma\right)^2 + \mathrm{const}. \tag{80}$$

doi: doi.org/10.52526/25792776-2021.68.2-186

This relation is, in essence, a prototype of the Q – integral obtained by Rybicki (1977). The above considerations imply that by its content the integral (80) is an analog of the momentum conservation law in mechanics and is due to the axes translation transformation.

For semi-infinite atmosphere $Y(\tau, \pm\varsigma, \mu) \to 0$ as $\tau \to \infty$ so that, const $= 0$, and we arrive at Eq. (53). More general relation for this case Eq. (71) may be derived in treating the problems differing with each other by the value of the parameter μ. It holds everywhere where λ does not vary with depth, i.e., if the medium is homogeneous.

The variational formalism suggested in the Byurakan observatory allows not only to elucidate the physical meaning of invariance principle but enables one to derive along with many known results a great number of new relations of great importance for the theory and applications. It allows also to find out some statistical characteristics of the diffusion process in the atmosphere (Nikoghossian, 1997, 2000). Some of the known non-linear relations possess a fairly obvious physical or/and probabilistic meaning and could be written immediately on the base of simple arguments. However, as we shall show below, by no means all of them follow from the variational principle, so they cannot be recognized as invariance relations or, even more, invariance principles.

xii. The polynomial distribution of sources. An important question to be answered is the applicability of the Lagrangian formalism to the transfer problems for atmospheres containing energy sources. Inasmuch as both the diffuse reflection and Milne problems obey the homogeneous integral-differential equation, the suitable quadratic and bilinear integrals are possible to write directly. In the case of the source-containing atmospheres we are led to the inhomogeneous integral-differential equations with appropriate source terms. Generally, the self-adjointness of the transfer equations may be violated so that the direct application of variational principle becomes impossible. Nevertheless, as it was shown by Nikoghossian (1999), in some cases such as the uniformly and exponentially distributed sources this difficulty was get over by using the apparent connection between these two problems treated in Sect. vii and the source-free problem. Now an additional possibility based on the conservation law (79) is appeared to reduce the source-containing problems to the source-free problem. As an example we shall briefly reproduce here the results obtained for the case of polynomial distribution of sources (Nikoghossian, 1999). The first attempt in this direction was made in (Rybicki, 1977). The approach proposed there was successful, however, for polynomials of the degree not higher than second, whereas, as it was shown in the mentioned Nikoghossian's paper, the Q-integrals exist for polynomials for arbitrary high order. Let we have the transfer equation of the form

$$\eta^2 \frac{d^2\Phi}{d\tau^2} = -\Phi(\tau, \eta) - \lambda \int_0^1 \Phi(\tau, \eta')\, d\eta' - 2g(\tau), \tag{81}$$

where

$$g(\tau) = (1 - \lambda) B(\tau), \qquad B(\tau) = \sum_{i=0}^{N} B_i \tau^i. \tag{82}$$

where N is the degree of polynomials, $B^{(m)} = d^m B / d\tau^m$. By introducing the functions

$$F_N(\tau, \eta) = 2 \sum_{k=0}^{[N/2]} B^{(2k)}(\tau)\, p_{2k}(\eta), \tag{83}$$

where brackets mean the integer part, one can check by direct substitution that F_N is a partial solution of Eq.(81) if only $p_{2k}(\eta)$ are polynomials of the order $2k$ (k=*1,2,...*) defined as follows

$p_{2k}(\eta) = \sum_{i=0}^{k} p_{2i}(0)\, \eta^{2(k-i)}$, (**??**)and

$$p_{2k}(0) = \frac{\lambda}{1-\lambda} \sum_{i=1}^{k} \frac{p_{2(k-i)}(0)}{2k+1}, \; p_0(\eta) = 1. \tag{84}$$

Having the rule for construction the function (84), one can derive the requisite Q-integrals for any source term with polynomial depth-dependence. Some results for small values of N are presented in (Nikoghossian, 1999).

xiii. The group of the RSF (reducible to the source-free) problems. Thus, one may conclude that there exists a group of different frequently occurring radiation transfer problems of astrophysical interest which admit quadratic and bilinear integrals. They can be reduced to the source-free problem. This group includes the Milne's problem, the problem of diffuse reflection (and transmission in the case of the atmosphere of finite optical thickness) as well as the problems with exponential and polynomial laws for the distribution of internal energy sources. An important special case of the last type of problems is the problem of the radiative transfer in an isothermal atmosphere (i.e. in atmosphere with homogeneous distribution of internal sources). This group of problems is characterized at least by three common features. First of all, the invariance principle implies bilinear relations connecting the solutions

doi: doi.org/10.52526/25792776-2021.68.2-186

of the listed problems. As it was shown in (Nikoghossian, 2011b), the group of the RSF-problems admits a class of integrals involving quadratic and bilinear moments of the intensity of arbitrarily high orders. Secondly, if the problem can be formulated for finite atmosphere then the principle allows connecting its solution with that of the proper problem for a semi-infinite atmosphere. Finally, knowledge of the φ-function reduces their solutions to the Volterra-type equation for the source function with the kernel-function (9). The author refers to these problems as the group of RSF-problems.

xiv. Arbitrarily varying sources. For further insight to the point can by given by considering the general treatment of the problem of sources. Consider the transfer of monochromatic radiation through semi-infinite homogeneous and plane-parallel atmosphere that contains energy sources varied arbitrarily with depth. The source function of this problem, as is known, satisfies integral equation

$$S(\tau) = \frac{\lambda}{2}\int_0^\infty \mathrm{Ei}\,(|\tau - t|)\,S(t)\,dt + g(\tau). \tag{85}$$

As it was shown in (Yengibarian, 1972, Yengibarian & Nikoghossian, 1973b), the solution of this equation is equivalent to the solution of the following coupled pair of the Volterra-type equations

$$S(\tau) = \omega(\tau) + \int_0^\tau L(\tau - t)\,S(t)\,dt, \tag{86}$$

$$\omega(\tau) = g(\tau) + \int_\tau^\infty L(\tau - t)\,\omega(t)\,dt. \tag{87}$$

As a matter of fact, the set of equations (86), (87) represents a kind of splitting the so-called Λ-operator (Hubeny, 1982) and may become useful in solving the transfer problems. Note that being applied to this system, the escape probability approach (Rybicky, 1984) leads, as could be expected, to sufficiently accurate results. For instance, when $B = const$, one may easily find for $\tau = 0$ that $\omega = g/(1-\lambda)$ and $S(0) = \omega = B\sqrt{1-\lambda}$. For deep interiors of the atmosphere it yields

$$\lim_{t\to\infty} S(\tau) = \lim_{t\to\infty}\frac{\omega}{L(\tau) + \sqrt{1-\lambda}} = B. \tag{88}$$

Thus in both cases his approach leads to exact values of the source function, whereas the same approach applied to Eq. (85) gives the rather crude estimate for the surface value: $S(0) = 2(1-\lambda)B/(2-\lambda)$. At the same time, it easy to see that the kernel splitting method provides correct values of $S(0)$ for all the treated special RSF-problems. This follows from the fact that in these cases Eq. (87) allows exact analytical solution so that the problems resolve themselves into the solution of a single Volterra-type equation (86) for the source function.

The approach described for the semi-infinite atmosphere is easy to apply to an atmosphere of finite optical thickness. In fact, the generalization of previous results for such atmosphere is attained trivially and resolves itself to determining the proper values of the integration constants. To proceed, we introduce by analogy to the semi-infinite atmosphere the quantities $Y(\tau, \pm\eta, \mu; \tau_0)$ with similar probabilistic meaning, characterizing the photon's exit from the boundary $\tau = 0$ of an atmosphere for the photon moving in direction $\pm\eta$ at depth τ (angular arguments are referenced with respect to the outward normal to the surface $\tau = 0$). This implies that

$$Y(0, \eta, \mu; \tau_0) = \delta(\eta - \mu), \qquad Y(\tau_0, \eta, \mu; \tau_0) = \mu q(\mu, \eta, \tau_0),$$
$$Y(0, -\eta, \mu; \tau_0) = \mu\rho(\mu, \eta, \tau_0), \qquad Y(\tau_0, -\eta, \mu; \tau_0) = 0, \tag{89}$$

where

$$q(\mu, \eta, \tau_0) = \eta^{-1}\delta(\eta - \mu)\,e^{-\frac{\tau_0}{\eta}} + \sigma(\mu, \eta, \tau_0), \tag{90}$$

is transmittance of the medium. Since the functions $Y(\tau, \pm\eta, \mu; \tau_0)$ satisfy the partition transfer equations Eqs. (**??**), the variational principle leads to the quadratic Q - integral Eq. (80) with the value $(\lambda/4)\,\psi^2(\mu, \tau_0)$ for the constant. It is apparent that with no more effort one may derive many different kind of bilinear and two-point bilinear relations linking with each other different quantities describing the field of radiation in different depths of the finite media of different optical thickness. Such relations for some of the RSF – problems for finite atmosphere are given in (Nikoghossian, 1999).

Of special interest are the nonlinear relations which establish connection between characteristics of the radiation transfer in finite and semi-infinite atmospheres. We limit ourselves to presenting here only two of them which will be mentioned below

doi: doi.org/10.52526/25792776-2021.68.2-186

$$\eta'\rho_\infty(\eta',\eta) = -\eta\rho(\eta,\eta',\tau) + \int_0^1 q(\eta,\varsigma,\tau)\,Y_\infty(\tau,-\varsigma,\eta')\,d\varsigma -$$
$$-\frac{\lambda}{2}\psi(\eta,\tau)\int_0^1 Y_\infty(\tau,\varsigma,\eta')\,d\varsigma - \frac{\lambda}{2}\varphi_\infty(\eta')\,\varphi(\eta,\tau), \tag{91}$$

$$Y_\infty(\tau,\eta,\eta') = q(\eta,\eta',\tau) - \eta\int_0^1 \rho(\eta,\varsigma,\tau)\,Y_\infty(\tau,-\varsigma,\eta')\,d\varsigma -$$
$$-\frac{\lambda}{2}\varphi(\eta,\tau)\int_0^1 Y_\infty(\tau,\varsigma,\eta')\,d\varsigma - \frac{\lambda}{2}\varphi_\infty(\eta')\,\psi(\eta,\tau), \tag{92}$$

where quantities pertaining to the semi-infinite atmosphere are marked by the sign of infinity.

xv. **The nature of some non-linear relations of the radiation transfer theory**. Invariant properties of the problems of radiation transfer in homogeneous atmospheres lead to a variety of non-linear relations. They are widely used and are especially efficient when being combined with other methods of solution. In light of the new results presented in the above cited works carried out in the Byurakan observatory, the question arises to what extent certain nonlinear relations in radiative transfer theory are connected with the variational principles resulting from invariance with respect to the translational transformation of the optical depth. Only those relations are implied here, which are used in connection with the invariance principle or with the method of adding layers. As it was shown by Nikoghossian (2009a,b), some nonlinear relations found in the theory sometimes are erroneously considered to be a consequence of the invariance properties of the problem. This question is crucial to the theory of radiative transfer, so it is expedient to summarize here the findings of the above mentioned works.

To begin, it is important to note that, for instance, Eqs. (10) - (13) in deriving the layers adding law have been written without invoking the invariance principle, to which they are, of course, not related. In fact, these formulas remain valid in general cases, when it is inappropriate to speak of invariance properties of the problem. For example, these equations remain in force even when the media are inhomogeneous, with, of course, their polarity property taken into account (see below).

We now rewrite Eqs. (10) - (13) for the three-dimensional plain-parallel homogeneous atmosphere. The initial problem can be re-formulated now in the following way: let a parallel beam of radiation with intensity I_0 be incident on the boundary $\tau = 0$ of a medium at an angle of $\arccos\varsigma$ to its inner normal (Fig. 9). The intensity of the reflected radiation is related to the reflection function $\rho(\eta,\varsigma,\tau_0)$ by $I(0,\eta,\varsigma) = I_0\rho(\eta,\varsigma,\tau_0)\,\varsigma$. In analogous fashion for transmitted radiation we have $I(\tau_0,\eta,\varsigma) = I_0 q(\eta,\varsigma,\tau_0)\,\varsigma$, in which we have retained the customary notation σ for the diffuse part of the transmitted radiation. For brevity, the dependence of the intensities on the optical thickness of the medium is left out of the arguments. Since the medium can now be regarded as consisting of two parts with respective thicknesses τ and $\tau_0-\tau$, relations analogous to Eqs. (10) - (13) can be written in the form (I_0 can be taken equal to unity without loss of generality).

$$\rho(\eta,\varsigma,\tau_0)\,\varsigma = \rho(\eta,\varsigma,\tau)\,\varsigma + I(\tau,\eta,\varsigma)\,e^{-\tau/\eta} + \int_0^1 \sigma(\eta,\eta',\tau)\,I(\tau,\eta',\varsigma)\,\eta'\,d\eta', \tag{93}$$

$$\sigma(\eta,\varsigma,\tau_0)\,\varsigma = \sigma(\eta,\varsigma,\tau_0-\tau)\,\varsigma e^{-\tau/\eta} + I^*(\tau,-\eta,\varsigma)\,e^{-(\tau_0-\tau)/\eta} +$$
$$\int_0^1 \sigma(\eta,\eta',\tau_0-\tau)\,I^*(\tau,-\eta',\varsigma)\,\eta'\,d\eta', \tag{94}$$

$$I(\tau,\eta,\varsigma) = \rho(\eta,\varsigma,\tau_0-\tau)\,\varsigma e^{-\tau/\varsigma} + \int_0^1 \rho(\eta,\eta',\tau_0-\tau)\,I^*(\tau,-\eta',\varsigma)\,\eta'\,d\eta', \tag{95}$$

$$I^*(\tau,-\eta,\varsigma) = \sigma(\eta,\varsigma,\tau)\,\varsigma + \int_0^1 \rho(\eta,\eta',\tau)\,I(\tau,\eta',\varsigma)\,\eta'\,d\eta', \tag{96}$$

where the diffuse part of the intensity of the downward moving radiation is indicated by an asterisk.

The nonlinear relations written down by Chandrasekhar in the 1950's and called invariance principles by him (Chandrasekhar, 1960) are well known in radiative transfer theory. These relations were examined by Nikoghossian (2009a,b) from the standpoint of their possible connection with the invariance principle.

The problem of diffuse reflection and transmission of radiation by a medium of finite optical depth examined by Chandrasekhar was stated as follows: on a medium of optical thickness τ_0 in direction $(-\mu_0,\varphi_0)$, falls a parallel beam of radiation with flux πF per unit area perpendicular to the direction of incidence. The reflection function S and the transmission function T are introduced so that

doi: doi.org/10.52526/25792776-2021.68.2-186

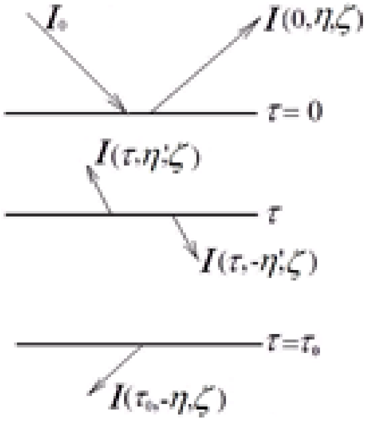

Figure 9: Diffuse reflection of light from a medium of finite thickness.

$$I\left(0,\mu,\varphi\right)=\frac{F}{4\mu}S\left(\tau_0,\mu,\varphi;\mu_0,\varphi_0\right),\qquad I^*\left(\tau_0,-\mu,\varphi\right)=\frac{F}{4\mu}T\left(\tau_0,\mu,\varphi;\mu_0,\varphi_0\right). \tag{97}$$

Chandrasekhar wrote down the following four nonlinear equations:

$$I\left(\tau,\mu,\varphi\right)=\frac{F}{4\mu}e^{-\tau/\mu_0}S\left(\tau_0-\tau,\mu,\varphi;\mu_0,\varphi_0\right)+$$

$$\frac{1}{4\pi\mu}\int_0^{2\pi}\mathrm{d}\varphi\int_0^1 S\left(\tau_0-\tau,\mu,\varphi;\mu',\varphi'\right)I^*\left(\tau,-\mu',\varphi'\right)\mathrm{d}\mu', \tag{98}$$

$$I^*\left(\tau,-\mu,\varphi\right)=\frac{F}{4\mu}T\left(\tau,\mu,\varphi;\mu_0,\varphi_0\right)+$$

$$\frac{1}{4\pi\mu}\int_0^{2\pi}\mathrm{d}\varphi\int_0^1 S\left(\tau,\mu,\varphi;\mu',\varphi'\right)I\left(\tau,\mu',\varphi'\right)\mathrm{d}\mu', \tag{99}$$

$$\frac{F}{4\mu}S\left(\tau_0,\mu,\varphi;\mu_0,\varphi_0\right)=\frac{F}{4\mu}S\left(\tau,\mu,\varphi;\mu_0,\varphi_0\right)+e^{-\tau/\mu}I\left(\tau,\mu,\varphi\right)+$$

$$\frac{1}{4\pi\mu}\int_0^{2\pi}\mathrm{d}\varphi\int_0^1 T\left(\tau,\mu,\varphi;\mu',\varphi'\right)I\left(\tau,\mu',\varphi'\right)\mathrm{d}\mu', \tag{100}$$

$$\frac{F}{4\mu}T\left(\tau_0,\mu,\varphi;\mu_0,\varphi_0\right)=\frac{F}{4\mu}e^{-\tau/\mu_0}T\left(\tau_0-\tau,\mu,\varphi;\mu_0,\varphi_0\right)+e^{-(\tau_0-\tau)/\mu}I\left(\tau,-\mu,\varphi\right)+$$

$$\frac{1}{4\pi\mu}\int_0^{2\pi}\mathrm{d}\varphi\int_0^1 T\left(\tau_0-\tau,\mu,\varphi;\mu',\varphi'\right)I^*\left(\tau,-\mu',\varphi'\right)\mathrm{d}\mu', \tag{101}$$

We now set ourselves the task of comparing Eqs. (98) - (101) with Eqs. (93) - (96) of the preceding section. To do this we neglect the azimuthal dependence in Eqs. (98) - (101), set $F = 1$, switch to the previous notation, and include the following easily verified relation between the corresponding coefficients of reflection and transmission:

$$(1/2)\,S\left(\tau_0,\eta,\varsigma\right)=\eta\varsigma\rho\left(\eta,\varsigma,\tau_0\right),\qquad (1/2)\,T\left(\tau_0,\eta,\varsigma\right)=\eta\varsigma\sigma\left(\eta,\varsigma,\tau_0\right) \tag{102}$$

Then it is easy to show that Eqs. (98) - (101) are the same as Eqs. (95), (96), (93), and (94), respectively. Thus, neither these, nor the previous equations have a direct connection to the invariance principle associated with a translational transformation of the optical depth, and so they cannot be derived from the corresponding conservation law.

These considerations imply that the nonlinear relations discussed above can be divided into two classes. The first includes those formulas which characterize only the radiative transfer process, itself, in a plane parallel atmosphere; these have great generality. Equations (10) - (13), (98) - (101), belong to this class. The second, narrower class includes equations that are a consequence of the invariance properties of the specific transfer problem at hand. Many equations of this type for groups of the RSF-problems have been derived in the first part of this review.

xvi. Inhomogeneous atmosphere. When interpreting the radiation from objects in space it is usually necessary to apply various simplifying assumptions regarding their geometry and physical properties. For example, it is often

doi: doi.org/10.52526/25792776-2021.68.2-186

assumed that a radiating medium is homogeneous and stationary, although it clearly has a rather complex structure and is subject to variation in time. This simplifies the problems to a great extent and makes it possible to estimate some characteristics of the radiating medium averaged in some sense. However, the high-resolution observational data available nowadays afford an opportunity for a more detailed investigation of astrophysical objects and analysis of their radiation. This leads to pressure to develop a suitable theory of radiation transfer trough an inhomogeneous atmosphere, providing new efficient methods of computations. Such attempts were made by a number of authors (see e.g., Jefferies, & Lindsey, 1988; Secchi-Pestelini & Barletti, 2001; Menkohn, & Richling, 2002). In connection with solar prominences, it was in (Nikoghossian, S. Pojoga, & Mouradian, 1997, 1998, 1999; Nikoghossian, & Mouradian, 2000) treated the effect of physical inhomogeneities related to the distribution of internal energy sources and to geometrical factors. In an analysis of multiple scattering at the line frequencies, the scattering coefficient was usually assumed to be constant inside the radiating volume. It is, however, evident that such an assumption may be rather crude for interpretation of radiation in the optically thick lines. Henceforth under inhomogeneous atmosphere we will mean atmosphere with the scattering coefficient arbitrarily varying with depth, though methods developed in these works remain in force also in the case of variation of other parameters which determine an elementary scattering event and the distribution of primary energy sources.

The complexity of the boundary-value transfer problems makes it necessary to develop appropriate analytical techniques in order to make it somehow easier to get a numerical solution. In each individual case, depending on the initial assumptions about the properties of the medium, of elementary scattering events, etc., specialized methods have been developed. One of the first methods of this type was the method based on invariance principle, i.e., on the symmetry properties of the problem, which avoided the above difficulties in the case of homogeneous atmospheres and allowed to determine the intensity of the emerging radiation without prior knowledge of the radiation field in the entire atmosphere. There has also been a natural drive to find an alternative statement of the classical problems of radiative transfer theory with the aim of reducing them to initial-value problems (so-called Cauchy problems). With the development of high speed electronic computers, research in this area have become especially important in connection with the fact that solving this kind of problem is more suited to the computers' capabilities. Among the first papers in this area, we note those of Bellman (1957) and Sobolev (1957, 1959, 1985) who developed a method based on extensive use of the "surface" resolvent function. The idea of this approach goes back to Krein's paper (1955).

Attempts to apply the invariance principle in solving the radiation transfer problems for inhomogeneous atmospheres were made by Sobolev (1956) (see also Yanovitskij, 1997). As it was above said, the method of invariant imbedding enables one to readdress standard problems in a way such as to reduce them to the initial value problems. Of the extensive literature in this area, besides the above cited works of Bellman's group of authors, we note also monographs (Scott, 1973; Casti & Kalaba, 1976).

The method descrybed in Nikoghossian (2004, 2004a,b,c; 2012a,b; 2013a) includes a simple, but, at the same time, universal computational scheme that can be used to determine the radiation field and various characteristics of the scattering process as solutions of corresponding initial-value problems. *The idea behind this method developed for solving a given linear problem of the radiation transfer involves a preliminary determination of the global optical properties of an atmosphere – the reflection and transmission coefficients, as well as some other related quantities, for a family of atmospheres with different optical thicknesses. This makes it possible to determine the radiation field inside the 1D inhomogeneous medium without solving any new equations.* However, as it was shown below, there exists another route that allows reducing the computational process to ordinary matrix multiplication. Regardless of the initial assumptions, the calculations are easily carried out on modern computers and, most importantly, are numerically stable.

Generalization of the layers adding law for the case of inhomogeneous atmospheres. As it was shown by Nikoghossian (2004), Ambartsumia's arguments and derivations described in Sect.3 for homogeneous atmosphere can be generalised by considering the division of the medium into two parts as a combination of two media generally of different optical properties.

For illustration of the basic idea, it is reproduced here the simplest scalar case involving the transfer of monochromatic radiation in a one-dimensional inhomogeneous atmosphere. As it was shown in (Nikoghossian, 2004), the inhomogeneous atmosphere exhibits the so-called polarity property with respect to the sense of the incoming illumination, i.e., its optical properties in the scalar case are described by three parameters: two reflection coefficients and one transmission coefficient.

Fig.10 is a schematic illustration of two cases where a photon is incident from outside on a composite medium formed as the result of adding two inhomogeneous scattering and absorbing media with optical thicknesses τ_1 and τ_2.

The formulas for addition in the case shown in the upper part of the figure are

doi: doi.org/10.52526/25792776-2021.68.2-186

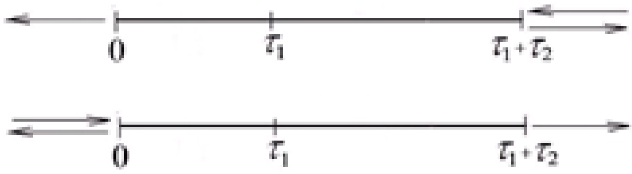

Figure 10: Reflection and transmission of a composite atmosphere.

$$q(\tau_1+\tau_2)=\frac{q(\tau_1)\,q(\tau_2)}{1-r(\tau_1)\,\bar{r}(\tau_2)},\qquad r(\tau_1+\tau_2)=r(\tau_2)+\frac{r(\tau_1)\,q^2(\tau_2)}{1-r(\tau_1)\,\bar{r}(\tau_2)},\tag{103}$$

where the barred values refer the direction inverse to that of radiation incidence. For the reflection coefficient of a composite atmosphere on the left (lower drawing of Fig.10) it was obtained

$$\bar{r}(\tau_1+\tau_2)=\bar{r}(\tau_1)+\frac{r(\tau_1)\,q^2(\tau_2)}{1-r(\tau_1)\,\bar{r}(\tau_2)}.\tag{104}$$

It should be noted that, in general, the two components of the composite medium differ one from another not only by optical thickness, but also by the form of the scattering coefficient. Even in the case of the scattering coefficient common for two components, their optical characteristics may differ by the range of variation of this coefficient. But this should not cause confusion in further discussion since henceforth τ_2 will be replaced by infinitely thin layer.

Now consider an atmosphere of thickness τ_0, where the inhomogeneity stems from variability of the scattering coefficient λ with depth, is divided into two parts. Then, the ordinary procedure of taking the limit, when the thickness of one of components tends to zero, leads to equations which coincides with those for homogeneous atmosphere (see, Eq. (16), Eq. (17)). For the inverse illumination one finds

$$\frac{d\bar{r}}{d\tau_0}=\frac{\lambda(\tau_0)}{2}q^2(\tau_0),\tag{105}$$

where we take into account that in the scalar case $\bar{q}=q$ (Nikoghossian, 1999, 2004b),

This is important that $r(\tau_0)$ satisfies a separate equation. It is a Riccati equation and can be solved by one of the standard numerical methods. Note that a fairly high accuracy is obtained even in the simplest case of solving Eq. (17) by the Euler method.

After finding the reflectance, $r(\tau_0)$, the transmission coefficient is determined explicitly using the formula (Nikoghossian, 2011c)

$$q(\tau_0)=\exp\left[-\int_0^{\tau_0}\varpi(\tau)\,d\tau\right],\tag{106}$$

where

$$\varpi(\tau_0)=1-\frac{\lambda(\tau_0)}{2}\left[1+r(\tau_0)\right].\tag{107}$$

It follows from Eqs. (106) and (105) that as $\tau_0\to\infty$, $r(\tau_0)$ and $q(\tau_0)$ correspondingly approach $\left(2-\lambda_\infty-2\sqrt{1-\lambda_\infty}\right)/\lambda_\infty$ and zero, where λ_∞ is the limiting value of the scattering coefficient.

An alternative approach to the theory of radiation transfer in inhomogeneous media was developed by Nikoghossian (2012b) by considering the new functions

$$P(\tau_0)=\frac{1}{q(\tau_0)},\qquad S(\tau_0)=\frac{r(\tau_0)}{q(\tau_0)}=r(\tau_0)\,P(\tau_0).\tag{108}$$

From Eq. (105) it is easy to obtain (see e.g., Nikoghossian, 2004, 2004a, b, c)

$$\frac{dP}{d\tau_0}=\left[1-\frac{\lambda(\tau_0)}{2}\right]P(\tau_0)-\frac{\lambda(\tau_0)}{2}S(\tau_0),\tag{109}$$

which is the first of the requisite equations. On the other hand, Eq. (17) and (109) imply

$$\frac{dS}{d\tau_0}=\frac{\lambda(\tau_0)}{2}P(\tau_0)-\left[1-\frac{\lambda(\tau_0)}{2}\right]S(\tau_0),\tag{110}$$

Equations (109) and (110) represent the required linear system of differential equations. It must be supplemented by initial conditions $P(0)=1$, $S(0)=0$, which follow from the similar conditions for the reflection and transmission

doi: doi.org/10.52526/25792776-2021.68.2-186

coefficients. Having solved the system, the quantities $r(\tau_0)$ and $q(\tau_0)$ are readily found from Eq. (108). The system of equations (109) and (110) plays an important role in the theory being put forward.

Note that, if $\lambda(\tau_0)$ is differentiable, Eqs. (109) and (110) may be used to obtain separate differential equations for determining the functions $P(\tau_0)$ and $S(\tau_0)$. Differentiating the mentioned equations, after some simple transformations, we arrive at the following linear differential equations of the second order (Nikoghossian, 2004)

$$\frac{d^2P}{d\tau_0^2} - \frac{\lambda'}{\lambda}\frac{dP}{d\tau} - \left(1 - \lambda - \frac{\lambda'}{\lambda}\right)P(\tau_0) = 0, \tag{111}$$

$$\frac{d^2S}{d\tau_0^2} - \frac{\lambda'}{\lambda}\frac{dS}{d\tau} - \left(1 - \lambda + \frac{\lambda'}{\lambda}\right)S(\tau_0) = 0, \tag{112}$$

respectively, with the initial conditions $P(0) = 1$, $P'(0) = 1 - \frac{\lambda(0)}{2}$, $S(0) = 0$, $S'(0) = \frac{\lambda(0)}{2}$.

In the case of homogeneous atmospheres these equations, like the corresponding density of the Lagrangian, do not contain τ_0 explicitly (i.e., τ_0 is a cyclical coordinate), so that translation of an optical thickness is a symmetry transformation for the system Eqs. (109), (110)). The variation approach proposed in (Krikorian & Nikoghossian, 1996; Nikoghossian, 1999) for equations of this type indicates that this system of equations allows a conservation law of the form

$$[P(\tau_0) - S(\tau_0)]^2 - (1-\lambda)[P(\tau_0) + S(\tau_0)]^2 = \text{const.} \tag{113}$$

The value of the constant is determined from the initial conditions for the functions $P(\tau_0)$ and $S(\tau_0)$ and equals λ. It can be expressed in terms of the reflection and transmission coefficients as

$$\lambda[1 + r(\tau_0)]^2 - 4r(\tau_0) = \lambda q^2(\tau_0). \tag{114}$$

If the explicit dependence of λ on τ_0 is known, then Eqs. (111) and (112) can be solved using one of the available computational schemes for the Cauchy problem for linear differential equations. In order to clarify the particularly mathematical aspect of these results, we must point out the relationship of these equations to Riccati equations. Thus, for example, solving system of Eqs. (109), (110) is equivalent to solving the second order differential equation

$$F''(\tau_0) - [1 - \lambda(\tau_0)]F(\tau_0) = 0 \tag{115}$$

For the function $F(\tau_0) = P(\tau_0) + S(\tau_0)$. The initial conditions will obviously be $F(0) = F'(0) = 1$. On the other hand, it is well known that the substitution $u = F'/F$ yields the following Riccati equation

$$u'(\tau_0) + u^2(\tau_0) = 1 - \lambda(\tau_0). \tag{116}$$

Equations (111), (112) also are reducible to this type of equation. In some cases, solving this system reduces to finding the solution of ordinary differential equations of known types, whose solutions are expressed in terms of special and elementary functions.

One criticism sometimes raised about the applicability of the methods of adding layers and invariant imbedding is that the latter are supposedly not effective for determining the radiation field inside a medium. Here we show that, in fact, these methods make it easy to determine this field as well as a number of other quantities which describe the process of multiple scattering inside a medium.

One can now write the transfer equations in terms of $U(\tau, \tau_0)$ and$V(\tau, \tau_0)$, which represent the probabilities that photon will move at the optical depth τ in the direction of decreasing and increasing optical depths, respectively (see Fig.11):

$$\frac{dU}{d\tau} = \left[1 - \frac{\lambda(\tau)}{2}\right]U(\tau, \tau_0) - \frac{\lambda(\tau)}{2}V(\tau, \tau_0), \tag{117}$$

$$\frac{dV}{d\tau} = \frac{\lambda(\tau)}{2}U(\tau, \tau_0) - \left[1 - \frac{\lambda(\tau)}{2}\right]V(\tau, \tau_0), \tag{118}$$

These equations satisfy the boundary conditions $U(\tau_0, \tau_0) = 1$, $V(0, \tau_0) = 0$. In classical astrophysical problems, the transfer equations are usually reduced to just these kind of boundary-value problems. It is easy to see on comparing the system of Eqs. (117) and (118) with Eqs. (109) and (110) that, as functions of optical depth, the functions U è V satisfy the same equations as the functions P è S of the optical thickness. However, in the first case, we have to deal with a boundary-value problem, and in the second, with an initial-value problem.

doi: doi.org/10.52526/25792776-2021.68.2-186

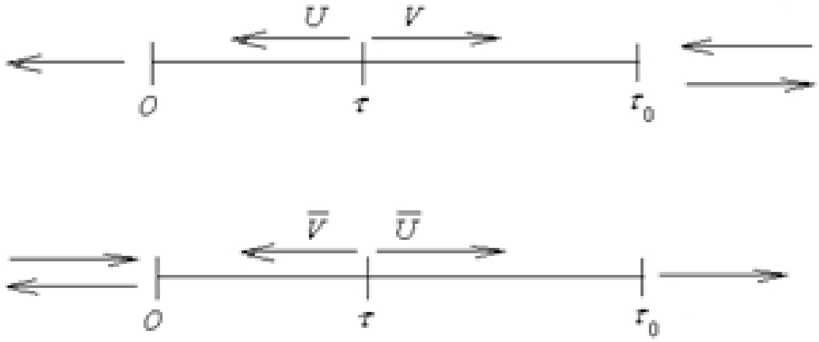

Figure 11: Schematic illustration of radiative transfer in a one-dimensional medium.

Based on some simple physical arguments it is easy to show that

$$q(\tau_0) = q(\tau)\, U(\tau, \tau_0), \qquad V(\tau, \tau_0) = r(\tau)\, U(\tau, \tau_0). \tag{119}$$

These equations follow mathematically by comparing the conditions at the boundary $\tau = 0$, $U(0, \tau_0) = q(\tau_0)$ and $V(0, \tau_0) = 0$, with the same conditions for the functions P and S. In fact, these equations need no proof, since the addition rules for the reflection and transmission coefficients have been derived from them.

Eq. (119) yields

$$U(\tau, \tau_0) = \exp\left[-\int_\tau^{\tau_0} \varpi(\tau')\, d\tau'\right], \qquad V(\tau, \tau_0) = r(\tau) \exp\left[-\int_\tau^{\tau_0} \varpi(\tau')\, d\tau'\right]. \tag{120}$$

Thus, for determining the radiation field inside a medium it is sufficient to first determine the reflectance of a family of atmospheres by solving Eq. (106). It should be noted that, as is clear from the above formulas, the variables τ and τ_0 in expressions for U and V are separated:

$$U(\tau, \tau_0) = q(\tau_0)\, P(\tau), \qquad V(\tau, \tau_0) = q(\tau_0)\, S(\tau). \tag{121}$$

These equations follow mathematically from a comparison of the conditions at the boundary, $U(0, \tau_0) = q(\tau_0)$ and $V(0, \tau_0) = 0$, with the same conditions for the functions P and S.

We see that the radiation field inside the atmosphere is determined entirely by the reflectance and transmittance of its individual parts. In other words, knowledge of the global optical properties for a family of atmospheres with different optical thicknesses, but with a given type of inhomogeneity, can be used for directly determining the radiation intensity at an arbitrary optical depth, without solving any new equations.

Furthermore, the fact that the variables in U and V are separable makes it substantially easier to find these intensities, since the required solution can be obtained immediately for a family of atmospheres with different optical thicknesses. Equations (121) clarify certain features of the radiation field in an atmosphere. Thus, for example, they imply that the radiation fluxes in both directions at some depth τ in atmospheres with different optical thicknesses are proportional to the transmittance of these atmospheres, while the intensities at different depths inside a given atmosphere are proportional to the corresponding opacity $q(\tau)$.

Knowledge of r makes it possible to find explicit solutions for a whole series of problems that are frequently encountered in astrophysical applications. Here we consider a few of them.

a. *Internal energy sources*. Suppose that an inhomogeneous atmosphere contains energy sources of power $B(\tau)$ and it is required to determine the intensity of the radiation emerging from the medium and the radiation field within the medium. If we denote the intensities emerging from the medium through the boundaries $\tau = \tau_0$ and $\tau = 0$ by $I_1(\tau_0)$ and $I_2(\tau_0)$, then, after some simple reasoning, we can write (Nikoghossian, 2004b)

$$I_1(\tau_0) = \frac{1}{2} q(\tau_0) \int_0^{\tau_0} [1 + r(\tau)]\, B(\tau)\, d\tau / q(\tau), \tag{122}$$

$$I_2(\tau_0) = \frac{1}{2} \int_0^{\tau_0} [\lambda(\tau)\, I_1(\tau) + B(\tau)]\, q(\tau)\, d\tau. \tag{123}$$

Knowledge of the latter is sufficient for determining the intensities $I^+(\tau, \tau_0)$, $I^-(\tau, \tau_0)$ of the radiation directed, respectively, toward decreasing and increasing depths, i.e.,

doi: doi.org/10.52526/25792776-2021.68.2-186

$$I^{+}(\tau,\tau_0)=[I_2(\tau_0)-I_2(\tau)]/q(\tau), \tag{124}$$

$$I^{-}(\tau,\tau_0)=r(\tau)I^{+}(\tau,\tau_0)+I_1(\tau). \tag{125}$$

b. *Average number of scattering events*. We introduce the notations $N_r(\tau_0)$, $N_q(\tau_0)$ for the MNSE, respectively, for two categories of photons: reflected and transmitted. It has been shown by (Nikoghossian, 2004b) that these quantities can be completely expressed in terms of the above reflection and transmission coefficients for the family of atmospheres by

$$N_r(\tau_0)=\frac{1}{2}\frac{q^2(\tau_0)}{r(\tau_0)}\int_0^{\tau_0}\lambda(\tau)\left[1+r^2(\tau)\right]\frac{d\tau}{q^2(\tau)}, \tag{126}$$

$$N_q(\tau_0)=\frac{1}{2}\int_0^{\tau_0}\lambda(\tau)\{1+r(\tau)[1+N_r(\tau)]\}\,d\tau. \tag{127}$$

c. *Reflection from the opposite boundary*. For completeness, here we also give the formula for the reflection coefficient of this medium when it is illuminated from the side of the boundary $\tau=0$ in Fig.10. It was shown (Nikoghossian, 2004, 2004a,b,c), that

$$\bar{r}(\tau_0)=\frac{1}{2}\int_0^{\tau_0}\lambda(\tau)q^2(\tau)\,d\tau=\frac{1}{2}\int_0^{\tau_0}\lambda(\tau)e^{-2\int_0^{\tau}\varpi(\tau')d\tau'}d\tau. \tag{128}$$

Thus, we can note the major conclusion of this section: *in order to solve the scalar problem of the radiation transfer in inhomogeneous atmosphere it is enough to know its reflectivity, since all the other quantities of interest are found explicitly.*

xvii. Group-theoretical description of radiative transfer.

Media composition groups. ***Scalar case***. Ambarsumian's method of addition of layers was further developed by Nikoghossian (2011a; 2014a,b; 2016, 2019), where, for the first time, the group theory was applied to solve the problems of radiative transfer in inhomogeneous absorbing and scattering atmospheres. It was introduced the concept of a composition or transformation of scattering and absorbing atmospheres, which involves the adding of an additional atmosphere to an initial one in the general case of an inhomogeneous atmosphere (or removing some part from an initial atmosphere). It was assumed that the added or subtracted parts do not contain primary energy sources. The transformations induced in this way form a group if the group product is taken to mean the resultant of two successive transformations. It is easy to see that the other conditions for formation of a group are satisfied. In particular, the role of a unit element is the identity transformation, which leaves the initial atmosphere unchanged, and the inverse elements are transformations which reverse the effect of one or another already performed transformation. The associativity of the group product is evident. This group of transformations was referred to as the GN2 group. It is easy to see that, in general, it is not commutative. Among this type of groups, an important role is played by groups associated with the formation of a multicomponent atmosphere. In that case, the transformation is taken to mean the addition (or removal) of a homogeneous medium characterized by an optical thickness and a scattering coefficient λ. This group (referred to as GNH2) is a two-parameter, noncommutative group. The special case where λ is the same for all the added or removed media (group GH2) yields the case of homogeneous atmospheres. In this case, the group is obviously commutative, i.e., is abelian (Wigner, 1961). It is also a one-parameter, infinite, and continuous group.

Every homogeneous medium of optical thickness τ_0 can be characterized by two quantities, the reflection $r(\tau_0)$ and transmission $q(\tau_0)$ coefficients, which have a probabilistic meaning. At the same time, it has been shown (Nikoghossian 2004, 2004a) that an inhomogeneous atmosphere has a polarity property, i.e., its optical properties are described by three parameters: two reflection coefficients and one transmission coefficient. Turning again to Fig.10 and the layers adding laws Eq. (103), Eq. (104), one can rewrite these laws in terms of functions P, S, $\bar{S}$. These were derived in (Nikoghossian, 2011a) and read as

$$P(\tau_1+\tau_2)=P(\tau_1)P(\tau_2)-S(\tau_1)\bar{S}(\tau_2), \tag{129}$$

$$S(\tau_1+\tau_2)=P(\tau_1)S(\tau_2)+S(\tau_1)M(\tau_2), \tag{130}$$

where $M(\tau)=[1-S(\tau)S(\tau)]/P(\tau)$. Similarly,

$$\bar{S}(\tau_1+\tau_2)=P(\tau_2)\bar{S}(\tau_1)+\bar{S}(\tau_2)M(\tau_1). \tag{131}$$

It can be confirmed by direct testing that there is also an addition law for $M(\tau)$,

doi: doi.org/10.52526/25792776-2021.68.2-186

$$M(\tau_1 + \tau_2) = M(\tau_1) M(\tau_2) - S(\tau_1) \bar{S}(\tau_2). \tag{132}$$

On introducing the matrices

$$A(\tau) = \begin{pmatrix} P(\tau) & -\bar{S}(\tau) \\ S(\tau) & M(\tau) \end{pmatrix}, \tag{133}$$

it is easy to confirm that they also constitute a group and form a representation of the group GN2. In fact, each element of the group GN2 corresponds to a transformation $T(g)$,

$$\begin{pmatrix} P(\tau_1+\tau_2) \\ S(\tau_1+\tau_2) \end{pmatrix} = \begin{pmatrix} P(\tau_2) & -\bar{S}(\tau_2) \\ S(\tau_2) & M(\tau_2) \end{pmatrix} \begin{pmatrix} P(\tau_1) \\ S(\tau_1) \end{pmatrix}, \tag{134}$$

if the medium is illuminated from the right, and $T'(g)$,

$$\begin{pmatrix} P(\tau_1+\tau_2) \\ \bar{S}(\tau_1+\tau_2) \end{pmatrix} = \begin{pmatrix} P(\tau_1) & -S(\tau_1) \\ \bar{S}(\tau_1) & M(\tau_1) \end{pmatrix} \begin{pmatrix} P(\tau_2) \\ \bar{S}(\tau_2) \end{pmatrix}, \tag{135}$$

in the opposite case.

In addition, the group product $g_1 \otimes g_2$ corresponds to the matrix product $A(\tau_1+\tau_2) = A(\tau_2) A(\tau_1)$, i.e., $T(g_1 \otimes g_2) = T(g_2) T(g_1)$, for illumination from the right and $\tilde{A}(\tau_1+\tau_2) = \tilde{A}(\tau_1) \tilde{A}(\tau_2)$, i.e., $T'(g_1 \otimes g_2) = T'(g_1) T'(g_2)$, for illumination from the left. (Here a tilde denotes the transposed matrix.) The identity transformation obviously corresponds to the unit matrix: $T(e) = \mathbf{E}$ and $T'(e) = \mathbf{E}$. The matrix $\mathbf{A}(\tau)$ is nonsingular (its determinant equals 1), so inverse matrices exist, with

$$A^{-1}(\tau) = \begin{pmatrix} M(\tau) & S(\tau) \\ -\bar{S}(\tau) & P(\tau) \end{pmatrix}, \tilde{A}^{-1}(\tau) = \begin{pmatrix} M(\tau) & \bar{S}(\tau) \\ -S(\tau) & P(\tau) \end{pmatrix}. \tag{136}$$

These two group representations are isomorphic, since the correspondence between the groups GN2 and $T(g)$, as well as between GN2 and $T'(g)$, are mutually unique.

The vector-matrix case. Up to now the discussion was restricted to the simplest scalar problem for one-dimensional media. It was shown by Nikoghossian (2014a,b,c) that the results can be generalized to the matrix case, which covers a wide range of astrophysical problems in which the spatial and frequency distributions of the radiation field are taken into account. Besides its purely theoretical significance, this generalization is of great practical importance since it makes it possible to develop new methods for numerical solution of many extremely complicated astrophysical problems. In particular, these include the formation of spectral lines in media with various kinds of inhomogeneities, particularly, in those with fine structure that can be observed with the aid of powerful modern instrumentation.

In general, the adding media can differ from one another in optical thickness, as well as in the character of their inhomogeneity related to variations in different parameters that control elementary scattering event, such as the absorption profile, scattering coefficient, scattering indicatrix, frequency distribution of the radiation, degree of polarization, etc. The matrix case described in the above-mentioned works includes both the diffusion of radiation in a three-dimensional plane-parallel medium, and in a one-dimensional medium where the frequency redistribution of the radiation is taken into account. The results were presented for the last of these two cases with partial frequency redistribution where the inhomogeneity of the atmosphere resulting from by variations in the scattering coefficient within it. As above, the composition or transformation of absorbing and scattering atmospheres was taken to mean adding another, generally, inhomogeneous atmosphere to one of the sides of an initial atmosphere. These transformations form a group if the group product (a binary operation) in it signifies the result of two successive transformations. Everything stated above for 1D case relating to the conditions for formation of a group in the scalar problem remains in force in the matrix case examined here. This generalized version of the composition group was referred nominally to as a GN(2,C) group which, like the GN(2) group in the scalar problem is infinite and, in general, noncommutative. The set of atmospheres obtained as a result of a described composition will evidently consist of multicomponent atmospheres with inhomogeneous components. There are two subgroups of GN(2,C), both of which are of independent interest. The first is related to the composition of *homogeneous* media, which differ from one another not only in thickness, but also in several optical properties that characterize the diffusion process in it. These groups referred to as GNH(2,C) are noncommutative and two, three-, or multicomponent, depending on the number of parameters that vary on going from one medium to another. This sort of multicomponent media, in which each component is homogeneous and differs from the others in its optical characteristics, can serve as a prototype for an entire series of real radiative media that are often encountered in astrophysical applications.

doi: doi.org/10.52526/25792776-2021.68.2-186

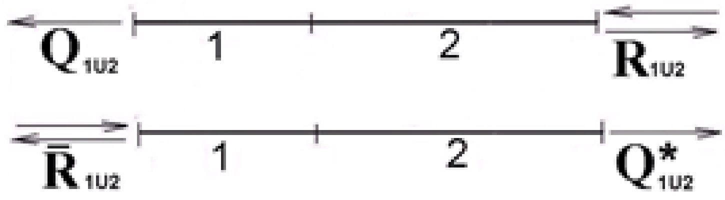

Figure 12: Reflection and transmission in an inhomogeneous two-component atmosphere.

The second subgroup is contained in the first and refers to the case when the added layers have the same properties and differ from one another only in their thicknesses (group GH(2,C)). Obviously, any transformation in this case yields only homogeneous media. This kind of group is commutative (abelian), one-parameter, infinite, and continuous with the continuously varying optical thickness.

Fig. 12 demonstrates a configuration consisting of two media, which differ from one another generally in optical thickness and in the functional behavior of their parameters which determine an elementary scattering event. This means that both components are inhomogeneous, so they have the property of polarity. As opposed to the scalar case, the reflection and transmission coefficients now depend on frequency (and also on direction in three-dimensional problems), as well as on thickness; thus, it is convenient to write them down in operator form. These coefficients are denoted, respectively, by $\mathbf{R}_i$, $\mathbf{Q}_i$ ($i = 1, 2$) when the medium is illuminated from the right (top drawing in Fig. 8) and by $\mathbf{R}_i$ and $\mathbf{Q}_i$ when the medium is illuminated from the left (bottom drawing). We recall also that $\mathbf{Q}_i = \mathbf{Q}_i^*$, where the asterisk denotes the transposed matrix. Thus, in the following discussion one shall adhere to the notation $\mathbf{Q}_i^*$.

Along with the transmission coefficients $\mathbf{Q}_i$, their inverse matrices $\mathbf{P}_i = \mathbf{Q}_i^{-1}$, $\mathbf{P}_i^* = \left(\mathbf{Q}_i^*\right)^{-1}$, (they exist because the matrix $\mathbf{Q}_i$ is nondegenerate) the matrices $\mathbf{S}_i = \mathbf{R}_i\mathbf{P}_i$ and $\mathbf{\bar{S}_i} = \mathbf{P_i\bar{R}_i}$ play an important role in the developed theory The matrix analogs of addition laws Eqs.(129, 130) are written as follows

$$\mathbf{P}_{1\cup 2} = \mathbf{P}_2\mathbf{P}_1 - \mathbf{\bar{S}}_2\mathbf{S}_1, \qquad \mathbf{S}_{1\cup 2} = \mathbf{S}_2\mathbf{P}_1 + \mathbf{M}_2\mathbf{S}_1 \tag{137}$$

where $\mathbf{M} = \mathbf{Q}^* - \mathbf{S}\mathbf{\bar{R}}$.

Using the concept of supermatrices (Berezin, 1986; Wigner, 1961), Eqs. (137) can be combined and written in the form

$$\begin{pmatrix} \mathbf{P}_{1\cup 2} \\ \mathbf{S}_{1\cup 2} \end{pmatrix} = \begin{pmatrix} \mathbf{P}_2 & -\mathbf{\bar{S}}_2 \\ \mathbf{S}_2 & \mathbf{M}_2 \end{pmatrix} \begin{pmatrix} \mathbf{P}_1 \\ \mathbf{S}_1 \end{pmatrix}. \tag{138}$$

It is introduced the notation

$$\mathbf{\tilde{A}} = \begin{pmatrix} \mathbf{P} & -\mathbf{\bar{S}} \\ \mathbf{S} & \mathbf{M} \end{pmatrix}, \tag{139}$$

where the tilde means that a quantity is a supermatrix (or, as it is still customarily called, a cell or block matrix).

One can see that the supermatrices $\mathbf{\tilde{A}_i}$ also form a group and are representations of the group GN(2,C) that maps it in a linear supervector space. It is important to note that the technique for composition of absorbing and scattering media described by $\mathbf{\tilde{A}_i}$ (the transformation g) does not depend on that what of some particular parameters is responsible for inhomogeneity. Thus, these results apply equally to the media with components that have of different kind inhomogeneity.

It is easy to understand that the transformation Eq.(138) only provides a partial answer about the optical properties of the resultant atmosphere. It can be used to determine the reflectivity and transmission of a medium only from the side on which it is illuminated; this can be regarded as sufficient only in the case of a homogeneous atmosphere. To find the lacking properties of the resultant atmosphere, we proceed as follows. It is evident that adding new media twice on the right to an initial layer is equivalent to taking the product of matrices (139). This yields the addition rules for $\mathbf{\bar{S}}$ and $\mathbf{M}$,

$$\mathbf{\bar{S}}_{1\cup 2} = \mathbf{P}_2\mathbf{\bar{S}}_1 + \mathbf{\bar{S}}_2\mathbf{M}_1, \qquad \mathbf{M}_{1\cup 2} = \mathbf{M}_2\mathbf{M}_1 - \mathbf{S}_2\mathbf{\bar{S}}_1. \tag{140}$$

Equations (xv.12) can now be written in vector-matrix form as

$$\begin{pmatrix} \mathbf{M}_{1\cup 2} \\ \mathbf{\bar{S}}_{1\cup 2} \end{pmatrix} = \begin{pmatrix} \mathbf{M}_2 & -\mathbf{S}_2 \\ \mathbf{\bar{S}}_2 & \mathbf{P}_2 \end{pmatrix} \begin{pmatrix} \mathbf{M}_1 \\ \mathbf{\bar{S}}_1 \end{pmatrix}. \tag{141}$$

Thus, we arrive at yet another representation of the transformation g by means of the supermatrix

doi: doi.org/10.52526/25792776-2021.68.2-186

$$\tilde{\mathbf{B}} = \begin{pmatrix} \mathbf{M} & -\mathbf{S} \\ \overline{\mathbf{S}} & \mathbf{P} \end{pmatrix}. \tag{142}$$

The notations $T(g)$and $\overline{T}(g)$ are introduced to denote the above representations of the group GN(2,C) corresponding to transformations of the initial medium from the right. Then the group products $g_1 \otimes g_2$ will correspond to the supermatrix products $\tilde{\mathbf{A}}_{1\bigcup 2} = \tilde{\mathbf{A}}_2\tilde{\mathbf{A}}_1$ and $\tilde{\mathbf{B}}_{1\bigcup 2} = \tilde{\mathbf{B}}_1\tilde{\mathbf{B}}_2$, i.e., $T(g_1 \otimes g_2) = T(g_2)\,T(g_1))$ and $\overline{T}(g_1 \otimes g_2) = \overline{T}(g_2)\,\overline{T}(g_1)$. The identity transformation e corresponds to the supermatrix

$$\tilde{\mathbf{E}} = \begin{pmatrix} \mathbf{I} & \mathbf{0} \\ \mathbf{0} & \mathbf{I} \end{pmatrix}, \tag{143}$$

where $\mathbf{I}$ is the unit matrix.

The representations Eq.(139) and Eq.(142) found above are isomorphic to the group GN(2,C), since the correspondence between this group and $T(g)$, $\overline{T}(g)$ is mutually unique and the product of any two elements from GN(2,C) corresponds to matrix multiplications of the corresponding representations of this group. These two representations can be combined and written in the form of the reducible representation

$$\begin{pmatrix} \mathbf{P}_{1\bigcup 2} \\ \mathbf{S}_{1\bigcup 2} \\ \mathbf{M}_{1\bigcup 2} \\ \overline{\mathbf{S}}_{1\bigcup 2} \end{pmatrix} = \begin{pmatrix} \mathbf{P}_2 & -\overline{\mathbf{S}}_2 & \mathbf{0} & \mathbf{0} \\ \mathbf{S}_2 & \mathbf{M}_2 & \mathbf{0} & \mathbf{0} \\ \mathbf{0} & \mathbf{0} & \mathbf{M}_2 & -\mathbf{S}_2 \\ \mathbf{0} & \mathbf{0} & \overline{\mathbf{S}}_2 & \mathbf{P}_2 \end{pmatrix} \begin{pmatrix} \mathbf{P}_1 \\ \mathbf{S}_1 \\ \mathbf{M}_1 \\ \overline{\mathbf{S}}_1 \end{pmatrix}, \tag{144}$$

with $\mathbf{P}(\mathbf{0}) = \mathbf{M}(\mathbf{0}) = \mathbf{I}$, $\mathbf{S}(\mathbf{0}) = \overline{\mathbf{S}}(\mathbf{0}) = \mathbf{0}$.

Therefore, it is concluded that the ordinary matrix multiplication can be used to determine the quantities expressing the reflectivity and transmittance of a composite atmosphere if these parameters of its components are known. Evidently, in the case of a homogeneous medium, it is sufficient to consider the transformation Eq. (138) instead of Eq. (144).

When the composite medium is illuminated from its left boundary (bottom drawing of Fig.12), the composition transformation reads

$$\begin{pmatrix} \mathbf{P}^*_{1\bigcup 2} \\ \overline{\mathbf{S}}^*_{1\bigcup 2} \end{pmatrix} = \begin{pmatrix} \mathbf{P}^*_1 & -\mathbf{S}^*_1 \\ \overline{\mathbf{S}}^*_1 & \mathbf{M}^*_1 \end{pmatrix} \begin{pmatrix} \mathbf{P}^*_2 \\ \overline{\mathbf{S}}^*_2 \end{pmatrix}. \tag{145}$$

Finally, instead of Eq. (141), it is obtained

$$\begin{pmatrix} \mathbf{M}^*_{1\bigcup 2} \\ \mathbf{S}^*_{1\bigcup 2} \end{pmatrix} = \begin{pmatrix} \mathbf{M}^*_1 & -\overline{\mathbf{S}}^*_1 \\ \mathbf{S}^*_1 & \mathbf{P}^*_1 \end{pmatrix} \begin{pmatrix} \mathbf{M}^*_2 \\ \mathbf{S}^*_2 \end{pmatrix}. \tag{146}$$

Thus, there was found two new representations of the group GN(2,C) that describe the transformation of the global optical characteristics of a composite atmosphere illuminated on its left boundary $\tau = 0$

$$\tilde{\mathbf{C}} = \begin{pmatrix} \mathbf{P}^* & -\mathbf{S}^* \\ \overline{\mathbf{S}}^* & \mathbf{M}^* \end{pmatrix}. \qquad \tilde{\mathbf{D}} = \begin{pmatrix} \mathbf{M}^* & -\overline{\mathbf{S}}^* \\ \mathbf{S}^* & \mathbf{P}^* \end{pmatrix}. \tag{147}$$

As it was proofed by Nikoghossian (2019), the superdeterminants (Berezinians) of all the supermatrices $\tilde{\mathbf{A}}$, $\tilde{\mathbf{B}}$, $\tilde{\mathbf{C}}$ and $\tilde{\mathbf{D}}$ are equal to unity, so that both two-sided inverse matrices of them exist. Here are these matrices

$$\tilde{\mathbf{A}}^{-1} = \begin{pmatrix} \mathbf{M}^* & \overline{\mathbf{S}}^* \\ -\mathbf{S}^* & \mathbf{P}^* \end{pmatrix}, \qquad \tilde{\mathbf{B}}^{-1} = \begin{pmatrix} \mathbf{P}^* & \mathbf{S}^* \\ -\overline{\mathbf{S}}^* & \mathbf{M}^* \end{pmatrix}, \qquad \tilde{\mathbf{C}}^{-1} = \begin{pmatrix} \mathbf{M} & \mathbf{S} \\ -\overline{\mathbf{S}} & \mathbf{P} \end{pmatrix}. \qquad \tilde{\mathbf{D}}^{-1} = \begin{pmatrix} \mathbf{P} & \overline{\mathbf{S}} \\ -\mathbf{S} & \mathbf{M} \end{pmatrix}. \tag{148}$$

These supermatrices are fundamental in the developed theory since they establish the laws of transformation of global optical characteristics in composing scattering and absorbing media. All of them have a number of common properties: they are non-singular (non-degenerate) and have invariant superdeterminants equal to unity. In other words, *the only global invariant during composition of media of arbitrary optical thickness is the superdeterminant of the corresponding transformation operator. Physically, this is a consequence of the invertibility property of optical phenomena.* This result can be illustrated using the geometric significance of the determinant of an ordinary two-dimensional matrix (Fig. 13).

The theory developed in (Nikoghossian, 2011, 2014a] has been applied to the problem of diffusive reflection of line radiation from an atmosphere of finite thickness with partial frequency redistribution. Transformations of the group GNH(2,C) make it possible to construct a multicomponent atmosphere with a certain optical thickness τ_0, the

doi: doi.org/10.52526/25792776-2021.68.2-186

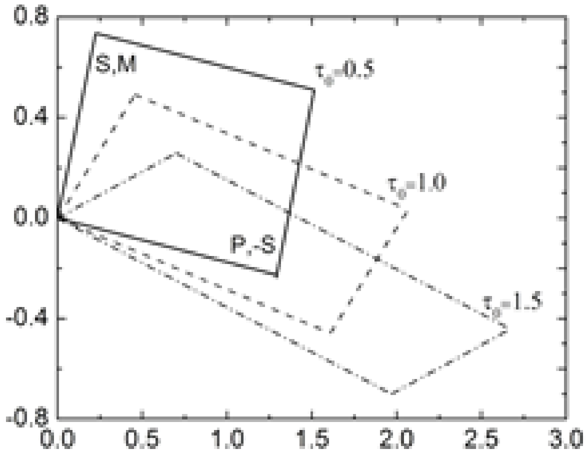

Figure 13: Geometrical interpretation of the determinant of a scalar matrix $\tilde{A}$ for several values of the optical thickness.

components of which can be distinguished by their physical characteristics. As an example, it was examined a one-dimensional, inhomogeneous medium illuminated on the side at a boundary $\tau = \tau_0$. It was assumed that medium is composed of components of equal and quite small thickness, which are characterized by constant values of the scattering coefficient λ such that it can be regarded as a continuous function of optical depth in the limit when the thickness of the components goes to zero. For the infinitesimal operator of the group $\tilde{A}$ with the parameter equal to τ_0, it was obtained

$$\tilde{\mathbf{\Xi}}(\tau_0) = \lim_{\Delta\tau_0 \to 0} \frac{\tilde{\mathbf{A}}(\tau_0 + \Delta\tau_0) - \tilde{\mathbf{A}}(\tau_0)}{\Delta\tau_0} = \begin{pmatrix} \mathbf{m}(\tau_0) & -\mathbf{n}(\tau_0) \\ \mathbf{n}(\tau_0) & -\mathbf{m}(\tau_0) \end{pmatrix}, \tag{149}$$

where

$$\mathbf{m}(\tau_0) = \boldsymbol{\alpha} - \frac{\lambda(\tau_0)}{2}\mathbf{\Gamma}, \qquad \mathbf{n}(\tau_0) = \frac{\lambda(\tau_0)}{2}\mathbf{\Gamma}. \tag{150}$$

and $\boldsymbol{\alpha}$ and $\mathbf{\Gamma}$ are the discrete analogs of the scattering coefficient profile in the line and the frequency redistribution law, respectively. It is assumed for simplicity that both of these quantities are independent of optical thickness. $\boldsymbol{\alpha}$ is a diagonal matrix with elements $\alpha_{\mathbf{i}} = \alpha(\mathbf{x_i})$.

Eq. (149) leads to the system of equations (Nikoghossian, 2013, 2014a]

$$\frac{d\mathbf{P}}{d\tau_0} = \mathbf{m}(\tau_0)\mathbf{P}(\tau_0) - \mathbf{n}(\tau_0)\mathbf{S}(\tau_0), \tag{151}$$

$$\frac{d\mathbf{S}}{d\tau_0} = \mathbf{n}(\tau_0)\mathbf{P}(\tau_0) - \mathbf{m}(\tau_0)\mathbf{S}(\tau_0), \tag{152}$$

with initial conditions $\mathbf{P}(0) = \mathbf{I}$ and $\mathbf{S}(0) = \mathbf{0}$, where $\mathbf{0}$ is the zero matrix.

The matrix $\mathbf{P}(\tau_0)$ obtained by solving the system of Eqs. (151), (152) can be inverted to determine the desired values of the reflection and transmission coefficients of the medium. The analogous system for the rest of other properties of the medium reads

$$\frac{d\mathbf{M}}{d\tau_0} = -\mathbf{m}(\tau_0)\mathbf{M}(\tau_0) - \mathbf{n}(\tau_0)\overline{\mathbf{S}}(\tau_0), \tag{153}$$

$$\frac{d\overline{\mathbf{S}}}{d\tau_0} = \mathbf{n}(\tau_0)\mathbf{M}(\tau_0) + \mathbf{m}(\tau_0)\overline{\mathbf{S}}(\tau_0). \tag{154}$$

with the initial conditions $\mathbf{M}(0) = \mathbf{I}$ and $\mathbf{S}(0) = \mathbf{0}$.

If the medium is homogeneous, then it is sufficient to limit ourselves to the system of Eqs. (151) and (152), the solution of which can be written in the form of a series expansion of the matrix exponential

$$\mathbf{P}(\tau_0) = \mathbf{I} + \left(\boldsymbol{\alpha} - \frac{\lambda}{2}\mathbf{\Gamma}\right)\frac{\tau_0}{1!} + \left[\boldsymbol{\alpha}^2 - \frac{\lambda}{2}(\mathbf{\Gamma}\boldsymbol{\alpha} - \boldsymbol{\alpha}\mathbf{\Gamma})\right]\frac{\tau_0^2}{2!} + \ldots, \tag{155}$$

doi: doi.org/10.52526/25792776-2021.68.2-186

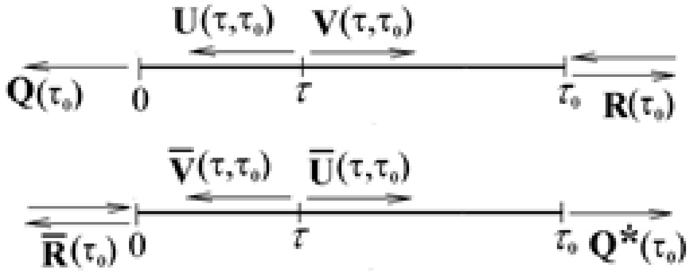

Figure 14: Illustrating the determination of a radiation field inside a medium.

$$\mathbf{S}(\tau_0) = \mathbf{R}(\tau_0)\,\mathbf{P}(\tau_0) = \frac{\lambda}{2}\boldsymbol{\Gamma}\frac{\tau_0}{1!} + \frac{\lambda}{2}(\boldsymbol{\Gamma}\boldsymbol{\alpha} - \boldsymbol{\alpha}\boldsymbol{\Gamma})\frac{\tau_0^2}{2!} + ..., \tag{156}$$

Depths translation groups. The group-theoretical description of radiation fields in inhomogeneous atmospheres was developed in (Nikoghossian, 2014b). A definition of the group of optical depth translations was given and demonstrated its equivalence to the group of compositions of atmospheres. The transition from one optical depth to another by attaching a new layer to it is, in fact, an infinite set of translations of this kind and forms a group, since if the group product is taken to be the result of two successive translations, then it will satisfy all the group postulates. In accord with the physical significance of the problem, the values of the optical depth obtained as the result of translations should not exceed the optical thickness of the medium being considered ($\tau \leq \tau_0$). This group, as a subset of the GN(2,C) group, is equivalent to the analogous subgroup introduced in the first part of this paper for a composition of media with different optical thicknesses.

The theory was applied, as above, to an inhomogeneous plane-parallel atmosphere of optical thickness τ_0 illuminated from the side of the boundary $\tau = \tau_0$ (top sketch in Fig. 14). In general, scattering in this medium can be accompanied by redistribution with respect to both frequency and direction. To describe the radiation field inside the atmosphere, it is introduced the matrices $\mathbf{U}(\tau, \tau_0)$ and $\mathbf{V}(\tau, \tau_0)$, which specify the probability that a photon with spatial - frequency characteristics (η, x) incident on the boundary at $\tau = \tau_0$ will, as a result of diffusion, end up at depth τ, moving, respectively, toward the boundaries $\tau = 0$. $\tau = \tau_0$ generally with some other characteristics $\eta\prime, x\prime$.

Given the probabilistic significance of $\mathbf{U}(\tau, \tau_0)$ and $\mathbf{V}(\tau, \tau_0)$, one can write

$$\mathbf{Q}(\tau_0) = \mathbf{Q}(\tau)\,\mathbf{U}(\tau, \tau_0), \qquad \mathbf{V}(\tau, \tau_0) = \mathbf{R}(\tau)\,\mathbf{U}(\tau, \tau_0), \tag{157}$$

which implies that

$$\mathbf{U}(\tau, \tau_0) = \mathbf{P}(\tau)\,\mathbf{Q}(\tau_0), \qquad \mathbf{V}(\tau, \tau_0) = \mathbf{S}(\tau)\,\mathbf{Q}(\tau_0). \tag{158}$$

It is seen that in a vector-matrix formulation, the variables in $\mathbf{U}(\tau, \tau_0)$ and $\mathbf{V}(\tau, \tau_0)$ are separated, which is one of the advantages of the approach we are using.

It follows directly from Eq. (158) that the subgroup of the representations $\Im(g)$ corresponding to the composition of media with different optical thicknesses is, at the same time, *the group of representations for translations of optical depths*. Note that, in this sense, a group of compositions of media with different thicknesses can be referred to nominally as a *group of translations of optical thicknesses*. Therefore, the supermatrix $\tilde{\mathcal{A}}$ plays a fundamental role, both when combining atmospheres with different optical thicknesses and for optical depths translation of radiation field inside a specified inhomogeneous atmosphere. In other words, it can be regarded simultaneously as the “composer” (former) of an inhomogeneous atmosphere and the “translator” for the transition from one depth of the medium to another.

It is important to note that, as Eq.(158) implies, in the transition from one depth to another only the global optical characteristics of the added layer are important, while the characteristics of the radiation field within the layer play no role in this transformation. Here it does not matter what particular parameter or parameters have changed to produce the inhomogeneity of the medium. Thus, the approach described here is also suitable for problems involving atmospheres that have different kinds of inhomogeneities and have arbitrary distributions.

Eq.(158) and translation rules ((151), (152)) lead to the ordinary transfer equations for the operator functions **U** and **V**,

$$\frac{d\mathbf{U}}{d\tau} = \mathbf{m}(\tau)\,\mathbf{U}(\tau, \tau_0) - \mathbf{n}(\tau)\,\mathbf{V}(\tau, \tau_0), \tag{159}$$

$$\frac{d\mathbf{V}}{d\tau} = \mathbf{n}(\tau)\,\mathbf{U}(\tau,\tau_0) - \mathbf{m}(\tau)\,\mathbf{V}(\tau,\tau_0)\,. \tag{160}$$

with initial conditions $\mathbf{U}(\mathbf{0},\tau_0) = \mathbf{Q}(\tau_0)$, $\mathbf{V}(\mathbf{0},\tau_0) = \mathbf{0}$.

It is easy to see that the group of translations of the optical depths in this problem is the same as the subgroup of the group of compositions of media GNH(2,C) introduced above. This implies that, when determining the radiation field inside a medium, it is possible to proceed without solving any new equations, since it can be found using the results obtained in constructing a given medium by composition of proper layers and multiplying the found value of $\mathbf{Q}(\tau_0)$ by the values of $\mathbf{P}$ and $\mathbf{S}$ obtained in intermediate calculations.

The far reaching analogy between the group GN(2,C) and the group of translations of optical depths makes it possible to transfer various results for the global optical characteristics of atmospheres to the case of quantities describing the radiation field within them.

Thus, the media composition groups and their representations generalize the layers adding method, which now covers inhomogeneous, particularly multi-component, atmospheres with allowance of the angle and frequency distribution of the radiation field. The group representations being expressed in terms of some combined discrete quantities allow to find the most general summation laws for reflectance and transmittance of the plane-parallel media. This confirms the importance of the approach proposed in (Nikoghossian, 2013b,c), according to which for determination of the radiation field in the medium one must preliminary find its global optical properties. This contrasted with the approach adopted in the classical transfer theory. Usage of composers facilitates solution of a rather broad class of the line-formation problems by reducing the most part of computations to the simple algebraic operations with matrices. The efficacy of the approach becomes more discernable in the case of multi-component atmospheres often encountered in astrophysical applications.

Employment of infinitesimal operators of the introduced groups makes it possible to establish the close connection of the introduced groups with the classical transfer equations and the equations ensuing from invariant imbedding. In fact, the first of them are connected with the depth translation groups, while the second - with composition groups for media of different optical thicknesses.

The developed theory facilitates solution of some other standard transfer problems of astrophysical importance as, for instance, the problem of multiple scattering in inhomogeneous atmosphere with internal energy sources or in a semi-infinite atmosphere, the problem of finding different statistical mean quantities, characteristics of the radiation diffusion and so on. The theory is of sufficiently great generality since it does not depend on the nature of inhomogeneity of the media, as well as on the angle and frequency distribution of the radiation field.

Hamilton's principle. It was shown (Nikoghossian, 2014b) that differential representations of composition and translation groups reduce the solution of the radiation transfer problems to systems of linear differential equations with initial conditions. The first of these for a homogeneous atmosphere is given by Eqs.(151,152), and the second by (Eqs. (159), (160)).

The linear system of Eqs. (151,152) is analogous to non-linear equations obtained by invariant imbedding (Chandrasekhar, 1960; Sobolev, 1963; Bellman & Wing, 1973). At the same time, (Eqs. (159), (160)) are the classical radiative transfer equations. If the first of these two systems is first solved and the transmission coefficient is known, then the transport problem (Eqs. (159), (160)) can be formulated as a problem with initial conditions. *Mathematically, we are dealing with one and the same system of equations with different initial conditions; this is because of the simple relationships coupling the global optical characteristics of the medium and the quantities describing the emission regime inside the medium.* Systems of equations of this type can be reduced to a second order matrix differential equation

$$\mathbf{\Phi}'' = \mathbf{k}^2\mathbf{\Phi}, \tag{161}$$

with appropriate initial conditions; then $k^2 = (\alpha - 2n)\,\alpha$. In the first case, here Φ signifies $\mathbf{P} + \mathbf{S}$ and, in the second, $\mathbf{U} + \mathbf{V}$. The operator acting in Eq. (161) is self-adjoint (potential), so a variational principle can be applied to this type of problem (Vainberg, 1964). This possibility is important for the theory of radiative transfer. A variational formulation of these problems of continuum physics is the shortest way to clarify the general physical laws of the phenomena being studied and interpret them. Generalized expressions for the Lagrangian density and the Euler-Lagrange equation can be written in this case for the matrix-vector operator in Eq. (161) (Nikoghossian, 2014a):

$$L(\mathbf{\Phi},\mathbf{\Phi}',\mathbf{k},\tau_0) = \mathbf{\Phi}^2 + \mathbf{k}^{-2}\mathbf{\Phi}'^2, \tag{162}$$

$$\frac{d}{d\tau}\frac{\partial L}{\partial \mathbf{\Phi}'} - \frac{\partial L}{\partial \mathbf{\Phi}} = 0. \tag{163}$$

doi: doi.org/10.52526/25792776-2021.68.2-186

For the two problems being discussed here, the Hamilton's principle (by analogy with the principle of the least action in analytic mechanics) is written in the form

$$\delta \int \Lambda\left(\Phi, \mathbf{\Phi}', \mathbf{k}, \tau_{\mathbf{0}}\right) d\tau_0 = 0, \qquad \delta \int \Lambda\left(\mathbf{\Phi}, \mathbf{\Phi}', \mathbf{k}, \tau\right) d\tau = 0, \tag{164}$$

where Λ is the Lagrangian.

It is easy to see that these generalized formulas have a significance analogous to that in the scalar problem. Mathematically, this general approach is extremely important, since it covers an extremely wide circle of physical problems. One example is the diffuse reflection and transmission of a three-dimensional medium with isotropic scattering considered in Sect. 5.xi (Nikoghossian, 1999).

Conservation laws. Quadratic and bilinear integrals. The characteristic feature of the matrix equation Eq. (161) is that the optical thickness of the medium and the optical depth do not appear explicitly in it. In other words, these quantities are cyclic coordinates, which leads to conservation laws expressed as constancy of the Hamiltonian, i.e.,

$$\sum \left(L - \frac{\partial L}{\partial \mathbf{\Phi}'}\mathbf{\Phi}'\right) = \text{const}, \tag{165}$$

or

$$\sum \left(\mathbf{\Phi}^2 - \mathbf{k}^{-2}\mathbf{\Phi}'^2\right) = \text{const}. \tag{166}$$

For the above three-dimensional problem of isotropic scattering, Eq. (166) takes the form

$$\int_0^1 \left[\Phi^2 - (\eta\Phi')^2 - \lambda\Phi J\right] d\eta = \text{const}. \tag{167}$$

In considering the internal radiation regime, we have $\Phi = U + V$, and $\eta\Phi' = U - V$, so that Eq. (161) yields

$$\int_0^1 U(\tau,\eta,\mu;\tau_0)\, V(\tau,\eta,\mu;\tau_0)\, d\eta - \frac{\lambda}{4}\left(\int_0^1 \left(U(\tau,\eta,\mu;\tau_0) + V(\tau,\eta,\mu;\tau_0)\right) d\eta\right)^2 = \text{const}. \tag{168}$$

This equation is the so-called Q integral of Rybicky (1977) written in our notation. The constant of integration is found from the boundary conditions: it equals

$$\text{const} = -\frac{\lambda}{4}\left(\int_0^1 Q(\eta,\mu,\tau_0)\, d\eta\right)^2, \tag{169}$$

for a finite medium and zero for an infinite medium. This dependence can be dealt with most easily in a physical sense if we examine the scalar analog of the problem. Then Eq. (168) yields

$$H^2(\tau) - (1-\lambda)\,\Phi^2(\tau) = \lambda Q^2(\tau_0), \tag{170}$$

where $H = U - V$ and $\Phi = U + V$. These quantities are related to the radiative flux and the integrated intensity (or source function), respectively. It shows that in a medium with a given optical thickness and a specified scattering coefficient at its every depth, a mutually unique relation develops between the integrated radiation field and its flux; i.e., when more radiative energy is confined in the medium, its flux is greater and *vice versa*. In particular, in the two limiting cases of $\lambda = 0$ and $\lambda = 1$, we have $H(\tau) = U(\tau)$ and $H(\tau) \equiv Q(\tau_0)$. Finally, in a semi-infinite atmosphere we have $H(\tau) = \sqrt{1-\lambda}\,\Phi(\tau)$. It should be specially noted that in this problem it is possible to derive a number of other integrals, in particular the R-integral. These integrals, however, are consequences of a conservation law and have no independent significance (Nikoghossian, 1999). In similar fashion, the Hamilton principle is applied for the global optical characteristics of a scattering atmosphere, when the cyclic coordinate in Eqs. (151, 152) is τ_0 according to the Lagrangian. In this case, the system of matrix equations (151) and (161) leads to the conservation law

$$\int_0^1 P(\tau_0,\eta,\mu)\, S(\tau_0,\eta,\mu)\, d\eta - \frac{\lambda}{4}\left(\int_0^1 \left[P(\tau_0,\eta,\mu) + S(\tau_0,\eta,\mu)\right] d\eta\right)^2 = -\frac{\lambda}{4}. \tag{171}$$

For a one-dimensional medium it takes the form

$$\lambda(1+R)^2 - 4R = \lambda Q^2. \tag{172}$$

This integral is well known in the classical theory of radiative transfer (Ambartsumian, 1960; Sobolev, 1963). It has a simple physical significance that indicates the relationship between the reflection and transmission capacities of a given atmosphere is fully determined by the magnitude of the scattering coefficient. The results shown in this

doi: doi.org/10.52526/25792776-2021.68.2-186

section answer the questions posed in (Rybicky, 1977) regarding the nature of the quadratic integrals of the transfer theory. The group approach also makes it possible to extend the results obtained there, as well as in (Ivanov, 1978; Janovitskij, 1997), to the quantities which determine the reflectivity and transmission of a scattering and absorbing atmosphere. The additivity of the linear operator in Eq. (161) shows possibility to derive so-called bilinear integrals, which connect with each other the solutions of different radiative transfer problems.

Multiparameter groups. The definition of the composition group for absorbing and scattering media given above is sufficiently general, since it imposes no limits on the physical and optical properties of the combined media. They can be inhomogeneous and have different optical thicknesses. Compositions of homogeneous media that differ from one another in several parameters characterizing the diffusion process in them are of special interest. Depending on the number of these parameters, the resulting groups are one-, two-, or three-parameter groups, etc. In the limiting transition to infinitesimal thicknesses, multicomponent groups usually lead to a linear partial differential equation of order determined by the number of parameters that vary independently of one another.

As examples, we point at two problems of the theory of radiative transfer which are reduced to solving equations of one and the same kind. The first is the nonstationary radiative transfer problem in a homogeneous medium of finite optical thickness. We shall be interested in the dependence of the reflection and transmission coefficients on the thickness of the medium and time under the assumption that as they diffuse, the photons spend time only in flight between two successive scattering events. The average time of flight T is determined by the density n of the medium and the average value of the absorption coefficient in the line k: $T = (ckn)^{-1}$. In the following we assume that the time ω is measured in units of T. The addition law for these media will again be given by Eq. (159), where the indices i (i = 1,2, 1U2) now belong both to the optical thickness $\tau_0$of the given medium and to the dimensionless time ω. For simplicity we consider the problem in a one-dimensional approximation assuming that scattering in the medium takes place with complete frequency redistribution when $\Gamma = \alpha_0\alpha_0'$, with the elements of the diagonal matrices α_0 α_0' being the values of the absorption coefficient in a spectrum line normalized in corresponding fashion. The addition law for this problem reduces to the following hyperbolic system of the linear partial differential equations of the first-order with two independent variables:

$$\frac{\partial \mathbf{P}}{\partial \tau_0} + \frac{\partial \mathbf{P}}{\partial \omega} = \mathbf{mP}(\omega, \tau_\mathbf{0}) - \mathbf{nS}(\omega, \tau_\mathbf{0}), \qquad \frac{\partial \mathbf{S}}{\partial \tau_\mathbf{0}} + \frac{\partial \mathbf{S}}{\partial \omega} = \mathbf{nP}(\omega, \tau_\mathbf{0}) - \mathbf{mS}(\omega, \tau_\mathbf{0}), \tag{173}$$

with the conditions $\mathbf{P}(\omega, \mathbf{0}) = \mathbf{I}$, $\mathbf{S}(\omega, \mathbf{0}) = \mathbf{0}$; $\mathbf{P}(\mathbf{0}, \tau_\mathbf{0})$, $\mathbf{S}(\mathbf{0}, \tau_\mathbf{0})$. Treating the left side of Eq. (173) as the derivative with respect to direction and making the corresponding parametrization, the unknown functions can be represented as functions of a single variable which vary in a direction perpendicular to the characteristic direction (Arsenin, 1984). Along this direction the equations have the same form as the equations discussed above. In particular, by analogy with Eq. (161) we have

$$\breve{\mathbf{\Phi}}''_s = \mathbf{k^2}\,\breve{\mathbf{\Phi}}(\mathbf{s}), \tag{174}$$

where $\breve{\Phi}(s) = \breve{\mathbf{P}}(s) + \breve{\mathbf{S}}(s)$ and $\mathbf{k^2} = \mathbf{m^2} - \mathbf{n^2}$. .

Using the variational principle along this direction makes it possible to introduce the Lagrangian density,

$$L = \left(\frac{\partial}{\partial \tau_0} + \frac{\partial}{\partial \omega}\right)\left[\mathbf{P^2} + \mathbf{S^2} - \frac{\lambda}{\mathbf{2}}(\mathbf{P} + \mathbf{S})^\mathbf{2}\right] \tag{175}$$

for this problem along with a conservation law in the form

$$\sum \left(\frac{\partial}{\partial \tau_0} + \frac{\partial}{\partial \omega}\right)\left[\frac{\lambda}{4}\boldsymbol{\alpha}_0(\mathbf{P} + \mathbf{S})^2 - \mathbf{PS}\right] = 0, \tag{176}$$

where the arguments of the unknown matrix-functions in Eqs. (175) and (176) have been left out for brevity. The sum in Eq. (176) is taken over one of the columns denoting the frequency of the reflected radiation. In the stationary problem the time dependence vanishes and we find

$$\sum \frac{\lambda}{4}\alpha_0(\mathbf{P} + \mathbf{S})^2 - \mathbf{PS} = \mathrm{const}. \tag{177}$$

The second problem involves determining the profiles of spectrum lines formed in a homogeneous scattering and absorbing atmosphere of finite thickness with developed homogeneous turbulence. Referring the reader to (Nikoghossian, 2017) for a statement of the problem and its physical aspect, here we note only that an approach based on the group properties of the quantities describing radiative transfer can be used in this problem as well if the spatial correlations of non-thermal motions are represented as a Markov process, which is described by Gaussian distributions in a plane. For this distribution in this case, the Chapman-Kolmogorov relation applies, i.e.,

doi: doi.org/10.52526/25792776-2021.68.2-186

$$G\left(u,u',\rho\left(l_1+l_2\right)\right)=\int_{-\infty}^{\infty}G\left(u,u'',\rho\left(l_1\right)\right)G\left(u,u'',\rho\left(l_2\right)\right)du''. \tag{178}$$

The distribution G has a probabilistic sense in that $G\left(u,u',\rho\left(l\right)\right)du$ is the probability that if at some depth τ' the non-thermal velocity equals u', then at depth τ it takes a value within the interval $(u,\ u+du)$. The correlation coefficient ρ for Markov process varies exponentially as $\rho\left(l\right)=\exp\left(-l/\Lambda\right)$, where Λ is the average optical correlation length. Then the addition law for two layers with optical thicknesses τ_1 and τ_2 is given by

$$\begin{pmatrix}\mathbf{P}_{1\bigcup 2}\left(\mathbf{u}\right)\\ \mathbf{S}_{1\bigcup 2}\left(\mathbf{u}\right)\end{pmatrix}=\begin{pmatrix}\mathbf{P}_2\left(u'\right) & -\overline{\mathbf{S}}_2\left(u'\right)\\ \mathbf{S}_2\left(u'\right) & \mathbf{M}_2\left(\mathbf{u}'\right)\end{pmatrix}G\left(\rho\left(\tau_1\right)\right)\begin{pmatrix}\mathbf{P}_1\left(u\right)\\ \mathbf{S}_1\left(u\right)\end{pmatrix}. \tag{179}$$

Here the variable u denotes the shift of the frequency at the right boundaries of these media. The system of vector-matrix differential equations generated by this rule is given by

$$\frac{\partial\mathbf{P}}{\partial\tau_0}+\frac{1}{\Lambda}\frac{\partial\mathbf{P}}{\partial u}=\mathbf{m}\left(u\right)\mathbf{P}\left(u,\tau_{\mathbf{0}}\right)-\mathbf{n}\left(u\right)\mathbf{S}\left(u,\tau_{\mathbf{0}}\right),$$

$$\frac{\partial\mathbf{S}}{\partial\tau_0}+\frac{1}{\Lambda}\frac{\partial\mathbf{S}}{\partial u}=\mathbf{n}\left(\mathbf{u}\right)\mathbf{P}\left(\mathbf{u},\tau_{\mathbf{0}}\right)-\mathbf{m}\left(\mathbf{u}\right)\mathbf{S}\left(\mathbf{u},\tau_{\mathbf{0}}\right), \tag{180}$$

with the initial conditions $\mathbf{P}(u,0)=\mathbf{I}$ and $\mathbf{S}(u,0)=\mathbf{0}$. $\mathbf{m}$ and $\mathbf{n}$ are specified by the same formulas as in the preceding example with the frequency shift taken into account. The system of Eqs. (180) is valid for any values of the correlation coefficient except $\Lambda=0$. This case, which corresponds to a microturbulent regime is generally examined separately (Nikoghossian, 2017). We can see that this system of equations differs in form from Eqs. (173) derived for the preceding problem in that the correlation coefficient Λ appears on its right hand side. Thus, both the methods for studying and solving it, as well as the possibility of using the variational principle with conservation laws, are fundamentally the same.

II. APLICATIONS TO ASTROPHYSICAL PROBLEMS. INTERPRETATION OF SPACE OBJECTS SPECTRA.

6. THEORETICAL PHYSICS

i. The relativistic Doppler broadening of the line absorption profile. The classical results of Doppler broadening of the spectral line absorption profile was generalized in (Kichenassami, Krikorian & Nikoghossian, 1982) in a relativistic gas in thermal equilibrium by taking into account the relativistic variance of the volume absorption coefficient of the gas, as derived in (Thomas, 1930). The latter was shown to be important, since the variance produces a small correction even in the non-relativistic approximation. The derived expression of the absorption coefficient χ_ν, has a form

$$\chi_\nu=\frac{n_0}{2}\frac{\sigma_0 f}{K_2\left(m\xi\right)}\frac{\Gamma}{\pi\nu^2}\int_{-\infty}^{\infty}\mathrm{e}^{-\frac{m\xi\left(x^2+\nu^2\right)}{2\nu x}}\frac{xdx}{\left(x-\nu\right)^2+\Gamma^2}, \tag{181}$$

where the following notations are used: n_0 is density of the gas in its rest frame, $\sigma_0=\pi e^2/m_e c$, $\xi=c^2/kT$, c is light velocity, $x=\gamma\nu\left(1+\beta\right)$, $\gamma=\left[1+\left(p/m\right)^2\right]^{1/2}$. The modified Bessel function of the second order $K_2(m\xi)$ is defined by

$$K_2(m\xi)=2\int_0^{\infty}\mathrm{e}^{-m\xi cht}chtdt. \tag{182}$$

For vanishing Γ Eq. (182) gives

$$\chi_\nu=n_0\sigma_0 f\frac{\nu_0}{2K_2\left(m\xi\right)\nu^2}\mathrm{e}^{-\frac{m\xi\left(\nu^2+\nu_0^2\right)}{2\nu\nu_0}}, \tag{183}$$

where ν_0 is the frequency in the center of the line.

ii. The photon scattering by electrons. Energy losses by electrons. A series of papers in Byurakan Observatory were devoted to derivation of the redistribution function (scattering kernel) describing the photons scattering on free electrons. The simplest special case of isotropic and low energetic photons scattering on the ensemble of electrons with the Maxwellian distribution of moments was considered above in Sect. 5.i (Harutyunian & Nikoghossian, 1980). The generalized problem for the redistribution law averaged over directions of monoenergetic electrons velocities in the observer's frame was treated in (Harutyunian & Nikoghossian, 1981, 1989; Dzhrbashian & Harutyunian, 1985). The explicit expression of this law is too cumbersome to be presented here. We limit ourselves with only mentioning that the first of the cited two papers uses the obtained results to formulate the problem of diffuse reflection of radiation from a semi-infinite absorbing and electron scattering atmosphere. Exact expressions for the energy losses during photons scattering is treated and investigated in (Harutyunian, Dzhrbashian & Nikoghossian, 1988).

The results of numerical calculations for the energy loss by electrons and photons depending on their energy are depicted in Fig.15. It is noteworthy the maxima of curves for the electrons energy loss.

doi: doi.org/10.52526/25792776-2021.68.2-186

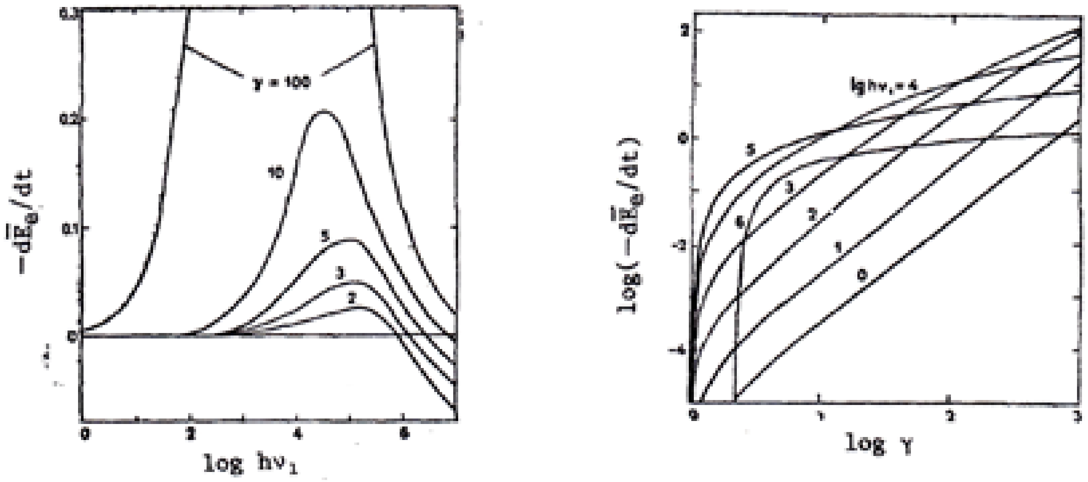

Figure 15: The angle-averaged value of the energy loss by electrons as a function of the energy of photons and electrons (left panel); the dependence of the energy loss by photons on the energy of the photons and electrons (right panel).

7. SOLAR PHYSICS

7.1. Quiescent prominences.

i. The research work on solar prominences carried out in collaboration with the Meudon observatory in Paris started in 1994. The cooperation involved Z. Mouradian (Meudon), A. Nikoghossian (Byurakan observatory) and their PhD student S. Pojoga (Romania). The first works used digital raster images of prominences obtained with the Harvard College Observatory (HCO) aboard ATM-Skylab, which represent a rich observational resource for investigating the statistical properties of the spectra formation in media with composite thread-like structure. Spatial and temporal variations of the prominences brightness in the EUV spectral domain were studied. The spatial brightness variations of prominences may have several reasons: differences in the line-of-sight number of structural elements and in the value of the filling factor, physical inhomogeneities of the structures, instrumental errors and so on. These factors are studied separately in order to determine the significance of each in establishing the variations.

ii. The theory developed in a series of papers by Nikoghossian, Mouradian & Pohoga (1997, 1998a, 1998b, 1999), Pojoga, Nikoghossian & Mouradian (1998), Nikoghossian & Mouradian (2000), Nikoghossian (2001), Nikoghossian, Aboudarham & Mouradian (2005) aimed at determining the mean intensity and the relative mean square deviation (RelMSD) for the line radiation emerging from an one-dimensional atmosphere with randomly distributed inhomogeneities. The idea of such statistical approach based on the study of spatial fluctuations of brightness goes back to Ambartsumian's classical works (1951, 1960) studying fluctuations of the Milky Way brightness in estimating the mean value of the opacity of interstellar matter.

iii. The theory developed in the cited papers both for spectral lines in the LTE and Non-LTE, allowed to make an idea on the processes leading at the observed spatial and temporal fluctuations of brightness, and then on the optical thicknesses, temperature and velocity field. Some information on the line-of-sight number of threads was obtained by theoretical treatment of dependence of the filling factor (coefficient of filling of the spectrograph slit in each pixel) on this number (Nikoghossian, 2001). It was shown that the role of the random variations in the filling factor is insignificant among the other factors producing brightness fluctuations for the regions of prominences having high and moderate packing of filaments. At the same time, this role may become important for rarified and weakly radiating regions. Note that analogous approach is applicable also in studying such multicomponent and non-steady formations in the solar atmosphere as chromospheric spicules and various coronal streams. Similar examples can also be cited from other fields of astrophysics.

iv. The classical method for determining the velocities of micro-turbulent motions in solar prominences (Tandberg-Hanssen, 1995) was generalized in (Nikoghossian & Mouradian 2010) to account for the possible opacity of the spectral lines. A new characteristic of a line was introduced, which, for a given line formation mechanism, allows also to determine the optical thickness of the emitting region. The method was applied to the spectral lines in the EUV region observed with the SUMER spectrograph as part of the SOHO space program. Comparison with observational data not only confirms the validity of this mechanism for the line formation, but also shows that the optical thickness of the medium is typically small for these lines. Difficulties involved in determining the kinetic temperature and, therefore, the micro-turbulent velocities, are mainly due to accuracy of the observational material. Based on the lines

doi: doi.org/10.52526/25792776-2021.68.2-186

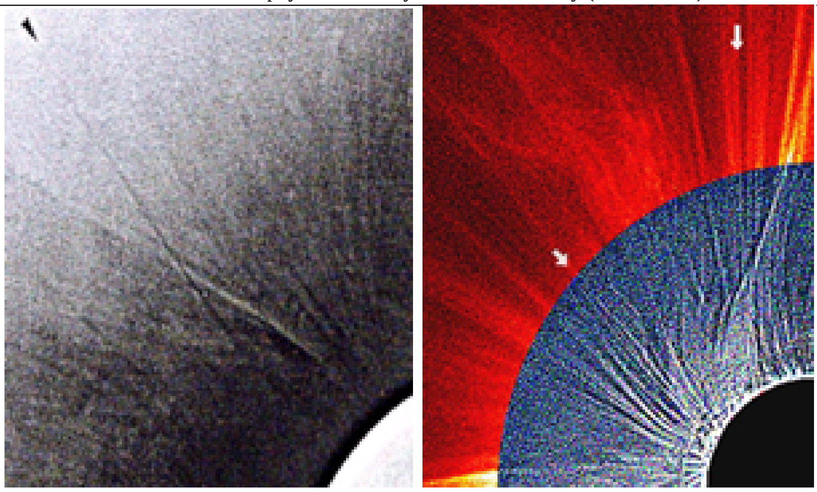

Figure 16: Early observation of a coronal linear (in dark) ray-thread showing a large aspect ratio. This is a greatly magnified negative print made by the team of the Kiev University (Ukraine) using a 10 cm diameter lens of 10 meters focal length and 30 s exposure time (left panel). Selected part of a composite (inner part is a W-L compressed image taken from Iran by the team of the Institut d'Astrophysique de Paris-CNRS using a radial filter; outer parts is the Lasco C2 image from SOHO taken simultaneously from space on July 11, 1999) to show the NE limb, right above a coming flaring active regions. High resolution images of the more inner parts of this limb did show many loops. Arrows are indicating the most obvious linear rays-threads. The one raising above the N-pole region was seen on both ground-based and space-born images (right panel).

of various ions, this velocity is estimated to be on the order of 30-40*km/s*. The cited paper presents a table of 20 spectral lines with the proper estimating values of the micro-turbulent velocity, opacity and kinetic temperature.

7.2. Coronal supra-thermal streams.

For a long time high resolution W-L eclipse images taken near the time of the solar maximum of activity did show multiple thread-like streams and/or straight and fine "diverging" rays of unknown origin. This structure is not anchored at the surface of the Sun but appears as a straight linear structure starting from a fraction of the solar radius and was sometimes called rays or "fan-streamer" (Vsessviatski & Bougoslavskaya 1944; Koutchmy 1969). They are typically seen above limb active regions which produced flares or at least sub-flares before. Coronal streams are one of the intriguing short-lived phenomena emerging from the magnetically dominated part of the inner atmosphere of the Sun; their typical linear structure, their large aspect ratio, and their dispersed directions with respect to the local radial direction strongly suggest that they largely ignore the outer background of the general coronal magnetic field which is usually computed using current-free or force-free extrapolations of the measured magnetic field at the solar surface. They probably represent fluxes of supra-thermal electrons (with velocities up to 10^5 km/s^{-1}) moving partly along spiral trajectories.

The theoretical works by Nikoghossian & Koutchmy (2001, 2002) aimed at revealing the role of the Compton effect when considering the W-L scattering of the solar photospheric radiation by coronal supra-thermal streams. The height-dependent model problem of Compton scattering on the beam of fast electrons gyrating around the lines of force of the magnetic field was considered. The resulting change in frequency averaged over the beam and the solid angle, within which the photospheric radiation falls, is computed for both sunward and anti-sunward directed streams. The dependence of the effect on the height above the solar surface, the speed of electrons and the slope angle were discussed. For illustration, it was assumed that the frequency distribution of the incident radiation is Planckian. The effective value of the cross-section of interaction was compared with that for the Thomson scattering.

The results may be summarized as follows. At the least, at high distances over the solar limb the frequency change in the suprathermal stream radiation resulting from the Compton scattering may be significant even for moderate energies of electrons. For electrons moving off the Sun, longwave-ward drifts of the spectrum are more likely, while opposite ones are due preferably to the opposite directed beams of electrons. The effect was expected to be detectable only if the fractional density of fast electrons is not very small.

The realistic height-dependent model problem was treated in (Nikoghossian & Koutchmy, 2002). The results of numerical calculations for the mean frequency change and the proper cross-section for both the sunward and anti-sunward directed beams of electrons were given as a function of height and the slope angle. It was concluded that, depending on the angle between directions of the initial outburst and magnetic field, the scattering on the beams moving away the Sun may produce measurable drifts in frequency to shortwave as well as to longwave domains of

doi: doi.org/10.52526/25792776-2021.68.2-186

the spectrum. At the same time, the sunward directed beams result only in an increase in the photon energy.

In order to verify the theoretical results obtained, observations were made during the total eclipse in Angola in 2001. The authors first document several examples of well observed cases of the linear W-L coronal threads extending above flaring active regions which are good candidates to give the signature known from the interpretation of radio type III bursts. There were performed measurements of the color index of the coronal supra-thermal streams. Observations imply that the color index of streams differs markedly from that for adjacent parts of the surrounding corona taken as reference (Koutchmy & Nikoghossian, 2005). The registered drifts to the longwave and shortwave domains of the spectrum are in agreement with theoretical results obtained by the authors.

8. STELLAR ASTROPHYSICS

8.1. Flare stars. A certain place in the works of the Department of Theoretical Astrophysics occupied the study of flare stars as a part of observational programs in the Byurakan Observatory

i. In the frameworks of this research field, a statistical analysis of the flare data obtained in 1967-1969 for the star UV Cet and in 1967-1970 of the star YZ CMi was carried out by Oskanian & Terebizh (1971a,b). They showed that the flare activity of these stars did not change during the mentioned periods. The detailed investigation of a number of flares showed that the succession of the flares on the stars are near the Poisson distribution law. The research work was continued by B-color photometric observations of the stars AD Leo, EV Lac, YZ CMi, UV Cet, The distribution of amplitudes, amounts of radiated energy and frequencies were studied. The influence of the observational selection on the detection of small-amplitudes flares as well as the problem of determination of the absolute flare activity of these stars were discussed in detail.

ii. The Ambartsumian paper appeared in 1978 is devoted to derivation of the frequency function of stellar flares in clusters. First, the problem of determining the total number of flare stars was considered on the example of Pleiades under assumption that all stars flare equally often. Assuming that the flares occur according to Poisson's law, the problem was solved by using the chronology of discoveries ("first flares") and the chronology of confirmation ('second flares'). For the expected number of stars in the aggregate that have not flashed in the entire time they were observed n_0, an estimate was obtained

$$n_0 = \frac{n_1^2}{2n_2}, \tag{184}$$

where n_1 and n_2 are expected numbers of stars that respectively flared once and twice.

If frequencies of flares are different for different stars, then this formula gives only the lower limit of this value. It has been shown that in the case of different frequencies, there are the following inequalities

$$\frac{n_1^2}{n_2} \geq n_0 \geq \frac{n_1^2}{2n_2}. \tag{185}$$

Further, as subtracted, the fraction of flare stars increases when getting to fainter stars, in other words, the flare activity previously decreases in more luminous stars.

iii. The possibility of interpretation of flare radiation of red dwarf stars with use of the inverse Compton scattering was discussed by Harutyunian, Krikorian & Nikoghossian (1979). They refined the expressions, adopted earlier for the law of the frequency redistribution during the scattering process and gave the formula for differential cross-section. It was indicated the importance of the geometry of the photon-electron interaction and showed that the interpretation of observational data by this mechanism meets considerable difficulties.

iv. Chavushian, Pikichyan et al. (2004) constructed the three-dimensional distribution of flare stars in the Pleiades cluster. For this purpose a one-dimensional distribution was first constructed from the observed two-dimensional distribution of the stars. It was shown that reliable construction of one-dimensional distribution requires solution of the Abel equation. The last one was used to determine the dependence of the real three-dimensional distribution of the density of flare stars on distance from the center of the cluster. This reveals a spherical layer of width 0.5 pc $2.8 \leq R \leq 3.5$pc with a deficit in the member of flare stars. A profile of the three-dimensional density distribution of flare stars was constructed in the region of deficit. The characteristics of this region were described.

v. The works by Hayrapetian & Nikoghossian (1989), Hayrapetian, Vikhrev & Nikoghossian (1989) showed that qualitative and quantitative comparison of the results of plasma experiments with observational data on stellar flares suggests that flares could be explained by the Pinch effect, i.e., by the plasma compression by magnetic field in the outer layers of these stars. A possible scenario of magnetic tubes floating from the convective zone with further stretching and arch structures formation was suggested.

vi. Hayrapetian & Nikogohossian (1988) showed that some spectral peculiarities of T Tau stars such as the values of half-widths of Balmer lines, the short-term variability of hydrogen lines, the values of Balmer jumps and shifts of the HeI lines, can be explained by generation of the quasi-stationary plasma turbulence in atmospheres of these stars.

doi: doi.org/10.52526/25792776-2021.68.2-186

vii. An inverse problem of determination of the total number, luminosity function and the variability characteristics of brightness of T Tau type stars in stellar aggregates was considered by Pikichyan (2018). It was demonstrated that the four observations of stellar aggregate make it possible to estimate the total number of irregular variable stars. By assuming that the random process is continuous and stationary, it was formulated an inverse problem for restoration of the star's luminosity function, as well as the distribution function of the brightness variability. The original information requires detailed photometry of two rather distant in time "pictures" of the aggregate stars. It is significant that the mentioned author with his co-author proposed a project aim at minimizing the effect of the astronomical dome and tower on the quality of the star image (Muradyan & Pikichyan, 1986). The new class of astronomical domes of changing geometry was suggested, which are smaller in size and simpler in constructing as compared to the classical ones with constant geometry.

8.2. LBV stars.

i. The spectral variability of P Cyg was investigated by Israelian & Nikoghossian (1993). The careful analysis of the CCD – spectra of P Cyg made it possible to identify 10 of the 43 lines that had been unidentified up to that time. The majority of identified lines belong to multiply ionized atoms. The conclusion was reached that there is anomalous heating in the certain layers of the stellar wind. There were presented facts that suggest variation in the degree of ionization of the stellar wind. Some forbidden lines were identified in the spectrum of P Cyg (see, also Israelian & De Groot, 1992).

ii. Based on the fact that the stellar winds of LBV stars are due to acceleration of matter resulting from radiation pressure in optically thin weak emission lines of metals in the Balmer continuum, Israelian, Nikoghossian & Tambovtseva (1993) constructed models of the winds of these stars for some specific cases. The obtained results are in satisfactory agreement with observational data.

iii. The papers by Nikoghossian & Israelian (1996), Israelian & Nikoghossian (1996) and Nikoghossian (2020) present a theoretical study of changes in some spectral characteristics of the early type supergiants due to the scattering of radiation in the continuous spectrum. Thomson scattering on free electrons was regarded as a scattering mechanism, although the approach used is fairly general. The cause of changes in the star's spectral class at constant bolometric luminosity and surface temperature was revealed, and conditions necessary for their implementation were given. The effect of scattering in the continuum on the magnitude of intensity jumps in the hydrogen spectrum depending on the degree of ionization was studied. The conditions under which the Schuster mechanism of emission lines formation starts to operate both in the isothermal atmosphere and in the atmosphere with temperature gradient were brought out.

iv. Possible reasons for displacement of the peak of an emission line of an object with an expanding shell were considered by Grigorian & Arshakian (1990). A new effect, a blue shift of the emission line peak, was established. It was shown that such peak arises because the simultaneously observed photons reached the observer from points of the shell at different distances emitted at different times of its expansion. The effect is more pronounced, the closer the speed of the ejected layers of the shell to the speed of light. The case of continuous shell isotropically expanding with velocities proportional to the distance from the star was treated. A method was proposed for determining the displacement of the emission peak and estimating the lower limit of the density of atoms emitted a given line. Application of this method to the supernova SN 1987A led to an estimate of the radial velocity (-170 km/s) corresponding to the lower limit of the displacement of the peak of the H_α line.

8.3. **Ap stars**.

In the context of the study of elemental diffusion in Ap stars, Alecian (Meudon Observatory in Paris) in cooperation with Harutyunian (2012), Haruthunian et al., (2016) treated the problem of radiative transfer in an inhomogeneous medium with the depth-dependent absorption coefficient. The corresponding equations are obtained to solve by numerical methods.

8.4. Pulsars.

The radio luminosities of pulsars were given by Andreasian & Arshakian (1993) as a function of their period and the time of its variation. The parameters of that dependence were calculated and independent distances were determined for 288 pulsars. The average electron densities toward the pulsars were determined from the known dispersion measures. The results obtained were used to study the large-scale electron density distribution in the Galaxy at a distance of 4-5 kps from the Sun. The distribution maximum has been found to lay at a distance of 9 kps from the center of the Galaxy in the vicinity of the Sagittarius spiral arm. They found that the electron density falls off exponentially in the regions between arms (toward the Perseus and Centaurus spiral arms).

9. EXTRAGALACTIC ASTROPHYSICS

i. The possibility of explaining the broad emission lines formation in quasars spectra by Cherenkov radiation was considered by Nikoghossian (1994). This idea was suggested and worked out by some authors in a number of papers, where, however, some effects, being essential for the line profile, were ignored. The classical Non-LTE line-formation

doi: doi.org/10.52526/25792776-2021.68.2-186

problem with allowance for the Cherenkov radiation was solved in the above-cited paper. The results obtained for the Lyman alpha line for the electron temperature $T_e \approx 1.5 \cdot 10^4$K show that the effect of this mechanism becomes measurable merely for unreasonably high densities of relativistic electrons $n_e \geq 10^{11} cm^{-3}$. **ii.** The statistics of interacting galaxies was treated by Karachentsev & Terebizh (1968). They used data for the systems of interacting galaxies brighter than $15^m.0$ spatial distribution. The results of statistical analysis have proved that the processes giving rise to interacting galaxies have been spontaneous and induced by internal causes.

iii. The source-count analysis and the V/V_m test in the study of the evolution of quasi-stellar radio sources was treated by Terebizh (1973). The exact expressions for V/V_m the distribution under arbitrary character of their evolution were derived. The dependence of different methods were quantitatively was estimated. Arguments were rendered in favor of the density evolution of quasi-stellar radio sources on the analysis of distribution of these objects on the luminosity-redshift diagram. The same author studied the luminosity functions of Seifert galaxies and quasars (Terebizh, 1975, 1980).

iv. The spectra of Arakelian galaxies with high surface brightness were obtained by Doroshenko & Terebizh (1975). A total 40 of 73 galaxies were with emission lines in the spectra. Red shifts and absolute magnitudes of galaxies were determined.

v. The large scale spatial orientation of the major axes of extended double radio sources was studied by Arshakian (1991). It was found the preferable orientation of the axes for 82 objects. Within limits of error the resulting direction was concluded to coincide with the direction of the regular metagalactic magnetic field. **vi.** The problem of finding the distribution of separation velocities of the components of classical double radio sources were solved by Arshakian & Andreasian (1993). Most of radio galaxies were found to have velocities in three intervals: $v \approx$-0.05c, -0.015c and -0.026c, where c is the speed of light. For quasars they are in two intervals with average separation velocities of 0.13c and 0.26c.

ANNEX

Almost simultaneously with opening the Department of Theoretical Astrophysics in the Byurakan Observatory, the international journal "Astrophysics" was founded. At different times, different members of the department were part of the editorial board of the journal, which soon gained wide recognition from the scientific community. In its turn, the appearance of the journal was an impetus for the development of theoretical astrophysics both in the observatory itself and in the Republic.

The contribution of the members of the Department to the teaching activity and training of scientific personnel in the republic is significant. The broad international cooperation of Department played an important role in the further development of some areas of theory in the observatory, as well as in the creation of new ones.

doi: doi.org/10.52526/25792776-2021.68.2-186

REFERENCES

V.A. Ambartsumian, The Light Scattering and Absorption in Atmospheres of Planets, Uch. Zap, LGU, No. 82, is. 11, 1941.

V.A. Ambartsumian, New Method for Studying the Light Scattering in the Foggy Medium, Izv. AN SSSR, serie Geogr. I Geophys., No. 3, 97-103, 1942.

V.A. Ambartsumian, On the Scattering of Light by the PlanetaryAtmospheres, *Astron. Zh*, **19**, 30-41, 1942.

V.A. Ambartsumian, On Diffuse Reflection of Light by Turbid Medium, *Dokl. Akad. Nauk. SSSR*, **38**, 257-261, 1943.

V.A. Ambartsumian, On the Problem of Diffuse Reflection of Light, *J. Exp. Theoret. Phys*., **13**, 323-334, 1943.

V.A. Ambartsumian, The Diffusion of Light through Scattering Medium of Large Optical Thickness, *Dokl. Akad. Nauk. SSSR*, **43**, 106-112, 1944.

V.A. Ambartsumian, On the One-Dimensional Case of the Problem of the Scattering and Absorbing Medium of Finite Optical Thickness, *Izv*. *AN ArmSSR*, No.1-2, 31-36, 1944.

V.A. Ambartsumian, On the Theory of the Brightness Fluctuations in the Milky Way, *Dokl. Akad. Nauk. SSSR*, **44**, 244-321, 1944.

V.A. Ambartsumian, On the Diffuse Reflection and Transmission of Light by an Anisotropic One-dimensional Scattering Medium of Finite Optical Thickness, *Izv. AN ArmSSR*, VII, No 5,199-202, 1947.

V.A. Ambartsumian, On the Number of Scatterings of Photons in Foggy Media, *Dokl. Akad. Nauk ArmSSR*, **8**, 101-105, 1948.

V.A. Ambartsumian, On the Theory of Fluctuations in the Stars Distribution on the Sky, Com. BAO, 2-59, 1951.

V.A. Ambartsumian, Scientific Papers, vol.1, Izd.AN. ArmSSR, Yerevan (1960).

V.A. Ambartsumian, On One Problem of the Non-linear Theory of the Light Scattering in Foggy Medium, *Dokl. Akad. Nauk ArmSSR*, **38**, 225–230, 1964a.

V.A. Ambartsumian, On One Case of Enlightenment of the Medium under the Influence of Radiation, *Dokl. Akad. Nauk ArmSSR*, **39**, 159–165, 1964b.

V.A. Ambartsumian, On the Problem of the Multiple Light Scattering in a Plane-parallel Medium with the Internal Reflection from the Boundary Surface, Trudi Astron. Obs.. LGU, **20**, 1964c.

V.A. Ambartsumian, Some Non-linear Problems in the Theory of Radiative Transfer, in: Theory of Stellar Spectra (in Russian), Nauka, Moscow, 225-235, 1966.

V.A. Ambartsumian, Derivation of the Frequency Function of Stellar Flares in a Star Cluster, *Astrophysics*, **14**, 209-217, 1978.

V.A. Ambartsumian, On Some Trends in the Development of Astrophysics, *Ann. Rev. Astron. Astrophys*. **18**, 1-13, 1980.

V.A. Ambartsumian, Scientific Papers, vol.3, Izd.AN.ArmSSR, Yerevan (1988).

V.A. Ambartsumian, On the Fluctuations of the Surface Brightness of Galaxies, *Astrophys. Sp, Sci*., **144**, 635 -638, 1988,

doi: doi.org/10.52526/25792776-2021.68.2-186

V.A. Ambartsumian, in: “A Life in Astrophysics. Selected papers of Viktor Ambartsumian”, Allerton press, NY (1998).

D. Anderson, Variational Principles for the Radiative Transfer Equation of Single Scattering, *J. Inst. Math. Applic.*, **12**, 55-62, 1973.

R.R. Andreasian, E.Kh. Danielian, On the Problem of Calculation of the Ambartsumianφ-Function, *Comm. BAO*, **50**, 114-117, 1978.

R.R. Andreasian, T.G. Arshakian, Radio Luminosities of Pulsar and the Electron Density Distribution in the Galaxy, *Astrophysics*, **36**, 229–234, 1993.

V.Ya. Arsenin, Methods of Mathematical Physics and Special Functions [in Russian], M.,Nauka (1984).

T.G. Arshakian, Large-scale Spatial Orientation of Major Axes of Extendid double Radio Sources, *Astrophysics*, **35**, 394-399, 1991.

T.G. Arshakian, R.R. Andreasian, The Discreteness of the Velocities of Separation of Components of Extended Double Radio Sources, *Astrophysics*, **36**, 235-240, 1993.

G. Batchelor, The Theory of Homogeneous Turbulence, Cambridge Univ. Press, 6th ed., 1970.

M.M. Basko, Frequency Redistribution and Diffusion of Radiation in Resonance X-ray Line, *J. Exp. Theoret. Phys*, **48**, 644-649, 1978.

R. Bellman, R. Kalaba, M. Wing, Invariant Imbedding and Mathematical Physics.I. Particle Processes, *J. Math. Phys*., 1, 280–308, 1960.

R. Bellman, R. Kalaba, M. Prestrud, Invariant Imbedding and Mathematical Physics, New York, American Elsevier (1963).

R. Bellman, Functional Equations in the Theory of Dynamic Programming.VII., A Partial Differential Equation for the Fredholm Resolvent, *Proc. Amer. Math. Soc*., **8**, 435-440, 1957.

R. Bellman & G.M. Wing, An Introduction to Invariant Imbedding, New York, Wiley & Sons (1973).

F.A. Berezin, The Method of Second Quantization, (in Russian), Nauka, M., (1986).

K.M. Case & P.F. Zweifel, Linear Transport Theory, Reading, MA, Addison-Weslay (1967).

J. Casti, R. Kalaba, Imbedding Methods in Applied Mathematics, (Russian transl.), M., Mir (1976).

S. Chandrasekhar, Radiative Transfer, New York, Dover (1960).

H.S. Chavushian, H. V. Pikichyan, A. V. Oskanian, G. H. Broutian, Reconstruction of The Three-dimensional Density Distribution of Flare Stars in the Pleiades *Astrophysics*, **47**, 313-323, 2004,

L.E. Cram, Multi-Component Models for the Formation of the Chromospheric Ca II K Line. II: The Effect of Velocity Fields, Sol. Phys., 22, 375-386, 1982. E.Kh. Danielian, Radiation Field in a Plane Layer Illuminated by Parallel Rays, *Astrophysics*, **12**, 378-385, 1976.

E.Kh. Danielian, H.V, Pikichian, Radiation Field in a Plane-Parallel Atmosphere Containing Energy Sources, *Astrophysics*, **13**, 147-154, 1977.

doi: doi.org/10.52526/25792776-2021.68.2-186

E.Kh. Danielian, Theory of Isotropic Scattering of Radiation in a Homogeneous Plane-Parallel Medium, *Astroohysics*, **19**, 194-202, 1983.

E.Kh. Danielian, On the Problem of Radiation Transfer With Three-demensionality of the Medium, *Dokl. Acad. Sci. ArmSSR*, **61**, 117-123.

V.A. Djrbashian. H.A. Harutyunian, Probability of Photon Scattering by Electrons. The Case of Randomlyly Moving Monoenergetic Electrons, *Astrophysics*, **22**, 228-232, 1985.

V.T. Doroshenko, V.Yu. Terebizh, UBV-Photometry of Seifert Galaxies, *Astrophysics*, **17**, 358-362, 1981.

I.M. Gelfand, S.V. Fomin, Calculus of Variation, Englewood Cliffs, N.J. Prentice-Hall (1965),

I.P. Grant, G.E. Hrant, Solution of Radiative Transfer Problems Using the Invariant S_n Method, *Mon. Not. Roy. Astr. Soc*., **14**1, 27–41, 1968.

A.E. Grigorian, T.G. Arshakian, Blue Shift of Supernova Emission Lines Due to Finiteness of the Speed of Light, *Astrophysics*, **33**, 513-517, 1990.

M. Gros & C. Magnan, The Method of Addition of Layers to Solve the Non-linear Transfer Problem, *Astron. Astrophys*., **93**, 150-154, 1981.

H.A. Harutyunian, A.G. Nikoghossian, The Contours of Spectral Lines for Non-Coherent Scattering, *DAN SSSR*, **242**, 66-69, 1978.

H.A. Harutyunian, A.G. Nikoghossian, Radiation Scattering for a General Law of Frequency Redistribution, *J. Quantit. Spectrosc. Radiat. Transfer,* **19**, 135–148, 1978.

H.A. Harutyunian, R.A. Krikorian & A.G. Nikoghossian, Interpretation of Flares of Red Dwarfs by Means of the Inverse Compton Effect, *Astrophysics*, **15**, 293-300, 1979.

H.A. Harutyunian, A.G. Nikoghossian, The Redistribution Function for the Scattering on Relativistic Electrons, *Dokl. Akad. Nauk SSSR*, **255**, 86–89, 1980.

H.A. Harutyunian, Spectral Line Formation in an Atmosphere with Exponential Distribution of Sources, *Dokl. Acad. Sci. ArmSSR*, **70**, 41, 1980.

H.A. Harutyunian, A Simple Method for Calculation of the Redistribution Function R_{III} (x',x) , *Comm. of BAO*, **52**. 137, 1980.

H.A. Harutyunian, A.G. Nikoghossian, The Application of the Invariance Principle to the Problems of Multiple Compton Scattering, Transact. of the All-Union Symp. "The Invariance Principle and Its Applications", 1981, Yerevan, 431-439.

H.A. Harutyunian, A.G. Nikoghossian, The Mean Number of Scatterings for Radiative Transfer with Frequency Redistribution, *Dokl. Akad. Nauk SSSR*, **268**, 1342 – 1346, 1983.

H.A. Harutyunian, Reflection from the Semi-infinite Inhomogeneous Atmosphere for the General Laws of Noncoherent Scattering, *Astrophysics*, **23**, 584-590, 1985.

H.A. Harutyunian, A.G. Nikoghossian, Statistical Description of Radiation Field on the Basis of the Invariance Principle. IV., The Results of Numerical Calculations, *Astrophysics*, **27**, 536–543, 1987.

H.A. Harutyunian, V.A. Djrbashian, A.G. Nikoghossian, Energy Losses for the Photon Scattering by Free Electrons, *Astrophysics*, **29**, 119-131, 1988.

doi: doi.org/10.52526/25792776-2021.68.2-186

H.A. Harutyunian, A.G. Nikoghossian, The Application of the Invariance Principle to the Multiple Compton Scattering Problem, in: Principle of Invariance and its Applications, Eds. M.A. Mnatsakanian & O.V. Pikichyan, 431-439, Izd. AN ArmSSR (in Russian), 1989.

H.A. Harutyunian, Formation of Spectral Lines in the Medium of Finite Thickness for Non-Coherent Scattering of Radiation, *Dokl. Acad. Nauk SSSR*, **320**, 1073-1077, 1991.

H.A. Harutyunian, Bilinear Expansion of the Frequency Redistribution Functions, 1991, *Dokl. Acad. Nauk SSSR*, **321**, 285-289, 1991.

H.A. Harutyunian, Radiative Transfer for Incoherent Scattering in a Semi-Infinite Atmosphere, Containing Energy Sources, *Astrophysics*, **36**, 335-342, 1993.

H.A. Harutyunian, The Expansion of the Voigt Function, *Astrophysics*, **39**, 370-374, 1996.

H.A. Harutyunian, Scattering of Radiation by Free Electrons. The Angle-averaged Redistribution Function, *Astrophysics*, **49**, 405-414, 2006.

H.A. Harutyunian & G. Alecian, Radiation Transfer in an Inhomogeneous Medium. Optical Depth Depending Absorption Coefficient, *Astrophysics*, **55**, 251-260, 2012.

H.A. Harutyunian, G.Alecian, K.G. Khachatryan, A.V. Vardanyan, Bilinear Expansion for Redistribution Functions, *J. Quantit. Spectrosc. Radiat. Transfer*, **189**, 64-69, 2016.

H.A. Harutyunian, H.A. Poghosyan Numerical Solution of the Ambartsumian Functional Equations for a Plane Medium with Finite Thickness, *Astrophysics*, **61**, 525-539, 2018.

V.S. Hayrapetian, A.G. Nikoghossian, Effect of the Plasma Turbulence in the Atmospheres of Active Stars, *Astrophysics*, **29**, 455-462, 1988.

V.S. Hayrapetian, V.V. Vikhrev, A.G. Nikoghossian, On the Generation of Magnetic Field in the Floating Strength Magnetic Tubes, *DAN Arm. SSR*,**87**, 171-173, 1989.

Hubeny, Probabilistic Interpretation of Radiative Transfer, I,II, *Astron. Astrophys*., **185**, 332, 1987a, **185**, 336, 1987b.

Hubeny, in: Atmospheres of Early Type Stars, U. Huber, U.S. Jeffery, ed., Lecture Notes in Physics, No. 401, p. 377, Berlin, Springer, 1982.

D.G. Hummer, Non-coherent scattering: I. The redistribution function with Doppler broadening. *Mon. Not. Roy Astron. Soc*., **125**, 21–37, 1962.

A.F. Illarionov, R.A. Sunyaev, Compton Scattering by Thermal Electrons in X-Ray Sources, *Astron. Zh.*, **49**, 581-587, 1972.

G.L. Israelian, M. De Groot, Forbidden Lines in the Spectrum of P Cyg, *Astrophysics*, **34**, 171-174, 1992.

G.L. Israelian, A.G. Nikoghossian, The Spectral Variations of P Cyg, *Astrophysics*, **36**, 119-121, 1993.

G.L. Israelian, L.V. Tambovtseva, A.G. Nikoghossian, Wind Dynamics of LBV-Stars, *Astron. Zh*, **70**, 976-983, 1993.

G.L. Israelian, A.G. Nikoghossian, On Schuster's Mechanism of Emission Line Formation, *J. Quantit. Spectrosc. Radiat. Transfer*, **56**, 509-512, 1996.

doi: doi.org/10.52526/25792776-2021.68.2-186

V.V. Ivanov, Nonlinear Equations in Linear Problems of Radiative Transfer in Plane Atmospheres, *Astron. Zh.*, **22**, 612-618, 1978.

V.V. Ivanov, Radiative Transfer and the Spectra of Celestial Objects (in Russian), M., Nauka, (1969).

J.T. Jefferies, C. Lindsey, Radiative Transfer in Inhomogeneous Atmospheres, A Statistical Approach, *Astrophys. J.*, **335**, 372-382, 1988.

I.D. Karachentsev, V.Yu. Terebizh, On the Statistics of “Interacting” Galaxies, *Astrophysics*, 4, 443-449, 1968.

S. Kichenessamy, R.A. Krikorian, A.G. Nikoghossian, The Relativistic Doppler Broadening of the Line Absorption Profile, *J. Quantit. Spectrosc. Radiat. Transfer*, **27**, 653-655, 1982.

M.G. Krein, On New Method of Solution of Linear Integral Equations of the First and the Second Kinds, *Dokl. Acad, Sci. SSSR*, **100**, 413-416, 1955.

R.A. Krikorian, A.G. Nikoghossian, On the Lagrangian Formalism in the Radiative Transfer Theory, *J. Quantit. Spectrosc. Radiat. Transfer*, **56**, 465-469, 1996.

S. Koutchmy. Some Morphological Pecularities of the Solar Corona on 22 September 1968, *Astrophys. Let.*, **3**, 215-2020, 1969

S. Koutchmy, A.G. Nikoghossian, Coronal Linear Threads: W-L Radiation of Supra-thermal Streams, *Astron. Astrophys.*, **395**, 983-989, 2002.

S. Koutchmy, A.G. Nikoghossian, Analysis of the Radiation of Coronal Suprathermal Streams, *Astrophysics*, **48**, 62-67, 2005.

W. Magnus, *Comm. Pure and Appl. Math.*, **VII** (**??**), 649, 1954.

C. Magnan, The Method of Addition of Layers for Non-linear Radiative Transfer Problems: practical applications, *Astron. Astrophys.*, 543-551, 1993.

E. Menkohn, S. Richling, Radiative Transfer with Finite Elements.II.Ly-alpha Line Transfer in Moving Transfer, *Astron. Astrophys.*, **392**, 827-880, 2002.

D. Mihalas, Stellar Atmospheres, Freeman & Co, San Francisco (1970).

I.N. Minin, On the Theory of the Radiation Diffusion in a Semi-infinite Medium, *Dokl. Akad. Nauk. SSSR*, **120**, 63-65, 1958.

M.A. Mnatsakanian, Quasiasymptotic Solutions of the Problem of Radiation in a Slab of Finite Thickness, I. *Astrophysics*, **11**, 434-447, 1975.

M.A. Mnatsakanian, Quasiasymptotic Solutions of the Problem of Radiation in a Slab of Finite Thickness, II. *Astrophysics*, **12**, 295-311, 1976.

R.A. Muradian, H.V. Pikichyan, The Possible Reduction of Dome Impact on Images of Stars, CommBAO, **58**, 100-107, 1986.

A.G. Nikoghossian, Non-Linear Problem of Polychromatic Diffuse Reflection from an Infinitely Deep One-Dimensional Medium, *Dokl. Akad. Nauk ArmSSR*, **39**, 227–233, 1964.

A.G. Nikoghossian, Polychromatic Diffuse Reflection of Light from an Infinitely Deep One-Dimensional Medium, *Astrophysics*, **1**, 285–296, 1965.

doi: doi.org/10.52526/25792776-2021.68.2-186

A.G. Nikoghossian, H.A. Haruthyunian, Spectral Lines Formation for a General Law of Redistribution, *Dokl. Akad. Nauk SSSR*, **229**, 583-586, 1976.

A.G. Nikoghossian, The Problem of Diffuse Reflection for Redistribution of Radiation over Frequencies and Directions, *Dokl. Akad. Nauk SSSR*, **235**, 786 -789, 1977.

A.G. Nikoghossian, H.A. Haruthyunian, Diffuse Reflection of Light in the Case of an Arbitrary Phase Function,Astrophysics, **14**, 223– 230, 1978.

A.G. Nikoghossian, H.A. Haruthyunian, The Radiation Field in a Semi-Infinite Atmosphere Containing Energy Sources, *Astrophys. Sp. Sci*., **64**, 285 -299, 1979.

A.G. Nikoghossian, Diffuse Reflection of Light from a Semi-Infinite Atmosphere for the Redistribution Law $r_{II}(x,x\prime,\gamma)$, *Dokl. AN Arm.SSR*, **68**, 176-182, 1979.

A.G. Nikoghossian, Statistical Description of Radiation Field on the Basis of the Invariance Principle I., The Mean Number of Scatterings in a Medium Illuminated from Outside, *Astrophysics*, **21**, 527–537, 1984.

A.G. Nikoghossian, Statistical Description of Radiation Field on the Basis of the Invariance Principle.II., The Mean Number of Scatterings in a Medium Containing Energy Sources, *Astrophysics*, **21**, 685–693, 1984.

A.G. Nikoghossian, ”Reflection” Function for an Infinite Atmosphere in the Case of Non-Coherent Scattering, *Astrophysics*, 1986, **25**, 596-602, 1986.

A.G. Nikoghossian, Statistical Description of Radiation Field on the Basis of the Invariance Principle.III., Average Time of Photon Travel in the Scattering Medium, *Astrophysics*, **24**, 89–99, 1986.

A.G. Nikoghossian, On the Problem of the Formation of Quasars Emission Lines by the Cherenkov Mechanism, *Astrophysics*, **37**, 247-255, 1994.

A.G. Nikoghossian, Some New Nonlinear Relations of the Radiative Transfer Theory, *Astrophysics*, 38, 577-586, 1995.

A.G. Nikoghossian, G.L. Israelian, The Effect of Strong Scattering Processes in the Continuum on the Stellar Emergent Energy Distribution, *J. Quantit. Spectrosc. Radiat. Transfer*, **56**, 501-507, 1996.

A.G. Nikoghossian, Invariance Principle and Bilinear Relations of the Radiative Transfer Astrophys. J., **483**, 849–856, 1997.

A.G. Nikoghossian, S. Pojoga, Z. Mouradian, On the Radiative Transfer in Atmospheres with Randomly Distributed Inhomogeneities, *Astron. Astrophys*, **325**, 813–818,1997.

A.G. Nikoghossian, S. Pojoga, Z. Mouradian A Statistical Approach to the Investigation of Fine Structure of Solar Prominences, *Astron. Astrophys.*, **332**, 325-338, 1998.

A.G. Nikoghossian, S. Pojoga, Z. Mouradian, A Statistical Investigation of Prominence Fine Structure in the EUV, In: IAU Coll. 167, in: New Perspectives on Solar Prominences, (Eds. Webb D., Shmieder. B. & Rust. D.), 59-65, 1998.

A.G. Nikoghossian, S. Pojoga, Z. Mouradian, Statistical Characteristics of Radiation Formed in Atmosphere with Randomly Distributed Inhomogeneities, *Astron. Astrophys*, **342**, 785–798, 1999.

A.G. Nikoghossian, The Variational Formalism and Bilinear Relations of the Radiative Transfer Theory. *J. Quantit, Specrosc. Radiat. Transfer*, **61**, 345–359, 1999.

doi: doi.org/10.52526/25792776-2021.68.2-186

A.G. Nikoghossian, Z. Mouradian, Profiles of the Spectral Lines Formed in Stochastic Multicomponent Atmosphere, *Astron. Astrophys*, **360**, 1086–1095, 2000.

A.G. Nikoghossian, Non-Linear Relations for Statistical Mean Quantities Describing the Multiple Scattering Process, *Astrophysics*, **43**, 337-342, 2000.

A.G. Nikoghossian, On a Covering Problem and its Astrophysical Application, *Astrophysics*, **44**, 131-136, 2001.

A.G. Nikoghossian, S. Koutchmy, On Interpretation of the Radiation of Coronal Suprathermal Streams. I, *Astrophysics*, **44**, 528-535, 2001.

A.G. Nikoghossian, S. Koutchmy On Interpretation of the Radiation of Coronal Suprathermal Streams.II., *Astrophysics*, **45**, 489-496, 2002.

A.G. Nikoghossian, Intensity Fluctuations of Radiation Escaping from a Multicomponent Stochastic Atmosphere. I,, *Astrophysics*, **45**, 223-231, 2002.

A.G. Nikogohossian, Radiative Transfer in One-dimensional Inhomogeneous Atmospheres *Astron. Astrophys*., **422**, 1059 -1066, 2004.

A.G. Nikoghossian, Radiative Transfer in Inhomogeneous Atmosphere, I, II, III, *Astrophisics***, 47**, 104–115,2004a, 248–259, 2004b..412–420, 2004c.

A.G. Nikoghossian, J. Aboudarham, Z. Mouradian, Fluctuations of the Radiation Intensity Outgoing from a Multicomponent Stochastic Atmosphere. II, *Astrophysics*, **48**, 253 – 261, 2005.

A.G. Nikoghossian, Spectral Line Formation in a Dynamically Active Multicomponent and Stochastic Atmosphere, *Astrophysics*, **50**, 94 - 104, 2007a.

A.G. Nikoghossian, Spectral Line Formation in a Mesoturbulent Atmosphere, *Astrophysics*, **50**, 175-186, 2007b.

A.G. Nikoghossian, Diffuse Reflection of the Line-radiation from a Semi-infinite Turbulent Atmosphere, *Astrophysics*, **50**, 321-332, 2007c.

A.G. Nikoghossian, Ambartsumian’s Methods in the Radiative Transfer Theory, **52**, 1 – 23, 2009a.

A.G. Nikoghossian, Ambartsumian’s Principle of Invariance and Some Non-linear Relations of the Radiative Transfer Theory, *Astrophysics*, **52**, 431–439, 2009b.

A.G. Nikogohossian, Z. Mouradian, On Determining the Microturbulent Velocities of Solar Prominences, *Astrophysics*, **53**, 387–395, 2010.

A.G. Nikogohossian, Group-theoretical Description of Radiation Transfer in One-dimensional Medium, *Astrophysics*, **54**, 126–138, 2011a.

A.G. Nikogohossian, Bilinear Integrals of the Radiative Transfer Equation, *Astrophysics*, **54**, 242-249, 2011b.

A.G. Nikogohossian, Solution of Linear Problems of the Radiation Transfer in Plane-parallel Atmosphere. I, *Astrophysics*, **54**, 553–567, 2011c.

A.G. Nikogohossian, Solution of Linear Problems of the Radiation Transfer in Plane-parallel Atmosphere. II., *Astrophysics*, **55,** 261-274, 2012a.

A.G. Nikoghossian, Ambartsumian’s Methods in the Theory of Radiative Transfer, in: Ambartsumian’s Legacy and Active Universe, Springer, 37-59, 2012b.

doi: doi.org/10.52526/25792776-2021.68.2-186

A.G. Nikoghossian, Solution of Linear Problems of the Radiation Transfer in Plane-parallel Atmosphere. III., *Astrophysics*, **56**, 130-141, 2013a.

A.G. Nikogohossian, On Some Trends in the Progress of Astrophysical Radiative Transfer, *Light Scat. Rev*., **8**, 377–426, 2013b.

A.G. Nikoghossian, On the Role of the Reflection Function in Describing the Diffusion in the Plane-parallel Inhomogeneous Atmosphere, *Astrophysics*, **56,** 553-560, 2013c.

A.G. Nikoghossian, Groups and their Representations in the Radiative Transfer Theory. I,II., *Astrophysics*, **57**, 272-286, 2014a, 375-383, 2014b.

A.G. Nikoghossian, Groups in the Radiative Transfer Theory, *J. Quantit. Spectrosc. Radiat. Transfer*, **183**, 90-99, 2016.

A.G. Nikoghossian, Radiation Diffusion in an Inhomogeneous Turbulent Atmosphere, *Astrophysics*, **60**, 380-392, 2017.

A.G. Nikoghossian, Groups and their Representations in the Radiative Transfer Theory. III, *Astrophysics*, **62**, 92-117, 2019.

A.G. Nikoghossian, Investigation of Some Manifestations of Non-Stationarity in the Spectra of the Early Type Supergiants, *Astrophysics*, **63**, 2020 (in print).

V.S. Oskanian, V.Yu. Terebizh, Some Characteristics of the Flare Activity of UV Ceti Type Stars, **7**, 48-54, 1971a, 287-294, 1971b.

A**.** Peraiah, Principles of Invariance in Radiative Transfer, *Sp. Sci. Rev*., **87**, 465 – 538, 1999.

H.V. Pikichyan, Green's Function of a Plane-parallel Layer in the Case of Incoherent Anisotropic Scattering, *Astrophysics*, **14**, 96-108, 1978a,

H.V. Pikichyan, The Problem of Diffuse Reflection for an Arbitrary Law of the Frequency Redistribution, *Dokl. Acad. Sci. ArmSSR*, **67**, 151-156, 1978b.

H.V. Pikichyan, Green's Function of an Optically Thick Layer, *Astrophysics*, **16**, 209-217, 1980,

H.V. Pikichyan, Determination of the Radiation Field in a Composite Medium by Known Solutions of the Transfer Problems for Arbitrarily Chosen macro-Parts, *Dokl. Acad. Sci. SSSR*, **263**, 601-606, 1982a.

H.V. Pikichyan. General Relations of Invariance in Investigating the Transfer Problems fot the Media of Arbitrary Geometrical and Physical Characteristics, *Dokl. Acad. Sci. SSSR*, 262, 860-863, 1982b.

H.V. Pikichyan, Solution of the Transfer Problem in an Isolated Part of the Volume by the Solution Known for the Whole Volume, *Dokl. Acad. Sci. SSSR*, **273**, 861-865, 1983.

H.V. Pikichyan, Invariance Principle in the Problems of Addition of Layers of Arbitrary Properties, CommBAO, **55**, 5-16, 1984.

H.V. Pikichyan, Nonlinear Diffuse Reflection and Transmission of Radiative Energy by a Layer of Finite Thickness, *Astrophysics*, **53**, 251-267, 2010.

H.V. Pikichyan, On the linear properties of the nonlinear radiative transfer problem. *J. Quantit. Spectrosc. Rad. Transfer*., **183**, 113-127, 2016a.

doi: doi.org/10.52526/25792776-2021.68.2-186

H.V. Pikichyan, Internal Radiation Field in the Nonlinear Transfer Problem for a One-dimensional Anisotropic Medium. I.II, *Astrophysics,* **59**, 114-125, 2016b, 272-284, 2016c.

H.V. Pikichyan, The Inverse Problem of Statistical Determination of the Total Number, Luminosity Function, and Brightness Variability Characteristics of T Tau Type Stars in Stellar Aggregates, *Astrophysics,* **61**, 333-346, 2018.

H.V. Pikichyan, Analytical Solution of the Nonlinear Problem of Radiation Diffusion in a Pure Scattering Medium, **62**, 387-401, 2019.

R.W. Preisendorfer, *Hydrologic Optics*, vol. **IV**, U.S. Dept. of Commerse, Honolulu, Hawaii (1976).

R. Redheffer, On the Relation of Transmission-line Theory to Scattering and Transfer, *J. Math.& Phys*., **41**, 1-41, 1962.

G.B. Rybicki, Integrals of the Transfer Equations, *Astrophys. J*., **213**, 165-176, 1977.

G.B. Rybicki, in: Methods on Radiative Transfer, W. Kalkofen, ed., 21-64, Cambridge, Cambridje Univ. Press. 1984.

M. Scott, Invariant Imbedding and its Applications to Ordinary Differential Equations. An Introduction, Reading, MA. Addison-Wesley (1973).

Secchi-Pestelini, L. Barletti, Radiative Transfer in Stochastic Universe. .I, *New Astron*., **6**, 151-163, 2001.

V.V. Sobolev, Light Scattering in Inhomogeneous Atmosphere, Dokl. Acad. Sci. SSSR, **111**, 1000-1003, 1956.

V.V. Sobolev, Radiation Diffusion in a Semi-infinite Medium, *Dokl. Acad, Sci. SSSR*, **116**, 45-48, 1957.

V.V. Sobolev, On the Theory of Radiation Transfer in Stellar Atmospheres, *Astron. Zh*., **36**, 573–578, 1959.

V.V. Sobolev, A Treatise on Radiative Transfer, Princeton: Van Nostrand (1963).

V.V. Sobolev, Course in Theoretical Astrophysics, (in Russian), M., Nauka (1985).

E. Tandberg-Hanssen, The Nature of Solar Prominences, Kluver, Dordrecht (1995).

M. Tavel, Application of Noether's Theorem to the Transport Equation, *Transport Theory Statist. Phys*., 1, 271-285, 1971.

V.Yu. Terebizh, Some Nonlinear Problems in the Theory of Radiative Transfer within Spectral Lines, *Astrophysics*, **3**, 129-132, 1967.

V.Yu. Terebizh, polychromatic Light Scattering in a Semi-infinite Medium, **5**, 359-370, 1969.

V.Yu. Terebizh, Softening of Radiation by Multiple Compton Scattering, **6**, 368-371, 1970.

V.Yu. Terebizh, Source Number as a Function of the Flux and the V/V_m Method in the Investigation of the Evolution of the Quasi-stellar Radio Sources, *Astrophysics*, **9**, 118-124, 1973.

V.Yu. Terebizh, Luminosity Function of Quasi-stellar Radio Sources, *Astrophysics*, **11**, 104-105, 1975.

V.Yu. Terebizh, Luminosity Function of Seyfert Galaxies, *Astrophysics*, **16**, 36-46, 1980.

L.H. Thomas, The Slow Contraction or Expansion of a Fluid Sphere, *Mon. Not. Roy. Astron. Sci*., **91**, 122-127, 1930.

doi: doi.org/10.52526/25792776-2021.68.2-186

M.M. Vainberg, Variational Methods for the Study of Non-Linear Operators, san Francisco, Holden Day (1964).

H.C. Van de Hulst, Light scattering Tables, Formulas and Applications, Vol.1, New York, Academic Press (1980).

S. Vsessviatski & E. Bougoslavskaya, The Solar Eclipse of 1936 June 19, *Mon. Not. Roy. Astr. Soc.*, **104**, 140-148, 1944.

E. Wigner, Group Theory [Russian translation], izd. IL, Moscow (1961).

E.G. Yanovitskij, Light Scattering in Inhomogeneous Atmospheres, New York, Springer (1997).

N.B. Yengibarian, A.G. Nikoghossian, Diffuse Reflection of Quanta from the Turbulent Medium, In: Stars, Nebulas, Galaxies,: Izd. Acad. Sci. Arm.SSR, Yerevan, pp.65-72 (1969).

N.B. Yengibarian, A.G. Nikoghossian, Incoherent Scattering. II, III., *Astrophysics*, **8**, 39-51, 1972a, 128-136, 1972b.

N.B. Yengibarian, A.G. Nikoghossian, Diffuse Reflection of the Resonant Radiation from a Semi-Infinite Medium, *Dokl. ANArmSSR*, **54**, 91-95, 1972c.

N.B. Yengibarian, On Factoriization of the Symmetric Integral Operators, *Dokl. Akad. Nauk SSSR*, **203**, 4-8, 1972.

N.B. Yengibarian, A.G. Nikoghossian, Incoherent Scattering. IV. Infinite Medium, *Astrophysics.* **9**, 41-50, 1973.

N.B. Yengibarian, A.G. Nikoghossian, Incoherent Scattering, *J. Quantit. Spectrosc. Radiat. Transfer*, **13**, 787-811, 1973.

N.B. Yengibarian, M.A. Mnatsakanian, *Dokl. Akad. Nauk. SSSR*, **217**, 106, 1974.

N.B. Yengibarian, A.G. Nikoghossian, M.S. Gevorkian, Incoherent Scattering. V. *Astrophysics.*, **11**, 303-315, 1975.

Ya.B. Zel'dovich, R.A. Sunyaev, *Astrophys. Space Sci.*, **4**, 301 (1969).

V.S. Hayrapetian, A.G. Nikoghossian, The Linear Z-Pinch and Stellar Flare Phenomena, *Astrophysics*, **30**, 329-336, 1989.

V.Yu. Terebizh, Non-stationary Diffusion of Radiation in a Gas, *Astrophysics*, **4**, 45-46, 1968.

doi: doi.org/10.52526/25792776-2021.68.2-186

Communications of BAO, Vol. 68, Issue 2, 2021, pp. 236-310

Ambartsumian's vision and further insight to key puzzles of ultra-high energy astrophysics

G.Ter-Kazarian*[1]

[1]Byurakan Astrophysical Observatory, 378433, Aragatsotn District, Armenia

Abstract

We review the Ambartsumian's cosmogony, which involves his fundamental ideas on Stellar Associations and eruptive Activity of Galactic Nuclei, where the creation process is at work. It is caused by the violent outburst events of transformations of superdense matter in supermassive compact bodies in galaxies, away from the accretion physics. We discuss the pioneering works of V.A. Armbartsumyan and G.S. Saakyan carried out at Byurakan Observatory in the earlier of 1960's towards the physics of equilibrium configurations of degenerate superdense gas of elementary particles, particularity, the hyperon configurations of stellar masses. These issues have been comprehensively developed later on by G.Ter-Kazarian in the proposed theory of *distortion of space-time continuum* (DSTC) at huge energies (respectively, at short distances < 0.4fm), which underlies the *microscopic theory of black hole* (MTBH). The MTBH has further proved to be quite fruitful for ultra-high energy astrophysics. The MTBH explores the most important process of spontaneous breaking of gravitation gauge symmetry at huge energies, and thereof for that of re-arrangement of vacuum state. As a corollary, MTBH has smeared out the central singularities of BHs, and makes room for their growth and merging behavior, with implications of vital interest for high energy astrophysics.

Keywords: *stellar associations—galaxy: galactic nuclei—distortion of space-time continuum—black hole physics—X-rays: binaries*

Contents

*gago_50@yahoo.com, Corresponding author

doi: 10.52526/25792776-2021.68.2-236

1. Introduction

As the title of the present article promises, the central theme is the Ambartsumian's cosmogony from its historical development up to current interests. It describes the phenomenon of Activity of Galactic Nuclei, the existence of supermassive compact celestial bodies, and the implications for stellar and extragalactic high energy astrophysics, and the (at least partial) observational confirmation of this astonishing fact. Following the historical evolution of Ambartsumian's views, we hope to give prominence to his fundamental ideas, which manifests itself in the many different routes leading to spectacular astrophysical predictions. This report serves as an accessible introduction to the field and presents a compact and modern up-to-date source of reference on a well-defined topic, which can be a source of advanced teaching material. The selection of topics treated in detail (and the omission of other items) may be somewhat unusual, but we think it is justified in view of the title of this report. Wherever possible, we emphasize the mutual dependence and interplay between different subjects.

The fundamental concept of activity of galactic nuclei have a long tradition of precursors that dates back to the pioneering seminal works by V.A. Ambartsumian in 1950-1965. Among others, he was credited with outstanding contributions to stellar and extragalactic astronomy. Our primary interest in present article is rather to review the original vision of Ambartsumian on the Stellar Associations (Ambartsumian, 1947, 1949, 1954, 1955, 1958c, 1960, 1971, 1984, 1985) for analysing the observational data of highly energetic starburst processes, and the existence of, so-called, *super-dense prestellar D-bodies* in the Universe causing a different forms of eruptive Activity of Galactic Nuclei (Ambartsumian, 1958a,b, 1961, 1962, 1965, 1966, 1968a,b), where the creation process is at work. We also review the pioneering works carried out by Armbartsumyan with his student - G.S. Saakyan (Ambartsumian & Saakyan, 1960, 1961a,b, 1965) at Byurakan Observatory in the earlier of 1960's towards the physics of equilibrium configurations of degenerate superdense gas of elementary particles, particularity, the hyperon configurations of stellar masses. Consequently, these ideas have been further developed by G.Ter-Kazarian in his later works on the DSTC (Ter-Kazarian, 1986, 1989c, 1997, 2010, 2011, 2012, 2015) at huge energies, which underlies the MTBH (Ter-Kazarian, 1989a,b, 1990, 1991, 1992, 2001, Ter-Kazarian & Yerknapetian, 1995) with implications of vital interest for high anergy astrophysics (Ter-Kazarian, 2014, 2015, 2016a,b, 2021a, Ter-Kazarian & Sargsyan, 2013, Ter-Kazarian & Shidhani, 2017, 2019, Ter-Kazarian et al., 2003, 2006, 2007). Rather, we try to impart some knowledge about the fundamental nature and structure of the physical space-time in a mostly non-technical, nevertheless hopefully precise and consistent language. We hope that even professional experts will find some new viewpoints and connections between different topics. There are also several closely related physical issues worked out in Byurakan Astrophysical Observatory, not touched upon here for brevity reasons. These issues reveal an interplay between novel aspects of geometry and high energy physics, spacetime deformation induced inertia effects, and intense radiation physics. We briefly outline these issues in our second report (Ter-Kazarian, 2021b), to which the interested reader is invited to consult for further details.

With this perspective in sight, we will proceed according to the following structure. To start with, Section 2 recounts some of the highlights behind of Ambartsumian's cosmogony. Astrophysics in the second half of the 20th century is saturated with seminal ideas of an outstanding astronomer V.A. Ambartsumian, who originated in astrophysics a new paths that expands over decades. He appreciated the empirical approach to the problems of the origin and evolution of stars and galaxies when one attempts to uncover the secrets of nature by observing the key points where they are hidden. He often claimed that we can hardly achieve this aim only by theorizing. Just this approach allowed Ambartsumian to develop the cosmogonic concept (Ambartsumian, 1947, 1949, 1954, 1955, 1958a,b,c, 1960, 1961, 1962, 1965, 1966, 1968a,b, 1971, 1984, 1985), according which the stars, different star groups, and the interstellar gas are formed from certain superdense prestellar bodies by the eruption of various quantities of matter. In order of magnitude the mass of the prestellar body must be greater than the mass of a star.

Ambartsumian also was first who applied the same arguments to what appear to be violent outbursts in the nuclei of galaxies, and called attention to the instability and activity of galactic cores and, thus, raised the issue of Activity of Nuclei of Galaxies. The nuclei determines the most important processes in the life of large galaxies, particularly, its activity is responsible for the formation of the

doi: 10.52526/25792776-2021.68.2-236

spiral arms and formation of stars and the stellar clusters of spherical components. His key assumption was that every nucleous contains, as a rule, a supermassive nonstellar body along with the stellar population and gas, and, that nucleous plays an essential if not dominant role in the evolution of each galaxy. These phenomena seem to occur at different stages of development and are accompanied by corresponding changes in the nuclei. The process of formation of given type of subsystem varies under different circumstances.

Section 3 deals with a discussion of the composition of a degenerate gas with a density of order of nuclear density or higher (Ambartsumian & Saakyan, 1960), but not in the sense of a systematic and complete, textbook-like presentation, but by focusing on some characteristic and fundamental topics within this immensely rich theory. Earlier, attempting to explain supernova explosions, Zwicki (Baade & Zwicky, 1934, Zwicky, 1938) concluded on the possible existence of superdence states of neutron stars. The corresponding theoretical model suggested by (Oppenheimer & Volkoff, 1939). They calculated the values of masses of neutronic stars to be falling in the rage of 0.3 to 0.7 the mass of the Sun, while radii lie within the range of 6 to 20km. But much earlier Landau (Landau, 1932) speculated on the possibility of superdense cores in massive stars. Cameron (Cameron, 1950) took into account further the forces of mutual repulsion between neutrons acting at close neighborhood. He has found that the masses of some configurations of neutronic stars may reach ~ 2 the mass of the Sun. The difference in the model context between the study (Ambartsumian & Saakyan, 1960) and those of Oppenheimer and Volkoff is the presence of hyperons in composition of particles at high density. It points out to a possible existence of equilibrium configurations with a large number of hyperons. The temperature is assumed so low that all types of fermions are degenerate. It is shown that, with increasing density, different hyperons are successively appear and increase in number. They should be stable because of Pauli's exclusion principle. The threshold densities of different hyperons are calculated. Paradoxically, the smallest threshold density does not correspond to the Λ-hyperon, having the smallest mass at rest, but to the Σ^--hyperon. This suggests that a sufficiently massive celestial body in gravitational equilibrium should consist of a hyperon core, a neutron layer, and an outer envelope with the usual composition made of electrons, protons and composite nuclei.

On these premises, we review in Section 4 the equilibrium configurations of superdense degenerate gas masses (Ambartsumian & Saakyan, 1961a). The equilibrium configurations of highly degenerate baryonic ideal and real Fermi gases of stellar masses with density of order of density of atomic nucleus are studied.

In Section 5 we give an outline of internal structure of hyperon configurations of stellar masses with density of order of density of atomic nucleus and higher (Ambartsumian & Saakyan, 1961b). The space metric inside the configuration deviates essentially from Euclidean metric. The total number of baryons in configuration is calculated. For large values of this number there are two solutions with different total energies. Therefore, a stable configuration should be those with a larger mass defect. The gravitational mass defect of baryon stars has been investigated. The authors undertook a treatment of the case of infinitely high density. However, the problem of the state of matter in such cases where the mean distances between particles become appreciably smaller than the radius of the pion cloud surrounding (1.4fm) the baryons is still is open question. In the cores are identical in all the baryons or at least in some of them, additional repulsive forces should strongly make themselves felt as soon as particles come close, as was quite correctly noted by Zel'dovich (Zel'dovich, 1959) in line with the Pauli exclusion principle. Taking this to be a valid assumption, the theory of superdense degenerate state as presented by (Ambartsumian & Saakyan, 1961a) can no longer considered applicable for the range $N \gtrsim 10^{41}\mathrm{cm}^{-3}$.

Section 6 offers a more detailed analysis of the absolute gravitational mass defect $\triangle M = nm_n - M$ of neutron configurations (Ambartsumian & Saakyan, 1961b, 1965), where M is the observed mass of the star, n is the number of neutrons in it, m_n is the neutron mass. The existence of baryon configurations with an anomalous (negative) mass defect was predicted in (Ambartsumian & Saakyan, 1961b). The essence of the anomaly is that the mass of a superdense body is greater than the sum of the rest masses of the baryons it contains. The same subject was later discussed by Zel'dovich (Zel'dovich, 1962). He demonstrated that $M < fnm_n$, where $f \approx 1.5\sqrt{g_{rr}(R)}$, g_{rr} is the spatial component of metric tensor, and R is the star radius. This estimate of the upper limit of mass does not exclude

doi: 10.52526/25792776-2021.68.2-236

the possibility of the existence of equilibrium configurations with mass $M > nm_n$. It is shown that in the case of central densities $\rho(0)$ exceeding nuclear density by an order of magnitude, $\triangle M$ exhibits anomalous behavior. The anomaly consists in that with increase in $\rho(0)$ the mass defect decreases and, in the case of central baryon densities exceeding $10^{40}\mathrm{cm}^{-3}$, becomes negative. This phenomenon is caused by the severe disruption of additivity of internal energy in an intense gravity field, where nonlinear effects are extremely important. The configurations with an anomalous value of the absolute mass defect should be of great importance to Ambartsumian's cosmogonic concept Ambartsumian & Saakyan (1961b), according which stars, different star groups, and the interstellar gas are formed from certain superdense prestellar bodies by the eruption of various quantities of matter. In order to relate the behavior of baryon configurations with an anomalous value of the absolute mass defect to the concept mentioned, it is necessary to construct models of superdense prestellar bodies with masses of a much greater order of magnitude than the solar mass. This would solve in principle the problem of *superdense* cosmogony. However, the construction of physical models of continuous superdense prestellar bodies of great mass involves difficulties. The solution of these difficulties may possibly involve the consideration of nonstationary and nonequilibrium models. Further consideration of the problems of superdense states of baryonic configurations Ambartsumian & Saakyan (1960, 1961a,b, 1965) would confront us with many confusing and puzzling aspects. It is obvious that the problems of the state of matter at such desirable high densities can only be tackled in the framework of a new, unknown yet, fundamental physical theory apart of standard views.

The Irony of Fate. Although both fundamental ideas of the *activity of galactic nuclei* and the existence of *supermassive bodies* in galactic centers are now commonly accepted but, by the irony of fate, with irrevocably distorted upside-down meaning that the truth is the exact opposite of these claims. There is a crucial difference between Ambartsumian's interpretation of phenomenon of activity of galactic nuclei and the views of the majority of theoreticians, which based on the *accretion* physics and *infinite collapse* as the major law of Nature. While Ambartsumian put forward unquenchable hypothesis that *the primary events are the outflow of matter and emission of energy from the active superdense prestellar body in nucleus*, which at the beginning was an isolated body and gradually created a galaxy around itself, the theoreticians attribute the outflow of matter and other signs of nuclear activity as *secondary events* to the *primary event* of hypothetical *accretion* of diffuse matter into the central mass of galaxy, which commonly believed is a supermassive black hole (SMBH), described by a phenomenological model as a peculiar repercussion of general relativity (GR).

One of the achievements of contemporary observational astrophysics is the development of a quite detailed study of the physical properties of growth and merging phenomena of astrophysical black holes, even at its earliest stages. But even thanks to the fruitful interplay between the astronomical observations, the theoretical and computational analysis, the scientific situation is, in fact, more inconsistent to day. Actually, the active galactic nuclei (AGNs) with typical bolometric luminosities$\sim 10^{45-48}$ erg s^{-1} are amongst the most luminous emitters in the Universe, particularly at high energies (gamma-rays) and radio wavelengths. From its historical development up to current interests, the efforts in the AGN physics have evoked the study of a major unsolved problem of how efficiently such huge energy release from compact regions of AGNs observed can be generated. This energy scale severely challenges conventional source models. The huge energy release from compact regions of AGN requires extremely high efficiency (typically $\geq$ 10 per cent) of conversion of rest mass to other forms of energy. This serves for the majority of theoreticians as the main argument in favour of SMBHs, with masses of millions to billions of times the mass of the Sun, as central engines of massive AGNs. Within this scenario, a BH has been formed as an almost inevitable endpoint of the gravitational collapse of a large fraction of total mass of supermassive configuration occurring after entire burning of the whole amount of spared intrinsic energy. The BHs are fueled steadily from the thick accretion disks. Such evolutionary processes of accretion onto massive BHs as the prime energy sources have immense emissive power. The astrophysical black holes come in a wide range of masses, from $\geq 3\,M_\odot$ for stellar mass black holes to $\sim 10^{10}\,M_\odot$ for SMBHs. Although direct evidence for existence of BHs still has been elusive, it is now recognized the BH signatures in AGNs, with the implication that BH and galaxy formation processes are closely linked. Demography of local galaxies suggests that most galaxies harbour quiescent SMBHs in their nuclei at the present time and that the

doi: 10.52526/25792776-2021.68.2-236

mass of the hosted black hole is correlated with properties of the host bulge. The visible Universe should therefore be contained at least 100 billion SMBHs. A large number of representative models towards this are available in literature, but all they are subject to many uncertainties. Specifically, the Hubble Space Telescope measurements of stellar kinematics highlight an evidence for the ubiquity of SMBHs. However, the most important characteristics of the AGN powerhouse, the central masses and structures, and the BH formation and growth processes are not understood well. This issue is many-sided and fundamental, and can be settled fairly only by more investigations to be done for its better understanding.

The fact that accretion processes really take place in AGNs is already established and proven by many observations. With these observational advances, a tacit assumption of theoretical interpretation of astrophysical scenarios is a general belief reinforced by statements in textbooks, that the long-standing phenomenological model of BH (PMBH) is capable to describe the growth and merging behavior of accreting BHs. Even though the PMBH, namely, the most general Kerr-Newman black hole model, with parameters of mass (M), angular momentum (J) and charge (Q) (*still has to put in by hand*), is being among the most significant advances in astrophysics, it is rather surprising that this model is routinely used to explore the growth and merging behavior of BHs. Altogether based on this belief, the question then arises: What procedure is in fact employed by the astronomers in the course of reaching the conclusion while estimating a growth of energy-mass of astrophysical BH? The following stepwise properties are commonly attributed to above procedure:

(i) At first, from observations of surroundings of the BH, the astronomers by means of simulation estimated a total amount of the outside mass that potentially can be swallowed driven by an accretion onto BH.

(ii) Secondly, this amount of mass, without any substantiation, is simply accepted as a real *physical* measure of growth of energy-mass of the astrophysical BH.

Although arguably all these reasonings seemed appealing and attractive, nevertheless there is no convincing reason to rely on a validity of such procedure and, therefore, we do not share this view. Such beliefs are suspect and should be critically re-examined. First among them is the fact that observed time-scales for flux variations of some objects are inconsistent with contemporary black hole accretion models. That is, on the basis of the diagram of the minimum variability time-scale versus the bolometric luminosity for 60 sources it has been shown that, in spite of auxiliary assumption of asymmetric emission geometry, a few BL Lac objects - B2 1308 + 72, 3C 66A, OJ 287, AO 0235 + 16 and Quasars - 3C 345, 3C 446, 3C 454.3, LB 9743 remained in forbidden zone (particularly the three of them) (Bassani et al., 1983a,b), namely their observed sizes appeared to be less than the sizes of corresponding spheres of the event horizon. In many of the more recent papers (Ter-Kazarian, 1989a,b, 1990, 1991, 1992, 2001, Ter-Kazarian & Yerknapetian, 1995, Ter-Kazarian et al., 2003) (and references therein) it has repeatedly been recognized that the PMBHs, at least at their current state of development, are quite incapable of making predictions of their growth and merging behavior.

In the framework of PMBHs there is no provision for growth and merging behavior of BHs because of the nasty inherent appearance of BH *singularities*, and that if the *infinite collapse to the singularity* inside the BH is accepted as a legitimate feature of Nature. Certainly, during a super-increasing of total mass of configuration one undoubtedly will arrive (irrelevant to gravitational theory in use) to a critical turning point of relativistic collapse, beyond which the gravitational forces of compression prevail over all the other forces. Than it is enough to add from the outside a small amount of energy near-by the critical point in order to begin a process of irresistible infinite catastrophic compression of configuration under the pressure of grand forces. This certainly inhibits one to answer quantitatively such purely academic question, say, what is a further evolution of the decrease of the energy and entropy carried by the accreting mass that was swallowed by the BH; or what is further evolution of the coalescence and merger of binary BHs at grazing collision of members, when triggered by the emission of gravitational waves their orbits will tighten by spiraling inwards. At this, immediately the question arises whether or not yet observationally unverifiable standard four laws of the mechanics for a stationary, asymptotically flat, black BH in four dimensions will be valid as well for non-stationary processes of BH formation and growth. To the best of our knowledge, the PMBH does not answer the questions invoked.

doi: 10.52526/25792776-2021.68.2-236

Notwithstanding, much remarkably efforts have been made in understanding of BH physics, many important issues still remain unresolved and, thus, a situation is unclear, than described so far. Therefore the purpose of Section 7 is to examine the meaning of such statements and to assess briefly the validity of the growth and merging properties of BHs within the PMBHs. The first goal is to review briefly the necessary ideas behind the various specific constructions and suggestions on the conceptual problems of GR, the singularities and the thermodynamics of BHs in semiclassical and quantum physics. The second goal encompasses the many discoveries which unlocked the mysteries or exposed some of the illusions of the considered field. Without it we cannot show how the matters stand, we almost bound of necessity to enter upon it, if we would write of them at all.

In this respect, we should deliberately refrain from presumption of such exotic hypothetical behaviors, which seem nowhere near true if one applies the phenomenological model. But, how one can be sure that some hitherto unknown source of internal pressure does not become important above such extreme densities and halt the collapse? The failure of the PMBH does not necessarily imply a failure of the BH concept in general. In spite of a thorough search no reason could be found to introduce the required huge energy scale in BH physics but considerable change of properties of space-time continuum in density range far above nuclear density. We believe that a complete, *self-consistent* gravitation theory will smear out singularities at huge energies. This may shed further light upon the growth and merging phenomena of astrophysical BHs.

To fill the void which the standard PMBH presents and to innovate the solution to alluded problems, in what follows, we should recount some of the highlights behind of MTBH, whereas the infrastructures will inevitably be accommodated inside the EH. To start with, in Section 8 we discuss the proposed general theory of DSTC (Ter-Kazarian, 1986, 1989c, 1997, 2010, 2011, 2012, 2015), underlying the MTBH. This theory, in particular, involves a drastic revision of a role of local internal symmetries in physical concept of curved geometry, and explores the most important processes of spontaneous breaking of gravitation gauge symmetry and rearrangement of vacuum state. Using the language of fundamental geometric structure - distortion gauge induced fiber-bundle, it leads to modified gravitational theory as a corollary of the spacetime deformation/distortion framework. We generalize the standard gauge scheme via the concept of distortion gauge field which acts on the external spacetime groups, and that accounts for *gravitation gauge group* G_R generated by hidden local internal symmetry implemented on the *maximally symmetric* (MS) - space. Thereby we construct a formalism of unitary mapping of the fields and their dynamics from the flat space to the curved space, and vice versa. In the framework of method of phenomenological Lagrangians, we relate the group G_R to non-linear realization of the Lie group G_D of *distortion* of local internal properties of the 12-dimensional M_{12} MS-space. We study the geometrical structure of the space of parameters in terms of Cartan's calculus of exterior forms introduced through the appropriate Maurer-Cartan's structure equations. The metric in our approach is no more a fundamental field. Hence, we extend the curvature of the spacetime continuum to general distortion as the theory of spontaneous breaking of distortion symmetry. The fundamental field is distortion gauge field and, thus, all the fundamental gravitational structures in fact - the metric as much as the coframes and connections - acquire a distortion-gauge induced theoretical interpretation. Particular attention is given to realization of the group G_R by the hidden local internal symmetry of abelian group $U^{loc} = U(1)_Y \times diag[SU(2)]$ implemented on the M_{12}, where Y is the hypercharge. We address the rearrangement of vacuum state in gravity resulting from these ideas. Spontaneous symmetry breaking is achieved by Higgs scalar. Two neutral gauge bosons were mixed to form the massless and massive components of distortion field. Hence, a massive distortion field component may cause an additional change of properties of the space-time continuum beyond gravity at huge energies. This theory is renormalizable, because gauge invariance gives conservation of charge, also ensures the cancelation of quantum corrections that would otherwise result in infinitely large amplitudes. Moreover, one of the underlying principles of MS-space interacting quantum field theory is that the vacuum is well-determined and unique, in particular, $|in>=|out>$ (up to a phase factor).

The available solar system observational verifications offer many opportunities to improve tests of relativistic gravity. We rather have shown that the agreement is satisfactory between the proposed theory of gravity and mentioned observational verifications. Thereby the free adjustable parameter

doi: 10.52526/25792776-2021.68.2-236

ε in metric component, in case of static spherically symmetrical system, $g_{00} \simeq 1 - \frac{R_g}{r} + \varepsilon\frac{R_g^2}{r^2}$, can be written in terms of Eddington-Robertson expansion parameters β and γ, as $\varepsilon = 2(\beta - \gamma)$. The best fit for satisfactory agreement between the proposed theory of gravity and observation is reached at $\varepsilon = (2.95 \pm 3.24) \times 10^{-5}$. Moreover, it is consistent with GR up to the limit of neutron stars. However, this theory manifests its virtues applied to the physics at huge energies. Whereas a significant change of properties of space-time continuum, so-called inner distortion (ID), arises simultaneously with the strong gravity.

In Section 9 we discuss some basic knowledge and a few more technical details of MTBH (Ter-Kazarian, 1989a,b, 1990, 1991, 1992, 2001, Ter-Kazarian & Yerknapetian, 1995), which would certainly be helpful for the reader. The MTBH is a first-principles treatment of a fundamental *superdense protomatter* physics, but it also has an actual physical realization of Ambartsumian's fundamental vision. We necessarily proceed with some preliminaries on generic of the MTBH as a guiding principle to make the rest of paper understandable. Exploring the most important process of a spontaneous breaking of gravitation gauge symmetry at huge energies, MTBH is an extension of the PMBH to huge energies. This has smeared out a central singularity of a BH at very strong gravitational fields, replacing it by the equilibrium *superdense proto-matter core* (SPC), subject to certain rules. Encapsulated in an entire set of equations of equilibrium configuration, the SPC is a robust structure that has stood the tests of the most rigorous theoretical scrutinies of a stability (Ter-Kazarian et al., 2007). This approach manifests its practical and technical virtue in the most remarkable drawback of MTBH, which is the fact that, instead of *infinite collapse* and *central singularity*, an inevitable end product of the evolution of massive object is the stable SPC. This will ultimately circumvent a principle problem of an observer's inability to access the degrees of freedom that are hidden beyond the horizon, and a necessity to assign the *elusive entropy to BH*. This in somehow or other implies that a physical entropy is assigned to SPC as a measure of the large number of thermodynamical real microstates of proto-matter, which is compatible with a concept of *ergodicity*. Due to it, MTBH is proved to be quite fruitful for the study of outlined below fundamental non-stationary ultra-high energy phenomena. We describe finite though unbelievably extreme conditions held in SPC, where, nevertheless, static observers are existed. The stable equilibrium holds as well in outward layers and, thus, an accumulation of matter is now allowed around the stable SPC. An external physics of accretion onto the SPC in the earlier half of its lifetime is identical to the processes in Schwarzschild's model. A crucial difference in the model context between the phenomenological and microscopic models of black hole comes in when one looks for the spontaneous breaking of gravitation gauge symmetry at huge energies, and thereof making room for growth and merging behavior of black holes. It should be emphasized that the key to our construction procedure is widely based on the premises of our experience of accretion physics. Therefore, what we have presented here has all the vices and virtues of the classical scenario of runaway core collapse which has always been a matter of uncertainties and controversies. Nevertheless, we caution that these entire constructions will be valid as well in the case if some hitherto unknown yet mechanism in Nature will in somehow or other way produce the superdense proto-matter, away from the accretion physics.

With this perspective in sight, in Section 10, we have undertaken a large series of numerical simulations with the goal to trace an evolution of the mass assembly history of 377 plausible accreting supermassive black hole seeds in AGNs to the present time and examine the observable signatures today (Ter-Kazarian, 2014, 2015, Ter-Kazarian et al., 2007). Given the redshifts, masses and luminosities of these black holes at present time collected from the literature, we compute the initial redshifts and masses of the corresponding seed black holes. For the present masses $M_{BH}/M_{\odot} \simeq 1.1 \times 10^6$ to 1.3×10^{10} of 377 black holes, the computed intermediate seed masses are ranging from: $M_{BH}^{Seed}/M_{\odot} \simeq 26.4$ to 2.9×10^5. We compute the fluxes of UHE neutrinos (Ter-Kazarian, 2001, 2014, 2015, Ter-Kazarian et al., 2007). The AGNs are favored as promising pure UHE neutrino sources, because the computed neutrino fluxes are highly beamed along the plane of accretion disk, peaked at high energies and collimated in smaller opening angle ($\theta \ll 1$). While hard to detect, the extragalactic ZeV-neutrinos may reveal clues on the puzzle of the origin of UHE-cosmic-rays with energies exceeding 1.0×10^{20} eV, as they have the advantage of representing unique fingerprints of hadron interactions and, therefore, can initiate the cascades of UHE-particles. We also study neutrino

doi: 10.52526/25792776-2021.68.2-236

cooling and fueling at disk accretion onto the SPC in AGN, and origin of UHE G.R.s (Ter-Kazarian, 2001, Ter-Kazarian et al., 2003).

In Section 11, we discuss the most striking recent revolutionary NuSTAR discovery of the first rare and mighty ultraluminous X-ray pulsations (Ter-Kazarian, 2016a,b). The pulsed luminosity of M82X-2 is the most extreme violation of the Eddington limit and could be reconciled with that in the model of magnetic neutron star pulsar only by very arbitrary assumptions on geometric beaming of accretion flow on neutron star. Instead of making such assumptions, we tackle the problem by the implications of MTBH, without the need for significant breaking of Eddington limit. The M82X-2 is assumed to be a spinning intermediate mass black hole resided in final stage of growth. As a corollary, the thermal blackbody X-ray emission, arisen due to the rotational kinetic energy of black hole, escapes from event horizon through the vista to outside world which is detected as ultraluminous X-ray pulsations. The M82X-2 indeed releases $\simeq 99.6$ of its pulsed radiative energy predominantly in the X-ray bandpass $0.3 - 30$ keV. We produce a coherent picture of the pulsed radiation of M82X-2: we derive a pulse profile and give a quantitative account of energetics and orbital parameters of the semi-detached X-ray binary containing a primary accretor M82X-2 of inferred mass $M \simeq 138.5 - 226 M_{\odot}$ and secondary massive, $M > 48.3 - 64.9 M_{\odot}$, O/B-type donor star with radius of $R > 22.1 - 25.7 R_{\odot}$, respectively. We compute the torque added to M82X-2 per unit mass of accreted matter which yields the measured spin-up rate.

However, we need to be more rigorous about a geometry which describes rotating axisymmetric black holes. Therefore, in Section 12 we analytically study the microscopic model of stationary and axisymmetric rotating black hole (Ter-Kazarian, 2016a). There are deep conceptual and technical problems involved, and these provide scope for the arguments discussed, which are carefully presented in both mathematical and physical terms. We derive field equations and obtain both internal and global vacuum spacetime solutions. The most remarkable feature of microscopic model of a rotating black hole is that, in earlier part of its lifetime, the external physics outside of outer oblate event horizon of accretion onto a black hole is identical to the processes in Kerr's model. But, there is also a crucial difference between internal physics of Kerr and microscopic rotating black hole models, that is, a central ring singularity of the Kerr black hole cannot occur, which is now replaced by finite though unbelievably extreme conditions held in the central part of rotating SPC, where the static observers exist. The corrections introduced by this theory to the characteristic phase profile of M82X-2 of previous model are calculated (Ter-Kazarian, 2016a, Ter-Kazarian & Shidhani, 2017).

In Section 13 we further expose the assertions made in MTBH, for the physics of intermediate mass black holes (IMBHs) (Ter-Kazarian & Shidhani, 2019). This allows to construct microscopic models of accreting IMBHs. The mass estimates collected from the literature of all the observational evidence for 137 IMBH-candidates,even though there are still large uncertainties, allow us to undertake a large series of numerical simulations to derive all their essential physical characteristics. We compute among the others the masses, redshifts and growth-time scales of seed BHs. The luminosities of IMBH-candidates are computed by using a derived new scaling mass-luminosity relation.

The physical outlook and concluding remarks are given in Section 14.

2. Ambartsumian's cosmogony

Prior to Ambartsumian's work, the astronomers were applying the kinematic theory of gases to stars. In reality, the stars interact in accordance with Newton's law and special physical statistics should be used for investigations of stellar systems. Ambartsumian laid the foundations of such statistics and applied it to multiple stars and star clusters. This becomes further the basis for the statistical mechanics of the stellar systems. He determined the distribution of elements of binary star orbits at equilibrium and suggested that such state has not yet arrived. He also studied the process of star cluster disintegration due to escape of high-velocity stars and discovered that the process did not yet go too far. This led to a conclusion that the age of the galaxies is less than 10^{10} years. It was assumed previously that the stars were much older. Ambartsumian clearly proved the *short scale* of galactic life in a dispute (1935-1937) with the known British astronomer Sir James Jeans. The main feature of proposed earlier models describing the origin and evolution of stars and galaxies is the

doi: 10.52526/25792776-2021.68.2-236

initial hypothetical state of tenuous gas, while stars originate through the condensation of this gas. The stellar matter remains a classical perfect gas throughout all of initial phases of evolution.

However, based on the observations in 1947 of stars of O and B spectral types and T Tauri and flare stars that cluster very loosely, he was first to suggest a concept of OB and T associations, coined by him as Stellar Associations (Ambartsumian, 1947, 1949, 1954, 1955, 1958c, 1960, 1971, 1984, 1985, ?). The observations indicate that in real stellar systems of the trapezium type one of the components belongs to O or B spectral types. Such stars are of recent formation and the number of revolutions they complete in the system is expected to be small. However, the observations show that a few multiple stars of later spectral classes also possess trapezium-like configurations. Of course, the configurations we observe on the sky are projections of true space configurations. Therefore, even if there are no real trapezium configurations of later- type stars, when they are projected on the sky a small percentage (8%) of apparent configurations of the trapezium type will appear. This is almost precisely the percentage of trapezium configurations observed in cases where the components of multiple stars do not belong to the O and B spectral types. In other words, there are no or almost no real configurations of the trapezium type among the late-type multiple stars. The analysis of observational data of young stars leads to the conclusion that very dense protostellar bodies give birth to more or less numerous groups of stars. These considerations prove that the ideas about the simultaneous emergence of stars and diffuse matter from denser and more massive bodies are more fruitful and correspond to reality. In these associations the stars differ from the surrounding stars by having a greater partial density (i.e., density of stars of a given spectral class).

On these premises, Ambartsumian explained relatively rarely observed forms of activity of a nearby red dwarf stars, which have evolutionary significance Ambartsumian (1971). These, first of all, are the transitions from a state of low luminosity to a state of higher luminosity, maintaining this for a long time. This was observed in the objects of FU Orion type (Fuors) and objects of Herbig-Haro. Fuors are the variable stars that can undergo unpredictable dramatic increases in brightness in the observed part by more than a hundred times in a short period of time, after which they retain increased luminosity for many years. Much attention is paid to the variable dwarfs among which the atmospheres of UV Ceti stars and T Tauri stars should be more attractive ones. In their spectra, bright lines and the emission of a continuous spectrum are observed, which are sometimes so strong that all absorption lines are veiled. The stars of type T Tauri are interesting as they meet in groups, forming associations. In 1953, Ambartsumian paid attention to the fact that in short burst periods, UV Ceti type variable stars acquire some features similar to characteristics of T Tauri stars, and that the T Tauri type stars along with continuous and irregular changes of brightness also show flare type changes. He concluded that these two types of objects are genetically related. The ultraviolet excess observed in some T Tauri stars has approximately the same energy distribution as the emission from flares of UV Ceti type stars. A comprehensive study of this phenomenon allows Ambartsumian in 1968 to conjecture that *the flare stars are the earliest evolutionary stages of the dwarf stars*. Moreover, he believes that the stage of a flare star follows a stage of T Tauri type at overlapping of these stages.

The nature of the source of non-thermal and corpuscular radiation of the prefuor is unknown. Ambartsumian argued that a superdense companion in the close neighborhood of that star (red dwarf) gives the thermal radiation of the prefuor. While it cannot be ruled out that the envelope is ejected by a super-dense companion. Proceeding from the fact that prefuors and flare stars are members of the same stellar associations, Ambartsumian concluded (Ambartsumian, 1971) that the processes of decay and release of energy in both cases have the same physical nature. Ambartsumian believes that each outburst is the result of the explosion (when brightness increase time is often measured in seconds) of a certain portion of the *prestellar superdense matter*, which came out from the inner layers of the star, where a prestellar matter remained for a relatively long time before explosion. A release of energy during decay processes of prestellar matter is reminiscent of the phenomena of radioactive decays. Ambartsumian, therefore, rejected the assumption of thermonuclear reactions as the main sources of this energy. Based on the idea that a portion of superdense prestellar matter transfers from the stellar interiors to the surface layers of young stars, Ambartsumian predicted the existence of *fast* and *slow* flares, which were later discovered, and gave an explanation to the Fuor phenomenon.

Ambartsumian predicted (Ambartsumian, 1949) the expansion of the associations, which was later

doi: 10.52526/25792776-2021.68.2-236

observed. A mere comparison of statistical data concerning clusters and associations revealed that much greater number of systems are originated with positive, than with negative energies. The associations with with positive energies are very unstable and should disintegrate rapidly. From the fact that they did not disintegrate until now, it was concluded that they are not more than few million years old. This conclusion about the youth of stars contained in associations is supported by a number of other features of associations. He thus concluded that stellar births of explosive events are ongoing in the galaxies where stars are born in groups. Ambartsumian's stemming idea of stellar association as a dynamical entity of groups of stars with positive total energy had far-reaching implications for subsequent star formation theories. These ideas have a subsequent influence in his interpretation of active galaxies.

Ambartsumian was first to show in the early 1950's that the so-called radiogalaxies are not a result of accidental collision of two gigantic star systems, but represent a definite stage of internal evolution of galaxies of very high luminosity. *Activity* of galaxies, which manifests in their radio emission, is intimately connected with new formations, such as jet ejections extending from the galactic nucleus, spiral arms, and new star systems emerging within old galaxy. Ambartsumian was also first to call attention to the instability and activity of galactic cores and, thus, raised the issue of Activity of Nuclei of Galaxies (Ambartsumian, 1958a,b, 1961, 1962, 1965, 1966, 1968a,b). In his report at the Solvay Conference on Physics (Brussels 1958), Armbartsumian claimed that the activity of the galactic nuclei determines the most significant processes in the evolution of galaxies. He argued that so-called *D-bodies* exist in nature, which are responsible for the activity of the nuclei of galaxies, and that galaxies are born from the explosion of such *D-bodies*. Indeed, the correctness of Ambartsumian's general conception was incorporated with the subsequent discovery of quasi-stellar radio sources (quasars), which are starlike objects of exceptionally high luminosity at cosmological distances. These objects exhibit extraordinary violent processes including very fast fluctuation of luminosity, jet ejection, and high motion velocities of luminescent gases. There is very likely a close connection between galactic nuclei and quasars, and thus formation of developed structure of galaxies is, apparently, connected with their nuclei (or, possibly, with quasars). The nuclei of galaxies are the places where new objects are generated, and the fact that the activity can be found in galaxies with a wide range of distances strongly suggests that the activity goes on at all epochs. Violent events in galaxies are manifestations of mass creation. From these events huge fluxes of relativistic particles and rapidly moving gas clouds are generated. Quasars with *intrinsic redshifts* are also ejected, and they are probably related to the mechanism through which new galaxies are formed. Following Armbartsumian, it is reasonable to consider the possibility that systems of galaxies with positive total energy also originate in this way. He didn't believe that all cases groups and clusters of galaxies are stable and bound. Note that a common point of view has been that in general such systems are bound by unseen matter. In some cases this is clearly true, but it is not a general rule. Thus, a large part of the argument for the presence of much dark matter goes away, since it is mostly based on the use of the virial theorem. As well as when the interacting systems of galaxies are detected there is no good reason to believe that they are merging. This is what all of the observers like to assume, but from an observational point of view they may well be coming apart. Presumably the prejudice towards merging is based on the idea that gravity is the only force acting. But if explosive events are clearly seen, even if we do not understand them, the possibility that objects are separating rather than merging must be considered. Only in the cases in which tidal effects can clearly be seen to be present, as in the classical case of NGC 4038-39, is it reasonable to accept the merging hypothesis. There is much direct evidence that coherent objects- galaxies, quasars, etc. do not originate from initial density fluctuations in the Universe, but are generated and ejected from galactic nuclei as was originally proposed by Ambartsumian. The rapid release of large amounts of energy from galactic nuclei arise from creation processes, which taking place here and now in the present epoch. Thus he concluded that there exist clusters which are in a particularly active phase of evolution when new galaxies originate within them. Ambartsumian believed, see e.g. (Ambartsumian, 1961), that a strong argument in support of this view is provided by the two galaxies (NGC 3651 and IC 1182) out of the nuclei of which jets are ejected containing blue condensations. These galaxies with blue jets are also among the brightest members in the corresponding clusters. Finally, there are cases when blue components occur in the vicinity of other

doi: 10.52526/25792776-2021.68.2-236

giant elliptical galaxies, which evidently represent a later stage in the evolution of the above blue condensations. The famous interacting galaxy pair NGC 3561 A&B sometimes described as a spiral and elliptical galaxy in collision with a tidally bound dwarf galaxy created in in the collision. The embedded nebulosity is attributed to tidal effects. Several other active galaxies have been found to exhibit the same effect. Ambartsumian pointed out that this system may equally well be the result of the ejection of one galaxy from another, along the lines of M87 and M84 with this debris extending over $\sim 100kpc$ with blue dwarf galaxies and starforming regions emerging out of the debris. Thus, he believed that this is an excellent example of one galaxy ejecting another, and the existence of much star formation and the high-redshift quasars shows that the creation process is at work. His view was that the galaxies which are expanding away from parent galaxy have been generated by processes in the nucleous of that galaxy. He gave as another example some of the small groups of galaxies and highly irregular clusters like the Hercules cluster, in which the kinetic energy of the visible galaxies is much greater than the potential energy. If this is so, Ambartsumian concluded that the phenomena all pointed to ejection from superdense state, and that the galactic nuclei must contain superdense bodies of huge mass and some kind of *non-stellar* objects of unknown nature. He, in fact, conjectured that such an eruptive activity is due to the violent outburst events of transformations of superdense matter in supermassive compact *D-bodies* in galaxies, away from the accretion physics, where the creation process is at work. This signifies that every nucleus is made up of three components: *stellar population, gas and supermassive body.* Dynamically, the nucleus evolves independently of the rest of the galaxy.

In all these ideas Ambartsumian was initially alone. For many researchers it is still not easy to admit the possibility of changing the traditional paradighm of the models of gravitational collapse, even that they leave an inexplicable gap in explaining how the stars and galaxies come into being. From their view point, the apparent difficulty with Ambartsumian's hypothesis (Ambartsumian, 1961) is coming from dynamical arguments that the time scale for such systems to disintegrate is $\leq 10^9$ years, a value much less than H_0^{-1}, and much less than the time scale associated with galaxy formation and evolution in the big-bang cosmology. For example, Ambartsumian's estimate of age of M 82 employed only the fact that it has velocity higher than the velocity of escape from the M 81 group. All the members of the group M 81- M 82 are well known and therefore the upper limit of luminous mass can be estimated for certain, while any estimate of non-luminous mass will be quite arbitrary. So he was concluded that M 81 may be much older than M 82 and only M 82 (and perhaps NGC 3077) is of recent origin. But, of course, one also may consider the possibility that in this system of galaxies there exists rather more mass than is indicated by the luminous galaxies. However, the pressure of the further observations does its work, slowly but steadily. Generally though, they produce almost innumerable evidence in favor of ejections and explosions and are rather scanty regarding the processes of condensation and collapse. The concept of AGNs was widely accepted a few years later. A thousands of galaxies with strong ultraviolet excess have been discovered ever since in Byurakan Observatory under his direction. Ambartsumian's student, B. Markarian (well known for Markarian galaxies), completed a brilliant survey of galaxies known by his name with UV excess using the 1-m Schmidt telescope of the Byurakan Observatory. A study of the structure of the irregular clusters of galaxies leads one to the conclusion that often they are made up of several superimposed groupings. An interesting example of such a grouping was pointed out by Markarian: the chain of bright galaxies in the Virgo cluster containing NGC 4374, 4406, 4438 and others. This wonderful arc of eight bright galaxies is presumed to represent a physical grouping within the Virgo cluster. On the other hand facts about the radial velocities of the members of this group undoubtedly establish its positive total energy. Such facts are pronouncing an indictment against the ideas supporting the condensation processes. Thus, his conclusion was that observations produce almost innumerable evidence in favor of ejections and explosions and are rather scanty regarding the processes of condensation and collapse. In the observable Universe the processes of expansion and diffusion are responsible for the majority of changes occur now. These violent explosions were the manifestations of mass creation events.

doi: 10.52526/25792776-2021.68.2-236

3. The degenerate superdense gas of elementary particles

Following Ambarstumian, three series of observational data providing an evidence in favor of superdense initial state are: (i) the galaxies and spiral arms are formed from their nuclei (Ambartsumian, 1958a,b), which have small sizes and high density; (ii) close groups of stars and Trapezium-type systems in associations and, in particular, in central regions of large gaseous nebulae found in O-associations; the phenomenon of flares in UV Cetl stars, and in many of the T-association members (Ambartsumian, 1958c). The most important property of superdense states, as will be seen from the following, must be the presence of hyperons in the star, in addition to neutrons. Let consider the processes releasing energy during transition from metastable state to stable one. Since, at sufficiently low temperatures, the nucleon (neutron or proton) gas is highly degenerate, hyperons with energies lower than a threshold value will become stable, because in accordance to Pauli's exclusion principle, the nucleons arising from their decay cannot find a place in phase space. For the same reason, the interconversion of different types of hyperons is also impossible. The hyperons present must also form a degenerate gas. Then, following Ambartsumian & Saakyan (Ambartsumian & Saakyan, 1960), we consider here a degenerate nucleon-electron gas with density of nuclear density, or higher, at a temperature $T = 0$. At densities above certain value, the threshold Fermi energies for nucleons and electrons become so high that to maintain minimum total energy of the gas it is favorable if some of the nucleons should have changed into hyperons. Here the authors are not interested in the way in which superdense states are formed. To determine the relative abundance of the various types of particles as a function of density, they used a table of elementary processes of all standard leptonic transitions in which nucleons (n,p) converse into Λ, Σ and subsequently Ξ-hyperons, to obtain respective relations between the chemical potentials μ_i of elementary particles $n, p, \Lambda, \Sigma, \Xi, e, \nu, \bar{\nu}$ as follows: $\mu_{\Xi^0} = \mu_{\Sigma^0} = \mu_\Lambda = \mu_n$, $\mu_{\Sigma^+} = \mu_p = \mu_n - \mu_e$, $\mu_{\Xi^-} = \mu_{\Sigma^-} = \mu_n + \mu_e$, which is valid for particles obeying Fermi statistics at $T = 0$. The chemical potentials μ of the particles equal to their threshold Fermi energies. The $e, \nu, \bar{\nu}$ denote electron, neutrino and antineutrino, respectively. Also $\mu_\nu = \mu_{\bar{\nu}} = 0$, because neutrinos and antineutrinos escape from the volume of the star as soon as they are generated without experiencing any interactions (the cross section for the interaction of neutrinos with electrons is of the order $10^{-44}\mathrm{cm}^2$). A derivation of concentrations of various particles in a highly degenerate baryon gas at absolute zero temperature is based on the following supplementary assumptions: (i) At equilibrium, the energy of the system should be a minimum. (ii) Conservation of the number of baryons in all the processes leading to establishment of a state of statistical equilibrium of configuration. (iii) The star as a whole, as well as its separate macroscopic regions, should be electrically neutral. Consequently, the problem is reduced to determining the minimum of the energy density of the medium of possible various particles, with the supplementary conditions stemming from the above assumptions. The accepted procedure for this is to equate to zero the derivatives of the resulting extended energy function with respect to the particle concentrations, one finds the necessary conditions for the energy of mass distribution to be a minimum. The final problem is now to find the variation of the particle concentrations as the total number of baryons N increases from zero to very high values. There will be a number of phase changes as N increases. However, to find the values of density attained in any given cosmic body, which is in equilibrium state under the action of its own gravitational forces, one should employ GR to derive the equation of state $\rho = \rho(P)$, or in parametric form. This reveals the overall scenario. At density $\rho < \rho_n = 1.28 \times 10^7\mathrm{gcm}^{-3}$, the gas consists of protons and electrons. At $\rho = \rho_n$ neutrons appear. At density $\rho > 10^8\mathrm{gcm}^{-3}$, the number of neutron is much larger that numbers of protons and electrons. The individual atomic nuclei will no longer play an important role. At baryon density $N \geq 6.4 \times 10^{38}\mathrm{cm}^{-3}$, i.e. $\rho = \rho_{\Sigma^-} = 1.1 \times 10^{15}\mathrm{gcm}^{-3}$, the first hyperons appear. Although the rest masses of the hyperons $\Lambda, \Sigma^+, \Sigma^0$ are smaller than that of the Σ^-, nevertheless first Σ^--hyperons appear. Highly degenerate matter contains hyperons and μ^--mesons in addition to nucleons. At $\rho = \rho_\Lambda$, Λ-hyperrons appear, and with a further increase of density, other heavier hyperons make an appearance altogether with . For baryons densities exceeding $5 \times 10^{16}\mathrm{gcm}^{-3}$, the following difficulties arise in the study of state equation: (i) very strong repulsive forces arise whose properties are not know well; (ii) the relative concentrations of various types of baryons can be strongly affected by the presence of higher hyperons having masses grater than that of the Ξ-hyperon. At still higher densities, π-mesons must also make their appearance as a Bose gas.

doi: 10.52526/25792776-2021.68.2-236

4. On equilibrium configurations of superdense degenerate gas masses

Continuing along this line, Ambartsumian & Saakyan (Ambartsumian & Saakyan, 1961a) seek to find the solution to Einstein's equations for spherically symmetric superdence configurations. Oppenheimer & Volkoff (Oppenheimer & Volkoff, 1939) have shown that the solution of Einstein's equations in the static case is reduced to solution of comparatively simple differential equations. The Oppenheimer & Volkoff's equations can be readily integrated for the case of configuration of ideal gas. Proceeding with the initial conditions $\rho = \rho(0)$ and $P(0) = P(\rho(0))$, where $\rho(0)$ is the central density of the given configuration, the integration is carried out step by step all the way up to boundary R, where $\rho = \rho(R) = P(R) = 0$. In this case, the numerical integration of the equations does not encumbered for the finite central densities. The calculations shown that the masses of equilibrium configurations of a non-rotating baryon ideal gas are of the ordder of a half of a solar mass, and that the radii reach out several kilometers. It would be of interest, however, to consider also the limiting case of $\rho(0) \to \infty$ when baryon gas becomes extremely relativistic $P \approx \rho/3$. At small interparticle distances ~ 0.4fm or less, strongly intense repulsive forces apparently come into action. The baryonic gas, therefore, can no longer be considered an ideal gas at baryon densities exceeding $10^{40}\mathrm{cm}^{-3}N$ which corresponds to the short distances $l < 0.5$fm. It is possible roughly take into account the potential $U(N)$ of interactions in state equation. The masses of the degenerate configurations calculated for a real Fermi gas of baryons under the assumption that repulsive forces are active between the baryons, are appreciably larger than the masses of configurations of an ideal gas. However, small masses of the order of a solar mass are also obtained in this case. Even if the law of repulsion should be altered, which assumed to prevail, this still be unable to leads to the masses far exceeding a solar mass. The sizes and masses of the outer regions of a baryon star, i.e. neutron or proton-electron layers, comprise a small part of the total mass and size of the star at fairly high central densities. The bulk of the star's mass in those cases goes into the hyperon core. Such configurations are coined hyperon-configurations. Configurations with slightly lower central densities $\rho < 10^{15}\mathrm{gcm}^{-3}$ lack hyperon cores and consists entirely of neutrons.

5. Internal structure of hyperon configurations of stellar masses

By numerical integration of equations determining the configuration of degenerate baryonic gas, all the necessary parameters specifying the internal structure of configurations of stellar masses are obtained in previous Section. Following Ambartsumian & Saakyan (Ambartsumian & Saakyan, 1961b), Fig. 1 gives in somewhat greater detail the plots of major characteristics of internal structure of configurations of ideal Fermi gas against the distance $\underline{r}$ from the center: (a) $t_n(\underline{r})$; $(b)U(\underline{r})$; metric components (c) $g_{rr}(\underline{r})$ and (d) $g_{00}(\underline{r})$, and (e) the dependence of mass of configuration on total number of baryons. Here and throughout we use following notational conventions: the particle concentrations are expressed in terms of parameter $t_k = 4arsh(p_k/m_k c)$, m_k is the mass of k-th particle, p_k is the critical Fermi momentum $p_k = (6\pi^2/a_k)^{1/3} h N_k^{1/3}$ for the k-th particle, $a_k = 2S_k + 1$ is the number of particle spin states, $\underline{r}$ is the distance from the center, the function $U(\underline{r})$ gives approximate idea of the mass, in units of solar mass, concentrated in a sphere of radius $\underline{r}$. Inside the configuration volume, the value of time component g_{00} of metric tensor achieved at accepting starting point that the matter exists in a state of thermodynamic and mechanical equilibrium. The numbers attached to the lines indicate the value of $t_n(0)$ for the given configuration. The corresponding characteristics of internal structure of configurations of real Fermi gas are not referred for obvious reason as the non-Euclidian nature of space in this case is more strongly pronounced in the volume of the configurations and adjacent regions. The study of the relationship between stellar parameters and total number of baryons in the star, and the dependence of that number on the density value at the center are problems of heightened interest. For example, plot (e) shows the dependence of mass of configuration on total number of baryons. Numbers next to circles indicate values of parameter t_n at the center for those points. Solid line refers to real gas models, and dashed line refers to ideal gas models. The range $0.6 < t_n(0) \lesssim 1.8$ is traced out in common by both curves. Models of an ideal gas corresponding to points on the lower branch of the graph are purely neutronic models. Points on the upper branch correspond to hyperon

doi: 10.52526/25792776-2021.68.2-236

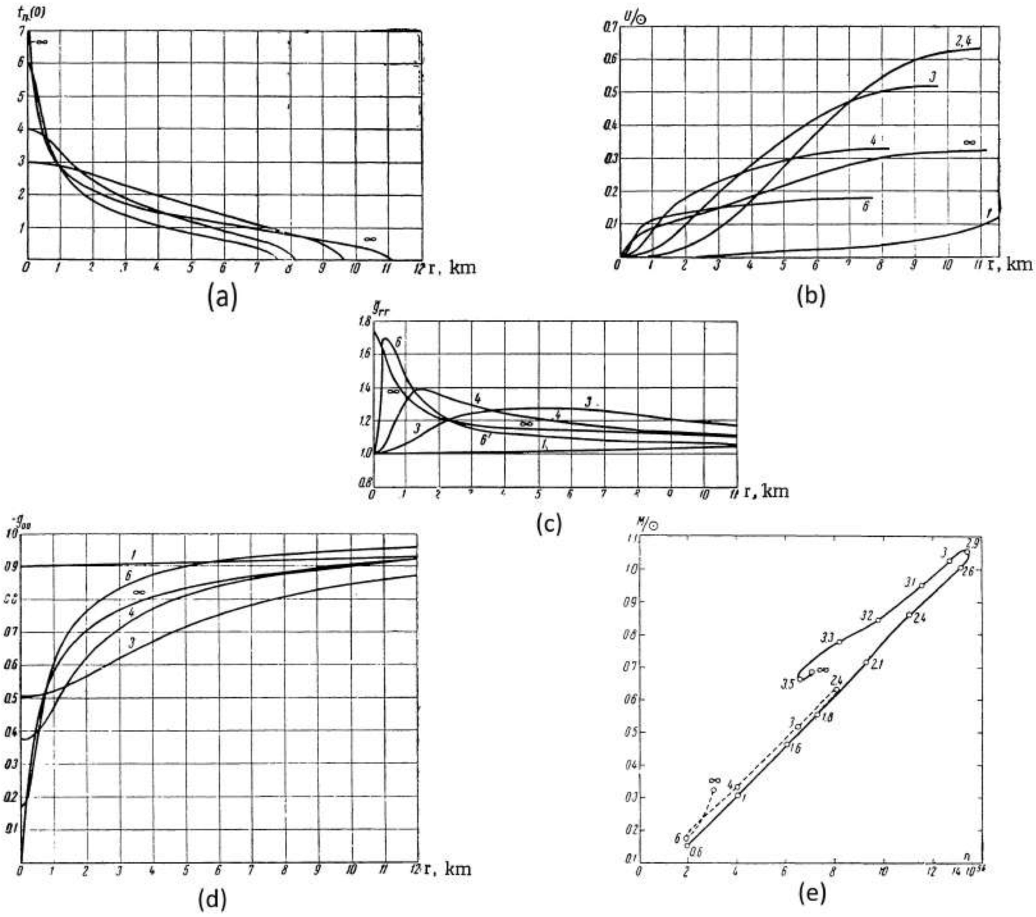

Figure 1. (a) The parameter $t_n(\underline{r})$ against the distance $\underline{r}$ from the center for four configurations corresponding to different central values of $t_n(0)$. (b) The function $U(\underline{r})$ which gives approximate idea of the mass, in units of solar mass, concentrated in a sphere of radius $\underline{r}$, for six different ideal gas states. The curves for $t_n(0) = 1$ extends out to $\underline{r} = 21.1$km. (c) Dependence of metric component g_{rr} on $\underline{r}$ for five different ideal gas states. As $\underline{r} \to \infty$, the function tends to its Euclidian value of unity. (d) Dependence of time component g_{00} of metric tensor on $\underline{r}$. The $g_{00} = 1$ corresponds to Euclidian value of unity. Distances are given in kilometers. (e) Dependence of mass of configuration on total number of baryons. Numbers next to circles indicate values of parameter t_n at the center for those points. Solid line refers to real gas models, and dashed line refers to ideal gas models. The range $0.6 < t_n(0) \lesssim 1.8$ is traced out in common by both curves.

configurations. In the case of real gas, hyperon configurations are found on both branches, but states corresponding to upper branch points contain still higher percentage of hyperons. Starting from some value $\underline{n}$ of number of baryons in the star (equal to 6.5×10^{56} for real gas) there correspond to each $\underline{n}$ two or three equilibrium configurations. It is obvious that the configuration of lesser mass will be the more stable. A large mass exhibits a high density at the center. This must signify a large gravitational mass defect, in consequence of which the total mass of the configuration should be smaller in this case. A star located on the upper branch of the curve must undergo a transition to a state belonging to lower branch, in response to certain perturbations. Such transition will be accompanied by the release of tremendous amount of energy from the star, an amount of the order of 10% of the star's intrinsic energy. Such question merit special scrutiny. The gravitational mass defect $\triangle M = nm_H - M$ of baryon stars has been investigated. Reviewing notations M is the mass of the star, n is the number of baryons present, and m_H is the mass of hydrogen atom. It is shown that the configuration with $t_n(0) \lesssim 2.4$ is absolutely stable in the case of ideal gas, while the configuration with $t_n(0) \lesssim 2.9$ is absolutely stable in the case of real gas. The rest of configurations are either metastable or unstable. There is one intriguing feature in the unstable branches, namely that for $t_n(0) \gtrsim 4.2$ in the case of ideal gas and for $t_n(0) \gtrsim 3.15$ in the case of real gas, the binding energy $\triangle M$ becomes negative (see also sect.5). Such states will be less stable than the others.

6. The mass defect of baryon stars

In this Section we outline the key points of a more detailed analysis of the absolute gravitational mass defect, $\triangle M = nm_n - M$l, of neutron configurations (Ambartsumian & Saakyan, 1961b, 1965). This is of particular interest to astrophysicists. Note that the value of the mass defect $\triangle M$ is to some degree dependent on the selection of the frame of reference and therefore is not an invariant characteristic of the star. Obviously, for ordinary celestial bodies in all case $\triangle M > 0$. The computations of baryon configurations have demonstrated that when central densities rise above a certain value $\rho_1(0)$ the absolute mass defect changes sign - it becomes negative. The value of $\rho_1(0)$ depends on the form of the equation of state for the baryon gas used in the computations. In models with a real baryon gas $\rho_1(0)$ has a lesser value than in models with an ideal gas. This can be attributed to the fact that in the case of a real gas, at densities greater than nuclear, the nuclear forces of repulsion between baryons is played important role. Naturally, the forces of repulsion facilitate the appearance of the considered effect. It follows that the value of gravitational mass defects for models with a real gas are not entirely correct, because in this case they are determined not only by gravitation but also by the effect of nuclear forces (attraction and repulsion). In order to exclude the influence of nuclear forces on the absolute mass defect and investigate the phenomenon in purer form, one will be concerned only with models of superdense stars consisting of an ideal baryon gas. The presence of hyperons and interaction between baryons were disregarded, in order to avoid complications unrelated to the considered problem. Thereby, at first, one uses Einstein's gravitational theory as a point of departure. Next, neutron configurations were also computed for the case when Newton's gravitational law is used as the point of departure. In this case one knowingly admitted a certain inconsistency, extending the computations to include configurations consisting of a relativistic neutron gas. However, in this case one had a definite purpose in mind: comparison of the exact and approximate computations in order to clarify the role of relativism of the baryon gas and the curvature of space and thereby determine the cause of the anomaly in the absolute gravitational mass defect. We shall note only a few common and important aspects of numerical computations. a) Although the results of computations of the parameters of neutron stars on the basis of Newton's and Einstein's gravity theories reveal an appreciable quantitative difference, nevertheless, in some most important respects there is good qualitative agreement. For example, Newton's theory of the mass, radius, and number of baryons in a star gives the correct orders of magnitude. b) According to both theories, all the parameters of the configurations are single-valued functions of the central den- sity $N(0)$. The opposite assertion is, in general, untrue. In certain regions the same value of some of the star parameters, such as mass, correspond to two (or even more) values of the central density. c) In the case of Newtonian models, the absolute gravitational mass defect for all possible static configurations has a positive value. The packing coefficient is in all cases an increasing function of the central density, with the exception of the region of extraordinarily high central densities , where a conspicuous minimum is recorded. d) In the case of relativistic models, the gravitational packing factor $\triangle M/M_0 = f(n)$ exhibits anomalous behavior. At first, it increases with increase in density, at $N(0) = 3 \times 10^{39}\mathrm{cm}^{-3}$ it attains a maximum and then begins to decrease. At $N(0) = 1.12 \times 10^{40}\mathrm{cm}^{-3}$ the packing factor becomes negative. At $N(0) = 2 \times 10^{41}\mathrm{cm}^{-3}$, there is a deep minimum, approximately equal to -0.1; then the packing factor, oscillating with a small and strongly damping amplitude and continuing to remain negative as $\rho(0) \to \infty$, tends to a limit of -0.069. The authors, therefore, conclude that the mass defect anomaly was caused by a catastrophic deviation from additivity of the internal energy due to warping of the spatial metric in the corresponding baryon configurations. In these configurations and in the Newtonian approximation the deviation from additivity (here the kinetic energy is additive and the potential energy is not) is strong, but inadequate for a change in the sign of the mass defect. Obviously, the configurations corresponding to the lower branch of the $f(n)$ curve when $3 < t_n(0) < 4.67$ are unstable in relation to the transitions to the upper branch, where the mass defect exhibits normal behavior. However, configurations with $t_n(0) > 4.67$, having a negative absolute mass defect, are unstable not

doi: 10.52526/25792776-2021.68.2-236

only in relation to transition to the upper branch, but also in relation to decay into a diffuse state. Since the mass defect is several percent of the mass of the star itself, an improbably large energy will be released in these transitions. The energy associated with one gram of star matter is an order of magnitude greater than the corresponding energy released in thermonuclear reactions in the combustion of hydrogen. It is important to note that the binding energy of each particle in a star is negative, so that the particles cannot escape individually to infinity. The escape of a certain number of baryons from a star requires the addition of supplementary energy to the remaining configuration from the outside. For this reason it cannot occur spontaneously. This means that transition of the system to a more stable state can occur only under the influence of very great perturbations. In this case expansion will occur, accompanied by heating of the celestial body. The corresponding transition will have the character of a cosmic explosion. These arguments concerning the fate of baryon configurations with an anomalous absolute mass defect were first presented in (Ambartsumian & Saakyan, 1961b). The configurations with an anomalous value of the absolute mass defect (we refer to the entire branch of the curve with $t_n(0) > 3$) should be of some importance to Ambartsumian's cosmogony. In order to relate the above considerations on the behavior of baryon configurations with an anomalous value of the absolute mass defect to the concept mentioned, it is necessary to construct models of superdense prestellar bodies with masses of a much greater order of magnitude than the solar mass.

7. Assessment of growth and merging properties of BHs within PMBH

Wheeler in 1967 coined a spacetime region, where the gravitational field is so strong that no information carrying objects and signals can escape it, by the term 'a black hole', although the possibility of the existence of such objects was discussed a long time before this. At the end of the eighteenth century Michell and Laplace independently came to the conclusion that if the mass of a star were large enough its gravity would not allow light to escape. Though this conclusion was based on the Newtonian theory the obtained result for the size of such 'dark stars' (the gravitational radius) coincides with the later prediction of Einstein's theory of gravity. A principle feature that makes GR distinctively different from other field theories is the occurrence of curvature singularities in spacetime. The singularities lead to regions of the universe that cannot be observed. This causes an observer's inability to access the degrees of freedom that are hidden beyond the horizon which, in turn, leads to thermodynamical behavior of BHs. The astrophysical significance of the issue, and the importance of considering the gravitational collapse of a matter cloud within the framework of the GR theory, with reasonable physical properties for the matter included, stems from the fact that GR predicts that a star more massive than about five to eight times the mass of the Sun, cannot stabilize to a neutron star final state at the end of its life cycle. It must collapse continually under the force of its own gravity on exhausting its internal nuclear fuel, and there are no known forces of nature that would halt such a collapse. GR predicts that such a star must then terminate into a spacetime singularity where densities and spacetime curvatures blow up and the physical conditions are extreme. The estimates on the mass limit for a star in order to collapse, of course, are indefinitely vary depending on different models for the star's interior and equation of state for matter at very high densities.

In this Section we would like briefly re-examine (critically) the past and present of the PMBHs, and attempt to chart the future of the subject. Within respect to standard models, a hard look at the PMBH physics reveals at least the following severe problems:

(i) The geometrical interpretation of gravitation, having arisen from the dual character of the metrical tensor in its metrical and gravitational aspects, is a noteworthy result of GR. Being among the most significant advances in solving the key problems of cosmology and astrophysics, the GR certainly can claim remarkable success in the experimental and observational tests too. Nevertheless such a distinction of the gravitational field among the fields yields the difficulties in the unified theories of all interactions of elementary particles, and in quantization of gravitation. Some conceptual problems of the energy-momentum conservation laws of gravitational interacting fields, the localization of energy of gravitation waves, the role of singularities, and also severe problems involved in quantum gravity are still plaguing GR. As a geometrized theory of gravitation, the GR clashes from the very outset with basic principles of the field theory. This rather stems from the fact that Riemannian geometry, in

doi: 10.52526/25792776-2021.68.2-236

general, does not admit a group of isometries, i.e., Poincaré transformations no longer act as isometries and, for example, it is impossible to define energy-momentum as Noether local currents related to exact symmetries. This posed severe problems in a Riemannian space interacting quantum field theory. The major unsolved problem is the non-uniqueness of the physical vacuum and the associated Fock space. Actually, a peculiar shortcoming of the interacting quantum field theory in curved spacetime is in the following two key questions to be addressed yet: a) the absence of the definitive concept of space-like separated points, particularly, in the canonical approach, and the *light-cone* structure at each spacetime point; b) the separation of positive- and negative-frequencies for completeness of the Hilbert-space description. Due to this, a definition of positive frequency modes, therefore, cannot be unambiguously fixed in the past and future, which leads to $|in> \neq |out>$, because the state $|in>$ is unstable against decay into many particle $|out>$ states due to interaction processes allowed by lack of Poincaré invariance. A non-trivial Bogolubov transformation between past and future positive frequency modes implies that particles are created from the vacuum and this is one of the reasons for $|in> \neq |out>$.

(ii) Conjectured in the framework of GR, the very source of gravitational field of a BH is a kind of meaningless curvature singularity at the central point of the stationary nonrotating Schwarzschild BH, or a ring singularity at the center of the rotating axisymmetric Kerr BH, which are hidden behind the event horizon (EH). The theory breaks down inside the EH which is causally disconnected from the exterior world. The Kruskal manifold is the maximal analytic extension of the Schwarzschild and Kerr solutions inside EH, so no more regions can be found by analytic continuation. Either the Kruskal continuation of the Schwarzschild ($J = 0$, $Q = 0$) metric, or the Kerr ($Q = 0$) metric, or the Reissner-Nordstrom ($J = 0$) metric, show that the static observers fail to exist inside the horizon. Any object that collapses to form a black hole will go on to collapse to a singularity inside the black hole. Any timelike worldline must strike the central singularity which wholly absorbs the infalling matter. Therefore, the ultimate fate of collapsing matter once it has crossed the black hole surface is unknown. The interior solution is not physically meaningful and essentially irrelevant. Black holes then present a major challenge that they render time reversibility impossible. Objects thrown into a BH can never be retrieved, because any timelike worldline must strike the central singularity which wholly absorbs the infalling matter. Any object that collapses to form a BH will go on to infinite collapse to a singularity inside the BH. The PMBH, therefore, ultimately precludes any accumulation of matter inside EH and, thus, neither the growth of BHs nor the increase of their mass-energy density could occur at accretion of outside matter, or by means of merger processes.

(iii) One of the most important open issues in the theory and astrophysical applications of modern day BH and gravitation physics is that of the Roger Penrose's Cosmic Censorship Conjecture (CCC). The CCC assumption that any physically realistic gravitational processes must not lead to the formation of a singularity which is not covered by an horizon, thus hiding it from external observers in the universe. This of course includes the complete gravitational collapse of a massive star which, if the CCC is true, must terminate generically into a BH final state only. Such a singularity is then crucial and is at the basis of much of the modern theory and astrophysical applications of BHs today. Despite the past four decades of serious efforts, we do not have as yet available any proof or even any mathematically precise formulation of the cosmic censorship hypothesis. The consideration of dynamical evolution of collapse is a crucial element of the CCC. Many solutions of Einstein field equations are known which present naked singularities (such as, for example, the super-spinning Kerr solutions), nevertheless almost none of these solutions can be obtained as the dynamically evolved final state of some initially regular matter configuration. For this reason, over the last decades a great deal of work has been done to test the CCC in the few dynamically evolving spacetimes we know. These are typically the scenarios that describe gravitational collapse in spherical symmetry, and some non-spherical collapse models have also been considered, for examples of critical collapse with angular momentum. In recent years, a wide variety of gravitational collapse models have been discovered where exact analytical calculations (e.g. (Joshi & Malafarina, 2013) and references therein) have meanwhile shown that mass concentrations collapsing under their own weight will no longer form BHs as collapse endstate, rather naked singularities, except for configurations of highest symmetry which are, however, of measure zero among all initial data. By this, even the theoretical existence of

doi: 10.52526/25792776-2021.68.2-236

BHs is no longer justified. The first examples were restricted to some classes of inhomogeneous dust collapse, and they were extended to the case of collapse in the presence of only tangential pressures, and perfect fluids. The existence of classes of pressure perturbations is shown explicitly, which has the property such that an injection of a small positive (or negative) pressure in the Oppenheimer, Snyder and Datt (OSD) model, or in a Tolman-Bondi-Lemaitre (TBL) inhomogeneous dust collapse to a BH (simplest generalization of the OS model), leads the collapse to form a naked singularity, rather than a BH (Joshi & Malafarina, 2013). The classic OSD scenario is the basic paradigm for BH physics today, and the TBL models describe the most general family of dust, i.e. pressureless, collapse solutions. This result is therefore intriguing, because it shows that arbitrarily close to the dust BH model, we have collapse evolutions with non-zero pressures that go to a naked singularity final state, thus proving a certain 'instability' of the OSD BH formation picture against the introduction of small pressure perturbations. In such a case, the super-ultra-dense regions, or the spacetime singularity, that forms at the end of collapse would be visible to faraway observers in the universe, rather than being hidden in a BH. Thus, rigorous calculations have shown that the expectations of the 1970s have been hasty, that CCC assumption has been premature, because while the CCC states that the OSD collapse final fate is necessarily replicated for any realistic stellar collapse in nature, the result here shows that an arbitrarily small pressure perturbation of the OSD model can change the final outcome of collapse to a naked singularity and therefore the OSD BH may be considered 'unstable' in this sense.

(iv) If the BH was being off the ordinary mass shell and carried no entropy, it would be possible to violate the cherished law of energy conservation and 2^{nd} law of thermodynamics, because the energy and entropy in the exterior spacetime could be decreased by throwing matter into a BH. In the framework of incomplete theory, therefore, there is nothing left but to admit stepwise, without any substantiation, that the BH resides on the *ordinary mass shell* and it has entropy. That is, the law of increase of area (Hawking's area theorem) looks like the 2^{nd} law of thermodynamics for the increase of entropy, if one assigns an entropy to BH that is proportional to its surface, and that the surface gravity stands for a temperature. Moreover, the GSL was needed to present the second law of thermodynamics as valid. This is because the 2^{nd} law of thermodynamics, as a result of the disappearance of entropy near the exterior of BHs, is not useful. Then the increase of these quantities may compensate the decrease of the energy and entropy carried by the mass that was swallowed. At first sight this definition of the laws of gravitation, and thereof for that of thermodynamics and entropy of BHs, seems quite natural, however, at closer inspection one finds that these intriguing ideas have encountered to the following severe objections:

a) The two features violate Hawking's area theorem - (1) in pair creation effectively a spacelike energy flux is involved - in contrast to the one of the essential postulates of the area theorem which requires that the energy-momentum tensor $T_{\mu\nu}$ should satisfy the dominant energy condition. This held if for all future-directed timelike vector fields v, the vector field $j(v) \equiv -v^{\mu}T_{\mu}{}^{\nu}\partial_{\nu}$ is future-directed non-spacelike, or zero, i.e. no spacelike energy fluxes are allowed; (2) the mass of BH decreases during evaporation by energy conservation, as well as inevitably do the surface area and entropy.

b) The entropy of a thermodynamic system is a measure of the large number of the *real physical microstates* that an observer would not be aware of when measuring macroscopic parameters, and so-called *no hair* theorems allow BH, in best case, to have only a single microstate.

(v) Yet about 47 years after its conjecturing, solid physical information regarding the physical origin of BH entropy is still lacking, which arises several puzzling questions. For example, since there is no unique rigid notion of *time translations* in a classical GR-dynamics, the BH entropy at least appears to be *incompatible* with any notion of *ergodicity*. Or, the equation for Hawking's black body radiation temperature, $T_H = c^3\hbar(8\pi k_B G_N M)^{-1}$, clearly shows that the more mass is radiated away from the black hole, the hotter this becomes. What then is the endpoint of BH evaporation? Moreover, the thermal properties of thermodynamic systems reflect the statistical mechanics of underlying microstates. Entropy is normally a measure of the degeneracy of microstates, Σ, in some underlying microscopic description of a physical system, determined by Boltzmann's formula $S = k_B log\Sigma$. Since the Bekenstein-Hawking entropy of generalized second law (GSL) of BH thermodynamics, $S_H k_B^{-1} = 4\pi G_N M^2(c\hbar)^{-1} = A_H(2l_{Pl})^{-2}$ of a BH, where A_H is the area of the horizon and

doi: 10.52526/25792776-2021.68.2-236

l_{Pl} is the Planck length $l_{Pl} = \sqrt{G_N \hbar / c^3} \approx 10^{-33}$ cm, is naturally a huge number, how can one exhibit such a wealth of microstates?

(vi) Certain gravitational backgrounds gave rise to thermal radiation from the vacuum. This provides an alternate conceptual means for understanding the physics of cosmological pair production at a wide variety of cosmological event horizons in exotic spacetimes. However, all these processes for certain do not give physical insight regarding the nature of the *microstates of a BH* and nor does it offer a substantiated reason for the *BH entropy* S_{BH}. Moreover, in semi-classical analysis of the Hawking evaporation process, if the correlations between the inside and outside of the BH are not restored during the evaporation process, then by the time that the BH has evaporated completely, an initial pure state will have evolved to a mixed state, i.e., *information* will have been lost in the process of BH formation and evaporation - the *BH information loss paradox*. If information is lost into the BH, which is ascribable to the propagation of the quantum correlations into the singularity within the BH, this put quantum field theory in curved spacetime in conflict with a basic principle of quantum mechanics, because of incompatibility with the unitary time evolution of a state vector in a Hilbert space. This violates the causality and energy-momentum conservation laws. The following three postulates of BH complementarity are not consistent with one another for a sufficiently old BH: (1) Hawking radiation is in a pure state, (2) the information carried by the radiation is emitted from the region near the horizon, with low energy effective field theory valid beyond some microscopic distance from the horizon, and (3) the infalling observer encounters nothing unusual at the horizon. These seem to require novel dynamics that nevertheless cause notable violations of semiclassical physics at macroscopic distances from the horizon. That is, one must sacrifice some principle: the equivalence principle, low energy effective field theory, or the nonexistence of high-entropy *remnants* at the end of BH evaporation.

(vii) The BH solutions to Einstein's equations, implying an existence of the event horizons, are defined only in asymptotically flat space-times. The Universe, in fact, is not asymptotically flat. So the event horizons, to which the laws of BH thermodynamics are referred, do not exist. The Schwarzschild BH, fixing its temperature at infinity, has negative heat capacity. Similarly, in an asymptotically anti-de-Sitter spacetime fixing the BH temperature via the normalization of the timelike Killing vector at infinity is not justified because there is no such physically distinguished Killing field. The BHS are localized objects, thus one must be able to describe their properties and dynamics even at the quasi-local level. These difficulties lead to the need of a quasi-local formulation of BH thermodynamics. The subject of the quasi-local formulations is to describe the properties and the evolution of the so-called *trapping horizon*, which is a quasi-locally defined notion, somewhat as an apparent horizon.

(viii) Although no results on BH thermodynamics have been subject to any experimental or observational tests, the attempts of theoretical interpretation of the BH thermodynamics provide a basis for further research and speculation on the nature of its quantum gravitational origin. In the entanglement entropy and thermal atmosphere approaches, the relevant degrees of freedom are those associated with the ordinary degrees of freedom of quantum fields outside of the BH. The string theory implies weak coupling states, so it is not clear what the degrees of freedom of these weak coupling states would correspond to in a low energy limit where these states may admit a BH interpretation. There is no indication in the calculations that these degrees of freedom responsible for BH entropy should be viewed as being localized near the BH horizon. It is far from clear as to whether one should think of these degrees of freedom as residing outside of the BH (e.g., in the thermal atmosphere), on the horizon (e.g., in Chern-Simons states), or inside the BH (e.g., in degrees of freedom associated with what classically corresponds to the singularity). Moreover, the entanglement mechanism is not specific to BHs but to any spacetime with a bifurcating Killing horizon.

(ix) The efforts to understand the mysterious statistical mechanical properties of BHs has led to many speculations about their quantum gravity origin. Though not yet fully understood in general, the holographic principle is central to theories like the AdS/CFT (anti-de Sitter spaces/conformal field theories) correspondence. The holographic scaling suggests that a BH has far fewer degrees of freedom than we might expect. For a comprehensive review of recent progresses on the holographic understandings of the entanglement entropy in the AdS/CFT correspondence, BH entropy and covariant formulation of holography. As notably pointed out by these authors, even after quite intense

doi: 10.52526/25792776-2021.68.2-236

efforts in AdS/CFT for recent years, fundamental mechanism of the AdS/CFT correspondence still remains a mystery. In particular, one cannot answer which region of AdS is responsible to particular information in the dual CFT. There is also an essential discrepancy between the entanglement entropy and the BH entropy, that the entanglement entropy is proportional to the number of matter fields, while the BH entropy is not. The former includes ultraviolet divergences as opposed to the latter.

(x) Within string theory, there is a class of BHs where some problems can be conveniently addressed, the so-called extremal BHs, for which the mass is tuned, so that the tendency to gravitational collapse is precisely balanced by the electrostatic repulsion. Consequently, the temperature vanishes and the black hole behaves somehow in this limiting case as if it were an elementary particle. These results, however, rely heavily on supersymmetry and serious difficulties are met in attempts to extend them to non-supersymmetric BHs. Up to date no one was able to make a convincing calculation of BH entropy based on statistical mechanics, which associates entropy with a large number of microstates being compatible with a concept of *ergodicity*. In this regard, proving the GSL is generally valid would require using quantum-statistical mechanics, but this discipline does not exist. So, due to existing discrepancies and absence of distinctive observationally tested predictions, there is no convincing reason to rely on the string theory in its present form. This then ruptures the familiar BH entropy illusion which has insufficient dimensions.

Only a true *internal* solution was able to give a reliable information on the thermodynamic behavior and entropy of BH if, and only if, it is known deep within the BH. At this point we cut short our discussion, and refer the interested reader to (Ter-Kazarian, 2021a, Ter-Kazarian & Shidhani, 2017) for more details.

8. The theory of distortion of the space-time continuum

A remarkable surge of activity of investigations towards an extension of GR has arisen recently. They are geometrically expressible in the language of the fundamental structure known as a fiber bundle. This provides an unified picture of gravity modified models based on several Lie groups. All the approaches have their own advantages, but in the same time they are subject to many uncertainties. Currently no single theory has been uniquely accepted as the convincing gauge theory of gravitation, which will be able successfully to address the aforementioned problems.

In this respect we advocate with alternative proposal of the new physical perception of space-time geometry - the *theory of distortion of space-time continuum* (DSTC) (Ter-Kazarian, 1986, 1989c, 1997, 2010, 2011, 2012, 2015) at huge energies (respectively, at short distances $<$ 0.4fm). As a corollary, in particular, DSTC leads to modified gravitational theory. The proposed gravitational theory involves a drastic revision of a role of local internal symmetries in physical concept of curved geometry, and explores the most important processes of spontaneous breaking of gravitation gauge symmetry and rearrangement of vacuum state. Much use has been made in proposed gravitation theory of the language of fundamental geometric structure - *a distortion gauge induced fiber-bundle* (Ter-Kazarian, 1986, 1989c, 1997, 2010, 2012), incorporating with the spacetime deformation/distortion-framework, (Ter-Kazarian, 2011, 2015) and references therein.

8.1. A first glance at spacetime deformations

In the framework of spacetime deformation theory, we consider a smooth deformation map $\Omega : M_4 \rightarrow \widetilde{\mathcal{M}}_4$, written in the terms of the *world-deformation* tensor Ω, the general, $\widetilde{\mathcal{M}}_4$, and the flat, M_4, smooth differential 4D-manifolds. A following notational conventions will be used throughout this paper. All magnitudes related to the space, $\widetilde{\mathcal{M}}_4$, will be denoted with an over $'\sim'$. We use the Greek alphabet $(\mu, \nu, \rho, ... = 0, 1, 2, 3)$ to denote the holonomic world indices related to $\widetilde{\mathcal{M}}_4$, and the second half of Latin alphabet $(l, m, k, ... = 0, 1, 2, 3)$ to denote the world indices related to M_4. The tensor, Ω, can be written in the form $\Omega = D\,\psi\,(\Omega^m_{\ l} = D^m_\mu\,\psi^\mu_l)$, provided with the invertible distortion matrix $D\,(D^m_\mu)$ and the tensor $\psi\,(\psi^\mu_l \equiv \partial_l\,\widetilde{x}^\mu$ and $\partial_l = \partial/\partial\,x^l)$. The principle foundation of a world-deformation tensor comprises the following two steps.

doi: 10.52526/25792776-2021.68.2-236

First step: The basis vectors e_m at given point ($p \in M_4$) undergo the distortion transformations by means of D: $\widetilde{e}_\mu = D^l_\mu\, e_l$.

Second step: The diffeomorphism $\widetilde{x}^\mu(x) : M_4 \to \widetilde{M}_4$ is constructed by seeking a new holonomic coordinates $\widetilde{x}^\mu(x)$ as the solutions of the first-order partial differential equations: $\widetilde{e}_\mu\, \psi^\mu_l = \Omega^m{}_l e_m$, here the conditions of integrability, $\partial_k\, \psi^\mu_l = \partial_l\, \psi^\mu_k$, and non-degeneracy, $\|\psi\| \neq 0$, necessarily hold. Next we write the norm $d\widetilde{s} \equiv i\widetilde{d}$ of the infinitesimal displacement $d\widetilde{x}^\mu$ on the $\widetilde{\mathcal{M}}_4$ in terms of the spacetime structures of M_4: $i\widetilde{d} = \widetilde{e}\,\widetilde{\vartheta} = \widetilde{e}_\mu \otimes \widetilde{\vartheta}^\mu = \Omega^m{}_l\, e_m \otimes \vartheta^l \in \widetilde{\mathcal{M}}_4$. The deformation $\Omega : M_4 \to \widetilde{\mathcal{M}}_4$ comprises the following two subsequent 4D deformations $\overset{\circ}{\Omega}$: $M_4 \to V_4$ and $\breve{\Omega} : V_4 \to \widetilde{M}_4$, where V_4 is the semi-Riemannian space, $\overset{\circ}{\Omega}$ and $\breve{\Omega}$ are the corresponding world deformation tensors.

The interested reader is invited to consult the original papers (Ter-Kazarian, 2011, 2015) for hard glance of the theory of spacetime deformation.

Finally, to complete this theory we need to determine $\widetilde{D}$ and $\widetilde{\psi}$. Keeping in mind aforesaid, we develop on the alternative framework of the *General Gauge Principle* (GGP), which is the *distortion gauge induced* fiber-bundle formulation of gravitation. In this, we restrict ourself to consider only the simplest spacetime deformation map, $\widetilde{\Omega} : M_4 \to V_4$ ($\breve{\Omega}^\mu{}_\nu \equiv \delta^\mu_\nu$).

8.2. GGP

We generalize the standard gauge scheme via the concept of distortion gauge field which acts on the external spacetime groups. Given the principal fiber bundle $\widetilde{P}(V_4,\, G_V; \widetilde{s})$ with the structure group G_V, the local coordinates $\widetilde{p} \in \widetilde{P}$ are $\widetilde{p} = (\widetilde{x},\, U_V)$, where $\widetilde{x} \in V_4$ and $U_V \in G_V$, the total bundle space $\widetilde{P}$ is a smooth manifold, the surjection $\widetilde{s}$ is a smooth map $\widetilde{s} : \widetilde{P} \to V_4$. The collection of matter fields of arbitrary spins $\widetilde{\Phi}(\widetilde{x})$ take values in standard fiber over $\widetilde{x}$: $\widetilde{s}^{-1}(\widetilde{\mathcal{U}}_i) = \widetilde{\mathcal{U}}_i \times \widetilde{F}_{\widetilde{x}}$. The action of the structure group G_V on $\widetilde{P}$ defines an isomorphism of the Lie algebra $\widetilde{\mathfrak{g}}$ of G_V onto the Lie algebra of vertical vector fields on $\widetilde{P}$ tangent to the fiber at each $\widetilde{p} \in \widetilde{P}$ called fundamental. The structure group G_V is generated by the hidden local internal symmetry of two-parameter abelian local group $U^{loc}(2) = U(1)_Y \times \overline{U}(1) \equiv U(1)_Y \times diag[SU(2)]$. The latter is implemented on the flat space, M_4. Involving a drastic revision of the role of gauge fields in the physical concept of the spacetime deformation, we generalize the standard gauge scheme by exploring a new special type of *distortion* gauge field $a(x)\,(\equiv\, a_n(x))$. This field takes values in the Lie algebra of the abelian group $U^{loc}(2)$ and acts on the external spacetime groups. Besides, we also consider the principle fiber bundle, $P(M_4,\, U^{loc}(2);\, s)$, with the base space M_4, the structure group $U^{loc}(2)$ and the surjection s. Hereinafter the quantities referring to V_4 are denoted by wiggles, and are left without wiggles if they correspond to M_4. The matter fields $\Phi(x)$ take values in the standard fiber which is the Hilbert vector space where a linear representation $U(x)$ of group $U^{loc}(2)$ is given. This space can be regarded as the Lie algebra of the group $U^{loc}(2)$ upon which the Lie algebra acts according to the law of the adjoint representation: $a \leftrightarrow ad\, a\;\, \Phi \to [a\,,\Phi]$.

Third step: The physical system of the fields $\widetilde{\Phi}(\widetilde{x})$ defined on V_4 must be invariant under the finite local gauge transformations U_V of the Lie group of gravitation G_V: $\widetilde{\Phi}'(\widetilde{x}) = U_V\,(\widetilde{x})\,\widetilde{\Phi}(\widetilde{x})$, and $[\widetilde{\gamma}^\mu(\widetilde{x})\,\widetilde{\nabla}_\mu\widetilde{\Phi}(\widetilde{x})]' = U_V\,(\widetilde{x})[\widetilde{\gamma}^\mu(\widetilde{x})\,\widetilde{\nabla}_\mu\widetilde{\Phi}(\widetilde{x})]$. The invariance of the Lagrangian of matter fields, $L_{\widetilde{\Phi}}$, under the infinite-parameter group of general covariance in V_4 implies an invariance of $L_{\widetilde{\Phi}}$ under the G_V group and vice versa if, and only if, the generalized local gauge transformations of the fields $\widetilde{\Phi}(\widetilde{x})$ and their covariant derivative $\widetilde{\nabla}_\mu\widetilde{\Phi}(\widetilde{x})$ are introduced by finite local $U_V \in G_V$ gauge transformations. The GGP scheme is

$$
\begin{array}{rcl}
\widetilde{\Phi}'(\widetilde{x}) = U_V\,\widetilde{\Phi}(\widetilde{x}) & \xleftarrow{\;U_V = R'_\psi\, U^{loc}\, R^{-1}_\psi\;} & \widetilde{\Phi}(\widetilde{x}) \\
R'_\psi(\widetilde{x},\, x)\ \Big\uparrow & & \Big\uparrow\ R_\psi(\widetilde{x},\, x) \\
\Phi'(x) = U^{loc}\,\Phi(x) & \xleftarrow{\;U^{loc}\;} & \Phi(x)
\end{array}
$$

Fourth step: In order the gauge transformations to be universally satisfied, we consider a following smooth unitary map of all the matter fields and their covariant derivatives: $R_\psi(a) : \Phi \to \widetilde{\Phi}$, and

doi: 10.52526/25792776-2021.68.2-236

$S(a)\,R_\psi(a) : (\gamma^k D_k \Phi) \to (\widetilde{\gamma}^\nu(\widetilde{x})\nabla_\nu \widetilde{\Phi})$, where $R_\psi(a)(\equiv R_\psi(\widetilde{x}, x))$ is the unitary map matrix, $S(F)$ denotes the gauge invariant scalar function. Reviewing notations the $\widetilde{\nabla}_\mu$ denotes the covariant derivative agreed with the metric, $\widetilde{g}^{\mu\nu} = (1/2)(\widetilde{\gamma}^\mu\,\widetilde{\gamma}^\nu + \widetilde{\gamma}^\nu\,\widetilde{\gamma}^\mu)$: $\widetilde{\nabla}_\mu = \widetilde{\partial}_\mu + \widetilde{\Gamma}_\mu$, where $\widetilde{\Gamma}_\mu(\widetilde{x}) = \frac{1}{2}\,J^{ab}\,\widetilde{e}_a{}^\nu(\widetilde{x})\widetilde{\partial}_\mu\,\widetilde{e}_{b\nu}(\widetilde{x})$ is the connection, J_{ab} are the generators of Lorentz group Λ. The tetrad components $\widetilde{e}_a{}^\mu(\widetilde{x})$ associate with the chosen representation $D(\Lambda)$ by which the $\widetilde{\Phi}(\widetilde{x})$ is transformed as $[D(\Lambda)]^{l'\cdots k'}_{l\cdots k}\widetilde{\Phi}(\widetilde{x})$, where $D(\Lambda) = I + \frac{1}{2}\widetilde{\omega}^{ab}J_{ab}$, $\widetilde{\omega}_{ab} = -\widetilde{\omega}_{ba}$ are the parameters of the Lorentz group. One has, for example, to set $\widetilde{\gamma}^\mu(\widetilde{x}) \to \widetilde{e}^\mu(\widetilde{x})$ for the fields of spin $(j = 0, 1)$; for vector field $[J_{ab}]^l_k = \delta^l_a\eta_{bk} - \delta^l_b\eta_{ak}$; but $\widetilde{\gamma}^\mu(\widetilde{x}) = \widetilde{e}_a{}^\mu(\widetilde{x})\,\gamma^a$ and $J_{ab} = -(1/4)[\gamma_a, \gamma_b]$ for the spinor field $(j = \frac{1}{2})$, where γ^a are the Dirac matrices. To determine $R(a)$ and $S(F)$, our strategy is as follows: (i) we may obtain the identity by inserting first relation into the second relation; (ii) we further equate in this identity the coefficients in front of Φ and $\partial\,\Phi$ to zero. In this way we have the two relations to determine $R(a)$ and $S(F)$. In case of zero curvature, one has $\psi^\mu_l = D^\mu_l = e^\mu{}_l = (\partial x^\mu/\partial X^l)$, $\quad \|D\| \neq 0$, where X^l are the inertial coordinates. In this, the conventional gauge theory given on the M_4 is restored in both curvilinear and inertial coordinates. Although the distortion gauge field (a_A) is a vector field, nevertheless only the gravitational attraction is presented in the proposed theory of gravitation. Although we have explored the simplest abelian symmetry U^{loc} as a hidden symmetry, however, one may envisage that a straightforward extension should be to achieve the full machinery of the GGP scheme for non-abelian symmetries.

8.3. Nonlinear realization of the Lie group, G_D

We connect the structure group G_V, further, to the nonlinear realization of the Lie group, G_D, of *distortion* of the spacetime, i.e. we extend the curvature of the spacetime continuum to general *distortion* as the theory of spontaneous breaking of *distortion* symmetry. The nonlinear realization technique, or the method of phenomenological Lagrangians, provides a way to determine the transformation properties of fields defined on the quotient space. We treat the distortion group G_D and its stationary subgroup $H = SO(3)$, respectively, as the dynamical group and its algebraic subgroup. The fundamental field is distortion gauge field and, thus, all the fundamental gravitational structures in fact - the metric as much as the coframes and connections - acquire a *distortion-gauge induced* theoretical interpretation. Constructing a non-linear realization of the Lie group of distortion G_D, first, within the scheme of the GGP we necessarily introduce the language of the conceptual six-dimensional geometry of M_6, which is assumed as a toy model underlying the M_4. This replacement appears to be indispensable in our discussion of the distortion of the local internal properties of the spacetime continuum. The space M_6 reads $M_6 = R^3_+ \oplus R^3_- = R^3 \oplus T^3, sgn(R^3) = (+++), \quad sgn(T^3) = (---)$. The $e_{(\lambda\alpha)} = O_\lambda \times \sigma_\alpha \quad (\lambda = \pm, \alpha = 1, 2, 3)$ are linearly independent unit basis vectors at the point (p) of interest of the given three-dimensional space R^3_λ. The unit vectors O_λ and σ_α imply $< O_\lambda, O_\tau >= {}^*\delta_{\lambda\tau}, \quad < \sigma_\alpha, \sigma_\beta >= \delta_{\alpha\beta}$, where $\delta_{\alpha\beta}$ is the Kronecker symbol, and ${}^*\delta_{\lambda\tau} = 1 - \delta_{\lambda\tau}$. Three spatial $e_\alpha = \xi \times \sigma_\alpha$ and three temporal $e_{0\alpha} = \xi_0 \times \sigma_\alpha$ components are the basis vectors, respectively, in spaces R^3 and T^3, where $O_\pm = (1/\sqrt{2})(\xi_0 \pm \xi), \quad \xi_0^2 = -\xi^2 = 1, \quad < \xi_0, \xi >= 0$. The 3D space $R^3_\pm$ is spanned by the coordinates $\eta_{(\pm\alpha)}$. In using the 6D language, we will be able to make a necessary reduction to the conventional 4D space which can be achieved in the following way.

(i) In case of free flat space M_6, the subspace T^3 is isotropic. And in so far it contributes in line element just only by the square of the moduli $t = |\mathbf{x}^0|$, $\mathbf{x}^0 \in T^3$, then, the reduction $M_6 \to M_4 = R^3 \oplus T^1$ can be readily achieved if we use $t = |\mathbf{x}^0|$ for conventional *time*.

(ii) In case of curved space, the reduction $V_6 \to V_4$ can be achieved if we use the projection $(\widetilde{e}_0)$ of the temporal component $(\widetilde{e}_{0\alpha})$ of basis six-vector $\widetilde{e}\,(\widetilde{e}_\alpha, \widetilde{e}_{0\alpha})$ on the given *universal* direction $(\widetilde{e}_{0\alpha} \to \widetilde{e}_0)$. By this we choose the *time* coordinate. Actually, the Lagrangian of physical fields defined on R_6 is a function of scalars such as $A_{(\lambda\alpha)}B^{(\lambda\alpha)} = A_\alpha B^\alpha + A_{0\alpha}B^{0\alpha}$, then upon the reduction of temporal components of six-vectors $A_{0\alpha}B^{0\alpha} = A^{0\alpha} < \widetilde{e}_{0\alpha}, \widetilde{e}_{0\beta} > B^{0\beta} = A^0 < \widetilde{e}_0, \widetilde{e}_0 > B^0 = A_0 B^0$ we may fulfill a reduction to V_4.

doi: 10.52526/25792776-2021.68.2-236

8.4. Lie group G_D of the distortion

A distortion of the basis comprises the following two steps. We, at first, consider distortion transformations of the ingredient unit vectors O_τ under the distortion gauge field (a): $\widetilde{O}_{(+\alpha)}(a) = \mathcal{Q}^{\tau}_{(+\alpha)}(a)\,O_\tau = O_+ + æ\, a_{(+\alpha)}O_-$, $\widetilde{O}_{(-\alpha)}(a) = \mathcal{Q}^{\tau}_{(-\alpha)}(a)\,O_\tau = O_- + æ\, a_{(-\alpha)}O_+$, where $\mathcal{Q}\,(= \mathcal{Q}^{\tau}_{(\lambda\alpha)}(a))$ is an element of the group Q. This , in turn, induces the distortion transformations of the ingredient unit vectors σ_β, which undergo the rotations, $\widetilde{\sigma}_{(\lambda\alpha)}(\theta) = \mathcal{R}^{\beta}_{(\lambda\alpha)}(\theta)\,\sigma_\beta$, where $\mathcal{R}(\theta) \in SO(3)$ is the element of the group of rotations of planes involving two arbitrary axes around the orthogonal third axis in the given ingredient space R^3_λ. Then, the resulting basis vectors $\widetilde{\sigma}_{(\lambda\alpha)}(\theta)$ of each three-dimensional ingredient space R^3_λ retain the orthogonality condition between themselves, but violate it with respect to the basis vectors of different ingredient spaces. That is, $< \widetilde{\sigma}_{(\lambda\alpha)}, \widetilde{\sigma}_{(\tau\beta)} >_{\alpha\neq\beta} \neq 0, \quad \text{at} \quad \lambda \neq \tau$. In fact, distortion transformations of basis vectors (O) and (σ) are not independent, but rather are governed by the spontaneous breaking of the distortion symmetry. To avoid a further proliferation of indices, thenceforth we will use upper case Latin (A) in indexing $(\lambda\alpha) \quad (\lambda = \pm; \alpha = 1, 2, 3)$, etc. The infinitesimal transformations read $\delta\, \mathcal{Q}^{\tau}_{A}(a) = æ\, \delta\, a_A X^{\tau}_{\lambda} \in Q$, $\delta\, \mathcal{R}(\theta) = -\frac{i}{2} M_{\alpha\beta}\delta\, \omega^{\alpha\beta} \in SO(3)$, provided by the generators $X^{\tau}_{\lambda} = {}^{*}\delta^{\tau}_{\lambda}$ and $I_i = \frac{\sigma_i}{2}$, where σ_i are the Pauli matrices, $M_{\alpha\beta} = \varepsilon_{\alpha\beta\gamma} I_\gamma$ and $\delta\, \omega^{\alpha\beta} = \varepsilon_{\alpha\beta\gamma}\delta\, \theta_\gamma$. The transformation matrix $D(a, \theta) = \mathcal{Q}(a) \times \mathcal{R}(\theta)$ is an element of the distortion group $G_D = Q \times SO(3)$: $D_{(d\,a^A,\, d\theta^A)} = I + d\, D_{(a^A,\, \theta^A)}$, $d\, D_{(a^A,\, \theta^A)} = i\left[d\, a^A X_A + d\, \theta^A I_A\right]$, where $I_A \equiv I_\alpha$ at given λ. The generators X_A of the group Q do not complete the group H to the dynamical group G_D, therefore, they cannot be interpreted as the generators of the quotien space G_D/H, and the distortion fields a_A cannot be identified directly with the Goldstone fields arisen in spontaneous breaking of the distortion symmetry G_D. These objections, however, can be circumvented, because, as it is shown by (Ter-Kazarian, 2010), the distortion group $G_D = Q \times SO(3)$ can be mapped in a one-to-one manner onto the group $G_D = SO(3) \times SO(3)$, which is isomorphic to the chiral group $SU(2) \times SU(2)$. The method of phenomenological Lagrangians is well known for this group. Hence we arrive at $\tan\theta_A = -æ\, a_A$. Given the distortion field a_A, this key relation uniquely determines six angles θ_A of rotations around each of six (A) axes. The fundamental field is distortion gauge field (a) and, thus, all the fundamental gravitational structures in fact - the metric as much as the coframes and connections - acquire a *distortion-gauge induced* theoretical interpretation. We study the geometrical structure of the space of parameters in terms of Cartan's calculus of exterior forms and derive the Maurer-Cartan structure equations, where the distortion fields (a) are treated as the Goldstone fields (Ter-Kazarian, 2010).

8.5. A spontaneous breaking of gravitation gauge symmetry

As alluded to above, in realization of the structure group G_V we implement the abelian local group $U^{loc} = U(1)_Y \times \overline{U}(1) \equiv U(1)_Y \times diag[SU(2)]$, on the space M_6 (spanned by the coordinates η), with the group elements of $exp\,[i\frac{Y}{2}\,\theta_Y(\eta)]$ of $U(1)_Y$ and $exp\,[iT^3\,\theta_3(\eta)]$ of $\overline{U}(1)$. The group $U^{loc}(2)$ has two generators, the third component T^3 of isospin $\vec{T}$ related to the Pauli spin matrix $\frac{\vec{\tau}}{2}$, and hypercharge Y implying $Q^d = T^3 + \frac{Y}{2}$, where Q^d is the *distortion charge* operator assigning the number -1 to particles, but +1 to anti-particles. The group $U^{loc}(2)$ entails two neutral gauge bosons of $\overline{U}(1)$, or that coupled to T^3, and of $U(1)_Y$, or that coupled to the hypercharge Y. The gauge invariant Lagrangian of the fermion field is given in the standard form by $\mathcal{L} = \overline{\psi}(\eta) i\gamma^A\, D_A\psi(\eta)$, provided the covariant derivative is $D_A\,\psi(\eta) = (\partial_A - ig\,T^3\,W^3_A - ig'\,(Y/2)\,B_A)\,\psi(\eta)$, and g, g' being the $\overline{U}(1)$, $U(1)_Y$ coupling strengths, respectively. Spontaneous symmetry breaking can be achieved by introducing the neutral complex scalar Higgs field (Ter-Kazarian, 2010): $\phi = \begin{pmatrix} 0 \\ \phi^0 \end{pmatrix}$, $\quad Y(\phi) = 1, \quad \phi^0 = \frac{1}{\sqrt{2}}(\phi_1 + i\phi_2)$, with the standard potential energy density function $V(\phi) = -\mu^2\phi^+\,\phi + \lambda(\phi^+\,\phi)^2$, where $\mu^2 > 0, \quad \lambda > 0$. This is an ingredient of the gauge invariant Lagrangian of Higgs field $\mathcal{L}_H = (D_A\,\phi)^+(D^A\,\phi) - V(\phi)$, where $D_A\,\phi(\eta) = (\partial_A - ig\,T^3\,W^3_A - ig'\,(Y/2)\,B_A)\,\phi(\eta)$. Minimization of the vacuum energy fixes the non-vanishing VEV: $< \phi >_0 \equiv < 0|\phi|0 > = \begin{pmatrix} 0 \\ \frac{v}{\sqrt{2}} \end{pmatrix}$, $\quad v = (\frac{\mu^2}{\lambda})^{1/2}$, leaving one Goldstone boson. The VEV of spontaneously breaks the theory, leaving the $U(1)_d$ subgroup intact. The unitary gauge

doi: 10.52526/25792776-2021.68.2-236

$\phi(\eta) = U^{-1}(\xi_3)\begin{pmatrix} 0 \\ \frac{v+\zeta(\eta)}{\sqrt{2}} \end{pmatrix}$, $U(\xi_3) = \exp\left[\frac{i\xi_3\cdot\tau^3}{v}\right]$, is parameterized by two real shifted fields ξ_3 and ζ, such that $< 0|\xi_3|0 >=< 0|\zeta|0 >= 0$. The gauge transformation $\phi' = U(\xi_3)\,\phi = \frac{v+\zeta}{\sqrt{2}}\,\chi$, $\chi = \begin{pmatrix} 0 \\ 1 \end{pmatrix}$, leads to $V(\phi') = \mu^2\zeta^2 + \lambda v\zeta^3 + (\lambda/4)\,\zeta^4$, which gives the mass of Higgs boson $M_H = \sqrt{2}\,\mu$. An examination of the v^2-terms in the kinetic piece of the Lagrangian $\mathcal{L}_H = (D_A\,\phi')^+(D^A\,\phi') - V(\phi')$ reveals the mass terms for the physical gauge bosons: $\frac{v^2}{2}\,\left|(i\frac{g}{2}\,\tau^3\,W'^3_A + ig'\,\frac{Y}{2}\,B'_A)\,\chi\right|^2 =$ $\frac{1}{2}\,(\bar{a}_A,\,a_A)\begin{pmatrix} M^2_{\bar{a}} & 0 \\ 0 & 0 \end{pmatrix}\begin{pmatrix} \bar{a}^A \\ a^A \end{pmatrix}$. The mass matrix can be diagonalized by the standard orthogonal transformations: $\bar{a}_A = \cos\theta_W\,W'^3_A + \sin\theta_W\,B'_A$, $a_A = \sin\theta_W\,W'^3_A + \cos\theta_W\,B'_A$, $M_{\bar{a}} = \frac{v}{2}\sqrt{g^2 + g'^2}$, $M_a = 0$, where $\tan\theta_W = g'/g$. Namely, the neutral gauge field W'^3_A mixes with the abelian gauge field B'_A to form the physical states $\bar{a}_A$ and a_A, with the masses $M_{\bar{a}} \neq 0$ and $M_a = 0$, respectively. For a neutral current we get $\mathcal{L}_{int} = æ\,(\mathcal{J}^{(0)}_A\,A^A + \mathcal{J}^{(M)}_A\,\bar{a}^A) \equiv æ\,(\mathcal{J}_A\,a^A)$, where $æ = g\,\sin\theta$, and $\mathcal{J}^{(0)}_A = \overline{\psi}(\eta)i\gamma_A\,Q^d\,\psi(\eta)$, $\mathcal{J}^{(M)}_A = \overline{\psi}(\eta)i\gamma_A\,Q^{(in)}\,\psi(\eta)$, $\mathcal{J}_A = \overline{\psi}(\eta)i\gamma_A\,\psi(\eta)$, $Q^{(in)} = \frac{T^3 - \sin^2\theta_W,\,Q^{gr}}{\sin\theta_W\,\cos\theta_W},$. That is, the left Goldstone boson is gauged away from the scalar sector, but it essentially reappears in the gauge sector providing the longitudinally polarized spin state of one of gauge bosons that acquires mass through its coupling to Higgs scalar. Consequently, the two neutral gauge bosons were mixed to form two physical orthogonal states of the massless component of *distortion* field, (a) $(M_a = 0)$, which is responsible for gravitational interactions, and its massive component, $(\bar{a})$ $(M_{\bar{a}} \neq 0)$, which is responsible for the ID-regime. Hence, a substantial change of the properties of the spacetime continuum besides the curvature may arise at huge energies. The theory is renormalizable, because gauge invariance gives conservation of charge, also ensures the cancelation of quantum corrections that would otherwise result in infinitely large amplitudes. Without careful thought we expect that in this framework the renormalizability of the theory will not be spoiled in curved space-time too, because, the infinities arise from ultra-violet properties of Feynman integrals in momentum space which, in coordinate space, are short distance properties, and locally (over short distances) all curved space-time look like maximally symmetric (flat) space.

8.6. The 12D smooth differentiable manifold $\widetilde{M}_{12}$

In pursuing our goal further, we are necessarily led to extend a whole framework of GGP to 12D smooth differentiable manifold $\widetilde{M}_{12}$. Consider the curve $\lambda(t) : R^1 \to \widetilde{M}_{12}$ passing through the point $p = \lambda(0) \in \widetilde{M}_{12}$ with tangent vector $\mathbf{A}|_{\lambda(t)}$. The $\{\zeta\}$ are local coordinates in open neighborhood of $p \in \mathcal{U}$. The 12-dimensional smooth vector field $\mathbf{A}_p = \mathbf{A}(\zeta)$ belongs to the section of tangent bundle $\mathbf{T}_p$ at the point $p(\zeta)$. The one parameter group of diffeomorphisms A^t for the curve $\zeta(t)$ passing through point p and $\zeta(0) = \zeta_p$, $\dot{\zeta}(0) = \mathbf{A}_p$, is written as $d\,A^t_p(\mathbf{A}) = \frac{d}{d\,t}\Big|_{t=0} A^t(\zeta(t)) = \mathbf{A}_p(\zeta)$, such that $d\,A^t : \mathbf{T}(\widetilde{M}_{12}) \to R(\mathbf{T}(\widetilde{M}_{12}) = \bigcup_{p(\zeta)} \mathbf{T}_p)$. The $e_{(\lambda,\mu,\alpha)} = O_{\lambda,\mu} \times \sigma_\alpha$ $(\lambda,\mu = 1,2;\quad \alpha = 1,2,3)$ are linear independent 12 unit basis vectors at the point $p \in \widetilde{M}_{12}$ provided by the unit vectors $O_{\lambda,\mu}$ and σ_α implying $< O_{\lambda,\mu}, O_{\tau,\nu} >= {}^*\delta_{\lambda\tau}{}^*\delta_{\mu\nu}$, $< \sigma_\alpha, \sigma_\beta >= \delta_{\alpha\beta}$, where $\delta_{\alpha\beta}$ is the Kronecker symbol, but ${}^*\delta_{11} = {}^*\delta_{22} = 0$ and ${}^*\delta_{12} = {}^*\delta_{21} = 1$. The basis vectors σ_α refer to given three dimensional ordinary space $R^3_{\lambda\mu}$. The metric on $\widetilde{M}_{12}$ reads $\hat{\mathbf{g}} : \mathbf{T}_p \times \mathbf{T}_p \to C^\infty(\widetilde{M}_{12})$. Let also the massless gauge field $a_A(\zeta)$ associates with connection in principle bundle $p : E \to M_{12}$ with a structure group U^{loc}, where the coordinates ζ exist in the whole region $\mathcal{U}$ of space $M_{12} = M_6 \oplus \bar{M}_6$. The M_6 relates to the spacetime, but the $\bar{M}_6$ is displayed as a space of inner degrees of freedom. In the framework of method of phenomenological Lagrangians, we address the non-linear realizations of the Lie group G of *distortion* of 12-dimensional space. One may now implement the matrix $D(a,\,\theta) = \mathcal{Q}(a) \times \mathcal{R}(\theta)$ of *distortion* group $G = Q \times SO(3)$ by which the basis vector e is transformed at point $p \in \widetilde{M}_{12}$. The infinitesimal transformations read $\delta\,\mathcal{Q}^{\tau,\nu}_A(a) = æ\,\delta\,a_A X^{\tau\nu}_{\lambda\mu} \in Q$, $\delta\,\mathcal{R}(\theta) = -\frac{i}{2}M_{\alpha\beta}\delta\,\omega^{\alpha\beta} \in SO(3)$, provided by the generators $X^{\tau\nu}_{\lambda\mu} = {}^*\delta^\tau_\lambda{}^*\delta^\nu_\mu$, and $I_i = \frac{\sigma_i}{2}$, where σ_i are the Pauli's matrices, such that $M_{\alpha\beta} = \varepsilon_{\alpha\beta\gamma}I_\gamma$, $\left[\frac{\sigma_i}{2}, \frac{\sigma_k}{2},\right] = i\varepsilon_{ikj}\frac{\sigma_j}{2}$, $\delta\,\omega^{\alpha\beta} = \varepsilon_{\alpha\beta\gamma}\delta\,\theta_\gamma$. Consequenttly, the infinitesimal action of the group on basis vectors e_A can be written as $d\,e_A = e_A\,d\,F_A = O_A(d) \times \sigma_A + O_A \times \sigma_A(d) =$ $i[\omega^A(d)\,X_A + \vartheta^A(d)\,I_A]\,e_A$,where we denote $e_A \equiv (\exp F_A)$. It is shown that the *distortion* group

doi: 10.52526/25792776-2021.68.2-236

$G = Q \times SO(3)$ can be mapped onto the group $G = SO(3) \times SO(3)$ in one-to-one manner. The latter is isomorphic to the isotopic chiral group $SU(2) \times SU(2)$, for which the method of phenomenological Lagrangians is well known. For the sake of simplicity, throughout this item we leave the Greek indices implicit unless otherwise stated, such that $A = (\lambda\mu i) \to i = 1, 2, 3,$. But it goes without saying that all the results obtained refer to the given three-dimensional ingredient space $R^3_{\lambda\mu}$. Three I_i among the six generators of the group correspond to isotopic transformations, and three K_i- to special chiral transformations mixing the states of different parities. They imply the conventional commutation relations of invariant subgroup $H = SO(3)$, with the generators I_i, and of quotien space G/H, with the generators K_i, where ε_{ijk} denotes the antisymmetric unit tensor. Three parameters $\overline{a}^i(a)$ of special chiral transformations, with respect to which the Lagrangian of physical fields is not invariant, can be identified with three Goldstone fields. Consequently we arrive at $\tan\theta_A = -æ\, a_A$. This key relation contains no new information, beyond the fact that it uniquely determines the 12 angles θ_A of rotations around each of 12 axes (A) at given distortion field a_A. The Maurer-Cartan's structure equations $(\omega^i)' = [\omega^k, \omega^i_k]$, and $(\omega^i_k)' = -R^l_{jki}[\omega^k, \omega^i]/2 + [\omega^k_j, \omega^l_k]$, describe the motion of the orthogonal reper joint to the given point of the group space, where $R^l_{jki} = -\varepsilon_{lj\gamma}\varepsilon_{\gamma ki}$ is the curvature of the group space. The forms ω^i and ω^i_k are interpreted as the transformations of translation and rotation of the orthogonal reper, such that the rotation $(\vartheta^l I_l)$ belongs to stationary group H while the translation reads as $(\omega^i K_i)$. Whereas, the invariant constraint means that there always exists the rotation transformation of stationary subgroup H annulling the change in equation of Cartan's forms arisen from the translation transformation of the quotien space $\overline{Q} = G/H$. A general transformation of the group G can be written as $G = \overline{Q}(\overline{a})H(\theta)$, where $\overline{Q}(\overline{a})$ is the transformation belonged to the left adjacent class G/H of the group G by subgroup H.

8.7. The extended field equations

The Lagrangian of Goldstone field $(\overline{a})$ can be identified with the square of interval of the geodesic line, with minimal number of derivatives, between the infinitely closed points $\overline{a}^i$ and $\overline{a}^i + d\,\overline{a}^i$ $L_{\overline{a}}(\zeta) = \frac{1}{2}\,\omega^i(\overline{a}, \partial_A\,\overline{a})\omega^i(\overline{a}, \partial_A\,\overline{a})$, where $\varepsilon_{\alpha il}\varepsilon_{l\alpha j} = -\delta_{ij}$ is the metric tensor of the group space. Since the massless gauge field (a) is associated with the gauge group U^{loc}, the Lagrangian should be equated to undegenerated Killing form defined on the Lie algebra of the group U^{loc} in adjoint representation $L_{\overline{a}}(\zeta) = L_a(\zeta) = -\frac{1}{4} < F_{AB}(a),\, F^{AB}(a) >_K$, where $F_{AB}(a)$ is the antisymmetric tensor of the gauge field (a). Thence the Goldstone field $(\overline{a})$ as a function of the gauge field (a) can be determined. The covariant derivatives of the matter fields Ψ interacting with the Goldstone fields $\overline{a}$ are determined by means of the form ϑ^α $L = L_0(\Psi, \partial_A\Psi + \vartheta^\alpha(\overline{a}, \partial_A\,\overline{a})T_\alpha\,\Psi)$, where $L_0(\Psi, \partial_A\Psi)$ is the Lagrangian of interacting matter fields classified by the linear representations T_α of the subgroup H. The Lagrangians above are invariant with respect to *distortion* translations and rotations. These also should be completed by the transformations $\Psi' = (\exp\,[i\eta'^\alpha(\overline{a}, g)T_\alpha])\,\Psi$.

The extended field equations followed at once in terms of Euler-Lagrange variations respectively on the M_{12} and $\widetilde{M}_{12}$ (Ter-Kazarian, 1986, 1989c, 1997, 2010, 2012): $S = S_a + S_{\widetilde{\Phi}} = \int \sqrt{-\eta}\, L_a\, d^{12}\zeta + \int \sqrt{-g}\, L_{\widetilde{\Phi}}\, d^{12}\widetilde{\zeta}$, where L_a is the Lagrangian of distortion field (a), $L_{\widetilde{\Phi}}$ is the Lagrangian of matter fields, whereas the dependence on the distortion gauge field comes only through the components of the metrical tensor. The L_a is invariant under Lorentz (Λ) and U^{loc} gauge groups. The Lagrangian $L_{\widetilde{\Phi}}$, in turn, is invariant under the gauge group of gravitation, G_R. In terms of the Euler-Lagrange variations in M_{12} and $\widetilde{M}_{12}$, we readily obtain $\frac{\delta(\sqrt{-\eta}\, L_a)}{\delta\, a_A} = -\frac{\partial\, g^{BC}}{\partial\, a_A}\frac{\delta(\sqrt{-g}\, L_{\widetilde{\Phi}})}{\delta\, g^{BC}} = -\frac{\sqrt{-g}}{2}\frac{\partial\, g^{BC}}{\partial\, a_A}\widetilde{T}_{BC}$, $\frac{\delta \widetilde{L}_{\widetilde{\Phi}}}{\delta\,\widetilde{\Phi}} = 0$, $\frac{\delta\, L_{\widetilde{\Phi}}}{\delta\widetilde{\overline{\Phi}}} = 0$, where $\widetilde{T}_{BC}$ is the energy-momentum tensor of the matter fields $\widetilde{\Phi}(\widetilde{\zeta})$. The Lagrangian of distortion gauge field $a_A = (a_{(\lambda\alpha)}, \bar{a}_{(\tau\beta)})$ defined on the flat space, yields $\partial^B\partial_B a_A - (1-\zeta_0^{-1})\,\partial_A\partial^B a_B = J_A = -\frac{1}{2}\sqrt{g}\frac{\partial g^{BC}}{\partial a_A}\widetilde{T}_{BC}$, where $F_{AB}(a)$ is the antisymmetrical tensor of gauge field (a), ζ_0 is the gauge fixing parameter. To render our discussion here more transparent, below we clarify the relation between gravitational and coupling constants. To assist in obtaining actual solutions from the field equations, we may consider the weak-field limit and shall envisage that the right hand side of should be in the form $-\frac{1}{2}\,(4\pi G_N)\,\sqrt{g(x)}\,\frac{\partial g^{BC}(x)}{\partial x_A}\widetilde{T}_{BC}$. Hence, we may assign to the Newton's gravitational constant G_N the value $G_N = æ^2/4\pi$.

doi: 10.52526/25792776-2021.68.2-236

Let consider, particularly, the static and spherically symmetrical physical system. In accord, the equation of distortion gauge field $a_A = (a_{(\lambda\alpha)}, \bar{a}_{(\tau\beta)})$ reads $\partial^B \partial_B a_A - (1 - \zeta_0^{-1})\,\partial_A \partial^B a_B = J_A = -\frac{1}{2}\sqrt{g}\frac{\partial g^{BC}}{\partial a_A} T_{BC}$, where T_{BC} is the energy-momentum tensor, ζ_0 is the gauge fixing parameter. To render our discussion here more transparent, below we clarify the relation between gravitational and coupling constants. To assist in obtaining actual solutions from the field equations, we may consider the weak-field limit and shall envisage that the right hand side should be in the form $-\frac{1}{2}\,(4\pi G_N)\,\sqrt{g(x)}\,\frac{\partial g^{BC}(x)}{\partial x_A}\widetilde{T}_{BC}$. Hence, we may assign to the Newton's gravitational constant G_N the value $G_N = æ^2/4\pi$. The curvature of manifold $M_6 \to \widetilde{M}_6$ is the familiar distortion induced by the extended field components $a_{(1,1,\alpha)} = a_{(2,1,\alpha)} \equiv \frac{1}{\sqrt{2}}a_{(+\alpha)}$, $a_{(1,2,\alpha)} = a_{(2,2,\alpha)} \equiv \frac{1}{\sqrt{2}}a_{(-\alpha)}$. The other regime of ID presents at: $a_{(1,1,\alpha)} = -a_{(2,1,\alpha)} \equiv \frac{1}{\sqrt{2}}\bar{a}(+\alpha)$, $a_{(1,2,\alpha)} = -a_{(2,2,\alpha)} \equiv \frac{1}{\sqrt{2}}\bar{a}_{(-\alpha)}$.

8.8. A hard look at spacetime deformation

The holonomic metric on $\widetilde{\mathcal{M}}_4$ can be recast in the form $\widetilde{g} = \widetilde{g}_{\mu\nu}\,\widetilde{\vartheta}^\mu \otimes \widetilde{\vartheta}^\nu = \widetilde{g}(\widetilde{e}_\mu,\, \widetilde{e}_\nu)\,\widetilde{\vartheta}^\mu \otimes \widetilde{\vartheta}^\nu$, with components, $\widetilde{g}_{\mu\nu} = \widetilde{g}(\widetilde{e}_\mu, \widetilde{e}_\nu)$ in the dual holonomic base $\{\widetilde{\vartheta}^\mu \equiv d\widetilde{x}^\mu\}$. It is well known that the notions of space and connections should be separated. The curvature and torsion are in fact properties of a connection, and many different connections are allowed to exist in the same spacetime. Therefore, when considering several connections with different curvature and torsion, one takes spacetime simply as a manifold, and connections as additional structures.

In order to relate local Lorentz symmetry to more general deformed spacetime, there is, however, a need to introduce the soldering tools, which are the linear frames and forms in tangent fiber-bundles to the external a general smooth differential manifold, whose components are so-called tetrad (vierbein) fields. The $\widetilde{\mathcal{M}}_4$ has at each point a tangent space, $\widetilde{T}_{\widetilde{x}}\widetilde{M}_4$, spanned by the anholonomic orthonormal frame field, $\widetilde{e}$, as a shorthand for the collection of the 4-tuplet $(\widetilde{e}_0, \cdots, \widetilde{e}_3)$, where $\widetilde{e}_a = \widetilde{e}_a{}^\mu\,\widetilde{\partial}_\mu$. The frame field, $\widetilde{e}$, then defines a dual vector, $\widetilde{\vartheta}$, of differential forms, $\widetilde{\vartheta} = \begin{pmatrix}\widetilde{\vartheta}^0\\ \vdots \\ \widetilde{\vartheta}^3\end{pmatrix}$, as a shorthand for the collection of the $\widetilde{\vartheta}^b = \widetilde{e}^b{}_\mu\, d\widetilde{x}^\mu$, whose values at every point form the dual basis, such that $\widetilde{e}_a \rfloor \widetilde{\vartheta}^b = \delta^b_a$. In components $\widetilde{e}_a{}^\mu\,\widetilde{e}^b{}_\mu = \delta^b_a$.

On the manifold, $\widetilde{\mathcal{M}}_4$, the tautological tensor field, $\widetilde{id}$, of type (1,1) can be defined which assigns to each tangent space the identity linear transformation. Thus for any point $\widetilde{x} \in \widetilde{\mathcal{M}}_4$, and any vector $\widetilde{\xi} \in \widetilde{T}_{\widetilde{x}}\widetilde{\mathcal{M}}_4$, one has $\widetilde{id}(\widetilde{\xi}) = \widetilde{\xi}$. In terms of the frame field, the $\widetilde{\vartheta}^a$ give the expression for $\widetilde{id}$ as $\widetilde{id} = \widetilde{e}\widetilde{\vartheta} = \widetilde{e}_0 \otimes \widetilde{\vartheta}^0 + \cdots \widetilde{e}_3 \otimes \widetilde{\vartheta}^3$, in the sense that both sides yield $\widetilde{\xi}$ when applied to any tangent vector $\widetilde{\xi}$ in the domain of definition of the frame field. One can also consider general transformations of the linear group, $GL(4, R)$, taking any base into any other set of four linearly independent fields. The notation, $\{\widetilde{e}_a,\, \widetilde{\vartheta}^b\}$, will be used below for general linear frames.

Let us introduce the so-called *first deformation matrices*, $(\pi(x)^m_k$ and $\widetilde{\pi}^a{}_l(\widetilde{x})) \in GL(4, \widetilde{M})\,\forall\,\widetilde{x}$, as follows: $\widetilde{D}^m_\mu = \widetilde{e}_\mu{}^k\,\pi^m{}_k$, $\quad \widetilde{\psi}^\mu_l = \widetilde{e}^\mu{}_k\,\pi^k{}_l$, $\quad \widetilde{e}_\mu{}^k\,\widetilde{e}^\mu{}_m = \delta^k_m$, $\widetilde{\pi}_a{}^m = \widetilde{e}_a{}^\mu\,\widetilde{D}^m_\mu$, $\quad \widetilde{\pi}^a{}_l = \widetilde{e}^a{}_\mu\,\widetilde{\psi}^\mu_l$, where $\widetilde{g}_{\mu\nu}\,\widetilde{e}_k{}^\mu\,\widetilde{e}_s{}^\nu = \eta_{ks}$, η_{ks} is the metric on M_4. Hence the deformation tensor, $\Omega^m{}_l = \pi^m{}_k\,\pi^k{}_l$, yields local tetrad deformations $\widetilde{e}_a = \widetilde{\pi}_a{}^m\,e_m$, $\quad \widetilde{\vartheta}^a = \widetilde{\pi}^a{}_l\,\vartheta^l$, $\bar{e}_k = \pi^m{}_k\,e_m$, $\quad \overline{\vartheta}^k = \pi^k{}_l\,\vartheta^l$, and that $\widetilde{id} = \widetilde{e}_a \otimes \widetilde{\vartheta}^a = \bar{e}_k \otimes \overline{\vartheta}^k \in \widetilde{\mathcal{M}}_4$. The *first deformation matrices* π and $\widetilde{\pi}$, in general, give rise to the right cosets of the Lorentz group, i.e. they are the elements of the quotient group $GL(4, \widetilde{M})/SO(3,1)$.

If we deform the co-tetrad, we have two choices to recast metric as follows: either writing the deformation of the metric in the space of tetrads or deforming the tetrad field: $\widetilde{g} = o_{ab}\,\widetilde{\vartheta}^a \otimes \widetilde{\vartheta}^b = o_{ab}\,\widetilde{\pi}^a{}_l\,\widetilde{\pi}^b{}_m\,\vartheta^l \otimes \vartheta^m = \gamma_{lm}\,\vartheta^l \otimes \vartheta^m$. where the *second deformation matrix*, γ_{lm}, reads $\gamma_{lm} = o_{ab}\,\widetilde{\pi}^a{}_l\,\widetilde{\pi}^b{}_m$. The deformed metric splits as $\widetilde{g}_{\mu\nu} = \Upsilon^2\,\eta_{\mu\nu} + \widetilde{\gamma}_{\mu\nu}$,where $\Upsilon = \widetilde{\pi}^a{}_a = \pi^k{}_k$, and $\widetilde{\gamma}_{\mu\nu} = (\gamma_{al} - \Upsilon^2\,o_{al})\,\widetilde{e}^a{}_\mu\,\widetilde{e}^l{}_\nu = (\gamma_{ks} - \Upsilon^2\,\eta_{ks})\,\widetilde{e}^k{}_\mu\,\widetilde{e}^s{}_\nu$. The anholonomic orthonormal frame field, $\widetilde{e}$, relates $\widetilde{g}$ to the tangent space metric, $o_{ab} = diag(+---)$, by $o_{ab} = \widetilde{g}(\widetilde{e}_a,\, \widetilde{e}_b) = \widetilde{g}_{\mu\nu}\,\widetilde{e}_a{}^\mu\,\widetilde{e}_b{}^\nu$, which has the converse $\widetilde{g}_{\mu\nu} = o_{ab}\,\widetilde{e}^a{}_\mu\,\widetilde{e}^b{}_\nu$ because $\widetilde{e}_a{}^\mu\,\widetilde{e}^a{}_\nu = \delta^\mu_\nu$. With this provision, we build up a *world-deformation* tensor Ω yielding a deformation of the flat space M_4. The γ_{lm} can be decomposed in terms of symmetric, $\widetilde{\pi}_{(al)}$, and antisymmetric, $\widetilde{\pi}_{[al]}$, parts of the matrix $\widetilde{\pi}_{al} = o_{ac}\widetilde{\pi}^c{}_l$ (or respectively in terms of $\pi_{(kl)}$ and $\pi_{[kl]}$,

doi: 10.52526/25792776-2021.68.2-236

where $\pi_{kl}=\eta_{ks}\,\pi^s{}_l)$ as $\gamma_{al}=\widetilde{\Upsilon}^2\,o_{al}+2\widetilde{\Upsilon}\,\widetilde{\Theta}_{al}+o_{cd}\,\widetilde{\Theta}^c{}_a\,\widetilde{\Theta}^d{}_l+o_{cd}\,(\widetilde{\Theta}^c{}_a\,\widetilde{\varphi}^d{}_l+\widetilde{\varphi}^c{}_a\,\widetilde{\Theta}^d{}_l)+o_{cd}\,\widetilde{\varphi}^c{}_a\,\widetilde{\varphi}^d{}_l$, where $\widetilde{\pi}_{al}=\widetilde{\Upsilon}o_{al}+\widetilde{\Theta}_{al}+\widetilde{\varphi}_{al}$, $\widetilde{\Upsilon}=\widetilde{\pi}^a{}_a$, $\widetilde{\Theta}_{al}$ is the traceless symmetric part and $\widetilde{\varphi}_{al}$ is the skew symmetric part of the first deformation matrix. The anholonomy objects defined on the tangent space, $\widetilde{T}_{\widetilde{x}}\widetilde{M}_4$, read $\widetilde{C}^a:\;=d\,\widetilde{\vartheta}^a=\frac{1}{2}\,\widetilde{C}^a{}_{bc}\,\widetilde{\vartheta}^b\wedge\widetilde{\vartheta}^c$, where the anholonomy coefficients, $\widetilde{C}^a{}_{bc}$, which represent the curls of the base members, are $\widetilde{C}^c{}_{ab}=-\widetilde{\vartheta}^c([\widetilde{e}_a,\,\widetilde{e}_b])=\widetilde{e}_a{}^\mu\widetilde{e}_b{}^\nu(\widetilde{\partial}_\mu\widetilde{e}^c{}_\nu-\widetilde{\partial}_\nu\widetilde{e}^c{}_\mu)=-\widetilde{e}^c{}_\mu[\widetilde{e}_a(\widetilde{e}_b{}^\mu)-\widetilde{e}_b(\widetilde{e}_a{}^\mu)]=2\,\pi^c{}_l\,\widetilde{e}_m{}^\mu\,(\pi^{-1m}{}_{[a}\widetilde{\partial}_\mu\,\pi^{-1l}{}_{b]})$. In particular case of constant metric in the tetradic space, the deformed connection can be written as $\widetilde{\Gamma}^a{}_{bc}=\frac{1}{2}\,(\widetilde{C}^a{}_{bc}-o^{aa'}\,o_{bb'}\,\widetilde{C}^{b'}{}_{a'c}-o^{aa'}\,o_{cc'}\,\widetilde{C}^{c'}{}_{a'b})$. All magnitudes related to the V_4 will be denoted with an over $'\circ'$. Now we have $\overset{\circ}{\Omega}{}^m{}_l=\overset{\circ}{D}{}^m{}_\mu\,\overset{\circ}{\psi}{}^\mu{}_l$ and $\breve{\Omega}^\mu{}_\nu=\breve{D}^\mu_\rho\breve{\psi}^\rho_\nu$, provided $\overset{\circ}{e}{}_\mu=\overset{\circ}{D}{}^l{}_\mu\,e_l$, $\overset{\circ}{e}_\mu\overset{\circ}{\psi}{}^\mu{}_l=\overset{\circ}{\Omega}{}^m{}_l\,e_m$, $\widetilde{e}_\rho=\breve{D}^\mu_\rho\,\overset{\circ}{e}_\mu$, $\widetilde{e}_\rho\,\breve{\psi}^\rho_\nu=\breve{\Omega}^\mu{}_\nu\,\overset{\circ}{e}_\mu$. The following relations hold: $\overset{\circ}{D}{}^m_\mu=\overset{\circ}{e}{}^k_\mu\,\overset{\circ}{\pi}{}^m{}_k$, $\overset{\circ}{\psi}{}^\mu_l=\overset{\circ}{e}{}^\mu{}_k\,\overset{\circ}{\pi}{}^k{}_l$, $\overset{\circ}{e}{}^k_\mu\,\overset{\circ}{e}{}^\mu{}_m=\delta^k_m$, $\overset{\circ}{\pi}{}_a{}^m=\overset{\circ}{e}{}_a{}^\mu\,\overset{\circ}{D}{}^m_\mu$, $\overset{\circ}{\pi}{}^a{}_l=\overset{\circ}{e}{}^a{}_\mu\,\overset{\circ}{\psi}{}^\mu_l$, where $\overset{\circ}{\Omega}{}^m{}_l=\overset{\circ}{\pi}{}^m{}_\rho\,\overset{\circ}{\pi}{}^\rho{}_l$, $\breve{\Omega}^\mu{}_\nu=\breve{\pi}^\mu{}_\rho\breve{\pi}^\rho{}_\nu$. So, $\overset{\circ}{g}_{\mu\nu}\,\overset{\circ}{e}{}_k{}^\mu\,\overset{\circ}{e}{}_s{}^\nu=\eta_{ks}$, and $\breve{D}^\mu_\rho=\breve{e}_\nu{}^\mu\,\breve{\pi}^\nu{}_\rho$, $\breve{\psi}^\rho_\nu=\breve{e}^\rho{}_\mu\,\breve{\pi}^\mu{}_\nu$, $\breve{e}_\nu{}^\mu\,\breve{e}^\nu{}_\rho=\delta^\mu_\rho$, $\breve{\pi}_a{}^\mu=\breve{e}_a{}^\rho\,\breve{D}^\mu_\rho$, $\breve{\pi}^a{}_\nu=\breve{e}^a{}_\rho\,\breve{\psi}^\rho_\nu$. The norm $d\,\overset{\circ}{s}\equiv i\,\overset{\circ}{d}$ of the infinitesimal displacement $d\,\overset{\circ}{x}{}^\mu$ on the V_4 can be written in terms of the spacetime structures of M_4 as $i\,\overset{\circ}{d}=\overset{\circ}{e}\,\overset{\circ}{\vartheta}=\overset{\circ}{\Omega}{}^m{}_l\,e_m\otimes\vartheta^l\in V_4$. The holonomic metric can be recast in the form $\overset{\circ}{g}=\overset{\circ}{g}_{\mu\nu}\,\overset{\circ}{\vartheta}{}^\mu\otimes\overset{\circ}{\vartheta}{}^\nu=\overset{\circ}{g}\,(\overset{\circ}{e}_\mu,\,\overset{\circ}{e}_\nu)\,\overset{\circ}{\vartheta}{}^\mu\otimes\overset{\circ}{\vartheta}{}^\nu$. The anholonomy objects defined on the tangent space, $\overset{\circ}{T}_{\overset{\circ}{x}}\,V_4$, read $\overset{\circ}{C}{}^a:\;=d\,\overset{\circ}{\vartheta}{}^a=\frac{1}{2}\,\overset{\circ}{C}{}^a{}_{bc}\,\overset{\circ}{\vartheta}{}^b\wedge\overset{\circ}{\vartheta}{}^c$, where the anholonomy coefficients, $\overset{\circ}{C}{}^a{}_{bc}$, which represent the curls of the base members, are $\overset{\circ}{C}{}^c{}_{ab}=-\overset{\circ}{\vartheta}{}^c([\overset{\circ}{e}_a,\,\overset{\circ}{e}_b])=\overset{\circ}{e}_a{}^\mu\overset{\circ}{e}_b{}^\nu\,(\overset{\circ}{\partial}_\mu\overset{\circ}{e}{}^c{}_\nu-\overset{\circ}{\partial}_\nu\overset{\circ}{e}{}^c{}_\mu)=-\overset{\circ}{e}{}^c{}_\mu[\overset{\circ}{e}_a\,(\overset{\circ}{e}_b{}^\mu)-\overset{\circ}{e}_b\,(\overset{\circ}{e}_a{}^\mu)]$. The (anholonomic) Levi-Civita (or Christoffel) connection can be written as $\overset{\circ}{\Gamma}{}_{ab}:\;=\overset{\circ}{e}_{[a}\rfloor d\,\overset{\circ}{\vartheta}_{b]}-\frac{1}{2}\,(\overset{\circ}{e}_a\rfloor\,\overset{\circ}{e}_b\rfloor d\,\overset{\circ}{\vartheta}_c)\wedge\overset{\circ}{\vartheta}{}^c$, where $\overset{\circ}{\vartheta}_c$ is understood as the down indexed 1-form $\overset{\circ}{\vartheta}_c=o_{cb}\,\overset{\circ}{\vartheta}{}^b$. The norm $i\widetilde{d}$ can then be written in terms of the spacetime structures of V_4 and M_4: $i\widetilde{d}=\widetilde{e}\widetilde{\vartheta}=\widetilde{e}_\rho\otimes\widetilde{\vartheta}^\rho=\widetilde{e}_a\otimes\widetilde{\vartheta}^a=\breve{\Omega}^\mu{}_\nu\,\overset{\circ}{e}_\mu\otimes\overset{\circ}{\vartheta}{}^\nu=\breve{\Omega}^a{}_b\,\breve{e}_a\,\breve{\vartheta}^b=\Omega^m{}_l\,e_m\otimes\vartheta^l\in\widetilde{\mathcal{M}}_4$, provided, $\breve{\Omega}^a{}_b=\breve{\pi}^a{}_c\breve{\pi}^c{}_b=\breve{\Omega}^\mu{}_\nu\,\overset{\circ}{e}{}^a{}_\mu\,\overset{\circ}{e}{}_b{}^\nu$, $\widetilde{e}_\rho=\breve{\pi}^\nu{}_\rho\,\overset{\circ}{e}_\nu$, $\widetilde{\vartheta}^\rho=\breve{\pi}_\mu{}^\rho\,\overset{\circ}{\vartheta}{}^\mu$, $\widetilde{e}_c=\breve{\pi}_c{}^a\,\overset{\circ}{e}_a$, $\widetilde{\vartheta}^c=\breve{\pi}^c{}_b\,\overset{\circ}{\vartheta}{}^b$. Under a local tetrad deformation, a general spin connection transforms according to $\widetilde{\omega}^a{}_{b\mu}=\breve{\pi}_c{}^a\,\overset{\circ}{\omega}{}^c{}_{d\mu}\breve{\pi}^d{}_b+\breve{\pi}_c{}^a\,\widetilde{\partial}_\mu\,\breve{\pi}^c{}_b=\pi_l{}^a\,\widetilde{\partial}_\mu\,\pi^l{}_b$. We have then two choices to recast metric as follows: $\widetilde{g}=o_{ab}\,\widetilde{\vartheta}^a\otimes\widetilde{\vartheta}^b=o_{ab}\,\breve{\pi}^a{}_c\breve{\pi}^b{}_d\,\overset{\circ}{\vartheta}{}^c\otimes\overset{\circ}{\vartheta}{}^d=\breve{\gamma}_{cd}\,\overset{\circ}{\vartheta}{}^c\otimes\overset{\circ}{\vartheta}{}^d$. In the first case, the contribution of the Christoffel symbols constructed by the metric $\breve{\gamma}_{ab}=o_{cd}\,\breve{\pi}^c{}_a\breve{\pi}^d{}_b$ reads $\widetilde{\Gamma}^a{}_{bc}=\frac{1}{2}\,(\overset{\circ}{C}{}^a{}_{bc}-\breve{\gamma}^{aa'}\,\breve{\gamma}_{bb'}\,\overset{\circ}{C}{}^{b'}{}_{a'c}-\breve{\gamma}^{aa'}\,\breve{\gamma}_{cc'}\,\overset{\circ}{C}{}^{c'}{}_{a'b})+\frac{1}{2}\,\breve{\gamma}^{aa'}\,(\overset{\circ}{e}_c\rfloor d\,\breve{\gamma}_{ba'}-\overset{\circ}{e}_b\rfloor d\,\breve{\gamma}_{ca'}-\overset{\circ}{e}_{a'}\rfloor d\,\breve{\gamma}_{bc})$.As before, the second deformation matrix, $\breve{\gamma}_{ab}$, can be decomposed in terms of symmetric, $\breve{\pi}_{(ab)}$, and antisymmetric, $\breve{\pi}_{[ab]}$, parts of the matrix $\breve{\pi}_{ab}=o_{ac}\breve{\pi}^c{}_b$. So, $\breve{\pi}_{ab}=\breve{\Upsilon}o_{ab}+\breve{\Theta}_{ab}+\breve{\varphi}_{ab}$, where $\breve{\Upsilon}=\breve{\pi}^a{}_a$, $\breve{\Theta}_{ab}$ is the traceless symmetric part and $\breve{\varphi}_{ab}$ is the skew symmetric part of the first deformation matrix. The deformed metric can then be split as $\widetilde{g}_{\mu\nu}(\breve{\pi})=\breve{\Upsilon}^2(\breve{\pi})\;\overset{\circ}{g}_{\mu\nu}+\breve{\gamma}_{\mu\nu}(\breve{\pi})$, where $\breve{\gamma}_{\mu\nu}(\breve{\pi})=[\breve{\gamma}_{ab}-\breve{\Upsilon}^2\,o_{ab}]\;\overset{\circ}{e}{}^a{}_\mu\;\overset{\circ}{e}{}^b{}_\nu$. The inverse deformed metric reads $\widetilde{g}^{\mu\nu}(\breve{\pi})=o^{cd}\,\breve{\pi}^{-1a}{}_c\,\breve{\pi}^{-1b}{}_d\;\overset{\circ}{e}{}_a{}^\mu\;\overset{\circ}{e}{}_b{}^\nu$, where $\breve{\pi}^{-1a}{}_c\,\breve{\pi}^c{}_b=\breve{\pi}^c{}_b\,\breve{\pi}^{-1a}{}_c=\delta^a_b$. The (anholonomic) Levi-Civita (or Christoffel) connection can be written as $\widetilde{\Gamma}_{ab}:\;=\widetilde{e}_{[a}\rfloor d\widetilde{\vartheta}_{b]}-\frac{1}{2}\,(\widetilde{e}_a\rfloor\widetilde{e}_b\rfloor d\widetilde{\vartheta}_c)\wedge\widetilde{\vartheta}^c$, where $\widetilde{\vartheta}_c$ is understood as the down indexed 1-form $\widetilde{\vartheta}_c=o_{cb}\,\widetilde{\vartheta}^b$. Hence, the usual Levi-Civita connection is related to the original connection by the relation $\widetilde{\Gamma}^\mu{}_{\rho\sigma}=\breve{\Gamma}^\mu{}_{\rho\sigma}+\breve{\Pi}^\mu{}_{\rho\sigma}$, provided $\Pi^\mu{}_{\rho\sigma}=2\widetilde{g}^{\mu\nu}\,\breve{g}_{\nu(\rho}\,\breve{\nabla}_{\sigma)}\,\breve{\Upsilon}-\breve{g}_{\rho\sigma}\,g^{\mu\nu}\,\breve{\nabla}_\nu\,\breve{\Upsilon}+\frac{1}{2}\,\widetilde{g}^{\mu\nu}\,(\breve{\nabla}_\rho\,\breve{\gamma}_{\nu\sigma}+\breve{\nabla}_\sigma\,\breve{\gamma}_{\rho\nu}-\breve{\nabla}_\nu\,\breve{\gamma}_{\rho\sigma})$, where $\breve{\nabla}$ is the covariant derivative. The contravariant deformed metric, $\widetilde{g}^{\nu\rho}$, is defined as the inverse of $\widetilde{g}_{\mu\nu}$, such that $\widetilde{g}_{\mu\nu}\,\widetilde{g}^{\nu\rho}=\delta^\rho_\mu$. Hence, the connection deformation $\Pi^\mu{}_{\rho\sigma}$ acts like a force that deviates the test particles from the geodesic motion in the space, V_4.

A metric-affine space $(\widetilde{M}_4,\;\widetilde{g},\,\widetilde{\Gamma})$ is defined to have a metric and a linear connection that need not dependent on each other. In general, the lifting of the constraints of metric-compatibility and symmetry yields the new geometrical property of the spacetime, which are the *nonmetricity* 1-form $\widetilde{N}_{ab}$ and the affine *torsion* 2-form $\widetilde{T}^a$ representing a translational misfit. These, together with the *curvature* 2-form $\widetilde{R}_a{}^b$, symbolically can be presented as $(\widetilde{N}_{ab},\,\widetilde{T}^a,\,\widetilde{R}_a{}^b)\;\sim\;\widetilde{\mathcal{D}}(\widetilde{g}_{ab},\,\widetilde{\vartheta}^a,\,\widetilde{\Gamma}_a{}^b)$, where $\widetilde{\mathcal{D}}$ is the *covariant exterior derivative*. If the nonmetricity tensor $\widetilde{N}_{\lambda\mu\nu}=-\widetilde{\mathcal{D}}_\lambda\,\widetilde{g}_{\mu\nu}\equiv-\widetilde{g}_{\mu\nu\,;\lambda}$ does not vanish, the general formula for the affine connection written in the spacetime components is

doi: 10.52526/25792776-2021.68.2-236

$\widetilde{\Gamma}^{\rho}{}_{\mu\nu} = \overset{\circ}{\Gamma}{}^{\rho}{}_{\mu\nu} + \widetilde{K}^{\rho}{}_{\mu\nu} - \widetilde{N}^{\rho}{}_{\mu\nu} + \frac{1}{2}\widetilde{N}_{(\mu\ \nu)}{}^{\rho}$, where $\overset{\circ}{\Gamma}{}^{\rho}{}_{\mu\nu}$ is the Riemann part, $\widetilde{K}^{\rho}{}_{\mu\nu} := 2\widetilde{Q}_{(\mu\nu)}{}^{\rho} + \widetilde{Q}^{\rho}{}_{\mu\nu}$ is the non-Riemann part - the affine *contortion tensor*. The torsion, $\widetilde{Q}^{\rho}{}_{\mu\nu} = \frac{1}{2}\widetilde{T}^{\rho}{}_{\mu\nu} = \widetilde{\Gamma}^{\rho}{}_{[\mu\nu]}$ given with respect to a holonomic frame, $d\,\widetilde{\vartheta}^{\rho} = 0$, is a third-rank tensor, antisymmetric in the first two indices, with 24 independent components.

In the presence of curvature and torsion, the coupling prescription of a general field carrying an arbitrary representation of the Lorentz group will be $\widetilde{\partial}_{\mu} \to \widetilde{\mathcal{D}}_{\mu} = \widetilde{\partial}_{\mu} - \frac{i}{2}(\widetilde{\omega}^{ab}_{\mu} - \widetilde{K}^{ab}{}_{\mu})J_{ab}$, with J_{ab} denoting the corresponding Lorentz generator. The Riemann-Cartan manifold, U_4, is a particular case of the general metric-affine manifold $\widetilde{\mathcal{M}}_4$, restricted by the metricity condition $\widetilde{N}_{\lambda\mu\nu} = 0$, when a nonsymmetric linear connection is said to be metric compatible. The Lorentz and diffeomorphism invariant scalar curvature, $\widetilde{R}$, becomes either a function of $\widetilde{e}^{a}{}_{\mu}$ only, or $\widetilde{g}_{\mu\nu}$: $\widetilde{R}(\widetilde{\omega}) \equiv \widetilde{e}_{a}{}^{\mu}\,\widetilde{e}_{b}{}^{\nu}\,\widetilde{R}_{\mu\nu}{}^{ab}(\widetilde{\omega}) = \widetilde{R}(\widetilde{g},\widetilde{\Gamma}) \equiv \widetilde{g}^{\rho\nu}\,\widetilde{R}^{\mu}_{\rho\mu\nu}(\widetilde{\Gamma})$.

8.9. Determination of $\widetilde{D}$ and $\widetilde{\psi}$ in standard theory of gravitation

Let $\widetilde{\omega}^{ab} = \widetilde{\omega}^{ab}_{\mu} \wedge d\,\widetilde{x}^{\mu}$ be the 1-forms of corresponding connections assuming values in the Lorentz Lie algebra. The action for gravitational field can be written in the form $\widetilde{S}_g = \overset{\circ}{S} + \widetilde{S}_Q$, where the integral $\overset{\circ}{S} = -\frac{1}{4æ}\int \star\, \overset{\circ}{R} = -\frac{1}{4æ}\int \star\, \overset{\circ}{R}_{cd} \wedge \widetilde{\vartheta}^{c} \wedge \widetilde{\vartheta}^{d} = -\frac{1}{2æ}\int \overset{\circ}{R}\,\sqrt{-\widetilde{g}}\,d\,\Omega$, is the usual Einstein action, with the coupling constant relating to the Newton gravitational constant $æ = 8\pi G_N/c^4$, S_Q is the phenomenological action of the spin-torsion interaction, $\star$ denotes the Hodge dual. This is a C^{∞}-linear map $\star : \Omega^{p} \to \Omega^{n-p}$, which acts on the wedge product monomials of the basis 1-forms as $\star(\widetilde{\vartheta}^{a_1\cdots a_p}) = \varepsilon^{a_1\cdots a_n}\,\widetilde{e}_{a_{p+1}\cdots a_n}$. Here $\widetilde{e}_{a_i}$ $(i = p+1,...,n)$ are understood as the down indexed 1-forms $\widetilde{e}_{a_i} = o_{a_i b}\,\widetilde{\vartheta}^{b}$ and $\varepsilon^{a_1\cdots a_n}$ is the total antisymmetric pseudo-tensor.

The variation of the connection 1-form $\widetilde{\omega}^{ab}$ yields $\delta\,\widetilde{S}_Q = \frac{1}{æ}\int \star\widetilde{\mathcal{T}}_{ab} \wedge \delta\widetilde{\omega}^{ab}$, where $\star\widetilde{\mathcal{T}}_{ab} := \frac{1}{2}\star(\widetilde{Q}_a \wedge \widetilde{e}_b) = \widetilde{Q}^{c} \wedge \widetilde{\vartheta}^{d}\,\varepsilon_{cdab} = \frac{1}{2}\,\widetilde{Q}^{c}{}_{\mu\nu} \wedge \widetilde{e}^{d}{}_{\alpha}\,\varepsilon_{abcd}\,\widetilde{\vartheta}^{\mu\nu\alpha}$, here we used the abbreviated notations for the wedge product monomials, $\widetilde{\vartheta}^{\mu\nu\alpha\ldots} = \widetilde{\vartheta}^{\mu} \wedge \widetilde{\vartheta}^{\nu} \wedge \widetilde{\vartheta}^{\alpha} \wedge ...$, defined on the U_4 space, and that $\widetilde{Q}^{a} = \widetilde{D}\,\widetilde{\vartheta}^{a} = d\,\widetilde{\vartheta}^{a} + \widetilde{\omega}^{a}{}_{b} \wedge \widetilde{\vartheta}^{b}$. The variation of the action describing the macroscopic matter sources $\widetilde{S}_m$ with respect to the coframe ϑ^{a}, and connection 1-form $\widetilde{\omega}^{ab}$ reads $\delta\,\widetilde{S}_m = \int \delta\,\widetilde{L}_m = \int(-\star\widetilde{\theta}_a \wedge \delta\,\widetilde{\vartheta}^{a} + \frac{1}{2}\star\widetilde{\Sigma}_{ab} \wedge \delta\,\widetilde{\omega}^{ab})$, where $\star\widetilde{\theta}_a$ is the dual 3-form relating to the canonical energy-momentum tensor, $\widetilde{\theta}^{\mu}_{a}$, by $\star\,\widetilde{\theta}_a = \frac{1}{3!}\,\widetilde{\theta}^{\mu}_{a}\,\varepsilon_{\mu\nu\alpha\beta}\,\widetilde{\vartheta}^{\nu\alpha\beta}$. and $\star\widetilde{\Sigma}_{ab} = -\star\,\widetilde{\Sigma}_{ba}$ is the dual 3-form corresponding to the canonical spin tensor, which is identical with the dynamical spin tensor $\widetilde{S}_{abc}$, namely $\star\widetilde{\Sigma}_{ab} = \widetilde{S}^{\mu}{}_{ab}\,\varepsilon_{\mu\nu\alpha\beta}\,\widetilde{\vartheta}^{\nu\alpha\beta}$. The variation of the total action, $\widetilde{S} = \widetilde{S}_g + \widetilde{S}_m$, with respect to the $\widetilde{e}_a$, $\widetilde{\omega}^{ab}$ and $\widetilde{\Phi}$ gives the field equations: 1)$\frac{1}{2}\ \overset{\circ}{R}_{cd} \wedge \widetilde{\vartheta}^{c} = æ\,\widetilde{\theta}_d = 0$, 2) $\star\,\widetilde{\mathcal{T}}_{ab} = -\frac{1}{2}\,æ\,\star\,\widetilde{\Sigma}_{ab}$, 3)$\frac{\delta\,\widetilde{L}_m}{\delta\widetilde{\Phi}} = 0$, $\frac{\delta\,\widetilde{L}_m}{\delta\overline{\widetilde{\Phi}}} = 0$.The DC-members $\widetilde{D}$ and $\widetilde{\psi}$ can readily be determined as follows: $\widetilde{D}^{l}_{a} = \eta^{lm} < \widetilde{e}_a,\, e_m >$, $\widetilde{\psi}^{a}_{l} = \eta_{lm}\,\widetilde{\vartheta}^{a}(\vartheta^{-1})^{m}$.

9. The microscopic theory of black hole: Preliminaries

The theoretical framework in which we shall tackle the problem in quest is the framework of GGP. Exploring a spontaneous breaking of gravitation gauge symmetry at huge energies, the GGP underlies the MTBH which, in turn, has proved to be quite fruitful for ultra-high energy astrophysics. Although the agreement is satisfactory between MTBH and the solar system observational verifications and, moreover, it is consistent with general relativity up to the limit of neutron stars, nevertheless, one of the most remarkable drawback of this theory is the fact that instead of *infinite collapse* and *central singularity*, an inevitable end product of the evolution of massive object is the stable SPC, where static observers exist.

For a benefit of the reader, as a guiding principle to make the rest of paper understandable, in this Section we necessarily recount some of the highlights behind of MTBH, which are in use throughout the paper. Needless to say that we will refrain from providing lengthy mathematical details of MTBH. We will not be concerned with the actual details here, but only use it as a backdrop to validate the MTBH with some observational tests. Although some key theoretical ideas were introduced with

doi: 10.52526/25792776-2021.68.2-236

a satisfactory substantiation, we have also attempted to maintain a balance between being overly detailed and overly schematic.

9.1. The equilibrium superdense proto-matter core

For brevity reasons, in our setting we proceed in relatively simple way toward first look at some of the associated physics, which is quick to estimate the physical properties of more realistic SPC-configurations. The equations describing the equilibrium SPC include the gravitational and ID field equations, the hydrostatic equilibrium equation, and the state equation of the spherical-symmetric distribution of baryonic-quark matter in many-phase stratified states specified for each domain. The state equation will be discussed separately step-by-step away from the domain of lower density up to the domain of higher density.

Field equations. The field equations follow at once from the total gauge invariant Lagrangian in terms of Euler-Lagrange variations, respectively on both the 4D semi-Riemannian space $V_4 = \widetilde{R}^3 \oplus \widetilde{R}^0$, and the 4D flat space $M_4 = R^3 \oplus R^0$. Hereinafter the quantities referring to V_4 are denoted by wiggles, and are left without wiggles if they correspond to M_4. We are interested in the case of a 1D spherical-symmetric gravitational field $(a_0(r)), (r \in R^3))$, in presence of 1D space-like ID-field $(\bar{a}(r))$. In the case at hand, one has the group of motions $SO(3)$ with 2D space-like orbits S^2 where the standard coordinates are $\widetilde{\theta}$ and $\widetilde{\varphi}$. The stationary subgroup of $SO(3)$ acts isotropically upon the tangent space at the point of sphere S^2 of radius $\widetilde{r}$. So, the bundle $p : V_4 \to \widetilde{R}^2$ has the fiber $S^2 = p^{-1}(\widetilde{x}), \quad \widetilde{x} \in V_4$ with a trivial connection on it, where $\widetilde{R}^2$ is the quotient-space $V_4/SO(3)$. Considering the equilibrium configurations of degenerate baryonic-quark matter, we assume a spherical-symmetric gravitational field $a_0(r)$ in presence of one-dimensional space-like ID-field $\bar{a}$. That is, $a_{(1,1,3)} = a_{(2,2,3)} = a_{(+3)} = \frac{1}{2}(-a_0 + \bar{a})$, $a_{(1,2,3)} = a_{(2,1,3)} = a_{(-3)} = \frac{1}{2}(-a_0 - \bar{a})$, $a_{(\lambda,\mu,1)} = a_{(\lambda,\mu,2)} = 0, \quad \lambda, \mu = 1, 2.$; an absence of transversal stresses and the transference of masses in the space V_4: $T_1^1 = T_2^2 = T_3^3 = -\widetilde{P}(\widetilde{r}), \quad T_0^0 = -\widetilde{\rho}(\widetilde{r})$, where T_ν^μ is taken to denote the components of energy stress tensor. The equations of gravitation, $x_0 := æ a_0$, and ID, $x := æ\bar{a}$, fields can be written in Feynman gauge as follows (Ter-Kazarian, 2014, 2015): $\Delta x_0 = -æ^2 \left\{ \frac{1-x_0}{(1-x_0)^2+x^2}\widetilde{\rho}(\widetilde{r}) + \frac{1+x_0}{(1-x_0)^2+x^2}\widetilde{P}(\widetilde{r}) \right\}$, $(\Delta - \lambda_a^{-2})x = æ^2 x \left\{ \frac{\widetilde{\rho}(\widetilde{r})}{(1-x_0)^2+x^2} - \frac{\widetilde{P}(\widetilde{r})}{(1-x_0)^2+x^2} \right\} \times \theta(\lambda_a - n^{-1/3})$. Reviewing notations æ is the coupling constant relating to the Newton gravitational constant (G) as $æ = 8\pi G/c^4$, $\widetilde{P}(\widetilde{r})$ and $\widetilde{\rho}(\widetilde{r}) \quad (\widetilde{r} \in \widetilde{R}^3)$ are taken to denote the internal pressure and macroscopic density of energy defined in proper frame of reference that is being used, $\widetilde{n}$ is the distorted concentration of particles, r is the radius-vector defined on flat space R^3, $\Delta \equiv \partial^2/\partial r^2$, $\theta(t)$ is the step function $\theta(t) = \begin{cases} 1 & t \geq 0 \\ 0 & t < 0 \end{cases}$, and λ_a is the Compton length of the ID-field: $\lambda_a = \hbar/m_a c \simeq 0.4\,\mathrm{fm}$. A diffeomorphism $\widetilde{r}(r) : M_4 \to V_4$ is defined as $r = \widetilde{r} - R_g/4$, where R_g is the gravitational radius of distribution of matter, $R_g = 2GM/c^2 = 2.95 \times 10^5\, M/M_\odot\,\mathrm{cm}$.

Phase transition of II-type. In case at hand, the aforementioned profound geometrical structures enable an insight to explore a novel aspects expected at distortion of basis vectors $(e_{\lambda\alpha}, \bar{e}_{\tau\beta})$ of $\widetilde{M}_{12}$, where $tan\theta_{(\pm3)} = æ(-a_0 \pm \bar{a})$. Namely, $\widetilde{e}_0 = e_0(1 - x_0) + \bar{e}_3\, x, \quad \widetilde{e}_3 = e_3(1 + x_0) - \bar{e}_{03}\, x, \quad \widetilde{e}_1 = \frac{1}{2}\{(\cos\theta_{(+3)} + \cos\theta_{(-3)})e_1 + (\sin\theta_{(+3)} + \sin\theta_{(-3)})e_2 + (\cos\theta_{(+3)} - \cos\theta_{(-3)})\bar{e}_{01} + (\sin\theta_{(+3)} - \sin\theta_{(-3)})\bar{e}_{02}\}$, $\widetilde{e}_2 = \frac{1}{2}\{(\cos\theta_{(+3)} + \cos\theta_{(-3)})e_2 - (\sin\theta_{(+3)} + \sin\theta_{(-3)})e_1 + (\cos\theta_{(+3)} - \cos\theta_{(-3)})\bar{e}_{02} - (\sin\theta_{(+3)} - \sin\theta_{(-3)})\bar{e}_{01}\}$,. This straightforwardly yields the transformations of Poincaré generators of translations, which, in turn, lead to the phase transition of each particle located in the ID-region: $\widetilde{E} = E, \quad \widetilde{P}_{1,2} = P_{1,2}\cos\widetilde{\theta}_3, \quad \widetilde{P}_3 = P_3 - \tan\widetilde{\theta}_3\, mc$, $\widetilde{m} = \left|(m - \tan\widetilde{\theta}_3\, \frac{P_3}{c})^2 + \sin^2\widetilde{\theta}_3\, \frac{P_1^2+P_2^2}{c^2} - \tan^2\widetilde{\theta}_3\, \frac{E^2}{c^4}\right|^{\frac{1}{2}}$, where $E, \vec{P}, m$ and $\widetilde{E}, \widetilde{\vec{P}}, \widetilde{m}$ are, respectively, ordinary and distorted energy, momentum and mass at rest, and $\tan\widetilde{\theta}_3 = -x, \quad \widetilde{\theta}_1 = \widetilde{\theta}_2 = 0$. Consequently, a whole matter found in the ID-region of spacetime continuum is undergone phase transition of II-type, while a shift of mass and energy-momentum spectra occurs upwards along the energy scale. The thermodynamics of a resulting matter, so-called *proto-matter*, is drastically differed from the thermodynamics of strongly compressed ordinary matter. It was in close analogy of well known Nambu-Jona-Lasinio model (Nambu & Jona-Lasinio, 1961) of elementary particle physics, to generate a fermion mass within the framework of gauge fields due to rearrangement

doi: 10.52526/25792776-2021.68.2-236

of vacuum state. The formation of *proto-matter* is a main reason for a sharply increase of energy density and internal pressure in the central part of proto-matter configuration , which is proportional to strong gravitational forces of compression. This halts the collapse and the central singularity would not occur. The resulting stable SPC is formed, which consists of the proto-matter core (PC) and the outer layers of ordinary matter. Thus, such phase-transition of matter has smeared out a central singularity of BH at very strong gravitational fields, replacing it by the equilibrium SPC.

The explicit form of the line element from the outside of configuration $\widetilde{r} > \widetilde{r}_b$, where $\widetilde{r}_b$ is the boundary of distribution of matter, reads $d\,s^2 = (1-x_0)^2 d\widetilde{t}^2 - (1+x_0)^2 d\widetilde{r}^2 - \widetilde{r}^2(\sin^2\theta d\,\varphi^2 + d\,\theta^2)$. Given the state equation, the hydrostatic equilibrium equation can be integrated. While an integration constant is determined from the condition of matching of internal and external metrics. Hence $g_{00}(r_f) = (1-\frac{R_g}{2r_b})^2 \exp\left[\int_0^{\widetilde{P}} \frac{2\widetilde{P}}{\widetilde{P}+\widetilde{\rho}}\right]$. Before proceeding further, and to make the reader fully understood, it is worthwhile to discuss in more detail one principle issue in use. Recall that according to the fundamental idea, conceived in the framework of GR, the EH is impenetrable barrier for crossing from inside the BH, because of a singularity arisen at Schwarzschild radius. But this barrier disappears in the framework of MTBH, when a matter, located in ID-region of the spacetime continuum, has undergone phase transition of II-type and, thus, it becomes a proto-matter. To obtain some feeling about this phenomena, note that, a singularity at intersection of proto-matter disk with the event horizon disappears where a massive component of ID-field is not zero, and hence the crossing event horizon from inside of BH at such conditions is allowed.

9.2. A research design and methods

We implement our scheme by considering the equilibrium configurations of non-rotating SPC of the two classes, with spherical-symmetric distribution of matter in many-phase stratified states. A layering of configuration is a consequence of the onset of different regimes in equation of state.
The I-class configurations include:
Domain $\rho < \rho_{drip} = 4.3\times 10^{11}\,\mathrm{g\,cm^{-3}}$ - the shell made of cold catalized matter, which is formed after nuclear burning in the density range below neutron drip (ρ_{drip}). Below $10^7\,\mathrm{g\,cm^{-3}}$, the $^{56}_{26}$Fe nuclei are dominating. In the inner crust, a Coulomb lattice of heavy nuclei co-exist in β- equilibrium with relativistic electrons.
Domain $\rho_{drip} \leq \rho < 4.5\times 10^{12}\,\mathrm{g\,cm^{-3}}$ inner crust-the electrons, nuclei and free neutrons co-exist in the medium.
Above the density $\rho > 4.5\times 10^{12}\,\mathrm{g\,cm^{-3}}$ the I-class configurations are thought to be composed of two phases of ideal cold n-p-e gas, which is mixture of neutrons, protons and electrons in complete β-equilibrium. The first phase state covers the intermediate density -
Domain $4.5\times 10^{12}\,\mathrm{g\,cm^{-3}} \leq \rho < \rho_d = 2.6\times 10^{16}\,\mathrm{g\,cm^{-3}}$ - which is the regular n-p-e gas in absence of ID. Second phase state is -
Domain $\rho > \rho_d$ - the n-p-e proto-matter at short nucleon-nucleon distances $r_{NN} \leq 0.4\,\mathrm{fm}$, in presence of ID.
For the II-class SPC configurations, up to the density range $\rho \leq \rho_{fl} = 4.1\times 10^{14}\,\mathrm{g\,cm^{-3}}$, to which the $r_{NN} \leq 1.6\,\mathrm{fm}$ nucloun-nucleon distances correspond, one has the same domains of I-class configurations. Above the density ρ_{fl}, we consider an onset of melting down of hadrons when nuclear matter consequently turns to quark matter. In the domain of $\rho_{fl} \leq \rho < \rho_{as} = m_n\,(0.25\,\mathrm{fm})^3 \simeq 1.1\times 10^{17}\,\mathrm{g\,cm^{-3}}$, where m_n is the neutron mass at rest, 0.25 fm is the string thickness, we consider two phase states of string flip-flop regimes.
Domain $\rho_{fl} \leq \rho < \rho_d$, to which the distances $0.4\,\mathrm{fm} < r_{NN} \leq 1.6\,\mathrm{fm}$ correspond - the regular string flip-flop, when ID is absent. This is a kind of tunneling effect when the strings joining the quarks stretch themselves violating energy conservation and after touching each other they switch on to the other configuration. We are interested in the individual particle approximation (Hartree approximation), where the Hartree potential is almost linearly proportional to the string length. The Y shape string is the most convenient for calculations, because the center of it almost equals to the center of gravity. At very first, we shall study the classical strings. In analogy to the case of ordinary quark matter, one may readily show that in order to have bound state the rising potential should be a scalar.

doi: 10.52526/25792776-2021.68.2-236

Similar to ordinary case a red quark searches for the nearest center and joins with it by a string and so on. One simplifies the calculations by assuming that the centers are uniformly distributed with a particle concentration. We assume that quarks have small ordinary mass $m_i \simeq m_u = 5MeV$. Next, we explore a tunneling effect of quantum fluctuations of string, and the negative potential energy caused by such a quantum jump. The basic technique adopted for calculation of transition matrix element $\widetilde{K}$ is the instanton technique (semi-classical treatment). Due to quantum string flip-flop, an attractive interaction between quarks is presented, when during the quantum transition from a state ψ_1 of energy $\widetilde{E}_1$ to another one ψ_2 of energy $\widetilde{E}_2$, the lowering of energy of system occurs. The quark matter acquires $\Delta\widetilde{E}$ correction to the classical string energy, such that the flip-flop energy lowers the energy of quark matter, consequently by lowering the critical density or critical Fermi momentum. The quark matter acquires $\Delta\widetilde{E}$ correction to the classical string energy, such that the flip-flop energy lowers the energy of quark matter, consequently by lowering the critical density or critical Fermi momentum. If one, for example, looks for the string flip-flop transition amplitude of simple system of $q\bar{q}q\bar{q}$ described by the Hamiltonian $\widetilde{H}$ and invariant action $\widetilde{S}$, then one has $< \;\Big|\, e^{-\widetilde{H}T} \,\Big|\; > \;=\; < \int [d\,\widetilde{\sigma}]\, e^{-\widetilde{S}} >$, where T is a (imaginary) time interval, $[d\,\widetilde{\sigma}]$ is the integration over all the possible string motion. The action $\widetilde{S}$ is proportional to the area $\widetilde{A}$ of the surface swept by the strings in the finite region of ID-region of V_4. The strings are initially in the configuration and finally in the configuration. Note that the maximal contribution to the path integral comes from the surface σ_0 of the minimum surface area (*instanton*). A computation of the transition amplitude is strightforward by summing over all the small vibrations around σ_0. Note that string has a finite thickness d, and the width of the area $\Delta\widetilde{A}$ cannot be less than d. This cutoff introduces a factor $\exp(-a_0\, d\, r_{NN})$, (where r_{NN} is the distance between two separated centers) in the amplitude $\widetilde{K}$ resulting in the finite-ranged potential. The interaction energy between two centers has a range of order $2\widetilde{\bar{r}}$ due to overlap of wave functions. A string thickness d can be estimated to be $0.25fm$.

Domain $\rho_d \leq \rho < \rho_{as}$- the string flip-flop regime in presence of ID at distances $0.25fm < r_{NN} \leq 0.4\,\mathrm{fm}$ - a system is made of quark proto-matter in complete β-equilibrium with rearrangement of string connections joining them.

Domain $\rho > \rho_{as}$- the system is made of quarks in one beg in complete β-equilibrium at presence of ID, under the weak interactions and gluons, including the effects of QCD-perturbative interactions. The QCD vacuum has a complicated structure due to the glueon-glueon interactions. The confinement of quarks is a natural feature of the exercising a pressure B on the surface of the local region of the perturbative vacuum to which quarks are confined. This is just the main idea of phenomenological MIT quark bag model, where quarks are assumed to be confined in a bag. Due to the screening of strong forces, the quarks are considered to be free inside the bag and to interact only in the surface region. The surface energy is estimated to be proportional to quark density. The stability of the hadron is ensured by the vacuum pressure B and surface tension. The surface energy is estimated to be proportional to quark density. In most applications, sufficient accuracy is obtained by assuming that all the quarks are almost massless inside a bag. Now, our purpose is to convert this picture to the medium of quark proto-matter. The quark proto-matter is in overall color singlet ground state, which is a non-interacting relativistic Fermi gas found in the ID-region of the spacetime continuum, at $r_{NN} \leq 0.25fm$. We consider the quark proto-matter of u, d and s flavors, in complete β-equilibrium. Now, let discuss the QCD interaction effects in approximation at hand, with extension to quark proto-matter. The first effect is the shift of the vacuum energy per unit volume. The bag constant $B \simeq 55MeV/fm^3$ of the MIT bag model must be added to the kinetic energy density. Including the gluon exchange perturbative interactions the energy density of quark proto-matter is then given by the non-interacting Fermi contribution plus bag constant $\widetilde{E}_0 = \sum_i \frac{3}{4}\widetilde{\nu}_i\widetilde{P}_{Fi}\widetilde{b}_I(\widetilde{N}, \alpha_c) + B$, where $\widetilde{P}_{Fi}$ is the distorted Fermi momentum of i flavor, $\widetilde{N}$ is the number of flavors present. The $\widetilde{N}$ and running coupling constant α_c takes into account the QCD perturbative interactions. The first correction to the free ground state is the ordinary exchange energy corresponding to the second order closed loop diagrams. Next correction is coming up from the sum of different ring diagrams. With equal numbers of quarks of each flavor presented, the modified function $\widetilde{b}_I(\widetilde{N}, \alpha_c)$ reads $\widetilde{b}_I(\widetilde{N}, \alpha_c) = (\widetilde{N}\left[1 + \frac{2\alpha_c}{3\pi} + \frac{\alpha_c^2}{3\pi^2}(\widetilde{N}\ln\frac{\alpha_c\widetilde{N}}{\pi} + 0.02\widetilde{N} + 6.75)\right]$. For numerical calculations it is sufficient to make use of the value $\alpha_c \simeq 2.2$ fitting the MIT bag model.

doi: 10.52526/25792776-2021.68.2-236

9.3. Simulations

Each configuration is defined by two free parameters of central values of particle concentration $\widetilde{n}(0)$ and ID-field $x(0)$. The interior gravitational potential $x_0^{int}(r)$ should be matched into the exterior one $x_0^{ext}(r)$. Checking it out one introduces the dimensionless sewing parameter $D(r_b) = \left|x_0^{int}(r_b) - x_0^{ext}(r_b)\right| / x_0^{int}(r_b)$, provided by the subsidiary sewing condition $D(r_b) = 0$ imposed at the boundary of configuration. The central value of the gravitational potential $x_0(0)$ can be found by reiterating integrations when the sewing condition.

Stability of SPC. In the relativistic case a total mass-energy M of configuration is the extremum in equilibrium for all configurations with the same total number of baryons. While the extrema of M and N occur at the same point in a one-parameter equilibrium sequence, therefore one can extremize $\widetilde{E} = \widetilde{M}\, c^2 - \widetilde{m}_B\, N$ on equal footing. Minimizing the energy will give the equilibrium configuration, and the second derivative of $\widetilde{E}$ will give stability information. For a spherical configurations of matter, instantaneously at rest, small radial deviations from equilibrium are governed by a Sturm-Liouville linear eigenvalue equation, with the imposition of suitable boundary conditions on normal modes with time dependence. A necessary and sufficient condition for stability is that the potential energy be positive defined for all initial data of small perturbations, namely, in first order approximation when one does not take into account the rotation and magnetic field, if the square of frequency of normal mode of small perturbations is positive. A relativity tends to destabilize configurations. For the SPC one should note that the total mass M is located in the region of $r \leq \bar{r}$, $\bar{r}$-is the boundary of distribution of protomatter, thus, the ID-field $x(r) \neq 0$ gives an additional contribution $(\nabla\, \widetilde{P} - \nabla\, P)$ to the potential energy of interaction, where $\nabla\, P$ is the gradient of internal pressure, and the quantities denoted by wiggles refer to SPC while the corresponding quantities of quark-star or neutron star are left without wiggles. The increase of distorted (effective) mass $\widetilde{m}$ of each particle of photometer at sufficiently strong $x(r) >> 1$ ID is governed by the rule $|\widetilde{m}| \sim x\, m >> m$. Since the internal pressure $\widetilde{P}$ and microscopic energy density $\widetilde{\rho}$ of degenerate superdence matter is proportional to the fourth degree of $\propto \widetilde{m}^4$, then their increase will be on the order of magnitude $\propto x^4$ with respect to the conventional value for neutron star. While the gradient of pressure should be increased as $\partial \widetilde{P}/\partial\, r \,\propto\, x^3\, (\partial\, x/\partial\, r)$. On the other hand, one has for the gravitational force $(\widetilde{P} + \widetilde{\rho})\, (g^{00}\, \partial g_{00}/2\, \partial\, r) \,\propto\, -x^3\, (\partial\, x_0/\partial\, r)$. From the field equation we find that $x_0 \simeq x >> 1$, $r \leq \bar{r}$ in central region of SPC, therefore $\widetilde{W} \approx W$ (W is the potential corresponding to neutron star) and, accordingly, this condition yields $\bar{\Gamma}_1 > 1.671$, which is analogous to the case of neutron star. Keeping in mind aforesaid, a numerical integrations (Ter-Kazarian et al., 2007) lead to the $\bar{\Gamma}_1 \approx 2.216$ for the SPC_I, while in the case of SPC_{II} we obtain $\bar{\Gamma}_1 \approx 2.4$, which clearly proves that the condition for stability of SPC is satisfied.

9.4. Results

The simulations confirm in brief the following scenario. The energy density and internal pressure have sharply increased in PC proportional to gravitational forces of compression in about 20-25 order of magnitude with respect to corresponding central values of neutron star. This counteracts the collapse and equilibrium holds even for the masses $\sim 10^{10} M_\odot$. The stable SPCs are formed, with radial distributions of density, internal pressure and a number of integral characteristics. Thereby the stable equilibrium holds for outward layers too. The SPC accommodates the highest energy scale up to hundreds ZeV in central proto-matter core. Without loss of generality, the typical features of SPC-configurations are summarised in the Fig. 2. The special units in use denote $P_{OV} = 6.469 \times 10^{36}\,\mathrm{erg\,cm^{-3}}$, $\rho_{OV} = 7.195 \times 10^{15}\,\mathrm{g\,cm^{-3}}$ and $r_{OV} = 13.68\,\mathrm{km}$. Moreover, above nuclear density, the SPC always resides inside the event horizon, therefore it could be observed only in presence of accreting matter in its close vicinities. This important feature can be seen even without addressing the exact theory. Actually, setting aside for the moment the details of superdense proto-matter physics, it is clear that the metric will necessarily be matched into Einstein's gravitation metric at weak gravitation limit on large distances far from the SPC of masses $\sim (10^8$ to $10^9)\ \mathrm{M}_\odot$ and respectively of small sizes $\sim (10^8$ to $10^{10})$ km. The latter suggests a presence of the coordinate singularity at $g_{00} = 0$. In contrast to Schwarzschild pseudo-singularity, in microscopic theory a true physical singularity occurred at the EH sphere of the radius $r = R_g/2$ such that the SPC is located inside the EH, where $R_g \simeq 2.95 \cdot 10^{13}\, M_8\, cm$

doi: 10.52526/25792776-2021.68.2-236

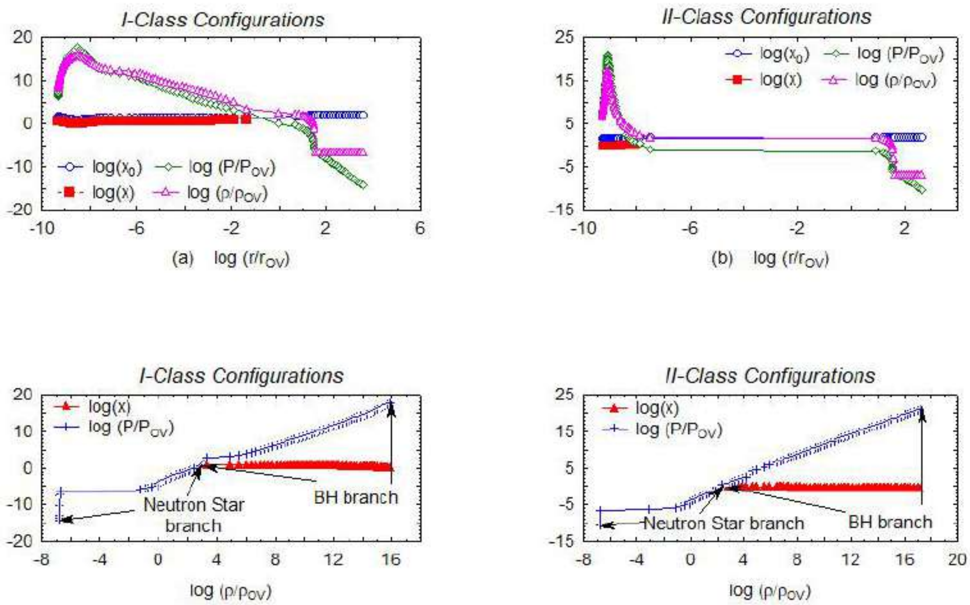

Figure 2. (a) The radial profiles of the pressure, the density, the dimensionless gravitational (x_0)- and ID (x)- potentials, and (b) the state equation, of the SPC of mass $\sim 1.49 \times 10^5\, M_\odot$.

is the gravitational radius and $M_8 = M/10^8 M_\odot$. The metric component g_{00} is equal zero on the EH where the curvature invariants are singular. The external physics of accretion onto the SPC in first half of its lifetime is identical to the processes in phenomenological BH models. In other words, there is no observable difference between the gravitational field of SPC and Schwarzschild BH but only one feature as follows. To make the reader fully understood, it is worthwhile before proceeding further to discuss in more detail one principle issue in use. Recall that according to the fundamental idea, conceived in the framework of GR, the EH is impenetrable barrier for crossing from inside the BH, because of a singularity arisen at Schwarzschild radius. But this barrier disappears in the framework of MTBH, when a matter, located in ID-region of the spacetime continuum, has undergone phase transition of II-type and, thus, it becomes a proto-matter. To obtain some feeling about this phenomena, note that (according to the field equations, a singularity at intersection of proto-matter disk with the event horizon disappears where a massive component of ID-field is not zero, and hence the crossing event horizon from inside of BH at such conditions is allowed.

A crucial difference in the model context between the phenomenological and microscopic black holes comes in when one looks for the spontaneous breaking of gravitation gauge symmetry at huge energies, and thereof making room for growth and merging behavior of black holes. We argue that the black hole seeds might grow driven by the accretion of outside matter when they were getting most of their masses. An infalling matter with time forms a thin proto-matter disk around the proto-matter core tapering off faster at reaching out the event horizon. The thickness of proto-matter disk at the edge of event horizon is of linear size d. Whereas a metric singularity inevitably disappears and the ZeV-neutrinos produced via simple or modified URCA processes in deep layers of SPC and proto-matter disk may escape from event horizon to outside world through a thin belt area $S = 2\pi R_g d$, even after the strong neutrino trapping. The neutrinos are collimated in very small opening angle $\theta_\nu \simeq \varepsilon_d = \frac{d}{2R_g} \ll 1$. To emphasize the distinction between phenomenological and microscopic black hole models, we present their schematic plots in Fig. 3, to guide the eye.

10. Growth of accreting supermassive black hole seeds and neutrino radiation

We further expose the assertions made in the framework of MTBH, to show that the seed black hole might grow up driven by the accretion of outside matter when it was getting most of its mass.

doi: 10.52526/25792776-2021.68.2-236

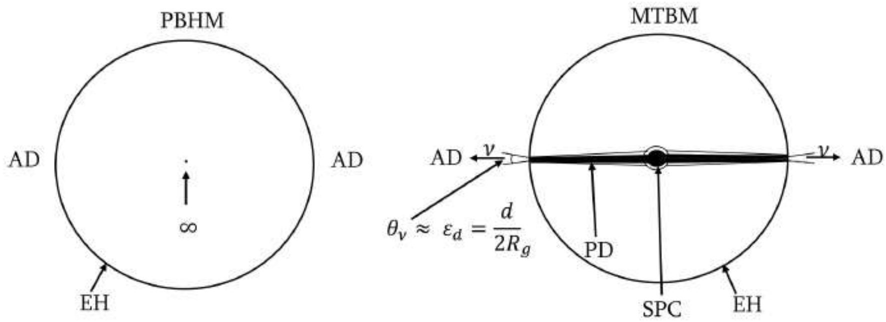

Figure 3. *Left panel*: Phenomenological model of non-spinning black hole. The meaningless singularity occurs at the center inside the black hole. *Right panel*: Microscopic model of non-spinning black hole, with the central stable SPC. An infalling matter with the time forms PD around the SPC. In final stage of growth, a PD has reached out the edge of the event horizon. Whereas a metric singularity inevitably disappears and UHE neutrinos may escape from event horizon to outside world through vista - a thin belt area $S = 2\pi R_g d$ - with opening angle θ_ν. Accepted notations: EH=Event Horizon, AD=Accretion Disk, SPC=Superdense Proto-matter Core, PD=Proto-matter Disk.

An infalling matter with time formes the proto-matter disk around the proto-matter core tapering off faster at reaching out the thin edge of the event horizon. At this, metric singularity inevitably disappears (see appendices) and the neutrinos may escape through vista to outside world, even after the neutrino trapping. We study the growth of proto-matter disk and derive the intermediate mass and initial redshift of seed black hole, as well as examine luminosities, neutrino surfaces for the disk. We review the mass assembly history of 377 plausible accreting supermassive black hole seeds. After the numerous reiterating integrations of the state equations of SPC-configurations, we compute their intermediate seed masses, M_{BH}^{Seed}, neutrino *pre-radiation times* (PRTs), initial redshifts, z^{Seed} and UHE-neutrino fluxes produced in the medium of the SPC via simple (quark and pionic reactions) or modified URCA processes, even after the neutrino trapping. The *trapping* is due to the fact that as the neutrinos are formed in proto-matter core at super-high densities they experience greater difficulty escaping from the proto-matter core before being dragged along with the matter, namely the neutrinos are *trapped* comove with matter. The part of neutrinos annihilate to produce, further, the secondary particles of expected ultra-high energies. In this model, of course, a key open question is to enlighten the mechanisms that trigger the activity, and how a large amount of matter can be steadily funneled to the central regions to fuel this activity. In high luminosity AGNs the large-scale internal gravitational instabilities drive gas towards the nucleus that trigger big starbursts, and the coeval compact cluster just formed. It seemed they have some connection to the nuclear fueling through mass loss of young stars as well their tidal disruption, and supernovae. Note that we regard the UHECR particles as a signature of existence of *superdence protomatter* sources in the universe. Since neutrino events are expected to be of sufficient intensity, our estimates can be used to guide investigations of neutrino detectors for the distant future.

10.1. Growth of black hole seed in mass

In the framework of MTBH, a growth behavior of IMBH-candidates widely based on the premises of runaway core collapse scenario. Matter pulled toward the seed BH (proto-matter core) loses angular momentum through viscous or turbulent processes in an intrinsic accretion disk. Within such a disc, friction would cause angular momentum to be transported outward, allowing matter to fall further inward, thus releasing potential energy and increasing the temperature of the proto-matter. One of the key objectives is then the increase of mass M^{seed} and gravitational radius R_g^{seed} of the seed BH at accretion of outside matter. Simultaneously with an increase of seed mass, an infalling matter formes intrinsic proto-matter disk around grown up proto-matter core tapering off faster at reaching out the thin edge of EH. The key objectives of the MTBH framework is then an increase of the mass, M_{BH}^{Seed}, and gravitational radius, R_g^{Seed}, of the seed black hole, BH^{Seed}, at accretion of outside matter. Thereby

doi: 10.52526/25792776-2021.68.2-236

an infalling matter formes proto-matter disk around proto-matter core tapering off faster at reaching out the thin edge of event horizon. So, a practical measure of growth $\mathrm{BH}^{Seed} \to \mathrm{BH}$ may most usefully be the increase of gravitational radius or mass of black hole $\Delta R_g = R_g^{BH} - R_g^{Seed} = \frac{2G}{c^2} M_d = \frac{2G}{c^2} \rho_d V_d$, and that $\Delta M_{BH} = M_{BH} - M_{BH}^{Seed} = M_{BH}^{Seed} \frac{\Delta R_g}{R_g^{Seed}}$, where M_d, ρ_d and V_d respectively are the total mass, density and volume of proto-matter disk. At the value $\hat{R}_g^{BH}$ of gravitational radius, when proto-matter disk has finally reached the event horizon of grown-up supermassive black hole, the volume $\hat{V}_d$, at $R_d \ll \hat{R}_g^{BH}$, is $\hat{V}_d \simeq \frac{\sqrt{2}\pi}{3} R_d (\hat{R}_g^{BH})^2$. From the first line, we obtain $\hat{R}_g^{BH} = k(1 \pm \sqrt{1 - \frac{2}{k} R_g^{Seed}})$, where $2/k = 8.73\,[\mathrm{km}]\, R_d\, \rho_d / M_\odot$, which is valid at $\frac{2}{k} R_g^{Seed} \leq 1$, namely $\frac{R_\odot}{R_d} \geq 2.09 \frac{[\mathrm{km}]}{R_\odot} \frac{\rho_d}{\bar{\rho}_\odot} \frac{R_g^{Seed}}{R_\odot}$.For the values $\rho_d = 2.6 \times 10^{16}\,[\mathrm{g\,cm}]^{-3}$ (see below) and $R_g^{Seed} \simeq 2.95\,[\mathrm{km}](10^3$ to $10^6)$, the inequality is reduced to $\frac{R_\odot}{R_d} \geq 2.34 \times 10^8 (1$ to $10^3)$ or $\frac{[\mathrm{cm}]}{R_d} \geq 0.34(10^{-2}$ to $10)$. This condition always satisfied, because for considered 377 black holes, with the masses $M_{BH}/M_\odot \simeq 1.1 \times 10^6$ to 1.3×10^{10}, we approximately have $\frac{R_d}{r_{OV}} \simeq 10^{-10}$ to 10^{-7}. Then the mass of seed black hole reads $\frac{M_{BH}^{Seed}}{M_\odot} \simeq \frac{M_{BH}}{M_\odot}(1 - 1.68 \times 10^{-6} \frac{R_d}{[\mathrm{cm}]} \frac{M_{BH}}{M_\odot})$.

10.2. The neutrino pre-radiation time

The PRT is referred to as a lapse of time, T_{BH}, from the birth of BH till neutrino radiation - the earlier part of the lifetime. A typical growth rate for a BH is then given by the time required to reach the final mass, M, and gravitational radius, $\hat{R}_g$, when proto-matter disk has finally reached the EH. In this framework we have introduced a notion of the pre-radiation time (PRT) of black hole which is referred to as a lapse of time T_{BH} from the birth of black hole till neutrino radiation - provision for the earlier half of the lifetime of black hole. The PRT-scale can be written (Ter-Kazarian, 2014, 2015) $T_{BH} = \frac{M_d}{\dot{M}}$, where $\dot{M}$ is the accretion rate. For given luminosity L, reads $T_{BH} \simeq 2.64\,(\frac{\epsilon}{0.1})\,\frac{R_d}{[\mathrm{cm}]}\,(\frac{M^{seed}}{M_\odot})^2\,\frac{10^{35}\,W}{L}\,[\mathrm{yr}]$, To give more credit to this view, next we would like to infer an analytical expression for the PRT-scale, T_{BH}. The order of magnitudes of the accretion rates can be derived if we assume that there is no shortage of the fuel around the BH. Actually, the BHs are fed by the accretion of gas in a process in which a small fraction of the energy of the accreted gas is released in the form of radiation of intensity L. The stars are sufficient to fuel some low luminosity dwarf nuclei: at high densities stellar collisions replenish the central density, and the nuclei can reach higher luminosities. If these conditions are fulfilled, the growth of massive BH can then be accretion-dominated. Thereby the mass accretion rate should be $\dot{M} \equiv \frac{dM}{dt} = \frac{L}{\epsilon c^2}$, where ϵ is the accretion efficiency to transform the gravitational energy into radiation. According to the canonical Bondi accretion rate, the luminosity has increased as $L \propto \dot{M} \propto M^2$. The Bondi rate should in general be considered an upper limit on the accretion rate, because it assumes free-fall of gas from the Bondi radius $R_B = GM/a_s^2$, where a_s is the sound speed of the gas. At some point, the BH growth seemed to slow down when approaching to quasar phase, for which the gas maximum rate accretion occurs nearly at the Eddington limit, and radiate at Eddington luminosity, $L_{Edd} = \frac{4\pi GMc}{k} = 1.3 \times 10^{38} (\frac{M}{M_\odot})\,[\mathrm{erg\,s}^{-1}]$ (above which the radiation pressure prevents the material to fall in), where $k = \sigma_T / m_p$ is the opacity. So, the $\dot{M}$ is expected to be limited by Eddington accretion rate $\epsilon\, c^2\, \dot{M} \leq L_{Edd}$. In the same time, it should be emphasized that the possibility of super-Eddington accretion has been also explored theoretically by many authors. A basic reason why this may be feasible is the photon trapping effect on small scales near the BH. That is, in a spherically symmetric accretion flow at a rate much greater than Eddington accretion, the emergent radiation flux is reduced by photon trapping in the optically-thick accreting matter. Such an effect operates when the radial gas in flow speed is faster than the outward photon diffusion speed. The photon trapping effect becomes physically relevant when, so-called, the "trapping radius" $R_{tr} = (k/4\pi c)\dot{M}$ is outside R_g. Note that the Bondi radius is generally much larger than the trapping radius. This idea dates back to the works by Begelman, who constructed in 1978 a global spherical accretion solution for ionized gas at super-Eddington value. The above scenarios holds, however, only in spherical symmetry, and ignores the question of the stability of the flow. The photon-trapping effect has more recently been incorporated into accretion disk models including direct radiation hydrodynamical simulations. These simulations find self-consistent super-Eddington accretion on small scales with lower values of the radiative efficiency below 10%, but are numerically

doi: 10.52526/25792776-2021.68.2-236

limited to model only short durations and small scales. The efficient growth phase can stably exist unless the outward momentum L/c dominates the inward ram pressure of the rapidly accreting gas. In summary, high accretion rates exceeding the Eddington value are possible but produce intense radiation flux toward the polar directions. These results, however, are valid only as long as a sufficient amount of gas at rates of $\dot{M} \gg \dot{M}_{Edd}$ is supplied from larger scales without being impeded by the strong radiation feedback.

In what follows, for simplicity reasons, the mass supply rate from large scales $\sim \dot{M}_{Edd}$ (precisely tracked as a BH grows by orders of magnitude in mass) is of particular interest to us. Then the Salpeter characteristic time-scale becomes as long as $T_s = \epsilon\, t_{Edd} = \epsilon\, \frac{kc}{4\pi G} = \frac{M}{\dot{M}_{Edd}} = (\frac{dt}{d\,log(M)})_{Edd} = \frac{M\epsilon c^2}{L_{Edd}} = (\frac{\epsilon}{0.1})\, 4.5\times 10^7$ [yr]. Thence $M(\frac{t}{[\mathrm{yr}]}) < M(0)\, exp(\frac{t}{T_s}) = M(0)\times 10^{\frac{t\,\log\,e}{T_s}} = M(0)\times 10^{\frac{0.434\,t}{T_s}}$, so that the characteristic minimum time, t_{min}, which takes at least BH of mass $M(0)$ to grow to mass, M, at the Eddington rate should be $t > t_{min} \equiv \frac{T_s}{0.434}\,\log(\frac{M}{M(0)})$ [yr] $= 1.037\times 10^8\, \log(\frac{M}{M(0)})$ [yr], where the value of efficiency is taken $\epsilon \simeq 0.1$ for high redshift quasars. For a seed mass, say, $M(0) \simeq 10^5 M_\odot$, the accretion of mass at the Eddington rate causes a BH mass to increase in time $t_{min} = 1.037\times 10^8 \times 4$ [yr] $=$ 4.148×10^8 [yr], to $\simeq 10^9 M_\odot$. This brings one back in time to an epoch when the Universe was very young and galaxies in their infancy. For example, the observation of luminous quasars well in excess of $\simeq 10^{47}$ [erg s^{-1}], at $z \simeq 6$, implies that the first SMBHs with masses $\sim 10^9 M_\odot$ must have formed already in place when the Universe is only 1 [Gyr] old.

The thickness of proto-matter disk at the edge of event horizon is of linear size d. Whereas a metric singularity inevitably disappears and the ZeV-neutrinos produced via simple or modified URCA processes in deep layers of SPC and proto-matter disk may escape from event horizon to outside world through a thin belt area $S = 2\pi R_g d$, even after the strong neutrino trapping. The neutrinos are collimated in very small opening angle $\theta_\nu \simeq \varepsilon_d = \frac{d}{2R_g} \ll 1$. Note that the spherical accretion onto black hole, in general, is not necessarily an efficient mechanism for converting rest-mass energy into radiation. Accretion onto black hole may be far from spherical accretion, because the accreted gas possesses angular momentum. In this case, the gas will be thrown into circular orbits about the black hole when centrifugal forces will become significant before the gas plunges through the event horizon. Assuming a typical mass-energy conversion efficiency of about $\epsilon \sim 10\%$, in approximation $R_d \ll R_g$, the resulting relationship of typical PRT versus bolometric luminosity becomes $T_{BH} \simeq 0.32 \frac{R_d}{r_{OV}} (\frac{M_{BH}}{M_\odot})^2 \frac{10^{39} W}{L_{bol}}$ [yr].

10.3. Redshift of seed black hole

To follow the history of the seed BH to the present time in the expanding Universe of a general recession of distant galaxies away from us in all directions, the radiation density at the present epoch can be neglected in comparison with the matter density in the Universe. So, the expansion rate of the Universe depends on the matter density, ρ, the cosmological constant, Λ, and the curvature, k, of the space. Interpreting the redshift as a cosmological Doppler effect, and that the Hubble law could most easily be understood in terms of expansion of the universe, we are interested in the purely academic question of principle, to ask what could be the initial redshift, z^{Seed}, of seed black hole if the mass, the luminosity and the redshift, z, of black hole at present time are known. To follow the history of seed black hole to the present time, let place ourselves at the origin of coordinates $r = 0$ (according to the Cosmological Principle, this is mere convention) and consider a light traveling to us along the $-r$ direction, with angular variables fixed. If the light has left a seed black hole, located at r_s, θ_s, φ_s, at time t_s, and it has to reach us at a time t_0, then a power series for the redshift as a function of the time of flight is $z^{Seed} = H_0\,(t_0 - t_s) + \cdots$, where t_0 is the present moment, H_0 is the Hubble's constant. Similar expression $z = H_0\,(t_0 - t_1) + \cdots$, can be written for the current black hole, located at r_1, θ_1, φ_1, at time t_1, where $t_1 = t_s + T_{BH}$, as seed black hole is a object at early times. Hence, in the first-order approximation by Hubble's constant, we may obtain the following relation between the redshifts of seed and present black holes: $z^{Seed} \simeq z + H_0\, T_{BH}$. This relation is in agreement with the scenario of a general recession of distant galaxies away from us in all directions, the furthest naturally being those moving fastest. This relation, incorporating with the value $H_0 = 70$[km]/[s Mpc] favored today yield $z^{Seed} \simeq z + 2.292\times 10^{28}\, \frac{R_d}{r_{OV}} (\frac{M_{BH}}{M_\odot})^2 \frac{W}{L_{bol}}$.

doi: 10.52526/25792776-2021.68.2-236

The general relation between the PRT-scale and the redshifts of BH and its seed is written (Ter-Kazarian, 2014, 2015): $H_0 T_{BH} = \int_z^{z^{seed}} \frac{dz'}{(1+z')\sqrt{\Omega_M(1+z')^3+\Omega_K(1+z')^2+\Omega_\Lambda}}$, where $\Omega_\Lambda = \frac{\Lambda}{3H_0^2}$, $\Omega_K = \frac{-k}{a_0^2 H_0^2}$, $\Omega_M = \frac{\rho}{\rho_{crit}}$, and the critical density is $\rho_{crit} = \frac{3H^2}{8\pi G}$. There are only two independent contributions to the energy density $\Omega_M + \Omega_\Lambda + \Omega_K = 1$. The expansion rate (Hubble's parameter) of the Universe at any epoch at redshift less than about 1000 can be related to the one at the present epoch by $H(z) = H_0 E(z)$, where $E(z) \equiv \sqrt{[\Omega_M(1+z)^3 + \Omega_K(1+z)^2 + \Omega_\Lambda]}$. Let the proper time, t, be the temporal measure. This is a convenient time measure because it is the proper time of comoving observers. The lookback time is the time difference between the present epoch, t_0, and the time of an event that happened at the redshift, z. From the definitions of Hubble's parameter and redshift it follows that $H = \frac{d}{dt}\log(\frac{R(t)}{R_0}) = \frac{d}{dt}\ln(\frac{1}{1+z}) = \frac{-1}{1+z}\frac{dz}{dt}$, where R is called the scale factor of the Universe, and increases as the Universe expands in a manner that depends upon the cosmological model selected. Hence, the lookback time from the present, as a function of the time of flight, reads $t_0 - t_1(z_1) = H_0^{-1} \times \int_0^{z_1} \frac{dz'}{(1+z')\sqrt{\Omega_M(1+z')^3+\Omega_K(1+z')^2+\Omega_\Lambda}}$. Relating the PRT-scale, T_{BH}, to the redshifts of BH, z, and its seed, z^{seed}, let we place ourselves at the origin of coordinates, $r = 0$, (according to the Cosmological Principle, this is mere convention). Consider a light traveling to us along the $-r$ direction, with angular variables fixed. If the light has left a seed BH, located at r_s, θ_s, φ_s, at time t_s, that happened at the redshift z^{seed}, and it has to reach us at present epoch t_0, at the redshift $z = 0$, then from the definition of the lookback time, it follows that $H_0(t_0 - t_s(z^{seed})) = \int_0^{z^{seed}} \frac{dz'}{(1+z')\sqrt{\Omega_M(1+z')^3+\Omega_K(1+z')^2+\Omega_\Lambda}}$. Similar expression can be written for the current BH, located at r_1, θ_1, φ_1, at time t_1, with redshift z: $H_0(t_0 - t_1(z)) = \int_0^{z} \frac{dz'}{(1+z')\sqrt{\Omega_M(1+z')^3+\Omega_K(1+z')^2+\Omega_\Lambda}}$. Taking into account that $t_1 = t_s + T_{BH}$, we arrived to the general relation between the PRT-scale and the redshifts of BH and its seed. As a supplement to this relation, we may derive z_s as a function of the quantities z and T_{BH}. According to the definitions of Hubble's parameter, we may write down $z + 1 = e^{H(z)(t_0-t_1)}$, for the BH, $z_s + 1 = e^{H(z_s)(t_0-t_s)}$, for the seed BH. Setting $H(z) \simeq H(z_s)$, and taking into account that $t_1 = t_s + T_{BH}$, we obtain $\frac{z+1}{z_s+1} = e^{-H(z)(t_1-t_s)} = e^{-H(z)\,T_{BH}}$. Hence, the function $z_s(z, T_{BH})$ reads $z_s = (z+1)e^{H(z)\,T_{BH}} - 1$.

High redshifts: At large redshifts $z >> \Omega_M, \Omega_\Lambda$, only third power of z in the square root becomes important, and thus we find $T_{BH} \simeq \int_z^{z^{seed}} \frac{dz}{H_0\sqrt{\Omega_M}(1+z)^{5/2}} \simeq \frac{2}{3H_0\sqrt{\Omega_M}}[\frac{1}{(1+z)^{3/2}} - \frac{1}{(1+z^{seed})^{3/2}}]$. Thus, in time to an epoch when the Universe was very young and galaxies in their infancy, the redshift of seed BH reads $z^{seed} \simeq [\frac{1}{(1+z)^{3/2}} - \frac{3\sqrt{\Omega_M}H_0 T_{BH}}{2}]^{-2/3} - 1$. Hence $z^{seed} \simeq [\frac{1}{(1+z)^{3/2}} - \frac{3\sqrt{\Omega_M}}{2}\,(18.25 \pm 0.351) \times (\frac{\epsilon}{0.1})\,\frac{R_d}{[\mathrm{cm}]}\,(\frac{M^{seed}}{M_\odot})^2\,\frac{10^{24}\,W}{L}]^{-2/3} - 1$.

Low redshifts: For low redshifts $z << 1$, as alluding to above, in the first-order approximation by the z, we obtain $z^{seed} \simeq z + H_0\,T_{BH}$. Hence $z^{seed} \simeq z + (18.25 \pm 0.351)\,(\frac{\epsilon}{0.1})\,\frac{R_d}{[\mathrm{cm}]}\,(\frac{M^{seed}}{M_\odot})^2\,\frac{10^{24}\,W}{L}$.

10.4. UHE cosmic-ray particles

The galactic sources like supernova remnants (SNRs) or micro-quasars are thought to accelerate particles at least up to energies of 3×10^{15} eV. The ultra-high energy cosmic-ray (UHECR) particles with even higher energies have since been detected. Although more than five decades passed since the famous first detection of cosmic rays with huge energies exceeding 1.0×10^{20} eV by the Volcano Ranch group led by John Linsley (Linsley, 1963), nevertheless, the solution to this outstanding puzzle had not been achieved yet, and this principle problem was ever since much the same as now. At present, about 20 events above $10^{20} eV$ have been reported worldwide by experiments such as the High Resolution Fly's Eye, AGASA, Fly's Eye, Haverah Park, Yakutsk, and Volcano Ranch, etc.. The cosmic-ray events with the highest energies so far detected have energies of 2×10^{11} GeV and 3×10^{11} GeV. These energies 10^7 times higher than the most energetic man-made accelerator, the LHC at CERN. These highest energies are believed to be reached in extragalactic sources like AGNs or gamma-ray bursts (GRBs). During propagation of such energetic particles through the universe, the threshold for pion photoproduction on the microwave background is $\sim 2 \times 10^{10}$ GeV, and at $\sim 3 \times 10^{11}$ GeV the energy-loss distance is about 20 Mpc. Propagation of cosmic-rays over substantially larger distances gives rise to a cutoff in the spectrum at $\sim 10^{11}$ GeV, so-called GZK-cutoff (Greisen-Zatsepin-Kuzmin) as was first shown by these

doi: 10.52526/25792776-2021.68.2-236

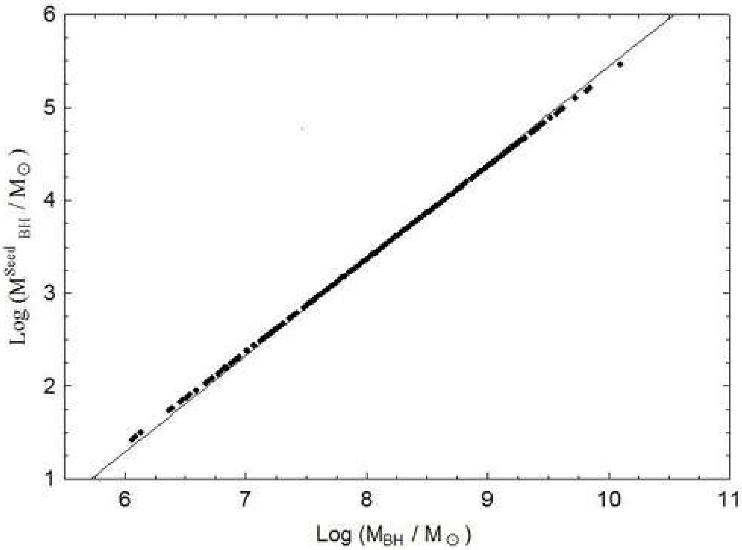

Figure 4. The $M^{Seed}_{BH}/M_\odot$ - $M_{BH}/M_\odot$ relation on logarithmic scales of 337 black holes. The solid line is the best fits to data of samples.

authors. The recent confirmation of GZK suppression in the cosmic-ray energy spectrum indicates that the cosmic-rays with energies above the GZK cutoff, $E_{GZK} \sim 40$ EeV, mostly come from relatively close (within the GZK radius, $r_{GZK} \sim 100$ Mpc) extragalactic sources. However, despite the detailed measurements of the cosmic-ray spectrum, the identification of the sources of the cosmic-ray particles is still an open question as they are deflected in the Galactic and extragalactic magnetic fields and hence have lost all information about their origin when reaching Earth. Only at the highest energies beyond $\sim 10^{19.6}$ GeV cosmic-ray particles may retain enough directional information to locate their sources. The latter must be powerful enough to sustain the energy density in extragalactic cosmic-rays of about $3\times10^{-19}\,\mathrm{erg\,cm^{-3}}$ which is equivalent to $\sim 8\times10^{44}$ erg $\mathrm{Mpc^{-3}\,yr^{-1}}$. Though it hasn't been possible up to now to identify the sources of Galactic or extragalactic cosmic-rays, general considerations allow to limit potential source classes. Eventually, the neutrinos will serve as unique astronomical messengers, and that they will significantly enhance and extend our knowledge on Galactic and extragalactic sources of the UHE universe. Indeed, except for oscillations induced by transit in a vacuum Higgs field, neutrinos can penetrate cosmological distances and their trajectories are not deflected by magnetic fields as they are neutral, providing powerful probes of high energy astrophysics in ways which no other particle can. Moreover, the flavor composition of neutrinos originating at astrophysical sources can serve as a probe of new physics in the electroweak sector. Therefore, an appealing possibility among the various hypotheses of the origin of UHECR is so-called Z-burst scenario. This suggests that if ZeV astrophysical neutrino beam is sufficiently strong, it can produce a large fraction of observed UHECR particles within 100 Mpc by hitting local light relic neutrinos clustered in dark halos and form UHECR through the hadronic Z (s-channel production) and W- bosons (t-channel production) decays by weak interactions. The discovery of UHE neutrino sources would also clarify the production mechanism of the GeV-TeV gamma-rays observed on Earth as TeV photons are also produced in the up-scattering of photons in reactions with accelerated electrons (inverse-Compton scattering). The direct link between TeV gamma-ray photons and neutrinos through the charged and neutral pion production, which is well known from particle physics, allows for a quite robust prediction of the expected neutrino fluxes provided that the sources are transparent and the observed gamma rays originate from pion decay. The weakest link in the Z-burst hypothesis are probably both unknown boosting mechanism of the primary neutrinos up to huge energies of hundreds ZeV and their large flux required at the resonant energy $E_\nu \simeq M_Z^2/(2m_\nu) \simeq 4.2\times10^{21}\,\mathrm{eV}\,(\mathrm{eV}/m_\nu)$ well above the GZK cutoff. Such a flux severely challenges conventional source models. Any concomitant photon flux should not violate existing upper limits. The obvious question is then arisen: Where in the Cosmos are these neutrinos coming from? It turns out that currently at energies in excess of 10^{19} eV, there are only two good candidate source classes for

doi: 10.52526/25792776-2021.68.2-236

UHE neutrinos: AGNs and GRBs. While hard to detect, neutrinos have the advantage of representing unique fingerprints of hadron interactions and, therefore, UHE neutrinos may initiate the cascades of UHE cosmic rays via very complex chains of Z-burst interactions. Some part of UHE neutrinos may produce, in accretion disk and in a torus of hot gas surrounding the AGN core, the secondary electrons with huge energies, which, in turn, may give rise a secondary flux of the GeV-TeV gamma-rays. Two basic event topologies can be distinguished: track-like patterns of detected Cherenkov light (hits) which originate from muons produced in charged-current interactions of muon neutrinos (muon channel); spherical hit patterns which originate from the hadronic cascade at the vertex of neutrino interactions or the electromagnetic cascade of electrons from charged current interactions of electron neutrinos (cascade channel). If the charged current interaction happens inside the detector or in case of charged current tau-neutrino interactions, these two topologies overlap which complicates the reconstruction. At the relevant energies, the neutrino is approximately collinear with the muon and, hence, the muon channel is the prime channel for the search for point-like sources of cosmic neutrinos. On the other hand, cascades deposit all of their energy inside the detector and therefore allow for a much better energy reconstruction with a resolution of a few 10%. Finally, a numerous reports are available at present in literature on expected discovery potential and sensitivity of experiments to neutrino point-like sources. Currently operating high energy neutrino telescopes attempt to detect UHE neutrinos, such as ANTARES which is the most sensitive neutrino telescope in the Northern Hemisphere, IceCube which is worldwide largest and hence most sensitive neutrino telescope in the Southern Hemisphere, BAIKAL, as well as the CR extended experiments of The Telescope Array, Pierre Auger Observatory, and JEM-EUSO mission, etc. Anyhow, with neutrino telescopes of the cubic-kilometer class we are now entering into a sensitivity region where exactly these discoveries will be made is hard to forsee as the predicted fluxes are at the edge of delectability and the uncertainties on the neutrino fluxes are still large. In this regard, it will be of vital interest to compute in the framework of MTBH the high-energy astrophysical neutrino fluxes from aforementioned IMBH-candidates too.

10.5. UHE neutrino fluxes

We are now in a position to discuss the predominant cooling mechanism of SPC in terms of neutrino emission. Namely, the neutrino created leave SPC carrying away energy and thus cooling of SPC. Both quark- and pion-condensed proto-matter core cool much more rapidly than (n-p-e)-proto-matter core, because of the reason that the simple URCA process can occur in the former both cases, while in (n-p-e)-proto-matter core it is very inefficient for phase space reasons (see below). As before, we denote the quantities referred to SPC by wiggles, while the corresponding quantities of neutron star or quark-star are left without wiggles. The interior temperature or temperature at the surface of proto-matter core is $\widetilde{T} > \frac{100\,\text{ZeV}}{k_B} \sim 1.2 \times 10^{27}$K (Ter-Kazarian, 2001). The SPC interiors are to a good approximation isothermal, but near the surface the temperature $\widetilde{T}_e$ drops rapidly. We may, therefore, adapt a standard discussion of the degenerate-nondegenerate transition region of a neutron star to the corresponding region of SPC. This is quick to estimate $\widetilde{T}_e$ and will guide us toward first look at some of the associated physics. So, given the surface temperature of the neutron star T_e: $\frac{T_e}{T} = 1 \times 10^{-2} T_9^{-5/8} (\frac{M}{M_\odot})^{1/4} (\frac{R}{10\,\text{km}})^{-1/2}$, where T_9 denotes the temperature in units of 10^9K, and using the approximate fit to Tsuruta's calculation $T_e \simeq (10T)^{2/3}$, one may expect that the rough qualitative behavior for the surface temperature $\widetilde{T}_e$ of the SPC can be given by $\frac{\widetilde{T}_e}{T_e} \simeq (\frac{\widetilde{T}}{T})^{3/8} (\frac{\widetilde{M}}{M})^{1/4} (\frac{\widetilde{R}}{R})^{-1/2}$. Therefrom, for the values $\widetilde{R} \simeq \frac{1}{4} R_g$ (?), $R \simeq 10$ km and $\widetilde{T} \simeq \widetilde{T}_{100\,\text{ZeV}}$, we obtain $\frac{\widetilde{T}_e}{T_e} \simeq 3.5 \times 10^7 (\frac{\widetilde{M}}{M_\odot})^{-1/4}$. Setting $T_e \simeq 2 \times 10^6$K, the average surface temperature for the SPCs with the masses $M_{BH} \sim (1.1 \times 10^6$ to $1.3 \times 10^{10})\, M_\odot$ will then be $\overline{\widetilde{T}}_e \simeq 1.2 \times 10^{12}$K.

10.6. URCA reactions

In contrast to simple URCA reactions $n \to p + e^- + \bar{\nu}_e$ and $e^- + p \to n + \nu_e$, the nucleon-modified URCA processes can occur only when a bystander neutron must be present to absorb momentum: $n + n \to n + p + e^- + \bar{\nu}_e$, and $n + e^- + p \to n + n + \nu_e$. Thereby the muon-neutrino emitting reactions may also occur whenever the chemical potential $\mu_e > m_\mu c^2$. But the $\tau-$neutrinos do not occur because of

doi: 10.52526/25792776-2021.68.2-236

$m_\tau c^2 = 1784\mathrm{MeV} \gg \mu_e$. Given a luminosity of the neutron star of mass M and a uniform density ρ by modified URCA reactions with no muons, it is straightforward to estimate a luminosity of SPC (Ter-Kazarian, 2014). Such approach is much less time-consuming than a direct calculation. Note that for each degenerate species of the proto-matter in SPC, only a fraction $\sim k\widetilde{T}/\widetilde{E}_F$ can effectively contribute to the cooling rate of SPC because of $d^3\widetilde{p}_i \to \widetilde{p}_F(i)^2 d\widetilde{E}_F(i) \propto \widetilde{T}$, which for five degenerate species gives $\propto \widetilde{T}^5$. Another factor, $\widetilde{T}^3$, is due to the antineutrino phase space: $d^3\widetilde{p}_{\bar{\nu}} \propto (\widetilde{E}_{\bar{\nu}})^2 d\widetilde{E}_{\bar{\nu}} \propto \widetilde{T}^3$. We also should take into account that the temperature that determines the thermal emission from SPC is that at the surface $\widetilde{T}_e$ rather than the interior temperature $\widetilde{T}$. The luminosity of SPC, therefore, can approximately be written $\widetilde{L}^{URCA}_{\nu\,\varepsilon} = \varepsilon\,\frac{\widetilde{M}}{M}(\frac{\widetilde{\rho}}{\rho})^{-1/3}(\frac{\widetilde{T}}{T})^8 L^{URCA}_\nu \simeq \varepsilon\,\frac{\widetilde{M}}{M}(\frac{\widetilde{\rho}}{\rho})^{-1/3}(\frac{\widetilde{T}_F}{T_F})^5(\frac{\widetilde{T}_e}{T_e})^3 L^{URCA}_\nu$. The coefficient ε reads $\varepsilon = \varepsilon_d\,\varepsilon_{trap}, \quad \varepsilon_d = \frac{d}{2R_g} \simeq \theta$, where d is the thickness of the proto-matter disk at the edge of even horizon, θ is a beaming angle, ε_{trap} is the neutrino trapping coefficient. The Fermi energy of each of five fermions, participating in the modified URCA reactions, is $\widetilde{E}_{F\,i} \sim \widetilde{T}_{F\,i} \sim \widetilde{\rho}^{1/3}$, as well as $E_{F\,i} \sim T_{F\,i} \sim \rho^{1/3}$. Then $\widetilde{L}^{URCA}_{\nu\,\varepsilon} = \varepsilon\,\frac{\widetilde{M}}{M_\odot}(\frac{\widetilde{\rho}}{\rho})^{4/3}(\frac{\widetilde{T}_e}{T_e})^3 L^{URCA}_\nu$. The trapping coefficient, ε_{trap}, arises as the neutrinos are trapped comove with matter and build up a semidegenerate Fermi sea. We might expect that the neutral current reactions will inhibit neutrino transport in SPC and enhance neutrino trapping. Neutrino trapping event forces the liberated energy to be emitted on a much larger diffusion timescale for neutrinos to diffuse out of the proto-matter core. This can be roughly estimated by assuming, in analogy of neutron star, that the coherent scattering in proto-matter core is the dominant opacity source. Namely, the heavy particle of proto-matter core acts nonlinearly as a single particle. Coherent scattering induces a random-walk trajectory for the neutrino in the proto-matter core and proto-matter disk without slightly changing its energy before reaching the surface of SPC. Furthermore, we assume that the mean energy of neutrinos generated via electron capture is comparable to the electron Fermi energy. Thus eventually the average neutrino trapping coefficient in proto-matter medium of SPCs with the masses $M_{BH} \sim (1.1\times10^6$ to $1.3\times10^{10})\,M_\odot$ is $\bar{\varepsilon}_{trap} \simeq 6.36\times10^{-20}$. We obtain then (Ter-Kazarian, 2014): $\widetilde{L}^{URCA}_{\nu\,\varepsilon} = 3.8\times10^{50}\,\varepsilon_d\,(\frac{M_\odot}{\widetilde{M}})^{1.75}\mathrm{erg\,s^{-1}}$. The average neutrino luminosity of considered SPCs is $\overline{\widetilde{L}}^{URCA}_{\nu\,\varepsilon} = 5.1\times10^{39}\,\varepsilon_d\,\mathrm{erg\,s^{-1}}$.

The flux can be written in terms of luminosity as $J_{\nu\,\varepsilon} = \widetilde{L}_{\nu\,\varepsilon}/4\pi\,D_L^2(z)\,(1+z)$, where z is the redshift, $D_L(z)$ is the luminosity distance depending on the cosmological model. The $(1+z)^{-1}$ is due to the fact that each neutrino with energy $\widetilde{E}'_\nu$ if observed near the place and time of emission t' will be red-shifted to energy $\widetilde{E}_\nu = \widetilde{E}'_\nu R(t_1)/R(t_0) = \widetilde{E}'_\nu\,(1+z)^{-1}$ of the neutrino observed at time t after its long journey to us, where $R(t)$ is the cosmic scale factor. Computing the UHE neutrino fluxes in the framework of MTBH, we choose the cosmological model favored today, with a flat universe, filled with matter $\Omega_M = \rho_M/\rho_c$ and vacuum energy densities $\Omega_V = \rho_V/\rho_c$, thereby $\Omega_V + \Omega_M = 1$, where the critical energy density $\rho_c = 3H_0^2/(8\pi G_N)$ is defined through the Hubble parameter H_0: $D_L(z) = 2.4\times10^{28}\,I(z)\,cm$. Here $I(z) = (1+z)\int_1^{1+z} dx/\sqrt{2.3+x^3}$, and that we have taken the values $H_0 = 70\mathrm{km/s\,Mpc}$, $\Omega_V = 0.7$ and $\Omega_M = 0.3$. Combining these equations, the resulting total UHE neutrino flux of cooling of the SPC via simple or modified URCA processes with no muons can be obtained as $J^{URCA}_{\nu\,\varepsilon} \simeq 5.22\times10^{-8}\,\frac{\varepsilon_d}{I^2(z)(1+z)}(\frac{M_\odot}{\widetilde{M}})^{1.75}[\mathrm{erg\,cm^{-2}\,s^{-1}\,sr^{-1}}]$, where the neutrino is radiated in a cone with the beaming angle $\theta \sim \varepsilon_d \ll 1$, $\;I(z) = (1+z)\int_1^{1+z} dx/\sqrt{2.3+x^3}$. As it is seen, the nucleon modified URCA reactions can contribute efficiently only for extragalactic objects with enough small redshift $z \ll 1$.

10.7. Pionic reactions

The pionic reactions allow both energy and momentum to be conserved in the reactions, which are known as an analogue of the simple URCA processes: $\pi^- + n \to n + e^- + \bar{\nu}_e$, $\pi^- + n \to n + \mu^- + \bar{\nu}_\mu$, and two inverse processes. As in the modified URCA reactions, the total rate for all four processes is essentially four times the rate of each reaction alone. Muons are already present when pions appear. Note that there are two fewer fermions participating in the reactions than in the modified URCA reactions. So the phase-space factor varies as T^6 rather than T^8. We may obtain then $\widetilde{L}^\pi_{\nu\,\varepsilon} = \varepsilon\frac{\widetilde{M}}{M}\,\frac{\varrho}{\widetilde{\rho}}(\frac{\widetilde{T}_F}{T_F})^3(\frac{\widetilde{T}_e}{T_e})^3 L^\pi_\nu$, where $\widetilde{T}_F = \widetilde{E}_F/k_B$, $\;L^\pi_\nu$ refers to the neutron star: $L^\pi_\nu \sim 1.5\times10^{46}\,\vartheta^2\,\frac{M}{M_\odot}\,\frac{\rho_{nuc}}{\rho}\,T_9^6\,\mathrm{erg\,s^{-1}}$, and $\vartheta \sim 0.3$ is an angle measuring the degree of pion condensation. Hence $\widetilde{L}^\pi_{\nu\,\varepsilon} = 5.78\times10^{58}\,\varepsilon_d\,(\frac{M_\odot}{\widetilde{M}})^{1.75} erg\,s^{-1}$,

doi: 10.52526/25792776-2021.68.2-236

and that the average neutrino luminosity of considered SPCs is $\widetilde{\overline{L}}^{\pi}_{\nu\,\varepsilon} = 7.7\times10^{47}\,\varepsilon_d\,\mathrm{erg\,s^{-1}}$. Therefrom the total UHE neutrino flux reads $J^{\pi}_{\nu\,\varepsilon} \simeq 7.91\,\frac{\varepsilon_d}{I^2(z)(1+z)}(\frac{M_\odot}{\widetilde{M}})^{1.75}\,\mathrm{erg\,cm^{-2}s^{-1}\,sr^{-1}}$. So, the average flux is $\overline{J}^{\pi}_{\nu\,\varepsilon} \simeq 1.1\times10^{-10}\,\varepsilon_d/I^2(z)(1+z)\,\mathrm{erg\,cm^{-2}s^{-1}\,sr^{-1}}$. As it is seen, the resulting total energy-loss rate will then be dramatically larger due to the pionic reactions rather than the modified URCA processes.

10.8. Quark reactions

In the superdense proto-matter medium the distorted quark Fermi energies are far below the charmed c-, t- , and b- quark production thresholds. Therefore, only up, down, and strange quarks are present. The β equilibrium is maintained by reactions like $d \to u + e^- + \bar{\nu}_e$, $\quad u + e^- \to d + \nu_e$, and $s \to u + e^- + \bar{\nu}_e$, $\quad u + e^- \to s + \nu_e$, which are β decay and its inverse. These reactions constitute simple URCA processes, in which there is a net loss of a $\nu_l\bar{\nu}_l$ pair at nonzero temperatures. In this application a sufficient accuracy is obtained by assuming β-equilibrium and that the neutrinos not to be retained in the medium of Λ-like proto-matter. The above quark reactions proceed at equal rates in β equilibrium, where the participating quarks must reside close to their Fermi surface. Hence, the total energy of flux due to simple URCA processes is rather twice than of each alone. Our purpose here is to adapt in sufficient approximation a discussion of ordinary quark matter in neutron star to the corresponding region of quark proto-matter in SPC, where a rearrangement of vacuum state causes a shift of zero point energy. Accordingly, the energy-loss rate of the SPC due to neutrino emission process $d \to u + e^- + \bar{\nu}_e$ can be generalized in the form $\widetilde{\epsilon}^{q}_{\bar{\nu}\,\varepsilon} = 6V^{-1}\varepsilon(\prod_{i=1}^{4} V\int\frac{d^3\widetilde{p}_i}{(2\pi)^3})\widetilde{E}_{\bar{\nu}}V(2\pi)^4\delta^{(4)}(\widetilde{p}_d - \widetilde{p}_{\bar{\nu}_e} - \widetilde{p}_u - \widetilde{p}_e)\frac{|M|^2}{\prod_{i=1}^{4}2\widetilde{E}_iV}\,S$. Here $\widetilde{p}_i$ and $\widetilde{E}_i$ denote the distorted momentum and energy of a particle of the given species of proto-matter. The four-vectors $\widetilde{p}_i$ are numbered as $i = 1,2,3,4 \equiv d, \bar{\nu}_e, u, e^-$, $\quad V$ is the normalization volume, $|\,M\,|^2$ is the squared invariant amplitude averaged over the initial d-quark spin and summed over the final spins of the u quark and the electron. Also, $S = f_d(1-f_u)(1-f_e)$ is the statistical factor, $f_i \equiv [\exp\widetilde{\beta}(\widetilde{E}_i - \widetilde{\mu}_i) + 1]^{-1}$ is the fraction of phase space occupied at energy $\widetilde{E}_i$ and distorted chemical potential $\widetilde{\mu}_i = (1 + 8\alpha_c/3\pi)\,c\widetilde{p}_{Fi}$, $\widetilde{p}_{Fi}$ is the Fermi momentum. This is given to lowest order in the QCD interaction coupling constant α_c. The blocking factors $1 - f_i$ accounting for the distribution of final states reduce the reaction rate, which ensure that the exclusion principle is obeyed; the factor 3 takes account of three color degrees of freedom, and 2 is the spin of the initial d quark. Since typical Fermi energies of quarks are higher than the electron rest mass, a slight difference between $\widetilde{\mu}_d$ and $\widetilde{\mu}_e$ (or $\widetilde{\mu}_s$ and $\widetilde{\mu}_u$) implies that the electrons will generally have a relativistic Fermi energy. The interaction Lagrangian density is given in the standard current-current form $\mathcal{L}^W_I = \frac{G}{\sqrt{2}}\cos\theta_C\,\bar{u}\gamma^\mu(1-\gamma_5)d\,\bar{e}\gamma_\mu(1-\gamma_5)\nu_e$, where the weak-coupling constant is $G \simeq 1.435\times 10^{-40}\mathrm{erg\,cm^3}$, $\quad\theta_C$ is the Cabibbo angle ($\cos^2\theta_C \simeq 0.948$). The squared invariant averaged amplitude can be calculated in case of proto-matter medium to be $\frac{1}{2}\sum_{\sigma_1,\sigma_3,\sigma_4}|\,M_{fi}\,|^2 = 64G^2\cos^2\theta_C(\widetilde{p}_1\cdot\widetilde{p}_2)(\widetilde{p}_3\cdot\widetilde{p}_4)$. As the neutrinos are produced thermally, we can neglect the neutrino momentum in the momentum conservation law, and that to the lowest order in α_c we can use an approximate formula $|\,M\,|^2 = \frac{1024\alpha_c}{3\pi}G^2\cos^2\theta_C\,\widetilde{E}_d\widetilde{E}_{\bar{\nu}}\widetilde{E}_u\widetilde{E}_e(1 - \frac{|\widetilde{\mathbf{p}}_d|}{\widetilde{E}_d}\cos\theta_{d\,\bar{\nu}})$, where $\cos\theta_{d\,\bar{\nu}} \equiv \hat{\widetilde{p}}_d\cdot\hat{\widetilde{p}}_{\bar{\nu}}$, $\quad\hat{p}_i \equiv \frac{\widetilde{\mathbf{p}}_\mathbf{i}}{|\widetilde{p}_i|}$. We may further set $\widetilde{E}_i \simeq \widetilde{p}_i$ because all the particles are relativistic, and that $\widetilde{p}_d \sim \widetilde{p}_u$ $\quad(\widetilde{p}_e << \widetilde{p}_d)$. Also all the $\widetilde{p}_i$ (except $\widetilde{p}_{\bar{\nu}}$) can be set equal $\widetilde{p}_F(i)$ and removed from the integral. To estimate the magnitude of the emissivity, we follow the original argument of (Ter-Kazarian, 2014), which can be applied to both neutron star and SPC, and that assume for distorted Fermi momenta $\widetilde{p}_F(d) \simeq \widetilde{p}_F(u) \simeq \widetilde{p}_F(s)$ as in non-interacting case, such that $\widetilde{p}_F(e) \simeq 3^{(1/3)}\widetilde{Y}_e^{(1/3)}\widetilde{p}_F(q)$, where $\widetilde{Y}_e \simeq \frac{\widetilde{n}_e}{\widetilde{n}_b}$, $\quad\widetilde{n}_i$ is the distorted concentration of particles. We may also set the value $\alpha_c \simeq 0.1$ as rather being a reasonable order of magnitude estimate, and $\widetilde{Y}_e \simeq 0.01$ as typical value of what is expected for superdense proto-matter. A standard evaluation of integrals in the complex plane, as well as taking into account that for each degenerate species only a fraction $\widetilde{T}/\widetilde{T}_F$ effectively contribute to the cooling rate, and that there are one such initial species and two such final species, finally we arrive at the spectral flux of the UHE antineutrinos $\frac{d\,J^{q}_{\bar{\nu}\,\varepsilon}}{d\,y_2} \simeq 0.41\,\frac{\varepsilon_d}{I^2(z)(1+z)}(\frac{M_\odot}{\widetilde{M}})^{1.75}\frac{y_2^3(\pi^2+y_2^2)}{e^{y_2}+1}\mathrm{erg\,cm^{-2}\,s^{-1}\,sr^{-1}}$.

Similar reasonings can be applied for the process $u + e^- \to d + \nu_e$, where $\widetilde{E}_d + \widetilde{E}_\nu = \widetilde{E}_e + \widetilde{E}_u$, $\widetilde{E}_d - \widetilde{E}_u \simeq \widetilde{E}_e\cos\theta_{e\,u} - \widetilde{E}_\nu\cos\theta_{d\,\nu}$. Taking into account that $d\Omega_e \simeq (1/\widetilde{E}_e)d\widetilde{E}_d d\varphi_e$, so

doi: 10.52526/25792776-2021.68.2-236

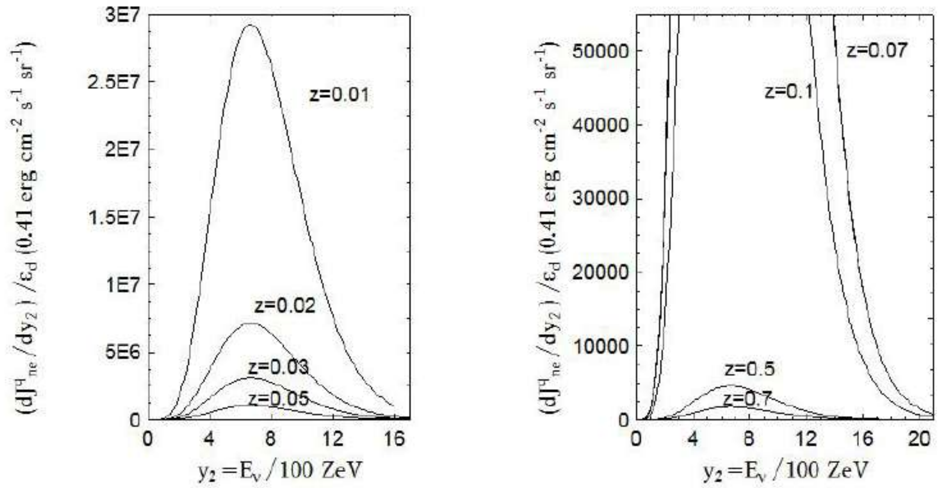

Figure 5. The spectral fluxes of UHE antineutrinos for different redshifts from quark reactions.

$\int \frac{\widetilde{p}_\nu \widetilde{p}_u \widetilde{p}_e}{\widetilde{E}_d} d\Omega_\nu\, d\Omega_u\, d\Omega_e\, d\widetilde{E}_\nu\, d\widetilde{E}_u\, d\widetilde{E}_e = \int \widetilde{E}_\nu\, d\varphi_e\, d\Omega_\nu\, d\Omega_u\, d\widetilde{E}_d\, d\widetilde{E}_\nu\, d\widetilde{E}_u\, d\widetilde{E}_e$, we obtain the resulting spectral UHE neutrino flux: $\frac{d\,J^q_{\nu\,\varepsilon}}{d\,y_1} \simeq 0.1\, \frac{\varepsilon_d}{I^2(z)(1+z)} (\frac{M_\odot}{\widetilde{M}})^{1.75} \frac{y_1^4(\pi^2+y_1^2)}{e^{y_1}+1}$ erg cm^{-2} s^{-1} sr^{-1}, where $y_1 \equiv \widetilde{E}_\nu\, \widetilde{\beta}$. A different $\widetilde{E}_\nu$ dependence is due to the partial restriction of the electron's phase space which introduces an extra factor of $(\widetilde{E}_e \widetilde{\beta})^{-1}$. But, as far as the neutrino flux is independent of the electron's Fermi energy, a potential source of ambiguity is eliminated. Consequently, both fluxes above yield the total UHE neutrino flux $J^q_{\nu\,\varepsilon} \simeq 70.68\, \frac{\varepsilon_d}{I^2(z)(1+z)} (\frac{M_\odot}{\widetilde{M}})^{1.75}$erg cm^{-2}s^{-1} sr^{-1}, and that eventually the average flux is $\overline{J}^q_{\nu\,\varepsilon} \simeq 9.46 \times 10^{-10}\, \varepsilon_d / I^2(z)(1+z)$ erg cm^{-2} s^{-1} sr^{-1}.

10.9. Simulation

For simulation we use the data of AGN/BH mass and luminosity estimates for 377 black holes which are mostly based on the virial assumption for the broad emission lines, with the broad-line region size determined from either reverberation mapping or optical luminosity. Additional black hole mass estimates based on properties of the host galaxy bulges, using either the observed stellar velocity dispersion or using the fundamental plane relation. Since the aim is to have more than a thousand of realizations, each individual run is simplified, with a use of previous algorithm of the SPC-configurations as a working model. Computing the corresponding PRTs, seed black hole intermediate masses and total neutrino fluxes, a main idea comes to solving an inverse problem. Namely, by the numerous reiterating integrations of the state equations of SPC-configurations we determine those required central values of particle concentration $\widetilde{n}(0)$ and ID-field $x(0)$, for which the integrated total mass of configuration has to be equal to the black hole mass M_{BH} given from observations. Along with all integral characteristics, the radius R_d also computed which is in use for calculating M^{Seed}_{BH}, T_{BH}, z^{Seed}, and $J^i_{\nu\,\varepsilon}$, respectively. The Fig. 4 gives the intermediate seed masses $M^{Seed}_{BH}/M_\odot$ versus the present masses $M_{BH}/M_\odot$ of 337 black holes, on logarithmic scales. For the present masses $M_{BH}/M_\odot \simeq 1.1 \times 10^6$ to 1.3×10^{10}, the computed intermediate seed masses are ranging from: $M^{Seed}_{BH}/M_\odot \simeq 26.4$ to 2.9×10^5.

The spectral fluxes of the UHE antineutrinos and neutrinos for different redshifts from quark reactions are plotted respectively on the Fig. 5 and Fig. 6. The computed neutrino fluxes are ranging from: 1) (quark reactions) - $J^q_{\nu\,\varepsilon}/\varepsilon_d$ [erg cm^{-2} s^{-1} sr^{-1}] $\simeq 8.29 \times 10^{-16}$ to 3.18×10^{-4}, with the average $\overline{J}^q_{\nu\,\varepsilon} \simeq 5.53 \times 10^{-10}\, \varepsilon_d$ [erg cm^{-2} s^{-1} sr^{-1}]; 2) (pionic reactions) - $J^\pi_{\nu\,\varepsilon} \simeq 0.112\, J^q_{\nu\,\varepsilon}$, with the average $J^\pi_{\nu\,\varepsilon} \simeq 3.66 \times 10^{-11}\, \varepsilon_d$ [erg cm^{-2} s^{-1} sr^{-1}]; and 3) (modified URCA processes) - $J^{URCA}_{\nu\,\varepsilon} \simeq 7.39 \times 10^{-11}\, J^q_{\nu\,\varepsilon}$, with the average $\overline{J}^{URCA}_{\nu\,\varepsilon} \simeq 2.41 \times 10^{-20}\, \varepsilon_d$ [erg cm^{-2} s^{-1} sr^{-1}]. To render our discussion

doi: 10.52526/25792776-2021.68.2-236

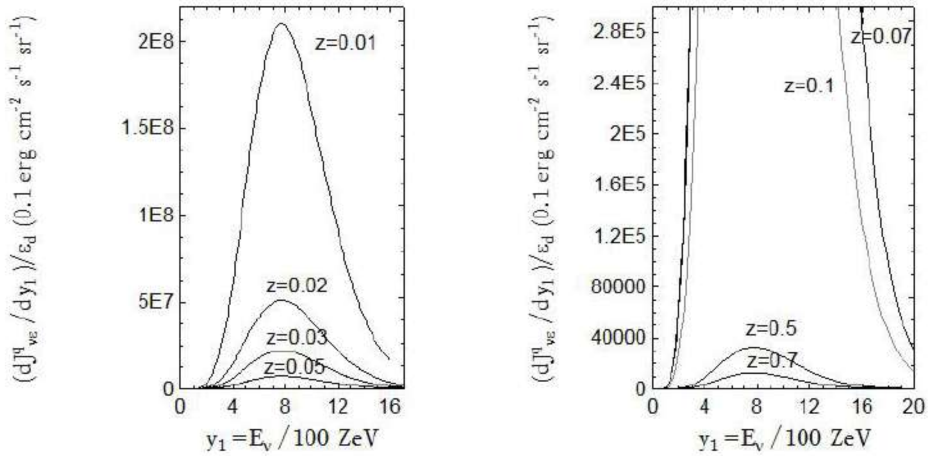

Figure 6. The spectral fluxes of UHE neutrinos for different redshifts from quark reactions.

here a bit more transparent and to obtain some feeling for the parameter ε_d we may estimate $\varepsilon_d \simeq 1.69 \times 10^{-10}$, just for example only, for the suppermassive black hole of typical mass $\sim 10^9 M_\odot$ $(2\,R_g = 5.9 \times 10^{14}\mathrm{cm})$, and so $d \sim 1\,\mathrm{km}$. But the key problem of fixing the parameter ε_d more accurately from experiment would be an important topic for another investigation elsewhere. Reflecting upon the results far obtained, we draw a statement that the AGNs are favored as promising pure neutrino sources because the computed neutrino fluxes are highly beamed along the plane of accretion disk, and peaked at high energies and collimated in smaller opening angle. The neutrinos are able to stream freely out of SPC, and the bulk of liberated binding energy of proto-matter must be converted into other forms of internal energy rather than being released immediately in the form of escaping neutrinos. Such neutrinos may initiate the cascades of UHE cosmic rays via very complex chains of Z-burst interactions. Some part of UHE neutrinos may produce, in accretion disk and in a torus of hot gas surrounding the AGN core, the secondary electrons with huge energies, which, in turn, may give rise a secondary flux of the GeV-TeV gamma-rays. Above said was sharpened by the recent surprising announcement of the first high-energy neutrino event by the IceCube Neutrino Observatory (Collaboration, 2018). With the very large volume neutrino telescope optimized for the TeV energy range, they have traced a neutrino with the energy approximately 300 TeV that hit their Antarctica-based detector in September 2017 back to its point of origin in a blazar, TXS 0506+056, the 3.7 billion light-years away. This constitutes the first use of a neutrino detector to locate an object in space.

11. On the physical nature of the source of ultraluminous X-ray pulsations

The physical nature of the accreting off-nuclear point sources in nearby galaxies, so-called the ultraluminous X-ray sources (ULXs), has been an enigma because of their high energy output characterized by super-Eddington luminosities up to two orders of magnitude higher than those observed from Galactic X-ray binaries, and unusual soft X-ray spectra with blackbody emission around $\lesssim 0.3$ keV and a downturn above ~ 5 keV. In spite of significant efforts in more than three decade since the discovery of ULXs, the astronomers have not yet clarified their nature. Without care of the historical justice and authenticity, it should be emphasized that the ULX sources have attracted a great deal of observational and theoretical attention, in part because their luminosities suggest that they may harbor intermediate mass black holes (IMBHs) with an ubiquitous feature of the mass fits of more than $10^2 - 10^4\,M_\odot$. A strong argument in favor of IMBHs is the presence of a soft, 0.1–0.2 keV

doi: 10.52526/25792776-2021.68.2-236

component in their spectra. The hyperluminous X-ray sources with luminosities $\geq 10^{41}\,\mathrm{erg\,s^{-1}}$ are thought to be amongst the strongest IMBH candidates. Assuming the emission is isotropic, in general, the extreme luminosities of ULXs suggest either the presence of IMBHs and sub-Eddington accretion, or stellar-mass black holes ($M \leq 10\,M_{\odot}$) that are either breaking or circumventing their Eddington limit via somewhat geometric beaming of accretion flow. The latter remains still a relatively poorly understood regime. The brightest ULXs (with $L_X > 5 \times 10^{40}\,\mathrm{erg\,s^{-1}}$), located within 100 Mpc, are identified in a cross correlation of the 2XMM-DR1 and RC3 catalogues. These objects seemed to be amongst the most plausible candidates to host larger, IMBHs. But, future improved observations are needed yet to decide on the issue. The quasi-periodic oscillations (QPOs) and frequency breaks in XMM-Newton power-density spectra of ULXs with luminosity, $L_X \geq 10^{40}\,\mathrm{erg\,s^{-1}}$, suggest that the black hole masses are more consistent with IMBHs than stellar-mass black holes. Or, using high sensitive dataset in the Fe K region obtained in scope of a long Suzaku program on Holmberg IX X-1 for any luminous, isolated ULX to date, it is found no statistically significant narrow atomic features in either emission or absorption across the 5–9 keV energy range. Therefore, the models of spherical super-Eddington accretion can be rejected, as can wind-dominated spectral models. The lack of iron emission implies that the stellar companion in sub-Eddington accretion onto an IMBH is unlikely to be launching a strong wind, and therefore the black hole must primarily accrete via roche-lobe overflow. There are also several other new results of more recent studies: for example, if the transferred mass is efficiently converted to X-ray luminosity (with disregard of the classical Eddington limit) or if the X-rays are focused into a narrow beam then binaries can form extreme ULXs with the X-ray luminosity of $L_X \gtrsim 10^{42}$ erg s^{-1}. It was envisaged that these systems are not only limited to binaries with stellar-origin black hole accretors, but also can be identified with neutron star systems. For the latter the typical donors are evolved low-mass ($2\,M_{\odot}$) helium stars with Roche lobe overflow rate of $\sim 10^{-2}\,M_{\odot}\mathrm{yr}^{-1}$. This study does not prove that any particular extreme ULX is a regular binary system. Combining binary population synthesis and detailed mass-transfer models, one concludes that the binary system that formed M82X-2 is most likely less than 50 Myr old and contains a donor star which had an initial mass of approximately $8 - 10\,M_{\odot}$, while the NS's progenitor star had an initial mass in the $8 - 25\,M_{\odot}$ range. The resulting luminosity of NS pulsars may can reach values of the order of 10^{40} erg s^{-1} for the magnetar-like magnetic field, since the equilibrium, where the Alfvén radius matches the co-rotation radius, indicates a magnetic field of $B \gtrsim 10^{14}$G, and long spin periods ($P \gtrsim 1.5s$). They conclude that a substantial part of ULXs are accreting neutron stars in binary systems.

All these proposals have own advantages and difficulties. Nevertheless, no single theory has been invented yet which successfully addresses the solution to the problems involved. The aforementioned studies are not exception to the rule that as phenomenological approaches they suffer from own difficulties. Namely, they are strongly model dependent and subject to many uncertainties. The physics is obscured by multiple assumptions and proliferation of a *priori* free parameters involved, while a consistent complete theory would not have so many free parameters. So, the issue is still controversial, and these exotic results and conclusions are still lame and for sure not proven by the authors. For example, one evokes the possibility that the transferred mass is efficiently accreted onto a compact object and converted to X-ray luminosity in the full range of possible mass accretion rates, which is in contrast with the generally accepted view that the conversion efficiency decreases with increasing mass accretion rate. Or, in case of model of the accretion column, a necessary condition for the X-ray luminosity to exceed the Eddington limit is a certain degree of asymmetry in the distribution of matter over the Alfven surface, which is a qualitative picture, perhaps, but not quantitative one, or a $B \gtrsim 10^{14}$ G magnetic field of a magnetar-like pulsar is rather above the quantum limit, etc. We will not be concerned here with the actual discussion of these results, which require further extensive and careful investigations, in order could verify the proposed estimates and constrain model parameters, and consequently could lead to a consistent theory. There were still many open key questions arisen inevitably that we have no understanding of ULX physics. A main physical issue whether ULXs are powered by IMBHs or normal stellar black holes to date is unresolved, primarily because we do not have dynamical mass measurements of the compact objects that power ULXs. So, it is premature to draw conclusions and only time will tell whether any of these intriguing proposals is correct and which

doi: 10.52526/25792776-2021.68.2-236

of the hypothesized ULX scenario is actually realized in nature.

11.1. The ultraluminous X-ray pulsations

The most striking is the recent revolutionary NuSTAR discovery of the first rare and mighty ultraluminous X-ray pulsations with the maximum luminosity $\widetilde{L}(3-30\text{keV}) = 4.9\times10^{39}\,\text{erg}\,\text{s}^{-1}$, of average period 1.37 s with a 2.5-day sinusoidal modulation, coming from an ultraluminous source, NuSTAR J095551+6940.8, located nearby starburst galaxy M82 (NGC 3034) (Ter-Kazarian, 2016b). The pulsed emission centroid is spatially consistent with the location of a variable M82X-2 which further secures the association of the pulsating source with M82X-2. The NuSTAR finding will significantly enhance our understanding of the ULX Universe which currently we do not have. Detection of coherent pulsations, a binary orbit, and spin-up behaviour indicative of an accretion torque unambiguously, allow to feature the M82X-2 as mass-exchange binary that contains a nondegenerate secondary donor star. Eventually, in addition to the orbital modulation, about an evident linear spin-up of the pulsar was reported, with $\dot{p}\simeq -2\times10^{-10}$s/s over the interval from modified Julian days 56696 to 56701 when the pulse detection is most significant. Phase connecting the observations enables detection of a changing secular spin-up rate over a longer timespan as well as erratic variations. Future observations will show whether the current spin-up rate is secular. The spin-up to luminosity ratio 10^{-50} $(\text{erg}\cdot\text{s})^{-1}$ is an order of magnitude lower than the typical ratio observed in the X-ray pulsars, which makes an interpretation of the data in terms of a strongly magnetized X-ray pulsar quite challenging. In absolute terms, this spin-up rate is orders of magnitude higher than the values measured in the usual accretion powered X-ray pulsars.

11.2. Key objectives

A current understanding of NuSTAR discovery is quite complicated. At first glance it seems as though the NuSTAR team has demonstrated that the super-Eddington accretion is also possible in ULXs hosting a neutron star, because it is generally believed that the pulsating X-ray sources are magnetic neutron stars which are accreting matter from a binary companion. Therefore, it seems that there is nothing left but M82X-2, which until recently astronomers had thought was a black hole, is the brightest magnetic neutron star system ever recorded. This point of view is widely quoted in literature and, at first sight, seems eminently reasonable. However, deeper examination raises several disturbing questions, if the above result is really valid. Even though, if for a moment we take the classical accreting neutron star pulsar system as a basic assumption, note that this model is not flawless. The actual mechanism by which pulsars convert the rotational energy of the neutron star into the observed pulses is poorly understood. Many theoretical models have been proposed that account for such features, but no single one is compelling.

Explaining periodic source M82X-2 that obviously has black hole energetics with a $\sim 1.4\,M_\odot$ compact object using the accreting neutron star pulsar systems is extremely challenging, because of several problems we encountered. The difficulty becomes apparent when one follows the three objections, which together constitute a whole against the claim that M82X-2, perhaps, is a common pulsar: 1) The NuSTAR team discovery is the most extreme violation of the so-called Eddington limit, i.e. the pulsed luminosity of M82X-2 reaches about ~ 26.9 times brighter than the theoretical threshold at the spherical accretion for $\sim 1.4\,M_\odot$ stellar-mass black holes where the outward pressure from radiation balances the inward pull of gravity of the pulsar. The accretion is inhibited once radiation force is equal or grater than gravity force. 2) The difficulty is brought into sharper focus by considering the association with M82X-2, which is featured with high luminosity ($\simeq 1.8\times10^{40}\,\text{erg}\,\text{s}^{-1}$) of additional persistent continuous broad X-ray radiation observed earlier from its active state. This more compelling argument in somehow or other implies the luminosity ~ 100 times if compared to the Eddington limit. Such a collimation (~ 100), which is comparable to that obtained for black holes (e.g., **??**), would be needed to explain M82X-2 as beamed radiation from neutron star. 3) Equally noteworthy that the centroid of the persistent X-ray emission is between M82X-2 and M82X-1. If M82X-1 is indeed harbors plausible IMBH, we expect the similarity of the persistent X-ray properties of the M82X-1 and M82X-2 to imply that the non-pulsed emission from the latter originates in the

doi: 10.52526/25792776-2021.68.2-236

accretion disc, as it must in the black hole M82X-1. In this sense, the NuSTAR discovery is unexpected and still hard to be explained in the context of magnetic neutron star pulsar model. The fraction of ULXs powered by neutron stars must be considered highly uncertain and many details of this scenario remain poorly understood. Added to this was the fact that NuSTAR finding may indeed not be rare in the ULX population. In the future astronomers also will look at more ULXs, and it is a matter of time until they could prove an expected ubiquitous feature of even more energetic ULX pulsations, as being common phenomena in the Universe. If confirmed, this would support a scenario in which the more ULXs beat with the pulse of black holes rather than magnetized neutron star systems. What if NuSTAR detection might radically change one's view of Nature. With this perspective in sight, it is wise to place constraints on the likelihood of the magnetic neutron star pulsar systems. So, it is becoming increasingly important that in the case of M82X-2 the model of common pulsar will be tested critically.

11.3. Result

Putting apart the discussion of inherent problems of the mass scaling of the black holes in ULXs, which is beyond the scope of this report, we approach the M82X-2 issue from the standpoint of black holes rather than magnetic neutron star pulsar systems (Ter-Kazarian, 2016b). To reconcile the observed unusual high pulsed luminosity with the above mentioned violation of the Eddington limit, we examine the physics which is at work in ultraluminous pulsations by assuming that M82X-2 is being a spinning intermediate-mass black hole (SIMBH). If a black hole of intermediate mass will be an exact law of Nature, it is certainly an attractive scenario. Fore example, it was suggested that the M82X-2 is a binary system with a black hole accretor. Assuming the persistent emission is isotropic, the X-ray luminosity $\simeq 10^{40}\,\mathrm{erg\,s^{-1}}$ implies that the compact object is a $> 100M_\odot$ IMBH in the low/hard state. However, one may be tempted to argue truly that most of the issues and objections raised above cannot be solved in the framework of PBHMs. The coherent periodicity obviously rules out PBHM, because 1) black holes do not radiate; 2) the spinning black holes are axisymmetric and have no internal structure on which to attach a periodic emitter. Orbital motion, whether modulating some emission mechanism directly or exciting short-period pulsations, would decay very quickly due to gravitational radiation. With this in mind, we revisited the MTBH which completes PBHM by exploring the most important processes of spontaneous breaking of gravitation gauge symmetry and rearrangement of vacuum state at huge energies. One of the purposes of the report (Ter-Kazarian, 2016b) is to motivate and justify the further implications of MTBH framework to circumvent the alluded obstacles without the need for significant breaking of Eddington limit.

11.4. Axisymmetric space V_4 in $3+1$ formalism

As in the case of neutron stars, we expect that accreting black holes are fast spinning objects. For the self-contained arguments, we need to extend the preceding algorithm of non-spinning MBHM to its spinning counterpart, which is almost a matter of routine, to change the geometry of static SPC to a more general one, describing axisymmetric rotating SPC. Here we will collect together the results which are required later. The non-spinning SPC is static and spherically symmetric. So, one needs to be clear about more general geometry which can describe rotating axisymmetric SPCs. The principle foundation of the spinning configurations first comprises the following additional distinctive features with respect to non-spinning ones: 1) Rapid rotation causes the shape of the SPC to be flattened by centrifugal forces - flattened at poles and buldged at equator (oblate spheroid, which is second order effect in the rotation rate). 2) A rotating massive SPC drags space and time around with it. The local inertial frames are dragged by the rotation of the gravitational field, i.e. a gyroscope orbiting near the SPC will be dragged along with the rapidly rotating SPC. This is probably the most remarkable feature that could serve as a link with the general description of spacetime. Beside the geodetic procession, a spin of the body produces in addition the Lense-Thirring procession. To look into the future, measurement of the gyrogravitational ratio of particle would be a further step towards probing the microscopic origin of gravity. Let the world coordinate $t(=x^0)$ be the time (in units of c), and $\phi(=x^1)$ be the azimuthal angle about the axis of symmetry. Moreover,

doi: 10.52526/25792776-2021.68.2-236

a metric of a two-space, (x^2, x^3), can always be diagonalized. Since the source of gravitational field has motions that are pure rotational about the axis of symmetry, then the energy-momentum tensor as the source of the metric will have the same symmetry. Namely, the space $\mathcal{M}_4$ would be invariant against simultaneous inversion of time t and azimuthal angle ϕ. The $3+1$ formalism is the most commonly used approach in which, as usual, spacetime is decomposed into the one parameter family of space-like slices - the hypersurfaces Σ_t. The study of a dragging effect is assisted by incorporating with the soldering tools in order to relate local Lorentz symmetry to curved spacetime. These are the linear frames and forms in tangent fiber-bundles to the external general smooth differential manifold, whose components are so-called tetrad (vierbein) fields. Whereas, the $\mathcal{M}_4$ has at each point a tangent space, $T_x\mathcal{M}_4$, spanned by the anholonomic orthonormal frame field, e, as a shorthand for the collection of the 4-tuplet $(e_0 = \exp(-\nu)\,(\partial_t + \omega\partial_\phi),\ e_1 = \exp(-\psi)\,\partial_\phi,\ e_2 = \exp(-\mu_2)\,\partial_2,\ e_3 = \exp(-\mu_3)\,\partial_3)$, where $e_a = e_a{}^\mu\,\partial_\mu$, $e_a{}^\mu$ is the the soldering form between the tangent space and the spacetime manifold. This is called a Bardeen observer, locally nonrotating observer, or the local Zero Angular-Momentum Observers (ZAMO), i.e. observers whose worldlines are normal to the hypersurfaces defined by constant coordinate time, $\widetilde{t} = const$, also called Eulerian observers. Here we use Greek alphabet $(\mu, \nu, \rho, ... = 0, 1, 2, 3)$ to denote the holonomic world indices related to V_4, and the first half of Latin alphabet $(a, b, c, ... = 0, 1, 2, 3)$ to denote the anholonomic indices related to the tangent space. The frame field, e, then defines a dual vector, ϑ, of differential forms, $\vartheta = \begin{pmatrix} \vartheta^0 = \exp\nu\, d\widetilde{t} \\ \vartheta^1 = \exp\psi\,(d\psi - \omega d\widetilde{t}) \\ \vartheta^2 = \exp\mu_2\, d\widetilde{x}^2 \\ \vartheta^3 = \exp\mu_3\, d\widetilde{x}^3 \end{pmatrix}$, as a shorthand for the collection of the $\vartheta^b = e^b{}_\mu\, d\widetilde{x}^\mu$, whose values at every point form the dual basis, such that $e_a \rfloor \vartheta^b = \delta^b_a$, where $\rfloor$ denoting the interior product, namely, this is a C^∞-bilinear map $\rfloor : \Omega^1 \to \Omega^0$ with Ω^p denotes the C^∞-modulo of differential p-forms on V_4. In components $e_a{}^\mu\, e^b{}_\mu = \delta^b_a$. One can also consider general transformations of a local Lorentz group, taking any frame field, e, into any other set, e', of four linearly independent fields: $e'_a = \Lambda^b_a e_b$. Here and throughout the notation, $\{e_a,\, \vartheta^b\}$, will be used for general linear frames. The norm $d\widetilde{s}$ then reads $d\widetilde{s} : \ = e_a\,\vartheta^a = e_\mu \otimes \vartheta^\mu \in V_4$, and the holonomic metric on the space V_4 can be recast into the form $g = o_{ab}\vartheta^a \otimes \vartheta^a = g_{\mu\nu}\,\vartheta^\mu \otimes \vartheta^\nu$, with the components $g_{\mu\nu} = g(e_\mu, e_\nu)$ in dual holonomic basis $\{\vartheta^\mu \equiv d\widetilde{x}^\mu\}$, and o_{ab} denotes $diag(+ - - -)$ metric. In the case at hand, the metric function ω is the angular velocity of the local ZAMO with respect to an observer at rest at infinity. Thereby the redshift factor $\alpha \equiv \exp\nu$ is the time dilation factor between the proper time of the local ZAMO and coordinate time t along a radial coordinate line, i.e. the redshift factor for the time-slicing of a spacetime.

Given a height-function $\widetilde{t}$, the time-like unit normal to Σ_t will be denoted by n^μ and the 3+1 decomposition of the evolution vector field by $\widetilde{t}^\mu = Nn^\mu + \beta^\mu$, where N is the lapse function and β^μ is the shift vector. The induced metric on the space-like 3-slice Σ_t is expressed as $\gamma_{\mu\nu} = g_{\mu\nu} + n_\mu n_\nu$, with D_μ the associated Levi-Civita connection and volume element ${}^3\epsilon = \sqrt{\gamma} d\widetilde{x}^1 \wedge d\widetilde{x}^2 \wedge d\widetilde{x}^3$, so that ${}^3\epsilon_{\mu\nu\rho} = n^\sigma {}^4\epsilon_{\sigma\mu\nu\rho}$. The extrinsic curvature of $(\Sigma_t, \gamma_{\mu\nu})$ in V_4 reads $K_{\mu\nu} := -(1/2)\mathcal{L}_n\gamma_{\mu\nu} = -\gamma_\mu{}^\rho\nabla_\rho n_\nu$, where $\mathcal{L}$ denotes Lie derivative. In accord, all the geometrical objects are split into corresponding components with respect to this time-slice of spacetime.

In particular, the splitting of manifold V_4 into a foliation of three-surfaces will induce a corresponding splitting of the affine connection, curvature and, thus, of the energy-momentum tensor. The 3+1 decomposition of the (matter) stress-energy tensor, measured by an adapted Eulerian observer of four-velocity n^μ in rest with respect to the foliation $\{\Sigma_t\}$, is $\widetilde{T}_{\mu\nu} = \widetilde{E}\, n_\mu n_\nu + \widetilde{p}_{(\mu} n_{\nu)} + \widetilde{S}_{\mu\nu}$, where the matter energy and momentum densities are given by $\widetilde{E} := \widetilde{T}_{\mu\nu} n^\mu n^\nu$ and $\widetilde{p}_\mu := -\widetilde{T}_{\nu\rho} n^\nu \gamma^\rho{}_\mu$, respectively, whereas the matter stress tensor is $\widetilde{S}_{\mu\nu} := \widetilde{T}_{\rho\sigma}\gamma^\rho{}_\mu\gamma^\sigma{}_\nu$. Latin indices running in $\{1, 2, 3\}$ will be employed in expressions only involving objects intrinsic to space-like Σ_t slices. That is, $\widetilde{T}^{\alpha\beta} = \widetilde{E} n^\alpha n^\beta + n^\alpha \widetilde{J}^\beta + \widetilde{J}^\alpha n^\beta + \widetilde{S}^{\alpha\beta}$. Here n^α is the unit orthogonal vector to the hypersurface Σ_t, whereas the spacetime metric g induces a first fundamental form with the spatial metric $\gamma_{\alpha\beta}$ on each Σ_t as $\gamma_{\alpha\beta} = g_{\alpha\beta} + n_\alpha n_\beta$. This form includes one gauge freedom for the coordinate choice. For the spherical type coordinates $\widetilde{x}^2 = \widetilde{\theta}$ and $\widetilde{x}^3 = \widetilde{r}$, for example, so-called quasi-isotropic gauge corresponds to $\gamma_{r\theta} = 0$ and $\gamma_{\theta\theta} = \widetilde{r}^2\gamma_{rr}$. Then, one may define the second fundamental form which associates with each vector tangent to Σ_t, and the extrinsic curvature of the hypersur-

doi: 10.52526/25792776-2021.68.2-236

face Σ_t as minus the second fundamental form. Aftermath, one can define the usual Lorentz factor $W = -n_\mu \widetilde{u}^\nu = \alpha \widetilde{u}^t$ for a fluid which is the source of the gravitational field, with conventional stress-energy tensor $\widetilde{T}^{\mu\nu} = (\widetilde{\rho} + \widetilde{P})\widetilde{u}^\mu \widetilde{u}^\nu + \widetilde{P} g^{\mu\nu}$, where $\widetilde{\rho}$ is the total energy density and $\widetilde{P}$ is the pressure. Hence $\widetilde{E} = W^2(\widetilde{\rho} + \widetilde{P}) - \widetilde{P}$ and $\widetilde{J}^i = (\widetilde{E} + \widetilde{P})\widetilde{v}^i$, where the fluid three-velocity $\widetilde{v}^i (i = 1, 2, 3)$ implies $\widetilde{u}^i = W(\widetilde{v}^i - \beta^i/\alpha)$. Thereby the resulting stress tensor can be written $\widetilde{S}_{ij} = (\widetilde{E} + \widetilde{P})\widetilde{v}_i \widetilde{v}_j + \widetilde{P}\gamma_{ij}$. The four-velocity for rotating fluid reads $\widetilde{u} = \widetilde{u}^i(\partial/\partial\widetilde{t}) + \Omega\partial/\partial\widetilde{\phi}$, where $\Omega = \widetilde{u}^\phi/\widetilde{u}^t$ is the fluid angular velocity as seen by an inertial observer at rest at infinity.

Consequently, the components of the energy - momentum tensor of matter with total density ρ and pressure P are given in the non-rotating anholonomic orthonormal frame as $\widetilde{T}^{(ab)} = e^a_\mu e^b_\nu \widetilde{T}^{\mu\nu}$, $\widetilde{T}^{(00)} = W^2(\widetilde{\rho} + \widetilde{P}V^2)$, $\widetilde{T}^{(11)} = W^2(\widetilde{\rho} + \widetilde{P}V^2)$, $\widetilde{T}^{(01)} = W^2(\widetilde{\rho} + \widetilde{P})V$ and $\widetilde{T}^{(22)} = \widetilde{T}^{(33)} = \widetilde{P}$, with its trace $\widetilde{T} = -\widetilde{\rho} + 3\widetilde{P}$, where V is the velocity (in units of c) with respect to the Bardeen observer $V = \varrho B(\Omega - \omega)/\alpha^2$, so $W = 1/\sqrt{1 - V^2}$.

The other physical features of SIMBH configuration also need to be accounted which comprise the whole of the case. The fact that the rotational energy has a steeper dependence on the radius of the compact object than the internal energy in the relativistic limit is quite significant. Equilibrium can always be achieved for massive configurations with nonzero angular momentum by decreasing its radius. Also, there are two characteristic features that distinguish a spinning relativistic SPC-configuration from its non-spinning counterpart: 3) The geodetic effect, as in case of a gyroscope, leads an accretion stream to a tilting of its spin axis in the plain of the orbit. Hence a proto-matter disk will be tilted from the plane of accretion on a definite angle δ towards the equator. 4) Besides the UHE neutrinos, produced in the deep interior layers of superdense proto-matter medium as in case of non-spinning model, the additional thermal defuse blackbody radiation is released from the outer surface layers of ordinary matter of spinning SPC and co-spinning proto-matter thin disk. All of the rotational kinetic energy is dissipated as thermal blackbody radiation. This is due to the physical condition that these layers optically thick and, eventually, in earlier half of the lifetime of spinning black hole, at times $< T_{BH}$, the strict thermodynamic equilibrium prevails for this radiation because there would be no net flux to outside of event horizon in any direction. That is, the emission from the isothermal, optically thick outer layers at surface is blackbody, which is the most efficient radiation mechanism. This radiation is free of trapping. All of the rotational energy of SIMBH is dissipated as thermal defuse blackbody X-ray radiation to outside world.

11.5. The X-ray radiation from SIMBH

If this were the case, eventually the spinning proto-matter core and a thin co-spinning proto-matter disk driven by accretion would be formed. The evolution and structure of a proto-matter disk is largely determined by internal friction. Before tempting to build a physical model in quest, the other features of SIMBH configuration also need to be accounted which comprise the whole of the case. The fact that the rotational energy has a steeper dependence on the radius of the compact object than the internal energy in the relativistic limit is quite significant. Equilibrium can always be achieved for massive configurations with nonzero angular momentum by decreasing its radius. Also, there are two characteristic features that distinguish a spinning relativistic SPC-configuration from its non-spinning counterpart: 3) The geodetic effect, as in case of a gyroscope, leads an accretion stream to a tilting of its spin axis in the plain of the orbit. Hence a proto-matter disk will be tilted from the plane of accretion on a definite angle δ towards the equator. 4) Besides the UHE neutrinos, produced in the deep interior layers of superdense proto-matter medium as in case of non-spinning model, the additional thermal defuse blackbody radiation is released from the outer surface layers of ordinary matter of spinning SPC and co-spinning proto-matter thin disk. All of the rotational kinetic energy is dissipated as thermal blackbody radiation. This is due to the physical condition that these layers optically thick and, eventually, in earlier half of the lifetime of spinning black hole, at times $< T_{BH}$, the strict thermodynamic equilibrium prevails for this radiation because there would be no net flux to outside of event horizon in any direction. That is, the emission from the isothermal, optically thick outer layers at surface is blackbody, which is the most efficient radiation mechanism. This radiation is free of trapping. With this guidelines to follow, we may proceed in relatively simple

doi: 10.52526/25792776-2021.68.2-236

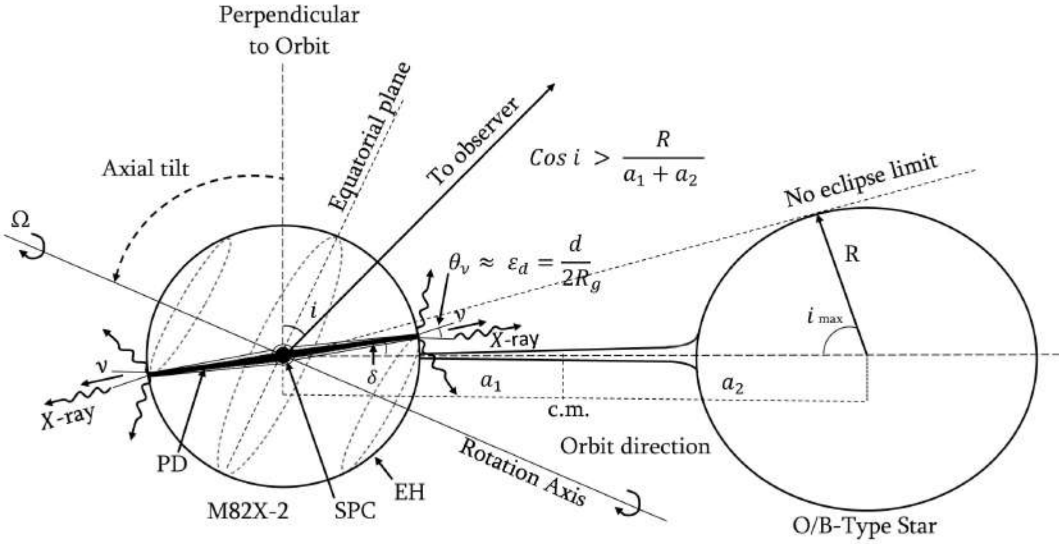

Figure 7. A schematic SIMBH model of M82X-2 constituting mass-exchange binary with the O/B-type donor star. The angle i is the binary inclination with respect to the plane of the sky. No eclipse condition holds. In final stage of growth, PD has reached out the edge of the EH. The thermal defuse blackbody X-rays beams may escape from SIMBH through a thin belt area $S = 2\pi R_g d$ to outside world that sweep past Earth like lighthouse beacons. Parameters of a binary system is viewed in the orbital plane. The picture is not to scale. Accepted notations: EH=Event Horizon, SPC=Superdense Proto-matter Core, PD=Proto-matter Disk.

way toward first look at some of the associated physics and can be quick to estimate the physical characteristics of mass-exchange X-ray binaries. Examining the pulsations revealed from M82X-2, as a working model we assume the source of the flashes to be a self-gravitating SIMBH resided in the final stage of growth. This implies that a thin co-spinning proto-matter disk has reached out the edge of the event horizon. Due to it a metric singularity inevitably disappears at the intersection of proto-matter disk with the event horizon. Hence, the crossing event horizon at such conditions from inside of black hole is allowed. This general behavior is very robust and depends very little on the details of the model of SPC. A principle physical properties of this phenomena for non-rotating SPC are already discussed. Without being carefully treated, even though these properties are of great significant as well for a rotating SPCs. Actually, they will retain for a more general geometry of rotating axisymmetric SPCs. We conclude on the basis of these observations that the energy can be carried away to outside world by the thermal defuse blackbody X-ray radiation through a thin belt area S. As M82X-2 spins, the pulse profile results from the axial tilt or obliquity. Hence the X-ray beams intercept Earth-like lighthouse beacons. The orbital motion causes a modulation in the observed pulse frequency.The SIMBH model of M82X-2 in binary system is schematically plotted in Fig. 7. No eclipse condition holds. The parameters of a binary system is viewed in the orbital plane. The Fig. 8 explains the "spherical triangle". No eclipse condition holds. The parameters of a binary system is viewed in the orbital plane.

11.6. Basic geometry: Implications on the pulse profile and mass scaling

To see where all this is leading to, let us consider next the real issue that of the physical description of M82X-2. A knowledge of the dynamical mass measurements of the compact objects that power ULXs is a primarily necessary prerequisite to the derivation of a complete picture about the physical nature of ULXs. Keeping in mind aforesaid, we are now in a position to derive a general pulse profile dependent upon the position angles, and give a quantitative account of a potential dynamical mass scaling of M82X-2 and other energetics. The most reliable method is to measure the mass function through the secondary mass and orbital parameters, which can be measured only if the secondary donor star is optically identified. In the absence of direct mass-function measurements from phase-

doi: 10.52526/25792776-2021.68.2-236

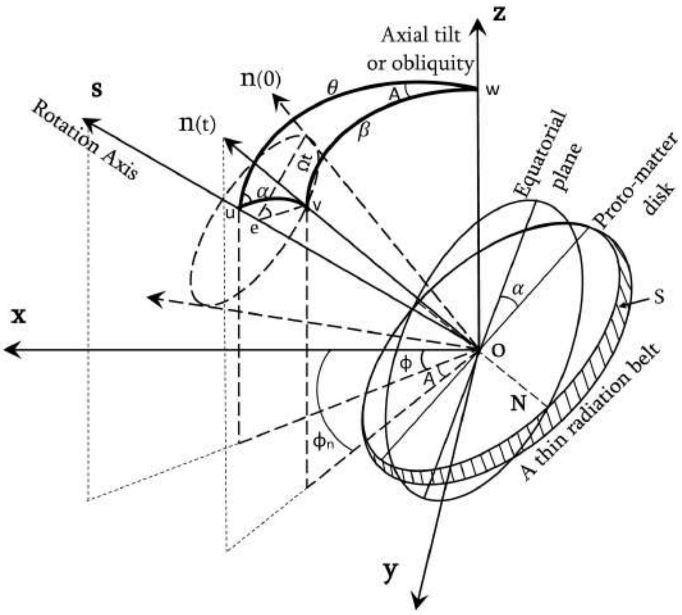

Figure 8. A schematic plot explaining the spherical triangle solved by the law of cosines. The space-fixed Cartesian coordinate system is labeled (z,x,y), with zx as a plane-of sight. Axis s of the M82X-2-fixed frame is rotation axis. The angles θ and ϕ are spherical polar coordinates. The line of nodes N is defined as the intersection of the equatorial and proto-matter disk planes. It is perpendicular to both the z axis and vector $\vec{n}(t)$, where $\vec{n}(t)$ is the normal to the plane of proto-matter disk at moment t. The $\vec{n}(0)$ lies in the plane of zs. The lengths of three sides of a "spherical triangle" (shown at top) are $\theta = \widehat{(z,s)}$, $\alpha = \widehat{(s,n)}$ and $\beta = \widehat{(z,n)}$. The vertex angle of opposite β is Ωt.

resolved optical spectroscopy, we still have to rely on X-ray spectral and timing modeling and other indirect clues. To bring this point sharply into focus note that in case of the first ultraluminous pulsar, only the X-ray mass function is measured, when the optical secondary is unknown and most of the orbital parameters are yet to be measured. However, exploring the key physical characteristics of a SIMBH model, let us consider the space-fixed Cartesian coordinate system labeled (z,x,y), with zx as a plane-of sight, and the axis s of the M82X-2-fixed frame as the rotation axis. A schematic plot is given in Fig. 8. Here and throughout we now use following notational conventions. The angles θ and ϕ are spherical polar coordinates. The observed pulses are produced because of periodic variations with time of the projection $d_{zx}(t)$ of the vector $\vec{d}(t)$ aligned with the $\vec{n}(t)$ ($\vec{d}(t) = d\,\frac{\vec{n}(t)}{|n(t)|}$) on the plane-of sight, where $\vec{n}(t)$ is the normal to the plane of the proto-matter disk at the moment t. The $\vec{n}(0)$ lies in the plane of zs. So, these pulsations are due to the fact that the visible surface is less at one moment than at another. The Fig. 8 explains the *spherical triangle*. That is, given a unit sphere, a *spherical triangle* on the surface of the sphere is defined by the great circles connecting three points u, v, and w on the sphere (shown at top). The lengths of these three sides are $\alpha = \widehat{(s,n)}$ (from u to v), the axial tilt $\theta = \widehat{(z,s)}$ (from u to w), and $\beta = \widehat{(z,n)}$ (from v to w). The angles of the corners u and e opposite β equal $u = e = \Omega t$. The proto-matter disk was shifted from the orbital direction on angle $\delta = \theta - \alpha$ towards the equator. The projection $d_{zx}(t)$ is written $d_{zx}(d,\theta,\phi,\alpha,t) = \sqrt{d_z^2(d,\theta,\alpha,t) + d_x^2(d,\theta,\alpha,\phi,t)}$, where $d_z(d,\theta,\alpha,t) \equiv \vec{d}(...,t)\cdot\vec{e_z} = d\cos\beta(\theta,\alpha,t)$, and $d_x(d,\theta,\alpha,\phi,t) \equiv \vec{d}(...,t)\cdot\vec{e_x} = d\,\sin\beta(\theta,\alpha,t)\cos\phi_n(\theta,\alpha,\phi,t)$. Here the $\vec{e}_z$ and $\vec{e}_x$ denote unit vectors along the axes z and x, respectively, $\phi_n = \phi + A$ is the azimuthal angle of vector $\vec{n}(t)$. The vertex angle opposite the side α is A. To the extent that all of the rotational energy of M82X-2 is dissipated as thermal defuse X-ray blackbody radiation, this may escape from the event horizon to outside world only through a thin belt area S. The radiation arisen from per area of surface is σT_s^4, where T_s is the surface temperature, σ is the Stefan-Boltzmann constant. Therefore, the pulsed luminosity $\widetilde{L}$ will be observed if and only if the projection of the belt area $S_{zx} = 2\pi R_g d_{zx}(d,\theta,\phi,\alpha,t)$ on the plane-of sight zx is not zero. So, pulsed luminosity reads $\widetilde{L}(R_g,d,T_s,\theta,\phi,\alpha,t) = S_{zx}\,\sigma T_s^4 =$

doi: 10.52526/25792776-2021.68.2-236

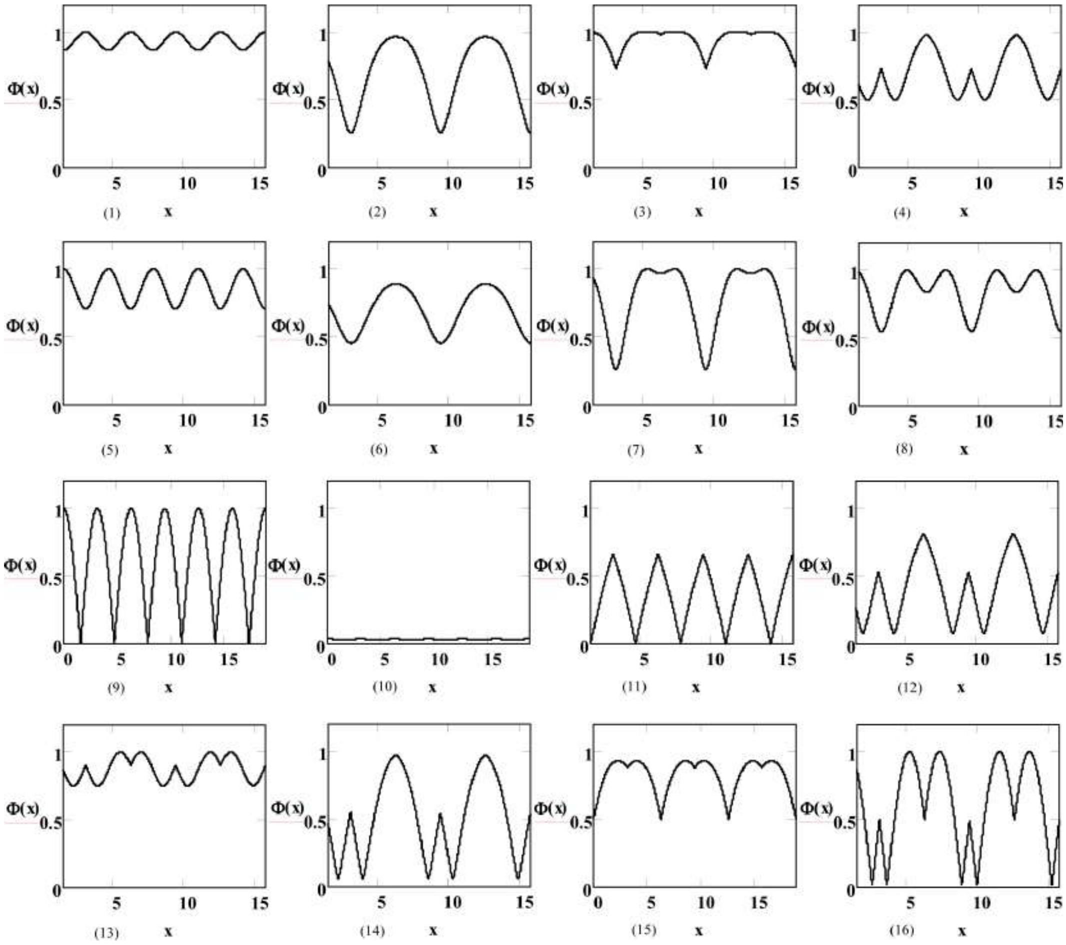

Figure 9. Characteristic phase profiles versus the time ($x \equiv \Omega t$), viewed at the following position angles (θ, α, ϕ): (1) $(45^0, 30^0, 0^0)$; (2) $(45^0, 30^0, 90^0)$; (3) $(45^0, 30^0, 135^0)$; (4) $(45^0, 30^0, 60^0)$; (5) $(45^0, 90^0, 90^0)$; (6) $(45^0, 18^0, 90^0)$; (7) $(45^0, 60^0, 90^0)$; (8) $(45^0, 78.3^0, 90^0)$; (9) $(90^0, 90^0, 180^0)$; (10) $(90^0, 0.6^0, 72^0)$; (11) $(90^0, 30^0, 60^0)$; (12) $(72^0, 30^0, 60^0)$; (13) $(60^0, 90^0, 60^0)$; (14) $(60^0, 45^0, 60^0)$; (15) $(60^0, 153^0, 60^0)$; (16) $(1.2^0, 90^0, 60^0)$.

$2\pi R_g d_{zx}(d, \theta, \phi, \alpha, t)\, \sigma T_s^4 \equiv L_0(M, d, T_s)\, \Phi(\theta, \phi, \alpha, t)$, where its amplitude and phase, respectively, are $L_0(M, d, T_s) \simeq 1.05 \times 10^4\, (\mathrm{erg\,s^{-1}}) \frac{M}{M_\odot} \frac{d}{\mathrm{m}} \frac{T_s^4}{K^4}$, $\Phi(\theta, \phi, \alpha, t) \equiv \sqrt{1 - \sin^2\beta \sin^2(\phi + A)}$. The *spherical triangle* is solved by the law of cosines $\cos\beta(\theta, \alpha, t) = \cos\theta\cos\alpha + \sin\theta\sin\alpha\cos\Omega t$, $\cos A(\theta, \alpha, t) = \frac{\cos\alpha - \cos\theta\cos\beta}{\sin\theta\sin\beta}$.

Consequently, the pulsed flux can be written in the form $\widetilde{F}(R_g, d, \theta, \phi, \alpha, t) = F_0(M, d)\, \Phi(\theta, \phi, \alpha, t)$. where, given the distance $D \simeq 3.6\,\mathrm{Mpc}$ to the galaxy M82, the flux amplitude is $F_0(M, d) = \frac{L_0(M,d)}{4\pi D^2} \simeq 6.8 \times 10^{-48}\, (\mathrm{erg\,s^{-1}cm^{-2}}) \frac{M}{M_\odot} \frac{d}{\mathrm{m}} \frac{T_s^4}{K^4}$. Thus, the theoretical model of periodic source M82X-2 left six free parameters: $(M, d, T_s, \theta, \phi, \alpha)$. The Fig. 9 reveals the diversity of the behavior of characteristic phase $\Phi(\theta, \phi, \alpha, x \equiv \Omega t)$ profiles versus the time, viewed at given position angles (θ, ϕ, α). The observed X-ray pulse is further determined by the complicated transfer of X-ray photons from the surface of M82X-2 through regions of external accreting plasma. At hard look, the position angles being the parameters of a model function can be adjusted via nonlinear regression analysis to the approximate solution of overdetermined systems to best fit a data set from observed pulsed profile of M82X-2. These missing ingredients are the shortcoming of present framework, which will be solved by iterative refinement elsewhere. For maximum value of pulsed luminosity either at $\beta = \pi s$ or $\phi + A = \pi s$ (s=0,1,2,...), we have $L_0(M, d, T_s) = \widetilde{L}(3 - 30\,\mathrm{keV}) = 4.9 \times 10^{39}\,\mathrm{erg\,s^{-1}}$ or $F_0(M, d) = \widetilde{F}(3 - 30\,\mathrm{keV}) \simeq 3.16 \times 10^{-12}\,\mathrm{erg\,s^{-1}cm^{-2}}$. Hence the surface temperature scales $\propto T_s^{-4}$ with the black hole mass: $\frac{M}{M_\odot} = \frac{4.66 \times 10^{35}\, K^4}{T_s^4} \frac{\mathrm{m}}{d}$. That is, a cooler radiation surface implies a bigger black hole. If we further assume that the persistent emission - $\overline{L}(0.3 - 10\,\mathrm{keV}) = 1.8 \times 10^{40}\,\mathrm{erg\,s^{-1}}$ - from M82X-2

doi: 10.52526/25792776-2021.68.2-236

is isotropic, we may impose a strict Eddington limit on the mass transfer rate that can be accepted by the black hole, $\overline{L} < L_{Edd} \simeq 1.3 \times 10^{38} \frac{M}{M_\odot}\,\mathrm{erg\,s^{-1}}$. This imposes stringent constraint on the lower limit of black hole mass $\frac{M}{M_\odot} > 138.5, \quad R_g > 408.6\,\mathrm{km}$, because for an accreting of ~ 10 per cent of the Eddington limit - a fairly typical accretion rate for a high-state black hole - this points towards a rough estimate of upper limit of mass $M < 1385\,M_\odot$.

11.7. More accurate determination of upper mass limit of M82X-2

For the knowledge of upper mass limit of M82X-2, a good progress can still be made by establishing a direct physical relation between masses of M82X-2 and M82X-1, and then one should rely on the available mass estimates of the latter (Ter-Kazarian, 2016b). The controversy, however, is with their mass range. As one may envisage, a different mass estimates of M82X-1 may yield different mass values of M82X-2. So, we should be careful in choosing the most accurate black hole mass measurement to-date. As the centroid of the persistent emission is between M82X-2 and M82X-1 which indicates that M82X-2 harbors an IMBH, likewise M82X-1, we suppose that accretion onto a black hole is well approximated by the relation $L_{acc} = \eta c^2 \dot{M} = \frac{GM}{R}\dot{M}$. This gives $\dot{M}_1/\dot{M} = \overline{L}_1/\overline{L} \simeq 5.556$. According to MTBH, we have $\dot{M} \propto M^2$ for both the collisionless and the hydrodynamic spherical accretions onto black hole . Making use of these relations, we then obtain $M_1 \simeq 2.357M$. The M82X-1 is a good candidate for hard state ULXs which may be one of the very few ULXs that change their spectral state during outbursts, switching from a hard to a thermal state. The "type-C" low frequency quasi-periodic oscillations and broadband timing noise, detected in the two XMM-Newton observations in 2001 and 2004, in the central region of M82 and later confirmed to originate from the M82X-1, suggest that the ULX harbors a massive black hole. The used mass estimate is based on the assumption that M82X-1 also follows well established relation of the photon spectral index versus QPO frequency, $\Gamma - \nu_{QPO}$, found for the Galactic X-ray binaries in their high or intermediate states. The resulting IMBH mass for M82X-1 is in the range of $25 - 520\,M_\odot$. However, there may be systematic errors in the photon indices measured with XMM-Newton and Rossi X-ray Timing Explorer (RXTE) due to contamination from nearby sources, as indicated by large apparent changes in the effective absorption column. Another mass estimate is inferred from the correlations with the X-ray luminosity and type C QPO frequency. This method is based on the correlation between characteristic frequencies, on the fundamental plane and on the variability plane of accreting black holes. Exploring this method, the black hole masses inferred from the characteristic frequencies are all about $10^3 - 10^4\,M_\odot$ indicating that ULXs contain IMBHs. But, these results were not without problems, notably pointed out by the same authors. Such mass estimates are based on scaling relations which use low-frequency characteristic timescales which have large intrinsic uncertainties. In particular, it was unclear whether these mHz oscillations are indeed the Type-C analogs of stellar mass black, and both the Type-C and the mHz oscillations are variable, resulting in a large dispersion in the measured mass of $25 - 1300\,M_\odot$. Positive identification of the emission states requires both timing and spectral information. Consequently, with simultaneous observations exploiting the high angular resolution of Chandra to isolate the ULX spectrum from diffuse emission and nearby sources and the large collecting area of XMM-Newton observations of M82 to obtain timing information, it is surprisingly found that the previously known QPOs in the source disappeared. The light curve was no longer highly variable and the power spectrum was consistent with that of white noise. The energy spectrum also changed dramatically from a straight power-law to a disk-like spectrum. The disappearance of QPOs and the low noise level suggest that the source was not in the hard state. All results are well consistent with that expected for the thermal state. The monitoring data from RXTE indicate that these Chandra and XMM-Newton observations were made during the source outbursts, suggesting that M82X-1 usually stays in the hard state and could transition to the thermal state during outbursts. The spectral fitting suggests that the ULX contains a close to Eddington ($L_{disk}/L_{Edd} \sim 2$) rapidly spinning IMBH of $200 - 800\,M_\odot$ masses. The thermal dominant states are all found during outbursts. Nonetheless, modeling of X-ray energy spectra during the thermal-dominant state using a fully relativistic multi-colored disk model has large uncertainties owing to both systematic and measurement errors. In addition to the large mass uncertainty associated with the modeling, the same authors also found that the energy spectra can be equally well-fit with a stellar-mass black hole accreting at a rate of roughly 160 higher than the Eddington limit. Also, the

doi: 10.52526/25792776-2021.68.2-236

X-rays from this source are known to modulate with an orbital periodicity of 62 days, which indicates to an intermediate-mass black hole with mass in the range of $200-5000\,M_\odot$. But, a recent study finds that this periodicity may instead be due to a precessing accretion disk in which case a stellar-mass black hole will suffice to explain the apparent long periodicity. Thus, the mass measurements above have large uncertainties. This makes black hole masses obtained by this method at the very least questionable. In what follows, therefore, we adopt an alternative and less ambiguous mass determination for intermediate-mass black holes, which seems to be a more reliable determinant of the mass of M82X-1. The searched was made of RXTE's proportional counter array archival data to look for 3 : 2 oscillation pairs in the frequency range of $1-16$ Hz which corresponds to a black hole mass range of $50-2000\,M_\odot$. In stellar-mass black holes, it is known that the high frequency quasi-periodic oscillations that occur in a 3 : 2 ratio ($100-450$ Hz) are stable and scale inversely with black hole mass with a reasonably small dispersion. It is reported of stable, twin-peak (3:2 frequency ratio) X-ray quasi-periodic oscillations from M82X-1 at the frequencies of 3.32 ± 0.06 Hz (coherence, Q = centroid frequency (ν)/width$(\nu) > 27$) and 5.07 ± 0.06 Hz ($Q > 40$). The discovery of a stable 3 : 2 high-frequency periodicity simultaneously with the low-frequency mHz oscillations allows for the first time to set the overall frequency scale of the X-ray power spectrum. This result not only asserts that the mHz quasi-periodic oscillations of M82X-1 are the Type-C analogs of stellar-mass black holes but also provides an independent and the most accurate black hole mass measurement to-date. Assuming that one can scale the stellar-mass relationship, they estimate the black hole mass of M82X-1 to be $428\pm105\,M_\odot$. They also estimate the mass using the relativistic precession model, which yields a value of $415\pm63\,M_\odot$. Combining the average 2-10 keV X-ray luminosity of the source of $5\times10^{40}\,\mathrm{ergs\,s^{-1}}$ with the measured mass suggests that the source is accreting close to the Eddington limit with an accretion efficiency of 0.8 ± 0.2.

Making use of the mass values $428\pm105\,M_\odot$, we provide the mass estimate for M82X-2: $M\simeq 138.5-226\,M_\odot$, $\quad R_g\simeq 408.6-666.7\,\mathrm{km}$, Rotation speed at surface of M82X-2 with upper limit mass $226\,M_\odot$ as rigidly spinning IMBH configuration of angular velocity Ω equals $v=R_g\Omega\simeq 3.06\times 10^8\,\mathrm{cm\,s^{-1}}$. We may also slightly improve the lower mass limit $323\,M_\odot$ of M82X-1, to now be $326.5\,M_\odot$. Combining all the results above, we obtain then $2.06\times10^{33} < \frac{T_s^4}{K^4}\frac{d}{\mathrm{m}} < 3.34\times10^{33}$. For reasons that will become clear below, next, in our setting we adopt the rather concrete proposal of non-spinning black holes, i.e. the neutrino flux from spinning M82X-2 might as well be highly beamed along the plane of proto-matter disk and collimated in very small opening angle. For the adopted values, this yields the constraints $7.5\times10^{-7}\,\frac{d}{\mathrm{m}} < \theta_\nu \sim \varepsilon_d < 1.2\times10^{-6}\,\frac{d}{\mathrm{m}}$. Besides, the ε_d is likely to be about an order of magnitude $\sim10^{-5}$ for M82X-2. Therefore, $d\simeq 61-100\,\mathrm{m}$, $\quad \varepsilon_d\simeq(4.6-7.5)\times10^{-5}$, is a good guess for the thickness of proto-matter disk at the edge of event horizon. This gives $T_s\simeq 7.6\times10^7$ K. Thus, M82X-2 indeed releases $\sim 99.6\%$ of its radiative energy predominantly in the X-ray bandpass of $0.3-30$ keV. However, its studies in other wavelengths well give us useful information on its physical nature and environment. From Wien's displacement law we obtain the wavelength $\lambda_{max}\simeq 0.381$nm at which the radiation curve peaks, which corresponds to energy $h\nu_{max}\simeq 3.2$ keV. As an immediate corollary to the assumption that the emission arisen from accretion is isotropic, we are able to infer the most important ratios of the pulsed and persistent luminosities to the isotropic Eddington limit for M82X-2: $\frac{\widetilde{L}}{L_{Edd}}\simeq 0.17-0.28$, $\frac{\overline{L}}{L_{Edd}}\simeq 0.63-1.03$, respectively, where $L_{Edd}\simeq(1.75-2.85)\times10^{40}\,\mathrm{erg\,s^{-1}}$. These properties appear consistent with the sub-Eddington hard state, which given the observed luminosities of M82X-2 suggests the presence of SIMBH with a dynamical mass. Given the angular velocity $\Omega=\frac{2\pi}{P}(P=1.37\,\mathrm{s})$, we may calculate the rotational kinetic energy $E_{rot}=\frac{1}{2}I\Omega^2$ of M82X-2, where $I=\frac{2}{5}MR_g^2$ is the moment of inertia if M82X-2 is regarded as the rigidly spinning *canonical* configuration of mass M and radius R_g. Hence $E_{rot}\simeq(3.72-16.17)\times10^{51}\,\mathrm{erg}$. When all energy thermalized, radiation emerges as a blackbody. A significant fraction of the accretor M82X-2 surface radiates the accretion luminosity at temperature $T_b=\left(\frac{L_{acc}}{4\pi R_g^2}\right)^{1/4}\simeq\left(\frac{L_{Edd}}{4\pi R_g^2}\right)^{1/4}$, such that $T_b\simeq(3.88-5.37)\times10^6 K$. The gravitational energy of each accreted electron-proton pair turned directly into heat at (shock) temperature T_{sh}: $3kT_{sh}=\frac{GMm_p}{R_g}$, so $T_{sh}\simeq 1.8\times10^{12}K$. Hence typical photon energies of persistent radiation lies between $kT_b\simeq 0.34\,\mathrm{keV}\le h\nu\le kT_{sh}\simeq 180\,\mathrm{MeV}$. So, M82X-2 is persistent X-ray and possibly gamma-ray emitter. Also, given the mass of the most brightest

doi: 10.52526/25792776-2021.68.2-236

source M82X-1 of persistent X-ray radiation, typical photon energies of persistent radiation lie in range $kT_{b(X1)} \simeq 0.3\,\mathrm{keV} \leq h\nu \leq kT_{sh} \simeq 180\,\mathrm{MeV}$.

11.8. The mass of companion star and orbit parameters

Once the mass scaling of M82X-2 is accomplished, this can potentially be used further to quantify the association between the M82X-2 and the optical secondary donor star in X-ray binary. The orbital period P_{or} is a key parameter for dynamical mass measurement. From Fig. 7, the separation of the two masses is a, and their distances from the center of mass are a_1 and a_2. The highly circular orbit, combined with the mass function $f(M,\, M_2,\, i) = 2.1 M_\odot$, the lack of eclipses and assumption of a Roche-lobe- filling companion constrain the inclination angle to be $i < 60^o$. These alow to determine the mass M_2 of donor star: $\frac{M_2}{M_\odot} > \begin{cases} 48.3, & \text{for} \quad M = 138.5\, M_\odot, \\ 64.9, & \text{for} \quad M = 226\, M_\odot. \end{cases}$ Thus, optical companion is a typical O/B supergiant, which evolves away from the main sequence in just a few million years. The binary separation can be computed with Kepler's Law $a^3 = \frac{G(M+M_2)}{4\pi^2} P^2_{or}$. The Doppler curve of the spectrum of NuSTAR J095551+6940.8 shows a $P_{or} = 2.5$-day sinusoidal modulation arisen from binary orbit. All these give the projection of the orbital velocity of M82X-2 along the line of sight $v_1 = \frac{2\pi}{P_{or}} a_1 \sin i \simeq 200.9 \frac{\mathrm{km}}{\mathrm{s}}$, and hence $a_1 \sin i \simeq 9.9 R_\odot$. The absence of eclipses implies $\cos i > \frac{R}{a}$, where R is the radius of companion donor star. Hence $R > \begin{cases} 22.1\, R_\odot, & \text{for} \quad M = 138.5\, M_\odot, \\ 25.7\, R_\odot, & \text{for} \quad M = 226\, M_\odot. \end{cases}$ As well as $a_1 > 11.4\, R_\odot$, $a_2 > 32.9\, R_\odot$ for $M/M_\odot = 138.5$; and a_1 is the same, $a_2 > 39.9\, R_\odot$ for $M/M_\odot = 226$. The Roche lobe radius R_L for donor star is $R_L > \begin{cases} 15\, R_\odot, & \text{for} \quad M = 138.5\, M_\odot, \\ 14.3\, R_\odot, & \text{for} \quad M = 226\, M_\odot. \end{cases}$ Thus, the M82X-2 and donor star constitute the semi-detached binary, accreting through Roche-lobe overflow. Donor star exceeds its Roche lobe ($R > R_L$), therefore its shape is distorted because of mass transfer from donor star through the inner Lagrange point L_1 to the M82X-2. The accretion stream is expected to be rather narrow as it flows through the L_1 point and into the Roche lobe of the primary.

11.9. Spin-up rate and the torque added to M82X-2

All accreting pulsars show stochastic variations in their spin frequencies and luminosities, including those displaying secular spin-up or spin-down on long time scales, blurring the conventional distinction between disk-fed and wind-fed binaries. Pulsed flux and accretion torque are strongly correlated in outbursts of transient accreting pulsars, but uncorrelated, or even anticorrelated, in persistent sources. The observed secular spin-up rate can be accounted for quantitatively if one assumes the reduction of the torque on the rapidly spinning object. Continuing on our quest, below we determine the conditions under which pulsed source M82X-2 spins up and hance gains rotational energy as matter is accreted, i.e. we discuss the relationship between the properties of the exterior flow and the measured rate of change of angular velocity $d\Omega/dt$. Although measurements of spin-up or spin-down appears to be the most promising method for determining the angular momentum transport by the inflowing matter, which in turn, may provide information about pattern of material flow outside the event horizon of SIMBH, the extraction of this information from such measurements clearly requires some care. We explore the relationship between the torque ($\equiv l$) flux through the event horizon, spin-up rate of SIMBH and the rate of change of its rotational energy. The rates of change of the SIMBH angular velocity and of the rotational energy can be related to the flux of torque across the event horizon boundary as follows. The rate of change of the torque is given by $\frac{d}{dt}(I\Omega) = \dot{M} l$, where I is the moment of inertia, and l is the torque added to the SIMBH per unit mass of accreted matter. This equation gives for the rate of change of angular velocity $\frac{d\Omega}{dt} = \frac{\dot{M}}{L_{bh}} \left[l\Omega - \Omega^2 R^2_{gir} (\frac{M}{I} \frac{dI}{dM}) \right]$, where $L_{bh} \equiv I\Omega$, and R_{gir} is the radius of gyration of SIMBH. The rate of change of the rotational energy is $\frac{dE_{rot}}{dt} = \frac{d}{dt}(\frac{1}{2} I \Omega^2)$. To make further progress we recast these equations into the form $\frac{dE_{rot}}{dt} = \dot{M} \left[l\Omega - \frac{1}{2} \Omega R^2_{gir} (\frac{M}{I} \frac{dI}{dM}) \right]$. When $\frac{M}{I} \frac{dI}{dM} > 0$, which is generally the case, the SIMBH's behavior can be conveniently characterized by the dimensionless parameter $\zeta \equiv \frac{l}{\Omega R^2_{gir}} (\frac{M}{I} \frac{dI}{dM})^{-1}$. Thus the black hole loses rotational energy and spins down for $\zeta < 1/2$, whereas it gains rotational energy and

doi: 10.52526/25792776-2021.68.2-236

spins up for $\zeta > 1$; for $1/2 < \zeta < 1$ the black hole spins down even though it is gaining rotational energy. The logarithmic derivative $\frac{M}{I}\frac{dI}{dM}$ for *canonical* configuration, i.e. spinning uniform-density sphere with mass M and radius R_g, is $\frac{d\ln I}{d\ln M} = \frac{d}{d\ln M}\ln(\frac{2}{5}MR_g^2) = 3$, so $\zeta = \frac{l}{3\Omega R_{gir}^2}$, where $R_{gir}^2 = I/M = \frac{2}{5}R_g^2$. For the spin up regime of M82X-2 when $\zeta \simeq 0.073\frac{l}{\Omega R_{gir}^2} > 1$, we obtain $l > 2.192 R_g^2\,\mathrm{s}^{-1}$, so $l > \{\ 3.7\times 10^5\,\mathrm{km^2 s^{-1}}$, for $M = 138.5\,M_\odot 9.7\times 10^5\,\mathrm{km^2 s^{-1}}$, for $M = 226\,M_\odot$. The time derivative of the angular velocity gives $l = \frac{4\pi R_g^2}{5P}(3 - \frac{\dot P}{P}\frac{M}{\dot M})$. Combing $\dot M \simeq 6.35\times 10^{-7}\,M_\odot\,yr^{-1}$, and a linear spin-up $\dot p$ of the NuSTAR J095551+6940.8 pulsar, we obtain the torques added to M82X-2 per unit mass of accreted matter, which satisfy the spin-up condition of $\zeta > 1$: $l \simeq \begin{cases} 1.1\times 10^{11}\,\mathrm{km^2 s^{-1}}, & \text{for}\quad M = 138.5\,M_\odot, \\ 9.8\times 10^{11}\,\mathrm{km^2 s^{-1}}, & \text{for}\quad M = 226\,M_\odot. \end{cases}$

12. Rotating black holes in microscopic theory: the implications for periodic source M82X-2

For rigorous theoretical solutions, we analytically treat the microscopic model of stationary and axisymmetric rotating black hole (Ter-Kazarian, 2016a). In particular, we derive field equations and obtain both internal and global vacuum spacetime solutions. A ring singularity of the Kerr black hole cannot occur, which is now replaced by equilibrium SPC. We calculate the corrections to previous model introduced by the rotation of the characteristic phase profile of M82X-2.

12.1. Axisymmetric distortion of $M_6 \to V_6$: A reduction to V_4

Before tempting to build an axisymmetric distorted Riemannian 4D space V_4, we need to consider an axisymmetric distortion of the 6D space $M_6 \to V_6$, and next reduce it to V_4. The element $D(a,\theta)$ of the distortion group G_D has induced a general distortion transformations of the six-basis vectors $e = O\times\sigma\,(\in M_6) \to \widetilde e = \widetilde O\times\widetilde\sigma\,(\in V_6)$: $2\widetilde e_{(0\alpha)} = \widetilde\xi_{(0\alpha)}\times(\widetilde\sigma_{(+\alpha)} + \widetilde\sigma_{(-\alpha)}) + \widetilde\xi_{(\alpha)}\times(\widetilde\sigma_{(+\alpha)} - \widetilde\sigma_{(-\alpha)})$, $2\widetilde e_{(\alpha)} = \widetilde\xi_{(\alpha)}\times(\widetilde\sigma_{(+\alpha)} + \widetilde\sigma_{(-\alpha)}) + \widetilde\xi_{(0\alpha)}\times(\widetilde\sigma_{(+\alpha)} - \widetilde\sigma_{(-\alpha)})$, where distortion transformations of the ingredient basis vectors (O) and (σ) are not independent. Hence $\delta\widetilde\xi_{(0\alpha)} = -\xi_0 x_{(0\alpha)} + \xi x_\alpha + \bar\xi_0\bar x_{(0\alpha)} - \bar\xi\bar x_\alpha$, $\delta\widetilde\xi_\alpha = \xi x_{(0\alpha)} - \xi_0 x_\alpha + \bar\xi_0\bar x_\alpha - \bar\xi\bar x_{0\alpha)}$, provided by $\delta\widetilde\sigma_A(\theta) = \delta\mathcal{R}_A^{\beta}(\theta)\,\sigma_\beta$. Let $\phi(= x^1)$ be the azimuthal angle about the axis of symmetry in R^3. The axisymmetric distortion of the space $M_6 \to V_6$ can be induced by the distortion gauge field a_A, with the only non-zero 1D components of $x_0 := x_{(03)} = æ a_{(\pm 3)}$ and $x_1 = \mp æ a_{(\pm 1)}$, in presence of ID-field, $\bar x := \bar x_{(03)} = æ\bar a_{(\pm 3)}$, where a coupling constant æ relates to the Newton's gravitational constant G_N. Then, the non-zero components of the transformation matrix D can be recast into the form $D^{(01)}_{(\tilde 0 1)} = 1$, $D^1_{(\tilde 0 1)} = x_1$, $D^{(02)}_{(\tilde 0 2)} = \cos\theta_1$, $D^3_{(\tilde 0 2)} = \sin\theta_1$, $D^{(03)}_{(\tilde 0 3)} = \cos\theta_1(1-x_0)$, $D^2_{(\tilde 0 3)} = -\sin\theta_1(1+x_0)$, $D^{\bar 3}_{(\tilde 0 3)} = -\cos\theta_1$, $D^{(\bar 0 2)}_{(\tilde 0 3)} = -\sin\theta_1$, $D^1_{\tilde 1} = 1$, $D^{(01)}_{\tilde 1} = -x_1$, $D^2_{\tilde 2} = \cos\theta_1$, $D^{(03)}_{\tilde 2} = \sin\theta_1$, $D^3_{\tilde 3} = \cos\theta_1(1+x_0)$, $D^{(02)}_{\tilde 3} = -\sin\theta_1(1-x_0)$, $D^{(\bar 0 3)}_{\tilde 3} = \cos\theta_1 x_1$, $D^{\bar 2}_{\tilde 3} = -\sin\theta_1 x_1$, where the rotation angles are determined as $\pm\,\theta_{(1)} := \tan\theta_{(\pm 1)} = \mp x_1$, $\tan\theta_{(\pm 3)} = x_{(0)}$, $\theta_{(+3)} = \theta_{(-3)}$. Then $\widetilde e_{(01)} = e_{(01)} + e_1 x_1$, $\widetilde e_{(02)} = e_{(02)}\cos\theta_1 + e_3\sin\theta_1$, $\widetilde e_{(03)} = \cos\theta_1[e_{(03)}(1-x_0) - \bar e_3\bar x] - \sin\theta_1[e_{(2)}(1+x_0) + \bar e_{(02)}\bar x]$, $\widetilde e_1 = e_1 - e_{(01)}x_1$, $\widetilde e_2 = e_2\cos\theta_1 + e_{(03)}\sin\theta_1$, $\widetilde e_3 = \cos\theta_1[e_3(1+x_0) + \bar e_{(03)}\bar x] - \sin\theta_1[e_{(02)}(1 - x_0) - \bar e_2\bar x]$. Consequently, the resulting deformed metric on V_6 in holonomic coordinate basis takes the form $g_{00} = \tau_1^2(1-\tan^2\theta_1) + \tau_2^2\cos 2\theta_1 + \tau_3^2\{\cos^2\theta_1[(1-x_0)^2 + \bar x^2] - \sin^2\theta_1[(1+x_0)^2 + \bar x^2]\}$, $g_{01} = -2\tau_1 x_1$, $g_{02} = 2\tau_3\sin 2\theta_1$, $g_{03} = -2\tau_2\sin 2\theta_1$, $g_{11} = -(1+\tan^2\theta_1)$, $g_{22} = -\cos 2\theta_1$, $g_{33} = -\cos^2\theta_1[(1+x_0)^2 + \bar x^2] +$
$\sin^2\theta_1[(1-x_0)^2 + \bar x^2]$, where, the 3D space T^3 is spanned by the coordinates $d\widetilde x^{(0\alpha)} = \tau_\alpha d\widetilde x^0$ ($\tau_1^2 + \tau_2^2 + \tau_3^2 = 1$). At reducing $V_6 \to V_4$, we may further fix the most convenient universal time direction by imposing the constraint $g_{02}d\widetilde x^2 + g_{03}d\widetilde x^3 = 0$, i.e., $\sin 2\theta_1(\tau_3 d\widetilde x^2 - \tau_2 d\widetilde x^3) = 0$.

(i) In the case of static spherical-symmetry when $\sin 2\theta_1 = 0$, the τ_α can be chosen as $\tau_1 = \tau_2 = 0$, $\tau_3 = 1$.

(ii) Let, in axisymmetric space V_4, the world coordinate $\widetilde t(= \widetilde x^0)$ be the time (in units of c), and $\widetilde\phi(= \widetilde x^1)$ be the azimuthal angle about the axis of symmetry. The space V_4 would be invariant against simultaneous inversion of time $\widetilde{t}$ and azimuthal angle $\widetilde{\phi}$. So, $\sin 2\theta_1 \neq 0$, and the τ_2 and τ_3 can be chosen to eliminate the term $(\tau_3 d\widetilde{x}^2 - \tau_2 d\widetilde{x}^3)$, which has the effect of introducing the following values into the problem: $\tau_2 = \tau_3 \frac{\widetilde{u}^2}{\widetilde{u}^3}$, at $\frac{\widetilde{u}^2}{\widetilde{u}^3} \leq 1$, $\tau_3 = \tau_2 \frac{\widetilde{u}^3}{\widetilde{u}^2}$, at $\frac{\widetilde{u}^3}{\widetilde{u}^2} \leq 1$. A velocity field at each point in V_4 is $\widetilde{u}^t = d\widetilde{t}/d\widetilde{s}$, with proper time $d\widetilde{s}$, $\widetilde{t}(= x^0)$ is the world time coordinate (in units of c), $\widetilde{u}^\phi = d\widetilde{\phi}/d\widetilde{s} = \Omega \widetilde{u}^t$ and $\widetilde{u}^t = d\widetilde{x}^C/d\widetilde{s} = \widetilde{u}^t \widetilde{v}^C$, and $\Omega = d\widetilde{\phi}/d\widetilde{t}$ is the angular velocity, as seen by an inertial observer at rest at infinity. The components $\widetilde{v}^C = d\widetilde{x}^C/d\widetilde{t}\,(C = 2, 3)$ denote the poloidal velocity. Hence the metric on axisymmetric space V_4 becomes $g_{00} = \tau_1^2(1 - \tan^2\theta_1) + \tau_2^2 \cos 2\theta_1 + \tau_3^2\{\cos^2\theta_1[(1-x_0)^2+\bar{x}^2] - \sin^2\theta_1[(1+x_0)^2+\bar{x}^2]\}$, $g_{01} = -2\tau_1 x_1$, $g_{11} = -(1+\tan^2\theta_1)$, $g_{22} = -\cos 2\theta_1$, $g_{33} = -\cos^2\theta_1[(1+x_0)^2 + \bar{x}^2] + \sin^2\theta_1[(1-x_0)^2 + \bar{x}^2]$. We define the five quantities ν, ψ, ω, μ_2 and μ_3 which are only functions of the coordinate $\widetilde{x}^2$ and $\widetilde{x}^3$: $\exp(2\psi)(\widetilde{x}^2, \widetilde{x}^3) := 1 + x_1^2$, $\omega(\widetilde{x}^2, \widetilde{x}^3) := -\frac{\tau_1 x_1}{1+x_1^2}$, $\exp(2\nu)(\widetilde{x}^2, \widetilde{x}^3) := \frac{1}{1+x_1^2}\{\tau_1^2(1 + x_1^2 - x_1^4) + \tau_2^2(1 - x_1^2) + \tau_3^2[(1 - x_0)^2 + \bar{x}^2] - \tau_3^2 x_1^2[(1 + x_0)^2 + \bar{x}^2]\}$, $\exp(2\mu_2)(\widetilde{x}^2, \widetilde{x}^3) := \frac{1-x_1^2}{1+x_1^2}$, $\exp(2\mu_3)(\widetilde{x}^2, \widetilde{x}^3) := \frac{1}{1+x_1^2}\{(1 + x_0)^2 + \bar{x}^2 - x_1^2[(1 - x_0)^2 + \bar{x}^2]\}$, where we seek a holonomic coordinates $\widetilde{x}^\mu(x)$, in our construction above, as the solutions of the first-order partial differential equations: $\frac{\partial \widetilde{x}^\mu}{\partial x^l} \equiv \psi^\mu_l = D^\mu_l(1 + \varpi(F))$. Provided, a world-deformation tensor is in the form $\Omega^m_l(F) = \delta^m_l(1 + \varpi(F))$, where $\varpi(F)$ is the scalar function of antisymmetric tensor of the gauge field. We do not at the moment specify the scalar function $\varpi(F)$ apart from the initial condition $\varpi(0) = 0$, which can be determined in intermediate stage of the analysis. Substituting these solutions into a bilinear form of norm $d\widetilde{s}^2$ of infinitesimal displacement on V_4, describing the stationary and axisymmetric spacetimes, we obtain $d\widetilde{s}^2 = \exp(2\nu)d\widetilde{t}^2 - \exp(2\psi)(d\widetilde{\phi} - \omega d\widetilde{t})^2 - \exp(2\mu_2)(d\widetilde{x}^2)^2 - \exp(2\mu_3)(d\widetilde{x}^3)^2$. Thus, we arrive at the metric of the stationary and axisymmetric space V_4 in the most commonly used $3 + 1$ formalism.

12.2. Field equations

In case of stationary and axisymmetric space V_4, the equations of 1D gravitation x_0, the frame-dragging potential x_1, and the ID field $\bar{x}$, generated by the stress-energy tensor of isolated spinning fluid, can be obtained in the Feynmann gauge: $\Delta x_0(x) = -\widetilde{J}_{(x_0)}(\widetilde{x})$, $\Delta x_1(x) = -\widetilde{J}_{(x_1)}(\widetilde{x})$, $(\Delta - \lambda_{\bar{x}}^{-2})\bar{x}(x) = -\widetilde{J}_{(\bar{x})}(\widetilde{x})$. Here the current $\widetilde{J}_{(\chi)}$ $(\chi := x_0, x_1, \bar{x})$ is referred to as $\widetilde{J}_{(\chi)} := (æ/2)\sqrt{-g}\, e^\mu_a e^\nu_b (\partial g_{\mu\nu}/\partial\chi)\widetilde{T}^{(ab)}$, provided, the Compton length of the ID-field $\bar{x}$ is $\lambda_{\bar{x}} = (\hbar/m_{\bar{a}}c) \simeq 0.4fm$. The system of non-linear differential field equations explicitly reads $\Delta x_0 = -\frac{æ}{2}\sqrt{-g}\,[\exp(-2\nu)\; W^2(\widetilde{\rho} + \widetilde{P}V^2) \times \frac{\partial g_{00}}{\partial x_0} + \exp(-2\mu_3)\widetilde{P}\frac{\partial g_{33}}{\partial x_0}]$, $\Delta x_1 = -\frac{æ}{2}\sqrt{-g}\,\exp(-\nu)\frac{\partial g_{01}}{\partial x_1}[\exp(-\nu)\omega \times W^2(\widetilde{\rho} + \widetilde{P}V^2) + \exp(-\psi)W^2(\widetilde{\rho} + \widetilde{P})V]$, $(\Delta - \lambda_{\bar{x}}^{-2})\bar{x} = -\frac{æ}{2}\sqrt{-g}\,[\exp(-2\nu)W^2(\widetilde{\rho} + \widetilde{P}V^2)\frac{\partial g_{00}}{\partial \bar{x}} + \exp(-2\mu_3)\widetilde{P}\frac{\partial g_{33}}{\partial \bar{x}}]$. These equations can be solved together with a diffeomorphism $\widetilde{x}^\mu(x) : M_4 \to V_4$. Adopting spherical polar coordinates (r, θ, ϕ) in flat space M_4, we then have $\frac{\partial \widetilde{r}}{\partial r} = \psi^{\widetilde{3}}_3 = D^{\widetilde{3}}_3(1 + \varpi)$, $\frac{\partial \widetilde{r}}{\partial \theta} = \psi^{\widetilde{3}}_2 = 0$, $\frac{\partial \widetilde{\theta}}{\partial r} = \psi^{\widetilde{2}}_3 = 0$, $\frac{\partial \widetilde{\theta}}{\partial \theta} = \psi^{\widetilde{2}}_2 = D^{\widetilde{2}}_2(1 + \varpi)$. Hence $d\widetilde{r} = \psi^{\widetilde{3}}_3(\widetilde{r}, \widetilde{\theta})\, dr$ and $d\widetilde{\theta} = \psi^{\widetilde{2}}_2(\widetilde{r}, \widetilde{\theta})\, d\theta$, which means that $r = r(\widetilde{r}, \widetilde{\theta})$ and $\theta = \theta(\widetilde{r}, \widetilde{\theta})$. Therefore, the stationary axisymmetric field components $\chi(r, \theta)$ are the solutions of the system of non-linear differential axisymmetric Poisson field equations. Recall that the infinite series expansion of the factor $1/|\mathbf{x} - \mathbf{x}'|$ in Green function of Poisson equation in spherical polar coordinates (r, θ, ϕ), in general, is $\frac{1}{|\mathbf{x}-\mathbf{x}'|} = \sum_{l=0}^{\infty} \frac{r^l_<}{r^{l+1}_>} P_l(\cos\theta)P_l(\cos\theta') + (\phi-$dependent terms), where P_l denotes a Legendre polynomial and $r_<(r_>)$ is the lesser (greater) of r and r'. By azimuthal symmetry, the ϕ-dependant terms do not contribute to this relation.

12.3. A global vacuum solution: horizons

The existence of a global vacuum solution, $\chi\,(\equiv x_0,\, x_1)$, outside of the matter, amounts to solving the field equations in a nearly Newtonian weak source limit: $\widetilde{T} \to 0$, $\bar{x} = 0$. In Lorentz gauge, it is given by means of fundamental solution of Poisson's equation as a retarded integral of the form familiar from linearized field equation theory: $\chi(\mathbf{x}) = \frac{1}{4\pi}\int \frac{\widetilde{J}^{ext}_{(\chi)}(|\mathbf{x}-\mathbf{x}'|)d^3x'}{|\mathbf{x}-\mathbf{x}'|}$, where the current $\widetilde{J}^{ext}_{(\chi)}(|\mathbf{x} - \mathbf{x}'|)$ denotes $\widetilde{J}^{ext}_{(\chi)}(|\mathbf{x} - \mathbf{x}'|) = 4\pi Q_{(\chi)}(|\mathbf{x} - \mathbf{x}'|)\delta(|\mathbf{x} - \mathbf{x}'|)$. The charge $Q_{(\chi)}(|\mathbf{x} - \mathbf{x}'|)$ is calculated in the spacetime region far outside the system, where we assume that the spacetime is almost Minkowski $g \simeq \eta$. The external metric $g^{ext} = g^{ext}(\chi)$ is then written $g^{ext}_{00} = \tau_1^2(1 - \tan^2\theta_1) + \tau_2^2\cos 2\theta_1 +$

doi: 10.52526/25792776-2021.68.2-236

$\tau_3^2[\cos^2\theta_1(1-x_0)^2-\sin^2\theta_1(1+x_0)^2]$, $g_{01}^{ext}=-2\tau_1 x_1$, $g_{11}^{ext}=-(1+\tan^2\theta_1)$, $g_{22}^{ext}=-\cos 2\theta_1$, $g_{33}^{ext}=-\cos^2\theta_1(1+x_0)^2+\sin^2\theta_1[(1-x_0)^2$. These Petrov type D vacuum solutions associate with the gravitational field of isolated massive stationary and axisymmetric rotating SPC. They completely characterized by its mass M_{SPC} and angular momentum J_{SPC}. The two double principal null directions define "radially" ingoing and outgoing null congruences near the SPC which is the source of the field. The horizon is a 2D surface of spherical topology, where the redshift factor $\alpha(r,\theta)$ vanishes $g_{00}^{ext}(r,\theta)=\alpha^2(r,\theta)=\tau_1^2(1-\tan^4\theta_1)+\tau_2^2(1-\tan^2\theta_1)+\tau_3^2[(1-x_0)^2-\tan^2\theta_1(1+x_0)^2]=0$. The gravitational infinite redshift suppresses any emission at the horizon. The solution, for given x_1, is $x_0^{(\pm)}=(\tau_3(1-x_1^2))^{-1}\{\tau_3(1+x_1^2)\pm\sqrt{\tau_3^2(1+x_1^2)^2-(1-x_1^2)(1-\tau_2^2x_1^2-\tau_1^2x_1^4)}\}$, where the discriminant has to be positive.

(i) At $x_1<1$, the gravitational field potentials $x_0^{(\pm)}$ yield two physical horizons. Their radii coincide with $r_g=R_g/2$ $(x_0^{(\pm)}=1)$ on the axis of rotation of SPC, located at $\theta=0$ (where $x_1=0$), where $R_g=2GM/c^2=2.95\times10^5\,M/M_\odot$ cm is the Schwarzschild radius (radius of a non-rotating black hole).

(ii) At $x_1(r_0)=1$, the outer oblate horizon can be formed only at infinity $r_0\to\infty$, where $x_0(r_0\to\infty)\to 0$.

(iii) For vanishing $x_1\to 0$, the solution, at $\tau_3\to 1$ ($\tau_2=\tau_1\to 0$), becomes static, spherically symmetric, yielding a single spherical event horizon $x_0^{(\pm)}(r)\to 1$ of previous model of non-rotating SPC.

The horizons are null surfaces because they are light-like. The hypersurfaces with $r_\pm$ are Killing horizons of the Killing vector field. A null hypersurface $\mathcal{N}$ is a Killing horizon of a Killing vector ξ if, on $\mathcal{N}$, ξ is normal to $\mathcal{N}$.

Suppose we adopt affine parametrization $l\cdot Dl^\mu=0$. Since $\xi=fl$ on $\mathcal{N}$ for some function f, it follows that $\xi\cdot D\xi^\mu=k\xi^\mu$ on $\mathcal{N}$, where $k=\xi\cdot\partial\ln|f|$ is called the surface gravity. Since ξ is normal to $\mathcal{N}$, Frobenius theorem implies that $\xi_{[\mu}D_\nu\xi_{\rho]}\big|_{\mathcal{N}}=0$, where '[...]' indicates total anti-symmetry in the enclosed indices. For a Killing vector field ξ, it implies $D_\mu\xi_\nu=D_{[\mu}\xi_{\nu]}$. Except at points for which $\xi=0$, one then has $k^2=(1/2)(D^\mu\xi^\nu)(D_\mu\xi_\nu)\big|_{\mathcal{N}}$. All points at which $\xi=0$ are limit points of orbits of ξ for which $\xi\neq0$, so continuity implies that this formula is valid even when $\xi=0$. One can then prove that k is constant on orbits of ξ: $\xi\cdot\partial k^2=-(D^\mu\xi^\nu)R_{\nu\mu\rho\sigma}\xi^\rho\xi^\sigma=0$, because of antisymmetry $R_{\nu\mu\rho\sigma}=-R_{\nu\mu\sigma\rho}$.

The surface gravity k is not a property of $\mathcal{N}$ alone, it also depends on the normalization of ξ, because if $\mathcal{N}$ is a Killing horizon of ξ with surface gravity k, then it is also a Killing horizon of $c\xi$ with surface gravity c^2k for any constant c. There is no natural normalization of ξ on $\mathcal{N}$ since $\xi^2=0$ there, but in an asymptotically flat spacetime there is a natural normalization at spatial infinity, e.g. for the time-translation Killing vector field k we choose $k^2\to-1$ as $r\to\infty$. This fixes k, and hence k, up to a sign, and the sign of k is fixed by requiring k to be future-directed.

12.4. External fields in the weak source limit

The external fields $\chi(|\mathbf{x}-\mathbf{x}'|)$ can be obtained straightforwardly in the weak source limit $\widetilde{T}\to0$, where the spacetime is almost Minkowski $g\simeq\eta$. It is sufficient then to consider an isolated system only in the asymptotic linearized regime. Without loss of accuracy, one can therefore keep only leading linear order-terms of fields, ignoring a second and higher order effects.

Linearized field equations guarantee conservation of 4-momentum and angular momentum of any body bounded by vacuum. So, we expand the solutions $\chi(|\mathbf{x}-\mathbf{x}'|)$ in powers of $x'/r=x'/|\mathbf{x}|$. It is convenient to perform calculation in the system's rest frame, where $P^j=\int T^{j0}d^3x=0$, with origin of coordinates at the system's center of mass $\int x^jT^{00}d^3x=0$. Hence, in suitable asymptotically Minkowski coordinates, where the stationary Killing vector is given by $m=\partial_t$, the resulting redshift factor $\alpha(M,r)$ and the frame-dragging potential $\omega(J,r)$ can be defined by means of the constants M and J, respectively, as the total mass and intrinsic angular momentum of the source.

These quantities are well substantiated by Komar integral. Recall that to every Killing vector field ξ in the volume V of spacetime on a spacelike hypersurface Σ, with boundary ∂V, one can associate the Komar integral $Q_\xi(V)=(q/16\pi G)\oint dS_{\mu\nu}D^\mu\xi^\nu$, for some constant q. Since Killing fields satisfy

doi: 10.52526/25792776-2021.68.2-236

the identity $D_\nu D_\mu \xi^\nu = R_{\mu\nu}\xi^\nu$, where $R_{\mu\nu}$ is the curvature tensor of V_4, then $Q_\xi(V) = \int_V dS_\mu J^\mu_{(\xi)}$, and the current $J^\mu_{(\xi)}$ is defined as follows: $J^\mu_{(\xi)} := qR^\mu_\nu \xi^\nu$. The current $J^\mu_{(\xi)}$ is conserved $D_\mu J^\mu_{(\xi)} = 0$, and the charge $Q_\xi(V)$ is time-independent, provided $J^\mu_{(\xi)}$ vanishes on the boundary ∂V.

If $\xi = k$, $q = -2$ is fixed by comparison with the formula derived for total mass (energy) in asymptotic expansion, the M integral can be recast into a coordinate-independent form $M = -(1/8\pi G)\oint_\infty dS_{\alpha\beta}\, D^\alpha k^\beta$.If $m = \partial_t$ is the Killing vector of axisymmetry, one obtains for $q = 1$ a coordinate-independent angular momentum integral $J = (1/16\pi G)\oint_\infty dS_{\alpha\beta}\, D^\alpha m^\beta$. For a weak source, $g \simeq \eta$, the total mass and angular momentum of an asymptotically flat spacetime is found by taking ∂V to be a 2-sphere at spatial infinity. If one chooses V to be on t constant hypersurface, then in Cartesian coordinates x^i $(i = 1, 2, 3)$, one has $dS_\mu m^\mu = 0$ and $m = x^1\partial_2 - x^2\partial_1$. For a weak source, therefore $J(V) \simeq \varepsilon_{3ij}\int_V x^i T^{j0}$.

Using Killing equations $D_{(\alpha}k_{\beta)} = 0 = D_{(\alpha}m_{\beta)}$, which lead to $D_\alpha D^\alpha k^\beta = R^\beta{}_\rho k^\rho$ and $D_\alpha D^\alpha m^\beta = R^\beta{}_\rho m^\rho$, the total mass and angular momentum above can be converted by means of Stoke's theorem as $M = -(1/4\pi G)\int_\Sigma R^\alpha{}_\beta k^\beta d\Sigma_\alpha$, $J = (1/8\pi G)\int_\Sigma R^\alpha{}_\beta m^\beta d\Sigma_\alpha$. The leading linear order-terms in asymptotic expansion of the redshift factor and the frame-dragging potential are given by $\alpha(R_g, r) \simeq 1 - R_g/2r + O(1/r^3)$, $\omega(J, r) = 2GJ/c^3r^3 + O(1/r^4)$. Equating these values respectively to the functions $[g^{ext}_{00}(M, r)]^{1/2}$ and $[-(1/2)\, g^{ext}_{01}(J, r)]$, where the components of the external metric, accurate to linearized order, become $g^{ext}_{00} \simeq 1 - 2\tau_3^2 x_0$, and $g^{ext}_{01} = -2\tau_1 x_1$, we finally obtain $x_0(r) = R_g/2\tau_3^2 r$, $\quad x_1(r) = 2GJ_{SPC}/\tau_1 c^3 r^3$. The potential of dragging of inertial frames ω drops very rapidly with increasing radius. The maximal frame-dragging effects therefore can only be observed in the immediate vicinity of the event horizon: $x_{1(H)} = \omega_H/\tau_1 \simeq 2GJ_{SPC}/\tau_1 c^3 R_g^3 = J_{SPC}c^3/4\tau_1 G^2 M^2$. In physical units the angular momentum $J_{SPC} = aM_{SPC}$ becomes $J_{SPC} = a_* M_{SPC}\frac{GM_{SPC}}{c^2}$, such that $x_{1(H)} = (2ca_*/\tau_1 GM_{SPC})$, where a_* is the dimensionless angular momentum $|a_*| \leq 1$. The special case $a = M_{SPC}$ is the extreme solution. From this we get the maximal specific angular momentum $J^{max}_{SPC} = (GM_{SPC}/c)$, and that $x_{1(H)} = 2a_*/\tau_1 J^{max}_{SPC} < 1$.

The Petrov type D vacuum solutions for stationary axisymmetric rotating SPC, therefore, satisfy the Robinson's theorem for Kerr solutions in vacuum: the solutions, (i)-are asymptotically flat, (ii)-contain a smooth convex horizon, (iii)- are nonsingular outside the horizon, and are uniquely specified by two parameters: the mass M_{SPC} and angular momentum J_{SPC}. The angular velocity of a SPC is the sum of two terms: the classical one given by the intrinsic angular velocity Ω and the frame dragging ω from the rotation of absolute space.

Near the horizon of SPC, for example, where the redshift tends to zero ($\alpha \to 0$), the angular velocity of matter Ω is completely dominated by the frame-dragging effect. Whatever the intrinsic angular momentum of the incoming matter is, this matter is forced to rotate with the local angular velocity ω, which is the maximal angular velocity at event horizon. When matter falls, say into a nonrotating black hole, it is forced to zero rotation near the horizon despite its angular momentum.

The event horizon is a Killing horizon for the Killing field $\xi = k + \Omega_H m$, with $\xi^2 = 0$, where Ω_H denotes the angular velocity of the horizon as it is rigidly rotating. Let $m = \partial_t$ be the axial Killing field, and $\widetilde{u} = \widetilde{u}^t(1, \Omega_H, 0, 0)$ be the four-velocity of SPC. We may choose $\tau_2 = 0$, $\tau_1 = \tau_3 = 1/\sqrt{2}$. Since $x_{1(H)} < 1$, analogous to the Kerr black hole, there are the outer horizon or event horizon by its radius r_+, and the inner horizon or Cauchy horizon by its radius r_-. The radii r_+ and r_- coincide with r_g $(x_0^{(\pm)} = 1)$ on the axis of rotation of SPC, located at $\theta = 0$ $(J_{SPC} = 0)$. The oblate event horizon is the surface of the oblate spheroid with the semimajor r_+ and semiminor r_g axes, respectively. Dependent of the value of the potential $x_{1(H)}$, the Cauchy horizon either is the surface of the prolate spheroid with the semimajor r_g and semiminor r_- axes, or oblate spheroid with the semimajor r_- and semiminor r_g axes, respectively. The radii of the oblate event horizon and the Cauchy horizon are given by $r_\mp = r_g/\tau_3^2 x_0^{(\pm)}$. These radii, as the function of $x_{1(H)}$, are plotted in Fig. 10. Since $\alpha(r_+) = 0$, any observer, but the ZAMO, rotates at the outer horizon with the angular velocity Ω_H. The angular velocity of ZAMO is $\Omega = \omega$, which will have vanishing specific angular momentum: $\widetilde{u}^\phi = g_{\phi\alpha}\widetilde{u}^\alpha = g_{\phi\phi}\widetilde{u}^\phi + g_{t\phi}\widetilde{u}^t = \widetilde{u}^t(\omega g_{\phi\phi} + g_{t\phi}) = \widetilde{u}^t g_{\phi\phi}(\omega + g_{t\phi}/g_{\phi\phi}) = 0$. It is therefore convenient to express physical observables with respect to ZAMO. In the slow-rotation limit, the angular momentum of SPC, as rigidly rotating body, can be given in the form $J = \int_{M_H}(\widetilde{\rho} + \widetilde{P})(\widetilde{u}^t)^2(g_{t\phi} + \Omega g_{\phi\phi})\sqrt{-g}d^3\widetilde{x} \simeq$

doi: 10.52526/25792776-2021.68.2-236

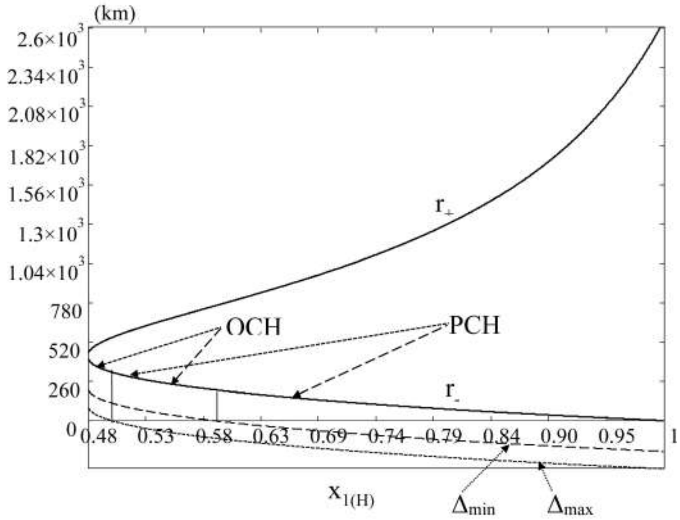

Figure 10. The radii $r_\pm$ of outer and inner horizons v.s. potential $x_{1(H)}$, for M82X-2, with the mass $M \simeq 138.5 - 226\, M_\odot$, i.e. $r_g = R_g/2 = r_g^{max} - r_g^{min} \simeq 204.3 - 333.4$km.
Abbreviated notations: $\Delta_{min} := r_- - r_g^{min}$, $\Delta_{max} := r_- - r_g^{max}$, OCH :=Oblate Cauchy Horizon, PCH :=Prolate Cauchy Horizon.

$\int_{M_H}(\widetilde{\rho}+\widetilde{P})(\widetilde{u}^t)^2 g_{\phi\phi}(\Omega_H - x_{1(H)}/\sqrt{2})\sqrt{-g}d^3\widetilde{x}$, which in leading order in the expansion for Ω_H reads $J \simeq \frac{8\pi}{3}\int_0^{R_{SPC}} r^4 \frac{(\rho+P)}{(1-r_g/r)\sqrt{1-2M(r)/r}}(\Omega_H - 2a_*/4J^{max}_{SPC})dr$, where R_{SPC} is the radius of SPC.

12.5. Microscopic model of stationary and axisymmetric rotating SPC

The key physical properties of SPC depend very little on the details of concrete SPC-model, as they are a direct consequence of the fundamental features of underlying gravitation theory. The latter explores a spontaneous breaking of gravitation gauge symmetry and a rearrangement of vacuum state. We therefore expect that the key physical properties of non-rotating SPC, outlined in Section 9, even though without being carefully treated, retain for a rotating SPC too. Some evidence for a simplified physical picture, for example, at $x_1 < 1$ in the weak source limit (iii), is highlighted in Fig. 11 to guide the eye, without loss of generality. *Model building of the periodic source M82X-2.* With this guidelines to follow, we may proceed to Fig. 12 and Fig. 13. Fig. 12 emphasizes an apparent distinction between Kerr model and rotating SPC in second half of its lifetime. Fig. 13 schematically plot the SIMBH model of the periodic ULX M82X-2, constituting mass-exchange binary with the O/B-type donor star. The OEH-surface of the spheroid has the polar equation $R = R(\vartheta)$, where $\frac{r_g^2}{R^2} = \cos^2\vartheta + (1-e^2)\sin^2\vartheta$, provided, ϑ is the reduced or parametric latitude $(-\pi/2 < \vartheta < \pi/2)$, e denotes the eccentricity $e := e(x_{1(H)}) = \sqrt{1 - r_g^2/r_+^2(x_{1(H)})}$, while $r_+(x_{1(H)})$ and $r_g := R(0)$ are the semimajor and semiminor axes, respectively, of the rotated ellipse of OEH.

12.6. Corrections to the characteristic phase profile of M82 X-2 introduced by OEH

The OEH introduces the corrections to the characteristic phase profile of previous model of X-ray radiation from M82X-2 derived in approximation of spherical EH. In the case of OEH, the pulsed luminosity reads (Ter-Kazarian & Shidhani, 2017): $\widetilde{L}(M,d,T_s,e,\theta,\phi,\alpha,t) = S_{zx}\,\sigma T_s^4 = L_0(M,d,T_s)\,\Phi'(e,\theta,\phi,\alpha,t)$, where the amplitude is $L_0(M,d,T_s) \simeq 1.05\times10^4\,(\mathrm{erg\,s^{-1}})\frac{M}{M_\odot}\,\frac{d}{\mathrm{m}}\,\frac{T_s^4}{K^4}$, and the corrected phase profile $\Phi'(e,\theta,\phi,\alpha,t)$ is $\Phi'(e,\theta,\phi,\alpha,t) = \Upsilon(e,\alpha)\,\Phi(\theta,\phi,\alpha,t)$. Provided, the correction function is denotetd by $\Upsilon(e,\alpha) := C_1(e,\alpha)/2\pi r_g$, $\Phi(\theta,\phi,\alpha,t)$ is the phase profile in case of spherical EH: $\Phi(\theta,\phi,\alpha,t) \equiv \sqrt{1-\sin^2\beta\sin^2(\phi+A)}$. Here the spherical triangle, with the lengths of three sides $\theta = \widehat{(z,s)}$, $\alpha = \widehat{(s,n)}$ and $\beta = \widehat{(z,n)}$, is solved by the law of cosines $\cos\beta(\theta,\alpha,t) = \cos\theta\cos\alpha + \sin\theta\sin\alpha\cos\Omega t$, $\cos A(\theta,\alpha,t) = \frac{\cos\alpha - \cos\theta\cos\beta}{\sin\theta\sin\beta}$. Consequently, the phase profile can be recast into the form $\Phi'(e,\theta,\phi,\alpha,t)$

doi: 10.52526/25792776-2021.68.2-236

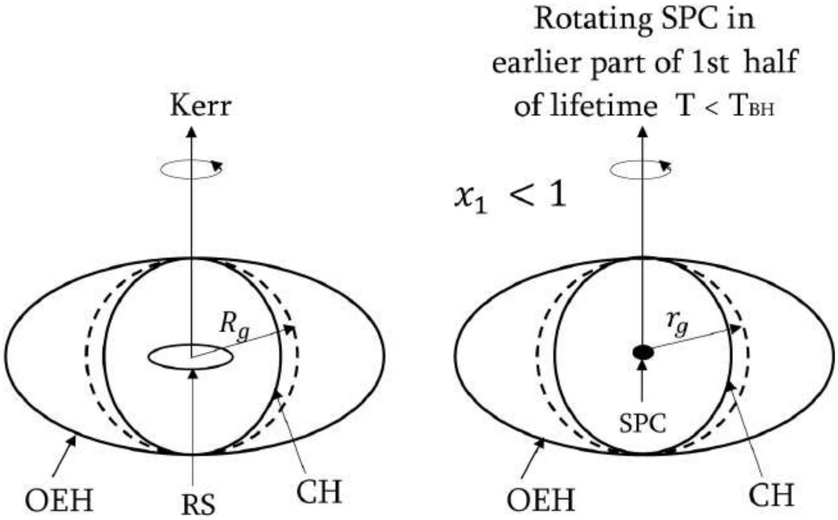

Figure 11. *Left panel*: Kerr model of spinning black hole. The meaningless ring singularity occurs at the center inside the black hole. *Right panel*: Microscopic model of rotating SPC in earlier part of first half of its lifetime $T < T_{BH}$. The picture is not to scale.
Abbreviated notations: OEH :=Oblate Event Horizon, SPC :=Superdense Proto-matter Core, RS :=Ring Singularity, PCH := Prolate Cauchy Horizon.

$= \frac{1}{\sqrt{1-e^2}}\left[1-\sum_{n=1}^{\infty}\left(\frac{(2n-1)!!}{2^n n!}\right)^2 \frac{e_1^{2n}(\alpha)}{2n-1}\right]\Phi(\theta,\phi,\alpha,t)$, where $n!!$ is the double factorial $n!! = \prod_{i=0}^{l}(n-2i)$, $l = [n/2]-1$. The Fig. 14 - Fig. 18 are the examples, revealing the diversity of the behavior of corrected phase profiles versus the time, viewed at given position angles, for different values of eccentricity.

13. A study of intermediate mass black hole-candidates

A good deal of evidence that IMBHs could be the seeds for the growth of SMBHs. The IMBHs are the long-sought missing population falling within the gap between stellar mass BHs, $\sim 3-100\,M_\odot$, and SMBHs. The *leftover* populations of IMBHs at low redshift, i.e. those seed BHs that did not grow into SMBHs (the *leftovers* of the early Universe), are expected to be found in the local Universe and up to $z \sim 2.4$, namely in dwarf star-forming galaxies, as these have undergone a quieter merging/accretion history; in nearby globular clusters; or in the form of off-nuclear ultraluminous and hyperluminous X-ray sources (ULXs and HLXs) in the halos and spiral arms of large galaxies. We need hardly add that the study of an accretion physics of IMBHs, incorporating their observed number so far available on over the last decades, has been a prompt for pushing forward many intriguing proposal towards formation and growth of initial seed BHs. These scenarios view IMBHs as a laboratory to giving hints as to the proper path toward the formation of the first galaxies and the quenching of star formation, for studies of the epoch of reionization, and for proving, in general, that a disk-jet coupling mechanism takes places in BHs of all masses. There are three formation scenarios for IMBHs: (i) the merging of stellar mass BHs and other compact objects; (ii) the runaway collision of massive stars in dense stellar clusters and the collapse of the collision product into an IMBH; (iii) they are primordial BHs formed in the early Universe being extremely dense. In such a dense medium, there must have been initial density perturbations that could then grow under their own gravity. Different models for the early universe vary widely in their predictions of the scale of these fluctuations.

Without care of the historical justice and authenticity, it should be emphasized that the ultraluminous X-ray sources (ULXs) have attracted a great deal of observational and theoretical attention, in part because their luminosities suggest that they may harbor IMBHs with an ubiquitous feature of the mass fits of more than $10^2 - 10^4\,M_\odot$. A strong argument in favor of IMBHs is the presence of a soft, $0.1-0.2$ keV component in their spectra. In addition to the search for HLXs, IMBHs can, in principle, be discovered in the center of low-luminosity active galactic nuclei (LLAGN), and *dwarf*

doi: 10.52526/25792776-2021.68.2-236

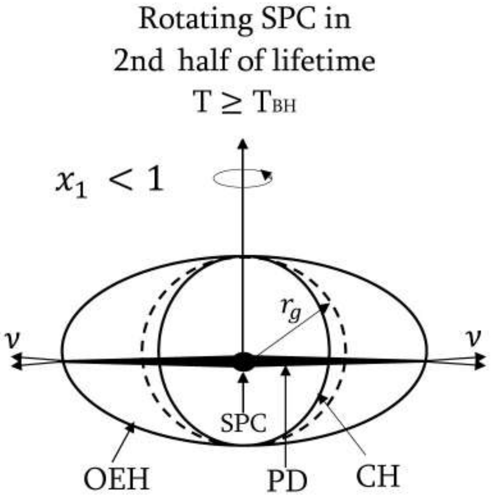

Figure 12. Microscopic model of rotating SPC in second half of its lifetime. An infalling matter already formed a thin co-spinning proto-matter disk which has reached out the edge of the outer oblate event horizon. A singularity inevitably disappears and the neutrinos escape to outside world through the vista.
Abbreviated notations: OEH :=Oblate Event Horizon, SPC :=Superdense Proto-matter Core, PCH := Prolate Cauchy Horizon, PD :=Proto-matter Disk.

galaxies. These low-mass galaxies are expected to have undergone quiet merger histories and are, therefore, more likely to host lower-mass central BHs, a fraction of which is expected to lie in the IMBH range. However, it is premature, therefore, to draw conclusions and only time will tell whether any of these intriguing proposals is correct and which of the hypothesized IMBH formation scenario is actually realized in nature.

The MTBH allows to construct also microscopic models of 137 plausible accreting IMBH-candidates (Ter-Kazarian & Shidhani, 2019). In the sequel we have established that versus a broad range of the central values of physical parameters, such configurations present the microscopic models of IMBHs. The mass estimates collected from the literature of all the observational evidence for 137 IMBH-candidates, even thought there are still large uncertainties, allow us to undertake a large series of numerical simulations to obtain all their physical characteristics. Below we briefly reflect upon a few key points.

13.1. Primer on the microscopic models of IMBHs

In our setting we retain the rather concrete proposal of preceding developments of the model of a non-rotating SPC described in Section 8, without going into the subtleties, as applied to the study of IMBHs. For brevity reasons, we proceed in relatively simple way toward first look at some of the associated physics, which is quick to estimate the physical properties of more realistic SPC-configurations. The equations describing the equilibrium SPC include the gravitational and ID field equations, the hydrostatic equilibrium equation, and the state equation of the spherical-symmetric distribution of baryonic-quark matter in many-phase stratified states specified for each domain. The last equation will be discussed separately in the next Section step-by-step away from the domain of lower density up to the domain of higher density. We implement our scheme by considering the equilibrium configurations of non-rotating SPC of the two classes as described in secttion 8, with spherical-symmetric distribution of matter in many-phase stratified states. A layering of configuration is a consequence of the onset of different regimes in equation of state.

doi: 10.52526/25792776-2021.68.2-236

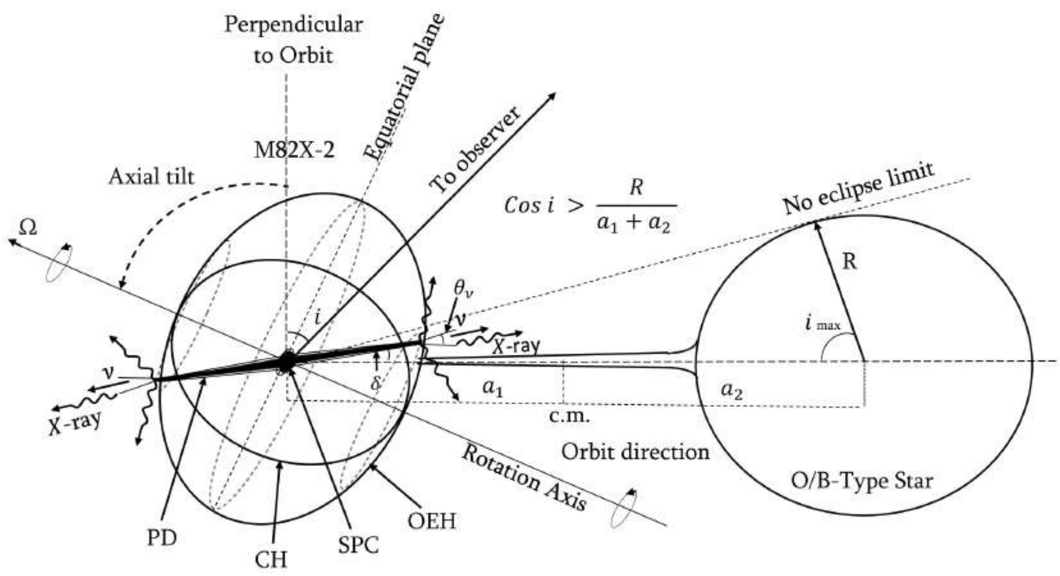

Figure 13. A schematic SIMBH model of M82X-2 constituting mass-exchange binary with the O/B-type donor star. The angle i is the binary inclination with respect to the plane of the sky. No eclipse condition holds. In final stage of growth, PD has reached out the edge of the OEH. The thermal defuse blackbody X-rays beams may escape from SIMBH through a thin belt area $S = 2\pi R(\theta)d$ to outside world that sweep past Earth like lighthouse beacons. Parameters of a binary system is viewed in the orbital plane. The picture is not to scale.
Abbreviated notations: OEH :=Oblate Event Horizon, SPC :=Superdense Proto-matter Core, PCH := Prolate Cauchy Horizon, PD :=Proto-matter Disk.

13.2. Simulations and the results

We are led to the numerical integration of equations of equilibrium SPC-configurations, including the state equation specified for each domain at ID-regime, leading from the center of configuration up to the surface. For the central parameters given in table 1 of (Ter-Kazarian & Shidhani, 2019), the results of the numerical integration of the equations of I-class configurations of 137 IMBHs are presented in table 2 of (Ter-Kazarian & Shidhani, 2019). Similar reasonings lead us also to compute corresponding characteristics referring to the II-class configurations. But it is not convenient to bring here the table data, as they are too large. Moreover, they are rather lame to specify completely all the relations between the integral characteristics. Therefore, the most straightforward and perhaps natural way to proceed is to present the figures, which clearly highlight a main difference between both classes. For 137 IMBHs of both class configurations, the masses M, M_1 and M_0, the number of baryons and the gravitational packing coefficients are given in Fig.17 versus central density and radius. The radial profiles of the pressure and the density; the gravitational (x_0)- and ID (x)- potentials; the g_{00} and g_{33} metric components; the ratios of electron-neutron (en), electron-proton (ep) and proton-neutron (pn) concentrations are plotted in Fig.18 for the sources M82X-1. The state equations for the sources M82 X-1 and IC 467 are presented in Fig.19. As in Section 10, the special units in use, denote $P_{OV} = 6.469 \times 10^{36}\,\mathrm{erg\,cm^{-3}}$, $\rho_{OV} = 7.195 \times 10^{15}\,\mathrm{g\,cm^{-3}}$ and $r_{OV} = 13.68\,\mathrm{km}$.

Cutting short where our analysis is leading to, we note that there is still very much to be gained by further study of the issues that we raised here.

doi: 10.52526/25792776-2021.68.2-236

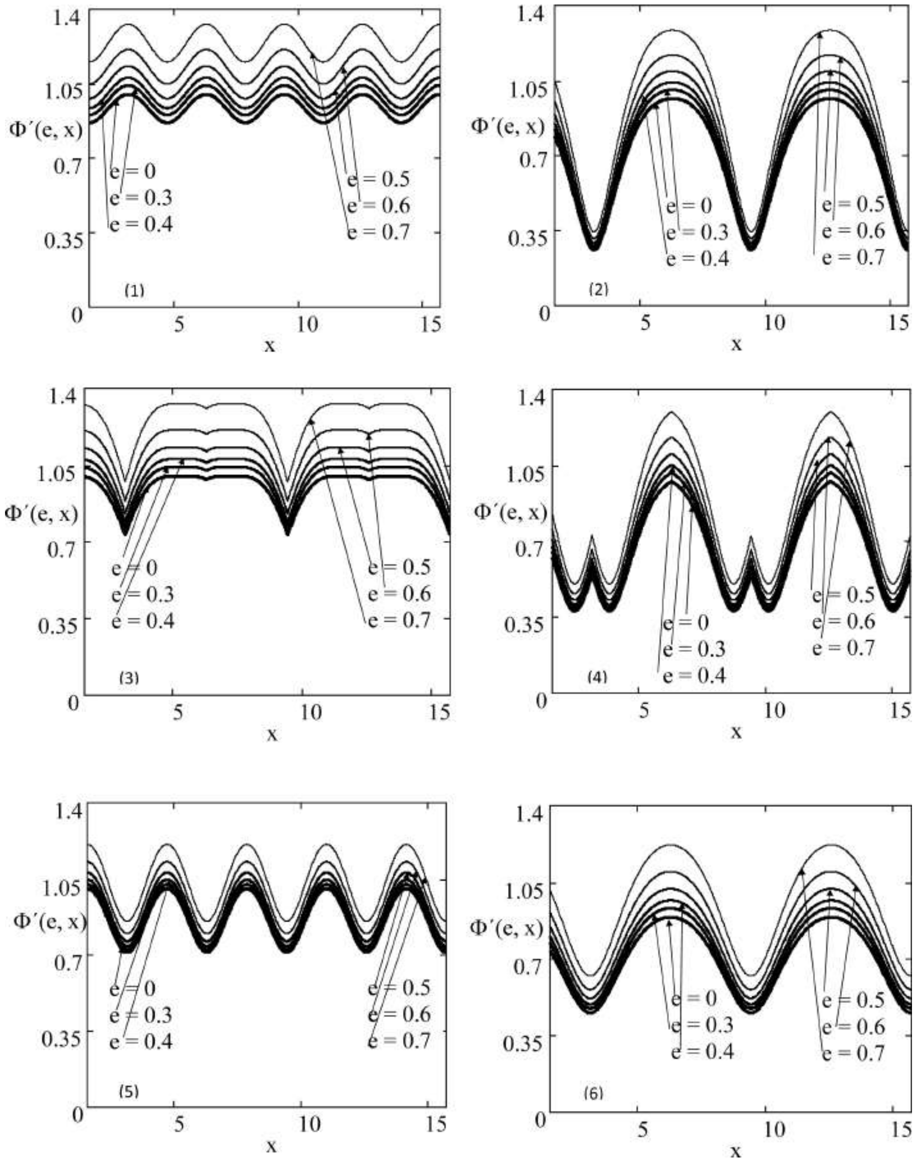

Figure 14. Corrected characteristic phase profiles versus the time ($x \equiv \Omega t$), viewed at the following position angles (θ, α, ϕ): (1) $(45^0, 30^0, 0^0)$; (2) $(45^0, 30^0, 90^0)$; (3) $(45^0, 30^0, 135^0)$; (4) $(45^0, 30^0, 60^0)$; (5) $(45^0, 90^0, 90^0)$; (6) $(45^0, 18^0, 90^0)$.

14. The physical outlook and concluding remarks

In this Section we briefly expose the main features of our physical outlook and draw a number of conclusions. The following items once again resume a whole physical picture.

• Ambartsumian's stemming idea of stellar association as a dynamical entity of groups of stars with positive total energy had far-reaching implications for subsequent star formation theories. Based on the observations in 1947 of stars of O and B spectral types and T Tauri and flare stars that cluster very loosely, Ambartsumian suggest a concept of OB and T associations, coined by him as Stellar Associations. These considerations prove that the ideas about the simultaneous emergence of stars and diffuse matter from denser and more massive bodies are more fruitful and correspond to reality. In these associations the stars differ from the surrounding stars by having a greater partial density.

In 1953, Ambartsumian paid attention to the fact that in short burst periods, UV Ceti type variable stars acquire some features similar to characteristics of T Tauri stars, and that the T Tauri type stars along with continuous and irregular changes of brightness also show flare type changes. He con-

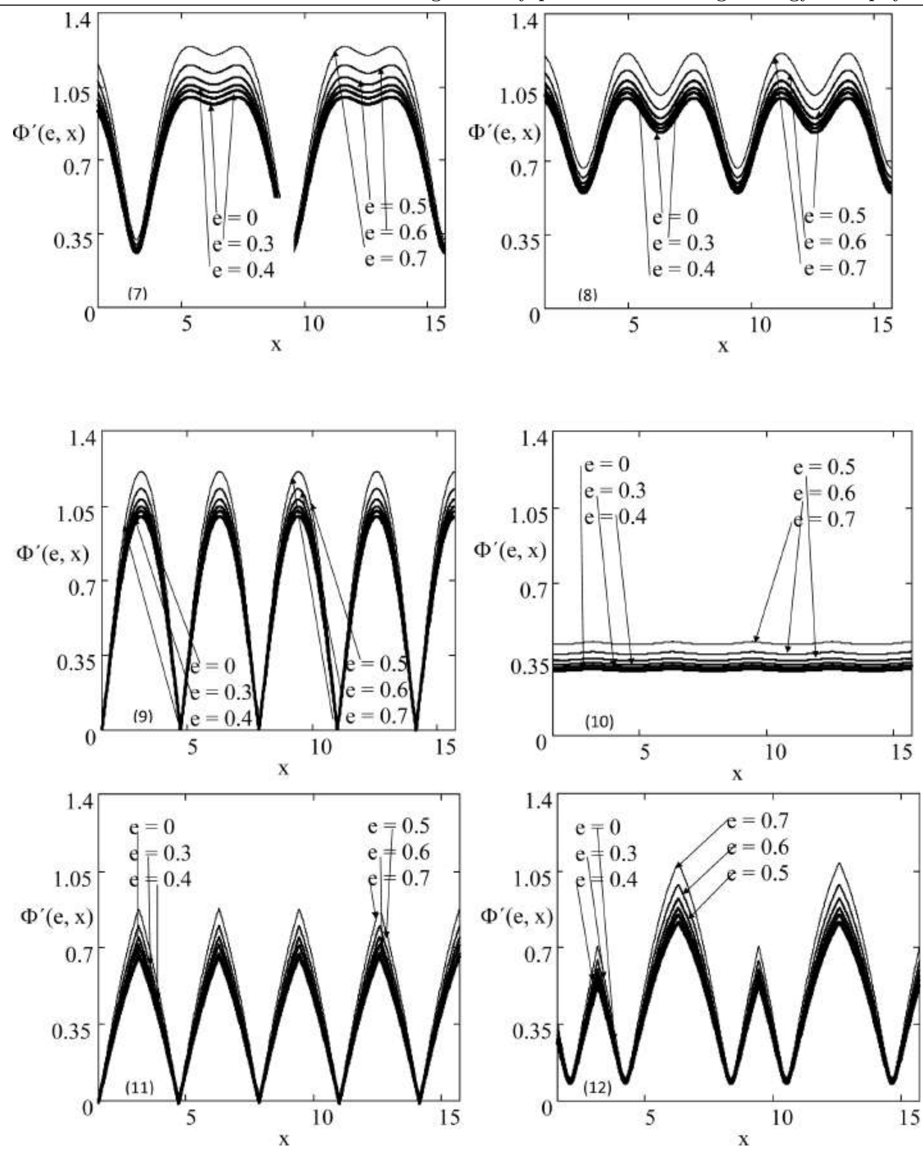

Figure 15. Corrected characteristic phase profiles versus the time ($x \equiv \Omega t$), viewed at the following position angles (θ, α, ϕ): (7) $(45^0, 60^0, 90^0)$; (8) $(45^0, 78.3^0, 90^0)$; (9) $(90^0, 90^0, 180^0)$; (10) $(90^0, 0.6^0, 72^0)$; (11) $(90^0, 30^0, 60^0)$; (12) $(72^0, 30^0, 60^0)$.

cluded that these two types of objects are genetically related. The ultraviolet excess observed in some T Tauri stars has approximately the same energy distribution as the emission from flares of UV Ceti type stars. A comprehensive study of this phenomenon allows Ambartsumian in 1968 to conjecture that *the flare stars are the earliest evolutionary stages of the dwarf stars*. Moreover, he believes that the stage of a flare star follows a stage of T Tauri type at overlapping of these stages.

• Ambartsumian argued that a superdense companion in the close neighborhood of that star (red dwarf) gives the thermal radiation of the prefuor. While it cannot be ruled out that the envelope is ejected by a super-dense companion. Proceeding from the fact that prefuors and flare stars are members of the same stellar associations, Ambartsumian concluded that the processes of decay and release of energy in both cases have the same physical nature. Ambartsumian believes that each outburst is the result of the explosion (when brightness increase time is often measured in seconds) of a certain portion of the *prestellar superdense matter*, which came out from the inner layers of the star, where a prestellar matter remained for a relatively long time before explosion.

Ambartsumian, therefore, rejected the assumption of thermonuclear reactions as the main sources

doi: 10.52526/25792776-2021.68.2-236

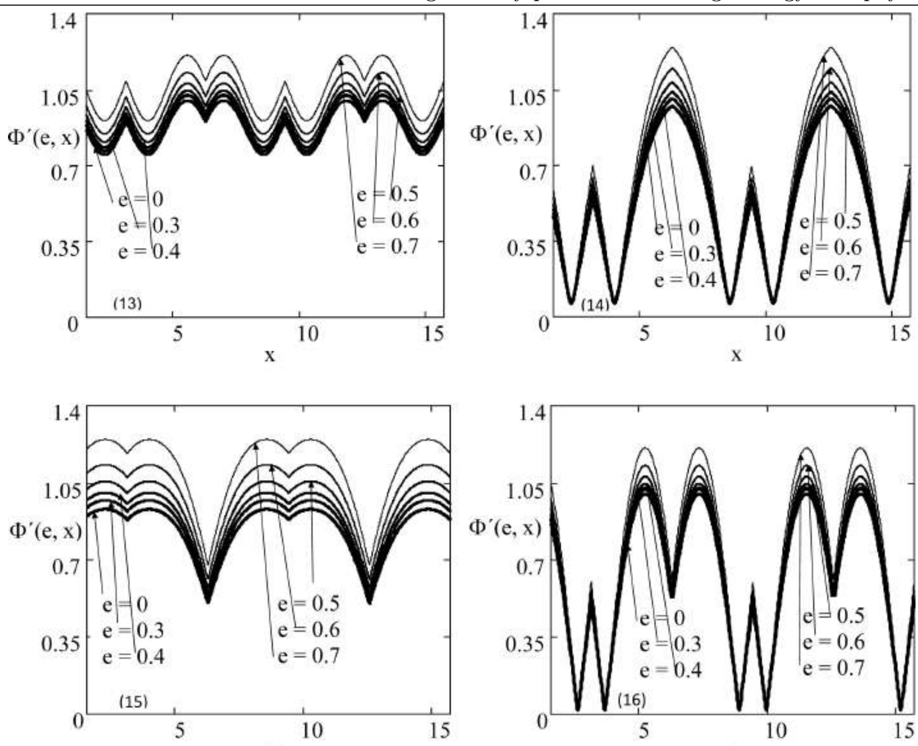

Figure 16. Corrected characteristic phase profiles versus the time ($x \equiv \Omega t$), viewed at the following position angles (θ, α, ϕ): (13) $(60^0, 90^0, 60^0)$; (14) $(60^0, 45^0, 60^0)$; (15) $(60^0, 153^0, 60^0)$; (16) $(1.2^0, 90^0, 60^0)$.

of this energy. Based on the idea that a portion of superdense prestellar matter transfers from the stellar interiors to the surface layers of young stars, Ambartsumian predicted the existence of *fast* and *slow* flares, which were later discovered, and gave an explanation to the Fuor phenomenon.

Ambartsumian predicted the expansion of the associations, which was later observed. These ideas have a subsequent influence in his interpretation of active galaxies.

Ambartsumian was also first to call attention to the instability and activity of galactic cores and, thus, raised the issue of Activity of Nuclei of Galaxies. In his report at the Solvay Conference on Physics (Brussels 1958), Armbartsumian claimed that the activity of the galactic nuclei determines the most significant processes in the evolution of galaxies. He argued that so-called *D-bodies* exist in nature, which are responsible for the activity of the nuclei of galaxies, and that galaxies are born from the explosion of such *D-bodies*. The nuclei of galaxies are the places where new objects are generated, and the fact that the activity can be found in galaxies with a wide range of distances strongly suggests that the activity goes on at all epochs. Violent events in galaxies are manifestations of mass creation. From these events huge fluxes of relativistic particles and rapidly moving gas clouds are generated. Quasars with *intrinsic redshifts* are also ejected, and they are probably related to the mechanism through which new galaxies are formed. Following Armbartsumian, it is reasonable to consider the possibility that systems of galaxies with positive total energy also originate in this way.

Ambartsumian concluded that the phenomena all pointed to ejection from superdense state, and that the galactic nuclei must contain superdense bodies of huge mass and some kind of non-stellar objects of unknown nature. He, in fact, conjectured that such an eruptive activity is due to the violent outburst events of transformations of superdense matter in supermassive compact D-bodies in galaxies, away from the accretion physics, where the creation process is at work. This signifies that every nucleus is made up of three components: *stellar population, gas and supermassive body.* Dynamically, the nucleus evolves independently of the rest of the galaxy. Thus, his conclusion was

doi: 10.52526/25792776-2021.68.2-236

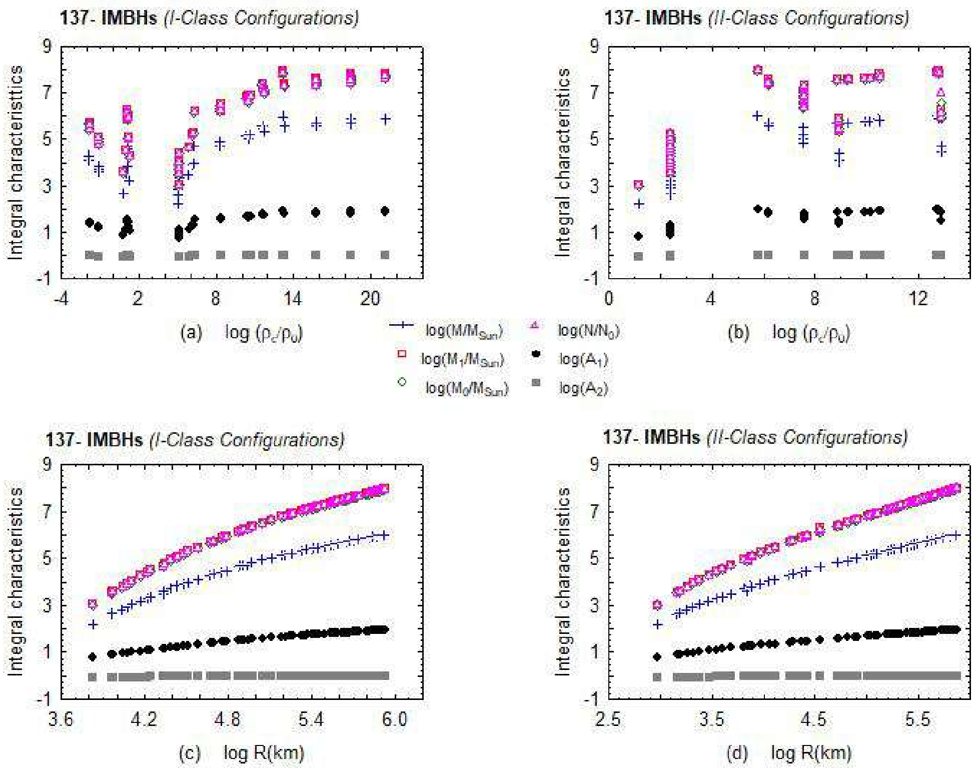

Figure 17. The 137 IMBH-configurations: the masses (over solar mass), number of baryons (over $N_0 = 10^{57}$) and gravitational packing coefficients versus central density and radius.

that observations produce almost innumerable evidence in favor of ejections and explosions and are rather scanty regarding the processes of condensation and collapse. In the observable Universe the processes of expansion and diffusion are responsible for the majority of changes occur now. These violent explosions were the manifestations of mass creation events.

A thousands of galaxies with strong ultraviolet excess have been discovered ever since in Byurakan Observatory under his direction. Ambartsumian's student, B. Markarian (well known for Markarian galaxies), completed a brilliant survey of galaxies known by his name with UV excess using the 1-m Schmidt telescope of the Byurakan Observatory.

• The most important property of superdense states, as shown by Ambartsumian and Saakyan, must be the presence of hyperons in the star, in addition to neutrons. The temperature is assumed so low that all types of fermions are degenerate. With increasing density, different hyperons are successively appear and increase in number. They should be stable because of Pauli's exclusion principle. Paradoxically, the smallest threshold density does not correspond to the Λ-hyperon, having the smallest mass at rest, but to the Σ^--hyperon. This suggests that a sufficiently massive celestial body in gravitational equilibrium should consist of a hyperon core, a neutron layer, and an outer envelope with the usual composition made of electrons, protons and composite nuclei. At density $\rho < \rho_n = 1.28 \times 10^7 \mathrm{gcm}^{-3}$, the gas consists of protons and electrons. At $\rho = \rho_n$ neutrons appear. At density $\rho > 10^8 \mathrm{gcm}^{-3}$, the number of neutron is much larger that numbers of protons and electrons. The individual atomic nuclei will no longer play an important role. At baryon density $N \geq 6.4 \times 10^{38} \mathrm{cm}^{-3}$, i.e. $\rho = \rho_{\Sigma^-} = 1.1 \times 10^{15} \mathrm{gcm}^{-3}$, the first hyperons appear. Although the rest masses of the hyperons $\Lambda, \Sigma^+, \Sigma^0$ are smaller than that of the Σ^-, nevertheless first Σ^--hyperons appear. Highly degenerate matter contains hyperons and μ^--mesons in addition to nucleons. At $\rho = \rho_\Lambda$, Λ-hyperrons appear, and with a further increase of density, other heavier hyperons make an

doi: 10.52526/25792776-2021.68.2-236

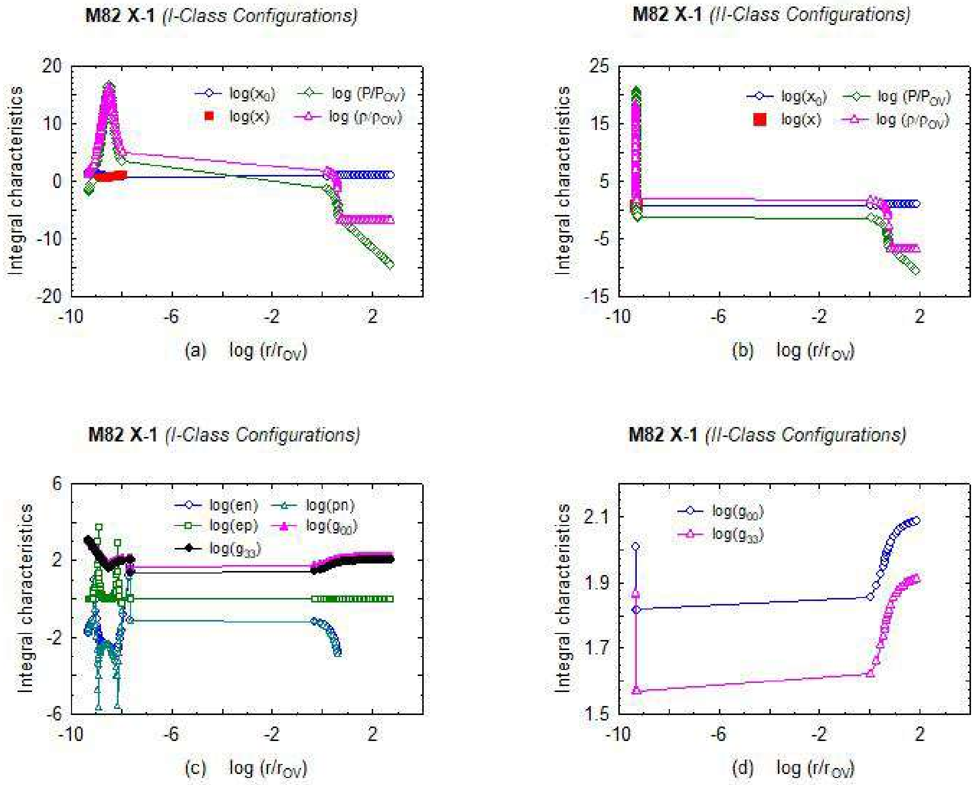

Figure 18. The M82X-1: the radial profiles of pressure and density; gravitational (x_0)- and ID (x)-potentials; g_{00} and g_{33} metric components; the ratios of electron-neutron (en), electron-proton (ep) and proton-neutron (pn) concentrations.

appearance altogether with . For baryons densities exceeding 5×10^{16}gcm^{-3}, the following difficulties arise in the study of state equation: (i) very strong repulsive forces arise whose properties are not know well; (ii) the relative concentrations of various types of baryons can be strongly affected by the presence of higher hyperons having masses grater than that of the Ξ-hyperon. At still higher densities, π-mesons must also make their appearance as a Bose gas.

• The calculations made by Ambartsumian and Saakyan shown that the masses of equilibrium configurations of a non-rotating baryon ideal gas are of the ordder of a half of a solar mass, and that the radii reach out several kilometers. At small interparticle distances $\sim$ 0.4fm or less, strongly intense repulsive forces apparently come into action. The baryonic gas, therefore, can no longer be considered an ideal gas at baryon densities exceeding 1040cm-3N which corresponds to the short distances $l <$ 0.5fm. The masses of the degenerate configurations calculated for a real Fermi gas of baryons under the assumption that repulsive forces are active between the baryons, are appreciably larger than the masses of configurations of an ideal gas. The sizes and masses of the outer regions of a baryon star, i.e. neutron or proton-electron layers, comprise a small part of the total mass and size of the star at fairly high central densities. The bulk of the star's mass in those cases goes into the hyperon core.

• The study of the relationship between stellar parameters and total number of baryons in the star, and the dependence of that number on the density value at the center are problems of heightened interest. The configuration of lesser mass will be the more stable. A large mass exhibits a high density at the center. This must signify a large gravitational mass defect, in consequence of which the total mass of the configuration should be smaller in this case. The gravitational mass defect $\triangle M = nm_H - M$ of baryon stars has been investigated. Reviewing notations M is the mass of the star, n is the number of baryons present, and m_H is the mass of hydrogen atom. It is shown that the configuration with

doi: 10.52526/25792776-2021.68.2-236

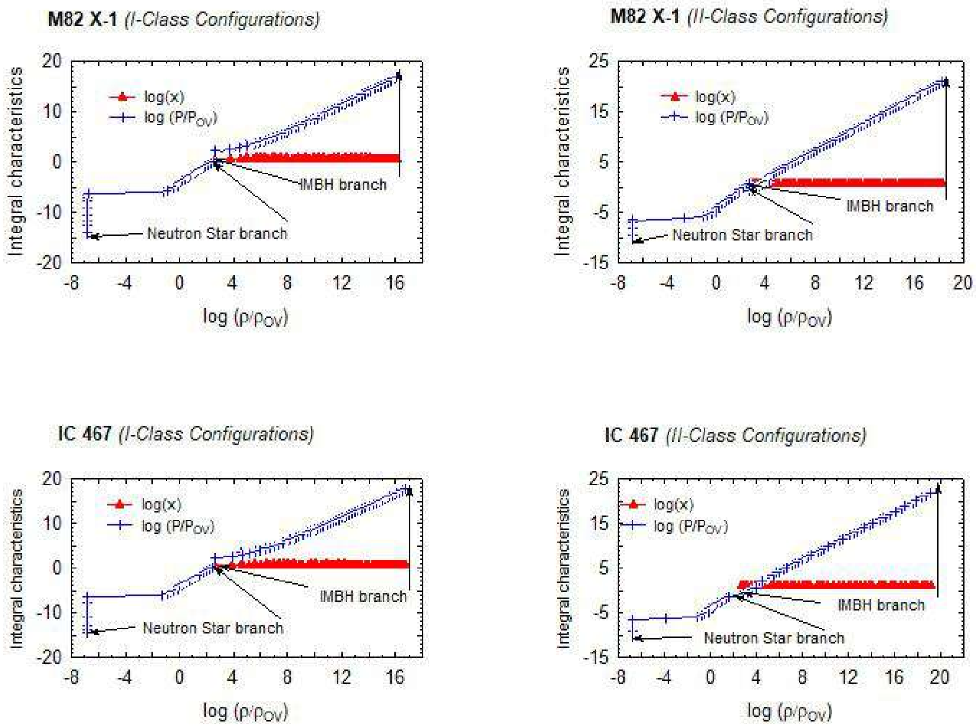

Figure 19. The state equations for M82 X-1 and IC 467.

$t_n(0) \lesssim 2.4$ is absolutely stable in the case of ideal gas, while the configuration with $t_n(0) \lesssim 2.9$ is absolutely stable in the case of real gas. The rest of configurations are either metastable or unstable. There is one intriguing feature in the unstable branches, namely that for $t_n(0) \gtrsim 4.2$ in the case of ideal gas and for $t_n(0) \gtrsim 3.15$ in the case of real gas, the binding energy $\triangle M$ becomes negative. Such states will be less stable than the others.

• A more detailed analysis of the absolute gravitational mass defect, $\triangle M$, of neutron configurations is of particular interest to astrophysicists. The computations of baryon configurations have demonstrated that when central densities rise above a certain value $\rho_1(0)$ the absolute mass defect changes sign - it becomes negative. The value of $\rho_1(0)$ depends on the form of the equation of state for the baryon gas used in the computations. In models with a real baryon gas $\rho_1(0)$ has a lesser value than in models with an ideal gas. This can be attributed to the fact that in the case of a real gas, at densities greater than nuclear, the nuclear forces of repulsion between baryons is played important role. The energy associated with one gram of star matter is an order of magnitude greater than the corresponding energy released in thermonuclear reactions in the combustion of hydrogen. It is important to note that the binding energy of each particle in a star is negative, so that the particles cannot escape individually to infinity. The escape of a certain number of baryons from a star requires the addition of supplementary energy to the remaining configuration from the outside. For this reason it cannot occur spontaneously. This means that transition of the system to a more stable state can occur only under the influence of very great perturbations. In this case expansion will occur, accompanied by heating of the celestial body. The corresponding transition will have the character of a cosmic explosion. These arguments concerning the fate of baryon configurations with an anomalous absolute mass defect were first presented by Ambartsumian and Saakyan. The configurations with an anomalous value of the absolute mass defect should be of some importance to Ambartsumian's cosmogony. In order to relate the above considerations on the behavior of baryon configurations with an anomalous value of the absolute mass defect to the concept mentioned, it is necessary to construct

doi: 10.52526/25792776-2021.68.2-236

models of superdense prestellar bodies with masses of a much greater order of magnitude than the solar mass. This would solve in principle the problem of `superdense´ cosmogony. However, the construction of physical models of continuous superdense prestellar bodies of great mass involves difficulties. The solution of these difficulties may possibly involve the consideration of nonstationary and nonequilibrium models.

• We briefly review the observable signature and computational efforts of growth and merging phenomena of astrophysical black holes. We examine the meaning, and assess the validity of such properties within theoretical framework of PMBHs. We provide a discussion of some key objectives with the analysis aimed at clarifying the current situation of the subject. It is argued that such exotic hypothetical behaviors seem nowhere near true if one applies the PMBH. We briefly re-examined (critically) the past and present of the GR and PMBHs, and attempted to chart the future of the subject.

• A principle feature that makes general relativity (GR) distinctively different from other field theories is the occurrence of curvature singularities in spacetime. The singularities lead to regions of the universe that cannot be observed. This causes an observer's inability to access the degrees of freedom that are hidden beyond the horizon which, in turn, leads to thermodynamical behavior of BHs. Notwithstanding, much remarkably efforts have been made in understanding of BH physics, many important issues still remain unresolved and, thus, a situation is unclear, than described so far. The astrophysical significance of the issue, and the importance of considering the gravitational collapse of a matter cloud within the framework of the GR theory, with reasonable physical properties for the matter included, stems from the fact that GR predicts that a star more massive than about five to eight times the mass of the Sun, cannot stabilize to a neutron star final state at the end of its life cycle. It must collapse continually under the force of its own gravity on exhausting its internal nuclear fuel, and there are no known forces of nature that would halt such a collapse. General relativity predicts that such a star must then terminate into a spacetime singularity where densities and spacetime curvatures blow up and the physical conditions are extreme. The estimates on the mass limit for a star in order to collapse, of course, are indefinitely vary depending on different models for the star's interior and equation of state for matter at very high densities. One of the most important open issues in the theory and astrophysical applications of modern day BH and gravitation physics is that of the Roger Penrose's Cosmic Censorship Despite the past four decades of serious efforts, we do not have as yet available any proof or even any mathematically precise formulation of the cosmic censorship hypothesis, which is at the basis of much of the modern theory and astrophysical applications of BHs today. In recent years, a wide variety of gravitational collapse models have been discovered where exact analytical calculations have meanwhile shown that mass concentrations collapsing under their own weight will no longer form BHs as collapse endstate, rather naked singularities, except for configurations of highest symmetry which are, however, of measure zero among all initial data. By this, even the theoretical existence of BHs is no longer justified. Some conceptual problems of the energy-momentum conservation laws of gravitational interacting fields, the localization of energy of gravitation waves, the role of singularities, and also severe problems involved in quantum gravity are still plaguing GR. Within respect to standard models, a hard look at the PMBH physics reveals at least severe principle difficulties. Although no results on BH thermodynamics have been subject to any experimental or observational tests, the attempts of theoretical interpretation of the BH thermodynamics provide a basis for further research and speculation on the nature of its quantum gravitational origin. The efforts to understand the mysterious statistical mechanical properties of BHs has led to many speculations about their quantum gravity origin. In particular, one cannot answer which region of AdS is responsible to particular information in the dual CFT. There is also an essential discrepancy between the entanglement entropy and the BH entropy, that the entanglement entropy is proportional to the number of matter fields, while the BH entropy is not. The former includes ultraviolet divergences as opposed to the latter. So, due to existing discrepancies and absence of distinctive observationally tested predictions, there is no convincing reason to rely on the string theory in its present form. This then ruptures the familiar BH entropy illusion which has insufficient dimensions. Thus we conclude

doi: 10.52526/25792776-2021.68.2-236

that PBHM, at least at its current state of development, is quite incapable of making predictions on growth and merging properties of the astrophysical BHs, because of the nasty inherent appearance of BH *singularities*, and that if the *infinite collapse to the singularity* inside the BH is accepted as a legitimate feature of Nature. Only a true internal solution was able to give a reliable information on the thermodynamic behavior and entropy of BH if, and only if, it is known deep within the BH.

• To fill the void which the standard PMBH presents, and to innovate the solution to alluded problems, we have recounted some of the highlights behind of MTBH, whereas the infra-structures will inevitably be accommodated inside the EH. To start with, we discuss the proposed general theory of distortion of space-time continuum at huge energies (respectively, at short distances < 0.4fm). As a corollary, in particular, DSTC leads to modified gravitational theory, underlying the MTBH. Much use has been made in proposed gravitation theory of the language of fundamental geometric structure - *a distortion gauge induced fiber-bundle*, incorporating with the spacetime deformation/distortion-framework. The general gauge principle innovates the solution to the problems of standard Riemannian (and its extensions) space interacting quantum field theory. Involving a drastic revision of the role of gauge fields in the physical concept of curved geometry, this theory generalizes the standard gauge scheme. The nonlinear realization technique or the method of phenomenological Lagrangians provides a way to determine the transformation properties of fields defined on the quotient space. We treat the distortion group and its stationary subgroup, respectively, as the dynamical group and its algebraic subgroup. The fundamental field is distortion gauge field (a) and, thus, all the fundamental gravitational structures in fact - the metric as much as the coframes and connections - acquire a distortion-gauge induced theoretical interpretation. We study the geometrical structure of the space of parameters in terms of Cartan's calculus of exterior forms and derive the Maurer-Cartan structure equations, where the distortion fields (a) are treated as the Goldstone fields. The available solar system observational verifications offer many opportunities to improve tests of relativistic gravity. Besides, the GGP explores the most important processes of spontaneous breaking of gravitation gauge symmetry and rearrangement of vacuum state. Spontaneous symmetry breaking can be achieved by introducing the neutral complex scalar Higgs field. Minimization of the vacuum energy fixes the non-vanishing vacuum expectation value, which spontaneously breaks the theory, leaving the U(1)d subgroup intact, i.e. leaving one Goldstone boson. The left Goldstone boson is gauged away from the scalar sector, but it essentially reappears in the gauge sector providing the longitudinally polarized spin state of one of gauge bosons that acquires mass through its coupling to Higgs scalar. The two neutral gauge bosons were mixed to form two physical orthogonal states of the massless component of distortion field, which is responsible for gravitational interactions, and its massive component, which is responsible for the ID-regime. Hence, a substantial change of the properties of the spacetime continuum besides the curvature may arise at huge energies. The theory is renormalizable, because gauge invariance gives conservation of charge, also ensures the cancelation of quantum corrections that would otherwise result in infinitely large amplitudes.

• To innovate the solution to aforementioned problems, we advocate with alternative proposal by utilizing the MTBH, which has explored a novel aspects expected from considerable change of properties of space-time continuum at spontaneous breaking of gravitation gauge symmetry far above nuclear density. The MTBH is a first-principles treatment of a fundamental *superdense protomatter* physics, but it also has an actual physical realization of Ambartsumian's fundamental vision. It may shed further light upon the growth and merging phenomena of astrophysical BHs.

The MTBH is an extension of PBHM and rather completes it by exploring the most important processes of spontaneous breaking of gravitation gauge symmetry at huge energies, and thereof for that of rearrangement of vacuum state. Whereas a significant change of properties of space-time continuum (ID-regime), arises simultaneously with the strong gravity. This manifests its virtues below the ID-threshold length (0.4fm), yielding the transformations of Poincar´e generators of translations. Accordingly, a matter found in ID-region of spacetime continuum is undergone phase transition of II-type, i.e., each particle goes off from the mass shell. Hence, a shift of mass and energy-momentum

doi: 10.52526/25792776-2021.68.2-236

spectra occurs upwards along the energy scale. The thermodynamics of a resulting matter, so-called proto-matter, is drastically differed from the thermodynamics of strongly compressed ordinary matter. The energy density and internal pressure have sharply increased in the central region of configuration, proportional to gravitational forces of compression up to $\sim 10^{25}$ order of magnitudes with respect to corresponding central values of neutron star. In the resulting so-called proto-matter, the pressure becomes dominant over gravitational force at very short distances when matter falls into central singularity as the collapse proceeds and, thus, it halts the infinite collapse. This supplies a powerful pathway to form a the equilibrium superdense proto-matter core. The stable equilibrium holds for outward layers too. This counteracts the collapse and equilibrium condition remains valid even for the masses up to $\sim 10^{10} M_{\odot}$. As a corollary, this theory has smeared out the central singularities of BH at very strong gravitational fields. One of the most remarkable drawback of MTBH is the fact that instead of infinite collapse and central singularity, an inevitable end product of the evolution of massive object is the stable SPC, where static observers exist. It will ultimately circumvent a principle problem of an observer's inability to access the degrees of freedom that are hidden beyond the horizon, and a necessity to assign the elusive entropy to BH. This in somehow or other implies that a physical entropy is assigned to SPC as a measure of the large number of thermodynamical real microstates of proto-matter, which is compatible with a concept of ergodicity. This may shed further light upon the growth and merging phenomena of astrophysical BHs, that are in evidence throughout the universe.

The ID mechanism accommodates the highest energy scale in central SPC. Encapsulated in an entire set of equations of equilibrium configuration, the SPC is a robust structure that has stood the tests of the most rigorous theoretical scrutinies of a stability. It also helps to reassure us that the stable equilibrium holds in outward layers too. In this way, an accumulation of matter is allowed about SPC. Moreover, above nuclear density, the SPC always resides inside the event horizon, therefore it could be observed only in presence of accreting matter. The external physics of accretion onto the SPC in first half of its lifetime is identical to the processes in phenomenological BH models. In other words, there is no observable difference between the gravitational field of SPC and Schwarzschild BH, so that the observable signature of BHs available in literature is of direct relevance for the SPC-configurations too. But MTBH manifests its virtue when one looks for the internal physics, accounting for growth and merging behavior of BHs. A crucial point of the MTBH is that a central singularity cannot occur, which is now replaced by SPC, where the static observers are existed. The seed BH might grow up driven by the accretion of outside matter when it was getting most of its mass.

• One of the achievements of contemporary observational astrophysics is the development of a quite detailed study of the physical properties of growth and merging phenomena of astrophysical black holes, even at its earliest stages. But even thanks to the fruitful interplay between the astronomical observations, the theoretical and computational analysis, the scientific situation is, in fact, more inconsistent to day. The growth of accreting supermassive black hole seeds and their neutrino radiation are found to be a common phenomena in the AGNs. We further expose the assertions made in the framework of microscopic theory of black hole via reviewing the mass assembly history of 377 plausible accreting supermassive black hole seeds. After the numerous reiterating integrations of the state equations of SPC-configurations, we compute their intermediate seed masses, M_{BH}^{Seed} , PRTs, initial redshifts, z^{Seed} and neutrino fluxes. All the results are presented in the Tables 1-5. The Fig. 8 gives the intermediate seed masses M_{BH}^{Seed} versus the present masses $M_{BH}/M_{\odot}$ of 337 black holes, on logarithmic scales. In accord, the AGNs are favored as promising pure UHE neutrino sources. Such neutrinos may reveal clues on the puzzle of origin of UHE cosmic-rays. We regard the considered black holes only as the potential neutrino sources. The obtained results, however, may suffer and that would be underestimated if not all 377 live black holes in the$M_{BH}/M_{\odot} \simeq 1.1 \times 10^{6}$ to 1.3×10^{10} mass range at present reside in final stage of their growth, when the proto-matter disk driven by accretion has reached out the event horizon.

• The analysis of periodic source M82X-2 in this paper goes contrary to the conventional wisdom. Namely, putting apart the discussion of inherent problems of the mass scaling of the black holes in

doi: 10.52526/25792776-2021.68.2-236

ULXs, we have focused on black hole rather than typical accreting pulsar models. It is, of course, impossible to explain the pulsed high luminosity in the framework of widely accepted conventional phenomenological black hole model because black holes do not radiate, also the spinning black holes are axisymmetric and have no internal structure on which to attach a periodic emitter. The new conceptual element of the implications of the framework of MTBH in tackling this problem is noteworthy. The MTBH explores the most important processes of spontaneous breaking of gravitation gauge symmetry and rearrangement of vacuum state at huge energies, making room for growth and merging behavior of black holes. We assume a source of flashes M82X-2 is being SIMBH, resided in the final stage of growth. If this were the case, eventually, a thin co-spinning proto-matter disk driven by accretion would be formed around the spinning proto-matter core, tilted from the plane of accretion on a definite angle δ towards the equator. It has reached out the edge of the event horizon where a metric singularity inevitably disappears. The energy is carried away then from event horizon through a thin belt area to outside world by both the ultra-high energy neutrinos produced in the superdense proto-matter medium, and the thermal defuse blackbody radiation released from the outer surface layers of ordinary matter of spinning SPC and co-spinning proto-matter disk. All of the rotational energy of SIMBH is dissipated as thermal defuse blackbody X-ray radiation to outside world. The manner in which we led the reader to the result, it should not come as a surprise. As M82X-2 spins, we see pulses because of the axial tilt or obliquity. That is to say, the M82X-2 is the emitter of both persistent continuous broad X-ray radiation and pulsating X-rays. We derive the general profiles of pulsed luminosity and X-ray flux of M82X-2. Thus, M82X-2 indeed releases 99.59% of its radiative energy predominantly in the X-ray bandpass of $0.3-30$ keV. Since there is not enough information to test the theory, i.e. in the absence of direct mass-function measurements from phase-resolved optical spectroscopy, we still have to rely on X-ray spectral and timing modeling and other indirect clues and, thus, the resulting theoretical model necessarily includes a number of poorly known parameters. We give a quantitative account of all the energetics, a potential dynamical mass scaling and orbital parameters of the semi-detached X-ray binary containing primary M82X-2 and the secondary massive O/B-type donor star, accreting through Roche-lobe overflow. These results have a heuristic value but are far from rigorous. At hard look, the position angles can be adjusted from rigorous comparison with the behavior of observed pulsed light curve of M82X-2, which will be discussed in a future publication.

- We supplement our previous investigation by more rigorous analytical treatment of rotating SPC. We analytically treat the microscopic model of stationary and axisymmetric rotating black hole. The non-spinning SPC is static and spherically symmetric. Therefore, we need to be clear about more general geometry which can describe rotating axisymmetric SPC. A rotating massive configuration drags space and time around with it (non-Newtonian gravitational effect). The local inertial frames are dragged by the rotation of the gravitational field, i.e. a gyroscope orbiting near the configuration will be dragged along with the rapidly rotating configuration. This is probably the most remarkable feature that could serve as a link with the general description of spacetime. Beside the geodetic procession, a spin of the body produces in addition the Lense-Thirring procession. The most remarkable feature of microscopic model of a rotating black hole is that, in earlier part of its lifetime, the external physics outside of outer oblate event horizon of accretion onto a black hole is identical to the processes in Kerr's model. But, there is also a crucial difference between internal physics of Kerr and microscopic rotating black hole models. That is, a central ring singularity of the Kerr black hole cannot occur, which is now replaced by finite though unbelievably extreme conditions held in the central part of rotating SPC, where the static observers exist. This has then made room for growth and merging properties of black holes. The rotating SPC necessarily introduces essential corrections to the astrophysical calculations of previous models. This was accounted, for particular example, in X-ray pulsations from M82X-2.

- For a broad range of parameters, the numerous reiterating integrations of the entire set of equations of equilibrium SPC-configurations allow to compute all the essential physical characteristics of 137 IMBH-candidates. The BH mass is an important parameter in this study. Of course, there are still large uncertainties in mass estimates collected from the literature of all the observational

doi: 10.52526/25792776-2021.68.2-236

evidence for 137 IMBH-candidates. However, for brevity reasons to save space, we retain rather a concrete proposal to proceed in relatively simple way. That is, we choose the computed mass values of the IMBH-candidates to be matched the mean values of observational mass estimates of corresponding objects. It is sensible to do so, especially since we have already reflected upon the matter. We comment on the observational mass uncertainties for some of these objects, and their validity or the confidence. In the same time, for overall details regarding this issue, we invite the interested reader to consult further the papers cited. We present the figures, which clearly highlight a main difference between both classes of discussed configurations.

Reflecting upon the results so far obtained, we demonstrate how much should be gained for high energy astrophysics by further study of the fundamental paths laid by Ambartsumian. That is, developing Ambartsumian's ideas, we consequently have arrived to a new physical perception of space-time geometry, namely the general theory of DSTC at huge energies (at short distances < 0.4fm). It leads to modified gravitational theory as a corollary of the particular case of spacetime deformation/distortion framework. This theory, in turn, underlies the MTBH, which has smeared out the central singularities of BHs, and makes room for their growth and merging behavior. The MTBH is a first-principles treatment of a fundamental *superdense protomatter* physics, but it also has an actual physical realization of Ambartsumian's fundamental vision, which enables an insight to key puzzles of ultra-high energy astrophysics. However, it should be emphasized that the key to our construction procedure is widely based on the premises of our experience of accretion physics. Therefore, what we have presented here has all the vices and virtues of the classical scenario of runaway core collapse which has always been a matter of uncertainties and controversies. Nevertheless, we caution that these entire constructions will be valid as well in the case if some hitherto unknown yet mechanism in Nature will in somehow or other way produce the superdense proto-matter, away from the accretion physics as Ambartsumyan has believed.

References

Ambartsumian V. A., 1947, The Evolution of Stars and Astrophysics, (in Russian). Armenian SSR Academy of Sciences Press, Yerevan

Ambartsumian V. A., 1949, Stellar Associations, Astronomicheskii Zhurnal, 26(1), 3

Ambartsumian V. A., 1954, The Phenomenon of Continuous Emission and Sources of Stellar Energy, ComBAO, 13, 3

Ambartsumian V. A., 1955, Stellar systems of positive total energy, The Observatory, 75, 72

Ambartsumian V. A., 1958a, in On the Evolution of Galaxies, XI Solvay Conf., Brussel. p. 241

Ambartsumian V. A., 1958b, On the Evolution of Galaxies, Izvest. Akad. Nauk ArmSSR, 11(5), 9

Ambartsumian V. A., 1958c, On the Problem of the Mechanism of the Origin of Stars in Stellar Associations, Reviews of Modern Physics, 30, Issue 3, 944

Ambartsumian V. A., 1960, On the Evolution of Stellar Systems, George Darwin Lectures, Quarterly Journal of the Royal Astronomical Society, 1, 152

Ambartsumian V. A., 1961, Instability phenomena in systems of galaxies, Astronomical Journal, 66, 536

Ambartsumian V. A., 1962, Problems of Extra-Galactic Research, Transactions of the International Astronomical Union, 11B, 145

Ambartsumian V. A., 1965, The Nuclei of Galaxies and Their Activity, The Structure and Evolution of Galaxies. Library of Congress Catalog Card No. 65-26979. Interscience Publishers, a division of John Wiley &Sons, Ltd., London

Ambartsumian V. A., 1966, Some remarks on the nature of the nuclei of galaxies,Transactions of the International Astronomical Union, 12B, 578

Ambartsumian V. A., 1968a, Galaxies and galactic evolution, "The Earth in the Universe". Israel Program for Scientific Translations, Jerusalem

Ambartsumian V. A., 1968b. The Pubblishing House of the Academy of Sciences of Armenian SSR, Yerevan, p. 521

Ambartsumian V. A., 1971, Fuors, Astrophysics, SSSR, 7, Issue 4, 557

Ambartsumian V. A., 1984, The questions of superdense celestial bodies, (in Russian). State Univ. press, Yerevan

doi: 10.52526/25792776-2021.68.2-236

Ambartsumian V. A., 1985, On the dynamics of open clusters, Dynamics of Star Clusters; IAU Symposium, May 29-June 1, 1984. Dordrecht, D. Reidel Publishing Co., Princeton, NJ

Ambartsumian V. A., Saakyan G. S., 1960, The Degenerate Superdense Gas of Elementary Particles, Astronomicheskii Zhurnal, 37, 193

Ambartsumian V. A., Saakyan G. S., 1961a, On Equilibrium Configurations of Superdense Degenerate Gas Masses, Astronomicheskii Zhurnal, 38, 785

Ambartsumian V. A., Saakyan G. S., 1961b, Internal Structure of Hyperon Configurations of Stellar Masses, Astronomicheskii Zhurnal, 38, 1016

Ambartsumian V. A., Saakyan G. S., 1965, The Mass Defect of Baryon Stars, Astrophysics, 1, Issue 1, 1

Baade W., Zwicky F., 1934, On super-nova, Proc. Nat. Acad. Sci., 20, 2599

Bassani L., Dean A. I., S S., 1983a, Preprint Univ. Southampton, Dept. Phys., Southampton, S09 5NH, UK

Bassani L., Dean A. I., S S., 1983b, Super-Eddington luminosity characteristics of active galactic nuclei, Astron. Astrophys., 125, 52

Cameron A. G. W., 1950, Neutron star models, Astrophys. J., 130, 884

Collaboration I., 2018, Multimessenger observations of a flaring blazar coincident with high-energy neutrino, IceCube-170922A, Science

Joshi P. S., Malafarina D., 2013, Instability of black hole formation under small pressure perturbations, Gen. Rel. Grav., 45, 305

Landau L., 1932, Neutron Star Structure and Equation of State, Phizik Z. Sowietunion, 1, 285

Linsley J., 1963, "Primary cosmic-rays of energy 10^{17} to 10^{20} ev, the energy spectrum and arrival directions", Proc. from the 8th International Cosmic Ray Conference, 4, 77

Nambu Y., Jona-Lasinio G., 1961, Dynamical model of elementary particles based on an analogy with superconductivity, Phys. Rev., 122, 345

Oppenheimer J. R., Volkoff G. M., 1939, On massive neutron cores, Phys. Rev., 55, 374

Ter-Kazarian G., 1986, Distortion of the Space-Time, Textbook:"Selected Questions of Theoretical and Mathematical Physics". Vol. N5322-B86, No1, 62-146, VINITI, Moscow, Russia

Ter-Kazarian G., 1989a, Supermassive Equilibrium Configurations of Superdense Matter, Akademiia Nauk SSSR, Doklady (ISSN 0002-3264), In Russian, 309, No.1, 97-101

Ter-Kazarian G., 1989b, On Study of Equilibrium Configuration of Protomatter, Part I, Astrofizika, 31, Issue 2, 345-358

Ter-Kazarian G., 1989c, The Theory of Distortion of Space-Time Continuum, ComBAO, 62, 1-123

Ter-Kazarian G., 1990, On Study of Equilibrium Configuration of Protomatter, Part II, Astrofizika, 33, 143-153

Ter-Kazarian G., 1991, On the study of internal structure of superdense celestial bodies. Astrofizika, 35, Issue 2,3, 335-372

Ter-Kazarian G., 1992, An Introduction to the Theory of Internal Structure of Supermassive Compact Celestial Bodies, Astrophysics & Space Sci., 194, No1, 1-129

Ter-Kazarian G., 1997, Gravitation Gauge Group, Nuovo Cimento, 112B, No 6, 825-838

Ter-Kazarian G., 2001, Protomatter and EHE C.R., Japan Phys. Soc. Jpn., 70, S. B., 84-98

Ter-Kazarian G., 2010, Gravitation and inertia; a rearrangement of vacuum in gravity; Astrophysics & Space Sci., 327, 91-109, arxiv:1001.2990[gr,qc]

Ter-Kazarian G., 2011, Two-step spacetime deformation-induced dynamical torsion, Class. Quantum Grav., 28, 055003 (19pp); stacks.iop.org/CQG/28/000000; arxiv:1102.24911[gr,qc]

Ter-Kazarian G., 2012, Spacetime deformation-induced inertia effects, Advances in Mathematical Physics, Article ID 692030, 1-41, http://dx.doi.org/10.1155/2012/692030

Ter-Kazarian G., 2014, Ultra-high energy neutrino fluxes from supermassive AGN black holes, Astrophys. & Space Sci., 349, 919-938

Ter-Kazarian G., 2015, Modified Theories of Gravitation behind the Spacetime Deformation, Physics Research International, 2015, Article ID 152846, 1-19, http://dx.doi.org/10.1155/2015/152846

Ter-Kazarian G., 2016a, Rotating black holes in microscopic theory: the implications for periodic source M82X-2, Advances in Astrophysics, 1, issue 3, 201-223

Ter-Kazarian G., 2016b, On the Physical Nature of the Source of Ultraluminous X-ray Pulsations, Astrophys. & Space Sci., 361, issue 1, 20pp, DOI 10.1007/s10509

doi: 10.52526/25792776-2021.68.2-236

Ter-Kazarian G., 2021a, Growth and merging phenomena of black holes: observational, computational and theoretical efforts, ComBAO, 68, issue 1, pp. 56-74, https://doi.org/10.52526/25792776

Ter-Kazarian G., 2021b, A new look at some aspects of geometry, particle physics, inertia, radiation and cosmology, ComBAO, 68, issue 2, pp. ??, https://doi.org/10.52526/25792776

Ter-Kazarian G., Sargsyan L., 2013, Signature of plausible accreting supermassive black holes in Mrk 261/262 and Mrk266, Advances in Astronomy, 2013, Article ID 710906, http://dx.doi.org/10.1155/2013/710906

Ter-Kazarian G., Shidhani S., 2017, Plausible Intermediate Mass Black Hole from M82X-2 X-Ray Pulsations, Advances in Astrophysics, 2, issue 3, 162-183

Ter-Kazarian G., Shidhani S., 2019, A study of 137 intermediate mass black hole candidates, Astrophys. Space Sci., 364, Issue 10, article id. 165, 23 pp

Ter-Kazarian G., Yerknapetian K., 1995, On the Internal Structure of Supermassive Compact Celestial Bodies, Astrofizika, 38, No4, 659-666

Ter-Kazarian G., Khachatryan V., Yerknapetyan K., 2003, Neutrino Cooling and Fueling at Disk Accretion Onto the SPC in AGN, and Origin of EHE G.R.s, "The Universe Viewed in Gamma-rays", ICRR, University of Tokyo. Universal Academy Press, Inc., BR-Hongo-5 Bldg., 6-16-2 Hongo Bunkyo-ku, Tokyo, Japan

Ter-Kazarian G., Terzyan Y., Khachikian E. e. a., 2006, On Multi-Nuclei Features of Some Markarian Galaxies, Monthly Notice of Royal Astron. Soc., 368, 461-470

Ter-Kazarian G., Shidhani S., Sargsyan L., 2007, Neutrino Radiation of the AGN Black Holes, Astrophys. & Space Sci., 310, issue 2, 93-110

Zel'dovich Y. B., 1959, Soviet Physics- JETP, 10, 409

Zel'dovich Y. B., 1962, Static solutions with energy excess in general relativity, Soviet Physics- JETP, 42, 1667

Zwicky F., 1938, On Collapsed Neutron Stars, Astrophys.J., 88, 522

A new look at some aspects of geometry, particle physics, inertia, radiation and cosmology

G.Ter-Kazarian*[1]

[1]Byurakan Astrophysical Observatory, 378433, Aragatsotn District, Armenia

Abstract

Continuing along the line of our previous report (Ter-Kazarian, 2021c), in present communication we briefly outline several closely related issues, carried out also in Byurakan Astrophysical Observatory, not touched in it for brevity reasons. These issues reveal and further develop novel aspects of the fundamental nature and structure of the space-time geometry and the high energy physics, the inertia effects, the intense radiation physics, and the notion of relative velocity in a curved space-time.

Keywords: *geometry—torsion—supersymmetric quantum mechanics—operator manifold—Standard Model of elementary particles—supersymmetric extension—inertia effects—radiation physics—cosmology*

Contents

*gago_50@yahoo.com, Corresponding author

doi: 10.52526/25792776-2021.68.2-311

1. Introduction

In our previous report (Ter-Kazarian, 2021c), among others, we have also developed on the new physical perception of space-time geometry - the *theory of distortion of space-time continuum* (DSTC) (Ter-Kazarian, 1986, 1989c, 1997, 2010) at huge energies (respectively, at short distances < 0.4fm). Using the language of fundamental geometric structure - distortion gauge induced fiber-bundle, it leads to modified gravitational theory as a corollary of the spacetime deformation/distortion framework. We generalize the standard gauge scheme via the concept of distortion gauge field which acts on the external spacetime groups. This theory, in turn, underlies the *microscopic theory of black hole* (Ter-Kazarian, 1989a,b, 1990, 1991, 1992, 2001a, Ter-Kazarian & Yerknapetian, 1995), which has smeared out the central singularities of BHs, and makes room for their growth and merging behavior. The MTBH is the first-principles treatment of a fundamental `superdense protomatter´ physics, but it also has an actual physical realization of Ambartsumian's fundamental vision, which enables an insight to key puzzles of ultra-high energy astrophysics (Ter-Kazarian, 2014, 2015, 2016a,b, Ter-Kazarian & Sargsyan, 2013, Ter-Kazarian & Shidhani, 2017, 2019, Ter-Kazarian et al., 2003, 2006, 2007).

Continuing along this line, in present communication we briefly outline several closely related issues, carried out also in Byurakan Astrophysical Observatory, not touched in previous paper for brevity reasons. These issues reveal novel aspects of the fundamental nature and structure of space-time geometry and high energy physics, inertia effects and intense radiation physics. In the same time, the interested reader is invited to consult for details the original papers as follows: Two-step spacetime deformation (TSSD)-induced dynamical torsion (Ter-Kazarian, 2011); TSSD-metric-affine gravity behind the spacetime deformation (Ter-Kazarian, 2015); Extended phase space SUSY (Ter-Kazarian, 2009, 2013a, Ter-Kazarian & Sobouti, 2008); The operator manifold approach to geometry and particle physics (Ter-Kazarian, 1884, 1996, 1999a); Microscopic theory of the Standard Model (MTSM) of elementary particles (Ter-Kazarian, 1999b, 2001b); and Supersymmetric extension of MTSM (Ter-Kazarian, 2001c); Spacetime deformation induced inertia effects (Ter-Kazarian, 2010, 2012)); Probing inertia behind the SUSY (Ter-Kazarian, 2001b); Einstein's transition coefficients for Compton scattering, the annihilation and creation of electron-positron pairs at intense radiation (Ter-Kazarian, 1984c,e); The theory of Multiphoton Comptonization (Ter-Kazarian, 1984a,b,d, 1987, 1989a,b); Unique definition of relative velocity of luminous source as measured along the observer's line-of-sight in a generic pseudo-Riemannian space-time (Ter-Kazarian, 2021b): The implications for the spatially homogeneous and isotropic Robertson-Walker space-time (Ter-Kazarian, 2021a).

With this perspective in sight, we will proceed according to the following structure. To start with, Section 2 recounts some of the highlights behind of the *TSSD-induced dynamical torsion* (Ter-Kazarian, 2011, 2015). We extend the geometrical ideas of the spacetime deformations (Ter-Kazarian, 2010, 2012) to study the physical foundation of post-Riemannian geometry. To this aim, we construct the theory of TSSD as a guiding principle. Through a non-trivial choice of explicit form of a *deformation* tensor, we have a way to derive different post Riemannian spacetime structures such as: (i) the Weitzenböck spacetime structure — (W_4) underlying a teleparallelism theory of gravity; (ii) the RC manifold — (U_4) underlying Einstein-Cartan theory also called Einstein-Cartan-Sciama-Kibble theory; (iii) or even the most general linear connection of metric-affine gravity (MAG) theory taking values in the Lie-algebra of the 4D-affine group, $A(4,R) = R^4 \otimes GL(4,R)$ (the semi-direct product of the group of 4D-translations and general linear 4D-transformations). We address the theory of teleparallel gravity and construct a consistent Einstein-Cartan (EC) theory with the *dynamical torsion*. We show that the equations of the standard EC theory, in which the equation defining torsion is the algebraic type and, in fact, no propagation of torsion is allowed, can be equivalently replaced by the set of *modified Einstein-Cartan equations* in which the torsion, in general, is a *dynamical*. The special physical ansatz for the spacetime deformations yields the short-range propagating torsion.

Having gained some insight into the physical foundation of the Einstein-Cartan theory, with *two-step spacetime deformation* induced dynamical torsion, TSSD-U_4 theory, in Section 3, we extend these ideas as applied to the more general *TSSD-metric-affine gravity* (Ter-Kazarian, 2015). The MAG theory is an extension of the Poincaré gauge theory of gravity, constructed in the Rieman-Cartan geometry, to the most general spacetime symmetry gauge theory. The MAG theory has the most general type of covariant derivative: in addition to curvature and torsion, the MAG also has nonmetricity, i.e.,

doi: 10.52526/25792776-2021.68.2-311

a nonmetric compatible connection. Hence parallel transport no longer preserves length and angle. The TSSD-MAG is constructed in the framework of the first order Lagrangian expressed in terms of the gauge potentials and their first derivatives. We show that, in this framework, the equations of the standard MAG theory which have no further propagating modes can be equivalently replaced by the set of the *modified equations* which, in the limit of reducing the affine group, may recover TSSD-U_4 theory, with propagating torsion. The special physical ansatz for the spacetime deformations yields the short-range propagating torsion. In testing the modified TSSD-MAG framework for different particular cases, the restrictions are imposed via the method of *Lagrange multipliers*. To pursue the TSSD-approach further, here we address the essential features of the MAG theory in context of the TSSD-construction of post-Riemannian geometry. A formulation of the major physical aspects of this theory will be given in the framework of the first order Lagrangian expressed in terms of the gauge potentials and their first derivatives. All the fundamental gravitational structures in fact - the metric as much as the coframes and connections - acquire a TSSD induced theoretical interpretation. It is remarkable that in the framework of the first order Lagrangian, the equations of the standard MAG theory which have no further propagating modes can be equivalently replaced by the set of the *modified equations* which, in the limit of reducing the affine group, may recover TSSD-U_4 theory, with a *dynamical* torsion.

In Section 4, we give an outline of the `extended phase space´ stochastic quantization of constrained hamiltonian systems (Ter-Kazarian & Sobouti, 2008). Exploring the concept of `actual and virtual paths´ in a phase space formalism, we address a stochastic quantization of Hamiltonian systems with first class holonomic constraints. Extended canonical transformations allows to go from one extended phase space to another. This unifying feature of the theory makes the comparison of the various functions existing in the literature possible and transparent. We have developed the stochastic quantization method (SQM) in extended phase space and shown how this method can be generalized to deal with systems subjected to first class constraints.

All this variety prompts us, in Section 5, to address the SUSY for an `extended phase space´ quantum mechanical system (Ter-Kazarian, 2009). We have concerned ourselves with the *extended* phase space quantum mechanics of particles which have both bosonic and fermionic degrees of freedom, i.e., the quantum field theory in (0+1)-dimensions in $q-$ (position) and $p-$ (momentum) spaces, exhibiting supersymmetry. We present (N=2)-realization of the supersymmetry algebra, and discuss the vacuum energy and the topology of super-potentials. We demonstrate the merits of shape-invariance of exactly solvable extended SUSY potentials, which has underlying algebraic structure, by obtaining analytic expressions for the entire energy spectrum of extended Hamiltonian with Scarf potential without ever referring to underlying differential equation. However, a shape-invariance is not the most general integrability condition as not all exactly solvable potentials seem to be shape-invariant. As an application we obtain analytic expressions for the entire energy spectrum of extended Hamiltonian with *Scarf* potential without ever referring to underlying differential equation.

In Section 6, we derive the classical analog of the `extended phase space´ SUSY quantum mechanics and obtain the integrals of motion (Ter-Kazarian, 2013a). Consequently, we describe the extended phase space (N=2)-SUSY algebra. In the second part, by means of an iterative scheme, first, we find the approximate groundstate solutions to the extended Schrödinger-like equation, and then calculate the parameters which measure the breaking of extended SUSY such as the groundstate energy. We calculate a more practical measure for the SUSY breaking, in particular in field theories which is the expectation value of an auxiliary field. We analyze non-perturbative mechanism for extended phase space SUSY breaking in the instanton picture and show that this has resulted from tunneling between the classical vacua of the theory. Finally, we deal with the independent group theoretical methods with nonlinear extensions of Lie algebras from the perspective of extended phase space SUSY quantum mechanics and, further, shows how it can be useful for spectrum generating algebra.

Section 7 offers a detailed analysis of the *operator manifold approach* to geometry and particle physics (Ter-Kazarian, 1884, 1996, 1999a). The fundamental question that guides our discussion is how did the geometry and particles come into being? To explore this query, the operator manifold (OM)-formalism enables the unification of the geometry and the field theory. It yields the quantization of geometry drastically different from earlier suggested schemes. It address itself to the question of the

doi: 10.52526/25792776-2021.68.2-311

prime-cause of origin of geometry and basic concepts of particle physics such as the fundamental fields of quarks and leptons with the spins and various quantum numbers, internal symmetries and so forth; also basic four principles of Relativity, Quantum, Gauge and Color Confinement, which are, as it was proven, all derivative and come into being simultaneously. The substance out of which the geometry and particles are made is a set of new physical structures. The most promising aspect of our approach so far is the fact that many of the important anticipated properties, basic concepts and principles of particle physics are appeared quite naturally in the framework of suggested theory. In pursuing the original problem further we have elaborated a new mathematical framework, which is, in fact, a still wider generalization of familiar methods of secondary quantization with appropriate expansion over the geometric objects. The OM formalism provides a natural unification of the geometry- yielding the special and general relativity principles, and the quantized fermion fields serving as the basis for the constituent subquarks.

In Section 8, we discuss the key points of field aspect of OM. The quantum field theory of the OM is equivalent to configuration space wave mechanics employing the antisymmetric state functions incorporated with geometric properties of corresponding objects. Therein, by applying the algebraic approach we reach to rigorous definition of the OM. Considering an arbitrary superposition of state vectors we get a whole set of explicit forms of the matrix elements of operator vector and covector fields.

In Section 9, we briefly outline the key points of differential geometric aspect of OM. The operators are the basis for all operator vectors of tangent section of principle bundle. The smooth field of tangent operator vector is a class of equivalence of the curves. For any function of the ordinary class of functions of smoothness, one may define an operator differential. Constructing matrix elements of operator tensors, one produces the Cartan's exterior forms. Whence, the matrix elements of symmetric operator tensors equal zero. The differential operator form at given point can be defined as the exterior operator form on tangent operator space of tangent operator vectors. The linear operator form of 1 degree is a linear operator valued function. The set of all linear operator forms defined at given point fill up the operator vector space. We consider the integration of operator form. Next, we apply the analog of exterior differentiation.

Section 10 deals with primordial structures and link establishing processes. It has cleared up the physical conditions in which the geometry and particles come into being.

These structures are thought to be the substance out of which the geometry and particles are made. There is not any restriction on the number of primordial structures of both types involved in the link establishing processes simultaneously. Only, in the stable system the link stability condition must be held for each linkage separately. The persistent processes of creation and annihilation of the primordial structures proceed in different states. The processes of creation and annihilation of `regular structures´ in lowest state are described by the OM formalism given above. In all higher states the primordial structures are distorted (interaction states) and described by distorted link functions defined on distorted manifolds. The `distorted ordinary structures´ emerge in geometry only in permissible combinations forming a stable system. Below, in simplified schematic way we exploit the background of the known colour confinement and gauge principles. Naive version of such construction still should be considered as a preliminary one, which will be further elaborated to introduce a basis for the subquarks. Due to the incompatibility commutation relations the transformation matrices generate the unitary groups of internal symmetries $U(1), SU(2)$, $SU(3)$ corresponding to one-, two- and three-dimensional rotations, while an action of physical system must be invariant under such transformations (gauge principle). The subquarks emerge in the geometry only in certain permissible combinations utilizing the idea of the subcolour (subquark) confinement principle, and have undergone the transformations yielding the internal symmetries and gauge principle.

In Section 11, we generalize the OM-formalism via the concept of operator multimanifold (OMM), which yields the multiworld (MW) geometry involving the spacetime continuum and internal worlds of given number. All this is not merely an exercise in abstract reasoning but presumably bears directly on the geometry of the universe in which we live. In an enlarged framework of the OMM we define and clarify the conceptual basis of subquarks and their characteristics stemming from the various symmetries of the internal worlds. The hypothesis of existence of the MW structures manifests

doi: 10.52526/25792776-2021.68.2-311

its virtue by solving some key problems of particle phenomenology, when we attempt to suggest a microscopic approach to the properties of particles and interactions.

A definite pattern for the theoretical description of particle physics has emerged based on the framework of the Standard Model (SM) of high energy physics, which is built up from observation for prediction and correlation of the new data. Although the SM has proven to be in spectacular agreement with experimental measurements and quite successful in a predicting a wide range of phenomena, however, it is not exception to the rule that as the phenomenological approach it suffers from own difficulties. There were still many open key questions arisen inevitably that we have no understanding why the SM is as it is? Why is the gauge symmetry? Why is this the particle spectrum? The mechanism of the electroweak symmetry breaking is a complete mystery. A phenomenological standard model (SM) of high energy physics with enormous success settles order in entangled experimental data. Although it has proven to be in spectacular agreement with experimental measurements and highly successful in a description and predicting a wide range of phenomena, however, it suffers from some vexing problems and many key questions of both the phenomenological and SUSY aspects have yet to be answered. To fill the void which the SM presents, and to innovate the solution to alluded problems, we will use OM-formalism as a backdrop to discuss in Section 12 the key points of *Microscopic theory of the Standard Model (MTSM) of elementary particles* (Ter-Kazarian, 1999b, 2001b). A theoretical significance of the MSM, first of all, resides in the microscopic interpretation of all physical parameters.

With this perspective in sight, in Section 13, we further expose the assertions made in OM-formalism, to recount some of the highlights behind of the supersymmetrization of MTSM (SuMTSM) (Ter-Kazarian, 2001c). We promote the MTSM into supersymmetric framework in order to solve its technical aspects of vacuum zero point energy and hierarchy problems, and attempt, further, to develop its realistic viable minimal SUSY extension. Among other things that - the MTSM provides a natural unification of geometry and the field theory, has clarified the physical conditions in which the geometry and particles come into being, in microscopic sense enables an insight to key problems of particle phenomenology and answers to some of its nagging questions - a present approach also leads to quite a new realization of the SUSY yielding a physically realistic particle spectrum. It stems from the special subquark algebra, from which the nilpotent supercharge operators are derived. The resulting theory makes plausible testable implications for the current experiments at LEP2, at the Tevatron and at LHC drastically different from those of the conventional MSSM models.

In Section 14, we further discuss the *Spacetime deformation induced inertia effects* (Ter-Kazarian, 2010, 2012). We construct a toy model of spacetime deformation induced inertia effects, in which we prescribe to each and every particle individually a new fundamental constituent of hypothetical 2D, so-called, *master-space* (MS), subject to certain rules. The MS, embedded in the background 4D-spacetime, is an indispensable companion to the particle of interest, without relation to every other particle. The MS is not measurable directly, but we argue that a deformation/(distortion of local internal properties) of MS is the origin of inertia effects that can be observed by us. With this perspective in sight, we construct the alternative *relativistic theory of inertia* (RTI) (Ter-Kazarian, 2010, 2012). We go beyond the hypothesis of locality with special emphasis on distortion of MS, which allows to improve essentially the standard metric and other relevant geometrical structures referred to a noninertial frame in Minkowski spacetime for an arbitrary velocities and characteristic acceleration lengths. We compute the inertial force exerted on the photon in a gravitating system in the semi-Riemann space. Despite the totally different and independent physical sources of gravitation and inertia, this approach furnishes justification for the introduction of the *weak* principle of equivalence (WPE), i.e., the universality of free fall. Consequently, we relate the inertia effects to the more general post-Riemannian geometry. We derive a general expression of the relativistic inertial force exerted on the extended spinning body moving in the Rieman-Cartan space.

In Section 15, we prob the inertia behind SUSY. We derive a standard Lorentz code (SLC) of motion by exploring rigid double transformations of, so-called, *master space-induced* supersymmetry (MS-SUSY), subject to certain rules (Ter-Kazarian, 2001b). The renormalizable and actually finite flat-space field theories with $N_{max} = 4$ supersymmetries in four dimensions, if only such symmetries are fundamental to nature, yield the possible *extension of Lorentz code* (ELC), at which the SLC violating new physics appears. In the framework of local MS-SUSY, we address the inertial effects.

doi: 10.52526/25792776-2021.68.2-311

We argue that a space-time deformation of MS is the origin of inertia effects that can be observed by us. We go beyond the hypothesis of locality. This allows to improve the relevant geometrical structures referred to the noninertial frame in Minkowski space for an arbitrary velocities and characteristic acceleration lengths. This framework furnishes justification for the introduction of the *weak* principle of equivalence, i.e., the *universality of free fall*. The implications of the inertia effects in the more general post-Riemannian geometry are briefly discussed.

In Section 16, we briefly outline the issues on the interaction of electrons with the intense radiation: Einstein's transition coefficients for Compton scattering, and the annihilation and creation of electron-positron pairs at intense radiation (Ter-Kazarian, 1984c,e). Einstein's ideas are developed for free-virtual, virtual-free and free-free transitions for electron-photon scattering at arbitrary intense radiation by splitting Compton scattering into two components. Whereas, we consider the general problem of interaction of electrons with the intense radiation via s-photon Compton scattering $s\gamma + e \to \gamma' + e'$. In doing this, we introduce a new concept of `effective photon´, and then instead of $s$-photon scattering by electron with an `effective´ four-momentum, with equal footing,, we should consider the scattering of one `effective photon´ by free electron. The Compton scattering is the s-channel of the photon-electron interaction. This formalism can be easily extended to the t-channel of the photon-electron interaction, namely to processes of annihilation and creation of electron-positron pairs. Certainly, since the Feynman diagram for these processes is topologically identical to the corresponding diagram of the s-channel of the photon-electron interaction, then the probability coefficients for the t-channel of the photon-electron interaction can be obtained directly from the Compton scattering by performing simple replacements. Determining the probability coefficients of transitions in the state of thermodynamic equilibrium, we readily derive the radiation transfer equation for nonequilibrium processes.

On this basis, in Section 17, we suggest the *theory of multiphoton comptonization* (Ter-Kazarian, 1984a,b,d, 1987, 1989a,b). Employing the method of `effective photons´, the integral kinetic equation is derived that describes the time variation of the distribution function of quanta of non-equilibrium intense radiation for their multiphoton Compton scattering on Maxwellian nonrelativistic electrons. This equation is the crux for the constructed theory of multiphoton comptonization, which determines the heating of thermal electrons during multiphoton induced Compton interaction. The integral kinetic equation allows one to describe the evolution of intense spectral lines of radiation, for any spectral widths, and any angular aperture of the radiation beam.

In Section 18, we discuss the unique definition of relative velocity of luminous source as measured along the observer's line-of-sight in a generic pseudo-Riemannian space-time. Using a way of separating the spectral shifts into infinitesimally displaced `relative´ spectral bins and sum over them, in Subsection 18.1, we overcome the ambiguity of the parallel transport of four-velocity, in order to give an unique definition of the so-called *kinetic* relative velocity of luminous source as measured along the observer's line-of-sight in a generic pseudo-Riemannian space-time (Ter-Kazarian, 2021b). A resulting relationship between the spectral shift and the *kinetic* relative velocity is utterly distinct from a familiar global Doppler shift rule. We show that such a performance of having found a *kinetic* relative velocity of luminous source, without subjecting it to a parallel transport, manifests its virtue in particular case when adjacent observers are being in free fall and populated along the null geodesic. So that the *kinetic* relative velocity is reduced to global Doppler velocity as studied by Synge (Synge, 1960).

In Section 19, we discuss the implications for the spatially homogeneous and isotropic Robertson-Walker space-time (Ter-Kazarian, 2021a), which leads to cosmological consequences that the resulting *kinetic* recession velocity of a galaxy is always subluminal even for large redshifts of order one or more, and thus, it does not violate the fundamental physical principle of *causality*.

The physical outlook and concluding remarks are given in Section 20.

2. Two-step spacetime deformation-induced dynamical torsion

The TSSD as a guiding principle. When considering several connections with different curvature and torsion, one takes spacetime simply as a manifold, and connections as additional structures. The

doi: 10.52526/25792776-2021.68.2-311

universality of gravitation allows the Levi-Civita connection to be interpreted as part of the spacetime definition. The form of Riemannian connection, which is a function of the tetrad fields and their derivatives, shows that the relative orientation of the orthonormal frame $\breve{e}_a(\breve{x}+d\,\breve{x})$ with respect to $\breve{e}_a(\breve{x})$(parallel transported to $(\breve{x}+d\,\breve{x})$ is completely fixed by the metric. Since a change in this orientation is described by Lorentz transformations, it does not induce any gravitational effects; therefore, from the point of view of the Principle of Equivalence, there is no reason to prevent independent (due to arbitrary deformations) Lorentz rotations of local frames in the space under consideration. If we want to use this freedom, the spin connection should contain a part which is independent of the metric, which will realize an independent Lorentz rotation of frames under parallel transport. In this way, we are led to a description of gravity which is not in Riemann space, but in the metric-affine geometry. If all inertial frames at a given point are treated on an equal footing, the spacetime has to have torsion, which is the antisymmetric part of the affine connection. Recall that the concept of a linear connection as an independent and primary structure of spacetime is the fundamental proposal put forward by Élie Cartan's geometrical analysis. Cartan gave a beautiful geometrical interpretation of torsion and curvature. Namely, the torsion is related to the translation of a vector, like curvature is related to the rotation of a vector, when it is displaced around an infinitesimal closed path - loop, and when this loop is developed in the flat space tangent to the manifold such that the tangent space rolls without gliding around the loop. At the end of the journey one has a rotation if there is only curvature, or the loop, mapped into the tangent space, has a small closure failure, i.e. a translational misfit, a translation if there is only torsion, or both if there is curvature and torsion. When torsion is nonvanishing, the affine connection is no longer coincident with the Levi-Civita connection, and the geometry is no longer Riemannian, but one has a Riemann-Cartan U_4 spacetime, with a nonsymmetric, but metric-compatible, connection. On the other hand, teleparallel gravity attributes gravitation to torsion, but in this case torsion accounts for gravitation not by geometrizing the interaction, but by acting as a force. This theory represented a new way of including torsion into general relativity, an alternative to the scheme provided by the usual Einstein-Cartan-Sciama-Kibble approach. However, for a specific choice of the free parameters, teleparallel gravity shows up as a theory completely equivalent to Einstein's general relativity, in which case it is usually referred to as the teleparallel equivalent of general relativity. From this point of view, curvature and torsion are simply alternative ways of describing the gravitational field, and consequently related to the same degrees of freedom of gravity. The fundamental difference between these two theories above was that, whereas in the former torsion is a propagating field, in the latter it is not, a point which can be considered a drawback of this model. This prompt us below to separate these two different cases.

2.1. Model building: spacetime deformations

When considering several connections with different curvature and torsion, one takes spacetime simply as a manifold, and connections as additional structures. From this view point, below we shall tackle the problem of spacetime deformation. To start with, let us consider the holonomic metric defined in the Riemann space, V_4, as $\breve{g} = \breve{g}_{\mu\nu}\,\breve{\vartheta}^\mu \otimes \breve{\vartheta}^\nu = \breve{g}(\breve{e}_\mu,\, \breve{e}_\nu)\,\breve{\vartheta}^\mu \otimes \breve{\vartheta}^\nu$, with components, $\breve{g}_{\mu\nu} = \breve{g}(\breve{e}_\mu, \breve{e}_\nu)$ in dual holonomic base $\{\breve{\vartheta}^\mu \equiv d\breve{x}^\mu\}$. All magnitudes related with the Riemann space, V_4, will be denoted with an over $'\,\breve{}\,'$. The space, V_4, has at each point a tangent space, $\breve{T}_{\breve{x}}V_4$, spanned by the four tetrad fields, $\breve{e}_a = \breve{e}_a{}^\mu\,\breve{\partial}_\mu$, which relate $\breve{g}$ to the tangent space metric, $o_{ab} = diag(+---)$, by $o_{ab} = \breve{g}(\breve{e}_a,\, \breve{e}_b) = \breve{g}_{\mu\nu}\,\breve{e}_a{}^\mu\,\breve{e}_b{}^\nu$. The coframe members are $\breve{\vartheta}^b = \breve{e}^b{}_\mu\, d\breve{x}^\mu$, such that $\breve{e}_a \rfloor \breve{\vartheta}^b = \delta^b_a$, where $\rfloor$ denotes the interior product, namely, this is a C^∞-bilinear map $\rfloor : \Omega^1 \to \Omega^0$ with Ω^p denotes the C^∞-modulo of differential p-forms on V_4. In components $\breve{e}_a{}^\mu\,\breve{e}^b{}_\mu = \delta^b_a$. One can consider general transformations of the linear group, $GL(4,R)$, taking any base into any other set of four linearly independent fields. The notation, $\{\breve{e}_a,\, \breve{\vartheta}^b\}$, will be used below for general linear frames. The converse metric is $\breve{g}_{\mu\nu} = o_{ab}\,\breve{e}^a{}_\mu\,\breve{e}^b{}_\nu$ because of $\breve{e}_a{}^\mu\,\breve{e}^a{}_\nu = \delta^\mu_\nu$. The anholonomy objects read $\breve{C}^a := d\,\breve{\vartheta}^a = \frac{1}{2}\,\breve{C}^a{}_{bc}\,\breve{\vartheta}^b \wedge \breve{\vartheta}^c$, where the anholonomy coefficients, $\breve{C}^a{}_{bc}$, which represent the curls of the base members are $\breve{C}^c{}_{ab} = -\breve{\vartheta}^c([\breve{e}_a,\, \breve{e}_b]) = \breve{e}_a{}^\mu\breve{e}_b{}^\nu(\breve{\partial}_\mu\breve{e}^c{}_\nu - \breve{\partial}_\nu\breve{e}^c{}_\mu) = -\breve{e}^c{}_\mu[\breve{e}_a(\breve{e}_b{}^\mu) - \breve{e}_b(\breve{e}_a{}^\mu)]$. The (anholonomic) Levi-Civita (or Christoffel) connection can be written as $\breve{\Gamma}_{ab} := \breve{e}_{[a}\rfloor d\breve{\vartheta}_{b]} - \frac{1}{2}\,(\breve{e}_a\rfloor\breve{e}_b\rfloor d\breve{\vartheta}_c) \wedge \breve{\vartheta}^c$ where $\breve{\vartheta}_c$ is understood as the down indexed one-form $\breve{\vartheta}_c = o_{cb}\,\breve{\vartheta}^b$. Next, we write a norm, ds, of

doi: 10.52526/25792776-2021.68.2-311

the infinitesimal displacement, dx^μ, on the general smooth differential 4D-manifold $\mathcal{M}_4$, in terms of the spacetime structures of V_4, as $ds = \Omega_\mu{}^\nu \breve{e}_\nu \breve{\vartheta}^\mu = \Omega_b{}^a\, \breve{e}_a\, \breve{\vartheta}^b = e_\rho\, \vartheta^\rho = e_a\, \vartheta^a \in \mathcal{M}_4$, where $\Omega_\mu{}^\nu$ is the world-*deformation tensor*, $\{e_a = e_a{}^\rho\, e_\rho\}$ is the frame and $\{\vartheta^a = e^a{}_\rho\, \vartheta^\rho\}$ is the coframe defined on $\mathcal{M}_4$, such that $e_a \rfloor \vartheta^b = \delta^b_a$, or in components, $e_a{}^\mu\, e^b{}_\mu = \delta^b_a$, also the procedure can be inverted $e^a{}_\rho\, e_a{}^\sigma = \delta^\sigma_\rho$. Provided, $\Omega_\mu{}^\nu = \pi_\mu{}^\rho\, \pi_\rho{}^\nu$, $\Omega_b{}^a = \pi_c{}^a\, \pi_b{}^c = \Omega_\mu{}^\nu\, \breve{e}^a{}_\nu\, \breve{e}_b{}^\mu$, $e_\rho = \pi_\rho{}^\nu\, \breve{e}_\nu \equiv \partial_\rho$, $\vartheta^\rho = \pi^\rho{}_\mu\, \breve{\vartheta}^\mu \equiv dx^\rho$, $x^\rho \in \mathcal{U} \in \mathcal{M}_4$. Hence the deformation tensor, $\Omega^a{}_b$, yields a local tetrad deformations $e_a \vartheta^a = \Omega^a{}_b\, \breve{e}_a\, \breve{\vartheta}^b$, $e_c = \pi_c{}^a\, \breve{e}_a$, $\vartheta^c = \pi^c{}_b\, \breve{\vartheta}^b$. A general spin connection then transforms according $\omega^a{}_{b\mu} = \pi_c{}^a \breve{\omega}^c{}_{d\mu} \pi^d{}_b + \pi_c{}^a\, \partial_\mu\, \pi^c{}_b$. The matrices, $\pi(\overline{x}) :\ \ = (\pi_b{}^a)(\overline{x})$, can be called *first deformation matrices*, and the matrices $\gamma_{cd}(x) = o_{ab}\, \pi_c{}^a(x)\, \pi_d{}^b(x)$, as the *second deformation matrices*. The matrices, $\pi^a{}_c(x) \in GL(4,R)\, \forall\, x$, in general, give rise to right cosets of the Lorentz group, i.e. they are the elements of the quotient group $GL(4,R)/SO(3,1)$.

2.2. The post-Riemannian geometry

In what follows, we deal with a more generic spacetime deformation $\pi(x)$, consisted of a double deformations $(\overset{\bullet}{\pi}(\overset{\bullet}{x}),\ \sigma(x))$ of the infinitesimal displacements described on a generic smooth differential 4D manifold in terms of the spacetime structures of a Riemann space. The first deformation matrix $\overset{\bullet}{\pi}(\overset{\bullet}{x})$, will be conveniently chosen in such a way that the deformed connection is set as the Weitzenböck connection, and the associated deformed spin-connection vanishes. the Weitzenböck connection is a connection presenting a non-vanishing torsion, but vanishing curvature. This recovers a particular case of the teleparallel gravity theory with the dynamical torsion. All magnitudes related with the teleparallel gravity will be denoted with an over '$\bullet$'. Then, we will be able, further, to generalize the Einstein-Cartan equations for which the spin generates a dynamical torsion part, associated with spacetime deformation $\sigma(x)$, in the canonical energy-momentum tensor producing a deviation from Riemannian geometry. Keeping in mind aforesaid, let a deformation $(\breve{e},\ \breve{\vartheta}) \to (e,\ \vartheta)$ be now performed in the *two-steps*:

$$\begin{tikzcd}
(\breve{e}(\breve{x}),\ \breve{\vartheta}(\breve{x})) \arrow[d, "\pi(x)"'] \arrow[dr, "\overset{\bullet}{\pi}(\overset{\bullet}{x})"] & \\
(e(x),\ \vartheta(x)) & (\overset{\bullet}{e}(\overset{\bullet}{x}),\ \overset{\bullet}{\vartheta}(\overset{\bullet}{x})) \arrow[l, bend left, "\sigma(x)"]
\end{tikzcd}$$

Two-step deformation map

where the first deformation matrix, $\overset{\bullet}{\pi}(\overset{\bullet}{x}) :\ \ = (\overset{\bullet}{\pi}{}_b{}^a)(\overset{\bullet}{x})$, is the solution of the following equation: $\overset{\bullet}{\pi}{}_c{}^a(\overset{\bullet}{x})\ \overset{\bullet}{\partial}_\mu\, \overset{\bullet}{\pi}{}^{-1}{}^c{}_b(\overset{\bullet}{x}) = \breve{\omega}^a{}_{b\mu}(\breve{x})$, where $\breve{\omega}^a{}_{b\mu}(\breve{x})$ is the spin connection defined in the Riemann space. We recall that for an arbitrary matrix M, $Tr\left\{M^{-1}\partial_\mu M\right\} = \partial_\mu \ln Det\, M$, where Det- denotes the determinant, Tr- the trace. Then, in matrix notation $\overset{\bullet}{\pi} := (\overset{\bullet}{\pi}{}_b{}^a)$ and $\breve{\omega}_\mu := (\breve{\omega}^a{}_{b\mu})$, we have $Tr\{\overset{\bullet}{\pi}(\overset{\bullet}{x})\ \overset{\bullet}{\partial}_\mu\, \overset{\bullet}{\pi}{}^{-1}(\overset{\bullet}{x})\} = -\ \overset{\bullet}{\partial}_\mu \ln Det\, \overset{\bullet}{\pi}(\overset{\bullet}{x}) = Tr\, \breve{\omega}_\mu(\breve{x})$, which gives $Det\, \overset{\bullet}{\pi}(\overset{\bullet}{x}) = Det\, \overset{\bullet}{\pi}_0$ $\exp\{-\int_0^{\overset{\bullet}{x}} Tr\, \breve{\omega}_\mu(\breve{x})\, d\overset{\bullet}{x}{}'^\mu\}$. Hence $\overset{\bullet}{\pi}(\overset{\bullet}{x}) = \overset{\bullet}{\pi}(0) \exp[-\int_0^{\overset{\bullet}{x}} \breve{\omega}_\mu(\breve{x})\, d\overset{\bullet}{x}{}'^\mu]$, where $\overset{\bullet}{\pi}(0) \equiv C\ \overset{\bullet}{\pi}_0$, C is an arbitrary proper constant matrix $|C| = 1$. Provided, $\overset{\bullet}{\Omega}{}_\mu{}^\nu = \overset{\bullet}{\pi}{}_\mu{}^\rho\ \overset{\bullet}{\pi}{}_\rho{}^\nu$, $\overset{\bullet}{\Omega}{}_b{}^a = \overset{\bullet}{\pi}{}_c{}^a\ \overset{\bullet}{\pi}{}_b{}^c = \overset{\bullet}{\Omega}{}_\mu{}^\nu\, \breve{e}^a{}_\nu\, \breve{e}_b{}^\mu$, $\overset{\bullet}{e}_\rho = \overset{\bullet}{\pi}{}_\rho{}^\nu\, \breve{e}_\nu \equiv \overset{\bullet}{\partial}_\rho = \frac{\partial}{\partial \overset{\bullet}{x}{}^\rho}$, $\overset{\bullet}{\vartheta}{}^\rho = \overset{\bullet}{\pi}{}^\rho{}_\mu\, \breve{\vartheta}^\mu \equiv d\,\overset{\bullet}{x}{}^\rho$. Under a local spacetime deformation $\overset{\bullet}{\pi}(\overset{\bullet}{x})$, the tetrad changes according to $\overset{\bullet}{e}_a\, \overset{\bullet}{\vartheta}{}^a = \overset{\bullet}{\Omega}{}^a{}_b\, \breve{e}_a\, \breve{\vartheta}^b$, $\overset{\bullet}{e}_c = \overset{\bullet}{\pi}{}_c{}^a\, \breve{e}_a$, $\overset{\bullet}{\vartheta}{}^c = \overset{\bullet}{\pi}{}^c{}_b\, \breve{\vartheta}^b$, and, the general deformed spin connection vanishes $\overset{\bullet}{\omega}{}^a{}_{b\mu} = \overset{\bullet}{\pi}{}_c{}^a\, \breve{\omega}^c{}_{d\mu}\ \overset{\bullet}{\pi}{}^d{}_b + \overset{\bullet}{\pi}{}_c{}^a\ \overset{\bullet}{\partial}_\mu\, \overset{\bullet}{\pi}{}^c{}_b = \overset{\bullet}{e}{}^a{}_\sigma\ \overset{\bullet}{\Gamma}{}^\sigma{}_{\rho\mu}\ \overset{\bullet}{e}{}_b{}^\rho + \overset{\bullet}{e}{}^a{}_\rho\ \overset{\bullet}{\partial}_\mu\, \overset{\bullet}{e}{}_b{}^\rho \equiv 0$. In fact, a general linear connection, $\overset{\bullet}{\Gamma}{}^\mu{}_{\rho\sigma}$, is related to the corresponding spin connection, $\overset{\bullet}{\omega}{}^a{}_{b\mu}$, through the inverse $\overset{\bullet}{\Gamma}{}^\mu{}_{\rho\sigma} = \overset{\bullet}{e}{}_a{}^\mu\ \overset{\bullet}{\partial}_\sigma\, \overset{\bullet}{e}{}^a{}_\rho + \overset{\bullet}{e}{}_a{}^\mu\ \overset{\bullet}{\omega}{}^a{}_{b\sigma}\ \overset{\bullet}{e}{}^b{}_\rho = \overset{\bullet}{e}{}_a{}^\mu\ \overset{\bullet}{\partial}_\sigma\, \overset{\bullet}{e}{}^a{}_\rho$, which is the the Weitzenböck connection revealing the Weitzenböck spacetime W_4 of the teleparallel gravity (see next subsect.). Thus,

doi: 10.52526/25792776-2021.68.2-311

$\overset{\bullet}{\pi}\,(\overset{\bullet}{x})$ can be referred to as the Weitzenböck deformation matrix. The above equations are simply different ways of expressing the property that the total—that is, acting on both indices—derivative of the tetrad vanishes identically. According to the two-step spacetime deformations map, the next first deformation matrices $\sigma(x) := (\sigma_b{}^a)(x)$, contribute to corresponding ingredient part, $\chi_b{}^d$, of general deformation tensor, $\Omega_b{}^a = \chi_b{}^d \overset{\bullet}{\Omega}{}_d{}^a = \chi_b{}^d \overset{\bullet}{\tilde{\Omega}}{}_\rho{}^\nu \breve{e}_\nu{}^a \breve{e}^\rho{}_d$, $\overline{\chi}_d{}^c = \sigma_e{}^c \sigma_d{}^e$, $\overline{\chi}_e{}^d \overset{\bullet}{\pi}{}_b{}^e = \chi_b{}^e \overset{\bullet}{\pi}{}_e{}^d$, or $\Omega_\mu{}^\nu = \chi_\mu{}^\rho \overset{\bullet}{\tilde{\Omega}}{}_\rho{}^\nu$, $\chi_\mu{}^\rho = \chi_b{}^d \breve{e}_d{}^\rho \breve{e}^b{}_\mu$. Under a deformation, $\sigma(x)$, in general, the tetrad changes according to $e_c = (\sigma_c{}^d \overset{\bullet}{\pi}{}_d{}^a)\,\breve{e}_a = \sigma_c{}^d \overset{\bullet}{e}_d$, $\vartheta^c = (\sigma^c{}_e \overset{\bullet}{\pi}{}^e{}_b)\,\breve{\vartheta}^b = \sigma^c{}_e \overset{\bullet}{\vartheta}{}^e$, $e_\rho = \sigma_\rho{}^\sigma \overset{\bullet}{e}_\sigma$, $\vartheta^\rho = \sigma_\sigma{}^\rho \overset{\bullet}{\vartheta}{}^\sigma$, $e_\rho = \sigma_\rho{}^c \overset{\bullet}{e}_c$, $\vartheta^\rho = \sigma_c{}^\rho \overset{\bullet}{\vartheta}{}^c$, $\sigma_\rho{}^c = \sigma_\rho{}^\sigma \overset{\bullet}{e}{}_\sigma{}^c$, $\sigma^\rho{}_c = \sigma^\rho{}_\sigma \overset{\bullet}{e}{}^\sigma{}_c$, $e_c\vartheta^c = \overline{\chi}_d{}^c \overset{\bullet}{e}_c \overset{\bullet}{\vartheta}{}^d = \Omega_b{}^a\, \breve{e}_a\, \breve{\vartheta}^b$. The corresponding second deformation matrices read $\gamma_{cd}(x) = \overline{\chi}_{ee'} \overset{\bullet}{\pi}{}_c{}^e \overset{\bullet}{\pi}{}_d{}^{e'}$, $\overset{\bullet}{\gamma}_{cd}\,(\overset{\bullet}{x}) = o_{ab} \overset{\bullet}{\pi}{}_c{}^a(\overset{\bullet}{x}) \overset{\bullet}{\pi}{}_d{}^b(\overset{\bullet}{x})$, where $\overline{\chi}_{ee'} = o_{ab}\, \sigma_e{}^a \sigma_{e'}{}^b$. Under a local tetrad deformation, a general spin connection transforms according to $\omega'^a_{b\mu} = \sigma_c{}^a \overset{\bullet}{\omega}{}^c{}_{d\mu} \sigma^d{}_b + \sigma_c{}^a \partial_\mu \sigma^c{}_b$, such that $\overset{(\sigma)}{\omega}{}^a{}_{b\mu} := \omega'^a_{b\mu} = \sigma_c{}^a \partial_\mu \sigma^c{}_b$, is referred to as the *deformation related frame connection*, which represents the *deformed properties of the frame* only. Then, it follows that the affine connection, Γ, related to tetrad deformations, transforms through $\Gamma^\mu{}_{\rho\sigma} = e_a{}^\mu \partial_\sigma e^a{}_\rho + e_a{}^\mu \overset{(\pi)}{\omega}{}^a{}_{b\sigma} e^b{}_\rho = \sigma_a{}^\mu \partial_\sigma \sigma^a{}_\rho + \sigma_a{}^\mu \overset{(\sigma)}{\omega}{}^a{}_{b\sigma} \sigma^b{}_\rho$, where $\sigma_a{}^\mu \sigma_\mu{}^b = \delta^b_a$, also the procedure can be inverted $\sigma_a{}^\mu \sigma_\nu{}^a = \delta^\mu_\nu$, and that $\overset{(\pi)}{\omega}{}^a{}_{b\mu} := \omega^a{}_{b\mu} = \pi^a{}_c \breve{\omega}^c{}_{d\mu} \pi^{db} + \pi^a{}_c \partial_\mu \pi^{cb}$, is the spin connection. Then, the line element, $d\,s^2$ may alternatively be recast in general form of the spacetime or frame objects, respectively, as $d\,s^2 = g_{\mu\nu}\, \vartheta^\mu \otimes \vartheta^\nu = g(e_\mu, e_\nu)\, \vartheta^\mu \otimes \vartheta^\nu = (\Omega_\mu{}^\nu \Omega_\rho{}^\sigma)\, \breve{g}_{\nu\sigma}\, \breve{\vartheta}^\mu \otimes \breve{\vartheta}^\rho = o_{ab}\, \vartheta^a \otimes \vartheta^b = (\Omega_a{}^c \Omega_b{}^d) o_{cd}\, \breve{\vartheta}^a \otimes \breve{\vartheta}^b = \gamma_{cd}\, \breve{\vartheta}^c \otimes \breve{\vartheta}^d$. For our convenience, the notation, $\{\overset{(A)}{e}{}_a, \overset{(A)}{\vartheta}{}^b\}\,(A = \pi, \sigma)$, will be used below for general linear frames $\{\overset{(A)}{e}{}_a, \overset{(A)}{\vartheta}{}^b\} = \{(\overset{(\pi)}{e}{}_a, \overset{(\sigma)}{e}{}_a), (\overset{(\pi)}{\vartheta}{}^b, \overset{(\sigma)}{\vartheta}{}^b)\} \equiv \{(e_a, \overset{\bullet}{e}_a), (\vartheta^b, \overset{\bullet}{\vartheta}{}^b)\}$, where $\overset{(A)}{e}{}_a \rfloor \overset{(A)}{\vartheta}{}^b = \delta^b_a$, or in components, $\overset{(A)}{e}{}_a{}^\mu \overset{(A)}{e}{}^b{}_\mu = \delta^b_a$, also the procedure can be inverted $\overset{(A)}{e}{}^a{}_\rho \overset{(A)}{e}{}_a{}^\sigma = \delta^\sigma_\rho$. Provided, $\overset{(A)}{e}{}_a{}^\mu = (\overset{(\pi)}{e}{}_a{}^\mu, \overset{(\sigma)}{e}{}_a{}^\mu) \equiv (e_a{}^\mu, \sigma_a{}^\mu)$. Hence, the affine connection can be re-written in the abbreviated form $\Gamma^\mu{}_{\rho\sigma} = \overset{(A)}{e}{}_a{}^\mu \partial_\sigma \overset{(A)}{e}{}^a{}_\rho + \overset{(A)}{e}{}_a{}^\mu \overset{(A)}{\omega}{}^a{}_{b\sigma} \overset{(A)}{e}{}^b{}_\rho$. Since the first deformation matrices $\pi(x)$ and $\sigma(x)$ are arbitrary functions, the transformed general spin connections $\overset{(\pi)}{\omega}\,(x)$ and $\overset{(\sigma)}{\omega}\,(x)$, as well as the affine connection, are independent of tetrad fields and their derivatives. In what follows, therefore, we will separate the notions of space and connections-the metric-affine formulation of gravity. A metric-affine space $(\mathcal{M}_4,\ g,\ \Gamma)$ is defined to have a metric and a linear connection that need not dependent on each other. The new geometrical property of the spacetime, are the *nonmetricity* one-form N_{ab} and the affine *torsion* two-form T^a representing a translational misfit. These, together with the *curvature* two-form $R_a{}^b$, symbolically can be presented as $(N_{ab},\ T^a,\ R_a{}^b) \ \sim\ \mathcal{D}(g_{ab},\ \vartheta^a,\ \Gamma_a{}^b)$, where $\mathcal{D}$ is the *covariant exterior derivative*. We may introduce the contortion tensors related to the *deformation related frame connection* and the spin connection: $\overset{(A)}{K}{}^c{}_{a\nu} = \overset{(A)}{\omega}{}^c{}_{a\nu} + \overset{(A)}{\Delta}{}^c{}_{a\nu}$, , where $\overset{(A)}{\Delta}{}_{\mu\rho\nu} = \overset{(A)}{e}{}_{\mu a} \overset{(A)}{e}{}^a{}_{[\rho,\nu]} - \overset{(A)}{e}{}_{\rho a} \overset{(A)}{e}{}^a{}_{[\mu,\nu]} - \overset{(A)}{e}{}_{\nu a} \overset{(A)}{e}{}^a{}_{[\mu,\rho]}$, is referred to as the the Ricci coefficients of rotation. Both the contortion tensor and spin connection are antisymmetric in their first two indices. The relations between the corresponding torsion and contortion tensors read $\overset{(A)}{K}{}^\rho{}_{\mu\nu} := 2\, \overset{(A)}{Q}{}_{(\mu\nu)}{}^\rho + \overset{(A)}{Q}{}^\rho{}_{\mu\nu}$, $\overset{(A)}{Q}{}^\rho{}_{\mu\nu} = \overset{(A)}{K}{}^\rho{}_{[\mu\nu]}$, where $\overset{(A)}{Q}{}^\rho{}_{\mu\nu} = \overset{(A)}{\omega}{}^\rho{}_{[\mu\nu]} + \overset{(A)}{e}{}^a{}_{[\mu,\nu]} \overset{(A)}{e}{}^\rho_a$. Let us define then a translation in the connection space. Suppose a point in this space will be a Lorentz connection, $\overset{(\pi)}{\omega}\,(x) := \overset{(\pi)}{\omega}{}^{bc}{}_\mu(x)\, J_{bc}\, d\,x^\mu$, presenting simultaneously curvature and torsion written in the language of differential forms as $\overset{(\pi)}{R} = d\, \overset{(\pi)}{\omega} + \overset{(\pi)}{\omega}\, \overset{(\pi)}{\omega} \equiv \mathcal{D}_{\overset{(\pi)}{\omega}}\, \overset{(\pi)}{\omega}$, $\quad \overset{(\pi)}{T} = d\,e + \overset{(\pi)}{\omega}\ e \equiv \mathcal{D}_{\overset{(\pi)}{\omega}}\, e$, where $\mathcal{D}_{\overset{(\pi)}{\omega}}$ denotes the covariant differential in the connection $\overset{(\pi)}{\omega}$. For more detail see (Ter-Kazarian, 2011).

2.3. Teleparallel gravity

The total covariant derivative of a geometrical object carrying both flat and curvilinear indices is covariant with respect to both diffeomorphism and local Lorentz symmetries. In both, W_4 and

doi: 10.52526/25792776-2021.68.2-311

U_4, spaces the total covariant derivative of the vierbein field, $e^a{}_\nu$, is assumed to vanish $\mathcal{D}_\mu e^a{}_\nu = \partial_\mu e^a{}_\nu - \Gamma^\rho{}_{\nu\mu} e^a{}_\rho + \omega^a{}_{b\mu} e^b{}_\nu = 0$, which provides a relation between both connections. We may now introduce the Weitzenböck torsion $\overset{\bullet}{T}{}^\rho{}_{\mu\nu} := \overset{\bullet}{\Gamma}{}^\rho{}_{\mu\nu} - \overset{\bullet}{\Gamma}{}^\rho{}_{\nu\mu}$, and the Weitzenböck contortion: $\overset{\bullet}{K}{}^\rho{}_{\mu\nu} := \frac{1}{2}(\overset{\bullet}{T}{}_\nu{}^\rho{}_\mu + \overset{\bullet}{T}{}_\mu{}^\rho{}_\nu + \overset{\bullet}{T}{}^\rho{}_{\mu\nu})$. We then obtain $\overset{\bullet}{T}{}^\rho{}_{\mu\nu} = T^\rho{}_{\mu\nu} - \omega^\rho{}_{\mu\nu} + \omega^\rho{}_{\nu\mu}$. and $\overset{\bullet}{K}{}^\rho{}_{\mu\nu} = K^\rho{}_{\mu\nu} + \omega^\rho{}_{\mu\nu}$. Below, we will concentrate on the specific space, W_4, of vanishing affine torsion in the class of frames, $\{\overset{\bullet}{e}_a\}$: $T^\rho{}_{\mu\nu} = 0$. While, the metricity condition holds: $\overset{\bullet}{N}_{ab} := -\overset{\bullet}{\mathcal{D}}\, g_{ab} = 0$, and that $\Gamma^\rho{}_{\mu\nu} = \overset{\circ}{\Gamma}{}^\rho{}_{\mu\nu}$, as in the Riemann space. Consequently, $K^\rho{}_{\mu\nu} = 0$, and $\overset{\bullet}{K}{}^\rho{}_{\mu\nu} = \omega^\rho{}_{\mu\nu}$. Hence, $\overset{\bullet}{\Gamma}{}^\rho{}_{\mu\nu} = \overset{\circ}{\Gamma}{}^\rho{}_{\mu\nu} + \overset{\bullet}{K}{}^\rho{}_{\mu\nu} = \Gamma^\rho{}_{\mu\nu} + \overset{\bullet}{K}{}^\rho{}_{\mu\nu}$, while, the Weitzenböck covariant derivative of the tetrad field vanishes identically: $\overset{\bullet}{\mathcal{D}}_\nu \overset{\bullet}{e}{}^a{}_\mu \equiv \overset{\bullet}{\partial}_\nu \overset{\bullet}{e}{}^a{}_\mu - \overset{\bullet}{\Gamma}{}^\rho{}_{\mu\nu} \overset{\bullet}{e}{}^a{}_\rho = 0$. This is the so called distant, or absolute parallelism condition. As a consequence of this condition, the corresponding Weitzenböck spin connection also vanishes identically: $\overset{\bullet}{\omega}{}^c{}_{a\nu} = \overset{\circ}{\omega}{}^c{}_{a\nu} + \overset{\bullet}{K}{}^c{}_{a\nu} \equiv 0$. Of course, these relations above are true only in one specific class of frames. In fact, since $\overset{\bullet}{\omega}{}^c{}_{a\nu}$ is the Weitzenböck spin connection, if it vanishes in a given frame, it will be different from zero in any other frame related to the first by a local Lorentz transformation. In teleparallel gravity, the coupling of spinor fields with gravitation is a highly controversial subject. However, it seems there is no compelling arguments supporting the choice of the Weitzenböck spin connection $\overset{\bullet}{\omega}{}^c{}_{a\nu}$ as the spin connection of teleparallel gravity, otherwise several problems are immediately encountered with such coupling prescription. The teleparallel gravity becomes consistent and fully equivalent with GR, even in the presence of spinor fields if we write the minimal coupling prescription as $\overset{\bullet}{\partial}_a \to \overset{\bullet}{\mathcal{D}}_a = \overset{\bullet}{e}{}_a{}^\mu\, \overset{\bullet}{\mathcal{D}}_\mu$ with $\overset{\bullet}{\mathcal{D}}_\mu$ the teleparallel Fock-Ivanenko derivative written in the form $\overset{\bullet}{\mathcal{D}}_\mu := \overset{\bullet}{\partial}_\mu - \frac{i}{2}\, \overset{\bullet}{\Omega}{}^a{}_{b\mu} J_a{}^b$, where the teleparallel spin connection, $\overset{\bullet}{\Omega}{}^a{}_{b\mu}$, reads $\overset{\bullet}{\Omega}{}^a{}_{b\mu} := 0 - \overset{\bullet}{K}{}^a{}_{b\mu}$. Field equations can be derived from the least action, $\delta\, \overset{\bullet}{S} = 0$, with the total invariant action of conventional theory of teleparallel gravity.

2.4. The TSSD-induced dynamical torsion in tensorial form

In this section we construct the TSSD-U_4 theory, which considers curvature and torsion as representing independent degrees of freedom. The RC manifold, U_4, is a particular case of general metric-affine manifold $\mathcal{M}_4$, restricted by the metricity condition $N_{\lambda\mu\nu} = 0$, when a nonsymmetric linear connection is said to be metric compatible. Taking the antisymmetrized derivative of the metric condition gives an identity between the curvature of the spin-connection and the curvature of the Christoffel connection $\overset{(A)}{R}{}_{\mu\nu}{}^{ab}(\overset{(A)}{\omega})\, \overset{(A)}{e}{}_{\rho b} - R^\sigma{}_{\rho\mu\nu}(\Gamma)\, \overset{(A)}{e}{}_\sigma{}^a = 0$, where $\overset{(A)}{R}{}_{\mu\nu}{}^{ab}(\overset{(A)}{\omega}) = \partial_\mu \overset{(A)}{\omega}{}_\nu{}^{ab} - \partial_\nu \overset{(A)}{\omega}{}_\mu{}^{ab} + \overset{(A)}{\omega}{}_\mu{}^{ac}\, \overset{(A)}{\omega}{}_{\nu c}{}^b - \overset{(A)}{\omega}{}_\nu{}^{ac}\, \overset{(A)}{\omega}{}_{\mu c}{}^b$, $R^\sigma{}_{\rho\mu\nu}(\Gamma) = \partial_\mu \Gamma^\sigma_{\nu\rho} - \partial_\nu \Gamma^\sigma_{\mu\rho} - \Gamma^\lambda_{\mu\rho}\Gamma^\sigma_{\nu\lambda} + \Gamma^\lambda_{\nu\rho}\Gamma^\sigma_{\mu\lambda}$. Hence, the relations between the scalar curvatures for an U_4 manifold read $\overset{(A)}{R}(\overset{(A)}{\omega}) \equiv \overset{(A)}{e}{}_a{}^\mu\, \overset{(A)}{e}{}_b{}^\nu\, \overset{(A)}{R}{}_{\mu\nu}{}^{ab}(\overset{(A)}{\omega}) = R(g,\Gamma) \equiv g^{\rho\nu} R^\mu_{\rho\mu\nu}(\Gamma)$. This means that the Lorentz and diffeomorphism invariant scalar curvature, R, becomes either a function of $\overset{(A)}{e}{}^a_\mu$ only, or a function of $g_{\mu\nu}$ only. Certainly, it can be seen by noting that the Lorentz gauge transformations can be used to fix the six antisymmetric components of $\overset{(A)}{e}{}^a_\mu$ to vanish. Then in both cases diffeomorphism invariance fixes four more components out of the six $g_{\mu\nu}$, with the four components $g_{0\mu}$ being non dynamical, obviously, leaving only two dynamical degrees of freedom. This shows the equivalence of the vierbein and metric formulations holds.

The total *Einstein-Cartan action* can be written in the terms of the spin connection, $\overset{(\pi)}{\omega}$ and the *deformation related frame connection*, $\overset{(\sigma)}{\omega}$, in the form $S = S_g^{(A)}(\overset{(A)}{\omega}) + S_m^{(\pi)}(\overset{(\pi)}{\omega}) = -\frac{1}{2æ}\int \overset{(A)}{R}\sqrt{-g}\, d\,\Omega + \int L_m^{(\pi)}(g,\,\Psi,\,\nabla\Psi)\sqrt{-g}\, d\,\Omega$, where $S_g^{(A)}$ $(A = \pi,\,\sigma)$ is the action for the gravitational field written in terms of scalar curvature $\overset{(A)}{R}(\overset{(A)}{\omega})$ for an U_4 manifold, while $S_m^{(\pi)}$ is the action for the matter fields, æ is the coupling constant relating to Newton gravitational constant $æ = 8\pi G/c^4$. The action regards the contortion tensor as a variational variable, in addition to the gravitational and matter fields. The gravitational action can be decomposed as $S_g^{(A)} = -\frac{1}{2æ}\int \overset{\circ}{R}\sqrt{-g}\, d\,\Omega + S_Q^{(A)}$, where the

doi: 10.52526/25792776-2021.68.2-311

torsional action reads $S_Q^{(A)} = \frac{1}{2æ}\int d\,\Omega\,\sqrt{-g}L_Q^{(A)}$ The coupling constant of the spin-tortion is the same of that of the mass-metric distortion field interaction. The dynamical spin density tensor, which is antisymmetric in the Lorentz indices, reads $\overset{(\pi)}{s}{}_{\mu}{}^{ab} = 2\frac{\delta(\sqrt{-g}\,L_m^{(\pi)})}{\delta\overset{(\pi)}{\omega}{}^{\mu}{}_{ab}} = 2\frac{\delta(\sqrt{-g}\,L_m^{(\pi)})}{\delta\overset{(\pi)}{K}{}^{\mu}{}_{ab}} = \sqrt{-g}\;\overset{(\pi)}{S}{}_{\mu}{}^{ab}$. The variation of the action have to be applied by independent variation of the fields g, $\overset{(\pi)}{\omega}(x)$ (or equivalently $\overset{(\pi)}{K}(x)$) and $\Psi(x)$, $\overline{\Psi}(x)$. In terms of the Euler-Lagrange variations, the least action $\delta S = 0$ gives $\delta g^{\mu\nu}$: $\overset{\circ}{G}_{\mu\nu} + \frac{\delta(\sqrt{-g}\,L_Q^{(A)})}{\delta g_{\mu\nu}} = -2æ\frac{\delta(\sqrt{-g}\,L_m^{(\pi)})}{\delta g^{\mu\nu}}$; $\delta\;\overset{(\pi)}{\omega}{}_{\nu}{}^{\mu\rho}$: $\frac{\partial\overset{(A)}{\omega}{}_{\nu'}{}^{\mu'\rho'}}{\partial\overset{(\pi)}{\omega}{}_{\nu}{}^{\mu\rho}}\frac{\delta}{\delta\overset{(A)}{\omega}{}_{\nu'}{}^{\mu'\rho'}}(\sqrt{-g}\,L_Q^{(A)}) = -\frac{\delta(\sqrt{-g}\,L_m^{(\pi)})}{\delta\overset{(\pi)}{\omega}{}_{\nu}{}^{\mu\rho}}$; $\delta\,\Psi$: $\frac{\delta\,(\sqrt{-g}\,L_m^{(\pi)})}{\delta\,\Psi} = 0$; $\delta\,\overline{\Psi}$: $\frac{\delta\,(\sqrt{-g}\,L_m^{(\pi)})}{\delta\overline{\Psi}} = 0$, where $\overset{\circ}{G}_{\mu\nu}$ is the Einstein tensor. Hence, the *first Einstein-Cartan equation* is written $\overset{\circ}{G}_{\mu\nu} =æ\;\overset{(A)}{\theta}{}_{\mu\nu}$, where including the spin contributions directly into the energy-momentum tensor, we introduce the canonical energy-momentum tensor $\overset{(A)}{\theta}{}_{\mu\nu}$: $= T_{\mu\nu} + \overset{(A)}{U}{}_{\mu\nu}$. For variations $\delta\;\overset{(\pi)}{K}{}^{\nu}{}_{\mu\rho}$ (or equivalently $\overset{(\pi)}{\omega}{}^{\nu}{}_{\mu\rho}$), the $\delta S = 0$ gives the *second Einstein-Cartan equation* $\frac{\partial\overset{(A)}{\omega}{}_{\nu'}{}^{\mu'\rho'}}{\partial\overset{(\pi)}{\omega}{}_{\nu}{}^{\mu\rho}}(\overset{(A)}{\mathcal{T}})\;\overset{(A)}{\mathcal{T}}{}^{\nu'}{}_{\mu'\rho'} = -\frac{1}{2}æ\;\overset{(\pi)}{S}{}^{\nu}{}_{\mu\rho}$,where the *modified torsion* reads $\overset{(A)}{\mathcal{T}}{}^{\nu}{}_{\mu\rho} := \frac{1}{2\sqrt{-g}}\frac{\delta(\sqrt{-g}\,L_Q^{(A)})}{\delta\overset{(A)}{\omega}{}_{\nu}{}^{\mu\rho}} = \overset{(A)}{Q}{}^{\nu}{}_{\mu\rho} + \delta^{\nu}_{\mu}\;\overset{(A)}{Q}{}_{\rho} - \delta^{\nu}_{\rho}\;\overset{(A)}{Q}{}_{\mu}$. Thus, the equations of the standard Einstein-Cartan theory can be recovered for $A = \pi$: $\overset{\circ}{G}_{\mu\nu} =æ\;\overset{(\pi)}{\theta}{}_{\mu\nu}$, $\quad\overset{(\pi)}{\mathcal{T}}{}^{\nu}{}_{\mu\rho} = -\frac{1}{2}æ\;\overset{(\pi)}{S}{}^{\nu}{}_{\mu\rho}$, in which the equation defining torsion is the algebraic type, such that torsion at a given point in spacetime does not vanish only if there is matter at this point, represented in the Lagrangian density by a function which depends on torsion. Unlike the metric, which is related to matter through a differential field equation, torsion does not propagate. However, these equations can be equivalently replaced by the set of *modified Einstein-Cartan equations* for $A = \sigma$: $\overset{\circ}{G}_{\mu\nu} =æ\;\overset{(\sigma)}{\theta}{}_{\mu\nu}$, $\quad\Theta^{\mu'\rho'\nu}_{\nu'\mu\rho}(\overset{(\sigma)}{\mathcal{T}})\;\overset{(\sigma)}{\mathcal{T}}{}^{\nu'}{}_{\mu'\rho'} = -\frac{1}{2}æ\;\overset{(\pi)}{S}{}^{\nu}{}_{\mu\rho}$, where $\frac{\partial\overset{(\sigma)}{\omega}{}_{\nu'}{}^{\mu'\rho'}}{\partial\overset{(\pi)}{\omega}{}_{\nu}{}^{\mu\rho}}(\overset{(\sigma)}{\mathcal{T}}) := \Theta^{\mu'\rho'\nu}_{\nu'\mu\rho}(\overset{(\sigma)}{\mathcal{T}}) \equiv \Theta^{\mu'\rho'\nu}_{\nu'\mu\rho}(\pi(x),\,\sigma(x))$, in which the torsion $\overset{(\sigma)}{\mathcal{T}}{}^{\nu}{}_{\mu\rho}$ is a *dynamical* if only $\Theta^{\mu'\rho'\nu}_{\nu'\mu\rho}(\pi(x),\,\sigma(x)) \neq \delta^{\mu'}_{\mu}\,\delta^{\rho'}_{\rho}\,\delta^{\nu}_{\nu'}$. Therefore, it is spin that generates a nonsymmetric part in the canonical energy-momentum tensor and then, produces a deviation from the Riemann geometry. The variation of $S_m^{(\pi)}$ with respect to the metric-compatible affine connection in the metric-affine variational formulation of gravity is equivalent to the variation with respect to the torsion (or contortion) tensor. Consequently, the dynamical spin density $\overset{(\pi)}{s}{}_{ab}{}^{\mu}$ is identical with $\overset{(\pi)}{\Sigma}{}_{ab}{}^{\mu} = \frac{\partial(\sqrt{-g}\,L_m)^{(\pi)}}{\partial\Psi_{,\mu}}\;\overset{(\pi)}{S}{}_{ab}\;\Psi$, referred to as the *canonical spin density*. The canonical tensor $e\;\overset{(A)}{\theta}{}_{\mu\nu} = \tau_{\mu\nu} = e_{a\nu}\,\tau_{\mu}{}^{a}$ is generally not symmetric, whereas the canonical energy-momentum density is identical with the dynamical tetrad energy-momentum density $e\;\overset{(A)}{\theta}{}_{\mu}{}^{a} = \tau_{\mu}{}^{a}$, where $e := det|e^{\mu}_{a}| = \sqrt{-g}$. The relation between the tetrad dynamical energy-momentum tensor and the metric dynamical energy-momentum tensor for matter fields is $\overset{(A)}{\theta}{}_{(\mu\nu)} = T_{\mu\nu}$. The Belinfante-Rosenfeld relation, between the dynamical metric and dynamical tetrad (canonical) energy-momentum tensors, can be written as $\overset{(A)}{\theta}{}_{\mu\nu} - T_{\mu\nu} = \frac{1}{2}\nabla^{*}_{\nu}(\overset{(\pi)}{S}{}_{\mu\rho}{}^{\nu} - \overset{(\pi)}{S}{}_{\rho}{}^{\nu}{}_{\mu} + \overset{(\pi)}{S}{}^{\nu}{}_{\mu\rho}) = \overset{(A)}{U}{}_{\mu\nu}$, where $\nabla^{*}_{\mu} = \nabla_{\mu} - 2\;\overset{(\pi)}{Q}{}_{\mu}$ is the *modified covariant derivative*. The conservation law for the spin density results from antisymmetrizing the Belinfante-Rosenfeld relation with respect to the indices μ,ρ: $\overset{(\pi)}{s}{}_{\mu\nu}{}^{\rho}{}_{;\rho} = \tau_{\mu\nu} - \tau_{\nu\mu} + 2\;\overset{(\pi)}{Q}{}_{\rho}\;\overset{(\pi)}{s}{}_{\mu\nu}{}^{\rho}$ or $\frac{1}{2}\nabla^{*}_{\rho}\;\overset{(\pi)}{S}{}_{\mu\nu}{}^{\rho} = \overset{(A)}{\theta}{}_{[\mu\nu]}$.

2.5. TSSD-U_4 theory in the language of the differential forms

In this subsection we re-derive the field equations of the TSSD-U_4 theory by using the exterior calculus. The fields have to be expressed in terms of differential forms in order to build the total

Lagrangian four-form as the appropriate integrand of the action. Let $\overset{(A)}{\omega}{}^{ab} = \overset{(A)}{\omega}{}^{ab}_{\mu} \wedge dx^{\mu}$ be the one-forms of corresponding connections assuming values in the Lorentz Lie algebra. The action for gravitational field can be written in the form $S_g = \overset{\circ}{S} + S_Q = -\frac{1}{4æ}\int \star \overset{\circ}{R} + S_Q$, provided, $\overset{\circ}{R} \equiv \overset{\circ\,(\sigma)}{R}{}_{cd} \wedge \overset{\bullet}{\vartheta}{}^{c} \wedge \overset{\bullet}{\vartheta}{}^{d} = \overset{\circ\,(\pi)}{R}{}_{cd} \wedge \vartheta^{c} \wedge \vartheta^{d}$. Consider a phenomenological action of the spin-torsion interaction, S_Q, such that the variation of the connection one-form $\overset{(A)}{\omega}{}^{ab}$ yields $\delta S_Q = \frac{1}{æ}\int \star \overset{(A)}{\mathcal{T}}{}_{ab} \wedge \delta \overset{(A)}{\omega}{}^{ab}$, where $\star \overset{(A)}{\mathcal{T}}{}_{ab}: \; = \frac{1}{2} \star (\overset{(A)}{Q}{}_{a} \wedge \overset{(A)}{e}{}_{b})$, and that $\overset{(A)}{Q}{}^{a} = \overset{(A)}{D} \overset{(A)}{\vartheta}{}^{a} = d \overset{(A)}{\vartheta}{}^{a} + \overset{(A)}{\omega}{}^{a}{}_{b} \wedge \overset{(A)}{\vartheta}{}^{b}$, with the wedge product monomial, $\overset{(A)}{\vartheta}{}^{\mu\nu\alpha}$, defined on the U_4 space. The variation of the action describing the macroscopic matter sources $S_m^{(\pi)}$ with respect to coframe ϑ^{a}, and connection one-form $\overset{(\pi)}{\omega}{}^{ab}$ reads $\delta S_m = \int \delta L_m = \int (-\star \overset{(A)}{\theta}{}_{a} \wedge \delta \overset{(A)}{\vartheta}{}^{a} + \frac{1}{2} \star \overset{(\pi)}{\Sigma}{}_{ab} \wedge \delta \overset{(\pi)}{\omega}{}^{ab})$, where $\star \overset{(A)}{\theta}{}_{a}$ is the dual three-form relating to the canonical energy-momentum tensor, $\overset{(A)}{\theta}{}^{\mu}_{a}$, by $\star \overset{(A)}{\theta}{}_{a} = \frac{1}{3!} \overset{(A)}{\theta}{}^{\mu}_{a} \varepsilon_{\mu\nu\alpha\beta} \overset{(A)}{\vartheta}{}^{\nu\alpha\beta}$. and $\star \overset{(\pi)}{\Sigma}{}_{ab} = -\star \overset{(\pi)}{\Sigma}{}_{ba}$ is the dual three-form corresponding to the canonical spin tensor, which is identical with the dynamical spin tensor $\overset{(\pi)}{S}{}_{abc}$, namely $\star \overset{(\pi)}{\Sigma}{}_{ab} = \overset{(\pi)}{S}{}^{\mu}{}_{ab} \varepsilon_{\mu\nu\alpha\beta} \vartheta^{\nu\alpha\beta}$. The integral $\overset{\circ}{S} = -\frac{1}{4æ}\int \star \overset{\circ}{R} = -\frac{1}{4æ}\int \star \overset{\circ\,(A)}{R}{}_{cd} \wedge \overset{(A)}{\vartheta}{}^{c} \wedge \overset{(A)}{\vartheta}{}^{d}$, is the usual Einstein action, written in the language of the exterior forms. Actually, writing explicitly the holonomic indices, we have $\overset{\circ}{S} = -\frac{1}{8æ}\int \overset{\circ\,(A)}{R}{}_{\mu\nu}{}^{ab} \overset{(A)}{e}{}^{c}_{\alpha} \overset{(A)}{e}{}^{d}_{\beta} \varepsilon_{abcd} \overset{(A)}{\vartheta}{}^{\mu\nu\alpha\beta} = -\frac{1}{8æ}\int \overset{\circ\,(A)}{R}{}_{\mu\nu}{}^{ab} \varepsilon_{ab\alpha\beta} \varepsilon^{\mu\nu\alpha\beta} d\Omega$. Also, one may readily verify that $\overset{\circ}{S} = -\frac{1}{2æ}\int \overset{\circ\,(A)}{R}{}_{\mu\nu}{}^{ab} \overset{(A)}{e}{}^{[\mu}_{\alpha} \overset{(A)}{e}{}^{\nu]}_{\beta} e\, d\Omega = -\frac{1}{2æ}\int \overset{\circ}{R} \sqrt{-g}\, d\Omega$. and $\delta S_Q = \frac{1}{æ}\int \overset{(A)}{\mathcal{T}}{}_{\mu\nu}{}^{\beta} \delta \overset{(A)}{\omega}{}^{\mu\nu}_{\beta}$. The variation of the total action, given by the sum of the gravitational field action and the matter action, with respect to the e^{a}, $\overset{(\pi)}{\omega}{}^{ab}$, and Ψ, gives 1) $\frac{1}{2} \overset{\circ\,(A)}{R}{}_{cd} \wedge \overset{(A)}{\vartheta}{}^{c} = æ \overset{(A)}{\theta}{}_{d}$, 2) $\frac{\partial \overset{(A)}{\omega}{}^{a'b'}}{\partial \overset{(\pi)}{\omega}{}^{ab}} \wedge \star \overset{(A)}{\mathcal{T}}{}_{a'b'} = -\frac{1}{2} æ \star \overset{(\pi)}{\Sigma}{}_{ab}$, 3) $\frac{\delta L_m^{(\pi)}}{\delta \Psi} = 0$, $\frac{\delta L_m^{(\pi)}}{\delta \bar{\Psi}} = 0$.

2.6. Short-range spin-spin interaction

In fact, torsion constitutes the more natural and simple way to introduce spin in general relativity. For that reason it is of fundamental importance to see if there are some experiences that indicate, if not directly at least indirectly, the presence of torsion. The most important experiments include neutron interferometry, neutron spin rotation induced by torsion in vacuum, anomalous spin-dependent forces with a polarized mass torsion pendulum, space-based searches for spin in gravity, etc. On the other hand, from the theoretical point of view, a problem of primary importance is to obtain the equation describing the short-range propagating torsion and showing the existence of torsion waves that may contribute a new special polarized effects in these experiments. A broad motivation of the present theoretical work just is the propagating torsion, which, in natural way, can be made a short-range propagating. We then see that it is the spin $\overset{(\pi)}{S}$ and spacetime deformations $\pi(x)$ and $\sigma(x)$ that define the torsion $\overset{(A)}{Q}$: $\overset{(A)}{Q}{}^{\nu}{}_{\mu\rho} = \overset{(A)}{\mathcal{T}}{}^{\nu}{}_{\mu\rho} + \frac{1}{2}\delta^{\nu}_{\mu} \overset{(A)}{\mathcal{T}}{}^{\lambda}{}_{\rho\lambda} - \frac{1}{2}\delta^{\nu}_{\rho} \overset{(A)}{\mathcal{T}}{}^{\lambda}{}_{\mu\lambda}$, which, in turn, defines the Einstein's field tensor $\overset{\circ}{G}$. This allows us to define the constraint, which, imposed upon the spacetime deformations $\pi(x)$ and $\sigma(x)$, yields the torsion and spin-spin interaction to be short-range propagating: $\Theta^{\mu'\rho'\nu}_{\nu'\mu\rho}(\pi(x), \sigma(x)) = (\Box + M^2_{\mathcal{T}}) \overset{(\sigma)}{\mathcal{T}}{}^{\nu}{}_{\mu\rho} (\overset{(\sigma)}{\mathcal{T}}{}^{-1})_{\nu'}^{\mu'\rho'}$, where $\Box$ is a generalization of the d'Alembertian operator for covariant derivatives defined on the RC manifold, U_4. Then, the set of *modified Einstein-Cartan equations* reduced to $\overset{\circ}{G}_{\mu\nu} = æ \overset{(\sigma)}{\theta}{}_{\mu\nu}$, $(\Box + M^2_{\mathcal{T}}) \overset{(\sigma)}{\mathcal{T}}{}^{\nu}{}_{\mu\rho} = -\frac{1}{2} æ \overset{(\pi)}{S}{}^{\nu}{}_{\mu\rho}$. At large distances $r > \lambda_{\mathcal{T}} \equiv \frac{\hbar}{M_{\mathcal{T}}c}$ (Compton length), torsion vanishes $\overset{(\sigma)}{\mathcal{T}}(r) = 0$, so in this case the torsion and spin-spin interaction are short-range propagating. To carry through TSSD-U_4 theory in full generality, below, for example, we may explicitly write the torsionic equation for the Dirac spinor matter source coupled to the metric and to the torsion, both contained implicitly in the connection

doi: 10.52526/25792776-2021.68.2-311

$\overset{(\pi)}{\omega}{}^{ba}{}_{\mu}$. The spinor connection $\overset{(\pi)}{\Gamma}_{\mu}$ is given, up to the addition of an arbitrary vector multiple of I, by the *Fock-Ivanenko coefficients*: $\overset{(\pi)}{\Gamma}_{\mu} = -\frac{1}{4}\overset{(\pi)}{\omega}{}_{ab\mu}\gamma^a\gamma^b = -\frac{1}{2}\overset{(\pi)}{\omega}{}_{ab\mu}S^{ab} = -\frac{1}{8}e^{\nu}_{c;\mu}[\overset{(\pi)}{g}{}_{\nu}, \gamma^c] = \frac{1}{8}[\overset{(\pi)}{g}{}^{\nu}{}_{;\mu}, \overset{(\pi)}{g}{}_{\nu}]$, with $S^{ab} = \frac{1}{2}\gamma^{[a}\gamma^{b]} = \frac{1}{4}(\gamma^a\gamma^b - \gamma^b\gamma^a)$ - the spinor representation, where γ^a are Dirac matrices, and $\overset{(A)}{g}{}^{\mu} = \overset{(A)}{e}{}_a{}^{\mu}\gamma^a$. Consequently, the torsionic equation can be recast into the form $(\Box + M^2_{\mathcal{T}})\overset{(\sigma)}{\mathcal{T}}{}^{\nu}{}_{\mu\rho} = -\frac{i}{4}æ\bar{\psi}\overset{(\pi)}{g}{}^{[\mu}\overset{(\pi)}{g}{}^{\nu}\overset{(\pi)}{g}{}^{\rho]}\psi$, where ψ satisfies the *Heisenberg-Ivanenko* non-linear equation: $i\overset{(\pi)}{g}{}^{\rho}\psi_{;\rho} - \frac{3æ}{8}(\bar{\psi}\overset{(\pi)}{g}{}_{\rho}\gamma^5\psi)\overset{(\pi)}{g}{}^{\rho}\gamma^5\psi = m\psi$. This is the Dirac equation written in the so-called second-order formalism, in which the contortion tensor is given explicitly in terms of the spin sources. In the limit when we neglect the usual Riemannian terms depending on the metric and the curvature ($\partial_{;\mu} \to \partial_{\mu}$), as we are interested only in the spin-torsion interaction, we have then $\overset{(\sigma)}{\mathcal{T}}{}^{\nu}{}_{\mu\rho}(x) = \frac{æ}{2}\int G_F(x, x')\overset{(\pi)}{S}{}^{\nu}{}_{\mu\rho}(x')\,d^4x'$ where the Feynman propagator reads $G_F(x, x') = -\frac{1}{4\pi}\delta(s) + \frac{M_{\mathcal{T}}}{8\pi\sqrt{s}}H^{(1)}_1(M_{\mathcal{T}}\sqrt{s})$ if $s \geq 0$; and $G_F(x, x') = -\frac{iM_{\mathcal{T}}}{4\pi^2\sqrt{-s}}K_1(M_{\mathcal{T}}\sqrt{-s})$ if $s < 0$, provided $s = (x - x')^2$, $H^{(1)}_1$ is the Hankel function of first kind and K_1 is a modified Bessel function. We emphasize that the short-range propagating torsion may contribute a new special polarized effects in the gravitational waves experiments. Neutron interferometry is powerful method to verification of gravitational spin-torsion interaction, whereas it was assumed that the neutron beams (I and II) are polarized in the antiparallel direction to the z axis. In the situation when one (or both) neutron beam(s) interact with torsion the states should be changed, and the interferences of these beams leads to the effect of the polarized rotation plane. So we can observe the effect of the polarized rotation plane due to quantum interferometry, which is caused by the interaction with torsion. At this point we cut short our discussion, and refer the interested reader to original paper (Ter-Kazarian, 2011) for more detail.

3. The TSSD-metric-affine gravity behind the spacetime deformation

At low energies the spacetime group associated the matter fields is the Poincaré group (PG). An extension of the Poincaré gauge theory of gravity constructed in the RC geometry, to the most general spacetime symmetry gauge theory, the MAG theory, has the most general type of covariant derivative: in addition to curvature and torsion, the MAG also has nonmetricity, i.e., a nonmetric compatible connection. Hence parallel transport no longer preserves length and angle.

3.1. Outline of the key points of TSSD-MAG

Note that there is only indications (but no conclusive evidence) for assuming invariance of physical systems under the action of the entire affine group, and that in MAG one is far from actually calculating S-matrix elements. Although the theoretical structure of this theory has been developed, we do not yet much understanding of what new physics is allowed by the MAG theory. One source of improved understanding is exact solutions, and references therein. But due to the highly nonlinear nature of theory, exact solutions are not easily found unless they have a great deal of symmetry. However, to carry in full generality through the extension of TSSD-ideas as applied to more general metric-affine gravity, it reasonable as a next step to gauge immediately the $4 + 16$ parameter *affine* group $A(4, R) = R^4 \otimes GL(4, R)$, which lacks a metric structure altogether and to introduce the metric *subsequently*. General affine invariance adds *dilation* and *shear* invariance as physical symmetries to Poincaré invariance, and both of these symmetries are of physical importance. Dilation invariance is a crucial component of particle physics in the high energy regime. Shear invariance was shown to yield representations of hadronic matter, the corresponding shear current can be related to hadronic quadrupole excitations. From this in the framework of the gauge theory of the affine group with a metric supplemented, as a physically meaningful field theory, it is speculated that the invariance under affine transformations played an essential part at an early stage of the universe, such that todays Poincaré invariance might be a remnant of affine invariance after some symmetry breaking mechanism.

doi: 10.52526/25792776-2021.68.2-311

Thus MAG encompasses the PG as a subcase. A brief outline of the key points of relevance to the context of TSSD can be stated here. To this aim, one enlarges at any point of the base manifold $x \in \widetilde{M}$ a tangent space $T_x\widetilde{M}$ to an *affine tangent space* $A_x\widetilde{M}$ by allowing to freely translate elements of $T_x\widetilde{M}$ to different points $p \in A_x\widetilde{M}$. The collection of all affine tangent spaces $A_x\widetilde{M}$ forms the *affine bundle* $A\widetilde{M}$. An *affine frame* of $\widetilde{M}$ at x is a pair $(\overset{(A)}{e}_a, p)$ (where as before $A = \pi, \sigma$) consisting of a linear frame $\overset{(A)}{e}_a \in L_x\widetilde{M}$ and a point $p \in A_x\widetilde{M}$. The origin of $A_x\widetilde{M}$ is that point $o_x \in A_x\widetilde{M}$ for which the affine frame $(\overset{(A)}{e}_a, o_x) \in A_x\widetilde{M}$ reduces to the linear frame $\overset{(A)}{e}_a \in L_x\widetilde{M}$. The transformation behavior of an affine frame $(\overset{(A)}{e}_a, p)$ under an affine transformation (Λ, τ) with $\tau = \tau^a \in T^4 \simeq R^4$ and $\Lambda = \Lambda_a{}^b \in GL(4, R)$ reads $(\overset{(A)}{e}, p) \overset{(\Lambda,\tau)}{\longrightarrow} (\overset{(A)}{e}{}', p') = (\overset{(A)}{e}\,\Lambda,\, p+\tau) = (\overset{(A)}{e}_b\,\Lambda_a{}^b,\, p+\tau^a\,\overset{(A)}{e}_a)$. The affine group acts transitively on the affine tangent spaces $A\widetilde{M}$: Any two affine frames of some $A_x\widetilde{M}$ can be related by a unique affine transformation. Consequently, the notion of an affine frame should be enlarged to include all $GL(4, R)$-representations needed. The gauging is accomplished by the introduction of the *generalized affine connection* as a prescription $(\overset{(A)}{\Gamma}{}^{(L)}, \overset{(A)}{\Gamma}{}^{(T)})$, which maps infinitesimally neighbouring affine tangent spaces $A_x\widetilde{M}$, $A_{\tilde{x}}\widetilde{M}$, where $\tilde{x} = x + dx$, by an $A(4, R)$-transformation onto each other. The generalized affine connection consists of a $GL(4, R)$-valued 1-form $\overset{(A)}{\Gamma}{}^{(L)}$ and an R^4-valued one form $\overset{(A)}{\Gamma}{}^{(T)}$, both of which generate the required $A(4, R)$-transformation. The two affine tangent spaces get now related by an affine transformation according to the prescription $dp = \overset{(A)}{\Gamma}{}^{(T)a}\,\overset{(A)}{e}_a$, $d\,\overset{(A)}{e}_a = \overset{(A)}{\Gamma}{}^{(L)b}_{a}\,\overset{(A)}{e}_b$. By introducing origins in $A_x\widetilde{M}$, i.e. by soldering $A_x\widetilde{M}$ to $\widetilde{M}$, one losts translational invariance in $A_x\widetilde{M}$ but gained a local one-to-one correspondence *between translations* in $A_x\widetilde{M}$ *and diffeomorphisms* on $\widetilde{M}$. However, one can introduce translational invariance by demanding diffeomorphism invariance instead and continue to work with this modified notion of translation invariance. The diffeomorphisms itself, as horizontal transformations in their active interpretation, cannot be gauged according to the usual gauge principle and thus do not furnish their own gauge potential.

3.2. Lagrangian formulation of the TSSD-MAG

In the Lagrangian formulation of a general metric-affine theory it was assumed that the matter fields are described in terms of manifields. Actually, the matter fields, denoted in the following by ψ, are supposed to be represented by vector- or spinor-valued p-forms. However, in MAG one goes beyond Poincaré invariance, assuming that matter fields might not only undergo Poincaré transformations but also the more general linear transformations. In this case, the unavailability of local Lorentz frames poses no problem in the context of boson fields. They are naturally constructed so as to be capable of carrying the action of $SL(4, R)$, instead of the Lorentz group, whether in a local frame or holonomically. However, this is not true of the conventional fermion fields one uses to represent matter, and a linear action should nevertheless be realized, through the use of infinite-component linear field representations of the double-covering of the linear, affine and diffeomorphism groups. More general spinor-representations than the Poincaré-representations have to be constructed. Such representations of the matter fields corresponding to the affine group must exist. Otherwise it does not make sense to demand $A(4, R)$-invariance of a non-vacuum field theory. The construction of the spinor representations of fermionic matter fields in MAG is called *manifields*. These representations turn out to be infinite dimensional, due to the non-compactness of the gauge (sub-)group $GL(4, R)$. Fermions are then assigned to spinor manifields. The restriction of $GL(4, R)$ to $SO(1, n-1)$ reduces the manifield representations to the familiar spinor representations. The actual gauging of the affine group introduced, in addition to the matter fields ψ, the gravitational gauge potentials $\overset{(A)}{\Gamma}{}^{(T)}$ and $\overset{(A)}{\Gamma}{}^{(L)}$. Following the common practice, we will use as gauge potential the translation invariant $\overset{(A)}{\vartheta}{}^a$ in place of the translational part $\overset{(A)}{\Gamma}{}^{(T)}$ of the affine connection, simply because it has the immediate interpretation as a reference (co-)frame. Expanded in a holonomic frame, the components of $\overset{(A)}{\vartheta}{}^a$ and $\overset{(A)}{\Gamma}{}^{(T)}$ differ just by a Kronecker symbol, as is clear from the definition of $\overset{(A)}{\vartheta}{}^a$. Also the homogeneous

doi: 10.52526/25792776-2021.68.2-311

transformation behavior of $\overset{(A)}{\vartheta}{}^{a}$ will turn out to be quite convenient. For the action of the $GL(4,R)$-gauge potential, below the shorthand notation $\overset{(A)}{\Gamma}{}_{a}{}^{b}$ is used instead of $(\overset{(A)}{\Gamma}{}_{c}{}^{(L)d}L^{c}{}_{d})_{a}{}^{b}$. The introduction of a metric into MAG is mandatory since we are interested in a realistic macroscopic gravity theory that contains GR in some limit. So, it was assumed a *metric* of the general form $\overset{(A)}{g} = \overset{(A)}{g}{}_{ab}\,\overset{(A)}{\vartheta}{}^{a}\otimes\overset{(A)}{\vartheta}{}^{b}$ with coefficients $\overset{(A)}{g}{}_{ab}$ which are independent of the coframe $\overset{(A)}{\vartheta}{}^{a}$. The gauge potentials $(\overset{(A)}{\vartheta}{}^{a}, \overset{(A)}{\Gamma}{}_{a}{}^{b})$ become true dynamical variables if one has to add to the minimally coupled matter Lagrangian $L^{(\pi)}_{m}$ a gauge Lagrangian V. Here, we restrict ourself considering only first order Lagrangian V, which must be expressed in terms of the gauge potentials and their first derivatives. The total action reads then $S = \int[V(\overset{(A)}{g}{}_{ab}, \overset{(A)}{\vartheta}{}^{a}, \overset{(A)}{N}{}_{ab}, \overset{(A)}{T}{}^{a}, \overset{(A)}{R}{}_{a}{}^{b}) + L^{(\pi)}_{m}(\overset{(A)}{g}{}_{ab}, \overset{(A)}{\vartheta}{}^{a}, \Psi, D\Psi)]$. If Ψ, as a p-form, represents a matter field (fundamentally a representation of the $SL(4,R)$ or of some of its subgroups), its first order Lagrangian $L^{(\pi)}_{m}$ will be embedded in metric-affine spacetime by the minimal coupling procedure, that is, exterior covariant derivatives feature in the kinetic terms of the Lagrangian instead of only exterior ones. Just as ordinary stress is the analogue of the (Hilbert) energy-momentum density, in MAG, one has, in addition, the spin current and the dilation plus shear currents inducing the torsion and nonmetricity fields, respectively. Both spin and dilation plus shear are components of the hypermomentum current, symmetric for dilation plus shear and antisymmetric for spin: *spin current* $\otimes$ *dilation current* $\otimes$ *shear current*. And these currents ought to couple to the corresponding post-Riemannian structures. In accord, the material currents are defined as follows: $\overset{(A)}{t}{}^{ab} := 2\,\frac{\delta L^{(\pi)}_{m}}{\delta \overset{(A)}{g}{}_{ab}}$, $\overset{(A)}{\theta}{}_{a} := \frac{\delta L^{(\pi)}_{m}}{\delta \overset{(A)}{\vartheta}{}^{a}}$, $\overset{(\pi)}{\Delta}{}^{a}{}_{b} := \frac{\delta L^{(\pi)}_{m}}{\delta \overset{(\pi)}{\Gamma}{}_{a}{}^{b}}$, where $\overset{(A)}{t}{}^{ab}$ is the metric (and symmetric) energy-momentum current of matter (`Hilbert current` ´), whereas one believes that $\overset{(A)}{\theta}{}_{a}$ should be the dual 3-form relating to the canonical energy-momentum tensor, $\overset{(A)}{\theta}{}^{\mu}{}_{a}$, by $\star\,\overset{(A)}{\theta}{}_{a} = \frac{1}{3!}\,\overset{(A)}{\theta}{}^{\mu}{}_{a}\,\varepsilon_{\mu\nu\alpha\beta}\,\overset{(A)}{\vartheta}{}^{\nu\alpha\beta}$, where we used the abbreviated notations for the wedge product monomials, $\overset{(A)}{\vartheta}{}^{\mu\nu\alpha\ldots} = \overset{(A)}{\vartheta}{}^{\mu}\wedge\overset{(A)}{\vartheta}{}^{\nu}\wedge\overset{(A)}{\vartheta}{}^{\alpha}\wedge\ldots$ and $\star$ denotes the Hodge dual (see Appendix). The canonical energy-momentum density is identical with the dynamical tetrad energy-momentum density $e\,\overset{(A)}{\theta}{}^{a}{}_{\mu} = \overset{(A)}{\tau}{}^{a}{}_{\mu}$, where $e := det|e^{\mu}_{a}| = \sqrt{-g}$, and that the canonical tensor $e\,\overset{(A)}{\theta}{}_{\mu\nu} = \overset{(A)}{\tau}{}_{\mu\nu} = \overset{(A)}{e}{}_{a\nu}\,\overset{(A)}{\tau}{}^{a}{}_{\mu}$ is generally not symmetric. The relation between the tetrad dynamical energy-momentum tensor and the metric dynamical energy-momentum tensor for matter fields is $\overset{(A)}{\theta}{}_{(\mu\nu)} = t_{\mu\nu}$. The canonical hypermomentum current $\overset{(\pi)}{\Delta}{}^{a}{}_{b}$, which couples to the linear connection, can be decomposed according to $\overset{(\pi)}{\Delta}{}_{ab} = \overset{(\pi)}{S}{}_{ab} + \frac{1}{4}\,\overset{(\pi)}{g}{}_{ab}\,\Delta + \widehat{\Delta}_{\alpha\beta}$, with $\overset{(\pi)}{S}{}_{ab} := \overset{(\pi)}{\Delta}{}_{[ab]}$ as (dynamical) spin current, $\Delta := \overset{(\pi)}{\Delta}{}^{c}{}_{c}$, as dilation current, and $\widehat{\Delta}_{ab}$ as symmetric and tracefree shear current, which is a bit more remote from direct observation than the other currents. From variation of a total action, we find the matter and the gauge field equations as follows: $D(\frac{\partial L^{(\pi)}_{m}}{\partial(D\Psi)}) - (-1)^{p}\,\frac{\partial L^{(\pi)}_{m}}{\partial\Psi} = 0$, $(matter)$, $D(2\,\frac{\partial V}{\partial \overset{(A)}{N}{}_{ab}}) + 2\,\frac{\partial V}{\partial \overset{(A)}{g}{}_{ab}} = -\,\overset{(A)}{t}{}^{ab}$, $(0th)$, $D(\frac{\partial V}{\partial \overset{(A)}{T}{}^{a}}) + \frac{\partial V}{\partial \overset{(A)}{\vartheta}{}^{a}} = -\,\overset{(A)}{\theta}{}_{a}$, $(1st)$, $\frac{\partial \overset{(A)}{\omega}{}_{a'}{}^{b'}}{\partial \overset{(\pi)}{\omega}{}_{a}{}^{b}} \wedge [D(\frac{\partial V}{\partial \overset{(A)}{R}{}_{a'}{}^{b'}}) + \overset{(A)}{\vartheta}{}^{a'} \wedge \frac{\partial V}{\partial \overset{(A)}{T}{}^{b'}} + 2\,\overset{(A)}{g}{}_{b'c}\,\frac{\partial V}{\partial \overset{(A)}{N}{}_{a'c}}] = -\,\overset{(\pi)}{\Delta}{}^{a}{}_{b}$, $(2nd)$, where we taken into account that the variation of $L^{(\pi)}_{m}$ with respect to the affine connection in MAG is equivalent to the variation with respect to the torsion (or contortion) or spin connection: $(\partial\,\overset{(A)}{\omega}{}_{a'}{}^{b'}/\partial\,\overset{(\pi)}{\omega}{}_{a}{}^{b} = \partial\,\overset{(A)}{\Gamma}{}_{a'}{}^{b'}/\partial\,\overset{(\pi)}{\Gamma}{}_{a}{}^{b})$. Note that, using the Noether identities, the zeroth field equation can be shown to be redundant, provided the matter equations hold. In first, the canonical energy-momentum of the translational gauge potential $\overset{(A)}{\vartheta}{}^{a}$ can be written in standard form $\frac{\partial V}{\partial \overset{(A)}{\vartheta}{}^{a}} = \overset{(A)}{e}{}_{a}\rfloor V - (\overset{(A)}{e}{}_{a}\rfloor\,\overset{(A)}{T}{}^{b}) \wedge \frac{\partial V}{\partial \overset{(A)}{T}{}^{b}} - (\overset{(A)}{e}{}_{a}\rfloor\,\overset{(A)}{R}{}_{b}{}^{c}) \wedge \frac{\partial V}{\partial \overset{(A)}{R}{}_{b}{}^{c}} - (\overset{(A)}{e}{}_{a}\rfloor\,\overset{(A)}{N}{}_{bc})\,\frac{\partial V}{\partial \overset{(A)}{N}{}_{bc}}$. Thus, the equations of the standard MAG theory written

doi: 10.52526/25792776-2021.68.2-311

in the framework of the first order Lagrangian, which is expressed in terms of the gauge potentials and their first derivatives, can be recovered for $A=\pi$. Consequently, the (2nd) equation defines a non-dynamical torsion, such that torsion at a given point in spacetime does not vanish only if there is matter at this point, represented in the Lagrangian density by a function which depends on torsion. Unlike the metric, which is related to matter through a differential field equation, torsion does not propagate. However, equations can be equivalently replaced by the set of *modified MAG equations* for $A=\sigma$: $D(\frac{\partial L_m^{(\pi)}}{\partial(D\Psi)})-(-1)^p\frac{\partial L_m^{(\pi)}}{\partial\Psi}=0$, $(matter)$, $D(2\frac{\partial V}{\partial \overset{(\sigma)}{N}_{ab}})+2\frac{\partial V}{\partial \overset{(\sigma)}{g}_{ab}}=-\overset{(\sigma)}{t}{}^{ab}$, $(0th)$, $D(\frac{\partial V}{\partial \overset{(\sigma)}{T}{}^a})+\frac{\partial V}{\partial \overset{(\sigma)}{\vartheta}{}^a}=-\overset{(\sigma)}{\theta}{}_a$, $(1st)$, $\Theta^{ab'}_{a'b}(\pi(x),\sigma(x))\wedge[D(\frac{\partial V}{\partial \overset{(\sigma)}{R}{}_{a'}{}^{b'}})+\overset{(\sigma)}{\vartheta}{}^{a'}\wedge\frac{\partial V}{\partial \overset{(\sigma)}{T}{}^{b'}}+2\overset{(\sigma)}{g}{}_{b'c}\frac{\partial V}{\partial \overset{(\sigma)}{N}{}_{a'c}}]=-\overset{(\pi)}{\Delta}{}^a{}_b$, $(2nd)$, where $\frac{\partial \overset{(\sigma)}{\omega}{}_{a'}{}^{b'}}{\partial \overset{(\pi)}{\omega}{}_a{}^b}:=\Theta^{ab'}_{a'b}(\pi(x),\sigma(x))$, in which the torsion is *dynamical* if only $\Theta^{ab'}_{a'b}(\pi(x),\sigma(x))\neq\delta^{a'}_a\,\delta^b_{b'}$. Actually, in testing the general MAG equations, we desire, in some limit, to recover the field equation for different (sub-)cases, then we have to put on *Lagrange multipliers*. Whereas, in the case of TSSD-PG, one has to kill nonmetricity; TSSD-EC is the TSSD-PG with the curvature scalar as gravitational Lagrangian; in the case of TSSD-teleparallel gravity (TSSD-GR$_{||}$) in a Weitzenböck spacetime, one has to remove nonmetricity and curvature; and, finally, in the case of GR in a Riemannian space, curvature scalar as Lagrangian, one has to remove nonmetricity and torsion.

Teleparallel gravity. Finally, we will concentrate on the other (sub-)case when $t^a{}_{bc}=\overset{(\pi)}{T}{}^a{}_{bc}-\overset{(\pi)}{C}{}^a{}_{bc}$, and the connection $\overset{(\pi)}{\omega}{}^a{}_{bc}$ vanishes, which characterizes teleparallel gravity. In this case, the field equations can be derived from the least action, $\delta\overset{\bullet}{S}=0$, with the Lagrangian of teleparallel gravity, where we take Lagrange multipliers for extinguishing nonmetricity, curvature, which holds when the deformation $\sigma(x)$ vanishes identically ($\sigma(x)\equiv 0$): $V_{||}=-\frac{1}{4æ}\overset{\bullet}{T}{}^a\wedge{}^*(-{}^{(1)}\overset{\bullet}{T}_a+2{}^{(2)}\overset{\bullet}{T}_a+\frac{1}{2}{}^{(3)}\overset{\bullet}{T}_a)+\frac{1}{2}\overset{\bullet}{N}_{ab}\wedge{}^{(1)}\lambda^{ab}+\overset{\bullet}{R}{}_a{}^b\wedge{}^{(2)}\lambda^a{}_b$, where the three irreducible pieces of the torsion $\overset{(A)}{T}{}^a={}^{(1)}\overset{(A)}{T}{}^a+{}^{(2)}\overset{(A)}{T}{}^a+{}^{(3)}\overset{(A)}{T}{}^a$ under $SO(1,3)$-decomposition are: ${}^{(1)}\overset{(A)}{T}{}^a:=\overset{(A)}{T}{}^a-{}^{(2)}\overset{(A)}{T}{}^a-{}^{(3)}\overset{(A)}{T}{}^a$,(tentor); ${}^{(2)}\overset{(A)}{T}{}^a:=\frac{1}{3}\overset{(A)}{\vartheta}{}^a\wedge(\overset{(A)}{e}{}_b\rfloor\overset{(A)}{T}{}^b)$, (trator); ${}^{(3)}T^a:=-\frac{1}{3}{}^*(\overset{(A)}{\vartheta}{}^a\wedge{}^*(\overset{(A)}{T}{}^b\wedge\overset{(A)}{\vartheta}{}_b))$, (axiator). The projective transformation $\overset{(A)}{\Gamma}{}_a{}^b\longrightarrow\overset{(A)}{\Gamma}{}_a{}^b+\delta^b_a P$, with arbitrary 1-form field P, leaves the Hilbert-Einstein type Lagrangian invariant, which leads to the connection determined up to a 1-form. Projectively related connections have the same (unparametrized) geodesics. So, only projectively invariant matter Lagrangians would be allowed. This necessitates to abandon this constraint, at the very least replacing semi-Riemann geometry by Weyl's. Namely, to remove this constraint from the gravitational Lagrangians, we may lift the Lagrange multiplier λ^{ab} and add a dilaton type massless scalar field to $V'=V+\frac{1}{2}d\Phi\wedge\star d\Phi$, in the context of the Weyl 1-form $\overset{(A)}{N}$, which is of the type of a gauge potential for dilations anyways: $V'_{\rm GR}=-\frac{1}{4æ}(\overset{(A)}{R}{}^{ab}\wedge\overset{(A)}{\eta}{}_{ab}+\beta\overset{(A)}{N}\wedge\star\overset{(A)}{N})+\overset{(A)}{T}{}^a\wedge{}^{(2)}\lambda_a$, and $V'_{\rm EC}=-\frac{1}{4æ}(\overset{(A)}{R}{}^{ab}\wedge\overset{(A)}{\eta}{}_{ab}+\beta\overset{(A)}{N}\wedge\star\overset{(A)}{N})$, respectively. Provided, the trace $\overset{(A)}{\Gamma}{}_c{}^c$ of a connection is closely related to the Weyl 1-form, as $\overset{(A)}{\Gamma}{}_c{}^c=2\overset{(A)}{N}+d\ln\sqrt{|\det\overset{(A)}{g}{}_{ab}|}$, $d\overset{(A)}{\Gamma}{}_c{}^c=\overset{(A)}{R}{}_c{}^c=2\,d\overset{(A)}{N}$. In case if matter is present and supplies energy-momentum and hypermomentum currents, then the *hypermomentum*, via the second field equation, turns out to be proportional to the *post*-Riemannian pieces of the connection.

In case of translational gauge with the most general term $V=d\overset{(A)}{\vartheta}{}^a\wedge\overset{(A)}{H}{}_a$, quadratic in $\overset{(A)}{\vartheta}{}^a$, the field equation $\delta L_{tot}/\delta\overset{(A)}{\vartheta}{}^a=0$ then becomes $\frac{\partial\overset{(A)}{\vartheta}{}_a}{\partial\overset{(\pi)}{\vartheta}{}^{a'}}\wedge[d\overset{(A)}{H}{}_{a'}-\overset{(A)}{E}{}_{a'}]=\overset{(A)}{\theta}{}_a$, where $\overset{(A)}{H}{}_a$ is linear in $d\overset{(A)}{\vartheta}{}^a$, and $\overset{(A)}{E}{}_a=(\overset{(A)}{e}{}_a\rfloor d\overset{(A)}{\vartheta}{}^b)\wedge\overset{(A)}{H}{}_b-\frac{1}{2}\overset{(A)}{e}{}_a\rfloor(d\overset{(A)}{\vartheta}{}^b\wedge\overset{(A)}{H}{}_b)=\frac{1}{2}[(\overset{(A)}{e}{}_a\rfloor d\overset{(A)}{\vartheta}{}^b)\wedge\overset{(A)}{H}{}_b-d\overset{(A)}{\vartheta}{}^b\wedge(\overset{(A)}{e}{}_a\rfloor\overset{(A)}{H}{}_b)]$, the energy-momentum current of the gauge field. This can be considered as a starting

doi: 10.52526/25792776-2021.68.2-311

point for turning to the Lagrangians with the quadratic ansatz for the kinetic term, i.e. quadratic in the field strengths, which would be an interesting topic not discussed in this paper. For more detail see (Ter-Kazarian, 2015).

4. An extended phase space stochastic quantization of constrained hamiltonian systems

In this section , we give a theory of the extended phase space stochastic quantization of constrained hamiltonian systems (Ter-Kazarian & Sobouti, 2008).

Objectives. The concept of an `extended´ Lagrangian, $\mathcal{L}(p,\, q,\, \dot{p},\, \dot{q})$ in phase space allows a subsequent extension of Hamilton's principle to actions minimum along the actual trajectories in $(p,\, q)-$, rather than in $q-$space. The following notational conventions are used throughout this paper: $\dot{p}$ denotes dp/dx_0 and so on, where x_0 is the real time. This extension, in turn, allows a definition of "second" momenta $\pi_p = \delta\,\mathcal{L}/\delta\,\dot{p}$ and $\pi_q = \delta\,\mathcal{L}/\delta\,\dot{q}$, and a subsequent introduction of an "extended" phase space $(p,\, q,\, \pi_p,\, \pi_q)$ and of an "extended" Hamiltonian, $\mathcal{H}(p,\, q,\, \pi_p,\, \pi_q)$. This simple formalism manifests its practical and technical virtue in the proposed canonical quantization in $(p,\, q)$ space that at once provides a framework for quantum statistical mechanics, for the classical statistical mechanics (Liouville's equation), for the conventional quantum mechanics as a special case, for von Neumann's density matrix and its equation of evolution as its inevitable corollaries. Wigner's distributions and the equation satisfied by them are also obtained by an appropriate canonical transformation in the proposed $(p,\, q,\, \pi_p,\, \pi_q)$-space.

Ordering of p and q factors in conventional quantum mechanics has always been a matter of debate. For, there is nothing in the basic postulates of quantum mechanics to decide on the issue. On the other hand the phase space quantization is constructed on the premises that p and q are independent variables. Thus, in reducing the theory to that of Schrödinger and/or Heisenberg, the standard ordering emerges as the rule of game. For example, qp in $q-$representation and pq in $p-$representation. For Wigner's distributions the appropriate ordering is the symmetric one. For example, $\frac{1}{2}(pq+qp)$ instead of pq or qp. This ordering is also obtained from the standard ordering by the same canonical transformation which transforms the state functions and evolution equations to those of Wigner.

Since Wigner's initial attempt, 1932, alternative phase space distributions have been proposed. Of these alternatives, the ones compatible with the uncertainty principle are obtainable from that by suitable canonical transformation in $(p,\, q,\, \pi_p,\, \pi_q)$-space. Husimi's all-positive distributions are, however, exceptions. For, his averaging of Wigner's distributions over small cells around phase space points makes the averaged distributions incompatible with the uncertainty principle.

The stochastic quantization method (SQM) of recent years is an alternative to the conventional canonical and path-integral quantizations. Conceptually and techniquewise it is versatile and powerful. Our interest here is to generalize SQM, to study the classical stochastic processes underlying the phase space quantization. In its present formulation, SQM exploits well-defined Markoffian process of Wiener's type with Gaussian white-noise. One may, however, envisage that different stochastic processes with respect to a fictitious time may yield different variations of quantum theories.

4.1. An Extended Phase Space Formulation of SQM

Consider a dynamical system with N degrees of freedom described by the 2N coordinates $q = (q_1, \dots q_N)$ and momenta $p = (p_1, \dots p_N)$ and a Lagrangian $\mathcal{L}^q(q,\, \dot{q})$ in $q-$representation and the corresponding $\mathcal{L}^p(p,\, \dot{p})$ in $p-$representation. In general, $\mathcal{L}^q$ and $\mathcal{L}^p$ are the Fourier transforms of each other. One may now defines an extended Hamiltonian $\mathcal{H}(p,\, q,\, \pi_p,\, \pi_q) = \sum_{n=1}\frac{1}{n!}\{\frac{\partial^n H}{\partial p^n}\pi_q^n - \frac{\partial^n H}{\partial q^n}\pi_p^n\}$, where $H(p,\, q) = p_i\dot{q}_i - \mathcal{L}^q = q_i\dot{p}_i - \mathcal{L}^p$ is the conventional Hamiltonian of the system. Introducing an imaginary time $x_4 = ix_0$, we define the Euclidian extended action as $S[p,\, q,\, \pi_p,\, \pi_q] = \int\left[-i\pi_{p_i}\frac{d\,p_i}{d\,x_4} - i\pi_{q_i}\frac{d\,q_i}{d\,x_4} + \mathcal{H}(p,\, q,\, \pi_p,\, \pi_q)\right]d\,x_4$. Following a general prescription of SQM, in case at hand the Parisi-Wu ansatz consists of proposing a Markoffian hypothetical stochastic process by the following set of Langevin equations: $\frac{d\,q_i}{dt} = -\frac{\delta\,S}{\delta\,q_i} + \xi_i^q(t)$, $\gamma\frac{d\,\pi_{q_i}}{dt} = -\frac{1}{\gamma}\frac{\delta\,S}{\delta\,\pi_{q_i}} + \eta_i^q(t)$, $\gamma\frac{d\,p_i}{dt} =$

doi: 10.52526/25792776-2021.68.2-311

$-\frac{1}{\gamma}\frac{\delta S}{\delta p_i}+\eta^p_i(t)$, $\frac{d\pi_{p_i}}{dt}=-\frac{\delta S}{\delta \pi_{p_i}}+\xi^p_i(t)$, where an additional "fictitious time" t is introduced, the $\xi^\nu_i(t)$ and $\eta^\nu_i(t)$ $(\nu = q, p)$ are Gaussian white-noise sources with $<\xi^\nu_i(t),\, \xi^{\nu'}_j(t')>= 2\,\delta_{ij}\,\delta_{\nu\nu'}\,\delta(t-t')$, $<\eta^\nu_i(t),\, \eta^{\nu'}_j(t')>= 2\,\delta_{ij}\,\delta_{\nu\nu'}\,\delta(t-t')$, $<\xi^\nu_i(t),\, \eta^{\nu'}_j(t')>= 0$, and γ is an arbitrary dimensional parameter. In this, we have only to look upon the fictitious time t as a mathematical tool, but need not to find its physical meaning. A remark on notation: Functional dependencies on variables are indicated by square brackets, such as $S[p, q, ...]$. The formalism being followed is based on a well-defined classical Wiener-Markoffian process. The Gaussian white-noises incorporated into equations above are designed to yield the quantum mechanics as its thermal equilibrium limit. Therefore, the task is to show that the dynamical system has an equilibrium distribution equivalent to the conventional path-integral measure. The procedure is (a) to define a Fokker-Planck Lagrangian, (b) to define Fokker-Planck momenta from this Lagrangian, (c) to compose a Fokker-Planck Hamiltonian, and finally (d) to set up the Fokker-Planck equation for the distribution of the system in the extended phase space. For example, the Fokker-Planck Hamiltonian is: $\mathcal{H}^F = \pi^F_{q_i}\frac{dq_i}{dt}+\pi^F_{\pi_{q_i}}\frac{d\pi_{q_i}}{dt}+\pi^F_{p_i}\frac{dp_i}{dt}+\pi^F_{\pi_{p_i}}\frac{d\pi_{p_i}}{dt}-\mathcal{L}^F$, provided, the Fokker-Planck equation for the probability distribution $\Phi[p,\, q,\, \pi_p,\, \pi_q,\, t]$ is $\frac{\partial}{\partial t}\,\Phi[p,\, q,\, \pi_p,\, \pi_q,\, t] = \mathcal{H}^F\,\Phi[p,\, q,\, \pi_p,\, \pi_q,\, t]$. Here we have replaced the canonical momenta $\pi^F_{q_i}$, $\pi^F_{\pi_{q_i}}$, $\pi^F_{p_i}$ and $\pi^F_{\pi_{p_i}}$ with $-\partial/\partial\, q_i$, $-\partial/\partial\, \pi_{q_i}$, $-\partial/\partial\, p_i$ and $-\partial/\partial\, \pi_{p_i}$, respectively. Then the equilibrium distribution clearly reads $\Phi[p,\, q,\, \pi_p,\, \pi_q] \propto \exp(-S[p,\, q,\, \pi_p,\, \pi_q])$. Thus, the Langevin equation give the same result as the conventional path-integral quantization method in extended phase space if only the drift forces $K_i(p,\ldots t) = -(\frac{\delta S[p,\ldots]}{\delta p_i})_{p=p(x_0,\,t)}$, etc., have a damping effect. Along the trajectories in $(p,\, q)$ space, however, it produces the state functions, $\chi(p,\, q,\, x_0)$: $i\hbar\,\frac{\partial}{\partial x_0}\chi = \mathcal{H}\,\chi$. Solutions are $\chi = a_{\alpha\beta}\,\psi_\alpha(q,\, x_0)\,\phi^*_\beta(p,\, x_0)\,e^{-i\,pq/\hbar}$, $a = a^\dagger$, positive definite, $tr\, a = 1$, where summation over repeated indices is implied, and ψ_α and ϕ^*_α are solutions of the conventional Schrödinger equation in $q-$ and $p-$representations, respectively. They are mutually Fourier transforms $\psi_\alpha(q,\, x_0) = (2\pi\hbar)^{-N/2}\int\,\phi_\alpha(p,\, x_0)\,e^{ipq/\hbar}\,d\,p$, $\phi_\alpha(p,\, x_0) = (2\pi\hbar)^{-N/2}\int\,\psi_\alpha(q,\, x_0)\,e^{-ipq/\hbar}\,d\,q$. Note that the α and β are not, in general, eigenindices. The normalization condition for χ, is $\int\,\chi\,d\,p\,d\,q = tr(a) = 1$.

4.2. Stochastic Quantization of Extended Dynamical Systems With Constraints

Here we discuss the SQM of an extended dynamical system with M first class independent and irreducible constraints $\phi^a(p,\, q,\, \pi_p,\, \pi_q) = 0$, $a = 1, 2, ..., M < N$. For reasons of simplicity let there also be M gauge conditions: $\chi^a(p,\, q,\, \pi_p,\, \pi_q) = 0$, $a = 1, 2, ..., M$. Equations obtained in previous subsection define a $(4N-2M)$ dimensional submanifold in phase space on which the system orbits dwell. For convenience we introduce the following new variables: $x_{q_i} = (q_1,\ldots,q_N,\pi_{p_1},\ldots,\pi_{p_N})$, $x_{p_i} = (p_1,\ldots,p_N,\pi_{q_1},\ldots,\pi_{q_N})$. The gauge conditions are such that $det\,\Delta^{ab} \neq 0$, where Δ^{ab} is the Poisson bracket of χ^a and ϕ^b $\Delta^{ab} = \frac{\partial\chi^a}{\partial x_{q_i}}\frac{\partial\phi^b}{\partial x_{p_i}} - \frac{\partial\chi^a}{\partial x_{p_i}}\frac{\partial\phi^b}{\partial x_{q_i}}$. The Euclidean path-integral measure for such a system can be obtained by the quantization procedure. The Faddeev-Popov path-integral formula for this system is $< f|\, i >= \frac{1}{2N}\int\,\mathcal{D}x_{q_i}\,\mathcal{D}x_{p_i}\,\delta(\phi^a)\,\delta(\chi^a)\,det\,\Delta^{ab}\,exp(-S[x_p,\, xq])$, where $S[x_p,\, x_q]$ is the extended Euclidian action. Our major goal is now to reproduce this equation from the standpoint of SQM in phase space in thermal equilibrium limit. Next we attempt to write the derived equations in a covariant form; that is, in a form invariant under general coordinate transformations. In this, we introduce the notation $(x^I) = (x_I) = (x_{qi}, x_{pi})$, $(X^I) = (Q^a, P^a, Q^\alpha, P^\alpha)$, $I = 1, ..., 4N$. Hereafter, the following convention will be observed in indexing the new variables. To begin with, the x-coordinates are Euclidean ones. It will not matter if they are indexed covariantly or contravariantly. The X-coordinates, on the other hand, are curvilinear ones. A contravariant index could be lowered by an appropriate metric tensor to be introduced shortly. The manifold M^{4N} spanned by X- coordinates could be split into two submanifolds M^{2M} and M^{4N-2M}. The X-coordinates spanning M^{2M} will be indexed by $A, B, ... = 1, ..., 2M$. Those spanning M^{4N-2M} will be indexed by $\Lambda, \Sigma, ... = 2M + 1, ..., 4N$. The indices $I, J, ...,$ will be reserved for the whole manifold M^{4N}. The contravariant metric tensor for the curvilinear X-coordinates is $g^{IJ} = \frac{\partial X^I}{\partial x^K}\frac{\partial X^J}{\partial x_K} = \left[\begin{array}{cc} g^{AB} & \\ & g^{\Lambda\Sigma}\end{array}\right]$, where the $2M\times 2M$ tensor g^{AB} is $g^{AB} = \frac{\partial X^A}{\partial x^K}\frac{\partial X^B}{\partial x_K} = \left[\begin{array}{cc} \{\phi^a,\phi^b\} & \{\phi^a,\chi^b\} \\ \{\chi^a,\phi^b\} & \{\chi^a,\chi^b\}\end{array}\right]$. The Poisson brackets, here,

doi: 10.52526/25792776-2021.68.2-311

are to be calculated in (x_{q_i}, x_{p_i})-coordinates, For conventional gauge conditions one has $\{\chi^a, \chi^b\} = 0$. The Laplace expansion of det g^{AB} then gives det $g^{AB} = -\det\{\phi^c, \chi^d\} det\{\chi^e, \phi^f\} = \det\{\phi^c, \chi^d\}^2$, det $g_{AB} = \det\{\phi^c, \chi^d\}^{-2}$. The expression for $g^{\Lambda\Sigma}$ is $g^{\Lambda\Sigma} = \frac{\partial X^\Lambda}{\partial x^K}\frac{\partial X^\Sigma}{\partial x_K}$; $\Lambda, \Sigma = 2M+1, \cdots, 4N$. For the present, there is no need to manipulate $g^{\Lambda\Sigma}$ beyond its definition. We are now in a position to write down the Langevin equations in manifest covariant forms. Then $\frac{dX^\Lambda}{dx^I}\frac{dX^A}{dx_I} = 0$, and $\frac{dX^A}{dt} = 0$. This gives $\frac{dX^\Lambda}{dt} = -g^{\Lambda\Sigma}\frac{\delta\widetilde{S}[X]}{\delta X^\Sigma} + \frac{\partial X^\Lambda}{dx^I}\zeta^I$, where $\zeta^I = (\xi^i, \eta^j)$, and $\widetilde{S}[X] = S[x(X)]$, is the action integral written in X-coordinates. This equation contains no new information, beyond the fact that ϕ^a, χ^a are to vanish along the phase space trajectories. Finally the form invariant Fokker-Planck equation emerges as $\frac{\partial\widetilde{\Phi}[X^\Lambda,t]}{\partial t} = \frac{1}{\sqrt{det\, g^{\Lambda\Sigma}}}\frac{\partial}{\partial X^\Lambda}[\sqrt{det\, g^{\Lambda\Sigma}}\, g^{\Lambda\Sigma}(\frac{\partial}{\partial X^\Sigma} + \frac{\delta\widetilde{S}[X]}{\delta X^\Sigma})\,\widetilde{\Phi}[X^\Lambda, t]]$. The stationary solution is $\widetilde{\Phi}_{eq}[X^\Lambda] = \frac{1}{\sqrt{det g^{\Lambda\Sigma}}}\, exp(-\widetilde{S}[X^\Lambda])$. In the limit of thermodynamic equilibrium the probability of finding the system on the constraint surface in the volume element $d^{(4N-2M)}X$ centered at X^Λ is $\frac{1}{\sqrt{det g^{\Lambda\Sigma}}}\, exp(-\widetilde{S}[X^\Lambda])\, d^{(4N-2M)}X = \frac{1}{\sqrt{det g^{\Lambda\Sigma}}}\, exp(-\widetilde{S}[X^I])\delta^{(2M)}(X^A)\, d^{(4N)}X$. Where $\delta^{(2M)}(X^A)$ is the Dirac delta function in M^{2M}. It is introduced to ensure that the system stays on the constraint surface. To transform back to the Euclidean coordinates $\{x^I\}$ we note that $\widetilde{S}[X]$ transform into $S[x]$, and the volume element $d^{(4N)}X$ transforms into $\sqrt{det\, g^{IJ}}\, d^{(4N)}x$, where $det(g^{IJ}) = det(g^{AB})\, det(g^{\Lambda\Sigma})$. Hence $\Phi_{eq}[x_p,\, x_q] = det\{\chi^a, \Phi^b\}\, \delta^{(M)}(\chi^c)\, \delta^{(M)}(\Phi^d)\, exp(-S[x_p,\, x_q])$. Thus, one of the most remarkable features of SQM is that one may quantize even dynamical systems with non-holonomic constraints as it is seen in the case of the stochastic gauge fixing.

5. An extended phase space SUSY quantum mechanics

In this section, we will concern ourselves with the *extended* phase space quantum mechanics of particles which have both bosonic and fermionic degrees of freedom (Ter-Kazarian, 2009), i.e., the quantum field theory in $(0+1)$-dimensions in $q-$ (position) and $p-$ (momentum) spaces, exhibiting supersymmetry. We present (N=2)-realization of the supersymmetry algebra, and discuss the vacuum energy and the topology of super-potentials. To demonstrate practical merits of shape-invariance of exactly solvable extended SUSY potentials which has underlying algebraic structure, as an application we obtain analytic expressions for the entire energy spectrum of extended Hamiltonian with *Scarf* potential without ever referring to underlying differential equation.

5.1. Extended phase space SUSY algebra

Practically and techniquewise the conventional SUSY method is versatile and powerful. Following a general prescription of SUSY quantum mechanics, we call an extended phase space quantum mechanical system characterized by an extended Hamiltonian H_{ext} acting in some Hilbert space $\mathcal{H}$ supersymmetric if there exist selfadjoint nilpotent operators $Q_i = Q_i^\dagger$, $\quad i = 1, 2, \ldots, N$, called *supercharges*, which also act on states in $\mathcal{H}$ and fulfill the following SUSY algebra: $\{Q_i,\, Q_j\} = Q_i\, Q_j + Q_j\, Q_i = 2H_{ext}\delta_{ij}$, $[Q_i,\, Q_j] = Q_i\, Q_j - Q_j\, Q_i = 0$, $i, j = 1, \ldots, N$. Pursuing the analogy with these ideas in outlined here approach let a selfadjoint operator $P = P^\dagger$ be *Witten operator* or *Witten parity*, which anticommutes with the supercharges, and therefore commutes with an extended Hamiltonian, and whose square is equal to the identity $\{Q_i,\, P\} = 0$, $[H_{ext},\, P] = 0$, $P^2 = 1$. This operator allows to introduce the notion of *bosonic* and *fermionic* states independently of an underlying space-time symmetry. The Witten parity can also be written in the form $P = (-1)^{n_F}$ where n_F is the fermion-number operator. Therefore, eigenstates of P with eigenvalue -1 correspond to *fermions* and those with $+1$ correspond to *bosons*. In accordance, the bosonic $\mathcal{H}_B$- and fermionic $\mathcal{H}_B$- subspaces read $\mathcal{H}_B = \{\chi \in \mathcal{H} | P\,\chi = +\chi\}$, $\mathcal{H}_F = \{\chi \in \mathcal{H} | P\,\chi >= -\chi\}$. Hence, any state $\chi \in \mathcal{H}$ can be decomposed into its bosonic and fermionic components as follows: $\chi = \begin{pmatrix} \chi_B \\ \chi_F \end{pmatrix}$. The Hilbert space may be written as a product space $\mathcal{H} = \mathcal{H}_0 \otimes \mathcal{C}^2$, and thus, the Witten operator is represented by the third Pauli matrix σ_3: $P = \mathbf{1} \otimes \sigma_3 = \begin{pmatrix} 1 & 0 \\ 0 & -1 \end{pmatrix}$. It will be more appropriate to use the notion *spin-up* and spin-

doi: 10.52526/25792776-2021.68.2-311

down states (of a fictitious spin-$\frac{1}{2}$-particle with mass $m>0$ moving along the d-dimensional Euclidean line $\mathcal{R}^d$ line) instead of bosonic and fermionic states, respectively. Having in addition only cartesian degrees of freedom $\mathcal{H}_0$ is given by the space of square-integrable functions over the d-dimensional Euclidean space $\mathcal{R}^d$, $\quad \mathcal{H}_0 = \mathcal{L}^2(\mathcal{R}^d)\otimes\mathcal{L}^2(\mathcal{R}^d), \quad d\in\mathbf{N}$. The SUSY has also implications on the spectral properties of the extended hamiltonian H_{ext}. First of all, we note $H_{ext}=Q_i^2\geq 0$. That is, the extended Hamiltonian has only non-negative eigenvalues. Suppose that χ_r is an eigenstate of H_{ext} with positive eigenvalue $E_r>0$. Then it follows immediately from the algebra that $\widetilde{\chi_r}(q,p)=\frac{1}{\sqrt{E_r}}\,Q_i\,\chi_r(q,p)$, $i=1,2\ldots,N$, is also an eigenstate with the same positive eigenvalue. Hence, all positive-energy eigenstates occur in spin-up (boson) spin-down (fermion) pairs. Actually, a multiplicity of degeneracy of the levels of Hamiltonian H_{ext} with the energy E equals to a dimension of invariant subspace with respect to the action of all the Q_i. If $E=0$, then the corresponding subspace is one-dimensional - a level of zero point energy. In general, the superalgebra defines the Clifford algebra with the basis of $q_i=\frac{Q_i}{\sqrt{E}}$ for non-zero-energy levels of H_{ext}, which is a key point in the SUSY theories. Due to it a definition of the multiplicity of degeneracy of the energy levels reduced to a definition of a dimension of the representations of the Clifford algebra, which is well-known. For the even and odd number N a dimension of the representation of Clifford algebra is given as $\nu=2^n=2^{[N/2]}$, where $[\ldots]$ means the integer part, namely the ν defines a number of states in given supermultiplet, Thus, the major law for the supermultiplets is that each of them contains an equal number of fermionic and bosonic degrees of freedom $n_B=n_F$. Certainly, re-writing the parity operator in the form $(-1)^{2S}$ where S is the spin angular momentum having eigenvalue $+1$ acting on a bosonic state and eigenvalue -1 acting on a fermionic state, we get $\sum_i <i\mid(-1)^{2S}H_{ext}\mid i>=\sum_i<i\mid(-1)^{2S}Q\,Q^\dagger\mid i>+\sum_i<i\mid(-1)^{2S}Q^\dagger Q\mid i>=\sum_i<i\mid(-1)^{2S}Q\,Q^\dagger\mid i>-\sum_j<j\mid(-1)^{2S}Q\,Q^\dagger\mid j>=0$. Here one has used the relation of completeness $\S_i\mid i><i\mid=1$ within the subspace of states invariant with respect to the action of Q and $Q^\dagger$, and the fact that the operator $(-1)^{2S}$ must anticommute with Q. The $\S_i<i\mid(-1)^{2S}H_{ext}\mid i>=E\,tr\left[(-1)^{2S}\right]$ is proportional to the number of bosonic degrees of freedom n_B minus the number of fermionic degrees of freedom n_F in the trace. Hence, this relation holds for any $E>0$ in each supermultiplet. This, however, is in general not true for possible zero-energy eigenstates. If the groundstate energy of H_{ext} is equal to zero, that is, exists a state $\chi_0\in\mathcal{H}_0\otimes\mathcal{C}^2$ such that $H_{ext}\,\chi_0=0$, then SUSY is said to be a good symmetry, i.e. the groundstate is invariant under SUSY transformations $Q_i\,\chi_0=0$. If the groundstate energy of H_{ext} is strictly positive then SUSY is said to be broken.

5.2. The (N=2)-SUSY in extended phase space

In constructing a particular (N=2)-realization of the SUSY algebra in the Hilbert space $\mathcal{H}=\mathcal{H}_0\otimes\mathcal{C}^2=[\mathcal{L}^2(\mathcal{R})\otimes\mathcal{L}^2(\mathcal{R})]\otimes\mathcal{C}^2$, let us first introduce a bosonic operators $B_\pm$ in $q-$ and p-representations and fermionic operator $\hat{f}$: $B_{q\mp}:\mathcal{L}^2(\mathcal{R})\to\mathcal{L}^2(\mathcal{R})$, $\quad B_{q\mp}=[p+\pi_q\pm iW(q)]$, $B_{p\mp}:\mathcal{L}^2(\mathcal{R})\to\mathcal{L}^2(\mathcal{R})$, $\quad B_{p\mp}=[q+\pi_p\pm iV(p)]$, and $\hat{f}:\mathcal{C}^2\to\mathcal{C}^2$, $\hat{f}=\frac{1}{2}[\hat{\psi}_+,\,\hat{\psi}_-]$. The $(\hat{\pi}_q,\,\hat{q})$ and $(\hat{\pi}_p,\,\hat{p})$ are usual bosonic momentum and coordinate operators respectively in $q-$ and $p-$ spaces, while $\hat{\psi}_\pm$ are two real fermionic creation and annihilation nilpotent operators describing the fermionic variables, $W(q):\mathcal{R}\to\mathcal{R}$ and $V(p):\mathcal{R}\to\mathcal{R}$ are the piecewise continuously differentiable functions called SUSY potentials. The $\hat{\psi}_\pm$, having anticommuting c-number eigenvalues, imply $\hat{\psi}_\pm=\sqrt{\frac{1}{2}}\,(\hat{\psi}_1\pm i\hat{\psi}_2)$, $\{\hat{\psi}_\alpha,\,\hat{\psi}_\beta\}=\delta_{\alpha\beta}$, $\{\hat{\psi}_+,\,\hat{\psi}_-\}=1$, $\hat{\psi}_\pm^2=0$. They can be represented by finite dimensional matrices $P=\mathbf{1}\otimes\sigma_3$, where $\sigma^\pm=\frac{\sigma_1\pm\sigma_2}{2}$ are the usual raising and lowering operators for the eigenvalues of σ_3. The fermionic operator commutes with the H_{ext} and is diagonal in this representation with conserved eigenvalues $\pm\frac{1}{2}$. Due to it the wave functions become two-component objects: $\chi(q,p)=\begin{pmatrix}\chi_{+1/2}(q,p)\\ \chi_{-1/2}(q,p)\end{pmatrix}=\begin{pmatrix}\chi_1(q,p)\\ \chi_2(q,p)\end{pmatrix}=\begin{pmatrix}\psi_1(q)\phi_1(p)\\ \psi_2(q)\phi_2(p)\end{pmatrix}$, where the states $\psi_{1,2}(q)$, $\phi_{1,2}(p)$ correspond to fermionic quantum number $f=\pm\frac{1}{2}$, respectively, in $q-$ and $p-$ spaces. Let us now to deal with abstract space of eigenstates of the conjugate operator $\hat{\psi}_\pm$ having anticommuting c-number eigenvalues. Suppose $|00->$ is the normalized zero-eigenstate of $\hat{q}$ and $\hat{\psi}_-$: $\hat{q}|00->=0$, $\quad \hat{\psi}_-|00->=0$. The state $|00+>$ is defined by $|00+>=\hat{\psi}_+|00->=0$, then $\hat{\psi}_+|00+>=0$, $\quad \hat{\psi}_-|00+>=|00->$. Taking into account that $\hat{\psi}_\pm^\dagger=\hat{\psi}_\mp$, we get $<\mp 00|\hat{\psi}_\pm=0$, $\quad <\mp 00|\hat{\psi}_\mp=<\pm 00|$. Now we may introduce

doi: 10.52526/25792776-2021.68.2-311

the notation $\alpha, \beta, \ldots$ for the anticommuting eigenvalues of $\hat{\psi}_\pm$. Consistency requires: $\alpha\hat{\psi}_\pm = -\hat{\psi}_\pm\alpha$, $\alpha|00\pm> = \pm|00\pm>\alpha$. The eigenstates of $\hat{q}, \hat{\psi}_-$ can be constructed as $|q\alpha-> = e^{-iq\hat{p}-\alpha\hat{\psi}_+}|00->$, and thus, $\hat{q}|q\alpha-> = q|q\alpha->$, $\quad \hat{\psi}_-|q\alpha-> = \alpha|q\alpha->$. Then, the $\hat{\pi}_q$ and $\hat{\psi}_+$ eigenstates are obtained by Fourier transformation. Thereby the completeness relations hold: $-\int d\alpha\, dq|q\alpha\pm><\mp\alpha^* q| = 1$, $-\int d\alpha\, \frac{d\pi_q}{2\pi}|\pi_q\alpha\pm><\mp\alpha^*\pi_q| = 1$, $-\int d\alpha\, dp|p\alpha\pm><\mp\alpha^* p| = 1$, $-\int d\alpha\, \frac{d\pi_p}{2\pi}|\pi_p\alpha\pm><\mp\alpha^*\pi_p| = 1$. If $|t>$ is the sate of the system at time t, then the wave function is obtained by expanding this state with respect to the coordinate basis in q- and p-spaces: $\chi_-(q\alpha\, p\gamma\, t) = \psi_-(q\alpha t)\,\phi_-(p\gamma t) =< +q\alpha^*|t><+p\gamma^*|t>$, and $\chi_+(q\beta\, p\delta\, t) = \psi_+(q\beta t)\,\phi_+(p\delta t) =< -q\beta^*|t><-p\delta^*|t>$, where $\psi_+(q\beta\, t) = -\int d\alpha\, e^{-\alpha\beta}\psi_-(q\alpha t)$, $\phi_+(p\delta\, t) = -\int d\gamma\, e^{-\gamma\delta}\phi_-(p\gamma\, t)$. On wave functions, the $\hat{\psi}_\pm$ are represented by anticommuting c-number operators: $\hat{\psi}_- = \zeta$, $\quad \hat{\psi}_+ = \partial/\partial\zeta$, provided $\chi(q,p,\zeta) = \psi(q,\zeta)\phi(p,\zeta) = [\psi_1(q) + \zeta\psi_2(q)][\phi_1(p) + \zeta\phi_2(p)]$. These operators allow us consequently to define a pair of appropriate nilpotent supercharges $Q_{q+} = B_{q-}\otimes\hat{\psi}_+ = \begin{pmatrix} 0 & B_{q-} \\ 0 & 0 \end{pmatrix}$, $Q_{q-} = B_{q+}\otimes\hat{\psi}_- = \begin{pmatrix} 0 & 9 \\ B_{q+} & 0 \end{pmatrix}$, $Q_{p+} = B_{p-}\otimes\hat{\psi}_+ = \begin{pmatrix} 0 & B_{p-} \\ 0 & 0 \end{pmatrix}$, $Q_{p-} = B_{p+}\otimes\hat{\psi}_- = \begin{pmatrix} 0 & 0 \\ B_{p+} & 0 \end{pmatrix}$, which obey the required relations $\{Q_\pm,\, Q_\pm\} = 0$. The operators $B_\pm$ can be presented as $B_\pm = B_1 \pm B_2$, where B_1 and B_2 are the hermitian operators. Accordingly, the operators Q_1 and Q_2 read $Q_{q1} = Q_{q+} + Q_{q-} = B_{q1}\sigma_1 + B_{q2}\sigma_2$, $Q_{q2} = -i(Q_{q+} - Q_{q-}) = B_{q1}\sigma_2 - B_{q2}\sigma_1$, and similar relations hold for the operators Q_{p1} and Q_{q2}. It is easily verified that $Q_{q\pm}$ are the generators of SUSY transformations between $\hat{q}$ and $\hat{\psi}$, as well as $Q_{p\pm}$ are the generators of SUSY transformations between $\hat{p}$ and $\hat{\psi}$: $[Q_{q\pm},\, \hat{q}] = -i\hat{\psi}_\pm$, $[Q_{q\pm},\, \hat{\pi}_q] = \mp W'_q(\hat{q})\,\hat{\psi}_\pm$, $\{Q_{q\pm},\, \hat{\psi}_\mp\} = \hat{p} + \hat{\pi}_q \pm iW(\hat{q})$, $\{Q_{q\mp},\, \hat{\psi}_\mp\} = 0$, and $[Q_{p\pm},\, \hat{p}] = -i\hat{\psi}_\pm$, $[Q_{p\pm},\, \hat{\pi}_p] = \mp V'_p(\hat{p})\,\hat{\psi}_\pm$, $\{Q_{p\pm},\, \hat{\psi}_\mp\} = \hat{q} + \hat{\pi}_p \pm iV(\hat{p})$, $\{Q_{p\mp},\, \hat{\psi}_\mp\} = 0$. The SUSY Hamiltonians read $2H_q = \{Q_{q1},\, Q_{q2}\} = \{Q_{q+},\, Q_{q-}\} = \{B_{q-},\, B_{q+}\} + [B_{q-},\, B_{q+}]\sigma_3$, $2H_p = \{Q_{p1},\, Q_{p2}\} = \{Q_{p+},\, Q_{p-}\} = \{B_{p-},\, B_{p+}\} + [B_{p-},\, B_{p+}]\sigma_3$. Along the trajectories in (p,q) space, however, this produces the extended Hamiltonian H_{ext}, $H_{ext} = \begin{pmatrix} H_+ & 0 \\ 0 & H_- \end{pmatrix} = \begin{pmatrix} H_{q+} - H_{p+} & 0 \\ 0 & H_{q-} - H_{p-} \end{pmatrix}$, where $H_q = \begin{pmatrix} H_{q+} & 0 \\ 0 & H_{q-} \end{pmatrix} = \frac{1}{2}\begin{pmatrix} B_{q-}B_{q+} & 0 \\ 0 & B_{q+}B_{q-} \end{pmatrix}$, $H_p = \begin{pmatrix} H_{p+} & 0 \\ 0 & H_{p-} \end{pmatrix} = \frac{1}{2}\begin{pmatrix} B_{p-}B_{p+} & 0 \\ 0 & B_{p+}B_{p-} \end{pmatrix}$. Then $H_{ext} = \frac{1}{2}[(p+\pi_q)^2 - (q+\pi_p)^2 + W^2(q) - V^2(p) + \sigma_3(p+\pi_q)W(q) - i\sigma_3(q+\pi_p)V(p)]$.

From now on we replace H_{ext} by $\overline{H}_{ext}$, and $\chi_r(q,p)$ by $\overline{\chi}_r(q,p)$, respectively, and retain former notational conventions. This realization characterizes two non-interacting point particles of equal mass $m = 1$ moving along the real line under influence of the external scalar potential $U_\pm = U_{q\pm} - U_{p\pm} \equiv W^2(q) - V^2(p) \pm (W'_q(q) - V'_p(p))$. The time evolution of the state $|t>$ is now given $\chi_-(q\alpha\, p\beta\, t) = -\int d\alpha'\, dq'\, d\beta'\, dp' K(q\alpha\, p\beta\, t|q'\alpha'\, p'\beta'\, t')$, provided by the kernel $K(q\alpha\, p\beta\, t|q'\alpha'\, p'\beta'\, t') = < +q\alpha^* p\beta^*|e^{-iH_{ext}(t-t')}|q'\alpha' p'\beta'>$, which can be evaluated by the path integral. Actually, an alternative approach to describe the state space and dynamics of the extended phase space quantum system is by the path integral, which reads $\mathcal{K}_{ff'}(qpt|q'p't') =< qpf|e^{-iH_{ext}(t-t')}|q'p'f'>$, where extended SUSY Hamiltonian can be represented as $H_{ext} = \frac{1}{2}(\hat{\pi}_q^2 + W^2(\hat{q}) + iW'_q(\hat{q})[\hat{\psi}_1,\, \hat{\psi}_2]) - \frac{1}{2}(\hat{\pi}_p^2 + V^2(\hat{p}) + iV'_q(\hat{p})[\hat{\psi}_1,\, \hat{\psi}_2])$. To infer the extended Hamiltonian equivalently one may start from the c-number extended Lagrangian of extended phase space quantum field theory in $(0+1)$-dimensions in $q-$ and $p-$ spaces: $\mathcal{L}_{ext}(p,\, q,\, \dot{p},\, \dot{q}) = -\dot{q}_i\, p_i - q_i\, \dot{p}_i + \frac{1}{2}[(\frac{dq}{dt})^2 - W^2(q)] + f\, W'_q(q) + \frac{1}{2}[(\frac{dp}{dt})^2 - V^2(p)] + f\, V'_p(p)$. With the Hamiltonian H_{ext}, the path integral is diagonal: $\mathcal{K}_{ff'}(qpt|q'p't') = \mathcal{K}_{ff'}(qt|q't')\,\mathcal{K}_{ff'}(pt|p't') = \delta_{ff'}\int_{q'}^{q} \mathcal{D}q \int_{p'}^{p} \mathcal{D}p\, \exp\,(i\int_{t'}^{t} \mathcal{L}_{ext}(p,\, q,\, \dot{p},\, \dot{q})dt)$. Knowing the path integral, it is sufficient to specify the initial wave function $\chi_f(q', p', t')$ to obtain all possible information about the system at any later time t, by $\chi_f(q,p,t) =$
$\sum_{f'}\int dq'\, dp'\, \mathcal{K}_{ff'}(qpt|q'p't')\,\chi_{f'}(q', p', t')$, The path integral becomes $\mathcal{K}(q\alpha p\beta t|q'\alpha' p'\beta' t') =$
$\int_{q',\alpha',p',\beta'}^{q,\alpha,p,\beta} \mathcal{D}q\,\mathcal{D}p\,\mathcal{D}\zeta\,\mathcal{D}\eta\, \exp\,(i\int_{t'}^{t} \mathcal{L}_{ext}(p,\, q,\, \dot{p},\, \dot{q})dt)$. The functional integral is taken over all trajectories from q', α' to q, α and p', β' to p, β between the times t' and t.

doi: 10.52526/25792776-2021.68.2-311

5.3. The vacuum energy and the topology of superpotential

The supersymmetry of quantum system is said to be a good symmetry (good SUSY) if the groundstate energy of H_{ext} vanishes. In the other case, $inf\, spec\, H_{ext} > 0$, SUSY is said to be broken. Let χ_r^+ and χ_r^- denote the eigenstates of H_+ and H_-, respectively, for the same positive eigenvalue $E_r > 0$: $H_\pm \chi_r^\pm = E_r \chi_r^\pm$. The SUSY transformation implies the relations $\chi_r^+ = \frac{1}{\sqrt{E_r}} B_+ \chi_r^-$, $\chi_r^- = \frac{1}{\sqrt{E_r}} B_- \chi_r^+$, where $B_+B_- = B_{q+}B_{q-} - B_{p+}B_{p-}$, $B_-B_+ = B_{q-}B_{q+} - B_{p-}B_{p+}$. Note that under the replacement of SUSY potentials, $W \to -W$ and $V \to -V$, $(U_\pm \to U_\mp)$, the roles of the two Hamiltonians H_+ and H_- are interchanged. Hence, the sign of the SUSY potentials may be fixed by some convention. For good SUSY the groundsate χ_0 of H_{ext} either belongs to H_+ or H_- $H_\pm \chi_0^\pm = 0 \Leftrightarrow B_\pm \chi_0^\pm = 0$, or $(H_{q\pm} - H_{p\pm})\chi_0^\pm = 0$. As far as $H_{q\pm}$ and $H_{p\pm}$ are independent, we have $H_{q\pm}\chi_0^\pm = 0$, $H_{p\pm}\chi_0^\pm = 0$, or $B_{q\pm}\chi_0^\pm = 0$, $B_{p\pm}\chi_0^\pm = 0$. Whence, $(\frac{d}{dq} \pm W(q))\psi_0^\pm(q) = 0$, $(\frac{d}{dp} \pm V(p))\phi_0^\pm(p) = 0$, $\chi_0^\pm(q,p) >\equiv \psi_0^\pm(q)\phi_0^\pm(p)$, and $< q|\psi_0^\pm >\equiv \psi_0^\pm(q)$, $< p|\phi_0^\pm >\equiv \phi_0^\pm(p)$. The functions $\psi_0^\pm(q)$ and $\phi_0^\pm(p)$ have to be square-integrable for SUSY to be a good symmetry. This requirement puts conditions on the SUSY potentials: $\int_0^\infty W(q')dq' \to \infty$ at $q \to \pm\infty$ for ψ_0^+, $\int_0^\infty W(q')dq' \to -\infty$ at $q \to \pm\infty$ for ψ_0^-, $\int_0^\infty V(p')dp' \to \infty$ at $p \to \pm\infty$ for ϕ_0^+, $\int_0^\infty V(p')dp' \to -\infty$ at $p \to \pm\infty$ for ϕ_0^-. Depending on the asymptotic behavior of the SUSY potentials one of the two functions $\chi_0^\pm$ will be normalizable (good SUSY) or both are not normalizable (broken SUSY). For continuous SUSY potentials $U_\pm(p,q)$ the functions $W(q)$ and $V(p)$ must have an odd number of zeros (counted with their multiplicity) for SUSY to be good. A continuous SUSY potentials with an even number of zeros necessarily leads to a broken SUSY. Consequently, if $W(q)$ and $V(p)$ have a well-defined parity, and odd $W(q)$ and $V(p)$ lead to good SUSY, whereas an even $W(q)$ and $V(p)$ break SUSY: $W(-q) = -W(q) \Rightarrow U_{q\pm}(-q) = U_{q\pm}(q)$ (SUSY and parity are good in q-subspace), $W(-q) = W(q) \Rightarrow U_{q\pm}(-q) \neq U_{q\pm}(q)$ (SUSY and parity are broken in q-subspace), and correspondingly the similar conditions hold for $V(p)$ and $U_{q\pm}(p)$. The spectra of H_+ and H_- are related as follows: $\mathrm{spec}(H_-)/\{0\} = \mathrm{spec}(H_+)$ (good SUSY), $\mathrm{spec}(H_-) = \mathrm{spec}(H_+)$ (broken SUSY).

Clearing up this situation the Witten index is turned out to be one of the useful tool which, according to the Atiyah-Singer index theorem associates with the operator index and depends only on the asymptotic values of SUSY potentials. This is a topological characteristic and does not vary with the variation of the parameters of theory. Thus, the Witten index reads $\Delta(\beta) = tr(P\, e^{-\beta H_{ext}}) = tr(P\, e^{-\beta(H_q - H_p)})$, $\beta > 0$. For a pure point spectrum of H_{ext} this index is the difference of the number of spin-up states $(\uparrow)$ and spin-down states $(\downarrow)$ with zero energy: $\Delta(\beta) = N_\uparrow(E=0) - N_\downarrow(E=0)$. Note that the factor $e^{-\beta H_{ext}}$ has only been introduced for regularization of the trace. The conditions of the positive-energy eigenstates cancel due to the pairwise degeneracy mentioned above. For a continuous spectrum this is not the case as the spectral densities for the spin-up and spin-down states are in general different due to which Witten index becomes β dependent. Therefore, for simplicity reasons we assume purely discrete spectra. Then, $\Delta = \mathrm{ind}\, B = \dim\ker H_- - \dim\ker H_+ = \dim\ker H_{q-} + \dim\ker H_{p+} - \dim\ker H_{q+} - \dim\ker H_{p-}$. Introducing a set of H_q and H_p upon reduction to the $q-$ or $p-$ space yields $\Delta = \frac{1}{2}[\mathrm{sgn}\, W(+\infty) + \mathrm{sgn}\, V(-\infty) - \mathrm{sgn}\, W(-\infty) - \mathrm{sgn}\, V(+\infty)]$. Hence for good SUSY one has $\Delta = \pm 1$ with the ground state belonging to $H_\pm$. For broken SUSY one has $\Delta = 0$. Although even small non-zero energy expectation value $\varepsilon = (\chi_1,\, H_{ext}\,\chi_1)$ gives direct evidence for the SUSY breaking in the extended phase space quantum mechanical system, a more practical measure for the SUSY breaking, in particular, in field theories is the expectation value of an auxiliary field, which can be replaced by its equation of motion right from the start: $< F >= (\chi_\uparrow,\, i\{Q_+, \sigma_-\}\chi_\uparrow)$, where as we mentioned above the solutions for non-zero energy come in pairs of the form $\chi_\uparrow(q,p)$ or $\chi_\downarrow(q,p)$ related by supersymmetry. Taking into account the relation $Q_+\chi_\uparrow = 0$, where Q_+ commutes with H_{ext} which means that the intermediate state must have the same energy as χ, the can be re-written in terms of a complete set of states: $< F >= i(\chi_\uparrow,\, Q_+\,\chi_\downarrow)(\chi_\downarrow,\, \hat{\psi}_-,\, \chi_\uparrow)$. We have $\varepsilon =< H_{ext} >= \frac{1}{2}(\chi_\uparrow,\, Q_+\,\chi_\downarrow)(\chi_\downarrow,\, Q_-\,\chi_\uparrow) = \varepsilon_q - \varepsilon_p =< H_q > - < H_p >= (\psi_\uparrow,\, H_q\,\psi_\uparrow) - (\phi_\uparrow,\, H_p\,\phi_\uparrow) = \frac{1}{2}(\psi_\uparrow,\, Q_{q+}\,\psi_\downarrow)(\psi_\downarrow,\, Q_{q-}\,\psi_\uparrow) - \frac{1}{2}(\phi_\uparrow,\, Q_{p+}\,\phi_\downarrow)(\phi_\downarrow,\, Q_{p-}\,\phi_\uparrow)$.

doi: 10.52526/25792776-2021.68.2-311

5.4. A shape-invariance of exactly solvable SUSY potentials

SUSY quantum mechanics provides an elegant and useful prescripton for obtaining closed analytic expressions both for the energy eigenvalues and eigenstates of a large class of Schrödinger-like equations. The key point in this are the SUSY partner Hamiltonians $H_- = B_-B_+$ and $H_+ = B_+B_-$. The operators in this factorization are expressed in terms of the SUSY potentials. The potentials for which the Schrödinger-like equations are exactly solvable share an integrability conditions called *shape-invariance*. The concept of shape-invariance in SUSY quantum mechanics has proven to be very useful because it leads immediately to exactly solvable potentials. An extended Hamiltonian H_{ext} of SUSY quantum mechanics can be treated as a set of two ordinary two-dimensional partner Hamiltonians $H_\pm = \frac{1}{2}[\pi_q^2 - \pi_p^2 + U_\pm(q,p)]$. Due to SUSY they have the same energy spactra at arbitrary functions $W(q)$ and $V(p)$, except the groundstate of H_- (defined in accordance with usual convention) which has no corresponding state in the spectra of H_+. The partner potentials $U_\pm(q,p)$ are called shape-invariant if they satisfy an integrability condition $U_\pm(a,q,p) = U_-(a_1,q,p) + R(a_1)$, $a_1 = f(a)$, where a and a_1 are a set of parameters that specify phase-space-independent properties of the potentials, and the reminder $R(a_1)$ is independent of (q,p). Although this looks like a satisfactory state of affairs, we may not always be so fortunate to have such potentials at our disposal. In fact a shape-invariance is not the most general integrability condition as not all exactly solvable potentials seem to be shape-invariant. Using the standard technique, we construct a series of Hamiltonians H_n, $n = 0,1,2,\dots$, $H_n = \frac{1}{2}[\pi_q^2 - \pi_p^2 + U_-(a_n,q,p) + \S_{k=1}^{n} R(a_k)]$, where $a_n = f^{(n)}(a)$ (n means the number of multiple applications.) Comparing the spectra H_n and H_{n+1}, we obtain $H_{n+1} = \frac{1}{2}[\pi_q^2 - \pi_p^2 + U_+(a_n,q,p) + \S_{k=1}^{n} R(a_k)]$. We see that the Hamiltonians H_n and H_{n+1} have the same energy spectra, except the groundstate of H_n, the energy of which is equal $\S_{k=1}^{n} R(a_k)$. Going through H_n to H_{n-1} and so on, we subsequently obtain the initial Hamiltonian $H_0 = H_- = \frac{1}{2}[\pi_q^2 - \pi_p^2 + U_-(a,q,p)]$, the groundstate of which is equal zero, but all the other energy levels coincide with the lower levels of Hamiltonians H_n. Continuing along this line, the entire energy spectrum of H_{ext} reads $\widetilde{E}_n = \S_{k=1}^{n} R(a_k)$. Hence the spectrum of Hamiltonian with the potential $U(a,q,p) = U_-(a,q,p) + C(a)$ has the form $E_n = \widetilde{E}_n + C(a) = \S_{k=1}^{n} R(a_k) + C(a)$. Instead of developing the full machinery here, we will illustrate this in passing in the following example.

Example: Scarf potential. To demonstrate practical merits of shape-invariance of exactly solvable extended SUSY potentials, we now obtain analytic expressions for the entire energy spectrum of one-dimensional problem with extended *Scarf* potential without ever referring to underlying differential equation. This potential $U(a,b,q,p) = U_q(a,b) - U_p(b,p) = -\frac{a(a+1)}{2ch^2 q} + \frac{b(b+1)}{2ch^2 p}$, will be of vital interest for the theory of solitons in extended phase space formalism. In case at hand we have $W(q) = a\, th\, q$ and $V(p) = b\, th\, p$, hence $U_\pm(a,b,q,p) = U_{q\pm}(a,q) - U_{p\pm}(b,p) = -\frac{a(a\mp1)}{2ch^2 q} + \frac{a^2}{2} + \frac{b(b\pm1)}{2ch^2 p} - \frac{b^2}{2}$. This yields $a_1 = f_1(a) = a-1$; $a_n = a-n$; $C_1(a) = -\frac{a^2}{2}$, $b_1 = f_2(b) = b-1$; $b_n = b-n$; $C_2(b) = -\frac{b^2}{2}$, $\sum_{k=1}^{n} R_1(a_k) = \frac{a^2-a_n^2}{2}$, $\sum_{k=1}^{n} R_2(b_k) = \frac{b^2-b_n^2}{2}$. The entire energy spectrum of the H_{ext} can be easily obtained as $E_n = E_{qn} - E_{pn} = -\frac{a_n^2}{2} + \frac{b_n^2}{2} = -\frac{(a-n)^2}{2} + \frac{(b-n)^2}{2}$. One final observation is worth recording. The shape-invariance has underlying algebraic structure of Lie algebras, which transform the parameters of the potentials. Shape-invariance algebra in general is an infinite-dimensional. However, under some conditions they become finite-dimensional. The Hamiltonian of exactly solvable systems can be written as a linear or quadratic function of an underlying algebra, and all the quantum states of these systems can be determined by independent group theoretical methods with a general change of parameters which involves nonlinear extensions of Lie algebras.

6. Classical analog of extended phase space SUSY and its breaking

It is certainly desirable to derive the classical analog of the extended phase space quantum mechanics of the particle with odd degrees of freedom directly from what may be taken as the first principle (**?**). Let us consider a nonrelativistic particle of unit mass with two ($\alpha = 1,2$) odd (Grassmann) degrees of freedom. The classical extended Lagrangian can be written $\mathcal{L}_{ext}(p,\, q,\, \dot p,\, \dot q) = -\dot q\, p - q\, \dot p + \frac{1}{2}\, \dot q^2 - F(q) + \frac{1}{2}\, \dot p^2 - G(p) - R(q,\, p)\, N + \frac{1}{2}\, \psi_\alpha \dot\psi_\alpha$, provided by $N = \psi_1\, \psi_2 = -i\, \psi_+\, \psi_-$. Here $F(q): \mathcal{R} \to \mathcal{R}$, $\quad G(p): \mathcal{R} \to \mathcal{R}$ and $R(q,\, p): \mathcal{R} \to \mathcal{R}$ are arbitrary piecewise continuously differentiable functions given over the 1-dimensional Euclidean space $\mathcal{R}$. The ψ_α are two odd (Grassmann)

doi: 10.52526/25792776-2021.68.2-311

degrees of freedom. The nontrivial Poisson-Dirac brackets of the system are $\{q,\, \pi_q\} = 1$, $\{p,\, \pi_p\} = 1$, $\{\psi_\alpha,\, \psi_\beta\} = \delta_{\alpha\beta}$, $\{\psi_+,\, \psi_-\} = 1$, $\psi_\pm^2 = 0$, $\psi_\pm = \frac{1}{\sqrt{2}}\,(\psi_1 \pm i\psi_2)$. The extended Hamiltonian H_{ext} reads $H_{ext}(p,\, q,\, \pi_p,\, \pi_q) = \frac{1}{2}\,(p+\pi_q)^2 + F^2(q) - \frac{1}{2}\,(q+\pi_p)^2 - G^2(p) + R(q,p)\,N$, which reduces to $H_{ext}(p,\, q,\, \pi_p,\, \pi_q) = \frac{1}{2}\,\pi_q^2 + F^2(q) - \frac{1}{2}\,\pi_p^2 - G^2(p) + R(q,p)\,N$. This Hamiltonian yields the following equations of motion: $\dot q = \pi_q$, $\dot p = \pi_p$, $\dot\pi_q = -F_q'(q) - R_q'(q,\, p)\,N$, $\dot\pi_p = -G_p'(p) + R_p'(q,\, p)\,N$, $\dot\psi_\pm = \pm iR(q,\, p)\,\psi_\pm$. A prime will indicate differentiation with respect either to q or p. Thus, N is the integral of motion additional to H_{ext}. Along the trajectories $q(t)$ and $p(t)$ in $(p,q)-$ spaces, the solution to equations of motion for odd variables is $\psi_\pm(t) = \psi_\pm(t_0)\, \exp[\pm i \int_{t_0}^t R(q(\tau),\, p(\tau))\, d\tau]$. Hence the odd quantities $\theta_\pm = \theta_\pm(t)\, \exp[\mp i \int_{t_0}^t R(q(\tau),\, p(\tau))\, d\tau]$ are nonlocal in time integrals of motion. In trivial case $R = 0$, we have $\dot\psi_\pm = 0$, and $\theta_\pm = \theta_\pm$. Suppose the system has even complex conjugate quantities $B_{q,p\pm}$, $(B_{q,p+})^* = B_{q,p-}$, whose evolution looks up to the term proportional to N like the evolution of odd variables. Then local odd integrals of motion could be constructed in the form $Q_{q,p\pm} = B_{q,p\mp}\,\psi_\pm$. Let us introduce the oscilliator-like bosonic variables $B_{q,p\pm}$ in $q-$ and p-representations $B_{q\mp} : \mathcal{L}^2(\mathcal{R}) \to \mathcal{L}^2(\mathcal{R})$, $B_{q\mp} = [p + \pi_q \pm iW(q)]$, $B_{p\mp} : \mathcal{L}^2(\mathcal{R}) \to \mathcal{L}^2(\mathcal{R})$, $B_{p\mp} = [q + \pi_p \pm iV(p)]$. The $W(q) : \mathcal{R} \to \mathcal{R}$ and $V(p) : \mathcal{R} \to \mathcal{R}$ are the piecewise continuously differentiable functions called SUSY potentials. In particular case if $R(q,\, p) = R_q(q) - R_p(p)$, for the evolution of $B_{q,p\pm}$ we obtain $\dot B_{q\mp} = [-(F_q' + R_q'\,N) \pm iW_q'(q)(p+\pi_q)]$, $\dot B_{p\mp} = [-(G_p' + R_p'\,N) \pm iV_p'(p)(q+\pi_p)]$. Consequently, $\dot Q_{q\pm} = \pm i[(W_q' - R_{q\pm}') \pm i(F_q' - WW_q')\,\psi_\mp]$, $\dot Q_{p\pm} = \pm i[(V_p' - R_{p\pm}') \pm i(G_p' - VV_p')\,\psi_\mp]$. This shows that either $\dot Q_{q\pm} = 0$ or $\dot Q_{p\pm} = 0$ when $W_q'(q) = R_{q\pm}'(q)$ and $F_q' = \frac{1}{2}(W^2)_q'$ or $V_p'(p) = R_{p\pm}'(p)$ and $G_p' = \frac{1}{2}(V^2)_p'$, respectively. Therefore, when the functions $R_{q,p}$ and $F(q)$, $G(p)$ are related as $R_{q\pm}'(q) = W_q'(q)$, $F_q = \frac{1}{2}(W^2) + C_q$, $R_{p\pm}'(p) = V_p'(p)$, $F_p = \frac{1}{2}(V^2) + C_p$, where $C_{q,p}$ are constants, then odd quantities $Q_{q,p\pm}$ are integrals of motion in addition to H_{ext} and N. Let us present H_{ext} in the form $H_{ext} = H_q - H_p$, where $H_q = \frac{1}{2}\,\pi_q^2 + F^2(q) + R_q\,N$, $H_p = \frac{1}{2}\,\pi_p^2 + G^2(p) + R_p\,N$. Then, $Q_{q,p\pm}$ and N together with the H_q and H_p form the classical analog of the extended phase space SUSY algebra $\{Q_{q,p+},\, Q_{q,p-}\} = -i(H_{q,p} - C_{q,p})$, $\{H_{q,p},\, Q_{q,p\pm}\} = \{Q_{q,p\pm},\, Q_{q,p\pm}\} = 0$, $\{N,\, Q_{q,p\pm}\} = \pm iQ_{q,p\pm}$, $\{N,\, H_{q,p}\} = 0$, with constants $C_{q,p}$ playing a role of a central charges in $(q,p)-$ spaces, N is classical analog of the grading operator. Putting $C_q = C_p = 0$, we arrive at the classical analog of the extended phase space SUSY quantum mechanics given by the extended Lagrangian $\mathcal{L}_{ext}(p,\, q,\, \dot p,\, \dot q) = \frac{1}{2}\,\pi_q^2 - \frac{1}{2}\,W^2(q) + \frac{1}{2}\,\pi_p^2 - \frac{1}{2}\,V^2(p) + \psi_1\psi_2(W_q' + V_p') + \frac{1}{2}\psi_\alpha\dot\psi_\alpha$. We conclude that the classical system is characterized by the presence of two additional local in time odd integrals of motion being supersymmetry generators. Along the actual trajectories in $q-$space, the lagrangian reproduces the results obtained in previous section.

6.1. Solution of the extended Schrödinger equation with small energy eigenvalue

First, we use the iterative scheme to find the approximate groundstate solutions to the extended Schrödinger-like equation $H_{ext}\,\chi(q,p) = (H_q - H_p)\,\chi(q,p) = \varepsilon\,\chi(q,p)$, with energy ε. We will then use these solutions to calculate the parameters which measure the breaking of extended SUSY such as the groundstate energy. The approximation, which went into the derivation of solutions meets our interest that the graoundstate energy ε is supposedly small. As we mentioned above the solutions for non-zero ε come in pairs of the form $\chi_\uparrow(q,p) = \begin{pmatrix} \chi_1(q,p) \\ 0 \end{pmatrix}$ or $\chi_\downarrow(q,p) = \begin{pmatrix} 0 \\ \chi_2(q,p) \end{pmatrix}$, related by supersymmetry, where $\chi_{1,2}(q,p) = \psi_{1,2}(q)\phi_{1,2}(p)$. The state space of the system is defined by all the normalizable solutions and the individual states are characterized by the energies ε_q and ε_q and the fermionic quantum number f. One of these solutions is acceptable only if $W(q)$ and $V(p)$ become infinite at both $q \to \pm\infty$ and $p \to \pm\infty$, respectively, with the same sign. If this condition is not satisfied, neither of the solutions is normalizable, and they cannot represent the groundstate of the system. The following relations between energy eigenstates with fermionic quantum number $\pm\frac{1}{2}$ hold: $\left[(\frac{\partial}{\partial q} + W_q(q)) - (\frac{\partial}{\partial p} + V_p(p))\right]\psi_1(q)\phi_1(p) = \sqrt{2\varepsilon_q}\psi_2(q)\phi_1(p) - \sqrt{2\varepsilon_p}\psi_1(q)\phi_2(p)$, and $\left[(-\frac{\partial}{\partial q} + W_q(q)) - (-\frac{\partial}{\partial p} + V_p(p))\right]\psi_2(q)\phi_2(p) = \sqrt{2\varepsilon_q}\,\psi_1(q)\phi_2(p) - \sqrt{2\varepsilon_p}\,\psi_2(q)\phi_1(p)$, where $\varepsilon = \varepsilon_q - \varepsilon_p$, ε_q and ε_p are the eigenvalues of H_q and H_p, respectively. The technique now is to devise an iterative approximation scheme by taking a trial wave function for $\chi_2(q,p)$, substitute this into the first equation

doi: 10.52526/25792776-2021.68.2-311

and integrate it to obtain an approximation for $\chi_1(q,p)$. This can be used as an ansatz in the second equation to find an improved solution for $\chi_2(q,p)$, etc. The procedure converges for well-behaved potentials with a judicious choice of initial trial function. If the W_q and V_p are odd, then $\psi_1(-q) = \psi_2(q)$, $\phi_1(-p) = \phi_2(p)$, since they satisfy the same eigenvalue equation. The independent nature of q and p gives the freedom of taking $q = 0, \quad p = 0$ which yield an expression for energies: $\sqrt{2\varepsilon_q} = W(0) + \psi_1'(0)\,/\psi_1(0)$, $\sqrt{2\varepsilon_p} = V(0) + \phi_1'(0)\,/\phi_1(0)$. Suppose the potentials $W_q(q)$ and $V_p(p)$ have a maximum, at q_- and p_-, and minimum, at q_+ and p_+, respectively. For the simplicity sake we choose the trial wave functions as $\psi^{(0)}_{1,2}(q) = \delta(q - q_\pm)$, $\phi^{(0)}_{1,2}(p) = \delta(p - p_\pm)$. The normalization constant N' is $N' = (\int_{q_-}^{\infty} dq\, e^{-2\int_0^{q} W(q')dq'} \int_{p_-}^{\infty} dp\, e^{-2\int_0^{p'} V(p')dp'})^{3/2}$. The energy expectation value $\varepsilon = (\chi_1,\, H_{ext}\,\chi_1)$ gives the same result as that obtained for odd potentials. Assuming the exponentials $e^{-2\int_{q_-}^{0} W(q)dq}$ and $e^{-2\int_{p_-}^{0} V(p)dp}$ to be small, which is correct to the same approximations, the difference is negligible and the integrals in both cases may be replaced by gaussians around q_+ and p_+, respectively. Hence, it is straightforward to obtain $\varepsilon = \frac{\hbar W'(q_+)}{2\pi}\, e^{-2\Delta W/\hbar} - \frac{\hbar V'(p_+)}{2\pi}\, e^{-2\Delta V/\hbar}$, which gives direct evidence for the SUSY breaking in the extended phase space quantum mechanical system. Here we have reinstated $\hbar$, to show the order of adopted approximation, and its non-perturbative nature. We also denoted $\Delta W = \int_{q_+}^{q_-} W(q)\,dq, \quad \Delta V = \int_{p_+}^{p_-} V(p)\,dp$. However, a more practical measure for the SUSY breaking, in particular, in field theories is the expectation value of an auxiliary field, which can be replaced by its equation of motion right from the start: $< F >= (\chi_\uparrow,\, i\{Q_+,\, \sigma_-\}\chi_\uparrow)$, etc. Hence we obtain $(\chi_\uparrow,\, Q_+\,\chi_\downarrow)(\chi_\downarrow,\, \hat{\psi}_-\,\chi_\uparrow) = 2i\sqrt{\varepsilon}\,[(\frac{\varepsilon_q}{\varepsilon})\,\sqrt{\varepsilon}_q\,\sqrt{\frac{W'(q_-)}{\pi}}\,\Delta\, q - (\frac{\varepsilon_p}{\varepsilon})\,\sqrt{\varepsilon}_p\,\sqrt{\frac{V'(p_-)}{\pi}}\,\Delta\, p]$, and that $< F >= -2\sqrt{\varepsilon}\,[(\frac{\varepsilon_q}{\varepsilon})\,\sqrt{\frac{W'(q_+)}{\pi}}\, e^{-2\Delta W}\Delta q - (\frac{\varepsilon_p}{\varepsilon})\,\sqrt{\frac{V'(p)}{\pi}}\, e^{-2\Delta V}\Delta p]$.

6.2. An extended SUSY breaking in the instanton picture

The matrix elements of $\hat{\psi}_\pm, Q_{q\pm}$ and $Q_{p\pm}$ can be calculated in the background of the classical solution $\dot{q}_c = -W_c$ and $\dot{p}_c = -V_c$. In doing this we re-write the matrix element in terms of eigenstates of the conjugate operator $\hat{\psi}_\pm$. In the limit $T \to -i\infty$, this reduces to $\sqrt{\varepsilon}\, < +0q_+p_+|Q_+|q_-p_-0- >< -0q_-p_-|\hat{\psi}_-|q_+p_+0+ >= \sqrt{\varepsilon_q}\, < +0q_+|Q_{q+}|q_-0- >< -0q_-|\hat{\psi}_-|q_+0+ > -\sqrt{\varepsilon_p}\, < +0p_+|Q_{p+}|p_-0- >< -0p_-|\hat{\psi}_-|p_+0+ >$, which, in turn, can be presented by path integrals defined in terms of anticommuting c-number operators ζ and η with Euclidean actions of the instantons in $q-$ and $p-$ spaces, respectively. These functional integrals include an integration over *instanton time* τ_0 which is due to the problem of zero modes of the bilinear terms in Euclidean actions. This arises from time-transformation of instantons, and SUSY transformations on them, respectively. The existence of zero modes gives rise to non-gaussian behaviour of the functional integral. Due to it the matrix elements above do not receive any contributions from either no-instanton or anti-instanton configurations. The zero mode problem is solved by introducing a collective coordinate τ_0 replacing the bosonic zero mode. Whereas, the funcional integrals depend only on the difference $\tau - \tau_0$. Note also that multi-instanton configurations could contribute in principle, provided they have not more than one normalizable fermionic zero mode. But, their contribution is clearly smaller with respect to $\sqrt{2\varepsilon_q}$ and $\sqrt{2\varepsilon_p}$. In the case when the SUSY potentials in $q-$ and $p-$ spaces have more than two extrema q_ν and p_μ, $\nu, \mu = 1, 2, \ldots, N$, one can put conditions on the SUSY potentials $\int_0^\infty W(q')dq' \to \infty$ at $q \to \pm\infty$ for ψ_0^+, $\int_0^\infty W(q')dq' \to -\infty$ at $q \to \pm\infty$ for ψ_0^-, and similar for $V(p)$, that the extrema are well separated: $\int_{q_\nu}^{q_\nu+1} W(q')dq' \gg 1$, and $\int_{p_\mu}^{q_\mu+1} V(p')dp' \gg 1$. Around each of the classical minima q_ν and p_μ of the potentials $W^2(q)$ and $V^2(p)$, respectively, one can approximate the theory by a suppersymmetric harmonic oscilliator. Then there are N ground states which have zero energy. These states are described by upper or lower component of the wave function, depending on whether ν and μ are odd or even. With this provision the functional integrals can be calculated, which allow us consequently to write down $< +0q_+|Q_{q+}|q_-0- >= i\sqrt{\frac{W_c'(q_+)}{\pi}}\, e^{-\Delta W_c}$, $< -0q_-|\hat{\psi}_-|q_+0+ >= \sqrt{\frac{W_c'(q_+)}{\pi}}\, e^{-\Delta W_c}\Delta q_c$, etc. Then, we arrive at the $< +0q_+p_+|Q_+|q_-p_-0- >< -0q_-p_-|\hat{\psi}_-|q_+p_+0+ >= 2i\sqrt{\varepsilon}\,[(\frac{\varepsilon_q}{\varepsilon})\,\sqrt{\varepsilon_q}\,\sqrt{\frac{W_c'(q_+)}{\pi}}\,\Delta q_c - (\frac{\varepsilon_p}{\varepsilon})\,\sqrt{\varepsilon_p}\,\sqrt{\frac{V_c'(p_+)}{\pi}}\,\Delta p_c]$, and, as its inevitable corollary, to final solution.

doi: 10.52526/25792776-2021.68.2-311

This proves that the extended SUSY breaking has resulted from tunnelling between the classical vacua of the theory. The corrections to this picture are due to higher order terms and quantum tunneling effects.

7. Operator manifold approach to geometry and particle physics

The operator manifold formalism enables the unification of the geometry and the field theory. It yields the quantization of geometry drastically different from earlier suggested schemes. We explored the query how did the geometry and fields, as they are, come into being. The substance out of which the geometry and fields are made is the `primordial structures´. The mathematical framework of the OM formalism reveals the fundamental concepts of the particle physics. The primordial structures are designed to posses certain physical properties. The processes of their creation and annihilation in the lowest state (the regular structures) just are described by the OM formalism. In all the higher states the primordial structures are distorted ones, namely they have undergone the distortion transformations. The distortion transformation functions are the operators acting in the space of the internal degrees of freedom (colours) and imply the fundamental Incompatibility relations, which hold for both the local and the global distortion rotations. They underly the most important symmetries such as the internal symmetries $U(1), SU(2), SU(3)$, the $SU(2)\otimes U(1)$ symmetry of electroweak interactions, etc. Our major purpose is to prove the idea that the Geometry and Fields, with the Internal symmetries and all interactions, as well the four major principles of Relativity (Special and General), Quantum, Gauge and Colour confinement are derivative, and they come into being simultaneously. For illustrative purposes below we briefly consider just only a few preliminary examples from the two important aspects of mathematical background of the OM-formalism (Ter-Kazarian, 1884, 1996, 1999a). Thereby we suppress the indices without notice.

7.1. Quantization of Geometry

Unifying the geometry and particles into one framework the OM formalism is analogous to the method of secondary quantization with appropriate expansion over the geometric objects. We proceed at once to the secondary quantization of geometry by substituting the basis elements for the creation and annihilation operators acting in the configuration space of occupation numbers. Instead of pseudo vectors O_λ we introduce the operators supplied by additional index (r) referring to the quantum numbers of corresponding state $\hat{O}^r_1 = O^r_1\alpha_1$, $\hat{O}^r_2 = O^r_2\alpha_2$, $\hat{O}^\lambda_r = {}^*\delta^{\lambda\mu}\hat{O}^r_\mu = (\hat{O}^r_\lambda)^+$, $\{\hat{O}^r_\lambda, \hat{O}^{r'}_\tau\} = \delta_{rr'}{}^*\delta_{\lambda\tau}I_2$. The matrices α_λ satisfy the condition $\{\alpha_\lambda, \alpha_\tau\} = {}^*\delta_{\lambda\tau}I_2$, where $\alpha^\lambda = {}^*\delta^{\lambda\mu}\alpha_\mu = (\alpha_\lambda)^+$, and $I_2 = \begin{pmatrix} 1 & 0 \\ 0 & 1 \end{pmatrix}$. For example $\alpha_1 = \begin{pmatrix} 0 & 1 \\ 0 & 0 \end{pmatrix}$, $\alpha_2 = \begin{pmatrix} 0 & 0 \\ 1 & 0 \end{pmatrix}$. The creation $\hat{O}^r_1$ and annihilation $\hat{O}^r_2$ operators are acting as follows: $\hat{O}^r_1 \mid 0 >= O^r_1 \mid 1 >$, $\hat{O}^r_2 \mid 1 >= O^r_2 \mid 0 >$, where $\mid 0 >\equiv \mid 0, 0, \ldots >$ and $\mid 1 >\equiv \mid 0, \ldots, 1, \ldots >$ are respectively the nonoccupied vacuum state and the one occupied state. Thus, $\hat{O}^r_1 \mid 1 >= 0$, $\hat{O}^r_2 \mid 0 >= 0$. A matrix realization of such states, for instance, can be: $\mid 0 >\equiv \chi_1 = \begin{pmatrix} 0 \\ 1 \end{pmatrix}$, $\mid 1 >\equiv \chi_2 = \begin{pmatrix} 1 \\ 0 \end{pmatrix}$. Hence $\chi_0 \equiv \mid 0 >= \prod_{r=1}^{N}(\chi_1)_r$ and $\chi_{r'} \equiv \mid 1 >= (\chi_2)_{r'} \prod_{r\neq r'}(\chi_1)_r$. Also, instead of ordinary basis vectors we introduce the operators $\hat{\sigma}^r_\alpha \equiv \delta_{\alpha\beta\gamma}\sigma^r_\beta\widetilde{\sigma}_\gamma$, where $\widetilde{\sigma}_\gamma$ are Pauli's matrices such that $< \sigma^r_\alpha, \sigma^{r'}_\beta >= \delta_{rr'}\delta_{\alpha\beta}$, $\hat{\sigma}^\alpha_r = \delta^{\alpha\beta}\hat{\sigma}^r_\beta = (\hat{\sigma}^r_\alpha)^+ = \hat{\sigma}^r_\alpha$, $\{\hat{\sigma}^r_\alpha, \hat{\sigma}^{r'}_\beta\} = 2\delta_{rr'}\delta_{\alpha\beta}I_2$. The vacuum state $\mid 0 >\equiv \varphi_{1(\alpha)}$ and the one occupied state $\mid 1_{(\alpha)} >\equiv \varphi_{2(\alpha)}$ read: $\varphi_{1(\alpha)} \equiv \chi_1$, $\varphi_{2(1)} = \begin{pmatrix} 1 \\ 0 \end{pmatrix}$, $\varphi_{2(2)} = \begin{pmatrix} -i \\ 0 \end{pmatrix}$, $\varphi_{2(3)} = \begin{pmatrix} 0 \\ -1 \end{pmatrix}$, thus, $\hat{\sigma}^r_\alpha\varphi_{1(\alpha)} = \sigma^r_\alpha\varphi_{2(\alpha)} = (\sigma^r_\alpha\widetilde{\sigma}_\alpha)\varphi_{1(\alpha)}$, $\hat{\sigma}^r_\alpha\varphi_{2(\alpha)} = \sigma^r_\alpha\varphi_{1(\alpha)} = (\sigma^r_\alpha\widetilde{\sigma}_\alpha)\varphi_{2(\alpha)}$. Whence, the single eigenvalue $(\sigma^r_\alpha\widetilde{\sigma}_\alpha)$ associates with different $\varphi_{\lambda(\alpha)}$, namely it is degenerate with degeneracy degree equal 2. Thus, among quantum numbers r there is also the quantum number of the half integer spin $\vec{\sigma}$ $(\sigma_3 = \frac{1}{2}s, \quad s = \pm 1)$. This consequently gives rise to the spins of particles. The one occupied state reads $\varphi_{r'(\alpha)} = (\varphi_{2(\alpha)})_{r'} \prod_{r\neq r'}(\chi_1)_r$. Next, we introduce the operators $\hat{\gamma}^r_{(\lambda,\mu,\alpha)} \equiv \hat{O}^{r_1}_\lambda \otimes \hat{O}^{r_2}_\mu \otimes \hat{\sigma}^{r_3}_\alpha$

doi: 10.52526/25792776-2021.68.2-311

and the state vectors $\chi_{\lambda,\mu,\tau(\alpha)} \equiv\mid \lambda,\mu,\tau(\alpha) >= \chi_\lambda\otimes\chi_\mu\otimes\varphi_{\tau(\alpha)}$, where $\lambda,\mu,\tau,\nu=1,2;\quad \alpha,\beta=1,2,3$ and $r\equiv(r_1,r_2,r_3)$. Omitting two valuedness of state vectors we apply $\mid \lambda,\tau,\delta(\beta) >\equiv\mid \lambda,\tau >$, and remember that always the summation must be extended over the double degeneracy of the spin states $(s=\pm1)$. The explicit matrix elements of basis vectors read $< \lambda,\mu \mid \hat{\gamma}^r_{(\tau,\nu,\alpha)} \mid \tau,\nu >= {}^*\delta_{\lambda\tau}{}^*\delta_{\mu\nu}e^r_{(\tau,\nu,\alpha)}$, $< \tau,\nu \mid \hat{\gamma}_r^{(\tau,\nu,\alpha)} \mid \lambda,\mu >= {}^*\delta_{\lambda\tau}{}^*\delta_{\mu\nu}e_r^{(\tau,\nu,\alpha)}$, for given λ,μ. The operators of occupation numbers $\hat{N_1}^{rr'}_{\alpha\beta}=\hat{\gamma}^r_{(1,1,\alpha)}\hat{\gamma}^{r'}_{(2,2,\beta)}$, $\hat{N_2}^{rr'}_{\alpha\beta}=\hat{\gamma}^r_{(2,1,\alpha)}\hat{\gamma}^{r'}_{(1,2,\beta)}$ have the expectation values implying Pauli's exclusion principle $< 2,2 \mid \hat{N_1}^{rr'}_{\alpha\beta} \mid 2,2 >=< 1,2 \mid \hat{N_2}^{rr'}_{\alpha\beta} \mid 1,2 >= \delta_{rr'}\delta_{\alpha\beta}$, $< 1,1 \mid \hat{N_1}^{rr'}_{\alpha\beta} \mid 1,1 >=< 2,1 \mid \hat{N_2}^{rr'}_{\alpha\beta} \mid 2,1 >= 0$. The operators $\{\hat{\gamma}^r\}$ are the basis for tangent operator vectors $\hat{\Phi}(\zeta)=\hat{\gamma}^r\Phi_r(\zeta)$ of the 12 dimensional flat OM: $\hat{G}$, where we introduce the vector function belonging to the ordinary class of functions of C^∞ smoothness defined on the manifold G: $\quad \Phi_r^{(\lambda,\mu,\alpha)}(\zeta)=\zeta^{(\lambda,\mu,\alpha)}\Phi_r^{\lambda,\mu}(\zeta),\quad \zeta\in G$. But, the operators $\{\hat{\gamma}_r\}$ is a dual basis for operator covectors $\hat{\bar{\Phi}}(\zeta)=\hat{\gamma}_r\Phi^r(\zeta)$, where $\Phi^r=\bar{\Phi}_r$ (charge conjugated). Hence $< \lambda,\mu \mid \hat{\Phi}(\zeta)\hat{\bar{\Phi}}(\zeta) \mid \lambda,\mu >= {}^*\delta_{\lambda\tau}{}^*\delta_{\mu\nu}\Phi_r^{(\tau,\nu,\alpha)}(\zeta)\Phi^r_{(\tau,\nu,\alpha)}(\zeta)$, for given λ,μ. Considering the state vectors $\mid \chi_\pm >$, we get the matrix elements $< \chi_+ \mid \hat{\Phi}(\zeta)\hat{\bar{\Phi}}(\zeta) \mid \chi_+ >\equiv \Phi_+^2(\zeta)=\quad \Phi_r^{(\lambda,1,\alpha)}(\zeta)\Phi^r_{(\lambda,1,\alpha)}(\zeta)$, $< \chi_- \mid \hat{\Phi}(\zeta)\hat{\bar{\Phi}}(\zeta) \mid \chi_- >\equiv \Phi_-^2(\zeta)=\Phi_r^{(\lambda,2,\alpha)}(\zeta)\Phi^r_{(\lambda,2,\alpha)}(\zeta)$. The basis $\{\hat{\gamma}^r\}$ decomposes into $\{\hat{\gamma_i}^r\}$ $(i=\eta,u)$, where $\hat{\gamma_i}^r_{(+\alpha)}=\frac{1}{\sqrt{2}}(\gamma^r_{(1,1\alpha)}+\varepsilon_i\gamma^r_{(2,1\alpha)})$, $\hat{\gamma_i}^r_{(-\alpha)}=\frac{1}{\sqrt{2}}(\gamma^r_{(1,2\alpha)}+\varepsilon_i\gamma^r_{(2,2\alpha)})$. The expansion of operator vectors $\hat{\Psi}_i\in\hat{G}_i$ and operator covectors $\hat{\bar{\Psi}}_i$ are written $\hat{\Psi}_i=\hat{\gamma_i}^r\Psi_{ir}$, $\hat{\bar{\Psi}}_i=\hat{\gamma}_{ir}\Psi_i{}^r$, where the following vector functions of C^∞ smoothness are defined on the manifolds G_i : $\Psi_{\eta r}^{(\pm\alpha)}(\eta,p_\eta)=\eta^{(\pm\alpha)}\Psi_{\eta r}^{\pm}(\eta,p_\eta)$, $\Psi_{ur}^{(\pm\alpha)}(u,p_u)=u^{(\pm\alpha)}\Psi_{ur}^{\pm}(u,p_u)$. Namely, the probability of finding the vector function in the state r with given sixvector of coordinate (η or u) and momentum (p_η or p_u) is determined by the square of its state wave function $\Psi_{\eta r}^{\pm}(\eta,p_\eta)$, or $Psi_{ur}^{\pm}(u,p_u)$. Due to the spin states, the $\Psi_{ir}^{\pm}$ can be regarded as the Fermi field of the positive and negative frequencies $\Psi_{ir}^{\pm}\equiv\Psi_{i\pm p}^{r}$.

7.2. Realization of the Flat Manifold G

The bispinor $\Psi(\zeta)$ defined on the manifold $G=G_\eta\oplus G_u$ can be written $\Psi(\zeta)=\Psi_\eta(\eta)\Psi_u(u)$, where Ψ_i is the bispinor defined on the manifold G_i. The free state of i-type fermion with definite values of momentum p_i and spin projection s is described by plane waves. The relations of orthogonality and completeness hold for the spinors. Considering also the solutions of negative frequencies, we make use of localized wave packets constructed by means of superposition of plane wave solutions furnished by creation and annihilation operators in agreement with Pauli's principle $\hat{\Psi}_i=\sum_{\pm s}\int\frac{d^3p_i}{(2\pi)^{3/2}}(\hat{\gamma}_{i(+\alpha)}\Psi_i{}^{(+\alpha)}+\hat{\gamma}_{i(-\alpha)}\Psi_i{}^{(-\alpha)})$, etc, where the summation is extended over all dummy indices. In such a manner we can treat as well the wave packets of operator vector fields $\hat{\Phi}(\zeta)$. While the matrix element of the anticommutator of expansion coefficients reads $< \chi_- \mid \{\hat{\gamma_i}^{(+\alpha)}(p_i,s),\,\hat{\gamma}_{j(+\beta)}(p'_j,s')\} \mid \chi_- >= \varepsilon_i\delta_{ij}\delta_{ss'}\delta_{\alpha\beta}\delta^{(3)}(\vec{p_i}-\vec{p'}_i)$. In the aftermath, we get the most important relation $\sum_{\lambda=\pm} < \chi_\lambda \mid \hat{\Phi}(\zeta)\hat{\bar{\Phi}}(\zeta) \mid \chi_\lambda >= \sum_{\lambda=\pm} < \chi_\lambda \mid \hat{\bar{\Phi}}(\zeta)\hat{\Phi}(\zeta) \mid \chi_\lambda >= -i\,\zeta^2\,G_\zeta(0)=-i\,(\eta^2\,G_\eta(0)-u^2\,G_u(0))$,where $G_i(0)\equiv\lim_{i\to i'}G_i(i-i'),\quad (i=\zeta,\eta,u,)$, etc., the Green's function $G_i(i-i')=-(i\hat{\partial}_i+m)\Delta_i(i-i')$ is provided by the usual invariant singular functions $\Delta_i(i-i')$. Realization of the flat manifold G ensued from the constraint imposed upon the matrix element that, as the geometric object, it is required to be finite $\sum_{\lambda=\pm} < \chi_\lambda \mid \hat{\Phi}(\zeta)\hat{\bar{\Phi}}(\zeta) \mid \chi_\lambda >< \infty$, which gives rise to $\zeta^2\,G_{\zeta F}(0)<\infty$, and $G_{\zeta F}(0)=G_{\eta F}(0)=G_{uF}(0)=\lim_{u\to u'}[-i\sum_{\vec{p}_u}\Psi_{up_u}(u)\,\bar{\Psi}_{up_u}(u')\,\theta(u_0-u'_0)+i\sum_{\vec{p}_u}\bar{\Psi}_{u-p_u}(u')\,\Psi_{u-p_u}(u)\,\theta(u'_0-u_0))$, where the $G_{\zeta F},G_{\eta F}$ and G_{uF} are causal Green's functions characterized by the boundary condition that only positive frequency occur for $\eta_0>0\quad(u_0>0)$, only negative for $\eta_0<0\quad(u_0<0)$. Here $\eta_0=\mid\vec{\eta}_0\mid$, $\eta_{0\alpha}=\frac{1}{\sqrt{2}}(\eta_{(+\alpha)}+\eta_{(-\alpha)})$ and the same holds for u_0. Satisfying the condition above, a length of each vector $\zeta=e\zeta\in G$ compulsory must be equaled zero $\zeta^2=\eta^2-u^2=0$, which is the condition of realization of the flat manifold G. The latter subsequently leads to Minkowski flat space M_4, the relativity principle holds $d\,\eta^2\big|_{6\to4}\equiv d\,s^2=d\,u^2=inv.$

doi: 10.52526/25792776-2021.68.2-311

8. OM: Field aspect

The quantum field theory of the OM is equivalent to configuration space wave mechanics employing the antisymmetric state functions incorporated with geometric properties of corresponding objects. Therein, by applying the algebraic approach we reach to rigorous definition of the OM: $\hat{G}$, construct the explicit forms of wave state functions and calculate the matrix elements of field operators. While, the $\hat{G}$ reads $\hat{G} = \sum_{n=0}^{\infty} \hat{G}^{(n)} = \sum_{n=0}^{\infty} (\hat{\mathcal{U}}^{(n)} \otimes \bar{\mathcal{H}}^{(n)})$, where $\hat{\mathcal{U}}^{(n)}_{(r_1,\ldots,r_n)} = \hat{\mathcal{U}}^{(1)}_{r_1}, \otimes \cdots \otimes \hat{\mathcal{U}}^{(1)}_{r_n}$ is the open neighbourhood of the n-points $\hat{\zeta}_{r_i}$ of the OM, $\bar{\mathcal{H}}^{(n)}_{(r_1,\ldots,r_n)} = \mathcal{H}^{(1)}_{r_1} \otimes \cdots \otimes \mathcal{H}^{(1)}_{r_n}$ is the Hilbert space for description of n particle system. To illustrate the point at issue, the operators $\{\hat{\gamma}^r\}$ are the basis for tangent operator vectors $\hat{\Phi}(\zeta) = \hat{\gamma}^r \Phi_r(\zeta)$ of the 12D flat OM: $\hat{G}$, where we introduce the vector function belonging to the ordinary class of functions of C^∞ smoothness defined on the 12D manifold G: $\Phi^{(\lambda,\mu,\alpha)}_r(\zeta) = \zeta^{(\lambda,\mu,\alpha)} \Phi^{\lambda,\mu}_r(\zeta)$, $\zeta \in G$ $(\lambda, \mu = 1, 2; \alpha = 1, 2, 3)$. But, the operators $\{\hat{\gamma}_r\}$ is a dual basis for operator covectors $\hat{\bar{\Phi}}(\zeta) = \hat{\gamma}_r \Phi^r(\zeta)$, where $\Phi^r = \bar{\Phi}_r$ (charge conjugated). The explicit matrix elements of basis vectors read $< \lambda, \mu \mid \hat{\gamma}^r_{(\tau,\nu,\alpha)} \mid \tau, \nu >= {}^*\delta_{\lambda\tau} {}^*\delta_{\mu\nu} e^r_{(\tau,\nu,\alpha)}$, $< \tau, \nu \mid \hat{\gamma}^{(\tau,\nu,\alpha)}_r \mid \lambda, \mu >= {}^*\delta_{\lambda\tau} {}^*\delta_{\mu\nu} e^{(\tau,\nu,\alpha)}_r$, for given λ, μ, and ${}^*\delta_{\lambda\tau} = 1 - \delta_{\lambda\tau}$. The operators of occupation numbers $\hat{N}_1{}^{rr'}_{\alpha\beta} = \hat{\gamma}^r_{(1,1,\alpha)} \hat{\gamma}^{r'}_{(2,2,\beta)}$, $\hat{N}_2{}^{rr'}_{\alpha\beta} = \hat{\gamma}^r_{(2,1,\alpha)} \hat{\gamma}^{r'}_{(1,2,\beta)}$, have the expectation values implying Pauli's exclusion principle $< 2, 2 \mid \hat{N}_1{}^{rr'}_{\alpha\beta} \mid 2, 2 >=< 1, 2 \mid \hat{N}_2{}^{rr'}_{\alpha\beta} \mid 1, 2 >= \delta_{rr'} \delta_{\alpha\beta}$, $< 1, 1 \mid \hat{N}_1{}^{rr'}_{\alpha\beta} \mid 1, 1 >=< 2, 1 \mid \hat{N}_2{}^{rr'}_{\alpha\beta} \mid 2, 1 >= 0$. And $< \lambda, \mu \mid \hat{\Phi}(\zeta) \hat{\bar{\Phi}}(\zeta) \mid \lambda, \mu >= {}^*\delta_{\lambda\tau} {}^*\delta_{\mu\nu} \Phi^{(\tau,\nu,\alpha)}_r(\zeta) \Phi^r_{(\tau,\nu,\alpha)}(\zeta)$, for given λ, μ. Meanwhile, one has to modify the basis operators (the creation $\hat{\gamma}_r \to \hat{\gamma}_{r_i}$ and annihilation $\hat{\gamma}^r \to \hat{\gamma}^{r_i}$ operators) in order to provide an anticommutation in arbitrary $(|>_{r_i})$ states. For example, acting on free state $\mid 0 >_{r_i}$ the creation operator $\hat{\gamma}_{r_i}$ now yields the one occupied state $\mid 1 >_{r_i}$ with the phase $'+'$ or $'-'$ depending of parity of the number of quanta in the states $r < r_i$. Modified operators satisfy the same anticommutation relations of the basis operators. It is convenient to make use of notation $\hat{\gamma}^{(\lambda,\mu,\alpha)}_r \equiv e^{(\lambda,\mu,\alpha)}_r \hat{b}^{\lambda\mu}_{(r\alpha)}$, and abbreviate the pair of indices $(r\alpha)$ by the single symbol r. Then for each $\Phi \in {}^A\mathcal{H}^{(n)}$ and any vector $f \in \mathcal{H}^{(1)}$ the operators $\hat{b}(f)$ and $\hat{b}^*(f)$ imply $\hat{b}(f)\Phi = \frac{1}{\sqrt{(n-1)!}} \sum_{\sigma \in S(n)} sgn(\sigma)(f\, \Phi^{(1)}_{\sigma(1)}) \Phi^{(1)}_{\sigma(2)} \otimes \cdots \otimes \Phi^{(1)}_{\sigma(n)}$, $\hat{b}^*(f)\Phi = \frac{1}{\sqrt{(n+1)!}} \sum_{\sigma \in S(n+1)} sgn(\sigma) \Phi^{(1)}_{\sigma(0)} \otimes \Phi^{(1)}_{\sigma(1)} \otimes \cdots \otimes \Phi^{(1)}_{\sigma(n)}$, where $\Phi^{(1)}_{(0)} \equiv f$. One continues the $\hat{b}(f)$ and $\hat{b}^*(f)$ by linearity to linear reflections, which are denoted by the same symbols acting respectively from ${}^A\mathcal{H}^{(n)}$ onto ${}^A\mathcal{H}^{(n-1)}$ or ${}^A\mathcal{H}^{(n+1)}$. They are limited over the values $\sqrt{n}|f|$ and $\sqrt{(n+1)}|f|$ and can be expanded by continuation up to the reflections acting from ${}^A\bar{\mathcal{H}}^{(n)}$ onto ${}^A\bar{\mathcal{H}}^{(n-1)}$ or ${}^A\bar{\mathcal{H}}^{(n+1)}$. Finally, they must be continued by linearity up to the linear operators acting from ${}^A\mathcal{F}$ onto ${}^A\mathcal{F}$ defined on the same closed region in ${}^A\bar{\mathcal{H}}^{(n)}$, namely in ${}^A\mathcal{F}$, which is invariant with respect to reflections $\hat{b}(f)$ and $\hat{b}^*(f)$. Hence, at $f_i, g_i \in \mathcal{H}^{(1)}$ $(i = 1, \ldots, n; j = 1, \ldots, m)$ all polynomials over $\{\hat{b}^*(f_i)\}$ and $\{\hat{b}(g_j)\}$ are completely defined on ${}^A\mathcal{F}$. While, for given λ, μ, one has $< \lambda, \mu \mid \{\hat{b}^{\lambda\mu}_r(f), \hat{b}^{r'}_{\lambda\mu}(g)\} \mid \lambda, \mu >= \delta^{r'}_r$. The mean values $< \varphi; \hat{b}^{\lambda\mu}_r(f)\, \hat{b}^r_{\lambda\mu}(f) >$ calculated at fixed λ, μ for any element $\Phi \in {}^A\mathcal{F}$ equal to mean values of the symmetric operator of occupation number in terms of $\hat{N}^r = \hat{b}_r(f)\, \hat{b}^r(f)$, with a wave function f in the state described by Φ. Here, as usual, it is denoted $< \varphi; A\Phi >= Tr\, P_\varphi A = (\Phi, A\Phi)$ for each vector $\Phi \in \mathcal{H}$ with $|\Phi| = 1$, while the P_φ is projecting operator onto one dimensional space $\{\lambda\Phi \mid \lambda \in C\}$ generated by Φ. Therewith, the probability of transition $\varphi \to \psi$ is given $Pr\{\varphi \mid \psi\} = |(\psi, \varphi)|^2$. The linear operator A defined on the elements of linear manifold $\mathcal{D}(A)$ of $\mathcal{H}$ takes the values in $\mathcal{H}$. The $\mathcal{D}(A)$ is an overall closed region of definition of A, namely the closure of $\mathcal{D}(A)$ by the norm given in $\mathcal{H}$ coincides with $\mathcal{H}$. Meanwhile, the $\mathcal{D}(A)$ included in $\mathcal{D}(A^*)$ and A coincides with the reduction of A^* on $\mathcal{D}(A)$, because $\mathcal{D}(A)$ is the symmetric operator such that the linear operator A^* is the maximal conjugated to A. That is, any operator A' conjugated to A - $(\Psi, A'\Phi) = (A'\Psi, \Phi)$ for all $\Phi \in \mathcal{D}(A)$ and $\Psi \in \mathcal{D}(A')$ coincides with the reduction of A^* on some linear manifold $\mathcal{D}(A')$ included in $\mathcal{D}(A^*)$. Thus, the operator A^{**} is closed symmetric expansion of operator A, namely it is a closure of A. Self conjugated operator A, the closure of which is self conjugated as well, allows only the one self conjugated expansion A^{**}. Hence, self conjugated closure $\hat{N}$ of operator $\sum_{i=1}^{\infty} \hat{b}^*(f_i)\, \hat{b}(f_i)$, where $\{f_i \mid i = 1, \ldots, n\}$ is an arbitrary orthogonal basis on $\mathcal{H}^{(1)}$, can be regarded as the operator of occupation number. For the vector $\chi^0 \in {}^A\mathcal{F}$ and $\chi^{0(n)} = \delta_{0n}$ one gets $< \chi^{0(n)}, \hat{N}(f) >= 0$ for all $f \in \mathcal{H}^{(1)}$. Thus, χ^0 is the

doi: 10.52526/25792776-2021.68.2-311

vector of vacuum state: $\hat{b}(f)\chi^0 = 0$ for all $f \in \mathcal{H}^{(1)}$. If $f = \{f_i \mid i = 1, 2, \ldots\}$ is an arbitrary orthogonal basis on $\mathcal{H}^{(1)}$, then due to irreducibility of operators $\hat{b}^*(f_i) \mid f_i \in f$, the ${}^A\mathcal{H}$ includes the 0 and whole space ${}^A\mathcal{H}$ as invariant subspaces with respect to all $\hat{b}^*(f)$. To define the 12 dimensional operator manifold $\hat{G}$ we consider a set $\hat{\mathcal{F}}$ of all the sequences $\hat{\Phi} = \{\hat{\Phi}^{(0)}, \hat{\Phi}^{(1)}, \ldots, \hat{\Phi}^{(n)}, \ldots\}$ with a finite number of nonzero elements provided by $\hat{\Phi}^{(n)}_{(r_1,\ldots,r_n)} = \hat{\Phi}^{(1)}_{r_1} \otimes \cdots \otimes \hat{\Phi}^{(1)}_{r_n} \in \hat{G}^{(n)}$, $\hat{\Phi}^{(1)}_{r_i} = \hat{\zeta}_{r_i}\Phi^{(1)}_{r_i} \in \hat{G}^{(1)}_i = \hat{\mathcal{U}}^{(1)}_i \otimes \mathcal{H}^{(1)}_i$, $\hat{\zeta}_{r_i} \equiv \sum_{\alpha_i=1}^3 \hat{\gamma}^{r_i}_{(\lambda_i,\mu_i,\alpha_i)}\zeta^{(\lambda_i,\mu_i,\alpha_i)}_{r_i} \in \hat{\mathcal{U}}^{(1)}_{r_i}$, $\hat{G}^{(n)} = \hat{\mathcal{U}}^{(n)} \otimes \bar{\mathcal{H}}^{(n)}$, $\hat{\mathcal{U}}^{(n)}_{(r_1,\ldots,r_n)} = \hat{\mathcal{U}}^{(1)}_{r_1}, \otimes \cdots \otimes \hat{\mathcal{U}}^{(1)}_{r_n}$. Then, the operator manifold $\hat{G}$ ensues $\hat{G} = \sum_{n=0}^\infty \hat{G}^{(n)} = \sum_{n=0}^\infty (\hat{\mathcal{U}}^{(n)} \otimes \bar{\mathcal{H}}^{(n)})$. To define the secondary quantized form of one particle observable A on $\mathcal{H}$, let consider a set of identical samples $\hat{\mathcal{H}}_i$ of one particle space $\mathcal{H}^{(1)}$ and operators A_i acting on them. To each closed linear operator $A^{(1)}$ in $\mathcal{H}^{(1)}$ with overall closed region of definition $\mathcal{D}(A^{(1)})$ following operators are corresponded: $A^{(n)}_1 = A^{(1)} \otimes I \otimes \cdots \otimes I, \ldots,$ $A^{(n)}_n = I \otimes I \otimes \cdots \otimes A^{(1)}$. The sum $\sum_{j=1}^n A^{(n)}_j$ is given on the intersection of regions of definition of operator terms including a linear manifold $\mathcal{D}(A^{(1)}) \otimes \cdots \otimes \mathcal{D}(A^{(n)})$ closed in $\hat{\mathcal{H}}^{(n)}$. While, the $A^{(n)}$ is a minimal closed expansion of this sum with $\mathcal{D}(A^{(n)})$. One considers a linear manifold $\mathcal{D}(\Omega(A))$ in $\mathcal{H} = \sum_{n=0}^\infty \hat{\mathcal{H}}^{(n)}$ defined as a set of all the vectors $\Psi \in \mathcal{H}$ such as $\Psi^{(n)} \in \mathcal{D}(A^{(n)})$ and $\sum_{n=0}^\infty \left|A^{(n)}\Psi^{(n)}\right|^2 < \infty$. The manifold $\mathcal{D}(\Omega(A))$ is closed in $\mathcal{H}$. On this manifold one defines a closed linear operator $\Omega(A)$ acting as $\Omega(A)^{(n)} = A^{(n)}\Psi^{(n)}$, namely $\Omega(A)\Phi = \sum_{n=0}^\infty A^{(n)}\Psi^{(n)}$, while the $\Omega(A)$ is self conjugated operator with overall closed region of definition, where $\Phi_i \in \mathcal{D}(A)$. Then, $< \varphi^{(n)}; A^{(n)} >= \sum_{i=1}^n < \varphi_i; A >$, which enables the expansion by continuing onto $\mathcal{D}(A)$. Thus, $A^{(n)}$ is the n particle observable corresponding to one particle observable A. So $< \varphi; \Omega(A) >= \sum_{n=0}^\infty < \varphi^{(n)}; A^{(n)} >$ for any $\Phi_i \in \mathcal{D}(\Omega(A))$. While, the $\Omega(A)$ reflects ${}^A\mathcal{D} = \mathcal{D}(\Omega(A)) \frown {}^A\mathcal{H}$ into ${}^A\mathcal{H}$. The reduction of $\Omega(A)$ on ${}^A\mathcal{H}$ is the self conjugated in the region ${}^A\mathcal{D}$, because ${}^A\mathcal{H}$ is the closed subspace of the $\mathcal{H}$. Hence, the $\Omega(A)$ is the secondary quantized form of one particle observable A on the $\mathcal{H}$. The vacuum state reads $\chi^0(\nu_1, \nu_2, \nu_3, \nu_4) =\mid 1, 1 >^{\nu_1} \cdot \mid 1, 2 >^{\nu_2} \cdot \mid 2, 1 >^{\nu_3} \cdot \mid 2, 2 >^{\nu_4}$, $\nu_i = \begin{cases} 1 & \text{if } \nu = \nu_i \quad \text{for some } i, \\ 0 & \text{otherwise,} \end{cases}$, where $\mid \chi_-(1) >\equiv \chi^0(1, 0, 0, 0)$, $\mid \chi_+(1) >\equiv \chi^0(0, 0, 0, 1)$, $\mid \chi_-(2) >\equiv \chi^0(0, 0, 1, 0)$, $\mid \chi_+(2) >\equiv \chi^0(0, 1, 0, 0)$, $< \chi_\pm(\lambda) \mid \chi_\pm(\mu) >= \delta_{\lambda\mu}$, and $< \chi_\pm(\lambda) \mid \chi_\mp(\mu) >= 0$, provided by $< \chi_\pm \mid A \mid \chi_\pm >\equiv \sum_\lambda < \chi_\pm(\lambda) \mid A \mid \chi_\pm(\lambda) >$ and the normalization condition $< \chi^0(\nu'_1, \nu'_2, \nu'_3, \nu'_4) \mid \chi^0(\nu_1, \nu_2, \nu_3, \nu_4) >= \prod_{i=1}^4 \delta_{\nu_i\nu'_i}$. The state vectors are introduced $\chi(\{n_r\}_1^N; \{m_r\}_1^M; \{q_r\}_1^Q; \{t_r\}_1^T; \{\nu_r\}_1^4) = (\hat{b}^{11}_N)^{n_N} \cdots (\hat{b}^{11}_1)^{n_1} \cdot (\hat{b}^{12}_M)^{m_M} \cdots (\hat{b}^{12}_1)^{m_1} \cdot (\hat{b}^{21}_Q)^{q_Q} \cdots (\hat{b}^{21}_1)^{q_1} \cdot \cdot (\hat{b}^{22}_T)^{t_T} \cdots (\hat{b}^{22}_1)^{t_1} \chi^0(\nu_1, \nu_2, \nu_3, \nu_4)$, where $\{n_r\}_1^N = n_1, \ldots, n_N$, etc., which are the eigenfunctions of modified operators. They form a whole set of orthogonal vectors $< \chi, \chi' >=$ $\prod_{r=1}^N \delta_{n_r n'_r} \cdot \prod_{r=1}^M \delta_{m_r m'_r} \cdot \prod_{r=1}^Q \delta_{q_r q'_r} \cdot \prod_{r=1}^T \delta_{t_r t'_r} \cdot \prod_{r=1}^4 \delta_{\nu_r \nu'_r}$. Considering an arbitrary superposition $\chi =$ $\sum^1_{a=\{n_r\}_1^N, \{m_r\}_1^M, \{q_r\}_1^Q, \{t_r\}_1^T = 0} c'(a)\, \chi(a)$, the coefficients c' of expansion are the corresponding amplitudes of probabilities. The nonvanishing matrix elements of operators $\hat{b}^{11}_{r_k}$ and $\hat{b}^{r_k}_{11}$ read

$< \chi(\{n'_r\}_1^N; 0; 0; 0; 1, 0, 0, 0) \mid \hat{b}^{11}_{r_k}\chi(\{n_r\}_1^N; 0; 0; 0; 1, 0, 0, 0) >=< 1, 1 \mid \hat{b}^{r'_1}_{11} \cdots \hat{b}^{r'_n}_{11} \cdot \hat{b}^{11}_{r_k} \cdot \hat{b}^{11}_{r_n} \cdots \hat{b}^{11}_{r_1} \mid 1, 1 >=$ $\begin{cases} (-1)^{n'-k'} & \text{if } n_r = n'_r \text{ for } r \neq r_k \text{ and } n_{r_k} = 0; n'_{r_k} = 1, \\ 0 & \text{otherwise,} \end{cases}$, etc., where one denotes $n = \sum_{r=1}^N n_r$, $\quad n' =$ $\sum_{r=1}^N n'_r$, the r_k and r'_k are k-th and k'-th terms of regulated sets of $\{r_1, \ldots, r_n\}$ $\quad (r_1 < r_2 < \cdots < r_n)$ and $\{r'_1, \ldots, r'_n\}$ $\quad (r'_1 < r'_2 < \cdots < r'_n)$, respectively. Continuing along this line we get a whole set of explicit forms of matrix elements of the rest of operators $\hat{b}_{r_k}$ and $\hat{b}^{r_k}$. Hence $\sum^1_{\{\nu_r\}=0} < \chi^0 \mid \hat{\Phi}(\zeta) \mid \chi >= \sum_{r=1}^N c'_{n_r} e^{n_r}_{(1,1,\alpha)} \Phi^{(1,1,\alpha)}_{n_r} + \cdots$, provided by $c'_{n_r} \equiv \delta_{1n_r} c'(0, \ldots, n_r, \ldots, 0; 0; 0; 0), \cdots$ Hereinafter we change a notation of the coefficients $\bar{c}(r^{11}) = c'_{n_r}$, $\bar{c}(r^{21}) = c'_{q_r}$, $\quad N_{11} = N$, $N_{21} = Q$, $\bar{c}(r^{12}) = c'_{m_r}$, $\bar{c}(r^{22}) = c'_{t_r}$, $N_{12} = M$, $N_{22} = T$, and make use of convention $F_{r^{\lambda\mu}} = \sum_\alpha e^{r^{\lambda\mu}}_{(\lambda,\mu,\alpha)} \Phi^{(\lambda,\mu,\alpha)}_{r^{\lambda\mu}}$, $\sum^1_{\{\nu_r\}=0} < \chi^0 \mid \hat{A} \mid \chi >\equiv< \chi^0 \parallel \hat{A} \parallel \chi >$, The matrix elements of operator vector and covector fields take the final forms $< \chi^0 \parallel \hat{\Phi}(\zeta) \parallel \chi >= \sum_{\lambda\mu=1}^2 \sum_{r^{\lambda\mu}=1}^{N_{\lambda\mu}} \bar{c}(r^{\lambda\mu})\, F_{r^{\lambda\mu}}(\zeta)$, $< \chi \parallel \bar{\hat{\Phi}}(\zeta) \parallel \chi^0 >=$ $\sum_{\lambda\mu=1}^2 \sum_{r^{\lambda\mu}=1}^{N_{\lambda\mu}} \bar{c}^*(r^{\lambda\mu})\, F^{r^{\lambda\mu}}(\zeta)$. In the following we shall use a convention: $\left\{\sum_{\lambda\mu}^2\right\}_1^n \equiv \sum_{\lambda_1\mu_1}^2 \cdots \sum_{\lambda_n\mu_n}^2$, $r_i^{\lambda\mu} \equiv r^{\lambda_i\mu_i}$ and $\bar{c}(r_1^{11}, \ldots, r_n^{11}) = c'(n_1, \ldots, n_N; 0; 0; 0)$, etc. The anticommutation relations ensue $<$ $\chi_- \mid \{\hat{b}^+_{ir}, \hat{b}^{r'}_{i+}\} \mid \chi_- >=< \chi_+ \mid \{\hat{b}^-_{ir}, \hat{b}^{r'}_{i-}\} \mid \chi_+ >= \delta^{r'}_r$, provided by $\hat{\gamma}^{(\lambda\alpha)}_{ir} = \hat{e}^{(\lambda\alpha)}_{ir}\, \hat{b}^{\lambda}_{i(r\alpha)}$, $\quad (r\alpha) \to r$.

doi: 10.52526/25792776-2021.68.2-311

The state functions $\chi = (\hat{b}^{+}_{\eta N})^{n_N}\cdots(\hat{b}^{+}_{\eta 1})^{n_1}\cdot(\hat{b}^{-}_{\eta M})^{m_M}\cdots(\hat{b}^{-}_{\eta 1})^{m_1}\cdot(\hat{b}^{+}_{uQ})^{q_Q}\cdots(\hat{b}^{+}_{u1})^{q_1}\cdot(\hat{b}^{-}_{uT})^{t_T}\cdots(\hat{b}^{-}_{u1})^{t_1}\cdot\chi_-(\lambda)\chi_+(\mu)$, form a whole set of orthogonal eigenfunctions of corresponding operators of occupation numbers $\hat{N}^{\lambda}_{ir} = \hat{b}_{ir}^{\lambda}\,\hat{b}^{r}_{i\lambda}$ with the expectation values $0, 1$.

For more detail see (Ter-Kazarian, 1884, 1996, 1999a).

9. OM: Differential geometric aspect

The operators $\{\hat{\gamma}^r\}$ are the basis for all operator vectors of tangent section $\hat{\mathbf{T}}_{\Phi_p}$ of principle bundle with the base $\hat{G}$ at the point $\mathbf{\Phi}_p = \mathbf{\Phi}(\zeta(t))|_{t=0} \in \hat{G}$. The smooth field of tangent operator vector $\hat{\mathbf{A}}(\mathbf{\Phi}(\zeta))$ is a class of equivalence of the curves $\mathbf{f}(\mathbf{\Phi}(\zeta))$, $\mathbf{f}(\mathbf{\Phi}(\zeta(0))) = \mathbf{\Phi}_p$. While, the operator differential $\hat{d}\,A^t_p$ of the flux $A^t_p : \hat{G} \to \hat{G}$ at the point $\mathbf{\Phi}_p$ with the velocity fields $\hat{\mathbf{A}}(\mathbf{\Phi}(\zeta))$ is defined by one parameter group of operator diffeomorphisms given for the curve $\mathbf{\Phi}(\zeta(t)) : R^1 \to \hat{G}$. Provided one has $\mathbf{\Phi}(\zeta(0)) = \mathbf{\Phi}_p$ and $\hat{\dot{\mathbf{\Phi}}}(\zeta(0)) = \hat{\mathbf{A}}_p$ $\hat{d}\,A^t_p(\mathbf{A}) = \frac{\hat{d}}{dt}\Big|_{t=0} A^t(\mathbf{\Phi}(\zeta(t))) = \hat{\mathbf{A}}(\mathbf{\Phi}(\zeta)) = \hat{\gamma}^r A_p$, where the $\{A_p\}$ are the components of $\hat{\mathbf{A}}$ in the basis $\{\hat{\gamma}^r\}$. According to eq.(3.2), in holonomic coordinate basis $\hat{\gamma}^r \to (\hat{\partial}\,/\,\partial\Phi_r(\zeta(t)))_p$ one gets $A_p = \frac{\partial\Phi_r}{\partial\zeta_r}\frac{d\zeta_r}{dt}\Big|_p$. Hence, for any function $f : \mathbf{R}^n \to \mathbf{R}^n$ of the ordinary class of functions of C^∞ smoothness on $\hat{G}$ one may define an operator differential $<\hat{d}\,f, \hat{\mathbf{A}}> = \widehat{(A\,f)}$, by means of smooth reflection $\hat{d}\,f : \hat{\mathbf{T}}(\hat{G}) \to \hat{R}$ $(\hat{\mathbf{T}}(\hat{G}) = \bigcup_{\Phi_p}\hat{\mathbf{T}}_{\Phi_p})$, where $<\chi\|\hat{d}\,f, \hat{\mathbf{A}}\|\chi^0> = \sum_{\lambda,\mu=1}^{2}\sum_{r^{\lambda\mu}=1}^{N_{\lambda\mu}}\hat{c}^*(r^{\lambda\mu}) <d\,f, \mathbf{A}>_{r^{\lambda\mu}} = \sum_{\lambda,\mu=1}^{2}\sum_{r^{\lambda\mu}=1}^{N_{\lambda\mu}}\hat{c}^*(r^{\lambda\mu})\,(\mathbf{A}\,f)_{r^{\lambda\mu}}$. In coordinate basis $<d\,\Phi^{\hat{\imath}}, \hat{\partial}\,/\,\partial\Phi^j> = \frac{\partial\Phi^{\hat{\imath}}}{\partial\Phi^j} = \delta^{\hat{\imath}}_j$, provided by $d\,\Phi^{\hat{\imath}} \equiv \hat{d}\Phi^i$ and $<\chi\|\hat{\delta}^{\imath}_j\|\chi^0> = \sum_{\lambda,\mu=1}^{2}\sum_{r^{\lambda\mu}=1}^{N_{\lambda\mu}}\hat{c}^*(r^{\lambda\mu})\delta^i_j$, where the i and j stand for a set of $(\lambda_i, \mu_i, \alpha_i)$. The operator tensor $\hat{\mathbf{T}}$ of $\widehat{(n,0)}$-type at the point $\mathbf{\Phi}_p$ is a linear function of the space $\hat{\mathbf{T}}^n_0 = \underbrace{\hat{\mathbf{T}}_{\Phi_p}\otimes\cdots\otimes\hat{\mathbf{T}}_{\Phi_p}}_{n}$, where the $\otimes$ denotes the tensor product. It enables a correspondence between the element $(\hat{\mathbf{A}}_1, \ldots, \hat{\mathbf{A}}_n)$ of $\hat{\mathbf{T}}^n_0$ and the number $T(\hat{\mathbf{A}}_1, \ldots, \hat{\mathbf{A}}_n)$ furnished by linearity. Constructing matrix elements of operator tensors of $\hat{G}$ one produces the Cartan's exterior forms. Whence, the matrix elements of symmetric operator tensors equal zero. The differential operator n form $\hat{\omega}^n|_{\Phi_p}$ at the point $\mathbf{\Phi}_p \in \hat{G}$ can be defined as the exterior operator n form on tangent operator space $\hat{\mathbf{T}}_{\Phi_p}$ of tangent operator vectors $\hat{\mathbf{A}}_1, \ldots, \hat{\mathbf{A}}_n$. That is, if the $\wedge\hat{\mathbf{T}}^*_{\Phi_p}(\hat{G})$ means the exterior algebra on $\hat{\mathbf{T}}^*_{\Phi_p}(\hat{G})$, then operator n form $\hat{\omega}^n|_{\Phi_p}$ is an element of n-th degree out of $\wedge\hat{\mathbf{T}}^*_{\Phi_p}$ depending of the point $\mathbf{\Phi}_p \in \hat{G}$. Hence $\hat{\omega}^n = \bigcup_{\Phi_p}\hat{\omega}^n|_{\Phi_p}$. Any differential operator n form of dual operator space $\underbrace{\hat{\mathbf{T}}^*_{\Phi_p}\otimes\cdots\otimes\hat{\mathbf{T}}^*_{\Phi_p}}_{n}$ may be written $\hat{\omega}^n = \sum_{i_1<\cdots<i_n}\alpha_{i_1\cdots i_n}(\Phi)d\,\Phi^{\hat{\imath}_1}\wedge\cdots\wedge d\,\Phi^{\hat{\imath}_n}$, provided by the smooth differentiable functions $\alpha_{i_1\cdots i_n}(\Phi) \in C^\infty$ and basis $d\,\Phi^{\hat{\imath}_1}\wedge\cdots\wedge d\,\Phi^{\hat{\imath}_n} = \sum_{\sigma\in S_n} sgn(\sigma)\gamma^{\sigma(\hat{\imath}_1\otimes\cdots\otimes\gamma^{\hat{\imath}_n})}$. The linear operator form of 1 degree $\hat{\omega}^1$ is a linear operator valued function on $\hat{\mathbf{T}}_{\Phi_p}$, namely $\hat{\omega}^1(\hat{\mathbf{A}}_p) : \hat{\mathbf{T}}_{\Phi_p} \to \hat{R}$, where $\hat{\mathbf{A}}_p \in \hat{\mathbf{T}}_{\Phi_p}$, and the operator $\hat{\omega}^1(\hat{\mathbf{A}}) = <\hat{\omega}^1, \mathbf{A}> \in \hat{R}$ corresponds to $\hat{\mathbf{A}}_p$ at the point $\mathbf{\Phi}_p$, provided, according to eq.(A.1.25), with $<\chi\|\hat{\omega}^1\|\chi^0> = \sum_{\lambda,\mu=1}^{2}\sum_{r^{\lambda\mu}=1}^{N_{\lambda\mu}}\hat{c}^*(r^{\lambda\mu})\,\omega^1_{r^{\lambda\mu}}$, where $\omega^1_{r^{\lambda\mu}} = e^{(\lambda,\mu,\alpha)}_{r^{\lambda\mu}}\omega^{r^{\lambda\mu}}_{(\lambda,\mu,\alpha)}$, the $<\omega^1_{r^{\lambda\mu}}, \mathbf{A}> = \omega^1_{r^{\lambda\mu}}(\mathbf{A})$ is a linear form on $\mathbf{T}_p$, and $\hat{\omega}^1(\lambda_1\hat{\mathbf{A}}_1 + \lambda_2\hat{\mathbf{A}}_2) = \lambda_1\hat{\omega}^1(\hat{\mathbf{A}}_1) + \lambda_2\hat{\omega}^1(\hat{\mathbf{A}}_2)$, $\quad\forall\lambda_1, \lambda_2 \in R, \quad \hat{\mathbf{A}}_1, \hat{\mathbf{A}}_2 \in \hat{\mathbf{T}}_{\Phi_p}$. The set of all linear operator forms defined at the point $\mathbf{\Phi}_p$ fill up the operator vector space $\hat{\mathbf{T}}^*_{\Phi_p}$ dual to $\hat{\mathbf{T}}_{\Phi_p}$. While, the $\{\hat{\gamma}_r\}$ serves as a basis for them. The operator n form is defined as the exterior product of operator 1 forms. Here as well as for the rest of this section we abbreviate the set of indices $(\lambda_i, \mu_i, \alpha_i)$ by the single symbol i. Let the $\hat{\mathcal{D}}_1$ and $\hat{\mathcal{D}}_2$ are two compact convex parallelepipeds in oriented n dimensional operator space $\hat{\mathbf{R}}^n$ and the $f : \hat{\mathcal{D}}_1 \to \hat{\mathcal{D}}_2$ is differentiable reflection of interior of $\hat{\mathcal{D}}_1$ into $\hat{\mathcal{D}}_2$ retaining an orientation, namely for any function $\varphi \in C^\infty$ defined on $\hat{\mathcal{D}}_2$ it holds $\varphi\circ f \in C^\infty$ and $f^*\varphi(\mathbf{\Phi}_p) = \varphi(f(\mathbf{\Phi}_p))$, where f^* is an image of function $\varphi(f(\mathbf{\Phi}_p))$ on $\hat{\mathcal{D}}_1$ at the point $\mathbf{\Phi}_p$. Hence, the function f induces a linear reflection $\hat{d}\,f : \hat{\mathbf{T}}(\hat{\mathcal{D}}_1) \to \hat{\mathbf{T}}(\hat{\mathcal{D}}_2)$ as an operator differential of f implying $\hat{d}\,f(\hat{\mathbf{A}}_p)\varphi = \hat{\mathbf{A}}_p(\varphi\circ f)$ for any operator vector $\hat{\mathbf{A}}_p \in \hat{\mathbf{T}}_{\Phi_p}$ and for any function $\varphi \in C^\infty$ defined in the neighbourhood of $\mathbf{\Phi}'_p = f(\mathbf{\Phi}_p)$. If the function f is

doi: 10.52526/25792776-2021.68.2-311

given in the form $\Phi'^i = \Phi'^i(\Phi_p)$ and $\hat{\mathbf{A}}_p = (A^i\,\hat{\partial}\big/\partial\Phi^i)_p$, then in terms of local coordinates one gets $(\hat{d}\,f)\hat{\mathbf{A}}_p = A^i(\frac{\partial\Phi'^j}{\partial\Phi^i})_p(\frac{\hat{\partial}}{\partial\Phi'^j})_{p'}$. So, if $f_1 : \hat{\mathcal{D}}_1 \to \hat{\mathcal{D}}_2$ and $f_2 : \hat{\mathcal{D}}_2 \to \hat{\mathcal{D}}_3$ then $\hat{d}\,(f_2 \circ f_1) = \hat{d}\,f_2 \circ \hat{d}\,f_1$. For any differential operator n form $\hat{\omega}^n$ on $\hat{\mathcal{D}}_2$ the reflection f induces the operator n form $\hat{f}^*\hat{\omega}^n$ on $\hat{\mathcal{D}}_1$ $(\hat{f}^*\hat{\omega}^n)\,(\hat{\mathbf{A}}_1,\ldots,\hat{\mathbf{A}}_n)\Big|_{\Phi_p} = \hat{f}_*\hat{\omega}^n\,(\hat{f}_*\hat{\mathbf{A}}_1,\ldots,\hat{f}_*\hat{\mathbf{A}}_n)\Big|_{f(\Phi_p)}$. We may consider the integration of operator n form implying $\int_{\hat{\mathcal{D}}_1}\hat{f}^*\hat{\omega}^n = \int_{\hat{\mathcal{D}}_2}\hat{\omega}^n$. In general, let $\hat{\mathcal{D}}_1$ is the limited convex n dimensional parallelepiped in the n dimensional operator space $\hat{\mathbf{R}}^n$. One defines the n dimensional i-th piece of integration path $\hat{\sigma}^i$ in $\hat{G}$ as $\hat{\sigma}^i = (\hat{\mathcal{D}}_i, f_i, Or_i)$, where $\hat{\mathcal{D}}_i \in \hat{\mathbf{R}}^n$, $f_i : \hat{\mathcal{D}}_i \to \hat{G}$ and the Or_i is an orientation of $\hat{\mathbf{R}}^n$. Then, the integral over the operator n form $\hat{\omega}^n$ along the operator n dimensional chain $\hat{c}_n = \sum m_i\hat{\sigma}^i$ may be written $\int_{\hat{c}_n}\hat{\omega}^n = \sum m_i\int_{\hat{\sigma}^i}\hat{\omega}^n = \sum m_i\int_{\hat{\mathcal{D}}_i}\hat{f}^*\hat{\omega}^n$, where the m_i is a multiple number. Next, we may apply the analog of exterior differentiation. We define the operator $(n+1)$ form $\hat{d}\,\hat{\omega}^n$ on $(n+1)$ operator vectors $\hat{\mathbf{A}}_1,\ldots,\hat{\mathbf{A}}_{n+1} \in \hat{\mathbf{T}}_{\Phi_p}$ by considering diffeomorphic reflection f of the neighbourhood of the point 0 in $\hat{\mathbf{R}}^n$ into neighbourhood of the point $\mathbf{\Phi}_p$ in $\hat{G}$. The prototypes of operator vectors $\hat{\mathbf{A}}_1,\ldots,\hat{\mathbf{A}}_{n+1} \in \hat{\mathbf{T}}_{\Phi_p}(\hat{G})$ at the operator differential of f belong to tangent operator space $\hat{\mathbf{R}}^n$ in 0. Namely, the prototypes are the operator vectors $\hat{\xi}_1,\ldots,\hat{\xi}_{n+1} \in \hat{\mathbf{R}}^n$. Let f reflects the parallelepiped $\hat{\mathbf{\Pi}}^*$, stretched over the $\hat{\xi}_1,\ldots,\hat{\xi}_{n+1}$, onto the $(n+1)$ dimensional piece $\hat{\mathbf{\Pi}}$ on the $\hat{G}$. While the border of the n dimensional chain $\partial\hat{\mathbf{\Pi}}$ in $\hat{\mathbf{R}}^{n+1}$ defined as follows: the pieces $\hat{\sigma}^i$ of the chain $\partial\hat{\mathbf{\Pi}}$ are n dimensional facets $\partial\hat{\mathbf{\Pi}}_i$ of parallelepiped $\partial\hat{\mathbf{\Pi}}$ with the reflections embedding the facets into $\hat{\mathbf{R}}^{n+1}$: $\quad f_i : \hat{\mathbf{\Pi}}_i \to \hat{\mathbf{R}}^{n+1}$, and the orientations Or_i has defined as $\partial\hat{\mathbf{\Pi}} = \sum\hat{\sigma}^i$, $\quad \hat{\sigma}^i = (\hat{\mathbf{\Pi}}_i, f_i, Or_i)$ Considering the curvilinear parallelepiped $F(\hat{\mathbf{A}}_1,\ldots,\hat{\mathbf{A}}_n) = \int_{\partial\hat{\mathbf{\Pi}}}\hat{\omega}^n$, one may state that the unique operator of the $(n+1)$-form $\hat{\Omega}$ exists on $\hat{\mathbf{T}}_{\Phi_p}$, which is the principle $(n+1)$ linear part in 0 of integral over the border of $F(\hat{\mathbf{A}}_1,\ldots,\hat{\mathbf{A}}_n)$, namely $F(\varepsilon\hat{\mathbf{A}}_1,\ldots,\varepsilon\hat{\mathbf{A}}_n) = \varepsilon^{n+1}\hat{\Omega}(\hat{\mathbf{A}}_1,\ldots,\hat{\mathbf{A}}_{n+1}) + O(\varepsilon^{n+1})$, where $\hat{\Omega}$ is independent of choice of the coordinates used in definition of F. The prove of it is the same to those of similar one given in the differential geometry.

At this point we cut short our discussion, and refer the interested reader to original papers (Ter-Kazarian, 1884, 1996, 1999a) for more detailed justification of some of the procedures and complete exposition of a lengthy mathematical apparatus of OM.

10. Primordial structures and link establishing processes

We have chosen a simple setting and considered the primordial structures designed to possess certain physical properties satisfying the stated general rules. These structures are thought to be the substance out of which the geometry and particles are made.

10.1. The Regular Primordial Structures

We distinguish η- and u-types primordial structures involved in the linkage establishing processes occurring between the structures of different types. The η-type structure may accept the linkage only from u-type structure, which is described by the link function $\psi_\eta(\eta)$ belonging to the ordinary class of functions of C^∞ smoothness, where $\eta = e_{\eta(\lambda\alpha)}\eta^{(\lambda\alpha)}$, $(\lambda = \pm; \alpha = 1,2,3)$, η is the link coordinate. Respectively the u-type structure may accept the linkage only from η-type structure described by the link function $\psi_u(u)$ (u-channel, $u = e_u u$), where ${\psi_\eta}^{(\pm\alpha)}(\eta,p_\eta) = \eta^{(\pm\alpha)}{\psi_\eta}^{\pm}(\eta,p_\eta)$, ${\psi_u}^{(\pm\alpha)}(u,p_u) = u^{(\pm\alpha)}{\psi_u}^{\pm}(u,p_u)$, a bispinor ${\psi_i}^{\pm}$ is the invariant state wave function of positive or negative frequencies, p_i is the corresponding link momentum. Thus, a primordial structure can be considered as a fermion. A simplest system made of two structures of different types becomes stable only due to the stable linkage $|p_\eta| = ({p_\eta}^{(\lambda\alpha)}, p_{\eta(\lambda\alpha)})^{1/2} = |p_u| = ({p_u}^{(\lambda\alpha)}, p_{u(\lambda\alpha)})^{1/2}$. Otherwise they are unstable. There is not any restriction on the number of primordial structures of both types involved in the link establishing processes simultaneously. Only, in the stable system the link stability condition must be held for each linkage separately. Suppose that persistent processes of creation and annihilation of the primordial structures proceed in different states $s, s', s'', ...$ The "creation" of structure in the given state (s) is due to its transition to this state from other states $(s', s'', ...)$, while the "annihilation" means a vice versa. Satisfying the stability condition the primordial structures from arbitrary states

doi: 10.52526/25792776-2021.68.2-311

can establish a stable linkage. Among the states $(s, s', s'', ...)$ there is a lowest one (s_0), in which all structures are regular, i.e., they are in free (pure) state and described by the plane wave functions ${\psi_\eta}^{\pm}(\eta_f, p_\eta)$ or ${\psi_u}^{\pm}(u_f, p_u)$ defined respectively on flat manifolds G_η and G_u. The index (f) specifies the points of corresponding flat manifolds $\eta_f \in G_\eta$, $u_f \in G_u$. Note that the processes of creation and annihilation of regular structures in lowest state are described by the OM formalism given above.

10.2. Distorted primordial structures

In all higher states the primordial structures are distorted (interaction states) and described by distorted link functions defined on distorted manifolds $\widetilde{G_\eta}$ and $\widetilde{G_u}$. The distortion $G \to \widetilde{G}$ with hidden Abelian local group $G = U^{loc}(1) = SO^{loc}(2)$ and one dimensional trivial algebra $\hat{g} = R^1$ is considered in (Ter-Kazarian, 2010). Within that scheme the basis e^f undergoes distortion transformation $e(\theta) = D(\theta)\, e^f$. The matrix $D(\theta)$ is in the form $D(\theta) = C \otimes R(\theta)$, where $O_{(\lambda\alpha)} = C^{\tau}_{(\lambda\alpha)} O_\tau$ and $\sigma_{(\lambda\alpha)}(\theta) = R^{\beta}_{(\lambda\alpha)}(\theta)\sigma_\beta$. Here $R(\theta)$ is the matrix of the group $SO(3)$ of ordinary rotations of the planes involving two arbitrary basis vectors of the spaces $R^3_{\pm}$ around the orthogonal third axes $(\pm k)$ through the angle $(\theta_{\pm k})$. The relation between the wave functions of distorted and regular structures reads ${\psi_u}^{\lambda}(\theta_{+k}) = f_{(+)}(\theta_{+k}){\psi_u}^{\lambda}$, $\psi_{u\lambda}(\theta_{-k}) = \psi_{u\lambda} f_{(-)}(\theta_{-k})$, where ${\psi_u}^{\lambda}$ $(\psi_{u\lambda})$ is the plane wave function of regular ordinary structure (antistructure). Next, we supplement the previous assumptions given in subsec.2.3 by the new one that now the η-type (fundamental) regular structure can not directly form a stable system with the regular u-type (ordinary) structures. Instead of it the η-type regular structure forms a stable system with the infinite number of distorted ordinary structures, where the link stability condition held for each linkage separately. Such structures take part in realization of flat manifold G. We employ the wave packets constructed by superposition of these functions furnished by generalized operators of creation and annihilation as the expansion coefficients. Geometry realization condition now should be satisfied for each ordinary structure in terms of $G^{\,\theta}_{uF}(0) = \lim_{\theta_+ \to \theta_-} G^{\,\theta}_{uF}(\theta_+ - \theta_-) = G_{\eta F}(0) = \lim_{\eta'_f \to \eta_f} G_{\eta F}(\eta'_f - \eta_f)$. Then $\sum_k \psi_u(\theta_{+k})\bar{\psi}_u(\theta_{-k}) = \sum_k {\psi_u}'(\theta'_{+k}){\bar{\psi}_u}{}'(\theta'_{-k}) = \cdots = inv$. Namely, the distorted ordinary structures emerge in geometry only in permissible combinations forming a stable system. Below, in simplified schematic way we exploit the background of the known colour confinement and gauge principles. Naive version of such construction still should be considered as a preliminary one, which will be further elaborated to introduce basis for subquarks.

10.3. Quarks and colour confinement

At the very first to avoid irrelevant complications, here, for illustrative purposes, we will attempt to introduce temporarily skeletonized `quark´ and `antiquark´ fields emerged in confined phase in the simplified geometry with the one-u channel given in the previous subsections. The complete picture of such a dynamics is beyond the scope of this subsection, but some relevant discussions on this subject will also be presented. We may think of the function ${\psi_u}^{\lambda}(\theta_{+k})$ at fixed (k) as being u-component of bispinor field of "quark" q_k, and of $\bar{\psi}_{u\lambda}(\theta_{-k})$ - an u-component of conjugated bispinor field of "antiquark" $\bar{q}_k$. The index (k) refers to colour degree of freedom in the case of rotations through the angles θ_{+k} and anticolour degree of freedom in the case of θ_{-k}. The η-components of quark fields are plane waves. There are exactly three colours. The rotation through the angle θ_{+k} yields a total quark field $q_k(\theta) = \Psi(\theta_{+k}) = {\psi_\eta}^0 \psi_u(\theta_{+k})$ where ${\psi_\eta}^0$ is a plane wave defined on G_η. This allows an other interpretation of quarks, which is absolutely equivalent to the former one and will be widely used throughout this article, i.e., $q_k(\theta) = {\psi_\eta}^0 q_{uk}(\theta) = q_{\eta k}(\theta){\psi_u}^0$, $q_{\eta k}(\theta) \equiv f_{(+)}(\theta_{+k}){\psi_\eta}^0$, where ${\psi_u}^0$ is a plane wave, $q_{uk}(\theta)$ and $q_{\eta k}(\theta)$ may be considered as the quark fields with the same quantum numbers defined respectively on flat manifolds G_u and G_η. Making use of the rules stated one may readily return to Minkowski space $G_\eta \to M_4$. In the sequel, a conventional quark fields defined on M_4 will be ensued $q_{\eta k}(\theta) \to q_k(x)$, $x \in M_4$. They imply $\sum_k q_{kp}\bar{q}_{kp} = \sum_k {q'}_{kp}{\bar{q}'}_{kp} = \cdots = inv$. It utilizes the idea of colour confinement principle: the quarks emerge in the geometry only in special combinations of colour singlets. Only two colour singlets are available $(q\bar{q}) = \frac{1}{\sqrt{3}}\delta_{kk'}\hat{q}_k\hat{\bar{q}}_{k'} = inv$, $(qqq) = \frac{1}{\sqrt{6}}\varepsilon_{klm}\hat{q}_k\hat{q}_l\hat{q}_m = inv$.

doi: 10.52526/25792776-2021.68.2-311

10.4. Gauge principle-internal symmetries

Each regular structure in the lowest state can be regarded as a result of transition from an arbitrary state, in which they assumed to be distorted. Hence, the following transformations may be implemented upon distorted ordinary structures ${\psi_u}'^{\lambda}(\theta'_{+l}) = f^{(+)}_{lk}{\psi_u}^{\lambda}(\theta_{+k}) = f(\theta'_{+l},\theta_{-k}){\psi_u}^{\lambda}(\theta_{+k})$, $f(\theta'_{+l},\theta_{-k}) = f_{(+)}(\theta'_l)f_{(-)}(\theta_k)$. The transformation functions are the operators in the space of internal degrees of freedom labeled by $(\pm k)$ corresponding to distortion rotations around the axes $(\pm k)$ by the angles $\theta_{\pm k}$. We make proposition that the distortion rotations are incompatible, namely the transformation operators $f^{(\pm)}_{lk}$ obey the incompatibility relations $f^{(+)}_{lk}f^{(+)}_{cd} - f^{(+)}_{ld}f^{(+)}_{ck} = \|f^{(+)}\|\varepsilon_{lcm}\varepsilon_{kdn}f^{(-)}_{nm}$, $f^{(-)}_{kl}f^{(-)}_{dc} - f^{(-)}_{dl}f^{(-)}_{kc} = \|f^{(-)}\|\varepsilon_{lcm}\varepsilon_{kdn}f^{(+)}_{mn}$, where $l,k,c,d,m,n = 1,2,3$. This relations hold in general for both local and global rotations. Then one gets the transformations implemented upon the quark field, which in matrix notation take the form $q'(\zeta) = U(\theta(\zeta))q(\zeta)$, $\bar{q}'(\zeta) = \bar{q}(\zeta)U^{+}(\theta(\zeta))$, where $q = \{q_k\}$, $\quad U(\theta) = \{f^{(+)}_{lk}\}$. Due to the incompatibility commutation relations the transformation matrices $\{U\}$ generate the unitary groups of internal symmetries $U(1), SU(2), SU(3)$ corresponding to one-, two- and three-dimensional rotations through the angles $\theta_{\pm k}$, while an action of physical system must be invariant under such transformations (gauge principle).

11. Operator Multimanifold $\hat{G}_N$

In the second part, we generalized the knowledge gained in outlined mathematical framework via the concept of operator multimanifold (OMM), which yields the multiworld (MW)-geometry. The latter involves the spacetime continuum and internal worlds of the given number.

11.1. Operator Vector and Covector Fields

The OM formalism of $\hat{G} = \hat{G}_\eta \oplus \hat{G}_u$ is built up by assuming an existence only of ordinary primordial structures of one sort (one u-channel). Being confronted by our major goal to develop the microscopic approach to field theory based on multiworld geometry, henceforth we generalize the OM formalism via the concept of the OMM. Then, instead of one sort of ordinary structures we are going to deal with different species of ordinary structures. But before proceeding further and to enlarge the previous model it is profitable to assume an existence of infinite number of ${}^iu$-type ordinary structures of different species $i = 1,2,\ldots,N$ (multi-u channel). These structures will be specified by the superscript i to the left. This hypothesis, as it will be seen in the subsequent part II, leads to the substantial progress of understanding of the properties of particles. At the very outset we consider the processes of creation and annihilation of regular structures of η- and ${}^iu$-types in the lowest state (s_0). The general rules stated in subsec 2.1 regarding to this change apply a substitution of operator basis pseudo vectors and covectors by a new ones $(i = 1,2,\ldots,N)$: ${}^i\hat{O}^{r_1 r_2}_{\lambda,\mu} = {}^i\hat{O}^{r_1}_{\lambda} \otimes {}^i\hat{O}^{r_2}_{\mu} \equiv {}^i\hat{O}^{r}_{\lambda,\mu} = {}^iO^{r}_{\lambda,\mu}(\alpha_\lambda \otimes \alpha_\mu)$, provided by $r \equiv (r_1, r_2)$ and ${}^iO^r_{1,1} = \frac{1}{\sqrt{2}}(\nu_i\, {O_{\eta}}^r_{+} + {}^i{O_u}^r_{+})$, ${}^iO^r_{2,1} = \frac{1}{\sqrt{2}}(\nu_i\, {O_{\eta}}^r_{+} - {}^i{O_u}^r_{+})$, ${}^iO^r_{1,2} = \frac{1}{\sqrt{2}}(\nu_i\, {O_{\eta}}^r_{-} + {}^i{O_u}^r_{-})$, ${}^iO^r_{2,2} = \frac{1}{\sqrt{2}}(\nu_i\, {O_{\eta}}^r_{-} - {}^i{O_u}^r_{-})$, where $< \nu_i, \nu_j >= \delta_{ij}$, $< {}^i{O_u}^r_{\lambda}, {}^j{O_u}^{r'}_{\tau} >= -\delta_{ij}\delta_{rr'}{}^*\delta_{\lambda\tau}$, $< {O_\eta}^r_{\lambda}, {}^i{O_u}^{r'}_{\tau} >= 0$. We consider then the operators ${}^i\hat{\gamma}^r_{(\lambda,\mu,\alpha)} = {}^i\hat{O}^{r_1 r_2}_{\lambda,\mu} \otimes \hat{\sigma}^{r_3}_{\alpha}$. and calculate nonzero matrix elements $< \lambda,\mu \mid {}^i\hat{\gamma}^r_{(\tau,\nu,\alpha)} \mid \tau,\nu >= {}^*\delta_{\lambda\tau}{}^*\delta_{\mu,\nu}\, {}^ie^r_{(\tau,\nu,\alpha)}$, where ${}^ie^r_{(\lambda,\mu,\alpha)} = {}^iO^r_{\lambda,\mu} \otimes \sigma_\alpha$. The operators $\{{}^i\hat{\gamma}^r\}$ are the basis for all the operator vectors $\hat{\Phi}(\zeta) = {}^i\hat{\gamma}^r\, {}^i\Phi_r(\zeta)$ of tangent section of principle bundle with the base of operator multimanifold $\hat{G}_N = (\sum_i^N \oplus {}^*\hat{R}^4_i) \otimes \hat{R}^3$. Here ${}^*\hat{R}_i{}^4$ is the 2×2 dimensional linear pseudo operator space, with the set of the linear unit operator pseudo vectors as the basis of tangent vector section, and $\hat{R}^3$ is the three dimensional real linear operator space with the basis consisted of the ordinary unit operator vectors $\{\hat{\sigma}^r_\alpha\}$. The $\hat{G}_N$ decomposes as follows: $\hat{G}_N = \hat{G}_\eta \oplus \hat{G}_{u_1} \oplus \cdots \oplus \hat{G}_{u_N}$, where $\hat{G}_{u_i}$ is the six dimensional operator manifold of the given species (i) with the basis $\left\{{}^i{\hat{\gamma}_u}{}^r_{(\lambda\alpha)} = {}^i{\hat{O}_u}{}^r_{\lambda} \otimes \hat{\sigma}^r_{\alpha}\right\}$. The expansions of operator vectors and covectors are written $\hat{\Psi}_\eta = \hat{\gamma}^r_\eta \Psi_{\eta r}$, $\hat{\Psi}_u = {}^i{\hat{\gamma}_u}^r\, {}^i\Psi_{ur}$, $\hat{\bar{\Psi}}_\eta = \hat{\gamma}_{\eta r}{\Psi_\eta}^r$, $\hat{\bar{\Psi}}_u = {}^i\hat{\gamma}_{ur}\, {}^i{\Psi_u}^r$, where the components $\Psi_{\eta r}(\eta)$ and ${}^i\Psi_{ur}(u)$ are respectively the link functions of η-type and ${}^iu$-type structures.

doi: 10.52526/25792776-2021.68.2-311

11.2. Realization of the Multimanifold G_N

Now, we consider the special system of the regular structures, which is made of one fundamental structure of η-type and infinite number of ${}^i u$-type ordinary structures of different species ($i = 1, \dots, N$). The primordial structures establish the stable linkage to form the stable system $p^2 = p_\eta^2 - \sum_{i=1}^N p_{u_i}^2 = 0$. The free field defined on the multimanifold $G_N = G_\eta \oplus G_{u_1} \oplus \cdots \oplus G_{u_N}$ is written $\Psi = \Psi_\eta(\eta)\Psi_u(u)$, $\Psi_u(u) = \Psi_{u_1}(u_1) \cdots \Psi_{u_N}(u_N)$, where Ψ_{u_i} is the bispinor defined on the internal manifold G_{u_i}. On analogy to above, we make use of localized wave packets by means of superposition of plane wave solutions furnished by creation and annihilation operators in agreement with Pauli's principle. Straightforward calculations now give $\sum_{\lambda=\pm} < \chi_\lambda \mid \hat{\Phi}(\zeta)\hat{\bar{\Phi}}(\zeta) \mid \chi_\lambda >= \sum_{\lambda=\pm} < \chi_\lambda \mid \hat{\bar{\Phi}}(\zeta)\hat{\Phi}(\zeta) \mid \chi_\lambda >= -i\,\zeta^2 G_\zeta(0) = -i\,(\eta^2 G_\eta(0) - \sum_{i=1}^N {u_i}^2 G_{u_i}(0))$. Along the same line the realization of the multimanifold stems from the condition as alluded to above. Let denote $u^2 G_u(0) \equiv \lim_{u_i \to u'_i} \sum_{i=1}^N (u_i u'_i) G_{u_i}(u_i - u'_i)$ and consider a stable system. Hence $G_{uF}(0) = G_{\eta F}(0) = G_{\zeta F}(0)$, where $G_{\eta F}, G_{uF}$ and $G_{\zeta F}$ are the causal Green's functions of the $\eta-, u-$ and ζ-type structures, and $m \equiv |p_u| = (\sum_{i=1}^N {p_{u_i}}^2)^{1/2} = |p_\eta|$. In the aftermath, the length of each vector $\zeta = {}^i e\, {}^i\zeta \in G_N$ should be equaled zero (subsec.2.2) $\zeta^2 = \eta^2 - u^2 = \eta^2 - \sum_{i=1}^N (u_i^G)^2 = 0$, where use is made of $(u_i^G)^2 \equiv u_i^2 \lim_{\substack{u_i \to u'_i \\ \eta \to \eta'}} G_{u_i F}(u_i - u'_i)\,/\,G_{\eta F}(\eta - \eta')$ and $u_i^G = {}^i\hat{e}_{u(\lambda,\alpha)}\, u_i^{G\,(\lambda,\alpha)}$. Thus, the multimanifold G_N comes into being, which decomposes as follows: $G_N = G_\eta \oplus G_{u_1} \oplus \cdots$ Meanwhile, the Minkowski flat space M_4 stems from the flat submanifold G_η , in which the line element turned out to be invariant. That is, the principle of relativity comes into being with the M_4 ensued from the MW geometry G_N. In the following we shall use a notion of the i-th internal world for the submanifold G_{u_i}.

11.3. The subquark algebra and supercharges

The following transformations are implemented upon the subquarks (antisubquarks) on the given (i) internal world: $q'_l = f_{lk}^{(+)}\, q_k$, $\bar{q}'_l = \bar{q}_k\, f_{kl}^{(-)}$, where as well for the next section we left implicit the MW-superscript (i) to the left. Then, the following composition rules hold for the transformation functions $f_{lk}^{(+)} = f_l \circ f_k^{-1}$, $f_{lk}^{(-)} = \bar{f}_l \circ \bar{f}_k^{-1}$, $(f_l \circ f_k^{-1})(f_c \circ f_d^{-1}) = (f_l\, f_c) \circ (f_k^{-1}\, f_d^{-1})$, where $l, k, c, d = 1, 2, 3$, the transformation functions $f_k \equiv f_{(+)}(\theta_{+k})$ and $\bar{f}_l \equiv f_{(-)}(\theta_{-k})$ are the operators in the space of internal degrees of freedom labeled by the subcolour index $(\pm k)$ such that the rotation through the angle $\theta_{\pm k}$ yields the subquark (antisubquark) field $q_k = f_k\, q_0$, $\bar{q}_k = \bar{q}_0\, \bar{f}_k$. The incompatibility commutation relations with the composition rule lead to the following commutation relations $[f_l, f_k] = \epsilon_{lkm}\, \bar{f}_m$. Whence, the subquarks imply $[q_l, q_k] = Q_0\, \epsilon_{lkm}\, \bar{q}_m$, $Q_0 \equiv q_0^2\,/\bar{q}_0$. The symmetries of the $C-$ $(C \equiv s, c, b, t)$ and $Q-$ worlds are assumed to be respectively global and local unitary $diag(SU(3))$ symmetries, for which $q_l\, q_k = Q'_0\, \epsilon_{lkm}\, \bar{q}_m$, while for the $W-$world with the unified symmetry $SU(2)_L \otimes U(1)$ it reduced to $[q_{1L}, q_{2L}] = Q_0\, \bar{q}_{2R}$, $[q_{2L}, q_{2R}] = Q_0\, \bar{q}_{1L}$, $[q_{2R}, q_{1L}] = Q_0\, \bar{q}_{2L}$, where the subcolour singlets are Q_{2R}, $[q_{1L}, q_{2L}]$ and $(q\,\bar{q})$. Hence, for the electron and corresponding neutrino one gets $[\nu_L, e_L] = Q_0\, \bar{e}_R$, $[e_L, e_R] = Q_0\, \bar{\nu}_L$, $[e_R, \nu_L] = Q_0\, \bar{e}_L$. The important relation between the fermionic (F) and bosonic (B) subcolour singlets reads $(qqq) \equiv \frac{1}{\sqrt{6}}\epsilon_{lkm}\, q_l q_k q_m = Q_{0u}\,(q\,\bar{q}) \equiv Q_{0u}\, \frac{1}{\sqrt{3}}(q_k\, \bar{q}_k)$, $F \to Q_{0u}\, B$, and vice versa, where $F \equiv (qqq)$, $B \equiv (q\,\bar{q})$, $Q_{0u} \equiv \frac{1}{\sqrt{2}}Q_0$. It means that considered physical system must respect the invariance under a symmetry group of the fermion-boson transformations occurred in the internal worlds. The latter is known as a "supersymmetry". It is why the basis vectors in the Hilbert space $\mathcal{H}$ have taken to be in the form $\mid n_B n_F >$, where the boson and fermion occupation numbers respectively are $n_B = 1, 2, ..., \infty$ and $n_F = 0, 1$. It is convenient, then, to describe such a quantum mechanical system as the spin-1/2 like supersymmetric particle with mass $m = \left(\frac{\hbar}{Q_{0u}}\right)^2$ moving along the one-dimensional Euclidean line $\mathcal{R}$. Therefore, one introduces a generalized bosonic operator b and a fermionic operator f acting on the Hilbert space $\mathcal{H} = L^2(\mathcal{R}) \otimes \mathcal{C}^2$: $b\,:\, L^2(\mathcal{R}) \to L^2(\mathcal{R})$, $b = \frac{1}{2}(\frac{\partial}{\partial u} + W(u))$, $f\,:\, \mathcal{C}^2 \to \mathcal{C}^2$, $f = \begin{pmatrix} 0 & 0 \\ 1 & 0 \end{pmatrix}$, where the supersymmetric potential $W(u)\,:\, \mathcal{R} \to \mathcal{R}$ defined on the given (i) internal world is assumed to be piecewise continuously differentiable function. The commutation and anticommutation relations for these operators

doi: 10.52526/25792776-2021.68.2-311

read $[b,\, b^+] = W'(u)$, $\{f,\, f^+\} = 1$. Employing standard technique, next we define the nilpotent supercharge operators $Q_u = Q_{0u}\, b \otimes f^+ = Q_{0u} \begin{pmatrix} 0 & b \\ 0 & 0 \end{pmatrix}$, ${Q_u}^+ = Q_{0u}\, b^+ \otimes f = Q_{0u} \begin{pmatrix} 0 & 0 \\ b^+ & 0 \end{pmatrix}$, which obey the anticommutation relations $\{Q_u,\, Q_u\} = \{{Q_u}^+,\, {Q_u}^+\} = 0$, and act as follows: $Q_u \mid n_B, n_F > \propto \mid n_B - 1, n_F + 1 >$, ${Q_u}^+ \mid n_B, n_F > \propto \mid n_B + 1, n_F - 1 >$.

11.4. The Primary Field

As alluded to above, we have chosen a simple setting and considered the `primordial´ structures, which are designed to posses certain physical properties satisfying the stated in (Ter-Kazarian, 1884, 1996, 1999a) general rules and have involved in the linkage establishing processes. The processes of their creation and annihilation in the lowest state (the `regular structures´) just are described by the OM formalism. In all the higher states the `primordial structures´ are distorted ones, namely they have undergone the distortion transformations. These transformations yield the `quark´ and ‘`antiquark´ fields defined on the simplified geometry (one $u$-channel), and skeletonized for illustrative purposes. Due to geometry realization conditions held in the stable systems of `primordial structures´ they emerge in confined phase. This scheme still should be considered as the preliminary one, which is further elaborated in this subsection to get the physically more realistic picture. The distortion transformation functions are the operators acting in the space of the internal degrees of freedom (colours) and imply the incompatibility relations (Ter-Kazarian, 1884, 1996, 1999a), which hold for both the local and the global distortion rotations. They underly the most important symmetries such as the internal symmetries $U(1), SU(2), SU(3)$, the $SU(2)\otimes U(1)$ symmetry of electroweak interactions, etc.

On these premises, in the enlarged framework of the OMM we define and clarify the fundamental conceptual basis of subquarks (instead of quarks) and their characteristics stemming from the various symmetries of the internal worlds. By this we have arrived at an entirely satisfactory answer to the question of the physical origin of the geometry and fields, the internal symmetries and interactions, as well the principles of relativity, quantum, gauge and subcolour confinement. The OMM formalism has the following features: All the fields including the leptons and quarks, along with the spacetime components have also the MW internal components made of the various constituent subquarks defined on the given internal worlds, such that the internal components are consisted of `distorted ordinary structures´: $\Psi(\theta) = \Psi_\eta(\eta)\Psi_Q(\theta_Q)\Psi_W(\theta_W)\Psi_B(\theta_B)\Psi_C(\theta^c)$. The components $\Psi_Q(\theta_Q), \Psi_W(\theta_W), \Psi_B(\theta_B)$ are primary massless bare Fermi fields. We assume that this field has arisen from primary field in the lowest state (s_0) with the same field components consisted of `regular ordinary structures´, subject to certain rules (Ter-Kazarian, 1884, 1996, 1999a). Therefore, the primary field defined on G_N $\Psi(0) = \Psi_\eta(\eta)\Psi_Q(0)\Psi_W(0)\Psi_B(0)\Psi_C(0)$ serves as the ready made frame into which the distorted ordinary structures of the same species should be involved. We apply the Lagrangian of this field possessed local gauge invariance written in the notations $\widetilde{L}_0(D) = \frac{i}{2}\{\bar{\Psi}_e(\zeta)\, {}^i\gamma D_i \Psi_e(\zeta) - D_i\bar{\Psi}_e(\zeta)\, {}^i\gamma\Psi_e(\zeta)\}$, with the vector indices contracted to form scalars, where $D_i = \partial_i - ig\mathbf{B_i}(\zeta)$, $\mathbf{B_i}$ are gauge fields. Since the components Ψ_B and Ψ_C will be of no consequence for a discussion, then we temporarily leave them implicit, namely $i = \eta, Q, W$. The equation of primary field of the MW- structure with nonlinear fermion interactions of the components may be derived from an invariant action in terms of local gauge invariant Lagrangian, which looks like Heisenberg theory: $\widetilde{L}(D) = \widetilde{L}_0(D) + \widetilde{L}_I + \widetilde{L}_B$, provided by the Lagrangians of nonlinear fermion interactions of the components $\widetilde{L}_I = \sqrt{2}\widetilde{O}_1 \otimes L_I$, and gauge field $\widetilde{L}_B = \sqrt{2}\widetilde{O}_1 \otimes L_B$. The binding interactions are in the form $L_I = L_{QI} + L_{WI}$, $L_{QI} = \frac{\lambda}{4}(J_{QL}J_{Q}{}^+_R + J_{QR}J_{Q}{}^+_L)$, $L_{WI} = \frac{\lambda}{2}S_W S_W^+$, $L_B = -\frac{1}{2}Tr(\mathbf{B}\bar{\mathbf{B}}) = -\mathbf{\frac{1}{2}Tr}\left(\mathbf{B_i B_i}\right)$, where $J_{QL,R} = V_Q \mp A_Q$, $V_{Q(\lambda\alpha)} = \bar{\Psi}_Q\gamma_{(\lambda\alpha)}\Psi_Q$, $V_{Q}{}^+_{(\lambda\alpha)} = {V_Q}^{(\lambda\alpha)} = \bar{\Psi}_Q\gamma^{(\lambda\alpha)}\Psi_Q A_{Q(\lambda\alpha)} = \bar{\Psi}_Q\gamma_{(\lambda\alpha)}\gamma_5\Psi_Q$, $A_{Q}{}^+_{(\lambda\alpha)} = {A_Q}^{(\lambda\alpha)} = \bar{\Psi}_Q\gamma^5\gamma^{(\lambda\alpha)}\Psi_Q$, $S_W = \bar{\Psi}_W\Psi_W$, γ_μ and $\gamma_5 = i\gamma_0\gamma_1\gamma_2\gamma_3$ are Dirac matrices. According to Fiertz theorem the interaction Lagrangian $L_{QI} = \frac{\lambda}{2}(VV^+ - AA^+)$ may be written $L_{QI} = -\lambda(S_Q S_Q^+ - P_Q P_Q^+)$, provided by $S_Q = \bar{\Psi}_Q\Psi_Q$, $\quad P_Q = \bar{\Psi}_Q\gamma_5\Psi_Q$. Hence $\widetilde{L}(D) = \sqrt{2}\widetilde{O}_1 \otimes L(D)$, $L(D) = L_\eta(D_\eta) - L_Q(D_Q) - L_W(D_W)$, where $L_\eta(D_\eta) = {L_\eta}'^{(0)}_0(D_\eta) - \frac{1}{2}Tr(\mathbf{B}_\eta\bar{\mathbf{B}}_\eta)$, $L_Q(D_Q) = {L_Q}'^{(0)}_0(D_Q) - L_{QI} - \frac{1}{2}Tr(\mathbf{B_Q}\bar{\mathbf{B}}_\mathbf{Q})$, $L_W(D_W) = {L_W}'^{(0)}_0(D_W) - L_{WI} - \frac{1}{2}Tr(\mathbf{B_W}\bar{\mathbf{B}}_\mathbf{W})$. Here ${L_\eta}'^{(0)}_0 = \frac{i}{2}\{\bar{\Psi}\ \gamma\overset{\frown}{D}_\eta\ \Psi - \bar{\Psi}\ \gamma\overset{\frown}{\overleftarrow{D}}_\eta\ \Psi\} = {\Psi_u}^+ L_{\eta 0}^{(0)}\Psi_u$,

doi: 10.52526/25792776-2021.68.2-311

${L_u}'^{(0)}_0 = \frac{i}{2}\{\bar{\Psi}\ \gamma\overset{\frown}{D}_u\ \Psi - \bar{\Psi}\ \gamma\overset{\frown}{\overleftarrow{D}}_u\ \Psi\} = {\Psi_\eta}^+ L_{u0}^{(0)}\Psi_\eta$, and $L_{\eta 0}^{(0)} = \frac{i}{2}\{\bar{\Psi}_\eta\ \gamma\overset{\frown}{D}_\eta\ \Psi_\eta - \bar{\Psi}_\eta\ \gamma\overset{\frown}{\overleftarrow{D}}_\eta\ \Psi_\eta\}$, $L_{u0}^{(0)} = \frac{i}{2}\{\bar{\Psi}_u\ \gamma\overset{\frown}{D}_u\ \Psi_u - \bar{\Psi}_u\ \gamma\overset{\frown}{\overleftarrow{D}}_u\ \Psi_u\}$. The total Lagrangian has the global γ_5 and local gauge symmetries. We consider only γ_5 symmetry in Q-world, namely $\mathbf{B_Q} \equiv 0$. According to the OMM formalism, it is important to fix the mass shell of the stable MW- structure. It means that we must take at first the variation of the Lagrangian with respect to primary field, then have switched on nonlinear fermion interactions of the components. In other words we take the variation of the Lagrangian with respect to the components on the fixed mass shell.

Reflecting upon the discussed in two previous subsections subject, we conclude that in the framework of MW-geometry, all the fields have composite nontrivial internal structure. The MW structure of primary field is described by the gauge invariant Lagrangian involving nonlinear fermion interactions of the internal field components somewhat similar to the theory by Heisenberg and his co-workers, but still it will be defined on the MW-geometry. This Lagrangian is the whole story since all the complexity of the leptons, quarks and their interactions arises from it. The number of free parameters in this Lagrangian is reduced to primary coupling constant of the nonlinear interaction and gauge coupling. All the fields along with the spacetime component have nontrivial composite internal MW structure. The possible elementary particles are thought to be composite dynamical systems in analogy to quantum mechanical stationary states of compound atom, but, now a dynamical treatment built up on the MW-geometry is quite different and more amenable to qualitative understanding (Ter-Kazarian, 1884, 1996, 1999a). The microscopic structure of leptons, quarks and other particles will be governed by the only possible conjunctions of constituent subquarks implying concrete symmetries.

The hypothesis of existence of the MW structures manifests its virtue by solving some key problems of particle phenomenology, when we attempt to suggest a microscopic approach to the properties of particles and interactions. We consider further the microscopic theory of the unified electroweak interactions (Ter-Kazarian, 1884, 1996, 1999a). It follows that contemporary phenomenological SM is an approximation to the suggested microscopic approach. The condition of realization of the MW connections is arisen due to the symmetry of Q-world of electric charge and embodied in the Gell-Mann-Nishijima relation. During the realization of the MW-structure the symmetries of corresponding internal worlds are unified into more higher symmetry including also the operators of isospin and hypercharge. Such approach enables to conclude that only possible at low-energy the three lepton generations consist of six lepton fields with integer electric and leptonic charges and being free of confinement. Also the three quark generations exist composed of six possible quark fields. They carry fractional electric and baryonic charges and obey confinement condition. The global group unifying all global symmetries of the internal worlds of quarks is the flavour group $SU_f(6)$. The Lagrangian of primary field contains only two free parameters, which are the coupling constants of nonlinear fermion and gauge interactions.

Hence, *the OMM formalism provides a natural unification of the geometry - yielding the 1) Special and 2) General relativity principles, and the fermion fields serving as the basis for the constituent subquarks.*

It has cleared up the physical conditions in which the geometry and particles come into being.

The subquarks emerge in the geometry only in certain permissible combinations utilizing the idea of the 3) Subcolour (subquark) confinement principle, and have undergone the transformations yielding the Internal symmetries and 4) Gauge principle.

Although within considered schemes the subquarks are defined on the internal worlds, however the resulting spacetime components of particles, which we are going to deal with to describe the leptons and quarks defined on the spacetime continuum, are affected by them in such a way that they carry exactly all the quantum numbers of the various constituent subquarks of the given composition. We discussed a class of models of internal symmetries, which reproduce the known phenomenology of electromagnetic, weak and strong interactions (Ter-Kazarian, 1884, 1996, 1999a). In order to save writing we guess it worthwhile to leave the other concepts such as the flavors and so forth with associated fundamental aspects of particle physics for an other treatment. It will not concern us here and must be further discussed. Surely this is an important subject for separate research.

doi: 10.52526/25792776-2021.68.2-311

12. Microscopic theory of the Standard Model of elementary particles

We attempt to develop, further, the *microscopic theory of the Standard Model of elementary particles* (Ter-Kazarian, 1999b, 2001b), which enables an insight to the key problems of particle phenomenology.

12.1. Objectives of MTSM

The most important open questions of the SM are as follows: We have no understanding why the SM is as it is? Why is the gauge symmetry? Why is this the particle spectrum? Why the electroweak symmetry breaking sector consists of just one $SU(2)_L$ doublet of Higgs bosons as it is in SM? The untested aspects of SM are the mass spectrum of the particles, the mixing patterns and the CP violation. The latter is introduced through complex Yukawa couplings of fermions to Higgs bosons, resulting in complex parameters in the CKM matrix. The SM contains a large number of arbitrary parameters, while a consistent complete theory would not have so many free parameters.

To address to some of these nagging questions of the SM, the MTSM is developed, wherein the proliferation of lepton and quark flavours prompts us to consider the fields as composites. Certainly, it may seem foolhardy to set up such a picture in the spacetime continuum. The difficulties arisen here are well-known. The first problem is closely related to the expected mass differences of particles, which in this case would be too large ($\geq 1TeV$). Another problem concerns the transformations of particles. Our idea is to remove these difficulties by employing MTSM, which is based on the MW-geometry. This theory attempts to answer to some of the above mentioned questions of particle phenomenology. The MTSM enables an insight to the key concepts of particle physics, and to conclude that the leptons are particles with integer electric and leptonic charges and free of confinement, while the quarks carry fractional electric and baryonic charges and imply the confinement. The theoretical significance of the MTSM resides in the microscopic interpretation of all physical parameters. We derive the Gell-Mann-Nishijima relation and the flavour group. The testable implications of the MTSM are given. Finally, we derive a physically more realistic mass spectrum of the leptons and quarks instead of the former one inferred within the simplified scheme.

A theoretical significance of the MTSM, first of all, resides in the microscopic interpretation of all physical parameters. Due to specific structure of the W-world of weak interactions implying the condition of realization of the MW-connections, the spanning takes place, which underlies the P-violation in W-world. It is expressed in the reduction of initial symmetry of the right-handed subquarks. Such reduction is characterized by the Weinberg mixing angle with the value fixed at 30^0. It gives rise to the expanded local symmetry $SU(2) \otimes U(1)$, under which the left-handed fermions transform as six independent $SU(2)$ doublets, while the right-handed fermions transform as twelve independent singlets. Due to vacuum rearrangement in Q-world the Yukawa couplings arise between the fermion fields and corresponding isospinor-scalar φ-meson in conventional form.

12.2. Higgs bosons and Electroweak symmetry breaking

We suggest the microscopic approach to Higgs bosons with self-interaction and Yukawa couplings. It involves the Higgs bosons as the collective excitations of bound quasi-particle iso-pairs. To obtain some feeling about this statement, below we give more detailed explanation.

Tracing a resemblance with the Cooper pairs, within the framework of local gauge invariance of the theory incorporated with the phenomenon of P-violation in weak interactions we suggest a mechanism providing the Bose-condensation of relativistic fermion pairs, which is due to effective attraction between the relativistic fermions caused by the exchange of the mediating induced gauge quanta in the W-world. The rationale for this approach is readily forthcoming from the consideration of gauge transformations of the fields under the P-violation in the W-world $\Psi'_L(x) = U_L(x)\Psi_L(x), \quad \Psi'_R(x) = U_R(x)\Psi_R(x)$, where the Fourier expansions carried out over corresponding gauge quanta with wave fourvectors q_L and q_R $U_L(x) = \int \frac{d^4q_L}{(2\pi)^4}\, e^{iq_Lx}\, U_L(q_L), \quad U_R(x) = \int \frac{d^4q_R}{(2\pi)^4}\, e^{iq_Rx}\, U_L(q_R)$, and $U_L(x) \neq U_R(x)$. They induce the gauge transformations implemented upon the φ-field $\varphi'(x) = U(x)\,\varphi(x)$.

doi: 10.52526/25792776-2021.68.2-311

The matrix of *induced gauge transformations* may be written down in terms of *induced gauge quanta* $U(x) \equiv U_L^+(x)\,U_R(x) = \int \frac{d^4q}{(2\pi)^4}\,e^{iqx}\,U(q)$, where $q = -q_L + q_R, \quad q(q^0, \vec{q})$. In momentum space one gets $\varphi'(k') = \int \frac{d^4q}{(2\pi)^4}\,U(q)\,\varphi(k'-q) = \int \frac{d^4k}{(2\pi)^4}\,U(k'-k)\,\varphi(k)$. Conservation of the fourmomentum requires that $k' = k + q$. Accordingly, we have $-p'_L + p'_R = -p_L + p_R + q = -p''_L + p_R = -p_L + p''_R$, where $p''_L = p_L - q, \quad p''_R = p_R + q$. Whence the wave vectors of fermions imply the conservation law $\vec{p}_L + \vec{p}_R = \vec{p}''_L + \vec{p}''_R$, characterizing the scattering process of two fermions with *effective interaction caused by the mediating induced gauge quanta*. We suggest the mechanism for the effective attraction between the fermions in the following manner: Among all induced gauge transformations with miscellaneous gauge quanta we distinguish a special subset with the induced gauge quanta of the frequencies belonged to finite region characterized by the maximum frequency $\frac{\widetilde{q}}{\hbar} \quad (\widetilde{q} = max\{q^0\})$ greater than the frequency of inducing oscillations fermion force $\frac{\bar{E_L} - \bar{E''_L}}{\hbar} < \frac{\widetilde{q}}{\hbar}$. To the extent that this is a general phenomenon, we can expect under this condition the effective attraction (negative interaction) arisen between the fermions caused by exchange of virtual induced gauge quanta if only the forced oscillations of these quanta occur in the same phase with the oscillations of inducing force (the oscillations of fermion density). In view of this we may think of isospinor Ψ_L and isoscalar Ψ_R fields as the fermion fields composing the iso-pairs with the same conserving net momentum $\vec{p} = \vec{p}_L + \vec{p}_R$ and opposite spin, for which the maximum number of negative matrix elements of operators composed by corresponding creation and annihilation operators $a^+_{\vec{p}''_R}\,a_{\vec{p}_R}\,a^+_{\vec{p}''_L}\,a_{\vec{p}_L}$ (designated by the pair wave vector $\vec{p}$) may be obtained for coherent ground state with $\vec{p} = \vec{p}_L + \vec{p}_R = 0$. In the mean time the interaction potential reads $V = \sum_{\vec{p}''_R,\,\vec{p}''_L,\,\vec{p}_R,\,\vec{p}_L}(a^+_{\vec{p}_L})^+ a^+_{\vec{p}''_R}(a^+_{\vec{p}''_L})a_{\vec{p}_R} = \sum_{\vec{p}''_R,\,\vec{p}''_L,\,\vec{p}_R,\,\vec{p}_L} a^+_{\vec{p}''_R}\,a^+_{\vec{p}''_L}\,a_{\vec{p}_R}\,a_{\vec{p}_L}$, implying the attraction between the fermions situated in the spherical thin shall near the Fermi surface $V_{\vec{p}\vec{p}'} = \begin{cases} -V & \text{at} \quad |\,E_{\vec{p}} - E_F\,| \leq \widetilde{q}, \quad |\,E_{\vec{p}'} - E_F\,| \leq \widetilde{q}, \\ 0 & \text{otherwise} \end{cases}$. The fermions filled up the Fermi sea block the levels below Fermi surface. Hence, the fermions are in superconducting state if this condition holds. Otherwise, they are in normal state described by Bloch individual particle model. Hence, the Bose-condensate arises in the W-world as the collective mode of excitations of bound quasi-particle iso-pairs described by the same wave function in the superconducting phase $\Psi =< \Psi_L\Psi_R >$, where $< \cdots >$ is taken to denote the vacuum averaging. The vacuum of the W-world is filled up by such iso-pairs at absolute zero $T = 0$. We make a final observation that $\Psi_R\Psi_R^+ = n_R$ is a scalar density number of right-handed particles. It readily follows that: $(\Psi_L\Psi_R)^+(\Psi_L\Psi_R) = \Psi_R^+\Psi_L^+\Psi_L\Psi_R = \frac{1}{n_R}\Psi_R^+\gamma^0(\gamma^0\Psi_L^+\Psi_R)(\Psi_R^+\Psi_L\gamma^0)\gamma^0\Psi_R = \varphi\varphi^+$, where $|\,\Psi\,|^2 =< \varphi\,\varphi^+ > = |< \varphi >|^2 \equiv |\,\varphi\,|^2$. It is convenient to abbreviate the $< \varphi >$ by the symbol φ. Hence the φ-meson actually arises as the collective mode of excitations of bound quasi-particle iso-pairs.

12.3. The Non-Relativistic Approximation

In the approximation to non-relativistic limit ($\beta \ll 1,\ \Psi_L \simeq \Psi_R,\ \gamma^0 \to 1$) by making use of Ginzburg-Landau's (GL) phenomenological theory, it is straightforward to write down the free-energy functional for the order parameter in equilibrium superconducting phase in presence of magnetic field. The self-consistent coupled GL-equations are differential equations like Schrödinger and Maxwell equations, which relate the spatial variation of the order parameter Ψ to the vector potential $\vec{A}$ and the current $\vec{j}_s$. By means of thermodynamic Green's functions in well defined limit, it is shown that GL-equations are a consequence of the BCS-Bogoliubov microscopic theory of superconductivity. The theoretical significance of these works resides in the microscopic interpretation of all physical parameters of GL-theory. Subsequently these ideas were extended to lower temperatures using a requirement that the order parameter and vector potential vary slowly over distances of the order of the coherence length and that the electrodynamics be local (London limit). Namely, the validity of derived GLG-equations is restricted to the temperature T, such $T_c - T \ll T_c$ and to the local electrodynamics region $q\xi_0 \ll 1$, where T_c is transition temperature, ξ_0 is coherent length characterizing the spatial extent of the electron pair correlations, q are the wave numbers of magnetic field $\vec{A}$. The most important order parameter Ψ, the mass m_Ψ and the coupling constant λ_Ψ figured in GLG-equations read $\Psi(\vec{r}) = \frac{(7\zeta(3)N)^{1/2}}{4\pi k_B T_c}\Delta(\vec{r})$, $\Delta(T) =\simeq 3.1 k_B T_c\left(1 - \frac{T}{T_c}\right)^{1/2}$, $\xi_0 =\simeq 0.18\frac{\hbar v_F}{k_B T_c}$, $m_\Psi^2 = 1.83\frac{\hbar^2}{m}\frac{1}{\xi_0^2}\left(1 - \frac{T}{T_c}\right)$,

doi: 10.52526/25792776-2021.68.2-311

$\lambda_\Psi^2 = 1.4\frac{1}{N(0)}\left(\frac{\hbar^2}{2m\xi_0^2}\right)^2\frac{1}{(k_BT_c)^2}$. Reviewing the notation $\Delta(\vec{r})$ is the energy gap, $e^* = 2e$ is the effective charge, $N(0)$ is the state density at Fermi surface, N is the number of particles per unit volume in normal mode, v_F is the Fermi velocity, $m \equiv \Sigma_Q = f_Q$ is the mass of fermion field. The transition temperature relates to gap at absolute zero Δ_0. The estimate for the pair size at $v_F \sim 10^8 cm/s, \quad T_c \sim 1$ gives $\xi_0 \simeq 10^{-4} cm$.

12.4. The Relativistic Treatment

We start with the Lagrangian of self-interacting fermion field in W-world, which is arisen from the Lagrangian of primary fundamental field after the rearrangement of the vacuum of the Q-world $L_W(x) = \frac{i}{2}\{\bar{\Psi}_W(x)\gamma^\mu\partial_{W\mu}\Psi_W(x) - \bar{\Psi}_W(x)\gamma^\mu\overleftarrow{\partial}_{W\mu}\Psi_W(x)\} - m\bar{\Psi}_W(x)\Psi_W(x) - \frac{\lambda}{2}\bar{\Psi}_W(x)\left(\bar{\Psi}_W(x)\Psi_W(x)\right)\Psi_W(x)$. Here, $m = \Sigma_Q$ is the self-energy operator of the fermion field component in Q-world, the suffix (W) just was put forth in illustration of a point at issue. For the sake of simplicity, we also admit $\mathbf{B_W}(x) = 0$, but, of course, one is free to restore the gauge field $\mathbf{B_W}(x)$ whenever it will be needed. In lowest order the relation $m \equiv m_Q \ll \lambda^{-1/2}$ holds. The Lagrangian $L_W(x)$ leads to the field equations $(\gamma p - m)\Psi(x) - \lambda\left(\bar{\Psi}(x)\Psi(x)\right)\Psi(x) = 0$, $\bar{\Psi}(x)(\gamma\overleftarrow{p} + m) + \lambda\bar{\Psi}(x)\left(\bar{\Psi}(x)\Psi(x)\right) = 0$, where the indices have been suppressed as usual. At non-relativistic limit the function Ψ reads $\Psi \to e^{imc^2t}\Psi$. In the following, we make use of conventional technique and evaluate the equations. The spirit of the calculation will be to treat interaction between the particles as being absent everywhere except the thin spherical shell $2\widetilde{q}$ near the Fermi surface. The Bose condensate of bound particle iso-pairs occurred at zero momentum. The scattering processes between the particles are absent. This method allows oneself to extend the study up to limit of temperatures, such that $T_c - T \ll T_c$, by making use of thermodynamic Green's function.

12.5. Lagrangian of Electroweak Interactions; The Transmission of the Electroweak Symmetry Breaking From the W-World to Spacetime Continuum

The results obtained within the previous subsections enable us to trace unambiguously rather general scheme of unified electroweak interactions, where the self-interacting isospinor scalar Higgs bosons have arisen as the collective modes of excitations of bound quasi-particle iso-pairs on the internal W-world. But, at the very first we remind some features allowing us to write down the final Lagrangian of electroweak interactions.

1. During the realization of the MW connections of weak interacting fermions under the action of the Q-world the P-violation compulsory occurred in the W-world incorporated with the symmetry reduction characterized by the Weinberg mixing angle with the fixed value at 30^0. This gives rise to the local symmetry $SU(2) \otimes U(1)$, under which the left-handed fermions transformed as six independent doublets, while the right-handed fermions transformed as twelve independent singlets.

2. Due to vacuum rearrangement in Q-world the Yukawa couplings arise between the fermion fields and corresponding isospinor-scalar φ- meson in conventional form.

3. In the framework of suggested mechanism providing the effective attraction between the relativistic fermions caused by the exchange of the mediating induced gauge quanta in W-world, the self-interacting isospinor-scalar Higgs bosons arise as Bose-condensate, namely the $SU(2)$ multiplets of spinless φ-meson fields coupled to the gauge fields in a gauge invariant way. Thus, in the Lagrangian of φ-meson with the degenerate vacuum of the W-world the symmetry-breaking Higgs boson is counted off from the gap symmetry restoring value as the point of origin.

In view of this the total Lagrangian ensues, and it is now invariant under the local symmetry $SU(2) \otimes U(1)$, where a set of gauge fields are coupled to various multiplets of fields among which is also a multiplet of Higgs boson. Subsequently, we separate a piece of Lagrangian containing only the fields defined on four dimensional Minkowski flat spacetime continuum M_4. To facilitate writing we shall forbear here to write out the piece of Lagrangian containing the terms of other fermion generations than one, as it is a somewhat lengthy and so standard. But, in the mean time, we shall retain the explicit terms of Higgs bosons arisen on the internal $W-$world to emphasize the specific mechanism of the electroweak symmetry breakdown discussed below. The resulting Lagrangian reads $L = -\frac{1}{2}TrG_{\mu\nu}G^{\mu\nu} - \frac{1}{4}F_{\mu\nu}F^{\mu\nu} + i\bar{L}\hat{D}L + i\bar{e}_R\hat{D}e_R + i\bar{\nu}_R\hat{D}\nu_R + |D_{W\mu}\varphi|^2 - \frac{1}{2}\lambda_\varphi^2\left(|\varphi|^2 - \frac{1}{2}\eta_\varphi^2\right)^2 -$

doi: 10.52526/25792776-2021.68.2-311

$f_e\left(\bar{L}\varphi e_R+\bar{e}_R\varphi^+L\right)-f_\nu\left(\bar{L}\varphi_c\nu_R+\bar{\nu}_R\varphi_c^+L\right)+$similar terms for other fermion generations. The gauge fields $\mathbf{A}_\mu(x)$ and $B_\mu(x)$ associate respectively with the groups $SU(2)$ and $U(1)$, where the gauge covariant curls are $F_{\mu\nu}, G_{\mu\nu}$. The corresponding gauge covariant derivatives are in standard form. One took into account corresponding values of the operators $\mathbf{T}$ and Y for left- and right-handed fields, and for isospinor φ-meson. The Yukawa coupling constants f_e and f_ν are inserted in subsec.6.10. Since the electroweak symmetry is at any rate only approximate, the test of the theory will depend on its ability to account for its breaking as well. here the MSM creates a particular incentive for the study of such a breaking. Then, just it remains to see how can such Higgs bosons arisen on the internal W-world break the gauge symmetry down in M_4 and lead to masses of the spacetime-components of the MW-fields? It is remarkable to see that the suggested MSM, in contrast to the SM, predicts the transmission of electroweak symmetry breaking from the $W-$world to the M_4 spacetime continuum. Actually, in standard scenario for the simplest Higgs sector, a gauge invariance of the Lagrangian is broken when the φ-meson fields acquire a VEV $\eta_\varphi\neq 0$ in the W-world. While the mass m_φ and coupling constant λ_φ are in the standard form. The spontaneous breakdown of symmetry is vanished at $\eta^2_\varphi(\lambda, T>T_{c\mu})<0$. When this doublet obtains a VEV, three of the gauge fields ${Z_W}^0_\mu$, ${W_W}^\pm_\mu$ acquire masses. These fields are the W-components of the mesons mediating the weak interactions. This mechanism does not disturb the renormalizability of the theory . In approximation to lowest order $f=\Sigma_Q\simeq m_Q\ll\lambda^{-1/2}\left(\lambda^{-1}=\frac{mp_0}{2\pi^2}\ln\frac{2\tilde{\omega}}{\Delta_0}\right)$, the Lagrangian produce the Lagrangian of phenomenological SM, where at $f\sim 10^{-6}$ one gets $\lambda\ll 10^{12}$. In standard scenario the lowest pole m_Q of the self-energy operator Σ_Q has fixed the whole mass spectrum of the SM particles. But, in general, one must also take into account the mass spectrum of expected various collective excitations of bound quasi-particle pairs produced by higher-order interactions as a `superconductive´ solution obtained from a nonlinear spinor field Lagrangian of the Q-component possessed γ_5 invariance. These states must be considered as a direct effect of the same primary nonlinear fermion interaction which provides the mass of the Q-component of Fermi field, which itself is a collective effect. They would manifest themselves as stable or unstable states. The general features of mass spectrum of the collective excitations and their coupling with the fermions are discussed through the use of the Bethe-Salpeter equation handled in the simplest ladder approximation incorporated with the self-consistency conditions, when one is still left with unresolved divergence problem. One can reasonably expect that these results for the bosons of small masses at low energy compared to the unbound fermion states are essentially correct in spite of the very simple approximations. Therein, some bound states are predicted too the obtained mass values of which are rather high, and these states should decay very quickly. The high-energy poles may in turn determine the low-energy resonances. All this prompt us to expect that the other poles different from those of lowest one in turn will produce the new heavy SM family partners. Hence one would expect a second important phenomenological implication of the MSM.

12.6. Quark flavour mixing and the Cabibbo angles

An implication of quark generations into general scheme will be carried out in the same way of the leptons. But before proceeding further that it is profitable to enlarge it by the additional assumption without asking the reason behind it:

The MW components imply ${}^i\bar{\psi_u}^A(\cdots,\theta_{i_1},\cdots\theta_{i_n},\cdots)\;{}^j{\psi_u}^B(\cdots,\theta_{i_1},\cdots\theta_{i_n},\cdots)=$ $\delta_{ij}\sum_{l=i_1,\ldots,i_n}f^{AB}_{il}\;{}^i(\bar{q}_l q_l)$, namely, the contribution of each individual subquark ${}^iq_l$, into the component of given world (i) is determined by the *partial formfactor* f^{AB}_{il}. Under the group $SU(2)\otimes U(1)$ the left-handed quarks transform as three doublets, while the right-handed quarks transform as independent singlets except of following differences:

1. The values of weak-hypercharge of quarks are changed due to their fractional electric charges $q_L: Y^w=\frac{1}{3},\quad u_R: Y^w=\frac{4}{3},\quad d_R: Y^w=-\frac{2}{3}$ etc.
2. All Yukawa coupling constants have nonzero values.
3. An appearance of quark mixing and Cabibbo angle, which is unknown in the scope of standard model.
4. An existence of CP-violating phase in unitary matrix of quark mixing. We shall discuss it in the

doi: 10.52526/25792776-2021.68.2-311

next section.

In previous section we attempt to give an explanation to quark mixing and Cabibbo angle. We consider this problem, for simplicity, on the example of four quarks u, d, s, c. The further implication of all quarks would complicate the problem only in algebraic sense. Instead of mixing of the d' and s' it is convenient to consider a quite equivalent mixing of u' and c'. Similar formulas can be worked out for the other mixings. Hence, the nonzero value of Cabibbo angle arises due to nonzero coupling constant $f_{u'c'}$. The problem is to calculate all coupling constants $f_{u'c'}, f_{c't'}$, and $f_{t'u'}$ generating three Cabibbo angles $\tan 2\theta_3 = \frac{2f_{u'c'}}{f_{c'}-f_{u'}}$, $\tan 2\theta_1 = \frac{2f_{c't'}}{f_{t'}-f_{c'}}$, $\tan 2\theta_2 = \frac{2f_{t'u'}}{f_{u'}-f_{t'}}$. Since the Q-components of the quark fields u', c' and t' contain at least one identical subquark, the partial formfactors $\bar{f}_i$, as well then all coupling constants, acquire nonzero values causing a quark mixing with the Cabibbo angles. Therefore, the unimodular orthogonal group of global rotations arises, and the quarks u', c' and t' come up in doublets (u', c'),(c', t'), and (t', u'). For the leptons these formfactors equal zero $\bar{f}_i^{lept} \equiv 0$, namely the lepton mixing is absent. In conventional notation $\begin{pmatrix} u' \\ d \end{pmatrix}_L, \begin{pmatrix} c' \\ s \end{pmatrix}_L, \begin{pmatrix} t' \\ b \end{pmatrix}_L \rightarrow \begin{pmatrix} u \\ d' \end{pmatrix}_L, \begin{pmatrix} c \\ s' \end{pmatrix}_L, \begin{pmatrix} t \\ b' \end{pmatrix}_L$, which gives rise to $f_{u'c'} \rightarrow f_{d's'}$, $f_{c't'} \rightarrow f_{s'b'}$, $f_{t'u'} \rightarrow f_{b'd'}$, $f_{u'} \rightarrow f_{d'}$, $f_{c'} \rightarrow f_{s'}$, $f_{t'} \rightarrow f_{b'}$, $f_d \rightarrow f_u$, $f_s \rightarrow f_c$, $f_b \rightarrow f_t$.

12.7. The CP-violating phase

The required magnitude of the CP-violating complex parameter ε depends upon the specific choice of theoretical model for explaining the $K_2^0 \rightarrow 2\pi$ decay. From the experimental data it is somewhere $|\varepsilon| \simeq 2.3 \times 10^{-3}$. In the framework of Kobayashi-Maskawa (KM) parametrization of unitary matrix of quark mixing, this parameter may be expressed in terms of three Eulerian angles of global rotations in the three dimensional quark space and one phase parameter. We attempt to derive the KM-matrix with an explanation given to an appearance of the CP-violating phase. Recall that during the realization of MW- structure the P-violation compulsory occurred in the W-world provided by the spanning. The three dimensional effective space $W_v^{loc}(3)$ arises as follows:

$$W_v^{loc}(3) \ni q_v^{(3)} = \begin{pmatrix} q_R^w(\vec{T}=0) \\ q_L^w(\vec{T}=\frac{1}{2}) \end{pmatrix} \equiv$$

$$\begin{pmatrix} u_R, d_R \\ \begin{pmatrix} u' \\ d \end{pmatrix}_L \end{pmatrix}, \begin{pmatrix} c_R, s_R \\ \begin{pmatrix} c' \\ s \end{pmatrix}_L \end{pmatrix}, \begin{pmatrix} t_R, b_R \\ \begin{pmatrix} t' \\ b \end{pmatrix}_L \end{pmatrix} \equiv \begin{pmatrix} q_3^w \\ \begin{pmatrix} q_1^w \\ q_2^w \end{pmatrix} \end{pmatrix}, \begin{pmatrix} q_1^w \\ \begin{pmatrix} q_2^w \\ q_3^w \end{pmatrix} \end{pmatrix}, \begin{pmatrix} q_2^w \\ \begin{pmatrix} q_3^w \\ q_1^w \end{pmatrix} \end{pmatrix},$$

where the subscript (v) formally specifies a vertical direction of multiplet, the subquarks $q_\alpha^w (\alpha = 1, 2, 3)$ associate with the local rotations around corresponding axes of three dimensional effective space $W_v^{loc}(3)$. The local gauge transformations f_{exp}^v are implemented upon the multiplet $q'^{(3)}_v = f_{exp}^v q_v^{(3)}$, where $f_{exp}^v \in SU^{loc}(2) \otimes U^{loc}(1)$. If for the moment we leave it intact and make a closer examination of the content of the middle row, then we distinguish the other symmetry arisen along the horizontal line (h). Hence, we may expect a situation similar to those of previous section will be held in present case. The procedure just explained therein can be followed again. We have to realize that due to the specific structure of W-world implying the condition of realization of the MW connections with $\vec{T} \neq 0, \quad Y^w \neq 0$, the subquarks q_α^w tend to be compulsory involved into triplet. They form one "doublet" $\vec{T} \neq 0$ and one singlet $Y^w \neq 0$. Then the quarks u'_L, c'_L and t'_L form a $SO^{gl}(2)$ "doublet" and a $U^{gl}(1)$ singlet $((u'_L, c'_L)\, t'_L) \equiv ((q_1^w, q_2^w)\, q_3^w) \equiv q_h^{(3)} \in W_h^{gl}(3)$, $(u'_L, (c'_L, t'_L)) \equiv (q_1^w, (q_2^w, q_3^w))$, $((t'_L, u'_L)\, c'_L) \equiv ((q_3^w, q_1^w), q_2^w)$. Here $W_h^{gl}(3)$ is the three dimensional effective space in which the global rotations occur. They are implemented upon the triplets through the transformation matrix f_{exp}^h: $q'^{(3)}_h = f_{exp}^h q_h^{(3)}$, which reads $f_{exp}^h = \begin{pmatrix} f_{33} & 0 & 0 \\ 0 & c & s \\ 0 & -s & c \end{pmatrix}$ in the notation $c = \cos\theta, \quad s = \sin\theta$. This implies the incompatibility relation $\|f_{exp}^h\| = f_{33}(f_{11}f_{22} - f_{12}f_{21}) = f_{33}\varepsilon_{123}\varepsilon_{123}\|f_{exp}^h\| f_{33}^*$. That is $f_{33}f_{33}^* = 1$, or $f_{33} = e^{i\delta}$ and $\|f_{exp}^h\| = 1$. The general rotation in $W_h^{gl}(3)$ is described by Eulerian three angles $\theta_1, \theta_2, \theta_3$. If we put the arisen phase only in the physical sector then a final KM-matrix of quark

doi: 10.52526/25792776-2021.68.2-311

flavour mixing would result. The CP-violating parameter ε approximately is written $\varepsilon \sim s_1 s_2 s_3 \sin\delta \neq 0$. Thus, while the spanning $W_v^{loc}(2) \to W_v^{loc}(3)$ underlies the P-violation and the expanded symmetry $G_v^{loc}(3) = SU^{loc}(2) \otimes U^{loc}(1)$, the CP-violation stems from the similar spanning $W_h^{gl}(2) \to W_h^{gl}(3)$ with the expanded global symmetry group.

12.8. Result

The testable solid implications. If the MTSM proves viable it becomes an crucial issue to hold in experiments the testable solid implications given in, which are drastically different from those of conventional models. Actually, the MTSM rejects drastically any expectation of discovery of any Higgs boson as an elementary particle in M_4, but in the same time it expects to include a rich spectrum of new particles at higher energies. Namely, if the MTSM proves viable it becomes an crucial issue to hold in experiments the following two solid tests:

1) The Higgs bosons never could emerge as an `elementary´ (apart the pole of composite structure) particle at experiments in spacetime continuum M_4, nor at any energy range, since these bosons have to arise only on the internal W-world and ,thus, they produced the electroweak symmetry breakdown in the W-world with the subsequent transmission of it to M_4.

2) For each of the three SM families of quarks and leptons there are corresponding heavy family partners with the same quantum numbers and common mass-shift coefficients $(1+k)$ given for the low-energy poles at $k_1 > \sqrt{2}$, $\quad k_2 = \sqrt{8/3}$ and $k_3 = 2$, lying far above the electroweak scale, respectively, at the energy threshold values: $E_1 > (419.6 \pm 12.0)GeV$, $\quad E_2 = (457.6 \pm 13.2)GeV$ and $E_3 = (521.4 \pm 15.0)GeV$.

To see its nature, now we may estimate the energy threshold of creation of such heavy family partners using the results far obtained (Nambu & Jona-Lasinio, 1961). It is therefore necessary under the simplifying assumption to consider in the Q-world a composite system of dressed fermion (N_*) made of the unbound fermion (N) coupled with the different kind two-fermion bound states $(N\bar{N})$ at low energy, which all together represent the primary manifestation of the fundamental interaction. Such a dressed fermion would have a total mass $m_* \simeq m_Q + \mu$, where m_Q and μ are the masses, respectively, of the unbound fermion and the bound state. According to the general discussion of the mass spectrum of the collective excitations given in (Nambu & Jona-Lasinio, 1961), here we are interested only in the following low-energy bound states written explicitly in spectroscopic notation $({}^1S_0)_{N=0}$, $\quad ({}^1S_0)_{N=\pm 2}$, $\quad ({}^3P_1)_{N=0}$ and $({}^3P_0)_{N=0}$ with the expected masses $\mu = 0$, $\; > \sqrt{2}m_Q$, $\sqrt{\frac{8}{3}}m_Q$ and $2\,m_Q$, respectively, where the subscript N indicates the nucleon number. One notes the peculiar symmetry existing between the pseudoscalar and the scalar states that the first has zero mass and binding energy $2m_Q$, while the opposite holds for the scalar state. When the next pole m_* to the lowest one m_Q will be switched on, then due to the Yukawa couplings the all fermions will acquire the new masses with their common shift $\frac{m_*}{m_Q} \equiv 1+k$ held upwards along the energy scale. To fix the energy threshold value all we have to do then is choose the heaviest member among the SM fermions, which is the top quark, and to set up the quite obvious formula $E \geq E_0 \equiv m_{t'}\,c^2 = (1+k)\,m_t\,c^2$, where m_t is the mass of the top quark. The top quark observed firstly in the two FNAL $p\,\bar{p}$ collider experiments in 1995, has the mass turned out to be startlingly large $m_t = (173.8 \pm 5.0)GeV/c^2$ compared to all the other SM fermion masses [125]. Thus, we get the most important energy threshold scale estimate where the heavy partners of the SM extra families of quarks and leptons likely would reside at: $E_1 > (419.6 \pm 12.0)GeV$, $\quad E_2 = (457.6 \pm 13.2)GeV$ and $E_3 = (521.4 \pm 15.0)GeV$, corresponded to the next nontrivial poles are written: $k_1 > \sqrt{2}$, $\quad k_2 = \sqrt{8/3}$ and $k_3 = 2$, respectively. We recognize well that the general results obtained in [95], however, model-dependent and may be considerably altered, especially in the high energy range by using better approximation. In present state of the theory it seemed to be a bit premature to get exact high energy results, which will be important subject for the future investigations. But, in the same time we believe that the approximation used in (Nambu & Jona-Lasinio, 1961) has enough accuracy for the low-energy estimate made above . Anyhow, it is for one thing, the new scale where the family partners reside will be much higher than the electroweak scale and thus these heavy partners lie far above the electroweak scale.

Remarks: As alluded to above, the Higgs boson does its work of breaking of the electroweak

doi: 10.52526/25792776-2021.68.2-311

symmetry in the W-world. The physical pole of formation of such a process, produced by *compositeness* of this boson in $W-$world, has afterwards transmitted to the M_4. Then, at the well known experiments performed by ATLAS and CMS Collaborations, announcing the discovery of Higgs boson in 2011- 2013 based on the finding of the excess of events over the background prediction around 125 GeV, one has just detected only this pole (maybe of composite structure) with the measurements of its subsequent decay to vector bosons in M_4, but not the Higgs as the *elementary particle* at all. It is similar to the case when quarks produced the reactions of elementary particles in M_4, but in the same time they obeyed Color Confinement principle, and that they appeared in spacetime continuum only in singlet combinations.

Regarding to the last phenomenological implication of the MTSM, it is remarkable that the similar in many respects prediction is made in somewhat different context by Adler (Adler, 2021) within a phenomenological scheme of a compositeness of the quarks and leptons. It based on the generic group theoretical framework of rishon type models exploring the preon constituents. But, therein a present, a bit premature, state of the theory does not allow the exact estimate of this scale. Although one admits that such a scale could be much higher than electroweak scale, however, it is also necessary special argumentations in support of validity of this prediction in the case if this scale has turned out to be low enough, namely, if these heavy partners lie not too far above the electroweak scale. Even thus, one must not worry for the existence of 6 heavy flavors, which is then marginally compatible with the current LEP data. Thus, which of these schemes above, if any, is realized either exactly or at least approximately in nature remains to be seen in the years to come.

Our approach still should be considered as a preliminary one, wherein we have contended ourselves with a rather modest task and do not profess to have any clear-cut answers to all the problems of particle physics, the complete picture of which is largely beyond the scope of the present paper. The only argument that prompts us to consider present approach seriously is the remarkable feature that the most important properties of particle phenomenology can be derived naturally within its framework. Therefore we hope that it will be an attractive basis for the future theory. Although many key problems are elucidated within outlined approach, nevertheless some issues still remain to be solved. For the details of theoretical apparatus of MTSM, see (Ter-Kazarian, 1999b, 2001b).

13. Supersymmetric Extension of MTSM

13.1. Objectives

There is an important line of reasoning which supports the side of supersymmetrization of the SM, i.e., there are two well known principal issues which remain open in the SM. The first is the vacuum zero point energy problem standing before any quantum field theory. Second is often referred to as the problem of quadratic divergences or the hierarchy and naturalness problem (the dimensional analysis problem) arisen as the quadratic growth of the Higgs boson mass beyond tree level in perturbation theory, namely, the extreme difference in energy scales in the theory is inconsistent in the fundamental scalar sector. This is strong indication for the physics beyond SM. These last two problems can be solved by extending the symmetry of the theory to supersymmetry, which is believed in conventional physics to be manifest at energies in the TeV range. Given the SUSY requiring doubling the number of all the particles by their SUSY partners (sparticles), the quantum radiative corrections may cancel because some loop diagrams vanish due to cancellation between bosons and fermions since they have opposite signs. Then, if the SUSY is present in the TeV range, the masses of the Higgs bosons are no more unstable than fermion masses, whose smallness is natural and hold due to the approximate chiral symmetries. In this manner, its simplest form, SUSY solves the technical aspects of the hierarchy problem as well as the zero point energy problem, when due to power of the boson-fermion cancellation the zero point energy of the fermions exactly cancels that of the bosons and the degeneracy is not arisen. Therefore, in usual, the SM should be regarded as an effective low energy field theory valid up to the energy range smaller than a few hundred GeVs.

However, the SUSY in turn introduces its own set of difficulties. Despite the beautiful mathematical features of SUSY theories and that the SUSY has been theoretically invented almost three decades ago, but a physically realistic realization of SUSY had not been achieved yet and this principal problem was

doi: 10.52526/25792776-2021.68.2-311

ever since much the same as now. In all suggested SUSY theories the supercharges have been inserted in *ad hoc* manner directly into the four-dimensional spacetime continuum adding a new structure, i.e., a new four odd fermionic dimensions. In fact, a physical essence of the basic concept of supercharge remains unknown and, therefore, the physical theory is beset by various difficulties. Perhaps the most discouraging and disturbing feature of the general class of proposed SUSY theories is the absence at the moment of a solid experimental motivation of supersymmetry, i.e., there is not a direct experimental evidence for the existence of any of the numerous new sparticles predicted by such theories. It is clear, then, that SUSY cannot be an exact symmetry in nature but has to be realized at least in broken phase. The last one is the least understood aspect of such theories. The spontaneously broken SUSY should be ruled out at once since it runs into phenomenological difficulties. One of the viable way out from this situation is an explicit breaking of the global SUSY. A generic parametrization of this phenomenon introduces the much larger free parameter space ($\simeq 124$) in the models of minimal supersymmetric extension of the SM (MSSM-124). Thus, it is important to develop the other schemes that attempt to reduce the number of free parameters. The conventional SUSY theories predict that the sparticles must reside in the TeV range. All such arguments that nature is supersymmetric, and that SUSY is broken at scales not too different than the weak scale, are theoretical. The next generation of experiments at Fermilab and CERN will explore this energy range, where at least some of sparticles are expected to be found. All this variety prompts us, further, to adopt the idea that perhaps a more deeper level of organization of physical world may be existed. In the light of current status of particle physics, any new more elaborated outlook seems worthy of investigation.

13.2. The superfield content of MSMSM and the resulting SUSY Lagrangian

The results obtained in the previous sections enable us to trace unambiguously rather general scheme of MSMSM, which is essentially a straightforward and viable supersymmetrization of the MSM where we want to keep the number of superfields and interactions as small as possible. To build up the MSMSM the major point is to define its superfield content. Below we recall some important features allowing us to write the resulting Lagrangian of MSMSM.

• Within the MSM, during the realization of MW connections of weak interacting fermions the P-violation compulsory occurred in W-world incorporated with the symmetry reduction. It has characterized by the Weinberg mixing angle with the fixed value at 30^0. This gives rise to the local symmetry $SU(2) \otimes U(1)$, under which the left-handed fermions transformed as six independent doublets, while the right-handed fermions transformed as twelve independent singlets.

• Due to vacuum rearrangement in Q-world the Yukawa couplings arise between the fermion fields and corresponding isospinor-scalar H-mesons in conventional form.

• In the framework of suggested mechanism, providing the effective attraction between the relativistic fermions caused by the exchange of the mediating induced gauge quanta in W-world, the two complex self-interacting isospinor-scalar Higgs doublets (H_u, H_d) as well as their spin-$\frac{1}{2}$ SUSY partners ($\widetilde{H}_u$, $\widetilde{H}_d$) Higgsinos arise as the Bose-condensate. Taking into account this slight difference from the MSM arisen in the field content of MSMSM in the Higgs sector, we must explicitly write in the supersymmetric Lagrangian also the piece containing these fields coupled to the gauge fields in a gauge invariant way, when the symmetry-breaking Higgs bosons are counted off from the gap symmetry-restoring value as the point of origin.

• The gauge group of MSMSM is the same $SU_c(3) \otimes SU(2)_L \otimes U(1)$ as in the MSM, which requires a colour octet of vector superfields V^a, a weak triplet $V^{(\delta)}$ and a hypercharge singlet V. Thus, the kinetic terms of all the fields now fixed by gauge invariance $L = \int d^4\theta\, \widetilde{\Phi}^+_{ch}\,(e^{g_1 V T + g_2 V^{(\delta)} T^{(\delta)} + g_3 V^a T^a})\,\widetilde{\Phi}_{ch} + [\int d^2\theta\, \frac{1}{4}(W W + W^{(\delta)} W^{(\delta)} + W^a W^a) + \text{h.c.}]$, where $\widetilde{\Phi}_{ch}$ is the matter superfields, T, $T^{(\delta)}$, T^a are the generators of appropriate representations of the gauge group. The superpotential determines the scalar potential $V(A, A^*) = \frac{1}{2} g_1^2 D^2 + \frac{1}{2} g_2^2 D^{\delta 2} + \frac{1}{2} g_2^2 D^{a 2} + |P|^2$, where the functions D and P are given above.

• By the index $I = 1, 2, 3$ in the MW-SUSY Lagrangian will be labeled the three families of chiral quarks q^I_L, u^I_R, d^I_R, and chiral leptons l^I_L, e^I_R, where all of them are Weyl fermions. A SUSY requires the presence of supersymmetric partners which form supermultiplets with known particles, i.e., for every field of SM there is a superpartner with the exact same gauge quantum numbers. Then, the

doi: 10.52526/25792776-2021.68.2-311

quarks and leptons are promoted to chiral multiplets by adding scalar (spin-0) squarks ($\widetilde{q}^I_L$, $\widetilde{u}^I_R$, $\widetilde{d}^I_R$) and sleptons ($\widetilde{l}^I_L$, $\widetilde{e}^I_R$) to the spectrum. The gauge bosons are promoted to vector supermultiplet by adding their SUSY partners gauginos (spin-$\frac{1}{2}$) ($\widetilde{G}$, $\widetilde{W}$ $\widetilde{B}$) to the spectrum. A content of superfields of MSMSM presents in Table 1:

	supermultiplet	F	B	$SU_c(3)$	$SU(2)_L$	$U(1)_Y$	$U(1)_{em}$
quarks	$Q^I_L = \begin{pmatrix} U^I_L \\ D^I_L \end{pmatrix}$	q^I_L	$\widetilde{q}^I_L$	3	2	1/6	$\begin{pmatrix} 2/3 \\ -1/3 \end{pmatrix}$
	U^I_R	u^I_R	$\widetilde{u}^I_R$	$\bar{3}$	1	− 2/3	−2/3
	D^I_R	d^I_R	$\widetilde{d}^I_R$	$\bar{3}$	1	1/3	1/3
leptons	$L^I_L = \begin{pmatrix} \mathcal{N}^I_L \\ E^I_L \end{pmatrix}$	l^I_L	$\widetilde{l}^I_L$	1	2	− 1/2	$\begin{pmatrix} 0 \\ -1 \end{pmatrix}$
	E^I_R	e^I_R	$\widetilde{e}^I_R$	1	1	1	1
Higgs	$H_d = \begin{pmatrix} H^0_d \\ H^-_d \end{pmatrix}$	$\begin{pmatrix} \widetilde{h}^0 \\ \widetilde{h}^- \end{pmatrix}$	$\begin{pmatrix} h^0_d \\ h^-_d \end{pmatrix}$	1	2	− 1/2	$\begin{pmatrix} 0 \\ -1 \end{pmatrix}$
	$H_u = \begin{pmatrix} H^+_u \\ H^0_u \end{pmatrix}$	$\begin{pmatrix} \widetilde{h}^+ \\ \widetilde{h}^0 \end{pmatrix}$	$\begin{pmatrix} h^+_u \\ h^0_u \end{pmatrix}$	1	2	1/2	$\begin{pmatrix} 1 \\ 0 \end{pmatrix}$
gauge bosons	G	$\widetilde{G}$	G	8	1	0	0
	W	$\widetilde{W}$	W	1	3	0	(0, ±1)
	B	$\widetilde{B}$	B	1	1	0	0

Table 1. Field content of MSMSM. The column below F(B) denotes its fermionic (bosonic) content.

Once the field content is fixed, putting it all together the most generic renormalizable MW-SUSY Lagrangian of MSMSM, defined on the SMM (SG_N), is now invariant under local gauge symmetry $SU_c(3) \otimes SU(2)_L \otimes U(1)$, where a set of gauge fields are coupled to various superfields among which is also Higgs supermultiplets. Furthermore, we especially separated from the rest the piece containing only the η-components of the particles defined on the supermanifold SG_η, which is important for the further discussion of a realistic realization of the MSMSM (next subsec.). Whereas, χ^I runs over all the particles, while A^J runs over all the sparticles, the index (a) labels the 3 different features in the gauge group, $V_d(H,\, H^*)$ is the scalar potential for each Higgs doublet $V_u(H_u,\, H_u{}^*) = -\frac{1}{2}\, m_u^2\, |H_u|^2 + \frac{1}{4}\, \lambda_u^2\, |H_u|^4$ $V_d(H_d,\, H_d{}^*) = -\frac{1}{2}\, m_d^2\, |H_d|^2 + \frac{1}{4}\, \lambda_d^2\, |H_d|^4$. A contribution of the "D" term to the Higgs potential has also taken into account $V_D = \frac{1}{2}\, D^{(a)}\, D^{(a)}$, $D^{(a)} = -g\, A^{I*}\, T^a_{IJ}\, A^J$, or $V_D = \frac{g^2+g'^2}{8}\,(|H_u|^2 - |H_d|^2 \bigoplus)^2 + \frac{1}{2}\, g^2\, |H_u\, H_d{}^*|^2$. The number of major free parameters in the Lagrangian are the primary coupling constants λ_Q and λ_W of nonlinear fermion interaction of the internal MW-components $i = Q, W$ and gauge couplings $g_1,\, g_2,\, g_3$. The SM relation $Q_e = g_1 \cos\theta_W$ holds, where θ_W is the weak mixing angle $\cos^2\theta_W = g^2 \big/ (g^2 + g'^2)$. The Yukawa couplings $(Y_l\, Y'_l)$ are given: $Y = f_Q = Z_Q$.

doi: 10.52526/25792776-2021.68.2-311

13.3. Higgs doublets in MW-SUSY and Higgs mechanism

Due to vacuum rearrangement in Q-world the Yukawa couplings arise between the fermion fields and corresponding isospinor-scalar H-mesons in conventional form. In the framework of suggested specific mechanism providing the effective attraction between the relativistic fermions caused by the exchange of the mediating induced gauge quanta in the W-world, the two complex self-interacting isospinor-scalar Higgs doublets $(H_u,\, H_d)$ as well as their spin-$\frac{1}{2}$ SUSY partners $(\widetilde{H}_u,\, \widetilde{H}_d)$ Higgsinos arise as the Bose-condensate. Taking into account this slight difference from the MTSM arisen in the field content of SuMTSM in the Higgs sector the supersymmetric Lagrangian now also contains these fields coupled to the gauge fields in a gauge invariant way, when the symmetry-breaking Higgs bosons are counted off from the gap symmetry-restoring value as the point of origin.

The Higgs mechanism does work in the following way: Before the symmetry was broken in the W-world, the 2 complex $SU(2)_L$ Higgs doublets had 8 degrees of freedom. Three of them were the would-be Nambu-Goldstone bosons G^0, $G^{\pm}$, which were absorbed to give rise the longitudinal modes of the massive W-components of the Z^0 and $W^{\pm}$ vector bosons, which simultaneously give rise the corresponding x- components too, leaving 5 physical degrees of freedom. The latter consists of a charged Higgs boson pairs $H^{\pm}$, a CP-odd neutral Higgs boson A^0, and CP-even neutral Higgs bosons h^0 and H^0. The mass eigenstates and would-be Nambu-Goldstone bosons are made of the original gauge-eigenstate fields, where the physical pseudoscalar Higgs boson A^0 is made of from the imaginary parts of h_u^0 and h_d^0, and is orthogonal to G^0; while the neutral scalar Higgs bosons are mixtures of the real parts of h_u^0 and h_d^0. The mass of any physical Higgs boson that is SM-like is strictly limited, as are the radiative corrections to the quartic potential terms. We calculated the tree-level masses for these Higgs states (sec.16) and shown that the h^0 Higgs boson arisen in the internal W-world is much heavier of that Z^0 boson. In contrast to the SM, the suggested microscopic approach predicts the electroweak symmetry breakdown in the W-world by the VEV of spin zero Higgs bosons and the transmission of electroweak symmetry breaking from the $W-$world to the M_4 spacetime continuum. The resulting Lagrangian of unified electroweak interactions of leptons and quarks ensues, which in lowest order approximation leads to the Lagrangian of phenomenological SM. In general, the self-energy operator underlies the Yukawa coupling constant, which takes into account a mass-spectrum of all expected collective excitations of bound quasi-particle pairs. If the MSM proves viable it becomes an crucial issue to hold in experiments the two testable predictions.

13.4. Realistic realization of the MW-SUSY: M$\not{S}$MSM

The MW-SUSY cannot be an exact symmetry of nature and has to be realized in its broken phase. The major point of our strategy is a realistic realization of the supersymmetric extension of the MSM. Thus, the test of the theory will depend on its ability to account for the breaking of the MW-SUSY as well. Here, suggested approach creates a particular incentive for its study. In previous sections we have made a headway of reasonable framework of exact MW-SUSY defined on the exact MW-supermanifold SG_N. Therefore, one will be able to verify its virtues manifested, first of all, in the power of boson-fermion cancellations. One of the two principal offshoots of the supersymmetrization of the MSM is the solution of the zero point energy problem. Also, in its unbroken form it solves the technical aspects of the naturalness and hierarchy problem, when in non-SUSY theories scalar fields receive large mass corrections even if the bare mass is set to zero, and small masses are `unnatural´. This applied to the Higgs bosons of the SM (as well as MSM) yields a difficulty in understanding of the smallness of M_Z and how it can be kept stable against quantum corrections in some extensions of the SM containing apart from the weak scale M_Z also a second larger scale $M_{GUT} >> M_Z$ [126,127], which holds in Grand Unified theories. The cancellation of quadratic divergences in SUSY theories is a consequence of general non-renormalization theorem, or the `taming´ of the quantum corrections, which stabilizes the Higgs mass and thus weak scale M_Z without fine-tuning. It is remarkable that these attractive features of the unbroken MSMSM can be maintained as well in the broken M$\not{S}$MSM. Achieving it one should perform an inverse passage $(SG_\eta \to G_\eta)$ to the $\not{S}$MM: $\not{S}G_N$. It is due to the fact that the most powerful boson-fermion cancellation can be regarded as a direct consequence of a constraint stemming from holomorphy, therefore, it should be held even in the $M\not{S}MSM$. Then the Lagrangian $L_{\not{S}G_N}$ of

doi: 10.52526/25792776-2021.68.2-311

the M$\not S$MSM ensues from the Lagrangian L_{SG_N} of the MSMSM: $L_{\not S G_N} = L_{SG_N} + L_{soft}$, where, one has $L_{soft} = (-m^2_{IJ}\, A^I\, A^J - \frac{1}{2}\, \widetilde{m}_{ab}\, \lambda^a\, \lambda^a - \frac{1}{2}\, m_u\, \widetilde{H_u}\, \widetilde{H_u} - \frac{1}{2}\, m_d\, \widetilde{H_d}\, \widetilde{H_d} + \text{h.c.}) + b\, \epsilon_{ij}\, ({H_u}^i {H_d}^j + \text{h.c.})$. Here m^2_{IJ} is the mass matrix for all the scalars of the chiral multiplets, $m \equiv (\widetilde{m}_{ab},\, m_u,\, m_d)$ is the mass matrix respectively for the gauginos of each factor of the gauge group, and Higgsinos. The last term of the interaction is induced because these doublets above in free states imply $\hat{m}^2_u = -m^2_u + \lambda^2_u\, v^2_u, = 0$, $\hat{m}^2_d = -m^2_d + \lambda^2_d\, v^2_d = 0$, where m^2, λ^2, v^2 are respectively the mass, the coupling constant and VEV of given doublet. In the case at hand, certainly, there is an interaction between the bosons H_u and H_d, when the strength of interaction b will be fixed through the minimization conditions of the total Higgs potential. This can be used to derive a more physical relationship among the physical parameters. The case $\hat{m}^2_u = -\hat{m}^2_d \neq 0$ corresponds to the situation when the axion A^0 ($m^2_{A^0} = 0$) has arisen after the breaking of electroweak gauge symmetry. But the other case of ($\hat{m}^2_u > 0, \quad \hat{m}^2_d > 0$) or ($\hat{m}^2_u < 0, \quad \hat{m}^2_d < 0$), implies an existence of the neutral physical particle of the mass $m^2_{A^0} = \hat{m}^2_u + \hat{m}^2_d \neq 0$. Note that such Higgs doublets arisen on equal footing have counted off from the same point of origin for the same vacuum, then we will be interested physically in the most important simplest case when the electroweak symmetry breaking is parametrized just only by the single Higgs VEV $v_u = v_d\,, \quad \hat{m}^2_u = \hat{m}^2_d > 0$. Of course, we shall carry out a computation in the generic case, but in the aftermath we shall turn to this case. The non-supersymmetric breaking terms do not spoil a condition of cancellation of quadratic divergences, i.e., a mass-squared sum rule $Str\, M^2 \equiv \sum^1_{J=0} (-1)^{2J} (2J+1) Tr\, M^2_J = const.$ where $\vec{J}$ is the spin of the particles. It holds independently of the values of the scalar fields. Eventually the mass terms for the scalars contribute a constant, field independent piece, while a generic mass matrix for the fermions reads $M_{1/2} = M^S_{1/2} + \delta\, M_{1/2}$, where $M^S_{1/2}$ is the supersymmetric part of $M_{1/2}$, when $\delta\, M_{1/2}$ is given $\delta\, M_{1/2} = \begin{pmatrix} \delta\, P_{IJ} & \delta\, D^b_I \\ \delta\, D^a_J & \delta\, \widetilde{m} \end{pmatrix}$. A computation for the considered fields gives $\delta\, P = 0 = \delta\, D$, while $\delta\, \widetilde{m}$ can be arbitrary.

13.5. The viable SUSY-MTSM

The realistic generating functional should be derived by passing back to the physical limit. Such a breaking of the MW-SUSY can be implemented by subtracting back all the explicit soft mass terms formerly introduced for the sparticles. These terms do not reintroduced the quadratic diagrams which motivated the introduction of SUSY framework. Therewith, the boson-fermion cancellation in the above-mentioned problems can be regarded as a consequence of a constraint stemming from holomorphy of the observables, therefore it will be held at the limit too. Thus, we extract the pertinent piece containing only the η-field components and then in afterwards pass to M_4 to get the final viable SUSY-MTSM (VMSM) yielding the realistic particle spectrum. Thus, if the VMSM proves viable it becomes an crucial issue to hold in the experiments at LEP2 and at the Tevatron three testable solid implications, which are drastically different from those of conventional MSSM models. The implication of quarks into the VMSM is carried out in the same way of leptons except that of appearance of quark mixing with Cabibbo angle and the existence of CP-violating complex phase in unitary matrix of quark mixing. The Q-components of the quarks contain at least one identical subquark, due to which the partial formfactors gain nonzero values. This underlies the quark mixing with Cabibbo angles. In lepton's case these formfactors are vanished and lepton mixing is absent. The CP-violation stems from the spanning. Adopting a simple viewpoint on Higgs sector the masses of leptons and quarks are obtained. We hope that the outlined VMSM, if it proves viable in the experiments at LEP2 and at the Tevatron, will be an attractive basis for the future theories. As yet no direct signal has been found in them, the absent of which has been cleared up the lower limits on Higgs bosons and sparticles masses. Furthermore, there is a tight upper limit ($m_{h^0} < 150GeV$) on the mass of the lightest Higgs boson h^0 among the 5 physical Higgs bosons predicted by the MSSM models. The current direct search limits from LEP2 give $m_{h^0} > 75GeV$. Therefore, the future searches for this boson (if the mass is below 150 GeV or so) would be a crucial point in testing the efforts made in the conventional models building as well in the present MTSM based on a quite different approaches. The testable prediction of MTSM above together with a new one that *the sparticles could never emerge in spacetime continuum since they have arisen only on the internal worlds, thus, they cannot be discovered in experiments nor at*

doi: 10.52526/25792776-2021.68.2-311

any energy range,
are the solid implications of the resulting VMSM for the experiments at LEP2, at the Tevatron and at LHC, which are drastically different from those of MSSM models. Which of these schemes, if any, is realized either exactly or at least approximately in nature remains to be seen in the years to come. For the theoretical apparatus of SUSY-MTSM, see (Ter-Kazarian, 2001c).

13.6. Three solid testable predictions of VMSM

Discussing now the relevance of our present approach to the physical realities we should attempt to provide some ground for checking the predictions of the VMSM against experimental evidence. It is remarkable that the resulting theory makes plausible following three testable implications for the current experiments, which are drastically different from the predictions of conventional models:

(1,2). The two important phenomenological implication of the MSM, given above, just are the first two testable predictions of the VMSM for the current experiments.

3. It is well known that once $SU(2)_L \otimes U(1)_Y$ is broken, the fields with different $SU(2)_L \otimes U(1)_Y$ quantum numbers can mix if they have the same $SU(3)_c \otimes U(1)_{em}$ quantum numbers. Such a phenomenon occurs in the sfermion sector of the M$\not{S}$MSM. If one ignore mixing between sfermions of different generations but will include the mixing between $SU(2)$ doublet and singlet sfermions then the sfermion mass matrix decomposes into a series of 2×2 matrices of the sfermions of a given flavour. The charginos are mixtures of the charged Higgsinos and the charged gauginos, and neutralinos are the mixture of neutral Higgsinos and the neutral gauginos, etc.. We can readily obtain the resulting explicit forms of corresponding mass matrices within standard technique. But shall forbear to write them out here as the sfermions are no longer of consequence for discussion of the final fields defined on M_4. The sparticles could never emerge in M_4 and will be of no interest for the future experiments. By this we arrived to the second principle point of drastic deviation of M$\not{S}$MSM from the conventional MSSM models. In MSSM models as well in any conventional SUSY theory the supersymmetry was implemented in the Minkowski space M_4 by adding a new four odd dimensions, and there are two major motivation for SUSY to be realized in the TeV range, i.e., the masses of sparticles are of the order of a few TeV or less. First one is a solution of the hierarchy problem, when in order to introduce no new fine-tunning all soft terms should be of the same order of magnitude at most in the TeV range-weak scale. The second motivation for low energy SUSY comes from the view point of gauge unification (a supersymmetric GUT). Since the current experiments will explore this energy range, then, the second great expectation of such theories arise that at least some of the sparticles can be found and their parameters like masses and coupling constants will also be measured (the precise measurements). Reflecting upon the results far obtained here, in a strong contrast to such theories the unbroken MW-SUSY is implemented on the MW-SMM: SG_N by, at first, lifting up $G_\eta \to SG_\eta$ and consequently making an inverse passage to the $\not{S}G_N$ $(SG_\eta \to G_\eta)$ on which the resulting theory M$\not{S}$MSM is defined. Applying the final passage $(G_\eta \to M_4)$ we arrive to the final VMSM, where only the particles will survive on the M_4 at the real physical limit under the R-parity conservation. Thus,

• *all the sparticles never could emerge in the M_4 neither at TeV range nor at any energy range at all.*

From the view point of achieving the final potentially realistic supersymmetric field theory this will be third crucial test in experiments above for verifying the efforts made either in MSSM model building (the conventional SUSY theories) or in suggested VMSM (the MW-SUSY), which are based on two quite different approaches. To sum up the discussion thus far, we have argued that, in strong contrast to conventional SUSY theories, if the VMSM given here proves viable it becomes an crucial issue to hold in experiments the above-mentioned three tests.

13.7. A brief outlook

Let us give a brief outlook on the key points of physical picture described in this subsection. We derive the MW-SUSY, which has an algebraic origin in the sense that it has arisen from the subquark algebra defined on the internal worlds, while the nilpotent supercharge operators are derived. Therefore, the MW-SUSY realized only on the internal worlds but not on the spacetime continuum.

doi: 10.52526/25792776-2021.68.2-311

Thus, it cannot be an exact symmetry of nature and has to be realized in its broken phase. Our purpose above is much easier to handle, by restoring in the first the `exact´ MW-SUSY. It can be achieved by lifting up each sparticle to corresponding particle state. This enables the sparticle to be included in the same supermultiplet with corresponding particle. Due to different features of particles and sparticles when passing back to physically realistic limit, one must have always to distinguish them by introducing an additional discrete internal symmetry, i.e., the multiplicative Z_2 R-parity.

We write then the most generic renormalizable MW-SUSY action involving gauge and supersymmetric matter frame fields, and, thus, the corresponding generating functional. Therein, we are led to the principal point of drastic change of the standard SUSY scheme to specialize the superpotential to be in such a form, which enables the microscopic approach to the key problems of particle phenomenology.

The realistic generating functional should be derived by passing back to the physical limit. Such a breaking of the MW-SUSY can be implemented by subtracting back all the explicit soft mass terms formerly introduced for the sparticles. These terms do not reintroduced the quadratic diagrams which motivated the introduction of SUSY framework. Therewith, the boson-fermion cancellation in the above-mentioned problems can be regarded as a consequence of a constraint stemming from holomorphy of the observables, therefore it will be held at the realistic physical limit too. Thus, we extract the pertinent piece containing only the η-field components and then in afterwards pass to M_4 to get the final VMSM yielding the realistic particle spectrum.

Thus, if the VMSM proves viable it becomes an crucial issue to hold in the current experiments three testable solid implications, which are drastically different from those of conventional MSSM models.

The implication of quarks into the VMSM is carried out in the same way of leptons except that of appearance of quark mixing with Cabibbo angle and the existence of CP-violating complex phase in unitary matrix of quark mixing. The Q-components of the quarks contain at least one identical subquark, due to which the partial formfactors gain nonzero values. This underlies the quark mixing with Cabibbo angles. In lepton's case these formfactors are vanished and lepton mixing is absent. The CP-violation stems from the spanning. Adopting a simple viewpoint on Higgs sector the masses of leptons and quarks are given.

We hope that the outlined VMSM, if it proves viable in the current experiments, will be an attractive basis for the future theories. As yet no direct signal has been found in them, the absent of which has been cleared up the lower limits on Higgs bosons and sparticles masses.

14. Spacetime deformation induced inertia effects

The principle of inertia, whose origin can be traced back to the works developed by Galileo and Newton, is one of the fundamental principles of the classical mechanics. This governs the *uniform motion* of a body and describes how it is affected by applied forces. The universality of gravitation and inertia attribute to the geometry but as having a different natures. However, despite the advocated success of general relativity (GR), the problem of inertia stood open and that this is still an unknown exciting problem to be challenged. The inertia effects cannot be in full generality identified with gravity within GR as it was proposed by Einstein in 1918, because there are many experimental controversies to question the validity of such a description, for details see e.g. (Ter-Kazarian, 2012) and references therein. The universality of the gravitation and inertia attributes to the *weak* principle of equivalence (WPE), which establishes the independence of free-fall trajectories of the internal composition and structure of bodies. Currently, the observations performed in the Earth-Moon-Sun system, or at galactic and cosmological scales, make it possible to probe the fundamental issue of gravitation/inertia more deeply by imposing the constraints of various analyses. The inertia effects in fact are of vital interest also for the phenomenological aspects of the long-standing problem of neutrino oscillations. All this variety has evoked the study of the inertial effects in an accelerated and rotated frame of stationary laboratories on Earth, relative to the local inertial frames. The standard extension of Lorentz invariance to accelerated observers in Minkowski spacetime is based on the hypothesis of locality, which in effect replaces the accelerated observer by a continuous infinity of

doi: 10.52526/25792776-2021.68.2-311

hypothetical momentarily comoving inertial observers along its wordline. This assumption, as well as its restricted version, so-called, clock hypothesis, which is a hypothesis of locality only concerned about the measurement of time, are reasonable only if the curvature of the wordline could be ignored. This question has become a major preoccupation of physicists. As long as all relevant length scales in feasible experiments are very small in relation to the huge acceleration lengths of the tiny accelerations we usually experience, the differences between observations by accelerated and comoving inertial observers will also be very small. However this works out, it is still reminds us of a puzzling underlying reality of the phenomenon of inertia. Beyond the WPE, there is nothing convincing in the basic postulates of physics for the origin and nature of inertia to decide on the issue.

On the other hand it seems that the inertia effects display no any physical characteristics of gravitation, because there are important reasons to question the validity of such a description. For example, there are a few experiments which tested the key question of anisotropy of inertia stemming from the idea that the matter in our galaxy is not distributed isotropically with respect to the earth, and hence if the inertia is due to gravitational interactions, then the inertial mass of a body will depend on the direction of its acceleration with respect to the direction towards the center of our galaxy. If the nuclear structure of Li^7 is treated as a single $P_{3/2}$ proton in a central nuclear potential, the variation Δm of mass with direction, if it exists, was found to satisfy $\frac{\Delta m}{m} \leq 10^{-20}$. This proves that there is no anisotropy of mass which is due to the effects of mass in our galaxy. Moreover, unlike gravitation, a curvature arisen due to acceleration of coordinate frame of interest, i.e. a `fictitious gravitation´ which can be globally removed by appropriate coordinate transformations, relates to this coordinate system itself and does not affect at once all the other systems or matter fields. Despite our best efforts, all attempts to obtain a true knowledge of the inertial effects and the geometry related to the noninertial reference frames of an arbitrary observer seem doomed, unless we find *a physical principle the inertia might refer to*, and construct the *relativistic theory of inertia*. Otherwise one wanders in a darkness.

It is the purpose of present section to carry out some details of the program of spacetime deformation theory to probe the origin and nature of the phenomenon of inertia. We ascribe the inertia effects to the geometry itself but as having a nature other than gravitation. To this aim, we propose a hypothetical space-companion to every particle. We explore the 2D, so-called, *master-space* (MS), subject to certain rules. The MS, embedded in the background 4D-space, is an indispensable individual companion to the particle of interest, without relation to the other matter. This notion is quite intuitive; in essence, it says that the particle apparently just has to live with MS-companion as an intrinsic property. This together with the heuristic idea that the inertia effects arise as a deformation/(distortion of local internal properties) of MS, are the highlights of the present paper. We will be brief and often ruthlessly suppress the indices without notice. Unless otherwise stated we take natural units, $h = c = 1$.

14.1. The hypothetical flat MS-companion: a toy model

As a preliminary step we now conceive of two different spaces, one would be 4D background Minkowski space, M_4, and another one should be MS embedded in the M_4, which is an indispensable individual companion to the particle, without relation to the other matter. The flat MS in suggested model is assumed to be 2D Minkowski space, M_2: $M_2 = R^1_{(+)} \oplus R^1_{(-)}$. The ingredient 1D-space R^1_A is spanned by the coordinates η^A, where we use the *naked* capital Latin letters $A, B, ... = (\pm)$ to denote the world indices related to M_2. The metric in M_2 is $\overline{g} = \overline{g}(\overline{e}_A, \overline{e}_B)\, \overline{\vartheta}^A \otimes \overline{\vartheta}^B$, where $\overline{\vartheta}^A = d\eta^A$ is the infinitesimal displacement. The basis $\overline{e}_A$ at the point of interest in M_2 consists of two real *null vectors*: $\overline{g}(\overline{e}_A, \overline{e}_B) \equiv < \overline{e}_A, \overline{e}_B >= {}^*o_{AB}$. The norm, $i\overline{d} \equiv d\hat{\eta}$, given in this basis reads $i\overline{d} = \overline{e}\overline{\vartheta} = \overline{e}_A \otimes \overline{\vartheta}^A$, where $i\overline{d}$ is the tautological tensor field of type (1,1), $\overline{e}$ is a shorthand for the collection of the 2-tuplet $(\overline{e}_{(+)}, \overline{e}_{(-)})$. We may equivalently use a temporal $q^0 \in T^1$ and a spatial $q^1 \in R^1$ variables $q^r(q^0, q^1)(r = 0, 1)$, such that $M_2 = R^1 \oplus T^1$. The norm, $i\overline{d}$, now can be rewritten in terms of displacement, dq^r, as $i\overline{d} = d\hat{q} = e_0 \otimes dq^0 + e_1 \otimes dq^1$, where e_0 and e_1 are, respectively, the temporal and spatial basis vectors. Then, a smooth map $f: \ M_2 \to M_4$ is defined to be an immersion- an embedding is a function that is a homeomorphism onto its image. In fact, we assume the particle has

doi: 10.52526/25792776-2021.68.2-311

to be moving simultaneously in the parallel *individual* M_2 space and the ordinary 4D background space (either Minkowskian or Riemannian). Let the non-accelerated observer uses the inertial coordinate frame $S_{(2)}$ for the position q^r of a free test particle in the flat M_2. We may choose the system $S_{(2)}$ in such a way as the time axis e_0 lies along the time axis of a comoving inertial frame S_4, such that the time coordinates in the two systems are taken the same, $q^0 = t$. Hence, given the inertial frames $S_{(4)}$, $S'_{(4)}$, $S''_{(4)}$,... in the M_4, in this manner we may define the corresponding inertial frames $S_{(2)}$, $S'_{(2)}$, $S''_{(2)}$,... in the M_2. Continuing on our quest, we next define the concepts of *absolute* and *relative* states of the ingredient spaces R^1_A. The measure for these states is the very magnitude of the velocity components v^A of the particle: *Definition:* The ingredient space R^1_A of the *individual MS-companion* of the particle is said to be in *absolute (abs) state* if $v^A = 0$, and in *relative (rel) state* if $v^A \neq 0$. Therefore, the MS can be realized either in the *semi-absolute* state (rel, abs), or (abs, rel), or in the *total relative* state (rel, rel). It is remarkable that the *total-absolute* state, (abs, abs), which is equivalent to the unobservable Newtonian *absolute* two-dimensional spacetime, cannot be realized because of the relation $v^{(+)} + v^{(-)} = \sqrt{2}$. An existence of the *absolute* state of the R^1_A is an immediate cause of the light traveling in empty space R^1 along the q-axis with a maximal velocity $v_q = c$ (we re-instate the factor (c)) in the $(+)-$direction corresponding to the state $(v^{(+)}, 0) \Leftrightarrow$ (rel, abs), and in the $(-)-$direction corresponding to the state $(0, v^{(-)}) \Leftrightarrow$ (abs, rel). The *absolute* state of R^1_A manifests its *absolute* character in the important for SR fact that the resulting velocity of light in the empty space R^1 is the same in all inertial frames $S_{(2)}$, $S'_{(2)}$, $S''_{(2)}$,..., i.e., in empty space light propagates independently of the state of motion of the source - if $v^A = 0$ then $v^{A\prime} = v^{A\prime\prime} = ... = 0$. This observation allows us to lay forth the *RLI-Conjecture: The non-zero local rate $\varrho(\eta, m, f)$ of instantaneously change of a constant velocity v^A (both magnitude and direction) of a massive (m) test particle under the unbalanced net force $(\vec{f})$ is the immediate cause of a deformation/(distortion of the local internal properties) of MS: $M_2 \to \widetilde{\mathcal{M}}_2$.* The MS-companion is not measurable directly, but in going into practical details, we will determine the function $\varrho(\eta, m, \vec{f})$ and show that a deformation/(distortion of local internal properties) of MS is the origin of inertia effects that can be observed by us.

14.2. Model building in the 4D background Minkowski spacetime

At first, we construct the RTI when the relativistic test particle accelerated in the Minkowski 4D background flat space, M_4, under an unbalanced net force other than gravitational. It proves necessary to provide, further, a constitutive ansatz of simple, yet tentative, linear *distortion transformations*, which, according to RLI-Conjecture, can be written in terms of *local rate* $\varrho(\eta, m, f)$ of instantaneously change of the measure v^A of massive (m) test particle under the unbalanced net force (f): $e_{(\tilde{+})}(\varrho) = D^{\ B}_{(\tilde{+})}(\varrho)\,\overline{e}_B = \overline{e}_{(+)} - \varrho(\eta, m, f)\,v^{(-)}\,\overline{e}_{(-)}$, and $e_{(\tilde{-})}(\varrho) = D^{\ B}_{(\tilde{-})}(\varrho)\,\overline{e}_B = \overline{e}_{(-)} + \varrho(\eta, m, f)\,v^{(+)}\,\overline{e}_{(+)}$. Clearly, these transformations imply a violation of the relation $e^2_{\tilde{A}}(\varrho) \neq 0$ for the null vectors $\overline{e}_A$. We parameterize the deformation tensor $\Omega_B^{\ A}$ in terms of the parameters τ_1 and τ_2 as $\Omega^{\ (+)}_{(+)} = \Omega^{\ (-)}_{(-)} = \tau_1(1 + \tau_2\,\overline{\varrho}^2)$, $\quad \Omega^{\ (-)}_{(+)} = -\tau_1(1 - \tau_2)\varrho v^{(-)}$, $\quad \Omega^{\ (+)}_{(-)} = \tau_1(1 - \tau_2)\varrho v^{(+)}$, where $\overline{\varrho}^2 = v^2\varrho^2$, $\quad v^2 = v^{(+)}v^{(-)} = 1/2\gamma_q^2$ and $\gamma_q = (1 - v_q^2)^{-1/2}$. Suppose a second observer, who makes measurements using a frame of reference $\widetilde{S}_{(2)}$ which is held stationary in deformed/distorted space $\widetilde{\mathcal{M}}_2$, uses for the test particle the corresponding spacetime coordinates $\widetilde{q}^{\tilde{r}}((\widetilde{q}^{\tilde{0}}, \widetilde{q}^{\tilde{1}}) \equiv (\widetilde{t}, \widetilde{q}))$. This gives the general transformation equations for spatial and temporal coordinates as follows ($\vec{e}_q \equiv e_1$, $q \equiv q^1$): $d\widetilde{t} = \tau_1\, dt$, $\quad d\widetilde{q} = \tau_1 \left[dq(1 + \frac{\tau_2\varrho v_q}{\sqrt{2}}) - \frac{\tau_2\varrho}{\sqrt{2}}dt\right] = \tau_1\,(dq - \frac{\tau_2\varrho}{\sqrt{2}\gamma_q^2}dt)$. The difference of the vector, $d\hat{q} \in M_2$, and the vector, $d\widetilde{\hat{q}} \in \widetilde{\mathcal{M}}_2$, can be interpreted by the second observer as being due to the deformation/distortion of flat space M_2. However, this difference with equal justice can be interpreted by him as a definite criterion for the *absolute* character of his own state of acceleration in M_2, rather than to any absolute quality of a deformation/distortion of M_2. To prove this assertion, note that the transformation equations give a reasonable change at low velocities $v_q \simeq 0$, as $d\widetilde{t} = \tau_1\, dt$, $\quad d\widetilde{q} \simeq \tau_1\,(dq - \frac{\tau_2\varrho}{\sqrt{2}}dt)$. This becomes conventional transformation equations to accelerated $(a_{net} \neq 0)$ axes if we assume $d(\tau_2\varrho)/\sqrt{2}dt = a_{net}$ and $\tau_1(v_q \simeq 0) = 1$, where a_{net} is a magnitude of proper net acceleration. In high velocity limit $v_q \simeq 1$, $\ \overline{\varrho} \simeq 0$, $(d\eta^{(-)} = v^{(-)}dt \simeq 0$, $\ v^{(+)} \simeq v \simeq \sqrt{2})$, we have $d\widetilde{t} = \tau_1\, dt \simeq \tau_1\, dq \simeq d\widetilde{q}$.

doi: 10.52526/25792776-2021.68.2-311

To this end, the inertial effects become zero. Let $\vec{a}_{net}$ be a local net 3-acceleration of an arbitrary observer with proper linear 3-acceleration $\vec{a}$ and proper 3-angular velocity $\vec{\omega}$ measured in the rest frame: $\vec{a}_{net} = \frac{d\vec{u}}{ds} = \vec{a} \wedge \vec{u} + \vec{\omega} \times \vec{u}$, where $\mathbf{u}$ is the 4-velocity. A magnitude of $\vec{a}_{net}$ can be computed as the simple invariant of the absolute value $|\frac{d\mathbf{u}}{ds}|$ as measured in rest frame: $|\mathbf{a}| = |\frac{d\mathbf{u}}{ds}| = (\frac{du^l}{ds}, \frac{du_l}{ds})^{1/2}$. We may introduce the very concept of the local *absolute acceleration* (in Newton's terminology) brought about via the Fermi-Walker transported frames as $\vec{a}_{abs} \equiv \vec{e}_q \frac{d(\tau_2 \varrho)}{\sqrt{2} ds_q} = \vec{e}_q\, |\frac{de_{\hat{0}}}{ds}| = \vec{e}_q\, |\mathbf{a}|$, where we choose the system $S_{(2)}$ in such a way as the axis $\vec{e}_q$ lies along the net 3-acceleration $(\vec{e}_q \,||\, \vec{e}_a)$, $\quad (\vec{e}_a = \vec{a}_{net}/|\vec{a}_{net}|)$. Hereinafter, we may simplify the flat-deformation tensor $\Omega_A{}^B$ by setting $\tau_2 = 1$, such that $\Omega_{(+)}{}^{(+)} = \Omega_{(-)}{}^{(-)} \equiv \Omega(\overline{\varrho}) = 1 + \overline{\varrho}^2$, $\quad \Omega_{(+)}{}^{(-)} = \Omega_{(-)}{}^{(+)} = 0$, and the general metric in $\widetilde{\mathcal{M}}_2$ reads $d\widetilde{s}_q^2 = \Omega^2(\overline{\varrho})\, ds_q^2$. Hence $\varrho = \sqrt{2}\int_0^{s_q} |\mathbf{a}| ds'_q$. Then we obtain the key relation between a so-called *inertial acceleration*, arisen due to the curvature of MS, $\vec{a}_{in} = \vec{e}_a\, a_{in}$, $\quad a_{in} = \frac{d^2\widetilde{q}}{d\widetilde{s}_q^2} = -\Gamma^1_{\tilde{r}\tilde{s}}(\varrho) \frac{d\widetilde{q}^{\tilde{r}}}{d\widetilde{s}_q} \frac{d\widetilde{q}^{\tilde{s}}}{d\widetilde{s}_q} = \frac{1}{\sqrt{2}}(\frac{d^2\widetilde{\eta}^{(+)}}{d\widetilde{s}_q^2} - \frac{d^2\widetilde{\eta}^{(-)}}{d\widetilde{s}_q^2})$, and a local *absolute acceleration* as follows: $\Omega^2(\overline{\varrho})\, \gamma_q\, \vec{a}_{in} = -\vec{a}_{abs}$, where $\Gamma^1_{\tilde{r}\tilde{s}}(\varrho)$ are the Christoffel symbols constructed by the metric. This provides a quantitative means for the *inertial force* $\vec{f}_{(in)}$: $\vec{f}_{(in)} = m\vec{a}_{in} = -m\,\Gamma^1_{\tilde{r}\tilde{s}}(\varrho) \frac{d\widetilde{q}^{\tilde{r}}}{d\widetilde{s}_q} \frac{d\widetilde{q}^{\tilde{s}}}{d\widetilde{s}_q} = -\frac{m\vec{a}_{abs}}{\Omega^2(\overline{\varrho})\,\gamma_q}$. Thus, it takes force to disturb an inertia state, i.e. to make the *absolute acceleration* $(\vec{a}_{abs} \neq 0)$. The *absolute acceleration* is due to the real deformation/distortion of the space M_2. The *relative* $(d(\tau_2\varrho)/ds_q = 0)$ acceleration (in Newton's terminology) (both magnitude and direction), to the contrary, has nothing to do with the deformation/distortion of the space M_2 and, thus, it cannot produce an inertia effects.

14.3. Beyond the hypothesis of locality

The hypothesis of locality represents strict restrictions, because in other words, it approximately replaces a noninertial frame of reference $\widetilde{S}_{(2)}$, which is held stationary in the deformed/distorted space $\widetilde{\mathcal{M}}_2 \equiv V_2^{(\varrho)}\ (\varrho \neq 0)$, with a continuous infinity set of the inertial frames $\{S_{(2)}, S'_{(2)}, S''_{(2)}, ...\}$ given in the flat $M_2\,(\varrho = 0)$. In this situation the use of the hypothesis of locality is physically unjustifiable. Therefore, it is worthwhile to go beyond the hypothesis of locality with special emphasis on distortion of MS, which we might expect will essentially improve the standard results. Therefore, our strategy now is to deform the metric by carrying out an additional deformation of semi-Riemannian 4D background space $V_4^{(0)} \rightarrow \widetilde{\mathcal{M}}_4 \equiv V_4^{(\varrho)}$, which, as a corollary, will recover the complete metric $g\quad (\varrho \neq 0)$ of the distorted MS- $V_2^{(\varrho)}$. The resulting deformed metric of the space $V_4^{(\varrho)}$ can be split as $g_{\mu\nu}(\varrho) = \Upsilon^2(\varrho)\, \breve{g}_{\mu\nu} + \gamma_{\mu\nu}(\varrho)$, provided $\gamma_{\mu\nu}(\varrho) = [\gamma_{\hat{a}\hat{b}} - \Upsilon^2(\varrho)\, o_{\hat{a}\hat{b}}]\, \breve{e}^{\hat{a}}{}_{\mu}\, \breve{e}^{\hat{b}}{}_{\nu}$, $\quad \gamma_{\hat{c}\hat{d}} = o_{\hat{a}\hat{b}}\, \pi_{\hat{c}}{}^{\hat{a}}\, \pi_{\hat{d}}{}^{\hat{b}}$, where $\Upsilon(\varrho) = \pi^{\hat{a}}_{\hat{a}}(\varrho)$ and $\gamma_{\hat{a}\hat{b}}(\breve{x})$ are the second deformation matrices. Hence, in general, the metric $g(\varrho)$ is decomposed in the form $g(\varrho) = \pi^2(\varrho)\, \breve{g} + \gamma(\varrho)$, where $\gamma(\varrho) = \gamma_{\mu\nu}(\varrho)\, d\breve{x}^\mu \otimes d\breve{x}^\nu$ and $\Upsilon(\varrho) = \pi^{\hat{a}}_{\hat{a}}(\varrho) = \pi(\varrho)$. A *generalized transport* for deformed frame $e_{\hat{a}}$, which includes both the Fermi-Walker transport and distortion of MS, can be written in the form $\frac{de^{\mu}{}_{\hat{a}}}{ds} = \widetilde{\Phi}_a{}^b\, e^{\mu}{}_{\hat{b}}$, where a *deformed acceleration tensor* $\widetilde{\Phi}_a{}^b$ concisely is given by $\widetilde{\Phi} = (d\,\ln\pi/ds) + \pi\,\Phi\,\pi^{-1}$.

14.4. Involving the background semi-Riemann space V_4

We can always choose *natural coordinates* $X^\alpha(T, X, Y, Z) = (T, \vec{X})$ with respect to the axes of the local free-fall coordinate frame $S_4^{(l)}$ in an immediate neighbourhood of any spacetime point $(\breve{x}_p) \in V_4$ in question of the background semi- Riemann space, V_4, over a differential region taken small enough so that we can neglect the spatial and temporal variations of gravity for the range involved. The values of the metric tensor $\breve{g}_{\mu\nu}$ and the affine connection $\breve{\Gamma}^\lambda_{\mu\nu}$ at the point $(\breve{x}_p)$ are necessarily sufficient information for determination of the natural coordinates $X^\alpha(\breve{x}^\mu)$ in the small region of the neighbourhood of the selected point. Then the whole scheme outlined above should hold in the frame $S_4^{(l)}$. The relativistic gravitational force $\breve{f}^\mu_g(\breve{x})$ exerted on the test particle of the mass (m) is given by $\breve{f}^\mu_g(\breve{x}) = m\frac{d^2\breve{x}^\mu}{d\breve{s}^2} = -m\breve{\Gamma}^\mu_{\nu\lambda}(a) \frac{d\breve{x}^\nu}{d\breve{s}} \frac{d\breve{x}^\lambda}{d\breve{s}}$. The frame $S_4^{(l)}$ will be valid if only the gravitational force given in this coordinate frame $f^\alpha_{g(l)} = \frac{\partial X^\alpha}{\partial \breve{x}^\mu} f^\mu_g$, could be removed by the inertial force. Whereas, as before, the two systems S_2 and $S_4^{(l)}$ can be chosen in such a way as the axis $\vec{e}_q$ of $S_{(2)}$ lies $(\vec{e}_q = \vec{e}_f)$ along the

doi: 10.52526/25792776-2021.68.2-311

acting net force $\vec{f} = \vec{f}_{(l)} + \vec{f}_{g(l)}$, where $\vec{f}_{(l)}$ is the SR value of the unbalanced relativistic force other than gravitational in the frame $S_4^{(l)}$, while the time coordinates in the two systems are taken the same, $q^0 = t = X^0 = T$. We now may write $\frac{1}{\sqrt{2}}\frac{d(\tau_2 \varrho)}{ds_q} = \frac{1}{m}|f^\alpha_{(l)} + f^\alpha_{g(l)}|$, such that the general *inertial force* reads $\breve{\vec{f}}_{(in)} = m\vec{a}_{in} = -\frac{m\vec{a}_{abs}}{\Omega^2(\overline{\varrho})\gamma_q} = -\frac{\vec{e}_f}{\Omega^2(\overline{\varrho})\gamma_q}|f^\alpha_{(l)} - m\frac{\partial X^\alpha}{\partial \breve{x}^\sigma}\breve{\Gamma}^\sigma_{\mu\nu}\frac{d\breve{x}^\mu}{dS}\frac{d\breve{x}^\nu}{dS}|$. Despite of totally different and independent sources of gravitation and inertia, at $f^\alpha_{(l)} = 0$, this establishes independence of free-fall ($v_q = 0$) trajectories of the mass, internal composition and structure of bodies. This furnishes a justification for the introduction of the WPE. A remarkable feature is that, although the inertial force has a nature different than the gravitational force, nevertheless both are due to a distortion of the local inertial properties of, respectively, 2D MS and 4D-background space.

14.5. The principle of equivalence in the RC space

The RC manifold, U_4, is a particular case of general metric-affine manifold $\widetilde{M}_4$, restricted by the metricity condition $N_{ab} = 0$, when a nonsymmetric linear connection, Γ, is said to be metric compatible. To avoid any possibility of confusion, here and throughout we again use the first half of Latin alphabet $(a, b, c, ... = 0, 1, 2, 3$ rather than $(\pm))$ now to denote the anholonomic indices referred to the tangent space, which is endowed with the Lorentzian metric $o_{ab} := diag(+---)$. The space, U_4, also locally has the structure of M_4. In the case of the RC space there also exist orthonormal reference frames which realize an `anholonomic´ free-fall elevator. That is, for any single point $P \in U_4$, there exist coordinates $\{x^\mu\}$ and an orthonormal frame $\{e_a\}$ in a neighborhood of P such that $e_a = \delta^\mu_a\,\partial_{x^\mu}$, and ${\Gamma_a}^b = 0$ at P, where ${\Gamma_a}^b$ are the connection 1-forms referred to the frame $\{e_a\}$. Therefore the existence of torsion does not violate the PE. Suppose that we have a tetrad $\{e_a(x)\}$ at the point P, and a tetrad $\{e_a(x + d\,x)\}$ at another point in a neighbourhood of P; then, we can apply a suitable Lorentz rotation to $e_a(x + d\,x)$, so that it becomes parallel to $e_a(x)$. Given a vector v at P, it follows that the components $v_c = v \cdot e_c$ do not change under parallel transport from x to $x + d\,x$, provided the metricity condition holds. Hence, the connection coefficients ${\omega^{ab}}_\mu(x)$ at P, defined with respect to this particular tetrad field, vanish: ${\omega^{ab}}_\mu(P) = 0$. This property is compatible with $g'_{ab} = o_{ab}$, since Lorentz rotation does not influence the value of the metric at a given point. In more general geometries, where the symmetry of the tangent space is higher than the Poincare group, the usual form of the PE is violated and local physics differs from SR. Taking this into account, we derive a general expression of the relativistic inertial force exerted on the extended spinning body moving in the Rieman-Cartan space (Ter-Kazarian, 2012).

15. Probing the inertia behind SUSY

The model discussed in previous section illustrates the problems of inertia effects described in the framework of classical physics, but it also hints at a possible complete solution. We will use this model as a backdrop to explore first the SLC in a new perspective of rigid double transformations of, so-called, *master space-induced* supersymmetry (MS-SUSY), subject to certain rules (Ter-Kazarian, 2013b). The theories with extended $N_{max} = 4$ supersymmetries, namely $N = 4$ super-Yang-Mills theories, if only such symmetries are fundamental to nature, lead to the model of ELC in case of the apparent violations of SLC, the possible manifestations of which arise in a similar way in all particle sectors. We show that in the ELC-framework the propagation of the superluminal particle could be consistent with causality, and give a justification of forbiddance of Vavilov-Cherenkov radiation/or analog processes in vacuum. However, we must be careful about the physical relevance of the standard theory of extended supersymmetry which does not allow for chiral fermions, and that its spectrum in no way resembles that of the observed in nature. Consequently, in the framework of local MS-SUSY, we address the *accelerated motion*, while, unlike gravitation, a curvature of space-time now arises entirely due to the inertial properties of the Lorentz-rotated frame of interest, i.e. a *fictitious gravitation* which can be globally removed by appropriate coordinate transformations. The only source of graviton and gravitino, therefore, is the acceleration of a particle.

doi: 10.52526/25792776-2021.68.2-311

15.1. A background `motion´ space $\underline{M}$

With regard now to our original question as to the understanding of the physical processes that underly the *motion*, we tackle the problem in the framework of quantum field theory (Ter-Kazarian, 2013b). Let us consider functional integrals for a quantum-mechanical system with one degree of freedom. Denote by $x(t)$ the position operator in the Heisenberg picture, and by $|x, t>$ its eigenstates. The probability amplitude that a particle which was at x at time t will be at point x' at time t', also called the Schwinger transformation function for these points, is $F(x't'; xt) =< x't'\,|xt>$. For a particle moving through the two infinitesimally closed points of original space, this in somehow or other implies the elementary act consisting of the *annihilation* of a particle at the point x and time t and, subsequently, its *creation* at the point x' and time t'. The particle can move with different velocities which indicates to existence of the intermediate, so-called, *motion* state. Then the *annihilation* of a particle at point x and time t can intuitively be understood as the transition from the initial state $|x, t>$ to the intermediate *motion* state, $|\underline{x}, \underline{t}>$, yet unknown, where $\underline{x}(\underline{t})$ represent atomic element of idealized *motion* point event. Meanwhile, the *creation* of a particle at infinitesimally closed final point x' and time t' means the subsequent transition from the intermediate *motion* state, $|\underline{x}, \underline{t}>$, to the final state, $|x', t'>$. So, the Schwinger transformation function for two infinitesimally closed points is written in terms of annihilation and creation processes of a particle as $F(x't'; xt) = \int d\underline{x} < x't'\,|\underline{x}\,\underline{t}>< \underline{x}\,\underline{t}\,|xt>$. It should be emphasized that since we do not understand the phenomenon of *motion*, then here it must suffice to expect that the state functions $|x, t>$ and $|\underline{x}, \underline{t}>$ are quite different. Therefore, the intermediate *motion* state, $|\underline{x}, \underline{t}>$, can be defined on say *motion* space, $\underline{M}$, the points $\underline{x}(\underline{t})$ of which are all the *motion* atomic elements, $(\underline{x}(\underline{t}) \in \underline{M})$. To express Schwinger transformation function, F, as a path integral, we divide the finite time interval into $n+1$ intervals: $t = t_0, t_1, \ldots, t_{n+1} = t'$; $t_k = t_0+k\varepsilon$, where ε can be made arbitrarily small by increasing n. In the limit $n \to \infty$, F becomes an operational definition of the path integral. Hence, in general, in addition to background 4D Minkowski space M_4, also a background *motion* space $\underline{M}$, or say *master space*, MS $(\equiv \underline{M})$ is required. So, we now conceive of the two different spaces M_4 and MS, where the geometry of MS is a new physical entity, with degrees of freedom and a dynamics of its own. The above example imposes a constraint upon MS that it was embedded in M_4 as an indispensable individual companion to the particle, without relation to the other matter. In going into practical details, we further adopt the model discussed in previous section, which illustrates the problems of inertia effects, but it also hints at a possible solution. In accord, MS is not measurable directly, but it was argued that a deformation of MS is the origin of inertia effects that can be observed by us. We will not be concerned with the actual details of this model here, but only use it as a backdrop to study the *motion* of a particle. In general case of 3D motion in M_4, a flat MS is the 2D Minkowski space $\underline{M}_2$. In deriving the final step, we should compare and contrast the particle states of quantum fields defined on the background spaces M_4 and $\underline{M}_2$, forming a basis in the Hilbert space. It is quite clear that the following properties, being the essence of the chain of transformations for the finite time interval, hold:

1. There should be a particular way of going from each point $x_{i-1}(t_{i-1}) \in M_4$ to the intermediate *motion* point $\underline{x}_{i-1}(\underline{t}_{i-1}) \in \underline{M}_2$ and back $x_i(t_i) \in M_4$, such that the net result of each atomic double transformations is as if we had operated with a space-time *translation* on the original space M_4. So, the symmetry we are looking for must mix the particle quantum states during the motion in order to reproduce the central relationship between the two successive transformations of this symmetry and the generators of space-time translations. Namely, the subsequent operation of two finite transformations will induce a translation in space and time of the states on which they operate.

2. These successive transformations induce in M_4 the inhomogeneous Lorentz group, or Poincaré group, and that an unitary linear transformation $|x, t>\to U(\Lambda, a)|x, t>$ on vectors in the physical Hilbert space.

Thus, the underlying algebraic structure of this symmetry generators closes with the algebra of *translations* on the original space M_4 in a way that it can then be summarized as a non-trivial extension of the Poincaré group algebra, including the generators of translations. The only symmetry possessing such properties is the SUSY, which is accepted as a legitimate feature of nature, although it has never been experimentally observed. Certainly we now need to modify the standard theory to have MS-SUSY, involving a superspace which is an enlargement of a direct sum of background

doi: 10.52526/25792776-2021.68.2-311

spaces $M_4 \oplus \underline{M}_2$ by the inclusion of additional fermion coordinates. Thereby an attempt will be made to treat the *uniform motion* of a particle as a complex process of the global (or rigid) MS-SUSY double transformations (Ter-Kazarian, 2013b). Namely a particle undergoes to *an infinite number of successive transitions from* M_4 *to* $\underline{M}_2$ *and back going permanently through fermion-boson transformations*, which can be interpreted as its *creation* and *annihilation* processes occurring in M_4 or $\underline{M}_2$. We derive the *Lorentz code* of motion in terms of spinors referred to MS. This allows to introduce the physical finite *time interval* between two events, as integer number of the *duration time* of atomic double transition of a particle from M_4 and back. While all the particles are living on M_4, their superpartners can be viewed as living on $\underline{M}_2$.

15.2. MS revisited

According to previous section, we assume that a flat MS is the 2D Minkowski space: $\underline{M}_2 = R^1_{(+)} \oplus R^1_{(-)}$. The ingredient 1D-space $R^1_{\underline{m}}$ is spanned by the coordinates $\eta^{\underline{m}}$. The following notational conventions are used throughout this paper: all magnitudes related to the space $\underline{M}_2$ will be underlined. In particular, the underlined lower case Latin letters $\underline{m}, \underline{n}, ... = (\pm)$ denote the world indices related to $\underline{M}_2$. The metric in $\underline{M}_2$ is $\underline{g} = \underline{g}(\underline{e}_{\underline{m}}, \underline{e}_{\underline{n}})\, \underline{\vartheta}^{\underline{m}} \otimes \underline{\vartheta}^{\underline{n}}$, where $\underline{\vartheta}^{\underline{m}} = d\eta^{\underline{m}}$ is the infinitesimal displacement. The basis $\underline{e}_{\underline{m}}$ at the point of interest in $\underline{M}_2$ is consisted of the two real *null vectors*: $\underline{g}(\underline{e}_{\underline{m}}, \underline{e}_{\underline{n}}) \equiv < \underline{e}_{\underline{m}}, \underline{e}_{\underline{n}} >= {}^*o_{\underline{m}\,\underline{n}}$, $\quad ({}^*o_{\underline{m}\,\underline{n}}) = \begin{pmatrix} 0 & 1 \\ 1 & 0 \end{pmatrix}$. The norm, $i\bar{d} \equiv d\hat{\eta}$, given in the basis reads $i\underline{d} = \underline{e}\underline{\vartheta} = \underline{e}_{\underline{m}} \otimes \underline{\vartheta}^{\underline{m}}$, where $i\underline{d}$ is the tautological tensor field of type (1,1), $\underline{e}$ is a shorthand for the collection of the 2-tuplet $(\underline{e}_{(+)}, \underline{e}_{(-)})$, and $\underline{\vartheta} = \begin{pmatrix} \underline{\vartheta}^{(+)} \\ \underline{\vartheta}^{(-)} \end{pmatrix}$. We may equivalently use a temporal $q^0 \in T^1$ and a spatial $q^1 \in R^1$ variables $q^r(q^0, q^1)(r = 0, 1)$, such that $\underline{M}_2 = R^1 \oplus T^1$. The norm, $i\underline{d}$, now can be rewritten in terms of displacement, dq^r, as $i\underline{d} = d\hat{q} = e_0 \otimes dq^0 + e_1 \otimes dq^1$, where e_0 and e_1 are, respectively, the temporal and spatial basis vectors: $e_0 = \frac{1}{\sqrt{2}}(\underline{e}_{(+)} + \underline{e}_{(-)})$, $e_1 = \frac{1}{\sqrt{2}}(\underline{e}_{(+)} - \underline{e}_{(-)})$, $\underline{g}(e_r, e_s) \equiv < e_r, e_s >= o_{rs}$, $(o_{rs}) = \begin{pmatrix} 1 & 0 \\ 0 & -1 \end{pmatrix}$. The $\underline{M}_2$-companion is smoothly (injective and continuous) embedded in the M_4. Suppose the position of the particle in the background M_4 space is specified by the coordinates $x^m(s)$ $(m = 0, 1, 2, 3)(x^0 = t)$ with respect to the axes of the inertial system $S_{(4)}$. Then, a smooth map $f:\ \underline{M}_2 \longrightarrow M_4$ is defined to be an immersion - an embedding which is a function that is a homeomorphism onto its image: $q^0 = \frac{1}{\sqrt{2}}(\eta^{(+)} + \eta^{(-)}) = t$, $q^1 = \frac{1}{\sqrt{2}}(\eta^{(+)} - \eta^{(-)}) = |\vec{x}|$. To motivate why is the MS two dimensional, we note that only two dimensional constructions of real *null vectors* are allowed as the basis at given point in MS, which can be embedded in the (3+1)-dimensional spacetime. This theory is mathematically somewhat similar to the more recent membrane theory, so the $\underline{M}_2$ can be viewed as 2D space living on the 4D world sheet. Given the inertial frame $S_{(4)}$ in M_4, we may define the corresponding inertial frame $S_{(2)}$ used by the non-accelerated observer for the position q^r of a free particle in flat $\underline{M}_2$. Thereby the time axes of the two systems $S_{(2)}$ and S_4 coincide in direction and that the time coordinates are taken the same, $q^0 = t$. For the case at hand, $v^{(\pm)} = \frac{d\eta^{(\pm)}}{dq^0} = \frac{1}{\sqrt{2}}(1 \pm v_q)$, $v_q = \frac{dq^1}{dq^0} = |\vec{v}| = |\frac{d\vec{x}}{dt}|$. So the particle may be viewed as moving simultaneously in M_4 and $\underline{M}_2$. Hence, given the inertial frames $S_{(4)}$, $S'_{(4)}$, $S''_{(4)}$,... in M_4, in this manner we may define the corresponding inertial frames $S_{(2)}$, $S'_{(2)}$, $S''_{(2)}$,... in $\underline{M}_2$. Suppose the elements of the Hilbert space can be generated by the action of field-valued operators $\phi(x)\,(\chi(x), A(x))$ $\ (x \in M_4)$, where $\chi(x)$ is the Weyl fermion and $A(x)$ is the complex scalar bosonic field defined on M_4, and accordingly, of field-valued operators $\underline{\phi}(\eta)\,(\underline{\chi}(\eta), \underline{A}(\eta))$ $\quad (\eta \in \underline{M}_2)$, where $\underline{\chi}(\eta)$ is the Weyl fermion and $\underline{A}(\eta)$ is the complex scalar bosonic field defined on $\underline{M}_2$, on a translationally invariant vacuum: $|x >= \phi(x)|0 >$, $\quad |x_1, x_2 >= \phi(x_1)\phi(x_2)|0 >$ $\quad$ referring to M_4, $|\eta >= \underline{\phi}(\eta)|0 >$, $\quad |\eta_1, \eta_2 >= \underline{\phi}(\eta_1)\underline{\phi}(\eta_2)|0 >$ $\quad$ referring to $\underline{M}_2$, etc. The displacement of the field takes the form $\phi(x_1 + x_2) = e^{ix_2^m P_m}\,\phi(x_1)\,e^{-ix_2^m P_m}$, $\underline{\phi}(\eta_1 + \eta_2) = e^{i\eta_2^{\underline{m}} \underline{P}_{\underline{m}}}\,\underline{\phi}(\eta_1)\,e^{-i\eta_2^{\underline{m}} \underline{P}_{\underline{m}}}$, where $P_m = i\partial_m$ is the generator of translations on quantum fields $\phi(x)$, and $\underline{P}_{\underline{m}} = i\underline{\partial}_{\underline{m}}$ is the generator of translations on quantum fields $\underline{\phi}(\eta) \equiv \underline{\phi}(t, q^1)$. According to the embedding map, the relation between the fields $\phi(x)$ and $\underline{\phi}(\eta)$ can be given by the a proper orthochronous Lorentz transformation. For a

doi: 10.52526/25792776-2021.68.2-311

field of spin-$\vec{S}$, the general transformation law reads $\phi'_\alpha(x') = M_\alpha{}^\beta\,\phi_\beta(x) = \exp(-\frac{1}{2}\theta^{mn}S_{mn})_\alpha{}^\beta\,\phi_\beta(x) = \exp(-i\vec{\theta}\cdot\vec{S} - i\vec{\zeta}\cdot\vec{K})_\alpha{}^\beta\,\phi_\beta(x)$, where $\vec{\theta}$ is the rotation angle about an axis $\vec{n}$ ($\vec{\theta} \equiv \theta\vec{n}$), and $\vec{\zeta}$ is the boost vector $\vec{\zeta} \equiv \vec{e}_v \cdot \tan h^{-1}\beta$, provided $\vec{e}_v \equiv \vec{v}/|\vec{v}|$, $\beta \equiv |\vec{v}|/c$, $\theta^i \equiv (1/2)\varepsilon^{ijk}\,\theta_k$ $(i, j, k = 1, 2, 3)$, and $\zeta^i \equiv \theta^{i0} = -\theta^{0i}$. The antisymmetric tensor $S_{mn} = -S_{nm}$, satisfying the commutation relations of the $SL(2.C)$, is the (finite-dimensional) irreducible matrix representations of the Lie algebra of the Lorentz group, and α and β label the components of the matrix representation space, the dimension of which is related to the spin $S^i \equiv (1/2)\varepsilon^{ijk}\,S_k$ of the particle. The spin $\vec{S}$ generates three-dimensional rotations in space and the $K^i \equiv S^{0i}$ generate the Lorentz-boosts. The fields of spin-zero ($\vec{S} = \vec{K} = 0$) scalar field $A(x)$ and spin-one $A^n(x)$, corresponding to the $(1/2.1/2)$ representation, transform under a general Lorentz transformation as $\underline{A}(\eta) = A(x)$, spin 0; $\underline{A}^m(\eta) = \Lambda^m{}_n\,A^n(x)$, spin 1, where the Lorentz transformation is written as $\Lambda^m{}_n(M) \equiv \frac{1}{2}\,Tr(\sigma_m M \sigma_n M^\dagger)$, provided, $\sigma^m \equiv (I_2, \vec{\sigma})$, $\vec{\sigma}$ are Pauli spin matrices. A two-component $(1/2, 0)$ Weyl fermion $\chi_\beta(x)$ transforms under Lorentz transformation, in accord to embedding map, as $\chi_\beta(x) \longrightarrow \underline{\chi}_\alpha(\eta) = (M_R)_\alpha{}^\beta\,\chi_\beta(x)$, $\alpha, \beta = 1, 2$ where the rotation matrix is given as $M_R = e^{i\frac{1}{2}\sigma_2\theta_2}e^{i\frac{1}{2}\sigma_3\theta_3}$. The matrix M_R corresponds to the rotation of an hermitian 2×2 matrix $p^n\sigma_n$: $p_q^m\sigma_m = M_R\,p^n\sigma_n\,M_R^\dagger$, by the angles θ_3 and θ_2 about the axes n_3 and n_2, respectively, where the standard momentum is $p^n \equiv m(ch\beta,\ sh\beta\sin\theta_2\cos\theta_3,\ sh\beta\sin\theta_2\sin\theta_3,\ sh\beta\cos\theta_2)$, and p_q^m is $p_q^m \equiv m(ch\beta,\ 0,\ 0,\ sh\beta)$. The two-component $(0, 1/2)$ Weyl spinor field is denoted by $\bar{\chi}^{\dot{\beta}}(x)$, and transforms as $\bar{\chi}^{\dot{\beta}}(x) \longrightarrow \underline{\bar{\chi}}^{\dot{\alpha}}(\eta) = (M_R^{-1})^{\dagger\dot{\alpha}}{}_{\dot{\beta}}\,\bar{\chi}^{\dot{\beta}}(x)$, $\dot{\alpha}, \dot{\beta} = 1, 2$ where we have used $(M^\dagger)^{\dot{\beta}}{}_{\dot{\alpha}} = (M^*)_{\dot{\alpha}}{}^{\dot{\beta}}$. The so-called \`dotted´ indices have been introduced to distinguish the $(0, 1/2)$ representation from the $(1/2, 0)$ representation. The "bar" over the spinor is a convention that this is the $(0, 1/2)$-representation. The infinitesimal Lorentz transformation matrices for the $(1/2, 0)$ and $(0, 1/2)$ representations, $M \simeq I_2 - \frac{i}{2}\vec{\theta}\cdot\vec{\sigma} - \frac{1}{2}\vec{\zeta}\cdot\vec{\sigma}$, for $(\frac{1}{2}, 0)$; $(M^{-1})^\dagger \simeq I_2 - \frac{i}{2}\vec{\theta}\cdot\vec{\sigma} + \frac{1}{2}\vec{\zeta}\cdot\vec{\sigma}$, for $(0, \frac{1}{2})$ give $S^{mn} = \sigma^{mn}$ for the $(1/2, 0)$ representation and $S^{mn} = \bar{\sigma}^{mn}$ for the $(0, 1/2)$ representation, where the bilinear covariants that transform as a Lorentz second-rank tensor read $(\sigma^{mn})_\alpha{}^\beta \equiv \frac{i}{4}(\sigma^m_{\alpha\dot{\alpha}}\,\bar{\sigma}^{n\dot{\alpha}\beta} - \sigma^n_{\alpha\dot{\alpha}}\,\bar{\sigma}^{m\dot{\alpha}\beta})$, $(\bar{\sigma}^{mn})^{\dot{\alpha}}{}_{\dot{\beta}} \equiv \frac{i}{4}(\bar{\sigma}^{m\dot{\alpha}\alpha}\,\sigma^n_{\alpha\dot{\beta}} - \bar{\sigma}^{n\dot{\alpha}\alpha}\,\sigma^m_{\alpha\dot{\beta}})$, provided $\bar{\sigma}^m \equiv (I_2; -\vec{\sigma})$, $(\sigma^{m\,*})_{\alpha\dot{\beta}} = \sigma^m_{\beta\dot{\alpha}}$ and $(\bar{\sigma}^{m\,*})^{\dot{\alpha}\beta} = \bar{\sigma}^{m\dot{\beta}\alpha}$.

15.3. MS-SUSY

As alluded to above (Ter-Kazarian, 2013b), a *creation* of a particle in $\underline{M}_2$ means its transition from M_4 to $\underline{M}_2$, while an *annihilation* of a particle in $\underline{M}_2$ means vice versa. The same interpretation holds for the *creation* and *annihilation* processes in M_4. Since all fermionic and bosonic states, taken together, form a basis in the Hilbert space, the basis vectors in the Hilbert space, therefore, can be written in the form $|\underline{n}_b,\, n_f >$ or $|n_b,\, \underline{n}_f >$, where the boson and fermion occupation numbers are n_b or $\underline{n}_b\,(= 0, 1, ..., \infty)$ and n_f or $\underline{n}_f\,(= 0, 1)$. So, we may construct the quantum operators, $(q^\dagger,\, \underline{q}^\dagger)$ and $(q,\, \underline{q})$, which replace bosons by fermions and fermions by bosons, respectively, $q^\dagger\,|\underline{n}_b,\, n_f > \longrightarrow |\underline{n}_b - 1,\, n_f + 1 >$, $q\,|\underline{n}_b,\, n_f > \longrightarrow\ |\underline{n}_b + 1,\, n_f - 1 >$, and that $\underline{q}^\dagger\,|n_b,\, \underline{n}_f > \longrightarrow\ |n_b - 1,\, \underline{n}_f + 1 >$, $\underline{q}\,|n_b,\, \underline{n}_f > \longrightarrow\ |n_b + 1,\, \underline{n}_f - 1 >$. This framework combines bosonic and fermionic states on the same footing, rotating them into each other under the action of operators q and $\underline{q}$. Consider two pairs of creation and annihilation operators $(b^\dagger,\, b)$ and $(f^\dagger,\, f)$ for bosons and fermions, respectively, referred to the background space M_4, as well as $(\underline{b}^\dagger,\, \underline{b})$ and $(\underline{f}^\dagger,\, \underline{f})$ for bosons and fermions, respectively, related to the background master space $\underline{M}_2$. Putting two operators in one $B = (\underline{b}$ or $b)$ and $F = (f$ or $\underline{f})$, the canonical quantization rules can be written most elegantly as $[B,\, B^\dagger] = 1$; $\{F,\, F^\dagger\} = 1$; $[B,\, B] = [B^\dagger,\, B^\dagger] = \{F,\, F\} = \{F^\dagger,\, F^\dagger\} = [B,\, F] = [B,\, F^\dagger] = [B^\dagger,\, F] = [B^\dagger,\, F^\dagger] = 0$, where we note that $\delta_{ij}\delta^3(\vec{p} - \vec{p}')$ and $\delta_{ij}\delta^3(\vec{p}_q - \vec{p}'_q)$ are the unit element 1 of the convolution product *, and according to embedding map we have $p_q = \pm|\vec{p}|$ and $p'_q = \pm|\vec{p}'|$. The operators q and $\underline{q}$ can be constructed as $q^\dagger = q_0\,\underline{b}\,f^\dagger$, $q = q_0,\underline{b}^\dagger f$, $\underline{q}^\dagger = q_0\,b\,\underline{f}^\dagger$, $\underline{q} = q_0\,b^\dagger\,\underline{f}$. So, we may refer the action of the supercharge operators q and $q^\dagger$ to the background space M_4, having applied in the chain of following transformations of fermion χ (accompanied with the auxiliary field F as it will be seen later on) to boson $\underline{A}$, defined on $\underline{M}_2$: $\cdots \longrightarrow \chi^{(F)} \longrightarrow \underline{A} \longrightarrow \chi^{(F)} \longrightarrow \underline{A} \longrightarrow \chi^{(F)} \longrightarrow \cdots$ Respectively, we may refer the action of the supercharge operators $\underline{q}$ and $\underline{q}^\dagger$ to the $\underline{M}_2$, having applied in the chain of following transformations of fermion $\underline{\chi}$ (accompanied with the auxiliary field $\underline{F}$) to boson A, defined

doi: 10.52526/25792776-2021.68.2-311

on the background space M_4: $\cdots \longrightarrow \underline{\chi}^{(F)} \longrightarrow A \longrightarrow \underline{\chi}^{(F)} \longrightarrow A \longrightarrow \underline{\chi}^{(F)} \longrightarrow \cdots$ Written in one notation, $Q = (q \text{ or } \underline{q})$, the operators become $Q = q_0\, B^\dagger F = (q \text{ or } \underline{q})$, $Q^\dagger = q_0\, BF^\dagger = (q^\dagger \text{ or } \underline{q}^\dagger)$. Due to nilpotent fermionic operators $F^2 = (F^\dagger)^2 = 0$, the operators Q and $Q\dagger$ also are nilpotent: $Q^2 = (Q^\dagger)^2 = 0$. Hence, the quantum system can be described in one notation by the selfadjoint Hamiltonian $\mathcal{H} = (H_q \equiv \{q^\dagger, q\}$ or $H_{\underline{q}} \equiv \{\underline{q}^\dagger, \underline{q}\})$, and that the generators Q and $Q^\dagger$ satisfy an algebra of anticommutation and commutation relations: $\mathcal{H} = \{Q^\dagger, Q\} \geq 0; \quad [\mathcal{H}, Q] = [\mathcal{H}, Q^\dagger] = 0$. This is a sum of Hamiltonian of bosonic and fermionic noninteracting oscillators, which decouples, for $Q = q$, into $H_q = q_0^2\,(\underline{b}^\dagger \underline{b} + f^\dagger f) = q_0^2\,(\underline{b}^\dagger \underline{b} + \frac{1}{2}) + q_0^2\,(f^\dagger f - \frac{1}{2}) \equiv H_{\underline{b}} + H_f$, or, for $Q = \underline{q}$, into $H_{\underline{q}} = q_0^2\,(b^\dagger b + \underline{f}^\dagger \underline{f}) = q_0^2\,(b^\dagger b + \frac{1}{2}) + q_0^2\,(\underline{f}^\dagger \underline{f} - \frac{1}{2}) \equiv H_b + H_{\underline{f}}$, with the corresponding energies: $E_q = q_0^2\,(\underline{n}_b + \frac{1}{2}) + q_0^2\,(n_f - \frac{1}{2})$, $E_{\underline{q}} = q_0^2\,(n_b + \frac{1}{2}) + q_0^2\,(\underline{n}_f - \frac{1}{2})$. This formalism manifests its practical and technical virtue in the proposed algebra, which becomes more clear in a normalization $q_0 = \sqrt{m}$: $\{Q^\dagger, Q\} = 2m; \quad \{Q, Q\} = \{Q^\dagger, Q^\dagger\} = 0$. The latter has underlying algebraic structure of the superalgebra for massive *one-particle* states in the rest frame of $N = 1$ SUSY theory without central charges. This is rather technical topic, and it requires care to do correctly. In what follows we only give a brief sketch. The extension of the MS-SUSY superalgebra in general case when $\vec{p} = i\vec{\partial} \neq 0$ in M_4 or $p_q = i\partial_q \neq 0$ in $\underline{M}_2$, and assuming that the resulting motion of a particle in M_4 is governed by the Lorentz symmetries, the MS-SUSY algebra can then be summarized as a non-trivial extension of the Poincaré group algebra thus of the commutation relations of the bosonic generators of four momenta and six Lorentz generators referred to M_4. Moreover, if there are several spinor generators ${Q_\alpha}^i$ with $i = 1, ..., N$ - theory with $N-$extended supersymmetry, can be written as a graded Lie algebra (GLA) of SUSY field theories, with commuting and anticommuting generators: $\{{Q_\alpha}^i, {\bar{Q}^j}_{\dot{\alpha}}\} = 2\delta^{ij}\, \sigma^{\hat{m}}_{\alpha\dot{\alpha}}\, p_{\hat{m}}$; $[p_{\hat{m}}, {Q_\alpha}^i] = [p_{\hat{m}}, {\bar{Q}^j}_{\dot{\alpha}}] = 0$, $\{{Q_\alpha}^i, {Q_\beta}^j\} = \{{\bar{Q}^i}_{\dot{\alpha}}, {\bar{Q}^j}_{\dot{\beta}}\} = 0$; $[p_{\hat{m}}, p_{\hat{n}}] = 0$. Here $\sigma^{(\pm)} = (1/2)(\sigma^o \pm \sigma^3)$, and in order to trace a maximal resemblance in outward appearance to the standard SUSY theories, we set one notation $\hat{m} = (m \quad \text{if} \quad Q = q, \text{ or } \underline{m} \quad \text{if} \quad Q = \underline{q})$, no sum over $\hat{m}$, and as before the indices α and $\dot{\alpha}$ go over 1 and 2. So for both supercharges, q and $\underline{q}$, we get a supersymmetric models, respectively: $\{{q_\alpha}^i, {\bar{q}^j}_{\dot{\alpha}}\} = 2\delta^{ij}\, \sigma^m_{\alpha\dot{\alpha}}\, p_m$; $[p_m, {q_\alpha}^i] = [p_m, {\bar{q}^j}_{\dot{\alpha}}] = 0$, $\{{q_\alpha}^i, {q_\beta}^j\} = \{{\bar{q}^i}_{\dot{\alpha}}, {\bar{q}^j}_{\dot{\beta}}\} = 0; \quad [p_m, p_n] = 0$. and $\{{\underline{q}_\alpha}^i, {\underline{\bar{q}}^j}_{\dot{\alpha}}\} = 2\delta^{ij}\, \sigma^{\underline{m}}_{\alpha\dot{\alpha}}\, p_{\underline{m}}$; $[p_{\underline{m}}, {\underline{q}_\alpha}^i] = [p_{\underline{m}}, {\underline{\bar{q}}^j}_{\dot{\alpha}}] = 0$, $\{{\underline{q}_\alpha}^i, {\underline{q}_\beta}^j\} = \{{\underline{\bar{q}}^i}_{\dot{\alpha}}, {\underline{\bar{q}}^j}_{\dot{\beta}}\} = 0$; $[p_{\underline{m}}, p_{\underline{n}}] = 0$. For the self-contained arguments, we should emphasize the crucial differences between the MS-induced SUSY and the standard theories as follows:

1) The standard theory can be realized only as a spontaneously broken symmetry since the experiments do not show elementary particles to be accompanied by superpartners with different spin but identical mass. The MS-SUSY, in contrary, can only be realized as an *unbroken SUSY*.

2) In the standard theory, the Q's operate on the fields defined on the single M_4 space. It is why the result of a Lorentz transformation in M_4 followed by a supersymmetry transformation is different from that when the order of the transformations is reversed. But, in the MS-SUSY theory, the Q-operators operate on the fields defined on both M_4 and $\underline{M}_2$ spaces, fulfilling a transition of a particle between these spaces ($M_4 \rightleftharpoons \underline{M}_2$). So after a Lorentz transformation in M_4 followed by a supersymmetry transformation (which, as we shall see below, now results to uniform motion of a particle with initial constant velocity) we have a particle moving with changed constant velocity. We obtain the same result if we reverse the order of the transformations, namely a Lorentz transformation changes the initial velocity and a supersymmetry transformation followed by a Lorentz transformation just keep the uniform motion with the changed velocity.

We shall forbear to write out further the unitary representations of supersymmetry, giving rise to the notion of supermultiplets, as they are so well known. Also, unless otherwise stated we will not discuss the theories with $N > 1$, because it is unlikely that they play any role in low-energy physics.

15.4. Wess-Zumino model

To obtain a feeling for this model we may consider first example of non-trivial linear representation of the MS-SUSY algebra in analogy of the Wess-Zumino toy model, which has $N = 1$ and $s_0 = 0$, and contains two spin states of a massive Majorana spinor $\psi(\chi, \underline{\chi})$ and two complex scalar fields $\mathcal{A}(A, \underline{A})$ and auxiliary fields $\mathcal{F}(F, \underline{F})$, which provide in supersymmetry theory the

doi: 10.52526/25792776-2021.68.2-311

fermionic and bosonic degrees of freedom to be equal. This model is instructive because it contains the essential elements of the MS-induced SUSY. Let us first introduce four additional, anti-commuting (Grassmann) parameters $\epsilon^\alpha(\xi^\alpha,\, \underline{\xi}^\alpha)$ and $\bar\epsilon^\alpha(\bar\xi^\alpha,\, \bar{\underline{\xi}}^\alpha)$: $\{\epsilon^\alpha,\, \epsilon^\beta\} = \{\bar\epsilon^\alpha,\, \bar\epsilon^\beta\} = \{\epsilon^\alpha,\, \bar\epsilon^\beta\} = 0$, $\{\epsilon^\alpha,\, Q_\beta\} = \cdots = [p_{\hat m},\, \epsilon^\alpha] = 0$, which allow to write the algebra (**??**) ($N = 1$) in terms of commutators only: $[\epsilon Q,\, \bar Q\bar\epsilon] = 2\epsilon\sigma^{\hat m}\bar\epsilon p_{\hat m}$, $[\epsilon Q,\, \epsilon Q] = [\bar Q\bar\epsilon,\, \bar Q\bar\epsilon] = [p^{\hat m},\, \epsilon Q] = [p^{\hat m},\, \bar Q\bar\epsilon] = 0$. Here we have dropped the indices $\epsilon Q = \epsilon^\alpha Q_\alpha$ and $\bar\epsilon\bar Q = \bar\epsilon_{\dot\alpha}\bar Q^{\dot\alpha}$. The infinitesimal supersymmetry transformations for $Q = q$ read $\delta_\xi \underline{A} = (\xi q + \bar\xi\bar q) \times \underline{A} = \sqrt{2}\xi\chi$, $\delta_\xi\chi = (\xi q + \bar\xi\bar q) \times \chi = i\sqrt{2}\sigma^m\bar\xi\partial_m\underline{A} + \sqrt{2}\xi F$, $\delta_\xi F = (\xi q + \bar\xi\bar q) \times F = i\sqrt{2}\bar\xi\bar\sigma^m\partial_m\chi$; and for $Q = \underline{q}$ are in the form $\delta_{\underline{\xi}} A = (\underline{\xi}\,\underline{q} + \bar{\underline{\xi}}\,\bar{\underline{q}}) \times A = \sqrt{2}\,\underline{\xi}\,\underline{\chi}$, $\delta_{\underline{\xi}}\,\underline{\chi} = (\underline{\xi}\,\underline{q} + \bar{\underline{\xi}}\,\bar{\underline{q}}) \times \underline{\chi} = i\sqrt{2}\,\sigma^{\underline{m}}\,\bar{\underline{\xi}}\,\partial_{\underline{m}}A + \sqrt{2}\underline{\xi}\,\underline{F}$, $\delta_{\underline{\xi}}\,\underline{F} = (\underline{\xi}\,\underline{q} + \bar{\underline{\xi}}\,\bar{\underline{q}}) \times \underline{F} = i\sqrt{2}\,\bar{\underline{\xi}}\,\bar\sigma^{\underline{m}}\,\partial_{\underline{m}}\,\underline{\chi}$, where $A = \underline{A}$. The first relation means that there should be a particular way of going from one subspace (bosonic/fermionic) to the other and back, such that the net result is as if we had operator of translation $p_{\hat m}$ on the original subspace. Actually, it can be checked that the supersymmetry transformations close supersymmetry algebra: $[\delta_{\epsilon_1},\, \delta_{\epsilon_2}]\mathcal{A} = -2i(\epsilon_1\sigma^{\hat m}\bar\epsilon_2 - \epsilon_2\sigma^{\hat m}\bar\epsilon_1)\,\partial_{\hat m}\mathcal{A}$, and likewise for ψ and $\mathcal{F}$. In the framework of MS-SUSY theory, the Wess-Zumino model has the following Lagrangians: $\mathcal{L}_{Q=q} = \mathcal{L}_0 + m\mathcal{L}_m$, $\quad \mathcal{L}_{Q=\underline{q}} = \underline{\mathcal{L}}_0 + m\underline{\mathcal{L}}_m$, provided, $\mathcal{L}_0 = i\partial_m\bar\chi\bar\sigma^m\chi + \underline{A}^*\underline{\Box}\,\underline{A} + F^*F$, $\mathcal{L}_m = \underline{A}\,F + \underline{A}^*\,F^* - \frac{1}{2}\chi\chi - \frac{1}{2}\bar\chi\bar\chi$, $\underline{\mathcal{L}}_0 = i\partial_{\underline{m}}\,\bar{\underline{\chi}}\bar\sigma^m\underline{\chi} + A^*\Box\,A + \underline{F}^*\underline{F}$, $\underline{\mathcal{L}}_{\underline{m}} = A\,\underline{F} + A^*\,\underline{F}^* - \frac{1}{2}\underline{\chi}\,\underline{\chi} - \frac{1}{2}\bar{\underline{\chi}}\,\bar{\underline{\chi}}$, where according to the embedding map, $\Box = \underline{\Box}$ and $A = \underline{A}$. Whereupon, the equations of motion for the Weyl spinor ψ and complex scalar $\mathcal{A}$ of the same mass m, are $(a)\,\left[i\bar\sigma^m\,\partial_m\,\chi + m\bar\chi = 0, \quad i\bar\sigma^{\underline{m}}\,\partial_{\underline{m}}\,\underline{\chi} + m\bar{\underline{\chi}} = 0, \quad F + m\underline{A}^* = 0\right]$, or $(b)\,[\underline{F} + mA^* = 0, \quad \Box\,\underline{A} + mF^* = 0, \quad \underline{\Box}\,A + m\underline{F}^* = 0]$. Respectively, (a) stands for $Q = q$ (referring to the motion of a fermion, χ, in M_4) and (b) stands for $Q = \underline{q}$ (so, of a boson, A, in M_4). Finally, the algebraic auxiliary field $\mathcal{F}$ can be eliminated to find $\mathcal{L}_{Q=q} = i\partial_m\bar\chi\bar\sigma^m\chi - \frac{1}{2}(\chi\chi + \bar\chi\bar\chi) + \underline{A}^*\underline{\Box}\,\underline{A} - m^2\underline{A}^*\underline{A}$, $\mathcal{L}_{Q=\underline{q}} = i\partial_{\underline{m}}\,\bar{\underline{\chi}}\bar\sigma^m\underline{\chi} - \frac{1}{2}(\underline{\chi}\,\underline{\chi} + \bar{\underline{\chi}}\,\bar{\underline{\chi}}) + A^*\Box\,A - m^2A^*\,A$.

15.5. General superfields

In the framework of standard generalization of the coset construction, we will take $G = G_q \times G_{\underline{q}}$ to be the supergroup generated by the MS-SUSY algebra (**??**). Let the stability group $H = H_q \times H_{\underline{q}}$ be the Lorentz group (as to M_4 and $\underline{M}_2$), and we choose to keep all of G unbroken. Given G and H, we can construct the coset, G/H, by an equivalence relation on the elements of G: $\quad \Omega \sim \Omega h$, where $\Omega = \Omega_q \times \Omega_{\underline{q}} \in G$ and $h = h_q \times h_{\underline{q}} \in H$, so that the coset can be pictured as a section of a fiber bundle with total space, G, and fiber, H. So, the Maurer-Cartan form, $\Omega^{-1}d\Omega$, is valued in the Lie algebra of G, and transforms as follows under a rigid G transformation, $\Omega \longrightarrow g\Omega h^{-1}$, $\quad \Omega^{-1}d\Omega \longrightarrow h(\Omega^{-1}d\Omega)h^{-1} - dh\,h^{-1}$, with $g \in G$. Also we consider a superspace which is an enlargement of $M_4 \oplus \underline{M}_2$ (spanned by the coordinates $X^{\hat m} = (x^m,\, \eta^{\underline{m}})$ by the inclusion of additional fermion coordinates $\Theta^\alpha = (\theta^\alpha,\, \underline{\theta}^\alpha)$ and $\bar\Theta_{\dot\alpha} = (\bar\theta_{\dot\alpha},\, \bar{\underline{\theta}}_{\dot\alpha})$, as to $(q,\, \underline{q})$, respectively. But note that the relation between the two spinors θ and $\underline{\theta}$ should be derived further from the embedding map (see next subsection). These spinors satisfy the following relations: $\{\Theta^\alpha,\, \Theta^\beta\} = \{\bar\Theta_{\dot\alpha},\, \bar\Theta_{\dot\beta}\} = \{\Theta^\alpha,\, \bar\Theta_{\dot\beta}\} = 0$, $[x^m,\, \theta^\alpha] = [x^m,\, \bar\theta_{\dot\alpha}] = 0$, $[\eta^{\underline{m}},\, \underline{\theta}^\alpha] = [\eta^{\underline{m}},\, \bar{\underline{\theta}}_{\dot\alpha}] = 0$. and $\Theta^{\alpha *} = \bar\Theta^{\dot\alpha}$. Points in superspace are then identified by the generalized coordinates $z^M = (X^{\hat m},\, \Theta^\alpha,\, \bar\Theta_{\dot\alpha})$. In case at hand we have then $\Omega(X,\, \Theta,\, \bar\Theta) = e^{i(-X^{\hat m}p_{\hat m} + \Theta^\alpha Q_\alpha + \bar\Theta_{\dot\alpha}\bar Q^{\dot\alpha})} = \Omega_q(x,\, \theta,\, \bar\theta) \times \Omega_{\underline{q}}(\eta,\, \underline{\theta},\, \bar{\underline{\theta}})$, where we now imply a summation over $\hat m$, etc., such that $\Omega_q(x,\, \theta,\, \bar\theta) = e^{i(-x^m p_m + \theta^\alpha q_\alpha + \bar\theta_{\dot\alpha}\bar q^{\dot\alpha})}$, $\Omega_{\underline{q}}(\eta,\, \underline{\theta},\, \bar{\underline{\theta}}) = e^{i(-\eta^{\underline{m}}p_{\underline{m}} + \underline{\theta}^\alpha\underline{q}_\alpha + \bar{\underline{\theta}}_{\dot\alpha}\bar{\underline{q}}^{\dot\alpha})}$. Supersymmetry transformation will be defined as a translation in superspace, specified by the group element $g(0,\, \epsilon,\, \bar\epsilon) = e^{i(\epsilon^\alpha Q_\alpha + \bar\epsilon_{\dot\alpha}\bar Q^{\dot\alpha})} = g_q(0,\, \xi,\, \bar\xi) \times g_{\underline{q}}(0,\, \underline{\xi},\, \bar{\underline{\xi}}) = e^{i(\xi^\alpha q_\alpha + \bar\xi_{\dot\alpha}\bar q^{\dot\alpha})} \times e^{i(\underline{\xi}^\alpha\underline{q}_\alpha + \bar{\underline{\xi}}_{\dot\alpha}\bar{\underline{q}}^{\dot\alpha})}$, with corresponding anticommuting parameters $\epsilon = (\xi$ or $\underline{\xi})$. To study the effect of supersymmetry transformations and $h = 1$, we consider $g(0,\, \epsilon,\, \bar\epsilon)\,\Omega(X,\, \Theta,\, \bar\Theta) = e^{i(\epsilon^\alpha Q_\alpha + \bar\epsilon_{\dot\alpha}\bar Q^{\dot\alpha})}\,e^{i(-X^{\hat m}p_{\hat m} + \Theta^\alpha Q_\alpha + \bar\Theta_{\dot\alpha}\bar Q^{\dot\alpha})}$. The multiplication of two successive transformations can be computed with the help of the Baker-Campbell-Hausdorf formula $e^Ae^B = e^{A+B+(1/2)[A,\,B]+\cdots}$. Hence the transformation above induces the motion $g(0,\, \epsilon,\, \bar\epsilon)\,\Omega(X^{\hat m},\, \Theta,\, \bar\Theta) \longrightarrow (X^{\hat m} + i\,\Theta\,\sigma^{\hat m}\,\bar\epsilon - i\,\epsilon\,\sigma^{\hat m}\,\bar\Theta,\, \Theta + \epsilon,\, \bar\Theta + \bar\epsilon)$, namely, $g_q(0,\, \xi,\, \bar\xi)\,\Omega_q(x,\, \theta,\, \bar\theta) \longrightarrow (x^m + i\,\theta\,\sigma^m\,\bar\xi - i\,\xi\,\sigma^m\,\bar\theta,\, \theta + \xi,\, \bar\theta + \bar\xi)$, $g_{\underline{q}}(0,\, \underline{\xi},\, \bar{\underline{\xi}})\,\Omega_{\underline{q}}(\eta,\, \underline{\theta},\, \bar{\underline{\theta}}) \longrightarrow (\eta^{\underline{m}} + i\,\underline{\theta}\,\sigma^{\underline{m}}\,\bar{\underline{\xi}} - i\,\underline{\xi}\,\sigma^{\underline{m}}\,\bar{\underline{\theta}},\, \underline{\theta} + \underline{\xi},\, \bar{\underline{\theta}} + \bar{\underline{\xi}})$. The superfield $\Phi(z^M)$, which has a finite number of terms in its expansion in terms of Θ and $\bar\Theta$ owing to their anticommuting property, can be considered as the generator of the various components of the supermultiplets. We will consider only a scalar superfield $\Phi'(z^{M\prime}) = \Phi(z^M)$, an infinitesimal supersymmetry transformation of which is given as $\delta_\epsilon \Phi(z^M) = (\epsilon^\alpha Q_\alpha + \bar\epsilon_{\dot\alpha} \bar Q^{\dot\alpha}) \times \Phi(z^M)$. Acting on this space of functions, the Q and $\bar Q$ can be represented as differential operators: $Q_\alpha = \frac{\partial}{\partial \Theta^\alpha} - i\sigma^{\hat m}_{\alpha\dot\alpha}\bar\Theta^{\dot\alpha}\partial_{\hat m}$, $\bar Q^{\dot\alpha} = \frac{\partial}{\partial \bar\Theta_{\dot\alpha}} - i\Theta^\alpha \sigma^{\hat m}_{\alpha\dot\beta}\varepsilon^{\dot\beta\dot\alpha}\partial_{\hat m}$, where, as usual, the undotted/dotted spinor indices can be raised and lowered with a two dimensional undotted/dotted $\varepsilon-$tensors, and the anticommuting derivatives obey the relations $\frac{\partial}{\partial\Theta^\alpha}\Theta^\beta = \delta^\beta_\alpha$, $\frac{\partial}{\partial\Theta^\alpha}\Theta^\beta\Theta^\gamma = \delta^\beta_\alpha\Theta^\gamma - \delta^\gamma_\alpha\Theta^\beta$, and similarly for $\bar\Theta$. In order to write the exterior product in terms of differential operators, one induces a new basis as $e^A(z) = dZ^M\, e_M^{\ A}(z)$, and that $D_A = e_A^{\ N}(z)\frac{\partial}{\partial z^N}$, where to be brief we left implicit the symbol $\wedge$ in writing of exterior product. The covariant derivative operators $D_{\hat m} = \partial_{\hat m}$, $D_\alpha = \frac{\partial}{\partial\Theta^\alpha} + i\sigma^{\hat m}_{\alpha\dot\alpha}\bar\Theta^{\dot\alpha}\partial_{\hat m}$, $\bar D^{\dot\alpha} = \frac{\partial}{\partial\bar\Theta_{\dot\alpha}} + i\Theta^\alpha\sigma^{\hat m}_{\alpha\dot\beta}\varepsilon^{\dot\beta\dot\alpha}\partial_{\hat m}$, anticommute with the Q and $\bar Q$ $\{Q_\alpha,\, D_\beta\} = \{\bar Q_{\dot\alpha},\, \bar D_{\dot\beta}\} = \{Q_\alpha,\, \bar D_{\dot\beta}\} = \{\bar Q_{\dot\alpha},\, D_\beta\} = 0$, and satisfy the following structure relations: $\{D_\alpha,\, D_{\dot\alpha}\} = -2i\sigma^{\hat m}_{\alpha\dot\alpha}\partial_{\hat m}$, $\{D_\alpha,\, D_\beta\} = \{\bar D_{\dot\alpha},\, \bar D_{\dot\beta}\} = 0$. Then we obtain

$$e_A^{\ M} = \begin{pmatrix} e_{\hat a}^{\ \hat m} = \delta^{\hat m}_{\hat a} & e_{\hat a}^{\ \mu} = 0 & e_{\hat a\,\dot\mu} = 0 \\ e_\alpha^{\ \hat m} = i\sigma^{\hat m}_{\alpha\dot\alpha}\bar\Theta^{\dot\alpha} & e_\alpha^{\ \mu} = \delta^\mu_\alpha & e_{\alpha\,\dot\mu} = 0 \\ e^{\dot\alpha\,\hat m} = i\Theta^\alpha\sigma^{\hat m}_{\alpha\dot\beta}\varepsilon^{\dot\beta\dot\alpha} & e^{\dot\alpha\,\mu} = 0 & e^{\dot\alpha}_{\ \dot\mu} = \delta^{\dot\alpha}_{\dot\mu} \end{pmatrix}, \text{ where } \hat a = (a \text{ or } \underline{a}),\; a = 0,1,2,3;\; \underline{a} = (+),(-).$$

The supersymmetry transformations of the component fields can be found using the differential operators. The covariant constraint $\bar D_{\dot\alpha}\Phi(z^M) = 0$, which does not impose equations of motion on the component fields, defines the chiral superfield, Φ. Under the supersymmetry transformation the chiral field transforms as follows: $\delta_\xi\Phi = (\xi q + \bar\xi\bar q)\times\Phi = \delta_\xi\,\underline{A}(\eta) + \sqrt{2}\theta\delta_\xi\chi(x) + \theta\theta\delta_\xi F(x) + \cdots$ in case of $Q = q$, and $\delta_{\underline{\xi}}\,\underline{\Phi} = (\underline{\xi}\,\underline{q} + \underline{\bar\xi}\,\underline{\bar q})\times\underline{\Phi} = \delta_{\underline{\xi}}\,A(x) + \sqrt{2}\underline{\theta}\delta_{\underline{\xi}}\,\underline{\chi}(\eta) + \underline{\theta}\,\underline{\theta}\delta_{\underline{\xi}}\,\underline{F}(\eta) + \cdots$ in case of $Q = \underline{q}$, where as before $A(x) = \underline{A}(\eta)$. The chiral superfield contains the same component fields as the Wess-Zumino model for MS-SUSY theory. The supervolume integrals of products of superfields constructed in the superspace $(x^m,\, \theta,\, \bar\theta)$ will lead to the supersymmetric kinetic energy for the Wess-Zumino model $\int d^4x\, d^4\theta\, \Phi^\dagger\Phi$, where the superspace Lagrangian reads $\Phi^\dagger\Phi = \underline{A}^*\,\underline{A} + \cdots + \theta\theta\bar\theta\bar\theta[\frac14\underline{A}^*\,\underline{\Box}\,\underline{A} + \frac14\underline{\Box}\,\underline{A}^*\,\underline{A} - \frac12\partial_{\underline{m}}\underline{A}^*\,\partial^{\underline{m}}\underline{A} + F^*F + \frac{i}{2}\partial_m\bar\chi\bar\sigma^m\chi - \frac{i}{2}\bar\chi\bar\sigma^m\partial_m\chi]$, where $\Box A = \underline{\Box}\,\underline{A}$ and $\partial_{\underline{m}}\underline{A}^*\,\partial^{\underline{m}}\underline{A} = \partial_m A^*\,\partial^m A$. Similarly, the supersymmetric kinetic energy for the Wess-Zumino model constructed in the superspace $(\eta^{\underline{m}},\, \underline{\theta},\, \underline{\bar\theta})$ for MS-SUSY theory is $\int d^2\eta\, d^4\underline{\theta}\,\underline{\Phi}^\dagger\,\underline{\Phi}$, where the superspace Lagrangian is written down $\Phi^\dagger\Phi = \underline{A}^*\,\underline{A} + \cdots + \theta\theta\bar\theta\bar\theta\,[\frac14\underline{A}^*\,\underline{\Box}\,\underline{A} + \frac14\underline{\Box}\,\underline{A}^*\,\underline{A} - \frac12\partial_{\underline{m}}\underline{A}^*\,\partial^{\underline{m}}\underline{A} + F^*F + \frac{i}{2}\partial_m\bar\chi\bar\sigma^m\chi - \frac{i}{2}\bar\chi\bar\sigma^m\partial_m\chi]$, To complete the model, we also need superspace expressions for the masses and couplings, which can be easily found in analogy of the standard theory, namely: 1) fermion masses and Yukawa couplings, $(\partial^2\mathcal{P}/\partial\mathcal{A}^2)\psi\psi$; and 2) the scalar potential, $\mathcal{V}(\mathcal{A},\,\mathcal{A}^*) = |\partial\mathcal{P}/\partial\mathcal{A}|^2$; where $\mathcal{P} = (1/2)\,m\,\Phi^2 + (1/3)\,\lambda\,\Phi^3$ is the most general renormalizable interaction for a single chiral superfield. Thereby, the auxiliary field equation of motion reads $\mathcal{F}^* + (\partial\mathcal{P}/\partial\mathcal{A}) = 0$. Similarly, we can treat the vector superfields, etc. Here we shall forbear to write them out as the standard theory is so well known.

15.6. Unaccelerated uniform motion; a foundation of SR

Let impose peculiar constraints upon the anticommuting spinors $(\underline{\xi},\, \underline{\bar\xi})$ and $(\xi,\, \bar\xi)$: $\underline{\xi}^\alpha = i\,\frac{\tau}{\sqrt2}\,\underline{\theta}^\alpha$, $\underline{\bar\xi}_{\dot\alpha} = -i\,\frac{\tau^*}{\sqrt2}\,\underline{\bar\theta}_{\dot\alpha}$, $\xi^\alpha = i\frac{\tau}{\sqrt2}\theta^\alpha$, $\bar\xi_{\dot\alpha} = -i\frac{\tau^*}{\sqrt2}\bar\theta_{\dot\alpha}$, and write down the infinitesimal displacement arisen in $\underline{M}_2$ as $\Delta\eta^{\underline{m}} = v^{\underline{m}}\tau = \underline{\theta}\,\sigma^{\underline{m}}\,\underline{\bar\xi} - \underline{\xi}\,\sigma^{\underline{m}}\,\underline{\bar\theta}$, where the parameter $\tau\,(=\tau^*)$ can physically be interpreted as the *duration time* of atomic double transition of a particle from M_4 to $\underline{M}_2$ and back. So, $v^{(+)}\tau = i(\underline{\theta}_1\,\underline{\bar\xi}_1 - \underline{\xi}_1\,\underline{\bar\theta}_1)$, $v^{(-)}\tau = i(\underline{\theta}_2\,\underline{\bar\xi}_2 - \underline{\xi}_2\,\underline{\bar\theta}_2)$, and that $v^2\tau^2 = v^{(+)}v^{(-)}\tau^2 = -(\underline{\theta}_1\,\underline{\bar\xi}_1 - \underline{\xi}_1\,\underline{\bar\theta}_1)(\underline{\theta}_2\,\underline{\bar\xi}_2 - \underline{\xi}_2\,\underline{\bar\theta}_2) = 4\underline{\theta}_1\,\underline{\bar\theta}_1\underline{\theta}_2\,\underline{\bar\theta}_2 \geq 0$. Hance $v^{(+)} = \sqrt2\,\underline{\theta}_1\,\underline{\bar\theta}_1 \geq 0$, $v^{(-)} = \sqrt2\,\underline{\theta}_2\,\underline{\bar\theta}_2 \geq 0$. According to embedding map, therefore, we may introduce the *velocity of light* (c) in vacuum as maximum attainable velocity for uniform motions of all the particles in the Minkowski background space, M_4: $c = \frac{1}{\sqrt2}(v^{(+)} + v^{(-)}) = \sqrt2\,(\underline{\theta}_1\,\underline{\bar\theta}_1 + \underline{\theta}_2\,\underline{\bar\theta}_2) = \sqrt2\,\underline{\theta}\,\underline{\bar\theta} = const$, $v_q = \frac{1}{\sqrt2}(v^{(+)} - v^{(-)}) = \sqrt2\,(\underline{\theta}_1\,\underline{\bar\theta}_1 - \underline{\theta}_2\,\underline{\bar\theta}_2) = \pm|\vec v| = const$, $|\vec v| \leq c$. The spinors $\theta(\underline{\theta},\, \underline{\xi})$ and $\xi(\underline{\theta},\, \underline{\xi})$ satisfy the embedding map (**??**), namely $\Delta q^0 = \Delta x^0$ and $\Delta q^2 = (\Delta\vec x)^2$, so we have $\underline{\theta}\,\sigma^0\,\underline{\bar\xi} - \underline{\xi}\,\sigma^0\,\underline{\bar\theta} = \theta\,\sigma^0\,\bar\xi - \xi\,\sigma^0\,\bar\theta$, $(\underline{\theta}\,\sigma^3\,\underline{\bar\xi} - \underline{\xi}\,\sigma^3\,\underline{\bar\theta})^2 = (\theta\,\vec\sigma\,\bar\xi - \xi\,\vec\sigma\,\bar\theta)^2$, such that $\underline{\theta}_1\,\underline{\bar\theta}_1 + \underline{\theta}_2\,\underline{\bar\theta}_2 = \underline{\theta}\,\underline{\bar\theta} = \theta\bar\theta$, $\underline{\theta}_1\,\underline{\bar\theta}_1 - \underline{\theta}_2\,\underline{\bar\theta}_2 = \pm\sqrt{\frac32}(-\theta\theta\bar\theta\bar\theta)^{1/2} = \pm\sqrt{\frac32}\,\theta\bar\theta$, where we use the following relations: $(\theta\sigma^m\,\bar\theta)(\theta\sigma^n\,\bar\theta) = \frac12\,\theta\theta\bar\theta\bar\theta\,\eta^{mn}$, $(-\theta\theta\bar\theta\bar\theta)^{1/2} = (\theta\bar\theta\theta\bar\theta)^{1/2} = \theta\bar\theta$.So, $\underline{\theta}_1\,\underline{\bar\theta}_1 = \frac12(1 \pm \sqrt{\frac32})\,\theta\bar\theta$, $\underline{\theta}_2\,\underline{\bar\theta}_2 = \frac12(1 \mp \sqrt{\frac32})\,\theta\bar\theta$. Hence we conclude that the *unaccelerated uniform motion of a particle in* M_4

doi: 10.52526/25792776-2021.68.2-311

is encoded in the spinors $\underline{\theta}$ and $\bar{\underline{\theta}}$ referred to the master space $\underline{M}_2$, which is an individual companion to the particle of interest. Therefore, to account for the most important two postulates constituting a foundation of SR, it would be necessary further to impose certain constraints upon the constant Lorentz spinors $\underline{\theta}$. Lorentz invariance is a fundamental symmetry and refers to measurements of ideal inertial observers that move uniformly forever on rectilinear timelike worldlines. In view of relativity of velocity of a particle, we are of course not limited to any particular spinor $\underline{\theta}(\vec{v})$, but can choose at will any other spinors $\underline{\theta}'(\vec{v'})$, $\underline{\theta}''(\vec{v''}), \ldots$ relating respectively to velocities $\vec{v'}, \vec{v''}, \ldots$, whose functional dependence (transformational law) on the original spinor $\underline{\theta}(\vec{v})$ is known. Of the various possible transformations, we must consider for a validity of SR only those which obey the following constraints: 1. $\underline{\theta}\,\bar{\underline{\theta}} = \underline{\theta}'\,\bar{\underline{\theta}}' = \underline{\theta}''\,\bar{\underline{\theta}}'' = \cdots = \frac{c}{\sqrt{2}} = const$; 2. $\underline{\theta}_1\,\bar{\underline{\zeta}}_1\underline{\theta}_2\,\bar{\underline{\zeta}}_2 = \underline{\theta}'_1\,\bar{\underline{\zeta}}'_1\underline{\theta}'_2\,\bar{\underline{\zeta}}'_2 = \cdots = inv$. According to first relation, we may introduce a notion of *time*, for the all inertial frames of reference S, S', S",..., we have then standard Lorentz code (SLC)-relations: $x^0 = ct$, $x^{0'} = ct'$, $x^{0"} = ct", \ldots$. This is a second postulate of SR (Einstein's postulate) that the velocity of light (c) in free space appears the same to all observers regardless the relative motion of the source of light and the observer. By virtue of second relation and equations above, we may derive the invariant interval between the two events defined in Minkowski spacetime: $8\underline{\theta}_1\,\bar{\underline{\theta}}_1\underline{\theta}_2\,\bar{\underline{\theta}}_2\,\Delta t^2 = 2v^2\Delta t^2 = (c^2 - v_q^2)\Delta t^2 = (c^2 - \vec{v}^2)\Delta t^2 = c^2\Delta t^2 - \Delta\vec{x}^2 \equiv \Delta s^2 = 8\underline{\theta}'_1\,\bar{\underline{\theta}}'_1\underline{\theta}'_2\,\bar{\underline{\theta}}'_2\,\Delta t'^2 = c^2\Delta t'^2 - \Delta\vec{x}'^2 \equiv \Delta s'^2 = \cdots = inv$, where we introduce the physical finite *time interval*, $\Delta t = k\tau$, between two events as integer number of the *duration time*, τ, of atomic double transition of a particle from M_4 to $\underline{M}_2$ and back, where k is the number of double transformations. Hence, an unaccelerated uniform motion, for example, of spin-0 particle in M_4 can be described by the chiral superfield $\underline{\Phi}(\eta^{\hat{m}}, \underline{\theta}, \bar{\underline{\theta}})$, while a similar motion of spin-1/2 particle in M_4 can be described by the chiral superfield $\Phi(x^m, \theta, \bar{\theta})$, etc. So, we may refer to all constant Lorentz spinors as the *SLC-spinors*, which constitute a foundation of SR. Hence, in view of the MS-SUSY mechanism of motion, the uniform motion of a particle in M_4 is encoded in the spinors $\underline{\theta}$ and $\bar{\underline{\theta}}$, which refer to $\underline{M}_2$. This will call for a complete reconsideration of our ideas of Lorentz motion code, to be now referred to as the *individual code of a particle*, defined as its intrinsic property.

15.7. Extended supersymmetry and ELC

In four dimensions, it is possible to have as many as eight supersymmetries: $N_{max} = 4$ for renormalizable flat-space field theories; $N_{max} = 8$ for consistent theories of supergravity. It has been shown that the N = 4 theory is not only renormalizable but actually finite. So, the theories with $N > 1$ may play a key role in high-energy physics. These models explore more than one distinct copy of the supersymmetry generators, $Q_{\alpha i}$, therefore, this perspective ultimately requires to relax the Einstein's postulate, because it is natural now to circumvent the limitations to any particular spinor $\underline{\theta}$, instead, considering $i(= 1, \ldots, 4)$-th ($N_{max} = 4$) copy of the spinors $\Theta^{\alpha i} \equiv (\theta^{\alpha i}$ or $\underline{\theta}^{\alpha i})$. Therefore, we now have a straightforward generalization: 1. $\underline{\theta}^i\,\bar{\underline{\theta}}^i = \underline{\theta}^{i\prime}\,\bar{\underline{\theta}}^{i\prime} = \underline{\theta}^{i\prime\prime}\,\bar{\underline{\theta}}^{i\prime\prime} = \cdots = \frac{c_i}{\sqrt{2}} = const$; (no sum over i), 2. $\underline{\theta}^i_1\,\bar{\underline{\zeta}}^i_1\underline{\theta}^i_2\,\bar{\underline{\zeta}}^i_2 = \underline{\theta}^{i\prime}_1\,\bar{\underline{\zeta}}^{i\prime}_1\underline{\theta}^{i\prime}_2\,\bar{\underline{\zeta}}^{i\prime}_2 = \cdots = inv$. This observation allows us to lay forth the extension of Lorentz code, at which SLC violating new physics appears. We may now consider the particles of $i(= 1, \ldots, 4)$-th *type* ($N_{max} = 4$). That is to say, *the i-th type particle in free Minkowski space carries an individual Lorentz motion code with its own maximum attainable velocity c_i, i.e., its own velocity of 'light-like' state*: $c_i = \frac{1}{\sqrt{2}}(v_i^{(+)} + v_i^{(-)}) = \sqrt{2}\,(\underline{\theta}_{1i}\,\bar{\underline{\theta}}_{1i} + \underline{\theta}_{2i}\,\bar{\underline{\theta}}_{2i}) = \sqrt{2}\,\underline{\theta}_i\,\bar{\underline{\theta}}_i = const$, (no sum over i), $v_{qi} = \frac{1}{\sqrt{2}}(v_i^{(+)} - v_i^{(-)}) = \sqrt{2}\,(\underline{\theta}_{1i}\,\bar{\underline{\theta}}_{1\,i} - \underline{\theta}_{2i}\,\bar{\underline{\theta}}_2) = \pm|\vec{v}_i| = const$, $|\vec{v}_i| \leq c_i$. A general solution to the Lorentz covariance in the theory can be easily accommodated if the \`time´ at which event occurs is extended by allowing an extra dependence on \`different type´ readings t_i referred to the particles of different type. They satisfy for all inertial frames of reference S, S', S",..., so-called 'ELC-relations': $x^0 \equiv c_1t_1 = \cdots = c_it_i = \ldots$, $x^{0'} \equiv c_1t'_1 = \cdots = c_it'_i = \ldots$, where $c_1 \equiv c$ is the speed of light in vacuum, and $c_i > c_1$, $(i = 2, 3, 4)$ are speeds of the additional \`light-like´ states, higher than that of light. The clock reading $t_i$ can be used for the $i-$th type particle, the velocity of which reads $v_i = x/t_i = c_ix/x^0$, so $\beta = v_1/c_1 = \ldots v_i/c_i = \cdots \equiv v/c = x/x^0$. If $v_i = c_i$ then $v_1 = c_1$, and the proper time of \`light-like´ states are described by the null vectors $ds_1^2 = \ldots ds_i^2 = \cdots = 0$. The extended Lorentz transformation equations for given i-th and j-th type clock readings can be written then in the form

doi: 10.52526/25792776-2021.68.2-311

$x' = \gamma(x - vt)$, $t'_i = \gamma\frac{c_j}{c_i}(t_j - \frac{v_j}{c_j^2}x)$, $y' = y$, $z' = z$, $\gamma \equiv 1/\sqrt{1-\beta^2}$. Hence, like the standard SR theory, regardless the type of clock, a metre stick traveling with system S measures shorter in the same ratio, when the simultaneous positions of its ends are observed in the other system S': $dx' = dx/\gamma$. Furthermore, a time interval dt_i specified by the $i-$th type readings, which occur at the same point in system S ($dx = 0$), will be specified with the $j-$th type readings of system S' as $dt'_j = \gamma(c_i/c_j)dt_i$. Here we have called attention to the fact that the mere composition of velocities which are not themselves greater than that of c_i will never lead to a speed that is greater than that of c_i. Inevitably in the ELC-framework a specific task is arisen then to distinguish the type of particles. This evidently cannot be done when the velocity ranges of different type particles intersect. To reconcile this situation, we note that, we may freely interchange the types of particles in the intersection. Therefore, we adopt following convention. With no loss of generality, we may re-arrange a general solution that the particles with velocities $v_1 < c_1$, regardless their type, will be treated as the 1-th type particles and, thus, a common clock reading for them and light will be set as t_1. This part of a formalism is completely equivalent to the SLC-framework. Successively, the particles, other than `light-like´ ones, with velocities in the range $c_{i-1} \leq v_i < c_i$, regardless their type, will be treated as the i-th type particles and, thus, a common clock reading for them and `light-like´ state (i) will be set as t_i. The invariant momentum $p_i^2 = p_{\mu i}p_i^{\mu} = (\frac{E_i}{c_i})^2 - \vec{p}_i^2 = m_{0i}^2c_i^2 = p_1^2 = p_{\mu 1}p_1^{\mu} = (\frac{E_1}{c_1})^2 - \vec{p}_1^2 = m_0^2c_1^2$, introduces a *modified dispersion relation* for $i-$th type particle: $E_i^2 = \vec{p}_i^2c_i^2 + m_{0i}^2c_i^4 = \vec{p}_i^2c_i^2 + m_{01}^2c_1^2c_i^2$, where the mass of $i-$th type particle has the value m_{0i}, when at rest, the positive energy is $E_i = m_ic_i^2 = \gamma m_{0i}c_i^2 = \gamma m_{01}c_1c_i$, and $\vec{p}_i = m_i\vec{v}_i = \gamma m_{0i}\vec{v}_i$ is the momentum. This relation modifies the well-known Einstein's equation that energy E always has immediately associated with it a positive mass $m_i = \gamma m_{0i}$, when moving with the velocity $\vec{v}_i$. Having set this theoretical background, one may find some consequences for the superluminal propagation of particles. In particular, in the ELC-framework of uniform motion, the time elapsing between the cause t_{iA} and its effect t_{iB} as measured for the $i-$th type superluminal particle is $\Delta t_i = t_{iB} - t_{iA} = \frac{x_B - x_A}{v_i}$, where x_A and x_B are the coordinates of the two points A and B. In another system S', which is chosen as before and has the arbitrary velocity $V \equiv V_j$ with respect to S, the time elapsing between cause and effect would be $\Delta t'_i = \frac{1 - \frac{V_j}{c_j}\frac{v_i}{c_i}}{\sqrt{1 - \frac{V_j^2}{c_j^2}}}\Delta t_i \geq 0$, where $t_{iB} = (c_j/c_i)t_{jB}$ and $t_{iA} = (c_j/c_i)t_{jA}$. That is, *the ELC-framework recovers the causality for a superluminal propagation*, so the starting of the superluminal impulse at A and the resulting phenomenon at B are being connected by the relation of cause and effect in arbitrary inertial frames. Furthermore, in this framework, we may give a justification of forbiddance of Vavilov-Cherenkov radiation/or analog processes in vacuum. Thereby, in this framework we have to set, for example, $k_1 = (\frac{\omega}{c_1}, \vec{k_1})$ for the 1-th type γ_1 photon, provided $\vec{k_1} = \vec{e}_k\frac{\omega}{c_1}$, and $p_2 = (\frac{E_2}{c_2}, \vec{p}_2)$ for the 2-nd type superluminal particle. Then the process $(l_2 \to l_2 + \gamma_1)$ becomes kinematically permitted if and only if $k_1p_2 = \frac{\omega}{c_1}\frac{E_2}{c_2}(1 - \vec{e}_k\frac{\vec{v}_2}{c_2}) = 0$, which yields $\omega \equiv 0$ because of $(1 - \vec{e}_k\frac{\vec{v}_{\nu 2}}{c_2}) \neq 0$. This evades constraints due to VC-like processes since the superluminal particle $\nu_{\mu 2}$ does not actually travel faster than the speed c_2. Finally, in ELC-framework we discuss the VC-radiation of the charged superluminal particle propagating in vacuum with a constant speed $v_2 > c_1$ higher than that of light. Recall that, for a charged particle ($e \neq 0$) moving in a transparent, isotropic and non-magnetic medium with a constant velocity higher than velocity of light in this medium the VC radiation is allowed. The energy loss per frequency is $dF = -d\omega\frac{ie^2}{2\pi}\sum\omega(\frac{1}{c^2} - \frac{1}{\varepsilon v^2})\int\frac{d\zeta}{\zeta}$, where the direction of the velocity $\vec{v}$ is chosen to be $x-$direction: $k_x = k\cos\theta = \omega/v$, $k = n\omega/c$ is the wave number $n = \sqrt{\varepsilon}$ is the real refractive index, ε is the permittivity. The summation is over terms with $\omega = \pm|\omega|$, and a variable $\zeta = q^2 - \omega^2(\frac{\varepsilon}{c^2} - \frac{1}{v^2})$ is introduced, provided $q = \sqrt{k_y^2 + k_z^2}$. The integrand is strongly peaked near the singular point $\zeta = 0$, for which $q^2 + k_x^2 = k^2$. Using standard technique, it can be easily transformed to be applicable in ELC-framework for the charged superluminal particle of 2-nd type propagating in vacuum (i.e. if $\varepsilon = 1$) with a constant speed v_2 higher than that of light ($c_1 \leq v_2 < c_2$): $dF = -d\omega\frac{ie^2}{2\pi}\sum\omega(\frac{1}{c_2^2} - \frac{1}{v_2^2})\int\frac{d\zeta}{\zeta}$. Hence $\zeta = q_1^2 - \omega^2(\frac{1}{c_2^2} - \frac{1}{v_2^2})$, where $q_1 = \sqrt{k_{y1}^2 + k_{z1}^2}$, $q_1^2 + k_{x1}^2 = k_1^2 = \omega^2/c_1^2$, and now $k_{x1}v_2 = \omega$. We have then $\zeta = \frac{\omega^2}{c_2^2}(\frac{c_2^2}{v_2^2\cos^2\theta} - 1) \neq 0$, because of $v_2 < c_2$, and that the integral is zero, since the integrand has no poles. Hence, as expected,

doi: 10.52526/25792776-2021.68.2-311

the *VC-radiation of a charged superluminal particle as it propagates in vacuum is forbidden.*

15.8. Accelerated motion and local MS-SUSY

In case of an accelerated ($a = |\vec{a}| \neq 0$) motion of a particle in M_4, we have then $\frac{i}{\sqrt{2}}(\underline{\theta}\,\sigma^3\frac{d^2\bar{\xi}}{dt^2} - \frac{d^2\xi}{dt^2}\sigma^3\bar{\underline{\theta}}) = \frac{d^2q}{dt^2} = a = \frac{1}{\sqrt{2}}(\frac{d^2\eta^{(+)}}{dt^2} - \frac{d^2\eta^{(-)}}{dt^2}) = \frac{1}{\sqrt{2}}(a^{(+)} - a^{(-)}),\ a^{(\pm)} = \frac{dv^{(\pm)}}{dt}$. So, we may relax the condition $\partial_{\hat{m}}\epsilon = 0$ and promote this symmetry to a local supersymmetry in which the parameter $\epsilon = \epsilon(X^{\hat{m}})$ depends explicitly on $X^{\hat{m}}$. Such a local SUSY can already be read off from the considered above algebra in the form $[\epsilon(X)Q, \bar{Q}\bar{\epsilon}(X)] = 2\epsilon(X)\sigma^{\hat{m}}\bar{\epsilon}(X)p_{\hat{m}}$, which says that the product of two supersymmetry transformations corresponds to a translation in space-time of which the four momentum $p_{\hat{m}}$ is the generator. Similar to the results of subsection F, the multiplication of two local successive transformations induces the motion $g(0, \epsilon(X), \bar{\epsilon}(X))\,\Omega(X^{\hat{m}}, \Theta, \bar{\Theta}) \longrightarrow (X^{\hat{m}} + i\,\Theta\,\sigma^{\hat{m}}\,\bar{\epsilon}(X) - i\,\epsilon(X)\,\sigma^{\hat{m}}\,\bar{\Theta},\ \Theta + \epsilon(X),\ \bar{\Theta} + \bar{\epsilon}(X))$, and, in accord, the transformation is expected to be somewhat of the form $[\delta_{\epsilon_1(X)}, \delta_{\epsilon_2(X)}]V \sim \epsilon_1(X)\sigma^{\hat{m}}\bar{\epsilon}_2(X)\,\partial_{\hat{m}}V$, that differ from point to point, namely this is the notion of a general coordinate transformation. Whereupon we see that for the local MS-SUSY to exist it requires the background spaces $(\widetilde{\underline{M}_2}, \widetilde{M_4})$ to be curved. Thereby, the space $\widetilde{M}_4$, in order to become on the same footing with the distorted space $\widetilde{\underline{M}}_2$, refers to the accelerated proper reference frame of a particle, without relation to other matter fields. A useful guide in the construction of local superspace is that it should admit rigid superspace as a limit. The reverse is also expected, since if one starts with a constant parameter ϵ and performs a local Lorentz transformation, then this parameter will in general become space-time dependent as a result of this Lorentz transformation. The mathematical structure of the local MS-SUSY theory has much in common with those used in the geometrical framework of standard supergravity theories. In its simplest version, supergravity was conceived as a quantum field theory whose action included the Einstein-Hilbert term, where the graviton coexists with a fermionic field called gravitino, described by the Rarita-Scwinger kinetic term. The two fields differ in their spin: 2 for the graviton, 3/2 for the gravitino. The different 4D $N = 1$ supergravity multiplets all contain the graviton and the gravitino, but differ by their systems of auxiliary fields. These fields would transform into each other under local supersymmetry. We may use the usual language which is almost identical to the vierbien formulation of GR with some additional input. In this framework supersymmetry and general coordinate transformations are described in a unified way as certain diffeomorphisms. The motion generates the super-general coordinate reparametrization $z^M \longrightarrow z'^M = z^M - \zeta^M(z)$, where $\zeta^M(z)$ arc arbitrary functions of z. The dynamical variables of superspace formulation are the frame field $E^A(z)$ and connection Ω. The superspace $(z^M, \Theta, \bar{\Theta})$ has at each point a tangent superspace spanned by the frame field $E^A(z) = dz^M E_M^{\ A}(z)$, defined as a 1-form over superspace, with coefficient superfields, generalizing the usual frame, namely supervierbien $E_M^{\ A}(z)$. Here, we use the first half of capital Latin alphabet $A, B, \ldots$ to denote the anholonomic indices related to the tangent superspace structure group, which is taken to be just the Lorentz group. The formulation of supergravity in superspace provides a unified description of the vierbein and the Rarita-Schwinger fields. They are identified in a common geometric object, the local frame $E^A(z)$ of superspace. Covariant derivatives with respect to local Lorentz transformations are constructed by means of the spin connection, which is a 1-form in superspace as well. Here we shall forbear to write the details out as the standard theory is so well known. The supervierbien $E_M^{\ A}$ and spin- connection Ω contain many degrees of freedom. Although some of these are removed by the tangent space and supergeneral coordinate transformations, there still remain many degrees of freedom. There is no general prescription for deducing necessary covariant constraints which if imposed upon the superfields of super-vierbien and spin-connection will eliminate the component fields. However, some usual constraints can be found using tangent space and supergeneral coordinate transformations of the torsion and curvature covariant tensors, given in appropriate supergauge. Together with other details of the theory, they can be seen in the textbooks. The final form of transformed super-vierbien, can be written as $E_A^{\ M}(z)\big|_{\Theta=\bar{\Theta}=0} = \begin{pmatrix} e_{\hat{m}}^{\ \hat{a}}(X) & \frac{1}{2}\psi_{\hat{m}}^{\ \alpha}(X) & \frac{1}{2}\bar{\psi}_{\hat{m}\dot{\alpha}}(X) \\ 0 & \delta_\alpha^\mu & 0 \\ 0 & 0 & \delta_{\dot{\alpha}}^\mu \end{pmatrix}$, where the fields of graviton $e_{\hat{m}}^{\ \hat{a}}$ and gravitino $\frac{1}{2}\psi_{\hat{m}}^{\ \alpha}$, $\frac{1}{2}\bar{\psi}_{\hat{m}\dot{\alpha}}$ cannot be gauged away. Provided, we

doi: 10.52526/25792776-2021.68.2-311

have $e_{\hat{a}}{}^{\hat{m}} e_{\hat{m}}{}^{\hat{b}} = \delta^{\hat{b}}_{\hat{a}}$, $\psi_{\hat{a}}{}^{\mu} = e_{\hat{a}}{}^{\hat{m}} \psi_{\hat{m}}{}^{\alpha} \delta^{\mu}_{\alpha}$, $\bar{\psi}_{\hat{a}\dot{\mu}} = e_{\hat{a}}{}^{\hat{m}} \bar{\psi}_{\hat{m}\dot{\alpha}} \delta^{\dot{\alpha}}_{\mu}$. The tetrad field $e_{\hat{m}}{}^{\hat{a}}(X)$ plays the role of a gauge field associated with local transformations. The Majorana type field $\frac{1}{2}\psi_{\hat{m}}{}^{\alpha}$ is the gauge field related to local supersymmetry. These two fields belong to the same supergravity multiplet which also accommodates auxiliary fields so that the local supersymmetry algebra closes. Under infinitesimal transformations of local supersymmetry, they transformed as $\delta e_{\hat{m}}{}^{\hat{a}} = i(\psi_{\hat{m}} \sigma^{\hat{a}} \zeta - \zeta \sigma^{\hat{a}} \bar{\psi}_{\hat{m}})$, $\delta\psi_{\hat{m}} = -2\mathcal{D}_{\hat{m}}\zeta^{\alpha} + i e_{\hat{m}}{}^{\hat{c}} \{\frac{1}{3} M (\varepsilon \sigma_{\hat{c}} \bar{\zeta})^{\alpha} + b_{\hat{c}} \zeta^{\alpha} + \frac{1}{3} b^{\hat{d}} (\zeta \sigma_{\hat{d}} \bar{\sigma}_{\hat{c}})\}$, etc., where M_4 and $b_{\bar{a}}$ are the auxiliary fields, and $\zeta^{\alpha}(z) = \zeta^{\alpha}(X)$, $\bar{\zeta}^{\alpha}(z) = \bar{\zeta}^{\alpha}(X)$ and $\zeta^{\bar{a}}(z) = 2i[\Theta \sigma^{\hat{a}} \bar{\zeta}(X) - \zeta(X) \sigma^{\hat{a}} \bar{\Theta}]$. The chiral superfields are defined as $\bar{\mathcal{D}}_{\dot{\alpha}} \Phi = 0$, therefore, the components fields are $\mathcal{A} = \Phi|_{\Theta=\bar{\Theta}=0}$, $\psi_{\alpha} = \frac{1}{\sqrt{2}} \mathcal{D}_{\alpha} \Phi|_{\Theta=\bar{\Theta}=0}$, $\mathcal{F} = -\frac{1}{4} \mathcal{D}^{\alpha} \mathcal{D}_{\alpha} \Phi|_{\Theta=\bar{\Theta}=0}$, which carry Lorentz indices. Under infinitesimal transformations of local supersymmetry, they transformed as $\delta\mathcal{A} = -\sqrt{2}\,\zeta^{\alpha}\psi_{\alpha}$, $\delta\psi_{\alpha} = -\sqrt{2}\,\zeta_{\alpha}\mathcal{F} - i\sqrt{2}\,\sigma_{\alpha\dot{\beta}}{}^{\hat{a}} \bar{\zeta}^{\dot{\beta}} \hat{\mathcal{D}}_{\hat{a}} \mathcal{A}$, $\delta\mathcal{F} = -\frac{1}{3}\sqrt{2}\, M^{*} \zeta^{\alpha} \psi_{\alpha} + \bar{\zeta}^{\dot{\alpha}} (\frac{1}{6}\sqrt{2}\, b_{\alpha\dot{\alpha}} \psi^{\dot{\alpha}} - i\sqrt{2}\, \hat{\mathcal{D}}_{\alpha\dot{\alpha}} \psi^{\alpha})$, where $\hat{\mathcal{D}}_{\hat{a}}$ is, so-called, super-covariant derivative $\hat{\mathcal{D}}_{\hat{a}} \mathcal{A} \equiv e_{\hat{a}}{}^{\hat{m}} (\partial_{\hat{m}} \mathcal{A} - \frac{i}{\sqrt{2}} \psi_{\hat{m}}{}^{\mu} \psi_{\mu})$, $\hat{\mathcal{D}}_{\hat{a}} \psi_{\alpha} = e_{\hat{a}}{}^{\hat{m}} (\mathcal{D}_{\hat{m}} \psi_{\alpha} - \frac{1}{\sqrt{2}} \psi_{\hat{m}\alpha} \mathcal{F} - \frac{i}{\sqrt{2}} \bar{\psi}_{\hat{m}}{}^{\dot{\beta}} \hat{\mathcal{D}}_{\alpha\dot{\beta}} \mathcal{A})$. The graviton and the gravitino form thus the basic multiplet of local MS-SUSY, and one expects the simplest locally supersymmetric model to contain just this multiplet. The spin 3/2 contact term in total Lagrangian arises from equations of motion for the torsion tensor, and that the original Lagrangian itself takes the simpler interpretation of a minimally coupled spin (2, 3/2) theory.

15.9. Inertial effects

We would like to place the emphasis on the essential difference arisen between the standard supergravity theories and some rather unusual properties of local MS-SUSY theory. In the framework of the standard supergravity theories, as in GR, a curvature of the space-time acts on all the matter fields. The source of graviton is the energy-momentum tensor of matter fields, while the source of gravitino is the spin-vector current of supergravity. In the local MS-SUSY theory, unlike the supergravity, a curvature of space-time arises entirely due to the inertial properties of the Lorentz-rotated frame of interest, i.e. a *fictitious gravitation* which can be globally removed by appropriate coordinate transformations. This refers to the particle of interest itself, without relation to other matter fields. The only source of graviton and gravitino, therefore, is the acceleration of a particle, because the MS-SUSY is so constructed as to make these two particles just as being the two bosonic and fermionic states of a particle of interest in the curved background spaces $\widetilde{M}_4$ and $\widetilde{\underline{M}}_2$, respectively, or vice versa. Whereas, in order to become on the same footing with the distorted space $\widetilde{\underline{M}}_2$, the space $\widetilde{M}_4$ refers only to the accelerated proper reference frame of a particle. With these physical requirements, a standard Lagrangian consisted of the classical Einstein-Hilbert Lagrangian plus a part which contains the Rarita-Schwinger field and coupling of supergravity with matter superfields evidently no longer holds. Instead we are now looking for an alternative way of implications of local MS-SUSY in the model of accelerated motion and inertial effects. For example, we may with equal justice start from the reverse, which as we mentioned before is also expected. If one starts with a constant parameter ϵ and performs a local Lorentz transformation, which can only be implemented if MS and space-time are curved (deformed/distorted) ($\widetilde{M}_2$, $\widetilde{M}_4$), then this parameter will in general become space-time dependent as a result of this Lorentz transformation, which readily implies *local* MS-SUSY. In going into practical details of the realistic local MS-SUSY model, it remains to derive the explicit form of the vierbien $e_{\hat{m}}{}^{\hat{a}}(\varrho) \equiv (e_m{}^a(\varrho), e_{\underline{m}}{}^{\underline{a}}(\varrho))$, which describes *fictitious graviton* as a function of *local rate* $\varrho(\eta, m, f)$ of instantaneously change of the velocity $v^{(\pm)}$ of massive (m) test particle under the unbalanced net force (f). At present, unfortunately, we cannot offer a straightforward recipe for deducing the alluded vierbien $e_{\hat{m}}{}^{\hat{a}}(\varrho)$ in the framework of quantum field theory of MS-supergravity. However, in previous section, it was described in the framework of classical physics. Together with other usual aspects of the theory, this illustrates a possible solution to the problems of inertia behind spacetime deformations. Thereby it was argued that a deformation/(distortion of local internal properties) of $\underline{M}_2$ is the origin of inertia effects that can be observed by us. Consequently, the next member of the basic multiplet of local MS-SUSY -*fictitious gravitino*, $\psi_{\hat{m}}{}^{\alpha}(\varrho)$, will be arisen under infinitesimal transformations of local supersymmetry, provided by the local parameters $\zeta^{M}(a)$.

doi: 10.52526/25792776-2021.68.2-311

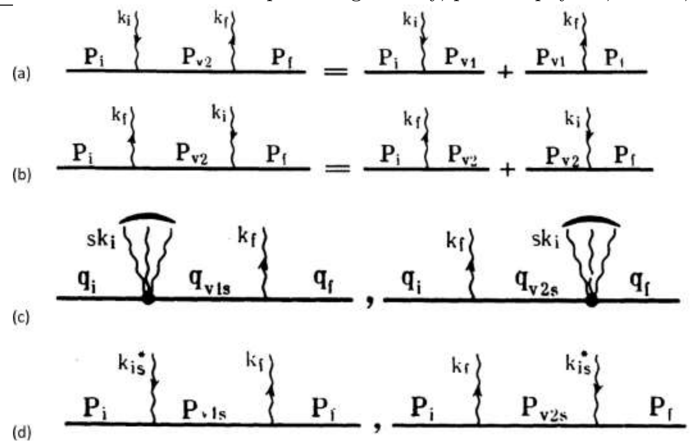

Figure 1. The amplitude of Compton scattering of a photon by an electron is represented by the sum of two amplitudes. The panels (a) and (b) stand for the case of weak and moderate radiation intensity $\xi_i^2 \ll 1$; The panels (c) and (d) stand for the case of intense radiation $\xi_i^2 \gtrsim 1$.

16. Einstein's transition coefficients for Compton scattering

The processes of interaction of electrons with intense radiation are of vital interest for interpretation of non-stationary phenomena occurring in a number of astrophysical objects. Then it is important to carry out a detailed analysis of nonlinear processes occurring at intense radiation that play a decisive role in the formation of the physical characteristics of these phenomena. Recently, with the increasing interest in non-stationary nonthermal phenomena occurring in recently discovered very interesting astrophysical objects, the research with the use of mechanisms of electron-photon interaction in cosmic plasma is being carried out more and more often and intensively. The Compton scattering is the s-channel of the photon-electron interaction, while the processes of annihilation and creation of electron-positron pairs is the t-channel. These processes of interactions are met both in weak, moderate, and in very intense radiation fields with the thermal and relativistic electrons.

The introduction of Einstein's transition coefficients is one of the outstanding events in the history of physics. There is no surprise that Milne's (see e.g. (Mihalas, 1978)) very important generalization of Einstein's relations to bound-free processes (photonionization) was dictated by the interests of astrophysical problems. Later, using the formal introduction of the indicated coefficients, by Pauli (Pauli, 1923) taken into account those quantum-theoretical properties of radiation, which in the wave theory are manifested in the form of interference fluctuations. A next important step was taken by Einstein and Ehrenfest (Einstein & Ehrenfest, 1923), by a clear separation of absorption and emission processes in the Compton scattering of quanta by molecules. However, for a deeper understanding of these processes, it needs further detailed analysis. In the papers (Ter-Kazarian, 1984c,e) Einstein's ideas are further developed for free-virtual, virtual-free and free-free transitions for electron-photon scattering at arbitrary intense radiation by splitting Compton scattering into two components.

To start with, we consider at first the case of weak and moderate radiation intensity $\xi_i^2 \ll 1$, where ξ_i is the parameter of intensity of radiation field of initial photons $\xi_i^2 = \frac{e^2 h n_\gamma}{\pi m_e^2 c^2 \nu_i}$, n_γ is the density of photons, and ν_i is their frequency. Let the electron-photon gas be in thermodynamic equilibrium. Meanwhile the distribution of electrons will be Maxwellian, and radiation will be Planckian. The amplitude of scattering of a photon by an electron is represented by the sum of two amplitudes $M = M_1 + M_2$. The amplitude M_1 corresponds to the process of scattering of a photon with four momenta k_i by an electron with four momenta p_i. After the act, they acquire impulses k_f and p_f. This act can be represented as the sum of two constituent processes: 1) the $(i \to v)$ transition of an electron from the initial free state (i) to the virtual (v) by absorbing the initial quantum; and 2) the transition $(v \to f)$ of an electron from the virtual state to the free state (f) by emission of a finite quantum. The corresponding Feynman diagram will have the form of panels (a, b) in Fig. 1. Note the following, it is unimportant that an electron can only have discrete states or energy values. If the density of states is a continuous function in the phase space, then we have the right to replace

doi: 10.52526/25792776-2021.68.2-311

these states with equiprobable, infinitesimal regions of states, between which a radiative transition is possible. Note also that when considering radiative transitions in molecules (Einstein & Ehrenfest, 1923), the `internal state´ of the molecule itself did not play any role. Although the virtual electron is `unusual´ (it was located outside the mass shell), without addressing questions about its `internal state´, we have the right to base this study on two quantum-theoretical hypotheses: 1) electrons can make free-virtual and virtually-free transitions both under the action of radiation field (induced) and spontaneous one; 2) at thermodynamic equilibrium, the principle of detailed equilibrium can also be applied to processes, where one of the states is virtual, i.e. any process, among those in the same frequency range and direction, is compensated by the opposite process. The simplicity of hypotheses, generality and ease of further consideration, as well as a natural transition to a well-known Pauli's hypothetical statistical law (Pauli, 1923) allows us to judge their correctness. We continue with two basic equations of the conservation law for the mean transitions for the states (i) and (f). Then, excluding the populations of the `internal states´, we obtain the conditions of detailed equilibrium for the transitions $(i_1 \to f_1$, $(i_2 \to f_2$ and $(i \to f$. Through the notation $B_{if} = B_{i_1v_1}B_{v_1f_1} + B_{i_2v_2}B_{v_2f_2}$, $B_{fi} = B_{f_1v_1}B_{v_1i_1} + B_{f_2v_2}B_{v_2i_2}$ - for induced coefficients; and $A_{if} = B_{i_1v_1}A_{v_1f_1} + A_{i_2v_2}B_{v_2f_2}$, $A_{fi} = B_{f_1v_1}A_{v_1i_1} + A_{f_2v_2}B_{v_2i_2}$- for spontaneous coefficients, the coefficients of probabilities of `real´ (free-free) transitions for processes $(i \to f$ are directly introduced, where $N_i/2 = N_{i_1} = N_{i_2}$, $N_f/2 = N_{f_1} = N_{f_2}$ (since the weights of the amplitudes M_1 and M_2 are the same), $n(\nu) = \frac{c^2}{2h\nu^3}\rho(\nu)$ is the number of fillings of the quanta of frequency ν. When considering the limiting case $T \to \infty$, it is easy to obtain relations between the coefficients of induced transitions. Finally, based on the fact that the energy `absorbed´ during the transition $(i \to f$ (in a unit volume of the phase space for the time $\triangle t$) can be represented as using the introduced coefficients, and by means of the usual quantum-mechanical scattering probability W, one can obtain the remaining relations between the coefficients of the transition probabilities. Similar reasoning for the `radiated´ energy in the transition $(f \to i$ gives additional relations. It should be noted that, in contrast to the coefficients of the probabilities of atomic transitions, here the values of the introduced coefficients are well defined, since the scattering probability W is well known.

Radiation transfer equation for nonequilibrium processes. Determining the probability coefficients of transitions in the state of thermodynamic equilibrium, it is easy to turn to the radiation transfer equation for nonequilibrium processes. For example, for free-free transitions, the corresponding equation has the form $(\frac{1}{c}\frac{\partial}{\partial t} + \frac{\partial}{\partial l})I_i = \int d\tau_i \int \frac{d\omega_f}{4\pi}\delta[-N_iI_i(B_{if}I_f + A_{if}) + N_fI_f(B_{fi}I_i + A_{fi})]$, where $d\tau_i$ is the element of the phase volume of the initial electrons.

16.1. Interaction of electrons with the intense radiation: `diagonal´ interaction

Next, we consider the general problem of interaction of electrons with the intense radiation $\xi_i^2 \gtrsim 1$ via s-photon Compton scattering $s\gamma + e \to \gamma' + e'$. Here it is necessary to highlight two type of interaction: c) `diagonal´, when an electron absorbs these $s$-quanta from one wave; d) `non-diagonal´, when the absorbed set of s-quanta includes all kinds of combinations of quanta from different waves. The corresponding diagram for `diagonal´ interaction will have the form of panel $(c)$ in Fig. 1 with four conservation laws: $q_i + shk_i = q_f + hk_f$, where $q_i^\mu = p_i^\mu + \frac{m_e^2c^4\xi_i^2}{2k_ip_i}k_i^\mu$, and $p_i^\mu$ is the four-momentum of an electron at time $t = -\infty$. If we introduce a new concept of `effective photon´ with four-momentum $k_{is}^* = s^*k_i$ where $s^* \equiv s + \frac{m_e^2c^4\xi_i^2}{2}(\frac{1}{k_ip_i} - \frac{1}{k_fp_f})$, then instead of s-photon scattering by electron with an effective four-momentum q_f, with equal footing we should consider the scattering of one `effective photon´ by free electron. Thereby the diagram (c) should be replaced with the (d) in Fig. 1. Consequently, the problem is wholly reduced to the above considered case of one-photon scattering. In this case, it should be assumed that the detailed balance condition is satisfied in the same frequency range for each fixed value of s, ψ_i, ψ_f, where $\psi_{i,\,f}$ is the angle between vectors k_i and $p_{i,f}$, and the parameters of `electronic medium´ (i.e., the coefficients A and B) will now depend on the intensity of the initial radiation fields.

*Interaction of electrons with the intense radiation: `non-diagonal´ interaction.* We now turn to the case of `non-diagonal´ interaction. Let N_i - electrons carry out the process of pumping between waves m_s (where $m_s = j_1, ..., j_s$, thus $\sum_{m_s}^{\infty} \equiv \sum_{j_1,...,j_s}^{\infty}$). Then it is easy to obtain results for this

doi: 10.52526/25792776-2021.68.2-311

case from the final expressions of the already considered problem of `diagonal´ interaction after making appropriate replacements $k_s^* \to k_{m_s}^*$, $W_s(I_i) \to W_{m_s}(I_{m_s i})$, etc. But for the probability of the process we no longer have an explicit expression $W_{m_s}(I_{m_s i})$, since the calculation of this quantity is associated with enormous difficulties. However, the complexity of the situation is to some extent compensated by the fact that the off-diagonal interaction involves only a tiny fraction of electrons, since the required conditions for electrons to be in the corresponding physical cones of formation pumping processes between different waves are very tough. For example, even in the simplest case of two $m_s = 2$ oncoming waves, the physical cone of the formation of the pumping process is already delta-shaped, and meets the condition $1 - \frac{v\cos\theta}{c}\frac{\nu_1+\nu_2}{\nu_1-\nu_2} = 0$, where angle between vectors is the velocity of the electron, θ is the angle between this velocity and $e_1 = -e_2$, ν_1, e_1 and ν_2, e_2 are the frequencies and the directional unit vectors of these waves. This means that the cone for cases $m_s > 2$ will be even more narrow and, thus, harder to be satisfied.

16.2. Transition coefficients for annihilation and creation of electron-positron pairs

The above formalism of the probability coefficients transitions can be easily extended to the t-channel of the photon-electron interaction, namely to processes of annihilation and creation of electron-positron pairs. Since the Feynman diagram for these processes is topologically identical to the corresponding diagram of the s-channel of the photon-electron interaction, then the probability coefficients for the t-channel of the photon-electron interaction can be obtained directly from those found above (in item 1) by performing simple replacements. For example, for the annihilation process we have: $i \to -$, $E_i \to E_-$, $\nu_i \to -\nu_1$, $I_i \to I_1$, and $f \to +$, $E_f \to -E_+$, $\nu_f \to \nu_2$, $I_f \to I_2$, where $(-)$ and $(+)$ indicate the electronic and positron states. Whereas, depending on the specific problem, for the probability W of the process one should take the probability of the process of annihilation or pairing. The interested reader is invited to consult the original papers (Ter-Kazarian, 1984c,e) for a complete set of derived explicit forms of Einstein's coefficients and the relations between them.

17. The theory of Multiphoton Comptonization

By means of the concept of `effective photons´, the integral kinetic equation was derived that describes the time evolution of the distribution function of quanta of non-equilibrium intense radiation for their multiphoton Compton scattering on Maxwellian nonrelativistic electrons (Ter-Kazarian, 1984a,b,d, 1987, 1989a,b). At first glance, it seems that the problem can hardly be reduced to the Fokker-Planck approximation, since the efficiency of electron acceleration in the field of an intense wave is large. Whereas, the thermal energy of electrons is much less than the energy acquired in the field of the intense wave. Therefore, consideration of issues of heat balance, etc. seems useless in this case. Moreover, one more difficulty arises regarding the distribution function of such electrons, which is essentially different from Maxwell's distribution function. To resolve these difficulties, the fact was used that the electron in both the initial and final states is in the field of initial radiation. Therefore, in multiphoton scattering, the process of transferring the energy of low-frequency photons to the short-wavelength part of the spectrum prevails. While the elementary act of stimulated multiphoton scattering by an electron with an effective four-momentum is replaced by another, completely equivalent to it, scattering of an `effective photon´ by a free electron, in a nonlinear mode, when the parameters of the electronic medium depend on the intensity of the initial radiation field. In the framework of this approach, the initial physical conditions of the problem are already imposed on the free states of electrons. The resulting Fokker-Planck approximation becomes valid when deriving an `intermediate´ kinetic equation for the distribution of `effective photons´. Subsequently, the transition to the kinetic equation for the distribution of ordinary photons is made. The rearrangement of spectrum in case of a wide, in comparison with the Doppler profile, emission spectrum $\delta \gg \triangle\omega_{Ds}^* = \omega_s^*\sqrt{2k_B T_e/m_e c^2}$ is described by means of this differential equation. While the particular problem of the relaxation of the nonequilibrium isotopic radiation interacting with nondegenerate nonrelativistic electrons via the multiphoton Compton scattering is studied. Whereas, it is shown that the kinetic equation satisfies Boltzman's $H-$theorem for the coupled electron-photon system. The equations of heating and cooling of electron gas are derived. In (Ter-Kazarian, 1987, 1989c), we

doi: 10.52526/25792776-2021.68.2-311

study this problem in detail, and make estimate of various physical characteristics of compact objects of superhigh luminosity, as well as the efficiency of comptonization as an energy exchange process compared with the bremsstrahlung. In (Ter-Kazarian, 1989a), it was shown that the interpretation of the observational characteristics of a certain class of astrophysical objects, such as BLL B211308 + 32, OJ 287, NP 0532 pulsar and radio pulsars, the mechanism of multiphoton stimulated Compton scattering by electrons plays an important role. However, under real physical conditions occurring in the compact objects of high luminosity, the radiation is concentrated in the high frequency range $\delta \gg \triangle\omega_D \leq \omega^*_{Ds}$ and solid angle $\Omega \ll 1$. Since scattering occurs only within the line, then due to the narrowness of the spectrum, the number of electrons involved in the process decreases and, consequently, the rate of the process decreases in comparison with a wide spectrum of radiation with the same brightness temperature. That is, with narrowing of the spectrum, both the transfer of radiation energy to electrons and the multiphoton induced pressure decrease. In (Ter-Kazarian, 1989b), we have continued the study of the process of relaxation of intense radiation on Maxwellian electrons in the general case of any spectral widths and any angular aperture of the radiation beam.

18. Unique definition of relative velocity of luminous source

For test particles and observers there is no unique way to compare four-vectors of the velocities at widely separated space-time events in a curved Riemannian space-time, because general relativity (GR) provides no *a priori* definition of relative velocity. This inability to compare vectors at different points was the fundamental feature of a curved space-time. Keeping in mind aforesaid, below we restrict our analysis to seeking solution for particular case when a test particle is being a luminous object. In this case, the problem of a definition of relative velocity can be significantly simplified because of available spectral shift measured by observer. The hope appears that a relative velocity of luminous source as measured along the observer's line-of-sight (speed) can be defined in unique way straightforwardly from kinematic spectral shift rule, which holds on a generic pseudo-Riemannian manifold (Synge, 1960). We extend those geometrical ideas developed by Synge, to build a series of infinitesimally displaced shifts and then sum over them in order to achieve an unique definition of the so-called *kinetic* relative velocity of luminous source, without subjecting it to a parallel transport, as measured along the observer's line-of-sight in a generic pseudo-Riemannian space-time. This provides a new perspective to solve startling difficulties of superluminal `proper´ recession velocities, which the conventional scenario of expanding universe of standard cosmological model presents. In some instances (in earlier epochs), the distant astronomical objects are observed to exhibit redshifts in excess of unity, and only a consistent theory could tackle the key problems of a dynamics of such objects.

18.1. The relative velocity of luminous source as measured along the observer's line-of-sight in a generic pseudo-Riemannian space-time

The principle foundation of our setup comprises the following steps. Let (o) and (s) be two world lines respectively of observer O and source S in the pseudo-Riemannian space-time. Suppose the passage of light signals from S to O is described by a single infinity of null geodesics $\Gamma(v)$ connecting their respective world lines. To clarify the issues further, it should help a few noteworthy points of Fig. 2. The $S_{(1)}$ and $S_{(2)}$ are two neighboring world points on (s). The parametric values for these geodesics are $v, v+\triangle v$, respectively, where $v = const$ and $\triangle v$ is infinitesimally small. Accordingly, the world line (s) is mapped pointwise on the (o) by a set of null geodesics $\Gamma(v)$. That is, a set of null geodesics are joining (s) to (o), each representing the history of a wave crest. The totality of these null geodesics forms a 2-space with equation $x^\mu = x^\mu(u, v)$, which is determined once (s) and (o) are given. The u denote the affine parameter on each of these geodesics running between fixed end-values $u = 0$ on (s) and $u = 1$ on (o). The $O_{(1)}$ and $O_{(2)}$ are corresponding world points on (o), where the null geodesics from $S_{(1)}$ and $S_{(2)}$ meet it. Also we will denote by τ_O and τ_S the proper times of the observer and the source, respectively, and $\triangle\tau_O$ and $\triangle\tau_S$ are the elements of proper time corresponding to the segments (the clock measures of) $O_{(1)}O_{(2)}$ and $S_{(1)}S_{(2)}$. Imagine now a dense family of adjacent observers O_j $(j = 1, ..., n-1)$ with the world lines (o_j) populated between the two world lines (o) and (s). Each

doi: 10.52526/25792776-2021.68.2-311

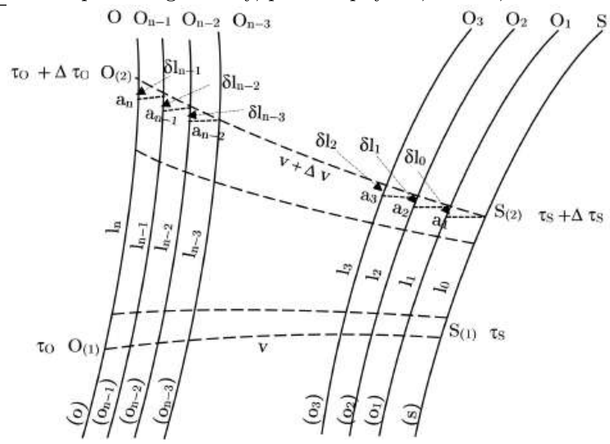

Figure 2. The infinitesimal spectral shifts as measured locally by emitter and adjacent receivers in a generic pseudo-Riemannian space-time. The (o) and (s) are two world lines respectively of observer O and source S. A dense family of adjacent observers O_j $(j = 1, ..., n-1)$ with the world lines (o_j) populated between the two world lines (o) and (s). A set of null geodesics (the dotted lines) is mapping (s) on (o), each representing the history of a wave crest. Each line segment l_{i-1} of proper space scale factor (at the affine parameter u_{i-1}) is identically mapped on the line segment $(l_i - \delta l_{i-1})$ of proper space scale factor (at infinitesimally close affine parameter u_i), such that $l_{i-1} \equiv (l_i - \delta l_{i-1})$, where δl_i denotes infinitesimal segment $a_i O_{i(2)}$.

observer O_j measures the frequency of light rays emitted by the source S as it goes by. The $O_{j(1)}$ and $O_{j(2)}$ are two neighboring world points on (o_j) where the null geodesics from $S_{(1)}$ and $S_{(2)}$ meet it. The u_j denote the values of affine parameter on each of the null geodesics chosen at equal infinitesimally small δu_i, so that $u = u_j$ on (o_j). The τ_{O_j} denotes the proper times of the adjacent observers, i.e. $\triangle\, \tau_{O_j}$ are the elements of proper time corresponding to the segment $O_{j(1)}O_{j(2)}$. Here and throughout we use the proper space scale factor l_i $(i = 0, 1, 2, ..., n)$ which encapsulates the beginning and evolution of the elements of proper time $\triangle\, \tau_S$ of source, namely $l_0 = c \triangle \tau_S$, $l_1 = c \triangle \tau_{O_{(1)}}$, $\ldots$, $l_{n-1} = c \triangle \tau_{O_{n-1}}$, $l_n = c \triangle \tau_O$. Each line segment l_{i-1} of proper space scale factor (at the affine parameter u_{i-1}) is identically mapped on the line segment $(l_i - \delta l_{i-1})$ of proper space scale factor (at infinitesimally close affine parameter u_i), such that $l_{i-1} \equiv (l_i - \delta l_{i-1})$, where δl_i denotes infinitesimal segment $a_i O_{i(2)}$. If there are N wave crests of the light, the wavelength of light λ_{O_i} at the observers O_i $(i = 1, ..., n$, where $O_n \equiv O)$, who measures the wavelength of light ray as it goes by, satisfies the following condition: $N = l_n/\lambda_n = l_{n-1}/\lambda_{n-1} = \cdots = l_1/\lambda_1 = l_0/\lambda_0$, where $\lambda_i (\equiv \lambda_{O_i})$. The spectral shift, z_i, then reads $z_i \equiv \lambda_i/\lambda_S - 1 = l_i/l_0 - 1 = \triangle\, \tau_{O_i}/ \triangle\, \tau_S - 1$. The spectral shift z_i, in general, can be evaluated straightforwardly in terms of the world function $\Omega(SO_i)$ for two points $S(x')$ and $O_i(x_{(i)})$ $(i = 1, ..., n)$ through an integral defined along the geodesic $\Gamma_{SO_i}(v)$ joining them (Synge, 1960), taken along any one of the curves $v = const$. The world function $\Omega(SO_i)$ can be defined for any of the geodesics in the family linking points on (o_i) and (s): $\Omega(SO_i) = \Omega(x' x_{(i)}) \equiv \Omega_i(v) = (1/2)(u_{Oi} - u_S)\int_{u_S}^{u_{Oi}} g_{\mu\nu} U^\mu U^\nu du$, taken along $\Gamma_{SO_i}(v)$ with $U^\mu = dx^\mu_{(i)}/du$, has a value independent of the particular affine parameter chosen. The holonomic metric $g = g_{\mu\nu}\, \vartheta\mu \otimes \vartheta^\nu = g(e_\mu, e_\nu)\, \vartheta^\mu \otimes \vartheta^\nu$, is defined in the Riemannian space-time, with the components, $g_{\mu\nu} = g(e_\mu, e_\nu)$ $(\mu = 0, 1, 2, 3)$ in the dual holonomic base $\{\vartheta^\mu \equiv dx^\mu\}$. For null geodesics $\Gamma_{S_{(1)}O_{i(1)}}(v)$ and $\Gamma_{S_{(2)}O_{i(2)}}(v + \triangle\, v)$, in particular, the world functions $\Omega_{(i)}(v)$ does not change in the interval v and $v + \triangle\, v$, therefore $\frac{\partial \Omega_{(i)}(v)}{\partial x^\mu}\frac{dx^\mu}{dv}\Big|_{O_i} + \frac{\partial \Omega_{(i)}(v)}{\partial x^\mu}\frac{dx^\mu}{dv}\Big|_S = 0$, which yields $1 + z_i = l_i/l_0 = p_{\mu(S)} V^\mu_{(S)}/p_{\mu(i)} V^\mu_{(i)}$, where $V^\mu_{(i)} = dx^\mu/d\tau_{O_i}|_{O_{i(1)}}$ and $V^\mu_{(S)} = dx^\mu/d\tau_S|_{S_{(1)}}$ are the respective four-velocity vectors of observer O_i and source S (or world lines (o_i) and (s)) at points $O_{i(1)}$ and $S_{(1)}$, $p^\mu_{(i)} = dx^\mu_{(i)}/du_i$ and $p^\mu_{(S)} = dx'^\mu/du_0$ are respective four-momenta of light ray (tangent to null geodesic) at the end points. For $i = n$, it becomes a well-known generalization of the overall spectral shift rule in a Riemannian space-time (Synge, 1960). Let us subject the vector $V^\mu_{(S)}$ to parallel transport along the null geodesic $\Gamma_{S_{(1)}O_{(1)}}(v)$ to the observer. This yields at $O_{(1)}$ the vector $\beta^\mu_{(S1)} = \mathrm{g}^{\mu\nu'}(O_{(1)}, S_{(1)}) V^{\nu'}_{(S1)}$,

doi: 10.52526/25792776-2021.68.2-311

where the two point tensor $g^{\mu\nu'}(O_{(1)}, S_{(1)})$ is the parallel propagator. The latter is determined only by the points $S_{(1)}$ and $O_{(1)}$. At $S_{(1)} \to O_{(1)}$, we have the coincidence limit $[g^{\mu\nu'}](O_{(1)}) = g^{\mu\nu}(O_{(1)})$. Then we obtain a relativistically invariant form of global Doppler shift (Synge, 1960): $z = 1 - [(1+\beta^2_{(O_{(1)})})^{\frac{1}{2}} + \beta_{R(O_{(1)})}]^{-1}$, where $c\beta^{\mu}_{(S1)} = v^{\mu}_{(S1)}$, $c\beta_{(O_{(1)})} = v_{(O_{(1)})}$, $c\beta_{R(O_{(1)})} = v_{R(O_{(1)})}$, and $v^2_{(O_{(1)})} = v_{(\alpha)(O_{(1)})}v^{(\alpha)}_{(O_{(1)})}$, $v_{(\alpha)(O_{(1)})} = v_{\mu(S1)}\xi^{\mu}_{(\alpha)(O_{(1)})}$, $v_{R(O_{(1)})} = v_{\mu(S1))}r^{\mu}_{(O_{(1)})} = v_{(\alpha)(O_{(1)})}v^{(\alpha)}_{(O_{(1)})}$. Reviewing notations the three-velocity of (s) relative (o) are defined by the tree invariant components $v_{(\alpha)(O_{(1)})}$, $v_{(S1)}$ is the relative speed, $v_{R(O_{(1)})}$ is the speed of recession of (s). Whereas $\xi^{\mu}_{(\alpha)(O_{(1)})}$ is the frame of reference on world-line (o) with $\xi^{\mu}_{0(O_{(1)})} = V^{\mu}_{(O_{(1)})}$, the unit vector $r^{\mu(O_{(1)})}$ at $O_{(1)}$ is orthogonal to world-line (o) $(r_{\mu(O_{(1)})}V^{\mu}_{(O_{(1)})} = 0)$ and lying in the 2-element which contains the tangent at $O_{(1)}$ to (o) and $S_{(1)}O_{(1)}$.

In studying further a set of null geodesics $\Gamma(v)$ with equations $x^{\mu}(u_i, v)$ (where $v = const$), we may deal with the deviation vector $\eta^{\mu}_{(i)}$ drawn from $O_{i(1)}S_{(1)}$ to $O_{i(2)}S_{(2)}$, and that we have along null geodesic $\eta_{\mu(i)}\partial x^{\mu}/\partial u_i = const$. Then the infinitesimal `relative´ spectral shift δz_i between the observers O_{i+1} and O_i will be $\delta z_i = p_{\mu(i)}V^{\mu}_{(i)}/p_{\mu(i+1)}V^{\mu}_{(i+1)} - 1 = \Omega_{\mu(i)}V^{\mu}_{(i)}/\Omega_{\mu(i+1)}V^{\mu}_{(i+1)} - 1$, where $E_i = p_{\mu(i)}V^{\mu}_{(i)}$ is the energy of light ray relative to an observer O_i, and $\Omega_{\mu(i)} = (u_{Oi} - u_S)U_{\mu}$. For definiteness, let consider case of $l_n > l_0$ (being red-shift, Fig. 1). In similar way, of course, we may treat a negative case of $l_n < l_0$ (being blue-shift), but it goes without saying that in this case a source is moving towards the observer. In first case, the observers at the points $O_{i(2)}$ $(i = 1, ..., n-1)$ should observe the monotonic increments of `relative´ spectral shifts $(\delta z_1, \delta z_2, \delta z_3, ..., \delta z_{n-1})$ when light ray passes across the infinitesimal distances $(O_{1(2)}, S_{(2)}), (O_{2(2)}, O_{1(2)}), ..., (O_{n(2)}, O_{(n-1)(2)})$. Thus, the wavelength of light emitted at $S_{(2)}$ is stretched out observed at the points $O_{i(2)}$. While weak, such effects considered cumulatively over a great number of successive increments of `relative´ spectral shifts could become significant. The resulting spectral shift is the accumulation of a series of infinitesimal shifts as the light ray passes from luminous source to adjacent observers along the path of light ray. This interpretation holds rigorously even for large spectral shifts of order one or more. If this view would prove to be true, then it would lead to the chain rule for the wavelengths $\frac{\lambda_{O_{(n2)}}}{\lambda_0} \equiv \frac{\lambda_n}{\lambda_1} = \frac{\lambda_n}{\lambda_{n-1}} \cdot \frac{\lambda_{n-1}}{\lambda_{n-2}} \cdots \frac{\lambda_2}{\lambda_1} \cdot \frac{\lambda_1}{\lambda_0} = \prod_{i=1}^{n-1}(1 + \delta z_i) = \prod_{i=1}^{n-1} p_{\mu(i)}V^{\mu}_{(i)}/p_{\mu(i+1)}V^{\mu}_{(i+1)} = \prod_{i=1}^{n-1} \Omega_{\mu(i)}V^{\mu}_{(i)}/\Omega_{\mu(i+1)}V^{\mu}_{(i+1)}$, where $\lambda_0 \equiv \lambda_{S_{(2)}}$. With no loss of generality, we may of course apply it all the way to $n \to \infty$. Let us view the increment of the proper space scale factor, $l_i = l(u_i)$, over the affine parameters u_i $(i = 1, 2, ..., n)$ as follows: $l_i = l_0 + i\varepsilon$, where ε can be made arbitrarily small by increasing n. In the limit $n \to \infty$, all the respective adjacent observers are arbitrarily close to each other, so that $\delta z_i = \delta l_i/l_i \simeq \varepsilon/l_0 \to 0$. This allows us to write the following relation for the infinitesimal `relative´ redshifts: $(\delta z_{n-1} = \delta z_{n-2} = \cdots = \delta z_1 = \varepsilon/l_0)_{n\to\infty} = \lim_{n\to\infty} \delta z^{(a)}_{(n-1)} \equiv \lim_{n\to\infty}(\frac{1}{n-1}\sum_{i=1}^{n-1}\delta z_i)$, provided, $\delta z^{(a)}_{(n-1)}$ is the average infinitesimal increment of spectral shift. Hence, $1 + z = \lim_{n\to\infty}(1 + \delta z^{(a)}_{(n-1)})^{n-1}$, where $\Omega_{\mu(O)} = (u_O - u_S)U_{\mu(O)}$ and $\Omega_{\mu(S)} = -(u_O - u_S)U_{\mu(S)}$. It should be emphasized that this general equation is the result of a series of infinitesimal stretching of the proper space scale factor in Riemannian space-time, whereas the path of a luminous source appears nowhere, thus this equation does not relate to the special choice of transport path. Then, the transformation of this equation by means of a particular definition of infinitesimal relative velocity of luminous source to observer in Riemannian space-time cannot be accepted in general, because in such approach there is no relative velocity without prior choice of transport paths. The statement attributing frequency shifts to the resulting relative velocity cannot be accepted either. To overcome the ambiguity of parallel transport of four-vectors in curved space-time, in what follows we advocate with alternative proposal. The infinitesimal increments of `relative´ spectral shifts $(\delta z_1, \delta z_2, \delta z_3, ..., \delta z_{n-1})$ can be derived from Doppler effect between adjacent emitter and absorber in relative motion measured in the respective tangent local inertial rest frames at infinitesimally separated space-time points. To obtain some feeling about this statement, below we give more detailed explanation. Imagine a family of adjacent observers $(O_{a_i}(u_i))$ situated at the points a_i $(i = 1, ..., n)$ on the world lines (o_i) at infinitesimal distances from the observers $(O_{i(2)})$, who measure the wavelength of radiation in relative motion which cause a series of infinitesimal stretching $(\delta l_0, ..., \delta l_{n-1})$ of the proper space scale factor. Since each line segment l_{i-1} of proper space scale factor

doi: 10.52526/25792776-2021.68.2-311

(at the affine parameter u_{i-1}) is identically mapped on the line segment $(l_i - \delta l_{i-1})$ (where δl_i denotes infinitesimal segment $a_i O_{i(2)}$) of proper space scale factor (at the affine parameter $u_i = u_{i-1} + \delta u_{i-1}$), the relative speed $v_{O_{i(2)}O_{a_i}}(u_i)$ of observer $(O_{i(2)}(u_i))$ to adjacent observer $(O_{a_i})(u_i)$ should be the same as it is relative to observer $(O_{(i-1)(2)}(u_{i-1}))$, that is $v_{O_{i(2)}O_{(i-1)}}(u_{i-1}) \equiv v_{O_{i(2)}O_{a_i}}(u_i)$. Continuing along this line, we may commit ourselves in the series of `relative´ spectral shifts, equivalently, a certain substitution of increments of relative speeds. Taking into account that the infinitesimal speeds of source (S) relative to observers $(O_{i(2)})$ arise at a series of infinitesimal stretching of the proper space scale factor δl_i $(i = 1, 2, ..., n)$ as it is seen from the Fig. 1, we may fill out the whole pattern of monotonic increments of `relative´ spectral shifts $(\delta z_1, \delta z_2, \delta z_3, ..., \delta z_{n-1})$ by, equivalently, replacing the respective pairs $(O_{1(2)}, S_{(2)}), (O_{2(2)}, O_{1(2)}), ..., (O_{n(2)}, O_{(n-1)(2)})$ with new ones $(O_{1(2)}, O_{a_1}), (O_{2(2)}, O_{a_2}), ..., (O_{n(2)}, O_{a_n})$, which attribute to the successive increments of relative speeds $v_{O_{1(2)}S}(u_1), ..., v_{O_{n(2)}O_{(n-1)(2)}}(u_n)$ of the source (S) away from an observer $(O_{n(2)})$ in the rest frame of $(O_{n(2)})$, viewed over all the values $(i = 1, ..., n)$. This framework furnishes justification for the concept of relative speed $c\beta_n \equiv v_{O_{n(2)}S_{(2)}}$, to be now referred to as the *kinetic* relative velocity, of the source (S) to observer $(O_{n(2)})$ along the line of sight. At the limit $n \to \infty$, the relative infinitesimal speeds tends to zero, $v_{O_{i(2)}O_{a_i}}(u_i) = c\delta\beta_i = c\delta z_i = c\delta l_i/l_i \simeq c\varepsilon/l_0 \to 0$, such that $v_{O_{i(2)}O_{a_i}}(u_i) = c\delta\beta_i = c\delta z_i = c\delta l_i/l_i \simeq c\varepsilon/l_0 \to 0$, such that $\lim_{n\to\infty} \delta\beta_{n-1} = \delta\beta^{(a)}(\equiv \lim_{n\to\infty}(n-1)^{-1}\sum_{i=1}^{n-1}\delta\beta_i) = \lim_{n\to\infty} n^{-1}\beta_n$.

Remark: Although we are free to deal with any infinitesimal `relative´ spectral shift δz_i for the pair $(O_{i(2)})$ and (O_{a_i}), in local tangent inertial rest frame of an adjacent observer (O_{a_i}), where we may approximate away the curvature of space in the infinitesimally small neighborhood, nevertheless, the infinitesimal relative velocities generally arise in RW space-time at a series of infinitesimal stretching of the proper space scale factor as alluded to above, so that the *SR law of composition of velocities cannot be implemented globally along non-null geodesic* because these velocities are velocities at the different events, which should be in a different physical frames, and cannot be added together.

Facilitating further the calculations of recession velocity (β_n) in quest, therefore, we may address the pair of observers at points $O_{(n)2}$ and a_n. Suppose $V^\mu_{O_{n(2)}}$ and $V^\mu_{O_{a_n}}$ be the unit tangent four-velocity vectors of observers $(O_{n(2)})$ and (O_{a_n}) to the respective world-lines in a general Riemannian space-time, thus in their respective rest frame we have $V^0_{O_{n(2)}} = 1$ and $V^0_{O_{a_n}} = 1$, as the only nonzero components of velocity. For comparing the vectors $V^\mu_{O_{n(2)}}$ and $V^\mu_{O_{a_n}}$ at different events, it is necessary to seek a useful definition of the relative velocity by bringing both vectors to a common event by subjecting one of them to parallel transport. Since all the paths between infinitesimally separated space-time points $O_{(n)2}$ and a_n are coincident at $n \to \infty$, for comparing these velocities there is no need to worry about specific choice of the path of parallel transport of four-vector. Therefore, we are free to subject further the unit tangent four-velocity vector $V^\mu_{O_{n(2)}}$ to parallel transport along the null geodesic $\Gamma_{O_{n(2)a_n}}$ to the point a_n. Thereby, the ray passes an observer $O_{a_n}(u_n)(\equiv O_{(n-1)(2)}(u_{n-1}))$ with the proper space scale factor l_{n-1} who measures the wavelength to be λ_{n-1}. The ray passes next observer $O_{n(2)}(u_n)$ with the proper space scale factor $l_n = l_{n-1} + \delta l_{n-1}$. The ray's wavelength measured by observer $O_{n(2)}(u_n)$ is increased by $\delta\lambda_{n-1} = \lambda_n - \lambda_{n-1}$ leading to infinitesimal `relative´ spectral shift δz_{n-1}. A parallel transport yields at O_{a_n} the vector $\beta_{\mu(O_{a_n})} = \mathrm{g}_{\mu\nu'}(O_{a_n}, O_{(n)2})V^{\nu'}_{O_{(n)2}}$, where the two point tensor $\mathrm{g}_{\mu\nu'}(O_{a_n}, O_{(n)2})$ is the parallel propagator as before, which is now determined by the points $O_{(n)2}$ and O_{a_n}. At $O_{(n)2} \to O_{a_n}$, we have the coincidence limit $[\mathrm{g}_{\mu\nu}](O_{a_n}) = g_{\mu\nu}(O_{a_n})$. As we have at point O_{a_n} two velocities $V^\mu_{O_{a_n}}$ and $\beta^\mu_{(O_{a_n})} = g^{\mu\nu}\beta_{\nu(O_{a_n})}$, we may associate Doppler shift δz_{n-1} to four-velocity $\beta^\mu_{(O_{a_n})}$ of observer O_n observed by an observer O_{a_n} with four-velocity $V^\mu_{O_{a_n}}$ as measured by the latter. Consequently, the three-velocity of an observer $(O_{n(2)})$ relative to observer at (O_{a_n}) is $v_{(\alpha)(O_{a_n})}$, the relative speed is $v_{(O_{a_n})}$, and $v_{R(O_{a_n})}$ is the speed of recession of (o_n). In the local inertial rest frame $\xi^\mu_{(\alpha)(O_{a_n})}$ of an observer (O_{a_n}), the velocity vector $\beta^\mu_{O_{a_n}}$ takes the form $(\gamma, \gamma\delta\beta_{(O_{a_n})}, 00)$, where an observer $(O_n(2))$ is moving away from the observer (O_{a_n}) with the relative infinitesimal three-velocity $\delta\beta_{(O_{a_n})}$ (in units of the speed of light) in a direction making an angel $\theta_{(O_{a_n})}$ with the outward direction of line of sight $\Gamma_{O_{n(2)O_{a_n}}}$ from $O_{(n)2}$ to O_{a_n}, and $\gamma = (1 - \delta\beta^2_{(O_{a_n})})^{-1/2}$. Hence, $\delta z_{n-1} = \delta\beta_{(O_{a_n})}\cos\theta_{(O_{a_n})}$. Thus, at $n \to \infty$, the wavelength measured by the observer $O_{n(2)}$ is increased by the first-order Doppler shift

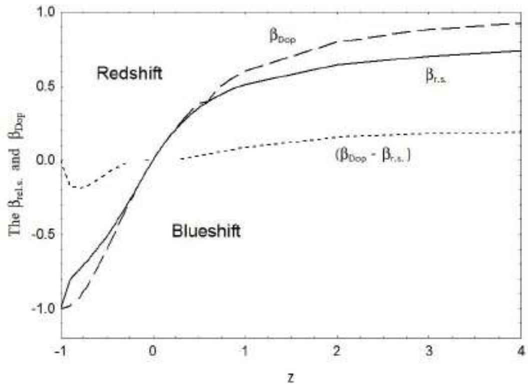

Figure 3. The relative velocity along the line of sight ($\beta_{r.s.}$) of luminous source (S) with $-1 \leq z \leq 4$ to observer (O), the global Doppler velocity (β_{Dop}), and their difference (in units of the speed of light).

caused unambiguously by the infinitesimal relative speed $\delta\beta^{(r)}_{n-1} \equiv \delta\beta_{(O_{a_n})}\cos\theta_{(O_{a_n})}$ along the line of sight with end-points $O_{(n)2}$ and O_{a_n}: $\delta z_{n-1} = \delta l_{n-1}/l_{n-1} = \delta\beta^{(r)}_{n-1}$. The SR law of composition of velocities along the line of sight can be implemented in the tangent inertial rest frame of an observer O_{a_n}: $\delta\beta^{(r)}_{n-1} = (\beta_n - \beta_{n-1})/(1-\beta_n\beta_{n-1}) \simeq \delta\beta_{n-1}/(1-\beta^2_{n-1})$, where $v_{n-1} = c\beta_{n-1}$ and $v_n = c\beta_n$ are, respectively, the three-velocities of observers O_{a_n} and O_n along the line of sight with end-points O_{a_n} and $O_{(n)2}$. Consequently, the relations presented above result in the straightforward kinematic relationship of the overall spectral shift, z, and the speed $\beta_{r.s.}$ (in units of the speed of light) of source (S) relative to observer ($O \equiv O_n$) in its rest frame along the line of sight in a general Riemannian space-time: $1+z = p_{\mu S}V^\mu_S/p_{\mu O}V^\mu_O = \Omega_{\mu(S)}V^\mu_{(S)}/\Omega_{\mu(O)}V^\mu_{(O)} = \exp\left[\beta_{r.s.})/(1-\beta^2_{r.s.})\right]$, where the relative speed $\beta_{r.s.} \equiv \lim_{n\to\infty}\beta_n$ in quest is marked with subscript $()_{r.s.}$. The relative speed of luminous source is plotted on the Fig. 3 for redshifts $-1 \leq z \leq 4$.

18.2. A global Doppler shift along the null geodesic

Suppose the velocities of observers say $O_{i(2)}$ $(i = 1, ..., n-1)$, being in free fall, populated along the null geodesic $\Gamma_{S_{(2)}O_{(2)}}(v+\triangle v)$ of light ray (Fig. 2), vary smoothly along the line of sight with the infinitesimal increment of relative velocity $\delta\beta^r_i$. The (i)-th observer situated at the point $i(2)$ of intersection of the ray's trajectory $\Gamma_{S_{(2)}O_{(2)}}(v+\triangle v)$ with the world line (o_i) at affine parameter u_i, and measures the frequency of light ray as it goes by. According to the equivalence principle, we may approximate away the curvature of space in the infinitesimally small neighborhood of two adjacent observers. We should emphasize that if we approximate an infinitesimally small neighborhood of a curved space as flat, the resulting errors are of order $(\delta l_i/l_n)^2$ in the metric. If we regard such errors as negligible, then we can legitimately approximate space-time as flat. The infinitesimal increment of spectral shift δz_i is not approximated away in this limit because it is in that neighborhood of leading order $(\delta l_i/l_i)$. That is, approximating away the curvature of space in the infinitesimally small neighborhood does not mean approximating away the infinitesimal increment δz_i. Imagine a thin world tube around the null geodesic $\Gamma_{S_{(2)}O_{(2)}}(v+\triangle v)$ within which the space is flat to arbitrary precision. Each observer has a local reference frame in which SR can be taken to apply, and the observers are close enough together that each one $O_{(i+1)(2)}$ lies within the local frame of his neighbor $O_{i(2)}$. This implies the vacuum value of a velocity of light to be universal maximum attainable velocity of a material body found in this space. Such statement is true for any thin neighborhood around a null geodesic. Only in this particular case, the relative velocity of observers can be calculated by the SR law of composition of velocities globally along the path of light ray. We may apply this law to relate the velocity β_{i+1} to the velocity β_i, measured in the i-th adjacent observer's rest frame. The end points of infinitesimal distance between the adjacent observers $O_{(i+1)(2)}$ and $O_{i(2)}$ will respectively be the points of intersection of the ray's trajectory with the world lines $o_{i+1}(u_{i+1})$ and $(o_i)(u_i)$. This causes a series of infinitesimal increment of the proper space scale factor from initial value $l_0 =\triangle\tau_S$ to the given value $l_i =\triangle\tau_{O_i}$, which in turn causes a series of infinitesimal increment of spectral shift

doi: 10.52526/25792776-2021.68.2-311

$\delta z_i = \delta\lambda_i/\lambda_i = \delta l_i/l_i$. Within each local inertial frame, there are no gravitational effects, and hence the infinitesimal spectral shift from each observer to the next is a Doppler shift. Thus, at the limit $n \to \infty$, a resulting infinitesimal frequency shift δz_i, can be unambiguously equated to infinitesimal increment of a fractional SR Doppler shift $\delta \bar{z}_i$ from observer $O_{i(2)}$ to the next $O_{(i+1)(2)}$ caused by infinitesimal relative velocity $\delta\bar{\beta}^r_i$: $(\delta z_i = \delta l_i/l_i)_{n\to\infty} = (\delta\bar{z}_i = \delta\bar{\beta}^r_i = (\bar{\beta}_{i+1} - \bar{\beta}_i)/(1 - \bar{\beta}_{i+1}\bar{\beta}_i) \simeq \delta\bar{\beta}_i/(1-\bar{\beta}^2_i))_{n\to\infty}$, where by $\bar{()}$ we denote the null-geodesic value, as different choice of geodesics yields different results for the motion of distant test particles relative to a particular observer. This relation can be transformed as follows: $(\delta z_{n-1} =)_{n\to\infty} = (\delta\beta_{n-1}/(1-\beta^2_n))_{n\to\infty} = (\delta\bar{z}^{(a)}_{(n-1)} = \delta\bar{\beta}^{r(a)}_{(n-1)} \equiv (n-1)^{-1}\sum^{n-1}_{i=1}\delta\bar{\beta}_i/(1 - \bar{\beta}^2_i))_{n\to\infty}$, which, for sufficiently large but finite n, gives $\bar{\beta}_n = (e^{\varrho_n}-1)/(e^{\varrho_n}+1), \quad \varrho_n \equiv 2\beta_n/(1-\beta^2_n)$. Hence the general solution is reduced to a global Doppler shift along the null geodesic $1 + z = \sqrt{1+\bar{\beta}_{r.s.}/1-\bar{\beta}_{r.s.}} = p_{\mu(O2)}V^{\mu}_{(S2)}/p_{\mu(O2)}V^{\mu}_{(O2)}$, where $\bar{\beta}_{rec} = \lim_{n\to\infty}\bar{\beta}_n$, $V^{\mu}_{(S2)}$ and $V^{\mu}_{(O2)}$ are the four-velocity vectors, respectively, of the source $S_{(2)}$ and observer $O_{(2)}$, $p_{\mu(S2)}$ and $p_{\mu(O2)}$ are the tangent vectors to the typical null geodesics $\Gamma_{S_{(2)}O_{(2)}}(v)$ at their respective end points. This procedure, in fact, is equivalent to performing parallel transport of the source four-velocity in a general Riemannian space-time along the null geodesic to the observer. Note that any null geodesic from a set of null geodesics mapped (s) on (o) can be treated in the similar way. In Minkowski space a parallel transport of vectors is trivial and mostly not mentioned at all. This allows us to apply globally the SR law of composition of velocities to relate the velocities $\bar{\beta}_{i+1}$ to the $\bar{\beta}_i$ of adjacent observers along the path of light ray, measured in the i-th adjacent observer's frame. Then, a global Doppler shift of light ray emitted by luminous source as it appears to observer at rest in flat Minkowski space can be derived by summing up the infinitesimal Doppler shifts caused by infinitesimal relative velocities of adjacent observers.

19. The implications for the spatially homogeneous and isotropic Robertson-Walker space-time

In the framework of RW-cosmological model, one assumes that the universe is populated with comoving observers (Ter-Kazarian, 2021a). In the homogeneous, isotropic universe comoving observers are in freefall, and obey Wayl's postulate: their all worldlines form a 3-bundle of non-intersecting geodesics orthogonal to a series of spacelike hypersurfaces, called comoving hypersurfaces. In case of expansion, all worldlines are intersecting only at one singular point. The clocks of comoving observers, therefor, can be synchronized once and for all. Let the proper time, t, of comoving observers be the temporal measure. Suppose $R(t)$ is the scale factor in expanding homogenous and isotropic universe. One considers in the so-called cosmological rest frame a light that travels from a galaxy to a distant observer, both of whom are at rest in comoving coordinates. As the universe expands, the wavelengths of light rays are stretched out in proportion to the distance $L(t)$ between co-moving points $(t > t_1)$, which in turn increase proportionally to $R(t)$. In this case, the role of proper space scale factor l_i is now destined to the scale factor $R(t_i) \propto L(t_i)$. The general solution, of course, does straightforwardly yield the particular solution as a corollary for the case of expanding RW-space-time of standard cosmological model. However, it is instructive to substantiate this principle statement further by the reasoning recast in more physical terms of, alternative, so-called *lookforward* history of expanding homogenous and isotropic universe. As a guiding principle, therefore, we briefly recount some of the highlights behind of this approach. The Fig. 4 illustrates the *lookforward* history, where $L_i \equiv L(t_i)$ is the \`proper distance´ between a galaxy (A_i) and observer (O_i), at given epoch (t_i), while the increase of the L_i is viewed over different epochs $(i = 1, 2, ..., n)$, with the infinitesimal time difference $((t_i - t_{i-1}) \to 0,\ n \to \infty)$. To give more credit to this view, we go ahead with the *lookforward* history of the proper distance $L_1 \equiv L(t_1)$ in the expanding universe, from initial epoch (t_1) to the present epoch (t). Thereby $t_n \equiv t$ and $L_n \equiv L(t)$. We assume that an observer (O_i) in its rest frame of reference measures the frequency of light rays emitted by a galaxy (A_i) viewed over different epochs $(1, ..., i)$ of expansion. Each proper distance $L_{A_{i-1}O_{i-1}}(t_{i-1})$ (at epoch t_{i-1}) is identically mapped on the line segment $L_{a_iO_i}(t_i)$ of proper distance (at infinitesimally close epoch t_i), such that $L_{a_iO_i}(ti) \equiv L_{A_{i-1}O_{i-1}}(t_{i-1})$. Null geodesic of a light signal from a galaxy (A_1) to the observers O_i $(O_n \equiv O)$ is also plotted. The picture on Fig. 4, of course, wholly agrees with the Cosmological Principle. The requirement for homogeneity and isotropy is implemented by this principle in order to

doi: 10.52526/25792776-2021.68.2-311

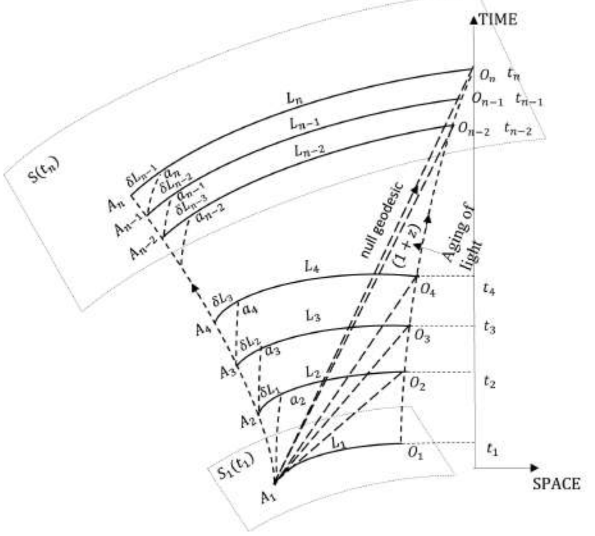

Figure 4. \`Lookforward´ history of expanding homogenous and isotropic universe.

avoid a privileged observer. In accord to modern cosmology, the universe does not expand in space, but consists of expanding space. It does not say anything about the point of origin of the universe, either it does not mean that every pair of galaxy (A_i) and observer (O_i) is in any specially favoured or unfavoured position in the universe: the universe is isotropic about this pair, which moving apart as universe expands. Keeping in mind aforesaid, now let us explore the definition of Hubble's parameter to write $H = \frac{d}{dt}\log(\frac{R(t)}{R_1}) = \frac{d}{dt}\ln(1+z) = \frac{1}{1+z}\frac{dz}{dt}$, which, incorporating with the relation $dt/dt_1 = 1+z$, yields $dL_1/dt_1 = \dot{L} - HL = 0$. The net result is as the relation $\lambda_{A_1} = \lambda_{O_{(1)}}$ holds for the wavelengths.

Imagine a family of comoving adjacent observers situated at the points a_i $(i = 2, ..., n)$ on the infinitesimal distances from the galaxies (A_i), who measure the frequency of light rays emitted by (A_i) as it goes by. Consequently, an observers should observe the successive increments of \`relative´ redshifts, $\delta z_1, \delta z_2, \delta z_3, ..., \delta z_{n-1}$, of the light when passing across the infinitesimal distances $(A_2, a_2), (A_3, a_3), ..., (A_n, a_n)$. Thus, the wavelength of light emitted at A_i is infinitesimally stretched out relative to the wavelength of light emitted at the adjacent point a_i. While weak, such effects considered cumulatively over a great number of successive increments of redshifts could become significant. The resulting redshift is the accumulation of a series of infinitesimal redshifts as the light passes from receding galaxy to adjacent observers along the line of sight. This interpretation holds rigorously even for large redshifts of order one or more. Continuing along this line, in what follows, the mathematical structure has much in common with those constructions of subsection 10.1. Here we shall forbear to write them out as they are explained so well. We finally achieve a general solution, which is now reduced to the straightforward kinematic relationship $1+z = R(t)/R(t_1) = \exp\left[\beta_{rec}/(1-\beta^2_{rec})\right]$. A crux is the more rigorous viable concept of *physical* recession velocity $(\beta_{rec} \equiv \beta_{rel.s.})$ of a comoving distant galaxy of redshift z, which crossed past light cone at time t_1, at point (A_1) away from comoving observer (O) at the present time t. This interpretation so achieved has physical significance as it agrees with a view that the light waves will be stretched by travelling through the expanding universe, and in the same time the *kinetic* recession velocity of a distant astronomical object is always subluminal even for large redshifts of order one or more. It, therefore, does not violate the fundamental physical principle of *causality*. This provides a new perspective to solve startling difficulties of superluminal \`proper´ recession velocities, which the conventional scenario of expanding universe of standard cosmological model presents. In some instances (in earlier epochs), the distant astronomical objects are observed to exhibit redshifts in excess of unity, and only a consistent theory could tackle the key problems of a dynamics of such objects. Moreover, the general solution is reduced to global Doppler shift along the null geodesic, studied by Synge. If, and only if, for the distances at which the Hubble empirical linear \`redshift-distance´ law $(cz = HL)$ is valid, the relationship between the *physical* recession velocity, v_{rec}, and the expansion rate, $\dot{L}$ $(= HL)$, reads $\beta_{rec} = [\sqrt{1+4\ln^2(1+\dot{L}/c)} - 1]/2\ln(1+\dot{L}/c)$.

doi: 10.52526/25792776-2021.68.2-311

20. The physical outlook and concluding remarks

The physical outlook and concluding remarks on suggested novel aspects of geometry and high energy physics, spacetime deformation induced inertia effects and intense radiation physics, are given in the following items in order to resume once again a whole physical picture.

• We show how the curvature and torsion, which are properties of a connection of geometry under consideration, will come into being? The theoretical significance resides in constructing the theory of the *two-step spacetime deformation* as a guiding principle. We construct the TSSD-versions of the theory of teleparallel gravity and the most important EC theory. It is remarkable that the equations of the standard EC theory, in which the equation defining torsion is the algebraic type and, in fact, no propagation of torsion is allowed, can be equivalently replaced by the set of *modified Einstein-Cartan equations* in which the torsion, in general, is a *dynamical*. The special physical constraint imposed upon the spacetime deformations yields the short-range propagating spin-spin interaction and the existence of torsion waves that may contribute a new special polarized effects in the neutron interferometry and gravitational waves experiments. We can observe the effect of the polarized rotation plane due to quantum interferometry, which would be an interesting topic not discussed in this paper. A detailed analysis and calculations on the more general MAG theory with dynamical torsion in context of TSSD formulation of post-Riemannian geometry will be presented in another paper to follow at a later date.

• In the same framework we shown that the equations of the standard MAG theory can be equivalently replaced by the set of *modified MAG equations* in which the torsion, in general, is *dynamical*. As an application we have to test the general TSSD-MAG framework in some limit, namely we have to put on Lagrange multipliers to recover the TSSD-versions of different (sub-)cases of Poincaré gauge theory (PG), Einstein-Cartan (EC) theory, teleparallel gravity ($GR_{||}$) and general relativity (GR). Moreover, we shown that by imposing different appropriate physical constraints upon the spacetime deformations, in this framework we may reproduce the term in the well known Lagrangian of pseudoscalar-photon interaction theory, or terms in the Lagrangians of pseudoscalar theories by Ni, or in modification of electrodynamics with an additional external constant vector coupling, as well as in case of intergrand for topological invariant, or in case of pseudoscalar-gluon coupling occurred in QCD in an effort to solve the strong CP problem.

• The new conceptual element in the extended phase space formulation is noteworthy. Extended canonical transformations allows to go from one extended phase space to another. This unifying feature of the theory makes the comparison of the various functions existing in the literature possible and transparent. We have developed the SQM in extended phase space and shown how this method can be generalized to deal with systems subjected to first class constraints. We have proved that Lagrange's method of undermined multipliers yields the quantization of constrained systems in SQM and, in a natural way, results in the Faddeev-Popov conventional path-integral measure for gauge systems. One of the most remarkable features of SQM is that one may quantize even dynamical systems with non-holonomic constraints as it is seen in the case of the stochastic gauge fixing.

• We construct (N=2)-realization of the extended phase space SUSY algebra, discuss the vacuum energy and the topology of super-potentials. The question of spontaneously breaking of extended SUSY deserves further investigation. Therefore, in subsequent paper we will analyze in detail the non-perturbative mechanism for extended phase space SUSY breaking in the instanton picture, and we will show that this indeed has resulted from tunnelling between the classical vacua of the theory. We demonstrate the merits of shape-invariance of exactly solvable extended SUSY potentials, which has underlying algebraic structure, by obtaining analytic expressions for the entire energy spectrum of extended Hamiltonian with Scarf potential without ever referring to underlying differential equation. However, a shape-invariance is not the most general integrability condition as not all exactly solvable potentials seem to be shape-invariant.

• We addressed the classical analog of (N=2)-realization of the supersymmetry algebra. We obtain the integrals of motion. We use the iterative scheme to find the approximate groundstate solutions to the extended Schrödinger-like equation and calculate the parameters which measure the breaking of extended SUSY such as the groundstate energy. The approximation, which went into the derivation of solutions meets our interest that the groundstate energy ε is supposedly small. This gives direct evidence for the SUSY breaking. However, we calculate a more practical measure for the SUSY breaking,

doi: 10.52526/25792776-2021.68.2-311

in particular in field theories which is the expectation value of an auxiliary field. We analyze in detail the non-perturbative mechanism for extended phase space SUSY breaking in the instanton picture and show that this has resulted from tunneling between the classical vacua of the theory. Finally, we present an analysis on the independent group theoretical methods with nonlinear extensions of lie algebras from the extended phase space SUSY quantum mechanics. Using the factorization procedure we explore the algebraic property of shape invariance and spectrum generating algebra. Most of these Hamiltonians posses this feature and hence are solvable by an independent group theoretical method. We construct the unitary representations of the deformed Lie algebra.

• The OM formalism is the mathematical framework for our physical outlook embodied in the idea that the geometry and fields, with the internal symmetries and all interactions, as well the four major principles of Relativity (Special and General), Quantum, Gauge and Colour Confinement, are derivative. They come into being simultaneously in the stable system of the underlying `primordial structures´ involved in the `linkage´ establishing processes. The OM formalism is the generalization of secondary quantization of the field theory with appropriate expansion over the geometric objects leading to the quantization of geometry drastically different from all existing schemes. We generalize the OM formalism via the concept of the OMM yielding the MW-geometry involving the spacetime continuum and the internal worlds of the given number. In an enlarged framework of the OMM we define and clarify the conceptual basis of subquarks and their characteristics stemming from the various symmetries of the internal worlds. They imply subcolour confinement and gauge principle. By this we have arrived at an entirely satisfactory answer to the question of the physical origin of the Geometry and Fields, the Internal symmetries and interactions, as well the fundamental principles of Relativity, Quantum, Gauge and Subcolour Confinement.

• The value of the hypothesis of existence of the MW-structures defined on the MW-geometry resides in solving of some key problems of the SM, wherein we attempt to suggest a microscopic approach to the properties of particles and interactions. Particularly, we derive the Gell-Mann-Nishijima relation and flavour group, infer the only possible low energy SM particle spectrum, and conclude that the leptons are particles with integer electric and leptonic charges, and free of confinement, while quarks carry fractional electric and baryonic charges, and imply the confinement. We suggest the microscopic theory of the unified electroweak interactions with a small number of free parameters, wherein we exploit the background of the local expanded symmetry $SU(2) \otimes U(1)$ and P-violation. The Weinberg mixing angle is shown to have fixed value at 30^o.

Due to the Bose-condensation of relativistic fermion pairs the Higgs bosons have arisen on an analogy of the Cooper pairs in superconductivity. It involves the Higgs bosons as the collective excitations of bound quasi-particle iso-pairs. In the framework of local gauge invariance of the theory incorporated with the P-violation in weak interactions we propose a mechanism providing the Bose-condensation of iso-pairs, which is due to effective attraction between the relativistic fermions caused by the exchange of the mediating induced gauge quanta in the W-world. We consider the four-component Bose-condensate, where due to self-interaction its spin part is vanished. Based on it we show that the field of symmetry-breaking Higgs boson always must be counted off from the gap symmetry restoring value as the point of origin. Then the Higgs boson describes the excitations in the neighbourhood of stable vacuum of the W-world. In contrast to the SM, the suggested approach predicts the electroweak symmetry breakdown in the W-world by the VEV of spin zero Higgs bosons and the transmission of electroweak symmetry breaking from the $W-$world to the M_4 spacetime continuum. The resulting Lagrangian of unified electroweak interactions of leptons and quarks ensues, which in lowest order approximation leads to the Lagrangian of phenomenological SM. In general, the self-energy operator underlies the Yukawa coupling constant, which takes into account a mass-spectrum of all expected collective excitations of bound quasi-particle pairs.

The implication of quarks into this scheme is carried out in the same manner except that of appearance of quark mixing with Cabibbo angles and the existence of CP-violating complex phase in unitary matrix of quark mixing. The Q-components of the quarks u', c' and t' contain at least one identical subquark, due to which the partial formfactors gain nonzero values. This underlies the quark mixing with Cabibbo angles. In the case of the leptons these formfactors are vanished and the mixing is absent. The CP-violation stems from the spanning incorporated with the expanded group of global

doi: 10.52526/25792776-2021.68.2-311

rotations. With a simple viewpoint on Higgs sector the masses of leptons and quarks are given.

• We derive the MW-SUSY, which has an algebraic origin in the sense that it has arisen from the subquark algebra defined on the internal worlds, while the nilpotent supercharge operators are derived. Our purpose at first is much easier to handle, by restoring in the first the `exact` ´ MW-SUSY. It can be achieved by lifting up each sparticle to corresponding particle state. This enables the sparticle to be included in the same supermultiplet with corresponding particle. Due to different features of particles and sparticles when passing back to physically realistic limit one must have always to distinguish them by introducing an additional discrete internal symmetry, i.e., the multiplicative Z_2 R-parity. The MW-SUSY has realized only on the internal worlds, but not on the spacetime continuum, which are all the ingredients of the broken super-multimanifold ($\not{S}$MM). Defined on the $\not{S}$MM it implies the super-algebra different from the conventional SUSY algebra. We write then the most generic renormalizable MW-SUSY action involving gauge and supersymmetric matter frame fields, and, thus, the corresponding generating functional. Therein, we are led to the principal point of drastic change of the standard SUSY scheme to specialize the superpotential to be in such a form, which enables within this framework, further, to build up the MTSM.

• We develop the microscopic approach to the isospinor Higgs boson with self-interaction and Yukawa couplings, wherein the two complex self-interacting isospinor-scalar Higgs doublets (H_u, H_d) as well as their spin-$\frac{1}{2}$ SUSY partners ($\widetilde{H}_u$, $\widetilde{H}_d$) Higgsinos have arisen on the W-world as the Bose-condensate. The Higgs mechanism does work in the following way: Before the symmetry was broken in the W-world, the 2 complex $SU(2)_L$ Higgs doublets had 8 degrees of freedom. Three of them were the would-be Nambu-Goldstone bosons G^0, $G^{\pm}$, which were absorbed to give rise the longitudinal modes of the massive W-components of the Z^0 and $W^{\pm}$ vector bosons, which simultaneously give rise the corresponding x- components too, leaving 5 physical degrees of freedom. The latter consists of a charged Higgs boson pairs $H^{\pm}$, a CP-odd neutral Higgs boson A^0, and CP-even neutral Higgs bosons h^0 and H^0. The mass eigenstates and would-be Nambu-Goldstone bosons are made of the original gauge-eigenstate fields, where the physical pseudoscalar Higgs boson A^0 is made of from the imaginary parts of h_u^0 and h_d^0, and is orthogonal to G^0; while the neutral scalar Higgs bosons are mixtures of the real parts of h_u^0 and h_d^0. The mass of any physical Higgs boson that is SM-like is strictly limited, as are the radiative corrections to the quartic potential terms. We calculated the tree-level masses for these Higgs states (sec.16) and shown that the h^0 Higgs boson arisen in the internal W-world is much heavier of that Z^0 boson. Such a breaking of the MW-SUSY can be implemented by subtracting back all the explicit soft mass terms formerly introduced for the sparticles. These terms do not reintroduced the quadratic diagrams which motivated the introduction of SUSY framework. Therewith, the boson-fermion cancellation in the above-mentioned problems can be regarded as a consequence of a constraint stemming from holomorphy of the observables, therefore it will be held at the limit too. Thus, we extract the pertinent piece containing only the η-field components and then in afterwards pass to M_4 to get the final VMSM yielding the realistic particle spectrum.

• The implication of quarks into the VMSM is carried out in the same way of leptons except that of appearance of quark mixing with Cabibbo angle and the existence of CP-violating complex phase in unitary matrix of quark mixing . The Q-components of the quarks contain at least one identical subquark, due to which the partial formfactors gain nonzero values. This underlies the quark mixing with Cabibbo angles. In lepton's case these formfactors are vanished and lepton mixing is absent. The CP-violation stems from the spanning. Adopting a simple viewpoint on Higgs sector the masses of leptons and quarks are given.

• Employing some features of the TSSD theory, we probe the origin and nature of the phenomenon of inertia effects. We construct the *relativistic theory of inertia*, which treats the inertia as a distortion of local internal properties of hypothetical 2D *master-space*. The MS is an indispensable companion of individual particle, without relation to the other matter, embedded in the background 4D-spacetime. The RTI allows to compute the *inertial force*, acting on an arbitrary point-like observer or particle due to its *absolute acceleration*. In this framework we essentially improve standard metric and other relevant geometrical structures referred to a noninertial frame for an arbitrary velocities and characteristic acceleration lengths. Despite the totally different and independent physical sources of gravitation and inertia, this approach furnishes justification for the introduction of the WPE. We relate the inertia ef-

doi: 10.52526/25792776-2021.68.2-311

fects to the more general post-Riemannian geometry. We derive a general expression of the relativistic inertial force exerted on the extended spinning body moving in the Rieman-Cartan space.

• We present a standard Lorentz code of motion in a new perspective of supersymmetry. In this, we explore the intermediate, so-called, *motion* state for a particle moving through the two infinitesimally closed points of original space. The Schwinger transformation function for these points is understood as the successive processes of annihilation of a particle at initial point and time, i.e. the transition from the initial state to the intermediate *motion* state, and the creation of a particle at final point and time, i.e. the subsequent transition from the intermediate *motion* state to the final state. The latter is defined on the *master space*, MS ($\equiv \underline{M}_2$), which is prescribed to each particle, without relation to every other particle. Exploring the rigid double transformations of MS-SUSY, we derive SLC as the individual code of a particle in terms of spinors referred to MS. This allows to introduce the physical finite *time interval* between two events, as integer number of the *duration time* of atomic double transition of a particle from M_4 to $\underline{M}_2$ and back. The theories with extended $N_{max} = 4$ supersymmetries, as renormalizable flat-space field theories, if only such symmetries are fundamental to nature, lead to the model of ELC in case of the apparent violations of SLC, the possible manifestations of which arise in a similar way in all particle sectors. We show that in the ELC-framework the propagation of the superluminal particle could be consistent with causality, and give a justification of forbiddance of Vavilov-Cherenkov radiation/or analog processes in vacuum. In the framework of local MS-SUSY, we address the inertial effects. The local MS-SUSY can only be implemented if $\widetilde{\underline{M}}_2$ and $\widetilde{M}_4$ are curved (deformed). Whereas the space $\widetilde{M}_4$, in order to become on the same footing with the distorted space $\widetilde{\underline{M}}_2$, refers to the accelerated reference frame of a particle, without relation to other matter fields. So, unlike gravitation, a curvature of space-time arises entirely due to the inertial properties of the Lorentz-rotated frame of interest, i.e. a *fictitious gravitation* which can be globally removed by appropriate coordinate transformations. The only source of graviton and gravitino, therefore, is the acceleration of a particle, because the MS-SUSY is so constructed as to make these two particles just as being the two bosonic and fermionic states of a particle of interest in the background spaces M_4 and $\underline{M}_2$, respectively, or vice versa. Therefore, a coupling of supergravity with matter superfields evidently is absent in resulting theory. Instead, we argue that a deformation/(distortion of local internal properties) of MS is the origin of inertia effects that can be observed by us.

• We briefly outline the issues on the interaction of electrons with the intense radiation: Einstein's transition coefficients for Compton scattering, and the annihilation and creation of electron-positron pairs at intense radiation. Einstein's ideas are developed for free-virtual, virtual-free and free-free transitions for electron-photon scattering at arbitrary intense radiation by splitting Compton scattering into two components. Whereas, we consider the general problem of interaction of electrons with the intense radiation via s-photon Compton scattering $s\gamma + e \to \gamma' + e'$. In doing this, we introduce a new concept of `effective photon´, and then instead of $s$-photon scattering by electron with an `effective´ four-momentum, with equal footing,, we should consider the scattering of one `effective photon´ by free electron. The Compton scattering is the s-channel of the photon-electron interaction. This formalism can be easily extended to the t-channel of the photon-electron interaction, namely to processes of annihilation and creation of electron-positron pairs. On the basis of the method of `effective photons´, the integral kinetic equation is derived that describes the time variation of the distribution function of quanta of non-equilibrium intense radiation for their multiphoton Compton scattering on Maxwellian nonrelativistic electrons. The equations of heating and cooling of electron gas are derived. We have continued the study of the process of relaxation of intense radiation on Maxwellian electrons in the general case of any spectral widths and any angular aperture of the radiation beam.

• Finally, we study the much-discussed in literature question of interpretation of the spectral shift of radiation from a distant object in a curved spacetime. We aim to provide a unique definition for the *kinetic* relative velocity between a source and the observer as measured along the observer's line-of-sight. Extending those geometrical ideas of well-known kinematic spectral shift rule to infinitesimal domain, we try to catch this effect by building a series of infinitesimally displaced shifts and then sum over them in order to find the proper answer to the problem that we wish to address. Thereby, the general equation is the result of a series of infinitesimal stretching of the proper space scale factor in Riemannian space-time, whereas the path of a luminous source appears nowhere, thus this equation

doi: 10.52526/25792776-2021.68.2-311

does not relate to the special choice of transport path. A resulting general relationship between the spectral shift and the *kinetic* relative velocity is utterly distinct from a familiar global Doppler shift. We discuss the implications for a particular case when adjacent observers are being in free fall and populated along the null geodesic, so that the *kinetic* relative velocity of luminous source is reduced to global Doppler velocity as studied by Synge. Moreover, the implications for the spatially homogeneous and isotropic Robertson-Walker space-time of standard cosmological model leads to cosmological consequences that resulting *kinetic* recession velocity of a distant astronomical object is always subluminal even for large redshifts of order one or more and, thus, it does not violate the fundamental physical principle of *causality*. That is, in the framework of `stretching of space´ point of view of the spatially homogeneous and isotropic RW space-time of standard cosmological model, we overcome an ambiguity of the procedure of parallel transport of four-velocity of source along the null geodesic to an observer by an alternative study of a `lookforward´ history of expanding universe. We use a way of separating the cosmological redshifts into infinitesimally displaced `relative´ redshift bins and sum over them to achieve an unique definition of the *kinetic* recession velocity of comoving astronomical object. A stemming relationship of overall cosmological redshift and *kinetic* recession velocity is utterly distinct from a familiar global Doppler shift formula. Nevertheless, in particular case of along the null geodesic, a general solution is reduced to a global Doppler shift.

References

Adler S. L., 2021, Int.J.Mod.Phys., A14, issue 12, 1911

Einstein A., Ehrenfest P., 1923, Z. Phys., Bd. 19, S. 301-306

Mihalas D., 1978, Stellar atmospheres, San Francisco: Freeman, W H

Nambu Y., Jona-Lasinio G., 1961, Dynamical model of elementary particles based on an analogy with superconductivity, Phys. Rev., 122, 345

Pauli W., 1923, Z. Phys., Bd. 18, S. 272-277

Synge J. L., 1960, *Relativity: The General Theory*, North-Hollaand, Amsterdam

Ter-Kazarian G., 1884, Operator Manifold Approach to Geometry and Particle Physics, I.C.T.P., Trieste, IC/94/290, No1, pp.1-76, Italy; [arXiv:hep,th/9510110]

Ter-Kazarian G., 1984a, Corrections to Inverse Compton Scattering, Astrofizika, 21, Issue 2, pp. , 345-352

Ter-Kazarian G., 1984b, The Energy Exchange Processes Between Electrons and Photons At the Intense Radiation, part I, Astrofizika, 21, pp. 609-625

Ter-Kazarian G., 1984c, The Einstein's Radiation Coefficients for the Compton Scattering, Akad. Nauk SSSR, Doklady, 276, No1, pp.598-603. In Russian

Ter-Kazarian G., 1984d, Electron's Motion Corrections to Inverse Compton Scattering, Akad. Nauk SSSR, Doklady (ISSN 0002-3264), 276, no. 1, 1984, p. 106-110. In Russian

Ter-Kazarian G., 1984e, The Einstein's Coefficients for the Compton Scattering, Communications of the Byurakan Astrophysical Observatory (ComBAO), 55, pp.65-69

Ter-Kazarian G., 1986, Distortion of the Space-Time, Textbook:"Selected Questions of Theoretical and Mathematical Physics". Vol. N5322-B86, No1, 62-146, VINITI, Moscow, Russia

Ter-Kazarian G., 1987, The Energy Exchange Processes Between Electrons and Photons At the Intense Radiation, part II., Astrofizika, 27, pp. 509-522

Ter-Kazarian G., 1989a, Supermassive Equilibrium Configurations of Superdense Matter, Akademiia Nauk SSSR, Doklady (ISSN 0002-3264), In Russian, 309, No.1, 97-101

Ter-Kazarian G., 1989b, On Study of Equilibrium Configuration of Protomatter, Part I, Astrofizika, 31, Issue 2, 345

Ter-Kazarian G., 1989c, The Theory of Distortion of Space-Time Continuum, ComBAO, 62, 1-123

Ter-Kazarian G., 1990, On Study of Equilibrium Configuration of Protomatter, Part II, Astrofizika, 33, 143-153

Ter-Kazarian G., 1991, On the study of internal structure of superdense celestial bodies. Astrofizika, 35, Issue 2,3, 335-372

Ter-Kazarian G., 1992, An Introduction to the Theory of Internal Structure of Supermassive Compact Celestial Bodies, Astrophysics & Space Sci., 194, No1, 1-129

doi: 10.52526/25792776-2021.68.2-311

Ter-Kazarian G., 1996, Operator Manifold Approach to Geometry and Particle Physics: General Gauge Principle & Gravitation, Astrophys. & Space Sci., 241, No2, pp.161-209

Ter-Kazarian G., 1997, Gravitation Gauge Group, Nuovo Cimento, 112B, No 6, 825-838

Ter-Kazarian G., 1999a, Operator Manifold Formalism, CPT-99/P.3918, CPT-CNRS, URL:www.cpt.univ-mrs.fr, Marseille, France, No1, pp.1-30; arxiv:9812181[hep,th]

Ter-Kazarian G., 1999b, Microscopic Theory of The Standard Model, CPT- 99/P.3919, CPT- CNRS, URL:www.cpt.univ-mrs.fr , Marseille, France, No1, pp.1-42; arxiv:9812182[hep-th]; arXiv:9710089[hep,th]

Ter-Kazarian G., 2001a, Protomatter and EHE C.R., Japan Phys. Soc. Jpn., 70, S. B., 84-98

Ter-Kazarian G., 2001b, Microscopic Theory of the Standard Model, CPT-2001/P.4269, CPT-CNRS, pp.1-35, URL:www.cpt.univ-mrs.fr, Marseille, France, arXiv:0007077[hep,ph]

Ter-Kazarian G., 2001c, Supersymmetric Microscopic Theory of the Standard Model, CPT-2001/P.4270, CPT-CNRS, pp.1-34, URL:www.cpt.univ-mrs.fr, Marseille, France, arXiv:0009046[hep,ph]

Ter-Kazarian G., 2009, An Extended Phase Space SUSY Quantum Mechanics, J. Phys. A: Math. Theor., 42, 055302

Ter-Kazarian G., 2010, Gravitation and inertia; a rearrangement of vacuum in gravity; Astrophysics & Space Sci., 327, 91-109, arxiv:1001.2990[gr,qc]

Ter-Kazarian G., 2011, Two-step spacetime deformation-induced dynamical torsion, Class. Quantum Grav., 28, 055003 (19pp); stacks.iop.org/CQG/28/000000; arxiv:1102.24911[gr,qc]

Ter-Kazarian G., 2012, Spacetime deformation-induced inertia effects, Advances in Mathematical Physics, Article ID 692030, 1-41, http://dx.doi.org/10.1155/2012/692030

Ter-Kazarian G., 2013a, Classical analog of extended phase space SUSY and its breaking, ISRN Mathematical Physics, 2013, Article ID 639424; http://dx.doi.org/10.1155/2013/639424

Ter-Kazarian G., 2013b, Is there an inertia due to the supersymmetry, 2013, arxiv:1303.3180[gr,qc]

Ter-Kazarian G., 2014, Ultra-high energy neutrino fluxes from supermassive AGN black holes, Astrophys. & Space Sci., 349, 919-938

Ter-Kazarian G., 2015, Modified Theories of Gravitation Behind the Spacetime Deformation, Physics Research International, 2015, Article ID 152846, 1-19,
http://dx.doi.org/10.1155/2015/152846

Ter-Kazarian G., 2016a, Rotating black holes in microscopic theory: the implications for periodic source M82X-2, Advances in Astrophysics, 1, issue 3, 201-223

Ter-Kazarian G., 2016b, On the Physical Nature of the Source of Ultraluminous X-ray Pulsations, Astrophys. & Space Sci., 361, issue 1, 20pp, DOI 10.1007/s10509

Ter-Kazarian G., 2021a, On the kinematic interpretation of cosmological redshifts, ComBAO, 68, issue 1, pp. 12-31, https://doi.org/10.52526/25792776

Ter-Kazarian G., 2021b, Unique definition of relative speed along the line of sight of a luminous object in a Riemannian space-time, ComBAO, 68, issue 1, pp. 38-49, https://doi.org/10.52526/25792776

Ter-Kazarian G., 2021c, Ambartsumian's cosmogony and the key mysteries of high energy astrophysics, ComBAO, to appear

Ter-Kazarian G., Sargsyan L., 2013, Signature of plausible accreting supermassive black holes in Mrk 261/262 and Mrk266, Advances in Astronomy, 2013, Article ID 710906, http://dx.doi.org/10.1155/2013/710906

Ter-Kazarian G., Shidhani S., 2017, Plausible Intermediate Mass Black Hole from M82X-2 X-Ray Pulsations, Advances in Astrophysics, 2, issue 3, 162-183

Ter-Kazarian G., Shidhani S., 2019, A study of 137 intermediate mass black hole candidates, Astrophys. Space Sci., 364, Issue 10, article id. 165, 23 pp

Ter-Kazarian G., Sobouti Y., 2008, An Extended Phase Space Stochastic Quantization Of Constrained Hamiltonian Systems, J. Phys. A: Math. Theor., 41, 315303

Ter-Kazarian G., Yerknapetian K., 1995, On the Internal Structure of Supermassive Compact Celestial Bodies, Astrofizika, 38, No4, 659-666

Ter-Kazarian G., Khachatryan V., Yerknapetyan K., 2003, Neutrino Cooling and Fueling at Disk Accretion Onto the SPC in AGN, and Origin of EHE G.R.s, "The Universe Viewed in Gamma-rays", ICRR, University of Tokyo. Universal Academy Press, Inc., BR-Hongo-5 Bldg., 6-16-2 Hongo Bunkyo-ku, Tokyo, Japan

Ter-Kazarian G., Terzyan Y., Khachikian E. e. a., 2006, On Multi-Nuclei Features of Some Markarian Galaxies, Monthly Notice of Royal Astron. Soc., 368, 461-470

Ter-Kazarian G., Shidhani S., Sargsyan L., 2007, Neutrino Radiation of the AGN Black Holes, Astrophys. & Space Sci., 310, issue 2, 93-110

doi: 10.52526/25792776-2021.68.2-311

The Digitized First Byurakan Survey (DFBS) as UNESCO Documentary Heritage

A. M. Mickaelian *[1], L. A. Sargsyan[1], G. A. Mikayelyan[1], K. S. Gigoyan[1], R. Nesci[2], and C. Rossi[2]

[1]NAS RA V. Ambartsumian Byurakan Astrophysical Observatory (BAO), Byurakan 0213, Aragatzotn province, Armenia
[2]Sapienza Università di Roma, Italy

Abstract

The famous Markarian Survey (or the First Byurakan Survey, FBS) was carried out in 1965-1980. Its 2000 plates were digitized in 2002-2007 and the Digitized FBS (DFBS, www.aras.am/Dfbs/dfbs.html) was created. New science projects have been conducted based on this low-dispersion spectroscopic material. The Armenian Virtual Observatory (ArVO, www.aras.am/Arvo/arvo.htm) database accommodates all new data. The project was conducted in collaboration with the Italian, USA and German scientists, as well as the Armenian Institute of Informatics and Automation Problems (IIAP) and continued during 6 years in 2002-2007. Markarian Survey and its digitized version were included in UNESCO Documentary Heritage *"Memory of the World"* International Register in 2011 as one of the rare heritage items from science.

Keywords: *photographic plates – astronomical plate archives – Markarian Survey – digitization – astrometry – photometry – spectroscopy – databases – Virtual Observatories.*

1. Introduction

Markarian survey (or the First Byurakan Survey, FBS) carried out by B. E. Markarian, V. A. Lipovetski, and J. A. Stepanian in 1965-1980 with BAO 1m Schmidt telescope and 1.5° prism, was one of the most efficient and important survey in astronomy. It was the first systematic objective-prism survey, the largest objective-prism survey of the Northern sky (17,000 sq. deg) and it was a new method of search for Active Galactic Nuclei (AGN). There are a total of $\sim$ 40,000,000 spectra for $\sim$ 20,000,000 objects in the entire survey (Markarian et al., 1989). The original aim was the search for galaxies with UV excess (Markarian et al., 1989, Mazzarella & Balzano, 1986). It resulted in discovery of 1515 UV-excess (UVX) galaxies, including more than 200 AGN and more than 100 SB galaxies. Markarian survey led to the classification of Seyferts into Sy1 and Sy2 (Weedman & Khachikyan, 1968), the definition of Starburst galaxies (Weedman, 1977), and several other projects, such as FBS Blue Stellar Objects (BSOs, Mickaelian 2008), late-type stars (Gigoyan & Mickaelian, 2012), optical identifications of IRAS sources (Byurakan-IRAS Galaxies (Mickaelian & Sargsyan, 2004) and Byurakan-IRAS Stars (Mickaelian & Gigoyan, 2006), BIG and BIS objects, respectively).

The Second Byurakan Survey (SBS) was also carried out with BAO 1m Schmidt and was the continuation of FBS to fainter magnitudes (Stepanian, 2005). FBS is now digitized and the Digitized First Byurakan Survey (DFBS, Massaro et al., 2008, Mickaelian et al., 2007) is available online. It provides 40,000,000 spectra for 20,000,000 objects at high Galactic latitudes. Detailed description of FBS, SBS and DFBS is given in Mickaelian (2016).

The huge amount of spectral information contained in the FBS plates allowed the development of several other projects based on the FBS, the most important is the discovery and investigation of blue stellar objects (Mickaelian, 2008), a survey for late-type stars (Gigoyan et al., 2003), and the optical identifications of sources from the IRAS catalogue. The sample of stellar objects is available at CDS (Byurakan-IRAS Stars, BIS; Mickaelian & Gigoyan, 2006), and a similar catalogue for IRAS galaxies (Byurakan-IRAS Galaxies, BIG; Mickaelian & Sargsyan, 2004) will soon appear at CDS. The number and classes of new objects discovered within the FBS made clear the need for open access to this information by the entire astronomical community.

*aregmick@yahoo.com, Corresponding author

doi: doi.org/10.52526/25792776-2021.68.2-390

2. Digitized First Byurakan Survey – DFBS

A number of digitization projects have been accomplished at BAO, including the most important one, **Digitized First Byurakan Survey** (**DFBS**; http://www.aras.am/Dfbs/dfbs.html; Massaro et al., 2008, Mickaelian et al., 2007) based on the digitization of the famous Markarian Survey (Markarian et al., 1989). It consisted of a number of steps:

- Development of technical principles of the Project, necessary Equipment
- Collection of all photographic plates of the Markarian Survey
- Revision and accounting of the plates and observing journals
- Scanning of a few dozens of plates to set up the necessary parameters for the scanning of all plates
- Input of data from observing journals; Creation of the DFBS Database (Mickaelian et al., 2006b)
- Creation of the DFBS Webpage and User Interface
- Scanning of photographic plates
- Archiving on HDDs and DVDs
- Astrometric plate solution; Extraction of images and spectra; Wavelength calibration; Density and flux calibration; Multiband (UBVR and POSS O/E) photometry
- Making up template low-dispersion spectra; Numerical classification of low-dispersion spectra
- DFBS catalogue and database, web page and user interface
- Visualization of DFBS on the sky map; creation of electronic interactive DFBS map and search system
- Proposing and discussing new research projects

The spectra extraction and analysis software is described in Mickaelian et al. (2010) and Knyazyan et al. (2011). DFBS plate database is available in Vizier, Strasbourg (Mickaelian et al., 2005a).

The DFBS project is relevant for preserving a very large database that was a milestone in the history of astronomy and to offer to the scientific community a new tool for investigating the properties of the nearby universe. The participating teams were: Byurakan Astrophysical Observatory (BAO, Armenia), Dipartimento di Fisica, 'La Sapienza' Università di Roma (Italy), Cornell University (Ithaca, NY, USA), MIGG Informatica & Ricerca (Italy), Hamburger Sternwarte (HS, Germany), and the Institute for Informatics and Automation Problems (IIAP, Yerevan, Armenia).

Digitization of the FBS plates started in 2002. After several test scans on a set of plates, all of the FBS plates were digitized with an Epson Expression 1680 Pro scanner at the Byurakan observatory. DFBS was the first digitization project conducted by scanner in Armenia, and its results allowed a number of other similar projects. The scanning resolution was 1600 dpi, so the pixel size is about 16 microns. The typical length of an FBS spectrum is $\sim$1.7mm, which gives 107 pixels along the wavelength direction. An 'ad hoc' program SCANFITS written by Stefano Mottola (DLR - Institute of Planetary Research, Berlin) allows the resulting image to be written directly in FITS format with corresponding information about the plate in the header. All 1874 plates in 1139 fields (Mickaelian et al., 2005b) were digitized and stored on DVDs.

The next steps were the **astrometric (plate) solution** (obtained with an accuracy of $\sim$1" rms or 0.6 pixel), automatic **extraction and classification of the spectral data** in a DFBS image, and **wavelength calibration** (only an approximate wavelength calibration scale was obtained because the dispersion is strongly non-linear, from about 22 Å/pixel at the blue edge of the spectrum to about 60 Å/pixel at the red edge, with mean dispersion 32.7 Å/pixel and dispersion of about 28.5 Å/pixel at Hγ).

Its main scanning and resulting features are given in Table 1.

The DFBS database presently is stored on a dedicated server at the 'La Sapienza' University in Rome and can be accessed through a web interface. Mirror sites are available in Yerevan at the IIAP, Trieste (Italy) and Observatoire de Paris (France). The database includes all the digitized plates and the automatically extracted spectra. Only for F-type plates (IIaF, IIAF, IIF, and 103aF) the automatic procedure do give reliable results, and for such plates approximate B and R magnitudes have also been computed and are

doi: doi.org/10.52526/25792776-2021.68.2-390

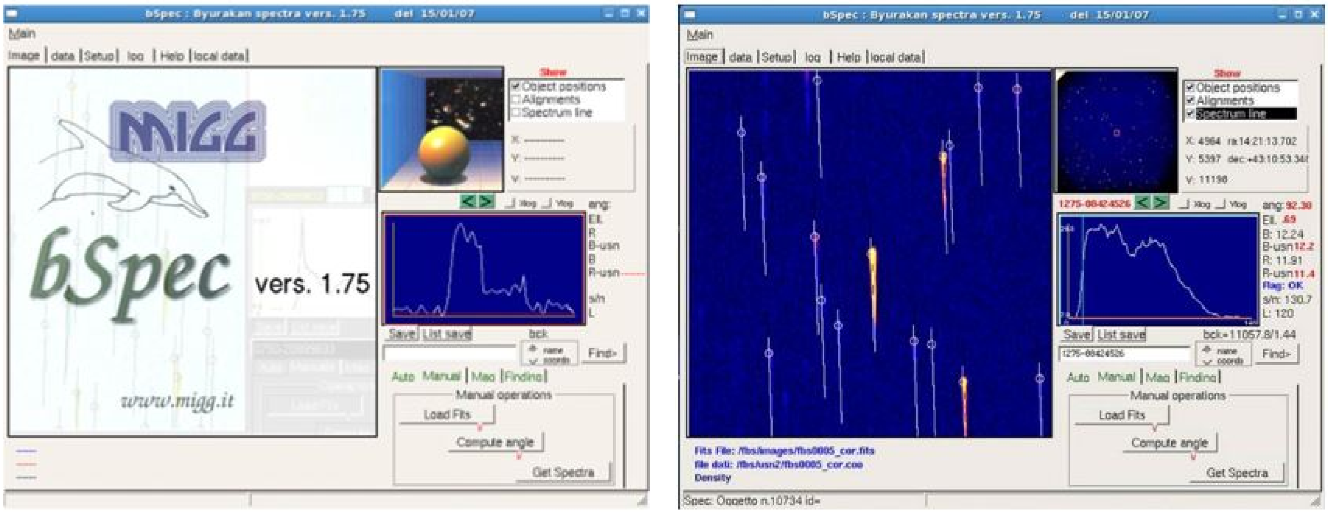

Figure 1. Dedicated software bSpec for the DFBS images and spectra extraction and analysis, an example of spectra extraction.

Table 1. Main scanning and resulting characteristics of the DFBS.

Items	**Description**
Teams	Byurakan Astrophys. Obs., Univ. Roma "La Sapienza", Cornell Univ.
Years	2002-2005
Instrument	Epson Expression 1680 Pro scanner
Scanning options	1600 dpi (15.875μ pix size), 16 bit, transparency mode, "scanfits"
Plate size	9601×9601 pix, 176 MB file
Spectra	107×5 pix (1700μ in length)
Dispersion	33 Å/pix average (22-60 Å/pix), 28.5 at Hγ
Spectral resolution	50Å(average)
Astrometric solution	1" rms accuracy
Scale	1.542 "/pix
Photometry	0.3^m accuracy
Data volume	1874 plates, $\sim$ 400 GB
Number of objects	$\sim$ 20,000,000 ($\sim$ 40,000,000 spectra)

available. Visual software named *bSpec* was created and implemented in order to get automated extraction and classification of the spectral data in a DFBS plate (Figure 1). This software performs all the operations necessary to build the DFBS database and was developed by Giuseppe Cirimele and the MIGG Informatica & Ricerca team.

A web page and user interface have been created to allow access to the DFBS database for the astronomical community. It can be queried at `http://byurakan.phys.uniroma1.it/` or `http://arvo.sci.am/ARVO/DFBS/`. The user interface provides an access to general information on the FBS and DFBS, an easy comparison of a spectroscopic DFBS plate with the corresponding direct plates from the DSS1 and DSS2, an access to the database and to the digitized plates. Users may download portions of the plates in FITS format and perform their own analysis. Each spectrum is identified by its coordinates in the USNO-A2 catalogue. Spectra can be downloaded as a single ASCII file containing all the selected spectra or as separate files for each spectrum (a tar or zip archive is actually downloaded). The user interface (the DFBS portal) presently allows the following operations to the guest user:

doi: doi.org/10.52526/25792776-2021.68.2-390

- **Get Image:** Allows users to select a portion of a plate (presently up to 1024×1024 pixels, i.e. about 26.5'×26.5') in FITS format and all spectra of this portion present in the database for downloading (spectra are ASCII files), as well as downloading of the whole selected field.

- **Get Spectra:** Allows downloading all the spectra in the database within a given distance from a selected central position (cone search); the query may be either interactive, by position, or made by uploading an ASCII file containing one or more positions (Figure 2, right panel). Objects may be selected by B, R or B-R values. If fewer than 50 objects are selected, the 2D images can also be downloaded by selecting a check box. The table containing the identifier and the main data for each spectrum can also be downloaded as an ASCII file.

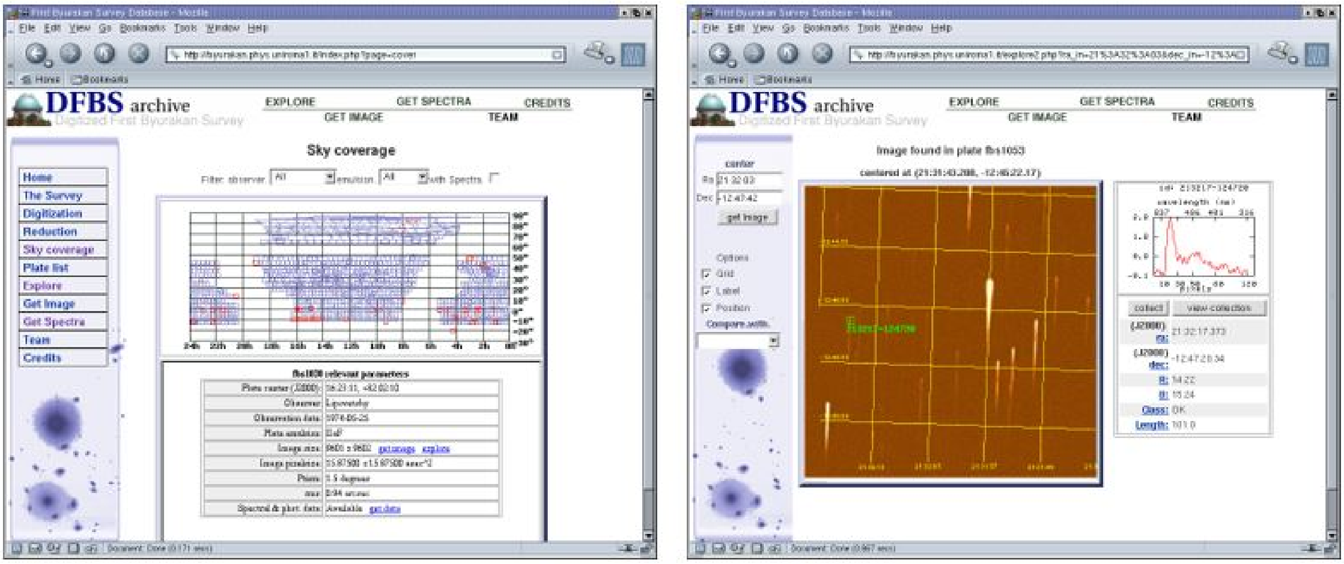

Figure 2. (left) DFBS Sky Coverage and (right) the operation "GETSPECTRA" showing the list of requested spectra and an extraction of a given spectrum on the right.

3. DFBS based Science Projects

In Figure 3 we give an example of extraction of an asteroid spectrum from DFBS using VO software SkyBoT proving how useful the DFBS plates can be for follow-up studies (Berthier et al., 2009, Sarkissian et al., 2012, Thuillot et al., 2007). The search for asteroids in DFBS jointly with IMCEE (Observatoire de Paris, France) colleagues was the most advanced research project. Bright ($<15^m$-16^m) asteroids observed in DFBS are being studied, which are divided into "fast" and "slow" ones depending on their motion during the typical DFBS plate exposure time (20 min), more or less than 3". All asteroid spectra are being extracted after they are found by means of SkyBoT. Sample spectra are being modelled similar to Solar spectra. Using these spectra and by means of comparisons with other catalogues, new candidate asteroids are being searched. Spectra analysis of asteroid spectra is being accomplished aimed at obtaining definite physical parameters.

The efficiency of studies of AGB stars based on DFBS low dispersion spectra and follow-up spectroscopy was shown by Nesci et al. (2014b). Gigoyan & Mickaelian (2007) have found a very high proper motion (PM) M7 type dwarf star, lying about 3 pc from the Sun, FBS 0250+167. Its PM is 5.050"/yr and it is in the list of the 10 known highest PM stars. Figure 4 shows that only existence of additional observational material, namely DFBS plates from 1969, linked measurements between DSS1 and DSS2 and helped identifying this object and measuring its PM.

The Second Byurakan Survey (SBS; Stepanian 2005) plates are also subject for digitization, as they are hypersensitized and their emulsion is more sensitive for deterioration. 180 plates have been digitized so far. Due to SBS smaller photographic grains, 2400 dpi ($10\mu m$ pixel size) is being used and 512 MB files are being obtained for each plate.

Having digitized plates and modern digital observational data, a number of efficient research projects have become possible, such as data discovery, spectral analysis, SED building and fitting, modelling, variability

doi: doi.org/10.52526/25792776-2021.68.2-390

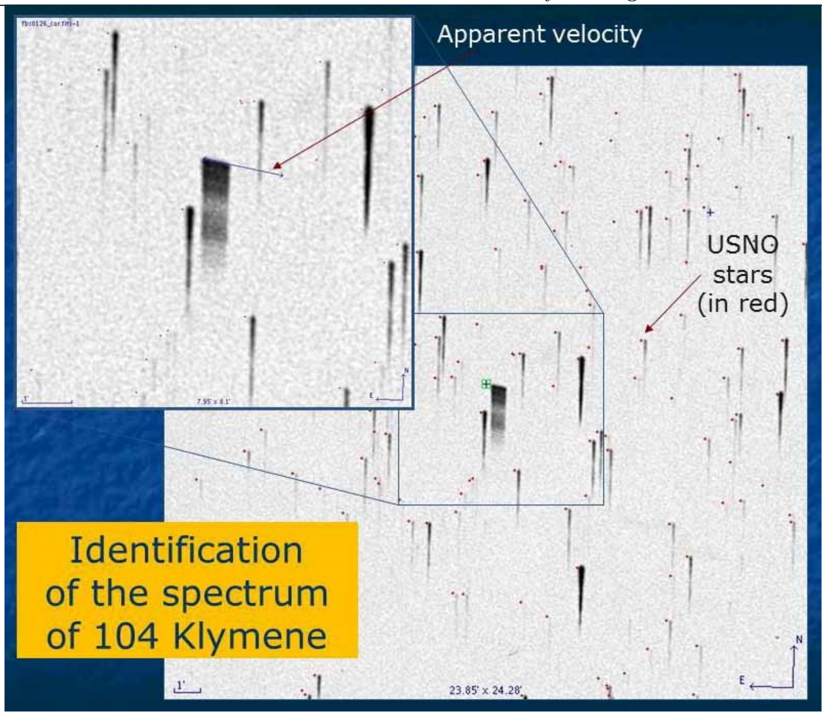

Figure 3. Extraction of an asteroid spectrum from DFBS using VO software SkyBoT.

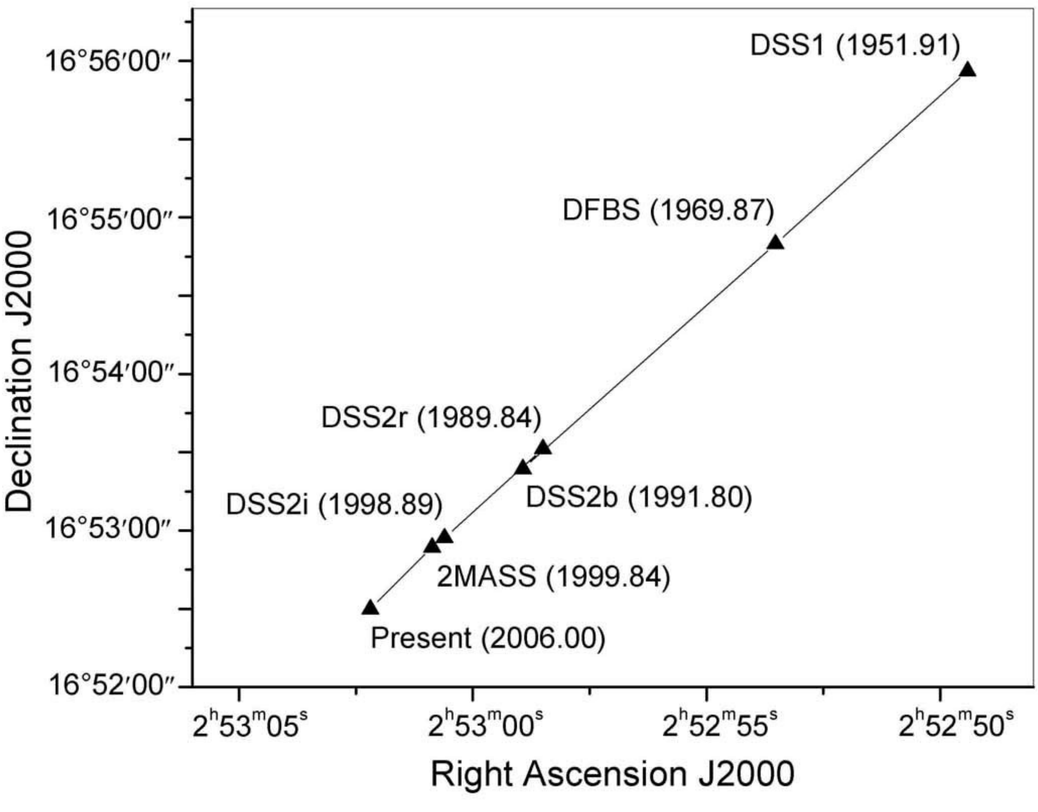

Figure 4. Direction of the motion of the high proper motion (PM=5.050"/yr) star FBS 0250+167, which was found due to DFBS plates.

studies, cross-matching, etc. Some examples are variability studies (Samus & Antipin, 2012), Cross-matching of Astronomical Catalogs (Malkov, 2012), Search for Asteroids and Exoplanets using VO tools (Sarkissian et al., 2012).

Our science projects are aimed at discoveries of new interesting objects searching definite types of low-dispersion spectra in the DFBS, by optical identifications of non-optical sources (X-ray, IR, radio) also using

doi: doi.org/10.52526/25792776-2021.68.2-390

the DFBS and DSS/SDSS, by using cross-correlations of large catalogs and selection of objects by definite criteria, etc.

4. DFBS as UNESCO "Memory of the World" documentary heritage

Markarian survey was an outstanding study for all extragalactic (as well as galactic) astronomy; its main features may be given as:

- Markarian survey is the first systematic objective-prism survey in the history of astronomy (later on, objective prism surveys became the main source for search and classification of thousands of objects having some peculiarities and for discovery of many new AGN, white dwarfs, H-alpha emission-line objects (both stars and nebulae), etc.).
- It is the largest objective-prism survey of the Northern sky (17,000 deg^2), thus providing the largest homogeneous material for unified research.
- It introduced and applied a new method of search for active galaxies, selection by UV-excess.
- Revelation of 1517 UVX galaxies: some 300 AGN and some 1000 HII galaxies.
- Classification of Seyferts into Sy1 and Sy2 types (Weedman & Khachikyan, 1968).
- Definition of Starburst (SB) galaxies (Weedman, 1977), active galaxies based on high star formation rate.
- Discovery of many new Blue Compact Dwarf Galaxies (BCDG).
- Revelation of 1103 FBS Blue Stellar Objects (BSOs; Mickaelian 2008) and 1471 Late-type Stars (Gigoyan et al., 2019) (2nd Part of the FBS).
- Optical identification of 1577 IRAS sources (samples of Byurakan-IRAS Galaxies (BIG; Mickaelian & Sargsyan 2004) and Byurakan-IRAS Stars (BIS; Mickaelian & Gigoyan 2006)); discovery of many new AGN and ULIRGs.
- Markarian survey led to many other objective prism surveys with better spectral resolution and deeper limiting magnitudes, including the Second Byurakan Survey (SBS, Markarian et al. 1983, Stepanian 2005).

Markarian galaxies are rather important for various extragalactic studies, such as: Mrk 231 is the most luminous infrared galaxy (ULIRG) in the Local Universe, Mrk 116 is the most metal-deficient blue compact dwarf galaxy (BCDG) (most of the BCDGs are Mrk and SBS galaxies), Mrk 421 and 501 are among the most powerful sources, etc.

Many more UVX and emission-line galaxies have been discovered in similar to Markarian surveys or by other studies. These are Arakelian galaxies having high surface brightness (Arakelian, 1975), Kazarian UVX galaxies (Kazarian et al., 2010), the University of Michigan emission-line galaxies (UM; MacAlpine & Williams 1981), Case Low-Dispersion Northern Sky Survey galaxies (CG; Pesch et al. 1991), the Montreal blue galaxies (Coziol et al., 1994), SBS UVX and emission-line galaxies (Stepanian, 2005), Kiso UV galaxies (KUG; Miyauchi-Isobe et al. 2010), Hamburg/SAO emission-line galaxies (Pustilnik et al., 2005), GALEX UV-luminous galaxies (Hoopes et al., 2007), etc.

Markarian survey led to the discovery of 1517 UVX galaxies, including some 300 AGN and some 1000 HII galaxies. Classification of Markarian galaxies provided Sy1 and Sy2 types and the definition of Starburst galaxies. Many new BCDG were discovered as well. The continuation of the FBS for stellar objects revealed FBS Blue Stellar Objects and FBS Late-type Stars, as well as optical identifications of IRAS sources have been carried out resulted in discovery of new ULIRGs and AGN. Markarian survey also led to many other objective prism surveys.

Markarian galaxies are reliable objects for MW studies of active galaxies, as they are bright enough and have been detected in all ranges of electromagnetic radiation; from gamma-ray to radio. The Spectral Energy Distribution (SED) provides a possibility to group objects by their shapes and compare to existing physical properties to find various relations and refine the AGN classifications.

doi: doi.org/10.52526/25792776-2021.68.2-390

The outstanding scientist Viktor Ambartsumian wrote about Markarian galaxies: *"The discovery of Markarian galaxies is a great achievement of our science. Now more and more astronomers both in our country and all over the world seek to study the nature of these objects in more details on the world largest telescopes..."*. Ambartsumian also compared Markarian survey plates with the treasures of Matenadaran – collection of ancient manuscripts.

In 2011, Markarian Survey and its digitized version, DFBS, entered **UNESCO's Documentary Heritage "Memory of the World" International Register**. It is one of the rarest science treasures that is included in UNESCO lists together with world cultural heritage masterpieces. We give in Figure 5 the related UNESCO Certificate.

The IAU Colloquium #184 in 2001 was dedicated to Markarian and the IAU Symposium #304 in 2013 was dedicated to Markarian's 100^{th} anniversary, both related to Markarian Survey and Multiwavelength AGN Surveys in general. The international symposium on *"Astronomical Surveys and Big Data"* in 2015 was dedicated to the 50^{th} anniversary of Markarian Survey and 10^{th} anniversary of Armenian Virtual Observatory (ArVO), based on DFBS, the digitized Markarian Survey.

Figure 5. UNESCO certificate awarded for its inscription in the "Memory of the World" documentary heritage International Register

5. Summary

There are a number of further **possible research projects** that will be conducted having the plates digitized:

- Correction of ephemerides of known asteroids and search for new asteroids (ex. Berthier et al. 2009, Thuillot et al. 2007)
- Discovery and study of variable stars (ex. Mickaelian et al. 2011, Nesci et al. 2009)
- Revealing high proper motion stars (ex. Mickaelian & Sinamyan 2010)
- Study of variability of known blazars and discovery of new blazars

doi: doi.org/10.52526/25792776-2021.68.2-390

- Revealing Novae and Supernovae progenitors
- Discovery of new QSOs
- Discovery of new white dwarfs (ex. Sinamyan & Mickaelian 2011)
- Discovery of new late-type stars (ex. Gigoyan et al. 2019)
- Discovery of optical sources of gamma-ray bursts
- Optical identifications of X-ray, IR and radio sources (ex. Hovhannisyan et al. 2009, Mickaelian & Gigoyan 2006, Mickaelian & Sargsyan 2004, Mickaelian et al. 2006c).

Acknowledgements

The work was supported by the Science Committee of RA, in the frames of the research project No. 21AG-1C053 *"Revelation of the early stages of galaxy evolution by means of multiwavelength study of active galaxies"*.

References

Arakelian M. A., 1975, Communications of the Byurakan Astrophysical Observatory, 47, 3

Berthier J., Sarkissian A., Mickaelian A., Thuillot W., 2009, in European Planetary Science Congress 2009. p. 526

Coziol R., Demers S., Pena M., Barneoud R., 1994, Astron. J. , 108, 405

Erastova L. K., 2004, Astrophysics, 47, 79

Gigoyan K. S., Mickaelian A. M., 2007, Astrophysics, 50, 54

Gigoyan K. S., Mickaelian A. M., 2012, Mon. Not. R. Astron. Soc. , 419, 3346

Gigoyan K. S., Abrahamyan H. V., Azzopardi M., Mauron N., Russeil D., Sinamyan P., 2003, Astrophysics, 46, 475

Gigoyan K. S., Sinamyan P. K., Engels D., Mickaelian A. M., 2010, Astrophysics, 53, 123

Gigoyan K. S., Mickaelian A. M., Kostandyan G. R., 2019, Mon. Not. R. Astron. Soc. , 489, 2030

Hoopes C. G., et al., 2007, Astrophys. J. Suppl. Ser. , 173, 441

Hovhannisyan L. R., et al., 2009, Astron. J. , 138, 251

Hudec R., 2014, in Astroplate 2014. p. 1

Kazantseva L., 2014, in Astroplate 2014. p. 13

Kazarian M. A., Adibekyan V. Z., McLean B., Allen R. J., Petrosian A. R., 2010, Astrophysics, 53, 57

Knyazyan A., Mickaelian A., Astsatryan H., 2011, International Journal "Information Theories and Applications, 18, 243

Knyazyan A. V., Astsatryan H. V., Mickaelian A. M., 2016, in Mickaelian A., Lawrence A., Magakian T., eds, Astronomical Society of the Pacific Conference Series Vol. 505, Astronomical Surveys and Big Data. p. 236

MacAlpine G. M., Williams G. A., 1981, Astrophys. J. Suppl. Ser. , 45, 113

Malkov O. Y., 2012, in Mickaelian A. M., Malkov O. Y., Samus N. N., eds, Fifty years of Cosmic Era: Real and Virtual Studies of the Sky. Conference of Young Scientists of CIS Countries. pp 48–55

Markarian B. E., Lipovetskii V. A., Stepanian D. A., 1983, Astrofizika, 19, 29

Markarian B. E., Lipovetsky V. A., Stepanian J. A., Erastova L. K., Shapovalova A. I., 1989, Soobshcheniya Spetsial'noj Astrofizicheskoj Observatorii, 62, 5

Massaro E., Mickaelian A. M., Nesci R., Weedman D., 2008, The Digitized First Byurakan Survey. ARACNE Editrice, Rome, 78p.

Mazzarella J. M., Balzano V. A., 1986, Astrophys. J. Suppl. Ser. , 62, 751

Mickaelian A. M., 2004, SCAN-IT No. 2, 2, 16

Mickaelian A. M., 2006, Romanian Astronomical Journal, 16, 23

Mickaelian A. M., 2007, Highlights of Astronomy, 14, 594

Mickaelian A. M., 2008, Astron. J. , 136, 946

Mickaelian A. M., 2012, in Mickaelian A. M., Malkov O. Y., Samus N. N., eds, Fifty years of Cosmic Era: Real and Virtual Studies of the Sky. Conference of Young Scientists of CIS Countries. pp 29–38

doi: doi.org/10.52526/25792776-2021.68.2-390

Mickaelian A., 2014a, in Astroplate 2014. p. 109

Mickaelian A. M., 2014b, in Mickaelian A. M., Sanders D. B., eds, Vol. 304, Multiwavelength AGN Surveys and Studies. pp 1–10, doi:10.1017/S1743921314003147

Mickaelian A. M., 2016, in Mickaelian A., Lawrence A., Magakian T., eds, Astronomical Society of the Pacific Conference Series Vol. 505, Astronomical Surveys and Big Data. p. 3

Mickaelian A. M., Gigoyan K. S., 2006, Astron. Astrophys. , 455, 765

Mickaelian A. M., Sargsyan L. A., 2004, Astrophysics, 47, 91

Mickaelian A. M., Sinamyan P. K., 2010, Mon. Not. R. Astron. Soc. , 407, 681

Mickaelian A. M., Hagen H. J., Sargsyan L. A., Mikayelyan G. A., 2005a, VizieR Online Data Catalog, p. VI/116

Mickaelian A. M., et al., 2005b, in Colless M., Staveley-Smith L., Stathakis R. A., eds, Vol. 216, Maps of the Cosmos. p. 230, doi:10.1017/S0074180900196676

Mickaelian A. M., Sargsyan L. A., Mikayelyan G. A., Erastova L. K., Sinamian P. K., 2006a, in Tsvetkov M., Golev V., Murtagh F., Molina R., eds, Virtual Observatory: Plate Content Digitization, Archive Mining and Image Sequence Processing. pp 82–92

Mickaelian A. M., Gigoyan K. S., Nesci R., Rossi C., 2006b, Mem.S.A.It., 77, 1159

Mickaelian A. M., Hovhannisyan L. R., Engels D., Hagen H. J., Voges W., 2006c, Astron. Astrophys. , 449, 425

Mickaelian A. M., et al., 2007, Astron. Astrophys. , 464, 1177

Mickaelian A. M., et al., 2008a, in Guainazzi M., Osuna P., eds, Astronomical Spectroscopy and Virtual Observatory. p. 29

Mickaelian A. M., et al., 2008b, Romanian Astronomical Journal, 18, 249

Mickaelian A. M., et al., 2009a, Proceedings of CSIT-2009 conference, 7, 420

Mickaelian A., et al., 2009b, CSIT 2009 Proceedings, 7, 424

Mickaelian A. M., Sargsyan L. A., Astsatryan H. V., Cirimele G., Nesci R., 2009c, Defense Science Journal, 8, 152

Mickaelian A. M., Sargsyan L. A., Nesci R., Cirimele G., Sarkissian A., 2010, in Mizumoto Y., Morita K. I., Ohishi M., eds, Astronomical Society of the Pacific Conference Series Vol. 434, Astronomical Data Analysis Software and Systems XIX. p. 325

Mickaelian A. M., Mikayelyan G. A., Sinamyan P. K., 2011, Mon. Not. R. Astron. Soc. , 415, 1061

Mickaelian A. M., Malkov O. Y., Samus N. N., eds, 2012, Fifty years of Cosmic Era: Real and Virtual Studies of the Sky

Mickaelian A. M., et al., 2016a, in Mickaelian A., Lawrence A., Magakian T., eds, Astronomical Society of the Pacific Conference Series Vol. 505, Astronomical Surveys and Big Data. p. 16

Mickaelian A. M., et al., 2016b, in Mickaelian A., Lawrence A., Magakian T., eds, Astronomical Society of the Pacific Conference Series Vol. 505, Astronomical Surveys and Big Data. pp 262–273

Mickaelian A. M., Sarkissian A., Berthier J., Meftah M., Thuillot W., Vachier F., 2019, Icarus, 330, 5

Miyauchi-Isobe N., Maehara H., Nakajima K., 2010, Publications of the National Astronomical Observatory of Japan, 13, 9

Nesci R., Rossi C., Sclavi S., Gaudenzi S., Mickaelian A. M., Sargsyan L. A., Erastova L. K., 2004, Baltic Astronomy, 13, 671

Nesci R., Mickaelian A., Rossi C., 2009, The Astronomer's Telegram, 2338, 1

Nesci R., Bagaglia M., Nucciarelli G., 2014a, in Astroplate 2014. p. 75

Nesci R., Gaudenzi S., Rossi C., Pezzotti C., Gigoyan K., Mauron N., 2014b, in Astroplate 2014. p. 91 (arXiv:1404.3842)

Osborn W., 2014, in Astroplate 2014. p. 15

Pesch P., Sanduleak N., Stephenson C. B., 1991, Astrophys. J. Suppl. Ser. , 76, 1043

Pustilnik S. A., et al., 2005, Astron. Astrophys. , 442, 109

Samus N. N., Antipin S., 2012, in Mickaelian A. M., Malkov O. Y., Samus N. N., eds, Fifty years of Cosmic Era: Real and Virtual Studies of the Sky. Conference of Young Scientists of CIS Countries. pp 39–47

Sarkissian A., Arzoumanian E., Mickaelian A. M., Berthier J., Thuillot W., Vachier F., 2012, in Mickaelian A. M., Malkov O. Y., Samus N. N., eds, Fifty years of Cosmic Era: Real and Virtual Studies of the Sky. Conference of Young Scientists of CIS Countries. pp 56–64

Sinamyan P. K., Mickaelian A. M., 2009, Astrophysics, 52, 76

Sinamyan P. K., Mickaelian A. M., 2011, Astrophysics, 54, 403

Sokolovsky K. V., Antipin S. V., Zubareva A. M., Kolesnikova D. M., Lebedev A. A., Samus' N. N., Sat L. A., 2014, Astronomy Reports, 58, 319

Stepanian J. A., 2005, Rev. Mex. Astron. Astrofis. , 41, 155

Stupka J., Benesova E., 2014, in Astroplate 2014. p. 31

Thuillot W., et al., 2007, Highlights of Astronomy, 14, 616

Tsvetkov M., Tsvetkova K., 2012, in Griffin E., Hanisch R., Seaman R., eds, Vol. 285, New Horizons in Time Domain Astronomy. pp 417–419, doi:10.1017/S1743921312001275

Véron-Cetty M. P., Véron P., 2010, Astron. Astrophys. , 518, A10

Weedman D. W., 1977, Vistas in Astronomy, 21, 55

Weedman D. W., Khachikyan E. E., 1968, Astrophysics, 4, 243

doi: doi.org/10.52526/25792776-2021.68.2-390

Twenty years of the Armenian Astronomical Society (ArAS)

A. M. Mickaelian [*], S. V. Farmanyan, and G. A. Mikayelyan

NAS RA V. Ambartsumian Byurakan Astrophysical Observatory (BAO), Byurakan 0213, Aragatzotn province, Armenia

Abstract

A review on the activities and achievements of the Armenian Astronomical Society (ArAS) and the Armenian astronomy in general is given on the occasion of the 20^{th} anniversary of the official foundation of ArAS. ArAS membership, ArAS electronic newsletters (ArASNews), ArAS webpage, Annual Meetings, Annual Prize for Young Astronomers (Yervant Terzian Prize) and other awards, international relations, participation in international organizations, Byurakan International Summer Schools (BISS), regional and local schools, Byurakan science camps, astronomical Olympiads and other events, other matters related to astronomical education, astronomical heritage, amateur astronomy, astronomy outreach and ArAS further projects are described and discussed.

Keywords: *Armenian Astronomical Society – electronic newsletter – annual meeting – summer schools – science camps – astronomical school lectures – annual prize – astronomical heritage – astronomical education – outreach.*

1. Introduction

The Armenian Astronomical Society (ArAS) was in fact created on 22 June 1999, when the first database of Armenian astronomers was collected, it was decided to create the society, By-Laws were developed and ArAS founding meeting was held. It is true that the Society was officially registered by the Armenian Ministry of Justice in two years, on 29 August 2001. Anyway, before that, actions were taken to involve astronomers in the membership, identify and organize the future activities of ArAS. After the official registration, the first steps were the affiliation to the European Astronomical Society (EAS) in September 2001, the creation of ArAS website in 2002, preparation and distribution of electronic newsletters ("ArASNews") since 2002 and establishment of the ArAS annual meetings since 2002. Since then, almost all events in Armenian astronomy are to a large extent connected with ArAS, and in the 2000s Armenian astronomy by its activeness has reached and in some ways exceeded the previous successes present during the Soviet Union years.

ArAS reports have also been published in some other papers (Mickaelian 2014, 2016, Mickaelian & Farmanyan 2018, Mickaelian et al. 2019, 2020).

[*]aregmick@yahoo.com

doi: doi.org/10.52526/25792776-2021.68.2-400

2. Membership

ArAS is an organization of exclusively professional astronomers (though a few exceptions are allowed), and also aims at establishing close ties with the Armenian foreign astronomers, inviting them to join and cooperate with astronomers in Armenia. ArAS founding members were 16 astronomers of the Byurakan Astrophysical Observatory (BAO). ArAS currently has 95 members (including 13 founding ones) representing 49 institutions from 21 countries (http://www.aras.am/Members/members.html), including: Armenia – 48 (BAO – 29, YSU – 4 and others), USA – 13, Germany – 6, Russia – 5, France – 3, Mexico – 3, Italy and Spain – 2 (each), Bulgaria, Canada, Chile, Greece, Hungary, India, Ireland, Netherlands, Portugal, Romania, Switzerland, Thailand, and UK – 1 (each). Among the famous ArAS members there are Michel Mayor (Switzerland), Brent Tully (USA), Vahe Petrosian (USA), Daniel Weedman (USA), Igor Karachentsev (Russia), Daniel Kunth (France), Massimo Turatto (Italy) and many others. We have created for each member a personal webpage containing basic information on his personal and professional data. ArAS has 2 Co-Presidents: Haik Harutyunian and Areg Mickaelian (Acting President), ArAS Vice-President: Tigran Magakian, ArAS Scientific Secretary: Elena Nikoghosyan, Treasurer: Marietta Gyulzadyan, ArASNews Editor: Meline Asryan, and ArAS Webpage Administrator: Gor Mikayelyan.

3. ArAS Electronic Newsletter

Until recently ArAS released periodically electronic newsletters (ArAS Newsletters, ArASNews; http://www.aras.am/ArasNews/arasnews.html) typically 8 times in a year (periodicity of 1.5 month). The Editors have been: Tigran Magakian (2002-2004, issues #1-12), Lusine Sargsyan (2005, issues #13-16), Lilit Hovhannisyan (2006-2007, issues #17-24), Areg Mickaelian (2008-2014, issues #25-76), Sona Farmanyan (2015-2020, issues #77-117) and Meline Asryan (since 2021, issues #141-145). Since 2015 the Newsletter became monthly, 12 issues in a year (however, in 2018-2020 it was mostly not published). In total, including the beginning of 2021, 122 issues have been prepared and released. In all ArASNews, already more than 1000 articles have been published with total some 1700 pages. ArAS Newsletters give news, announcements, articles on Armenian astronomy and BAO, ArAS new members, international and local meetings, summer/winter schools and participation of Armenian astronomers in them, astronomical education in Armenia, Armenian archaeoastronomy and astronomy in culture, anniversaries, scientific, scientific-popular, information materials, etc. A Reference List of ArASNews articles (http://www.aras.am/ArasNews/arasnewsreference.html) has been also created allowing easy access to all articles related to any subject.

4. ArAS webpage

ArAS webpage (http://www.aras.am/) was created in February 2002, at first to give the necessary information about ArAS, including ArAS objectives and forms of activities, list of ArAS members, annual meetings and other events, etc.

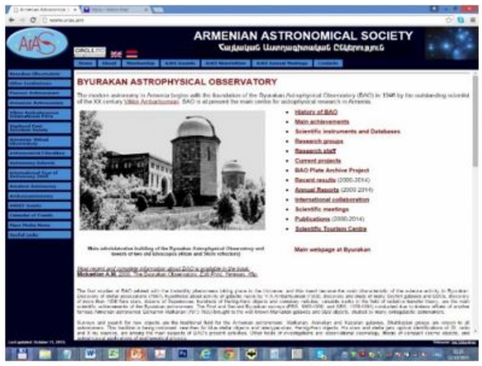

In early 2009, in connection with the International Year of Astronomy (IYA-2009), ArAS webpage was fundamentally enriched and renewed and became a repository containing full information on Armenian astronomy. There is information about BAO history, achievements, current projects and international collaboration, received grants, all publications since 2000 have been installed, all meetings with individual

doi: doi.org/10.52526/25792776-2021.68.2-400

pages, new sections have been opened for other scientific institutions in Armenia related to astronomy, 21 famous Armenian astronomers, database of 257 Armenian astronomers throughout the world, astronomical education, amateur astronomy, archaeoastronomy, etc. Without any exaggeration, in terms of the amount of information, ArAS webpage is the richest one among all Armenian scientific organizations and one of the best in the world. We also published in ArAS website Calendars of Astronomical Events of 2014-2021.

5. Participation in international organizations

Armenia is one of 82 member-states of the International Astronomical Union (IAU), as well as ArAS is recognized by IAU. Areg Mickaelian is the Secretary and the Acting President of the IAU National Committee for Astronomy (NCA) in Armenia. ArAS is one of EAS 28 affiliated societies, and by its activities it seconds only the most powerful countries in Europe: UK, Germany, France, Italy and some others. ArAS is also the official representative of the Euro-Asian Astronomical Society (EAAS) in Armenia. Areg Mickaelian is one of the EAAS Vice-Chairs and is a member of the EAAS International Bureau, and Tigran Magakian is a member of the EAAS Scientific-Technical Committee. Together with the Ministry of Education, Science, Culture, and Sports, ArAS is also one of the official representatives of International Astronomical Olympiads (IAO) in Armenia. Armenia joined the international Galileo Teachers Training Program (GTTP) with its official representatives Areg Mickaelian (Ambassador in Armenia) and Marietta Gyulzadyan (Armenian Coordinator). Armenia is an associate member of the Sub-Regional European Astronomical Committee (SREAC) acting in Southeast Europe and an associate member of the International Planetary Data Alliance (IPDA). The last EAS Annual Meeting (European Week of Astronomy and Space Science, EWASS) was virtually held in 2021; ArAS Acting President Areg Mickaelian and other Armenian astronomers took part from Armenia.

6. ArAS awards

ArAS has 5 kinds of awards given at ArAS webpage (http://www.aras.am/Prize/awards.htm):

- ArAS Annual Prize for Young Astronomers (Yervant Terzian Prize) (since 2004)
- ArAS/BAO Awards (2009)
- ArAS Certificates
- Scientific Journalism Prizes (since 2009), including ArAS/OxArm (Oxford Armenian Society) awards in 2011
- Galileo Teachers Training Program (GTTP) Certificates (since 2011)

Since 2004, ArAS awards Annul Prize for Young Astronomers (since 2009 it was renamed to Yervant Terzian Prize). It is being awarded to the most active young astronomers (younger 35) taking into account all annual activities. The award is sponsored by ArAS Co-President *Prof.* Yervant Terzian and BAO. At present it totals USD 500, and it is being awarded with ArAS Certificate. The full list of ArAS Annual Prize is given below:

In 2020, the GTTP international certificates was awarded to Ewelina Gradzka (Poland) who organized 2 events in Armenia: *"Young Explorers Club" and "Under Armenian Sky"*.

7. ArAS meetings and other events

Since 2002, ArAS holds regular annual meetings, however some of them were associated or combined with other conferences and events, where ArAS acted as co-organizer.

ArAS XIII annual meeting was unprecedented in its theme. It took place on 7-10 October 2014 in Byurakan and was called *"Relation of Astronomy to Other Sciences, Culture and Society"* (RASCS, http://www.aras.am/Meetings/RASCS/index.html). In addition to astrophysical issues it included Philosophical Problems of Astronomy, Astrobiology, Astroinformatics, Astronautics, Archaeoastronomy, Astronomical Education, Amateur Astronomy, Scientific Tourism and other topics related to astronomy. It brought together astronomers, philosophers, historians, archeologists, philologists, artists and representatives of other fields. ArAS dedicates small-scale events (one-day conferences or seminars) to the anniversaries of famous astronomers.

doi: doi.org/10.52526/25792776-2021.68.2-400

Year	Winners	Affiliation	Country
2020	Hasmik ANDREASYAN / Gor MIKAYELYAN	BAO / BAO	Armenia / Armenia
2019	Naira AZATYAN	BAO	Armenia
2018	Sona FARMANYAN	BAO	Armenia
2017	Naira AZATYAN	BAO	Armenia
2016	Anahit SAMSONYAN	BAO	Armenia
2015	Artur HAKOBYAN	BAO	Armenia
2014	Gurgen PARONYAN	BAO	Armenia
2013	Hayk ABRAHAMYAN / Avet HARUTYUNYAN	BAO / TNG	Armenia / Italy
2012	Vardan ADIBEKYAN	CAUP	Portugal
2011	Marine AVTANDILYAN	YSPU	Armenia
2010	Parandzem SINAMYAN	BAO	Armenia
2009	Lusine SARGSYAN	BAO	Armenia
2008	Vardan ADIBEKYAN / Artur HAKOBYAN	BAO / BAO	Armenia / Armenia
2007	Igor CHILINGARIAN	SAI MSU / CRAL	Russia / France
2006	Lilit HOVHANNISYAN / Parandzem SINAMYAN	BAO / BAO	Armenia / Armenia
2005	Artak HARUTYUNYAN / Elena HOVHANNESSIAN	BAO / BAO	Armenia / Armenia
2004	Lusine SARGSYAN	BAO	Armenia

8. Summer Schools and Science Camps

Since 2006, ArAS and BAO organize regular Byurakan International Summer Schools (BISS, http://www.aras.am/Meetings/meetingsSummerSchools.html), once every two years. In 2018, during the IAU General Assembly XXX in Vienna, Austria, BISS were announces as one of the top-3 international astronomical schools (along with ISYAs and Vatican Observatory Summer Schools, VOSS). Since 2005, local summer schools for YSU Physics Department students are being organized to cause and increase interest to astronomy. They are the continuation of the initiative started in 1995. ArAS has also organized a Conference for Young Astronomers in 2011. A Regional Astronomical Summer School (RASS) on Space Sciences and Technologies was organized in 2019 to establish the Armenia's first steps to this area. RASS also became a series and the 2^{nd} one was organized in 2021.

Armenian young astronomers regularly attend several international schools and conferences: IAU International Schools for Young Astronomers (ISYA), European NEON/OPTICON schools, Vatican Observatory Summer Schools (VOSS), Virtual Observatory (VO) training schools, and a number of others. ArAS website holds a directory table of the most important regular international schools (http://www.aras.am/SS2010/ss_other_schools.htm) which helps young astronomers and students to follow and find their respective schools based on the level of the students, location, subject, etc.

Since 2014, on the initiative of Sona Farmanyan, ArAS also organizes Byurakan Science Camps (BSC) for school pupils aged 12-15. Fund for Armenian Relief (FAR) partially sponsors these camps. In 2021, the 7^{th} Byurakan Science Camp (7BSC) was organized.

9. Astronomical Olympiads

Since 1996, International Astronomical Olympiads (IAO) and since 2007, International Olympiads on Astronomy and Astrophysics (IAOO) are being organized. Armenian pupils have regularly taken part in both of them and have achieved excellent results. In total, they have won 10 Gold, 7 Silver and 24 Bronze medals. Marietta Gyulzadyan has especially big contribution in the achievements of our team; she has been the team leader since 2006. Among the most successful participants are: Zhirayr Avetisyan and Mkrtich Soghomonyan (each have won one I, one II, and one III rank prizes), Tigran Shahverdyan (one II and one III rank prizes), Tigran Nazaryan, Hayk Saribekyan, Hayk Tepanyan, Hayk Hakobyan and Edgar Vardanyan have one I rank prize each. Igor Chilingarian from Russia has won I rank prize as well.

doi: doi.org/10.52526/25792776-2021.68.2-400

Year	No.	ArAS annual meeting description and other related conferences
2002	I	Scientific Sessions and Annual Report
2003	II	Scientific Sessions combined with Armenian-Georgian Colloquium
2004	III	Scientific Sessions and Annual Report
2005	IV	Scientific Sessions and Annual Report
2006	V	Scientific Sessions combined with BAO 60^{th} Anniversary Meeting
2007	VI	Scientific Sessions combined with 15^{th} EAS Annual Meeting (JENAM-2007)
2008	VII	Scientific Sessions combined with Ambartsumian's 100^{th} Anniversary Meeting
2009	VIII	Scientific Sessions related to IYA-2009 (incl. Astrobiology and Archaeoastronomy)
2010	IX	Scientific Sessions and Annual Report
2011	X	Scientific Sessions and Annual Report
2012	XI	Scientific Sessions combined with Anania Shirakatsi 1400 meeting
2013	XII	Annual Report and Summary of Astronomical Year 2013
2014	XIII	Scientific Sessions combined with RASCS meeting
2015	XIV	Scientific Sessions combined with Armenian-Iranian Astronomical Workshop
2016	XV	Annual Report and Summary of Astronomical Year 2016
2017	XVI	Scientific Sessions combined with the International Conference *"Astronomical Heritage of the Middle East"*
2018	XVII	IAU South West and Central Asian 2^{nd} Regional Astronomical Workshop
2019	XVIII	IAU South West and Central Asian 3^{rd} Regional Astronomical Workshop
2020	XIX	Scientific Sessions combined with the International Symposium *"Astronomical Surveys and Big Data 2"*
2021	XX	BAO seminar on ArAS 20-years celebration

10. ArAS School Lectures

ArAS Co-President Yervant Terzian and some other American sponsors of Armenian origin, co-finance a program of ArAS School Lectures, which runs jointly with the Armenian Ministry of Education and Science (MES). The lecturers are professional astronomers and their visits leave vivid impression for the school children. Schools are also given astronomical materials (books, booklets, sky maps, calendars, etc.), connection is being established with gifted children. In 2012, 2013, 2014, 2016, 2018, 2019, 2020 and 2021 such a program was implemented in Armenia and Artsakh schools.

11. Other matters of astronomical education

Armenia actively participates in the IAU Astronomy Education programs. The IAU Office for Astronomy Education (OAE) has been established in Heidelberg, Germany. The Armenian National Astronomy Education Coordinator Team (NAEC Team) consists of: Marietta Gyulzadyan, Sona Farmanyan and Armine Patatanyan.

ArAS tries to contribute to the astronomical education matters in Armenia. Summer Schools, Science Camps and Olympiads are also in this field. Network for Astronomy School Education (NASE) program was implemented in Armenia in 2019. Projects *"Under the Common Skies"* and *"Young Explorers Clubs"* were organized in 2018 and 2019 in collaboration with Poland (Ewelina Gradzka) and support from the USA. Other activities include installation of various information on ArAS webpage, preparation and release of educational CD/DVDs (recently released *"Astronomy for schools"* and *"Astronomy for students"* DVDs, which are collections of astronomical textbooks, books, dictionaries, encyclopedias, articles, reports, photos, videos, software, etc.). In November 2014, on the initiative of Sona Farmanyan ArAS founded Facebook group *"Junior Astronomer's Club"* (JAC). *"Viktor Ambartsumian's Descendants"* Educational Charitable Foundation was founded in August 2014.

doi: doi.org/10.52526/25792776-2021.68.2-400

Year	Summer school name	Short
2005	1^{st} Byurakan Summer School for YSU PhysDep students	1BSS
2006	1^{st} Byurakan International Summer School	1BISS
2008	2^{nd} Byurakan International Summer School	2BISS
2009	2^{nd} Byurakan Summer School for YSU PhysDep students	2BSS
2010	3^{rd} Byurakan International Summer School / IAU International School for Young Astronomers	3BISS/ISYA
2011	FSU countries Young Scientists Conference	FSU-YSC
2012	4^{th} Byurakan International Summer School	4BISS
2013	3^{rd} Byurakan Summer School for YSU PhysDep students / IAU S304 training	3BSS
2016	5^{th} Byurakan International Summer School	5BISS
2018	6^{th} Byurakan International Summer School	6BISS
2019	Regional Summer School on Space Sciences and Technologies	1RASS
2020	7^{th} Byurakan International Summer School	7BISS
2021	2^{nd} Regional Astronomical Summer School	2RASS

12. Archaeoastronomy and Astronomy in Culture

To coordinate issues related to Archaeoastronomy, an appropriate section was opened on ArAS webpage (http://www.aras.am/Archaeoastronomy/astronomyancientarmenia.html). These questions are currently given great importance in the world, in particular, they are in the focus of international organizations such as UNESCO (*"Astronomy and World Heritage"* project), IAU (Working Group *"Astronomy and World Heritage"*), International Council of Monuments and Sites (ICOMOS), European Society for Astronomy in Culture (Société Européenne pour l'Astronomie dans la culture, SEAC), "Starlight" initiative and others. In 2014, IAU created a new working group (WG) *"Archaeoastronomy and Astronomy in Culture"* (AAC). Already several related meetings have been organized in Armenia in 2011, 2012, 2014, 2015, 2016, 2017 and 2021. ArAS Newsletter now has a permanent section *"Archaeoastronomy and Astronomy in Culture"*. Areg Mickaelian is an Organizing Committee member of the newly founded (in 2018) IAU WG *"Astronomy and World Heritage"*.

13. Astronomy outreach

Armenia actively participates in the IAU Astronomy for Development (we have established a regional office in Armenia; see the corresponding article) and Astronomy Outreach programs. The IAU Office for Astronomy Outreach (OAO) has been established in Tokyo, Japan. The Armenian National Coordinator of the latter for a number of years has been Sona Farmanyan and recently Lilit Darbinyan also joined.

ArAS gives importance to the development of amateur astronomy. There is *"Goodricke John"* amateur astronomers organization created by Ruben Buniatyan, which put efforts and reached the recognition of 18 September (Viktor Ambartsumian's birthday) as Astronomy Day in Armenia since 2009. ArAS created on its webpage a section for amateur astronomy (further to establish Armenian Amateur Astronomical Society, ArAAS), as well as a Facebook group, where one can register as an amateur astronomer.

In December 2010, to promote scientific, especially astronomical journalism, the group of Scientific Journalists in Armenia was formed, which includes more than 160 journalists. ArAS periodically prepares and disseminates press releases, organizes press conferences, interviews, and scientific journalism seminars. Press releases contain astronomical news, events organized by ArAS and BAO and held in BAO, occurred and expected celestial phenomena, as well as scientists anniversaries, Armenian and other international scientific news. Astronomers hold public lectures at different organizations. On ArAS webpage, online *"Astghagitak" ("Astronomy Expert")* popular astronomical journal was created, where materials in Armenian are being placed for those interested in astronomy.

ArAS publishes a number of books (Proceedings of its Annual Meetings), popular booklets, calendars, sky maps and other promotional material.

doi: doi.org/10.52526/25792776-2021.68.2-400

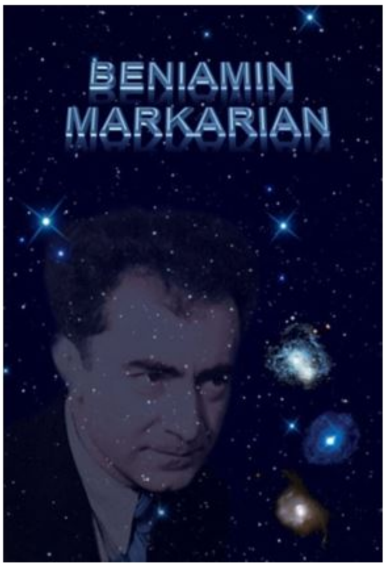

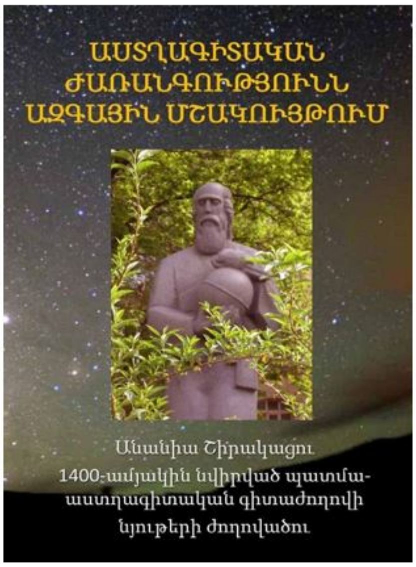

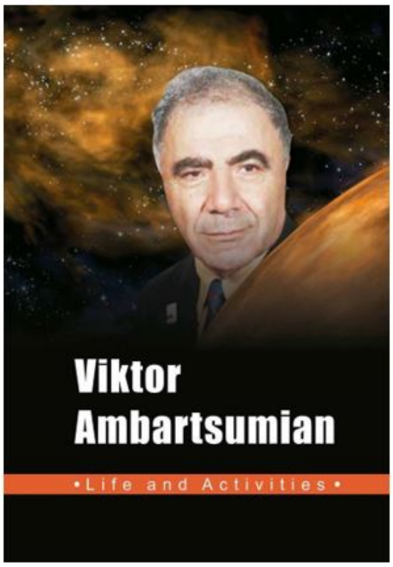

14. Further plans

More serious attention should be paid to *"Astronomy and World Heritage"* program. In particular, it is planned to implement a global program on Archaeoastronomy and History of Astronomy, Astronomy in Culture, as well as global programs on Amateur Astronomy and Astronomy Education. In parallel to the UNESCO World Heritage list, the IAU WG *"Astronomy and World Heritage"* has established a list of *Outstanding Astronomical Heritage* (OAH), and our aim is to include in it a number of Armenian astronomical items, particularly the Armenian ancient calendar and chronology, Armenian astronomical rock art, Zorats Karer (or Karahunge, the "Armenian Stonehenge"), Metzamor Hill astronomical platform, Anania Shirakatsi's astronomical heritage, and the architectural ensemble of the Byurakan Astrophysical Observatory (BAO).

Yet in deficient condition is the amateur astronomy; amateur telescopes, observational programs, amateur astronomers meetings, educational programs, and wider publicizing of astronomy are needed. Global programs are aimed at coordinating the whole area in Armenia. We intend to create new sections on ArAS webpage, namely Armenian duplicates of the *"Portal To The Universe"* (PTTU) and other webpages.

References

Mickaelian A. M., 2014, in Harutyunian H. A., Mickaelian A. M., Parsamian E. S., eds, Vol. 1400, Astronomical Heritage in the National Culture. pp 198–212

Mickaelian A. M., 2016, in Mickaelian A. M., Khosroshahi H. G., Harutyunian H. A. E. ., eds, Proceedings of Armenian-Iranian Astronomical Workshop (AIAW). pp 37–45

Mickaelian A. M., Farmanyan S. V., 2018, Communications of the Byurakan Astrophysical Observatory, 65, 99

Mickaelian A. M., Farmanyan S. V., Mikayelyan G. A., 2019, in Farmanyan S. V., Mickaelian A. M., McKim Malville J., Bagheri M., eds, Astronomical Society of the Pacific Conference Series Vol. 520, Astronomical Heritage of the Middle East. p. 295

Mickaelian A. M., Farmanyan S. V., Mikayelyan G. A., 2020, Communications of the Byurakan Astrophysical Observatory, 67, 75

doi: doi.org/10.52526/25792776-2021.68.2-400

Communications of BAO, Vol. 68, Issue 2, 2021, pp. 407-416

Outline of Calendar Studies Conducted at the Byurakan Astrophysical Observatory in 1983-2021

H.A. Malkhasyan *

NAS RA V. Ambartsumian Byurakan Astrophysical Observatory (BAO), Armenia

Abstract

The calendar studies conducted at the Byurakan Astrophysical Observatory in 1983-2021 are the result of Grigor Broutian's initiation and scientific activity. The approaches used by him have raised a number of new issues and provided extremely important results that are a serious incentive for the future development of this multilayered and multifaceted field in terms of astronomy and historical culture.

Almost all the problems of the Armenian and adjacent calendars of the Christian period have been discussed and finally resolved. The Armenian calendar attributed to Hayk Nahapet has been thoroughly researched and brought to an astronomically grounded comprehensive solution. The preliminary, so-called Protohaykian calendar has been revealed with its main and key aspects, and received astronomical as well as archaeological real evidence. All in all, in general the 11000-year-old Armenian calendar-astronomical traditional historical culture has been deciphered in its continuity. Some new data have been obtained in favor of the existence of an earlier, the so-called "Initial Calendar" as well. Moreover, common close relations have been revealed in the field of natural-philosophical-religious and their historical-cultural-astronomical traditional perception of the creation of the ancient Armenian "Vishap" ("dragon") stone monuments, the "Zorats Qarer" megalithic ensemble, the "Sasnay Tsrer" (Daredevils of Sassoun) epic poem, the Armenian folk tales and archaeological materials.

Keywords: *Armenian Calendar History: Archeoastronomy: Grigor Broutian: Zorats Qarer: Virgo: Haykian Calendar: Protohaykian Calendar: Cultural astronomy: Armenian folklore:*

1. Introduction

Archaeoastronomy and Cultural Astronomy department of the Byurakan Astrophysical Observatory was created in 2017 under the supervision of an astronomer, calendar scientist, PhD in phys.math. sciences Grigor Broutian. Until then, from the 60-70s, H. Badalian's and B. Tumanyan's research and monograph[1] in the field of calendar studies were known. Separate works of E. Parsamian on the archaeological site of Metzamor Astronomical Platform[2] and "Zorats Qarer" monument[3] were printed as well. Unfortunately, the mentioned period is not covered further in this paper and requires a complete

*hayk_malkhasyan@bao.sci.am

[1] Tumanyan B., History of Armenian Astronomy, vol. 1. "Mitq", Yerevan, 1964 (in Armenian)
Tumanyan B., Manual Calendar, Acad. Sci. of ARM SSR Publishing-House, Yerevan, 1965 (in Armenian)
Tumanyan B., History of Armenian Astronomy, vol. 2. "Mitq", Yerevan, 1968 (in Armenian)
Badalian H., History of Calendar, Acad. Sci. of ARM SSR Publishing-House, Yerevan, 1970 (in Armenian)
Tumanyan B., History of Calendar, "Mitq", Yerevan, 1972 (in Armenian)
Badalian H., History of Armenian Calendar, Acad. Sci. of ARM SSR Publishing-House, Yerevan, 1976 (in Armenian)
Tumanyan B., Mirzoean L., Astronomy, Yerevan University Publishing House, Yerevan, 1978 (in Armenian)
Tumanyan B., History of Armenian Calendar, Yerevan University Publishing House, Yerevan 1985 (in Armenian)

[2] Parsamian E., Astronomical Significance of the platforms of Small Hill, Khanzadian E.V., Mkrtchian K.H., Parsamian E.S., Metsamor, Acad. Sci. of ARM SSR Publishing-House, Yerevan, 1973, pp.142-149 (in Armenian)

[3] Parsamian E.S., On Possible Astronomical Significance of Megalithic Rings of Angelacot. Communications of BAO, 1985, vol. 57, pp. 101-103.

separate research and presentation. Thus, only the first research period of Gr. Broutian's calendar studies will be discussed here (1983-2021).

In modern life, the calendar is viewed merely as an instrument for time measurement. In our daily lives we clarify the date and check digital watches for unlimited times, while until the past centuries the traditional use of sundials was preserved in Armenia. The principle of the latter's operation, as we know, is the shadow change during the Sun's daily rotation period. This is a simple argument in favor of the fact that **the ancient Armenian (as well as of other nations) calendars must have had the observational basis[4].**

Unfortunately, we have no information about Armenian calendars of pre-Christian times, however, Armenian medieval bibliographic material of the Christian period is quite rich with data on calendars. Meanwhile, our knowledge in only calendars used through the rich history of Armenia is not enough to get a clear idea on their origin, structural features, changes and religious and cultural manifestations. In general, to form a general understanding about any calendar the following questions[5] should at least be answered:

1) When was the calendar founded (and by whom)?
2) What structure did it have?
3) When did the years count start? (what's the inception of the calculations)
4) What changes did it undergo later (when and who was the initiator)?

The answers to these quite important questions were sought in the historical-cultural studies of the Byurakan Astrophysical Observatory during the last decades.

These studies were conducted in "reverse chronological" sequence taking Bibliographic heritage of the Middle Ages as an inception. In natural sciences this research method is known as a "reverse problem"[6]. The non-singularity of this kind of problems are solved via supplementary information that can often come from completely other spheres (Folklore, Ethnography, Agriculture, Archeology, Mythology, etc.).

In this regard, it would be natural to present the results of the research on the Armenian calendars in the reverse chronology as well (from the most recent times to the early and "ancient" millennia). Conditionally, we will divide the calendar history into two periods: Christian and pre-Christian, considering 301 AD (the introduction of Christianity in Armenia) as the transition point. For this kind of "chronological chain" the calendar, its issues and "pillars" of the research will be discussed separately to present the results of calendar studies in a logical and a simplified manner possible. **The obtained results will be provided in the form of answers to the 4 questions listed above.**

2. Period of Christianity

It is known, that prior to 553 AD, the 200 year-long chart created by Andreas Byzantine was used to determine Christian holidays, while before that 95-year long holiday calendars of Ghevondes, Vorogines and Anatolios were used. These all were composed according to a fixed, non-Armenian calendar system like the Julian calendar. Only in the mid. 6^{th} century, when the above-mentioned Byzantine's lit of Eater dates came to its end, the Armenian church aimed at establishing independent church calendar, and resulted in Armenian Major Calendar.

[4]Gr. Broutian, On Some Questions about Armenian Calendar, the Armenian Calendar and Celestial Bodies, "Etchmiadzin", 1995, Issue 1, pp. 47-60 (in Armenian)

[5]Gr. Broutian, The Armenian Calendar from Its Foundation to the Present, NAS RA Byurakan Astrophysical Observatory, Yerevan, "Yanos", 2018, p.21 (in Armenian)

[6]Ambartsumian V., The reverse problems in the natural science, Acad. Sci. of ARM SSR Publishing-House, Yerevan, 1983

2.1. Armenian Major Calendar

In the Middle ages, until the 19^{th} century, the Armenian Major Calendar[7] was widely used in Armenia. Although the information about this calendar is relatively rich, the answers to the foregoing questions are often contradictory among the authors of the 10-11^{th} centuries. The foundation of this calendar is connected to the names of three different Catholicoses, thus dates differ. Later to overcome these difficulties modern researchers presented the foundation of this calendar in two stages: the establishment process itself and its official verification. The questions on its structure also received two different and contradictory answers. Some authors considered the Armenian Major Calendar fixed, while others argued it being a calendar of 365 days with movable beginning of the year. There are also two different beliefs on the beginning of the years count July 11, 552 AD and a year later (553 AD). The situation is clearer in regards to the changes of this calendar, in which case the opinions mostly coincide. Almost all agree that the Armenian Major Calendar was reformed by Anania Shirakouni (Shirakatsi) in the 7^{th} century.

To clarify disagreements of this kind we conducted in depth studies of the calendar tables authored by Anania Shirakouni, namely Revelation and Easter addresses (532-year tables), Hovhannes Sarkavag's calendar copy, The interpretation of the Armenian calendar, etc. Main results are obtained primarily due to the analysis of these works, and presented as a sequel of papers[8].

Below you can find the results on the Armenian Major Calendar in the form of answers to the above-mentioned questions:

1) It was founded by the order of Armenian Catholicos Movses Eghivandetsi in 552 AD. Athenas Taroneci was the author.

2) The duration of the year was always 365 days without leap years. A year, i.e. 360 days (12x30) and additional 5 days (Aveleac). With the movable beginning of the year with Navasard[9] 1.

3) According to Athenas the beginning of the years count was July 11, 552 AD, while according to the reforms made by Anania Shirakouni it was on January 6, 553 AD (with fixed start of the year).

4) It was reformed by Anania Shirakouni in 666-667 by the order of Anastas A (1st) Akoreci catholicos[10]. The beginning of the year was separated from Navasard 1 and was fixed prior to January 6.

Next reform of the Armenian calendar was made by Hovhannes Sarkawag in the 12^{th} century and this new calendar: Armenian Minor Calendar was put into practice.

---

[7]In the literataure on Calendar studies this calendar is known by different names: The Armenian Date, Haykazian Date, The Main Armenian Date, Asqanazian Date etc.

[8]Gr. Broutian, On Some Questions about Armenian Calendar: Armenian Major Calendar, "Etchmiadzin", 1983, Issue 8, pp.41-44 (in Armenian)

Gr. Broutian, On Some Questions about Armenian Calendar: the Armenian Calendar until Armenian Major Calendar, "Etchmiadzin", 1984, Issue 5, pp.54-58 (in Armenian)

Gr. Broutian, On Some Questions about Armenian Calendar: the Improvement of the Armenian Calendar and the List of Catholicoses with Dates, "Etchmiatdzin", 1994, Issue 8, pp.30-48 (in Armenian)

Gr. Broutian, The Circle 532 of Anania Shirakouni According to the Ancient Armenian Paper Manuscript, "Etchmiadzin", 1998, Issue 1, pp.125-143 (in Armenian)

Gr. Broutian, "Kharnakhoran" by Anania Shirakouni, Ed. Art. Matevosyan, Mother See of Holy "Etchmiadzin", 1999 (in Armenian)

Gr. Broutian, About a new component of the calendar of Anania Shirakouni, "Bazmavep", 2011, vol. 1-2, pp.181-215 (in Armenian).

Gr. Broutian, The Construction of "Tomar" (the Calendar) of Anania Shirakouni, "Bazmavep", 2013, vol. 3-4, pp.11-27 (in Armenian)

Gr. Broutian, The Construction of Calendars of Anania Shirakouni and Yovhannes Sarkawag and Their Relation, "Bazmavep", 2014, vol. 3-4, pp.11-24 (in Armenian)

[9]Gr.Broutian, On Some Questions about Armenian Calendar. The Main Armenian Holiday, "Etchmiadzin", 1995, Issues 10-12, pp.130-153 (in Armenian)

[10]Gr. Broutian, On the circumstances of the creation of Anania's K'NNIKON, "Bazmavep", 2016, vol. 1-2, pp.11-30 (in Armenian)

2.2. Armenian Minor Calendar

The fixed calendar created by Hovhannes Sarkawag is known as "Sarkawagadir Karg"[11] (Discipline of Sarkawag)[12]. It's in detail explanation can be found in calendrical "PATCHEN" ("The Copy"), and there are two main works related to it: Editing of "KHARNAKHORAN" by Sarkawag by Anania Shirakouni and famous calendar tables titled "Haysmavoracuyc" by Hovhannes Sarkawag. Unlike Anania Shirakouni, who in order to fix the calendar separated the start of the year from Navasard 1 and placed it on January 6, **Sarkawag introduced a leap day to the Armenian calendar for the first time** seeking the same purpose, which supplements 365 days of the Armenian calendar every 4 years. For a long time, there was an opinion in the Armenian calendar studies that Sarkawag added the leap day to the end of the year, after 5 days that are called Aveleac, however, it's not evidenced by any fact. The comprehensive research of Sarkawag's calendar studies reveals information on the position of the leap day. In "KHARNAKHORAN" edited by Hovhannes Sarkawag, in front of March 8 prior to Month Areg it's written, *"Hayq (the Armenians) place the unnecessary leap day here"*. In the paper of "PATCHEN TOMARI" (The Copy of the Calendar) it says, *"The leap year's month of Mehekan is 31. . . "*. This means that in "Sarkawagadir Karg" the leap day is placed between the months of Mehekan and Areg (before March 8).

Apart from fixation, Sarkawag changed the position of the start of the year as well, placing it on August 11. This change is probably the most discussed one by calendar scientists. They attempted to explain it as the main day of the start of the year in the Armenian calendar of the ancient times, and connect it to Hayk Nahapet's deeds: the victory over Bel and etc. Nevertheless, Sarkawag explained in his papers the reason he chose August 11 as the start of the year. He mentioned that the translations of the Bible and of some other books done in the beginning of the 5^{th} century served as a basis. Even during the first translations of these books the movable start of the year coincided with August 11. Having no other principle or an inception point except the date comparisons in the above-mentioned translations and seeking to fix the calendar, Hovhannes Imastaser chose the start of the year so that the letter was in harmony with the existing dates. **Hence, it should be noted that this is a common Roman date to which coincided the Armenian movable start of the year: Navasard 1, 428-431 AD. August 11 has no other significance other than this, and giving it another meaning or definition is wrong.**

All in all, as a result of the study of the Armenian Minor Calendar we learn that:

1) It was founded by the Armenian Catholicos Gregory II Vkayaser and compiled by Hovhannes Sarkawag in 1112 AD.

2) The medium duration of the year was 365,25 days (12x30, Aveleac 5 days and the added leap day every four years). The leap day was placed between the months of Mehekan and Areg before March 8 (every 4 years Mehekan lasted 31 days).

3) The beginning of the years count was August 11 (Navasard 1) 1084 AD with fixed start of the year.

4) It didn't undergo changes.

Though the Armenian Minor Calendar had limited use, it was applied as a church calendar till the 19^{th} century. Parallel to it already in the 18^{th} century the Roman calendar was put into practice.

3. Pre-Christian Period

We haven't received any direct evidence of the Armenian calendar of the pre-Christian period. We can understand the nature of that calendar by analysing the structure of the Armenian traditional calendar and other realities associated with the calendar.

[11] This Calendar is also known as "Mtruk"

[12] Gr. Broutian, On Some Questions about Armenian Calendar. Armenian Minor Calendar (Sarkawagadir Calendar), "Etchmiadzin", 1994, Issues 4-5, pp.100-116 (in Armenian)

Gr. Broutian, The Chronological System of Hovhannes Sarkawag, "Magaghat" Publishing House, Yerevan, 1999. (in Armenian)

3.1. Armenian Haykian Calendar

According to medieval calendar scientists, the foundation of the Armenian calendar is associated with Hayk Nahapet. It's also known that the Armenians named one of the brightest constellations, the famous Orion, in the name of Hayk. The analyses of the various data indicate that the heliacal rising[13] of the main **Betelgeuse star ("Hayk's Eastern Shoulder", α *Orionis*) of this constellation had close connection to the Armenian Holiday of Navasard.** Thus, it becomes possible to specify the time of this astronomical phenomenon and combine it with the already known historical data. The calculations have shown that from the center of Armenian Highland (39,5° latitude North) the heliacal rising of the above-mentioned star was seen **in the period of summer solstice, 8 days prior to it to be more precise.** Conducting a calendar countdown and comparing it to the well-known historical events, it became known that the beginning of the Haykian calendar is 2341 BC. This date was grounded quite well[14]. This is evidenced by detailed analyses of many bibliographic, historical, mythological, ethnographic, archaeological and other realities. In particular historical facts known from the Cuneiform sources were compared to the information Armenian historians conveyed. Complete parallels and stylized canonical identifications[15] were obtained between the story of **Hayk and Bel and the conflict between Sargon (I) the Great, ruler of northern Mesopotamia, and Lugalzagesi, the last ruler of the Early Dynastic period of Sumer.**

What is generally known about the Haykian Calendar?

1) It was founded in 2341 BC by Hayk Nahapet (most probably by Sargon I the Great)
2) It was composed of 12 months of 30 days (360 days) and additional 5 days, which were called Aveleac. The start of the year was movable. **The fixed holiday of Navasard was celebrated by the observation of the heliacal rising of the Betelgeuse star of Hayk constellation (Hayk's Eastern Shoulder, α *Orionis*).**
3) The years count began in 2341 BC, 8 days prior to summer solstice, **June 14 (Navasard 1).**
4) Most probably it didn't undergo any changes and was also parallely used[16] after the introduction of Christianity until 552 AD.

It is natural that before Hayk Nahapet's arrival to the country of Ararat from Babylon, the inhabitants of the land should have had their culture, the inseparable part of which is the calendar. It was conditionally called Protohaykian calendar considering its usage before Hayk Napahet's arrival.

3.2. Protohaykian Calendar

Many medieval authors (Anania Shirakouni, Hovhannes Sarkawag, Grigor Tatevatsi, Hovhannes Vanakan (Monk) et al.) conveyed that months of the Armenian calendar were named after Hayk's children. **All of them mention that Hayk had 10 children and only 10 months bore their names**. The other 2 months were called *"i gortsoc" ("of works")* or *"i veray yeghanakacd"* ("on top of the seasons"). The study of the above-mentioned sources on Hayk's 10 children has shown that **Hayk had 3 sons and 7 daughters**. This coincides with the fact that the main star of the Hayk constellation was seen 295 days, while it was beneath the horizon and invisible during the other 70 days. These 295 days correspond to the sum of 10 lunar months (10 x 29,5 days). This fact (also other supporting materials) allow us to conclude that the main year in Hayk's calendar consisted of 10

[13]Gr. Broutian, Relations of the Oldest Armenian Calendars with Hevenly Bodies, "Bazmavep", 2017, vol. 1-2, pp.39-59 (in Armenian)

[14]Gr. Broutian, On Some Questions of Armenian Calendar: The Main Armenian Date, "Etchmiadzin", 1985, Issue 1, pp.51-57 (in Armenian)

Gr. Broutian, On Some Questions of Armenian Calendar: Analysis of 2341 BC, "Etchmiadzin", 1985, Issues 2-3, pp.72-80 (in Armenian)

Gr. Broutian, The Armenian Calendar, "Etchmiadzin", 1997, Chapter 7, pp.211-246 (in Armenian)

[15]Gr. Broutian, On Some Questions of Armenian Calendar: the beginning of the Armenian Main Calendar and Historical Facts, "Etchmiadzin", 1997, Issues 2-3, pp.144-155 (in Armenian)

[16]Gr. Broutian, On Some Questions of Armenian Calendar: the Structure of the Protohaykian Calendar, "Etchmiadzin", 1996, Issue 12, pp.135-164 (in Armenian)

months, the remaining 65-70 days were considered out of the year, as the main star of Father God was not visible in the sky. This structure[17] of Protohaykian calendar was later approved by the analysis[18] of the archaeological material ((ornaments of the black polished ware (the end of IV millennium BC) excavated from Keti archaeological site, Shirak Region, Republic of Armenia). It was also discovered that the canonical duration of the calendar was not 295, but 300 days, and the 5-day difference was meantime considered as a part of the year and separate.

This calendar impacted every aspect[19] of Armenian culture (as well as of other nations). We have received only fragments in the materials of folklore, ethnography, historiography and archeology. The study and analysis[20] of all these has revealed that the Protohaykian calendar is closely related to cereal cultivation (agriculture). Such an extensive analysis has led us to conclude that the main star of this calendar was the brightest **Spica (α *Virginis*) in the constellation Virgo.** In the Sumerian astronomical catalog, the name of this star ^{mul}AB.SIN$_2$ is translated as "groove, ridge" and is linked[21] to the culture of agriculture and the name of the virgin goddess Sillia. And the observation of the heliacal rising of this very star, the start of the year, the main Armenian holiday Navasard, was celebrated. The most significant event in farmers' lives was the autumn cereal harvest, which takes place close to summer solstice. Therefore, it was not difficult to calculate in what year the heliacal rising of the main star of the Virgo constellation preceded the summer solstice for 8 days. This revealed the beginning[22] of the Protohaykian calendar, which is 9000 BC (with a possible mistake of 80 years). It is interesting that the same year was obtained by the astronomical examination[23] of one of the platforms of the ancient site of Metzamor as well. By this it has also been found out that heliacal rising of Pleiades was most probably observed in 9000 BC. Very recently this date was approved during the astronomical study[24] of "Zorats Qarer" megalithic monument. **We discovered that on one of the central stones (N 198) there is a specially cut corner the direction of which corresponds to the point of the sky, by which the Spica star of Virgo constellation (α *Virginis*) passed on summer solstice right before sunrise in 9000 BC (Figure 1).** The dates obtained in two different ways are in accord, which can be considered as an exceptionally accurate result for such ancient times. Due to its respectable antiquity, the Protohaykian calendar should be the subject of further studies as well. We do not have the opportunity to discuss historical figures and events in detail here, simple because we have no direct evidence of them. So, let's see what is already known and what is yet to learn about this calendar.

1) It was founded in 9000 BC (with possible mistake of 80 years) by the unknown farmers.
2) It's composed of the main year of 300 days and 65-70-day out of the year period. The start of the year is relatively fixed (1 day in about 100 years due to the Earth's precession and the angular velocity of the star's proper motion) 8 days prior to the summer solstice (Navasard 1 - June 14). 5 out of 300 days of the year were considered both as part of the year and out of it. Structurally it is a lunisolar calendar.
3) The year count started probably at the same time.

[17]Gr. Broutian, Ancient Armenian Calendar Ideas According to "Armenian History" by Agatangeglos, "Etchmiadzin", 1998, Issue 6, pp.45-53 (in Armenian)

[18]Gr. Broutian, The Oldest Armenian Calendar Concept According to the Analyze of the Ornaments of a Vessel from 28-27th c. B.C., "Bazmavep", 2007, pp. 149-163 (in Armenian)

Gr. Broutian, The Armenian Calendar of the Early Bronze Age According to Ornaments of the Black Polished Ware of Keti, 254 pages (unpublished monograph)

[19]See as an example: Gr. Broutian, The Concepts of the Oldest Armenian Calendar in Greek Epic Poem about Basil Digenis Akritas, "Bazmavep", 2004, vol. 3-4, pp.5-16 (in Armenian)

[20]Gr. Broutian, The Beginning of the Protohaykian Calendar, "Bazmavep", 2016, vol. 3-4, pp.11-63 (in Armenian)

[21]Davtyan A., Armenian Stellar Mythology, Yerevan, 2004, pp.158-161 (in Armenian)

[22]Gr. Broutian, The Beginning of Protohaykian Calendar, Non-stable Universe: Energetic Resources, Activity Penomena, and Evolutionary Processes, Proceedings of an International Symposium dedicated to the 70th anniversary of the Byurakan Astrophysical Observatory held at NAS RA, Yerevan and Byurakan, Armenia 19-23 September 2016, Edited by A. Mickaelian, Astronomical Society of the Pacific, Conference Series, vol. 511, San Francisco, 2017, pp. 296-302

[23]Gr. Broutian, "Bazmavep", 2017, Ibid.

[24]Gr. Broutian, H. Malkhasyan, About Some Preliminary Results Based on the Last Measerments of "Zorats Qarer" Megalithic Monument, "Bazmavep", 2021 (accepted)

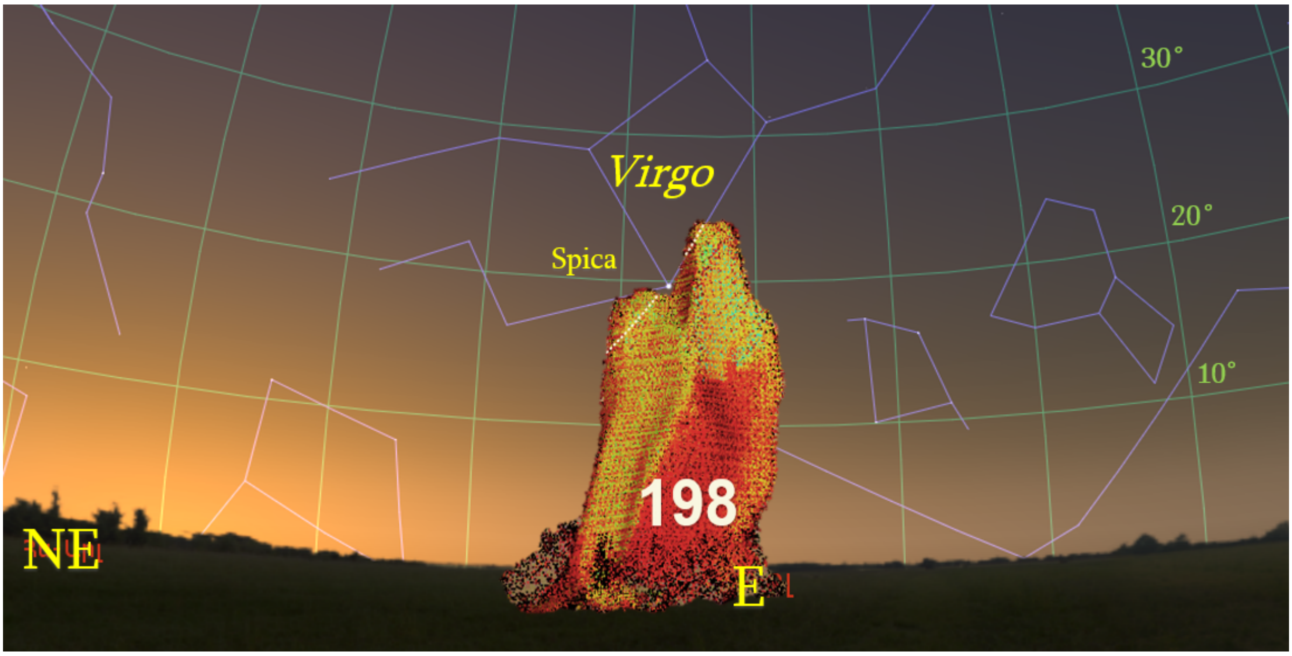

Figure 1. The megalithe with special angle N 198 (the direction of the angle - Azimuth=262°50′ from the South point, Elevation=19°34′). "Zorats Qarer" megalithic monument (Armenia, 39°33′ latitude North), 9000 BC (the beginning of Armenian Protohaykian Calendar). Summer solstice, before sunrise. Reconstructed in Stellarium v0.20.4 (http://www.stellarium.org).

4) There is a strong doubt that this calendar underwent changes in **the first half of the VI millennium BC**[25]. The observed main star, **Spica (α *Virginis*), was replaced by Sirius**[26] **(α *Canis Majoris*) to keep the start of the year fixed.** There is no information about the structural or any other changes of the mentioned calendar yet.

As we see, the structure of the Protohaykian calendar is quite complex. Despite its extreme antiquity, this kind of structural complexity implies that it must have developed for millennia.

3.3. The Preliminary Calendar

What was the calendar like before the foundation of the Protohaykian calendar? For now, we can only have hypotheses and suggestions. However, the existence of a calendar prior to the foundation of the Protohaykian cannot be ruled out. To this one the term Preliminary Calendar[27] is applied. Nevertheless, our knowledge of the latter is very poor. Thus, the lack of answers to the above 4 questions implies the continuation of the study in this area. Entirely convinced of the need for further research of the field, Gr. Broutian developed and published a scientific-methodological manual[28] dedicated to the basic knowledge and research methodology required for the research of the Armenian calendars.

In the table 1 you can find the calendars that were used in Armenia and discussed in this paper with their application periods[29].

It is obvious from the table that the Protohaykian calendar is "the most longevous" of all presented (66.5 centuries).

[25] Gr. Broutian, H. Malkhasyan, Ibid.

[26] It should be noted here that in Mesopotamian sources this star ^{mul}GAG.SI.DI is translated as "arrow", and it's interesting that there is a deity named "Arrow" in the Sumerian sources, who guards the doors of the underworld. See for example Davtyan A., 2004, Ibid, p. 163 (in Armenian)

[27] Gr. Broutian, The Armenian Calendar, "Etchmiadzin", 1997, pp.430-433 (in Armenian)

[28] Gr. Broutian, The Armenian Calendar Studies, Mkhitarian Publishing House, Yerevan, 2016 (in Armenian)

[29] Gr. Broutian, Knowledge of the ancient national calendars as a means of patriotism in the publications of the Mother See, "Etchmiadzin", 2020, Issue 12, pp. 24-33 (in Armenian)

	Calendar Name	Period of application	Duration
a.	Protohaykian Calendar	9000 - 2341 BC	66,5 centuries
b.	Haykian Calendar	2341 BC - 552 AD	28 centuries
c.	Armenian Major Calendar	552 AD - 20^{th} century	14 centuries
d.	Armenian Minor Calendar	1112 AD - 19^{th} century	7,5 centuries
e.	Roman Calendar	1774 AD - to our days	2,5 centuries

Table 1. The chronology of the Armenian Calendars.

"The period of the Protohaykian calendar coincides with the most ancient period of Armenian history, which was also the most significant period in terms of cultural and civilizational achievements. Such civilizational achievements as obtaining cultivated species of cereal and some other crops, the domestication of some pets, the division of the starry sky into constellations, the invention of primary writing, the invention of the mining and processing of bronze, and then iron, and more are related to this calendrical period.

Thus, based on all these, we can conclude that the Protohaykian calendar was better suited to the natural course of the (Armenian) people's lifestyle and the manifestation of his creative powers."[30]

Grigor Broutian

4. The Results of Other Studies in the Field of Cultural Astronomy

It should be especially noted that such calendar studies include a large amount of detailed analyses from the related fields. As it was mentioned earlier, in the course of the work an attempt is made to supplement the answers to the questions of interest by obtaining and importing additional information from various spheres of Armenian folklore, ethnography and cultural heritage, that concern our issues. Such an exploration leads to new discoveries in these areas. The results of the discoveries have been published in a number of publications over the past decades. Let us review the most important ones.

1) **The start of the year (Holiday of Navasard) in the Pre-Christian Armenian calendars was clarified.** There are different opinions about the position of Navasard, yet, as the examination[31] of numerous calendrical, astronomical and ethnographic facts shows, **the original position of Navasard was in the middle of the astronomical spring and summer, 8 days before the summer solstice.** Such a position of Navasard, among many other facts, is also confirmed by the testimony of Agatangelos that Navasard was considered the **"Festival of New Harvest".** Indeed, in Armenia the first harvest ripens during the beginning of summer season. It's especially important to note that during these days winter wheat also grows which has been the basis of the prosperity of the Armenian farmers for thousands of years. As it was already mentioned above, in the Haykian calendar as well this day was determined by the observation of the heliacal rising of the main star of the Hayk constellation at the 10^{th} hour in the Aravot (Morning), which is about 1,5 hours before sunrise. Special rituals and a celebration[32] were held during the holiday.

2) **In the meantime, cosmic[33] calendar[34] realities were revealed in many examples of Armenian folk tales.** The information contained in Armenian fairy tales, first of all, provides insight into the worldview of their creators. It is in these perceptions that we find some answers to the questions that we are interested in and use them as auxiliary information to make the

[30] Gr. Broutian, BAO, 2018, Ibid. pp. 174-175 (in Armenian)

[31] Gr. Broutian, "Etchmiadzin", 1995, Issues 10-12, pp.130-153 (in Armenian)

[32] Gr. Broutian, "Etchmiadzin", 1992, Issues 4-5, pp.95-118 (in Armenian)

[33] Gr. Broutian, "Etchmiadzin", 2008, Issue 2, pp.49-66 (in Armenian). Gr. Broutian, The Understanding of Time and Space According to Armenian Fairy Tales, "Bazmavep", 2011, vol. 3-4, pp.459-484 (in Armenian)

[34] Gr. Broutian, "Etchmiadzin", 2009, Issue 12, pp.62-83 (in Armenian). Gr. Broutian, "Etchmiadzin", 2010, Issue 6, pp.22-44 (in Armenian)

result of some "reverse problem's" solution univocal. Hayk's children can be regarded as the clearest example. To find out how many of Hayk's 10 children are sons, among other sources, we get help from tales, in which the protagonists are the king's three sons, the youngest of whom becomes the father's heir, as was the case with Hayk's youngest son Aramanyak[35].

3) **Numerous manifestations of astronomical and calendar realities have been revealed in the Armenian "Sasnay Tsrer" Epic poem**[36]. The parallels between the main characters of the epic poem and the constellations of the Zodiac have been clarified. In particular, the analysis has shown that the most discussed hero's, Davids' character paralleled the *Sagittarius* constellation and the planet Lusntag (*Jupiter*). The Elder-Pisces (based on the Mesopotamian constellation A-nu-ni-tu, which is located in the current region of *Pisces*), Pokr (Small) Mher - *Aries*, Dzenov Ohan - *Taurus*, Sanasar and Baghdasar - *Gemini*, Tzran Vergo - Tzir (present *Cancer* Zodiac sign), Mets (Big) Mher - *Leo* and other comparisons are also important. These, in fact, are adjacent constellations in the Zodiac. On the basis of such realities an attempt was made to date the Epic poem. Calendar parallels[37] with the celestial realities of considerable antiquity have been obtained (17700 BC). The poem's episode[38] in which Tsovinar (*Virgo*) advises his twin sons to escape from Baghdad, taking the bright star for direction, has also been examined. The work is based on two starting points: a) only a Pole star (or very close to the North Pole) can indicate a direction, as fixed; b) based on religious beliefs (worship of the cross) the main star of the Vulture (*Cygnus*) constellation, Deneb (α *Cygnus*) was taken as such. As a result, the possible date of this episode of the Epic poem has been estimated to 15500 BC. This is the time when the mentioned star was the closest to the North Pole.

4) **A significant change in the classification of Armenian "Vishap" (dragon) stones has been proposed on an astronomical basis.** It was generally accepted to classify these "Dragon Stones" into three types: fish-shaped, with the image of cattle (these are sometimes called bull heads) and with mixed images. **With the detailed analysis of the "Vishap" stone sculptures, it was possible to distinguish their 5 types: a) with the head of a wild donkey, b) depicting a pair of storks, c) with the bull head, d) with the head of a ram and e) in the form of fish.** This series, obviously, repeats a part of neighboring constellations of the zodiac: a) *Cancer* (wild donkey, donkey), b) *Gemini*, c) *Taurus*, d) *Aries*, e) *Pisces* respectively. Based on such correspondence, an attempt has been made[39] to date these monuments astronomically. As a result, the time related to them was set 28500-19900 BC, moreover, according to the type of the "Vishap" stone classification the approximate chronology has been calculated separately. It is also important to emphasize that **the imagery of the Gemini constellation has been revealed in the form of a pair of storks.**

5) **Based on the structure of the Armenian calendar, some circumstances about a number of calendars of neighboring nations have been explained**[40]. In particular, the main year the ancient Roman calendar being of 10-month (304-day) long (as well as many other features) is explained[41] by the direct or mediated borrowing of the Armenian Protohaykian calendar. This borrowing is also evidenced by a detailed examination[42] of all the expressions

[35] Gr. Broutian, The Armenian Calendar, "Etchmiadzin", 1997, Chapter 2, pp.386-399 (in Armenian)

[36] Gr. Broutian, Some Astronomical-Cosmic Realities in the Armenian Epic "Sasnay Tsrer", Astronomical Heritage of the Middle East, ASP Conference Series, Astronomical Society of the Pasific, 2019, Vol. 520, pp. 191-198

[37] Gr. Broutian, An attempt to determine the time of an episode of the Armenian "Sasnay Tsrer" epic through astronomical realities, "Etchmiadzin", 2021, (accepted)

[38] Gr. Broutian, An Astronomical Attempt to Determine the Temporal Origin of an Episode of the Armenian Epic "Sasnay Tsrer" Communications of BAO, Vol. 68, Issue 1, 2021, pp. 105-113 doi:https://doi.org/10.52526/25792776-2021.68.1-105

[39] Gr. Broutian, "Etchmiadzin", 2020, Issue 4, pp.44-65 (in Armenian)

[40] Gr. Broutian, Georgian and Alouanian calendars as presented in Anania Shirakouni's Tomar (Calendar): Some problems concerning their origin and structure, Armenia and Christian Caucasus, Republican Conference devoted to the 1700-th Anniversary of adoption of Christianity in Caucasian Albania and Georgia, Yerevan, 15-16 December 2015, Papers and abstracts of papers, pp. 58-68

[41] Gr. Broutian, "Etchmiadzin", 2019, Issue 7, pp.64-84 (in Armenian)

[42] Gr.Broutian, Armen deacon Khachatryan, Certain Issues Related to the Calendar in the Holy Bible, "Bazmavep",

with time-related words contained in the Book of Exhodus of the Torah. More than 20 significant similarities have been identified between the testimonies of the 7-day ritual of the main Jewish holiday (which was also the main point of the Exodus of the Jews from Egypt) and the Navasard celebrations in the Protohaykian calendar.

6) **Extensive astronomical research on the Armenian megalithic monuments has begun.** The comparative analysis of perhaps the most well-known and discussed monument in Armenia, the baseline structure of the "Zorats Qarer" and the arrangement of the stars of the Eagle-Cygnus constellation, has shown an almost complete correspondence in 30300-29300 BC millennial domain[43]. This examination differed from the previous ones as more than one baseline data were taken into account. The task was to find the time when all the dimensional data of the plan of the monument and the geographical location coincide with the equatorial coordinates of the constellation stars. Given the result, it became necessary to thoroughly research the monument from an astronomical point of view. For this purpose, within the framework of the cooperation agreement signed between the Byurakan Astrophysical Observatory (BAO) and the National University of Architecture and Construction of Armenia, a 1-week scientific expedition was carried out in July, 2020. **The aim of the scientific expedition was to examine the "Zorats Qarer" monument from an astronomical point of view and obtain a complete measurement data using modern digital measuring devices (an area of about 20 ha was measured to the nearest 1 mm in length and an angular dimension of 10 arc seconds).** A detailed examination revealed **specially cut angular stones** (Figure 1) and **platforms**, which, as it was discovered later, **had special observational importance.** In addition, the first results[44] showed the connection of this monument with the Haykian and Protohaykian calendars discussed above. In general, **the preliminary data show that the monument is multi-layered (9000 BC, 5800 BC and 2341 BC)**. Moreover, it should be emphasized that the observational realities revealed in the monument within the mentioned dates also show the continuation of the logical sequential development of the same cultural manifestations over the millennia. These studies are currently in progress and their results will be published in the near future[45]. The other megalithic monument which attracted our attention during the preliminary examination, is **the archaeological site near the village of Hartashen, Shirak Region.** The very first observations of this monument revealed some patterns which speak of its possible connection with astronomical phenomena. To study these assumptions in depth, measurements of the Hartashen monument were needed. This work began in June 2021 within the framework of the above-mentioned cooperation agreement and it still continues.

The foregoing results, as we see in 3, 4 and 6 sub-items, refer to the events of enormous antiquity (30000-15000 BC), information about which has not reached us. However, as it was mentioned, this period preceded the beginning of the Protohaykian calendar 9000 BC. Thus, the astronomical-calendrical notions of such antiquity probably refer to the Preliminary Calendar. Let us single out only one coincidence, which is obvious from 3 and 4 sub-items. We see almost the same span and time sequence of the constellations compared to the types of "Vishap" (dragon) stones and the main characters of the "Sasnay Tsrer" epic poem, which raises the need to answer a number of questions. The time "Zorats Qarer" megalithic monument was dated, on the other hand, also leaves many questions unanswered. All in all, we see that we are dealing with the multifaceted, millennial heritage of our ancestors that belong to the same culture. So, it is obvious that this field requires special attention, and future research with the introduction of wide opportunities is of great importance.

2008, pp. 83-100 (in Armenian)

[43] Malkhasyan H. A., The observation of Angegh-Vulture (Cygnus) constellation in Armenia 32 000 years ago, Communications of BAO, Vol. 67, Issue 1, 2020, pp. 27-36. doi: 10.52526/25792776-2020.67.1-27

[44] Gr. Broutian, H. Malkhasyan, Ibid.

[45] Malkhasyan H.A., Some New Results of the Study of "Zorats Qarer" Megalithic Monument (Platform 2), "Bazmavep", 2021, (accepted)

Communications of BAO, Vol. 68, Issue 2, 2021, pp. 417-424

The synchrotron mechanism and the high energy flare from PKS 1510-089

Z.N. Osmanov [*1,2]

[1]School of Physics, Free University of Tbilisi, 0183, Tbilisi, Georgia
[2]E. Kharadze Georgian National Astrophysical Observatory, Abastumani, 0301, Georgia

Abstract

In order to understand the role of the synchrotron emission in the high energy gamma-ray flares from PKS 1510-089, we study generation of the synchrotron emission by means of the feedback of cyclotron waves on the particle distribution via the diffusion process. The cyclotron resonance causes the diffusion of particles along and across the magnetic field lines. This process is described by the quasi-linear diffusion (QLD) that leads to the increase of pitch angles and generation of the synchrotron emission. We study the kinetic equation which defines the distribution of emitting particles. The redistribution is conditioned by two major factors, QLD and the dissipation process, that is caused by synchrotron reaction force. The QLD increases pitch angles, whereas the synchrotron force resists this process. The balance between these two forces guarantees the maintenance of the pitch angles and the corresponding synchrotron emission process. The model is analyzed for a wide range of physical parameters and it is shown that the mechanism of QLD provides the generation of high energy (HE) emission in the GeV energy domain. According to the model the lower energy, associated with the cyclotron modes, provokes the synchrotron radiation in the higher energy band.

Keywords: *blazars: individual: PKS 1510-089 – radiation mechanisms: non-thermal – plasmas.*

1. Introduction

During the last decade the observations in the high and the very high energy domains have stimulated theoretical studies of the corresponding astrophysical objects. Recently the AGILE (Astrorivelatore Gamma a Immagini LEggero) collaboration announced the discovery of the high energy (HE) γ-rays of PKS 1510-089 (D́Ammando et al., 2010), which is a nearby blazar ($z = 0.361$) belonging to the class of the flat radio quasars. The observations on the mentioned source was performed in the period $9 - 30$ March 2009. According to the observational data, PKS 1510-089 showed extreme variability in γ-rays. It was found that the HE photon spectrum can be well described by the photon index $\Gamma = 1.95 \pm 0.15$, the following average integral flux above 100MeV, $(311 \pm 21) \times 10^{-8}$photons cm^{-2}s^{-1}, and a peak integral flux $(702 \pm 131) \times 10^{-8}$photons cm^{-2}s^{-1} detected on 25 of March (D́Ammando et al., 2010). The monitoring of the blazar between September 2008 and June 2009 was performed by the Fermi-LAT telescope and a complex variability at optical, UV and γ-ray bands was found (Abdo et al., 2010). During this period three γ-ray flares have been detected, with the brightest isotropic luminosity 2×10^{48}erg/s on 2009 March 26. It has been found that the flux for energies above 200MeV reaches its peak value 2.4×10^{-7} photons $^{-2}$s^{-1}.

Obviously it is assumed that the HE emission is produced by the inverse Compton mechanism (Blandford et al., 1990) or curvature radiation (Gangadhara, 1996, Thomas & Gangadhara, 2005). The synchrotron process is supposed to be responsible only for producing relatively low energy photons, because in strong magnetic fields the cooling timescale is small compared with the kinematic timescale, that leads to the transition of relativistic electrons to their ground Landau states, resulting in the damping of the emission process.

[*]z.osmanov@freeuni.eduge

Unlike the standard mechanism explaining the HE radiation, we apply the so-called quasi-linear diffusion (QLD) that prevents the pitch angles from damping, sustaining the synchrotron process. In particular, it is believed that plasmas in pulsar magnetospheres with strong magnetic fields may induce the unstable cyclotron waves (Kazbegi et al., 1991). These unstable modes in turn feedback on relativistic electrons and by means of the diffusion influence the particle distribution along and across the magnetic field lines (Lominadze et al., 1979, Machabeli & Usov, 1979). Under certain conditions the physical system reaches the balance between the dissipation factors and the diffusion, leading to saturation of the pitch angles. Therefore, despite the efficient synchrotron losses, the pitch angles are maintained, which provides a continuous emission process.

The mechanism of QLD was successfully applied to pulsars (Chkheidze et al., 2007, 2011, Machabeli et l., 2010, Machabeli & Osmanov, 2010, Malov & Machabeli, 2001), anomalous pulsars (Osmanov, 2021), the black hole located in the center of Milky Way, SgrA* (Gogaberishvili et al., 2021) and active galactic nuclei (AGN) (Osmanov, 2011, 2010, Osmanov & Machabeli, 2010). In these papers it is shown that the QLD might provide the simultaneous generation of relatively low frequency waves and the HE γ-rays. On the other hand, it is observationally evident that some AGN reveal the strong correlation of HE and low frequency emission Bloom (2008), Giroletti et al. (2010), therefore the role of the QLD might be important for these sources. In particular, in Ref. Osmanov & Machabeli (2010) the excitation of X-rays connected to the radio waves has been studied. The similar method was developed to examine the possibility of strong correlation of HE emission and submillimeter/infrared radiation (Osmanov, 2010) and study the generation of high and very high energy γ-rays strongly connected to radio emission (Osmanov, 2011).

Unlike the aforementioned articles, in the present work we focus on the concrete AGN. According to the observational data presented by AGILE collaboration (D́Ammando et al., 2010), the HE flare was detected during 9-30 March 2009 from blazar PKS 1510-089. We apply the mechanism of the QLD to the mentioned AGN and analyze the synchrotron radiation processes in producing the observed HE (> 100MeV) photons. According to the standard theory of the synchrotron emission, it is assumed that the magnetic field is chaotic along the line of sight, therefore, in the framework of this approach the pitch angles vary in the broad interval, $0, \pi$ (Ginzburg, 1981). Contrary to this scenario, the QLD prevents the pitch angles from damping, restricting their values.

The paper is arranged in the following way. In section II, we introduce the theory of the QLD. In section III, we apply the model to the blazar PKS 1510-089 and in section IV, we summarize our results.

2. Main Consideration

In this section we present our model and apply it to BL Lac PKS 0548-322. This is a low redshift blazar with the central supermassive black hole (SMBH) having the following mass $M \approx 5.4 \times 10^8 M_\odot$ (Abdo et al., 2010), where $M_\odot \approx 2 \times 10^{33}$g is the solar mass. Around the SMBH, in a region of the lengthscale, $l \sim 10^{14-15}$cm, the magnetic field is strong enough to provide the frozen-in condition. In the magnetospheres of AGNs, Lorentz factors of the magnetospheric plasma particles lie in a broad interval, ranging from ~ 1 to 10^8 (Osmanov et al., 2007, Rieger & Aharonian, 2008). For simplicity we consider two component plasma: the relatively low energy electron-positron plasma component (γ_p) and the highly relativistic electrons - the so-called beam component (γ_b). As we have already mentioned, the relativistic particles will undergo strong synchrotron losses. In particular, the synchrotron cooling timescale for the beam electrons is given by the following expression $t_{syn} \sim \gamma_b mc^2/P_{syn}$, where m is the electron's mass, c is the speed of light, $P_{syn} \approx 2e^4\gamma_b^2 B^2/3m^2c^3$ is the single particle synchrotron emission power, e is the electron's charge and B is the magnetic induction. By considering the relativistic electrons one can show that the synchrotron cooling timescale, t_{cool}, is of the order of $0.05 \times \gamma_{b8}^{-2} B_{10}^{-2}$s ($\gamma_{b8} \equiv \gamma_b/10^8$, $B_{10} \equiv B/10G$), whereas the kinematic timescale, $t_{kin} \sim l/c \approx 3000 \times l_{14}$s ($l_{14} \equiv l/10^{14}cm$), for reasonable parameters is much smaller than t_{syn}. Moreover, the condition $t_{cool}/t_{syn} \ll 1$ becomes more strict for higher luminosity sources, or during γ-ray flares, since the equipartition magnetic field becomes higher in these cases. Therefore, due to the strong magnetic field, the synchrotron emission in the magnetosphere of PKS 1510-089 is strongly suppressed by the energy losses and the particles rapidly transit to their ground Landau states and generation of radiation is stopped.

The situation drastically changes by means of the excited cyclotron waves. This problem was considered for pulsars by Kazbegi et al. (1991). In particular, since the magnetic field near the pulsar's surface is very strong, any transverse momenta of relativistic electrons are lost and the corresponding distribution function of electrons from the very beginning of motion becomes one-dimensional and anisotropic. Kazbegi et al. (1991) showed that for the aforementioned conditions the anomalous Doppler effect leads to the generation of the pure transversal cyclotron modes

$$\omega_t \approx kc\left(1-\delta\right), \qquad \delta = \frac{\omega_p^2}{4\omega_B^2\gamma_p^3}, \tag{1}$$

where k is the modulus of the wave vector, $\omega_p \equiv \sqrt{4\pi n_p e^2/m}$ is the plasma frequency, n_p is the plasma number density and $\omega_B \equiv eB/mc$ is the cyclotron frequency. We assume that energy in plasmas is distributed uniformly, $n_p \approx n_b\gamma_b/\gamma_p$ (n_b is the number density of the beam electrons). As it was shown in (Machabeli & Usov, 1979) the mentioned cyclotron wave is characterized by the following frequency

$$\nu \approx \frac{\omega_B}{2\pi\delta\cdot\gamma_b}. \tag{2}$$

The major requirement for excitation of the cyclotron modes is considerably strong magnetic field, so that the magnetic energy density, W_B, can exceed the plasma energy density, W_p. One can straightforwardly show that for the light cylinder lengthscales the mentioned condition $W_B/W_p > 1$ writes as

$$\frac{W_B}{W_p} \approx 100 \times \frac{10^8}{\gamma_b} \times \frac{100cm^{-3}}{n_b} > 1. \tag{3}$$

This in turn means that the maximum value of the beam number density, allowing the excitation of the cyclotron waves is of the order of $2\times 10^4\text{cm}^{-3}$. If this condition is satisfied, the unstable cyclotron waves are excited, which by means of the feedback, through the diffusion process, affect the distribution of particles, creating the pitch angles.

On the other hand, since the emitting particles are extremely energetic they undergo the synchrotron radiation reaction force (Landau & Lifshitz, 1971)

$$F_\perp = -\alpha\frac{p_\perp}{p_\parallel}\left(1+\frac{p_\perp^2}{m^2c^2}\right), F_\parallel = -\frac{\alpha}{m^2c^2}p_\perp^2. \tag{4}$$

Unlike the role of the diffusion, this force is responsible for the dissipation process, decreasing the pitch angle. Here $\alpha = 2e^2\omega_B^2/3c^2$ and $p_\perp$ and $p_\parallel$ are transversal and longitudinal components of momentum respectively. The corresponding kinetic equation governing the mentioned mechanism is given in a series of works (Chkheidze et al., 2011)

$$\begin{aligned}\frac{\partial f^{\,0}(\mathbf{p})}{\partial t} + \frac{\partial}{\partial p_\parallel}\left\{F_\parallel f^{\,0}(\mathbf{p})\right\} + \frac{1}{p_\perp}\frac{\partial}{\partial p_\perp}\left\{p_\perp F_\perp f^{\,0}(\mathbf{p})\right\} = \\ = \frac{1}{p_\perp}\frac{\partial}{\partial p_\perp}\left\{p_\perp\left(D_{\perp,\perp}\frac{\partial}{\partial p_\perp} + D_{\perp,\parallel}\frac{\partial}{\partial p_\parallel}\right)f^{\,0}(\mathbf{p})\right\} + \\ + \frac{\partial}{\partial p_\parallel}\left\{\left(D_{\parallel,\perp}\frac{\partial}{\partial p_\perp} + D_{\parallel,\parallel}\frac{\partial}{\partial p_\parallel}\right)f^{\,0}(\mathbf{p})\right\},\end{aligned} \tag{5}$$

where $f^{\,0}(\mathbf{p})$ is the distribution function,

$$\begin{pmatrix} D_{\perp,\perp} \\ D_{\perp,\parallel} = D_{\parallel\perp} \\ D_{\parallel,\parallel}\end{pmatrix} = \begin{pmatrix} D\delta|E_k|^2 \\ -D\psi|E_k|^2 \\ D\psi^2\frac{1}{\delta}|E_k|^2\end{pmatrix}, \tag{6}$$

are the diffusion coefficients (Chkheidze et al., 2011), E_k is the electric field, square of which is given by $|E_k|^2 = mc^3 n_b\gamma_b/(4\pi\nu)$ (Malov & Machabeli, 2001), $\psi = p_\parallel/p_\perp$ is the pitch angle and $D = e^2/8c$.

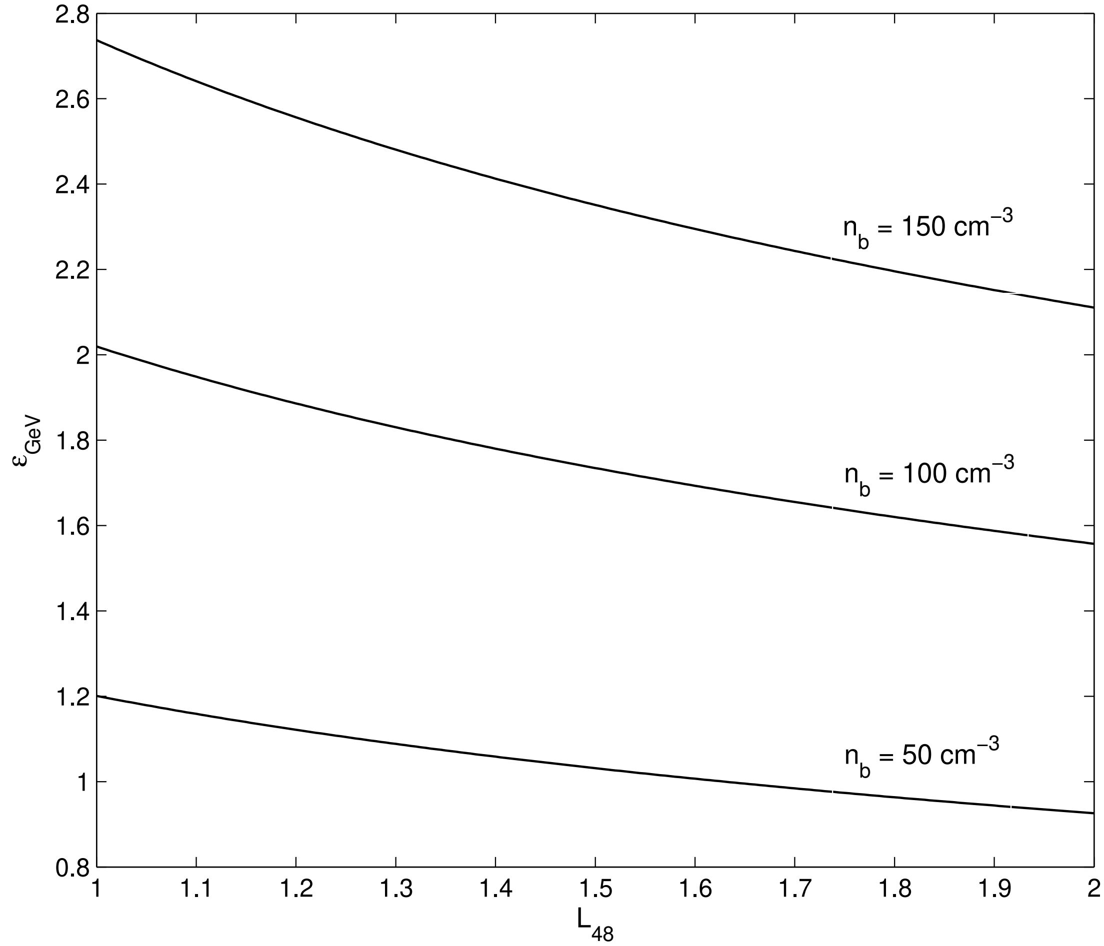

Figure 1. Behaviour of ϵ_{GeV} with respect to the dimensionless luminosity L_{48}. The set of parameters is: $M \approx 5.4 \times 10^8 M_{\odot}$, $r = 70R_g$, $n_b \in [50; 100; 150]$ cm^{-3}, $\gamma_p \approx 1$ and $\gamma_b = 2 \times 10^8$.

Normally the pitch angles are very small, $\psi \ll 1$, therefore, one can reduce Eq. (5) by using the relation $\partial/\partial p_{\perp} >> \partial/\partial p_{\|}$ (Chkheidze et al., 2011)

In the framework of the model the pitch angles saturate due to the balance between the diffusion and the dissipation factors. This leads to the stationary regime ($\partial/\partial t = 0$) and the solution of Eq. (9) writes as

$$f(p_{\perp}) = Cexp\left(\int \frac{F_{\perp}}{D_{\perp,\perp}} dp_{\perp}\right) = Ce^{-\left(\frac{p_{\perp}}{p_{\perp 0}}\right)^4}, \tag{7}$$

where

$$p_{\perp_0} = \left(\frac{4\gamma_b m^3 c^3 D_{\perp,\perp}}{\alpha}\right)^{1/4}. \tag{8}$$

$$\frac{\partial f^0}{\partial t} + \frac{1}{p_{\perp}} \frac{\partial}{\partial p_{\perp}} \left(p_{\perp} F_{\perp} f^0\right) = \frac{1}{p_{\perp}} \frac{\partial}{\partial p_{\perp}} \left(p_{\perp} D_{\perp,\perp} \frac{\partial f^0}{\partial p_{\perp}}\right). \tag{9}$$

It is evident from Eq. (7) that only a tiny fraction of electrons have the transversal momentum sufficiently exceeding the value of $p_{\perp_0}$. Therefore, it is worth estimating the average value of $p_{\perp}$

$$\langle p_{\perp} \rangle = \frac{\int_0^{\infty} p_{\perp} f(p_{\perp}) dp_{\perp}}{\int_0^{\infty} f(p_{\perp}) dp_{\perp}} \approx \frac{p_{\perp_0}}{2}, \tag{10}$$

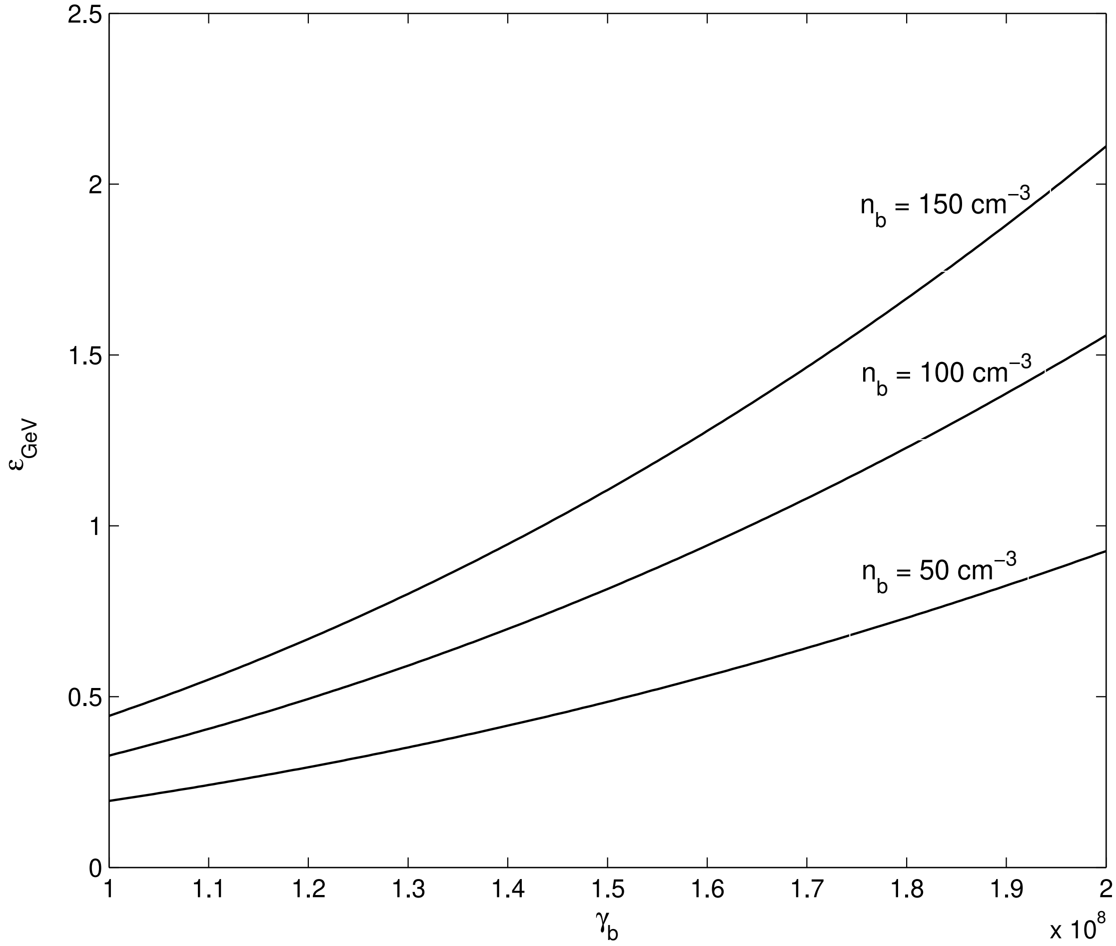

Figure 2. Behaviour of ϵ_{GeV} with respect to the Lorentz factor of relativistic electrons. The set of parameters is: $M \approx 5.4 \times 10^8 M_\odot$, $r = 70R_g$, $n_b \in [50; 100; 150]$ cm^{-3}, $\gamma_p \approx 1$, $L = 2 \times 10^{48}$erg/s.

which naturally describes the mean value of the pitch angles, $\langle\psi\rangle = \langle p_\perp\rangle/p_\parallel$, and the corresponding photon energy produced by the synchrotron emission (Rybicki & Lightman, 1979)

$$\epsilon_{MeV} \approx 2.5 \times 10^{-15} \frac{\gamma_b p_{\perp 0} B}{mc}. \tag{11}$$

Generally speaking, strong magnetic field leads to efficient energy losses, resulting in one-dimensional distribution function. This in turn, creates all necessary conditions for excitation of the cyclotron waves, leading to the final result of this complex process: the creation of the pitch angles, that inevitably causes synchrotron radiation. Therefore, as it is clear from the consideration, the strong synchrotron energy losses do not impose any constraints.

3. Discussion

In this section we study properties of the HE emission of the blazar PKS 1510-089. According to Abdo et al. (2010), between September 2008 and June 2009 the Fermi LAT has detected three γ-ray flares. The most luminous isotropic flare with the estimated luminosity 7×10^{47}erg/s was detected during 2009-03-10 and 2009-04-09, with the brightest daily luminosity of the order of 2×10^{48}erg/s (March 29 2009). The equipartition magnetic field depends on the source luminosity, $B \approx \sqrt{2L/(r^2c)}$ (r is the distance from blazar). Therefore, effectiveness of the QLD strongly depends on the flare efficiency, since the diffusion coefficient depends on B (see Eq. 6).

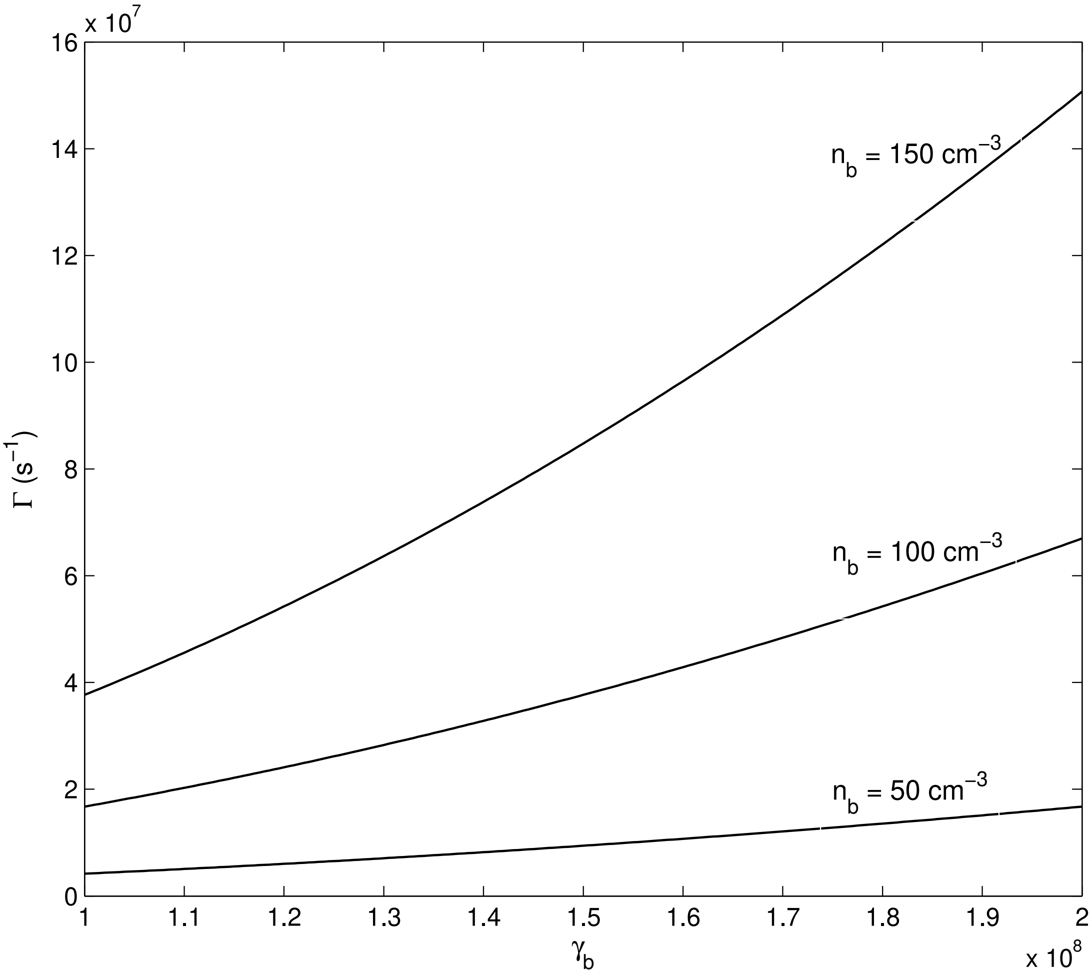

Figure 3. Behaviour of Γ with respect to the Lorentz factor of relativistic electrons. The set of parameters is: $M \approx 5.4 \times 10^8 M_{\odot}$, $r = 70R_g$, $n_b \in [50; 100; 150]$ cm^{-3}, $\gamma_p \approx 1$, $L = 2 \times 10^{48}$erg/s.

In Fig. 1 we show the dependence of ϵ_{GeV} on the dimensionless luminosity, $L_{48} \equiv \frac{L}{10^{48} erg/s}$ for different densities of the beam electrons. The set of parameters is: $M \approx 5.4 \times 10^8 M_{\odot}$, $r = 70R_g$, $n_b \in [50; 100; 150]$ cm^{-3}, $\gamma_p \approx 1$ and $\gamma_b = 2 \times 10^8$. As it is evident from the figure, the photon energy is a continuously decreasing function of the source luminosity. This is a direct consequence of the following behaviour $p_{\perp 0} \propto L^{-5/8}$ (see Eq. 6), which means that for more luminous sources the pitch angles, $\langle\psi\rangle \propto p_{\perp 0}$, and the corresponding synchrotron photon energies will be lower. As it is clear from the plots, by increasing the density, the corresponding photon energy increases as well. In particular, by taking into account Eqs. (8-11) one can see that $\epsilon_{MeV} \propto n_b^{1/2}$. From the plots we see that the QLD may provide HE emission in the GeV energy domain if the beam electrons' Lorentz factors and number density are of the order of 2×10^8 and $50; 100; 150$cm^{-3}, respectively and $\gamma_p \approx 1$.

In Fig. 2 we show the dependence of the photon energy on the Lorentz factors of the beam electrons. The set of parameters is the same as for Fig. 1, except $L = 2 \times 10^{48}$erg/s and $\gamma_b \in [1 - 2] \times 10^8$. As we see from the figures, the QLD may provide the synchrotron emission from multi MeV to several GeV, which is in a good agreement with the observations (Abdo et al., 2010, D́Ammando et al., 2010). On the other hand, it is worth noting that according to the multifrequency campaigns, the spectral energy distribution (SED) of the blazar PKS 1510-089 shows two clear peaks, one in the GeV energy domain and another peak near 10^{13}Hz. This particular peak is formed by mildly relativistic electrons in a different location, where magnetic induction is supposed to be of the order of 3G. In particular, by assuming that the corresponding emission is produced by the synchrotron mechanism, one can straightforwardly show from $\nu_1 \approx 2.9 \times 10^6 \gamma^2 B$Hz (Rybicki & Lightman, 1979) that the mildly relativistic electrons with $\gamma \sim 50$ can explain the first peak of SED. On the other hand, it is clear that energy losses in this case are not efficient, because $t_{syn} \sim 10^6$s exceeds the kinematic timescale and hence the synchrotron process does not require any additional mechanism for maintaining the radiation. Therefore, according to our model, the HE emission comes from the nearby zone of the light cylinder surface $r \sim 5.6 \times 10^{15}$cm (inner magnetosphere), whereas the first peak with 10^{13}Hz is formed in an outer magnetosphere of PKS 1510-089, where the magnetic field is lower.

Since the mechanism of the QLD is driven by the unstable cyclotron waves, it is important to investigate the effectiveness of the instability and the corresponding growth rate. Kazbegi et al. (1991) has shown that the increment of the cyclotron instability is given by

$$\Gamma = \frac{\omega_b^2}{2\nu\gamma_p}, \tag{12}$$

where $\omega_b \equiv \sqrt{4\pi n_b e^2/m}$ is the plasma frequency of beam electrons. In Fig. 3 we show the behaviour $\Gamma(\gamma_b)$. The list of parameters is the same as for Fig. 2. As it is clear from the plots, depending on the physical parameters, the Growth rate varies in a broad interval $[5 \times 10^6 - 1.5 \times 10^8]\text{s}^{-1}$, leading to the following timescales $t_{ins} \sim 1/\Gamma \sim [7 \times 10^{-9} - 2 \times 10^{-7}]$s. On the other hand, the kinematic timescale $t_{kin} \sim r/c$ is of the order of 2×10^5s, which exceeds that of the instability by many orders of magnitude. Therefore, the cyclotron instability is extremely efficient to provide the excitation of the cyclotron waves and maintain the synchrotron emission regime.

4. Summary

1) We study the recently detected (by AGILE and Fermi-LAT) HE γ-ray emission from the blazar PKS 1510-089. Applying the mechanism of the QLD we argue that in spite of the strong synchrotron energy losses, the diffusion is effective enough to provide the observed energies of the source.

2) It is shown that the excited unstable cyclotron waves strongly influence the distribution function of relativistic electrons by means of the quasi-linear diffusion. This in turn maintains the pitch angles from damping and provides the continuous synchrotron emission process.

3) We found that under favorable conditions the QLD may guarantee the HE emission with energies from multi MeV to several GeV, that is in a good agreement with the observations of AGILE and Fermi-LAT.

As we see, the synchrotron mechanism may guarantee emission in the HE domain. Another important issue that we would like to address is the emission spectrum. As we have already mentioned in the introduction, according to the standard theory of the synchrotron radiation (Ginzburg, 1981) the magnetic field is chaotic along the line of sight, therefore, the corresponding values of the pitch angles lie in a broad interval, $\psi \in (0;\pi)$. Unlike this case, in the framework of the QLD the pitch angles are restricted by the dissipation factors leading to a certain spectral picture. Therefore, sooner or later we are going to examine this particular problem as well.

Acknowledgments

The author is grateful to Prof. George Machabeli for valuable discussions and helpful suggestions.

References

Abdo, A.A. et al. (Fermi collaboration), 2010, ApJ, 721, 1425

D́Ammando et al. (AGILE collaboration), 2010, A&A, 521, 69

Blandford, R. D., Netzer, H., & Woltjer, L. 1990, Active Galactic Nuclei, Springer-Verlag

Bloom, S. D. 2008, AJ, 136, 1533

Chkheidze N. & Machabeli G., 2007, A&A, 471, 599

Chkheidze, N., Machabeli, G. & Osmanov, Z., 2011, ApJ, 721, 318

Gangadhara, R. T. 1996, A&A, 314, 853

Ginzburg, V. L. 1981, "Teor. Fizika i Astrofizika", Nauka M. 1981

Giroletti, M., Reimer, A., Fuhrmann, L. et al. 2010, [arXiv:astro-ph/1001.5123]

Gogaberishvili, G., Osmanov, Z.N. & Mahajan S.M., 2021, MNRAS, 503, 3592

Hartman, R. C., et al. 1999, ApJS, 123, 79

Kazbegi, A. Z., Machabeli, G. Z., & Melikidze, G. I. 1991, MNRAS, 253, 377

Landau, L. D., & Lifshitz, E. M. 1971, Classical Theory of Fields (London: Pergamon)

Lominadze J.G., Machabeli G.Z. & Mikhailovsky A.B., 1979, J. Phys. Colloq., 40, No. C-7, 713

Machabeli G. & Osmanov Z., 2009, ApJL, 700, 114

Machabeli G. & Osmanov Z., 2010, ApJ, 709, 547

Machabeli G.Z. & Usov V.V., 1979, AZhh Pis'ma, 5, 445

Malov I.F. & Machabeli G.Z., 2001, ApJ, 554, 587

Osmanov, Z.N., 2021, Com. BAO, 68, 114

Osmanov, Z., 2011, A&A, 530, 75

Osmanov, Z., 2010, ApJ, 721, 318

Osmanov Z. & Machabeli G., 2010, A&A, 516, A12

Osmanov, Z., Rogava, A. D., & Bodo, G. 2007, A&A, 470, 395

Rieger, F. M., & Aharonian, F. A. 2008, A&A, 479, L5

Rybicki, G.B. & Lightman, A. P., 1979, Radiative Processes in Astrophysics. Wiley, New York

Thomas, R. M. C., & Gangadhara, R. T. 2005, A&A, 437, 537

The Impact of Eruptions from Young Stars on Environments of Rocky Exoplanets

Vladimir S. Airapetian[1,2]

[1]NASA Goddard Space Flight Center, Greenbelt, MD USA
[2]American University, Washington, DC, USA

Abstract

Kepler and TESS missions have discovered over 4500 extra solar (exoplanets) around F, G, K and M dwarfs. They also revealed frequent superflares on planet hosting stars, providing a mechanism by which host stars may have profound effects on the physical and chemical evolution of exoplanetary atmospheres. While we can only infer the course of the Sun's early evolution and how it might have affected the early evolution of the Earth, possibly setting the stage for the origin of life, the observation of planets around sun-like stars allows us to directly observe events which likely took place in our own solar system. A major question this leads to is: what effects do extreme energy fluxes from eruptive events during evolution of G-K planet hosts have on prebiotic chemistry and primitive life forms on primitive planets? To address this question, I will describe recent observations of young solar-like stars as inputs for our 3D MHD models of the corona, the wind and transient events (flares, coronal mass ejections and solar energetic particle events) and discuss their impact on atmospheric erosion and chemistry of our planet. I will then use these constrained energy fluxes to describe our recent atmospheric chemistry models impacted by energetic particles from the young Sun and formation and precipitation of biologically relevant molecules. I will then highlight our results of laboratory experiments of proton irradiation of mildly reduced gas mixtures and their implications to the climate, prebiotic chemistry and the rise of habitability on early Earth and young exoplanets.

Keywords: *Solar-like Stars, Coronae, Winds, Coronal Mass Ejections, Stellar Energetic Particle Events, Exoplanets, Atmospheric Chemistry*

1. Introduction

The search for habitable planets and signatures of extraterrestrial life is one of the most ambitious and consequential endeavors of our civilization. Explosion of Kepler and current Transiting Exoplanets Survey Satellite (TESS) led detection of Earth-sized exoplanets within habitable zones opened a new avenue in physical characterization of their atmospheres with the goal to search for the signatures of life. Current data suggest that rocky exoplanets should be common around G-M dwarfs (Zink et al. 2019). Detection of rocky exoplanets within habitable zones around active planet hosting stars suggests that many rocky exoplanets can be exposed to large fluxes of ionizing radiation from coronae and flare activity of planet hosts. This raises the science question we will explore in this project: What is the impact of stellar ionizing radiation fluxes on habitability of rocky worlds around active G-K stars? Our team has recently presented the roadmap for the 31 study of various aspects of star-planet interactions in a global exoplanetary system environment with a systematic, integrated approach using theoretical modeling, observational and laboratory methods combining tools and methodologies of astrophysics, heliophysics, planetary and Earth science as shown in Figure 1 (Airapetian et al. 2020).

To address this question, we need to reconstruct the properties of eruptive events from active G-K dwarfs. Unlike the Sun and solar-type (G-type) stars, K dwarfs can retain their magnetic activity for billions of years (Loyd et al. 2016). Most of young solar-like (G and K-type) stars show signatures of powerful flares with energy exceeding the largest solar flares by a factor of ¿ 10 (referred to as superflares; Airapetian et al. 2020). Flare driven X-ray and Extreme UV (referred to as XUV, 1-120 nm), CME driven shocks and associated SEP fluxes can have a crucial impact on atmospheric escape 22 and chemistry, and thus on climate evolution and habitability of young exoplanets around active planet hosts (Cohen et al. 2014; Airapetian et al. 2016; 2017a; 2017b; 2020; Airapetian 2017; Garcia-Sage et al. 2017; Dong et al. 2018).

doi: doi.org/10.52526/25792776-2021.68.2-426

Recent Kepler, TESS and XMM-Newton, CHANDRA and NICER observations suggest that young solar-like (G and K type) stars show large starspots covering up to 10% of a stellar surface, strong surface magnetic fields up to a few hundred Gauss, The strong surface magnetic flux drives dense hot X-ray bright coronae and massive fast winds, while coronal active regions supply energy for energetic flares (Sanz-Forcada et al. 2011; 2019; Gudel 2007; Maehara et al. 2012; Kochukhov et al. 2020; Notsu et al. 2019; Airapetian et al. 2020).

While these processes can be important for evolution of stellar angular momentum and their contribution to magnetic breaking and activity, explosive events can impact environments of rocky exoplanets in the habitable zones around these stars and present challenges for their habitability (see Dong et al. 2018; Yamashiki et al. 2019; Airapetian et al. 2017; 2020 in references herein). Specifically, ionizing radiation fluxes in the X-ray [0.1-10 nm] and Extreme UV (EUV, 10-91.2 nm) bands (referred to as the XUV band) can deposit heating via photoinization in the exospheres of exoplanets, and thus cause atmospheric escape (Cohen et al. 2014; Johnstone et al. 2019; Airapetian et al. 2020; Vidotto & Cleary 2020). The moderate ionizing fluxes (about 10 times of the current Sun's EUV flux) can also erode planetary atmospheres via production of photoelectrons that drive polarization electric field, the source of ion outflows from exoplanets (Airapetian et al.2017; Garcia-Sage et al. 2017). The recent model of Johnstone et al. 2019 suggest that as stellar XUV fluxes greater than 60 times of the current Sun significantly increases neutral temperature with overall exospheric expansion transitioning to the hydrodynamic escape. Massive and magnetized stellar winds from young stars can exert dynamic pressure on exoplanetary magnetospheres, and thus leading to the expansion of the the polar cap area as well as generate ionospheric currents that can dissipate their energy via Joule heating, which is another factor of atmospheric escape via thermal plasma expansion (Cohen et. al. 2014; 2018). Thus, accurate knowledge of the XUV and wind fluxes are critical factors in assessing the atmospheric escape rates, and thus atmospheric evolution of Venus, Earth and Mars and exoplanets.

The XUV fluxes are enhanced by a factor of 10-100 during large stellar flares, and thus exoplanetary atmospheres around young stars irradiated with frequent flare events can be subject to high escape fluxes and rapid loss of atmospheres. However, coronal mass ejections associated with stellar flares can drive formation of particles up to a few GeV in their shocks that can modify the atmospheric chemistry of exoplanets via formation of biologically relevant molecules that can precipitste to the exoplanetary surfaces. Here, we provide a brief review of our recent results in modeling coronal stellar environments and their impact on chemistry of exoplanets.

2. Coronae and Winds of Active Solar-like Stars

Coordinated multi-wavelength multi-observatory efforts based on HST, XMM-Newton, Chandra, NICER, and ground-based photometric, spectropolarimetric observations are a crucial program for the characterization of input magnetic field and energy fluxes from G-M dwarfs required for their theoretical modeling. This is because stellar surface magnetic field and Zeeman Doppler Images based on spectropolarimetric observations of young G, K and M dwarf stars provide information about large scale structures of the surface magnetic field. They reveal magnetic field strengths much greater than that observed on the Sun (e.g. Rósen et al. 2016; See et al. 2019). The photospheric magnetic field strengths span the range between 10 G to several 100 G in young Sun-like stars, and up to a few 1000 G for M-dwarfs (Kochukhov et al. 2021). They also shows a great diversity of geometry of large-scale stellar magnetic fields varying from poloidal to toroidal configurations (Vidotto et al. 2014). Recent observations revealed that the geometry of global magnetic fields and associated Poynting fluxes may vary on time scales of a few days to years such as BE Cet, HN Peg, eps Eri, κ^1 Cet, EK Dra, AU Mic, Proxima Cen (Boro Saikia et al. 2015; Rosen et al. 2016; Waite et al. 2017). The total unsigned magnetic flux accounts for over 90% of the magnetic flux and is mostly concentrated in stellar starspots (Kochukhov et al. 2020).

It is generally understood that the magnetic field is the ultimate source of energy for coronal heating and wind acceleration, the details of how magnetic energy is transferred from the solar photosphere into the corona remain poorly known. One promising heating mechanism involves the generation and propagation of the Alfvénor magnetosonic waves driven by photospheric motions depositing their energy into the chromosphere, transition region and corona via resonant absorption, phase mixing, or turbulent dissipation (). Solar observations provide evidence for energy transport via upward-propagating large-amplitude Alfvénwaves in the solar chromosphere, transition region, and corona, where the wave amplitudes are inferred from the Doppler line-of-sight velocity perturbation and non-thermal broadening of optically thin

doi: doi.org/10.52526/25792776-2021.68.2-426

emission lines (Cranmer & Winebarger 2019)

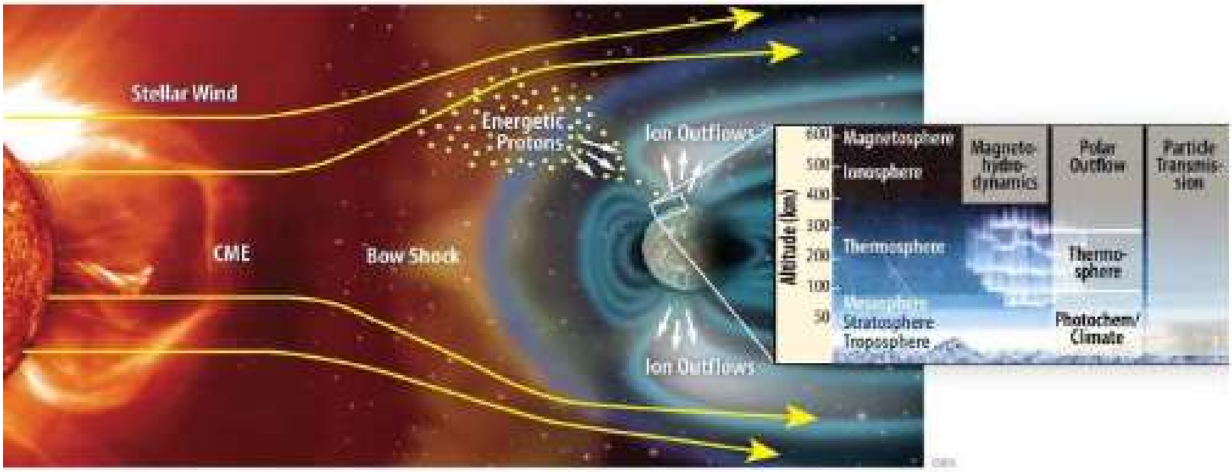

Figure 1. Schematic view of the complex exoplanetary space weather system that incorporates the physical processes driving stellar flares, coronal mass ejections (CMEs), their interactions with an exoplanetary atmosphere. While stellar winds and CMEs affect the shape of an exoplanetary magnetosphere, X-ray and Extreme Ultraviolet Emission (XUV) and stellar energetic particles (SEP) accelerated by coronal flares or CME-driven shocks enter the atmosphere.

Recently, Alvarado-Gomez et al. 2016; 2018; De Nascimento et al. 2016 Boro Saikia et al. (2020) used AlfvénWave Solam Model (AWSoM) constrained with ZDI magnetograms of active stars as boundary for realistic three-dimensional magnetohydrodynamic models of the coronae and winds of active solar-like stars. Airapetian et al. (2021) have extended these models by using fully resolved profiles of chromospheric lines from the Hubble Space Telescope observations that constrain the energy flux of Alfvénwaves at the upper chromosphere that propagate upward and dissipate energy in the upper layers forming the stellar corona.

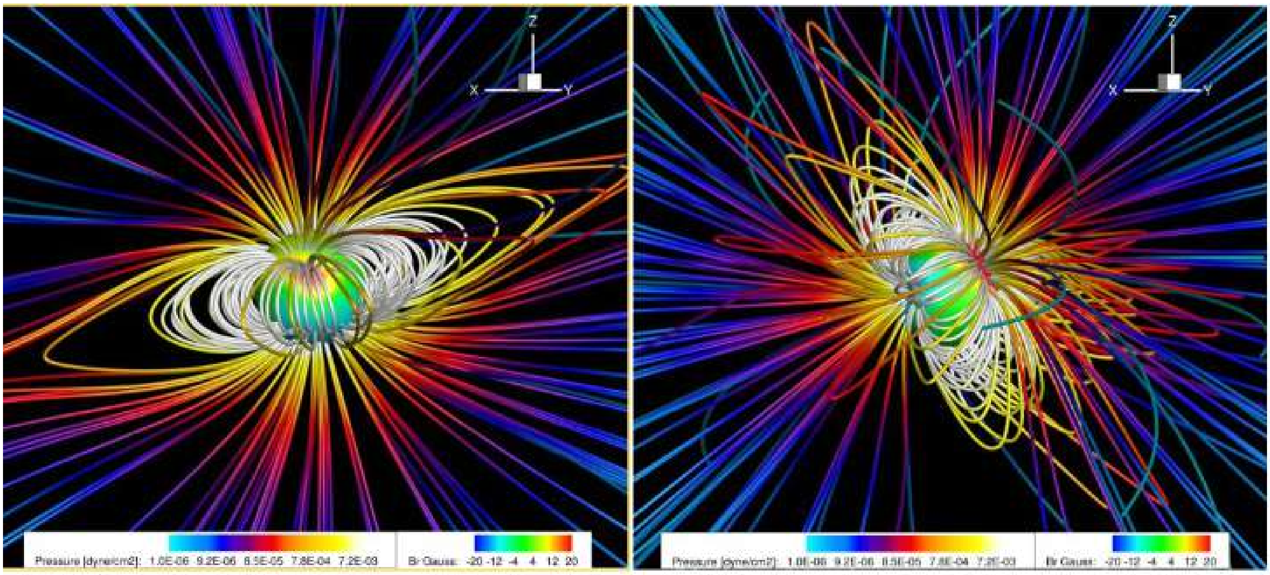

Figure 2. Global structure of the stellar magnetic corona of κ^1 Ceti at 2012.9 (left panel) and 2013.8 (right panel) with the superimposed plasma pressure along the field lines specified by the color bars.

.

The coronal models of κ^1 Ceti developed by Airapetian et al. (2021) is presented in Figure 2. The figure shows that the converged (steady) solution for the global magnetic coronal structure of the star at 2012.8 epoch, which is mostly represented by a dominant dipolar field tilted at 90 (dipole strength of 15.38 G vs 5.1 G and 7.99 G for quadrupole and octupole respectively at 2013.7) and resembles the current Sun's coronal state at minimum of the solar cycle. The right panel demonstrates the magnetic filed topology 11 months later suggesting that the stellar dipole magnetic field has undergone a dramatic transition from a simple

doi: doi.org/10.52526/25792776-2021.68.2-426

dipole to 450 tilted dipolar magnetic field with over 2/3 of the contribution from quadrupolar and octupal components).

The MHD model also provides steady wind solutions for 2012.8 and 2013.7 epochs. The global wind shows the two-component stellar wind of κ^1 Ceti. The plasma accelerated from giant coronal holes (see Figure 4) is driven by the Alfvénwave ponderomotive force, while slow wind is formed due to the thermal pressure gradient. At 2012.8 epoch, the fast wind reaches its terminal velocity of 1152 km/s within the first 15 R_{star}, while the slow and dense component of the wind originates from the regions associated with the equatorial streamer belt structures at 696 km/s.

The simulated stellar wind density is $\sim$50-100 times greater than that of the current Sun's wind and faster by a factor of 2, which produces a massive wind with the mass loss rates of 2.8 $\times 10^{-12}$ M_{sun}, which is 100 times greater than that observed from the current Sun. As high-speed solar wind originating in the stellar coronal hole structures interacts with the preceding slower wind formed along the equatorial regions of the stellar corona, it forms a region of compressed plasma, SIR, along the leading edge of the stream, which, due to the rotation of the star at 9.2 days, is twisted approximately into an Archimedean (or Parker, 1958) spiral. Because the coronal holes may persist for many months, the interaction regions and high-speed streams tend to sweep past an exoplanet at regular intervals of approximately the half of the stellar rotation period forming Corrotating Interaction Regions (CIRs) along the Parker spirals.

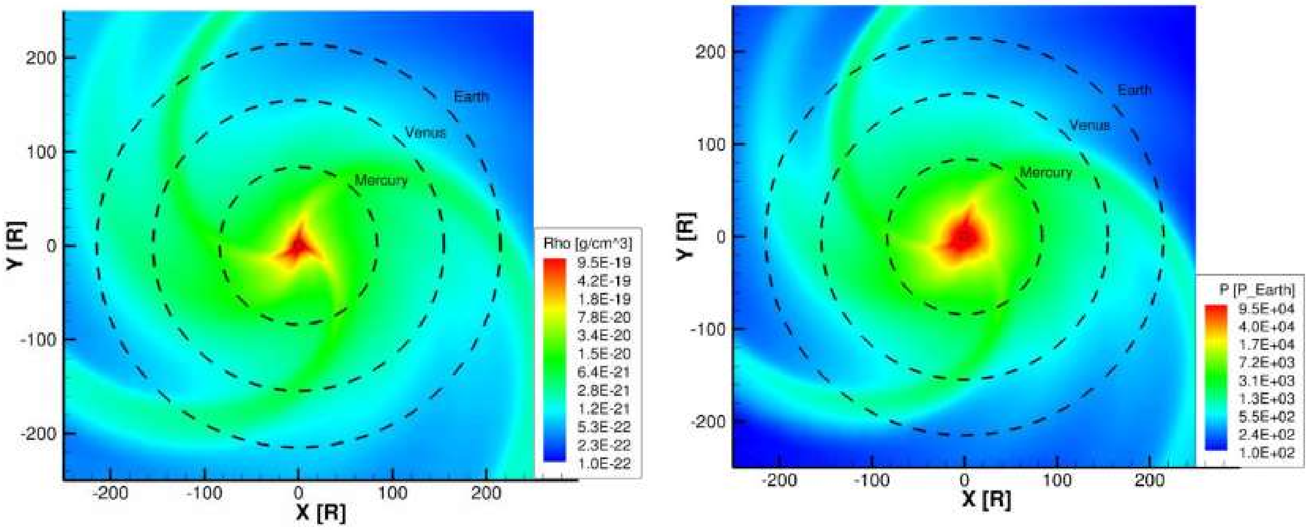

Figure 3. The top panel: 2D slice of the X-Y plane (Z=0) of the plasma density and the dynamic pressure of CIRs from κ_1 Ceti formed at 2012.8 epoch. Black dashed lines show the orbits of Mercury, Venus and Earth respectively.

The CIR wind densities are about 300 greater than the solar wind's density measured by Parker Solar Probe. These results can be applied to characterization of physical conditions at orbital distances of close-in exoplanets around G and K -types stars including eps Eri b (Benedict et al. 2016), K2-229b (Santerne et al. 2018), K2-198b.c, K2-168b,c (Hedges et al. 2016), HD 189733b (Barth et al. 2021). The simulated dynamic pressure exerted by CIRs at close-in exoplanets reaches 5,000-10,000 times at 0.05 AU and 1300 times greater at 1 AU than that exerted to the magnetosphere of the current Earth. The dynamic pressure from stellar CIRs would compress the magnetospheres of Earth-like exoplanets (at the current Earth's magnetic moment) to the standoff distance of $\sim 3R_{Earth}$, and thus ignite strong geomagnetic currents in the early Earth atmosphere.

3. Superflares, Coronal Mass Ejections and Stellar Energetic Particle Events

The evolution of stellar magnetic field has dramatic effects on the frequency and energy of stellar superflares from active stars driven by the rapid release of free magnetic energy stored in the sheared and/or twisted strong fields typically associated with sunspots and active regions (e.g. Shibata & Magara 2011; Maehara et al. 2020; Kazachenko et al. 2012). The maximum energy of superflares from young G-K

doi: doi.org/10.52526/25792776-2021.68.2-426

stars decreases with age from from 1036 ergs (young stars with periods of 1-3 days) to 10^{34} ergs (> 20 days). Because large (white-light) solar flares are accompanied by CMEs with the energy comparable (or exceeding) to solar flares, we can expect that stellar superflares from young solar-like stars should also be associated with energetic CMEs with energies up to 1036 ergs (Gopalswamy et al. 2005). Frequent and energetic CMEs from active stars can also contribute to the stellar angular momentum loss (Drake et al. 2013; Osten & Wolk 2015; Odert et al. 2017). The interaction of frequent and energetic CMEs with magnetically dominated regions of exoplanetary atmospheres (magnetospheres) can cause generation of electric currents that heat upper atmospheres and cause atmospheric escape and chemical changes (Cohen et al. 2014; 2018; Airapetian et al. 2017a;b; Garcia-Sage et al. 2017; Dong et al. 2017; 2018). The relationship between the eruptive flare and its resulting CME is well understood theoretically (Forbes 2000; Lynch et al. 2016; 2019). Because over 95% of powerful solar flares are accompanied by CMEs, and the physics of this correlation is understood (as discussed earlier), we will follow other teams to assume that active G-K stars with their frequent and powerful flares could also have correspondingly numerous energetic CMEs. Thus, the frequency of occurrence and energies of flares can characterize the frequency of occurrence and energies of associated CMEs (Gopalswamy et al. 2005; Odert et al. 2017; Lynch et al. 2019). Theoretical models of solar CMEs suggest that they are driven by the evolution and interaction between the low-lying energized and overlying restraining magnetic fields in solar and stellar coronae (Lynch et al. 2008, 2009; 2016; Karpen et al. 2012; Masson et al. 2013). Our team has recently modelled an energetic CME (7 × 1033 erg) from a young solar-like star, κ^1 Cet, based on the observationally derived k1 Cet magnetogram (Lynch et al. 2019). Magnetic reconnection during the stellar flare creates the twisted flux rope structure of the ejecta and the $\sim$2000 km/s CME eruption of magnetic flux forms a strongly magnetized shock.

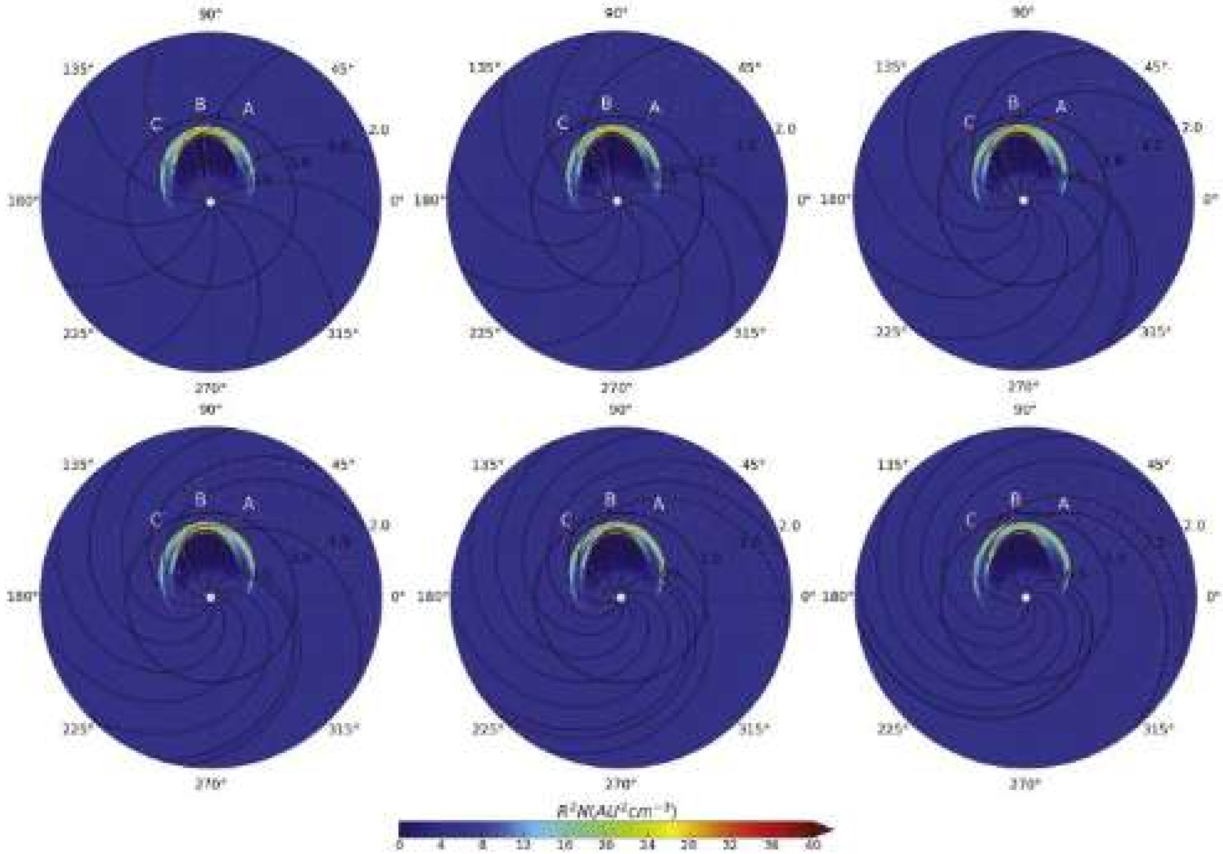

Figure 4. . Configuration for the CME-driven shock under six stellar rotation scenarios at t = 30.2 hr after CME eruption. The shock is initiated with the nose toward f=100°. The top row, from left to right, shows Ω=0.5 $\Omega_\odot$ (case I), 1.0 $\Omega_\odot$ (case II), and 1.5 $\Omega_\odot$ (case III), respectively; the bottom row, from left to right, shows Ω=2.0 $\Omega_\odot$ (case IV), 2.5 $\Omega_\odot$ (case V), and 3.0 $\Omega_\odot$ (case VI), respectively. The color scheme is for the normalized density nr2. The reference points labeled as A, B, and C are located at longitudes of 70°, 100°, and 130°, respectively.

doi: doi.org/10.52526/25792776-2021.68.2-426

Strong shocks are the sites of particle acceleration at the shock front via the diffusive shock acceleration (DSA) mechanism (e.g. Zank et al. 2000). Because the shocks are spatially extended and the acceleration often lasts over an extended period, accelerated particles can be observed at multiple locations that are longitudinally well separated, and the time-intensity profile of these events are "gradual" in nature. Our improved Particle Acceleration and Transport in Heliosphere (iPATH) model successfully explains SEP energy flux evolution in time, fluence, F (the total number of particles per unit area), the energy spectra and their maximum energy. Recent studies suggest that if SEPs with hard energy spectra (F $E^{-\gamma}$, γ ¡ -2) from the young solar-like stars penetrate into the lower layers of exoplanetary atmospheres, they become instrumental in initiating chemical reactions producing complex biomolecules in the atmospheres of early Earth and young exoplanets (Fu et al. 2019; Hu et al. 2021; Airapetian et al. 2016; 2020). Thus, the mechanisms that drive hard energy spectra and high fluence SEPs are of critical importance for understanding atmospheric chemistry of rocky exoplanets around active stars.

Specifically, we studied the role of a CME shock geometry on the fluences and spectra of SEP event cause by a CME with the speed of 1500 km/s. The shape of the shock for a given CME is determined by the geometry of the global magnetic field of the star, which in turn depends on the stellar rotation rate. We have studied 6 case of stellar rotation periods in the range between 0.5 to 3 times the current solar rotation rate on the fluences and spectra of SEP event cause by a CME with the speed of 2000 km/s. To evaluate the effect of the CME shock geometry, we kept the stellar magnetic field fixed and equal to the strength of the current Sun. As the star rotates faster, its interplanetary magnetic field (IMF) is described by a tighter Parker spiral presented in Fig. 4.

Our results suggest that the rotation rate alters the shock geometry. The maximum energy gained by a particle at the shock front also depends on the shock geometry. In addition, the observed time-intensity profiles and event-integrated spectra depend on the stellar rotation rate. Our results provide the first insight into the SEP properties in response to various magnetic field geometries and form a framework to study stellar SEPs including their fluence, spectra, and maximum energy from young magnetically active planet hosting stars.

4. Impact of Stellar Energetic Particles on Atmospheric Chemistry

Exoplanetary atmospheric chemistry is affected by many internal and external factors including the combined effect of XUV-UV and SEP driven particle precipitation into an exoplanetary atmosphere. The initial atmospheric chemical composition is defined by the interplay between the atmospheric escape and volcanic outgassing of species including SO2, H2, CO2, H2S, and H2O, among other species, driven by the internal planetary dynamics (see review paper, Airapetian et al. 2020). The interaction of internal and external energy sources such as meteor impacts, lightning, gamma rays, and SEPs can significantly modify atmospheric chemistry and impact the production rate of prebiotic atmospheric chemistry (Airapetian et al. 2016; and review in Airapetian et al. 2020; Patel et al. 2015). The atmospheric synthesis of molecules of astrobiological interest is influenced by the amount of energy available to drive such chemistry and by the altitude at which that energy is delivered. The main source of external energy, stellar XUV-UV ($1-300$ nm) radiation, will be augmented by reactions induced by other nonthermal processes: ionization, dissociation, and excitation of atomic/molecular species by energetic particles. Of critical importance to the origin of life are processes that dissociate N2 and produce 'fixed nitrogen' that can be used biologically. Stellar EUV radiation can do so, but that process typically happens high up in a planet's atmosphere (see, e.g., Zahnle, 1986; Airapetian et al. 2020). SEPs are much more penetrating and can dissociate N2 all the way down into the exoplanetary troposphere (Airapetian et al., 2016; 2020). Galactic Cosmic Rays and lightning can also cause N2 dissociation at low altitudes, but these sources have been studied previously (Chameides and Walker, 1981; Wong et al., 2017) and will be only used as a comparison against the solar induced production in our modeling.

Given a range of computed atmospheric compositions (see Table 1), we can calculate the steady-state concentrations of species that might have played a role in prebiotic chemistry. These include formaldehyde, H2CO (Pinto et al., 1980) and HCN (Zahnle, 1986), along with various oxides of nitrogen. The main species that we expect to produce initially from SEP bombardment are nitric oxide, NO, and carbon monoxide, CO, as it follows from the reaction

$$\frac{1}{2}N_2 + CO_2 -> NO + CO[R1] \tag{1}$$

doi: doi.org/10.52526/25792776-2021.68.2-426

As mentioned earlier, energetic particles break the N2 triple bond, producing N atoms which can then strip oxygen from CO2 to produce NO and CO. CO itself is interesting in a prebiotic context, as it is a high-energy compound that could have accumulated to substantial concentrations in the early planetary atmosphere (Kasting, 1990). It could have provided a free energy source for early metabolism by way of the water-gas shift reaction: CO + H_2O + CO_2 + H_2 (Kasting, 2014). CO also plays a role in some models of the origin of life (Huber and Wachtershauser, 1997, 1998). These authors envisioned an origin of life in hydrothermal vent systems; however, the free energy from the water-gas shift reaction should also have been available in surface environments. Other sources of energy could also have driven reaction R1, breaking N2 bonds. Previously recognized processes for doing this include lightning (Yung & McElroy 1979; Kasting Walker 1981; Navarro-Gonzalez et al. 1998; Wong et al. 2017), bolide impacts (McKay et al. 1988), and hot volcanic vents (Mather et al. 2004). But model calculations based on Airapetian (2016, 2020) suggest that hard spectra SEP bombardment may have been more effective than any of these other processes in producing NO.

The NO produced by reaction R1 could have played an important role in prebiotic chemistry. In the atmosphere, NO would have been converted to HNO and, to a lesser extent, HNO_2 and HNO_3 (Kasting Walker 1981; Wong et al. 2017). These hydrated forms of NO are all highly soluble and would have rained out into the early ocean. Once there, HNO would then have undergone dissociation, homologation, and decay reactions, ultimately yielding nitrite (NO_2), nitrate (NO_3), and gaseous N_2O (Mancinelli & McKay, 1988; Summers & Khare, 2007; Hu and Diaz, 2019). The N2O would have escaped to the atmosphere, where most of it should have been photodissociated but where, on exoplanets, it could also be confused as a biosignature. Meanwhile, nitrate and nitrite are implicated in a wide range of prebiotic chemistries (Laneuville et al. 2018; Ranjan et al. 2019; Mariani et al. 2018; Becker et al. 2019). Recent work suggests that their concentrations would have been low in the early oceans because of reaction with dissolved ferrous iron, but they could have been more abundant in prebiotic lakes (Ranjan et al., 2019). These predictions are broadly consistent with recently derived isotopic constraints (Homann et al. 2018). NO itself could have participated in prebiotic chemistry by serving as a strong electron sink (Ducluzeau et al., 2009).

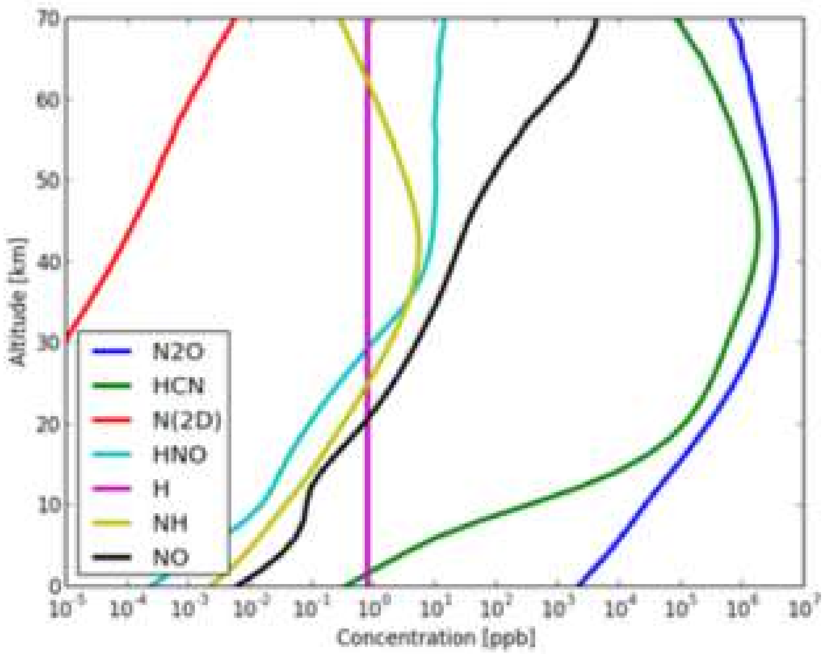

Figure 5. Vertical profiles of biologically important molecules produced by an SEP irradiation of a N_2-CO_2 rich atmosphere.

Another key molecule of interest is HCN, which serves as a precursor for many different biomolecules and prebiotic compounds. The main source of HCN on the early Earth has been considered to be recombination of N2+ in the ionosphere, producing N atoms. These flow down into the stratosphere where they react with the byproducts of methane photolysis to produce HCN, e.g.: CH3 + N + HCN + H_2; $3CH_2$ + N + HCN + H (Zahnle, 1986; Tian et al., 2011). HCN can also be produced in lightning discharges but only if the

doi: doi.org/10.52526/25792776-2021.68.2-426

atmospheric C:O ratio is > 1 (Chameides and Walker, 1981; Rimmer and Rugheimer, 2019). In practice, this requires CH4:CO2 ¿ 1, which is not thought to be true for realistic prebiotic atmospheres, for which researchers struggle to justify CH4 concentrations ¿10-100 ppmv (Kasting and Catling, 2003). Impacts are a more likely source of HCN because of the reduced nature of the gases within the impact plume (Ferus et al., 2017; Ritson et al., 2018). Once formed, HCN would have rained out of the atmosphere and entered the oceans, where it would have participated in numerous reactions. The hydrolysis rate of HCN as a function of pH and temperature has been carefully measured (Miyakawa et al. 2002).

Our updated model accounts for a number of factors including eddy diffusion and convection effects, concentration of hazes or Rayleigh scattering of solar EUV radiation in the atmosphere that significantly reduces photo-destruction of N_2O, and therefore increases its production. Typical fluence of SEP events from the young Sun and magnetically active G-M dwarfs could have been a factor of 10-100 greater than that conservatively assumed in our model.

Laboratory experiments report the production of nitrogen oxides, including N2O, when N2-CO2 mixtures that simulate primitive early Earth atmosphere were exposed to lightning or coronae discharges (Nna-Mvondo et al. 2005). Enhanced production of N_2O in lighting experiments were explained by energetic electrons accelerated in the discharge and UV emission. The production of CH, NH and NO sets stage for the formation of HCN=, and other N-containing species in the lower parts of the atmosphere, which may subsequently rain out into surface reservoirs and engage in higher order chemistry producing more complex organics. The calculated production rate of HCN in the low atmosphere is driven by three major reactions: CH+N + HCN, CH_3+N + HCN + H_2 and CH_2+N + HCN + H. This implies the production rate of HCN about 10^3 Tg/yr. Further HCN polymerization is known to produce various amino acids, the building blocks of proteins (Miyakawa et al. 2002; Coustenis et al. 2007), and is a starting material in the synthesis of purine and pyrimidine nucleobases in addition to sugars via a Kiliani-Fischer mechanism. Production of other types of soluble N-containing species (such as NH_3 and NOx) by SEPs may have provided a massive dose of nitrogen “fertilizer” to early surface biology on terrestrial planets. Our new concept of SEP mediated chemistry challenges the current view of the early Earth atmosphere and predicts new avenues for prebiotic chemistry of young exoplanets around active G-K stars. This model suggests the crucial role of N2O in warming the early Earth and young rocky exoplanets providing new pathway for formation of HCN and other nitrogen bearing molecules conducive to prebiotic chemistry as well as the resolution of the FYS paradox (Feulner 2012; Airapetian et al. 2020).

5. Conclusion

Here we described a novel approach in assessing the drivers and products of atmospheric chemistry of rocky exoplanets exposed to high XUV and SEP fluxes associated with flares from their active planet hosts. We applied an MHD codem AWSoM, to model the quiescent solar corona and the wind from young solar-like stars. This plasma and magnetic background was then used to study the properties of stellar energetic particles by using a proven heliophysics tool, iPATH, for a wide range of stellar environments, an unexplored source of chemical changes in exoplanetary atmospheres. This study will also have a major impact on our understanding of the rise of prebiotic atmospheric chemistry on Earth and rocky exoplanets, associated effects on climate, chemical synthesis and habitability of rocky planets, by placing them in a more complete context with respect to the history of magnetic activity of their host stars. The future work will study how high-energy events in young and active G-K stars may affect evolution of prebiotic and primitive biospheric chemistry and atmospheric warming mechanisms of rocky exoplanets.

doi: doi.org/10.52526/25792776-2021.68.2-426

6. References

Hu, J., Airapetian, V. S., Li, G., Zank, G., Jin, M. 2021, Extreme Energetic Particle Events by Superflare Associated CMEs from Solar-like Stars, Science Advances.

Airapetian, V. S., Jin, M., Lüftinger, T., Boro Saikia, S., Kochukhov, O., Gudel, M., B. Van DerHolst 2021, One Year in the Life of Young Suns, Astrophys. J., 916, 96.

Airapetian, V. S., Barnes, R., Cohen, O. et al. 2020, Int. J. of Astrobio. 19(2), 136.

Airapetian, V. S. 2017, in Extreme Events in Geospace: Origins, Predictability, and Consequences, Chapter 25. p. 611-632.

Airapetian, V. S., Glocer, A., Khazanov, G. V. et al. 2017a, Astrophys.-J. Lett., 836, L3.

Airapetian, V. S., Jackman, C. H., Mlynczak, M., Danchi, W., Hunt, L. 2017b, Atmospheric Beacons of Life from Exoplanets Around G and K Stars, Nature Scientific Reports, 7, 14141.

Airapetian, V. S., Glocer, A., Gronoff, G., E. Hébrard, E., Danchi, W. 2016, Nature Geoscience, 9, 452.

Airapetian, V. & Usmanov, A. 2016, Astrophys. J. Lett., 817, L24.

Alvarado-Gomez, J. D., Hussain, G. A. J., Cohen, O., et al. 2016, Astron. Astrophys., 588, A28

Barth, P., Helling, Ch., Stüeken, E. E. et al. 2021, Mon. Not. R. Astron. Soc., 502, 6201.

Beard, D. B. 1960, J. Geophys. Res., 65(11), 3559, 10.1029/JZ065i011p03559.

Benedict, G. F., McArthur, B. E., Gatewood, G., et al. 2006, Astron. J, 132, 2206

Boro Saikia, S., Jin, M., Johnstone, C. P. et al. 2020. Astron. Astrophys., 635, A178.

Boro Saikia, S., Jeffers, S. V., Petit, P., et al. 2015, Astron. Astrophys., 573, A17.

Cohen, O., Drake, J. J., Glocer, A. et al. 2014, Astrophys. J., 790, article id. 57, 13.

Cranmer, S. R. and Saar, S. H. 2011, Astrophys. J., 741, 54.

Do Nascimento, Jr. J-D, Vidotto, A. A., Petit, P. et al. 2016, Astrophys. J. Lett., 820, L15.

Dong, C. F., Jin, M., Lingam, M., Airapetian, V. S., Ma, Y. J., van der Holst, B. 2018, Proc. Nat. Acad. Sci., 115, 260.

Fu, S., Jiang, J., Airapetian, V., Hu, J., Li, G., and Zank, G., 2019, Astrophys. J. Lett., 878, L36.

Garcia-Sage, K., Glocer, A., Drake, J. J. et al. 2017, Astrophys. J. Lett., 844, L13.

Güdel, M. 2020, Space Science Reviews, 216, article id.143.

Johnstone, C., Khodanchenko, M. and Lüftinger, T. et al. 2019, Astron. Astrophys., 624, L10.

Kochukhov, O., Hackman, T., Lehtinen, J. J. 2020, Astron. Astrophys., 635, 142.

Lynch, B. J., Airapetian, V. S., DeVore, C. R. et al. 2019, Astrophys. J., 880, 97-109.

Maehara H., Shibayama T., Notsu S. et al 2012, Nature 485, 478.

Parker, E. N. 1958, Astrophys. J., 128, 664.

Patel, B. H., Percivalle, C., Ritson, D. J., Duffy, C. D., & Sutherland, J. D. 2015, Nature Chemistry, 7, 301.

Ribas, I., Guinan, E. F., Gudel, M. et al. 2005, Astrophys. J., 622, 680.

Rosen, L., Kochukhov, O., Hackman, T.,& Lehtinen, J. 2016, Astron. Astrophys,, 593, A35.

Sanz-Forcada, J., Micela, G., Ribas, I. et al. 2011, Astron. Astrophys., 532, A6.

doi: doi.org/10.52526/25792776-2021.68.2-426

See, V., Matt, S. P., Folsom, C. P. et al. 2019, Astrophys. J., 876, 118.

Vidotto, A. 2021, Living Reviews in Solar Physics, in press, 10.1007/s41116-021-00029- w

Vidotto, A. & Cleary, A. 2020, Mon. Not. R. Astron. Soc., 494, 2417.

Waite I. A., Marsden, S. C., Carter, B. D. et al., 2017, Mon. Not. R. Astron. Soc., 465, 2076.

doi: doi.org/10.52526/25792776-2021.68.2-426

Narrow band imaging survey of dark clouds

Movsessian T.A.*[1], Magakyan T.Yu.†[1], Dodonov S.N.‡[2], and Andreasyan H.R.§[1]

[1]Byurakan Astrophysical Observatory, Aragatsotn reg., Byurakan, 0213 Armenia
[2]Spetial Astrophysical Observatory, N.Arkhyz, Karachaevo-Cherkesia, 369167 Russia

Abstract

We present new results obtained in frames of the Byurakan Narrow Band Imaging Survey (BNBIS). Observations were carried out with upgraded 1 m Schmidt telescope of Byurakan Observatory. Main task of this survey is to search and to study the new Herbig-Haro objects and collimated outflows using narrow-band Hα and [S II] images of some fields in dark clouds of Galaxy. And, because, Herbig-Haro objects are the main indicators of active starformation processes to fined regions where going on active starformation processes. Main targets of this survey are R associations, young stellar objects associated with compact reflection nebulae, but here we will mainly focused on deeply embedded infrared sources in molecular clouds.

During this survey we plan to significantly expand the list of HH objects by using the high quantum efficiency of the system and the telescopes high focal ratio (F/2), which allows detecting low surface brightness objects as well as large field of view of Schmidt telescope.

Keywords: *Starformation, Herbig-Haro objects, jets and outflows*

1. Introduction

Herbig-Aro objects are formed by the interaction of collimated outflows from young stellar objects with the circumstellar medium and, in some cases, represents the brightest parts of optical jets. It is considered proven that the presence of Herbig-Haro objects is one of the main signs of an active star formation process in dark clouds (Reipurth & Bally, 2001). In most cases the sources of Herbig-Haro objects are stars which are bright in the infrared region of the spectrum, and only a small part of them are optically bright stars, which are mainly classical stars of the Tau class. Discovering of new HH objects are important as for the further studies of the phenomenon of directed outflows from young stars in various evolutionary stages, as well as for the searches for new star forming regions and groups.

The presence of deeply embedded sources with an infrared excess, characteristic of young stellar objects, can also be considered as a sign of star formation. Such sources are divided into three classes according to their infrared excess calculated by their spectral indexes. Currently, three classes have been identified, Class I - considered candidates for protostars, class II - T Tau stars and class III WTTs-type stars. In addition to these three classes, Class 0 has been proposed as evolutionary precursors of Class I protostars (Andre, Ward-Thompson, & Barsony, 1993, Andre & Montmerle, 1994). The work of (Bontemps et al., 1996) and (Saraceno et al., 1996). However, some Class I objects that are observed at a high inclination may look 'Class 0-like' due to the high optical thickness associated with absorption in a dense circumstellar disk (Masunaga & Inutsuka, 2000). This circumstance further complicates the distinction between Class 0 and Class I objects, however, there are sources associated with reflection nebulae, which helps clarify the nature of the source. The presence of such nebulae indicates that the optical radiation of the source is obscured not only by a dark cloud, since a reflective nebula is visible, but also by a dense circumstellar disk.

Taking this into account, we have included dark clouds with bright infrared sources and especially those associated with compact reflective nebulae in the list of studied areas.

*tigmov@bao.sci.am, Corresponding author
†tigmag@sci.am
‡dodo@sao.ru
§D.D@university.edu

doi: doi.org/10.52526/25792776-2021.68.2-436

2. Observations

The images were obtained on the nights of Feb. 3–4 2019 with 1m Schmidt telescope of Byurakan observatory, which was upgraded during 2013–2015 and equipped with CCD detector. Reworked 4K×4K Apogee (USA) liquid-cooled CCD camera was used as a detector with a pixel size of 0.868" and field of view of about 1 square degree (Dodonov et al., 2017).

Narrow-band filters centered on 6560 Å and 6760 Å, both with a FWHM of 100 Å, were used to obtain Hα and [S II] images, respectively. A midband filter, centered on 7500 Å with a FWHM of 250 Å, was used for the continuum imaging.

A dithered set of 5 min exposures was obtained in each filter. Ususal effective exposure times were about 3600-7200 sec in Hα and [S II] filters. Images were reduced in the standard manner using IDL package developed by one of authors (SND), which includes bias subtraction, cosmic ray removal, and flat fielding using "super flat-field", constructed by several images.

3. Results

3.1. Mon R1-first success

R1 association located not far from Mon OB1 (see Dahm (2003), for a detailed review) but unlike of it has not been investigated in sufficient detail. In frames of BNBIS in the Mon R1 were discovered several new HH objects as well as two collimated outflow systems, one form which belongs to giant HH outflows with size of 1.6pc. Detailed description of newly discovered HH objects and outflow systems can be found in Movsessian, Magakian, & Dodonov (2021). Narrow band image, which is covering one square degree field of Mon R1 region with newly discovered HH objects, is shown on the Fig. 1 in mentioned paper.

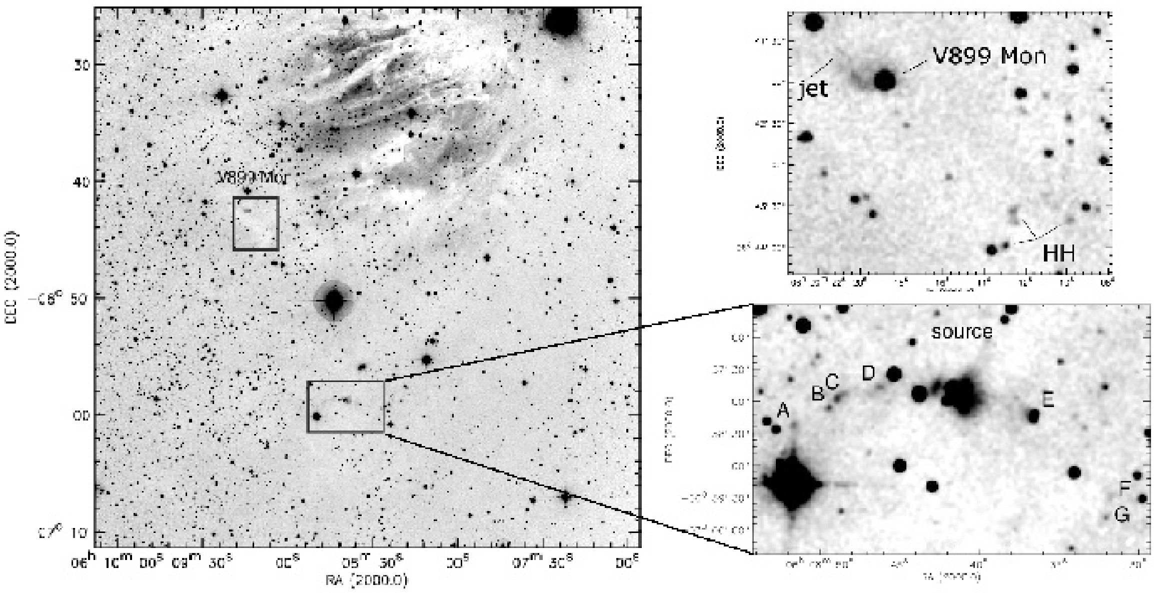

Figure 1. Whole observed field of Mon R2 south Mon in Hα+[S II] emission, where the areas including newly discovered HH objects and outflows, are shown by rectangles (left panel). V899 Mon with associated HH objects and narrow jet (right top) and curved HH outflow system from 2MASS 06084223-0657385 infrared source associated with bipolar reflection nebula (right bottom).

3.2. RNO 66 and V899 Mon field

This field located about one degree south from Mon R2 association. Mon R2 association is a well studied region of star formation which contains early-type stars (Racine, 1968), molecular outflows (Meyers-Rice & Lada, 1991), an embedded HII region (Downes et al., 1975) and clusters of infrared sources (Thronson et al., 1980). However there is little research on the search for HH objects, and were found some on the Eastern

doi: doi.org/10.52526/25792776-2021.68.2-436

side of Mon R2 (Carballo & Eiroa, 1993). Our attention was drawn to the area South of the Central part of Mon R2, where several nebulous objects and an eruptive star V899 Mon are located.

A Hα+[S II] image, which is covering one square degree field of the Mon R2 region, is shown on Fig.1 (left panel). The zones with newly discovered HH objects and HH flows are marked by rectangles.

3.2.1. V899 Mon

A possible FUor-type eruption of V899 Mon(IRAS 06068-0641) located near the Monoceros R2 region (d≈900 pc; (Lombardi, Alves, & Lada, 2011) was first discovered by the Catalina Real-time Transient Survey (CRTS) and reported by Wils et al. (2009). They announced the source as a FUor candidate based on the constant brightening it has been undergoing since 2005. The spectrum published by Wils et al. (2009) showed strong Hα and CaII IR triplet lines, which identify the outbursting source as a YSO.

Further optical and NIR spectroscopy of V899 Mon confirms it to be a member of the FUors/EXors family of outbursts. Photometrically and spectroscopically V899 Mon's properties lie between EXors and classical FUors. But it is probably more similar to EXors than classical FUors.

On the distance of about 2,5 arcmin in south-west from V899 Mon four HH knots were discovered which can probably associated with V899 Mon, besides narrow jet was detected in [S II] by the axis of the reflection nebula associated with V899 Mon Fig.1 (right top panel). All data suggest that V899 Mon is a source of collimated and possibly bipolar outflow and HH objects can represents counter flow from it. However, the newly found HH objects could be result of activity of other infrared sources in this area.

3.2.2. Curved HH flow

Abut 20 arcmin south-west from V899 Mon were revealed several HH knots near the 2MASS 06084223-0657385 infrared source associated with bipolar reflection nebula. HH objects lies on a parabolic curve at the apex of which the infrared source is located Fig.1 (right bottom panel). Therefore, it can be argued that we are dealing with a bipolar outflow with an unusual arc-shaped structure. Such a morphology is typical for so named irradiated jets or outflows from the sources with high proper motion. We incline to the second scenario, because irradiated outflows represents very thin emission structures without prominent knotty structures (Bally & Reipurth, 2001). Taking this scenario into account we estimated the proper motion value of the source which is about 50 km s^{-1}, which is quite acceptable. Estimated total length of this bipolar outflow will be about 1.5 pc for the distance of 900 pc. This outflow system represents giant or so called parsec scale HH flow as well as HH 1196 in Mon R1.

3.3. IRAS 06212-1049

The infrared source IRAS 06212-1049 is associated with a cone-shaped reflective nebula, the axis of which is oriented to the southeast. The deep images of the PanSTARRS survey show a faint nebula in the opposite direction from the source, which indicates the bipolar morphology of the nebula. The object is located near the dark cloud LDN 1652 which is located at a distance of 830 pc. It can be assumed that IRAS 06212-1049 is located in this group and, therefore, its distance can be considered the same. On the images obtained in the Hα and [S II] emission lines were detected HH knots, which are directed along the axis of the reflection nebula Fig.2 and, obviously, represent a collimated optical flow. If we take a distance of about 800 pc, the total length of the outflow will be about 0.9 pc.

A detailed analysis of the entire field made it possible to detect two more Herbig-Aro objects, which are shown in Fig.2. The first object is an isolated emission knot near which there is no any infrared source that could be its source. The second, a faint somewhat extended object with a length of about 6", is located near the infrared source IRAS 06216-1044 and is barely visible on the red maps of DSS2. The distance of this object from IRAS 06216-1044, which can be its source, is about 12" or 0.05 pc.

3.4. New HH objects near IRAS sources

As was already mentioned we choose some infrared sources as a targets for narrow band survey. All these sources have considerable infrared excess characteristic for young stellar objects. Some of targets are associated with small reflection nebulae with characteristic cone shape. On the Fig.3 some examples of such a sources are presented where HH objects are shown by arrows.

doi: doi.org/10.52526/25792776-2021.68.2-436

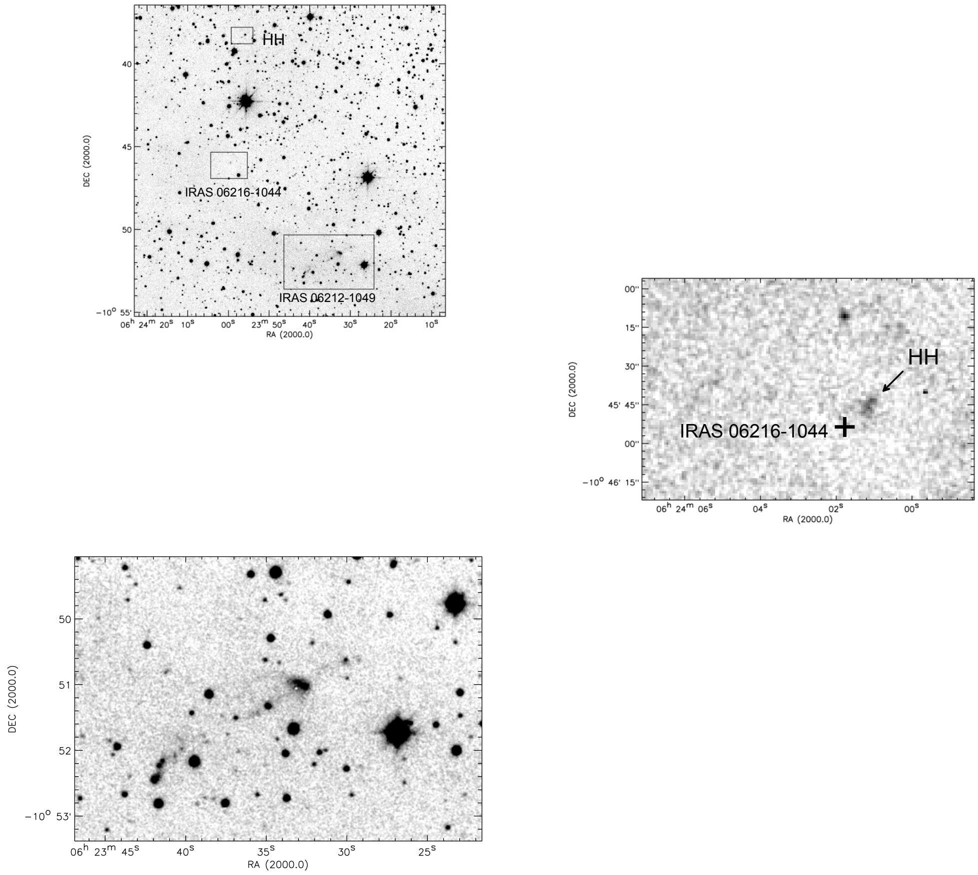

Figure 2. Whole observed field of IRAS 06212-1049 in Hα+[S II] emission. The areas including newly discovered HH objects and outflows, are shown by rectangles (left panel). Hα+[S II] and [S II] image of IRAS 06212-1049 (bottom panel)and IRAS 06216-1044 (left panel).

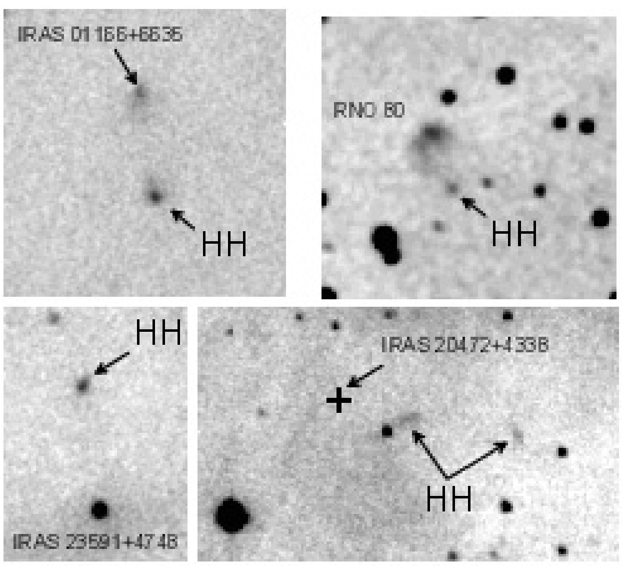

Figure 3. Infrared sources associated with Herbig-Haro objects

doi: doi.org/10.52526/25792776-2021.68.2-436

3.5. Conclusion

Since the beginning of 2019, when this survey began, more than 100 new HH objects and outflow systems have been found. Among them should be mention several giant outflow systems, narrow jets as well as curved HH flow.

Besides, several new HH objects were discovered near IRAS sources. Analysis of SED's these sources reveal its classes, which are mainly belongs to class I young stellar objects, but some of them have properties of class 0. Taking in account association of those objects with compact reflection nebulae, we incline to consider them as class I sources, which are surrounded by dense disc and oriented edge on.

In addition to all the results presented above, this work demonstrates that the 1-m Schmidt telescope of Byurakan Observatory, which was used several decades ago for well-known surveys of active galaxies such as the First Byurakan Survey and Second Byurakan Survey, can still lead to important discoveries.

References

Andre P., Ward-Thompson D., Barsony M., 1993, ApJ, 406, 122. doi:10.1086/172425

Andre P., Montmerle T., 1994, ApJ, 420, 837. doi:10.1086/173608

Bally J., Reipurth B., 2001, ApJ, 546, 299. doi:10.1086/318258

Bhadari N. K., Dewangan L. K., Pirogov L. E., Ojha D. K., 2020, ApJ, 899, 167. doi:10.3847/1538-4357/aba2c6

Bontemps S., Andre P., Terebey S., Cabrit S., 1996, A&A, 311, 858

Carballo R., Eiroa C., 1993, ASSL, 213. doi:10.1007/978-94-011-1924-$5_3$7

Dahm S.E, 2008, in Reipurth B., ed., Handbook of Star Forming Regions, Vol. I, Astron. Soc. Pac., p. 966

Lombardi M., Alves J., Lada C. J., 2011, A&A, 535, A16. doi:10.1051/0004-6361/201116915

Dodonov S.N., Kotov S.S., Movsesyan T.A., Gevorkyan M. 2017, Astrophysical Bulletin, 72, 473

Downes D., Winnberg A., Goss W. M., Johansson L. E. B., 1975, AA, 44, 243

Masunaga H., Inutsuka S.-. ichiro ., 2000, ApJ, 531, 350. doi:10.1086/308439

Meyers-Rice B. A., Lada C. J., 1991, ApJ, 368, 445. doi:10.1086/169709

Movsessian T. A., Magakian T. Y., Dodonov S. N., 2021, MNRAS, 500, 2440. doi:10.1093/mnras/staa3302

Reipurth B., Bally J., 2001, ARA&A, 39, 403. doi:10.1146/annurev.astro.39.1.403

Racine R., 1968, AJ, 73, 233

Saraceno P., Andre P., Ceccarelli C., Griffin M., Molinari S., 1996, A&A, 309, 827

Thronson H. A., Gatley I., Harvey P. M., Sellgren K., Werner M. W., 1980, ApJ, 237, 66. doi:10.1086/157844

Wils P., Greaves J., Drake A. J., Catelan M., 2009, CBET, 2033

doi: doi.org/10.52526/25792776-2021.68.2-436

Communications of BAO, Vol. 68, Issue 2, 2021, pp. 441-446

Study of radio properties of active galaxies

H. V. Abrahamyan [*], A. M. Mickaelian [†], G. M. Paronyan [‡], G. A. Mikayelyan [§] and A. G. Sukiasyan [¶]

NAS RA V. Ambartsumian Byurakan Astrophysical Observatory (BAO), Byurakan 0213, Aragatzotn Province, Armenia

Abstract

In this paper we investigate radio properties of active galaxies taken from Véron-Cetty & Véron (2010) catalogue. The galaxies are limited to magnitudes in the range of 12^m-19^m. We have cross-correlated the list with radio catalogues and selected those galaxies, which have data on 5 radio fluxes at different wavelengths. For all the objects we have built radio spectra and estimate radio spectral indices. As a result, we have $\alpha_{average}$=-0.5036±0.0717.

Keywords: *active galaxies, AGN, radio galaxies, QSO, Seyfert, LINER, radio spectral index.*

1. Introduction

In terms of activity, most of the galaxies in the Universe are considered as "normal", without any prominent activity manifestation. Normal galaxies have total luminosities up to about $10^{11} \times L_{Sun}$. For example, all galaxies in the Local Group (including the Milky Way and Andromeda Galaxy) are normal ones. In spectra of normal galaxies, we observe the sum of spectra of all the stars the galaxy contains. The luminosity of normal galaxies does not change much in short periods of time.

Active galaxies are among the most interesting objects in the Universe. They have higher luminosities than normal galaxies. It is important that active galaxies have brighter nuclei than normal ones. In these galaxies, large amounts of energy fall out from such small areas as the galactic nuclei. It is considered that there is a massive or supermassive black hole in the center of each of these galaxies. Some active galaxies have gigantic jets in optical and more often in radio ranges. The luminosity of an active galaxy can change twice and even more times during a short period of time, for instance, some active galaxies show variability during a period of a few days.

Active galaxies are of different types: radio galaxies, Seyfert galaxies, quasars, blazars, LINERs, and others. Radio galaxies are elliptical galaxies. All galaxies radiate some radio waves. In case of normal galaxies, radio emission corresponds to a small fraction of the total energy radiated by the galaxy. The energy for radio galaxies radiated at radio wavelengths is 0.1 to 10 times more than the energy radiated at visible wavelengths. Seyfert galaxies were discovered by Carl Seyfert in 1943. These galaxies have broad emission-line spectra indicating cores of hot, low-density ionized gas. The "typical" members of the class (Seyfert 1 and 2) were described by Khachikian & Weedman (1971), and Khachikian & Weedman (1974).

This work is dedicated to radio properties of active galaxies. In the radio range, radio spectra of these objects are very interesting. The radio emission of a distant galaxy consists of thermal and synchrotron contributions. The thermal emission is radiation from HII regions while the nonthermal synchrotron emission is generated by Supernova remnants (Biermann (1976); Condon (1992); De Young (1976); Blandford & Königl (1979)), as well as by the core. These emission components are characterized by different spectral indices and, therefore, the total spectral index depends on their relative contributions. The radio spectral index is a powerful probe for classifying cosmic radio objects and understanding the origin of the radio emission.

[*]abrahamyanhayk@gmail.com, Corresponding author
[†]aregmick@yahoo.com
[‡]paronyan_gurgen@yahoo.com
[§]gormick@mail.ru
[¶]andranik.suqiasyan.1995@mail.ru

doi: doi.org/10.52526/25792776-2021.68.2-441

To understand physical properties of some active galaxies, we have built radio spectra for our objects (spectral energy distribution, SED) and estimate radio spectral indices (Hawkins (2002), Ulrich (1999)). Radio spectral index is the most important property of radio sources in the radio range.

There are many papers devoted to radio investigation of active galaxies. Below, we present some of the recent works, which we have used, and made comparisons with.

In this work we have investigated 116 active galaxies which also have activity in radio range.

2. Investigated data

We use data from the Véron-Cetty & Véron (2010) catalogue (VCV-13). This catalogue includes 133,336 quasars, 1374 BL Lac objects, and 34,231 active galaxies (including 16,517 Seyfert 1.0). We have considered 34,231 active galaxies for our research. More information on these objects is given in table 1.

Table 1. Active galaxies in VCV-13 by activity types, excluding quasars.

Activity type	**Number**
Seyfert	23258
LINER	907
HII	167
Unk.	9899
Total	**34231**

VCV-13 catalogue was published by Véron-Cetty & Véron (2010) in 2010. It is a unique catalogue that includes objects having active galaxy types. Active galaxies collected until 2010 are given. After that no similar catalogue, that included active galaxies, was published. In 2019, Souchay et al. (2019) created LQAC-5 catalogue, which included all quasars discovered by all surveys. But it comprised only those active galaxies that were given in VCV-13. So far, we have the list of active galaxies from VCV-13.

For investigation, galaxies having magnitudes in the range of 12^m-19^m. have been taken. In the next step we have cross-correlated (Abrahamyan et al. (2015)) these objects with radio catalogues: FIRST (Helfand et al. (2015)), NVSS (Condon et al. (1998)), 87GB (Gregory & Condon (1991)), GB6 (Gregory et al. (1996)), 3C (Edge et al. (1959)), 4C (Pilkington & Scott (1965)), 7C (Hales et al. (2007)), 8C (Hales et al. (1995)), 9C (Waldram et al. (2003)), 10C (Consortium et al. (2011)), SUMSS (Mauch et al. (2003)), WISH (De Breuck et al. (2002)), WENSS (de Bruyn et al. (1998)), Molonglo Reference Catalogue of Radio Sources (Large et al. (1991)), Texas Survey of radio sources at 365 MHz (Douglas et al. (1996)), Miyun 232 MHz survey (Zhang et al. (1997)), CLASS survey of radio sources (Myers et al. (2003)), 74 MHz VLA Low-frequency Sky Survey Redux (Lane et al. (2014)) and The GMRT 150 MHz all-sky radio survey (Intema et al. (2017)).

As a result, we have 4437 objects which have identification in radio (table 2).

Table 2. Number of identifications for active galaxies.

Identification number with radio catalogue	**Number of objects**
10	6
9	10
8	33
7	58
6	91
5	116
4	139
3	361
2	629
1	2994
Total	**4437**

As seen from table 2, 4437 objects have from 1 to 10 radio fluxes at different wavelengths. In this work, radio catalogues that cover 38 MHz to 15.7 GHz frequency range have been taken. Abrahamyan in

doi: doi.org/10.52526/25792776-2021.68.2-441

2020 (Abrahamyan (2020)) taken and investigated objects which have 6 or more radio fluxes at different wavelengths. For our investigation we have taken objects which have 5 radio fluxes at different wavelengths. So, we have 116 objects with 5 or more radio fluxes.

3. Investigated data

The same method which given by Abrahamyan in 2020 (Abrahamyan (2020)), we estimated radio spectral indices for our objects.

Active galaxies are very interesting objects in the Universe. In order to understand some physical properties, we must identify which properties our objects have in radio range. We have 116 active galaxies having 5 at different wavelengths. A very important radio property for radio objects is the radio spectral index. It shows steep radio spectra. Having 5 frequencies we have built graph for all 116 galaxies (lg[flux] versus lg[frequencies]). Having lg[flux] versus lg[frequencies] graph for each source we have made linear fitting. The software "Origin" gives formula for each linear fit and using that we have counted radio spectral index for each source. The plot shows steep radio spectra for each line, and that is considered as radio spectral index. As examples, we give average radio spectra for our objects in Figure 1.

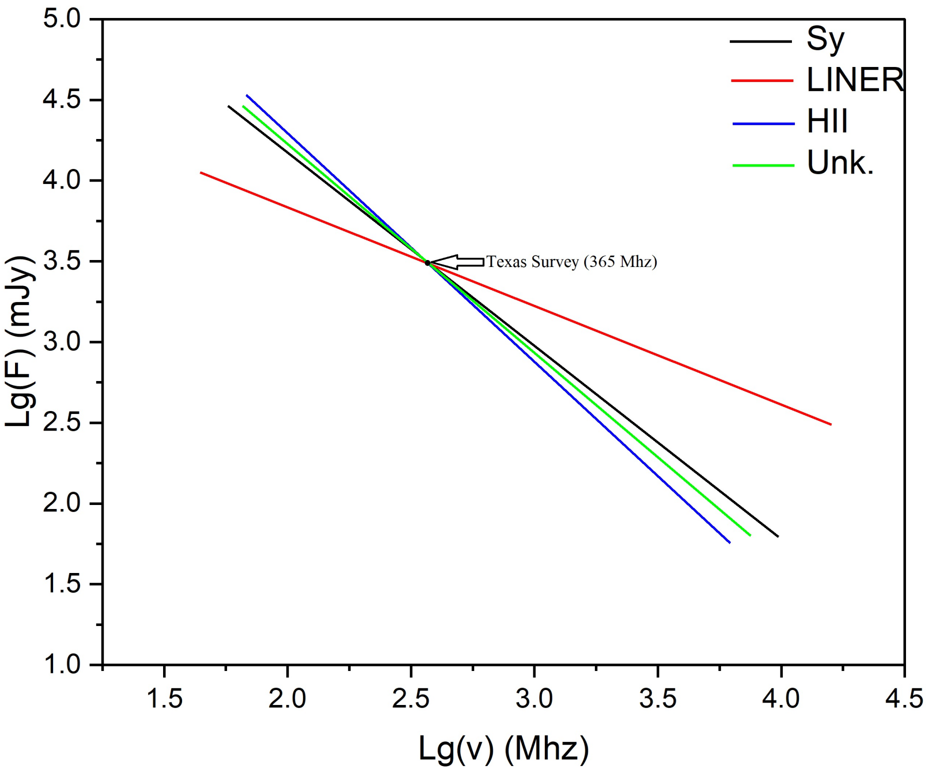

Figure 1. Average radio spectra for our object.

A number of authors have estimated radio spectral index for quasars and radio galaxies. In our work we have estimated radio spectral indices for 116 radio objects and compared our results with some authors (for example with Abrahamyan et al. (2014),Tiwari (2019), etc).

Using 116 spectra of our radio objects we have estimated radio spectral indices. For radio spectral index errors, in the first step we have counted each point's (radio flux) shift from fitting line in spectra. Having shift of each point we have estimated error in radio spectral index using Formula 1.

$$\sigma_{error} = \sqrt{\frac{\sum_{i=1}^{n} x_n^2}{n}} \tag{1}$$

where σ_{error} is the error of radio spectral index, x_n-shift of each point from fit (Figure 1), n – number of measurements.

Table 3 illustrates the average information of radio spectral indices.

Figure 2 shows graphical dependence of radio spectral index on redshift.

doi: doi.org/10.52526/25792776-2021.68.2-441

Table 3. Spectral indices for 116 radio sources

Activity type	**Average radio spectral index**	**Numbers of object**
Seyfert	-0.5442±0.0773	92
LINER	-0.3428±0.0489	12
HII	-0.5774±0.0824	1
Unknown	-0.5499±0.0785	11
All	**-0.5036±0.0717**	**116**

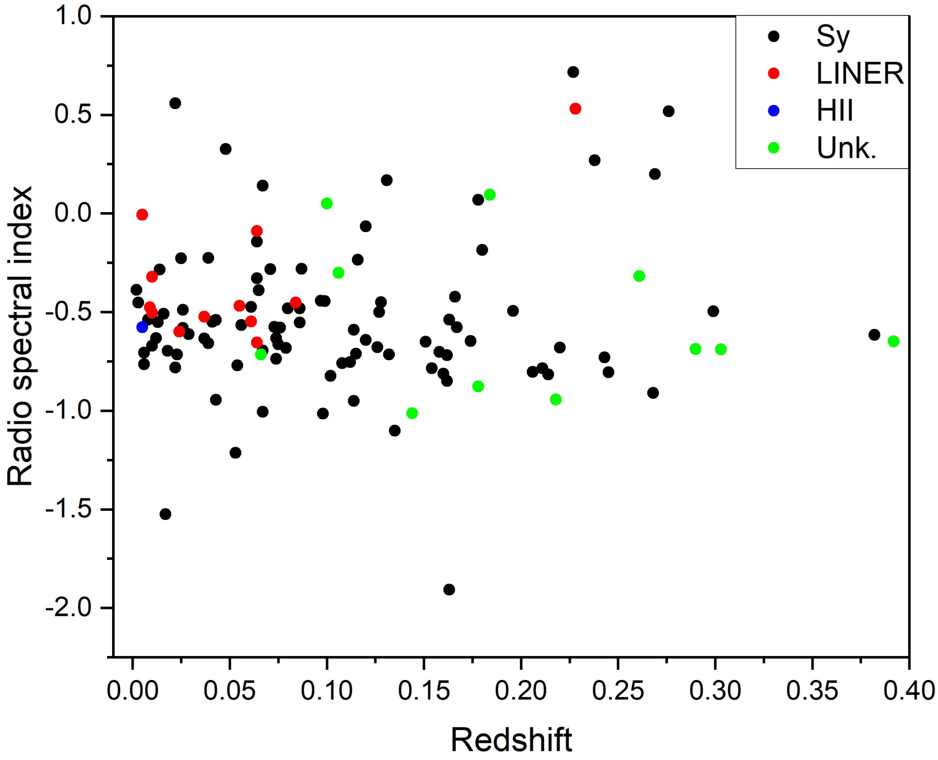

Figure 2. Radio spectral index vs. redshift.

4. Results

Presently, we wish to understand what radio properties active galaxies have. For that reason, we have created list of radio objects which have 12^m-19^m magnitudes and each object has 5 radio fluxes at different wavelengths. With this method we have distinguished 116 active galaxies. Using that we have estimated radio spectral indices for all the objects.

Similar work was carried out by Abrahamyan et al. (2014). Authors investigated 7C (Hales et al. (2007)) catalogues and separated 26 radio galaxies, as well as estimated radio spectral indices of those objects. We have compared our list to the list proposed by Abrahamyan et al. (2014). As a result, the objects have not been identified. In mentioned work, average radio spectral index for radio galaxies had α=-0.806, which is a little different from our present results. In this work radio objects have been selected by another method; errors are not estimated and they have redshifts up to z=3.

Laing & Bridle (2013) presented accurate, spatially resolved imaging of radio spectra at the bases of jets in eleven low-luminosity (Fanaroff–Riley I) radio galaxies, derived from Very Large Array (VLA) observations. Authors showed images and profiles of spectral index over the frequency range 1.4–8.5 GHz, together with values integrated over fiducial regions defined by relativistic models of the jets. The mean spectral indices given by the authors is 0.66±0.01. We have compared our result to those of Laing & Bridle (2013) and they appear to be similar.

So far, we have given some new results for properties of active galaxies:

- 79.3 % of our 116 active galaxies are Seyfert galaxies;
- We have built radio spectra and estimated radio spectral indices for 116 active galaxies ($\overline{\alpha}$=-0.5036±0.0717, $\overline{\alpha}_{Sy}$=-0.5442±0.0773, $\overline{\alpha}_{LINER}$=-0.3428±0.0489, $\overline{\alpha}_{HII}$=-0.5774±0.0824, $\overline{\alpha}_{Unk.}$=-0.5499±0.0785).

doi: doi.org/10.52526/25792776-2021.68.2-441

Acknowledgements

The work was supported by the Science Committee of RA, in the frames of the research project No. 21AG-1C053 “Revelation of the early stages of galaxy evolution by means of multiwavelength study of active galaxies”.

References

Abrahamyan H., 2020, Astronomische Nachrichten, 341, 703

Abrahamyan H. V., Andreasyan R. R., Hovhannisyan M. A., Paronyan G. M., 2014, Astrophysics, 57,3, 359

Abrahamyan H. V., Mickaelian A. M., Knyazyan A. V., 2015, Astronomy & Computing, 10, 99

Abrahamyan H. V., Mickaelian A. M., Paronyan G. M., Mikayelyan G. A., 2019, AN, 340,5, 437

Abrahamyan H. V., Mickaelian A. M., Paronyan G. M., Mikayelyan G. A., 2020, Astrophysics, submitted

Aghanim N., Akrami Y., Ashdown M., Aumont J., Baccigalupi C., et al. 2018, eprint arXiv:1807.06209, https://arxiv.org/abs/1807.06209

Aguado D. S., Ahumada R., Almeida A., Anderson S. F., et al. 2019, A&AS, 240,2, id.23

Biermann P., 1976, A&A, 53, 295

Blandford R. D., Königl A., 1979, ApJ, 232, 34

Condon J. J., 1992, ARA&A, 30, 575

Condon J. J., Cotton W. D., Greisen E. W., Yin Q. F., Perley R. A., et al. 1998, AJ, 115,5, 1693

Consortium D. M. L., Franzen T. M. O., Waldram E. M., Grainge K. J. B., et al. 2011, MNRAS, 415,3, 2708

Coppejans R., van Velzen S., Intema H. T., et al. 2017, MNRAS, 462,2, 2039

De Breuck C., Tang Y., de Bruyn A. G., Rottgering H., van Breugel W., 2002, A&A, 394, 59

De Young D. S., 1976, ARA&A, 14, 447

Douglas J. N., Bash F. N., Bozyan F. A., Torrence G. W., Wolfe C., 1996, AJ, 111, 1945

Edge D. O., Shakeshaft J. R., McAdam W. B., Baldwin J. E., Archer S., 1959, Memoirs of the Royal Astronomical Society, 68, 37

Gregory P. C., Condon J. J., 1991, AJS, 75, 1011

Gregory P. C., Scott W. K., Douglas K., Condon J. J., 1996, AJS, 103, 427

Hales S. E. G., Waldram E. M., Rees N., Warner P. J., 1995, MNRAS, 274,2, 447

Hales S. E. G., Riley J. M., Waldram E. M., Warner P. J., Baldwin J. E., 2007, MNRAS, 382,4, 1639

Hawkins M. R. S., 2002, MNRAS, 329, 1, 76

Heckman T. M., 1980, A&A, 87, 152

Helfand D. J., White R. L., Becker R. H., 2015, AJ, 501,1, id. 26

Intema H. T., Jagannathan P., Mooley K. P., Frail D. A., 2017, A&A, 598, id.A78

Khachikian E. E., Weedman D. W., 1971, Astrophysics, 7, 231

Khachikian E. E., Weedman D. W., 1974, ApJ, 192, 581

Laing R. A., Bridle A. H., 2013, MNRAS, 432, 1114

Laing R. A., Bridle A. H., 2014, MNRAS, 437, 3405

Lane W. M., Cotton W. D., van Velzen S., Clarke T. E., Kassim N. E., et al. 2014, MNRAS, 440,1, 327

Large M. I., Cram L. E., Burgess A. M., 1991, The Observatory, 111, 72

Massaro E., Maselli A., Leto C., Marchegiani P., Perri M., Giommi P., Piranomonte S., 2015, Astrophysics and Space Science, 357,1, id.75

Mauch T., Murphy T., Buttery H. J.and Curran J., Hunstead R. W., Piestrzynski B., Robertson J. G., Sadler E. M., 2003, MNRAS, 342,4, 117

McMahon R. G., McMahon R.G.and Irwin M. M., 2000, he APM-North Catalogue

Mickaelian A. M., Harutyunyan G. S., Sarkissian A., 2018, Astronomy Letters, 44, 6

Myers S. T., Jackson N. J., Browne I. W. A., de Bruyn A. G., et al. 2003, MNRAS, 341,1, 1

Pilkington J. D. H., Scott J. F., 1965, Memoirs of the Royal Astronomical Society, 69, 183

doi: doi.org/10.52526/25792776-2021.68.2-441

Reines A. E., Greene J. E., M. G., 2013, AJ, 755, 2

Riess A. G., Strolger L.-G., Tonry J., et al. 2004, ApJ, 607, 665

Seyfert C. K., 1943, AJ, 97, 28

Souchay J., Gattano C., Andrei A. H., Souami D., et al. 2019, A&A, 624, id.A145

Tiwari P., 2019, RAA, 19,7, 96

Ulrich M.-H., 1999, Contribution for the Encyclopedia of Astronomy and Astrophyisics, Oxford Institute of Physics and MacMillan

Véron-Cetty M. P., Véron P., 2010, A&A, A10, 518

Waldram E. M., Pooley G. G., Grainge K. J. B., Jones M. E., Saunders R. D. E., Scott P. F., Taylor A. C., 2003, MNRAS, 342,3, 915

Weedman D. W., 1977, Vistas in Astronomy, 21, 55

Zajaček M., Busch G., Valencia-S M., et al. 2019, A&A, A83, 630

Zhang X., Qing-Guo 2018, eprint arXiv:1812.01877, https://arxiv.org/abs/1812.01877

Zhang X., Zheng Y., Chen H., Wang S., Cao A., Peng B., Nan R., 1997, A&AS, 121, 59

de Bruyn G., Miley G., Rengelink R., Tang Y., et al. 1998, VizieR On-line Data Catalog: VIII/62. Originally published in: WENSS Collaboration NFRA/ASTRON and Leiden Observatory

de Gasperin F., Intema H. T., Frail D. A., 2017, MNRAS, 474,4, 5008

Composition of super-Earths, super-Mercuries, and their host stars

V. Adibekyan*[1, 2], N. C. Santos[1, 2], C. Dorn[3], S. G. Sousa[2], A. A. Hakobyan[4], B. Bitsch[5], Ch. Mordasini[6], S. C. C. Barros[1,2], E. Delgado Mena[1], O. D. S. Demangeon[1,2], J. P. Faria[1,2], P. Figueira[7,1], B. M. T. B. Soares[1,2], and G. Israelian[8,9]

[1]Instituto de Astrofísica e Ciências do Espaço, Universidade do Porto, CAUP, Rua das Estrelas, 4150-762 Porto, Portugal
[2]Departamento de Física e Astronomia, Faculdade de Ciências, Universidade do Porto, Rua do Campo Alegre, 4169-007 Porto, Portugal
[3]University of Zurich, Institut of Computational Sciences, Winterthurerstrasse 190, CH-8057, Zurich, Switzerland
[4]Center for Cosmology and Astrophysics, Alikhanian National Science Laboratory, 2 Alikhanian Brothers Str., 0036 Yerevan, Armenia
[5]Max-Planck-Institut für Astronomie, Königstuhl 17, 69117, Heidelberg, Germany
[6]Physikalisches Institut, University of Bern, Gesellschaftsstrasse 6, 3012, Bern, Switzerland
[7]European Southern Observatory, Alonso de Córdova 3107, Vitacura, Región Metropolitana, Chile
[8]Instituto de Astrofísica de Canarias, E-38205 La Laguna, Tenerife, Spain
[9]Departamento de Astrofisica, Universidad de La Laguna, E-38206 La Laguna, Tenerife, Spain

Abstract

Because of their common origin, it was assumed that the composition of planet building blocks should, to a first order, correlate with stellar atmospheric composition, especially for refractory elements. In fact, information on the relative abundance of refractory and major rock-forming elements such as Fe, Mg, Si has been commonly used to improve interior estimates for terrestrial planets. Recently Adibekyan et al. (2021) presented evidence of a tight chemical link between rocky planets and their host stars. In this study we add six recently discovered exoplanets to the sample of Adibekyan et al. and re-evaluate their findings in light of these new data. We confirm that i) iron-mass fraction of rocky exoplanets correlates (but not a 1:1 relationship) with the composition of their host stars, ii) on average the iron-mass fraction of planets is higher than that of the primordial $f_{\rm iron}^{\rm star}$, iii) super-Mercuries are formed in disks with high iron content. Based on these results we conclude that disk-chemistry and planet formation processes play an important role in the composition, formation, and evolution of super-Earths and super-Mercuries.

Keywords: *exoplanets, composition, stars*

1 Introduction

The study of only a few giant planets was enough to notice that presence of these planets correlates with stellar metallicity (Gonzalez, 1997, Santos et al., 2001). Since these pioneering works, different research groups tried to link the chemical composition of stars with the properties of planets (Adibekyan, 2019, Adibekyan et al., 2013, 2015a, Brewer et al., 2018, Delgado Mena et al., 2010, Hinkel et al., 2019, Suárez-Andrés et al., 2017, Teske et al., 2019, Unterborn et al., 2018).

With the increased precision of mass and radius measurements of planets, it become possible to characterize the interiors and bulk composition of low-mass exoplanets (Helled et al., 2021, Nettelmann & Valencia, 2021). Several attempts have been made in the last years trying to link the composition of low-mass planets and their host stars. However, these attempts were either based on single planetary systems (Lillo-Box et al., 2020, Mortier et al., 2020), on a small sample of planets (Plotnykov & Valencia, 2020, Santos et al., 2015, Schulze et al., 2021), or on a comparison of the overall properties of planets and overall properties of planet host stars in a population sense (Plotnykov & Valencia,

*vadibekyan@astro.up.pt, Corresponding author

doi: doi.org/10.52526/25792776-2021.68.2-447

2020). As a result, it was not possible to reach a firm conclusion either because of low-number statistics or because the results were not as informative (especially if the composition of the stars are not derived in a homogeneous way) as they would be if a direct star-planet comparison was performed.

On the contrary, Adibekyan et al. (2021, hereafter A21) adopted a different approach and looked for compositional relation between rocky exoplanets and their host stars. This approach overcomes the following potential issues:

- When performing a direct comparison of star-planet compositions for individual systems, large uncertainties in the compositions of planets and/or stars will naturally result in indistinguishable composition of the two.
- Because the uncertainties in planetary compositions are typically much larger than those in host star abundances (A21, Schulze et al., 2021), the necessity of exact chemical characterization of planet host stars can be overlooked (Schulze et al., 2021).
- Finally, it is impossible to make a general conclusion about the existence of a compositional link between stars and their planets by comparing the compositions of individual planet-star systems.

The main findings of A21 can be summarized as follows. The authors selected 22 low-mass exoplanets ($M < 10\ M_\oplus$) with precise mass and radius measurements (uncertainty both in mass and radius below 30%) orbiting around solar-type stars. For the sample planets they determined their normalized planet density ($\rho/\rho_{\rm Earth-like}$)[1] and the iron mass fraction ($f_{\rm iron}^{\rm planet}$) using the planet interior models of Dorn et al. (2017) and Agol et al. (2021). Based on the chemical abundances of the host stars and using the stoichiometric model from Santos et al. (2015, 2017) they also estimated the iron-to-silicate mass fraction ($f_{\rm iron}^{\rm star}$) of planetary building blocks. Based on these data the authors found: i) the normalized density and iron-mass fraction of exoplanets strongly correlate with the $f_{\rm iron}^{\rm star}$; ii) the relation between $f_{\rm iron}^{\rm planet}$ and $f_{\rm iron}^{\rm star}$ is not 1-to-1 (exoplanets have on average higher $f_{\rm iron}$ than what is expected from the host star composition), and iii) super-Earths (with $f_{\rm iron}^{\rm planet} \lesssim 50\%$) and super-Mercuries (with $f_{\rm iron}^{\rm planet} \gtrsim 60\%$) appear to be distinct populations in therm of compositions.

In this paper, we add six recently discovered exoplanets to the A21 sample and re-evaluate their claims and findings. The distribution of the exoplanets on a mass-radius diagram is shown in Fig. 1 where we single out the newly added planets.

2 Properties of planets and their host stars

To determine the properties of the new planets and their host stars we closely followed the work of A21. Below we provide a brief summary of the methods.

2.1 Exoplanet properties

We computed the bulk density (ρ) and the normalized density ($\rho/\rho_{\rm Earth-like}$) of the planets from their mass and radius and the Earth-like composition model of Dorn et al. (2017). From the mass and radius of planets we also estimated their expected iron fraction $f_{\rm iron}^{\rm planet}$, which is defined as $(M_{\rm Fe,mantle} + M_{\rm core})/M_{\rm pl}$, where $M_{\rm Fe,mantle}$ and $M_{\rm core}$ are the masses of iron in mantle and core, respectively. For the planet interiors, we assume a pure iron core and a silicate mantle; We neglected possible volatile atmospheric layers.

2.2 Host properties

We used publicly available high-resolution spectra for Kepler-37 (FIES, Telting et al., 2014), K2-36 (HARPS-N, Cosentino et al., 2012), K2-199 (HARPS-N, Cosentino et al., 2012), and HD 80653

[1]The normalization parameter $\rho_{\rm Earth-like}$, is the density of a planet with Earth-like composition (Dorn et al., 2017) for a given mass. The normalization is to take into account the dependence of planet density on planet mass for a given composition.

doi: doi.org/10.52526/25792776-2021.68.2-447

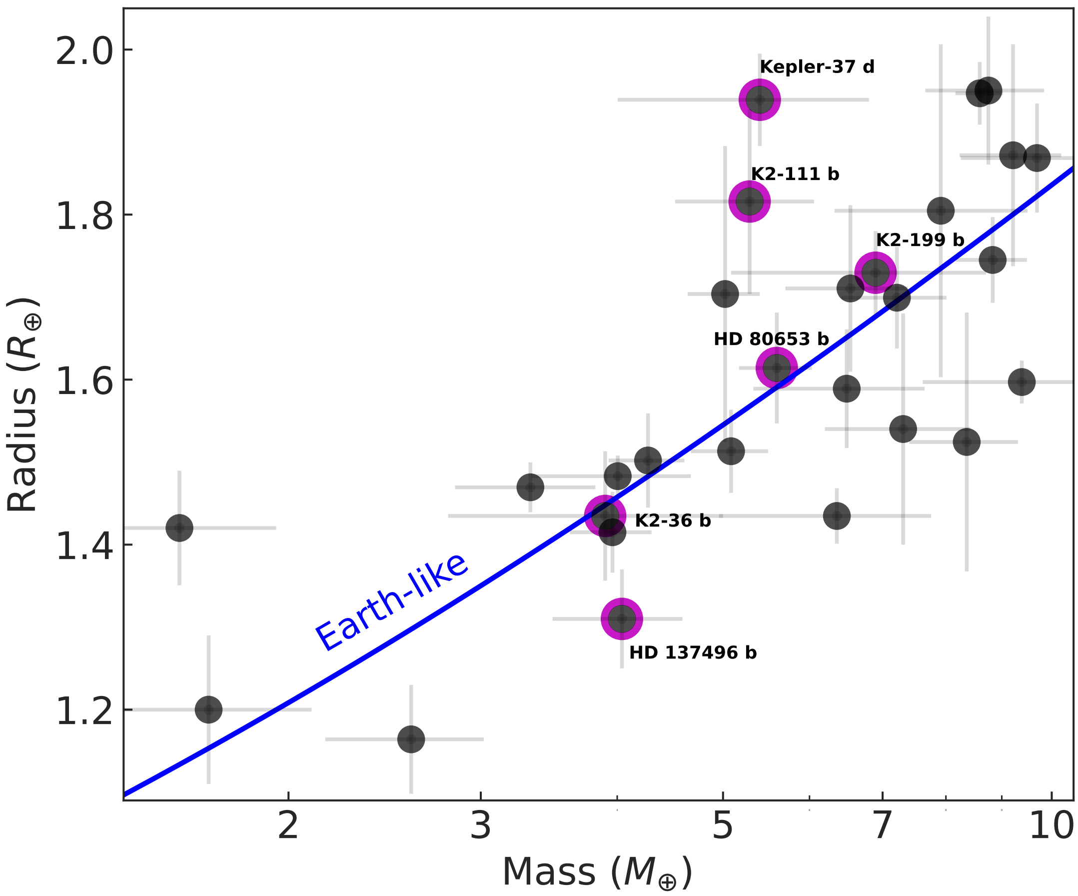

Figure 1: Mass-radius diagram for RV-detected planets with masses below 10 $M_\oplus$ and radii below 2 $R_\oplus$ for which the uncertainty both in mass and radius is below 30%. The blue curve shows the mass-radius relationship for Earth-like composition (32% Fe + 68% $MgSiO_3$) from Dorn et al. (2017). The six newly added planets are shown in black circles surrounded by a magenta ring. The names of these new planets are also displayed.

(UVES, Dekker et al., 2000) to determine the stellar parameters and abundances of Mg, Si and Fe. The stellar atmospheric parameters ($T_{\rm eff}$, $\log g$, microturbulence (Vmic), and [Fe/H]) of the stars have been determined following the methodology described in our previous works (Santos et al., 2013, Sousa, 2014). For the derivation of chemical abundances we closely followed the methods described in Adibekyan et al. (2012, 2015b). The stellar parameters and abundances of Mg, Si, and Fe of HD 137496 are taken from Silva et al. (2021) and for K2-111 are taken from Mortier et al. (2020)[2].

Based on the abundances of Mg, Si, and Fe, and using the stoichiometric models of Santos et al. (2015) we estimated the iron-to-silicate mass fraction ($f_{\rm iron}^{\rm star}$) of planetary building blocks under assumption that the stellar atmospheric composition reflects the composition of the proto-stellar (proto-planetary) disk where the star and the planets are formed.

3 Results

Fig. 2 shows the $\rho/\rho_{\rm Earth-like}$ as a function of $f_{\rm iron}^{\rm star}$. The figure reveals a clear correlation between these two quantities indicating that the final planetary density is a function of the composition of the planetary building blocks. We performed an orthogonal distance regression (ODR) and t-statistics to quantify the relation and to assess the significance of the relation. The test suggests that the observed correlation is statistically significant with a p-value of $\sim 3\text{x}10^{-6}$. For the same relation, the sample of A21 revealed a p-value of $\sim 7\text{x}10^{-6}$. The slopes of the relations obtained for A21 and the extended

[2]The adopted abundances are determined from the ESPRESSO spectrum.

doi: doi.org/10.52526/25792776-2021.68.2-447

samples agree withing one-sigma: 0.051±0.008 vs. 0.061±0.009.

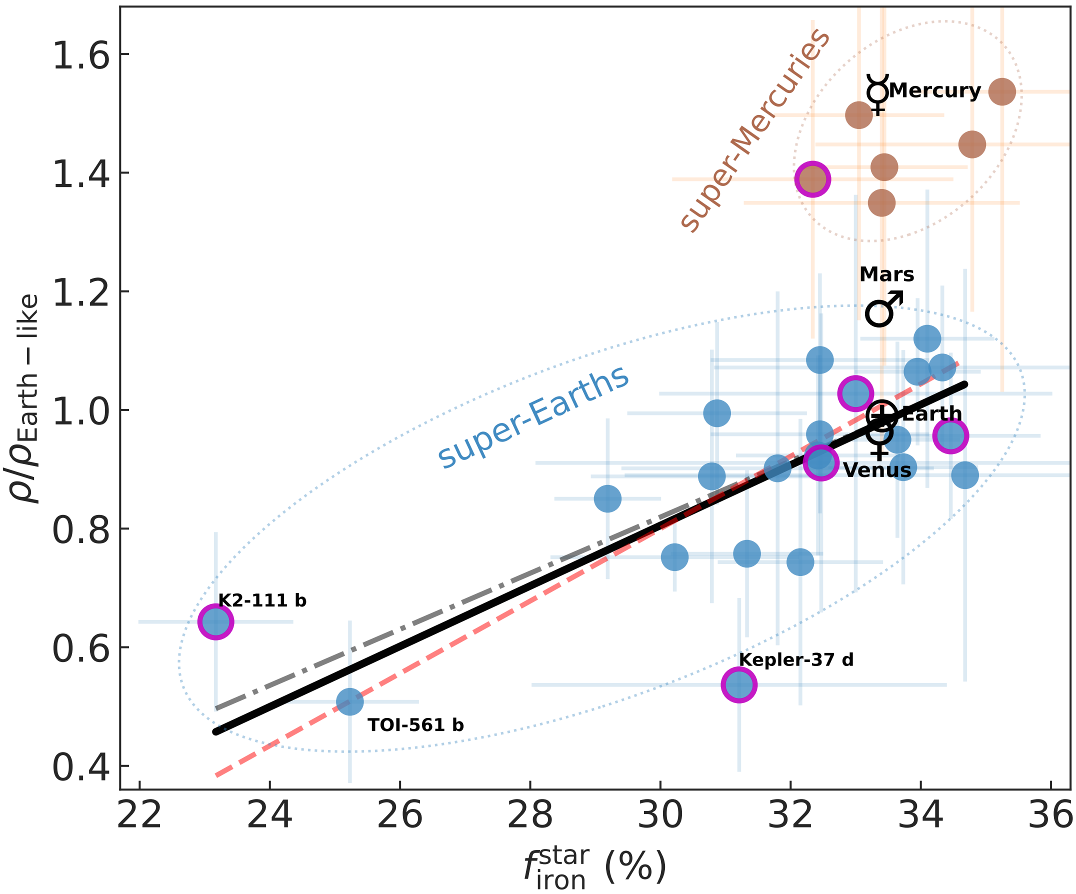

Figure 2: Normalized density of the planets as a function of iron mass fraction of planet building blocks estimated from the host star chemistry. The super-Earths and super-Mercures are shown in blue and brown colors. The positions of K2-111 b and TOI-561 b - planets orbiting around metal-poor stars - are indicated. The positions of the Solar System rocky planets are indicated with their respective symbols in black. The red dashed line represent the results of the ODR fit for the super-Earths of the sample of A21. The black solid and dotted-dashed lines show the ODR results for the super-Earths with and without considering Kepler-37 d, respectively. The Solar System planets are not considered in the linear regressions. All error bars show one standard deviation.

The largest deviation from the fit is observed for Kepler-37 d. Kepler-37 is orbited by three[3] transiting small planets. Kepler-37 d is the largest planet of the system, the mass of which was very recently determined by Rajpaul et al. (2021) using radial velocity (RV) observations. The authors obtained a RV based mass of 5.4±1.4 $M_\oplus$ and a dynamical mass of $\sim$ 4 $M_\oplus$. From the low density of the planet, Rajpaul et al. (2021) concluded that either Kepler-37 d is a water-world (> 25% H_2O) or has a gaseous envelope[4]. In either case, the planet is most probably not a rocky planet consisting of only metallic core and silicate mantle. The exclusion of Kepler-37 d from the ODR slightly reduces the value of the slope (0.047±0.007) and makes the significance of the relation slightly higher (p-value of $\sim$ 1x10^{-6}). The results of the ODR fit without considering Kepler-37 d is shown with a dotted-dashed line in Fig. 2.

We also study the relation between $f_{\mathrm{iron}}^{\mathrm{planet}}$ and $f_{\mathrm{iron}}^{\mathrm{star}}$ in Fig. 3. We performed an ODR and t-statistics to the super-Earths and found a p-value of $\sim$ 6x10^{-5}, which is even smaller than the p-value (1x10^{-4}) obtained for the A21 super-Earths sample. The slopes of the relations obtained for the A21 and the extended samples agree withing one-sigma: 0.36±0.9 vs. 4.3±0.8.

[3]The presence of a forth, non-transiting planet is unlikely (Rajpaul et al., 2021).

[4]Note, that the equilibrium temperature of Kepler-37 d is about 500K which is the coldest planet in the sample.

doi: doi.org/10.52526/25792776-2021.68.2-447

Two planets, 55 Cnc e and Kepler-37 b, show $f_{\rm iron}^{\rm planet}$ smaller than $f_{\rm iron}^{\rm star}$ of their host stars. We already discussed the possibility for Kepler-37 b to have a significant amount of volatiles or atmosphere. 55 Cnc multi-planetary system is one of the well studied ones (Bourrier et al., 2018). Several works suggested that 55 Cnc e may have volatile (e.g. Lopez, 2017) and/or hydrogen (e.g. Hammond & Pierrehumbert, 2017) layers which could explain the low density of the planet. In addition, it was proposed that 55 Cnc e can have Ca- and Al-rich interior without a significant iron core (Dorn et al., 2019).

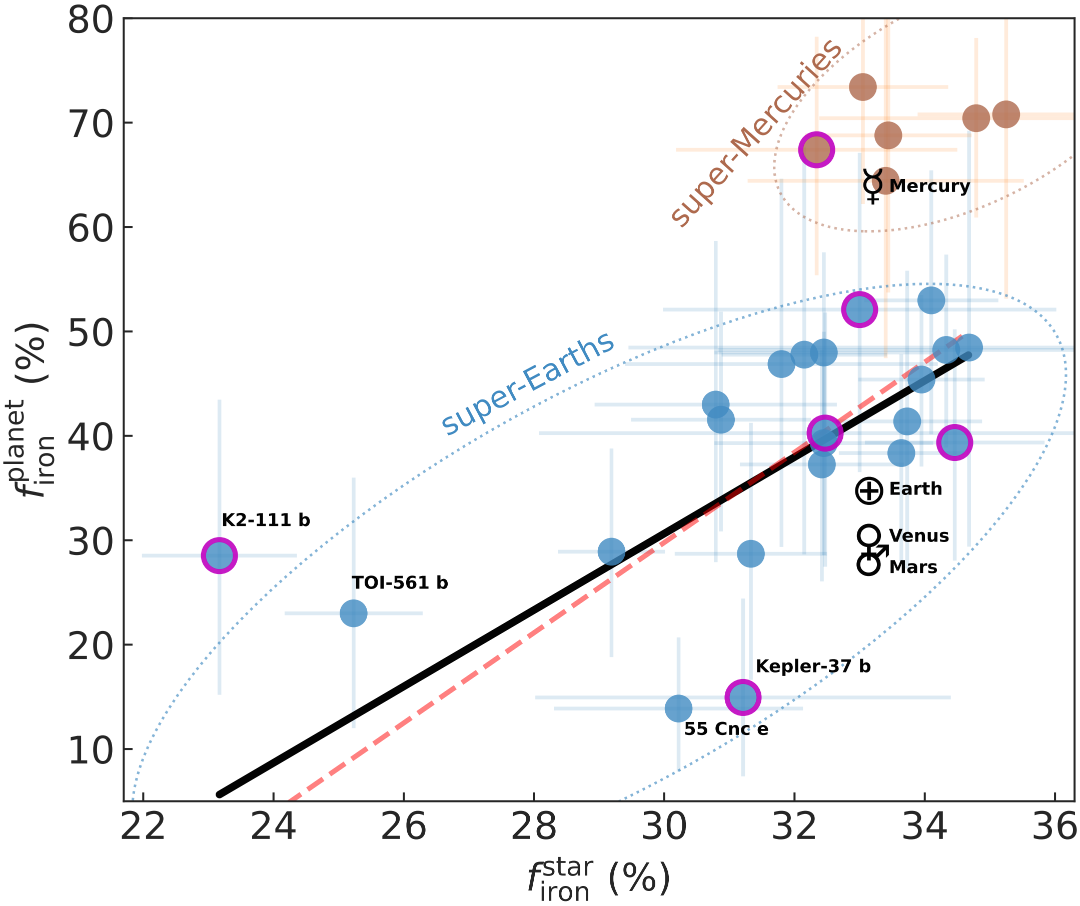

Figure 3: Iron mass fraction of planet building blocks ($f_{\rm iron}^{\rm star}$) versus iron mass fraction of the planets ($f_{\rm iron}^{\rm planet}$). The meaning of the symbols and lines are the same as in Fig. 2. The error bars of $f_{\rm iron}^{\rm star}$ show one standard deviation. The error bars of $f_{\rm iron}^{\rm planet}$ cover the interval between the 16th and the 84th percentiles.

.

4 Discussion

It is interesting to see that similarly to TOI-561 b, the newly added planet - K2-111 b, orbiting a metal-poor star, is also a low-density planet with low iron content. The low $f_{\rm iron}$ of rocky planets was proposed in Santos et al. (2017) where the authors studied the potential composition of planet building blocks around stars from different Galactic stellar populations. The stoichiometric model of Santos et al. (2015, 2017) also suggest a high water-mass-fraction for planets orbiting around metal-poor stars. It is thus possible that both TOI-561 b and K2-111 b have a non-negligible volatile layers, which we ignored in our analysis. In a subsequent paper, we plan to model the planet interiors considering also volatile layers and evaluate the presence of correlations between water-mass fraction of the planets and their host stars.

One of the newly added planets, HD 137496 b, is a super-Mercury. It is intriguing to see that this planet, just like the other five super-Mercuries of A21, has a high $f_{\rm iron}^{\rm star}$. A21 suggested that the

doi: doi.org/10.52526/25792776-2021.68.2-447

high iron content of super-Mercuries might be related to the protoplanetary disk composition, and not solely to a giant impact.

5 Summary

In this work we extended the sample of Adibekyan et al. (2021) by adding six recently discovered rocky exoplanets and studied the compositional link between rocky exoplanets and their host stars. The main results which confirm the recent findings of A21 are summarized below:

- The density ($\rho/\rho_{\mathrm{Earth-like}}$) of super-Earths correlates with the iron content ($f_{\mathrm{iron}}^{\mathrm{star}}$) of the protoplanetary disk.
- There is a non 1-to-1 relation between $f_{\mathrm{iron}}^{\mathrm{planet}}$ and $f_{\mathrm{iron}}^{\mathrm{star}}$. $f_{\mathrm{iron}}^{\mathrm{planet}}$ of super-Earths is larger than the iron content expected from the exoplanet host stars' composition.
- Super-Mercuries are formed in the disks with high $f_{\mathrm{iron}}^{\mathrm{star}}$ suggesting that protoplanetary disk composition might be important for the formation/evolution of these planets.

Studying the relationship between the compositions of planets and their host stars yields a wealth of information on the processes that occur during the formation and evolution of planets. As the number of newly discovered rocky exoplanets continues to increase, we will be able to better understand the origins of these compositional links.

Acknowledgements

This work was supported by FCT - Fundação para a Ciência e Tecnologia (FCT) through national funds and by FEDER through COMPETE2020 - Programa Operacional Competitividade e Internacionalização by these grants: UID/FIS/04434/2019; UIDB/04434/2020; UIDP/04434/2020; PTDC/FIS-AST/32113/2017 & POCI-01-0145-FEDER-032113; PTDC/FIS-AST/28953/2017 & POCI-01-0145-FEDER-028953. V.A., E.D.M, N.C.S., and S.G.S. also acknowledge the support from FCT through Investigador FCT contracts nr. IF/00650/2015/CP1273/CT0001, IF/00849/2015/CP1273/CT0003, IF/00169/2012/CP0150/CT0002, and IF/00028/2014/CP1215/CT0002, respectively, and POPH/FSE (EC) by FEDER funding through the program "Programa Operacional de Factores de Competitividade - COMPETE". V.A., E.D.M, N.C.S., and S.G.S. acknowledge support from FCT through Investigador FCT contracts nr. IF/00650/2015/CP1273/CT0001, IF/00849/2015/CP1273/CT0003, IF/00169/2012/CP0150/CT0002, and IF/00028/2014/CP1215/CT0002, respectively, and POPH/FSE (EC) by FEDER funding through the program "Programa Operacional de Factores de Competitividade - COMPETE". C.D. acknowledges support from the Swiss National Science Foundation under grant PZ00P2_174028, and the National Center for Competence in Research PlanetS supported by the SNSF. B.B., was supported by the European Research Council (ERC Starting Grant 757448-PAMDORA). O.D.S.D. and J.P.F. are supported by contracts (DL 57/2016/CP1364/CT0004 and DL57/2016/CP1364/CT0005, respectively) funded by FCT.

References

Adibekyan V., 2019, Geosciences, 9, 105

Adibekyan V. Z., Sousa S. G., Santos N. C., Delgado Mena E., González Hernández J. I., Israelian G., Mayor M., Khachatryan G., 2012, Astron. Astrophys. , 545, A32

Adibekyan V. Z., et al., 2013, Astron. Astrophys. , 560, A51

Adibekyan V., et al., 2015a, Astron. Astrophys. , 581, L2

Adibekyan V., et al., 2015b, Astron. Astrophys. , 583, A94

Adibekyan V., et al., 2021, Science, 374, 330

Agol E., et al., 2021, Planet. Sci. J., 2, 1

Bourrier V., et al., 2018, Astron. Astrophys. , 619, A1

Brewer J. M., Wang S., Fischer D. A., Foreman-Mackey D., 2018, Astrophys. J. Lett. , 867, L3

Cosentino R., et al., 2012, in McLean I. S., Ramsay S. K., Takami H., eds, Society of Photo-Optical Instrumentation Engineers (SPIE) Conference Series Vol. 8446, Ground-based and Airborne Instrumentation for Astronomy IV. p. 84461V, doi:10.1117/12.925738

Dekker H., D'Odorico S., Kaufer A., Delabre B., Kotzlowski H., 2000, in Iye M., Moorwood A. F., eds, Society of Photo-Optical Instrumentation Engineers (SPIE) Conference Series Vol. 4008, Optical and IR Telescope Instrumentation and Detectors. pp 534–545, doi:10.1117/12.395512

doi: doi.org/10.52526/25792776-2021.68.2-447

Delgado Mena E., Israelian G., González Hernández J. I., Bond J. C., Santos N. C., Udry S., Mayor M., 2010, Astrophys. J. , 725, 2349

Dorn C., Venturini J., Khan A., Heng K., Alibert Y., Helled R., Rivoldini A., Benz W., 2017, Astron. Astrophys. , 597, A37

Dorn C., Harrison J. H. D., Bonsor A., Hands T. O., 2019, Mon. Not. R. Astron. Soc. , 484, 712

Gonzalez G., 1997, Mon. Not. R. Astron. Soc. , 285, 403

Hammond M., Pierrehumbert R. T., 2017, Astrophys. J. , 849, 152

Helled R., et al., 2021, Experimental Astronomy,

Hinkel N. R., Unterborn C., Kane S. R., Somers G., Galvez R., 2019, Astrophys. J. , 880, 49

Lillo-Box J., et al., 2020, Astron. Astrophys. , 640, A48

Lopez E. D., 2017, Mon. Not. R. Astron. Soc. , 472, 245

Mortier A., et al., 2020, Mon. Not. R. Astron. Soc. ,

Nettelmann N., Valencia D., 2021, arXiv e-prints, p. arXiv:2111.09357

Plotnykov M., Valencia D., 2020, Mon. Not. R. Astron. Soc. ,

Rajpaul V. M., et al., 2021, Mon. Not. R. Astron. Soc. , 507, 1847

Santos N. C., Israelian G., Mayor M., 2001, Astron. Astrophys. , 373, 1019

Santos N. C., et al., 2013, Astron. Astrophys. , 556, A150

Santos N. C., et al., 2015, Astron. Astrophys. , 580, L13

Santos N. C., et al., 2017, Astron. Astrophys. , 608, A94

Schulze J. G., Wang J., Johnson J. A., Gaudi B. S., Unterborn C. T., Panero W. R., 2021, Planet. Sci. J., 2, 113

Silva T. A., et al., 2021, arXiv e-prints, p. arXiv:2111.08764

Sousa S. G., 2014, ARES + MOOG: A Practical Overview of an Equivalent Width (EW) Method to Derive Stellar Parameters. pp Springer International Publishing (Cham), Edited by Ewa Niemczura, Barry Smalley and Wojtek Pych, pp. 297–310, doi:10.1007/978-3-319-06956-2˙26

Suárez-Andrés L., Israelian G., González Hernández J. I., Adibekyan V. Z., Delgado Mena E., Santos N. C., Sousa S. G., 2017, Astron. Astrophys. , 599, A96

Telting J. H., et al., 2014, Astronomische Nachrichten, 335, 41

Teske J. K., Thorngren D., Fortney J. J., Hinkel N., Brewer J. M., 2019, Astron. J. , 158, 239

Unterborn C. T., Desch S. J., Hinkel N. R., Lorenzo A., 2018, Nature Astronomy, 2, 297

doi: doi.org/10.52526/25792776-2021.68.2-447

Communications of BAO, Vol. 68, Issue 2, 2021, pp. 454-463

On the origin of runaway binaries: the case of the HMXB 4U 2206+54/BD +53 2790

V. Hambaryan [*1,2], K. A. Stoyanov[†3], M. Mugrauer[‡1], R. Neuhäuser[§1], W. Stenglein[¶1], R. Bischoff[‖1], K.-U. Michel[**1], M. Geymeier[††1], A. Kurtenkov[‡‡3], and A. Kostov[§§3]

[1]Astrophysikalisches Institut und Universitäts-Sternwarte Jena, Schillergäßchen 2-3, 07745 Jena, Germany
[2]Byurakan Astrophysical Observatory, Byurakan 0213, Aragatzotn, Armenia
[3]Institute of Astronomy and National Astronomical Observatory, Bulgarian Academy of Sciences, Tsarigradsko Chaussee 72, BG-1784 Sofia, Bulgaria

Abstract

We present most probable place and time of the origin of the runaway high-mass X-ray binary 4U 2206+54 based on its *Gaia EDR3* astrometric parameters and our new systemic radial velocity. We studied the trace back motion of the system and propose that it originated in the subgroup of the Cepheus OB1 association (Age∼4-10 Myr) with its brightest star BD+53 2820 (B0V; $\mathcal{L}\sim 10^{4.7}\mathcal{L}_\odot$). The kinematic age of 4U 2206+54 is about 2.8 ± 0.4 Myr, it is at a distance of 3.1-3.3 kpc and has a space velocity of 75-100 km/s with respect to this member star (BD+53 2820) of the Cep OB1 association. This runaway velocity indicates that the progenitor of the neutron star hosted by 4U 2206+54 lost about 4-9 $\mathcal{M}_\odot$ during the supernova explosion and the latter one received a kick velocity of at least 200-350 km/s . The high-mass X-ray binary 4U 2206+54/BD+53 2790 was born as a member of a subgroup of the Cep OB1 association, the initially most massive star in the system terminated its evolution within $\lesssim 7-9$ Myr, corresponding to an initial mass $\gtrsim 32\ \mathcal{M}_\odot$.

Keywords: *astrometry, stars: individual: 4U 2206+54/BD +53 2790, Cep OB1, stars: HMXB, neutron, supernovae.*

1. Introduction

It is generally accepted that most stars are formed in compact groups in gravitationally bound clusters with space densities >1 $\mathcal{M}_\odot$ pc^{-3} (Lada & Lada (2003)) or in extended gravitationally unbound stellar associations with lower space densities <0.1 $\mathcal{M}_\odot$ pc^{-3} (Wright (2020)).

Star clusters form within giant molecular clouds and remain embedded in clouds for $\sim 2-5$ Myr before the combination of massive stellar winds and Supernovae drive out the gas. The stars that are left behind after the gas expulsion relax to the new potential and attempt to return to virial equilibrium (Baumgardt & Kroupa, 2007, Goodwin & Bastian, 2006).

Ward et al. (2020) argue that the formation of OB associations did not follow this scenario and show that they are formed in-situ as relatively large-scale and gravitationally-unbound structures. The OB-associations may contain multiple groups/cores of young stars, having characteristic population of

*Valeri.Hambaryan@uni-jena.de, Corresponding author
†kstoyanov@astro.bas.bg
‡markus@astro.uni-jena.de
§ralph.neuhaeuser@uni-jena.de
¶wolfgang.stengleinr@uni-jena.de
‖richard.bischoff@uni-jena.de
**kai-uwe.michel@uni-jena.de
††michael.geymeier@uni-jena.de
‡‡akurtenkov@astro.bas.bg
§§akostov@astro.bas.bg

doi: doi.org/10.52526/25792776-2021.68.2-454/

the massive, early spectral O-B type and also containing numerous low-mass stars. They exhibit some spatial and kinematic concentration of short-lived OB stars, a fact first realized by Ambartsumian (1947, 1955), which provided the first evidence that formation of single, double and multiple stars still ongoing in the Galaxy. Their dimensions can range from a few to a few hundred pc (for recent review see, e.g., Wright, 2020).

However, there is also a significant number (10–30%, see, e.g., Renzo et al., 2019, Stone, 1979) of young massive stars which are observed in the Galactic general field and called "Runaway stars", a term first introduced by Blaauw (1961). Runaway stars are thought to have formed in the stellar associations and have been ejected into the general Galactic field by two proposed mechanisms: dynamical ejection or binary supernova. The first mechanism, proposed by Ambartsumian (1954) in a Trapezium type (non-hierarchical) young multiple, dynamically non-stable systems, was further developed by Poveda et al. (1967). In contrary, the binary ejection mechanism was first proposed by Blaauw (1961) to explain the ejection of runaway O and B stars out of galactic plane. In this scenario the secondary star of a close binary becomes unbound when the primary explodes as a supernova (SN). Note, also, on the possibility of the so-called two-step-ejection scenario, i.e. massive binary ejection from star clusters and a second acceleration of a massive star during a subsequent supernova explosion (Dorigo Jones et al., 2020, Pflamm-Altenburg & Kroupa, 2010). In this case it will be very hard to identify the parent star clusters by traced back motion study of the binary system or single runaway star.

However, depending on separation and component masses prior to the explosion and the amount of asymmetry involved (i.e. the magnitude of the kick velocity imparted to the neutron star during the explosion), the binary will either get unbound (ejecting a single runaway star and neutron star) or it will remain bound (see, e.g., Tauris & Takens, 1998). In case of the latter, its center of gravity will be accelerated and one could expect to observe a binary system, either as a member of a stellar association or runaway close binary nearby to a parental stellar group, comprised by a neutron star and a normal star as High- or Low-Mass X-ray Binary (HMXB or LMXB, respectively), if the separation is sufficiently small for accretion to occur. Note that the magnitude of the kick velocity also depends on the evolutionary status of the pre-explosion close binary system (dynamical stability of mass transfer to the secondary, see, e.g., Hainich et al., 2020).

The proper motion of a runaway star or binary system often points exactly away from a stellar association, of which the star was formerly a member.

Note, also, on the possibility of the so-called two-step-ejection scenario, i.e. massive binary ejection from star clusters and a second acceleration of a massive star during a subsequent supernova explosion (Dorigo Jones et al., 2020, Pflamm-Altenburg & Kroupa, 2010). In this case it will be very hard to identify the parent star clusters by a traced back motion study of the binary system or single runaway star.

In this context, it is very interesting to identify the parent stellar group of HMXBs in the Galaxy (see, e.g., Ankay et al., 2001, van der Meij et al., 2021).

In this work, we concentrate on the kinematic study of the unique HMXB binary 4U 2206+54, which has been suspected to contain a neutron star accreting from the wind of its optical companion BD +53 2790. This optical counterpart was identified by Steiner et al. (1984) as the early-type star. Further analysis of many space and ground based observations showed that the system hosts a neutron star accreting from the wind of its companion, BD +53 2790 (see, e.g., Finger et al., 2010, Reig et al., 2009, Torrejón et al., 2018), which also exhibits a radial velocity modulation (Stoyanov et al., 2014, see further).

The neutron star in the system is probably a magnetar - a class of rare, strongly magnetized neutron stars. The strength of the surface characteristic magnetic field is estimated of the order of $B_S \sim 2 \times 10^{13} - 10^{14}$ G of this neutron star with the very slow spin period of – $P_{spin} \sim (5540 - 5570)$ s and the rapid spin-down rate of $\dot{P_{spin}} = 5.6 \times 10^{-7} ss^{-1}$ (Finger et al., 2010, Reig et al., 2009, Torrejón et al., 2018). Currently, the 4U 2206+54 is only known HMXB system hosting accreting magnetar with or without fallback disk (Alpar et al., 2013, Özsükan et al., 2014). The donor star does not meet the criteria for a classical Be V star, but rather is a peculiar O9 V star with higher than normal helium abundance (Blay et al., 2006) and the double peaked H_α emission line, as typical for the decretion disks (Hainich et al., 2020). The 4U 2206+54 with the orbital period of 9.5 days is one of the shortest

doi: doi.org/10.52526/25792776-2021.68.2-454/

orbital periods among known HMXBs.

2. The birth place of 4U 2206+54

In order to identify the possible birth place of 4U 2206+54 one needs to determine its possible membership to a stellar group either currently or in the past. The latter also requires to perform their trace back motion study in the Galaxy to test the concept: 4U 2206+54 and a stellar group or some of its members in the past were "in the same place at the same time".

It is obvious, that using as an input astrometric and kinematic parameters and their uncertainties of both one can get, in principle, only certain number of trajectories satisfying some of the criteria (e.g., minimum separation) of the close stellar passage. In each case, one clearly gets a probabilistic output (see, e.g., Hoogerwerf et al., 2000, 2001, Neuhäuser et al., 2020, Tetzlaff et al., 2010). Whether this number is expected from a real pair or by chance, i.e. occurred in the same volume of the space during some time interval in the past, needs further statistical analysis, given the above mentioned uncertainties of parameters (for details, see, Hambaryan et al., 2021, and further Sec. 2.1 and Fig. 3). Finally, further consistency checks must be performed as listed in Neuhäuser et al. (2020).

First, we have cross-matched the optical companion BD+53 2790 of the HMXB with possible candidate counterparts in *Gaia DR2 and EDR3* and identified it with the source 2005653524280214400 (see, also Arnason et al., 2021).

Table 1. The parameters of the optical companion BD +53 2790 of 4U 2206+543 and its probable birth counterparts — the member stars of Cep OB1 association (BD +53 2820 or HD 235673).

Name	*Gaia EDR3* Source ID	d** [pc]	ϖ [mas]	$\mu_\alpha cos\delta$ [mas/yr]	μ_δ [mas/yr]	RV*** [km/s]
BD +53 2790	2005653524280214400	$3167.4^{+165.3}_{-120.1}$	0.3051±0.0136	-4.173±0.015	-3.317±0.014	-62.7±8.8
BD +53 2820*	2005418950349782272	$3545.4^{+286.8}_{-225.5}$	0.2681±0.0169	-2.973±0.018	-3.350±0.016	15.8±32.3
HD 235673	1981443102866159232	$4201.6^{+827.1}_{-489.4}$	0.2240±0.0292	-3.828±0.030	-3.390±0.026	-40.0±10.0

* Radial velocity of BD +53 2820 is variable, may be double–lined spectroscopic binary (Abt & Bautz, 1963).
** Distance estimates are provided by Bailer-Jones et al. (2021) using parallaxes and additionally the G magnitudes.
*** Radial velocities and their standard deviations are given according to the SIMBAD astronomical database (Wenger et al., 2000) and corresponding bibliographic entries (Abt & Bautz, 1963, Wilson, 1953).

Next, we performed a preliminary selection of the possible birth place (i.e. a stellar group) of HMXB 4U 2206+54, according to its position and distance, as well as, upper limits of the age and runaway velocity (e.g., $\sim$ 10-20 Myr and $\sim$ 100-150 km/s corresponding to the distance of $\sim$ 1-2 kpc), from the recent catalogues of members of stellar associations (Melnik & Dambis, 2020) and open clusters (Cantat-Gaudin et al., 2020).

The selection criteria are as follows: Galatic longitude between 80° and 120°, latitude between -10° and 10° and distance between 1500 pc and 5000 pc. With this first step of selection the list consists of 143 stellar clusters and 11 associations. Taking into account the direction of relative motion of BD+53 2790 to these stellar groups (3D or proper motion) and the most probable upper limit of its age (see, e.g., Ekström et al., 2012, Meynet & Maeder, 2003, Spectral type O9.5V, $\mathcal{M}\sim\gtrsim 15.5\ \mathcal{M}_\odot$) the reduced list includes 62 open clusters and only one stellar association (see, Fig. 1) which can be considered as the probable place of the origin of the HMXB 4U 2206+54.

For these birth place counterparts, we estimated the membership probability/likelihood of BD+53 2790 by comparison with the bona fide members of stellar groups given the astrometric and kinematic parameters and their uncertainties by *Gaia EDR3*. For this purpose we used (for details, see, Hambaryan et al., 2021) a multivariate Gaussian distribution in the five dimensional space (position, parallax and proper motions)*.

*Unfortunately, the overwhelming majority, in average $\gtrsim$ 98% (Cantat-Gaudin et al., 2020), of bona fide members

doi: doi.org/10.52526/25792776-2021.68.2-454/

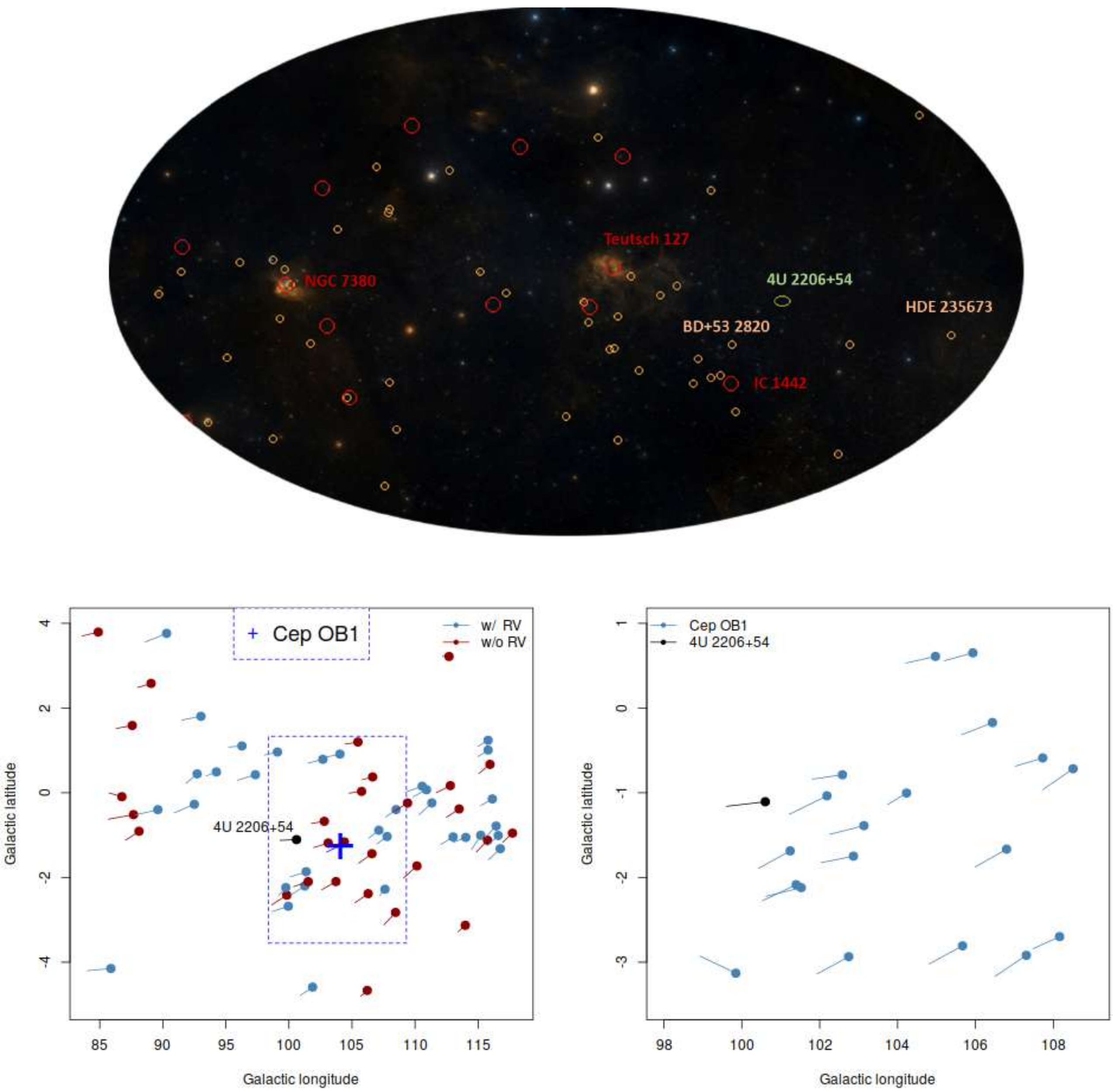

Figure 1. *Top panel:* Digitized (DSS2) color image of the region of the HMXB 4U 2206+54 (green oval) in the galactic coordinates, prepared with Aladin Desktop (Bonnarel et al., 2000). The positions of stellar clusters (large red circles, Cantat-Gaudin et al., 2020) and the Cep OB1 association member stars (brown circles, Melnik & Dambis, 2020) are also indicated. Most relevant objects for this study are annotated (for details, see text). *Bottom panel:* Galactic positions and proper motions of stellar clusters with the Cep OB1 in the center (left panel); the Cep OB1 association members are shown in the right panel, they can be considered as most probable birth counterparts of 4U 2206+54/BD+53 2790.

doi: doi.org/10.52526/25792776-2021.68.2-454/

It turned out, that BD+53 2790 has a very low probability to be considered as a member one of them. The logarithm of the ratio of the mean likelihoods of BD+53 2790 in comparison to the members of a stellar group is in the range of -11 to -183. Note that for the case of the Cep OB1 stellar association (the single one in the list) the logarithm of likelihood ratio is equal to -61.2.

Hence, we need to study trace back motions of this HMXB and its above mentioned probable counterparts of the place of origin, i.e. whether 4U 2206+54/BD+53 2790 and a stellar group or one of its member were in the same place at the same time in the past. In order to study the Galactocentric motion of the HMXB 4U 2206+54 for an input we used the astrometric parameters of the optical counterpart BD+53 2790 of the system presented in *Gaia EDR3*, as well as its systemic radial velocity. For the latter one, we performed additional spectral observations (Échelle spectrograph FLECHAS at the 90 cm telescope of the University Observatory Jena, Hambaryan et al., 2021, Mugrauer et al., 2014) and analyzed the combined radial velocity data set (Abt & Bautz, 1963, Stoyanov et al., 2014).

The fitted systemic velocity $\gamma = -61.5 \pm 1.55$ km/s together with other astrometric parameters presented in *Gaia EDR3* intended to serve as an input to retrace its orbits back in time to investigate the probable birth place and kinematic age of HMXB 4U 2206+54. However, to be conservative, for the study of trace back motion of HMXB 4U 2206+54 for the input parameter systemic radial velocity we used a relatively large interval, i.e. the randomly generated V_{sys} values were drawn from Gaussian distribution with the mean value equal to the fitted systemic velocity $V_{sys} \equiv \gamma = -61.5$ km/s with standard deviation of $SD_{V sys} = 15.0$ km/s .

2.1. Motion of 4U 2206+54 in the Galaxy

To study the Galactocentric motion of a single point mass (a star, binary or cluster) we use a numerical integration of its equations of motion in the gravitational field of the Galaxy expressed in a rectangular Galactocentric frame. Namely, for the Galactocentric motion of 4U 2206+54/BD+53 2790, the possible parental stellar cluster and association we make use of the code described in Neuhäuser et al. (2020), which computes the orbits by a numerical integration of their equations of motion as defined by the Galactic gravitational potential consisting of a three component (bulge, disk and halo) axisymmetric model (Model III from Bajkova & Bobylev, 2017). In addition, the Galactic gravitational potential is supplemented with the more realistic, non-axisymmetric and time dependent terms, which take into account the influence of the central bar and the spiral density wave (Bajkova & Bobylev, 2019, Fernández et al., 2008, Palous et al., 1993).

In order to take account of the uncertainties in the astrometric parameters of the star and stellar group, each one was replaced by a large number of clones, each with astrometric parameters drawn from a multivariate normal distribution. This is done by making use of the covariance matrix of the astrometric parameters from *Gaia EDR3* for the star and from a stellar cluster/association centroid parameters (Cantat-Gaudin et al., 2020, Melnik & Dambis, 2020, Soubiran et al., 2018) or the astrometric parameters of the individual member star (Gaia Collaboration, 2020, Gaia Collaboration et al., 2018). Such a procedure is superior to the individual, independent random drawing of each parameter that ignores their mutual dependence and result in to the more realistic probability distribution functions of the separation between 4U 2206+54 and the centre of stellar group or any member star (see, e.g., Fig. 3 and Sec. 2.2). For numerical integration we utilise the fast and accurate Gauss-Everhart orbit integrator provided by Avdyushev (2010).

Based on the *Hipparcos* proper motion of the HMXB HD153919/4U1700-37 Ankay et al. (2001) propose that it originates in the OB association Sco OB1 within $\lesssim$6 Myr (kinematic age being $\tau = 2.0 \pm 0.5$ Myr). We applied our approach to this system based on the more precise *Gaia EDR3* data and confirmed that both the place of origin in Sco OB1 and the kinematic age of HMXB HD153919/4U1700-37 ($\tau = 2.33 \pm 0.05$ Myr).

2.2. Results

Our trace back motion study of 4U 2206+54 and its possible parental stellar groups (see, Sec. 2) revealed that only the association Cep OB1 can be considered as a candidate. The astrometric and

of the stellar groups have no significant number of radial velocity measurements.

doi: doi.org/10.52526/25792776-2021.68.2-454/

kinematic parameters of its centroid was determined by member stars (Melnik & Dambis, 2020) present in the *Gaia EDR3* catalogue. Note, that the used distances of member stars and their uncertainties are provided by Bailer-Jones et al. (2021) using parallaxes and additionally the G magnitudes. It turned out that the trace back times of the pair (i.e. the HMXB 4U 2206+54 within the association Cep OB1, $\sim$ 150 pc) are distributed almost uniformly over a range from 1.3 Myr to 15 Myr. Given the fact that Cep OB1 association has a relatively large size (with a distance $\sim$ 2.7-3.5 kpc and several degrees on the sky), and that it is very elongated in the direction of the Galactic longitude (see Fig. 1), suggesting that it may include a chain of OB associations (Melnik & Dambis, 2020) or cores of different ages (see, Sec. 3), we performed also a trace back motion study of 4U 2206+54 and each member star to identify the most probable common birth place inside of the Cep OB1 association. Note that from 58 member stars (Melnik & Dambis, 2020) of Cep OB1 46 have an entry in *Gaia EDR3* and only 23 have also radial velocity measurements. It turned out that only 2 member stars, HD 235673 and BD+53 2820, with spectral types of O6.5V and B0V, respectively, show a significant number of close passages with BD+53 2790. Namely, from 1 million Monte-Carlo simulations 1234 (0.12%) and 52936 (5.3%) rated as success, i.e. the minimum separation does not exceed 15 pc within 20 Myr in the past, accordingly.

Moreover, the distributions of the trace back times of these “small” fractions of successful cases are unimodal (see, e.g., Fig.3) and a significant amount of them, namely 692 ($\sim$56%) and 36929 ($\sim$70%), is concentrated within relatively narrow time intervals δt=2.8 (12.4-15.2) Myr and δt=0.8 (2.4-3.2) Myr in the past, respectively.

In order to compare the obtained numbers of successful cases with the expected numbers of cases when our HMXB and a Cep OB1 member star (4U 2206+54–BD+53 2820 or 4U 2206+54–HD 235673) in reality were at the same place at the same time, we created virtual pairs inside the Cep OB1 association at the positions corresponding to BD+53 2820 and HD 235673. We ran them forward with the kinematic properties (proper motions and RVs, see Table 1) of flight times from 2.4 to 3.2 Myr and from 12.4 to 15.2 Myr in steps of 0.05 Myr. For each of the times in the interval, we traced back the pair starting from their virtual positions and using the kinematic properties (proper motions and RVs) – and varying them within their measurement uncertainties (i.e. according to the covariance matrices provided in *Gaia EDR3*, including as well corresponding parallax/distance errors) for 1 million trials each. For each such trial, we then obtained as usual the minimum distance between pairs. This procedure thus yields the number of expected close approaches (within e.g. 15 pc) for the above mentioned time intervals. As a result, with 95% confidence interval under the assumption of binomial distribution, we obtained (and, thus, expect at least) close meetings within 15 pc in 2.3 (2.0-2.7)% and 0.29 (0.21-0.33)% cases from of 1 million runs corresponding to the pairs 4U 2206+54–BD+53 2820 and 4U 2206+54–HD 235673, accordingly. Shortly, these fractions can be considered as lower thresholds in favour of the hypothesis that a pair of HMXB and member star of the Cep OB1 were at the same place during the above mentioned time intervals.

Also, we simulated a large number of random ”HMXB”s with mean astrometric and kinematic parameters and their covariance matrices of neighboring stars of 4U 2206+54/BD+53 2790 within 10 arcmin extracted from *Gaia EDR3* and calculated traced back orbits and compared them with the real trajectories of BD+53 2820 and HD 235673. It turned out that for such a “random” 4U 2206+54 in one million trials only 8 and 2 cases are successful ones (i.e. separation not exceeding 15 pc) with BD+53 2820 and HD 235673 in the trace back time range of 2.4-3.2 Myr and 12.4-15.2 Myr, respectively, i.e. with 95% confidence interval under the assumption of binomial distribution, we expect close meetings within 15 pc in 0.0008 (0.0003-0.001)% and 0.0002 (0.00002-0.0007)% successful cases even with this conservative randomization.

Thus, statistically the vicinity of both member stars (BD+53 2820 and HD 235673) of the Cep OB1 association in the past can be considered as probable place of the origin of the HMXB 4U 2206+54, thus indicating the probable coeval formation of the progenitor binary system and one of these stars. Note, that the case of BD+53 2820 can be considered as more probable one than the one of HD 235673 (see, further Sec. 3).

In Figure 2, the past 3D trajectories are displayed for the member star BD+53 2820 of Cep OB1 and for BD+53 2790 itself. The analysis of separations and corresponding times (see, Fig. 3) shows

doi: doi.org/10.52526/25792776-2021.68.2-454/

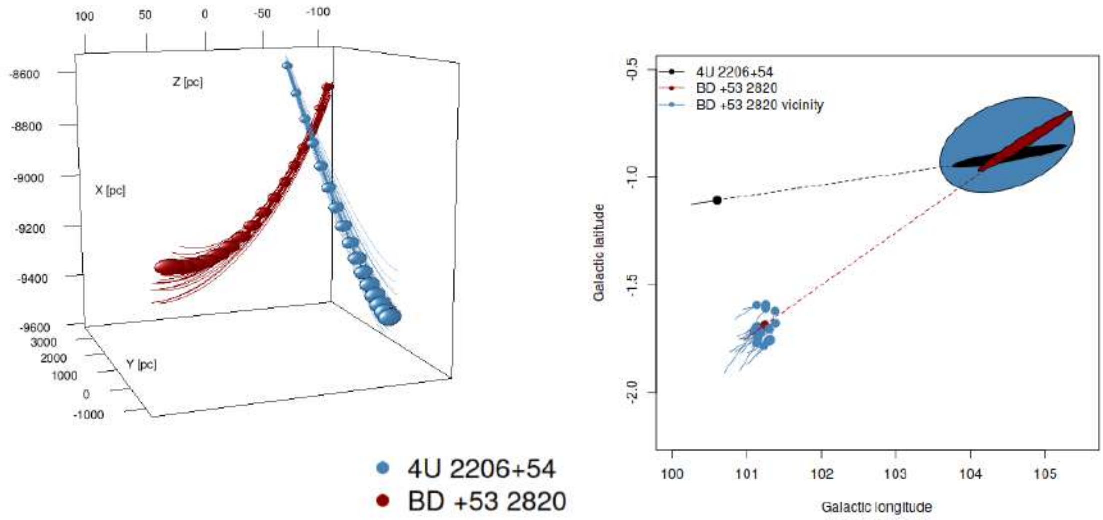

Figure 2. *Left panel:* The 3D trajectories of 4U 2206+54/BD+53 2790 and BD +53 2820 ≡ Gaia EDR3 2005418950349782272, a member of the Cep OB1 association, in Galactocentric Cartesian coordinates in the past. *Right panel:* The positions and proper motions of 4U 2206+54/BD+53 2790 and subgroup of stars in the Cep OB1 association with its brightest star BD +53 2820 in Galactic coordinates. With filled colors of ellipses are indicated the most probable positions of corresponding stars at 2.4-3.2 Myr ago.

that BD+53 2790 and BD+53 2820 in reality were both inside of the same volume (sphere with radius of $\sim$ 15pc) $\tau = 2.8 \pm 0.4$ Myr ago. We observe a similar picture for the neighboring stars of BD+53 2820 in the projection on the sky, i.e. purely using position, distance and proper motions of them (see, Fig. 2, left panel).

Figure 3 shows the distribution of the minimum separations, $D_{\min}(\tau_0)$, and the kinematic ages, τ_0, of the 52 936 simulations mentioned above.

In addition, we studied also the trace back motion of the pair (4U 2206+54–BD+53 2820) with number of input systemic radial velocities corresponding to the observed mean radial velocity values and standard deviations with different instruments Note that these parameters serving for an input to generate random systemic velocity are independent of the fitting results and cover a relatively large interval (see, e.g. Table 4 Hambaryan et al., 2021). It turned out that all of these cases confirmed our previous result, i.e. very similar kinematic age of the 4U 2206 and statistically significant success rate (Hambaryan et al., 2021).

3. Discussion

Based on the parameters of BD+53 2790 provided by *Gaia EDR3*, we calculated its absolute magnitude $M_V = -4.44 \pm 0.70$ mag (V = 9.84±0.2 mag, B = 10.11±0.19 mag, d = 3135.8±91.7 pc, Av = 1.8±0.70 mag, Reig & Fabregat, 2015) at first. Taking into account the bolometric correction (BC = -3.2 mag, see, e.g., Pecaut & Mamajek, 2013) for an O9.5V spectral type star we estimated the mass to be $\mathcal{M}= 23.5^{+14.5}_{-8.0}\mathcal{M}_{\odot}$using the luminosity-mass relation for main-sequence stars selected from the components of detached eclipsing spectroscopic binaries in the solar neighborhood (Eker et al., 2018, $\log \mathcal{L} = (2.726 \pm 0.203) \times \log \mathcal{M} + (1.237 \pm 0.228)$). With this initial mass there may be an upper limit for its lifetime in the range of 10-12 Myr according to non-rotating and rotating stellar evolution models (Ekström et al., 2012, Meynet & Maeder, 2003, Weidner & Vink, 2010). Hence, the primary of the progenitor of 4U 2206+54 may have an upper lifetime limit of 7-9 Myr.

Already Humphreys (1978) lists 11 O-stars within the large Cep OB1 association, which is located

doi: doi.org/10.52526/25792776-2021.68.2-454/

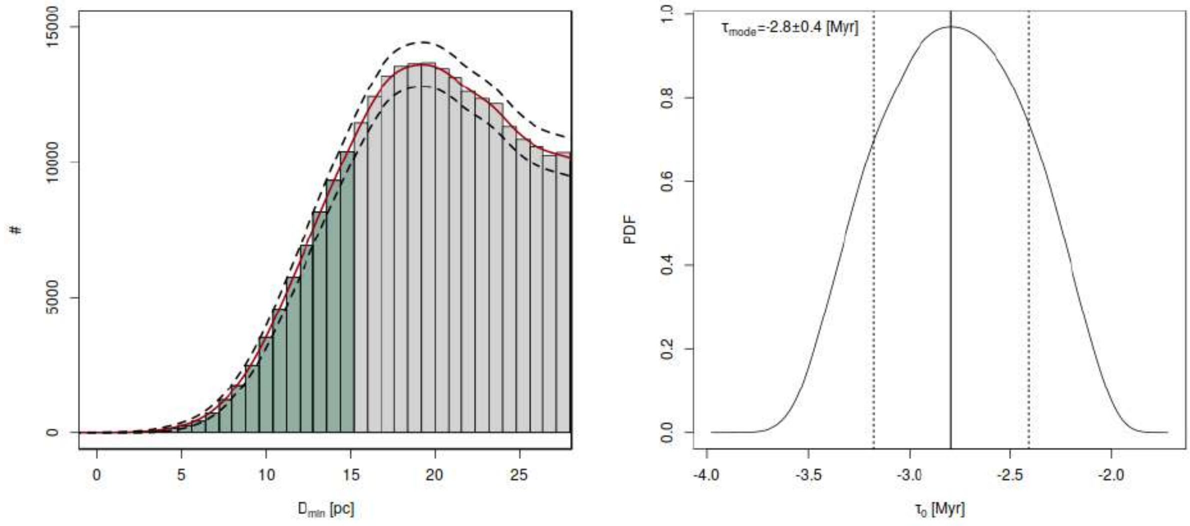

Figure 3. Distributions of minimum separations (D_{min}) and corresponding flight times (τ_0) of closest stellar passage of 4U 2206+53 and BD+53 2820 ($\leq$ 15 pc separation, rated as success, marked as filled green area) according to the trace back motion study of them in the Galaxy. The red curve with enveloping dashed curves show the fit of expected distribution of minimum separations for the 3D case (Eq. A3 in Appendix, Hoogerwerf et al., 2001). The highest posterior density (HPD) interval, 68% of area, is determined as a probabilistic region around a posterior mode of kinematic age of 4U 2206+53 and depicted as vertical dashed-lines (for details, see in the text).

at a distance of 3470 pc. According to Massey et al. (1995) the stellar association Cep OB1/NGC 7380 containing the highest mass stars has formed over a short time span, no longer than 4-6 Myr. Despite the fact that most of the massive stars are born during a period of $\Delta\tau$ <3 Myr in this association, some star formation has clearly preceded this event, as evidenced by the presence of evolved ($\tau \sim 10$ Myr) 15 $\mathcal{M}_{\odot}$ stars (Massey et al., 1995). Most recently Melnik & Dambis (2020) studied the motions inside 28 OB associations with the use of Gaia DR2 proper motions and lists 58 member stars of the Cep OB1 association having luminosity classes in the range of I to V, with spectral types of O6.5-M4. On the other hand, Kharchenko et al. (2005a,b) identifies 3 ionising star clusters related to the Cep OB1 association: NGC 7380, IC 1442, and MWSC 3632. Moreover, according to the most recent catalogues of stellar groups (Cantat-Gaudin et al., 2020, Soubiran et al., 2018) in the region of the Cep OB1 there are more groups in the age range of 4-10 Myr (see, Fig. 1).

The estimated ages of the Cep OB1 and 4U 2206+54 already are excluding HD 235673 as a birth counterpart owing to the longer flight time ($\tau = 13.2^{+2.0}_{-0.8}$ Myr, Sec. 2.2). Moreover, if this O6.5V spectral type star and the progenitor of 4U 2206+54 were born together then for the primary mass we would expect at least 40 $\mathcal{M}_{\odot}$and maximum lifetime of 4-10 Myr, much shorter than the flight time of 4U 2206+54 and HD 235673 to the hypothetical place of the common origin.

Thus, $\tau = 2.8 \pm 0.4$ Myr can be considered as the most probable kinematic age of 4U 2206+54, which suggests a coeval formation of the progenitor binary system of that HMXB and a subgroup of stars from the Cep OB1 association with its brightest member BD+53 2820.

Having estimates of the age range of the Cep OB1, the conservative lifetime of the donor star of the HMXB BD+53 2790 and the flight time to the probable birth place, we estimated the upper limit of the lifetime and hence, the initial mass of the primary before the SN for all models provided by Ekström et al. (2012), Meynet & Maeder (2003) to be $\mathcal{M}_{initial} \sim$ 32-60 $\mathcal{M}_{\odot}$.

It is difficult to reconstruct the evolution of the massive binary before the SN explosion. Nevertheless, with our results for the kinematic age and the orbital parameters of 4U 2206+54 we may put some constraints on it (Hambaryan et al., 2021, Hurley et al., 2002, Nelemans et al., 1999, Postnov & Yungelson, 2014, Tauris & Takens, 1998, van den Heuvel et al., 2000).

doi: doi.org/10.52526/25792776-2021.68.2-454/

Our analysis of motion shows that 4U 2206+54 originates in the OB association Cep OB1, from which it escaped about 2.8±0.4 Myr ago due to the SN of 4U 2206+54's progenitor. Using parameters of calculated 36 929 traced back orbits for the relative space velocity one obtains $\vartheta \equiv \mathrm{V_{relative}} = 92.6^{+14.6}_{-16.2}$ km/s with respect to BD+53 2820 or its vicinity stars and hence, the mass of the ejected material during the SN event $\Delta\mathcal{M} = 5.6^{+3.6}_{-2.2}\ \mathcal{M}_{\odot}$ for the neutron star of mass $\mathcal{M}_2 = 1.4\ \mathcal{M}_{\odot}$. Note, that the estimate of $\Delta\mathcal{M}$ is not changing significantly depending on the mass of a neutron star (1.2-2.2 $\mathcal{M}_{\odot}$). Thus, at the moment of the SN instantaneous explosion the collapsing core would have a mass of $7.0^{+4.2}_{-2.6}\ \mathcal{M}_{\odot}$, which explodes as a SN, becomes a neutron star or black hole, and receives a velocity kick, due to any asymmetry in the explosion. Evidence for such a kick for non-disrupted systems are large eccentricities of X-ray binary systems (see, e.g., Kaspi et al., 1996) or observed velocities of radio pulsars (Lyne & Lorimer, 1994). Clearly, the state of the binary after the SN depends on the orbital parameters at the moment of explosion and the kick velocity. For the case of 4U 2206+54 we estimated the required minimum kick velocity of a typical neutron star (Eq. A14 in Appendix, Hurley et al., 2002) $\sim$ 200–350 km/s for the simple case, i.e. imparted in the orbital plane and in the direction of motion of the pre-SN star, for parameters of the mass range of BD+53 2790, mass of the ejected material $\Delta\mathcal{M}$, orbital velocity (465-530 km/s) of the binary at the moment of explosion and post–SN runaway systemic velocity ($\mathrm{V_{relative}}$) of 4U 2206+54. Note that the above estimated kick velocity of a neutron star is compatible with kick velocities expected from a unimodal or bimodal Maxwellian distribution of pulsars (see, e.g., Hobbs et al., 2005, Igoshev, 2020).

On the other hand, the evolution of massive close binaries is driven by case B mass transfer (van den Heuvel et al., 2000). In this case, the mass transfer starts after the primary star has finished its core-hydrogen burning, and before the core-helium ignition. Resulting from the mass transfer, the remnant of the primary star is its helium core, while its entire hydrogen-rich envelope has been transferred to the secondary star, which became the more massive component of the system (conservative mass transfer as the dominant mode, see, e.g., van den Heuvel et al., 2000). Following Iben & Tutukov (1985) for the initial mass ($\geq$32 $\mathcal{M}_{\odot}$) of a star that will explode as a SN with helium core mass $\mathcal{M}_{He} \geq 13.4\ \mathcal{M}_{\odot}$ and $\mathcal{M}_{lost} \geq 6.4\ \mathcal{M}_{\odot}$ (the fraction of mass lost $\sim$ 0.2 van den Heuvel et al., 2000).

4. Summary

We presented the following study and results:

- We found that the member star of the Cep OB1 association BD+53 2820 (spectral type B0 and luminosity class IV) and runaway HMXB 4U 2206+54/BD+53 2790 pair satisfies all our criteria for a close meeting in the past, namely they were at the same time (2.8 ± 0.4 Myr ago) at the same place (distance of 3435 ± 67 pc). It is therefore most likely, that at this location and time, a SN in a close massive binary took place and can be considered as the place and time of the origin of the currently observed HMXB. For the HMXB 4U 2206+54/BD+53 2790, we obtained a runaway velocity of 75-100 km/s at the moment of SN explosion. Our conclusions hold for a wide range of radial velocity of BD+53 2820 of 23 ± 16 km/s.

- Given current orbital parameters of the HMXB 4U 2206+54/BD+53 2790 and using approaches described by Hurley et al. (2002), Nelemans et al. (1999), Postnov & Yungelson (2014), Tauris & Takens (1998), van den Heuvel et al. (2000) we estimated a number of parameters of the progenitor binary system, i.e. mass of the SN progenitor: $\gtrsim 32\ \mathcal{M}_{\odot}$ ($\mathcal{M}_{He} \geq 13.4\ \mathcal{M}_{\odot}$, $\mathcal{M}_{lost} \geq 6.4\ \mathcal{M}_{\odot}$), mass of the ejected SN shell $\Delta\mathcal{M} \gtrsim 5\ \mathcal{M}_{\odot}$, required minimum kick velocity of the produced neutron star $\mathrm{v}_{kick} \sim$200-350 km/s.

Acknowledgements

We acknowledge financial support from the Deutsche Forschungsgemeinschaft in grant NE 515/61-1. KAS acknowledge support from grant КП-06-Н28/2 08.12.2018 "Binary stars with compact object" (Bulgarian National Science Fund). AK acknowledges support from the Bulgarian Ministry of Education and Science under the National Research Programme "Young scientists and post-doctoral students" approved by DCM #577/17.08.2018. This work has made use of data from the European Space Agency (ESA) mission *Gaia* (`https://www.cosmos.esa.int/gaia`), processed by the *Gaia* Data Processing and Analysis Consortium (DPAC, `https://www.cosmos.esa.int/web/gaia/dpac/consortium`).

doi: doi.org/10.52526/25792776-2021.68.2-454/

References

Abt H. A., Bautz L. P., 1963, Astrophys. J. , 138, 1002

Alpar M. A., Çalışkan Ş., Ertan Ü., 2013, in Zhang C. M., Belloni T., Méndez M., Zhang S. N., eds, IAU Symposium Vol. 290, Feeding Compact Objects: Accretion on All Scales. pp 93–100 (arXiv:1211.4721), doi:10.1017/S1743921312019291

Ambartsumian V. A., 1947, The evolution of stars and astrophysics

Ambartsumian V. A., 1954, Communications of the Byurakan Astrophysical Observatory, 15, 3

Ambartsumian V. A., 1955, The Observatory, 75, 72

Ankay A., Kaper L., de Bruijne J. H. J., Dewi J., Hoogerwerf R., Savonije G. J., 2001, Astron. Astrophys. , 370, 170

Arnason R. M., Papei H., Barmby P., Bahramian A., Gorski M. D., 2021, Mon. Not. R. Astron. Soc. , 502, 5455

Avdyushev V. A., 2010, Vychisl. Tekhnol. (Computational Technologies), 15, 31

Bailer-Jones C. A. L., Rybizki J., Fouesneau M., Demleitner M., Andrae R., 2021, VizieR Online Data Catalog, p. I/352

Bajkova A., Bobylev V., 2017, Open Astronomy, 26, 72

Bajkova A. T., Bobylev V. V., 2019, Mon. Not. R. Astron. Soc. , 488, 3474

Baumgardt H., Kroupa P., 2007, Mon. Not. R. Astron. Soc. , 380, 1589

Blaauw A., 1961, Bull. Astron. Inst. Neth. , 15, 265

Blay P., Negueruela I., Reig P., Coe M. J., Corbet R. H. D., Fabregat J., Tarasov A. E., 2006, Astron. Astrophys. , 446, 1095

Bonnarel F., et al., 2000, Astron. and Astrophys. Suppl. Ser. , 143, 33

Cantat-Gaudin T., et al., 2020, Astron. Astrophys. , 640, A1

Dorigo Jones J., Oey M. S., Paggeot K., Castro N., Moe M., 2020, Astrophys. J. , 903, 43

Eker Z., et al., 2018, Mon. Not. R. Astron. Soc. , 479, 5491

Ekström S., et al., 2012, Astron. Astrophys. , 537, A146

Fernández D., Figueras F., Torra J., 2008, Astron. Astrophys. , 480, 735

Finger M. H., Ikhsanov N. R., Wilson-Hodge C. A., Patel S. K., 2010, Astrophys. J. , 709, 1249

Gaia Collaboration 2020, VizieR Online Data Catalog, p. I/350

Gaia Collaboration et al., 2018, Astron. Astrophys. , 616, A1

Goodwin S. P., Bastian N., 2006, Mon. Not. R. Astron. Soc. , 373, 752

Hainich R., et al., 2020, Astron. Astrophys. , 634, A49

Hambaryan V., et al., 2021, Mon. Not. R. Astron. Soc. , in press

Hobbs G., Lorimer D. R., Lyne A. G., Kramer M., 2005, Mon. Not. R. Astron. Soc. , 360, 974

Hoogerwerf R., de Bruijne J. H. J., de Zeeuw P. T., 2000, Astrophys. J. Lett. , 544, L133

Hoogerwerf R., de Bruijne J. H. J., de Zeeuw P. T., 2001, Astron. Astrophys. , 365, 49

Humphreys R. M., 1978, Astrophys. J. Suppl. Ser. , 38, 309

Hurley J. R., Tout C. A., Pols O. R., 2002, Mon. Not. R. Astron. Soc. , 329, 897

Iben I. J., Tutukov A. V., 1985, Astrophys. J. Suppl. Ser. , 58, 661

Igoshev A. P., 2020, Mon. Not. R. Astron. Soc. , 494, 3663

Kaspi V. M., Bailes M., Manchester R. N., Stappers B. W., Bell J. F., 1996, Nature. , 381, 584

Kharchenko N. V., Piskunov A. E., Röser S., Schilbach E., Scholz R. D., 2005a, Astron. Astrophys. , 438, 1163

Kharchenko N. V., Piskunov A. E., Röser S., Schilbach E., Scholz R. D., 2005b, Astron. Astrophys. , 440, 403

Lada C. J., Lada E. A., 2003, Ann. Rev. Astron. Astrophys. , 41, 57

Lyne A. G., Lorimer D. R., 1994, Nature. , 369, 127

Massey P., Johnson K. E., Degioia-Eastwood K., 1995, Astrophys. J. , 454, 151

Melnik A. M., Dambis A. K., 2020, Mon. Not. R. Astron. Soc. , 493, 2339

Meynet G., Maeder A., 2003, Astron. Astrophys. , 404, 975

Mugrauer M., Avila G., Guirao C., 2014, Astronomische Nachrichten, 335, 417

Nelemans G., Tauris T. M., van den Heuvel E. P. J., 1999, Astron. Astrophys. , 352, L87

Neuhäuser R., Gießler F., Hambaryan V. V., 2020, Mon. Not. R. Astron. Soc. , 498, 899

Özsükan G., Ekşi K. Y., Hambaryan V., Neuhäuser R., Hohle M. M., Ginski C., Werner K., 2014, Astrophys. J. , 796, 46

Palous J., Jungwiert B., Kopecky J., 1993, Astron. Astrophys. , 274, 189

Pecaut M. J., Mamajek E. E., 2013, Astrophys. J. Suppl. Ser. , 208, 9

Pflamm-Altenburg J., Kroupa P., 2010, Mon. Not. R. Astron. Soc. , 404, 1564

Postnov K. A., Yungelson L. R., 2014, Living Reviews in Relativity, 17, 3

Poveda A., Ruiz J., Allen C., 1967, Boletin de los Observatorios Tonantzintla y Tacubaya, 4, 86

Reig P., Fabregat J., 2015, Astron. Astrophys. , 574, A33

Reig P., Torrejón J. M., Negueruela I., Blay P., Ribó M., Wilms J., 2009, Astron. Astrophys. , 494, 1073

Renzo M., et al., 2019, Astron. Astrophys. , 624, A66

Soubiran C., et al., 2018, Astron. Astrophys. , 619, A155

Steiner J. E., Ferrara A., Garcia M., Patterson J., Schwartz D. A., Warwick R. S., Watson M. G., McClintock J. E., 1984, Astrophys. J. , 280, 688

Stone R. C., 1979, Astrophys. J. , 232, 520

Stoyanov K. A., Zamanov R. K., Latev G. Y., Abedin A. Y., Tomov N. A., 2014, Astronomische Nachrichten, 335, 1060

Tauris T. M., Takens R. J., 1998, Astron. Astrophys. , 330, 1047

Tetzlaff N., Neuhäuser R., Hohle M. M., Maciejewski G., 2010, Mon. Not. R. Astron. Soc. , 402, 2369

Torrejón J. M., Reig P., Fürst F., Martinez-Chicharro M., Postnov K., Oskinova L., 2018, Mon. Not. R. Astron. Soc. , 479, 3366

Ward J. L., Kruijssen J. M. D., Rix H.-W., 2020, Mon. Not. R. Astron. Soc. , 495, 663

Weidner C., Vink J. S., 2010, Astron. Astrophys. , 524, A98

Wenger M., et al., 2000, Astron. and Astrophys. Suppl. Ser. , 143, 9

Wilson R. E., 1953, Carnegie Institute Washington D.C. Publication, p. 0

Wright N. J., 2020, New Astron. Rev., 90, 101549

van den Heuvel E. P. J., Portegies Zwart S. F., Bhattacharya D., Kaper L., 2000, Astron. Astrophys. , 364, 563

van der Meij V., Guo D., Kaper L., Renzo M., 2021, arXiv e-prints, p. arXiv:2108.12918

doi: doi.org/10.52526/25792776-2021.68.2-454/

Perseverance Rover and Its Search for Life On Mars

James L. Green

NASA Headquarters, Washington D.C. USA

Abstract

Mars orbiters, landers, and rovers have made extraordinary discoveries about the evolution of Mars and its potential for life. At this time, it is clear, that the potential of ancient life on Mars has increased based on several discoveries. There have been many observed signs of ancient liquid water: surface and underground. There are past geological environments on Mars that had reasonable potential to have preserved the evidence of life, had it existed. The detection of complex organics by Curiosity has increased the potential for preserving "fingerprints of life" that may be locked away in the rock record. These and other factors have led NASA, with the support of other space agencies, to mount a Mars sample return (MSR) campaign. The first mission of MSR is the Perseverance rover. Designed to core and store rock, soils, and atmospheric samples in sealed tubes for later return, Perseverance landed in Jezero crater in February 2021 near an extensive ancient river delta. Other missions will follow to bring these samples back to Earth for further analysis. In addition, Perseverance carried the Ingenuity helicopter as a technology demonstration which has been tremendously successful and may lead to other future ariel missions on the red planet.

Keywords: *Mars, habitability, sample return*

1. Introduction

Today there is a fantastic array of operating missions at the planet Mars that include: orbiters, landers, rovers, and a helicopter. The operating missions at Mars shown in Figure 1, are from several international space agencies and represent the greatest armada of simultaneous active scientific instruments ever to be deployed at a planet beyond the Earth. In addition to the NASA orbiters, Mars Odyssey, Mars Reconnaissance Orbiter, and the MAVEN spacecraft, the European Space Agency (ESA) manages Mars Express and Trace Gas Orbiter, the Indian Space Research Organization manages the Mars Orbiter Mission, the United Arab Emirates manages the HOPE mission, and the China National Space Agency (CNSA) manages the Tiawen-1 orbiter. On the surface, the operating missions include NASA's Curiosity rover, the InSight lander, the Perseverance rover, and the Ingenuity helicopter joined by the CNSA lander and Zhurong rover. The purpose of this paper is to set the stage for the upcoming missions to Mars that will return rock cores, soils, and atmospheric samples as a step toward understanding the evolution of Mars and determining if Mars may have harbored life in its past.

2. Past Observations

From the array of orbiting missions at Mars it has been determined that Mars was a blue planet early on in its history with more than two-thirds of its northern hemisphere under water, but over time it lost this ocean. Mars also lost its intrinsic dynamo field about 4 billion years ago. A magnetosphere is known to provide resilience against solar storms removing the outer layers of the atmosphere (Dong et al., 2020). There is compelling evidence that Mars has lost a significant amount of atmosphere to outer space due to the direct solar wind interaction with the ionosphere and upper atmosphere thereby disrupting the water cycle and allowing its ocean to evaporate without replenishment (Jakosky & Edwards, 2018, Lillis et al., 2015).

Today, partial protection of the Martian atmosphere from the solar wind is provided by the strong, localized remnant crustal magnetic fields (Dong et al., 2015, Ma et al., 2014). Current monitoring of Mars shows an ongoing loss of key atmospheric elements, such as oxygen, due to solar short wavelength radiation (EUV and X-rays) and solar wind energy inputs (Brain et al., 2015). The current NASA rovers on Mars

doi: doi.org/10.52526/25792776-2021.68.2-464

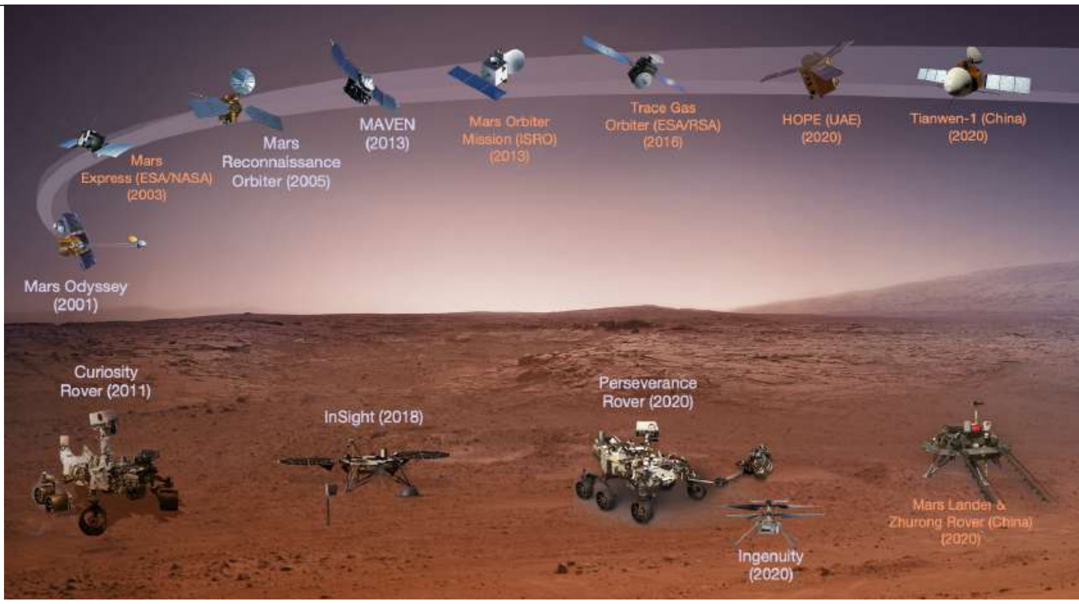

Figure 1. The international fleet of operating missions at Mars.

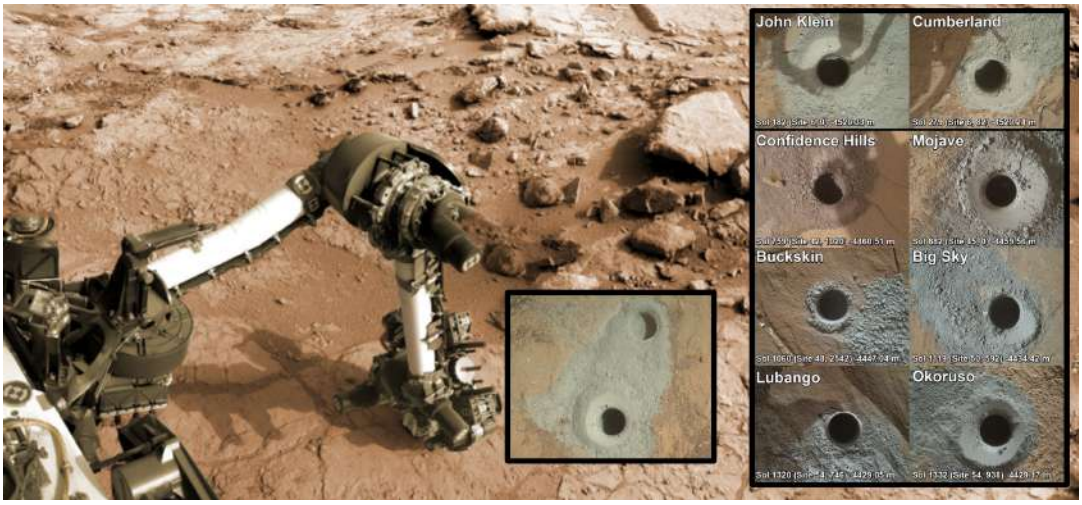

Figure 2. Mars subsurface material generated by the pulverizing drill on the Curiosity rover.

.

were designed to determine the habitability of past Mars by interrogating the soils and creating samples designed to be returned to Earth for future analysis.

The Curiosity rover, which landed in Gale Crater in August 2011, has uncovered a trove of important clues about Mars' distant past (Vasavada, 2015). For example, it is clear from the sedimentary material in Gale Crater that a significant amount of water filled the crater. Curiosity has a percussive drill allowing material to be pulverized for analysis. Drilling below the surface, about a centimeter to a centimeter and a half, the soils on Mars are very different than the oxidized surface. As shown in Figure 2, there's quite an array of different colored soils. Curiosity scoops up the pulverized soil material analyzing it in the Sample Analysis on Mars or SAM instrument. The key elements found in the soils by SAM include the chemical elements for life such as carbon, hydrogen, nitrogen, oxygen, phosphorus, and sulfur. The soils are moist, and they have nitrates.

Since Mars had a lot of water in its past, it must have had a significant atmosphere, and supported a significant greenhouse effect to keep the planetary surface warm to maintain a liquid ocean. Would it be also habitable for life at that time? Curiosity also found complex benzene and propane molecules as part of a larger macro molecule structure called kerogens (Eigenbrode et al., 2018). On Earth, typically organic constituents of kerogen are found in algae and woody plant products. These complex macro molecules tell us that the early Mars environment could have indeed been habitable. About 3 billion years ago, Mars went through a time of rapid climate change until it became the very dry and arid planet it is today. From this

doi: doi.org/10.52526/25792776-2021.68.2-464

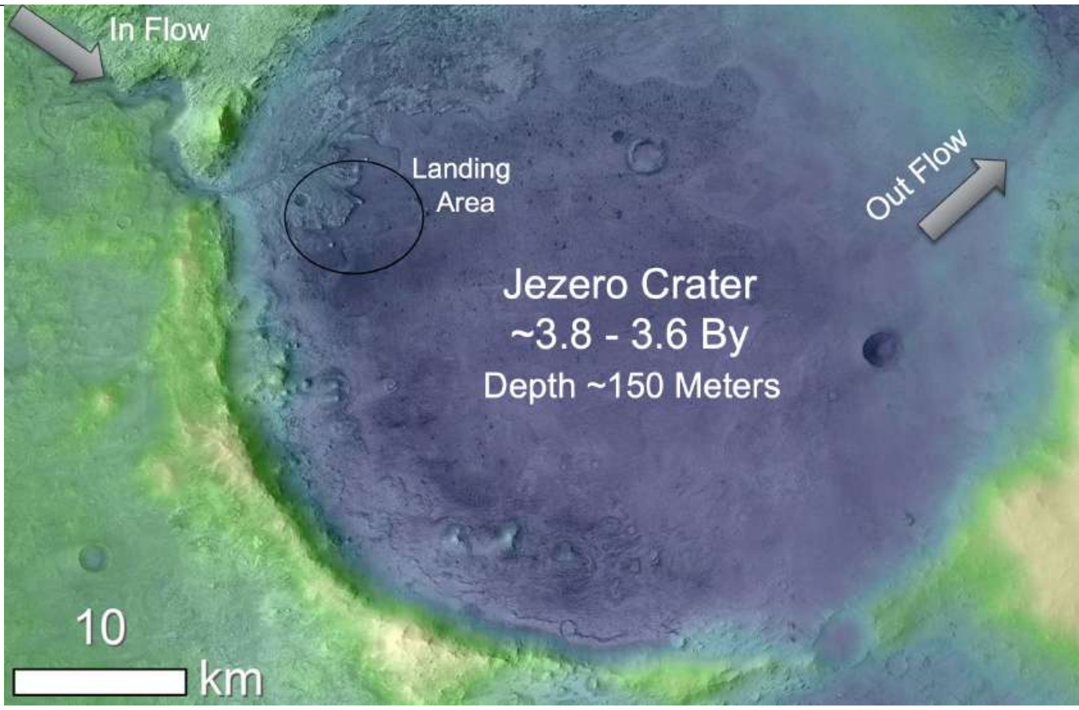

Figure 3. The Jezero crater and landing site of the Perseverance rover.

perspective, when we land our rovers on the surface of Mars today, the geology, the mineralogy, and its composition can be examined as if we are looking at early Mars. It is also important to note that about 3.6 billion years Earth life began. Could it also have begun on Mars and about the same time and if so, how can we find out? It is believed that a detailed rock record may hold the key to answering that question.

3. Where are These Discoveries Leading Us?

The recent Mars discoveries are leading us to conclude, that ancient life could have started on Mars, perhaps at the same time it started on Earth, because we've found the signs of past liquid water on its surface, strong indications of groundwater, and a past geological environment having a reasonable potential to preserve that evidence. A strong assumption in the past was that cosmic rays would break up organic material making it too difficult to find the macromolecules. But fortunately, we've been able to detect some of them. Now the detection of complex organics has increased the potential for finding, preserved in the soils and rocks, the "fingerprints of life." In summary, with our detailed knowledge of Mars, we now have a means to prioritize candidate sites and reason to believe that the evidence we are seeking may be preserved and that it is within reach of our exploration systems. The next logical step is for a Mars sample return (MSR) campaign to bring back the right samples.

4. A River Delta in Jezero Crater: The Right Location

About 4 billion years ago, the large ocean in the northern hemisphere on Mars was fed by a several rivers. At about 3.8 billion years a huge impact occurred on the ancient shoreline of this ocean creating a crater we named Jezero. The river flowed into the newly formed crater, as shown in the upper left corner of Figure 3, filling it up, until the water broke over its eastern crater wall (right corner of Figure 3) and into the Isidis Basin the lower extension of the ancient ocean. It is clear, as indicated from MRO images taken from orbit, that the rapid flowing river water upon meeting the rather still water within Jezero crater, dropped its sediments forming the extensive delta at this juncture we see today. The delta built up over time, with a diameter of approximately 10 km and a height of up to 65 meters.

Here on Earth, our own dried-up river delta's and ancient ocean shores preserve evidence of past life such as stromatolites that are 4 billion years old. Stromatolites are microbial mats that are built up over time in distinctive layers. Perhaps we will find similar types of signatures of life on Mars. On Earth there are over 5780 known minerals and about 337 of these are formed by the interactions with organic remains.

doi: doi.org/10.52526/25792776-2021.68.2-464

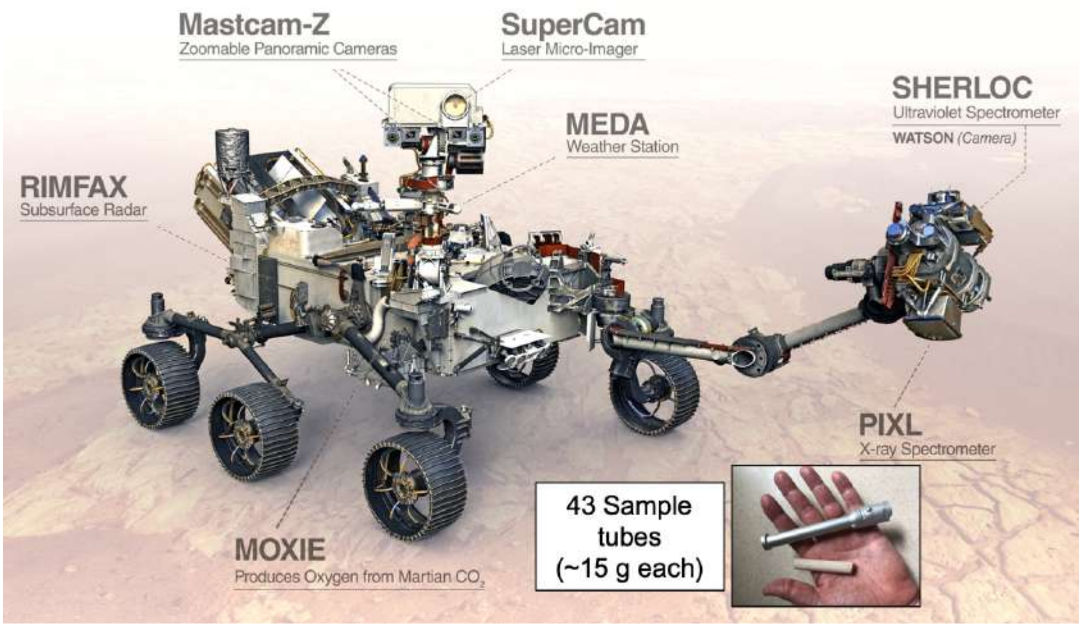

Figure 4. Perseverance rover instrumentation.

Once the Mars samples are returned to Earth for extensive analysis, not only will scientists be looking for the mineralogy as it may relate to the potential of past life, but also how the climate changed on Mars. It is believed that the climate change rapidly on Mars, but it is not known if that occurred over 10s of millions of years or several 100 million years.

After much deliberation, the landing site or ellipse for the Perseverance rover was determined to be just below the river delta in Jezero crater as shown in Figure 3. From orbit, MRO and Mars Express observed a variety of geological formations, not only the basaltic material from the adjacent volcano (west of the crater) thrown into the crater, but also olivine-carbonate bearing rock material. It will be up to Perseverance to validate these measurements, a process called ground-truth.

5. Perseverance Rover: The Starting Point of MSR

On February 18, 2021, NASA successfully landed the Perseverance rover while also carrying the Ingenuity helicopter, within the eastern portion of the landing ellipse on the Jezero crater floor just southeast and beyond the river delta. The purpose of NASA's Perseverance Rover is to create and cache critical samples for later return (Farley et al., 2020). Figure 4 is an overview of the instruments on the rover. Perseverance has many international instruments along with 23 cameras (9 engineering, 7 science, and 7 that were used during its entry, descent, and landing). The international instruments include: RIMFAX from Norway; SuperCam: NASA and France; MEDA from Spain; and a small retroreflector (not shown) from Italy. On the arm of the rover is a powerful drill designed to core rock, even as hard as granite, about the size of a chalkboard marker that is then placed into a metal tube producing a cache of samples. The rover has instruments that are designed to also provide a significant amount of contextual data about the geology, fine-scale mineralogy, chemistry, and atomic and molecular composition of targeted areas. This information is critical in determining where samples will be taken and how they may be interpreted once they have been returned to Earth and analyzed.

In addition to providing supporting sample information, Perseverance has the MEDA weather station (measuring temperature, pressure, wind velocity), a human exploration instrument, and a first ever Mars flying helicopter named Ingenuity. The average pressure of Mars is about 7 mb and is composed of 95.9% CO2, 2% argon, 1.9% nitrogen, and several other trace gases. The Mars Oxygen In-situ Resource Utilization Experiment (MOXIE) is designed to demonstrate production of molecular oxygen (O2), which can be breathed by humans or used as rocket fuel, by electrochemically splitting the Mars carbon dioxide (CO2) atmosphere into carbon monoxide (CO) and O2. MOXIE has worked perfectly and can generate 6-10 grams of propellant grade O2 per hour from the Mars atmosphere.

Another technology demonstration that was successfully accomplished was the Ingenuity helicopter. To

doi: doi.org/10.52526/25792776-2021.68.2-464

date (November 2021), Ingenuity has successfully flown its 5 test fights and 10 additional flights supporting Perseverance as an advance scout. Ingenuity has two cameras, one outward looking, and one downward looking and has flown to a maximum height of 10 meters and maximum distance of 271 meters. These flights and the demonstrated ability to easily maneuver in the thin Martian air indicates that flying technologies can be used successfully for future missions to the surface of Mars.

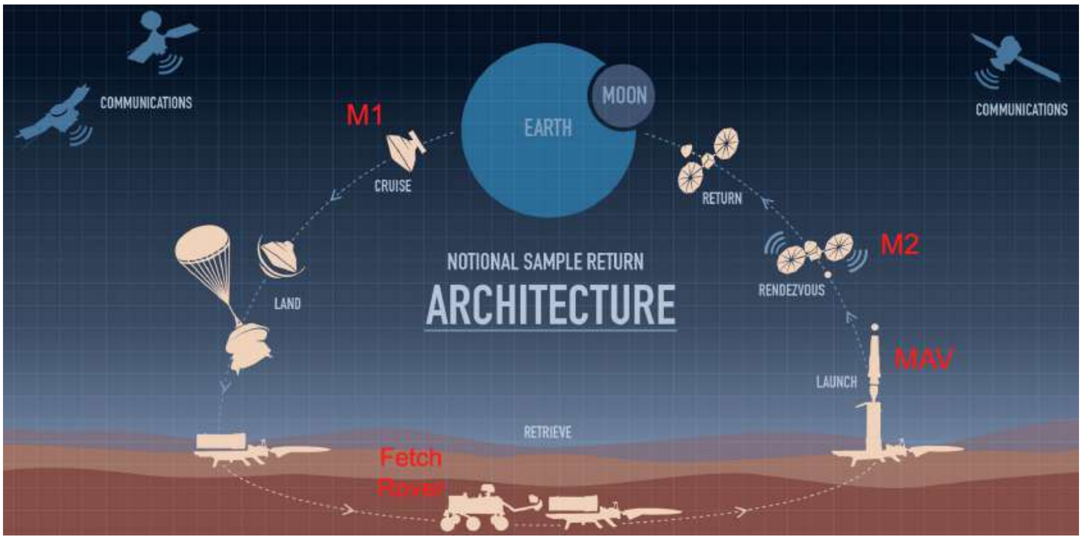

Figure 5. The notional Mars sample return architecture.

Perseverance has a total of 43 super clean sealed metallic sample tubes that can be filled over the next several years and will be placed on the surface in several piles for later pick-up and return. Currently (November 2021), Perseverance has already taken a total of 5 samples, which include 4 rock cores and one atmospheric sample. After exploring Jezero crater floor, Perseverance will climb up the delta, taking samples all along the way, depositing them in a few strategically placed stacks, and move into Nili Planum the high plains above the crater. Nili Planum gives Perseverance another opportunity at searching for signs of life in the rock record because it will be in an area of ancient hydrothermal systems and deep aquifers in the crust.

6. The Sample Return Missions

Shown in Figure 5 is the notional mission architecture for returning the cached samples which will start in 2026 and will consist of a series of missions from NASA and ESA. NASA's first mission (M1) will land a Mars Ascent Vehicle or MAV, along with a fetch rover. The rover will collect those samples, returning and loading them into the upper stage storage unit of the MAV. The MAV will then be erected and launched delivering the storage unit into low Mars orbit, where the second mission (M2), developed by ESA, will capture the sample storage unit and return it to the Earth. The sample storage unit will land in the desert of Utah in the United States and will immediately go into a biosafety facility to be curated, studied, and where the initial analysis will be completed. It is expected that at an appropriate time these samples will be released to the international science community for detailed analysis.

7. Conclusion

About 4 billion years ago, like the Earth, Mars was a blue planet, with a significant ocean and a thick atmosphere at the same time that life started on Earth. One of the challenges in searching for past life on Mars is that, while we know that the ancient surface had habitable conditions, we don't really know for how long and how rapidly it changed to the arid planet we see today. This situation calls into question whether Mars had time for life to spring up or not. The Perseverance rover has started the process of a sample return campaign that is designed to answer how the Red planet evolved over time and potentially, whether it harbored life in its past.

doi: doi.org/10.52526/25792776-2021.68.2-464

References

Brain D. A., et al., 2015, Geophysical Research Letters, 42, 9142

Dong C., et al., 2015, Journal of Geophysical Research (Space Physics), 120, 7857

Dong C., Jin M., Lingam M., 2020, Astrophys. J. Lett. , 896, L24

Eigenbrode J. L., et al., 2018, Science, 360, 1096

Farley K. A., et al., 2020, Space Science Reviews, 216, 142

Jakosky B. M., Edwards C. S., 2018, Nature Astronomy, 2, 634

Lillis R. J., et al., 2015, Space Science Reviews, 195, 357

Ma Y., Fang X., Russell C. T., Nagy A. F., Toth G., Luhmann J. G., Brain D. A., Dong C., 2014, Geophysical Research Letters, 41, 6563

Vasavada A., 2015, EOS, March15, 16

Communications of BAO, Vol. 68, Issue 2, 2021, pp. 470-477

On the Magnetic Fields of Galaxies

R.R. Andreasyan *

Byurakan Astrophysical Observatory NAS Armenia, Byurakan, Aragatsotn prov., 0213, Armenia

Abstract

We bring results of some our investigations of magnetic field of our Galaxy and extragalactic radio sources. For the study were used data of Faraday rotation of pulsars and extragalactic radio sources as well as data of physical and morphological properties of more than 500 radio galaxies of different morphological classes.

Keywords: *Magnetic field, Radio-galaxy, Active Galaxies*

1. Introduction

The study of the magnetic fields of galaxies and, in particular, of our Galaxy has a great importance for explaining many dynamical and active processes taking place in these objects. The presence of the magnetic field of the Galaxy can explain the transportation of cosmic rays through the interstellar medium, as well as synchrotron background radiation in the Galaxy (Fermi, 1949). The considering the role of the magnetic field in the process of star formation has a great importance in galaxies. All of this show that it is fundamental to understand the strength and direction of the magnetic field in the ISM, as well as its morphology across the entire Galaxy.

2. The magnetic field of the Galaxy

The magnetic field of our Galaxy was studied using observational data of various types, such as interstellar polarization of starlight (more than 9000 stars); Zeeman splitting of spectral lines of HI and different molecules in the radio range that provides detailed information about the line-of-sight magnetic field in the ISM. But the most effective method for the study of Galactic magnetic field is based on the use of data on Faraday rotation of polarized radio emission of extragalactic radio sources (now available for about 40000 objects) and pulsars (more than 1200). It is well known that pulsars, for which numerous and diverse observational data were obtained, can be considered probes for studying the interstellar medium. In particular, data on dispersion measures (DM), which practically are known for all known pulsars, and about measures of Faraday rotation (RM) are very important for studying the magnetic field of the Galaxy. These data are directly derived from observations of pulsars. Theoretically they are expressed by the electron density n_e in the interstellar medium through which the polarized radio emission of the pulsar passes and the projection of the magnetic field B_L (in Gauss) in this medium, using the following formulas:

$$DM = \int n_e dL \tag{1}$$

.

$$RM = \alpha \int n_e B_L dL, (\alpha = 8.1 * 10^5) \tag{2}$$

.

In these formulas, integration is carried out over the entire traversed path of radiation (L in parsecs) from the pulsar to the observer. If the sign of RM is positive, it means that projection of the magnetic field B_L is directed to observer. Formula 1 makes it possible to determine the distance of a pulsar with the

*randrasy@bao.sci.am

doi: doi.org/10.52526/25792776-2021.68.2-447

known electron density distribution in the Galaxy, and formula 2 together with formula 1 makes possible to determine the average component of the tension of interstellar magnetic field [B$_L$] on the line of sight in micro gauss (μG).

$$[B_L] = \frac{1}{\alpha}\frac{RM}{DM} = 1.23\frac{RM}{DM} \tag{3}$$

.

All of these data were used to study the structure and magnitude of the magnetic field of the Galaxy, since the seventies of the last century, when the rotation measures and other data were known for only a few tens of objects. As the amount of important data increases, more detailed studies have been carried out and various models have been proposed for the plane component of the Galactic magnetic field, as well as for the magnetic field in the Halo of the Galaxy. Here we present some of the results that we obtained in this area.

Andreasyan & Makarov (1989a) used the data of 185 RM data of pulsars for the study of magnetic field in the plan of Galaxy. Was construct the map of RM distribution in the galactic plan.

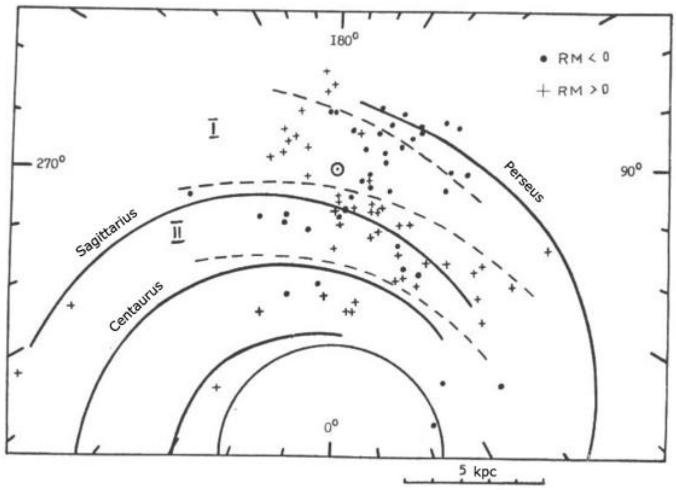

Figure 1. Distribution of RM signs for pulsars in the ±400 pc Galactic layer.

There are two well-defined areas in the picture. In the first area I (the local Orion arm and Perseus arm area) the magnetic field has anti clockwise direction. In the area II the magnetic field has opposite clockwise direction. It means that there is an inversion of the direction of magnetic field when passing from one spiral arm of the Galaxy to another.

Andreasyan & Makarov (1989b) for the study of Galactic magnetic field used star light interstellar polarization data of 7500 objects. In fig. it is shown a distribution of averaged star light polarization in the layer of ± 250 parsec near the Galactic plan.

From the picture evidences in favor of the presently accepted model of the magnetic field of the Galaxy were obtained. The magnetic fields in the Galaxy plane are mostly concentrated in the spiral arms and are directed along the axes of the corresponding arms.

Our investigation confirms the model of the two-component magnetic field of our Galaxy proposed in Andreasyan & Makarov (1989a). For the first time it was shown that the data on the rotation measures of pulsars and extragalactic radio sources are in good agreement with the model when the magnetic field of the plane component of the spiral arms is embedded in the magnetic field of the galactic halo with dipole configuration, which is deformed due to the differential rotation of the Galaxy.

In Andreasyan et al. (2011) a method is introduced for constructing two-color maps. Using the formulas 1 and 2 we obtain

$$B_L(DM) = \frac{1}{\alpha}\frac{dRM}{dDM} \tag{4}$$

.

$$B_L(R)n_e(R) = \frac{1}{\alpha}\frac{dRM}{d(R)} \tag{5}$$

.

where B$_L$(DM) is the line of sight component of magnetic field strength at the point with a given value of

doi: doi.org/10.52526/25792776-2021.68.2-447

DM, $B_L(R)$ is the line of sight component of magnetic field strength at the point with a distance R from the Sun. It means, that using the RM-DM and RM-R dependences for a given direction, it is possible to find $B_L(DM)$ for each value of DM, and $B_L(R)n_e(R)$ for each value of R. We can find the RM-DM and RM-R dependences for all directions in the plan of Galaxy using averaging procedure. In fact we are solving the inverse problem to construct 2-dimensional maps for plane component of Galactic magnetic field with coordinates (l;DM), or (l;R). Using the data of RM, DM and the distance of pulsars, we constructed a two-color map of the plane component of the magnetic field of the Galaxy, on which large-scale regions with regular magnetic fields, approximately corresponding to the spiral structure of the Galaxy, were clearly distinguished. Some results of calculations are given on the maps of $B_L(R)n_e(R)$ and $B_L(DM)$.

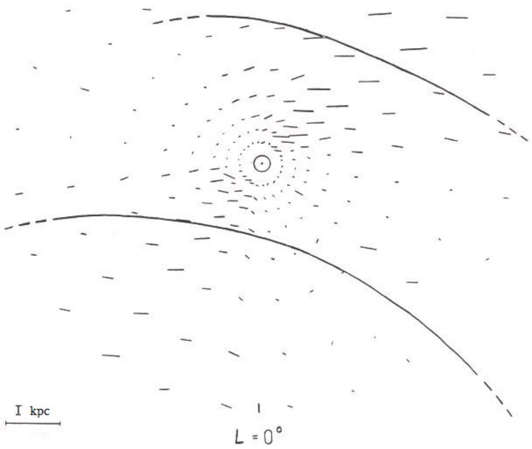

Figure 2. Star light interstellar polarization parameters of space groups of stars in the ± 250 pc layer. The directions of the spiral arms of Perseus and Sagittarius-Carina are also shown.

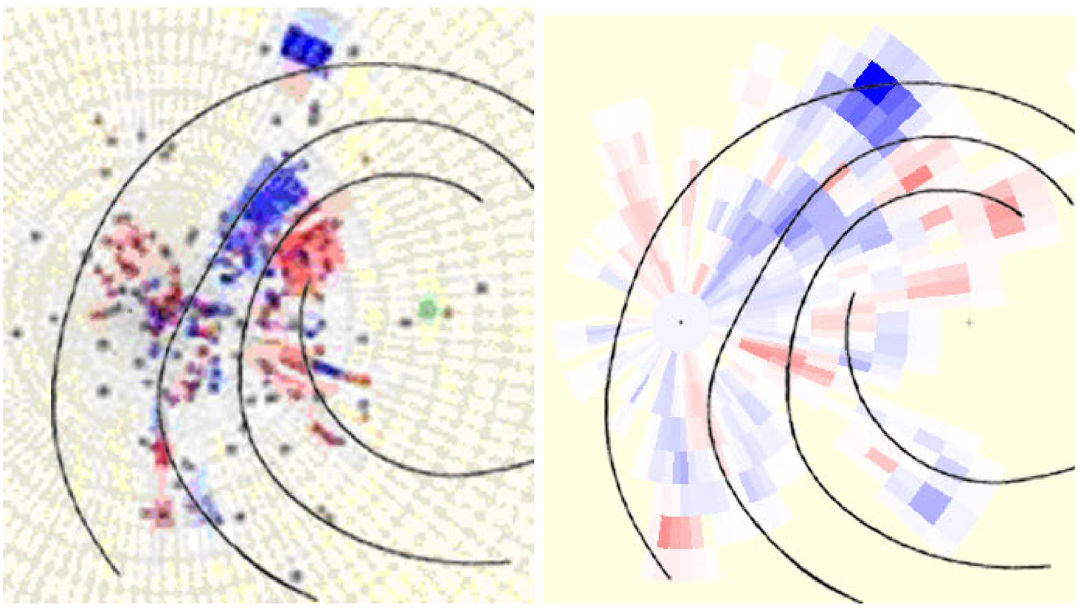

Figure 3. The distributions of $B_L(R)n_e(R)$ (with pulsars) in coordinates (l;R) (the left picture), and $B_L(DM)$ in coordinates (l;DM) (right picture) with the spiral arms of the Galaxy, red color for magnetic field directed to observer and blue color for the field directed from the observer. The intensity of the color shows the strength of the field) for the plane component of the magnetic field of our galaxy in (R, l) and (DM, l) coordinates. The sun is on the distance of 8.5 kpc to the left side from the Galactic center.

Using these pictures, identifying some details on two distributions it is possible to find the magnetic field strength in every point of Galactic plan.

In Andreasyan et al. (2020) is modeled reversals of Galactic magnetic field using the so-called no-z approximation based on the fact that the galactic disk is sufficiently thin. The magnetic field generation that exhibit both single and double sign changes with distance from the center is observed. There are

doi: doi.org/10.52526/25792776-2021.68.2-447

numerous arguments in favor of the fact that the magnetic field exhibits so-called reversals associated with a direction change from one region to another. A study of the pulsar distribution with large Faraday rotation measures ($RM > 300$ rad/m^2) was presented. The results indicate that there is a region of the Galaxy (the galactocentric ring inside ≈ 5kpc and 7kpc), in which the magnetic field is oriented counterclockwise.

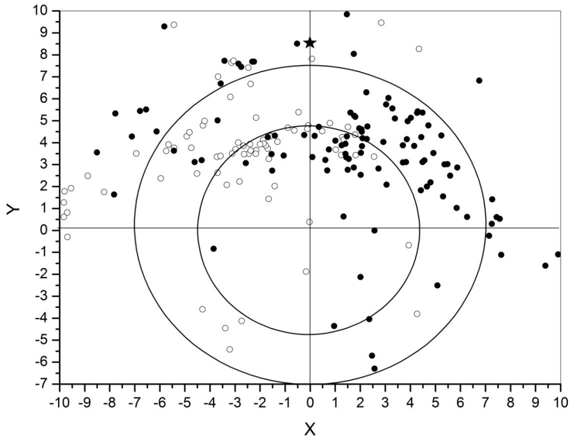

Figure 4. Distribution of rotation measures of pulsars in the plane of the Galaxy.

On the Fig. 4 black circles denote pulsars in $RM > 300$ rad/m^2 (the projection of the magnetic field on the line of sight is directed toward the observer), white circles - in which RM <-300 rad/m^2 (the projection of the magnetic field is directed from the observer). At the ring edges (≈ 5kpc and 7kpc) the magnetic field reverses its direction. These results are in close agreement with our theoretical concepts. As we see from the observations it can be studied the configuration and strength of Galactic magnetic field. The generation of these fields is explained by the dynamo mechanism associated with motions of the interstellar medium in appropriate objects. The growth of magnetic fields is exponential and these become stabilized when the equipartition of energy between magnetic fields and turbulent motions is reached. But for starting this generation mechanism, some initial "seed" magnetic fields are necessary, and these fields are not explained within the dynamo theory. The so-called Biermann battery mechanism is very good for the formation of "seed" magnetic fields. If we have an outflow of plasma in rotating interstellar medium of galaxies, then because of the large differences between scattering time of expanding electrons and protons with the rotating medium, in every point of galaxy the rotation velocity of scattered electrons and protons will correspond to the rotation velocity of their last scattering point and will be different. In the result of forming of circular electric currents in galaxies evaluates dipolar magnetic fields. Some simple estimates of the strength of such a field in active galaxies were found in our earlier works. Now we have constructed a self-consistent model and derived an integral equation, which permits both to determine the order of magnitude of the initial magnetic field and to study in detail its spatial structure. These magnetic fields evaluate to large-scale magnetic fields by Dinamo mechanisms. In this way can be generated large-scale dipolar magnetic fields.

3. Extragalctic radio sources

The dipolar configuration of large-scale magnetic fields of active galaxies was the main suggestion for the mechanism of the formation and evolution of extragalactic radio sources (Andreasyan, 1983). In frame of this mechanism extragalactic radio sources are formed from relativistic plasma clouds, ejected from the central part of the optical galaxy and moving in large-scale dipolar magnetic field of parent galaxy. The behaviors of relativistic plasma cloud, ejected in the direction of the dipole axis, depends on the ratio Q of the kinetic energy density of the plasma to the magnetic field energy density,

- If the ratio Q is greater than unity the clouds of charged particles, expanding, travels large distances from the optical galaxy, carrying with them the magnetic field lines. Similar features we observe in extragalactic radio sources of FRII classes (Fanaroff & Riley (1974), edge brightened, more powerful objects).
- If the ratio Q of energy densities is less than unity, the charged particles will move along the field lines of the dipole magnetic field of the galaxy. In this case will be evaluate extragalactic radio sources of

doi: doi.org/10.52526/25792776-2021.68.2-447

FRI classes (edge darkened less powerful objects)

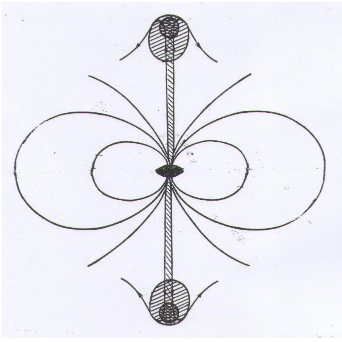

Figure 5. The ratio Q is greater than unity ($Q > 1$).

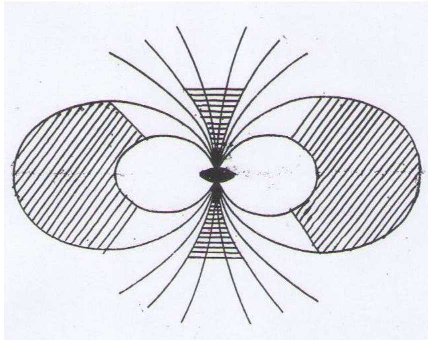

Figure 6. The ratio Q is less than unity ($Q < 1$).

In Andreasyan (1984, 1985) parallel to the well-known Fanaroff-Riley classification we bring also a simple classification of extragalactic radio sources by the elongation parameter K (the ratio of the largest dimension of radio image to the perpendicular dimension).

3.1. Observational data

For the study it was used data for 267 nearby radio galaxies identified with elliptical galaxies brighter than $18^t h$ magnitude (sample1) (Andreasyan & Sol, 1999), and 280 extragalactic radio sources with known position angles between the integrated intrinsic radio polarization and radio axes (sample 2) (Andreasyan et al., 2002). Here there are some results (physical and morphological differences in different classes of extragalactic radio sources) obtained in our study (Andreasyan & Sol, 1999, 2000, Andreasyan et al., 2002, 2013).

3.2. The correlation of radio axis with the optical axis in nearby radio galaxies

Data from sample of 267 nearby radio galaxies were used to study the correlations of radio axes with the optical axes of parent galaxies. Were constructed histograms separately for radio galaxies classified by elongation and for radio galaxies with FR classes. On the figures the difference between the radio and optical position angles (dPA) is laid out along the horizontal axis and the number of radio galaxies along the vertical axis.

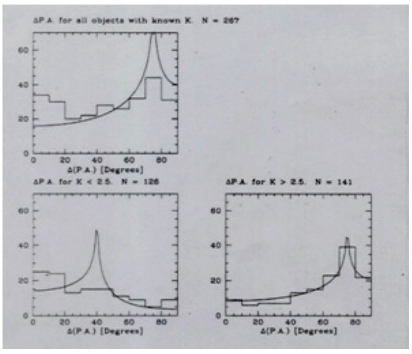

Figure 7. The distribution of (dPA) for K classes.

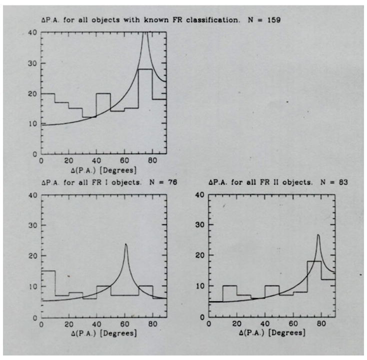

Figure 8. The distribution of (dPA) for FR classes.

From the figures we found, that more elongated and FRII type radio galaxies are in most cases directed as minor axes or rotation axes of host elliptical galaxies, while the less elongated and FRI ones are directed perpendicular to these axes. This result is in a good agreement with our conclusions.

3.3. The ellipticity of elliptical galaxies identified with the different types of extragalactic radio sources

In the Sample 1 we have data of the optical ellipticity (E) of 154 elliptical galaxies. For all of them we have the elongation parameters K and for 95 - the Fanaroff-Riley classes. We use this data to study the

doi: doi.org/10.52526/25792776-2021.68.2-447

distribution of ellipticities of parent optical galaxies for different FR types and for different classes of our K classification.

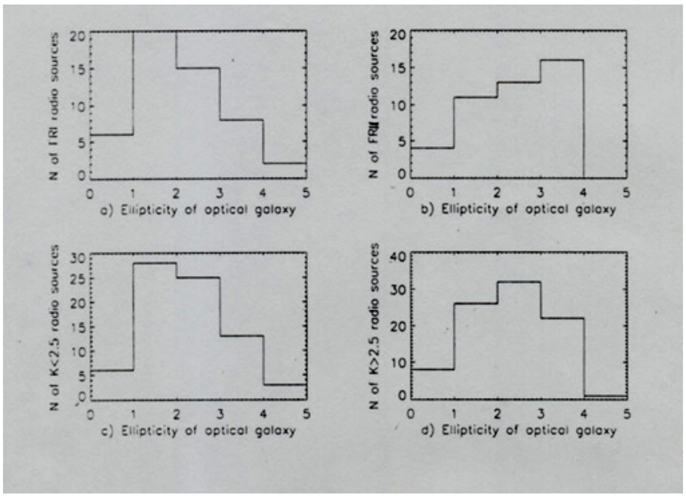

Figure 9. The ellipticities of optical parent galaxies for different FR types and for different classes of K classification.

From the Fig. 9 it is clear that the host elliptical galaxies of less elongated extragalactic radio sources and radio sources of FRI type have less ellipticity (E $\approx$ 1 to 2) than these of radio sources of large elongation and radio galaxies FRII type (E $\approx$ 3 to 4). The fact that host elliptical galaxies of FRI type radio sources have less ellipticities can be explained in two ways: It is primordial and in some way is responsible for the formation of FRI types, or it is from the orientation effect. In both cases, the fact of different ellipticities of different FR types is interesting for the understanding of formation of radio sources.

3.4. The correlation of the radio polarization angle with the radio axes of extragalactic radio sources

The data of 280 extragalactic radio sources of sample 2 were used for the study of distribution of angles Δ(PA) between directions of integrated intrinsic radio polarization and the major axes for different type radio sources, classified by their elongation and FR classification. The histograms of angles between radio and polarization axes are shown on pictures.

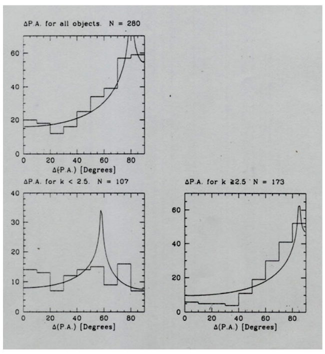

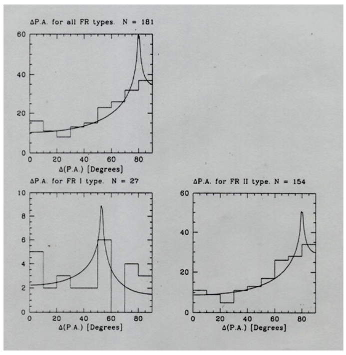

Figure 10. The distribution of Δ(PA) for K classes. Figure 11. The distribution of Δ(PA) for FR classes.

We see that for elongated and FRII sources, their intrinsic integrated polarization is perpendicular to their major radio axes. As the magnetic fields in optically thin synchrotron radio sources are perpendicular to the polarization of electric vector, the main result of this study is that integrated magnetic fields can be described as intrinsically aligned with major radio axes for elongated and FRII radio sources, while they are not correlated with radio axes for stocky and FRI radio sources.

doi: doi.org/10.52526/25792776-2021.68.2-447

3.5. Distribution of the elongation parameter of the extragalactic radio sources for the different FR classes

Here we study the distribution of the elongations of the radio images for radio sources in the two FR classes. Data from samples 1, 2, are used to construct the distribution functions f (K) of the elongation parameter K which are shown in the following figures.

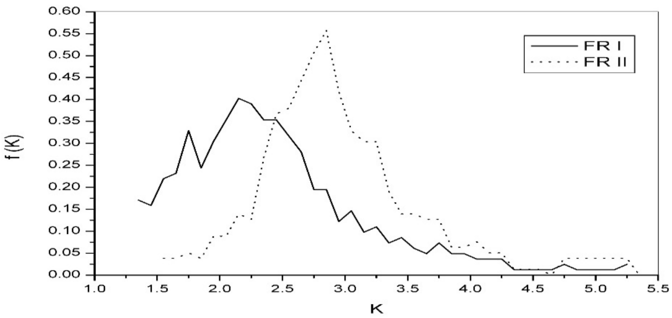

Figure 12. The distribution functions of the parameter K (using 82 FRI radio sources and 79 FRII radio sources).

These figures show that the peak of the distribution of FRII radio sources is at about K $\approx$ 3, while for the FRI sources the peak is at roughly K $\approx$ 2 that is, the FRII radio sources are, on the average, more elongated than the FRI sources. We believe that another important difference between the distributions of FRI and FRII extragalactic radio sources is that the FRI distribution has two peaks.

doi: doi.org/10.52526/25792776-2021.68.2-447

Acknowledgements

The work was supported by the Science Committee of RA, in the frames of the research project No. 21AG-1C053 “Revelation of the early stages of galaxy evolution by means of multiwavelength study of active galaxies”.

References

Andreasyan R. R., 1983, Astrophysics, 19, 245

Andreasyan R. R., 1984, Astrophysics, 21, 409

Andreasyan R. R., 1985, Astrophysics, 23, 404

Andreasyan R. R., Makarov A. N., 1988, Astrophysics, 28, 247

Andreasyan R. R., Makarov A. N., 1989a, Astrophysics, 30, 101

Andreasyan R. R., Makarov A. N., 1989b, Astrophysics, 31, 560

Andreasyan R. R., Sol H., 1999, Astrophysics, 42, 275

Andreasyan R. R., Sol H., 2000, Astrophysics, 43, 413

Andreasyan R. R., Appl S., Sol H., 2002, Astrophysics, 45, 198

Andreasyan R. R., Balayan S. K., Movsesyan V. H., 2011, Astrophysics, 54, 177

Andreasyan R. R., Hovhannisyan M. A., Paronyan G. M., Abrahamyan H. V., 2013, Astrophysics, 56, 382

Andreasyan R. R., Mikhailov E. A., Andreasyan H. R., 2020, Astronomy Reports, 64, 189

Fanaroff B. L., Riley J. M., 1974, MNRAS, 167, 31

Fermi E., 1949, PhysRev, 75, 1169

Communications of BAO, Vol. 68, Issue 2, 2021, pp. 478-483

Variability study of the FBS M giants

K. S. Gigoyan *[1] and G. R. Kostandyan †[1]

[1]V .A. Ambartsumian Byurakan Astrophysical Observatory, Armenia

Abstract

We study in this paper variability of the late-type M giants found in the First Byurakan Survey (FBS) spectroscopic data base. We used phase dependent light – curves from large sky area variability data bases such as Catalina Sky Survey (CSS) and All-Sky Automated Survey for Supernovae (ASAS-SN). We used also the distance information derived from Gaia EDR3 to construct the Galactic distribution of the M – type giants from the second edition of the FBS Late-Type Stars catalogue including various kinds of long period variables.

Keywords: *Late – type stars: Astronomical data bases-Variability*

1. Introduction

The study of variable stars is one of the most popular and dynamic areas of the modern astronomical research. Variability is a property of most stars, and as such it has a great deal to contribute to our understanding of them. It provides researchers with many additional and important parameters (periods, amplitudes, etc.) which are not available for non – variable stars. These important physical parameters can be used to deduce characteristics of the stars. The study of variability also allows us to directly observe changes in the stars: both the rapid and sometimes violent changes associated especially with stellar birth and death, and also the slow changes associated with normal stellar evolution. An overview of variable stars, including an introduction to variable stars in general, the techniques for discovering and many-sided studying variable stars, and description of the main types of variable stars are presented in more detail in the book by Percy (2007).

Determination of the correct classes of variables can be very important for studies of stellar populations. Some types of variable stars, such as RR Lyrae stars and Cepheids, are an excellent tool for studying our Galaxy. Being nearly standard candles (as distance indicators) and being intrinsically bright, they are a particularly suitable tracer of Galactic structure (Sesar et al., 2007, Tammann et al., 2003, 2008). Long period variables (LPV, $\Delta V > 2.5$ mag., or Miras), which are Asymptotic Giant Branch (AGB) stars, are also very important distance indicators for old and intermediate age populations (Whitelock et al., 2008).

The First Byurakan Spectral Sky Survey (henceforth FBS) low-resolution spectral plates have been used long period to search and study faint late M – type and C -type (carbob) stars (Late-Type Stars, LTSs) at high galactic latitudes. This objective-prism survey was carried out by Markarian and associates (Markarian et al., 1989) over the 1965 – 1980 period using the 1 m Schmidt telescope of the Byurakan Astrophysical Observatory (BAO, Armenia). The FBS survey covers total of 17000 deg^2 segmented in 24 parallel zones (see (Markarian et al., 1989)). Low-resolution photographic plates were obtained using 1.5^o objective-prism giving a reciprocal dispersion of 1800 Å/mm near Hγ throughout a useful field of 4^o×4^o. During the observations, various Kodak emulsions were used (IIF, IIAF, IIaF and 103aF) providing a 3400 – 6900 Å spectral range with a wide gap at 5300 Å. The FBS original goal was to identify objects with strong UV-excess in a region set by $\delta >$ -15^o and IbI > 15^o.

*kgigoyan@bao.sci.am
†kgayane@gmail.com

doi: doi.org/10.52526/25792776-2021.68.2-478

All FBS plates have been digitized, resulting in the creation of the Digitized First Byurakan Survey (DFBS) data base (Mickaelian et al., 2007). Its images and spectra are available on the DFBS web portal in Trieste (Italy)(accessed via https:// ia2-byurakan.oats.inaf.it/). All DFBS plates ($\sim$ 2000) were analyzed for LTSs. The second version of the "Revised And Updated Catalogue of the First Byurakan Survey of Late-Type Stars", containing data for 1471 M -and C-stars (130 C-type stars, 241 M dwarfs, and 1100 M -type giants) was generated (Gigoyan et al., 2019). Moderate-resolution CCD spectra were obtained for a large fraction of the FBS LTSs at different epochs and with various telescopes (Gigoyan et al., 2019).

2. Variability study of the FBS M giants

To determine the variability types of the FBS M – giants, we exploit data from two primary sources, namely the Catalina Sky Survey (CSS, second public data release CSDR2, accessed via http://nesssi.cacr.caltech.edu/DataRelease/) and the All – Sky Automated Survey for Supernovae (ASAS-SN, accessed via https://asas-sn.osu.edu/variables/, Jayasinghe et al. (2018), Kochanek et al. (2017), Shappee et al. (2014)). The CSS comprises two main parts surveying the Northern (Drake et al., 2014) and Southern (Drake et al., 2017) sky, respectively. Both surveys were analyzed by the Catalina Real-Type Transient Survey (CRTS) in search for optical transient ($V < 21.5$ mag.) phenomena. The ASAS-SN project is an all-sky optical monitoring to a photometric depth $V \leq 17.0$ mag. providing variability classification. Consequently, ASAS-SN was used as the primary source for attributing variability types, periods, and amplitudes to the FBS M-giants. For the some amounts of the objects missing in the ASAS-SN data base, variability parameters were determined from CSDR2 light curves using the VStar – data visualization and analysis tool (online at http://www.aavso.org/, Benn (2012)).

Our final sample consists of 690 SR (Semi – Regular) – type, 300 L – type (irregular) and 110 Mira – type variables.

In Figure1 presented ASAS-SN phase dependence light curves for objects FBS 1808+313 and FBS 2023+029, classified consequently as a Mira -type and Semi-Regular (SR) variables.

Figure 2 presents CSS phase dependence light curve for M giant FBS 2349+181.

Figure 3 presents the distribution of periods for 110 FBS M – type Mira – variables.

Figure 4 present Galactic distribution of the FBS M giants. We used the distance information from early installment of the third Gaia data release (Gaia EDR3) by Bailer-Jones et al. (2021), CDS VizieR Catalogue I/352/gedr3dis).

3. Discussion and conclusion

In this paper we explored the sample of 1100 M -giants from the second edition of the FBS LTS catalogue various kind of long period variables. For this study, we cross-correlated our sample with the Catalina Sky Survey (CSS) and All-Sky Automated Survey for Supernovae (ASAS-SN). These two large sky - area data bases allowed to characterize more detail the variability nature of M giants. Most of our FBS M – giants are found at typical distances of 1 kpc above or below the Galactic plane. No difference between Miras and SRVs has been found. Many-sided investigations based on modern optical and all-sky infrared astronomical data bases will allow to construct the spectral energy distribution (SED) and estimate important physical parameters for them. An analysis of the multiwavelength properties is now being carried out and the results will appear soon for all FBS M giants.

References

Bailer-Jones C. A. L., Rybizki J., Fouesneau M., Demleitner M., Andrae R., 2021, , 161, 147

Benn D., 2012, , 40, 852

doi: doi.org/10.52526/25792776-2021.68.2-478

Drake A. J., et al., 2014, , 213, 9

Drake A. J., et al., 2017, , 469, 3688

Gigoyan K. S., Mickaelian A. M., Kostandyan G. R., 2019, MNRAS, 489, 2030

Jayasinghe T., et al., 2018, , 477, 3145

Kochanek C. S., et al., 2017, , 129, 104502

Markarian B. E., Lipovetsky V. A., Stepanian J. A., Erastova L. K., Shapovalova A. I., 1989, Soobshcheniya Spetsial'noj Astrofizicheskoj Observatorii, 62, 5

Mickaelian A. M., et al., 2007, , 464, 1177

Percy J., 2007, Understanding Variable Stars. Cambridge University Press, https://books.google.am/books?id=GQzCDQI3YP4C

Sesar B., et al., 2007, , 134, 2236

Shappee B. J., Prieto J. L., Grupe D., Kochanek C. S., Stanek K. Z.and Walker Z., Yoon Y., 2014, , 788, 48

Tammann G. A., Sandage A., Reindl B., 2003, , 404, 423

Tammann G. A., Sandage A., Reindl B., 2008, , 679, 52

Whitelock P. A., Feast M. W., Van Leeuwen F., 2008, , 386, 313

doi: doi.org/10.52526/25792776-2021.68.2-478

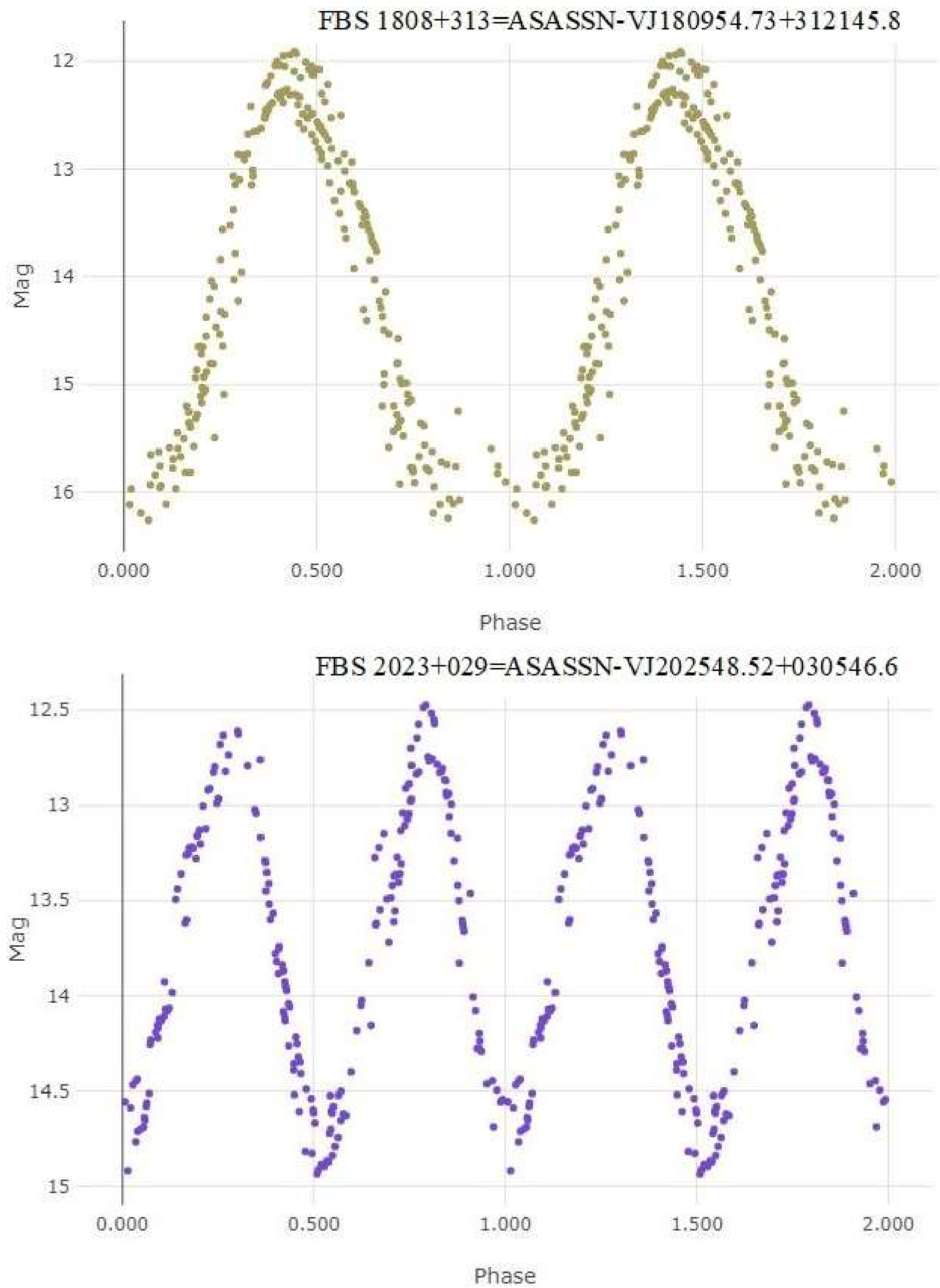

Figure 1. Phased ASAS-SN light curves for two M -giants, FBS 1808+313=ASASSN-VJ180954.73+312145.8, classified as a Mira-type variable (Vmean = 13.98 mag., ampl. = 3,82 mag., P = 240.422 days) and for FBS 2023+029=ASAS-SN-VJ202548.52+030546.6, classified as a SR variable (Vmean = 13.74 mag., ampl.= 2.21 mag., P = 619.654 days).

doi: doi.org/10.52526/25792776-2021.68.2-478

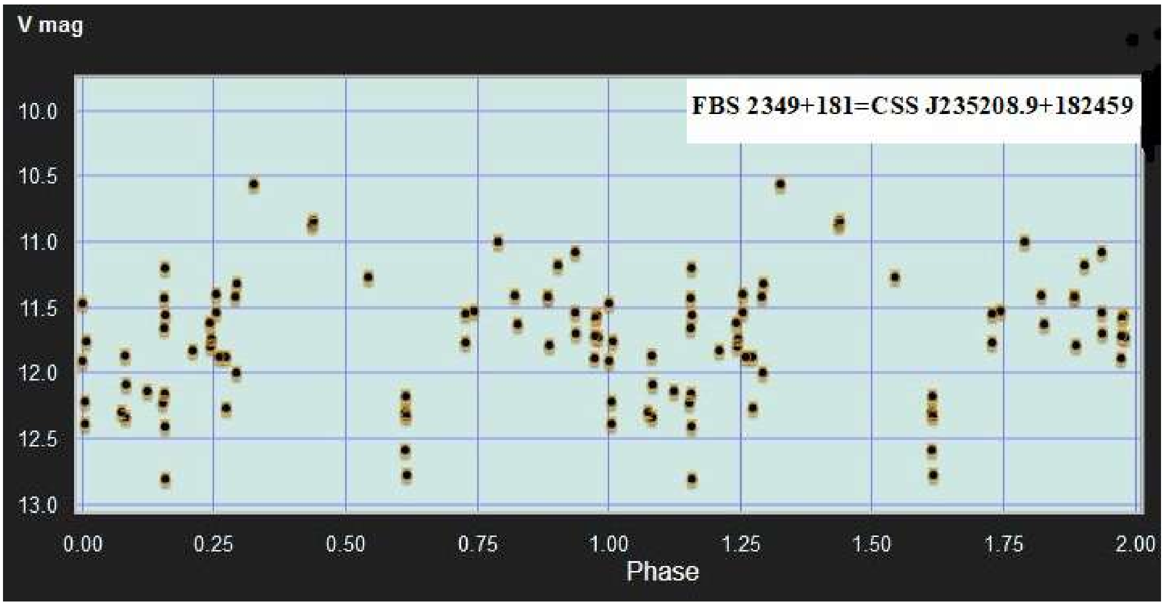

Figure 2. CSS phase dependence light curve for FBS 2349+181=CSS J235208.0+182459. This object classified as a irregular (L) variable.

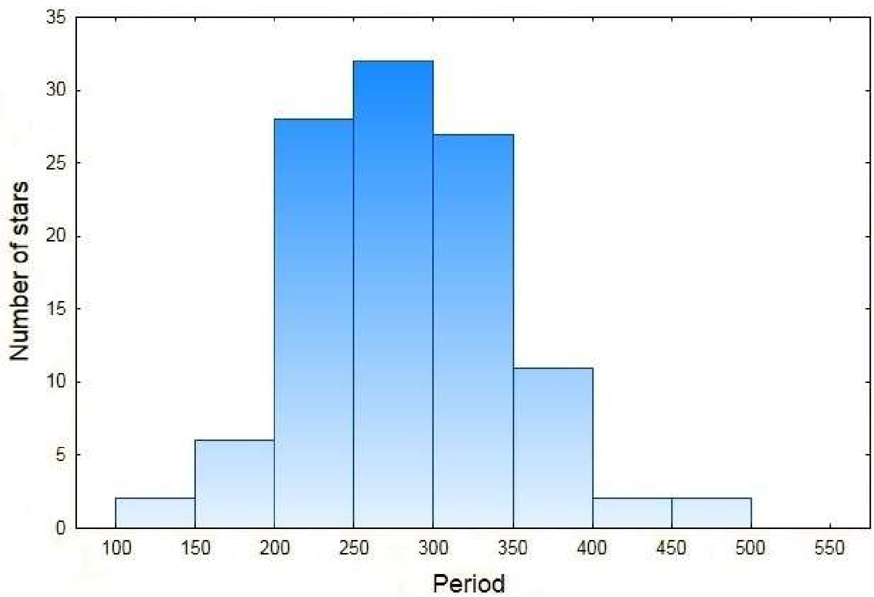

Figure 3. Period distribution of the 110 FBS M – type Mira variables based on ASAS-SN periods.

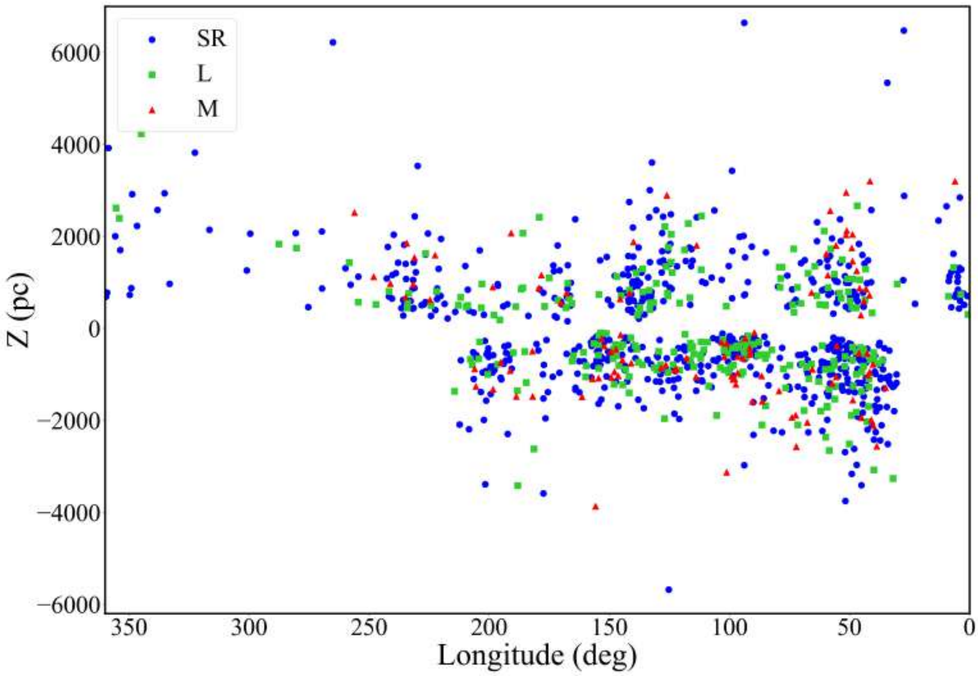

Figure 4. Galactic distribution of the FBS M giants. Symbols are: filled blue squares-SR-variables, filled green squares-irregular (L) variables, and red triangles-Mira-type variables. .

doi: doi.org/10.52526/25792776-2021.68.2-478

Communications of BAO, Vol. 68, Issue 2, 2021, pp. 484-489

Testing the evolution of the absolute magnitude of type Ia supernovae and cosmological parameters

Mahtessian A.P.*[1], G.S. Karapetian , M.A. Hovhannisyan [2], V.H. Movsisyan , and L.A. Mahtessian [2]

[1]NAS RA V. Ambartsumian Byurakan Astrophysical Observatory (BAO), Armenia
[2]NAS RA Institute of Applied Problems of Physics, Armenia

Abstract

Computer simulations show that, in estimating cosmological parameters, the best agreement between theory and observation is achieved by assuming the evolution of the absolute magnitude of type Ia supernovae. This requires only 0.3m of evolution for the time corresponding to z = 1. This leads to zero density of hidden energy in the Universe.

Keywords: *cosmological models - supernovae - dark energy - dark matter: general*

1. Introduction

One of the tasks in observant cosmology is to test cosmological hypotheses. Now, the most common hypothesis the Lambda CDM model, or the Friedman model. Cosmological models allow us to estimate the distance of distant objects in the universe. To test these models, you need distance standards. Such standards are considered type Ia supernovae.

To determine the distance using a simple formula:

$$M = m - 5lgD_L - 25, \tag{1}$$

where m is the apparent magnitude, M is the absolute magnitude, and D_L is the luminosity distance. In the flat Friedman Universe, the luminosity distance of an object at a given z is estimated by the following formula (Carroll et al., 1992, Weinberg, 2008) :

$$D_L = \frac{C(1+z)}{H_0}\int_0^z dz\left[(1+z)^2(1+\Omega_M z) - z(2+z)\Omega_\Lambda\right]^{-1/2} \tag{2}$$

Where $\Omega_\Lambda + \Omega_M = 1$. Ω_Λ is the fraction of dark or hidden energy and Ω_M is the mass fraction (hidden + visible mass).

We need one more formula for the model of the Universe with a zero cosmological constant (Ω_Λ=0). In this case, Mattig (1958) precisely solved the Einstein field equations and obtained the following relation:

$$D_L = \frac{C}{H_0 q_0^2}\left[q_0 z + (q_0 - 1)\left(\sqrt{1+2q_0 z} - 1\right)\right] \tag{3}$$

Where q_0 is the deceleration parameter, in this case:

$$q_0 = \frac{\Omega_M}{2}$$

In the case of a flat universe

$$q_0 = \frac{\Omega_M}{2} - \Omega_\Lambda$$

When calculating the distance according to the formula $M = m - 5lgD_L - 25$ it is necessary to accurately assess the value of the apparent magnitude of the object (taking into account galactic absorption, K-correction, spectral region, etc.). The absolute magnitude must be known either from theoretical approaches or from empirical dependencies.

*amahtes@bao.sci.am, Corresponding author

doi: doi.org/10.52526/25792776-2021.68.2-484

2. Results

2.1. The case of the distance-independent absolute magnitude of supernovae SNe Ia

In Figure 1 shows the Hubble diagram for the Union2 sample used by Amanullah et al. (2010). The sample consists of 557 stars, the observational data of which are carefully processed. We used exactly the same stars with the same observational data, i.e., we did not revise anything in the observational aspect. For the best approximation of the observational data, the authors obtained

$$\Omega_\Lambda = 0.73, \Omega_M = 0.27$$

Now let's see this result, how much is consistent with the assumption that type Ia supernovae are distance indicators. In Figure 2 shows the dependence of the absolute magnitude of these stars on the redshift for the obtained model parameters.

As you can see there is a clear dependence.

Now we find the value of these parameters at which the absolute magnitude of these stars does not depend on redshift.

In Figure 3 shows the dependence of the absolute magnitude of these stars on the redshift for the case $\Omega_\Lambda = 0.42, \Omega_M = 0.58$

Apparently there are no dependencies.

Now back to the Hubble diagram. It is clear from the diagram that the sum of the squared deviations of the observational data from the theoretical curve is clearly less for the case $\Omega_\Lambda = 0.42, \Omega_M = 0.58$ (Chi2 = 83.96), compared with the case $\Omega_\Lambda = 0.73, \Omega_M = 0.27$ (Chi2 = 90.37) . (This means that the authors did not conduct the most probable curve within the framework of the model under discussion.)

On the Hubble diagram, a model of the Universe with a zero cosmological constant is also discussed. Approximation gives $q_0 = 0.184$. Let's see what the diagram of the dependence of the absolute magnitude on the redshift for this model will give (Fig. 4).

It turns out that there is also no dependency between these quantities. Also, a smaller standard deviation is obtained than for the model with $\Omega_\Lambda = 0.73, \Omega_M = 0.27$.

Thus, we can say that the study of the dependence of the absolute magnitude of type Ia supernovae (also of any objects that are considered distance indicators) on redshift within the framework of the model under discussion is very important. This diagram and the Hubble c diagram complement each other and give consistent results. A comparison of two models (the Friedman's model of a flat universe and the model of the Universe with a zero cosmological constant) based on different subsamples of supernova stars from the Union (Kowalski et al., 2008) and Union2 (Amanullah et al., 2010) compilations using our absolute magnitude test was carried out in detail by Mahtessian et al. (2020).

Thus, assuming that the absolute magnitude of the supernova SNe Ia does not depend on distance (i.e. does not evolve), we get:

1. In the flat Universe of Friedman, the widespread opinion about the prevalence of hidden energy over mass is rejected. The maximum possible fraction of hidden energy is 0.5 (Mahtessian et al., 2020).

2. The model of the Universe with a zero cosmological constant at least describes the Universe no worse than the generally accepted Friedmann model of a flat Universe with a positive cosmological constant.

2.2. The case of the distance-depending absolute magnitude of supernovae SNe Ia

Let us assume that the absolute magnitude of SNe Ia supernovae is not constant, but changes with distance (there is an evolution of supernova luminosities). Let's see how the agreement between the observed and theoretical data improves? We will assume that the dependence on the distance of the absolute magnitude of supernovae is linear, i.e.

$$M = M_0 + \epsilon_c z$$

Where $M_0 = M(z = 0)$.

We will study the SNe Ia Union2 sample (Amanullah et al. 2010). Computer simulation data are given in Tables 1 and 2. In the first case (Table 1), the case is considered without assuming the evolution of the absolute magnitude of supernovae. And in the second (Table 2) with the assumption of the evolution of the absolute magnitude of supernovae.

It can be seen from Tables 1 and 2 that under the assumption of the evolution of supernovae Ia, the observational data agree better with the theory (Chi2 is smaller) than under the assumption of a constant

doi: doi.org/10.52526/25792776-2021.68.2-484

absolute magnitude. In this case, the density of the hidden energy turns out to be 0, that is, the Universe consists only of gravitational matter. The same is obtained for the model of the Universe with zero cosmological constant (Tables 3 and 4).

In the framework of the ΛCDM model, in the case of a flat universe, the influence of the absolute magnitude M of type Ia supernovae on cosmological parameters has also been investigated. In particular, it was found that a change in this value by only 0.4^m leads to a change in the parameters from $\Omega_\Lambda = 0.7$ and $\Omega_M = 0.3$ to $\Omega_\Lambda = 0$ and $\Omega_M = 1$.

According to numerous studies, M_0 fluctuates in a very wide range from -18 to -19.5. It is clear that with such a strong dependence of Ω_Λ and Ω_M on M, this interval is very wide. This means that a correct estimate of the absolute magnitude M of type Ia supernovae is extremely important for estimating cosmological parameters.

As seen above, for the best agreement between the observational data and theory, the evolution of the absolute magnitudes of type Ia supernovae is required by only 0.3m at a distance of z = 1. (Such a value of the evolution of the absolute magnitudes of supernovae is consistent with many observational results (for example, Kang et al., 2020), which is much less than the value of this interval. In this case, it turns out that the density of hidden energy in the universe is zero.

3. Conclusion

Thus, the universe is mainly composed of gravitational matter. Space is flat - Euclidean. The existence of hidden energy is rejected.

References

Amanullah R., et al., 2010, Astrophys. J. , 716, 712

Carroll S. M., Press W. H., Turner E. L., 1992, Ann. Rev. Astron. Astrophys. , 30, 499

Hubble E., 1929, Proceedings of the National Academy of Science, 15, 168

Kang J.-G., Gong Y., Cheng G., Chen X., 2020, Research in Astronomy and Astrophysics, 20, 055

Kowalski M., et al., 2008, Astrophys. J. , 686, 749

Mahtessian A. P., Karapetian G. S., Movsisyan V. H., Mahtessian L. A., 2020, Advances in Astrophysics, 5, 18

Mattig W., 1958, Astronomische Nachrichten, 284, 109

Perlmutter S., et al., 1999, Astrophys. J. , 517, 565

Riess A. G., et al., 1998, Astron. J. , 116, 1009

Sandage A., Tammann G. A., 1982, Astrophys. J. , 256, 339

Weinberg S., 2008, Cosmology, Oxford University Press

doi: doi.org/10.52526/25792776-2021.68.2-484

Table 1. The result of searching for the values of the parameters M_0, Ω_Λ, Ω_M for a Flat Universe ($\Omega_\Lambda+\Omega_M=1$) without assuming the evolution of the absolute magnitude of supernovae.

Parameter	Variable	Search range	Parameter search range	Chi^2	R^2
M_0	Yes	$-19.5 \div -18.0$	-18.903		
ϵ_c	No	0	0.000	83.74	0.9836
Ω_Λ	Yes	$0 \div 1$	0.397		
Ω_M	Yes	$0 \div 1$	0.603		

Table 2. The result of searching for the values of the parameters M_0, Ω_Λ, Ω_M for a Flat Universe ($\Omega_\Lambda+\Omega_M=1$) with assuming the evolution of the absolute magnitude of supernovae.

Parameter	Variable	Search range	Parameter search range	Chi^2	R^2
M_0	Yes	$-19.5 \div -18.0$	-18.875		
ϵ_c	Yes	$-1 \div 1$	0.304	83.23	0.9837
Ω_Λ	Yes	$0 \div 1$	0.000		
Ω_M	Yes	$0 \div 1$	1.000		

Table 3. The result of searching for the values of the parameters M_0, q_0 for a universe with zero cosmological constant without the assumption of the evolution of the absolute magnitude of supernovae.

Parameter	Variable	Search range	Parameter search range	Chi^2	R^2
M_0	Yes	$-19.5 \div -18.0$	-18.881		
ϵ_c	No	0	0.000	83.28	0.9837
q_0	Yes	$0 \div 0.5$	0.184		

Table 4. The result of searching for the values of the parameters M_0, q_0, ϵ_c for a universe with zero cosmological constant with the assumption of the evolution of the absolute magnitude of supernovae.

Parameter	Variable	Search range	Parameter search range	Chi^2	R^2
M_0	Yes	$-19.5 \div -18.0$	-18.875		
ϵ_c	Yes	$-1 \div 1$	0.304	83.23	0.9837
q_0	Yes	$0 \div 0.5$	0.500		

doi: doi.org/10.52526/25792776-2021.68.2-484

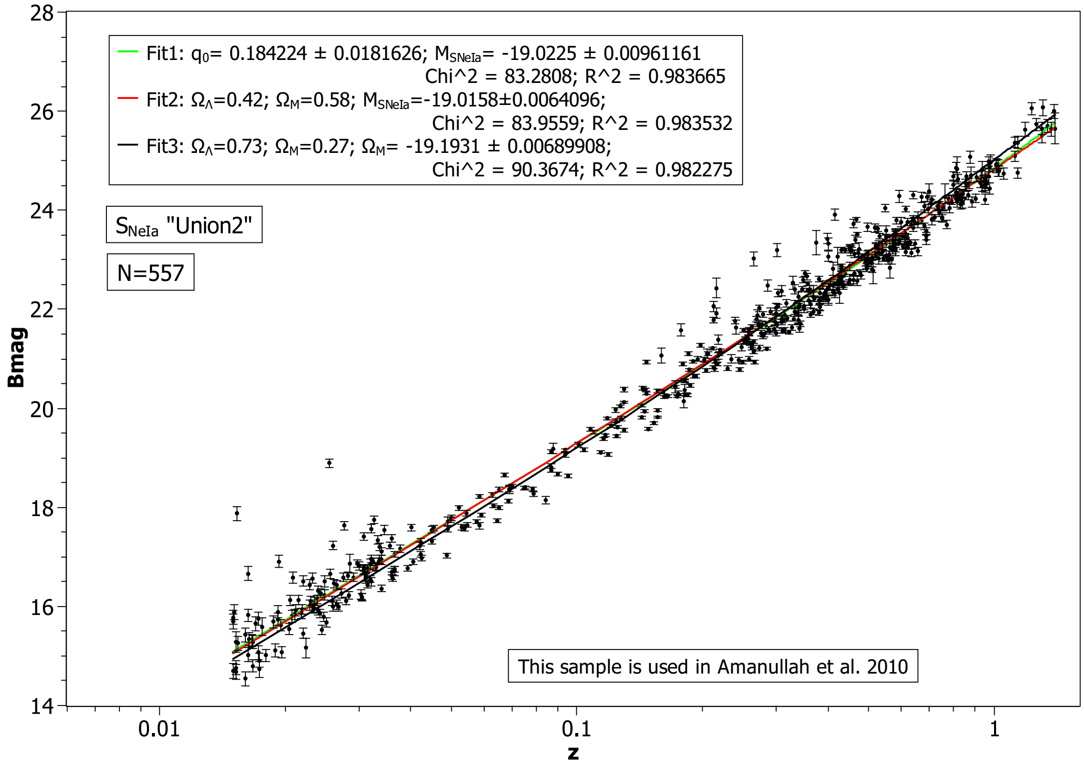

Figure 1. Hubble diagram for SNIa Amanullah et al. (2010) sample.

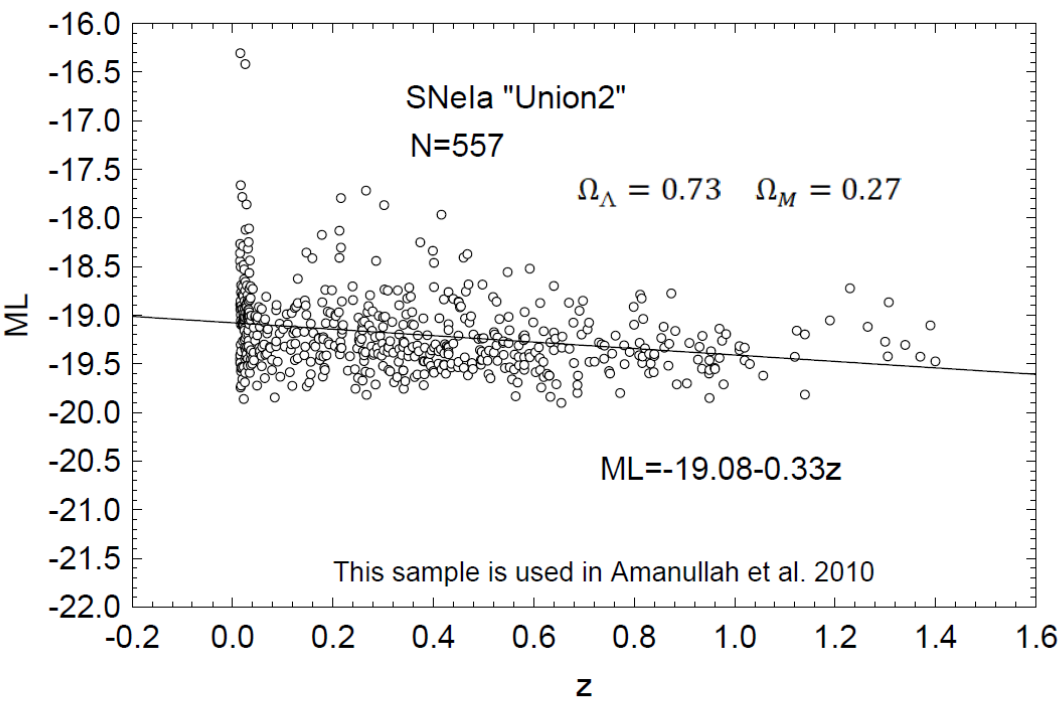

Figure 2. Absolute magnitude dependence on redshift forAmanullah et al. (2010) sample.

doi: doi.org/10.52526/25792776-2021.68.2-484

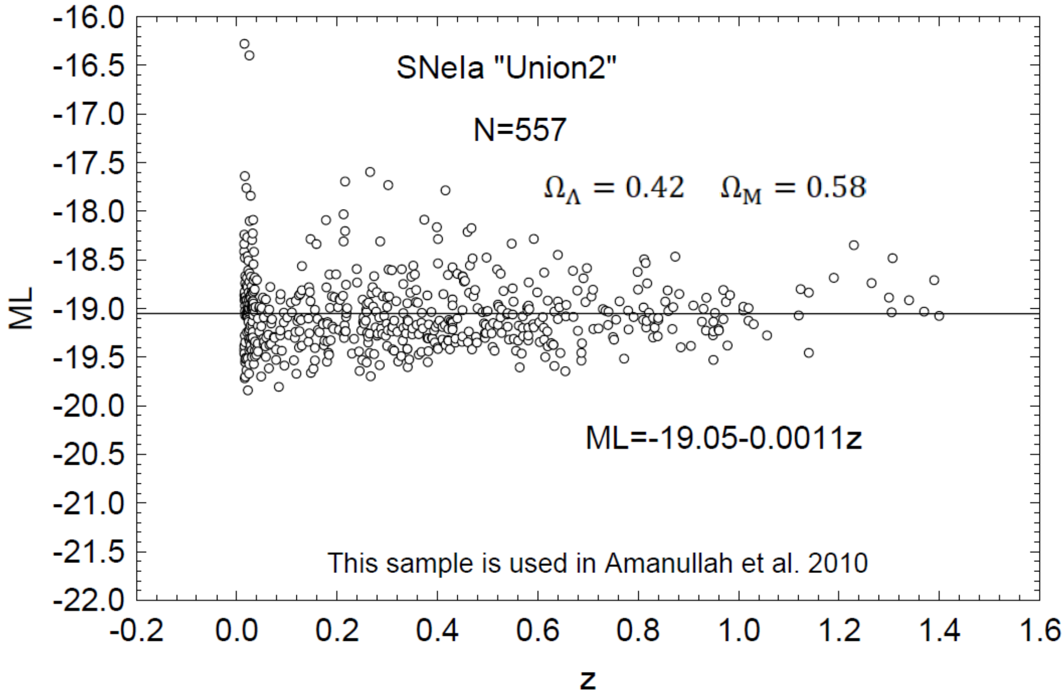

Figure 3. Absolute magnitude dependence on redshift for Amanullah et al. (2010) sample for the case $\Omega_\Lambda = 0.42, \Omega_M = 0.58$.

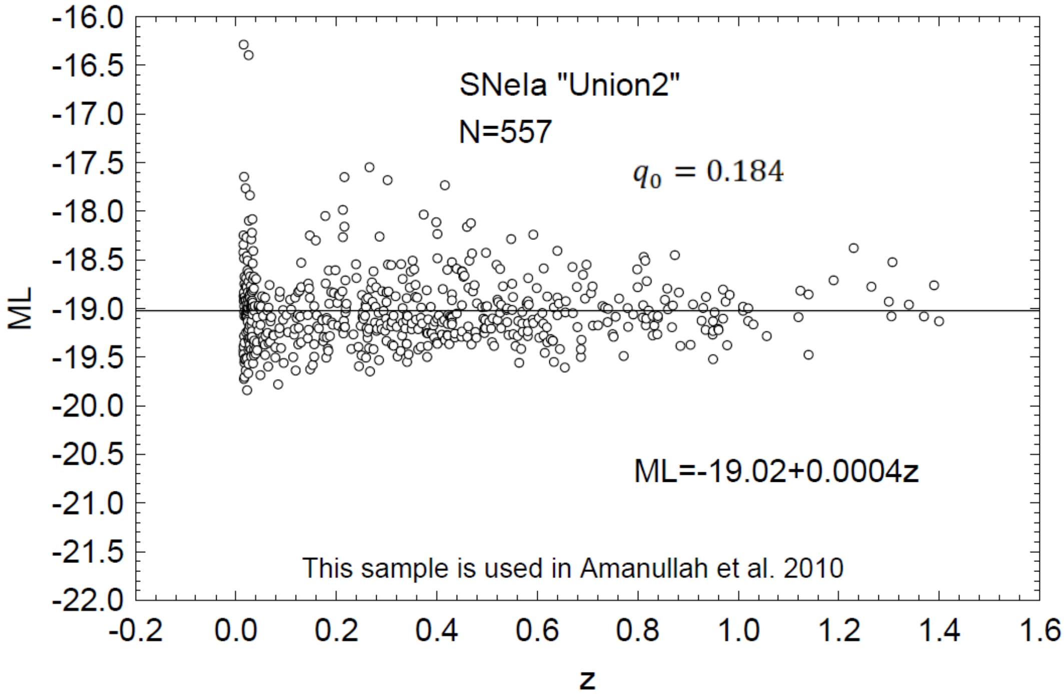

Figure 4. Absolute magnitude dependence on redshift for Amanullah et al. (2010) sample for a model of the Universe with a zero cosmological constant.

doi: doi.org/10.52526/25792776-2021.68.2-484

No-z model: results and perspectives for accretion discs

E.A. Mikhailov *[1,2] and M.V. Pashentseva†[1]

[1]M.V.Lomonosov Moscow State University, Moscow, Russia
[2]P.N.Lebedev Physical Institute, Moscow, Russia

Abstract

Accretion discs surround different compact astrophysical objects such as black holes, neutron stars and white dwarfs. Also they are situated in systems of variable stars and near the galaxy center. Magnetic fields play an important role in evolution and hydrodynamics of the accretion discs: for example, they can describe such processes as the transition of the angular momentum. There are different approaches to explain the magnetic fields, but most interesting of them are connected with dynamo generation. As for disc, it is quite useful to take no-z approximation which has been developed for galactic discs to solve the dynamo equations. It takes into account that the disc is quite thin, and we can solve the equations only for two plane components of the field. Here we describe the time dependence of the magnetic field for different distances from the center of the disc. Also we compare the results with another approaches which take into account more complicated field structure.

Keywords: *accretion discs, dynamo, magnetic field*

1. Introduction

The accretion discs are situated near different compact objects in space. First of all, we should mention black holes, white dwarfs and neutron stars. Usually such discs are quite thin and rotate with keplerian law: their angular velocity is proportional to $r^{-3/2}$, where r is the distance from the center. Even pioneer works connected with accretion discs supposed that they have large-scale magnetic field Shakura & Sunyaev (1973). They can describe a lot of hydrodynamical processes. For example, they can explain transtion of the angular momentum. Also they are closely connected with generation of jets Balbus & Hawley (1991) and hydrodynamical winds Pudritz & Norman (1986). Another important examples of the accretion discs are associated with central parts of the galaxies: now there are interesting results about the Faraday rotation measurements in the central part of the M87 galaxy Kravchenko et al. (2020). It can describe the magnetic field in the accretion disc surrounding the central black hole in this object. The next important example is connected with the accretion discs which are associated with eruptive stars Andreasyan et al. (2021).

There are different approaches which try to describe the mechanism of generating these magnetic fields. First of all, some authors try to explain the field evolution using the transport of accreting matter Lubow et al. (1994). Unfortunately, it cannot describe the transition of the regular field structures because of the dissipative effects and mixing of the medium. Another important works describe the field generation using the interaction between the disc and the central object. However, Brandenburg with co-authors showed that the magnetic field in the accretion discs are connected with the dynamo action Brandenburg & Donner (1994).

The dynamo mechanism is connected with two basic effects. First of all, it is based on differential rotation which shows changing angular velocity of the object. Then, the dynamo mechanism contains alpha-effect which describes the helicity of the turbulent motions: the vorticity has non-zero average projection on the velocity vector. Both of these effects produce the magnetic field, and they compete with turbulent diffusion which tries to destroy the magnetic field. So the magnetic field generation is a threshold effect, and it can grow only for some special cases, else it decays Sokoloff (2015).

The magnetic field generation in dynamo theory is described by the Steenbeck – Krause – Rädler effect. It is obtained by averaging the magnetohydrodynamics equations on distances associated with turbulent

*ea.mikhajlov@physics.msu.ru, Corresponding author
†pashentseva.mv17@physics.msu.ru

doi: doi.org/10.52526/25792776-2021.68.2-490

lengthscales. They are quite difficult to be solved, and there are different models which take into account the geometrical shape of the astrophysical object. For example, for the Sun we can take the Parker dynamo model Parker (1955). As for accretion discs, we can take the no-z model which has been developed for galactic discs Moss (1995). It takes into account that the disc is quite thin. So, the plane components of the magnetic field are much larger than the vertical one. It leads us to neglecting the z-part of the magnetic field and reduce its z-derivative by the solenoidality condition. As for the z-dependence of the magnetic field components a cosine law is taken, so second z-derivatives of the main magnetic fields can be changed by the algebraic expressions. This approach is widely used for modeling magnetic fields of galaxies and give an opportunity to find fields in different cases Andreasyan et al. (2020). The accretion discs also are quite thin and we can take there no-z approximation, too. This approach was firstly used by Moss et al. (2016). It gave quite important results, but it was a problem connected with the maximum value of the field, which was larger than the equipartition value. (So, the electromagnetic force is too much and can destroy the structure of motions.) This problem was solved by Boneva et al Boneva et al. (2021), and it was shown that the no-z approximation is quite useful for accretion discs.

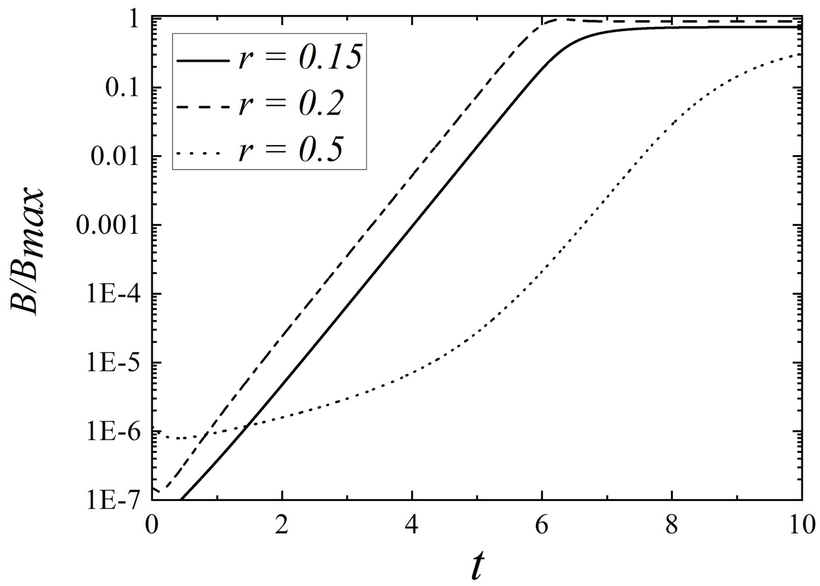

Figure 1. Magnetic field for different r obtained by no-z model.

It is also necessary to take into accont that for some cases the thickness of the disc can be quite comparable with its radius. So for this case it is quite difficult to apply the no-z approximation: we should use more difficult models for the field structure. For example, we can take the rz-model which uses the magnetic field as a combination of the azimuthal component and the rotor of azimuthal part of the vector potential of the magnetic field. This model was firstly developed as a torus dynamo model, which can be taken for outer rings of galaxies, where the width is comparable with thickness Mikhalov (2018). After that it was taken for main part of the galaxy Mikhalov (2021). Also we can take this model for the magnetic field of the accretion discs which can be very useful for the objects which have thickness comparable with the radius of the object.

In these paper we describe the magnetic field evolution using these two different models and compare their results.

2. Basic equations

The magnetic field evolution described by the dynamo theory is connected with the Steenbeck – Krause – Rädler equation Krause & Rädler (1980):

$$\frac{\partial \vec{B}}{\partial t} = \nabla \times \left(\alpha \vec{B}\right) + \nabla \times \left(\vec{V} \times \vec{B}\right) + \eta \nabla^2 \vec{B};$$

doi: doi.org/10.52526/25792776-2021.68.2-490

where $\vec{B}$ is the magnetic field induction, η is the turbulent diffusivity coefficient, $\vec{V}$ is the large-scale velocity and α characterizes the alpha-effect.

For large-scale velocity we can assume that $\vec{V} = r\Omega\vec{e}_\varphi$. As for the angular velocity we shall take the keplerian rotation law Shakura & Sunyaev (1973):

$$\Omega = \frac{\sqrt{GM}}{r^{3/2}};$$

where M is the mass of the central object.

The alpha-effect characterizes the helicity of the turbulent motions Krause & Rädler (1980):

$$\alpha = -\frac{\tau}{3} < \vec{v} \cdot \nabla \times \vec{v} >$$

where $\vec{v}$ is the small-scale velocity and τ is the timescale of the turbulence. As for disc objects it can be shown that:

$$\alpha \approx \frac{\Omega l^2}{h^2} \sin\left(\frac{\pi z}{2h}\right);$$

where l is the lengthscale of the turbulence.

The magnetic field cannot grow infinitely, so it is necessary to take the nonlinear saturation of the alpha-effect Boneva et al. (2021):

$$\alpha \sim 1 - \frac{B^2}{B^2_{max}(r)},$$

where $B_{max}(r)$ is the so-called equipartition value which shows the case when the kinetic energy of the turbulent motion is the same as the energy of the magnetic field.

This equation is quite difficult to be solved in 3D case. It needs quite large computational resources, and it is also difficult to make any analytical approximations. So, it is necessary to take the 2D-models which give us an opportunity to simplify the problem.

3. No-z model

One of the most important models which has been developed for thin discs is the no-z approximation Moss (1995). It takes the following approximation for the magnetic field:

$$B_{r,\varphi}(r,z,t) = B_{r,\varphi}(r,0,t)\cos\left(\frac{\pi z}{2h}\right).$$

So the magnetic field evolution is described by the equations Moss (1995):

$$\frac{\partial B_r}{\partial t} = -R_\alpha B_\varphi \left(1 - \frac{B^2}{B^2_{max}(r)}\right) - \frac{\pi^2 B_r}{4} + \lambda^2 \left(\frac{\partial^2 B_r}{\partial r^2} + \frac{1}{r}\frac{\partial B_r}{\partial r} - \frac{B_r}{r^2}\right);$$

$$\frac{\partial B_\varphi}{\partial t} = -\frac{3}{2r^{3/2}} R_\omega B_r - \frac{\pi^2 B_\varphi}{4} + \lambda^2 \left(\frac{\partial^2 B_\varphi}{\partial r^2} + \frac{1}{r}\frac{\partial B_\varphi}{\partial r} - \frac{B_\varphi}{r^2}\right).$$

Here time is measured in units of $\frac{h^2}{\eta}$ and distances are measured in units of radius of the disc. R_α characterizes the alpha-effect, R_ω shows the differential rotation and λ is connected with dissipation in the disc plane.

The results of the magnetic field modelling is shown on Figure 1. We describe the field evolution for different distances from the center of the discs.

4. Model with z-dependence

If we take into account more complicated z-structure of the field, the magnetic field can be described as:

$$\vec{B} = B\vec{e}_\varphi + \nabla \times (A\vec{e}_\varphi)$$

The field equations will be Mikhalov (2021):

doi: doi.org/10.52526/25792776-2021.68.2-490

$$\frac{\partial A}{\partial t} = -R_\alpha z \frac{\partial B}{\partial z}\left(1 - \frac{B^2}{B^2_{max}(r)}\right) + \lambda^2 \left(\frac{\partial^2 A}{\partial z^2} + \frac{\partial^2 A}{\partial r^2} + \frac{1}{r}\frac{\partial A}{\partial r} - \frac{A}{r^2}\right);$$
$$\frac{\partial B}{\partial t} = -\frac{3}{2r^{3/2}} R_\omega \frac{\partial A}{\partial z} + \lambda^2 \left(\frac{\partial^2 B}{\partial z^2} + \frac{\partial^2 B}{\partial r^2} + \frac{1}{r}\frac{\partial B}{\partial r} - \frac{B}{r^2}\right).$$

The results for this case are shown on Figure 2.

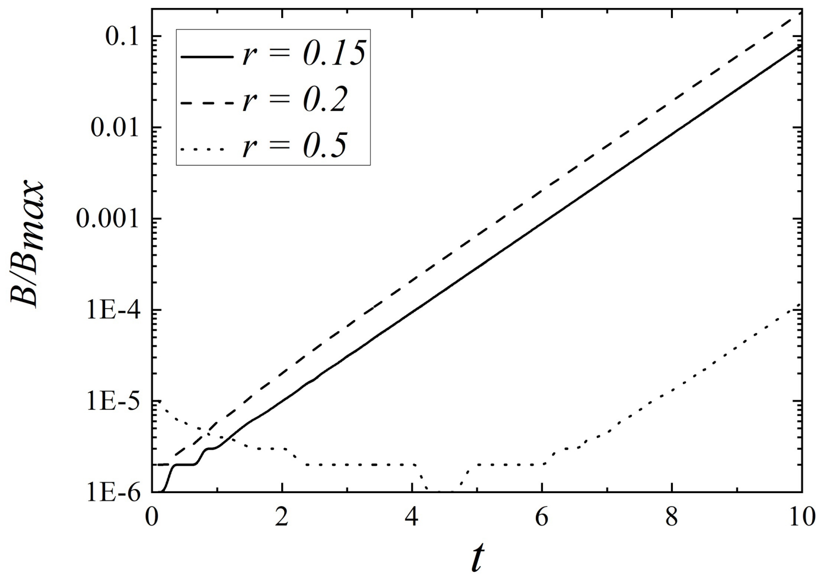

Figure 2. Magnetic field for different r obtained by rz-model.

5. Conclusions

We have studied the magnetic field evolution using the no-z model and the rz-approximation. The typical rate of the magnetic field growth differs, but basic features are the same. Also we have shown that the magnetic field can be generated by the dynamo model.

6. References

References

Andreasyan R. R., Mikhailov E. A., Andreasyan H. R., 2020, Asronomy Reports, 64, 189

Andreasyan H. R., Magakian T. Y., Movsessian T. A., Moiseev A. V., 2021, Astrophysics, 64, 187

Balbus S. A., Hawley J. F., 1991, Astrophysical Journal, 376, 214

Boneva D., Mikhalov E., Pashentseva M., Sokoloff D., 2021, Astronomy and Astrophysics, 652, A38

Brandenburg A., Donner K. J., 1994, MNRAS, 288, L29

Krause F., Rädler K. H., 1980, Mean-field magnetohydrodynamics and dynamo theory. Pergamon, Oxford

Kravchenko E., Giroletti M. F., Hada K., et al. 2020, Astronomy and Astrophysics, 637, L6

Lubow S. H., Papaloizou J. C. B., Pringle J. E., 1994, MNRAS, 267, 235

Mikhalov E. A., 2018, Astrophysics, 61, 147

Mikhalov E. A., 2021, Research in Astronomy and Astrophysics, 21, 056

Moss D., 1995, MNRAS, 191, 275

Moss D., Sokoloff D., Suleimanov V., 2016, Astronomy and Astrophysics, 588, A18

doi: doi.org/10.52526/25792776-2021.68.2-490

Parker E. N., 1955, Astrophysical Journal, 122, 293

Pudritz R. E., Norman C. A., 1986, Astrophysical Journal, 301, 571

Shakura N. I., Sunyaev R. A., 1973, Astronomy and Astrophysics, 500, 33

Sokoloff D. D., 2015, Physics-Uspekhi, 58, 601

doi: doi.org/10.52526/25792776-2021.68.2-490

Communications of BAO, Vol. 68, Issue 2, 2021, pp. 495-501

Proper motion of the spectrally selected structures in Herbig-Haro flows

T.A. Movsessian *and T.Yu. Magakyan †

Byurakan Astrophysical Observatory, Aragatsotn reg., Byurakan, 0213 Armenia

Abstract

We present some results of the investigations of proper motions of spectrally separated structures in the Herbig-Haro (HH) outflows with the aid of Fabry-Perot scanning interferometry. This project was started more than twenty years ago on the 2.6m telescope of Byurakan Observatory and afterwards was continued on 6m telescope (Russia). We describe the progress of research in the frames of this project and focus in more detail on the results of the latest observations of HH 83 outflow system.

The method of Fabry-Perot scanning interferometry allowed to reveal the morphology of high and low velocity structures not only inside the terminal working surfaces of the jets but also in their internal knots. As the great advance we consider the development of a methodology for measuring proper motions of already separated kinematical structures using observations in two epochs, which made it possible to reveal the physical nature of these structures.

Concerning the HH 83 collimated outflow it should be noted that our first observations of HH 83 revealed two structures in its working surface with strongly different radial velocities, and the second epoch data allowed to measure their proper motions. The proper motions of these structures are nearly equal, which points that they are physically connected and represents forward and reverse shock regions in the terminal working surface of HH 83.

Keywords: *Star formation, Herbig-Haro objects, jets and outflows*

1. Introduction and previous achievements

High proper motions (PM) of Herbig-Haro (HH) objects were discovered about 40 years ago. Orientation of PM vectors of HH objects, which represent shocked excitation regions, revealed the bipolar nature of high velocity flows, responsible for their formation (Herbig & Jones, 1981, Jones & Herbig, 1982). Further discoveries of highly collimated jets from young stellar objects indicated that HH objects actually are the brightest parts of these flows (Reipurth et al., 1986, 1993); in subsequent studies they usually are generically called HH jets and flows.

Further investigations of HH flows revealed their complex morphology. In particular, high and low excitation zones were separated by ground based and HST narrow band imagery (Hartigan et al., 2011, Reipurth et al., 1997) as well as by long-slit spectroscopy (Hartigan et al., 2011, Heathcote & Reipurth, 1992, Reipurth et al., 1997). High and low velocity components in the terminal working surfaces (WS) and inside the certain knots in the jets were found. By the methods of spectra-imagery full morphology and kinematics of these structures was revealed. Low radial velocity components appear as bow shape structures, while in high velocities the compact knots are detected (Hartigan et al., 2000, Movsessian et al. , 2000, Movsessian et al., 2009).

To clarify the physical nature of these two kinematical structures we decided to measure proper motions of these structures using two epoch of observations with scanning Fabry-Perot interferometer (FPI). Already the first attempt was very successful: two epoch study of HL Tau jet, based on the observations in 2001 and 2007, allowed to estimate the PM of spectrally separated structures in the jet. This method, probably for the first time applied to HH jets, demonstrated that the structural components inside the jet, divided by low and high radial velocity, have, nevertheless, very similar values of PM (Movsessian et al., 2012). This

*tigmov@bao.sci.am, Corresponding author
†tigmag@sci.am

doi: doi.org/10.52526/25792776-2021.68.2-495

important result was confirmed also for the components inside the FS Tau B jet system (Movsessian et al., 2019).

Generally speaking, inside the terminal WS (this is the common term for the regions, where supersonic flow slams directly into the undisturbed ambient medium: Reipurth & Bally 2001), as well as in the internal WS of jets knots, two principal shock structures form. They include a 'reverse shock', which decelerates the supersonic flow, and a 'forward shock', which accelerates the material with which it collides (e.g. Hartigan, 1989).

HH 83 represents a wiggling knotty jet emerging from IRAS 05311−0631 source. This source, being deeply embedded in a molecular cloud, is not visible in optical range, but it illuminates edges of a conical cavity, formed by the outflow (Reipurth, 1989). At the distance of 105 arcsec from the beginning of the jet, a bow shock structure was found, which is visible in Hα emission, but not in [SII] lines (Reipurth, 1989).

Our first observations of HH 83 with FPI revealed the separated structures with strongly different radial velocities in the terminal working surface (more than 250 km s^{-1}), as well as confirmed the steady increase of velocities along the jet depending on the distance from the source (Movsessian et al., 2009).

HH 83 system represented itself the suitable object for the second epoch spectra-imagery observations, especially in view of discovery of two separated kinematical structures in its WS. However, HH 83 is much more distant object than, for example, Taurus dark cloud. Taking this into account we decided to enlarge the time between two epochs up to 15 years.

2. Observations and Data Reduction

Observations were carried out in the prime focus of the 6 m telescope of Special Astrophysical Observatory of the Russian Academy of Sciences in two epoches: 10 Feb. 2002 and 2 Feb. 2017, in good atmpospheric conditions (seeing was about 1 arcsec). We used a FPI placed in the collimatedl beam of the SCORPIO (Afanasiev & Moiseev, 2005) and SCORPIO-2 (Afanasiev & Moiseev, 2011) multi-mode focal reducers in 2002 and 2017, respectively. The capabilities of these devices in the scanning FPI observational mode are presented by Moiseev (2002, 2015). Description of the first epoch observations was presented in Movsessian et al. (2009).

During the second epoch observations the detector was a EEV 40-90 2×4.5K CCD array. The observations were performed with $4{\times}4$ pixel binning, so for each spectral channel 512×512 pixel images were obtained. The field of view was 6.1 arcmin with a scale of 0.72 arcsec per pixel. Second epoch observations provided more deep images and higher spectral resolution.

The scanning interferometer was ICOS FPI operating in the 751st order of interference at the Hα wavelength, providing spectral resolution of FWHM $\approx$ 0.4Å (or $\approx$20 km s^{-1}) for a range of $\Delta\lambda$=8.7Å (or $\approx$390 km s^{-1}) free from order overlapping. The number of spectral channels was 40 and the size of a single channel was $\Delta\lambda \approx$ 0.22Å ($\approx$10 km s^{-1}).

In both epochs an interference filter with FWHM$\approx$15 Å centered on the Hα line was used for pre-monochromatization.

We reduced our interferometric observations using the software developed at the SAO (Moiseev, 2002, 2015, Moiseev & Egorov, 2008) and the ADHOC software package[1]. After primary data reduction, subtraction of night-sky lines, and wavelength calibration, the observational material represents "data cubes". We applied optimal data filtering, which included Gaussian smoothing over the spectral coordinate with FWHM = 1.5 channels and spatial smoothing by two-dimensional Gaussian with FWHM = 2–3 pixels. The FPIs, used in two epochs of observations, had different spectral resolutions. Therefore the rebinned data cubes were created for both epochs to bring them into the same velocity steps. It allows to achieve the better comparison of morphological details, which have same radial velocities.

Using these data cubes, we spectrally separated the details with different radial velocity in the outflow system. Then PM were measured for the selected structures using observations in both epochs.

3. Results

During the observations the field of view of the SCORPIO focal reducer covered the entire HH 83 outflow system including the jet, the working surface and the reflection nebula around the source (which actually

[1]The ADHOC software package was developed by J. Boulestex (Marseilles Observatory) and is publicly available in the Internet.

doi: doi.org/10.52526/25792776-2021.68.2-495

Table 1. Proper motions and radial velocities of knots in the HH 83 outflow

Knot	Distance (arcsec)	$V_{tan}{}^{a}$ (km s^{-1})	PA (deg)	V_r (km s^{-1})	V_{abs} (km s^{-1})
D	13.5	120 ± 30	310	-130	177
F	19.3	142 ± 35	327	-140	200
G	27.8	135 ± 40	319	-165	213
WS $_{high\ vel}$	117.0	160 ± 23	282	-312	351
WS $_{low\ vel}$	119.4	145 ± 30	277	-50	153^{b}
counter bow	96	180 ± 45	135	$+180$	255

(a) Tangential velocities correspond to 450 pc as a distance of the flow
(b) Values of these velocities will be discussed below

represents the illuminated cavity walls). Below we will discuss all these parts of HH 83 separately and compare the observations of 2002 and 2017.

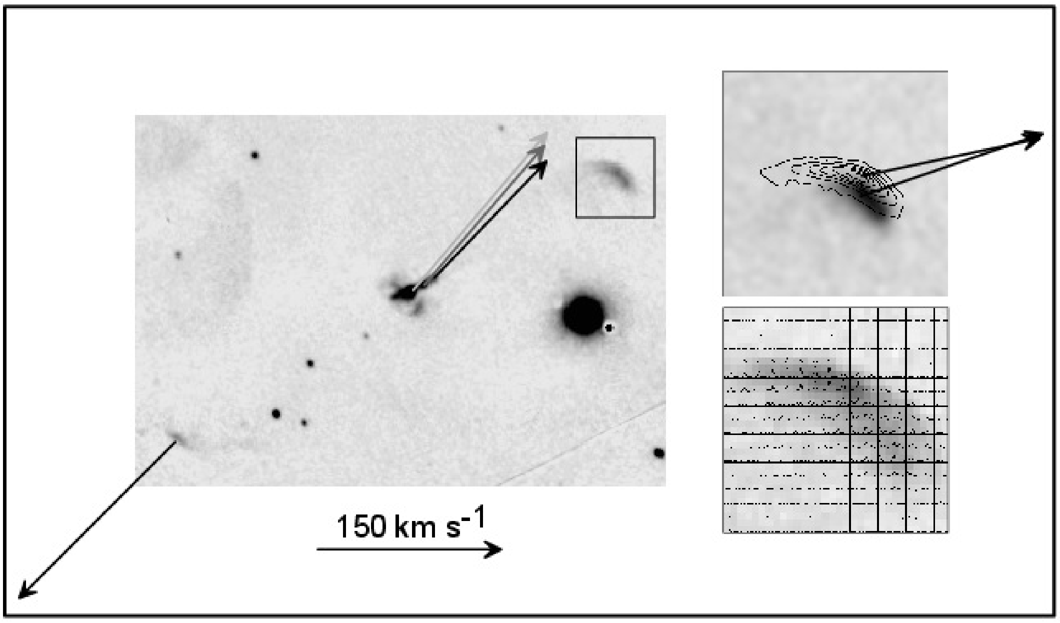

Figure 1. On the left panel the integrated over all velocity channels image of HH 83 outflow system with overlapped PM vectors in the jet knots and counterflow is presented. On the right bottom panel the grid of Hα profiles in the working surface, which indicates significant split of profiles in high and low velocity structures, is shown. On the right top panel the integrated over gaussian fitted profiles of low velocity component (grey scale) and high velocity one (contours) with PM vectors are presented.

3.1. The terminal working surfaces, their proper motions and kinematical structures

Besides of the already known WS (further denoted as NW-bow) which lies in about 2 arcmin distance from the source, our image clearly shows the second bow-shape structure in the opposite direction from the source, not described previously (Fig. 1, left panel). This structure lies on the axis of outflow system in the nearly same distance from the source as a main NW-bow. After re-examining of the first data, we found its faint traces in the same place. In contrast with the NW-bow this bow-shock has the positive radial velocity. It undoubtedly represents the terminal WS of the counter flow (further SE-bow), confirming the bipolar and symmetric nature of this outflow system.

As was already mentioned above, our previous data demonstrated that NW-bow in the HH 83 system is divided into two distinct components, which are well separated spectrally as well as spatially (see Fig. 6 in Movsessian et al., 2009). After gaussian fitting of the both components of Hα emission we restored images

doi: doi.org/10.52526/25792776-2021.68.2-495

of these components for each observational epoch. Using these images we measured the PM of high and low radial velocity structures in NW-bow.

The results of our PM measurements are presented on Fig. 1. In particular, PM vectors for the both low and high radial velocity structures of NW-bow of HH83 flow are shown in the inset. It is obvious that both structural components have very similar values of proper motion, despite the large difference in the radial velocities. We also estimated the distance between these structures during the second epoch observations and it turned out to be the same as for the first epoch (1000 AU). This is an additional evidence of their equal PM values. We will discuss this result in more detail in the next section.

On same Fig. 1 we show the PM vectors for the three brightest knots in the HH 83 jet, for the separated structures in the NW-bow as well as for the SE-bow, i.e. for the counter bow-shock. It worth to mention that this bow-shock has nearly the same range of radial velocities (in absolute values) as NW-bow, but, unlike the latter, it does not show neither spectral nor spatial inner separation. In any case, we were able to measure PM of this structure, even though it was significantly fainter in the first epoch data.

The numerical results are given in Table 1 where the distances for each structure, measured from the source position, values of tangential velocities (computed for the distance of 450 pc), position angles (PA) of PM vectors, radial velocities as well as the calculated absolute spatial velocities are presented.

3.2. PM of the knots in the jet

We measured PM of several bright knots in the HH 83 jet, namely knots D, G and F (according to the nomenclature of Reipurth, 1989). These knots also show high values of PM (see Table 1), similar to PM of high and low velocity structures in the terminal WS. It should be noted, however, that although the geometric axis of the jet coincides with NW-bow, the position angles of PM vectors of the jet knot significantly differ from those for the structures in NW-bow. Actually they are turned in the northern direction for about 14 degrees. Spatial velocities of the knots, calculated from their radial and tangential velocities, increase along with the distance from the source. Same trend also is observed in their radial velocities (see Table 1). We discuss this effect in the next section.

The knots in the HH 83 jet did not demonstrate the distinct division to high and low radial velocity components; consequently it was impossible to reveal the morphological structures with different radial velocities inside them.

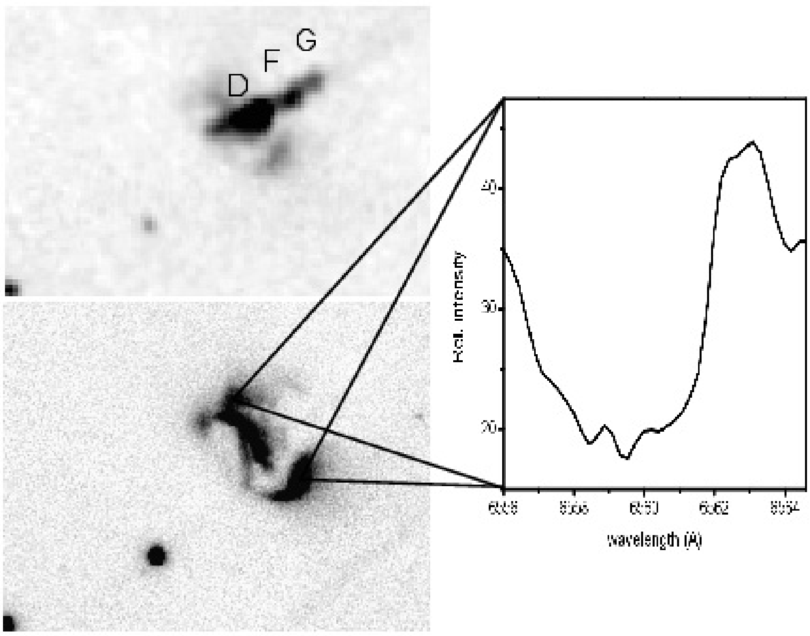

Figure 2. Integrated profile of the Hα line in the reflected light of the source of HH 83. In the left side the enlarged image of the central part of HH 83 system is shown in Hα emission (the integrated FP image from 2017, upper panel) and in i band (PanSTARRS survey, lower panel)

doi: doi.org/10.52526/25792776-2021.68.2-495

3.3. The reflection nebula

Observations show that HH 83 jet is propagating through the evacuated conical cavity, formed by wide-angle wind from the deeply embedded infrared source (Reipurth et al., 2000). The walls of this cavity are illuminated by light from this source. In the optical range they form two reflection lobes around the narrow jet. In the high-resolution infrared images (Reipurth et al., 2000) one can get impression of several spiral or helical arms on the cone walls. On the PanSTARRS i band image (see Fig. 2, lower panel) these two lobes are connected with bar-like structure, which probably represents one of the above mentioned arms. On the restored Hα image (Fig. 2, upper panel) these details are practically invisible, which confirms their reflection nature.

Above mentioned high quality of the new data allows the attempt to obtain the profile of Hα line in the spectrum of the central star through the scattered light of the source, deeply embedded in the dark cloud.To study the profile of Hα line in the reflected light we used the advantages of spectra-imagery, which allows to summarize data and to construct the total line profiles for any selected area. To avoid the contamination from the jet radiation and to deal with pure continual (i.e. reflected) light, we integrated profiles from the two side lobes only, excluding the bar-like structure, which is superimposed on the D knot of the jet. Resulting integrated Hα profile is presented in the right side of Fig. 2. This profile has strong and wide ($\sim$300 km s^{-1}) blue-shifted absorption with weak emission component near the zero radial velocity. We assume that it corresponds to the invisible IR source.

4. Discussion and conclusion

4.1. Working surface

Comparing the inner structures in the WS of HH 83 and in the knots in the HL Tau jet, we see that in both cases two emission structures with strongly different radial velocities were discovered. However, in the HL Tau jet these structures differ not only by their radial velocities but also by excitation, while in the parts of HH 83 WS the excitation level does not change, and these structures are visible mainly in Hα (Reipurth, 1989).

Their radial velocities differ in more than 250 km s^{-1}. This is an unique case: for example, two velocity components in the WS of HH 111 differ for about 60 km s^{-1} only (Reipurth et al., 1997) and in the HL Tau jet – about 100 km s^{-1}. This large difference in speed cannot be explained by existence of two separate outbursts, which formed two bow-shape structures with strongly different radial velocities, because in this case the high velocity structure will catch up the low velocity one in 15 years; besides, our new observations reveal that proper motions of these structures are the same.

Thus, we can come to conclusion that we observe in the terminal working surface of HH 83 physically connected structures, which can be designated as 'reverse shock' and 'forward shock'. The observed large difference in the radial velocities of these structures can form in very extremal conditions. For example, in the case of HL Tau jet the bright low velocity structures in front of the high velocity knots appear only in the region where the collisional interaction between the jet and wide outflow from XZ Tau is taking place (Movsessian et al., 2007).

In the case of HH 83 the asymmetry of bow-shock as well as the turning of it PM vectors compared to that of jet knots are the further indications of the encounter between the jet and the dense cloud core.

Taking into account the simple bow-shock and Mach disk model of Hartigan (1989), such values of velocities difference could occur when the ratio of ambient medium to jet densities will be near 100, and with the jet velocity more than 300 km s^{-1}.

If our conclusion is right and the high velocity structure in the WS indeed represents 'reverse shock', than we detect emission of the decelerated flow matter; the ratio of pattern speed to flow speed in this structure by definition will be equal one. On the contrary, for the 'forward shock', which represents the accelerated matter of ambient medium, this ratio will be much higher due to the lower radial velocities of the emitting particles. The spatial velocities of the flow structures, presented in the Table 1, correspond to the moving matter, while in the case of the forward shock this value does not have physical meaning, being strongly dependent on the ambient medium conditions. On the other hand, since the velocity in the 'reverse shock' region corresponds to the real matter movement, it is possible to compute the inclination angle between the line of sight and the jet, which turns out to be near 27 degrees. Using all these values, one can estimate the kinematical age of the outflow about 1500 year.

doi: doi.org/10.52526/25792776-2021.68.2-495

4.2. The source IRAS 05311−0631

The analysis of the reflected spectrum of the HH 83 source shows that it has Hα line profile of P Cyg type, with a wide, nearly rectangular absorption and faint secondary blue-shifted peak. Such profiles are likely to be formed in a strong wind with optical depth sufficient to produce the deep blueshifted absorption component (e.g. Muzerolle et al., 2011). They are very typical for the FU Ori type eruptive stars; on the other hand, only a few T Tauri stars show such well developed P Cygni profiles at Hα line. The blue edge of the absorption trough indicates wind velocities of up to 300 km s^{-1}. This value is nearly the same as the velocity of powerful wind that emanates from FU Orionis (e.g. Herbig et al., 2003).

As another argument for the FU Ori-type nature of IRAS 05311−0631 the detection of faint CO absorption bands at 2.3 μm by Davis et al. (2011) can be considered. Such absorption bands, though usually more strong, are typical for FUors (e.g. Reipurth & Aspin, 1997) .

On the other hand, FU Ori phenomenon in nearly all cases is associated with HH outflows (Audard et al., 2014). Moreover, the spacing of structure details in some HH outflows corresponds to the statistical estimates of the supposed recurrence of the FUor events (Herbig et al., 2003). 2003). In this case, the bright WS of HH 83 flow could be result of FU Ori-type outburst, which took place about 1500 year ago, judging from kinematical age of the outflow.

This work was supported by the Science Committee of RA, in the frames of the research project [1]18T-1C329. Observations with the SAO RAS telescopes are supported by the Ministry of Science and Higher Education of the Russian Federation (including agreement No05.619.21.0016, project ID RFMEFI61919X0016).

References

Afanasiev V.L., & Moiseev A.V., 2005, Astronomy Letters, 31, 194

Afanasiev V.L., & Moiseev A.V., 2011, Baltic Astronomy, 20, 363

Audard, M., Ábrahám, P., Dunham, M.M. et al. 2014, in Protostars and Planets VI, Univ. Arizona Press, eds. H. Beuther et al., 387

Davis, C.J., Cervantes, B.,Nisini, B. et al., 2011, Astron. Astrophys. , 528, A3

Hartigan, P., 1989, ApJ, 339, 987

Hartigan, P., Morse, J., Palunas, P., et al. 2000, Astron. J. , 119, 1872

Hartigan, P., Frank, A., Foster, J. M., et al. 2011, Astrophys. J. , 736, 29

Heathcote, S. & Reipurth, B. 1992, Astron. J. , 104, 2193

Herbig, G. H., & Jones, B. F. 1981, Astron. J. , 86, 1232

Herbig, G. H., Petrov, P. P., & Duemmler, R. 2003, Astrophys. J. , 595, 384

Jones, B. F., & Herbig, G. H. 1982, Astron. J. , 87, 1223

Moiseev, A.V., 2002, Bull. Spec. Astrophys. Obs., 54, 74

Moiseev, A.V., 2015, Bull. Spec. Astrophys. Obs.,70, 94

Moiseev, A.V., & Egorov, O.V. 2008, Bull. Spec. Astrophys. Obs., 63, 181

Movsessian, T. A., Magakian, T. Y., Amram, P., et al. 2000, Astron. Astrophys. , 364, 293

Movsessian, T. A., Magakian, T. Y., Bally, J., et al. 2007, Astron. Astrophys. , 470, 605

Movsessian, T. A., Magakian, T. Yu., Moiseev, A. V., & Smith, M. D., 2009, Astron. Astrophys. , 508, 773

Movsessian, T. A., Magakian, T. Y., & Moiseev, A. V. 2012, Astron. Astrophys. , 541, A16

Movsessian, T. A., Magakian, T. Y., Burenkov, A. N. 2019, Astron. Astrophys. , 827, A94.

Muzerolle, J., Calvet, N., Hartmann, L. 2001, Astrophys. J. , 550, 944.

doi: doi.org/10.52526/25792776-2021.68.2-495

Reipurth, B., Bally, J., Graham, J. A., et al. 1986, Astron. Astrophys. , 164, 51

Reipurth, B., 1989, A&A 220, 249

Reipurth, B. 1989, European Southern Observatory Conference and Workshop Proceedings, 247

Reipurth, B., Raga, A. C., & Heathcote, S. 1996, Astron. Astrophys. , 311, 989

Reipurth, B., Raga, A. C., & Heathcote, S. 1992, Astrophys. J. , 392, 145

Reipurth, B., & Heathcote, S. 1992, Astron. Astrophys. , 257, 693

Reipurth, B., Heathcote, S., Roth, M., et al. 1993, Astrophys. J. Lett. , 408, L49

Reipurth, B., Hartigan, P., Heathcote, S., Morse, J., & Bally, J. 1997, Astron. J. , 114, 757

Reipurth, B., Hartigan, P., Heathcote, S., et al. 1997, Astron. J. , 114, 757

Reipurth, B., & Aspin, C.A. 1997, Astron. J. , 114, 2700

Reipurth, B., Yu, K. C., Heathcote, S., et al. 2000, Astron. J. , 120, 1449

Reipurth, B., & Bally, J. 2001, Ann. Rev. Astron. Astrophys. , 39, 403

doi: doi.org/10.52526/25792776-2021.68.2-495

On the property of "statistical identity" of solutions to some classical problems of the radiative transfer theory

H. V. Pikichyan*

Byurakan Astrophysical Observatory, 378433, Aragatsotn District, Armenia

Abstract

A probabilistic interpretation of the classical solution of the diffuse reflection problem (DRP) of radiation from a semi-infinite homogeneous scattering-absorbing medium on the language of random events in the simple case of monochromatic and isotropic scattering is constructed. A certain property of the so-called "statistical identity" is specially defined. By using these two circumstances, it is possible to construct a simple symbolic scheme for the direct transformation of the solution mentioned above in the particular case of DRP into solutions to more general cases of DRP, which taking into account the anisotropy and incoherence of scattering, as well as the temporal dependence of the task on the act of absorption. Moreover, some generalization of the primary scheme makes it possible to directly obtain solutions of the DRP also for non-homogeneous media and for general case of time dependence (on absorption acts and free flights between them) for the quanta diffusion process. At the same time, both the well-known results of the DRP decisions and some new ones were obtained.

Keywords: *radiative transfer— probabilistic interpretation—diffuse reflection problem*

1. Introduction and purpose of the work

In 1942-44 by introducing the principle of invariance and the layer addition method into the theory of radiative transfer, Ambartsumian (Ambartsumian, 1942, 1943a,b, 1944a,b) obtained precise solutions to a number of diffuse reflection problems (DRP) from a semi-infinite medium and reflection-transmission for a layer of finite optical thickness. A significant advantage here in comparison with the traditional approach of applying the integro-differential equation of radiative transfer was to determine the diffuse radiation leaving the medium without the need to find the field inside the medium. Further, these considerations were widely used by many authors to analyze problems of varying complexity. However, it is well known that, both through the radiation transfer equation (Boltzmann's kinetic equation for a photonic gas) and through the application of invariance and layer addition considerations, analytical and numerical-analytical studies of transfer problems are associated with complex mathematical calculations. At the same time, with the complication of physical situations in the studied problems, both the number of independent variables and the cumbersomeness of the mathematical procedures used increase. Therefore, it is very advisable to search for more simplified private methods for analyzing such problems.

The purpose of the presented work is, using the example of a well-studied early DRP from a semi-infinite medium, to illustrate the possibility of obtaining solutions and corresponding functional equations of physically more general and complex DRP by direct transformation of a known solution corresponding to them more particular and simple DRP. At the same time, we will proceed from the probabilistic interpretation and statistical description of transport phenomena using the highlighted below property of the so-called "statistical identity" between the corresponding solutions and functional equations of more "particular" and more "general" problems.

*hovpik@bao.sci.am, hovpik@gmail.com

doi: doi.org/10.52526/25792776-2021.68.2-502

2. Property of statistical identity

In 1951, Sobolev introduced the concept of the exit probability of an absorbed quantum from the medium and the approach of statistical interpretation of radiative transfer processes (see, for example, (Sobolev, 1956a)). It is well known that this made it very easy to write down some of the relations and integral equations of the radiation transfer theory directly from the probabilistic reasons, bypassing the mathematical calculations of their derivation from the equation of radiative transfer. For example, in the classical DRP of a unit quantum from a semi-infinite scattering-absorbing homogeneous medium, in the case of monochromatic and isotropic scattering, the expression is directly recorded from the probabilistic reasons is

$$\rho(\mu \leftarrow \mu') = \int_0^\infty p(\mu,\tau) \cdot e^{-\frac{\tau}{\mu'}} \cdot \frac{d\tau}{\mu'}. \tag{1}$$

Indeed, the probability of diffuse reflection $\rho(\mu \leftarrow \mu')\,d\mu$ in the direction of μ, inside the solid angle $2\pi d\mu$ of a unit quantum falling on the boundary of the medium, from the direction $arccos\mu'$ with respect to its normal, is formed from the sequential realization of three independent events. The first event - entering the medium quantum first with probability $e^{-\frac{\tau}{\mu'}}$ flies some optical distance $\frac{\tau}{\mu'}$ freely. The second event - then the quantum is absorbed in the "infinitely thin" layer $d\tau$ of the depth τ, with a probability of $\frac{d\tau}{\mu'}$. As a result, after this first act of absorption, there is a quantum absorbed at depth τ in the medium, which with probability $p(\mu,\tau)\,d\mu$ (in the direction of μ, inside the solid angle $2\pi d\mu$) will realize the final third "complex event" - the process of its exit through the outer boundary of the semi-infinite medium after arbitrary wanderings in it. Since the above-mentioned first act of absorption can occur at any current value of τ, the integral over the entire interval of change of these values $[0,\infty]$ is obviously taken. For an unknown in (1) quantity $p(\mu,\tau)$ in the same simple way - directly for probabilistic reasons, the integral equation defining it is written (Sobolev, 1956a).

It is very important to note that the underlying statistical sequence of the three random events listed above is universal, that is, it is valid outside the specific physical properties of the elementary act of scattering. Therefore, the structure of expression (1) will not change if, taking into account the corresponding new physical variables of the problem. This expression is also rewritten for more general assumptions about the properties of the elementary act of scattering. In the case of non-coherent non-isotropic scattering, the expression (1) will take the form

$$\rho(\mu,x \leftarrow \mu',x';\varphi-\varphi') = \int_0^\infty p(\mu,x \leftarrow \mu',x';\varphi-\varphi';\tau) \cdot e^{-\alpha(x')\frac{\tau}{\mu'}} \alpha(x') \cdot \frac{d\tau}{\mu'}, \tag{2}$$

where the same three events are presented, indicating only the quantities describing the new physical situation: directions - (μ,φ), (μ',φ') and the dimensionless frequencies - x, x' related to the quant entering and leaving the medium, respectively, as well as the absorption coefficient profile - $\alpha(x')$. Indeed, the expression (2) is not different in structure from (1). Here, the same three random events appear, only taking into account the characteristics of a new, more complex physical situation.

Definition: The structural unity of the probabilistic interpretation (in the sense of identity and sequence of realized random events) of relations describing different relative to the elementary act of scattering (i.e., simpler and more complex) problems, conditionally called the property of the **statistical identity** of these relations or tasks.

Obviously, the ratios (1) and (2) in the sense of the formulated definition are statistically identical.

doi: doi.org/10.52526/25792776-2021.68.2-502

3. Probabilistic interpretation of the classical solution of the DRP from a semi-infinite medium

The classical solution of the DRP from a homogeneous semi-infinite medium in the case of monochromatic and isotropic scattering is of the form (Ambartsumian, 1942, 1943b)

$$\rho(\mu,\mu') = \frac{\lambda}{2}\mu\frac{\varphi(\mu)\varphi(\mu')}{\mu+\mu'}, \quad \varphi(\mu) = 1 + \int_0^1 \rho(\mu,\mu')\,d\mu', \tag{3}$$

$$\varphi(\mu) = 1 + \frac{\lambda}{2}\mu\int_0^1 \frac{\varphi(\mu')}{\mu+\mu'}d\mu'. \tag{4}$$

To use in (3), similarly to (1) and (2), the statistical identity property defined above, it is first necessary to find out the probabilistic meaning of the solution itself (3). It's not hard to see if it can be rewritten as

$$\left(\frac{1}{\mu}+\frac{1}{\mu'}\right)\cdot\rho(\mu,\mu') = p(0,\mu)\cdot\tilde{p}(0,-\mu'), \tag{5}$$

where the factors

$$\tilde{p}(0,-\mu') = \frac{\varphi(\mu')}{\mu'}, \quad p(0,\mu) = \frac{\lambda}{2}\varphi(\mu) \tag{6}$$

describe the probabilities of two "optically inverse" to each other processes. Indeed, the right factor on the right side of (5)- $\tilde{p}(0,-\mu')\,d\tau$, represents the probability of absorption (directly or by arbitrary wandering) of a unit quantum on the "infinitely thin" boundary $d\tau$ layer of the medium, provided that this quantum initially fell from the outside to the boundary of the medium from the direction of μ' to its external normal (Pikichyan 1980). The left multiplier - $p(0,\mu)\,d\mu$, represents the probability of the quantum initially absorbed at the boundary of the medium, which arbitrarily (after re-emission - directly, or by generally speaking multiple scatterings) will leave the medium in the direction of μ, inside the solid angle $2\pi d\mu$ (λ - the probability of re-emission of the quantum after absorption). The probabilistic interpretation of formula (5), taking into account the above, states the **equivalence** of two complex events - processes represented in two parts of this equation. The left part in the form of two multipliers represents the probability of joint realization of two random events. The first is the direct absorption in an infinitely thin boundary layer of the medium of a quantum with a probability of $\left(\frac{1}{\mu}+\frac{1}{\mu'}\right)d\tau$ when it enters the medium or when it leaves it. The second is the diffuse reflection of the quantum from the medium, after arbitrary wanderings in it, with a probability of $\rho(\mu,\mu')\,d\mu$. The right part of (5) describes the joint sequential implementation of the two mentioned above, generally speaking, diffusion processes with probabilities $\tilde{p}(0,-\mu')\,d\tau$ and $p(0,\mu)\,d\mu$.

4. Scheme of statistical identity for the DRP

The above statistical interpretation of the DRP (5) in the language of random events is generally more appropriate to present in the form of a simple symbolic scheme

$$(a+\tilde{a})\cdot R = \left\langle A\cdot\tilde{A}\right\rangle = Q. \tag{7}$$

Here, the values $a, \tilde{a}$ describe the probabilities of events: single elementary acts of direct absorption of the quantum at the boundary of the medium, R represents the complete process of diffuse reflection of the quantum from the medium, and the bracket $\left\langle A\cdot\tilde{A}\right\rangle$ represents the sequence of two described above - optically inverse to each other, generally speaking, diffusion processes $\tilde{A}$ and A . Accounting for changes in physical parameters in the elementary act (more generally than (5)) of scattering, on which the necessary integrations should be carried out, is indicated in parentheses - $\langle\ldots\rangle$ (see below). The right part of (7) can be perceived as a single specific statistical process Q where the quantum in its path necessarily undergoes, generally speaking, an intermediate -"diffusion" act of scattering at

doi: doi.org/10.52526/25792776-2021.68.2-502

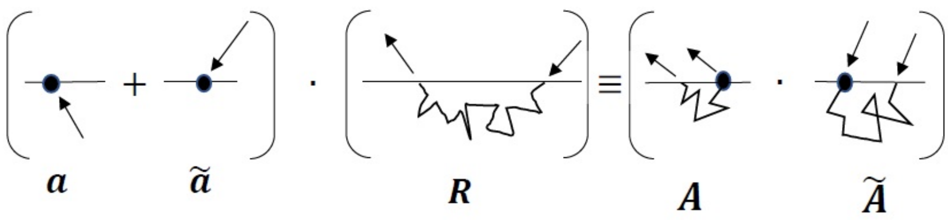

Figure 1.

the boundary of the medium. The formula (7), with the corresponding letter designations of events, in a diagramic way is shown in Fig. 1. The horizontal line indicates the boundary of the medium, below it a semi-infinite scattering-absorbing medium is implied, broken ones symbolically indicate the trajectories of the quantum, the points are the act of absorbing the quantum, and the arrows are the initial or final directions of motion of the quantum.

5. Examples of the application of the statistical identity property in the DRP

Here are examples of the application of the statistical identity property according to the scheme (7) with various assumptions more general than (5) regarding the elementary act of scattering. It is important to note that the corresponding symmetry of the diffuse reflection function, deriving, as is well known, from the identical symmetry of the elementary act of scattering, is taken into account in all DRP below. The expression (3) in the case of non-coherent isotropic scattering, with the frequencies redistribution function $r\left(x'',x'\right)$ of radiation, by means of (7) is directly transformed into a solution of known from (Pikichyan, 1978, 1980)

$$\left[\frac{\alpha(x)}{\mu}+\frac{\alpha(x_0)}{\mu_0}\right]\rho\left(\mu,x\leftarrow\mu_0,x_0\right)=\frac{\lambda}{2\mu_0}\int\int_{-\infty-\infty}^{+\infty+\infty}\varphi\left(\mu,x;x''\right)r\left(x'',x'\right)\varphi\left(\mu_0,x_0;x'\right)dx''dx',$$

$$\varphi\left(\mu,x;x''\right)=\delta\left(x-x''\right)+\int_0^1\rho\left(\mu,x\leftarrow\mu'',x''\right)d\mu'', \tag{8}$$

which was obtained earlier by the standard technique of the principle of invariance. In the more general case of redistribution of radiation by frequencies and directions (i.e., in non-coherent non-isotropic scattering), the use of scheme (7) directly leads to the functional equation

$$\frac{4\pi\mu'}{\lambda}\left[\frac{\alpha(x)}{\mu}+\frac{\alpha(x')}{\mu'}\right]\rho(M,M')=r(M,-M')+$$

$$\begin{gathered}\iiint\rho(M,M''')r(-M'''\leftarrow M')d^3M'''+\iiint r(M,M'')\rho(M',M'')d^3M''+\\ \iiint\iiint\left[\rho(M,M''')r(-M''',M'')\rho(M',M'')\right]d^3M''d^3M''',\end{gathered} \tag{9}$$

$$\pm M\equiv\{x,\pm\mu,\varphi\},\ \iiint d^3M\equiv\int_{-\infty}^{+\infty}\dots dx\int_0^{2\pi}\dots d\varphi\int_0^1\dots d\mu, \tag{10}$$

which was obtained in (Yengibaryan & Nikoghosyan, 1972) by applying the principle of invariance. This is the "non-coherent analogue" of Ambartsumian's functional equation obtained by him in the case of anisotropic monochromatic scattering in pioneer work (Ambartsumian, 1943a). In a non-stationary DRP of an "instantly emitting external source", taking into account the time losses only for

doi: doi.org/10.52526/25792776-2021.68.2-502

acts of absorption-re-emission of the quantum, the scheme (7) directly gives a solution that coincides in form with ours, obtained by the wound in the work (Ueno, 1962):

$$\left(\frac{1}{\mu}+\frac{1}{\mu_0}\right)\rho(\mu,\mu_0;u-u_0)=\frac{\lambda}{2\mu_0}\int_{u_0}^{u}e^{-(u-z)}dz\int_{u_0}^{z}\varphi(\mu;z-u')\varphi(\mu_0;u'-u_0)\,du', \tag{11}$$

$$\varphi(\mu;u-u_0)=\delta(u-u_0)+\frac{\lambda}{2}\mu\int_{u_0}^{u}e^{-(u-z)}dz\int_{u_0}^{z}\varphi(\mu;z-u')\,du'\int_0^1\frac{\varphi(\mu';u'-u_0)}{\mu+\mu'}d\mu'. \tag{12}$$

for another special case, the accounting of time costs only for free flights of the quantum between "instantaneous" acts of scattering. Indeed, the wound was aware (see, for example, (Minin, 1988)) that the solutions to these two special cases of non-stationary DRP coincide in form. Here, the values of u_0 and u represent the starting and ending moments of the dimensionless entry and output times of the quantum, respectively.

6. Generalization of the scheme of statistical identity

Examples of a homogeneous medium were considered above, while in the problem with a time dependence, the case of the time spent only on the act of absorption-re-emission of the quantum was considered. For taken into account both the non-homogeneity of the medium and of time spent on free flights between scattering acts require a generalization of the scheme (7). Let the boundary layer $[\alpha,\alpha+\tau]$ with the current thickness of τ be highlight in the original semi-infinite inhomogeneous medium $[\alpha,\infty]$ (here α the truncation parameter of the original inhomogeneous medium). The quantum entering the medium let this layer pass freely - without scattering, and reach its lower boundary $\alpha+\tau$. Then consider the DRP of this quantum from the underlying "current" semi-finite medium $[\alpha+\tau,\infty]$ by means of the above-defined process Q . After this specific process of diffuse reflection from this "particular" medium, let the quantum pass the $[\alpha,\alpha+\tau]$ layer again without scattering. As a result, we will have a quantum that has finally left the original medium $[\alpha,\infty]$. If, by integrating all the values of τ , all the "current" semi-infinite partial media are now taken into account, then obviously the solution of the original DRP will be obtained. The generalized scheme of statistical identity in this case will take the form

$$R=\left[EQ\tilde{E}\right]\equiv\left[E\left\langle A\cdot\tilde{A}\right\rangle\tilde{E}\right], \tag{13}$$

where the values $\tilde{E}$ and E describe the probabilities of free flight when entering and exiting the original medium, and the square brackets describe the integration operation for all values of the parameter τ . It is not difficult to ascertain that in the more specific DRP discussed in paragraph 5, the scheme (13) naturally turns into - (7).

7. Examples of application of the generalized scheme (13)

In the DRP of non-homogeneous medium with isotropic scattering equation (13) directly gives a well-known from the works (Bellman & Kalaba, 1956, Sobolev, 1956b, Sobolev & Yanovitsky, 1978) solution

$$\rho(\mu,\mu_0;\alpha)=\int_{\alpha}^{\infty}\frac{\lambda(\alpha')}{2}\varphi(\mu,\alpha')\varphi(\mu_0,\alpha')e^{-(\alpha'-\alpha)\left(\frac{1}{\mu}+\frac{1}{\mu_0}\right)}\frac{d\alpha'}{\mu_0}, \tag{14}$$

$$\varphi(\mu,\alpha')=1+\int_0^1\rho(\mu,\mu';\alpha')d\mu', \tag{15}$$

Where $\lambda(\alpha')$ is the probability of re-emission of the quantum after absorption at the depth of α' , α - is the parameter of truncation of the non-homogeneous medium. In the case of anisotropic scattering in an non-homogeneous medium, the scheme (13) directly gives an analogue of Ambartsumian's functional equation:

$$\rho(M,M_0;\alpha)=\frac{1}{4\pi\mu_0}\int_\alpha^\infty \lambda(\alpha')e^{-(\alpha'-\alpha)\left(\frac{1}{\mu}+\frac{1}{\mu_0}\right)}Q(M,M_0;\alpha')d\alpha', \tag{16}$$

$$Q(M,M_0;\alpha')=\chi(M,-M_0;\alpha')+$$
$$\int\int\rho(M,M';\alpha')\chi(-M',-M_0;\alpha')d^2M'+\int\int\chi(M,M';\alpha')\rho(M_0,M';\alpha')d^2M'+$$
$$\int\int\int\int[\rho(M,M'';\alpha')\chi(-M'',M';\alpha')\rho(M_0,M';\alpha')]d^2M''d^2M'. \tag{17}$$

Notations are used:

$$\pm M\equiv\{\pm\mu,\varphi\},\quad \int\int d^2M\equiv\int_0^{2\pi}\dots d\varphi\int_0^1\dots d\mu, f(M,M')\equiv f(\mu,\mu';\varphi-\varphi'). \tag{18}$$

In the general problem with time dependence in the mutual accounting of time costs both in the acts of scattering and in free flights between them in the case of monochromatic and isotropic scattering of radiation in the homogeneous medium, the ratio (13) directly gives a solution

$$\left(\frac{1}{\mu}+\frac{1}{\mu_0}\right)\rho(\mu,\mu_0;t)=\frac{\lambda}{2\mu_0}\int_0^t K(t-z)\,dz\int_0^z\varphi(\mu;z-z')\varphi(\mu_0;z')dz', \tag{19}$$

$$\varphi(\mu;t)=\delta(t)+\frac{\lambda}{2}\mu\int_0^t K(t-z)\,dz\int_0^z\varphi(\mu;z-z')\,dz'\int_0^1\frac{\varphi(\mu';z')}{\mu+\mu'}d\mu'. \tag{20}$$

Here the quantities are: t - is the total time of the quantum in the medium, t_1 - is the average time the quantum in the absorbed state in a unit scattering act, t_2 -is the average time of the free run of the quantum between the two scattering acts. The core of the equation is obtained in the form of

$$K(x)\equiv\frac{e^{-\frac{x}{t_2}}-e^{-\frac{x}{t_1}}}{t_2-t_1}. \tag{21}$$

The expressions (19) - (21) are new and represent a direct generalization of the corresponding formulas of Ueno (1962) obtained by him by applying the principle of invariance of Ambartsumian in the special case of taking into account the time costs of the quantum only during free flight between scatters. It is noteworthy that the expressions (19) - (21) in their simplicity differ favorably from the solution of the same general problem obtained by Minin using the Laplace transform (Minin, 1964), see also (Minin, 1988), in which derivatives of the first and second degrees from some auxiliary function of four variables appeared. The solution of the "instantaneous" illumination problem close to the considered (19) - (21), the DRP when illuminating the medium in the "finite time interval" was obtained earlier in the work of Matsumoto (Matsumoto, 1974). Obviously, in order to move from the solution (19) - (21) of the problem of "instantaneous source" to the case with the source of the "finite time interval" of radiation, it is enough to integrate the formulas (19) - (20) according to the corresponding time interval (see (Matsumoto, 1974)) . In the more general case of anisotropic scattering for the "instantaneous" source discussed above, we directly arrive at the expressions by means of scheme (13):

$$\left(\frac{1}{\mu}+\frac{1}{\mu_0}\right)\rho(M,M_0;t)=\frac{\lambda}{2\mu_0}\int_0^t K(t-z)\,Q(M,M_0,z)\,dz, \tag{22}$$

$$Q(M,M_0,z)=\delta(z)\,\chi(M,-M_0)+$$
$$+\int\int\rho\left(M,M'';z\right)\chi\left(-M'',-M_0\right)d^2M''+\int\int\chi\left(M,M'\right)\rho\left(M_0,M';z\right)d^2M'+$$

doi: doi.org/10.52526/25792776-2021.68.2-502

$$\int\int\int\int\chi\left(-M^{''},M^{'}\right)d^2M^{''}d^2M^{'}\int_0^z\rho\left(M,M^{''};z-z^{''}\right)\rho\left(M_0\leftarrow M';z^{''}\right)dz^{''}, \tag{23}$$

where the symbols (18) are used. The expressions (22) - (23) are new and together represent an analogue of the Ambartsumyan’s functional equation (Ambartsumian, 1943b) in the non-stationary problem of diffuse reflection from a homogeneous semi-infinite medium in the case of anisotropic scattering, taking into account the time losses both on scattering acts and on free flights between them.

8. Conclusion

In the presented work, a probabilistic interpretation of the classical solution of the problem of diffuse reflection of radiation from a semi-infinite homogeneous scattering-absorbing medium is constructed in the language of random events in the simple case of monochromatic and isotropic scattering. A certain property of the so-called ”statistical identity” is specially defined. By using these two circumstances, it is possible to construct a simple scheme for the direct transformation of the solution mentioned above in the particular case of the DRP into solutions to more general cases of DRP, taking into account the anisotropy and incoherence of scattering and the temporal dependence of the act of absorption. Moreover, some generalization of the primary scheme also makes it possible to directly obtain solutions to the DRP of non-homogeneous media and the general case of time-dependence (acts of absorption and free flights between them) of the process of diffusion of quanta in it. At the same time, both the well-known results of the DRP decisions and some new ones were obtained.

References

Ambartsumian V. A., 1942, Astronomicheskii Zhurnal (in Russian), 19, No 5, 30

Ambartsumian V. A., 1943a, Jurnal Teoreticheskoy i Eksperimentalnoy Fiziki (in Russian), 13, No. 9-10, 323

Ambartsumian V. A., 1943b, DAN SSSR, 38, No 8, 257

Ambartsumian V. A., 1944a, DAN SSSR (in Russian), 43, No 3, 106

Ambartsumian V. A., 1944b, Izvestiya. AN ArmSSR, Natural Sci. (in Russian), No. 1-2, 31

Bellman R. E., Kalaba R. E., 1956, Proc. Nat. Acad. Sci. USA, 42, 629

Matsumoto M., 1974, Publ. Astron. Soc. Japan, 26, 241

Minin I. N., 1964, DAN SSSR (in Russian), 154, No. 5, 1059

Minin I. N., 1988, Theory of Radiation Transfer in the Atmospheres of Planets. Nauka, Moscow

Pikichyan O. V., 1978, DAN Arm. SSR, (in Russian), 67, No. 3, 151

Pikichyan O. V., 1980, Soobshcheniya BAO (in Russian), 52, 148

Sobolev V. V., 1956a, Transfer of radiant energy in the atmospheres of stars and planets (in Russian). Gostekhizdat, Moscow

Sobolev V. V., 1956b, DAN USSR (in Russian), 111, No. 5, 1000

Sobolev V. V., Yanovitsky E. G., 1978, in Voprosy fiziki i evolutsii kosmosa. Izd. AN ArmSSR, Yerevan

Ueno S., 1962, Journal of math. analysis and applications, 4, 1

Yengibaryan N. B., Nikoghosyan A. G., 1972, DAN AN Arm SSR (in Russian), 54, No. 2, 91

doi: doi.org/10.52526/25792776-2021.68.2-502

Communications of BAO, Vol. 68, Issue 2, 2021, pp. 509-514

An Integral Approach to the Theory of Classical Polytropes

G.A.Saiyan

Kelly Serrvices Incorporation, Educational Staffing, 66210, Kansas,USA

Abstract

A nonlinear Volterra integral equation of the second kind is used instead of conventional Lane-Emden differential equation to represent an alternative approach to finding exact solutions and analytical approximations to solutions of the Lane-Emden equation for classical polytropic models. This approach enables us to reproduce the well - known Lane- Emden (or, just Emden) functions for polytropic indices n=0,1,5 directly or by making use of the Laplace transform, and, being combined with some heuristic reasonings, derive analytical approximations to exact solutions for n = 1.5, 2 and ∞ in closed forms. The proximity of all suggested analytical approximations to the exact solutions are evaluated with the use of the mean square error estimator. Standard deviations are found to be of 10^{-3} by the order of magnitude. The approximating function of the isothermal density distribution enables us to calculate a theoretical rotation curve that reproduces main features of rotation curves of a set of spiral galaxies. Detailed mathematical calculations will be introduced in an extended paper which is under preparation.

Keywords:*polytropes – polytropic index-Lane-Emden equation-Emden function; Volterra non-linear integral equation – Laplace transform - analytical approximations- dimensionless density distributions*

1. Introduction

Polytropes are self-gravitating gas systems characterized by a specific relationship between the gas pressure (P) and its density (ϱ): $P = K\varrho^{1+\frac{1}{n}}$, where n is the polytropic index and K is the coefficient of proportionality, dependent on the central density and the central velocity dispersion (or the central value of the gravitational potential). Polytropes have been intensively used in the study of stellar structure, theory of stellar evolution (Chandrasekhar (1939), Horedt (2004) (see references therein)), studies of the structure of globular clusters, clusters of galaxies and dark matter distribution. The mathematical foundation of the theory of classical polytropes is the well-known Lane – Emden differential equation, the solutions of which is called Lane-Emden (or, just Emden) function, derived from Poisson equation and the equation of hydrostatic equilibrium, in which the polytropic relation mentioned above is used. The Lane-Emden differential equation can be written in the standard or alternative form (Ivanov, 2018):

$$\frac{1}{\xi^2}\frac{\partial}{\partial}(\xi^2\frac{\partial\theta}{\partial\xi}) = -\theta^n \quad or \quad \frac{d^2(\xi\theta)}{d\xi^2} = -\xi\theta^n \tag{1}$$

where $\theta(\xi)=\frac{\varphi}{\varphi_c}$ dimensionless potential Emden (also Lane-Emden) function, that is the gravitational potential φ, divided by its central value), $\xi = \frac{r}{r_0}$ (r – distance from the center, r_0 - the characteristic radius in a polytropic model) and n as a polytropic index, supplied by the boundary conditions $\theta(0)$=1, $\theta'(0) = 0$. The equation has exact solutions only for n=0,1,5. For all other polytropic models their analytical solutions in closed form do not exist Medvedev & Rybicki (2001) and need to be found via numerical integration. Despite methods of numerical integration have achieved very high level of precision (Horedt (1986), Horedt (2004)) in computing Emden functions the analytical approach is still in demand (see Mach (2012), Milgrom (2021), Motsa & Shateyi (2012)) and references therein), may have a direct relation to physical aspects of the problem Horedt (1987), cast new light on old problems and reduce time for numerical integration. The main goal in this paper is to introduce an integral approach to the theory of classical polytropes as an alternative view on the well-known problem which can be used as an additional tool to the conventional Lane-Emden equation.

doi: doi.org/10.52526/25792776-2021.68.2-509

2. Volterra non-linear integral equation of the second kind

The Lane-Emden equation (1) with boundary conditions states the Cauchy problem in mathematical physics, the solution of which can be written in the form of Volterra non-linear integral equation of the second kind:

$$\theta(\xi) = 1 - \int_0^{\xi} \theta^n(x) x (1 - \frac{x}{\xi}) dx \tag{2}$$

for all n $< \infty$. It is required that $\theta(\xi_0) = 0$, ξ_0 - radius of the polytrope which is finite for n < 5 and infinite for n ≥ 5 . Only the functions satisfying all the conditions mentioned above are thought to be physically acceptable. In case of an isothermal sphere (n $= \infty$) the corresponding differential equation can be written in the form $d^2(\xi\psi)/d\xi^2 = \xi e^{-\psi(\xi)}$, supplied by the boundary conditions $\psi(0) = 0$, $\psi'(0) = 0$, and can be converted into the following Volterra homogenous non-linear integral equation of the second kind

$$\psi(\xi) = \int_0^{\xi} e^{-\psi(\xi)} x (1 - \frac{x}{\psi}) dx \tag{3}$$

The exponential term in (3) represents the dimensionless density distribution in the isothermal sphere $\rho(\xi) = exp(-\psi(\xi))$.
It is obvious that all polytropic solutions are symmetric $\theta(\xi) = \theta(-\xi)$ and their expansions into power series or Pade approximations must include only even powers of ξ (see, for example, **??**. In addition to this we can state that for a large domain of polytropic indices density distributions should have an inflection point. This may be incorrect for some polytropic models (such as $0 \leq$ n < 1).
The integral equations presented above were derived in Saiyan (1997) (not published), then by Shaudt (2000), who considered the existence and uniqueness as well as regularity of the general Lane-Emden solution within the fixed-point problem. Horedt (2004) refers to this result in his book and shows how the equations can be derived from general considerations by making use of Green's formula.

3. Exact solutions

3.1. n=0

This is a model of incompressible liquid ($\varrho = const$). The solution can be obtained via direct simple integration of (2), which gives well - known function $\theta(\xi) = 1 - \frac{\xi^2}{6}$.

3.2. n=1

The equation (3), after being multiplied by ξ, takes the form

$$\xi\theta(\xi) = \xi - \int_0^{\xi} \theta(x) x (\xi - x) dx \tag{4}$$

with the convolution term in the righthand integral. This is the standard linear Volterra integral equation of the second kind for the function $\xi\theta(\xi)$ and can easily be solved by applying direct and then inverse Laplace transforms or by Picard approximations. Its solution is $\sin\xi$. Thus, we derived Ritter's solution $\theta(\xi) = \frac{\sin(\xi)}{\xi}$, which is the Bessel spherical function $\mathrm{j}_0(\xi)$.

3.3. n=5

This case is more challenging in terms of direct calculations because of extreme non-linearity of the Volterra equation (2). We assume that the functions $\theta(\xi)$ and $\theta^5(\xi)$ themselves are Laplace images of the originals $F(t)t^{\nu}$ and $\Phi(t)t^{\mu}$, continuous on $\mathbf{R^1}$ and have appropriate rates of exponential growth

$$\theta(\xi) = C_1 \int_0^{\infty} F(t) t^{\nu} e^{-\xi t/\alpha} dt \qquad \theta^5(\xi) = C_2 \int_0^{\infty} \Phi(t) t^{\mu} e^{-\xi t/\alpha} dt \tag{5}$$

Here C_1 and C_2 are constants to be chosen and α is a free parameter to be defined. Taking derivatives by ξ in (6) and substituting them in the Lane-Emden equation, one can show that if functions $F(t)$ and $\Phi(t)$ are Bessel J- functions $F(t) = J_0(t)$, $\Phi(t) = J_2(t)$ and $C_1 = C_2\alpha^2 = 1$ for simplicity, as well as ν=0, $\mu = \frac{n-1}{2} = 2$, then the Lane -Emden equation turns into the following recurrence relation for Bessel functions

doi: doi.org/10.52526/25792776-2021.68.2-509

$tJ_1(t) = 2J_2(t) + tJ_2'(t)$. Thus, we have the following representations for $\theta(\xi)$ and $\theta^5(\xi)$ (Bateman & Erdelyi, 1974):

$$\theta(\xi) = \int_0^\infty e^{-\xi t/\alpha} J_0(t) t^\nu dt = \frac{1}{\sqrt{1+\xi^2/\alpha^2}}, \qquad \theta^5(\xi) = \frac{1}{\alpha^2}\int_0^\infty e^{-\xi t/\alpha} J_2(t) t^2 dt = \frac{3}{\alpha^2(1+\xi^2/\alpha^2)^{\frac{5}{2}}} \tag{6}$$

By comparing last integrals, we see that one can make (8) 5th power of (7) if $\alpha = \sqrt{3}$. Thus, we arrive at the following final representation $\theta(\xi) = \frac{1}{\sqrt{1+\xi^2/3}}$ and $\theta^5(\xi) = \frac{1}{(1+\xi^2/3)^{5/2}}$. This is the Emden-Schuster solution for n=5 polytrope with the finite mass, but infinite radius. In the meantime, the formula describes Plummer- Schuster model of globular clusters.

4. Approximate solutions

4.1. n=1.5 and n=2

As we know the case n=1.5 describes internal structure of white dwarfs of low mass with degenerate nonrelativistic electronic gas, fully convective star cores, and the quasi-stationary stellar systems with local thermodynamic equilibrium (Gurzadyan & Kechek (1979)). The case n=2 is within the range acceptable for common stars ($1.5 \leq$ n ≤ 3). The integral equations of these models are complex, but their linear approximation encourage us to search for possible solutions in the form close to $j_0(\xi/\sqrt{n})$, where $j_0(x)$ is a spherical Bessel function. By multiplying this function by correction term in the form of quadratic expression $\theta(\xi)$=$j_0(\xi/\sqrt{n})(1-\frac{\xi^2}{\xi_1^2})$ for n=1.5 and varying the free parameter ξ_1 we could find very good approximations for the Emden function of the polytrope. For n =1.5 ξ_1= 4.47456182 (the radius of the polytrope is found to be 3.8476, the real radius is 3.6538). For n=2 the correction factor is used in the form $1/[1+\xi^2/\xi_1^2]$ and gives $\xi_1 = 3.6$ (the radius obtained is 4.443 against the real 4.353). Graphs of the approximations to Emden functions are shown on Fig.1 and compared with results of numerical integration of the Lane – Emden equation Horedt (1986). The standard deviation of the suggested functions from exact solution is $8.087{\cdot}10^{-3}$ for n=1.5 and $4.12321{\cdot}10^{-3}$ for n=2.

4.2. Isothermal model (n=∞)

This model is of particular interest in astrophysics and stellar dynamics and has been studied in detail by Chandrasekhar (1939). Equation (3) gives us another opportunity to study some basic features of the model, such as the density distribution near the center of isothermal spheres and the main term of its asymptotic behavior. For $\xi \ll 1$ the exponential term in (3) can be replaced by 1 as a first approximation and we obtain $\psi(\xi) = \frac{\xi^2}{6}$ Thus, the density distribution near the center is $\rho(\xi) \approx exp(-\frac{\xi^2}{6}) \approx 1 - \frac{\xi^2}{6}$, which slightly differs from the density of incompressible liquid. The analysis of the equation (3) for the asymptotic behavior of the dimensionless potential and density distribution boils down to the simple equation:

$$\psi(\xi) = \int_0^\xi e^{-\psi(x)} x dx \tag{7}$$

that contains Emden's main asymptotic term $\psi(\xi)$ =$2ln\xi - ln2$ Chandrasekhar (1939), Ivanov (2018) which gives $e^{-\psi(\xi)} {\sim} \frac{2}{\xi^2}$ for the density distribution (solution for a singular isothermal sphere). Because the exact non-singular solution of the equation (6) is unknown, we can find its acceptable approximation by making use of heuristic reasoning and knowing the behavior of the distribution density in the vicinity of the center of the isothermal model and, also, its asymptotic behavior. Here we assume that in the most general form, for n ≥ 5, polytropic models with infinite radii can be described by functions of the type $\theta(\xi)$= $\frac{1}{(1+\delta x^2)^\beta}$, where values of the constants δ his gives δ=1/2 and β= 1/3 at $\xi{\to}0$ and β=1 at $\xi{\to}\infty$. In other words, we accept the possibility that β is a function of the dimensionless distance, which on the entire real axis varies within short range from 1/3 to 1. From the symmetry requirement of the function $\theta(\xi)$ it follows that in the simplest case it must depend on ξ^2. We have tested a set of functions with this property and have found that the best approximation for $\beta(\xi)$ (according to the mean square error estimator) is

$$\beta(\xi) = \frac{1+\frac{\xi^2}{4}}{3+\frac{\xi^2}{4}} \tag{8}$$

doi: doi.org/10.52526/25792776-2021.68.2-509

which results in the following expression for the density distribution:

$$e^{-\psi(\xi)} \approx \varrho(\xi) = (1 + \frac{\xi^2}{2})^{-\beta(\xi)} \tag{9}$$

The mean square deviation of its graph from the exact density distribution for the isothermal sphere, obtained by numerical integration, is $2.685 \cdot 10^{-3}$ (Fig.1). The dimensionless potential $\psi(\xi)$ and the acceleration (a(ξ)) in this case are determined by the following formulas:

$$\psi(\xi) = \frac{1 + \frac{\xi^2}{4}}{3 + \frac{\xi^2}{4}} ln(1 + \frac{\xi^2}{2}) \qquad \alpha(\xi) = \frac{\xi}{3 + \frac{\xi^2}{4}} [\frac{1 + \frac{\xi^2}{4}}{1 + \frac{\xi^2}{2}} + \frac{ln(1 + \frac{\xi^2}{2})}{3 + \frac{\xi^2}{4}}] \tag{10}$$

At large distances ($\xi \to \infty$) the acceleration decreases inversely proportional to the distance: a(ξ) $\sim \frac{1}{\xi}$. For a circular rotational motion then its orbital velocity at large distances reaches at saturation level $v^2 \sim \xi a(\xi) =$ const, while at short distances the velocity changes linearly $v \sim \xi$ wiith the distance from the center, which is in compliance with the properties of the rotation curves of spiral galaxies (see, for example, Wojnar et al. (2018) and references therein). The fact that centers of those galaxies rotate as a rigid body implies that they can be approximately described by the model of an incompressible liquid, which is typical for the central regions of all polytropic models. More detailed discussions of the results obtained as well as comparison with observational data and other theoretical rotation curves will be presented in a later paper.

5. Discussion

The Volterra nonlinear integral equation of the second kind is suggested as an alternative approach to the theory of classical polytropic models in finding exact solutions and analytical approximations to Emden functions that have been obtained so far via numerical integration. The equation is invariant with respect to homology transform. The approach reproduces main solutions of the classical polytropic theory (except for singular solutions which are disallowed by Volterra equation (2)) and helps in finding analytical approximations in closed forms to polytropic models with n=1.5,2 and isothermal spheres. The calculated theoretical rotation curves in the framework of an isothermal model reproduce main features of typical rotation curves of spiral galaxies (Fig 2).

doi: doi.org/10.52526/25792776-2021.68.2-509

References

Bateman H., Erdelyi A., 1974, Higher Transcedental Functions.II. Nauka, Moscow,Russia

Chandrasekhar S. R., 1939, An Introduction to the Study of StellarStructure. The University of Chicago Press, Chicago, Illiinois, USA

Gurzadyan V. G., Kechek A. G., 1979, Preprint, Lebedev Institute AN SSSRl, 180, 13

Horedt G. P., 1986, Astrophys.Space.Sci., 126, 357

Horedt G. P., 1987, A&A, 172, 359

Horedt G. P., 2004, Polytropes-Applications in Astrophysics and related fields. Kluwer Academic Publisher, Dordrecht, Netherlands

Ivanov V., 2018, Astrophysics of stars. Sant-Petersburg State University, Sant-Petersburg, Russia

Mach P., 2012, J.Math.Phys, 53, 1

Medvedev M. E., Rybicki G., 2001, ApJ, 555, 863

Milgrom M., 2021, Phys.Rev.D,, 103, 1

Motsa S. S., Shateyi S., 2012, Mathematical Problems in engineeringl, 2012, 1

Saiyan G. A., 1997, PhD Disertation. National Academy of Sciences of the Republic of Armenia, Yerevan, Armenia

Shaudt U. M., 2000, Ann.Henri Poincarel, 1, 945

Wojnar A., Sporea C. A., A. B., 2018, Galaxiesl, 6, 13

doi: doi.org/10.52526/25792776-2021.68.2-509

Appendices

Appendix A Graphs of analytical approximations in closed forms

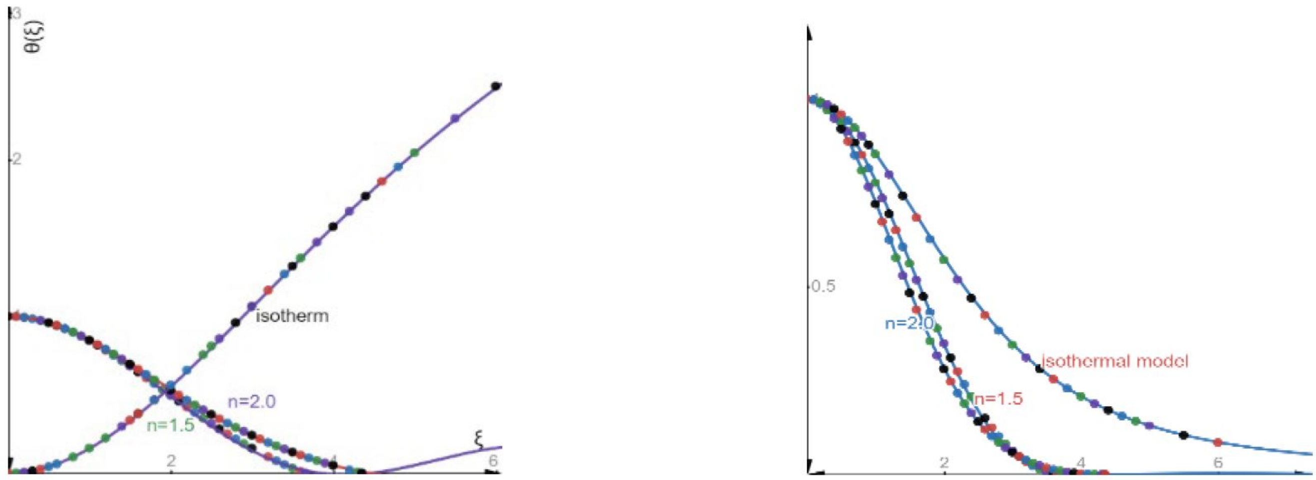

Figure 1. Continuous curves represent analytical approximations of Emden functions (left-hand graph) and density distributions for polytropic models with n = 1.5,2.0,∞. Dots represent exact solutions, obtained by Horedt (1986) via numerical integration.

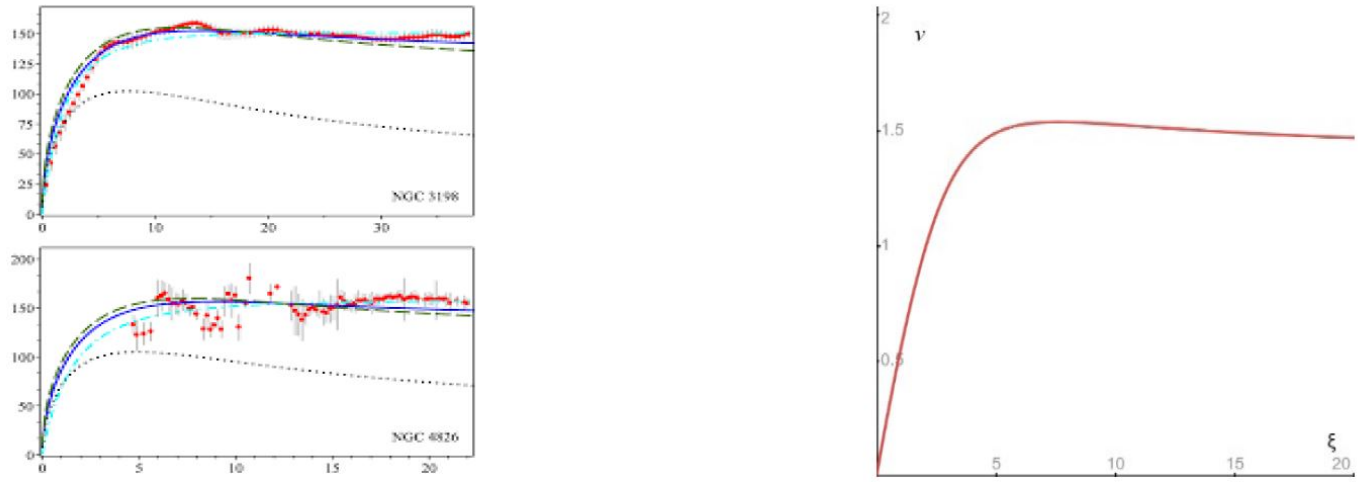

Figure 2. The rotation curves of spiral galaxies (NGC 3198, NGC 4826 from Wojnar et al. (2018) (left-hand graph) and the theoretical rotation curve for an isothermal sphere with the dimensionless gravitational potential in (10).

doi: doi.org/10.52526/25792776-2021.68.2-509

On the STEM Concept Projection on the Field of Astronomical Knowledge

L.A. Gheonjian *[1, 2]

[1]Tamar the King University, Tbilisi, Georgia
[2]Ivane Javakhishvili Tbilisi State University, Faculty of exact and Natural Sciences, Faculty Institute of Electrical and Electronics Engineering, Tbilisi, Georgia

Abstract

Astronomy, as the result of activity and development of the technology of human cognition of his existence environment, should be considered as the basis for an effective educational approach. The STEM (Science, Technology, Engineering and Mathematics) approach has failed because of limitations caused by the focus on the needs of engineering education only. The STEM projection on the field of astronomical knowledge, technology of means, engineering of instrumentation and mathematical modeling as science and technology language, removes limitations and solves the task to form an educated person. This idea finds solid ground if from philosophy, as a tool for unification, we turn to psychology which studies systems organized around the phenomenon of memory with the goal to reflect and comprehend reality in order to create a new reality and environment for preservation of the viability of human being. This approach is present and developed in different aspects of The General Psychological Theory of Set of Dimitri Uznadze. Based on Uznadze, education is an organized process of accumulation in memory of information that we unconsciously, but adequately use in situations of reality recognizing them as already known. Consciousness serves the memory to create new sets of behavior in new previously unknown situations. Education seems to be ideal, if one step by step organizes situations-tasks of consciousness "switching on" to search for solutions in own memory, in external source or experimentally. If one uses the Psychology of Set as a model of the educational process, astronomy is the best information environment for it.

Keywords: *Astronomical knowledge, Astronomical Education, STEM concept.*

1. Formulation of the problem

Astronomy has reached an unprecedented heyday relying on technological progress and setting technological super-tasks of obtaining observational data from the Earth and orbital observatories.We can say that we have come close to creating a model of the universe and are already trying to comprehend the available knowledge for this purpose. Any knowledge, in any field, presupposes bringing information into a certain optimal form suitable both for its storage and for convenient use. As a rule, the task of optimizing the use of information involves the creation of an educational information environment as a springboard for training future professional researchers, but it is equally important to offer this information as a part of the cultural environment taken on trust and stimulating interest in science. In both cases, it is very important to build some information sequences that are easy to understand. However, the construction of each such sequence is not an easy task of adequate information transfer in order to achieve a certain goal.

It would seem that this has long been engaged in education, which has its own specific tools. It also would seem that it is the University that is intended to fulfill this task, and this is its mission. The idea of an ideal university model was introduced in 1944 by Jose Ortega y Gasset (1991). The author found invariants of the model that remain unchanged today. The university is, first and foremost, the higher education that the average person should receive. First of all, the average person should be made a cultural personality, raising him to the level of time. Thus, the first and central function of the university is to familiarize with significant cultural areas of knowledge. The physical image of the World is one of these significant areas. Therefore, when putting in order astronomical knowledge, it is necessary to remember this important goal.

*lev.gheonjian@gmail.com

doi: doi.org/10.52526/25792776-2021.68.2-515

The reality that exists around us, created by our civilization, which distinguishes us from the animal and plant world, is created and is created by the development of engineering approaches. Both the "extraction" and "implementation" of our knowledge into reality is largely due to the purposefulness of engineering approaches and a systematic approach developed in this area for identifying problems and solving them (Ackoff & Emery, 2009). The concept of purposeful systems, brought to an idealized design algorithm (Ackoff et al., 2006), is based on an understanding of the psychology of human activity and is a very effective tool. Moreover, the concept of a purposeful system practically does not differ from the operational definition of intelligence developed in psychology. Apparently the time has come to use the above-mentioned engineering approaches to build a system of astronomical knowledge that is close to the ideal of perception.

This idea finds solid ground if from philosophy, as a tool for unification, we turn to psychology which studies systems organized around the phenomenon of memory with the goal to reflect and comprehend reality in order to create a new reality and environment for preservation of the viability of human being. This approach is present and developed in different aspects of The General Psychological Theory of Set of Dimitri Uznadze (Uznadze (1995), Uznadze (2004)).

2. Ways to solve the problem

It is necessary to solve such problems of systematization and ordering of knowledge in a wide variety of areas. We have to admit that the STEM (Science, Technology, Engineering and Mathematics) approach has failed in school and higher education because of limitations caused by the focus on the needs of engineering education only. The engineering approach itself has been misinterpreted. The standardization required for production technology was unsuccessfully projected onto science, mathematics, and engineering itself as a selection of necessary recipes. The creativity of engineering activity turned out to be unaccounted for.

Another thing is the astronomical knowledge at our disposal, which in the very process of its historical development contained a striving for knowledge, supported by the engineering and technology of creating a wide variety of observational means. Mathematics should be considered as a language for modeling objects of observation, and engineering solutions and technology for the implementation of astronomic engineering projects. The entire history of astronomy is a confirmation of this continuously operating approach-algorithm for obtaining knowledge about the world around us.

One of the successful attempts to implement the described approach can be considered a presentation of the evolution of approaches and solutions related to metrology (Hebra (2010)). When reading this book, there is a temptation to build a physics course based on primary metrological standards and to present physics in a new way for engineers and technologists. Other outstanding examples are also known, for example Zeldovich & Yaglom (1987). Such attempts are always successful when authors consider related fields as tools for obtaining new knowledge in their field.

From the point of view of the cultural value of astronomical knowledge, it would be very useful to build the entire body of astronomical knowledge using the metaphor of our Civilization as the crew of the Spaceship called the Earth, and present astronomers and their activities as the professional activity of navigators and navigators of this ship. The author of this publication consistently and successfully uses this metaphor in public lectures. It is accepted without objection by any audience and listeners of any age. As a rule, one single question-statement arises - is it not so !?

References

Jose Ortega y Gasset 1991, Mission of the University. Routledge

Ackoff R. L., Emery F., 2009, On purposeful systems: An Interdisciplinary Analysis of Individual and Social Behavior as a System of Purposeful Events. Transaction Publishers, Rutgers - The State University, 35 Berrue Circle, Pisccataway, New Jersey.

Ackoff R. L., Magidson J., Addison H., 2006, Idealized Design: How to Dissolve Tomorrow's Crisis Today . Prentice Hall, Upper Saddle River, New Jersey.

Hebra A., 2010, The Physics of Metrology: All about Instruments - From Trundle Wheels to Atomic Clock . Springer

Uznadze D., 1995, Psychology of Set. Springer

Uznadze D., 2004, General Psychology (in russian). Smisl, Moscow-50, a/b 158.

Zeldovich Y., Yaglom I., 1987, Higher Math for Beginners (Mostly Physicists and Engineers). Mir Publishers

doi: doi.org/10.52526/25792776-2021.68.2-515

Communications of BAO, Vol. 68, Issue 2, 2021, pp. 517-521

Preliminary Statistical Analysis of Lambda Bootis Stars

S. Ghazaryan *[1], G.Alecian[2], E.Paunzen[3], and A.A. Hakobyan[4]

[1]Byurakan Astrophysical Observatory, 0213 Byurakan, Aragatsotn province, Armenia
[2]LUTH, CNRS, Observatoire de Paris, PSL University, Universite Paris Diderot, Meudon, France
[3]Department of Theoretical Physics and Astrophysics, Masaryk University, Brno, Czech Republic
[4]Center for Cosmology and Astrophysics, Alikhanian National Science Laboratory, Armenia

Abstract

To enlarge our database of Chemically Peculiar stars, we compiled published data concerning the Lambda Bootis stars observed by high-resolution spectroscopy techniques during last decades. In total, 62 Lambda Bootis stars have been added to the database. To deepen our knowledge on statistical overview of the abundance anomalies versus the physical parameters of stars, our data were compared with previous compilations, as well as with Gaia DR2 data. Different statistical tests were applied on our data for 20 chemical elements for the search of interesting correlations for different physical parameters in the atmospheres of those stars. We confirmed all previous results and obtained correlations between different physical parameters, but because of the lack of the data, we could not find new correlations. We hope, that Gaia EDR3 data, on which we are working now, will help us to improve our database and to understand the nature of all Chemically Peculiar stars.

Keywords: *stars: abundances – stars: chemically peculiar – stars: λ Bootis – methods: statistical – techniques: spectroscopic – catalogue*

1. Introduction

Statistical study of Chemically Peculiar stars we started during last year of my PhD thesis in 2012 with my supervisor from Paris Observatory/Meudon - Georges Alecian and continue to work on that project till nowadays. Later on, we enlarge our collaboration and include on it Artur Hakobyan (2018) - former BAO senior researcher and Ernst Paunzen (2020) from Masaryk University- an expert of λ Bootis stars. During these years we published several articles and catalogues based on the statistical study of different type of Chemically Peculiar stars (Ghazaryan & Alecian, 2016, Ghazaryan et al., 2018, 2019).

So, what we know about λ Bootis stars? First λ Bootis stars was discovered by Jesuit Father Angelo Secchi the Director of Vatican Observatory in 1860s', an excellent spectroscopist, who analysed more than 4000 stars spectroscopically and was very famous astronomer.

Later on, a few women- Morgan and Kellman in collaboration with Philip Kunan produced Henry Drapper Catalogue published between 1918-1924, giving spectroscopic classifications for more than 225.000 and in 1943 they published "An Atlas of Stellar Spectra" (Morgan et al., 1943). In fact, from that Atlas the study of λ Bootis stars begins.

What Morgan and Kellman denote in "An Atlas of Stellar Spectra" about λ Bootis stars, is that the spectral type of λ Bootis stars in near A0, as far as can be determined. The spectral lines, while not unusually broad, are very weak, so that the only features easily visible are as weak K line and the Balmer series of hydrogen.

This idea was a key for Ernst Paunzen and Richard Gray to think that λ Bootis stars may be peculiar ones and to think about the origin of that peculiarity.

At the end of twentieth century Gray showed that there is a so called "garbage bag" between Population I and Population II type stars and that bag is filled by λ Bootis stars. In 1997 Gray showed an example of λ Bootis star spectrum itself sandwiched in between the spectra of normal or standard stars (Gray, 1997). You can see a figure from Gray's paper (see Figure 1), where above the λ Bootis star spectrum is HR 3314 star's spectrum and below β Leo's spectrum. Effective temperature in the atmospheres of both stars is

doi: doi.org/10.52526/25792776-2021.68.2-517

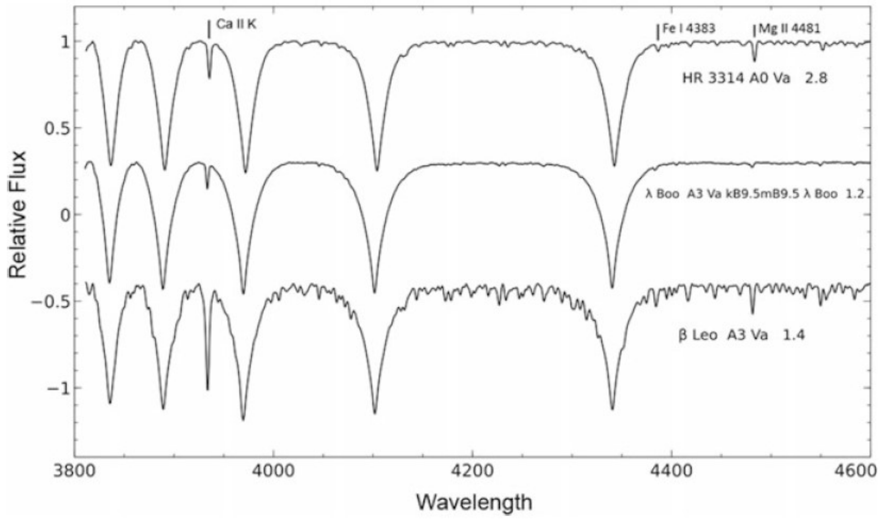

Figure 1. Montage of λ Boo with an MK standard star above and below. The spectra are from the Dark Sky Observatory.

10,000 K. By comparison the spectral lines we see that for λ Bootis stars they are broad, which means that those stars are fast rotators.

Bringed example of λ Bootis star's spectrum shows that it is an A type star belonging to the V class fusing hydrogen to helium in its core, like the Sun. It can also be referred as a main sequence star. It has broad wings to it's hydrogen lines. "kB9.5" refers to the strength of the ionized calcium K line (CaII K) on the left side of the spectrum. Compare it to the substantial CaII K line in β Leo, to which it should match given its' A3 temperature type, and to the still significant one in HR 3314. It is a bit weaker in λ Boo even than A0, and if we took a look at late B-type stars, it would fit with a B9.5 spectrum. "mB9.5" is short for looking at the metal lines due to other elements, particularly iron. There are the tiny "wriggles" in the spectrum, which are weak like CaII K line, again having about the same strength matching a B9.5 star. A λ Boo star is weak-lined, at least regarding to the strength of lines corresponding to its' temperature type, in this case A3. "λ Boo" is the final judgement that this star doesn't just have weak metal lines, but that the weakness is itself peculiar and initiates the prototype, λ Boo. A place to look for this is by comparing the ratio between the MgII λ4481 line and the nearby FeI λ4383 line. That ratio, which is equal to 1.2, appears at the end of the classification in Fig. 1 given by Gray in 1997. In λ Boo the MgII line is noticeably weaker than the iron lines nearby, when compared with the spectrum corresponding to its metal lines, and that is the real clincher.

Unfortunately, even since the time of Gray's definition, not everyone was as careful as he is classifying a star as a λ Bootis star and the "garbage bag" was filled with a lot of non-members of λ Bootis stars group.

In 2015 Murphy published a catalogue of probably candidates of λ Bootis stars, from which only 64 are proofed λ Bootis stars, 103 being definitely non-members and the membership status for 45 of them is still unclear (Murphy et al., 2015).

If we have a look to the plot of chemical abundances of λ Bootis stars given by Ernst Paunzen after Heiter in 2002 (see Figure 2), we see that four elements, which are shaded - carbon, nitrogen, oxygen and sulfur, compared to the standard stars abundances, have near normal abundances, whereas others can range to quite low values - especially for iron-peak elements (Heiter, 2002).

By summarizing the known facts about λ Bootis stars, we can tell that they are A type stars, and the effective temperature in their atmospheres is found in the range of 7,500 - 9,000 K. There are strong underabundances of iron-peak elements in their atmospheres. Carbon, nitrogen, oxygen and sulfur are in the same amount as in the atmospheres of normal stars. They have high rotation velocities, small magnetic fields, and are found in the range of zero age mass stars.

*satenikghazarjan@yahoo.de, Corresponding author

doi: doi.org/10.52526/25792776-2021.68.2-517

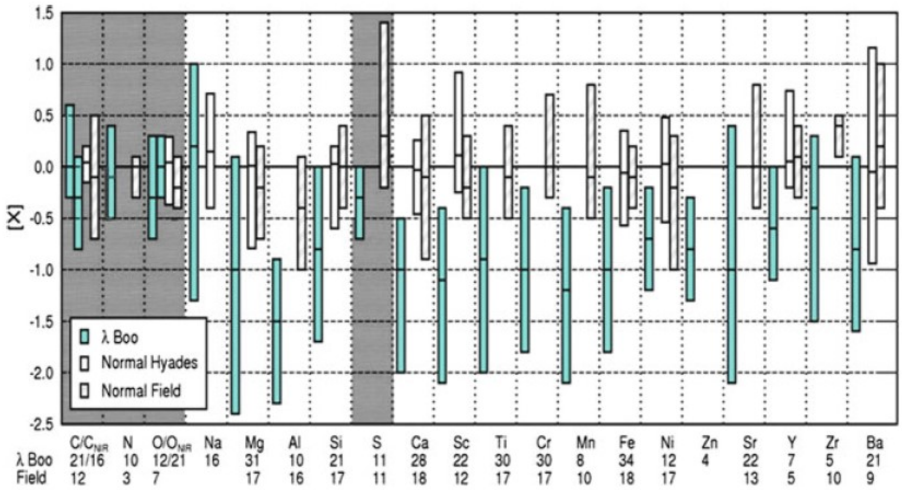

Figure 2. Abundance pattern for λ Boo stars. Plot is created by Paunzen after Heiter (2002).

2. Statistical study

To do statistical analysis we combined from literature all λ Bootis stars, which were observed by high resolution techniques. They were 65 in total. We combined their chemical abundances, known physical parameters - spectral type, effective temperature (T_{eff}), gravity (log g), rotational velocity (v sin$i$) and multiplicity from the papers from which their chemical abundances were taken, and did statistics on them. We applied Spearman Rank and Kendall τ correlation tests widely used on astronomy on chemical abundances, T_{eff}, log g and on v sin$i$ of λ Bootis stars to see the correlation between chemical abundances and physical parameters of those stars. To remind you what those tests are (Feigelson & Babu, 2012), we should tell that Spearman's Rank correlation test performs a hypothesis test on pair of two variables with null hypothesis that they are independent, and alternative hypothesis that they are not. Usually, one accepts the alternative hypothesis of the test than p-value is less than 5 percent. We also pay attention to those cases when the p-values are close to the adopted threshold between 5 and 6 percent (marginal cases). Spearman's coefficient ρ is a non-parametric measure of rank correlation ($\rho \in [-1; 1]$); it assesses how well the relationship between two variables can be described using a monotonic function. When each of the variables is a perfect monotonic function of the other, Spearman's coefficient ρ is +1 or -1.

Kendall τ test is also non-parametric test for statistical dependence based on the τ coefficient. It measures the rank correlation: the similarity of the orderings of the data when ranked by each of the quantities. The Kendall correlation between two variables will be high, when observations have a similar rank (correlation quantity is 1) between the two variables, and low, when observations have a dissimilar rank (correlation factor is -1) between the two variables.

The results, which we obtained, are plotted below (see Figure 3). We found

1) a strong correlation between carbon abundance and gravity,

2) an another strong correlation between oxygen abundance and rotational velocity,

3) a correlation between magnesium abundance and rotational velocity,

4) a correlation between silicon abundance and effective temperature,

5) a correlation between strontium abundance and gravity,

6) a correlation between yttrium abundance and gravity, and finally,

7) a correlation between zirconium abundance and effective temperature and also for gravity.

doi: doi.org/10.52526/25792776-2021.68.2-517

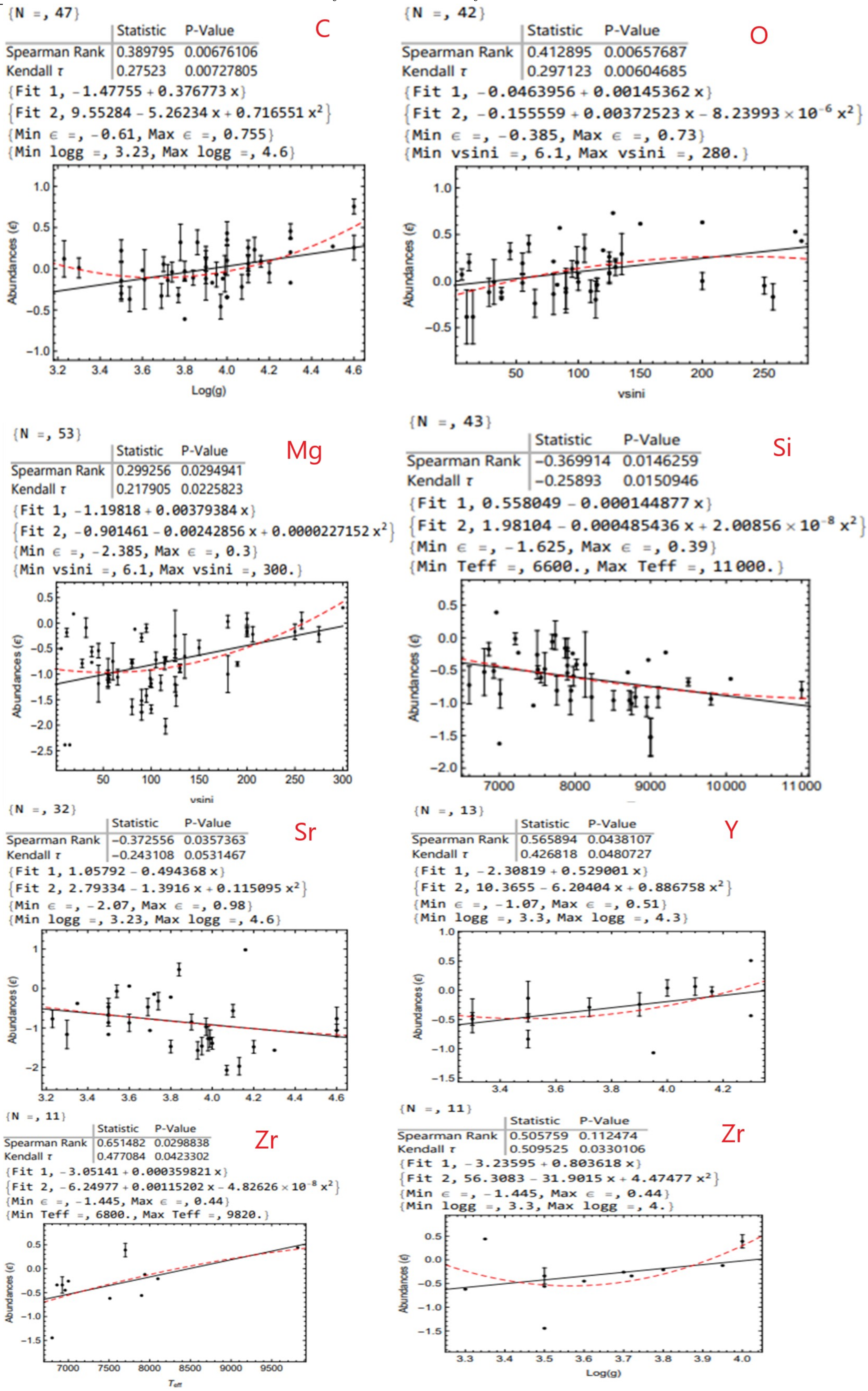

Figure 3. Correlations between λ Boo stars chemical abundances and physical parameters.

3. Conclusions

As you can see from bringed plots, we have perfect correlations between different chemical abundances of λ Bootis stars and their physical parameters. What we are going to do the next? It is, of course, to look to Gaia EDR3 data, which will help us to add much more confirmed λ Boo stars to our database, including

doi: doi.org/10.52526/25792776-2021.68.2-517

their physical parameters. In that case we can make our database homogenous and hopefully get better statistical results. They can help us to understand the nature of λ Boo stars and summing up our whole research - the nature of all Chemically Peculiar stars.

Acknowledgements

SG would like to thank to all coauthors for fruitful discussions and collaboration.

References

Feigelson E. D., Babu G. J., 2012, Modern Statistical Methods for Astronomy

Ghazaryan S., Alecian G., 2016, Mon. Not. R. Astron. Soc. , 460, 1912

Ghazaryan S., Alecian G., Hakobyan A. A., 2018, Mon. Not. R. Astron. Soc. , 480, 2953

Ghazaryan S., Alecian G., Hakobyan A. A., 2019, Mon. Not. R. Astron. Soc. , 487, 5922

Gray R. O., 1997, in Philip A. G. D., Liebert J., Saffer R., Hayes D. S., eds, The Third Conference on Faint Blue Stars. p. 237

Heiter U., 2002, A&A, 381, 959

Morgan W. W., Keenan P. C., Kellman E., 1943, An atlas of stellar spectra, with an outline of spectral classification

Murphy S. J., et al., 2015, PASA, 32, e036

Features of a Sample of Star-forming Galaxies in two Adjacent SBS Fields

S.A. Hakopian *

V.Ambartsumian Byurakan Astrophysical Observatory (BAO), Armenia

Abstract

Some results are presented on studies of a sample of about hundred galaxies ("100SBS") from two adjacent fields of SBS (Second Byurakan Survey), which have spectral data in SDSS (Sloan Digital Sky Survey-www.sdss.org).The work is carried out as a part of the long-term program (Hakopian, 2013) for in-depth study of the galaxies in seven selected SBS fields (including the two under investigation).

Comparative analysis was done between two classifications that the 100SBS objects got - from one side Starburst or Starforming in SDSS, from the other - SfGcont and SfGneb, with a possibility of further detailing in accordance to our scheme for SfG, i.e. star-forming galaxies. Obtained results showed good perspectives in using of our scheme for differentiation of activity phases of SfGs and for better statistics and comprehensive studies. Space distribution of 100 SBS galaxies,what is important, homogeneously selected in continuous (32 sq.deg) area, was obtained using uniformly determined in SDSS redshift values.As it follows from the graphs plotted at 0.01 intervals the maximum of the distribution, with an equal number of Staforming and Starburst galaxies falls on the range $0.01 < z < 0.019$. The minimum of the distribution falls on the range $0.02 < z < 0.029$ and more expressed for Starbursts. Also some difference is discerned in a diversity of morphological appearance of the galaxies composing two neighboring to it intervals.

Keywords: *SBS survey : Star-forming galaxies: Classificatons: Space ditribution.*

1. Introduction

The Second Byurakan Survey (SBS) (Markarian & Stepanian, 1983) was undertaken as a continuation of the Markarian/First Byurakan Survey (FBS) (Markarian et al., 1977) in a searching of active galaxies. Table 1 provides basic information on the survey conduction and the objects selection. Improved methods allowed a fainter limit on photographic plates to be reached, so more objects were detected, in particular, galaxies with emission lines. Most of them are currently being studied as galaxies of star-formation activity, which due to spatial distribution can be considered carriers of the main characteristics of the nearby Universe.

Comprehensive study of star-forming galaxies is an important part of our long-term program. The key role in it is played by SBS galaxies in separate fields, as namely these subsamples can be considered the most homogeneous in the survey. Seven fields were selected (see Fig. 1) out of 65 due to the higher level of completeness by the V/V_{max} test and other details. In the first phase of the program, the follow-up spectroscopy of all approximately 500 objects, constituting seven subsamples, was completed and their basic data, such as redshift values and type of activity, were obtained in accordance with a classification scheme adapted to the spectral material. About 80% of the objects got classification SfG - star-forming galaxy.

To designate the fields, we use a serial number from 1 to 7, based on the order in which the RA values of their centers increase. In a focus of this work are the samples of the 4th and 5th selected fields, which are highlighted in Fig. 1 by a red circle.

2. SfG sample in two adjacent fields of SBS

The 4th and 5th selected fields with centers at 11h 30m +59deg and 12h0m +59deg, respectively, are located side by side and cover a continuous area of the celestial sphere of approximately 32 square degrees. Classification SfG, i.e. star-forming galaxy got 116 out of 158 in all in the fields and approximately a hundred

*susannahakopian@yahoo.com

doi: doi.org/10.52526/25792776-2021.68.2-522

Table 1. The Second Byurakan Survey

OBSERVATIONS	
Byurakan 1-m Schmidt telescope	OBJECT SELECTION
Low-dispersion prisms (deg): 1.5, 3 , 4	Two samples of candidates for active galaxies:
Photographic plates: Kodak IIIa-(J, J, F)	diffuse morphology (d),
(hypersensibilization)	starlike morphology (s).
Filters: no, GG495, RG2	Criteria:
Dispersion (Å mm): 1800 (Hγ), 850 (Hγ), 1100 (Hα)	emission lines (e, e:),
Spectral range(nm): 350-540, 490–540, 630–690	uv-continuum (1,2,3).
Fields: 65×16 sq.deg (1000 sq.deg area)	App.Mag limit (pg): 18.5-19.5

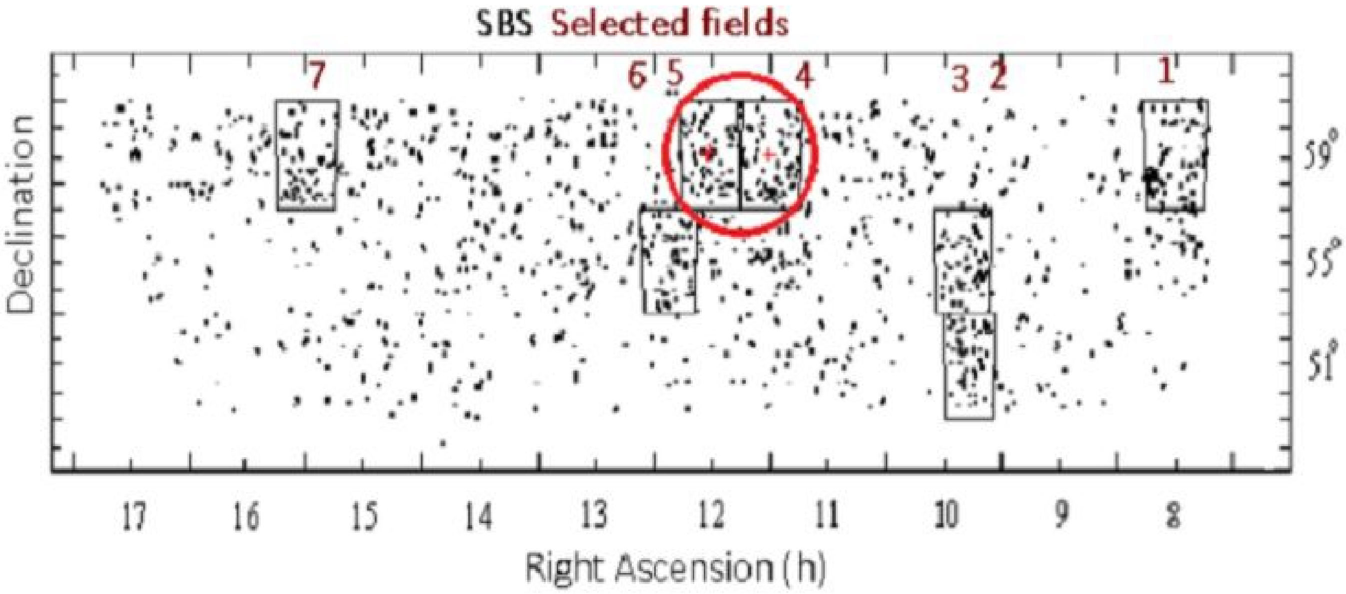

Figure 1. SBS galaxies and seven selected fields.

of 116 (further 100 SBS) are registered in SDSS (DR 16) with one at least associated spectrum (tied to the SBS designations in NED and/or LEDA).The uniformly obtained data of 100 SBS we use in comprehensive analysis. Some preliminary results, which obtained after comparative studies in spectral classifications and to get precise space distribution of the galaxies are given below.

2.1. Spectral classifications

We use the abbreviation SfG for star-forming galaxies to reference specifically to our classification scheme. In general, there is no unified approach to the use of the existing designations indicating the star formation of galaxies. This, in particular, makes it difficult to use them for statistical research or affects the results. Through our studies of homogeneous samples of such objects, we hope to make headway in improving classification schemes.

In our working classification scheme SfGs are divided on two types – SfGcont, i.e. star-forming in continual phase and SfGneb, i.e. star-forming in nebular phase (in some analogy with (Terlevich, 1997). Five numbered subclasses, from 1 to 5, are envisaged for each type in depend of available spectral detailing. The classification is based on the ascending of values of intensity and equivalent width of Balmer Hα line, begining from EW(Hα) = 5 Å for SfGcont_1 and EW(Hα) = 100 Å for SfGneb_1, taking into account the degree of manifestation of absorption lines.

Activity types that assigned in SDSS to 100 SBS galaxies in accordance to their spectra and imply activity of processes are two - Starforming or Starburst. In our scheme we also have two types (see above), but for each of them more detailing presupposed and the results we obtain in comparison show good effectiveness for spectral classification. Data on 5 chosen as examples galaxies are used to illustrate in short how SfG classification works in use.

Figure 2 shows spectra lined up from left to right in the order of increasing activity in correspondence

doi: doi.org/10.52526/25792776-2021.68.2-522

to the SfG classifications, given below each.The image of the galaxy, each spectrum is associated, is shown directly below, in the upper row of images. The 15 galaxies imaged in three rows of Fig. 2 are all those from 100SBS which have $z < 0.09$. The colour of frames of all SDSS images used through the paper indicates, by implication, SDSS activity type – brown means Starforming galaxy, blue - Starburst. A certain tendency can be traced visually along the sequence of spectra, at the same time considerable differences are seen both between spectra of two Starforming galaxies, and between the spectra of three Starbursts.Two other spectra classified as SfGcont_1 and SfGneb_5, i.e. completing the row on both sides, perfectly complement this sequence. They are shown in Fig. 3 together with images of the galaxies, which redshift values lie in the interval $0.01 < z < 0.019$.

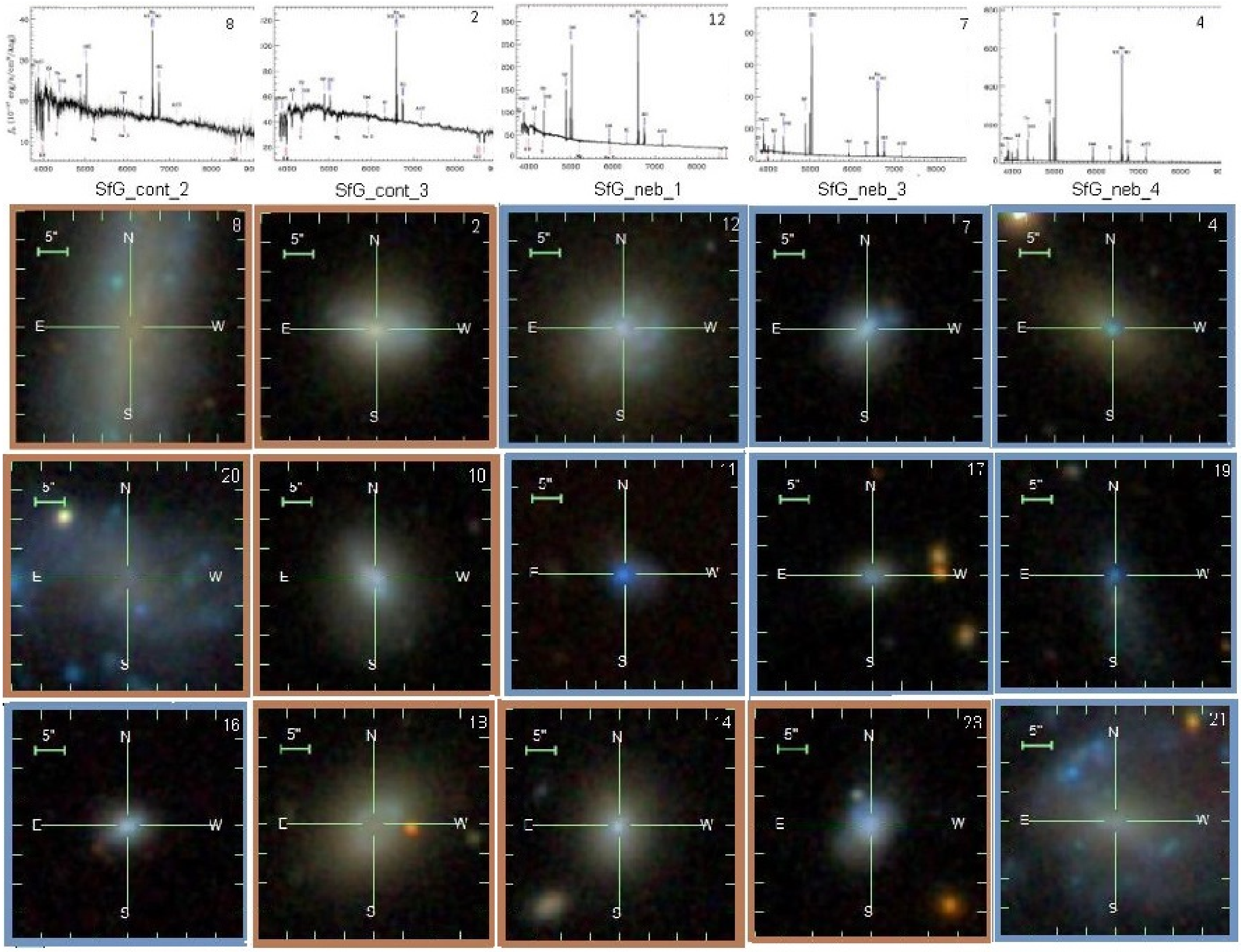

Figure 2. Some SDSS spectra and images of all 15 galaxies from 100 SBS with $z < 0.01$.

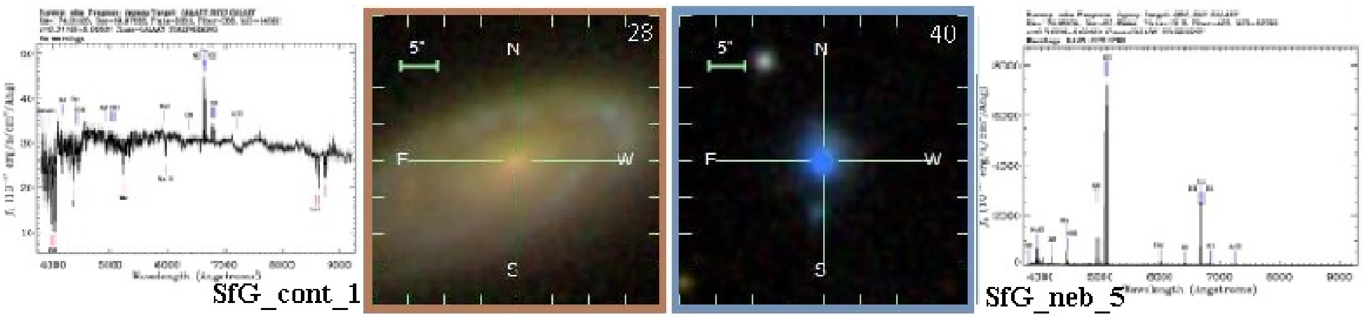

Figure 3. SDSS spectra and images of 2 galaxies from 100 SBS with $0.01 < z < 0.019$.

Thus, it can be assumed that SfG classification has good perspectives. SDSS data on 100 SBS will be an excellent base to make significant improvements in the scheme concerning the quantitative parameters

doi: doi.org/10.52526/25792776-2021.68.2-522

of the spectral lines and other features, including morphological structure of the galaxies.

Also, after the discussion on spectral classifications some clarifications are important.In the sample 100 SBS, which includes only those from SfG galaxies of the two fields classified Starforming or Starburst. Among 16, which remain out of it, 6 also have spectra in SDSS, but classified as Galaxy. Four of them are SfGcont_1, two – SfGcont_2 according to our scheme. It means, that a search in SDSS of starforming (in a wide meaning) galaxies (when completeness is important) by Starforming and Starburst types would be insufficient, and adding Galaxy type in search – meaningless. In this situation we see a manifestation of efficiency of the Second Byurakan Survey in its conduct and selection of objects.

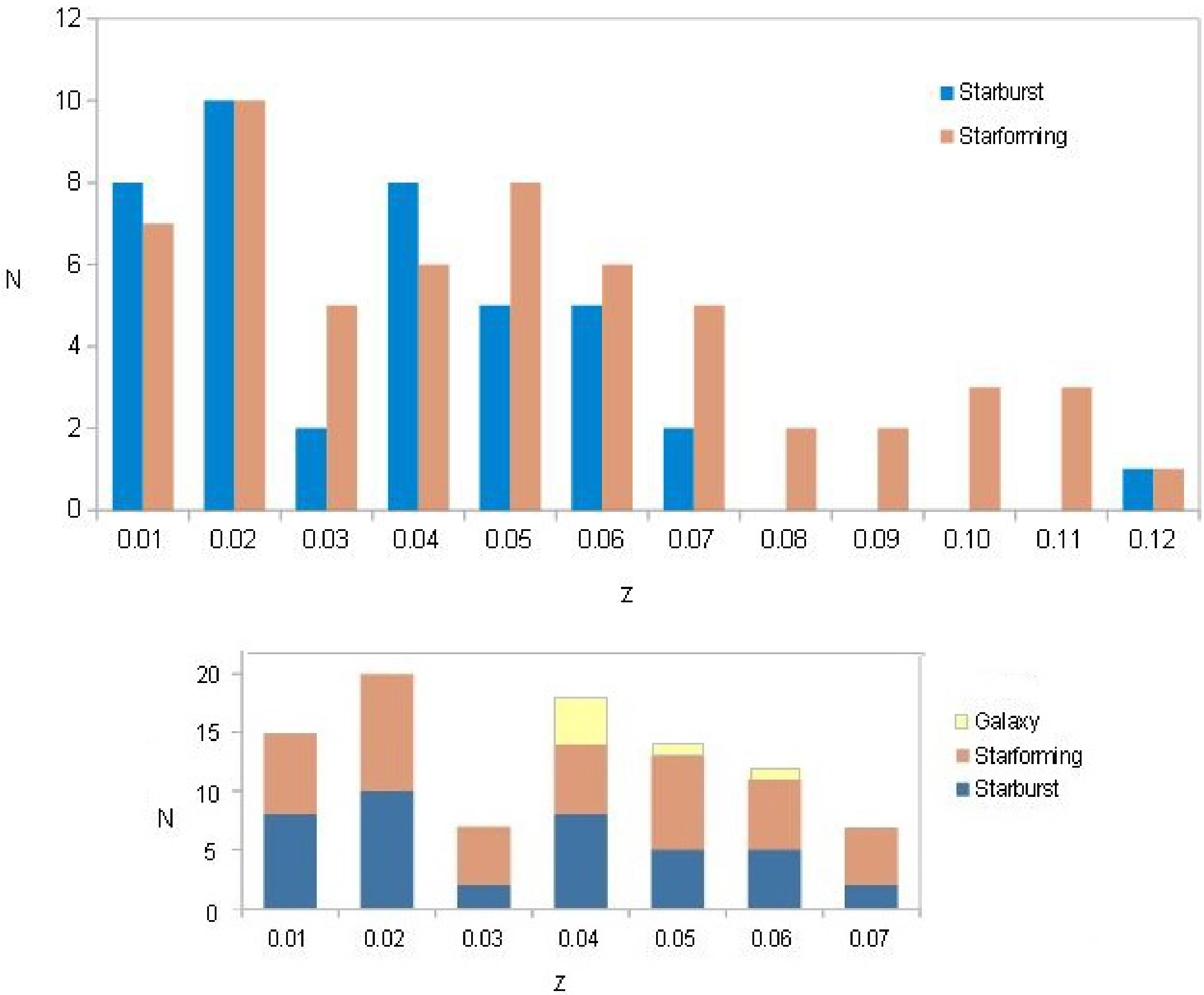

Figure 4. Two graphs of z-distribution of 100 SBS galaxies according to SDSS data

2.2. Space distribution of 100 SBS galaxies

We used the uniformly determined SDSS redshift values to get as precise as possible space distribution of the 100SBS galaxies. By two columns of the upper histogram of Fig.4 the distribution illustrated separately for Starforming and Starburst galaxies up to z = 0.12 with an interval of 0.01. It should be borne in mind that the level of redshift completeness is achieved approximately at 0.07. It depends on the details of the survey realization, such as spectral ranges of the used photographic plates, the registered emission lines and other (see Table 1).

Smaller number of Starbursts in comparison with Starformings at the values of $z > 0.04$ is one of the features of the distribution, which is not clear, as usually Starburst are much brighter. So, that can be question on their space distribution. But the main feature in the range of reliability of the distribution,

doi: doi.org/10.52526/25792776-2021.68.2-522

which is hard not to notice, - that the numbers of galaxies of both types in the range $0.02 < z < 0.03$ is considerably less than in the neighboring intervals. And this minimum in the distribution looks deeper if we add z - values of separately mentioned above objects that remain outside of 100 SBS because of SDSS type Galaxy. This is clearly seen in the diagram in the lower part of Fig. 4.

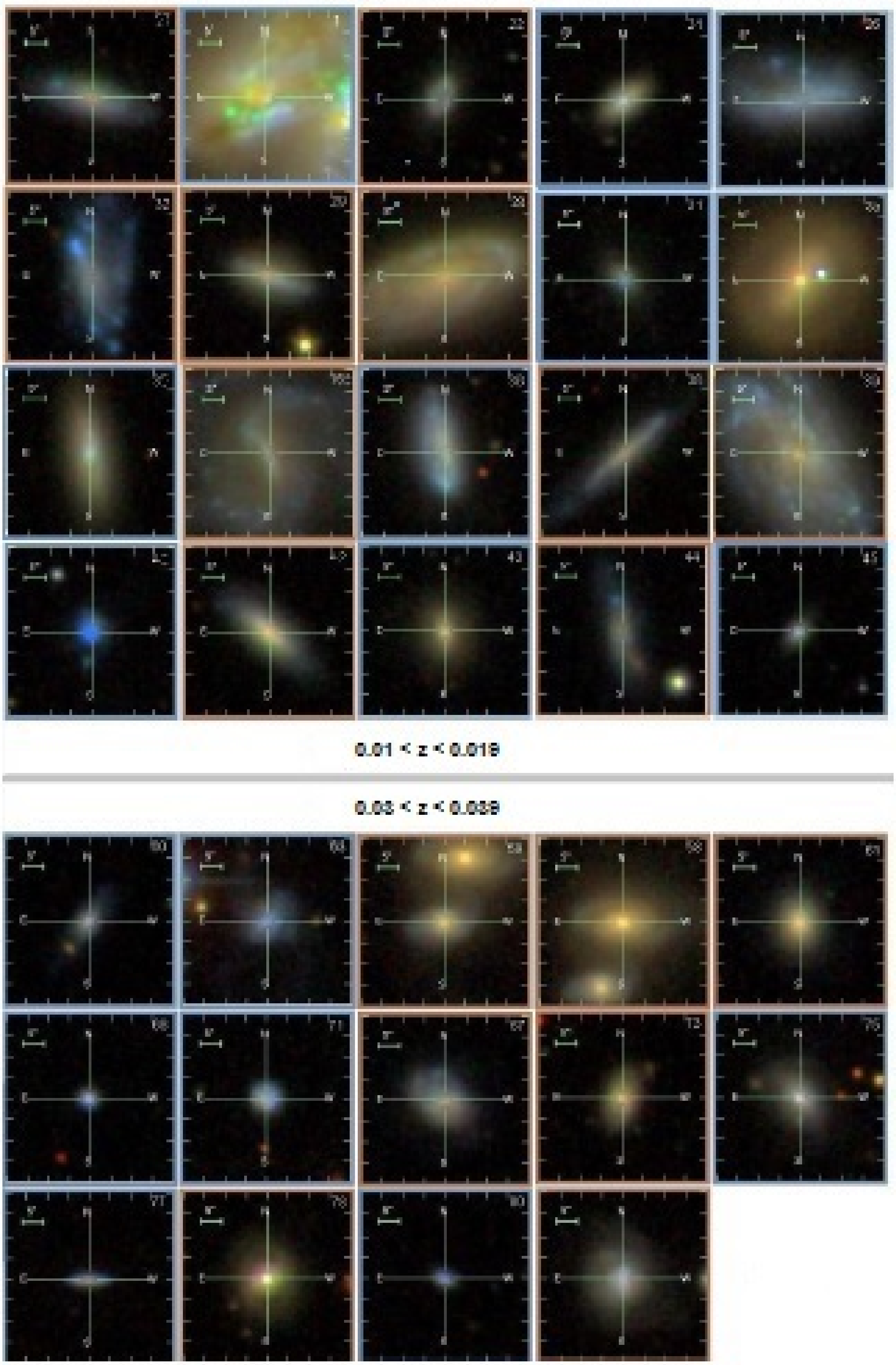

Figure 5. SDSS images of the galaxies from 100 SBS with $0.01 < z < 0.019$ in the upper part, with $0.03 < z < 0.039$ in the lower part of the figure.

doi: doi.org/10.52526/25792776-2021.68.2-522

The peak in the redshifts distribution falls on the interval $0.01 < z < 0.019$ with the same number of Starforming and Starburst galaxies, as it seen from the graphs of Fig. 4. The spectra of two of these objects were discussed above (see Fig. 3). Images of all 20 galaxies from this section are shown in the upper part of Fig.5, in the ascending order of z values – from left to right, row by row, starting from the top. Galaxies filling the interval $0.03 < z < 0.039$ are shown in a similar sequence in the lower part of the Fig. 5. Attentive comparing of the images of galaxies in the upper part of Fig. 5 with the images in the lower part by a visual inspection allows us to make a preliminary assumption that there is some difference between appearance of the galaxies on either side of the interval with minimum of the z – distribution. On the left of it, among the closer objects, including the galaxies in Fig. 2, we see all the diversity of morphology and different spatial orientations.The galaxies on the other side of the minimum look pretty similar and this only applies to the interval $0.03 < z < 0.039$. Among more distant galaxies again more diversity is observed – bright compact objects, developed structures, elongated shapes. Further studies will show how well this assumption is justified.

The dependence of the morphology and orientation of SfG galaxies on the spatial distribution is one of the questions of interest to us, directly related to the evolutionary chain of events.

3. Conclusions

Some results of a study of a sample of about 100 star-forming galaxies using SDSS data are presented.The sample (100 SBS) consists of SBS galaxies selected in two selected survey fields with common continuous area of 32 sq.deg. The list of 100 SBS designations and their data will be published subsequently.Comparing and juxtaposing of classifications that the galaxies got in SDSS with those in accordance to our scheme, which we name SfG classification, showed effectiveness and boundaries of the use of the latter. In the space distribution obtained with SDSS redshift values some peculiarities were revealed, which are required in further studies promising interesting results.More analysis on morphological and other features equally important for understanding of the formation and evolution of star-forming galaxies will be considered in following papers.

Acknowledgements

Funding for the Sloan Digital Sky Survey IV has been provided by the Alfred P. Sloan Foundation, the U.S. Department of Energy Office of Science, and the Participating Institutions. SDSS-IV acknowledges support and resources from the Center for High Performance Computing at the University of Utah. The SDSS website is www.sdss.org.

References

Hakopian S. A., 2013, arXiv:1403.0127,

Markarian B. E., Stepanian D. A., 1983, Astrofizika, 19, 14

Markarian B. E., Lipovetskii V. A., Stepanian D. A., 1977, Astrofizika, 13, 397

Terlevich R., 1997, in Franco J., Terlevich R., Serrano A., eds, Vol. 6, Revista Mexicana de Astronomia y Astrofisica Conference Series. p. 1

doi: doi.org/10.52526/25792776-2021.68.2-522

Communications of BAO, Vol. 68, Issue 2, 2021, pp. 528-533

Study of the X-ray properties of blazars, based on BZCAT catalogue

G. M. Paronyan*, A. M. Mickaelian†, H. V. Abrahamyan‡,

G. A. Mikayelyan § and A. G. Sukiasyan¶

NAS RA V. Ambartsumian Byurakan Astrophysical Observatory (BAO), Armenia

Abstract

The analysis of blazars' parameters from BZCAT leads to a conclusion that they do not have the same properties. The preliminary criterion to include an object in the catalog was the strong radio emission; however, two type of radio sources were selected: BL Lacertae (BLL) objects and Flat Spectrum Radio Quasars (FSRQ). As a number of properties are typical of blazars (strong radio emission, optical variability, continuum optical spectra, polarization, high luminosity, etc.), using the X-ray data, we investigate them to clarify which property plays the most significant role in their classification as blazars.In addition, 48 % of blazars have detected radiation in X-ray have detected. We give the average statistical characteristics of blazars based on our analysis and calculations.

Keywords: *active galactic nuclei, blazar, BLLac, quasar, X-ray*

1. Introduction

Among the Active Galactic Nuclei (AGN) having SuperMassive Black Hole (SMBH), most interesting are blazars, a combination of two subtypes, BL Lac (BLL) objects and Optically Violent Variable/Highly Polarized Quasars (QSOs). A blazar is characterized as a very compact quasar associated with a presumed SMBH at the center of an active, giant elliptical galaxy. Blazars are probably the most energetic phenomena in the Universe. Some rare objectsmay be considered as "intermediate blazars" that have a mixture of properties from both Optically Violent Variable (OVV) or Highly Polarized Quasars (HPQ) and BLL. OVV quasars are similar to BLL but with a normal QSO spectrum (having emission lines). BLL are radio loud. HPQs have polarization typically more than 3 %. They are combined with OVV quasars as a single class. HPQs are made of FR II type radio galaxies. Originally,the BL Lac object has been discovered by Hoffmeister (1929) as a variable star. Later, it was identified by Schmitt (1968) with an extragalactic source.

Blazars are believed to be objects with strong relativistically beamed jets in the line of sight. It is the case when the angle between the relativistic jet axis and the line of sight is small, and the jet is Doppler boosted by a large factor and the whole spectrum (from radio to γ - ray) is dominated by a compact,highly polarized, highly variable, superluminal, almost featureless continuum. The jet accounts for the rapid variability and compact features of both types of blazars (BLL and OVV/HPQ). The generally accepted picture is that OVV quasars are relatively powerful radio galaxies, while BLLs are relatively weak radio galaxies. In both cases, the host galaxies are giant ellipticals.

However, the definition of a blazar is still not well established. These two types have many common and different physical properties. There are many parameters that may be regarded as criteria for definition of blazars, such as high luminosity, radio flat spectrum, presence of X-ray and γ - ray,optical and/or radio variability, polarization, etc.

*paronyan_gurgen@yahoo.com, Corresponding author
†aregmick@yahoo.com
‡abrahamyanhayk@gmail.com
§gormick@mail.ru
¶andranik.suqiasyan.1995@m

doi: doi.org/10.52526/25792776-2021.68.2-528

Many astronomers have made long-term observations to detect the variability of blazars. Most of the works were done for small numbers of blazars and here we compare our list with them. Below, we present the works with which we have made comparisons.

Kurtanidze et al. (2007) investigated 9 X-ray selected blazars using ST-6 CCD camera attached to the Newtonian focus of the 70 cm meniscus telescope in Abastumani Astrophysical Observatory.

Gupta et al. (2008) investigated five blazars using data from a 1.02m optical telescope equipped with a CCD detector and BVRI Johnson broadband filters at Yunnan Astronomical Observatory, China. His observation was between October 27, 2006 and March 20, 2007. In our list,we have five variable blazars from Gupta, Alok C. et al.

Zhang et al. (2015) investigated 71 blazars (49 flat spectrum radio quasars and 22 BL Lac objects) and for the fractional variability, amplitudes of each source have been calculated in both the optical R band and infrared J band. In our list, we have 68 variable blazars from Bing-Kai Zhang et al.

Gaur et al. (2012) investigated 11 blazars using six optical telescopes, four in Bulgaria, one in Greece, and one in India during 2009–2011.

Hovatta et al. (2014) using Palomar Transient Factory (PTF) and the Catalina Real-Time Transient Survey (CRTS) divided 1,958 blazars to study the variability of γ - ray.

Sandrinelli et al. (2014) investigated seven blazars using data from the Rapid Eye Mount telescope telescope located at the European Southern Observatory premises of La Silla (Chile). Light curves were gathered in the optical/near-infrared VRIJHK bands from April 2005 to June 2012.

Liu et al. (2017) investigated five blazars using many telescopes in different areas (Weihai 1 m, Urumqi 1 m, and Abastumani 70 cm, University of Athens Observatory 40 cm).

2. Properties of BLAZARs

To understand some properties of blazars, we used Roma Multifrequency Catalog of Blazars (BZCAT) 5th version (Massaro et al., 2015). Altogether, 3561 objects are given as BLL, BLQ, BLG, or BLU corresponding to BLL, FSR quasars, galaxies, and blazars of uncertain/transitional type (Table 1). BLU are adopted for sources with peculiar characteristics but also showing blazar activity: occasional presence/ absence of broad spectral lines or features, transition objects between a radio galaxy and a BLL, etc.

Table 1. Distribution of types of objects in BZCAT catalog

N	Type	Number	Percentage
1	BLL	1151	32.3
2	BLG	274	7.7
3	BLQ	1909	53.6
4	BLU	227	6.4
5	All	3561	100

In Figure 1, we give redshift distribution of BZCAT blazars (Abrahamyan et al., 2019).

In BZCAT catalog, there is information on magnitude in the R band and redshift. Having this, we counted absolute magnitudes for blazars using formula 1 (Véron-Cetty & Véron, 2010).

$$M = m + 5 - 5 \times LogD - f(z) + \Delta m(z), \tag{1}$$

where D is the luminosity distance as defined by Riess et al. (2004):

$$D = \frac{c \times (1+z)}{H_0} \times \int_0^z [(1+z)^3 \times \Omega_M + \Omega_\Lambda]^{-0.5} dz, \tag{2}$$

z is the redshift, $f(z) = -2.5 \times log(1+z)^{1-\alpha}$ the $f(z)$ correction, $\Delta m(z)$ is a correction to $f(z)$ considering that the spectrum of quasars is not strictly a power law of the form $S \sim \theta^{-\alpha}$ ($\alpha = -0.3$, Paronyan et al. (2021), Véron-Cetty & Véron (2010)). The following values were taken for the cosmological constants in the calculations: $\Omega_M = 0.29$, $\Omega_\Lambda = 0.71$, and $H_0 = 71 km \times s^{-1}/Mpc$.

In Figure 2, we give graphs of the absolute magnitude versus redshift. Basically, three separated areas (BLL, BLG, and BLQ) are observed. Three types of blazars (BLL, BLG, and BLQ) are mostly separated, but there is overlap with each other to some extent.

doi: doi.org/10.52526/25792776-2021.68.2-528

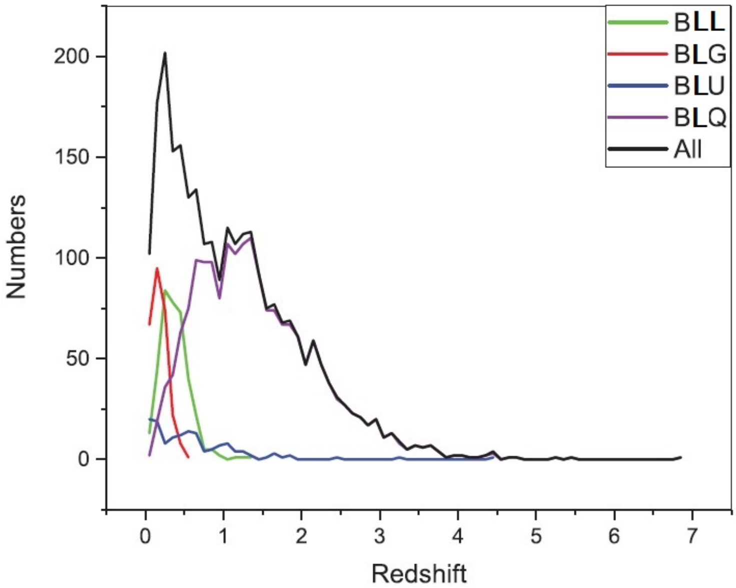

Figure 1. Redshift distribution of BZCAT blazars.

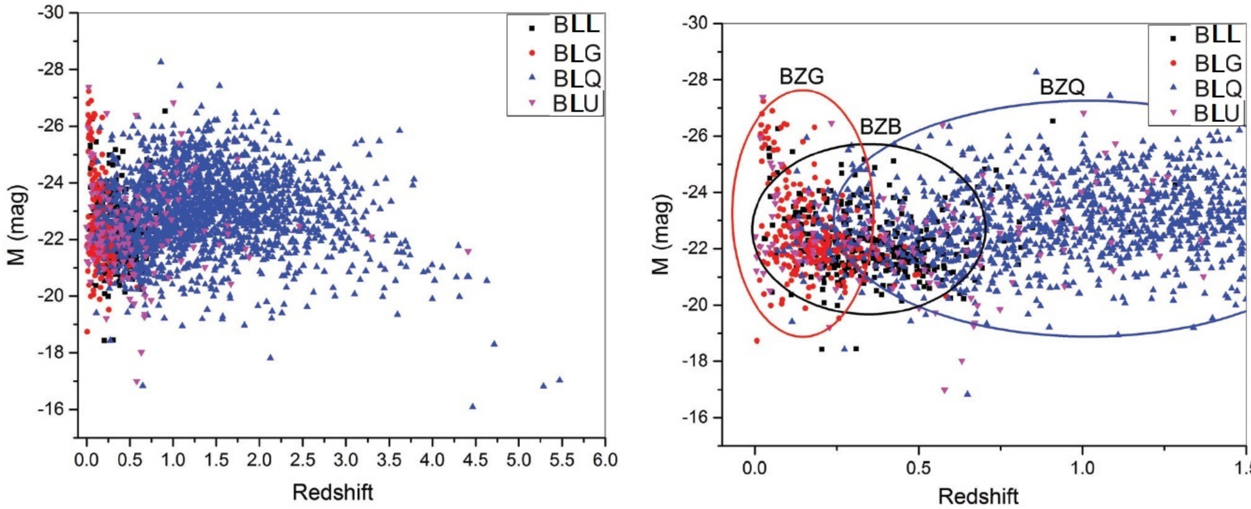

Figure 2. Absolute magnitude *vs*. redshift

.

Having the absolute magnitude, we calculated luminosities for blazars using formula 3.

$$L = L_{\odot} \times 2.512^{M_{\odot} - M}, \tag{3}$$

where $L_{\odot}$ and $M_{\odot}$ are luminosity and absolute magnitude of Sun ($L_{\odot} = 3.83 \times 10^{33}$ erg s^{-1}, $M_{\odot} = 4.83$). In Table 2, we give the luminosity range, average luminosity, absolute magnitude range, and average absolute magnitudes for different types of BLLs and FSRQs from the blazars catalog.

Note that the luminosity and absolute magnitude of galaxies have also contribution from the host galaxies, while BLLs and QSOs are typically pure nuclei. The numbers are approximately similar, so we do not find any significant difference between the BLL and FSRQ.

3. Cross-correlations with X-ray catalogs and collection data

Having 3561 blazars that have radio variability.

We cross-correlated these radio sources with X-ray catalogs: ROSAT (Boller et al., 2016), Swift-BAT (Oh et al., 2018), Chandra (Evans et al., 2010), XMM (Webb et al., 2020). In Table 3 given information of the cross-correlation X-ray catalogs.

In Table 4 information is given of the cross-correlation of optical catalogs (Abrahamyan et al., 2015).

doi: doi.org/10.52526/25792776-2021.68.2-528

Table 2. Luminosity range, average luminosity, absolute magnitude range, and absolute magnitude for different types of objects from the Blazars catalog

N	Type	Luminosity range (W)	**Average** luminosity (W)	**Absolte** magnitude range	**Average** absolute magnitude
1	BLL	$8.05 \times 10^{28} \div 5.32 \times 10^{41}$	3.45×10^{39}	$-15.09 \div -30.18$	-23.75
2	BLG	$6.54 \times 10^{35} \div 1.38 \times 10^{39}$	7.85×10^{37}	$-18.86 \div -27.08$	-22.76
3	BLQ	$5.63 \times 10^{35} \div 7.46 \times 10^{41}$	4.11×10^{39}	$-18.15 \div -30.52$	-25.27
4	BLU	$3.58 \times 10^{30} \div 9.53 \times 10^{40}$	1.18×10^{39}	$-18.16 \div -28.68$	-23.65
5	All	$8.05 \times 10^{28} \div 7.46 \times 10^{41}$	3.37×10^{39}	$-15.09 \div -30.52$	-24.57

Table 3. Identifications of blazars with X-ray catalogs

Name	**Band**	**Number of sources**	**Name**	**Band**	**Number of sources**
ROSAT			XMM-NEWTON		
R_b	0.1 - 2.0 kev	1590	N1	0.2 - 0.5 kev	94
Chandra			N2	0.5 - 1.0 kev	94
b	0.5 - 7.0 kev	234	N3	1.0 - 2.0 kev	94
h	2.0 - 7.0 kev	218	N4	2.0 - 4.5 kev	94
m	1.2 - 2.0 kev	226	N5	4.5 - 12.0 kev	94
s	0.5 - 1.2 kev	234	SWIFT		
u	0.2- 0.5 kev	219	S_b	14 - 195 kev	116
w	0.1 - 10.0 kev	9			

4. Study of the X-ray data

In Table 5, we give average X-ray luminosity and HR1, HR2 data for different types our blazars. From the table, we can say that, on average, BLQ is have highth luminous than BLL and BLG (BLQ > BLL > BLG). There is a difference for the values HR1 and HR2 (HR1; BLG > BLQ > BLL), (HR2; BLQ > BLG > BLL).

Having X-ray luminosity, we have built the dependence of luminosity on redshift graph (Figure 3).

In Figure 3, we can see that, on average, BLG are closer than BLQ, and BLQ blazars are brighter than BLG on average.

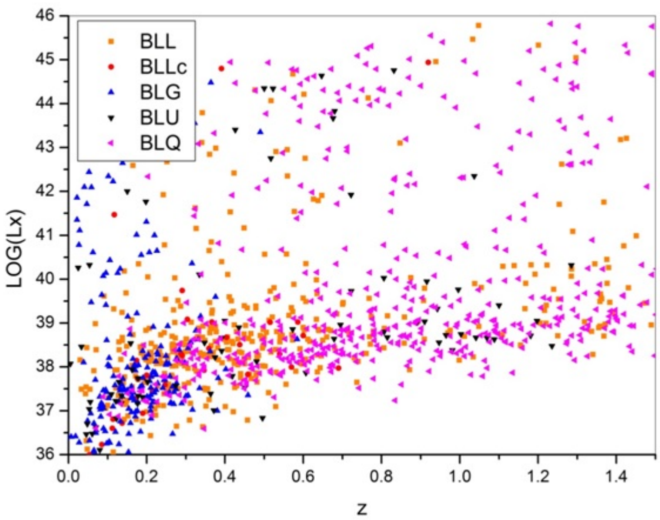

Figure 3. Distribution of redshift to X-ray luminosity BZCAT blazars.

In Table 6, we give the ratio optical luminosity to X-ray luminosity for different types blazars. From the table, we can say that, on average, BLQ is have highth value than BLL and BLG (BLQ > BLL > BLG).

Active galaxies are very interesting objects in the Universe. In order to understand some physical properties, we must identify which properties our objects have in X-ray range. We have 1718 active galaxies

doi: doi.org/10.52526/25792776-2021.68.2-528

Table 4. Optical identifications of blazars

N	Catalogs	Epoch	Photobands	Identified objects
1	APM	POSS1	b,r	1977
2	USNO A2.0	POSS1	B1, R1	3151
3	USNO B1.0	POSS1/POSS2	B1, R1/B2, R2	3492
4	GSC 2.3.2	POSS2	F, j	3501
5	SDSS DR16		u,g,r,i,z	1446

Table 5. X-ray Luminosity range, average luminosity, HR1 range, and HR2 range for different types of objects from the Blazars catalog

N	Type	**Luminosity** range (W)	**Average** luminosity (W)	**Average** HR1 range	**Average** HR2 range
1	BLL	$8.90 \times 10^{31} \div 1.45 \times 10^{46}$	8.89×10^{43}	0.218	0.151
2	BLG	$1.51 \times 10^{35} \div 3.01 \times 10^{44}$	2.83×10^{42}	0.415	0.199
3	BLQ	$3.89 \times 10^{36} \div 1.07 \times 10^{47}$	1.05×10^{45}	0.328	0.203
4	BLU	$9.02 \times 10^{30} \div 5.72 \times 10^{44}$	1.89×10^{43}	0.434	0.177
5	All	$9.02 \times 10^{30} \div 1.07 \times 10^{47}$	5.31×10^{44}	0.308	0.181

with X-ray fluxes at different wavelengths. A very important X-ray property for objects is the X-ray spectral index. It shows steep spectra. Using more bands, we have developed a graph for all galaxies (lg[flux] vs. lg[frequencies]). Using an lg[flux] versus lg[frequencies] graph for each source, we have made linear fitting. The software "Origin" gives the formula for each linear fit, and using that, we have measured the X-ray spectral index for each source. The plot shows steep spectra for each line, and that is considered spectral index. As examples, we give average X-ray spectra for our objects in Figure 4.

In Figure 4, average X-ray spectra for different types of our objects are given. It is obvious that BLQ on average, have steeper X-ray spectra than BLL, BLU and BLGs (Table 7).

Table 7 illustrates the average information of spectral indices.

Using information from Table 7, we can see that BLL and BLG have the same spectra on average, but BLQ has steeper spectra than BLL and BLG.

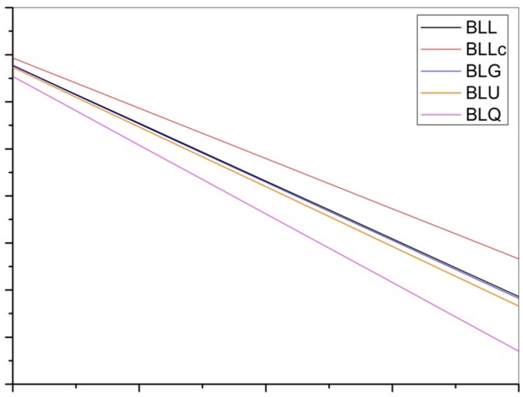

Figure 4. Distribution of X-ray spectral index BZCAT blazars.

5. Summary and Conclusion

We have analyzed flux and luminosities for 1572 blazars (ROSAT 0.1-2.0 kev band) (L_{BLL}= 8.89 $\times10^{43}$ W, L_{BLG} =2.83 $\times10^{42}$ W, L_{BLQ} =1.05 $\times10^{45}$ W , L_{BLU}=1.89 $\times10^{43}$ W, L_{BLLc}= 4.69 $\times10^{43}$ W).

We have analyzed absolute magnitudes and luminosities for 3117 blazars (SDSS DR16 r band) (M_{BLL} = -23.75, M_{BLG} = -22.76 , M_{BLQ}= -25.27, M_{BLU} = -23.65, M_{BLLc}= -22.58, L_{BLL}= 3.45 $\times10^{39}$ W, L_{BLG} = 7.85 $\times10^{37}$ W, L_{BLQ} = 4.11 $\times10^{39}$ W , L_{BLU}= 1.89$\times10^{37}$ W, L_{BLLc}=3.14 $\times10^{38}$ W).

We analyzed X-ray spectral indices for 1572 blazars (α_{BLL}= -3,075, α_{BLLc} = -3,054, α_{BLG} = -3,095, α_{BLU} = -3,168, α_{BLQ}= -3,659). On average, BLL and BLG have the same X-ray spectra, whereas BLQ has

doi: doi.org/10.52526/25792776-2021.68.2-528

Table 6. Distribution of dependence SDSS r band luminosity to ROSAT X-ray luminosity for Blazars (Lg (Lr/Lx))

N	Type	Min	Max	Average
1	BLL	-7.35	2.16	-1.09
2	BLG	-6.89	3.39	-0.71
3	BLQ	-7.84	1.96	-1.58
4	BLU	-6.84	2.31	-0.83

Table 7. Distribution of X-ray spectral index

N	Type	X-ray index
1	BLL	-3.075
2	BLG	-3.095
3	BLQ	-3.659
4	BLU	-3.168

steeper X-ray spectra than BLL and BLG.

We have estimated physical sizes for our objects. That objects of various activity types statistically have the same average sizes. However, due to small number of objects, this result is statistically not substantiated; hence, we need further studies using bigger numbers of objects to follow the real differences in distributions of physical sizes for different types of Blazars.

Acknowledgements

The work was supported by the Science Committee of RA, in the frames of the research project No. 21AG-1C053 " Revelation of the early stages of galaxy evolution by means of multiwavelength study of active galaxies".

References

Abrahamyan H. V., Mickaelian A. M., Knyazyan A. V., 2015, Astronomy and Computing, 10, 99

Abrahamyan H. V., Mickaelian A. M., Paronyan G. M., Mikayelyan G. A., 2019, Astronomische Nachrichten, 340, 437

Boller T., Freyberg M. J., Trümper J., Haberl F., Voges W., Nandra K., 2016, Astron. Astrophys. , 588, A103

Evans I. N., et al., 2010, Astrophys. J. Suppl. Ser. , 189, 37

Gaur H., et al., 2012, Mon. Not. R. Astron. Soc. , 425, 3002

Gupta A. C., Fan J. H., Bai J. M., Wagner S. J., 2008, Astron. J. , 135, 1384

Hoffmeister C., 1929, Astronomische Nachrichten, 236, 233

Hovatta T., et al., 2014, Mon. Not. R. Astron. Soc. , 439, 690

Kurtanidze O. M., Nikolashvili M. G., Kimeridze G. N., Sigua L. A., Kapanadze B. Z., 2007, in Karas V., Matt G., eds, Vol. 238, Black Holes from Stars to Galaxies – Across the Range of Masses. pp 399–400, doi:10.1017/S1743921307005649

Liu X., et al., 2017, Mon. Not. R. Astron. Soc. , 469, 2457

Massaro E., Maselli A., Leto C., Marchegiani P., Perri M., Giommi P., Piranomonte S., 2015, Astrophys. Space. Sci. , 357, 75

Oh K., et al., 2018, Astrophys. J. Suppl. Ser. , 235, 4

Paronyan G. M., Mickaelian A. M., Abrahamyan H. V., Mikayelyan G. A., 2021, Astrophysics, 64, 277

Sandrinelli A., Covino S., Treves A., 2014, Astron. Astrophys. , 562, A79

Schmitt J. L., 1968, Nature. , 218, 663

Véron-Cetty M. P., Véron P., 2010, Astron. Astrophys. , 518, A10

Webb N. A., et al., 2020, Astron. Astrophys. , 641, A136

Zhang B.-K., Zhou X.-S., Zhao X.-Y., Dai B.-Z., 2015, Research in Astronomy and Astrophysics, 15, 1784

doi: doi.org/10.52526/25792776-2021.68.2-528

Investigation of DFBS late type stars at high galactic latitudes.

G. R. Kostandyan*

V .A. Ambartsumian Byurakan Astrophysical Observatory, Armenia

Abstract

We study in this thesis relatively bright late-type giants found in the First Byurakan Survey (FBS) data base.We present the 2nd version of the catalogue of FBS LTS with new data (FBS LTS v2), 1471 objects. It is a homogeneous and complete database for high- Galactic late-type stars, including M and C types. Since 2007, all FBS low-resolution spectral plates are digitized. All DFBS spectral plates are analyzed with FITSView and SAO Image ds9 and numerous relatively faint LTS were discovered. We have made cross-correlation with DFBS, USNO-B1.0, 2MASS, AllWISE, IRAS PSC/FSC, AKARI, ROSAT BSC/FSC, GCVS, SDSS and added updated SIMBAD data. For numerous new detected objects, we present accurate DSS2 positions, approximate spectral subtypes refined from the DFBS low-dispersion spectra, luminosity classes estimated from 2MASS colours, and available proper motions for 1471 FBS LTS. The Revised and Updated Catalogue v2 lists a large number of completely new objects, which promise to extend very significantly the census of M giants, faint N-type AGB carbon stars, CH-type carbon giants at high Galactic latitudes, also M dwarfs in the Solar vicinity up to 16.0m-17.0m in visual. Phase dependent light-curves from large sky area variability data bases such as Catalina Sky Survey (CSS) and All-Sky Automated Survey for Supernovae (ASAS-SN), and the early installment of the third *Gaia* data release (Gaia EDR3) photometric and astrometric data have been used to characterize our sample of 1100 M-type giants found and 130 C-type stars at high latitudes. We show the behaviour of our sample stars in a *Gaia* DR2 color–absolute magnitude diagram (CaMD), the *Gaia*-2MASS-diagram, including two alternative versions, and the logP-K-diagram. In this way we explore the potential of these diagrams and their combination for the analysis and interpretation of datasets of LPVs. We show the possibility to classify stars into M- and C-types and to identify the mass of the bulk of the sample stars.

Keywords: *carbon stars: surveys: late – type stars*

1. Introduction

The First Byurakan Survey (FBS, known also as a Markarian survey) is an objective – prism low – resolution (lr) survey. It is performed with the Byurakan Observatory 1 m Schmidt telescope, which covers about 17.000 sq. deg. of the Northern sky and part of the Southern sky at high Galactic latitudes defined by δ > -15^o and IbI > 15^o. The FBS was originally conducted for galaxies with ultraviolet excess (UVX) Markarian et al. (1989). Since 1990s, the lr plates of the FBS was used to select comparatively faint (fainter than 12 mag. in visual) late – type stars (LTS, M and carbon (C) stars) at high latitudes. The large spectral range of the FBS (λ 3400 – 6900 Å) is well suited to identify cool M – type or C – type stars. C stars can be identified through the presence of Swan bands of C_2 molecule at 4737, 5165, and 5636 Å (N – type C stars). Several objects showing the C_2 band-head at 4382 Å are early – type C stars (R or CH type stars). M – type stars can easily be distinguished because of the titanium oxide (TiO) molecule absorption bands at 4584, 4762, 4954, 5167, 5500 and 6200 Å Gigoyan & Mickaelian (2012). The eye – piece search (with magnification 15x) near 2000 FBS lr plates resulted to discovery 1045 new LTS. On the base of this selection the “Revised And Updated

*kgayane@gmail.com

doi: doi.org/10.52526/25792776-2021.68.2-534

Catalogue of the First Byurakan Survey of LTS" was generated Gigoyan & Mickaelian (2012). Now the entire plate set of the FBS has been digitized (1874 plates for 1139 fields) leading to the Digitized First Byurakan Survey (DFBS) Mickaelian et al. (2007) (online at http://byurakan.phys.uniroma.it or http://www.ia2-byurakan.oats.it /).

We present in this this thesis the 2nd revised and updated version of the FBS LTS Catalogue at high Galactic latitudes, which is a comprehensive list of 1471 objects (compared to 1045 objects in FBS LTS v1),the methods of selecting and spectral classification of the late type stars of the First Byurakan Survey, the photometric study of the FBS late type stars in the infrared range, GAIA study of the FBS late type stars and the variability study of the FBS late type stars based on CATALINA, NSVS and ASAS-SN. The CATALINA and LINEAR long periodic variables are also studied.

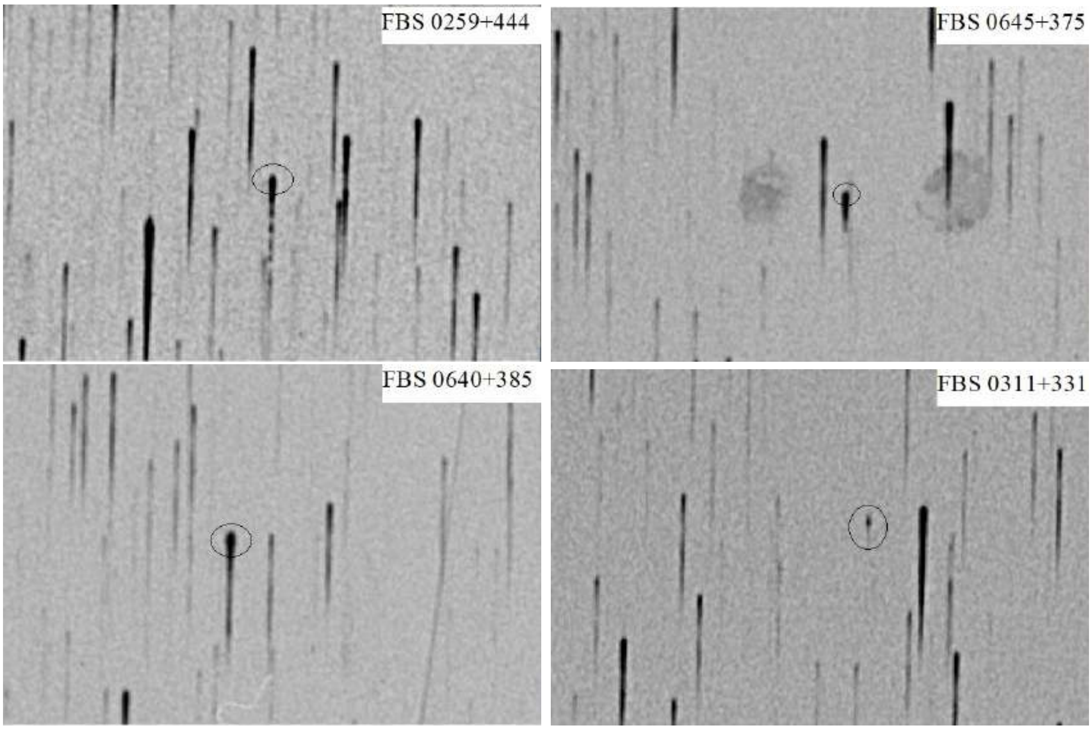

Figure 1. Two-dimensional low-resolution spectral shapes for the newly discovered DFBS objects.

2. Revised and updated catalogue of the First Byurakan Survey late-type stars. 2nd edition

All DFBS spectral plates (near 1800) are analyzed with the help of standard image analysis software (FITSView and SAOImage ds9). This visualization allows us to detect very red and faint candidate stars close to the limit in each DFBS plate (particularly, the range ~6500-6900 Å for the very late subclasses of the N-type and M-type stars and to perform a better selection of red objects using the possibilities of the analysis software (zooming the frame region et al.) compared to the eye-piece (lens) search used before. The second and very significant advantage is using the image analysis software for comparatively bright ($m_v \sim 12 - 13^m$) early type C stars, for which in the blue part of the low-resolution spectra the C_2 absorption bands are not easy detect due to saturation. Such visualization allowed us to detect additional 426 new faint objects, 27 C stars of early and late-subtypes, and also 399 stars of M classes.

Figure 1 shows examples of two-dimensional low-resolution spectral shapes for the newly discovered DFBS objects .

For FBS LTS medium-resolution spectra were obtained on diferent epochs with the BAO 2.6m telescope (UAGS, ByuFOSC2 and SCORPIO spectrographs; Abramyan & Gigoyan (1993)). C - rich nature for FBS candidates were confirmed also by moderate and high-resolution CCD spectroscopy,

doi: doi.org/10.52526/25792776-2021.68.2-534

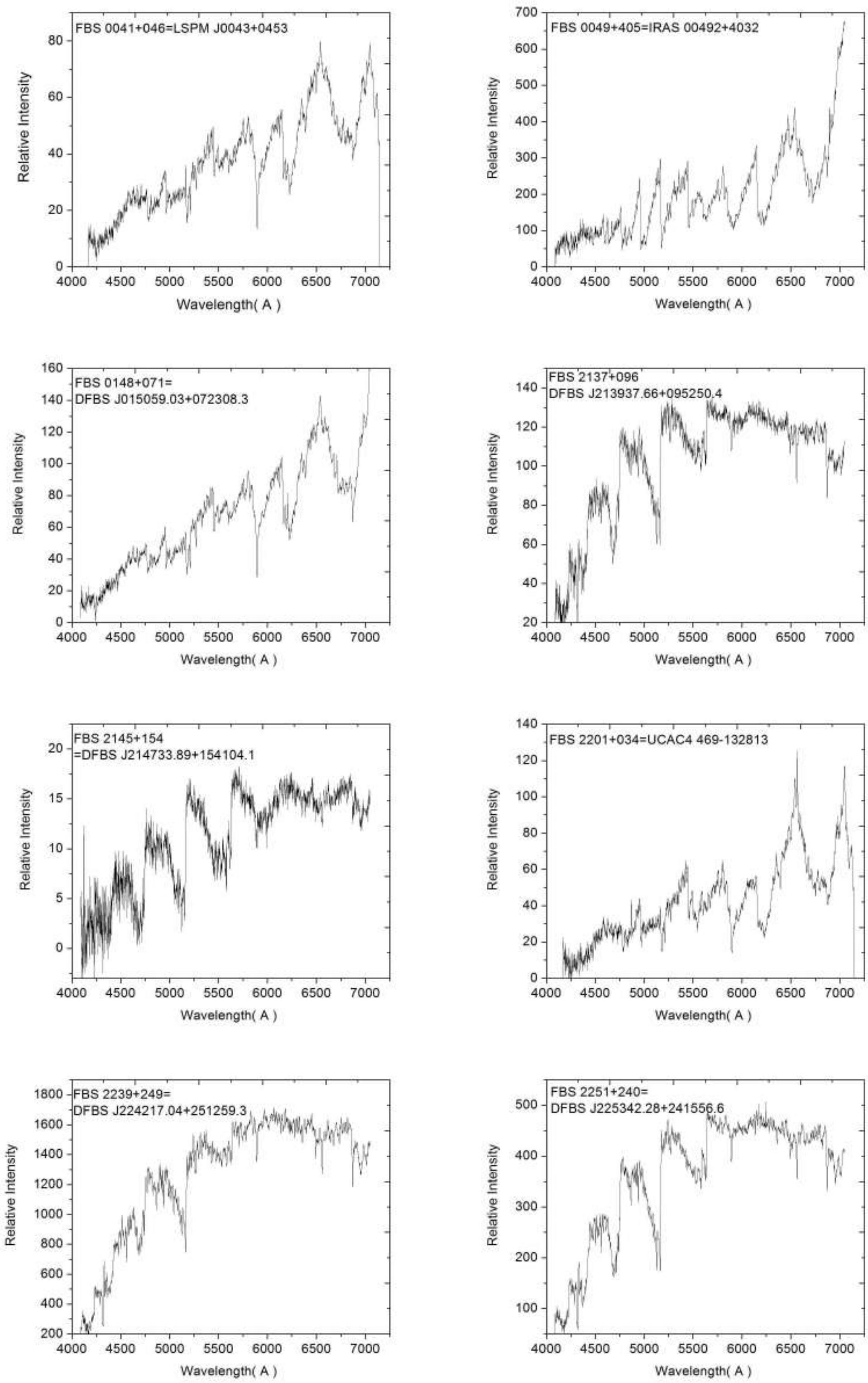

Figure 2. 2.6 m BAO telescope moderate-resolution CCD spectra for objects Table 1

doi: doi.org/10.52526/25792776-2021.68.2-534

Table 1. Data for 8 FBS Late-Type Stars

FBS Number	Other Association	Exp. time (sec)	Sp. class	Lum. Cl.
0041+046	LSPM J0043+04531	300	M	Dwarf
0049+405	IRAS 00492+40322	120	M	Giant
0148+071	DFBS J015059.03+072308.33	600	M	Dwarf
2137+096	DFBS J213937.66+095250.43	300	C-CH	Giant
2145+154	DFBS J214733.89+154104.13	600	C-CH	Giant
2201+034	UCAC4 469-1328134	120	M	Dwarf
2239+249	DFBS J224217.04+251259.33	120	C-CH	Giant
2239+249	DFBS J224217.04+251259.33	120	C-CH	Giant

obtained with the Observatory de Haute-Provence (OHP, France) 1.93m telescope (CARELEC spectrograph; Gigoyan et al. (2001)). For some amount of FBS C stars medium-resolution CCD spectra also were obtained at the Cima-Ekar 1.83m telescope of the Padova Astronomical Observatory (Italy) equipped with the Asiago Faint Objects Spectrometer and Camera (AFOSC) and with the 1.52m Cassini telescope of the Bologna Astronomical Observatory at Loiano (Italy) equipped with the Bologna Faint Objects Spectrometer and Camera (BFOSC; Gigoyan et al. (2008)). All CCD observations, confirms reliability of our preliminary low-resolution spectral class determinations on the FBS plates. Optical spectra for some number of the new detected LTS spectra were obtained also on 8/9 September 2016 with the SCORPIO spectrograph and EEV 42-40 2048x2048 CCD (pixel size is 13.5m, resolution $\sim$ 6Å spectral range 4000-7250 Å using 600 lines mm^{-1} grism. Observations were reduced using standard MIDAS techniques. These observations are summarized in Table 2, where column 1 presents the FBS Number; column 2-other associations in SIMBAD data base, column 3-exposure time, column 4 and 5-spectral class and luminosity class of the objects. Figure 2 presents 2.6m BAO telescope moderate-resolution CCD spectra for some objects of the Table 1.

As a result, a second version of the FBS catalog of late-type stars was generated. It consists of 1471 late-type stars, including the spectral types and luminosities of these stars. Accurate optical positions for all 1471 FBS LTS determined in the POSSI (DSS1) and POSSII (DSS2) digitized sky surveys made it possible to correctly cross-correlate the sample with all available modern astronomical catalogues and data bases, namely USNO-B1.0, SDSS DR15, Gaia DR2, 2MASS, AllWISE and IRAS PSC/FSC. The catalog is available at https://vizier.u-strasbg.fr/viz-bin/VizieR-3?-source=J/MNRAS/489/2030.

3. Investigation of infrared photometry of late type stars from FBS

Photometric studies of late-type DFBS stars were carried out in the infrared range. Two-color diagrams of 2MASS, IRAS, AKARI9 and WISE were constructed, which once again confirm the accuracy of spectroscopic classification. Class M dwarfs are very well separated on the 2MASS JHK color-color diagram in the infrared (NIR).

Figure 3 presents the 2MASS J-H versus H-K_s colour-colour diagrams for all 1471 FBS LTS. Objects having J-$H > 0.8$ and H-$K_s > 0.2$ in the colour-colour diagram, usually are AGB stars. M dwarfs show proper motions and are very well separated on *JHK* Near-IR colour-colour diagram usually J-$H < 0.7$ and H-$K_s > 1.5$, see paper for more details (Bessell & Brett, 1988). 235 stars (out of 1471) show significant proper-motions and are classified as M dwarfs in FBS new LTS Catalogue.

Figure 4 presents the WISE colour-colour diagrams for all 1471 FBS LTS. On the WISE two-color diagram CH, R carbon stars have the same color as early M-class stars. M-class giants and dwarfs - appear on the diagram in the same compact range. Color indices criteria based on WISE data allow the selection of AGB stars with gas and dust envelopes and to distinguish between C and M stars.

doi: doi.org/10.52526/25792776-2021.68.2-534

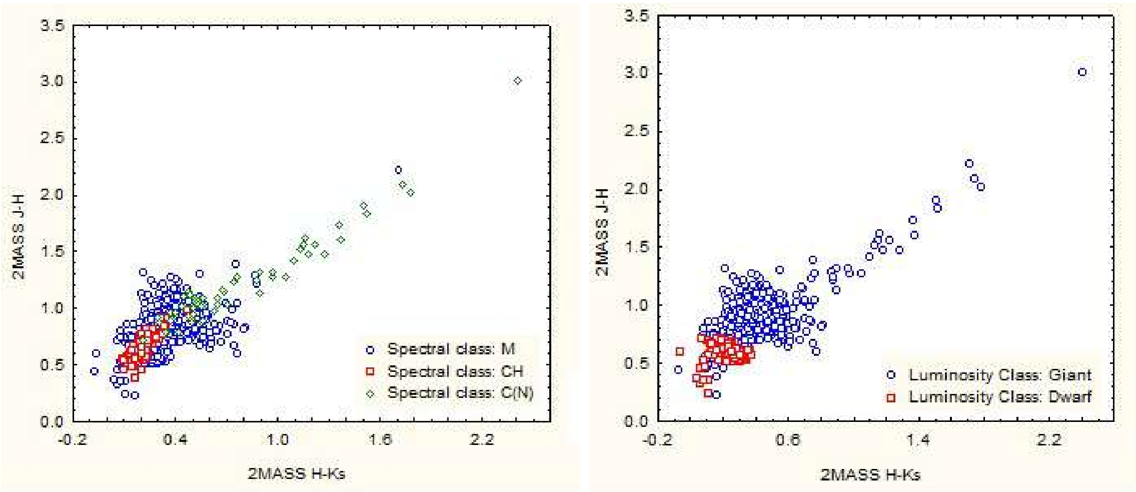

Figure 3. The 2MASS J-H versus H-K_s colour-colour diagrams for 1471 FBS LTSs stars.

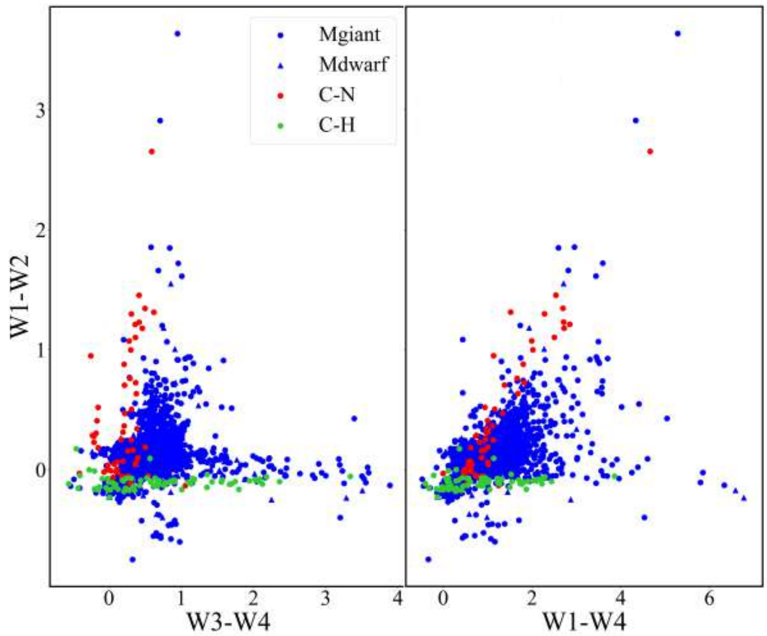

Figure 4. The WISE colour-colour diagrams for 1471 FBS LTSs stars.

4. Investigation of *Gaia* photometry of late type stars from FBS

The *Gaia* study was also conducted. The color - absolute magnitude and Teff - the absolute magnitude of the Hertzsprung–Russell diagram were plotted based on the distance data. Figure 5 show positions on colour – absolute M_G magnitude Gaia DR2 G – band absolute magnitude Hertzsprung – Russell diagram for 127 FBS C stars, also for near 150 M dwarfs from the “FBS Late – Type Stars Catalogue” Gigoyan et al. (2019). All N - type AGB stars are distributed in the brightest region, where Long – Period Variables (Miras, Semi – Regular variables, slow irregular variables, and small – amplitude red giant) are located and Figure 2 and 3 by Gaia Collaboration et al. (2019). Absolute G – band magnitude was estimated via the usual equation Gaia Collaboration et al. (2019);

$$M_G = G - 5Logr + 5 - A_G, \tag{1}$$

Combining near-infrared (NIR) and *Gaia* photometric information, Lebzelter et al. (2018) constructed a new diagram as an analysis tool for red giants. For this, they combined Wesenheit functions in the NIR and in the *Gaia* range. The 2MASS J and Ks NIR Wesenheit function is defined as Soszynski et al. (2005);

doi: doi.org/10.52526/25792776-2021.68.2-534

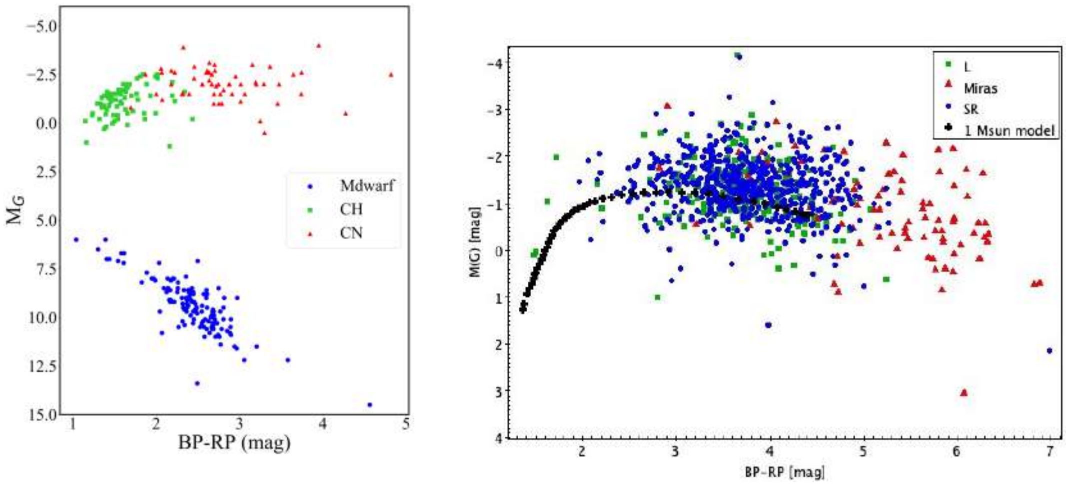

Figure 5. The Hertzsprung–Russell diagrams of FBS C stars and M gaints.

$$W_{K,J-Ks} = Ks - 0.686(J - Ks), \tag{2}$$

whereas the Wesenheit function for *Gaia* BP and RP magnitudes (Lebzelter et al., 2018) is defined as

$$W_{RP,BP-RP} = G_{RP} - 1.3(G_{BP} - G_{RP}) \tag{3}$$

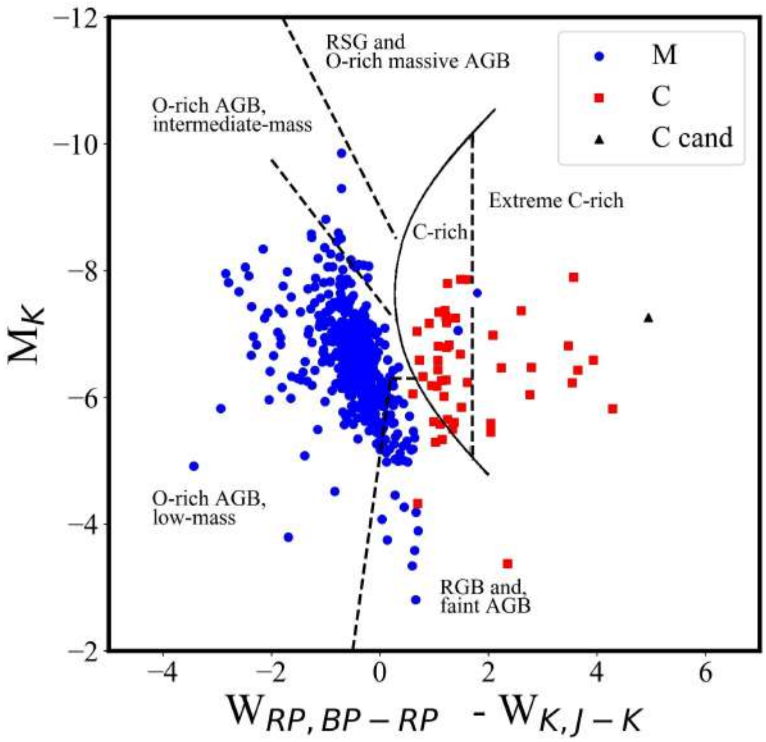

Figure 6. $W_{RP,BP-RP}$ - $W_{Ks,J-Ks}$ versus M_{Ks} diagram for FBS M and C giants.

In Figure 6 we show the application of this diagram to spectroscopically confirmed M and C giants with *Gaia* distances within our sample. Lebzelter et al. (2018) constructed this diagram for Large Magellanic Cloud (LMC) long period variables (LPVs) and demonstrated that it allows to identify subgroups among Asymptotic Giant Branch (AGB) stars according to their mass and chemistry. Six

doi: doi.org/10.52526/25792776-2021.68.2-534

distinct groups of red giants with their boundaries had been identified therein (for the definition of the borders of the groups see Table A.1 in Lebzelter et al. (2018)). For Figure 4, these boundaries were shifted according to the distance modulus of the LMC of 18.45 mag (Elgueta et al., 2016). With the help of synthetic stellar population models (based on the TRILEGAL code, Girardi et al. (2005), Marigo et al. (2017)), Lebzelter et al. (2018) showed that these groups correspond to low-mass, intermediate-mass, and massive O-rich AGB stars as well as RSG (Red Supergiants) and extreme C-rich AGB stars, the specific stellar mass range in each of these groups depending on the stellar metallicity (see Fig. 3 in Lebzelter et al. (2018) for details).

Figure 6 nicely confirms the ability of the *Gaia*-2MASS-diagram to distinguish between M- and C-stars. The majority of the FBS giants occupies the region of low mass, oxygen-rich AGB stars in this diagram. It thus seems likely that the FBS sample primarily consists of stars with M $<$ 2 $M_{\odot}$. Besides that, the diagram reveals a few candidates for intermediate mass AGB stars. The lack of the RSG and massive AGB stars among the sample of the FBS M giants is clearly evident.

5. Investigation of optical variability of late type stars from FBS

To study optical variability for FBS late-type stars, the basic data coming from the most prominent and wide-area sky were used and considered the CATALINA, NSVS, ASAS-SN, and LINEAR databases. The light curve analysis confirms nine stars as Mira-type variables, 43 as Semi-Regulars (SR) with very well expressed periodicity, and two objects as Irregular (Irr)-type variables for C stars. According to the ASAS-SN light curves, 690 of the giant M stars are classified as SR, 294 stars as L (Irr) variables, and 112 stars as Mira type.

A list of 1184 CRTS LINEAR objects was compiled, for which P $\geq$ 10 days. It is available at https://vizier.u-strasbg.fr/viz-bin/VizieR-3?-source=J/other/Ap/64. Spectral grades approved for over 625 PV. These are class F, G, K and M giants and dwarfs, as well as N-class stars at high galactic latitudes. For a large number of the PVs, we confirm spectral classes for objects presented in the "General Catalogue of Variable Stars: Version GCVS 5.1". Our list should be very useful for future versions of the GCVS. Nearly 100 LPV stars and 25 objects with very large Gaia DR2 BP - RP colors still need to be confirmed spectroscopically, and they will be included in our future observations.

6. Discussion and conclusion

We revised, updated and generated the new version of the FBS LTS catalogue. The second version of the catalogue contains main available data for 1471 objects. In revised catalogue we present DSS1/DSS2 accurate positions, USNO-B1.0 catalogue optical photometry and proper motions, WISE IR photometry, et al. for 1471 objects. Among 1471 objects, 127 are carbon stars of early and late subclasses. 235 LTS are M dwarfs. The remaining objects are M giants. Large number of the FBS LTS are completely new objects, which promise to expand the census of M giants and M dwarfs in the Solar vicinity. Two-color diagrams of 2MASS, IRAS, AKARI9 and WISE were constructed, which once again confirm the accuracy of spectroscopic classification. Class M dwarfs are very well separated on the 2MASS JHK color-color diagram in the infrared (NIR). *Gaia*-2MASS-diagram was constructed. Spectroscopically confirmed FBS O-rich and C-rich giants show the same separation in the Gaia-2MASS-diagram according to their chemistry as the LPVs of the LMC originally used to construct this diagnostic tool, providing another confirmation of its reliability. The discrimination between O-rich and C-rich objects becomes even more visible when using the $W_{RP,BP-RP} - W_{Ks,J-Ks}$ versus Gaia BP-RP colour or 2MASS J-Ks versus BP-RP. This offers the opportunity to use the difference of Wesenheit indices $W_{RP,BP-RP} - W_{Ks,J-Ks}$ also for chemistry classification in samples with unknown distances while losing the ability of the Gaia-2MASS diagram to separate the stars according to mass. To study optical variability for FBS late-type stars, the basic data coming from the most prominent and wide-area sky were used and considered the CATALINA, NSVS, ASAS-SN, and LINEAR databases. The light curve analysis confirms nine stars as Mira-type variables, 43 as Semi-Regulars (SR) with very well expressed periodicity, and two objects as Irregular (Irr)-type variables for C stars. According to

doi: doi.org/10.52526/25792776-2021.68.2-534

the ASAS-SN light curves, 690 of the giant M stars are classified as SR, 294 stars as L (Irr) variables, and 112 stars as Mira type. A list of 1184 CRTS LINEAR objects was compiled, for which P $\geq$ 10 days. It is available at https://vizier.u-strasbg.fr/viz-bin/VizieR-3?-source=J/other/Ap/64. Spectral grades approved for over 625 PV. These are class F, G, K and M giants and dwarfs, as well as N-class stars at high galactic latitudes.

References

Abramyan G. V., Gigoyan K. S., 1993, Astrophysics, 36, 114

Babusiaux C., van Leeuwen F., Barstow M. A., Jordi C., Zucker S., Zurbach C., Zwitter T., 2018, aap, 616, A10

Bailer-Jones C. A. L., Rybizki J., Fouesneau M., Mantelet G., Andrae R., 2018a, VizieR Online Data Catalog, p. I/347

Bailer-Jones C. A. L., Rybizki J., Andrae R., Fouesneau M., 2018b, A&A, 616, A37

Benn D., 2012, Journal of the American Association of Variable Star Observers (JAAVSO), 40, 852

Bessell M. S., Brett J. M., 1988, pasp, 100, 1134

Drake A. J., et al., 2014, apjs, 213, 9

Drake A. J., et al., 2017, mnras, 469, 3688

Elgueta S. S., et al., 2016, aj, 152, 29

Feast M. W., Glass I. S., Whitelock P. A., Catchpole R. M., 1989, mnras, 241, 375

Gaia Collaboration et al., 2018, A&A, 616, A1

Gaia Collaboration et al., 2019, A&A, 623, A110

Gaia Collaboration et al., 2021, aap, 650, C3

Gigoyan K. S., Mickaelian A. M., 2012, MNRAS, 419, 3346

Gigoyan K. S., Abrahamyan H. V., Azzopardi M., Russeil D., 2001, Astrophysics, 44, 328

Gigoyan K. S., Engels D., Mauron N., Hambaryan V. V., Rossi C., Gualandi R., 2008, Astrophysics, 51, 209

Gigoyan K. S., Russeil D., Mickaelian A. M., Sarkissian A., Avtandilyan M. G., 2012, A&A, 544, A95

Gigoyan K. S., Sarkissian A., Russeil D., Mauron N., Kostandyan G., Vartanian R., Abrahamyan H. V., Paronyan G. M., 2014, Astrophysics, 57, 510

Gigoyan K. S., Sarkissian A., Russeil D., Mauron N., Kostandyan G., Vartanian R., Abrahamyan H. V., Paronyan G. M., 2015, Astrophysics, 58, 369

Gigoyan K. S., Sarkissian A., Rossi C., Russeil D., Kostandyan G., Calabresi M., Zamkotsian F., Meftah M., 2017, Astrophysics, 60, 70

Gigoyan K. S., Mickaelian A. M., Kostandyan G. R., 2019, MNRAS, 489, 2030

Girardi L., Groenewegen M. A. T., Hatziminaoglou E., da Costa L., 2005, aap, 436, 895

Grady J., Belokurov V., Evans N. W., 2019, mnras, 483, 3022

Grady J., Belokurov V., Evans N. W., 2020, mnras, 492, 3128

doi: doi.org/10.52526/25792776-2021.68.2-534

Groenewegen M. A. T., et al., 2020, aap, 636, A48

Hughes S. M. G., Wood P. R., 1990, aj, 99, 784

Jayasinghe T., et al., 2018, mnras, 477, 3145

Kochanek C. S., et al., 2017, pasp, 129, 104502

Lebzelter T., Mowlavi N., Marigo P., Pastorelli G., Trabucchi M., Wood P. R., Lecoeur-Taïbi I., 2018, aap, 616, L13

Lebzelter T., Trabucchi M., Mowlavi N., Wood P. R., Marigo P., Pastorelli G., Lecoeur-Taïbi I., 2019, aap, 631, A24

Luo A. L., Zhao Y. H., Zhao G., et al. 2019, VizieR Online Data Catalog, p. V/164

Marigo P., et al., 2017, apj, 835, 77

Markarian B. E., Lipovetsky V. A., Stepanian J. A., Erastova L. K., Shapovalova A. I., 1989, Soobshcheniya Spetsial'noj Astrofizicheskoj Observatorii, 62, 5

Mickaelian A. M., et al., 2007, A&A, 464, 1177

Nicholls C. P., Wood P. R., Cioni M. R. L., Soszyński I., 2009, mnras, 399, 2063

Palaversa L., et al., 2013, aj, 146, 101

Prusti T., et al., 2016, aap, 595, A1

Rossi C., Dell'Agli F., Di Paola A., Gigoyan K. S., Nesci R., 2016, mnras, 456, 2550

Saio H., Wood P. R., Takayama M., Ita Y., 2015, mnras, 452, 3863

Shappee B. J., Prieto J. L., Grupe D., Kochanek C. S., Stanek K. Z.and Walker Z., Yoon Y., 2014, apj, 788, 48

Skrutskie M. F., et al., 2006a, aj, 131, 1163

Skrutskie M. F., et al., 2006b, AJ, 131, 1163

Soszynski I., et al., 2005, actaa, 55, 331

Soszynski I., et al., 2007, actaa, 57, 201

Whitelock P. A., Feast M. W., Van Leeuwen F., 2008, mnras, 386, 313

Wood P. R., et al., 1999, in Le Bertre T., Lebre A., Waelkens C., eds, Vol. 191, Asymptotic Giant Branch Stars. p. 151

doi: doi.org/10.52526/25792776-2021.68.2-534